JOHANNES GUTENBERG
UNIVERSITÄT MAINZ

Nachhaltige organische Synthesen sowie computergestützte Mechanismus- und Naturstoffaufklärung

Dissertation
zur Erlangung des Grades
»Doktor der Naturwissenschaften«
im Promotionsfach Chemie

am Fachbereich Chemie, Pharmazie, Geographie und Geowissenschaften
der Johannes Gutenberg-Universität Mainz

Jonathan Groß
geboren in Ludwigshafen am Rhein

Mainz, 2024

Die vorliegende Arbeit wurde im Zeitraum von Januar 2019 bis März 2023 im Arbeitskreis von Prof. Dr. Till Opatz am Department Chemie der Johannes Gutenberg-Universität Mainz angefertigt.

-D77-

Dekanin:	[redacted]
1. Berichterstatter:	Prof. Dr. Till Opatz
2. Berichterstatter:	[redacted]
Prüfungsvorsitz:	[redacted]
Datum der mündlichen Prüfung:	30. April 2024

Inhaltsverzeichnis

Danksagung

[redacted]

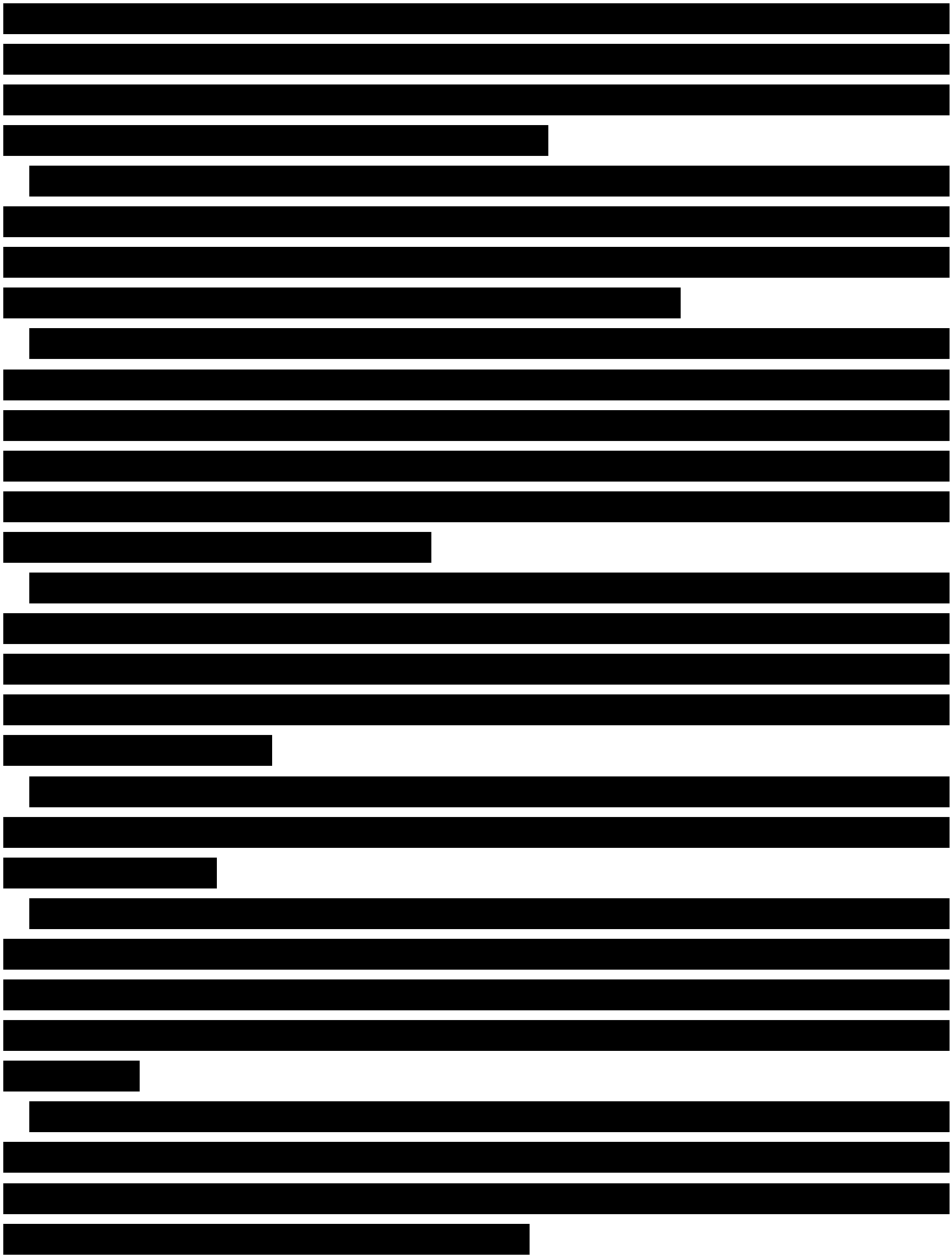

Zusammenfassung

Die chemische Industrie versucht durch ihre Transformation in den Bereichen Nachhaltigkeit und Umweltschutz einen wichtigen Beitrag zu der politisch angestrebten vollständigen Klimaneutralität zu leisten. Eine Möglichkeit bietet die Verwendung von Biomasse als erneuerbare Rohstoffquelle, jedoch sind kontinuierliche Prozessentwicklungen im Sinne der grünen Chemie nötig, um bestehende Prozesse sicherer, effizienter und ökologischer zu gestalten. Im ersten Teil dieser Arbeit wurden nachhaltige organische Synthesen unter Beachtung der Grundprinzipen der grünen Chemie erforscht. Die Verwendung einer Kugelmühle in Kombination mit rotem Blutlaugensalz als ungiftige Cyanidquelle erlaubte eine lösungsmittelfreie Umwandlung organischer Thiole in die entsprechenden Thiocyanate, wobei höhere Ausbeuten und deutlich geringere Reaktionszeiten im Vergleich zu dem komplementären Prozess im zweiphasigen Lösungsmittelgemisch erzielt werden konnten. Neben der Darstellung von 27 Substraten konnte die Reaktion erfolgreich in der ersten Totalsynthese des Naturstoffs Psammaplin B angewendet werden.

Performante Prozessoren und Grafikkarten ermöglichen seit einigen Jahren die Durchführung quantenmechanischer Berechnungen für große organische Systeme in kurzer Zeit und mit hoher Genauigkeit. Die implementierten Modelle aus dem Gebiet der theoretischen Chemie lassen sich für die Simulation von Reaktionsmechanismen anwenden, welche ein besseres Verständnis der auf molekularer Ebene ablaufenden Prozesse erlauben, die oft experimentell nicht zugänglich sind. Im Rahmen der vorliegenden Arbeit ermöglichte der Einsatz quantenchemischer Berechnungen auf Dichtefunktionaltheorie (DFT)- und *coupled-cluster* (CC)-Level die Simulation von Reaktionspfaden einer formalen [3+2]-Cycloaddition sowie einer Diels-Alder-Reaktion, womit einerseits auftretende angeregte Zustände und andererseits eine beobachtete Diastereoselektivität erklärt werden konnten. Des Weiteren wurde das unterschiedliche Polymerisationsverhalten substituierter *N*-Carbonsäureanhydride untersucht, allerdings ergaben die *in silico* Modellierungen keine

konsistenten Ergebnisse. Außerdem konnten bei einer photochemischen Dehydrierung von N-Heterozyklen niedrige Umsätze ausgewählter Substrate durch Substituenteneinflüsse und den daraus resultierenden verringerten Orbitalüberlapp erklärt werden.

Die Erforschung und Nutzbarmachung von Naturstoffen ist ein wichtiges Teilgebiet der organischen Chemie und besitzt seit jeher eine große Bedeutung für die Menschheit, insbesondere bei der Entwicklung von neuen Materialien oder Wirkstoffen. Die Isolierung und Strukturaufklärung unbekannter Sekundärmetaboliten aus Pilzen und Pflanzen sowie die Untersuchung ihrer inhärenten biologischen Aktivitäten kann die Suche nach potentiellen Leitstrukturen für die pharmazeutische Anwendung unterstützen. Da die dabei erhaltenen Substanzmengen häufig nicht für eine vollständige Charakterisierung, insbesondere die Bestimmung der Konfiguration chiraler Moleküle, ausreichen, können spektroskopische Methoden in Verbindung mit quantenmechanischen Berechnungen zu Hilfe genommen werden. Im Rahmen der vorliegenden Arbeit konnten diese sowohl bei synthetischen Molekülen als auch isolierten Naturstoffen angewendet werden. Der systematische Vergleich von simulierten *vibrational circular dichroism* (VCD)-Spektren mit aufgenommenen Spektren ausgewählter Moleküle ermöglichte eine Bewertung der Genauigkeit verschiedener Kombinationen von DFT-Funktionalen, Basissätzen und Solvatationsmodellen. Diese Methode wurde außerdem genutzt, um sowohl in der Synthese des Humanen Immundefizienz-Virus (HIV)-Integrase-Inhibitors Dolutegravir zwischen potentiell auftretenden Diastereomeren zu unterscheiden, als auch bei der Totalsynthese eines Makrozyklus aus der Gruppe der Oxacyclododecindione die absolute Konfiguration zu bestimmen. Darüber hinaus wurden DFT-Berechnungen zur Strukturaufklärung isolierter Verbindungen aus Pilz- und Pflanzenextrakten eingesetzt. Neben der Bestimmung der absoluten Konfiguration zweier Perylenstrukturen, die in einem Pilz der Gattung *Alternaria* vorkommen, konnte auch die Struktur eines Dihydroxanthons, das aus einem Pilz der Gattung *Diaporthe* isoliert wurde, vollständig charakterisiert werden. Für ein neuartiges Sesquiterpenlacton, das aus der zentralafrikanischen Pflanze *Vernonia tufnelliae* extrahiert wurde, konnte mit Hilfe der *diastereomeric probability 4+* (DP4+)-Methode die wahrscheinlichste relative Konfiguration vorhergesagt werden.

Abstract

Through its transformation in the areas of sustainability and environmental protection, the chemical industry is endeavouring to make an important contribution to the political goal of complete climate neutrality. One approach is the use of biomass as a renewable source of raw materials, whereas continuous process developments in the sense of green chemistry are necessary to make existing processes safer, more efficient and ecological. The first part of this thesis focussed on research regarding sustainable organic syntheses in accordance with the principles of green chemistry. The use of a ball mill in combination with Prussian red as a non-toxic cyanide source allowed a solvent-free conversion of organic thiols into the corresponding thiocyanates, resulting in higher yields and significantly shorter reaction times compared to the complementary batch process in a two-phase solvent mixture. In addition to the preparation of 27 substrates, the reaction was successfully applied in the first total synthesis of the natural product psammaplin B.

In recent years, high-performance processors and graphic cards have enabled quantum mechanical calculations for large organic systems in a short time and with high accuracy. The implemented models from the field of theoretical chemistry can be used for the simulation of reaction mechanisms, which allow a better understanding of processes occurring at the molecular level that are often not accessible experimentally. In the present work, the use of quantum chemical calculations at the density functional theory (DFT) and coupled-cluster (CC) level enabled the simulation of reaction pathways of a formal [3+2] cycloaddition and a Diels-Alder reaction, which allowed to explain the excited states that occur in the former reaction and the observed diastereoselectivity in the latter. Moreover, the different polymerisation rate of substituted *N*-carboxyanhydrides was investigated, but the *in silico* modelling did not provide consistent results. Furthermore, low conversions of selected substrates during a photochemical dehydrogenation of N-heterocycles could be explained by substituent influences and the resulting reduced orbital overlap.

The research and utilisation of natural products is an important field of organic chemistry and has always been of great importance to mankind, especially in the development of new materials or active pharmaceutical ingredients. The isolation and structural elucidation of unknown secondary metabolites from fungi and plants as well as the investigation of their inherent biological activities can support the search for potential lead structures for pharmaceutical applications. As the quantities of substances obtained are often not sufficient for a complete characterisation, in particular the determination of the configuration of chiral molecules, spectroscopic methods can be leveraged in conjunction with quantum mechanical calculations. In this dissertation, computer-aided spectroscopy methods were applied to both synthetic molecules and isolated natural substances. The systematic comparison of simulated vibrational circular dichroism (VCD) spectra and recorded spectra of selected molecules allowed an evaluation of the accuracy of different combinations of DFT functionals, basis sets and solvation models. This method was also used to distinguish between potentially occurring diastereomers in the synthesis of the human immunodeficiency virus (HIV) integrase inhibitor dolutegravir and to determine the absolute configuration of a macrocycle from the oxacyclododecindione family subsequent to its total synthesis. In addition, DFT calculations were applied to elucidate the structure of isolated compounds from fungal and plant extracts. The absolute configurations of two perylene structures found in a fungus of the genus *Alternaria* as well as the structure of a dihydroxanthone isolated from a fungus of the genus *Diaporthe* were fully characterised. For a novel sesquiterpene lactone extracted from the Central African plant *Vernonia tufnelliae*, the most probable relative configuration was predicted using the diastereomeric probability 4+ (DP4+) method.

Eigenständigkeitserklärung

Hiermit erkläre ich, dass ich die vorliegende Arbeit selbstständig verfasst habe. Ich versichere, dass wörtlich oder sinngemäß übernommenes Gedankengut als solches kenntlich gemacht wurde. Es wurden nur die Quellen und Hilfsmittel benutzt, die in der Arbeit angegeben sind.

Ort, Datum

Jonathan Groß

Bemerkungen

Im Rahmen dieser Dissertation wurde eine Vielzahl wissenschaftlicher Fragestellungen von großer thematischer Vielfalt bearbeitet, wofür diverse Kooperationen innerhalb der Arbeitsgruppe Opatz, insbesondere aber auch mit anderen Forschungsgruppen, unabdingbar waren. Die jeweiligen Beiträge der Kooperationspartner sowie eine Erlaubnis des entsprechenden Verlags zum Abdrucken in dieser Arbeit sind in den Kapiteln „Resultate und Diskussion“ aufgeführt. Das dazugehörige Zusatzmaterial befindet sich im Teil „Anhang“. Die Molekülnummerierung in den einzelnen Publikationen ist getrennt von den übrigen Kapiteln in dieser Arbeit zu betrachten. Abgeschlossene Projekte dieser Promotion wurden bereits in folgenden Publikationen veröffentlicht:

- **Structure elucidation and biological activities of perylenequinones from an *Alternaria* species**
  A. Kiefer, M. Arnholdt, V. Grimm, L. Geske, J. Groß, N. Vierengel, T. Opatz, G. Erkel, *Mycotoxin Res.* **2023**, *39*, 303–316.

- **An In Vitro Study of Local Oxygen Therapy as Adjunctive Antimicrobial Therapeutic Option for Patients with Periodontitis**
  L. K. Müller-Heupt, A. Eckelt, J. Eckelt, J. Groß, T. Opatz, N. Kommerein, *Antibiotics* **2023**, *12*, 990.

- **Comparison of Different Density Functional Theory Methods for the Calculation of Vibrational Circular Dichroism Spectra**
  J. Groß,[†] J. Kühlborn,[†] S. Pusch, C. Weber, L. Andernach, G. Renzer, P. Eckhardt, J. Brauer, T. Opatz, *Chirality* **2023**, *35*, 1–13.

[†] Geteilte Erstautorenschaft

- **Diplomeroterpenoid G: An unusual meroterpenoid from *Mimosa pudica* Linn. (Mimosaceae)**
  C. F. Kenmogne, P. Eckhardt, R. T. Tchuenguem, J. Groß, F. T. Ngouafong, B. K. Ponou, J. P. Dzoyem, R. B. Teponno, T. Opatz, L. A. Tapondjou, *Tetrahedron* **2023**, 154451.

- **Oxygen-Releasing Hyaluronic-Acid Based Dispersion with Controlled Oxygen Delivery for Enhanced Periodontal Tissue Engineering**
  L. K. Müller-Heupt, N. Wiesmann-Imilowski, S. Schröder, J. Groß, P. C. Ziskoven, P. Bani, P. W. Kämmerer, E. Schiegnitz, A. Eckelt, J. Eckelt, U. Ritz, T. Opatz, B. Al-Nawas, C. Synatschke, J. Deschner, *Int. J. Mol. Sci.* **2023**, *24*, 5936.

- **Total Synthesis and Biological Evaluation of the Anti-Inflammatory (13*R*, 14*S*, 15*R*)-13-Hydroxy-14-deoxyoxacyclododecindione**
  K. Seipp, J. Groß, A. Kiefer, G. Erkel, T. Opatz, *J. Nat. Prod.* **2023**, *86*, 924–938.

- **Complementary Mechanochemical and Biphasic Approaches for the Synthesis of Organic Thiocyanates using Hexacyanoferrates as Non-Toxic Cyanide Sources**
  C. Grundke,† J. Groß,† N. Vierengel, J. Sirleaf, M. Schmitz, L. Krieger, T. Opatz, *Org. Biomol. Chem.* **2023**, *21*, 644–650.

- **Extracts of *Rheum palmatum* and *Aloe vera* Show Beneficial Properties for the Synergistic Improvement of Oral Wound Healing**
  L. K. Müller-Heupt, N. Wiesmann, S. Schröder, Y. Korkmaz, N. Vierengel, J. Groß, R. Dahm, J. Deschner, T. Opatz, J. Brieger, B. Al-Nawas, P. W. Kämmerer, *Pharmaceutics* **2022**, *14*, 2060.

- **Ethyl Hydroxyethyl Cellulose—A Biocompatible Polymer Carrier in Blood**
  A. Eckelt, F. Wichmann, F. Bayer, J. Eckelt, J. Groß, T. Opatz, K. Jurk, C. Reinhardt, K. Kiouptsi, *Int. J. Med. Sci.* **2022**, *23*, 6432.

- **Constituents of *Desmodium salicifolium* (Poir.) DC (Fabaceae) with antifungal activity**
  A. P. T. Donkia, P. Eckhardt, B. T. Tsafack , R. T. Tchuenguem, J. Groß, B. K. Ponou, R. B. Teponno, J. P. Dzoyem, T. Opatz, L. Barboni, L. A. Tapondjou, *Phytochem. Lett.* **2022**, *50*, 100–105.

- **Sesquiterpene Lactones from *Vernonia tufnelliae*: Structural Features, Stereochemistry, and Biological Evaluation**
  G. Bitchagno, A. Schueffler, J. Groß, M. Krumb, P. Tané, T. Opatz, *J. Nat. Prod.* **2022**, *85*, 1681–1690.

- **Antiplanktonic and Antibiofilm Activity of *Rheum palmatum* against *Streptococcus oralis* and *Porphyromonas gingivalis***
  N. Kommerein, N. Vierengel, J. Groß, T. Opatz, B. Al-Nawas, L. K. Müller-Heupt, *Microorganisms* **2022**, *10*, 965.

- **Vinylcyclopropane [3+2] Cycloaddition with Acetylenic Sulfones Based on Visible Light Photocatalysis**
  A. Luque, J. Groß, T. J. B. Zähringer, C. Kerzig, T. Opatz, *Chem. Eur. J.* **2022**, *28*, e2021043.

- **Antimicrobial Activity of *Eucalyptus globulus, Azadirachta indica, Glycyrrhiza glabra, Rheum palmatum* Extracts and Rhein against *Porphyromonas gingivalis***
  L. K. Müller-Heupt, N. Vierengel, J. Groß, T. Opatz, J. Deschner, F. D. von Loewenich, *Antibiotics* **2022**, *11*, 186.

- **Xylochemicals and Where to Find Them**
  J. Groß,† C. Grundke,† J. Rocker,† A. J. Arduengo III, T. Opatz, *Chem. Commun.* **2021**, *57*, 9979–9994.

- **Anti-inflammatory dihydroxanthones from a Diaporthe species**
  M. Rohr, U. Kauhl, J. Groß, T. Opatz, G. Erkel, *Biol. Chem.* **2022**, *403*, 89–101.

- **Six-Step Gram Scale Synthesis of the HIV Integrase Inhibitor Dolutegravir Sodium**
  J.-P. Dietz, T. Lucas, J. Groß, S. Seitel, J. Brauer, D. Ferenc, B. F. Gupton, T. Opatz, *Org. Process Res. Dev.* **2021**, *25*, 1898–1910.

† Geteilte Erstautorenschaft

- **C-28/C-30 oxidized cycloartanes from the leaves and twigs of *Caloncoba dusenii* Gilg**
  L. Zeufack Nguetsa, J. D. Simo Mpetga, G. T. M. Bitchagno, J. Delain Tadjuidje, J. Groß, B.N. Lenta, T. Opatz, N. Sewald, M. Tene, *Phytochem. Lett.* **2021**, *43*, 145–149.

- **Diels-Alder Reaction of β-Fluoro-β-nitrostyrenes with Cyclic Dienes**
  S. A. Ponomarev, R. V. Larkovich, A. S. Aldoshin, A. A. Tabolin, S. L. Ioffe, J. Groß, T. Opatz, V. G. Nenajdenko, *Beilstein J. Org. Chem.* **2021**, *17*, 283–292.

- **An insight into the synthesis of *N*-methylated polypeptides**
  C. Muhl, L. Zengerling, J. Groß, P. Eckhardt, T. Opatz, P. Besenius, M. Barz, *Polym. Chem.* **2020**, *11*, 6919–6927.

- **Antimicrobial secondary metabolites from the medicinal plant *Crinum glaucum* A. Chev. (Amaryllidaceae)**
  B. Y. Kianfé, J. Kühlborn, R. T. Tchuenguem B. T. Tchegnitegni, B. K. Ponou, J. Groß, R. B. Teponno, J. P. Dzoyem, T. Opatz, L. A. Tapondjou, *S. Afr. J. Bot.* **2020**, *133*, 161–166.

- **Applications of Xylochemistry from Laboratory to Industrial Scale**
  J. Groß,† J. Kühlborn,† T. Opatz, *Green Chem.* **2020**, *22*, 4411–4425.

- **Making Natural Products from Renewable Feedstocks: Back to the Roots?**
  J. Kühlborn,† J. Groß,† T. Opatz, *Nat. Prod. Rep.* **2019**, *37*, 380–424.

- **Structure, Biosynthesis, and Bioactivity of Photoditritide from *Photorhabdus temperata* Meg1**
  L. Zhao, R. M. Awori, M. Kaiser, J. Groß, T. Opatz, H. B. Bode, *J. Nat. Prod.* **2019**, *82*, 3499–3503.

- **Synthesis of 2,3-Dihydro-4-Pyridones, 4-Quinolones and 2,3-Dihydro-4-Azocinones by Visible-Light Photocatalytic Aerobic Dehydrogenation**
  A. Sevenich, P. S. Mark, T. Behrendt, J. Groß, T. Opatz, *Eur. J. Org. Chem.* **2020**, *82*, 1505–1514.

† Geteilte Erstautorenschaft

Abkürzungsverzeichnis

αNNCA	α-substituiertes und *N*-methyliertes NCA
A	Absorbanz
A, **B**	Orbitalrotationshessematrizen (TD-DFT)
Ac	Acetyl
AI	*artificial intelligence*
AIBN	Azobis(isobutyronitril)
Ar	Aryl
ARE	*antioxidant response element*
ATR	*attenuated total reflection*
aug-cc-pVTZ	*augmented correlation-consistent polarized valence triple-zeta*
$\vec{B}$	Magnetfeld
B3LYP	Becke 3-Parameter Lee-Yang-Parr
BFGS	Broyden-Fletcher-Goldfarb-Shanno
Bn	Benzyl
Boc	*tert*-Butyloxycarbonyl
BODIPY	Bordipyrromethin
c	Lichtgeschwindigkeit
C	Koeffizientenmatrix
CAM	*Coulomb-attenuating method*
CAS	*complete active space*
CASPT2	CAS *second-order perturbation theory*
CC	*coupled-cluster*
CCS	CC *singles*
CCSD	CC *singles-doubles*
CCSD(T)	CCSD + *triples correction*

cc-pVDZ	*correlation-consistent polarised valence double-zeta*
CD	*circular dichroism*
CI	*configuration interaction*
CIS	CI *singles*
CIS(D)	CIS + *doubles correction*
CMAE	*corrected* MAE
CNSL	*cashew nut shell liquid*
COSMO	*conductor-like screening model*
CP3	*comparison parameter 3*
CPCM-X	*extended conductor-like polarisable continuum solvation model*
δ, d	chemische Verschiebung
D	Dipolstärke
DAMN	Diaminomaleonitril
def2-SVP	*definition 2 split-valence polarisation*
DFT	Dichtefunktionaltheorie
DIIS	*direct inversion of the iterative subspace*
DIPEA	Diisopropylethylamin
DLPNO	*domain based local pair-natural orbital*
DMF	*N*,*N*-Dimethylformamid
DNA	Desoxyribonukleinsäure
DP4	*diastereomeric probability 4*
dr	*diastereomeric ratio*
ε	molarer Extinktionskoeffzient (Spektroskopie), Orbitalenergie (Computerchemie)
$\boldsymbol{\varepsilon}$	Diagonalmatrix der Orbitalenergien
ε_0	elektrische Feldkonstante
e	Elektron
e	Elementarladung
ee	*enantiomeric excess*
E	Energie, Energieeigenwerte (Computerchemie)
$\vec{E}$	Elektrisches Feld
ECD	*electronic* CD

E_{el}	elektronische Energie
E_{h}	Hartree-Energie
EnT	Energietransfer
EOM-CC	*equation of motion* CC
ESI	*enantiomeric similarity index*
Et	Ethyl
eV	Elektronenvolt
E_{xc}	Austausch-Korrelations-Funktional
f	Oszillatorstärke, Ähnlichkeitsfaktor (SpecDis)
$\hat{F}$	Fock-Operator
$\mathbf{F}$	Fock-Matrix
γ	Halbwertsbreite
$\mathbf{g}$	Gradient
G	Gibbs-Energie
GGA	*generalised gradient approximation*
GIAO	*gauge-including atomic orbital*
h	Plancksches Wirkungsquantum
$\hbar$	reduziertes Plancksches Wirkungsquantum
$\hat{H}$	Hamiltonoperator
$\hat{H}'$	gestörter Hamiltonoperator
$\hat{H}_{\mathrm{el}}$	elektronischer Hamiltonoperator
$\mathbf{H}$	Hesse-Matrix
HF	Hartree-Fock
HI	Humanes Immundefizienz-Virus
HOMO	*highest occupied molecular orbital*
i	iso
IBWF	Institut für Biotechnologie und Wirkstoffforschung
IC_{50}	mittlere inhibitorische Konzentration
IEFPCM	*integral equation formalism* PCM
Im	Imaginärteil
IR	Infrarot
IRC	*intrinsic reaction coordinate*

$\mathcal{J}$	Kopplungskonstante, elektrostatische Abstoßung (Computerchemie)
JAK	Januskinasen
k	Geschwindigkeitskonstanten
k_B	Boltzmann-Konstante
K	Kern
KS	Kohn-Sham
λ	Wellenlänge
L	Ligand
LC-ωPBE	*long-range corrected* ω Perdew-Burke-Ernzerhof
LCAO	*linear combination of atomic orbitals*
LDA	*local density approximation*
LED	*light-emitting diode*
LR	*linear response*
LUMO	*lowest unoccupied molecular orbital*
μ	Mittelwert
$\hat{\vec{\mu}}$	elektrischer Übergangsdipolmomentoperator
m	Masse, meta
M	Molare Masse
$\vec{m}$	magnetisches Moment
$\hat{\vec{m}}$	magnetischer Übergangsdipolmomentoperator
M06-2X	Minnessota-'06 *double exchange*
MAE	*mean absolute error*
MCT	*mercury cadmium telluride*
MD	Molekulardynamik
m_e	Elektronenmasse
Me	Methyl
mGGA	*meta* GGA
MMFF	*Merck molecular force field*
MO	Molekülorbital
MOF	*metal-organic framework*
mRNA	*messenger ribonucleic acid*
MP	Møller-Plesset-Störungstheorie

mPW1PW91	modifiziert Perdew-Wang 1-Parameter Perdew-Wang-'91
∇	Nabla-Operator
ν	Freiheitsgrad
$\tilde{\nu}$	Wellenzahl
N_A	Avogadro-Konstante
NBO	*natural bonding orbital*
NCA	*N*-Carbonsäureanhydrid
NEVPT2	*N-electron valence state second-order perturbation theory*
NFκB	*nuclear factor kappa-light-chain enhancer of activated B-cells*
NMMet	*N*-Methyl-L-methionin NCA
NMR	*nuclear magnetic resonance*
Nrf2	*nuclear factor erythroid-derived 2*
ω	range-separation parameter (DFT-Funktionalen), Anregungs- bzw. Abregungsenergien (TD-DFT)
ωB97X-D	ω Becke-'97 *exchange* Dispersion
o	*ortho*
ϕ	Ortsorbital
φ	Spinorbital
ψ	Wellenfunktion
p	*para*
P	Wahrscheinlichkeit
$\hat{\vec{P}}, \hat{\vec{p}}$	Impulsoperator
PBE	Perdew-Burke-Ernzerhof
PBE0	Perdew-Burke-Ernzerhof, parameterfrei
PCM	*polarisable continuum model*
PEM	photoelastischer Modulator
PES	*potential energy surface*
Ph	Phenyl
PM6	*parametrisation method 6*
ppm	*parts per million*
Pr	Propyl
QST	*quadratic synchronous transit*

ρ	Elektronendichte
r	Abstand, Korrelationskoeffizient (Computerchemie)
$\vec{R}, \vec{r}$	Ortsvektor
$\boldsymbol{r}$	Elektronenkoordinaten
$\mathbf{R}$	Kernkoordinaten
R	Rotationsstärke
RPA	*radnom phase approximation*
rt	Raumtemperatur
σ	Standardabweichung
$\vec{\sigma}$	chemischer Verschiebungstensor
s	skaliert
$\mathbf{S}$	Überlappungsmatrix
SCF	*self-consistent field*
*s*DP4+	*scaled* DP4+
SET	*single electron transfer*
SMD	*solvation model based on density*
sod3	*superoxide dismutase 3*
SOMO	*singly occupied molecular orbital*
SSSET	*solid-state* SET
STAT	*signal transducers and activators of transcription*
T	Temperatur, kinetische Energie (theoretische Chemie), kumulierte t-Verteilungsfunktion (Computerchemie)
$\hat{T}$	kinetischer Energie-Operator
TD	*time-dependent*
TDA	*Tamm–Dancoff approximation*
TD-PT	TD *pertubation theory*
THF	Tetrahydrofuran
TMS	Tetramethylsilan
TMSCN	Trimethylsilylcyanid
TS	*transition state*
U	*unrestricted*
*u*DP4+	*unscaled* DP4+

UV	Ultraviolett
V	potentielle Energie
$\hat{V}$	potentieller Energie-Operator
VCD	*vibrational* CD
Vis	*visible*
VPT2	*vibrational* PT2
Z	Kernladungszahl

Teil I

Grüne Chemie

1 Einleitung

Der durch die Menschen hervorgerufene Klimawandel stellt eine potentiell irreversible Bedrohung für die Existenz von Pflanzen, Tieren und Menschen auf dem Planeten Erde dar. Seit Beginn der Industrialisierung kam es in Folge des exzessiven Verbrauchs fossiler Rohstoffe und des damit einhergehenden Ausstoßes von Treibhausgasen zu einer globalen Erwärmung der erdnahen Atmosphäre sowie der Meere. Bereits im späten 20. Jahrhundert zeichneten sich gravierende Veränderungen der Vegetation, des Bodens, des globalen Wasserhaushalts sowie der Zusammensetzung der Atmosphäre ab.[1] Um das Klima und die Umwelt vor weiteren schädlichen Konsequenzen zu schützen und die Auswirkungen der bisherigen Klimaveränderungen einzudämmen, wurden internationale Vereinbarungen wie das Kyoto-Protokoll (1997), das Übereinkommen von Paris (2015) oder der Europäische Grüne Deal (2019) verabschiedet.[2–4] Das von der Europäischen Kommission ausgegebene Ziel ist es, bis zum Jahr 2050 eine vollständige Klimaneutralität zu erreichen. Einen wichtigen Beitrag soll dabei die Reduktion von Treibhausgas-Emissionen leisten, sodass sich die globale Durchschnittstemperatur im Vergleich zum vorindustriellen Niveau[1] um maximal 1,5 °C erhöht.[5] Neben und in Überschneidung mit den Bereichen Handel, Verkehr sowie Land- und Forstwirtschaft kann die chemische Industrie für dieses Ziel einen wichtigen Beitrag leisten.[4]

1.1 Grüne Chemie

Der Bereich der grünen Chemie beschäftigt sich mit der Entwicklung chemischer Produkte und Verfahren, die ökologisch nachhaltig sind.[6,7] Das beinhaltet nicht nur die Verwendung oder Erzeugung von Stoffen einzuschränken oder ganz zu vermeiden, die gefährlich für den Menschen oder die Umwelt sind, sondern auch Reagenzien und Lösungsmittel so zu wäh-

[1] Das vorindustrielle Niveau wird aus dem Mittelwert der Jahre 1850–1900 gebildet.[5]

len, dass sie wenn möglich recycelbar sind. Darüber hinaus sind die Nutzung erneuerbarer Ressourcen, die Verringerung des Energieverbrauchs und der Abfallproduktion sowie die Vermeidung von Umweltverschmutzung von zentraler Wichtigkeit.[8,9] Zudem steht im Gegensatz zur konventionellen Beseitigung von Abfällen am Ende der Produktionskette die Vorbeugung im Vordergrund.[10]

Die Grundprinzipien für diese Ausrichtung der Chemie wurden von Anastas und Warner im Jahr 1998 in Form der zwölf Grundsätze der grünen Chemie formuliert und seitdem weltweit in Bildungseinrichtungen und Unternehmen implementiert:[11]

1. Abfallvermeidung
2. Maximierte Atomökonomie
3. Einsatz ungefährlicher Chemikalien
4. Entwicklung von umweltfreundlichen Produkten
5. Sichere Lösungsmittel und Auxiliare
6. Effiziente Energienutzung
7. Verwendung von nachwachsenden Rohstoffen
8. Minimierung von Derivatisierungen
9. Katalytische Verfahren
10. Biologische Abbaubarkeit
11. Echtzeitanalysen
12. Risikominimierung

Die klassische Produktion in der chemischen Industrie folgt in der Regel einem linearen Pfad, bei dem die erzeugten Produkte häufig nur einem einzigen Zweck dienen, bevor sie entsorgt werden. Die benötigten Rohstoffe, meist fossilen Ursprungs, werden mit hochreaktiven Reagenzien umgesetzt, die oft toxisch sind und eine hohe Persistenz aufweisen. Die Menge des dabei generierten Abfalls ist regelmäßig deutlich größer als die produzierte Menge des Zielprodukts. Alternativ zu solchen geradlinigen Produktionsketten wurde von Zimmerman *et al.* ein systematischer Ansatz vorgeschlagen, wie der Chemiesektor auf Grundlage bisheriger Erfolge im Bereich der grünen Chemie und deren technischen Umsetzung zu einem nachhaltigeren, zyklisch ausgerichteten System transformiert werden kann. Dies erfordert einen Wandel der gesamten Wertschöpfungskette hin zu mehr Nachhaltigkeit, beispielsweise durch die Verwendung erneuerbarer Ressourcen, einem neuar-

tigen Produktdesign sowie verbesserte Wiederverwendung, Recycling oder Downcycling des Produkts vor der Entsorgung.[12]

1.1.1 Metriken der grünen Chemie

In den letzten Jahrzehnten wurden verschiedene Metriken entwickelt, um chemische Reaktionen unter dem Gesichtspunkt der grünen Chemie zu quantifizieren, sodass für jede Interessengruppe geeignete Modelle zur Auswahl stehen.[13] Besonders hervorzuheben ist das von Trost entwickelte Konzept der Atomökonomie, das durch die Molmasse des Produktes im Verhältnis zur Molmasse aller Reaktanden definiert ist:[14]

$$\text{Atomökonomie} = \frac{M_{\text{Produkt}}}{M_{\text{Reaktanden}}} \cdot 100$$

Daneben ist auch der von Sheldon im Jahr 1992 eingeführte *E*-Faktor (*environmental factor*), der die Aufmerksamkeit auf das Problem der Abfallerzeugung bei der Herstellung von Chemikalien lenkt, hervorzuheben.[15–18] Hierbei wird auch der Vermeidung von Abfällen ein Wert beigemessen und die Effizienz chemischer Prozesse nicht mehr ausschließlich auf Grundlage der chemischen Ausbeute bewertet.[18,19] Der *E*-Faktor wird berechnet, indem die Masse aller Abfälle mit der Masse des Produktes ins Verhältnis gesetzt wird:

$$E\text{-Faktor} = \frac{m_{\text{Abfall}}}{m_{\text{Produkt}}}$$

1.1.2 Einfluss von Lösungsmitteln

Während sich die Herstellung von Grundchemikalien durch einen niedrigen *E*-Faktor auszeichnet, steigt dieser für die Herstellung von Feinchemikalien oder Pharmazeutika drastisch an. Dies ist eine Folge des weit verbreiteten Einsatzes stöchiometrischer Mengen von Reagenzien wie anorganischen Oxidations- und Reduktionsmitteln sowie Säuren und Basen, wodurch große Mengen an Abfällen generiert werden.[10] Insbesondere in der pharmazeutischen Industrie, bei der Herstellung aktiver pharmazeutischer Wirkstoffe, besitzen Lösungsmittel einen hohen Anteil an der verwendeten nicht wässrigen Masse (bis zu 90%) und somit auch an den Gefahren und Sicherheitsrisiken für den Menschen und die Umwelt.[8,9,20] Von verschiedenen Pharmafirmen wie GSK, Pfizer und Sanofi, aber auch Kooperationsgruppen wie der *American Chemical Society Green Chemistry Institute Pharma-*

ceutical Roundtable oder die europäische *Innovative Medicines Initiative* wurden Leitfäden herausgegeben, die eine Bewertung der Lösungsmittel sowie der verwendeten Reagenzien und Auxiliare auf Grundlage der ihrer inhärenten Probleme in Bezug auf Abfallentsorgung, Umwelt, menschliche Gesundheit und Sicherheit ermöglichen.[13,21–25] Dies stellt ein wichtiges Instrument bei der Versuchsplanung und der Auswahl der verwendeten Materialien (und daraus generierten Abfällen) dar. Im Idealfall wird kein Lösungsmittel benötigt, aber wenn es nicht vermieden werden kann, sollte es sicher zu verwenden sein, eine effiziente Abtrennung der Produkte erlauben und wiederverwendbar sein.[10] Mögliche Alternativen zu konventionellen organischen Lösungsmitteln stellen überkritische Lösungsmittel, ionische Flüssigkeiten oder Salzschmelzen dar.[26–29] Zweiphasige Lösungsmittelsysteme sowie homogene Mehrphasen-Katalysatoren erlauben eine einfache Abtrennung der Produkte und eine Rückgewinnung des Katalysators aus dem Reaktionsgemisch.[30]

1.1.3 Erneuerbare Ressourcen und Xylochemie

Die grüne Chemie gewinnt noch immer in vielen Bereichen wie der Pharmazie, der Landwirtschaft und der verarbeitenden Industrie an Bedeutung, wobei die Vereinbarkeit innovativer Ansätze mit bestehenden Synthesewegen bzw. ganzen Prozessen stark von der wirtschaftlichen Wettbewerbsfähigkeit abhängt.[31,32] Eine Kombination aus der Nutzung erneuerbare Rohstoffe mit umweltfreundlichen Lösungsmitteln und Reagenzien kann zu industriellen Prozessen mit minimalen Auswirkungen auf das globale Ökosystem führen. Durch stetige Forschung werden neue Quellen für erneuerbare Ressourcen gewonnen. So lassen sich die landwirtschaftlichen oder tierischen Abfallprodukte nutzen, um organische Grundchemikalien zu gewinnen. Einige Beispiele aus der Lebensmittelindustrie sind die Schalen von Krustentieren, gebrauchtes Frittierfett, Apfeltrester oder Treber bei der Bierherstellung.[33–36]

Der Begriff Xylochemie wurde von Arduengo und Opatz erstmals im Jahr 2015 beschrieben und kann als ein Teilbereich der grünen Chemie gesehen werden. Bestandteile von Holz oder Biomasse auf Pflanzenbasis dienen hierbei als Rohstoffquelle für die chemische Synthese anstelle von fossilen Kohlenstoffquellen.[37] Diese natürliche Palette an Chemikalien stellt eine Fülle an Funktionalitäten bereit, die in Petrochemikalien erst material- und energieintensiv über teils mehrere Syntheseschritte wieder eingeführt werden muss. Neben aromatischen und aliphatischen Verbindungen, die verschiedene funk-

tionelle Gruppen tragen können und Kohlenstoffatome in unterschiedlichen Oxidationsstufen besitzen können, sind auch enantiomerenreine Grundchemikalien zugänglich. Infolgedessen ergeben sich verkürzte oder alternative Syntheserouten zu organischen Molekülen mit biologischer Aktivität oder Naturstoffen.[38–47] Da es sich bei Xylochemikalien um nicht essbare Ausgangsmaterialen oder Abfallströme handelt, gibt es keine Überschneidungen mit der Lebensmittel- oder Futterindustrie, sodass keine ethischen Probleme wie die „Tank, Trog oder Teller"-Debatte entstehen.[48–50] Die aktuellste und ausführlichste Liste mit über 100 Xylochemikalien und deren respektiven natürlichen Quellen wurde im Jahr 2021 veröffentlicht.[47] Primäre Xylochemikalien lassen sich direkt aus Pflanzen- oder Holzextrakten isolieren, wohingegen sekundäre Xylochemikalien eine Umwandlung aus primären Spezies erfordern (Abbildung 1.1).[47]

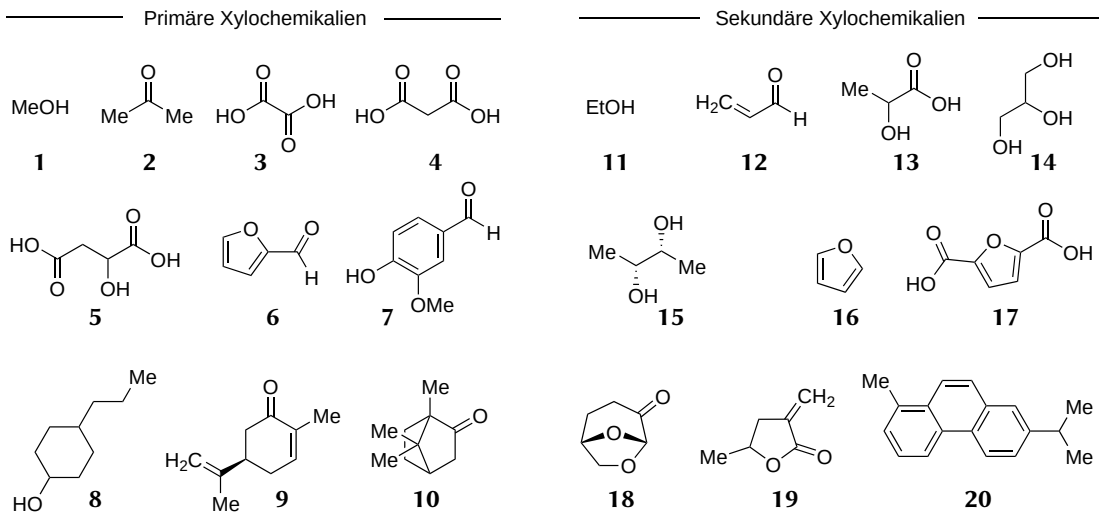

Abbildung 1.1: Eine Auswahl an primären und sekundären Xylochemikalien, die bereits zugänglich sind.[47]

Es existieren bereits viele technische Lösungen, um aus den verschiedenen Holzbestandteilen Plattformchemikalien zu gewinnen.[32,51–55] Prominente Beispiele sind die selektive Vanillin (**7**)-Isolierung durch den elektrochemischen Abbau von Kraft-Lignin, oder die Gewinnung oxygenierter, elektronenreicher Aromaten aus Sägespänen.[56–58] Die aus Lignocellulose gewonnenen Zucker lassen sich durch Fermentation in eine Vielzahl von Alkoholen, Carbonsäuren und weiteren Plattformchemikalien wie beispielsweise Furfural (**6**) transformieren.[10,51,59,60] Glycerin (**14**) fällt als Co-Produkt bei der Herstellung von Bio-Diesel als Abfall an und kann zu den Plattformchemikalien Epichlorhydrin oder Acro-

lein (**12**) umgesetzt werden.[10] Aus den nicht verzehrbaren Abfällen der Cashewnuss-Industrie (>1 Mt p.a.) lässt sich durch das Pressen der Schale bei erhöhten Temperaturen das Öl der Cashewnuss gewinnen. Dieses enthält langkettige alkylsubstituierte Salicylsäuren und Phenole.[61,62] Eine weitere Möglichkeit, Abfälle der Lebensmittelindustrie nutzbar zu machen, ist die Gewinnung von Monoterpenen, Pektinen und Flavonoiden aus den Schalen von Zitrusfrüchten oder von Polyhydroxyalkanoaten als biobasierte Polyester aus nicht mehr zum Verzehr geeigneten Pflanzenölen.[36,63,64] Auch organische Lösungsmittel lassen sich auf diese Weise gewinnen. Methyltetrahydrofuran (Me-THF) lässt sich entweder durch die Hydrierung von Furfural (**6**) oder aus Lävulinsäure darstellen, die im industriellen Maßstab aus Cellulose und Hemicellulose gewonnen werden kann.[55,65] Aus Cellulose kann darüber hinaus Cyren (**18**) gewonnen werden, das als Alternative zu *N*,*N*-Dimethylformamid (DMF) oder *N*-Methyl-2-pyrrolidon (NMP) verwendet werden kann.[66–69]

Die Verwendung erneuerbarer Grundchemikalien, Lösungsmittel und Reagenzien wurde in den letzten Jahren in verschiedenen Bereichen der chemischen Forschung implementiert. Neben vollständig auf Xylochemikalien basierenden Totalsynthesen wurde auch die Darstellung zahlreicher Anwendungsprodukte wie UV-Absorber, Farbstoffe und Polymere (Schema 1.1) beschrieben.[38–41,43,44,70–77] Im Teilbereich der Polymerchemie lassen sich als Alternative zu Methylmethacrylaten erneuerbare cyclische Vinyllactone polymerisieren, wie es von Manzer mit Tulipalin A (**21**) demonstriert wurde.[78] Ein eindrucksvolles Beispiel aus der Farbstoff-Chemie wurde von Opatz *et al.* beschrieben, die in einer dreistufigen Synthese Veratrumaldehyd (**23**) und Nitromethan (**24**) in die Leukoform zweier Indigofarbstoffe **25** und **26** transformierten, die so direkt für das Färben von Naturfasern verwendet werden können.[39] Sperry *et al.* zeigten die Nutzbarmachung der Polysaccharide Chitin und Chitosan als erneuerbare Quelle von stickstoffhaltigen Verbindungen.[79–81] Eine weitere Möglichkeit, ein Abfallprodukt in die Wertschöpungskette zu integrieren wurde ausgehend von Cashewnussschalenöl in technischer Qualität entwickelt. In einer umweltfreundlichen und abfallminimierten Synthese können Cardanolderivate **29**–**32**, durch katalytische reduktive Aminierung und anschließende Umsetzung, in neutrale, zwitterionische und kationische Tenside **35**, **36** und **37** überführt werden. Die Synthese von Gooßen *et al.* zeichnet sich durch einen niedrigen *E*-Faktor aus, während vergleichbare oder bessere Eigenschaften im Bereich der Oberflächenspannung oder des Aggregationsverhaltens der

erhaltenen Tenside **35**, **36** und **37** gegenüber modernen und kommerziell erhältlichen Tensiden erzielt werden.[82] Außerdem wurde die Darstellung von UV-Absorbern sowie eine Nutzung als Härterkomponenten in Epoxidharzen demonstriert.[44,83,84]

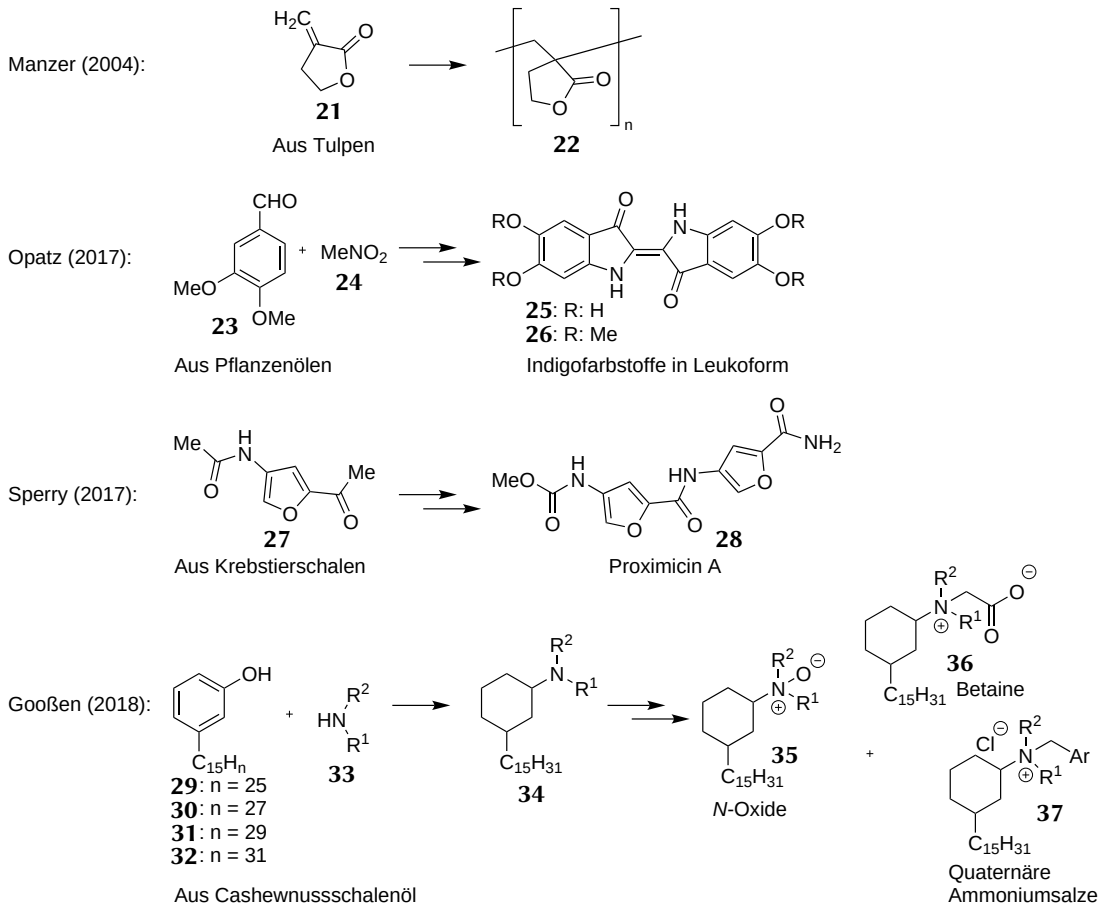

Schema 1.1: Verwendungsbereiche von erneuerbaren Ressourcen und Xylochemikalien zur Darstellung verschiedenster Verbindungsklassen.[39,78,79,82]

Ausgehend von Xylochemikalien können verschiedene Naturstoffe dargestellt werden.[46,47] Schäfer, Waldvogel und Opatz *et al.* entwickelten eine enantioselektive Totalsynthese des Opioids (–)-Thebain (**40**), die von den Xylochemikalien Methylgallat (**38**), Methanol (**1**) und Homoveratrylamin (**39**) ausgeht (Schema 1.2). Aufbauend auf diesem Naturstoff, der in Mohnpflanzen vorkommt, lassen sich diverse weitere analgetische Arzneimittel darstellen.[40] Aus den Knospen der Balsam-Pappel (*Populus balsamifera*) können verschiedene Balsakon-Naturstoffe gewonnen werden.[85–87] Die Darstellung der Substanzen **43**–**45**, die eine antibakterielle Wirkung gegen grampositive Erreger besitzen, wur-

de von der Arbeitsgruppe Pichette in einer einstufigen, metall- und schutzgruppenfreien Synthese veröffentlicht.[88] In verschiedenen Berichten konnten Opatz *et al.* die Sekundärmetaboliten **49**–**52** von Orchideen totalsynthetisch darstellen und auf biologische Eigenschaften testen.[45,89]

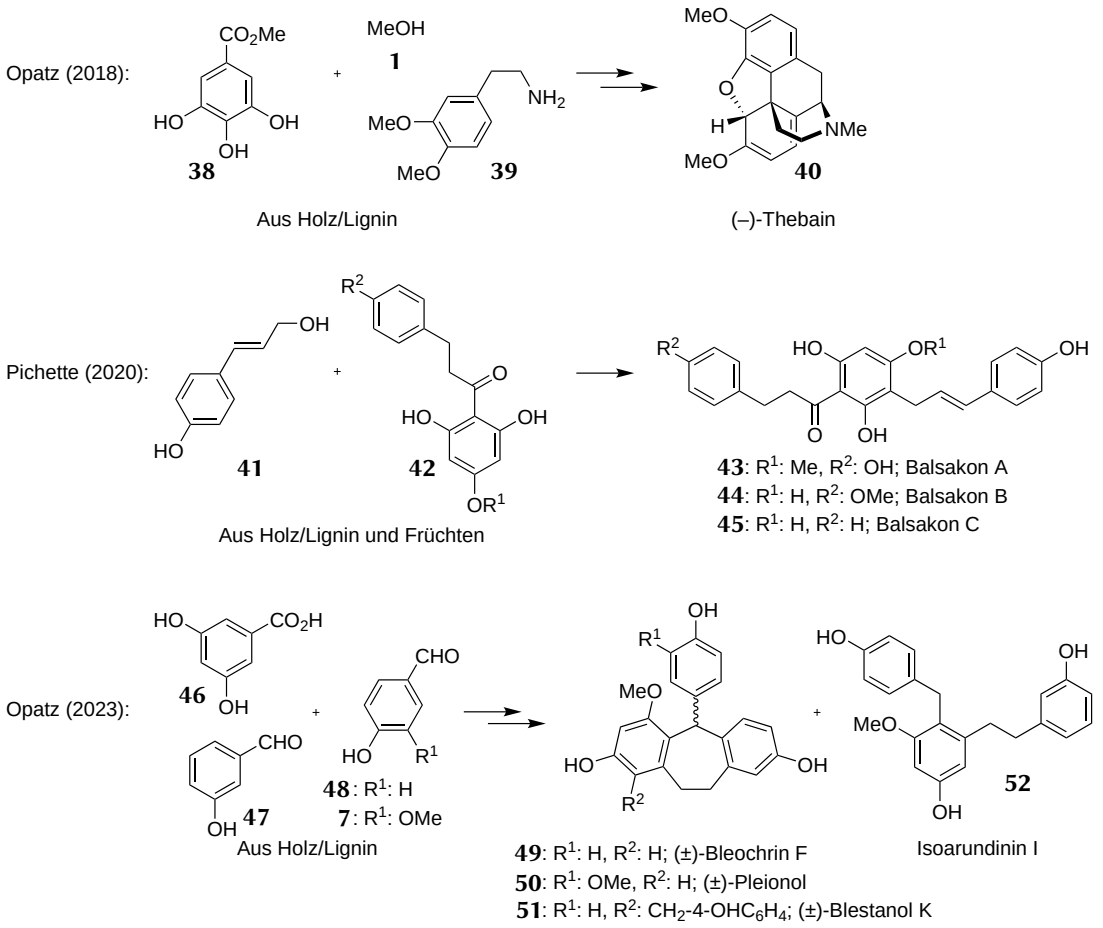

Schema 1.2: Totalsynthese verschiedener Naturstoffmotive ausgehend von Xylochemikalien.[40,45,88,89]

Neben der Auswahl der Reagenzien und der Lösungsmittel können auch unterschiedliche Methoden eingesetzt werden, um Reaktionen im Sinne der grünen Chemie nachhaltig durchzuführen. In der synthetischen organischen Chemie können Reaktionen nicht nur durch Temperatur, Licht oder Strom induziert werden, sondern auch auf mechanochemischer, lösungsmittelfreier Basis durchgeführt werden.

1.2 Mechanochemie

Die Mechanochemie befasst sich mit der chemischen Umwandlung von Stoffen, die durch einen mechanischen Energieeintrag wie Kompression, Reibung oder Scherung ausgelöst wird.[90] Die Entdeckung der Nutzbarkeit von mechanischer Energie zu diesem Zweck lässt sich nicht genau datieren, aber bereits in der Steinzeit wurden Mörser und Pistill für die Zubereitung von Nahrungsmitteln verwendet.[91] Diese Technik wurde später auf andere Materialien wie Mineralien, Farben oder Arzneimittel ausgedehnt. Da es damals unmöglich war, die rein physikalische Zerkleinerung von chemischen Umwandlungen zu unterscheiden, ist heute unklar, zu welchem Zeitpunkt die chemische Wirksamkeit des Feinmahlens erkannt wurde. Das älteste erhaltene Dokument in diesem Zusammenhang wurde um 315 v. Chr. von Theophrastus von Eresus, Aristoteles' Schüler, verfasst und enthält einen Verweis auf die Reduktion von Cinnabarit (HgS) zu elementarem Quecksilber, wenn das Mineral in einem aus Kupfer gefertigten Mörser und Pistill verrieben wird.[92,93]

Der Fokus der Mechanochemie lag lange Zeit auf anorganischen Materialien, im Bergbau und der Metallurgie.[94] Anfang des 20. Jahrhunderts definierte Ostwald die Mechanochemie als eine der vier Unterdisziplinen der Chemie mit unterschiedlichen Energiequellen, neben der Thermochemie, Elektrochemie und Photochemie.[95,96] Die ersten wissenschaftlichen Veröffentlichungen zu *mechanochemistry* in der Literaturdatenbank SciFinder^n reichen bis in das Jahr 1897 zurück.[97] Mit dem Beginn des 21. Jahrhunderts war die Mechanochemie nicht mehr nur auf Co-Kristallisationsreaktionen limitiert, sondern fand vermehrt Anwendung in der organischen Synthese.[98,99] Aufbauend auf den ersten Reaktionen mit Mörser und Pistill, wurden sicherere und effizientere Maschinen wie Kugelmühlen oder Doppelschneckenextruder entwickelt, die den Prinzipien der grünen Chemie folgen.[102,105,107] Vorteile sind ausbleibende Löslichkeitsbeschränkungen bei erheblicher Verringerung der anfallenden Abfälle. Weiterhin können Reaktionen unter Luftatmosphäre durchgeführt werden, die im konventionellen Lösungsmittelsystem eine Schutzgasatmosphäre benötigen und der Umgang mit Gefahrstoffen wird erleichtert.[94,103] Darüber hinaus lassen sich sowohl verbesserte als auch komplementäre Selektivitätsprofile und verkürzte Reaktionszeiten realisieren.[104,105] Wichtige industrielle Aspekte sind ein geringer Energieverbrauch, geringe CO_2-Emissionen und niedrige Betriebskosten.[100,101]

Auch wenn die Mechanochemie gemessen an ihrem Potenzial, die chemische Synthese voranzubringen, noch in den Kinderschuhen steckt, zeigt sich doch ein klarer Trend.[106]

Aus der Anzahl der Publikationen zu *ball mill* wird das gestiegene Interesse an Kugelmühlen ersichtlich. Werden die Veröffentlichungen gegen das entsprechende Erscheinungsjahr der letzten 50 Jahre aufgetragen (Abbildung 1.2) lässt sich ein starker Anstieg vor allem während der letzten 20 Jahren beobachten. Im Jahr 2019 wurde die Mechanochemie als eine der zehn aufstrebenden Zukunftstechnologien in der Chemie von der IUPAC benannt.[106] Wichtig wird es in der Zukunft sein, Methoden zur effizienten Skalierung mechanochemischer Reaktionen sowie praktikabler *in situ* Analysetechniken zu entwickeln.[107]

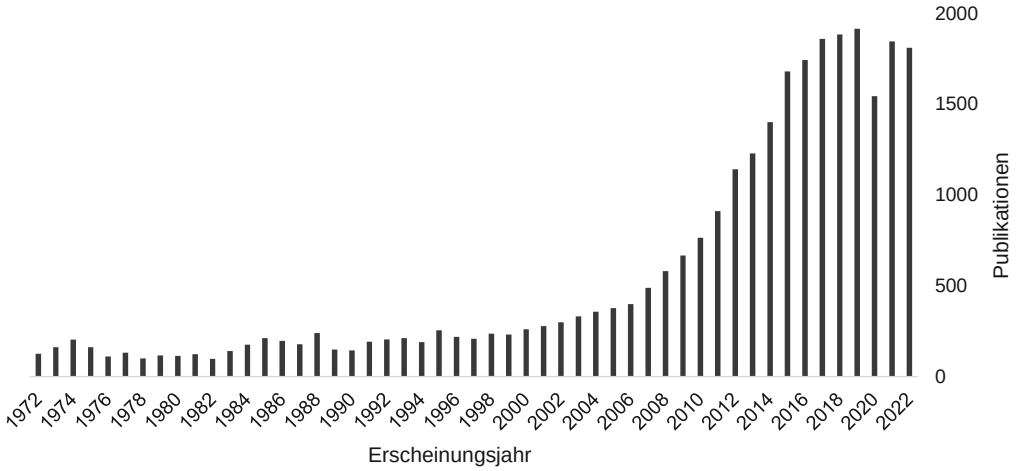

Abbildung 1.2: Auftragung der gelisteten Publikationen zu dem Suchbegriff *ball mill* in SciFinder^n gegen die Erscheinungsjahre der letzten 50 Jahre.[97]

1.2.1 Aufbau und Funktion verschiedener Mühlen

Heutzutage kann die Technik des Zermahlens vereinfacht und automatisiert in Mühlen durchgeführt werden. Durch ein genaues Einstellen der Parameter (z. B. Energie- und Geschwindigkeitskontrolle) wird eine höhere Reproduzierbarkeit erreicht und größere Maßstäbe sowie längere Mahlzeiten im Vergleich zu Mörser und Pistill können realisiert werden.[99,108] Die intensive Mischwirkung überwindet die Beschränkungen des Massentransports im festen Zustand und kann die Reaktionszeiten erheblich verkürzen.[105] Die Mischungsprobleme bei der Arbeit mit hydrophilen und lipophilen Verbindungen werden minimiert und die Verwendung biphasischer Lösungsmittelsysteme, phasenwechselnder Reagenzien oder Phasentransferkatalysatoren ist nicht erforderlich.[109] Darüber hinaus senkt die verringerte Verwendung flüchtiger organischer Lösungsmittel das Risikopoten-

zial. Aufgrund der effizienten Energieübertragung auf das Reaktionsgemisch sind Reaktionen in Mühlen durch eine geringe Energieintensität gekennzeichnet und erlauben eine Anwendbarkeit auf eine breite Palette von Materialien, z. B. kleine organische Moleküle, Katalysatoren, Mineralien, Metalloxide, Pigmente oder (Bio-)Polymere.[99,108] Um die in den Mühlen ablaufenden Prozesse beschreiben zu können, wurden in der Literatur bereits mehrere theoretische Modelle vorgeschlagen, auf die an dieser Stelle nur verwiesen wird.[127–129] Basierend auf ihrem Funktionsprinzip, dem direkten und indirekten Mahlen, können die Mühlen in zwei Gruppen unterteilt werden und eine Auswahl ist in Abbildung 1.3 gezeigt.

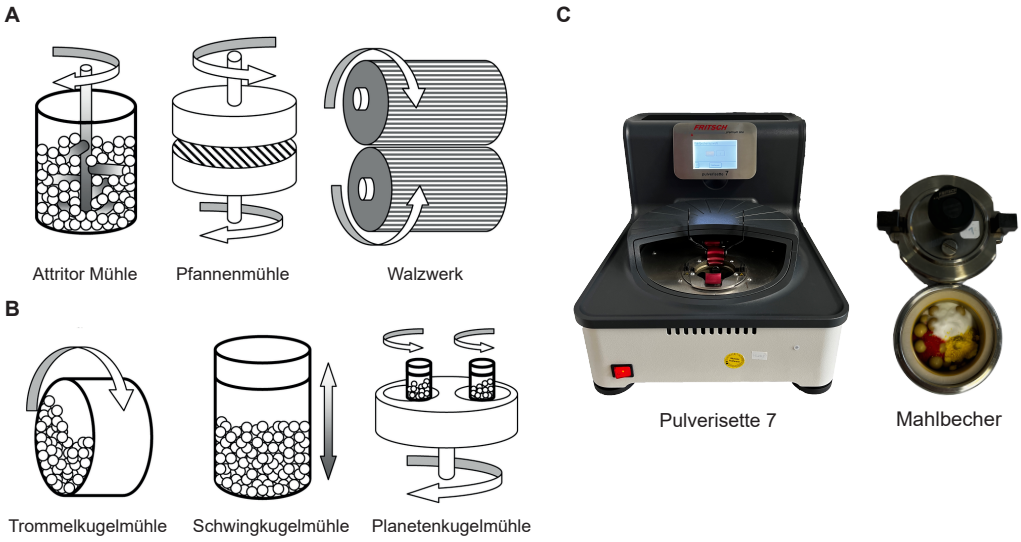

Abbildung 1.3: Schematische Darstellung verschiedener Mühlen, die das direkte (**A**) und indirekte (**B**) Mahlen von Stoffen erlauben, abgewandelt von Gorrasi *et al.*[110] Bei der Pulverisette 7 (**C**) handelt es sich um eine kommerzielle Planetenkugelmühle der Firma Fritsch GmbH & Co. KG, abgebildet mit beladenen Zirkonoxid Mahlbechern.

Beim direkten Mahlen wirken mechanische Wellen oder Walzen auf das Mahlgut ein und übertragen so die kinetische Energie direkt in Form von Druck-, Scher- und Schlagkräften auf das Mahlgut.[105] Beispiele hierfür sind die Attritor Mühle, die Pfannenmühle oder das Walzwerk (Abbildung 1.3 **A**).[110] Die Attritor Mühle besteht aus einem vertikalen stationären Behälter, der mit dem zu mahlenden Stoff gefüllt ist. Das Gemisch wird von einer vertikalen Welle mit horizontalen Armen vermengt. Je nach Anforderung kann diese Mühle unter einer Vielzahl von Bedingungen betrieben werden, wobei die Größe und Menge der Mahlkörper, die Mahlgeschwindigkeit und die Temperatur variiert werden können. Die

Pfannenmühle besteht aus zwei Mahltellern, wobei die Bewegung gegeneinander zu einer Zerkleinerung der dazwischen liegenden Materialien führt. Ein Walzwerk besteht aus zwei horizontalen Stahlwalzen mit gleichem Durchmesser und gleicher Länge. Der Spalt zwischen den thermisch regulierbaren Walzen kann mechanisch oder hydraulisch eingestellt und gehalten werden.[110,111]

Beim indirekten Mahlen wird die kinetische Energie zunächst auf den Mahlkörper und anschließend durch Reibung auf das Mahlgut übertragen, welches dadurch Gravitations- und Zentrifugalkräften ausgesetzt wird. Beispiele dafür sind Trommel-, Schwing- sowie Planetenkugelmühlen (Abbildung 1.3 **B**).Durch klar definierte Parameter wie die Kugelgröße, die Mahlzeit und die Frequenz lässt sich eine hohe Reproduzierbarkeit erreichen.[99] Die Kugeln und Mahlbecher können aus verschiedenen Materialien wie Zirkonoxid oder Wolframcarbid gefertigt werden, aus denen unterschiedliche Energieüberträge resultieren, was eine substratspezifische Auswahl ermöglicht.[94] Kugelmühlen erlauben die einfachere Verwendung toxischer Substanzen, da moderne Mahlbecher hermetisch verschlossen werden können. Dies ermöglicht auch Reaktionen zwischen Reaktanden in unterschiedlichen Aggregatszuständen.[112] Ein Nachteil beim Betrieb einer Kugelmühle ist, dass sich zwei wichtige Parameter, Temperatur und Druck, im Labormaßstab nur schwer messen lassen.[99] Eine Trommelkugelmühle besteht aus einem rotierenden horizontalen Zylinder, der mit Kugeln gefüllt ist und um seine Längsachse gedreht wird. Dabei fallen die Kugeln kontinuierlich auf das Mahlgut und zerkleinern dieses. Schwingkugelmühlen finden oft im Labormaßstab bei systematischen Testverfahren Einsatz. Dabei wird die mit Kugeln und Mahlgut beschickte Mahlkammer eingespannt und in hoher Frequenz hin- und hergeschwungen, um Stoßkräfte zu induzieren. Diese Mühlen können mit einer Kühlung ausgestattet werden, wodurch eine Verlängerung der Mahldauer ermöglicht oder die sichere Nutzung thermisch empfindlicher Reaktionspartner erleichtert wird.[109] Bei der Planetenkugelmühle stehen die Mahlkammern auf einer rotierenden Trägerscheibe und drehen sich zusätzlich um ihre eigene Achse.[110,113]

Nennenswerte Beispiele der erfolgreichen Anwendung der Mechanochemie sind die kontinuierliche Synthese von Ammoniak, einem der wichtigsten stickstoffhaltigen Grundstoffe, bei Raumtemperatur und atmosphärischem Druck in einer Schwingkugelmühle oder die Bildung von Co-Kristallen für die pharmazeutische Anwendung.[114–118] Darüber hinaus verdeutlichen die Herstellung von Legierungen, Oxiden oder (Nano)Kompositen, die

Darstellung von metallorganischen Gerüstverbindungen oder supramolekularen Systemen sowie die Funktionalisierung von Biopolymeren die vielfältige Nutzbarkeit der Mechanochemie.[110,113,119–122]

1.2.2 Anwendung der Kugelmühle in der organischen Synthese

Viele konventionelle organischen Synthesen konnten bereits auf diese lösungsmittelfreie Technik übertragen werden.[94,100,123–126] Dazu zählen übergangsmetallkatalysierte Kreuzkupplungsreaktionen wie die Sonogashira-, die Suzuki-Miyaura- und die Negishi-Kupplung sowie die Heck-Reaktion.[130–135] Auch direkte C–H-Aktivierungen, asymmetrische Synthesen sowie die Darstellung von Heterozyklen konnten durchgeführt werden.[99,100,109,130,136] Neben Kondensations-, Halogenierungs- und Aminohalogenierungsreaktionen sind auch Cycloadditionsreaktionen möglich.[137] Ausgewählte Anwendungsbeispiele der letzten Jahre sind in Schema 1.3 dargestellt.

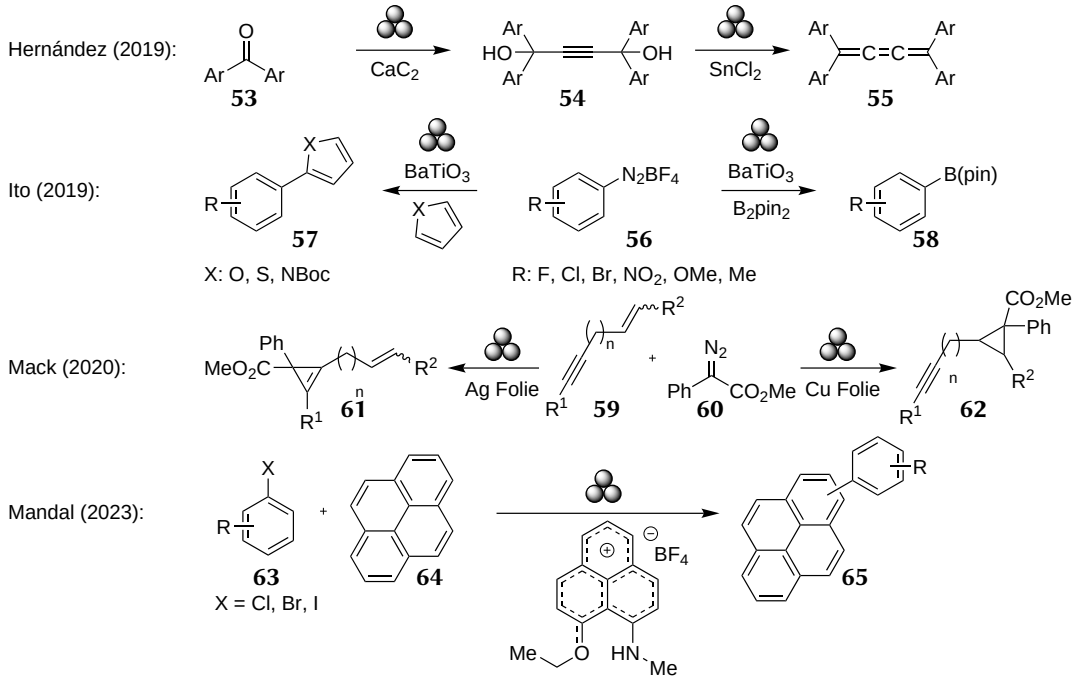

Schema 1.3: Organische Reaktionen die in den letzten Jahren in einer Kugelmühle durchgeführt wurden. Eine mechanochemische Reaktion wird symbolisch durch drei Kugeln dargestellt.[138–141]

Durch die mechanochemische Umsetzung von Diarylketonen **53** mit Calciumcarbid in Form einer Faworsky-Reaktion zu den entsprechenden Propargylalkoholen **54** konnten Hernández *et al.* den anschließenden Zugang zu Tetraaryl[3]kumulenen **55** demonstrieren. Vorteil dieser Art der Darstellung von Propargylalkoholen ist, dass auf die konventionell benötigten (Erd-)Alkaliacetylide verzichtet werden kann. Festes Calciumcarbid (CaC_2) kann als sichere Alternative zu Acetylen in der chemischen Synthese verwendet werden und die Herstellung ist unabhängig von fossilen Ressourcen. Darüber hinaus kann nicht umgesetztes Carbid einfach regeneriert und wiederverwendet werden und bietet sich somit für ein nachhaltiges Kohlenstoffkreislaufsystem an.[142] Die erhaltenen Propargyldiole **54** können in einer säure- und lösungsmittelfreien Zinnchlorid-vermittelten reduktiven Eliminierung zu Tetraaryl[3]kumulenen **55** umgesetzt werden.[138]

Durch Ausnutzung des piezoelektrischen Effektes von Bariumtitanat ($BaTiO_3$)-Nanopartikeln konnten Ito *et al.* eine komplementäre Methode zur Photoredox-Katalyse entwickeln, die die Mechanoredox-Aktivierung von organischen Molekülen ermöglicht. Diese Umsetzung wurde mit Aryldiazoniumsalzen **56** in Arylierungs- und Borylierungsreaktionen im Grammmaßstab gezeigt. Der mechanische Energieeintrag während des Mahlens erzeugt zeitweise sehr stark polarisierte Partikel, die als starkes Reduktionsmittel fungieren und einzelne Elektronen auf die Diazoverbindungen **56** übertragen, wodurch elementarer Stickstoff freigesetzt wird und die entsprechenden Arylradikale generiert werden. Nach Addition an einen Heteroaromaten oder ein Diboronat agiert das Elektronenloch des mechanisch aktivierten $BaTiO_3$ anschließend als Oxidationsmittel, wodurch der Katalysator zurückgebildet wird. Für die gezeigte Umsetzung werden weder absolutierte oder entgaste Lösungsmittel noch Schutzgasatmosphäre benötigt.[139]

Um ein neuartiges Katalysekonzept handelt es sich bei der direkten Mechanokatalyse, bei der die Oberfläche der Mahlkugeln als Katalysator agiert. Dies birgt den Vorteil, dass die Rückgewinnung des Katalysators einfach und effizient ist.[143] Im Jahr 2009 wurde von Mack *et al.* eine mechanochemische Sonogashira-Reaktion von *para*-substituierten Arylhalogeniden mit Acetylenen unter atmosphärischen Bedingungen beschrieben, bei der Palladium zwar als Katalysator zugegeben wurde, aber die Kupfermahlkugeln als Co-Katalysator fungierten.[132] Seitdem wurden weitere Beispiele beschrieben, die Kugeln aus Metallen wie Nickel, Silber, Palladium, Chrom oder Legierungen dieser Metalle als Katalysator verwendeten.[143] Im Rahmen weiterer Studien konnte die Gruppe um Mack verschie-

dene Selektivitäten in einer [2+1]-Cycloadditionsreaktion von Alkeninen **59** mit Diazoverbindungen **60** bestimmen. Unter Verwendung von Silber findet die Reaktion ausschließlich an der Dreifachbindung statt, wohingegen bei Verwendung von Kupfer die Doppelbindung selektiv reagiert.[140]

Eine weiteres Beispiel für eine C–C-Kreuzkupplungsreaktion unter lösungsmittel- und übergangsmetallfreien Bedingungen wurde von Mandal *et al.* gezeigt. Die Autoren setzten ein Phenalenylsalz ein, um Arylhalogenide **63** durch Festkörpereinzelelektronentransfer (*solid-state single electron transfer*, SSSET) unter Einfluss mechanischer Energie zu aktivieren und mit polycyclischen aromatischen Kohlenwasserstoffen **64** umzusetzen. Durch zweifachen Elektronenübertrag ausgehend von *in situ* generierten organischen Elektronendonoren wird das zweifach reduzierte Phenalenylanion erhalten, das im festen Zustand als Superreduktionsmittel agiert und die eingesetzten Arylhalogenide **63** zu entsprechenden Arylradikalen transformiert, die die C–C-Bindungsknüpfung eingehen.[141]

1.3 Darstellung von Thiocyanaten

Organische Thiocyanate sind wichtige synthetische Zwischenprodukte und ermöglichen den Zugang zu weiteren schwefelhaltigen Verbindungen.[144] Sie gehören zur Klasse der organischen Chalkogen-Cyanate (R–X–CN, X = O, S, Se, Te) bzw. den organischen Pseudo-Halogeniden (R–X, X = CN, N_3, OCN, NCO, SCN, NCS, SeCN). Zur Darstellung dieser Verbindungen können zwei Hauptstrategien verfolgt werden (Schema 1.4).

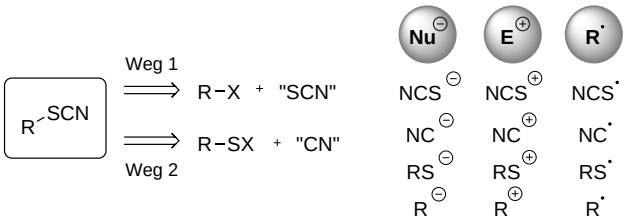

Schema 1.4: Verschiedene Darstellungsmöglichkeiten von organischen Thiocyanaten sowie die involvierten reaktiven Spezies. Von Donnard und Gulea *et al.* abgewandeltes Schema.[144]

Die erste Darstellungsmöglichkeit besteht aus der Reaktion halogenenierter Alkyl- oder Arylsubstrate, die keinen Schwefel enthalten, mit einem Thiocyanat-Ion (Weg 1, Sche-

ma 1.4). Alternativ kann das Substrat bereits einen elektrophilen oder nukleophilen Schwefel enthalten, der mit einem Cyanierungsmittel umgesetzt wird (Weg 2, Schema 1.4).[145] Verschiedene nukleophile, elektrophile und radikalische (Thio)-Cyanierungsmittel stehen für die Darstellung von organischen Thiocyanaten zur Verfügung.[144–146] Salze wie NaSCN, KSCN oder NH_4SCN dienen in nukleophilen Substitutionsreaktionen als Rhodanid-Quelle.[147–149] Unter oxidativen Bedingungen kann ein Thiocyanat-Radikal gebildet werden, das mit C=C-Bindungen umgesetzt werden kann.[150–153] In elektrophilen Additions- und Substitutionsreaktionen kann Dirhodan $(SCN)_2$, *N*-Thiocyanatosaccharin oder *N*-Thiocyanatosuccinimid verwendet werden.[154–157]

Ist ein elektrophiler Schwefel im Molekül vorhanden ist, beispielsweise bei einem Disulfid (RSSR) oder einem Sulfenylhalogenid (RSX), finden KCN, NaCN oder TMSCN als nukleophile Cyanid-Quelle Anwendung.[144,158] Unter aeroben Bedingungen und Kupfer-Katalyse können CN-Radikale gebildet werden, die ebenfalls mit Disulfiden zu den entsprechenden Thiocyanaten reagieren.[159] Es konnte gezeigt werden, dass ungiftige Substanzen wie Kaliumhexacyanoferrat-Salze oder Azobis(isobutyronitril) (AIBN) als sichere Cyanid-Quelle eingesetzt werden können, da sie Cyanid erst *in situ* freisetzen.[160–162] Unter oxidativen oder elektrochemischen Bedingungen können Thiole (RSH) direkt umgesetzt werden.[158,163] Elektrophile Cyanid-Quellen können Halogencyane (XCN; X = Br, Cl) oder hypervalente Iodverbindungen sein.[144,164,165]

Thiocyanat-Substituente können Einsatz bei der Feinabstimmung von Farbstoffen finden, z. B. bei Fluoreszenzsensoren, die auf Bordipyrromethin-Verbindungen (BODIPY), basieren, oder wurden auf ihren Anwendbarkeit als Insektizide getestet.[166–170] Darüber hinaus ermöglicht eine Thiocyanat-Funktionalität in Molekülen eine Vielzahl an weiteren synthetischen Umsetzungen, die in Schema 1.5 dargestellt sind.[144,171–174] Pericyclische Reaktionen mit Aziden sind in Form von [2+3]-Cycloadditionen möglich, wohingegen mit Alkinen [2+2+2]-Cycloadditionen stattfinden.[175,176] Bei der Umsetzung mit reduktiven Verbindungen werden Thiole **68** erhalten, wobei eine Racemisierung durch eine selektive Wahl des Reduktionsmittels verhindert werden kann.[177] Die Umsetzung mit aromatischen Grignard-Verbindungen führt zu Diarylthioethern, die anschließend zu den entsprechenden Sulfoxiden **69** oxidiert werden können.[178] Benzoisothiazolinone **70** können aus *o*-Brombenzamiden und Kaliumrhodanid mit einer sich anschließenden Tandem-Zyklisierung dargestellt werden.[179] Durch den Umsatz mit dem Treibhausgas Fluoro-

form (HCF_3),[2] werden Trifluormethylsulfide **71** erhalten, die sich durch einen der höchsten Hansch-Parameter, also eine sehr starke Lipophilie, auszeichnen.[180,183]

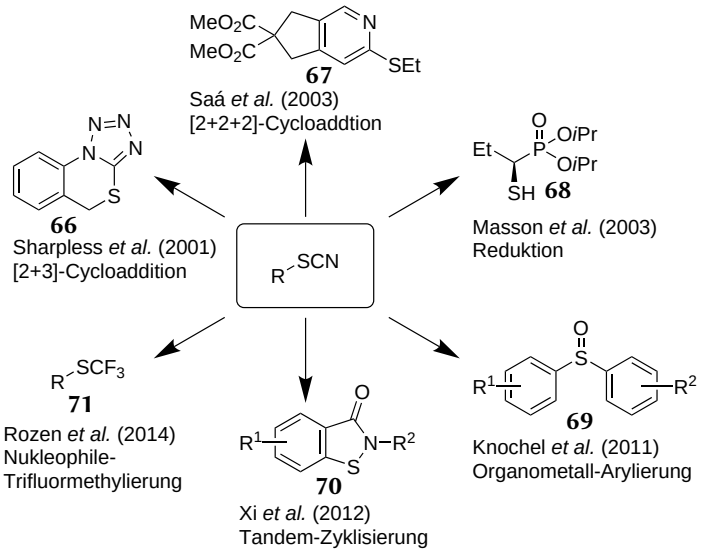

Schema 1.5: Ausgewählte Folgereaktionen an Thiocyanaten, bei denen das Schwefelatom im Molekül verbleibt.[175–180]

1.3.1 Thiocyanate in Naturstoffen

Bisher wurde die funktionelle Gruppe der Thiocyanate nur in wenigen Naturstoffen, meist in Sekundärmetaboliten mariner Lebensformen, identifiziert (Abbildung 1.4).[184] Aufgrund der beobachteten biologischen und pharmakologischen Aktivität dieser Verbindungen, z. B. eine antimykotische oder krebshemmende Wirkung, wurden diese und ähnliche Strukturmotive (total)-synthetisch dargestellt.[144,185–187] Die Verwendung als bisher wenig verbreitetes Strukturmotiv in pharmazeutischen Wirkstoffen kann den immer häufiger auftretenden Arzneimittelresistenzen entgegenwirken.[188–190]

Die Thiocyanatine A–E_2 (**72**–**78**) wurden aus einem marinen Schwamm der Gattung *Oceanapia* vor der Südküste Australiens von Capon *et al.* isoliert und bestehen aus einem 1,16-disubstituierten *n*-Hexadecan-Grundgerüst, das sich in seinem Substitutionsmuster oder der Position einer Doppelbindung unterscheidet. Die Verbindungen sind synthetisch zugänglich und die Vertreter **72** und **75**–**78** stellen eine bis dahin unbekannte Klasse

[2] Fluoroform fällt in über 20 000 t a^{-1} als Nebenprodukt bei der Produktion von Teflon®, Polyvinylidenfluorid (PVDF), Kühlschränken und Feuerlöschern an. Die Entsorgung als Abfallstoff ist äußerst kosten-, material- und energieintensiv und die Nutzung als Reagenz ist bisher nur wenig erforscht.[181,182]

von Nemataziden dar.[191,192] Ebenfalls in marinen Schwämmen wurden Neopupukeananе **79** und **80** sowie Cavernothiocyanat (**81**) nachgewiesen, die ein terpenoides Grundgerüst besitzen und sich strukturell ähneln.[193–196] Von der Gruppe um Srikrishna wurden die ersten enantioselektiven Synthesen von 2-Thiocyanatoneopupukeanan (**79**) und 4-Thiocyanatoneopupukeanan (**80**), jeweils ausgehend von (*R*)-Carvon (**9**), beschrieben.[197,198] Ein weiterer Sekundmetabolit, der aus marinen Schwämmen isoliert werden kann, ist Psammaplin B (**82**). Dieser Naturstoff setzt sich aus Bromtyrosin und einem modifizierten Cystein zusammen und zeigt Aktivität als Histon-Deacetylase sowie als DNA-Methyltransferase-Inhibitor.[196,199,200] Aus Seeschnecken oder Seescheiden können Fasicularin (**83**) und Cylindricine **84**–**87** isoliert werden, die ein trizyklisches Grundgerüst besitzen und totalsynthetisch zugänglich sind.[195,201–204]

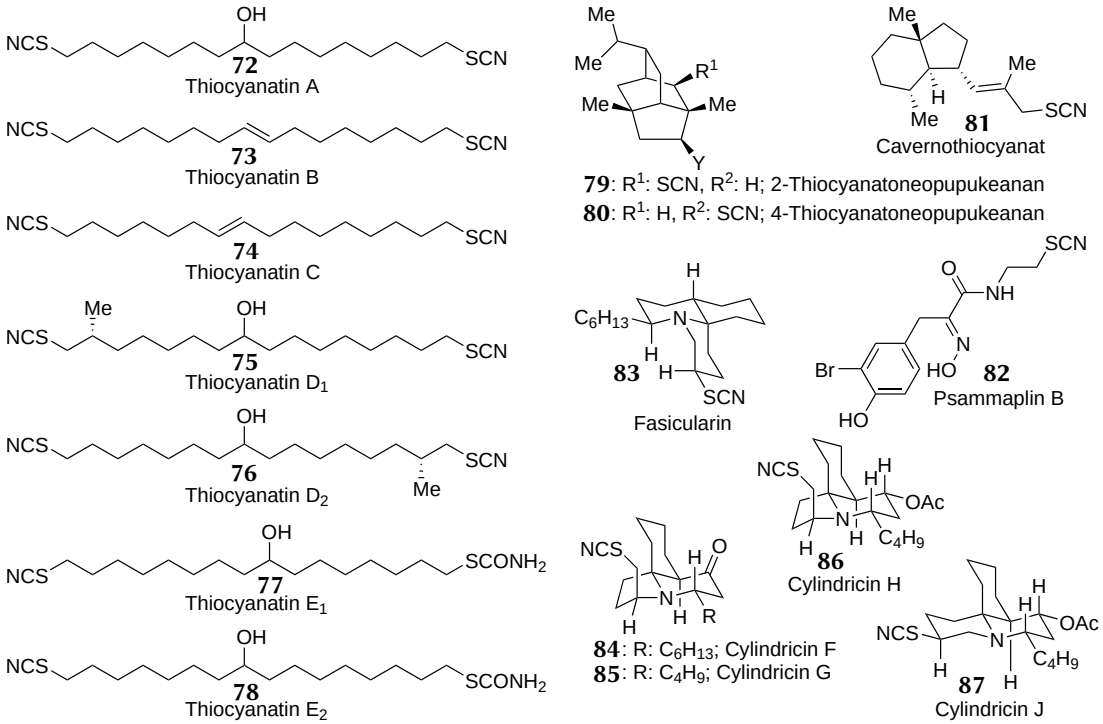

Abbildung 1.4: Eine Auswahl an Naturstoffen, die das Thiocyanat-Strukturmotiv tragen.[191–204]

2 Zielsetzung

2.1 Darstellung organischer Thiocyanate unter grünen Reaktionsbedingungen

Cyanide sind einer der wichtigsten C_1-Bausteine für die organische Synthese und werden trotz der hohen Toxizität klassisch verwendeter Reagenzien wie HCN (**94**), TMSCN oder NaCN sowohl im Labormaßstab als auch in der chemischen Industrie eingesetzt.[205,206] Der Großteil der bisher bekannten Cyanierungsreaktionen zielt auf den Aufbau neuer Kohlenstoff-Kohlenstoff-Bindungen, wohingegen die Einführung von Heteroatom-Kohlenstoff-Bindungen weniger erforscht ist. Ein interessantes Strukturmotiv der letzteren Klasse sind organische Thiocyanate, da sich die SCN-Funktionalität einerseits auf die biologische Aktivität eines Moleküls auswirken kann, andererseits aber auch vielfältige Folgereaktionen ermöglicht.[144,176,185,186,207]

Auf Grundlage der von Bolm *et al.* berichteten mechanochemischen Verwendung von Hexacyanoferrat-Salzen als ungiftige Cyanidquelle wurde in der Arbeitsgruppe Opatz diese Freisetzung genutzt, um eine säurekatalysierte Strecker-Reaktion im zweiphasigen Lösungsmittelgemisch zu erforschen. In einer weiteren Studie wurde der Mechanismus der Bildung von Diaminomaleonitril (DAMN, **97**) aus Cyanwasserstoff (**94**) mittels Massenspektrometerie untersucht und die Cyanierung eines Disulfids **96** als wichtige Zwischenstufe identifiziert (Schema 2.1).[162,208,209]

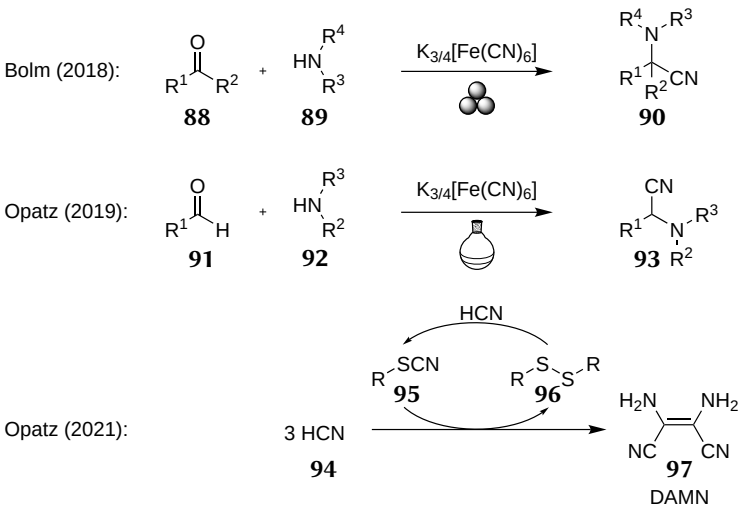

Schema 2.1: Literaturbekannte Verwendung von Blutlaugensalzen als Cyanidquelle sowie mechanistische Untersuchungen zur Tetramerisierung von HCN (**94**) unter Verwendung von Organoschwefelkatalysatoren. Ein zweiphasiges Lösungsmittelgemisch wird symbolisch durch den Kolben dargestellt.[162,208,209]

Diese Vorarbeiten bilden den Startpunkt für die Umsetzung kommerziell erhältlicher Thiole **98** und Disulfide **99** zu organischen Thiocyanaten **100**, die in dieser Arbeit systematisch untersucht werden soll (Schema 2.2). Besonderer Fokus liegt auf der Beachtung der Prinzipien der Grünen Chemie sowie der Nutzung nachhaltiger Synthesemethoden. Dies schließt die Verwendung eines organisch-wässrigen Zweiphasen-Systems sowie eine mechanochemische Umsetzung in einer Kugelmühle ein, da so geringere Lösungsmittelmengen als bei konventionellen Batchreaktionen benötigt werden. Nach der Optimierung der Reaktionsparameter für beide Methoden, sollen diese an verschiedenen Substraten getestet und in der Totalsynthese von Psammaplin B (**82**) eingesetzt werden.

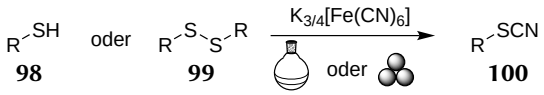

Schema 2.2: Geplante Umsetzung von Thiolen **98** oder Disulfiden **99** zu Thiocyanaten **100** unter Einsatz nicht giftiger Cyanidquellen, entweder im zweiphasigen Lösungsmittelgemisch oder in einer Kugelmühle.

3 Resultate und Diskussion

3.1 Darstellung organischer Thiocyanate unter grünen Reaktionsbedingungen

Die Reaktionsbedingungen für die Darstellung organischer Thiocyanate, unter Verwendung ungiftiger Blutlaugensalze als Cyanidquelle, wurden mittels eines zweiphasigen Lösungsmittelgemisches und einer Planetenkugelmühle jeweils an 2-Mercaptopyrimidin (**101**, in der Publikation **16**) optimiert. Die breite Anwendbarkeit beider Methoden wurde an insgesamt 27 Substraten erfolgreich demonstriert und in der ersten Totalsynthese des Naturstoffs Psammaplin B (**82**, in der Publikation **1**) angewendet (Abbildung 3.1).

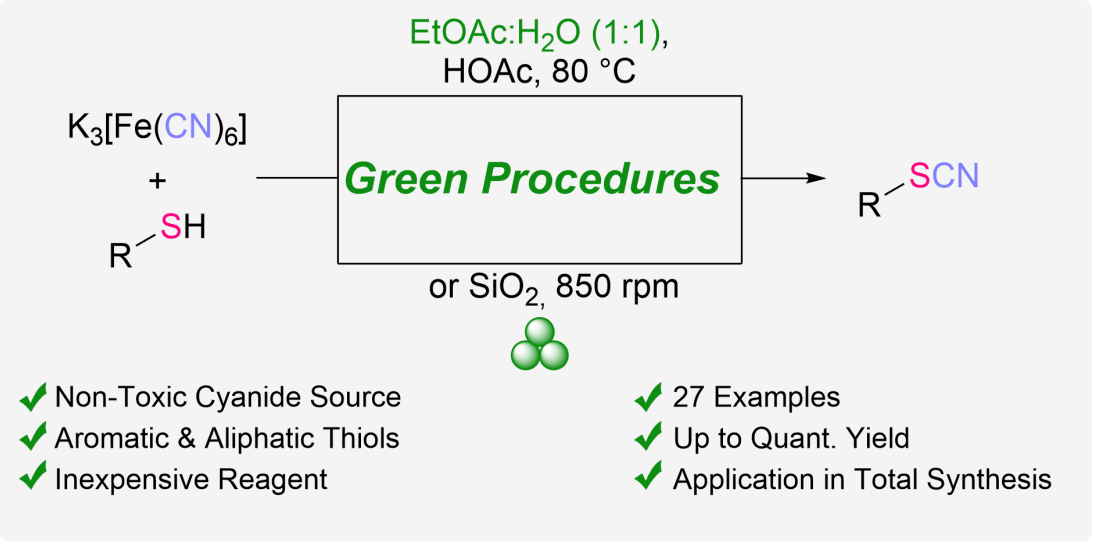

Abbildung 3.1: *Graphical abstract* der Publikation „Complementary Mechanochemical and Biphasic Approaches for the Synthesis of Organic Thiocyanates using Hexacyanoferrates as Non-Toxic Cyanide Sources“.[210]

Um die Reaktion nachhaltig zu gestalten, wurden verschiedene Techniken für die Isolierung der gebildeten Produkte untersucht, die alternativ zur Säulenchromatographie eingesetzt werden können. Die Anwendungsbereiche, Folgereaktionen sowie Limitierungen wurden in der Publikation beschrieben.[210]

Das zweiphasige Reaktionssystem wurde von [redacted] entwickelt und in Zusammenarbeit mit [redacted] und [redacted] angewendet. Die Übertragung der initialen Reaktionsbedingungen auf die Kugelmühle, deren Optimierung sowie die Darstellung des Substratspektrums und die Auswertung der analytischen Daten wurde von J. Groß durchgeführt. Die Isolierung und Reinigung einiger Produkte wurde von [redacted] in ihrer Funktion als wissenschaftliche Hilfskraft durchgeführt. Die Darstellung des Naturstoffs Psammaplin B (**82**, in der Publikation **1**) wurde von [redacted] durchgeführt. Das Manuskript wurde von [redacted], J. Groß, [redacted] und T. Opatz erstellt.[3]

[3] *Reproduced from C. Grundke, J. Groß, N. Vierengel, J. Sirleaf, M. Schmitz, L. Krieger, T. Opatz, Org. Biomol. Chem., 2023, 21, 644–650 with permission from the Royal Society of Chemistry.*

Organic & Biomolecular Chemistry

ROYAL SOCIETY OF CHEMISTRY

PAPER

View Article Online
View Journal | View Issue

Cite this: *Org. Biomol. Chem.*, 2023, **21**, 644

Complementary mechanochemical and biphasic approaches for the synthesis of organic thiocyanates using hexacyanoferrates as non-toxic cyanide sources†

Caroline Grundke,‡ Jonathan Groß,‡ Nina Vierengel, Jason Sirleaf, Matthias Schmitz, Leonie Krieger and Till Opatz *

Received 4th December 2022,
Accepted 19th December 2022

DOI: 10.1039/d2ob02216h

rsc.li/obc

Herein, we describe two complementary approaches towards various organic thiocyanates that are affordable, reliable and follow the principles of sustainable chemistry, starting from commercially available thiols or disulfides. Additionally, the application of this mild method to the first total synthesis of psammaplin B is demonstrated. Non-toxic and inexpensive ferricyanide is used as the cyanide source, which can be activated either in a mechanochemical, solvent-free approach, or in a biphasic solvent system allowing easier work-up. A total of 27 examples is demonstrated, with up to quantitative yields.

Introduction

Climate change and its increasing impact on human society such as sea level rise, weather disasters and long term changes in the atmosphere's composition, in soil and vegetation, have already emerged in the late 20th century.[1] In response to a probable human contribution to the phenomenon, the 12 principles of green chemistry were proclaimed by Anastas and Warner in 1998, to reach a paradigm shift in the chemical community.[2,3] One of the most important guidelines to develop more eco-friendly methodologies is to minimize the amount of toxic and harmful chemical reagents as well as the amount of solvents required. Cyanide is one of the most important C_1 building blocks in the organic laboratory as well as in industry,[4] but frequently applied cyanide sources such as HCN, TMSCN, metal cyanides or ketone cyanohydrins show very high toxicities. Therefore, their replacement with non-toxic alternatives that are not inferior to conventional agents on either reactivity or economic aspects, is highly desirable. In this respect, non-toxic and inexpensive potassium hexacyanoferrate II/III (oral LD_{50} in mice of $K_3[Fe(CN)_6]$ = 5110 mg kg^{-1}, oral LD_{50} in mice of NaCl = 3000–3750 mg kg^{-1})[5,6] became of increasing interest during the last few years, in particular in combination with palladium and copper catalysis for various cyanation reactions (see Scheme 1), but most of them require high reaction temperatures.[7–15] To produce less solvent waste, the application of biphasic solvent systems was recognized as a versatile tool, since the individual reactants can be dissolved in their preferred solvent instead of forcing them both into a suboptimal one through the use of large volumes. To this end, the Opatz group reported the implementation of a classical Strecker protocol in a biphasic solvent system consisting of water and ethyl acetate, while applying non-toxic ferri/ferrocyanide for the efficient synthesis of α-aminonitriles following a green protocol (Scheme 2b).[16]

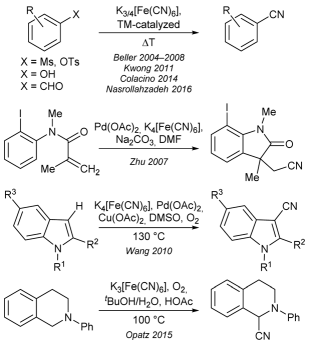

Scheme 1 Selected examples of various cyanation reactions using ferro-/ferricyanide as non-toxic cyanide sources.

Department of Chemistry, Johannes Gutenberg-University, Duesbergweg 10–14, 55128 Mainz, Germany. E-mail: opatz@uni-mainz.de

†Electronic supplementary information (ESI) available. CCDC 2206744. For ESI and crystallographic data in CIF or other electronic format see DOI: https://doi.org/10.1039/d2ob02216h

‡Shared first authorship.

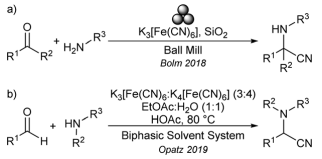

Scheme 2 Synthesis of α-aminonitriles *via* a ferri/ferrocyanide initiated Strecker-type reaction in a ball mill (a) and in a biphasic solvent system (b).

Mechanochemistry, which doesn't require additional thermal activation, has received increasing interest as a green synthesis alternative, mainly because of its significant advantages such as significantly shorter reaction times, higher selectivity and lower waste production, since the reactions are carried out solvent-free.[17] Various mechanochemical transformations have been reported, such as mechanochemical Friedel–Crafts alkylations,[18] diverse amino acid and peptide syntheses,[19,20] C–C bond formations[21–24] and even fullerene syntheses.[25–27] The Bolm group reported Strecker reactions furnishing α-aminonitriles by applying KCN as the cyanide source in 2016,[28,29] which the group further evolved by the application of hexacyanoferrates as less toxic cyanide sources in mechanochemistry two years later (Scheme 2a).[30]

However, the majority of such reactions focus on building new C–C bonds, whereas the formation of heteroatom–carbon bonds from non-toxic cyanide sources tends to be overlooked, even though the resulting products such as thiocyanates are useful intermediates in a variety of transformations.[31–34] Organic thiocyanates are a versatile compounds class and can serve as building blocks or precursors for various sulfur-containing heterocycles.[31] Moreover, the functional group itself can confer diverse biological activities to organic compounds containing it, creating for example anticancer or antifungal agents.[35,36] Efforts have been made to synthesize such compounds economically and sustainably, especially regarding potential drug motifs able to overcome increasing resistances towards frequently used drugs.[37–39] Besides, a variety of natural products with the thiocyanate structural motif have been isolated, such as psammaplin B (**1**),[40] fasicularin (**2**),[41] thiocyanatins (**3–5**),[36,42] neopupukeananes and congeners (**6–8**)[43,44] or other terpenoids (**9–12**)[45,46] (see Fig. 1).[47]

In the synthesis of organic thiocyanates, two main strategies are generally followed, the first one starting from different alkyl/aryl precursors and a thiocyanating agent, while the second uses a sulfur-containing substrate in combination with a cyanating agent. The most commonly used cyanating agents are still based on toxic metal cyanides such as KCN or NaCN, yet alternatives such as TMSCN, BrCN or some hypervalent iodine species are still highly toxic or need to be elaborately prepared. Likewise, commonly used thiocyanating reagents such as NH_4SCN (750 mg kg^{-1})[48] or KSCN (854 mg kg^{-1})[49] still show significantly lower oral LD_{50} values in mice than $K_3[Fe(CN)_6]$.[31,50–54] In this respect, we sought to study the

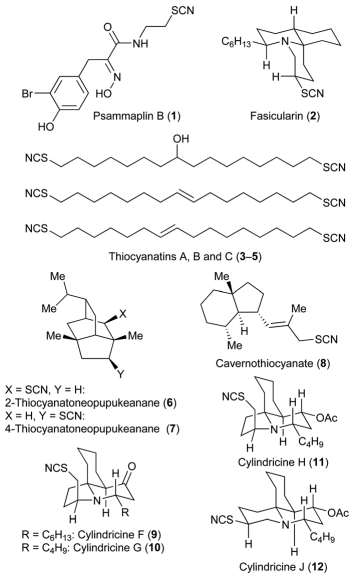

Fig. 1 Examples of thiocyanates as a structural motif in multiple natural products.

application of this affordable and essentially non-toxic cyanide source in the direct nucleophilic cyanation of thiols as, to the best of our knowledge, no such methodology has been reported. Herein, the efficient and sustainable synthesis of multiple thiocyanates using $K_3[Fe(CN)_6]$ in a biphasic solvent system or *via* mechanochemical activation in a ball mill is described. Additionally, the reported synthesis procedure was applied in the green and hitherto first total synthesis of the natural product psammaplin B, starting from 4-hydroxyphenylpyruvic acid (**54**) *via* late-stage functionalization of psammaplin A through application of the newly developed protocol in four steps.

Results and discussion

Based on the previously published biphasic reaction system using hexacyanoferrates for the synthesis of α-aminonitriles reported by the Opatz lab,[16] initial optimization experiments for the biphasic synthesis of thiocyanates have been performed using diphenyl disulfide (**13**), 2,2′-dipyridyldisulfide (**14**) or 2,2′-dipyrimidyldisulfide (**15**) as substrates. As the pyrimidyl substrate **15** showed the highest initial yield, further optimization focused on this as starting material.

Since $K_3[Fe(CN)_6]$ itself is a known oxidizing agent, a direct application of thiols instead of disulfides was investigated in this reaction setup (see Scheme 3). Pyrimidine-2-thiol (**16**) was successfully used as starting material, furnishing the respective thiocyanate product **16a** in quantitative yield after little

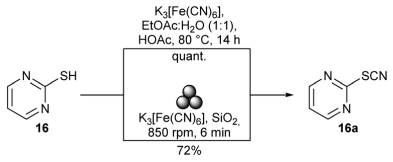

Scheme 3 Optimized reaction conditions for the synthesis of thiocyanates in batch as well as in a ball mill.

further optimization (please see Table T1 in the ESI† for more details). Besides the application of a biphasic reaction system, adaption of this new protocol to a mechanochemical, solvent-free approach has been investigated. After optimization of the amount of the CN source, the reaction time and potential grinding auxiliaries, optimum reaction conditions with a drastically reduced reaction time could be achieved. Furthermore, no additional chemicals for the required acidic activation are needed, as the ideal grinding auxiliary already provides the necessary acidity. Under these conditions, the respective 2-thiocyanatopyrimidine (**16a**) could be obtained in 72% yield (see Scheme 3). Both procedures can also be performed on gram scale, yielding 49% and 15% for the batch and ball mill approach, respectively (ESI Tables T1 and T2†).

With the optimized reaction conditions for both procedures in hand, the respective substrate scope was investigated (see Scheme 4). All yields are those of the isolated products unless stated otherwise, with column chromatography as the standard purification method to ensure comparability. Considering the sustainability of the developed procedures, alternative purification methods such as crystallisation, distillation and continuous extraction have exemplarily been applied to some of the substrates, proving that comparable yields can be obtained, provided that the alternative purification is adapted to the individual substrate (please see the ESI for further information†).

Switching from pyrimidine to pyridine thiols, the respective 2- and 4-substituted thiocyanate products **17a** and **18a** could

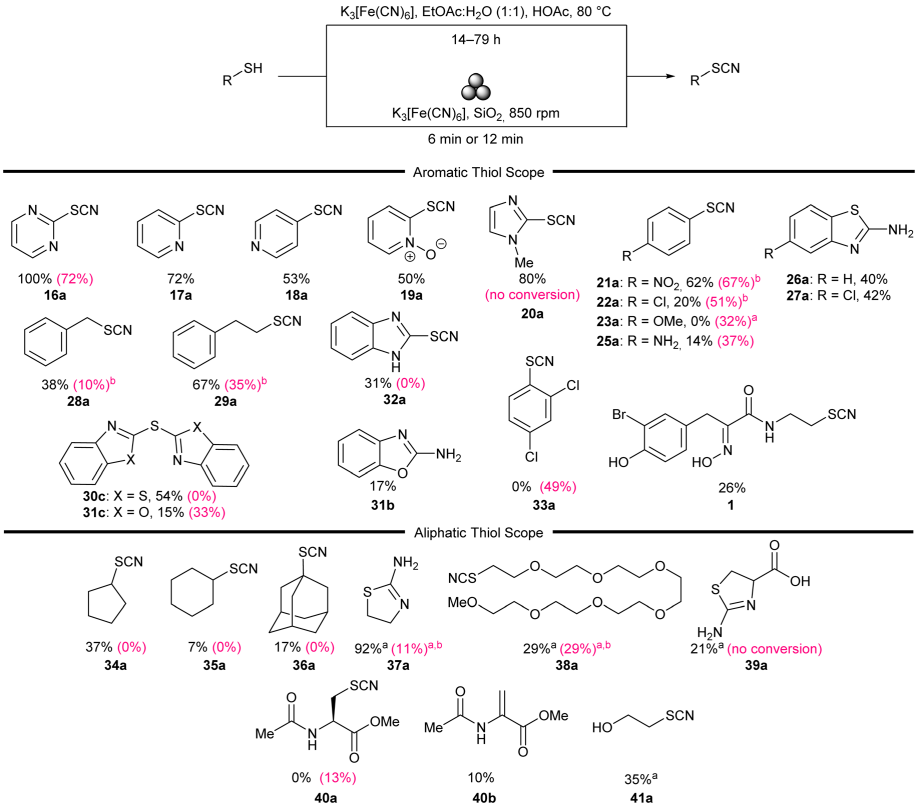

Scheme 4 Scope of aromatic and aliphatic substrates. Isolated yields unless stated otherwise. Yields in parenthesis are those of the mechanochemical procedure. [a]Yield determined *via* ^{1}H-NMR (internal standard). [b]Reaction time was extended to 12 min.

be obtained in yields of 72% and 53%, respectively. This might be due to better resonance stabilizing effects in the 4-substituted derivative **18a**. With 50% yield, 2-mercaptopyridine-*N*-oxide (**19**) as the thiol reagent could be converted to the respective thiocyanate product **19a**. The use of the electron-rich 2-mercapto-1-methylimidazole (**20**) under the biphasic conditions led to the respective thiocyanate (**20a**) in 80% yield, whereas subjection to the ball milling conditions did not lead to any conversion of the starting material. The influence of various substituents on the thiophenol core was investigated, with product formation of **21a** in 62% yield under the biphasic conditions if an electron-withdrawing nitro substituent is attached in *p*-position. Upon mechanochemical activation, a small increase in yield up to 67% could be observed when the reaction mixture was ground for 12 min. For the *p*-chloro derivative **22**, ball milling yielded the respective thiocyanate **22a** in 51% after 12 min of grinding time, whereas the biphasic reaction conditions furnished **22a** in only 20% yield. Through ball milling, 4-methoxythiophenol **23** could be converted to the respective thiocyanate derivative **23a** in 32% NMR-yield, whereas 4-methylthiophenol (**24**) yielded the corresponding disulfide **24b** in 49% yield.

Conversion of a substrate with a free amino group in *p*-position yielded the respective product **25a** in 14% yield under biphasic conditions, which could be increased significantly to 37% by mechanochemistry.

Shifting the amino group from the *para*- to the *ortho*-position led to a direct *in situ* cyclization of the intermediately formed thiocyanate to either the respective unsubstituted benzothiazol-2-amine product **26a** (40% yield) or the chlorinated benzothiazole-2-amine derivative **27a** in 42% yield. Benzylmercaptan (**28**) and 2-phenylethan-1-thiol (**29**) were also used as thiol reagents, furnishing the respective thiocyanate products **28a** in 38% and **29a** in 67% yield in the developed biphasic reaction protocol. Adaption to ball milling conditions led to a decrease in yield to 10% for **28a**, although the reaction time was slightly extended, and a 35% yield for **29a** could be observed with 12 min of grinding time. Under batch reaction conditions, the formation of the disulfide **30b** and thioether **30c** in 42% and 54% yield could be observed starting from 2-mercaptobenzothiazole **30**. The same applies to 2-mercaptobenzoxazole (**31**) as the thiol (desired product **31a**, 0%), with the unexpected 2-amino substituted product **31b** (17% yield) and the respective thioether **31c** (15% yield) being the isolated products. Product formation of 2-mercaptobenzimidazole (**32**) towards the desired thiocyanate **32a** could be achieved in 31% yield in the biphasic solvent system. When introduced to mechanochemical conditions, for the application of 2-mercaptobenzoxazole (**31**), thioether **31c** was obtained as the only product in an increased yield of 33% compared to the biphasic approach. 2,4-Dichlorothiophenol (**33**) was converted to the respective thiocyanate **33a** in 49% yield under ball milling conditions. Besides aromatic thiol derivatives, aliphatic substrates have also been investigated under both reaction conditions. Cyclic thiols such as cyclopentanethiol (**34**), cyclohexanethiol (**35**) and adamantane-1-thiol (**36**) yielded the desired thiocyanate products in 37% (**34a**), 7% (**35a**) and 17% yield (**36a**) under biphasic conditions, whereas under mechanochemical conditions, the cycloalkanes **34**, **35** and **36** furnished exclusively the respective disulfides. For these substrates, distillation as purification method furnished the desired products in comparable yields. Application of cysteamine (**37**) in the developed batch protocol followed an already observed *in situ* cyclization towards the respective 4,5-dihydrothiazole derivative **37a** in 92% NMR-yield after continuous extraction of the aqueous phase with ethyl acetate, whereas under mechanochemical conditions, an NMR-yield of only 11% could be achieved. Conversion of 2,5,8,11,14,17,20-heptaoxadocosane-22-thiol (**38**) to the respective thiocyanate **38a** was achieved in 29% NMR-yield after work-up as an inseparable product mixture together with disulfide **38b** (7% yield). In contrast, **38a** could be exclusively obtained under ball milling conditions (29% NMR-yield). Application of L-cystine (**39**) as a naturally occurring disulfide yielded the *in situ* cyclized product **39a** in 21% NMR-yield under batch conditions, after continuous extraction of the aqueous phase with ethyl acetate. Application of methyl acetyl-L-cysteinate **40** yielded the respective thiocyanate product **40a** in 14% yield after mechanochemical activation. In contrast, formation of methyl 2-acetamidoacrylate **40b** in 10% yield could be detected as the sole defined reaction when **40** was applied to the biphasic reaction conditions, probably due to elimination of H_2S or HSCN. The presence of a free hydroxy group was tolerated in the biphasic procedure, yielding the respective product **41a** in 35% NMR-yield. Conversion of 1,4-dimercaptobutane-2,3-diol (**42**) did not lead to any product formation. The significantly lower yields for aliphatic thiols that are only poorly soluble in water indicate that hydrophilicity of the substrates seems to play an important role for successful conversion into the respective thiocyanate products, particularly in the biphasic reaction protocol. Selected polar and protic solvent systems were investigated during optimization (see Table T1 in the ESI†).

As shown in Scheme 5, the scope of the developed procedures is limited through exclusive disulfide formation in 12% (**43b**) yield and 36% (**44b**) yield when applying either methyl 2-mercaptoacetate (**43**) or methyl 3-mercaptopropanoate (**44**) as thiol components. Application of (4-methoxyphenyl) methanethiol (**45**) to biphasic conditions resulted in the formation of the respective disulfide **45b** in 6% and *p*-anisyl alcohol (**45c**) in 27% yield, probably due to nucleophilic displacement by water, whereas under mechanochemical conditions, **45b** was formed after 6 min of grinding time (16%). Unsubstituted thiophenol (**46**) could not be converted into the respective thiocyanate under both sets of conditions, as well as α-lipoic acid (**47**), 3-mercaptopropionic acid (**48**), L-cystein (**49**), *N*-acetyl-L-cystein (**50**) and glutathione (**51**). Linear unsubstituted alkanethiols **52** and **53** could also not be transformed into their respective thiocyanate derivatives in the batch protocol, whereas formation of didecyldisulfide **53b** in 58% yield was observed after subjection of decanethiol (**53**) to the ball milling conditions (either 6 or 12 min).

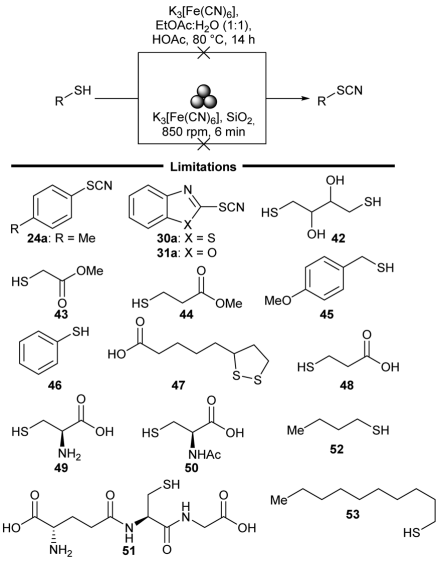

Scheme 5 Limitations of aromatic and aliphatic substrates in both protocols.

Total synthesis of psammaplins

The developed protocols were further applied in the total synthesis of psammaplin B (**1**, Scheme 6) through activation of the disulfide bond present in psammaplin A (**55**), a marine natural product first isolated in 1987 from the sponge *Psammaplysilla purpurea* which has interesting biological activities.[55–60] There are already various approaches towards psammaplin A by Nicolaou, Hoshino and others,[55,58–60] but none of them, to the best of our knowledge, includes psammaplin B as a synthesis target, even though it is a bromotyrosine-containing metabolite of the *Psammaplysilla purpurea* sponge.[40]

This synthesis approach is based on the report of *Sufrin et al.* starting from 4-hydroxyphenylpyruvic acid (**54**) to furnish psammaplin A (**55**) in four steps.[55] After oximation of the commercially available starting material **54** with hydroxylamine hydrochloride to oxime **56** in 63% yield, bromination with NBS yielded the mono- and dibrominated compounds **57** and **58** in 39% and 10% yield, respectively. Both substrates were coupled with cysteamine (**37**) to furnish psammaplin A (**55**) in 24% yield and the corresponding tetrabrominated psammaplin A derivative **59** in 13% yield. Psammaplin A was then subjected to the developed ball milling procedure, but only decomposition of the starting material could be observed. Subjection to a modified biphasic synthesis protocol (7.5 eq. CN source, 71 h of heating) yielded the natural product psammaplin B (**1**) in 26% isolated yield. It should be mentioned that, even though the reaction in the biphasic system proceeded rather slowly, no side product formation could be observed in the course of the reaction and only selective conversion of psammaplin A (**55**) to psammaplin B (**1**) occurred.

Thus, the developed protocol proved to be mild enough to even allow the transformation of highly functionalized substrates.

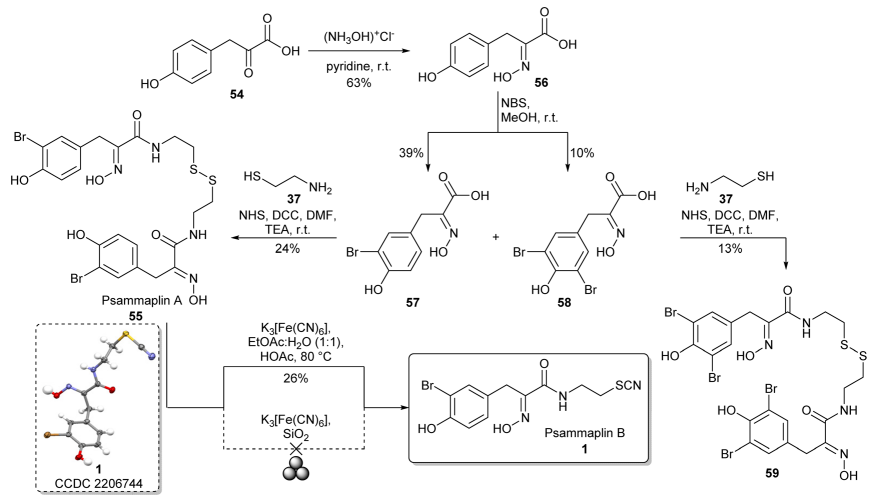

Scheme 6 Total synthesis of psammaplin A (**55**) and its tetrabrominated derivative **59** based on the sequence of Sufrin *et al.*[55] as well as further conversion of psammaplin A (**55**) to psammaplin B (**1**) with the newly developed synthesis procedure in batch.

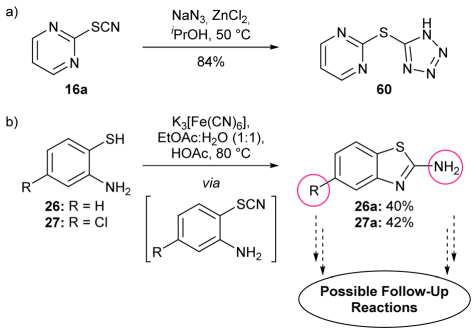

Scheme 7 (a) [3 + 2]-Cycloaddition of sodium azide to the thiocyanate moiety furnishing the corresponding sulfur-bridged tetrazole **60**. (b) Potential further functionalization of benzothiazoles **26** and **27** derived from *o*-amino thiocyanate intermediates **26a** and **27a** with the developed procedure.

Follow-up reactions

Tetrazoles are bioisosteric to the carboxy group and are therefore frequently applied as surrogates in biologically active synthetic compounds. They are metabolically stable to many of the biological transformations taking place in the liver to which carboxylic acids are way more susceptible.[61] Therefore, tetrazoles increasingly gained interest as pharmacologically significant scaffolds during the past decades.[62,63] Furthermore, they can be considered as useful ligands in organometallic chemistry.[31] The transformation of the newly introduced SCN moiety of pyrimidine-2-ylthiocyanate (**16a**) towards the respective sulfur-bridged tetrazole derivative **60** has been performed as a follow-up [3 + 2]-cycloaddition reaction using NaN_3 and $ZnCl_2$ in isopropanol. The desired product **60** could be obtained in 84% yield (see Scheme 7a). As described before, direct *in situ* cyclization of *o*-aminothiophenol derivatives **26** and **27** could be observed, furnishing the respective 2-aminobenzothiazole derivatives **26a** and **27a**, which could potentially be further functionalized either on the amino group or any other substituent (see Scheme 7b) to afford compounds with relevance for medicine and agrochemistry.[64,65] The developed reaction protocol thus also permits the construction of sulfur-containing heterocycles in short reaction times and under environmentally friendly conditions.

Conclusion

A green and economic synthesis of organic thiocyanates was developed, starting from commercially available thiols or disulfides. Ferricyanide could be applied as a non-toxic CN source, with an LD_{50} value even higher than that of sodium chloride. Two different approaches were used that follow the principles of green chemistry, the first one applying a biphasic solvent system consisting of water and ethyl acetate, the second one using a mechanochemical and solvent-free reaction setup with significantly decreased reaction time. Even gram scale can be realized for both systems, however, further optimisation is required in this case to improve the yields. For most of the reported substrates, column chromatography could be replaced by alternative purification methods such as crystallisation, distillation and continuous extraction without decrease in product yields and selected follow-up reactions could be demonstrated. Additionally, the first total synthesis of the natural product psammaplin B (**1**) could be achieved by successfully applying a biphasic solvent system.

Conflicts of interest

There are no conflicts to declare.

Acknowledgements

The authors sincerely thank Leander Geske for help with structure elucidation as well as Dr Johannes C. Liermann for NMR spectroscopy and Dr Christopher J. Kampf for mass spectrometry (all JGU Mainz).

References

1 G. H. Brundtland, *Environ. Conserv.*, 1987, **14**, 291–294.
2 P. T. Anastas and J. C. Warner, *Green Chemistry: Theory and Practice*, Oxford University Press, New York, 1998.
3 P. T. Anastas, T. C. Williamson, D. Hjeresen and J. J. Breen, *Environ. Sci. Technol.*, 1999, **33**, 116A–119A.
4 I. C. M. Institute, The Cyanide Code – Use in mining, **https://cyanidecode.org/cyanide-facts/**, (accessed 07.04.2022).
5 **https://www.sigmaaldrich.com/DE/en/sds/aldrich/208019**, Material Safety Data Sheet Potassium Hexacyanoferrate (III), (accessed 07.04.2022).
6 E. Boyd and M. Shanas, *Arch. Int. Pharmacodyn. Ther.*, 1963, **144**, 86–96.
7 T. Schareina, A. Zapf and M. Beller, *Chem. Commun.*, 2004, 1388–1389.
8 P. Y. Yeung, C. P. Tsang and F. Y. Kwong, *Tetrahedron Lett.*, 2011, **52**, 7038–7041.
9 G. Giachi, M. Frediani, W. Oberhauser, F. Lamaty, J. Martinez and E. Colacino, *ChemSusChem*, 2014, **7**, 919–924.
10 P. Y. Yeung, C. M. So, C. P. Lau and F. Y. Kwong, *Angew. Chem., Int. Ed.*, 2010, **49**, 8918–8922.
11 C. Zhao, W.-Y. Fang, K. P. Rakesh and H.-L. Qin, *Org. Chem. Front.*, 2018, **5**, 1835–1839.
12 M. Nasrollahzadeh, M. Atarod and S. M. Sajadi, *J. Colloid Interface Sci.*, 2017, **486**, 153–162.
13 G. Yan, C. Kuang, Y. Zhang and J. Wang, *Org. Lett.*, 2010, **12**, 1052–1055.

14 A. M. Nauth, N. Otto and T. Opatz, *Adv. Synth. Catal.*, 2015, **357**, 3424–3428.
15 A. Pinto, Y. Jia, L. Neuville and J. Zhu, *Chem. – Eur. J.*, 2007, **13**, 961–967.
16 C. Grundke and T. Opatz, *Green Chem.*, 2019, **21**, 2362–2366.
17 S. L. James, C. J. Adams, C. Bolm, D. Braga, P. Collier, T. Friščić, F. Grepioni, K. D. M. Harris, G. Hyett, W. Jones, A. Krebs, J. Mack, L. Maini, A. G. Orpen, I. P. Parkin, W. C. Shearouse, J. W. Steed and D. C. Waddell, *Chem. Soc. Rev.*, 2012, **41**, 413–447.
18 E. Troschke, S. Grätz, T. Lübken and L. Borchardt, *Angew. Chem., Int. Ed.*, 2017, **56**, 6859–6863.
19 C. Bolm and J. G. Hernández, *ChemSusChem*, 2018, **11**, 1410–1420.
20 V. Declerck, P. Nun, J. Martinez and F. Lamaty, *Angew. Chem., Int. Ed.*, 2009, **48**, 9318–9321.
21 G. Kaupp, M. R. Naimi-Jamal and J. Schmeyers, *Tetrahedron*, 2003, **59**, 3753–3760.
22 E. M. Gérard, H. Sahin, A. Encinas and S. Bräse, *Synlett*, 2008, 2702–2704.
23 J. Mack and M. Shumba, *Green Chem.*, 2007, **9**, 328–330.
24 V. P. Balema, J. W. Wiench, M. Pruski and V. K. Pecharsky, *J. Am. Chem. Soc.*, 2002, **124**, 6244–6245.
25 K. Koichi, F. Koichi and M. Yasujiro, *Chem. Lett.*, 2000, **29**, 1016–1017.
26 K. Komatsu, Y. Murata, G.-W. Wang, T. Tanaka, N. Kato and K. Fujiwara, *Fullerene Sci. Technol.*, 1999, **7**, 609–620.
27 Y. Murata, N. Kato and K. Komatsu, *J. Org. Chem.*, 2001, **66**, 7235–7239.
28 J. G. Hernández, M. Turberg, I. Schiffers and C. Bolm, *Chem. – Eur. J.*, 2016, **22**, 14513–14517.
29 S. Dabral, M. Turberg, A. Wanninger, C. Bolm and J. G. Hernández, *Molecules*, 2017, **22**, 146.
30 C. Bolm, R. Mocci, C. Schumacher, M. Turberg, F. Puccetti and J. G. Hernández, *Angew. Chem.*, 2018, **130**, 2447–2450.
31 T. Castanheiro, J. Suffert, M. Donnard and M. Gulea, *Chem. Soc. Rev.*, 2016, **45**, 494–505.
32 X. Lu, H. Wang, R. Gao, D. Sun and X. Bi, *RSC Adv.*, 2014, **4**, 28794–28797.
33 J. A. Varela, L. Castedo and C. Saá, *J. Org. Chem.*, 2003, **68**, 8595–8598.
34 Z. P. Demko and K. B. Sharpless, *Org. Lett.*, 2001, **3**, 4091–4094.
35 V. A. Kokorekin, A. O. Terent'ev, G. V. Ramenskaya, N. É. Grammatikova, G. M. Rodionova and A. I. Ilovaiskii, *Pharm. Chem. J.*, 2013, **47**, 422–425.
36 M. P. Fortes, P. B. N. da Silva, T. G. da Silva, T. S. Kaufman, G. C. G. Militão and C. C. Silveira, *Eur. J. Med. Chem.*, 2016, **118**, 21–26.
37 G. E. Linares, E. L. Ravaschino and J. B. Rodriguez, *Curr. Med. Chem.*, 2006, **13**, 335–360.
38 P. Ahmad, C. A. Fyfe and A. Mellors, *Biochem. Pharmacol.*, 1975, **24**, 1103–1109.
39 F.-Y. Lin, Y.-L. Liu, K. Li, R. Cao, W. Zhu, J. Axelson, R. Pang and E. Oldfield, *J. Med. Chem.*, 2012, **55**, 4367–4372.
40 C. Jiménez and P. Crews, *Tetrahedron*, 1991, **47**, 2097–2102.
41 S. M. Weinreb, *Chem. Rev.*, 2006, **106**, 2531–2549.
42 R. J. Capon, C. Skene, E. H.-T. Liu, E. Lacey, J. H. Gill, K. Heiland and T. Friedel, *J. Org. Chem.*, 2001, **66**, 7765–7769.
43 C. Li and A. Blackman, *Aust. J. Chem.*, 1994, **47**, 1355–1361.
44 C. Li and A. Blackman, *Aust. J. Chem.*, 1995, **48**, 955–965.
45 A. Srikrishna and S. J. Gharpure, *J. Chem. Soc., Perkin Trans. 1*, 2000, 3191–3193.
46 N. Fusetani, H. J. Wolstenholme, K. Shinoda, N. Asai, S. Matsunaga, H. Onuki and H. Hirota, *Tetrahedron Lett.*, 1992, **33**, 6823–6826.
47 J. Emsermann, U. Kauhl and T. Opatz, *Mar. Drugs*, 2016, **14**, 16.
48 **https://www.sigmaaldrich.com/DE/en/sds/sigald/a7149**, Material Safety Data Sheet of Ammonium Thiocyanate, (accessed 11.04.2022).
49 **https://www.sigmaaldrich.com/DE/en/sds/sigald/p3011**, Material Safety Data Sheet of Potassium Thiocyanate, (accessed 11.04.2022).
50 T. Castanheiro, M. Gulea, M. Donnard and J. Suffert, *Eur. J. Org. Chem.*, 2014, 7814–7817.
51 W. Fan, Q. Yang, F. Xu and P. Li, *J. Org. Chem.*, 2014, **79**, 10588–10592.
52 J. Yadav, B. Reddy and M. K. Gupta, *Synthesis*, 2004, 1983–1986.
53 K. Yamaguchi, K. Sakagami, Y. Miyamoto, X. Jin and N. Mizuno, *Org. Biomol. Chem.*, 2014, **12**, 9200–9206.
54 R. Frei, T. Courant, M. D. Wodrich and J. Waser, *Chem. – Eur. J.*, 2015, **21**, 2662–2668.
55 A. M. Godert, N. Angelino, A. Woloszynska-Read, S. R. Morey, S. R. James, A. R. Karpf and J. R. Sufrin, *Bioorg. Med. Chem. Lett.*, 2006, **16**, 3330–3333.
56 E. Quiñoà and P. Crews, *Tetrahedron Lett.*, 1987, **28**, 3229–3232.
57 I. C. Piña, J. T. Gautschi, G.-Y.-S. Wang, M. L. Sanders, F. J. Schmitz, D. France, S. Cornell-Kennon, L. C. Sambucetti, S. W. Remiszewski, L. B. Perez, K. W. Bair and P. Crews, *J. Org. Chem.*, 2003, **68**, 3866–3873.
58 S. Hong, M. Lee, M. Jung, Y. Park, M.-H. Kim and H.-G. Park, *Tetrahedron Lett.*, 2012, **53**, 4209–4211.
59 O. Hoshino, M. Murakata and K. Yamada, *Bioorg. Med. Chem. Lett.*, 1992, **2**, 1561–1562.
60 K. Nicolaou, R. Hughes, J. A. Pfefferkorn, S. Barluenga and A. Roecker, *Chem. – Eur. J.*, 2001, **7**, 4280–4295.
61 Y. Zou, L. Liu, J. Liu and G. Liu, *Future Med. Chem.*, 2020, **12**, 91–93.
62 E. A. Popova, R. E. Trifonov and V. A. Ostrovskii, *Russ. Chem. Rev.*, 2019, **88**, 644–676.
63 L. V. Myznikov, S. V. Vorona and Y. E. Zevatskii, *Chem. Heterocycl. Compd.*, 2021, **57**, 224–233.
64 T. L. Dadmal, S. D. Katre, M. C. Mandewale and R. M. Kumbhare, *New J. Chem.*, 2018, **42**, 776–797.
65 S. Bondock, W. Fadaly and M. A. Metwally, *J. Sulfur Chem.*, 2009, **30**, 74–107.

4 Zusammenfassung

4.1 Darstellung organischer Thiocyanate unter grünen Reaktionsbedingungen

Aufbauend auf den Vorarbeiten von Bolm *et al.* und Opatz *et al.* konnte im Rahmen dieser Dissertation die Synthese organischer Thiocyanate **100** erfolgreich von der Umsetzung in einem zweiphasigen Lösungsmittelgemisch auf eine lösungsmittelfreie mechanochemische Umsetzung in einer Planetenkugelmühle übertragen werden, wobei ungiftiges rotes Blutlaugensalz als Cyanidquelle genutzt wurde. Die Ergebnisse zeigten, dass sich die beiden entwickelten Methoden komplementär ergänzen. Hinsichtlich der Reaktion in der Kugelmühle konnte durch eine Optimierung der mechanochemischen Reaktionsbedingungen die benötigte Reaktionszeit stark verkürzt werden und durch die Verwendung von Silica als Schleifmittel auf den Zusatz von Essigsäure verzichtet werden, wodurch die Aufarbeitung deutlich vereinfacht wurde (Schema 4.1). Außerdem konnte für beide Methoden gezeigt werden, dass Reaktionen im Grammmaßstab prinzipiell möglich sind, aber jeweils eine eigene Optimierung benötigen. Die Methode zur Cyanierung von Disulfiden **99** im zweiphasigen Lösungsmittelgemisch konnte erfolgreich in der ersten Totalsynthese von Psammaplin B (**82**) angewendet werden. Ziel für die Zukunft ist es, eine (noch) breitere Anwendbarkeit für beide Methoden zu entwickeln und zu untersuchen, ob sich diese Cyanierungsreaktion auf weitere Heteroatome übertragen lässt. Dies kann durch eine Variierung der Mahlzeit und Rotationsgeschwindigkeit der Kugelmühle, die Verwendung von Mahlbechern und Kugeln aus anderen Materialien oder durch die Zugabe weiterer Additive getestet werden.

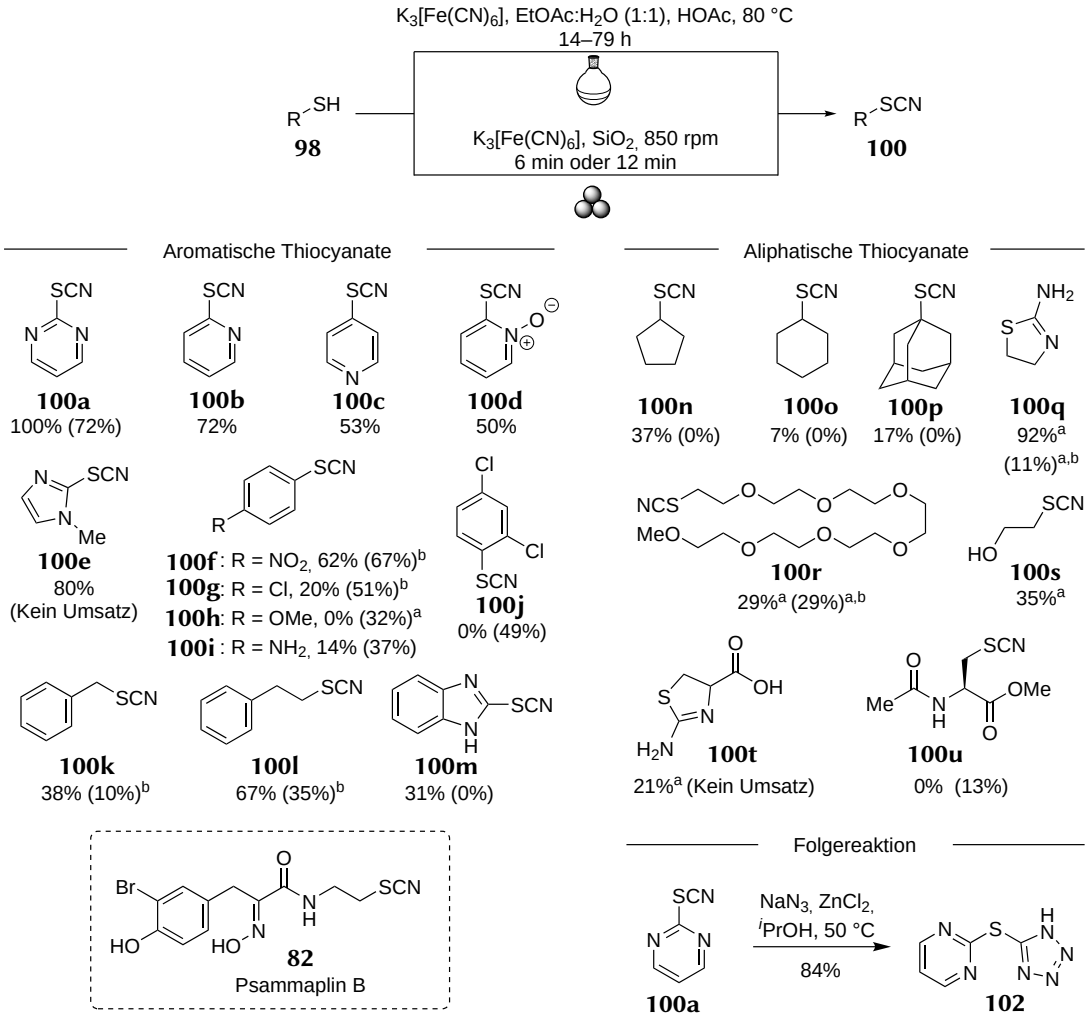

Schema 4.1: Die optimierten Parameter für die Darstellung organischer Thiocyanate **100a–u** unter Verwendung von rotem Blutlaugensalz als Cyanidquelle sowie das Substratspektrum ausgehend von aromatischen und aliphatischen Thiolen **98**. Darüber hinaus konnte der Naturstoff Psammaplin B (**82**) erfolgreich dargestellt werden und eine Folgereaktion an dem gebildeten Thiocyanat **100a** demonstriert werden. () Die Ausbeute unter mechanochemischen Bedingungen in der Kugelmühle. [a] Die Ausbeute wurde mittels internem Standard und ^{1}H-NMR bestimmt. [b] Die Mahlzeit wurde auf 12 min verlängert.

Teil II

Computerchemie und Spektroskopie

5 Einleitung

5.1 Naturstoffe

Die Naturstoffchemie beschäftigt sich mit der Extraktion und Isolierung, der Strukturaufklärung sowie der Synthese von Naturstoffen, die in lebenden Organismen gebildet werden.[211] Diese Moleküle lassen sich in Primär- und Sekundärmetaboliten einteilen. Während Primärmetaboliten sowohl für Wachstum und Lebenserhaltung (Anabolismus) als auch bei Abbauprozessen im Stoffwechsel (Katabolismus) produziert werden, sind Sekundärmetaboliten nicht essentiell, sondern verschaffen dem Organismus einen evolutionären Vorteil. Dieser kann in der gezielten Nutzung solcher Moleküle bei der Verteidigung gegen konkurrierende Organismen (z.B. antibiotische Wirkung) oder der Nutzung als Botenstoff liegen.[212] Diese sekundären Stoffwechselprodukte haben sich im Laufe von Millionen von Jahren entwickelt und besitzen häufig eine sehr komplexe Molekülstruktur, die sich in der Vielfalt ihrer biologischen Aktivitäten und inhärenten Eigenschaften niederschlägt.[213] Zu den bedeutendsten Klassen von Naturstoffen zählen die Alkaloide, die Polyketide sowie die Terpene.[214,215]

5.1.1 Bedeutung von Naturstoffen für den Menschen

Seit jeher macht sich die Menschheit die einzigartigen Eigenschaften von Sekundärmetaboliten zu Nutze und setzt diese unter anderem als Bestandteil traditioneller Medizin, durch Verwendung als Gift oder unter Ausnutzung der berauschenden Wirkung ein.[215–217] Eine Auswahl an Naturstoffen von großem pharmakologischen Interesse für die Menschheit ist in Abbildung 5.1 dargestellt.[218] Bei Morphin (**103**) handelt es sich um ein starkes Schmerzmittel und es war das erste Alkaloid, das im Jahr 1806 in Reinform isoliert werden konnte.[219] Die Gruppe der Penicilline zeichnet sich durch eine β-Lactam-Struktur aus und gehört zu den am längsten bekannten und vielfach gegen grampositive Bakterien

eingesetzten Antibiotika, weshalb es nicht überraschend ist, dass klinisch vorkommende Erreger bereits Resistenzen gegenüber solchen Strukturen entwickelt haben.[220,221] Eine Alternative, falls Allergien oder Resistenzen bestehen, ist Erythromycin A (**105**), das trotz des unterschiedlichen Makrolacton-Grundgerüsts, dessen Biosynthese über den Polyketid-Weg verläuft, ein vergleichbares antibiotisches Wirkungsspektrum bietet.[222,223] Es werden stetig Antibiotika mit neuen Wirkmechanismen gesucht, die immer häufiger auftretende Multiresistenzen von infektiösen Keimen überwinden können.[224–227] Darüber hinaus finden diverse Naturstoffe aufgrund ihrer einzigartigen Wirkmechanismen auch Anwendung als Zytostatika zur Behandlung verschiedener Krebsarten, wobei Paclitaxel (**106**) einer der am erfolgreichsten und am häufigsten verwendeten Naturstoffe aus der Stoffgruppe der Terpene ist.[228–230]

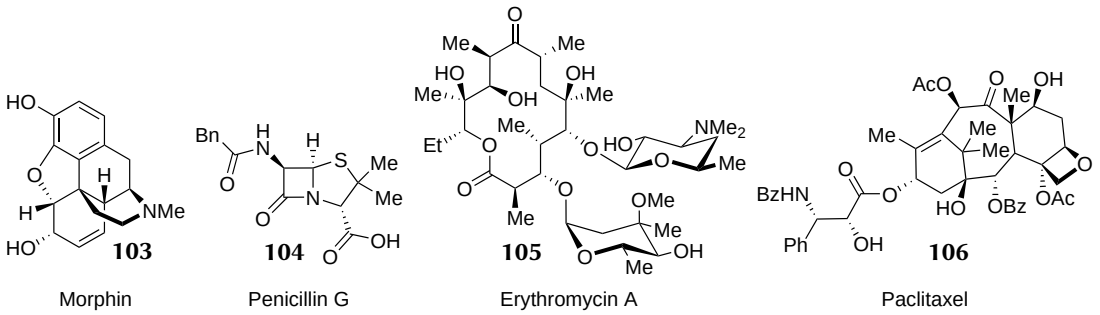

Abbildung 5.1: Für die Menschheit bedeutsame Naturstoffe **103**–**106**.

Die Suche nach spezifisch wirksamen und besser verträglichen Arzneimitteln gegen bisher unheilbare oder nicht behandelbare, lebensbedrohliche Krankheitserreger ist noch immer Gegenstand aktueller Forschung.[231–235] In der modernen Pharmakologie nehmen Naturstoffe eine wichtige Stellung bei der Identifizierung neuer Wirkstoffkandidaten ein, indem sie häufig als Leitstruktur dienen und das Grundgerüst für die Optimierung pharmakologischer Eigenschaften stellen.[236–238] Dabei versucht die Pharmaindustrie die Struktur so abzuwandeln, dass die Wirkung verbessert und auftretende Nebenwirkungen minimiert werden.[239] Da die aus der Natur isolierten Mengen häufig sehr gering sind, werden Totalsynthesen entwickelt, um diese Verbindungen sowie Derivate vollständig zu charakterisieren und ausgiebig auf ihre physiologischen und biologischen Eigenschaften untersuchen zu können.[236,240] Aufgrund des gleichzeitigen Vorhandenseins verschiedener aktiver Verbindungen in Naturstoffextrakten sind synergistische Effekte möglich, die in ihrer pharmako-

logischen Wirkung vollsynthetischen Wirkstoffen überlegen sein können.[240] Obwohl die Erforschung neuartiger Totalsynthesen komplexer Moleküle zeit- und ressourcenintensiv ist, helfen sie doch, Reaktivitäten besser zu verstehen sowie neue chemische Reaktionen und Prozesse zu entwickeln.[237,241,242]

5.1.2 Strukturaufklärung von Naturstoffen

Die Strukturaufklärung ist ein zentrales Thema bei der Erforschung von Naturstoffen. Unter den hierfür zur Verfügung stehenden Methoden liefert die Einkristall-Röntgenanalyse zwar die eindeutigsten Ergebnisse, ihre breite Anwendung ist in der Praxis aber durch die Zugänglichkeit geeigneter Kristalle eingeschränkt.[243–245] So konnte sich aufgrund ihrer sehr universellen Eignung die Kernspinresonanz (NMR)-Spektroskopie als führende Technik zur Aufklärung organischer Moleküle etabilieren.[246] Trotz Durchführung verschiedenster 1D- und 2D-NMR-Experimente, kann es infolge menschlicher Fehler, hoher molekularer Komplexität, Mehrdeutigkeit einzelner Signale und Probenverunreinigungen zu fehlerhaften Zuordnungen kommen, die oft erst durch die Darstellung der entsprechenden Struktur im Labor aufgedeckt werden.[247–253] Computer und Algorithmen können dazu beitragen, solche Fehlzuordnungen zu minimieren und so die Qualität von Strukturaufklärungsarbeiten zu verbessern. Die vorhergesagten spektroskopischen Daten können sowohl zur Validierung von Strukturen verwendet werden, als auch zur Durchführung von ansonsten unmöglichen strukturellen Zuordnungen.[254] Durch anhaltende Forschung und Optimierung nimmt die Zuverlässigkeit der quantenmechanischen Vorhersage chiroptischer Eigenschaften kontinuierlich zu und die Kombination solcher Berechnungen mit spektroskopischen Methoden spielt eine entscheidende Rolle bei der Bestimmung der absoluten Konfiguration von organischen Molekülen und unbekannten Naturstoffen.[245,255]

5.2 Grundlagen der Computerchemie

Das Ziel der Computerchemie ist es, die physikalischen Eigenschaften einer Substanz oder die Wechselwirkungen zwischen Molekülen vorherzusagen und experimentelle Befunde durch *in silico* Simulationen zu erklären. Durch die stetige Weiterentwicklung theoretischer Methoden im Bereich der Computerchemie können molekulare Systeme durch eine Vielzahl von Verfahren untersucht werden. Performantere Hochleistungsrechner mit

höheren Datenverarbeitungsgeschwindigkeiten sowie die Verfügbarkeit neuer Prozessoren und Grafikkarten ermöglichen die Berechnung und Analyse zunehmend komplexerer chemischer Strukturen und Systeme.[4] Geeignete Programme für quantenmechanische Berechnungen sind unter anderem Amsterdam Modeling Suite, CFOUR, Dalton, Gaussian, ORCA, QChem, Spartan sowie TURBOMOLE.[257–264]

Die klassische Computerchemie geht von der zeitunabhängigen Schrödinger-Gleichung aus, um Vielteilchensysteme näherungsweise zu berechnen, indem die Eigenwerte E des Hamiltonoperators $\hat{H}$ zu der Wellenfunktion ψ gesucht werden:

$$\hat{H}\psi = E\psi.$$

Der Hamiltonoperator eines Moleküls ergibt sich aus den Operatoren der kinetischen Energie $\hat{T}$ und den Potentialen der Coulomb-Wechselwirkungen $\hat{V}$ jeweils für die Kerne K und die Elektronen e in allgemeiner Form:

$$\hat{H} = \hat{T}_\mathrm{K} + \hat{T}_\mathrm{e} + \hat{V}_\mathrm{KK} + \hat{V}_\mathrm{Ke} + \hat{V}_\mathrm{ee}.$$

Eine analytische Lösung der Schrödinger-Gleichung ist nur bei Betrachtung sehr einfacher und kleiner Systeme möglich und auch numerische Lösungen sind aufgrund der hohen Dimensionalität nur eingeschränkt zugänglich. Dementsprechend müssen Näherungsverfahren wie die Born-Oppenheimer-Näherung herangezogen werden, die eine Separierung von Kern- und Elektronenbewegungen, erlaubt. Diese begründet sich auf der deutlich größeren Masse von Atomkernen im Vergleich zu Elektronen und führt zu guten Ergebnissen für Moleküle im Grundzustand. In dieser Näherung werden die Kerne als klassische Punktladungen betrachtet.[265] Dementsprechend ergibt sich der elektronische Hamiltonoperator $\hat{H}_\mathrm{el}$ in ausgeschriebenen Form:

$$\hat{H}_\mathrm{el} = \underbrace{-\sum_i \frac{\hbar^2}{2\,m_\mathrm{e}}\nabla_i^2}_{\hat{T}_\mathrm{e}} \quad \underbrace{-\frac{e}{4\,\pi\,\varepsilon_0}\sum_{i,I}\frac{Z_I}{|\vec{r}_i - \vec{R}_I|}}_{\hat{V}_\mathrm{Ke}} \quad \underbrace{+\frac{e}{4\,\pi\,\varepsilon_0}\sum_{i<j}\frac{1}{|\vec{r}_i - \vec{r}_j|}}_{\hat{V}_\mathrm{ee}}.$$

[4] Mit ca. 1,2 ExaFLOPS ist OLCF-5, auch Frontier genannt, im Juni 2023 der offiziell schnellste Hochleistungsrechner der Welt.[256]

In den Operatoren entspricht $\hbar$ der reduzierten Planck-Konstante, ε_0 der elektrischen Feldkonstante, ∇ dem Nabla-Operator und m_e der Elektronenmasse sowie e der respektiven Elementarladung. I und i, j zählen die Kerne beziehungsweise Elektronen, $\vec{R}_I$ und $\vec{r}_i$ bezeichnen die jeweiligen Ortsvektoren und Z_I entspricht der Kernladungszahl. Aus dem elektronischen Hamiltonoperator ergibt sich die vereinfachte, elektronische Schrödinger-Gleichung, die nur noch eine parametrische Abhängigkeit der Elektronenbewegung von den Kernpositionen enthält und mit Hilfe von Computern auch für große molekulare Systeme lösbar ist.[265]

5.2.1 Hartree-Fock-Methode

Ein Standardverfahren zur näherungsweisen Lösung der elektronischen Schrödinger-Gleichung ist die Hartree-Fock (HF)-Methode. Dabei handelt es um ein *ab initio* Verfahren, das nur Naturkonstanten benötigt und ohne empirische Parameter auskommt.

Zunächst wird die Wellenfunktion in ein antisymmetrisches Produkt von orthonormierten Einelektronenfunktionen zerlegt. Jeweils zwei dieser Spinorbitale φ_i lassen sich aus je einem räumlichen Orbital ϕ_i konstruieren, woraus sich die übliche Besetzungsregel von einem Elektronenpaar pro Orbital ergibt. Da es sich bei Elektronen um identische Teilchen und um Fermionen handelt, die nicht unterscheidbar sind, muss sich das Vorzeichen bei der Paarvertauschung zweier Teilchen ändern, um eine konsistente Beschreibung der Wellenfunktion zu erhalten. Eine molekulare N-Elektronen Wellenfunktionen lässt sich als Slater-Determinante darstellen:[266,267]

$$\psi_{\mathrm{HF}}(1,2,...,N) = \frac{1}{\sqrt{N!}} \begin{vmatrix} \varphi_1(1) & \varphi_2(1) & \cdots & \varphi_N(1) \\ \varphi_1(2) & \varphi_2(2) & \cdots & \varphi_N(2) \\ \vdots & \vdots & \ddots & \vdots \\ \varphi_1(N) & \varphi_2(N) & \cdots & \varphi_N(N) \end{vmatrix}.$$

Die Reihen der Slater-Determinante sind den Elektronen zugeordnet, während die Spalten den Spinorbitalen zugeordnet sind und $1/\sqrt{N!}$ entspricht der Normierungskonstante. Es kann kein Spinorbital zweimal auftreten, da die Slater-Determinante ansonsten zwei gleiche Spalten hätte und in $\psi = 0$ resultieren würde. Somit genügt dieser Ansatz dem Pauli-Prinzip.[268]

Für geschlossenschalige Systeme lassen sich aus der elektronischen Schrödinger-Gleichung die Hartree-Fock-Gleichungen herleiten:[269–271]

$$\hat{F}\phi_i = \varepsilon_i\phi_i.$$

$\hat{F}$ ist der Fock-Operator, der sich aus dem Einelektronen-, dem Coulomb- und dem Austauschoperator zusammensetzt. ϕ_i sind die optimalen Molekülorbitale und ε_i die dazugehörigen Orbitalenergien. Ziel ist es, mit Hilfe des Variationsverfahrens die optimalen Orbitale zu ermitteln, die den Energie-Erwartungswert der Slater-Determinante minimieren.

Für die Molekülorbitale wird angenommen, dass sie in Kernnähe Atomorbitalen ähneln und sich deshalb über eine Linearkombination aus diesen sowie den entsprechenden Koeffizienten beschreiben lassen (*linear combination of atomic orbitals*, LCAO-Ansatz).[272–274] Als Basisfunktionen finden normalerweise Linearkombinationen von Gaußfunktionen Anwendung. Aus der Wahl der Basisfunktionen für besetzte Atomschalen ergeben sich unterschiedliche Basissätze. Bekannte und weit verbreitete Basissätze sind die von Pople (z.B. 6-31G), die Ahlrichs- beziehungsweise Karlsruhe-Basen (z.B. SVP) sowie die korrelationskonsistenten Basen von Dunning (z.B. cc-pVDZ).[275–277]

Bei den Hartree-Fock-Gleichungen handelt es sich um ein nichtlineares Eigenwertproblem. Durch Überführung der Gleichungen in eine Matrixdarstellung lassen sich diese zu einem Pseudoeigenwertproblem, den sogenannten Roothaan-Hall-Gleichungen, vereinfachen. Diese können sehr effizient iterativ mittels eines *self-consistent field* (SCF)-Verfahrens von Computern gelöst werden:[278,279]

$$\mathbf{FC} = \mathbf{SC}\boldsymbol{\varepsilon}.$$

Dabei entspricht **F** der Fock-Matrix, **C** der Koeffizientenmatrix, **S** der Überlappungsmatrix und $\boldsymbol{\varepsilon}$ der Diagonalmatrix der Orbitalenergien.

Neben *ab initio* Verfahren existieren Methoden die (teilweise) auf empirischen Parametern oder Vereinfachungen basieren. Für sehr große Systeme (z.B. Proteinfaltung, Diffusion in Flüssigkeiten, Kristalle) kann eine parametrisierte Potentialhyperfläche verwendet werden. Dieser Ansatz entspricht dem klassischen Masse-Feder-Modell und ist auch als Kraftfeldmethode bekannt, um bestimmte molekulare Eigenschaften wie Geometrien und Schwingungsfrequenzen zu reproduzieren.[280–283] Bei semiempirischen Methoden handelt

es sich um vereinfachte Versionen der HF-Theorie, bei denen Näherungen auf Ebene der Fock-Matrix eingeführt werden. Mit Hilfe von experimentellen Daten oder Ergebnissen aus hochgenauen Berechnungen von Modellsystemen findet eine Parametrisierung statt, welche trotz deutlich geringerem Rechenaufwand genauere Ergebnisse als die HF-Methode ergibt. Beispiele für typische Näherungen sind die Beschränkung auf Valenzelektronen, das Verwenden einer minimalen Basis oder die Hückel-Theorie.[284–288]

Durch eine andere Herangehensweise lassen sich die erhaltenen HF-Energien mittels einer genaueren Beschreibung der Elektronenkorrelation verbessern. Während die Austausch-Korrelation der Elektronen im HF-Ansatz berücksichtigt wird, wird die Coulomb-Korrelation vernachlässigt. Die Wechselwirkung eines Elektrons mit allen anderen Elektronen wird lediglich über ein gemitteltes Feld der Ladungsdichte beschrieben. Zu den sogenannten *post*-HF-Methoden, die die Coulomb-Korrelation berücksichtigen, zählen das Konfigurationswechselwirkung-Verfahren (*Configuration Interaction*, CI), die *coupled-cluster* (CC)-Methode oder die Møller–Plesset-Störungstheorie.[289–298]

Durch Molekulardynamik (MD)-Simulationen lassen sich chemische Prozesse dynamisch beschreiben. Es wird eine deterministische Trajektorie des Systems erstellt und Zeitmittelwerte entlang dieser Trajektorie gebildet. Das System kann aus Atomen oder Molekülen bestehen, die sich unter dem Einfluss von Kräften bewegen und als Massenpunkte betrachtet werden. Bei der Berechnung werden die Newtonschen Bewegungsgleichungen für das wechselwirkende Vielteilchensystem ohne (direkte) Berücksichtigung von quantenmechanischen Effekten numerisch gelöst.[299–302]

5.2.2 Dichtefunktionaltheorie

Darüber hinaus existiert auch die Dichtefunktionaltheorie (DFT), bei der es sich in der Formulierung von Kohn[5] und Sham um die am häufigsten genutzte Methode der Quantenchemie handelt.[303–306] Analog zu den Hartree-Fock-Gleichungen werden die Kohn-Sham (KS)-Gleichungen durch ein selbstkonsistentes Verfahren innerhalb der Born-Oppenheimer-Näherung gelöst, die Orbitale aus Gaußfunktionen aufgebaut und die Molekülorbitale über den LCAO-Ansatz konstruiert. Trotz moderater Anforderungen an die Hardwareressourcen ist die Genauigkeit von DFT-Methoden dem HF-Ansatz klar überlegen.

[5] Walter Kohn wurde für seine Entwicklung der DFT zusammen mit John A. Pople im Jahr 1998 mit dem Nobelpreis für Chemie ausgezeichnet.

Während die HF-Methode auf einer Vielteilchenwellenfunktion basiert, die abhängig von N-Elektronen und den entsprechenden Orbitalen ist und die Elektronenkorrelation nur durch ein gemitteltes Feld berücksichtigt, wird bei der DFT nur die ortsabhängige Elektronendichte benötigt, um den elektronischen Grundzustand eines Vielelektronensystems und die Elektronenkorrelation indirekt zu beschreiben. Dies vereinfacht den konzeptionellen Umgang und die praktische Umsetzung.[304,307,308]

Die Grundlage für diesen Ansatz bilden die zwei Hohenberg-Kohn-Theoreme.[309] Das erste Theorem besagt, dass eine eindeutige Zuordnung zwischen der Elektronendichte des elektronischen Grundzustandes eines Systems und dem Coulomb-Potential (bis auf eine Konstante) existiert. Daraus folgt, dass in der Schrödinger-Gleichung dieses Systems der Hamiltonoperator und alle seine Eigenschaften festgelegt sind.[307] Das zweite Theorem besagt, dass für erlaubte Dichten das Variationsprinzip gilt, sodass die exakte Energie der elektronischen Schrödinger-Gleichung eine untere Schranke bildet. Folglich können bei bekannter Elektronendichte ρ alle weiteren physikalischen Eigenschaften des Moleküls im Grundzustand bestimmt werden.

Die Gesamtenergie eines Moleküls kann als Funktional der Elektronendichte $E[\rho]$ geschrieben werden, das sich aus der Summe der kinetischen Energie $T_\mathrm{e}[\rho]$, der Kern-Elektron- und der Elektron-Elektron-Wechselwirkung $V_\mathrm{Ke}[\rho]$ und $V_\mathrm{ee}[\rho]$ ergibt:

$$E[\rho] = T_\mathrm{e}[\rho] + V_\mathrm{Ke}[\rho] + V_\mathrm{ee}[\rho] .$$

Entsprechend der Kohn-Sham-Theorie lässt sich die kinetische Energie hinreichend gut durch Einelektronenorbitale mittels einer Slater-Determinante (Kohn-Sham-Determinante, ψ_KS) approximieren:[310]

$$T_\mathrm{e}[\rho] \approx T_\mathrm{S}[\psi_\mathrm{KS}] .$$

Trotz dieser Näherung lässt sich die Gesamtenergie unter Einbeziehung der elektrostatischen Abstoßung zwischen den Elektronen $J[\rho]$ weiterhin als exakter Ansatz ausdrücken. Alle kinetischen ($T_\mathrm{e}[\rho] - T_\mathrm{S}[\psi_\mathrm{KS}]$) und Austausch-Korrelationseffekte ($V_\mathrm{ee}[\rho] - J[\rho]$) lassen sich zu E_xc zusammenfassen, dessen Beitrag zur Gesamtenergie hinreichend klein ist, so-

dass auch Näherungen physikalisch sinnvolle Ergebnisse liefern. $T_\mathrm{S}\left[\psi_\mathrm{KS}\right]$, $J\left[\rho\right]$ und $V_\mathrm{Ke}\left[\rho\right]$ steuern große Beiträge zur Gesamtenergie bei und können explizit betrachtet werden:

$$E\left[\rho\right] = T_\mathrm{S}\left[\psi_\mathrm{KS}\right] + J\left[\rho\right] + V_\mathrm{Ke}\left[\rho\right] + E_\mathrm{xc}\left[\rho\right],$$
$$E_\mathrm{xc}\left[\rho\right] = T_\mathrm{e}\left[\rho\right] - T_\mathrm{S}\left[\psi_\mathrm{KS}\right] + V_\mathrm{ee}\left[\rho\right] - J\left[\rho\right].$$

Die unbekannte Größe $E_\mathrm{xc}\left[\rho\right]$ kann unterschiedlich komplex approximiert werden, um die Energie möglichst exakt zu berechnen. Eine Möglichkeit der Klassifikation ist die von Perdew *et al.* eingeführte Metapher der *Jacob's Ladder*.[311] Mit jeder weiteren Sprosse werden dem Funktional zusätzliche Variablen hinzugefügt, wodurch potentiell bessere, aber auch ressourcenintensivere Funktionale erhalten werden. Beginnend mit dem niedrigsten Funktional, welches lediglich die lokale Dichteapproximation (LDA) beinhaltet, nähert man sich durch sukzessives Einbeziehen von Dichtegradienten (GGA) und der kinetischen Energiedichte (mGGA) der chemisch exakten Lösung an.[310,312–321] Durch Hybrid- und Doppel-Hybrid-Methoden[322–327] werden explizit besetzte und virtuelle Orbitale berücksichtigt, während die letzte Sprosse vollständig nicht-lokale Funktionale (RPA) bilden.[328–331]

5.2.3 Angeregte Zustände

In der organischen Chemie nehmen elektronisch angeregte Zustände in vielen Bereichen eine wichtige Rolle ein. Klassische Bereiche sind photochemisch induzierte Reaktionen, photophysikalische Eigenschaften oder Farbstoffe. Durch theoretische Modellierungen lassen sich detaillierte mechanistische Einsichten zu den angeregten Zuständen gewinnen, die experimentell oft nur schwer zugänglich sind, aber wesentlich zum Verständnis beitragen können.[332,333]

Für eine gute Beschreibung von angeregten Zuständen ist eine einzelne Determinante oft nicht mehr ausreichend. Die Potentialhyperflächen angeregter Zustände liegen häufig energetisch eng beieinander. Somit müssen mehrere solcher Flächen, deren Kreuzpunkte (z.B. konische Durchschneidungen) und die entsprechenden Kopplungsmatrixelemente (nicht adiabatische Kopplung, Spin-Bahn-Kopplung) betrachtet werden. Um angeregte Zustände vorherzusagen, können verschiedene Level der Theorie verwendet werden. Semiempirische Verfahren sind rechnerisch deutlich weniger anspruchsvoll als die

wellenfunktionsbasierten Ansätze sowie DFT-Methoden und können recht genaue Schätzungen für die Eigenschaften großer Moleküle liefern.[288,334,335]

Die erste gängige *ab initio* Methode für angeregte Zustände war das Konfigurationswechselwirkung mit Einfachanregungen (CIS)-Verfahren, das Anfang der 1970er Jahre entwickelt wurde.[336] Hierbei wird die Wellenfunktion aus Linearkombinationen von Slater-Determinanten, also durch verschiedene Elektronenkonfigurationen, aufgebaut. Die Anregungsenergien werden häufig stark überschätzt und die angeregten Zustände falsch zugeordnet, wodurch die Verwendung von CIS als quantitative quantenchemische Methode ausgeschlossen ist. Von Head-Gordon *et al.* wurde die CIS(D)-Methode entwickelt, die eine Störungskorrektur zweiter Ordnung zur CIS hinzufügt und dadurch die Fehlergröße im Vergleich zur CIS erheblich reduziert.[337,338] Bei dem hochgenauen *complete active space* (CAS)-Verfahren werden die Molekülorbitale in inaktive, aktive und virtuelle Orbitale unterteilt. So können innerhalb des aktiven Raums alle Konfigurationswechselwirkungen bestimmt werden. Dies ermöglicht eine Untersuchung verschiedener elektronischer Konfigurationen, die nahezu entartet sind. Die richtige Wahl des aktiven Raums ist jedoch oft schwierig und wird schnell zum limitierenden Faktor im Bezug auf die benötigte Rechenzeit.[339] Außerdem wird die dynamische Elektronenkorrelation bei CASSCF vernachlässigt und bei *complete active space second-order perturbation theory* (CASPT2) nur störungstheoretisch in zweiter Ordnung behandelt.[340–342] Trotzdem können diese Ansätze sehr genaue Ergebnisse für molekulare angeregte Zustände ergeben.[333,343] Durch die Entwicklung der *N-electron valence state second-order perturbation theory* (NEVPT2)-Methode konnten einige der wichtigsten theoretischen Mängel der CASPT2 behoben werden, wie beispielsweise die Größenkonsistenz.[344] Darüber hinaus existieren weitere Ansätze, die die Nutzung von multikonfigurationellen Methoden auch für größere Moleküle oder stark korrelierte Systeme ermöglichen.[345–349]

Analog zu den Hohenberg-Kohn-Theoremen und den Ansätzen von Kohn und Sham wurde von Runge und Gross ein zeitabhängiges (TD)-Theorem für DFT veröffentlicht.[350] Mit der Veröffentlichung eines linearen Antwortfunktion (LR)-Formalismus von Casida für die Berechnung von Anregungsspektren entwickelte sich TD-DFT schnell zur am häufigsten verwendeten Theorie für (mittel)große organische Moleküle.[351] Analog zu der Implementierung von LR-TD-HF leitete Casida die Gleichung für ein N-Elektronensystem im Grundzustand her, das einer zeitabhängigen Störung, wie zum Beispiel der Wechselwir-

kung mit elektromagnetischer Strahlung, ausgesetzt ist. Die dynamische Antwort der KS-Dichtematrix bei einer infinitesimal kleinen Störung lässt sich als Matrix-Pseudoeigenwertproblem ausdrücken:[351]

$$\begin{bmatrix} \mathbf{A} & \mathbf{B} \\ \mathbf{B}^* & \mathbf{A}^* \end{bmatrix} \begin{pmatrix} \vec{X}_I \\ \vec{Y}_I \end{pmatrix} = \omega_I \begin{bmatrix} \mathbf{1} & \mathbf{0} \\ \mathbf{0} & -\mathbf{1} \end{bmatrix} \begin{pmatrix} \vec{X}_I \\ \vec{Y}_I \end{pmatrix}.$$

Für die Zustände I werden die Eigenwerte, also die Anregungs- bzw. Abregungsenergien ω_I, die sich nur im Vorzeichen unterscheiden, berechnet, wobei $(\vec{X}_I, \vec{Y}_I)^{\mathrm{T}}$ den zugehörigen Eigenvektoren der Orbitalrotationshessematrizen $\mathbf{A}$ und $\mathbf{B}$ entsprechen. Aufbauend auf dieser Gleichung wurde von Hirata und Head-Gorden die Tamm-Dancoff-Näherung[6] eingeführt, die die $\mathbf{B}$ Matrix vernachlässigt, wodurch Anregungen und Abregungen entkoppelt werden und sich die Gleichung zu einem Eigenwertproblem vereinfacht:[352,353]

$$\mathbf{A}\vec{X}_I = \omega_I \vec{X}_I.$$

Die zeitabhängige DFT besitzt eine hohe Berechnungseffizienz, die es ermöglicht, ausgedehnte molekulare Systeme zu behandeln und genaue Anregungsenergien in kurzer Rechenzeit zu generieren.[298,333] Außerdem bietet dieser Ansatz sowohl erste als auch zweite analytische Ableitungen, die für eine schnelle Geometrieoptimierung angeregter Zustände und Schwingungsfrequenzberechnungen benötigt werden.[354–360] Für eine Beschreibung von Ladungstransferzuständen, Rydberg-Zuständen, konischen Durchschneidungen und Doppelanregungen sind TD-DFT-Methoden in adiabatischer Näherung jedoch nicht geeignet.[361–367]

Neben der LR-TD-DFT existieren verschiedene weitere Ansätze, um diese Nachteile effizient auszugleichen.[368–371] Trotz der Entwicklung robusterer Funktionale ist es noch immer schwierig, ein für alle Anregungsfälle geeignetes Funktional auszuwählen.[372–379] Die Lösung des systematischen Delokalisierungsfehlers ist eine der größten Herausforderungen der DFT.[380–383] Darüber hinaus lassen sich weder die TD-DFT- noch die DFT-Methoden systematisch verbessern, wodurch deren Anwendbarkeit erschwert wird.[333]

Im Rahmen der *coupled-cluster*-Theorie können angeregte Zustände seit Anfang der 2000er Jahre mittels der *equation of motion*-Methode mit Einzel- und Doppelanregungen

[6] Im Rahmen von TD-HF entspricht diese Näherung der CIS-Methode.

(EOM-CCSD) simuliert werden.[295,384–386] Bei EOM-CCSD sind die Fehler klein und ionisierte Zustände können beschrieben werden, allerdings werden die vertikalen Übergangsenergien typischerweise überschätzt.[387] Die ursprünglichen CC-Methoden wurden schnell durch eine approximierte und rechnerisch leichtere Variante ergänzt (CC2 und CC3).[388,389]

Infolge der enormen Verbesserungen der Computerleistung, der Parallelisierung der Algorithmen sowie der Verfügbarkeit von relativ benutzerfreundlichen Softwarepaketen können quantenmechanische Berechnungen für elektronisch angeregte, mittelgroße organische Moleküle heutzutage einfach durchgeführt werden.[254,379,390,391] Es existieren systematische Benchmarkstudien und Referenzenergien sowohl zu den vertikalen Anregungsenergien und den Triplett-Zuständen mittelgroßer organischer Moleküle als auch experimentelle 0–0-Übergänge aus dem Bereich der organischen Photochemie.[392–399] So kann die Genauigkeit verfügbarer Methoden neben ihren formalen rechnerischen Skalierungen für angeregte Zustände auch über den typischen Fehlerbereich einzelner Anregungen verglichen werden.[333]

5.3 Berechnung spektroskopischer Eigenschaften

Experimentelle Spektren ergeben sich aus der Summe aller konformellen Anordnungen eines Moleküls, die unter den gegebenen Bedingungen eingenommen werden können. Um dies bei der *in silico* Vorhersage zu berücksichtigen und den bestmöglichen Vergleich zwischen experimentellen und theoretischen Spektren zu ermöglichen, ist es wichtig, nicht nur das energetisch tiefliegendste Konformer zu betrachten, sondern die Spektren für ein (möglichst) vollständiges Ensemble an Konformeren zu berechnen und auf Grundlage der Energie der einzelnen Konformere eine Boltzmann-Gewichtung vorzunehmen. Werden bei der experimentellen Messung Lösungsmittel verwendet, können diese durch implizite Solvatationsmodelle (z.B. SMD, IEFPCM, COSMO oder CPCM-X) in Form eines polarisierbaren Kontinuums modelliert werden.[400–405] Mit spektroskopischen Techniken lassen sich molekulare Systeme nicht invasiv untersuchen und ihre Struktur, Eigenschaften und Dynamik in unterschiedlichen Umgebungen und unter verschiedenen physikochemischen Bedingungen erforschen. Die große Vielfalt spektroskopischer Techniken, die verschiedene Bereiche des elektromagnetischen Feldes abdecken, können in Kombination mit der Massenspektrometrie zu einem umfassenderen Bild der untersuchten Moleküle führen. Zu

den spektroskopischen Moleküleigenschaften, die durch quantenmechanische Berechnungen vorhergesagt werden können, zählen die Kernresonanz-, Rotations- und Schwingungsspektroskopie sowie Techniken, die auf elektronischen Anregungen bzw. angeregten Zuständen basieren. Die moderne Spektroskopie besitzt eine so hohe Auflösung, dass eine Vielzahl von Signalen detektiert wird, die ohne die Unterstützung von quantenmechanischen Methoden kaum noch auswertbar ist.[406,407]

5.3.1 Geometrieoptimierung und Frequenzberechnung

Die Struktur eines Moleküls lässt sich durch Angabe der Positionen der Atome im Raum genau spezifizieren. Für eine bestimmte Struktur und einen bestimmten elektronischen Zustand besitzt ein Molekül eine definierte potentielle Energie und die Änderung der Energie eines Moleküls in Abhängigkeit der Struktur lässt sich über eine Potentialhyperfläche darstellen. Die Gleichgewichtsgeometrie eines Moleküls entspricht einem (lokalen) Minimum auf der Potentialhyperfläche. Bevor die physikalischen Eigenschaften eines Moleküls berechnet werden können, muss ein stationärer Punkt auf der Potentialhyperfläche identifiziert werden, der einem (lokalen) Minimum oder Sattelpunkt entspricht. Für alle stationären Punkte gilt, dass der Gradient, also die erste Ableitung der Energie nach allen Kernkoordinaten, gleich Null ist. Damit es sich um ein (lokales) Minimum handelt, darf die zweite Ableitung (Hesse-Matrix) nur Eigenwerte größer Null enthalten.[408] Die Struktur wird so lange optimiert bis diese entweder zu einer Gleichgewichtsgeometrie konvergiert, oder zuvor festgelegte Grenzwerte erreicht werden. Für jede Geometrie des Moleküls wird die elektronische Energie mittels SCF-Verfahren berechnet. Je nach Molekülgröße und geforderter Genauigkeit können hierfür Kraftfeld-, semiempirische oder quantenmechanische Methoden verwendet werden.

Das Newton-Raphson- und Quasi-Newton-Verfahren sind die effizientesten und am weitesten verbreiteten Verfahren zur Optimierung von Gleichgewichtsgeometrien und können auch zur Ermittlung von Sattelpunkten wirksam eingesetzt werden.[409] Bei dem Newton-Raphson-Verfahren werden die neuen Kernkoordinaten $\mathbf{R}$ iterativ über die Hesse-Matrix $\mathbf{H}$ und den Gradient $\mathbf{g}$ bestimmt:

$$\mathbf{R}_{k+1} = \mathbf{R} - \mathbf{H}^{-1}\mathbf{g}_k.$$

Neben der Wahl der Anfangsstruktur hängt die Effizienz und Stabilität einer Geometrieoptimierung von der Start-Hesse-Matrix, der Aktualisierungsmethode sowie der Schrittweite ab.[410] Bei der Quasi-Newton-Methode wird die inverse Hesse-Matrix approximiert, daraus der Gradient bestimmt und die Hesse-Matrix über die vorherigen Hesse-Matrizen sowie die Gradienten aktualisiert.[411–414] Diese Aktualisierungen der Hesse-Matrix finden häufig nach dem Broyden-Fletcher-Goldfarb-Shanno (BFGS)-Verfahren statt.[415–418] Darüber hinaus existieren verschiedene Verfahren für das Auffinden von Minima einer Potentialhyperfläche, wie das Liniensuchverfahren, das Verfahren der konjugierten Gradienten oder der Berny-Algorithmus.[409,410,419–421]

Im Gegensatz zu einer Minimierung muss die Optimierung eines Sattelpunktes (Übergangsstruktur) sich in eine Richtung der Potentialhyperfläche bergauf und in alle anderen orthogonalen Richtungen bergab bewegen, da die Hesse-Matrix genau einen negativen Eigenwert enthält. Oft ist die Richtung der Steigung nicht im Voraus bekannt und muss im Laufe der Optimierung bestimmt werden.[409] Hierfür zur Verfügung stehende Verfahren lassen sich grob in Methoden unterteilen, die entweder von einem oder zwei Startpunkten ausgehen.[422] Einseitige Methoden beginnen mit einer Ausgangsstruktur und variieren diese in Richtung der Übergangsstruktur. Dazu gehören Quasi-Newton-Methoden in optionaler Kombination mit einer quadratischen Synchronübergangs (*quadratic synchronous transit*, QST2 oder QST3)-Methode, die direkte Inversion des iterativen Unterraums (DIIS), die Sattelpunktnäherung oder der Berny-Algorithmus.[409,419,423–431] Zu den Methoden, die von zwei Startgeometrien ausgehen, gehören verschiedene *chain of state*-Methoden, die mittels einer Reihe von Punkten das Edukt mit dem Produkt auf der Potentialhyperfläche verbinden und so den Reaktionsweg diskretisieren, wie es beispielsweise bei der *nudged elastic band*-Methode[432–434] oder der *(growing) string*-Methode, der Fall ist.[435–439] Ein identifizierter Sattelpunkt wird durch die Analyse der Eigenwerte der Hesse-Matrix als Übergangszustand verifiziert. Ob diese Struktur tatsächlich Edukt und Produkt verbindet, lässt sich über die Berechnung der intrinsischen Reaktionskoordinate (IRC) bestätigen. Hierbei wird, ausgehend von der Geometrie des Übergangszustandes, das Energieprofil der Reaktionskoordinate in beide Richtungen mit definierter Schrittanzahl und entsprechenden geometrischen Parametern (Bindungslänge und Bindungswinkel) berechnet.[440,441]

Die Schwingungsfrequenzen werden berechnet, indem die Eigenvektoren der Hesse-Matrix in massengewichtete Koordinaten transformiert werden.[442] Da diese Transforma-

tion nur für stationäre Punkte gültig ist, muss die Berechnung der Frequenz auf demselben Level der Theorie wie die Geometrieoptimierung durchgeführt werden. Anharmonische Korrekturen können störungstheoretisch berücksichtigt werden.[443]

5.3.2 NMR-Spektroskopie

Aus der NMR-Spektroskopie lassen sich Informationen über die elektronische Umgebung und die geometrische Struktur einer Verbindung erhalten. Durch die Auswertung der chemischen Verschiebung und des Aufspaltungsmusters, hervorgerufen durch die Kopplung der Kerne untereinander, lässt sich eine Strukturformel sowie die relative Konfiguration einer Verbindung bestimmen.[444] Die NMR-Spektroskopie ist eines der wichtigsten Experimente, um unbekannte Verbindungen in der präparativen organischen Synthese sowie bei isolierten Naturstoffen aufzuklären.

Die Grundlage der NMR-Spektroskopie bildet die direkte Wechselwirkung des magnetischen Moments eines Atomkerns $\vec{m}_K$ mit einem äußeren Magnetfeld $\vec{B}$, die zu einer Aufspaltung der Kernenergieniveaus (Zeeman-Effekt)[7] mit der Energiedifferenz ΔE führt:

$$\Delta E = -\vec{m}_{\mathrm{K}}\vec{B}.$$

Entsprechend dem Biot-Savart-Gesetz induziert das Magnetfeld in einem Molekül einen Strom, der wiederum ein magnetisches Feld erzeugt, das das angelegte Feld überlagert.[446] An einem Kern wirkt somit ein effektives Feld $\vec{B}_{\mathrm{eff}}$ und der durch die Elektronen induzierte Anteil kann mittels des chemischen Verschiebungstensors $\vec{\sigma}_K$ charakterisiert werden:

$$\begin{aligned}\Delta E &= -\vec{m}_{\mathrm{K}}\vec{B}_{\mathrm{eff}},\\ \Delta E &= -\vec{m}_{\mathrm{K}}\left(1-\vec{\sigma}_{\mathrm{K}}\right)\vec{B}.\end{aligned}$$

Bei der experimentellen Messung von chemischen Verschiebungen mittels NMR-Spektroskopie wird eine Referenzsubstanz verwendet (für ^{1}H- und ^{13}C-Verschiebungen Tetrame-

[7] Die unterschiedlichen Verschiebungen von Energieniveaus einzelner Zustände führen zu einer Aufspaltung von Spektrallinien durch ein äußeres Magnetfeld. Dieser Effekt wurde im Jahr 1896 von Pieter Zeeman nachgewiesen und von Hendrik A. Lorentz drei Jahre später erklärt, wofür beide 1902 mit dem Nobelpreis für Physik ausgezeichnet wurden.[445]

thylsilan (TMS)) und die relative chemische Verschiebung δ ausgewertet:

$$\delta = \vec{\sigma}_{\mathrm{ref}} - \vec{\sigma}_{\mathrm{K}}.$$

Mit Hilfe quantenmechanischer Methoden kann die chemische Verschiebung unterschiedlicher Atomkerne aus den entsprechenden Abschirmungskonstanten berechnet werden. Diese ergeben sich aus der zweifachen Ableitung der Energie nach dem magnetischen Kernmoment und nach dem externen magnetischen Feld. Für die Berechnung der Spin-Spin-Kopplungskonstanten wird die zweifache Ableitung der Energie nach beiden magnetischen Kernmomenten berechnet. Um eichursprungsinvariante Ergebnisse zu erhalten, finden häufig lokale Eichursprünge auf der Ebene individueller Atomorbitale Anwendung (*gauge-including atomic orbital*, GIAO).[447–449]

Anfang der 2000er Jahre hat das Interesse an der *ab initio* Vorhersage von chemischen Verschiebungen zur Unterstützung der Strukturaufklärung insbesondere durch die Arbeiten von Bifulco *et al.* deutlich zugenommen.[450–452] Dabei handelt es sich um keine triviale Aufgabe, da die Übereinstimmung zwischen berechneten und experimentellen Daten nicht für jeden Kern ideal ist. Um diese Abweichung zu quantifizieren, wurden zunächst verschiedene Parameter, wie der Korrelationskoeffizient (*r*), der mittlere absolute Fehler (MAE) oder der korrigierte MAE (CMAE) verwendet.[450,451,453–456] Smith und Goodman leisteten mit der Entwicklung des *comparison parameter* (CP3)-Parameters und der *diastereomeric probability* (DP4)-Wahrscheinlichkeit Pionierarbeit auf diesem Gebiet. Der CP3-Parameter ermöglicht es, zwei experimentelle Datensätze zwei möglichen diastereomeren Strukturen zuzuordnen und bietet damit eine Herangehensweise für Situationen, die bei stereoselektiven Reaktionen auftreten können. Hierfür werden die Abweichungen in den berechneten chemischen Verschiebungen beider Stereoisomere mit den entsprechenden Unterschieden der experimentellen Verschiebungen verglichen. Diese Methode erfordert allerdings, dass für alle Diastereomere experimentelle Daten zur Verfügung stehen, was insbesondere in der Naturstoffaufklärung oder bei organischen Reaktionen mit sehr hoher Stereoselektivität zu Problemen führen kann.[452]

Im Gegensatz zum CP3-Parameter, ist für die DP4-Wahrscheinlichkeit nur ein Satz von experimentellen Daten notwendig, um die korrekte Struktur unter vielen plausiblen Isomeren zu identifizieren.[457] Smith und Goodman zeigten, dass der Fehler zwischen experimentellen (d_{exp}) und berechneten, skalierten (d_{s}) chemischen Verschiebungen für einen Satz

organischer Moleküle einer kumulierten Student *t*-Verteilung T^{ν} entspricht. Für ein gegebenes Molekül mit *N* Kernen wird die Wahrscheinlichkeit für jeden *i*-ten Fehler berechnet. Die Multiplikation der einzelnen *i*-ten Wahrscheinlichkeiten, unter der Annahme, dass die einzelnen Fehler unabhängige Zufallsvariablen sind, ergibt die Gesamtwahrscheinlichkeit für eine Kandidatenstruktur. Mit Hilfe des Bayes-Theorems werden die prozentualen Wahrscheinlichkeiten für alle Kandidatenstrukturen ermittelt. Mathematisch lässt sich die DP4-Wahrscheinlichkeit wie folgt berechnen:

$$\mathrm{P}(i) = \frac{\prod_{\mathrm{K}=1}^{N} \left(1 - T^{\nu}\left(d^{i}_{\mathrm{s,K}} - d_{\mathrm{exp,K}}\right)/\sigma\right)}{\sum_{j=1}^{m}\left[\prod_{\mathrm{K}=1}^{N}\left(1 - T^{\nu}\left(d^{j}_{\mathrm{s,K}} - d_{\mathrm{exp,K}}\right)/\sigma\right)\right]}.$$

P(*i*) entspricht der Wahrscheinlichkeit, dass es sich bei Isomer *i* aus *m* möglichen Strukturen um den korrekten Strukturvorschlag handelt. T^{ν} ist die kumulierte *t*-Verteilungsfunktion mit ν Freiheitsgraden. Bei ν handelt es sich zusammen mit der Standardabweichung σ um Schlüsselparameter bei der Berechnung der DP4-Wahrscheinlichkeit, die durch Anpassen des Fehlers e zwischen skalierten und experimentellen chemischen Verschiebungen eines großen Datensatzes an eine *t*-Verteilung von den Autoren ermittelt wurden. $\delta_{\mathrm{s},k}$ entspricht der berechneten, skalierten chemischen Verschiebung für Kern K. Die Skalierung wird durch das Auftragen von δ_{calc} gegen δ_{exp} erhalten und soll systematische Fehler ausgleichen. Die quantenmechanischen Berechnungen werden mittels der GIAO-Methode auf B3LYP/6-31G**//MMFF-Niveau in der Gasphase durchgeführt.[457]

Um die korrekte Zuordnung durch weitere Informationen zu unterstützen, wurde als Erweiterung die $\mathcal{J}$-DP4-Methode entwickelt, die es erlaubt, skalare H–H-Kopplungskonstanten von vicinalen Protonen ($^{3}\mathcal{J}_{\mathrm{HH}}$) einzubeziehen, um die Performanz bei gleichen oder geringeren Berechnungskosten zu verbessern.[458]

Es wurde anhand vieler Beispiele gezeigt, dass die DP4-Wahrscheinlichkeit inkonsistente und unzuverlässige Ergebnisse liefern kann oder sogar die experimentellen Daten einer falschen Kandidatenstruktur zuordnet.[459–461] Sarotti *et al.* gelang es, mit dem Theorieniveau sowie der ausschließlichen Verwendung von skalierten chemischen Verschiebungen, zwei potenzielle Schwachstellen in der DP4-Methode zu identifizieren. Auf der einen Seite lässt sich eine erhöhte Genauigkeit bei der Berechnung der chemischen Verschiebungen erreichen, indem die Molekülgeometrien auf B3LYP/6-31G*-Niveau berechnet werden

und für die Berechnung der Abschirmungstensoren mittels PCM/mPW1PW91/6-31+G** ein höheres Theorielevel verwendet wird, da gezeigt wurde, dass selbst kleine Fehler in der Ausgangsgeometrie zu erheblichen Fehlern in den berechneten chemischen Verschiebungen führen können.[462–464] Auf der anderen Seite werden lineare Skalierungen eingesetzt, um systematische Fehler zu entfernen, sodass die korrigierten Verschiebungen näher an den experimentellen Werten liegen.[452,457,465] Diese Praxis setzt jedoch voraus, dass die Größe eines Fehlers unabhängig von der chemischen Umgebung (z. B. der Kohlenstoff-Hybridisierung) ist, was bei der NMR-Spektroskopie nicht der Fall ist.[450,451,466,467] Darüber hinaus besteht bei der Datenkorrelation von Isomeren mit ähnlichen berechneten chemischen Verschiebungen immer das Risiko falsch positiver Ergebnisse, da einer der falschen Kandidaten eine (zufällig) bessere Anpassung als das richtige Isomer bieten könnte.[468] Aus diesem Grund haben Sarotti *et al.* die unskalierten chemischen Verschiebungen in die Methode für die Berechnung der verbesserten, sogenannten *diastereomeric probability 4+* (DP4+)-Wahrscheinlichkeiten mit einbezogen, um die strukturellen Unterschiede zwischen den plausiblen Kandidatenstrukturen besser abzubilden.[469] Die DP4+-Wahrscheinlichkeit P(*i*) für die Zuordnung eines Satzes experimenteller Daten zu einem Kandidat *i* aus einer Auswahl von *m* Isomeren ist durch eine Funktion f der Wahrscheinlichkeiten der entsprechenden skalierten und unskalierten chemischen Verschiebungen ($\mathrm{P}(i)_\mathrm{s}$ und $\mathrm{P}(i)_\mathrm{u}$) gegeben:

$$\mathrm{P}(i) = f\left[\mathrm{P}(i)_\mathrm{s}; \mathrm{P}(i)_\mathrm{u}\right].$$

Um die DP4+-Wahrscheinlichkeit zu berechnen, wurden die statistischen Parameter T_s^ν, e_s, σ_s, T_u^ν, e_u und σ_u mit einem genaueren Level der Theorie unter Berücksichtigung eines Solvatationsmodells für einen großen Datensatz von kleinen bis mittelgroßen Molekülen berechnet. Dabei zeigte sich, dass die unskalierten Kerne (^{1}H und ^{13}C) von sp^2- und sp^3-hybridisierter Kohlenstoffen (spx) isoliert betrachtet zwei *t*-Verteilungen mit jeweiligem Mittelwert $\mu_\text{u-spx}$ entsprechen. Daraus ergibt sich die finale DP4+-Wahrscheinlichkeit:[469]

$$\mathrm{P}(i) = \frac{\prod_{\mathrm{K}=1}^{N}\left[1 - T_\mathrm{s}^\nu\left(e_{\mathrm{s,K}}^i/\sigma_\mathrm{s}\right)\right]\left[1 - T_\text{u-spx}^\nu\left(\left(e_{\mathrm{u,K}}^i - \mu_\text{u-spx}\right)/\sigma_\text{u-spx}\right)\right]}{\sum_{j=1}^{m}\prod_{\mathrm{K}=1}^{N}\left[1 - T_\mathrm{s}^\nu\left(e_{\mathrm{s,K}}^j/\sigma_\mathrm{s}\right)\right]\left[1 - T_\text{u-spx}^\nu\left(\left(e_{\mathrm{u,K}}^j - \mu_\text{u-spx}\right)/\sigma_\text{u-spx}\right)\right]}.$$

In den letzten Jahren wurden zahlreiche weitere effiziente und genaue Methoden für die computergestützte Strukturaufklärung mittels NMR entwickelt.[246,470–477] Dazu zählen DP4-AI von Goodman *et al.*, die eine automatisierte Verarbeitung und Zuordnung von ^{1}H- und ^{13}C-NMR-Rohdaten erlaubt. Diese Methode ermöglicht Hochdurchsatzanalysen von Datenbanken und erreicht eine deutliche Steigerung der Verarbeitungsgeschwindigkeit.[478] Ein Ansatz, der nicht auf der linearen Regressionskorrektur basiert, wurde von Grimme *et al.* beschrieben. Durch maschinelles Lernen gelang es den Autoren, auf DTF-Niveau berechnete chemische Verschiebungen zu korrigieren, sodass bei deutlich geringerer Rechenzeit Abweichungen zu experimentellen Werten auf CCSD(T)-Niveau erreicht werden können.[479]

5.3.3 CD-Spektroskopie

Die Eigenschaft chiraler Verbindungen, die Polarisationsrichtung von Licht zu beeinflussen, wird als optische Aktivität bezeichnet. Verschiedene verlustfreie chiroptische Methoden wie beispielsweise die Polarimetrie, die optische Rotationsdispersion, die Raman optische Aktivität und die Zirkulardichroismus (CD)-Spektroskopie nutzen diese Eigenschaft, um chirale Verbindungen zu charakterisieren, zwischen Enantiomeren zu unterscheiden oder einen Enantiomerenüberschuss (*ee*) zu bestimmen.[480–482]

Die CD-Spektroskopie beruht auf der Differenz der unterschiedlichen molaren Extinktionskoeffizienten ε eines chiralen Moleküls, wenn es zirkular polarisiertem Licht ausgesetzt wird (die Indizes L und R entsprechen links- bzw. rechtshändiger Polarisation):

$$\Delta\varepsilon = \varepsilon_{\mathrm{L}} - \varepsilon_{\mathrm{R}}.$$

Da die molaren Extinktionskoeffizienten über das Lambert-Beer-Gesetz mit der gemessenen Absorption verknüpft sind, besitzen Enantiomere immer spiegelbildliche Spektren.[443]

Das erste elektronische CD (ECD)-Spektrum wurde im Jahr 1895 von Cotton[8] aufgezeichnet.[483] Während die Empfindlichkeit des ECD im Vergleich zu Schwingungszirkulardichroismus (VCD) um zwei Größenordnungen höher ist, muss der Analyt ein Chromophor in der Nähe der stereogenen Zentren oder anderer stereogener Elemente aufweisen, damit die ECD-Spektroskopie zuverlässig für die Bestimmung der absoluten Konfiguration angewendet werden kann. Im Gegensatz dazu enthält ein VCD-Spektrum deutlich mehr Banden und ist auch für gesättigte Kohlenwasserstoffe geeignet.[481,484,485] Die ersten VCD-Spektren wurden 1974 von Holzwarth *et al.* aufgenommen und ein Jahr später von Stephens *et al.* unabhängig bestätigt.[486,487]

VCD-Spektren können durch das Lösen der Schrödinger-Gleichung innerhalb der Born-Oppenheimer-Näherung vorhergesagt werden. Um den Einfluss der Zeit zu berücksichtigen, kann die zeitabhängige Störungstheorie (TD-PT) verwendet werden.[488] Die Lichtabsorption von Molekülen wird durch die Wechselwirkung des elektrischen und magnetischen Feldes des Lichts mit den Elektronen und Kernen des Moleküls beschrieben. Aus quantenmechanischer Sicht ergibt sich die Störung $\hat{H}'$ eines Moleküls, das homogenen elektrischen $\vec{E}$ und magnetischen Feldern $\vec{B}$ ausgesetzt ist unter Berücksichtigung der elektrischen und magnetischen Übergangsdipolmomentoperatoren $\hat{\vec{\mu}}$ und $\hat{\vec{m}}$ wie folgt:[489]

$$\hat{H}' = -\hat{\vec{\mu}} \cdot \vec{E} - \hat{\vec{m}} \cdot \vec{B}.$$

Die Operatoren setzen sich jeweils aus den einzelnen Beiträgen der Elektronen und Kerne zusammen und werden durch die folgenden Gleichungen beschrieben:[490]

$$\hat{\vec{\mu}} = \hat{\vec{\mu}}_{\mathrm{e}} + \hat{\vec{\mu}}_{\mathrm{K}},$$
$$\hat{\vec{\mu}}_{\mathrm{e}} = -\sum_{i}^{N_{\mathrm{el}}} e\,\vec{r}_i,$$
$$\hat{\vec{\mu}}_{\mathrm{K}} = \sum_{j}^{N_{\mathrm{K}}} Z_j e\,\vec{R}_j.$$

[8] Aimé Cotton berichtete über die charakteristische Änderung der optischen Drehung bzw. des CD-Signals in der Wellenlängenregion, in der Licht absorbiert wird (Cotton-Effekt). Ein positiver Cotton-Effekt ist gegeben, wenn die optische Drehung bei kleiner werdenden Wellenlänge zunächst steigt, am Absorptionsmaximum die Abszisse schneidet und anschließend sinkt.

Die Summe der einzelnen Beiträge $\hat{\vec{\mu}}_\mathrm{e}$ und $\hat{\vec{\mu}}_\mathrm{K}$ des elektrischen Dipolmoments $\hat{\vec{\mu}}$ ergeben sich jeweils als Produkt aus der Ladung der Elektronen e und der Kerne $Z_j e$ sowie deren Ortsvektoren $\vec{r}_i$ und $\vec{R}_j$.

Gleichermaßen ergibt sich das magnetische Übergangsdipolmoment $\hat{\vec{m}}$ als Summe der Einzelbeiträge von Elektronen und Kernen $\hat{\vec{m}}_\mathrm{e}$ und $\hat{\vec{m}}_\mathrm{K}$. Das Kreuzprodukt aus den Ortsvektoren und den Impulsoperatoren $\hat{\vec{p}}_i$, $\hat{\vec{P}}_\lambda$ der Teilchen sowie der entsprechenden Massen m_el und M_λ und der Lichtgeschwindigkeit im Vakuum c ergeben das jeweilige magnetische Dipolmoment $\hat{\vec{m}}$:

$$\begin{aligned}
\hat{\vec{m}} &= \hat{\vec{m}}_\mathrm{e} + \hat{\vec{m}}_\mathrm{K}, \\
\hat{\vec{m}}_\mathrm{e} &= -\sum_i^{N_\mathrm{el}} \frac{e}{2\, m_\mathrm{el}\, c} \vec{r}_i \times \hat{\vec{p}}_i, \\
\hat{\vec{m}}_\mathrm{K} &= \sum_j^{N_\mathrm{K}} \frac{Z_j e}{2\, M_j\, c} \vec{R}_j \times \hat{\vec{P}}_j.
\end{aligned}$$

Da der Beitrag des elektrischen Übergangsdipolmoments $\hat{\vec{\mu}}$ zur Störung deutlich größer ist als der des magnetischen Übergangsdipolmoments $\hat{\vec{m}}$, kann letzterer bei der Simulation von Schwingungsanregungen in der Regel vernachlässigt werden. Innerhalb dieser sogenannten elektrischen Dipolnäherung kann der molare Extinktionskoeffizient $\varepsilon(\tilde{\nu})$ für unpolarisiertes Licht bei gegebener Wellenzahl $\tilde{\nu}$ und unter Einbeziehung der Avogadro-Konstante N_A, des Planckschen Wirkungsquantums h sowie der Lichtgeschwindigkeit im Vakuum c berechnet werden:

$$\varepsilon(\tilde{\nu}) = \frac{8\,\pi^3 N_\mathrm{A}\,\tilde{\nu}}{3000\; h\; c\,\ln(10)} \sum_k D_k f_k(\tilde{\nu}, \tilde{\nu}_k).$$

Die Dipolstärke D_k der Anregung in den Zustand k ergibt sich aus dem Betragsquadrat des elektrischen Übergangsdipolmoments:

$$D_k = \left| \hat{\vec{\mu}}_k \right|^2.$$

Mit der Halbwertsbreite γ_k lassen sich Infrarot (IR)- und VCD-Banden als Lorentzkurven darstellen, die entsprechend folgender Gleichung aus den simulierten Linienübergängen berechnet werden können:

$$f_k(\tilde{\nu}_k, \tilde{\nu}) = \frac{1}{\pi} \frac{\gamma_k}{\left(\tilde{\nu} - \tilde{\nu}_k\right)^2 + \gamma_k^2}.$$

Für die Berechnung der CD-Intensität muss zusätzlich zum elektrischen Übergangsdipolmoment der Beitrag des magnetischen Übergangsdipolmoments zum Störoperator berücksichtigt werden. Somit ergibt sich $\Delta\varepsilon(\tilde{\nu})$ durch folgende Gleichung:

$$\Delta\varepsilon(\tilde{\nu}) = \frac{32\ \pi^3 N_\mathrm{A}\ \tilde{\nu}}{3000\ h\ c\ \ln(10)} \sum_k R_k f_k(\tilde{\nu}, \tilde{\nu}_k).$$

Die Wechselwirkung zwischen den beiden Übergangsdipolmomenten im Winkel ϕ ergibt die Rotationsstärke R_k des Übergangs zwischen dem Grundzustand und einem angeregten Zustand k und lässt sich entsprechend der Rosenfeld-Gleichung quantenmechanisch als Imaginärteil des Skalarproduktes von $\hat{\vec{\mu}}$ und $\hat{\vec{m}}$ berechnen:[491]

$$R_k = \mathrm{Im}\left[\hat{\vec{\mu}}_k \cdot \hat{\vec{m}}_k\right] = |\vec{\mu}| \cdot |\vec{m}| \cos\phi.$$

Die Vorhersage der Rotationsstärken ist auf DFT-Level durch die Verwendung von GIAO-Basissätzen in Kombination mit analytischen Ableitungsmethoden implementiert. Hierbei werden die harmonischen Kraftfelder, die atomaren Polartensoren und die atomaren Axialtensoren kosteneffizient berechnet.[492–497] Um hochgenaue Vorhersagen zu erhalten und willkürliche Wellenzahlverschiebungen zu vermeiden, können anharmonische Korrekturen auf der Ebene der Schwingungsstörungstheorie zweiter Ordnung (VPT2) angewendet werden.[498–500] Des Weiteren können MD-Simulationen zur expliziten Beschreibung von Lösungsmitteleffekten durchgeführt werden.[501] Auch durch die Verwendung von Algorithmen, die auf maschinellem Lernen basieren, kann die Vorhersage der absoluten Konfiguration verbessert werden.[502]

Um elektronische Anregungen in organischen Molekülen zu induzieren, kann Licht aus dem UV/Vis-Spektrum (180–800 nm) verwendet werden. Für die *in silico* Berechnung sol-

cher angeregter Zustände sowie den entsprechenden Rotationsstärken stehen sehr schnelle, semiempirische bis hochgenaue CC-basierte Methoden zur Verfügung.[388,443,503–507] Am verbreitetsten ist die Betrachtung mittels TD-DFT.[508,509] Neben der Berechnung von Absorptionsspektren, können damit auch ECD-Spektren simuliert werden.[505,510] Für die Berechnung des Vorzeichens und der Stärke einzelner elektronischer Übergänge ist eine akkurate Beschreibung der jeweiligen Grundzustände und der dazugehörigen angeregten Zustände nötig. Im Gegensatz zur Berechnung von VCD-Intensitäten wird dafür ein höheres Level der quantenmechanischen Methode benötigt.[443]

Sind für ein flexibles Molekül mehrere konformelle Zustände mit unterschiedlicher Energie besetzt, ergibt sich das gemittelte Spektrum entsprechend der Boltzmann-Statistik. Das Verhältnis der Besetzungszahl einer konformellen Struktur $N(c)$ zur Gesamtanzahl N ergibt den Boltzmann-Faktor jedes Konformers, der mit dem jeweiligen Spektrum multipliziert wird:

$$\frac{N(c)}{N} = \frac{e^{-\Delta G(c)/k_\mathrm{B}T}}{\sum_a e^{-\Delta G(a)/k_\mathrm{B}T}}.$$

$\Delta G(c)$ entspricht der freien Gibbs-Energie, k_B der Boltzmann-Konstante und T der Temperatur.

Der visuelle Vergleich von gemessenen und berechneten VCD-Spektren ist oft ausreichend für eine qualitative Zuordnung der absoluten Konfiguration eines chiralen Moleküls. Ein quantitativer Vergleich kann auf der Basis von Algorithmen und Computerprogrammen erfolgen und erlaubt so auch die Unterscheidung von Diastereomeren.[511,512] Im Jahr 2010 veröffentlichten Shen *et al.* mit SimVCD eine der ersten Methoden für quantitative Vergleiche, gefolgt von CDSpecTech von Covington und Polavarapu sowie SpecDis von Bruhn und Mitarbeitern.[512–515] Letztere wurde zunächst für den Vergleich von experimentellen und berechneten UV- und ECD-Spektren entwickelt, dann aber auch auf IR und VCD ausgeweitet. Die Ähnlichkeitsfaktoren f und f^* (enantiomeres f) wurden eingeführt, um den Grad der Übereinstimmung von zwei Spektren innerhalb eines bestimmten Wellenlängenbereichs zu quantifizieren. Ihre Werte reichen von 0 bis 1, wobei 1 für eine ideale Übereinstimmung steht. Der absolute Wert der Differenz ($|f\text{-}f^*|$) der Ähnlichkeitsfaktoren beider Enantiomere wird als Δ-Wert oder enantiomerer Ähnlichkeitsindex (*enantiomeric similarity index*, ESI) bezeichnet, der von Bultinck *et al.* eingeführt wurde und als nützliches Maß zur Unterscheidung zwischen zwei Enantiomeren dient.[514,516–518]

In einem VCD-Spektrometer wird aus unpolarisiertem Licht einer Infrarotquelle erst linearisierte und anschließend zirkular polarisierte elektromagnetische Strahlung erzeugt. Der photoelastische Modulator (PEM) moduliert zwischen links und rechts zirkular polarisiertem Licht mit einer bestimmten Frequenz vor der Probenkammer. Das austretende Licht wird über einen *mercury cadmium telluride* ($Hg_{1-x}Cd_xTe$, MCT)-Detektor aufgenommen, das Eingangssignal mittels eines Lock-in-Verstärkers mit der Schaltung des PEM korreliert und die Daten an einen PC zur Darstellung gesendet (Abbildung 5.2).

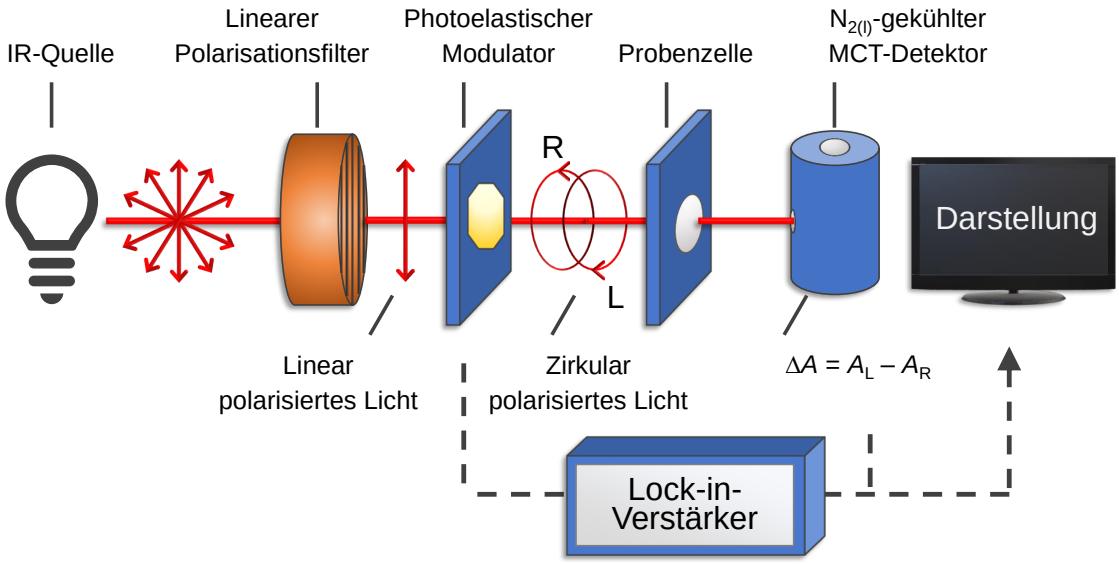

Abbildung 5.2: Schematischer Aufbau eines VCD-Spektrometers in Anlehnung an Nafie *et al.*[519]

6 Zielsetzung

6.1 *In silico* Betrachtung von Reaktionsmechanismen

Im Rahmen dieser Arbeit sollen quantenmechanische Berechnungen eingesetzt werden, um in verschiedenen Projekten innerhalb der Arbeitsgruppe sowie mit externen Kooperationspartnern experimentelle Befunde zu erklären. Dafür sollen vorwiegend *ab inito* Methoden verwendet werden, um Reaktivitäten, Übergangszustände oder Reaktionspfade vorherzusagen.

6.1.1 Simulation des Reaktionspfads einer photokatalysierten [3+2]-Cycloaddition von Vinylcyclopropanen mit Acetylenen

Die Arbeitsgruppe Opatz berichtete im Jahr 2021 von einer UV-katalysierten Norrish-Yang-Zyklisierung, durch die sich Cyclopropane **108** aus α-Mesyloxyketonen **107** darstellen lassen.[520] Diese substituierten Dreiringe **108** lassen sich in einer metallfreien, photochemischen Ringöffnung mit terminalen Alkinen **109** zu Cyclopentenen **110** oder mit Cyanopyridin **111** zu γ-Heteroarylketonen **112** umsetzen (Schema 6.1).

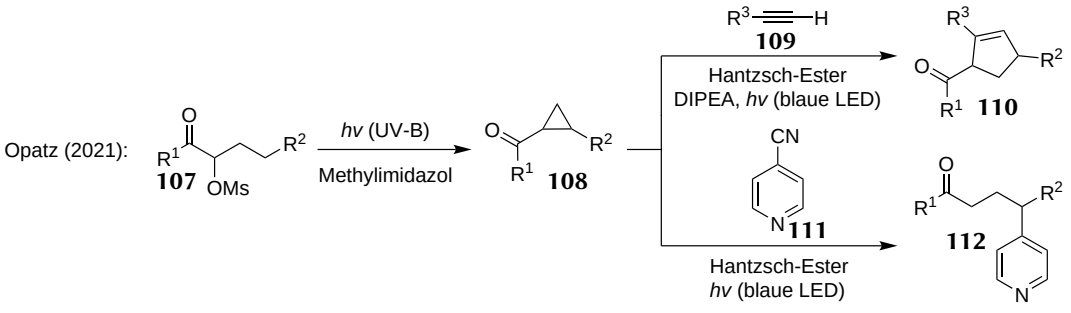

Schema 6.1: Photochemische Umsetzung von Cyclopropanen **108** zu Cyclopentenen **110** und γ-Heteroarylketonen **112**, ausgehend von α-Mesyloxyketonen **107**.[520]

Auf Grundlage dieser Reaktion soll der synthetische Zugang zu hoch substituierten Cyclopentenen **116** innerhalb eines polyzyklischen Gerüsts untersucht werden. Durch die Bestrahlung von Allylbenzylmethansulfonamid **113** mit UV-C-Strahlung soll ein *meta*-Photocycloaddukt **114** mit einer Vinylcyclopropan-Struktur erhalten werden. Anschließend soll dieses mit Sulfon-substituierten Alkinen **115** durch Bestrahlung mit sichtbarem Licht und unter Zusatz eines Iridium-Photokatalysators in einer formalen [3+2]-Cycloadditionsreaktion umgesetzt werden. Diese Methode soll die intrinsische Ringspannung von **114** als thermodynamische Triebkraft für die Ringerweiterung zur Bildung neuartiger Tetrazyklen **116** nutzen (Schema 6.2).

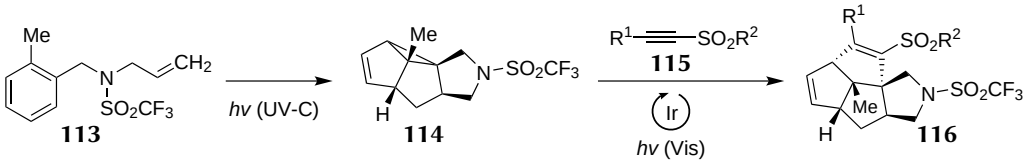

Schema 6.2: Geplante Darstellung von Vinylcyclopropan **114** mit anschließender Umsetzung in einer formalen [3+2]-Cycloadditionsreaktion zu Tetrazyklen **116**.

Um ein besseres Verständnis des Reaktionsmechanismus zu erlangen, sollen neben spektroskopischen Untersuchungen und Radikalfänger-Experimenten auch DFT-Berechnungen eingesetzt werden, um die auftretenden angeregten Zustände zu simulieren. So soll aufgeklärt werden, ob ein Elektronen- oder Energietransfer (EnT) von dem Photokatalysator auf eines der Edukte stattfindet.

6.1.2 Selektivitätsuntersuchung einer Diels-Alder-Reaktion eines β-Fluor-β-nitrostyrols mit Cyclopentadien

Fluorierte organische Verbindungen nehmen in verschiedenen Bereichen von Wissenschaft und Technik eine wichtige Rolle ein. Fluor als Substituent kann die pharmakokinetischen und physikochemischen Eigenschaften organischer Moleküle erheblich beeinflussen und deren metabolische sowie chemische Stabilität verbessern.[521–525]

Ziel ist es, in Kooperation mit der Arbeitsgruppe um [redacted] von der [redacted], ein synthetisches Protokoll zu entwickeln, das auf monofluorierten Edukten basiert und eine Alternative zu *late-stage* Fluorierungen bietet. Als Grundlage für den Aufbau fluorierter Bizyklen soll hierbei die Diels-Alder-Reaktion

dienen, welche sich durch ihre breite Anwendbarkeit auszeichnet.[526] Für die Darstellung fluorierter Norbornen-Strukturen soll Cyclopentadien (**118**) mit *Z*-konfigurierten 2-Fluor-2-nitrostyrolen **117** umgesetzt werden (Schema 6.3). Letztere sind durch radikalische Nitrierung von 2-Brom-2-fluornitrostyrolen zugänglich, die aus den jeweiligen Carbonylverbindungen und CBr_3F aufgebaut werden können.[527–529]

Schema 6.3: Anvisierte Syntheseroute für die Darstellung monofluorierter Norbornene **119**.

Bei der Diels-Alder-Reaktion mit zyklischen 1,3-Dienen können sowohl das *endo*- als auch das *exo*-Isomer des Produkts **119** gebildet werden. Die kinetischen Daten dieser Cycloaddition sollen experimentell bestimmt werden, um die Aktivierungsbarriere zu berechnen. Darüber hinaus soll die energetische Lage der Edukte, Produkte sowie der entsprechenden Übergangszustände auf DFT-Level berechnet werden, um die daraus erhaltene Reaktionsrate mit dem experimentellen Wert zu vergleichen.

6.1.3 Reaktivität verschiedener *N*-Carbonsäureanhydride in einer ringöffnenden Synthese von Polypeptiden

In Kooperation mit den Arbeitsgruppen um [redacted] und [redacted] soll die ringöffnende Polymerisation von *N*-Carbonsäureanhydriden (NCAs) **120** untersucht werden (Schema 6.4). Verschiedene Parameter wie die Polarität des Lösungsmittels, der sterische Anspruch des Initiators **121** sowie eine Substitution am Stickstoffatom oder in der α-Position der NCAs **120** besitzen einen Einfluss auf die Polymerisationskinetik.[530] In Abhängigkeit der zugrunde liegenden Aminosäuren beziehungsweise des Substitutionsgrades können sich die so erhaltenen (Bio-)Polymere in ihren Eigenschaften wie Lipophilie, Membranpermeabilität oder metabolische Stabilität unterscheiden und Anwendung in biomedizinischen Feldern finden.[531–534]

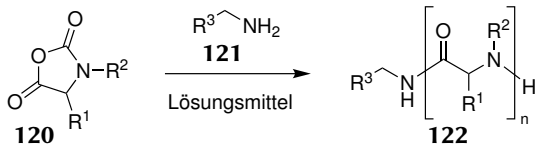

Schema 6.4: Geplante ringöffnende Polymerisation verschiedener *N*-Carbonsäureanhydride **120**.

Durch quantenmechanische Berechnungen soll die energetische Lage der an der Polymerisation beteiligten Molekülorbitale bestimmt werden. Auf Grundlage der Klopman-Salem-Gleichung sollen Unterschiede in der chemischen Reaktivität von NCAs **120** mit verschiedenen *N*-Substituenten erklärt werden.[535,536]

6.1.4 Bestimmung des Substituenteneinflusses bei der photochemischen Dehydrierung von N-Heterozyklen

In der Arbeitsgruppe Opatz soll eine Methode entwickelt werden, die unter Verwendung von sichtbarem Licht die photochemische Dehydrierung von N-Heterozyklen **123** zu zyklischen Enaminonen **124** ermöglicht. Ziel ist es, milde Reaktionsbedingungen und ökologisch unbedenkliche Reagenzien zu finden, die ohne stöchiometrische Oxidantien oder den Einsatz von Metallkatalysatoren auskommen (Schema 6.5).

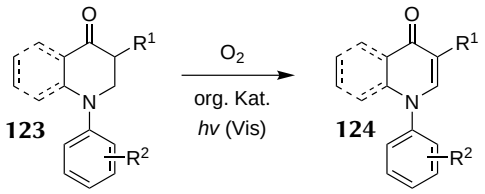

Schema 6.5: Verwendung von Sauerstoff als terminales Oxidationsmittel für die angestrebte photochemische Dehydrierung verschiedener N-Heterozyklen **123**.

Durch quantenmechanische Berechnungen auf DFT-Level soll untersucht werden, welchen Einfluss *N*-Aryl-Gruppen mit *ortho*-Substituent auf den Umsatz unter den optimierten Reaktionsbedingungen aufweisen.

6.2 Computergestützte Strukturaufklärung kleiner organischer Moleküle

Um die Strukturaufklärung synthetischer Moleküle zu ermöglichen, sollen verschiedene spektroskopische Techniken in Kombination mit quantenmechanischen Berechnungen angewendet werden.[407]

6.2.1 Benchmarkstudie über die Genauigkeit von DFT-Methoden in der VCD-Spektroskopie

Ziel dieses Projekts ist es, einen systematischen Vergleich der Genauigkeit einer großen Anzahl von DFT-Methoden für die Berechnung von VCD-Spektren verschiedener kleiner organischer Moleküle anhand ausgewählter Moleküle **125**–**130** durchzuführen (Abbildung 6.1). Dafür sollen die experimentellen Spektren aufgenommen und mit allen Kombinationen aus Funktionalen, Basissätzen und Solvatationsmodellen simuliert werden. Durch eine Quantifizierung des spektralen Überlapps sollen die Ergebnisse gegenübergestellt und die Kombinationen herausgearbeitet werden, die hohe Übereinstimmungen ergeben. Einerseits soll analysiert werden, welche Kombinationen für die einzelnen Moleküle **125**–**130** besonders geeignet sind, andererseits bestimmt werden, welche Kombinationen für unterschiedliche Moleküle universell einsetzbar sind und eine hohe Ähnlichkeit aufweisen.

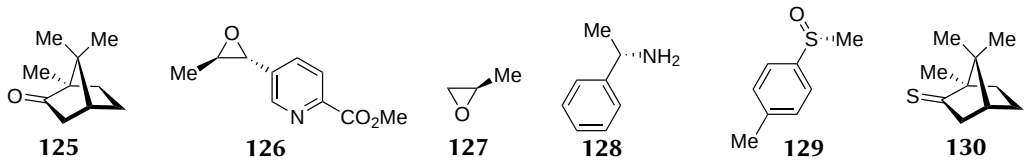

125 **126** **127** **128** **129** **130**

Abbildung 6.1: Ausgewählte Moleküle **125**–**130** für den geplanten systematischen Vergleich experimenteller und simulierter VCD-Spektren.

Für die Berechnung der Rotationsstärken der Verbindungen **125**–**130** auf DFT-Level sollen verschieden Klassen von Funktionalen und Basissätzen verwendet werden, um den Einfluss der Genauigkeit und Recheneffizienz auf die VCD-Signale zu bewerten. Die Übereinstimmung der simulierten Spektren mit den experimentellen Spektren soll mittels der Software SpecDis quantifiziert werden.[514,515]

6.2.2 Differenzierung von Diastereomeren in der Synthese eines HIV-Integrase-Inhibitors

Um die globale Verfügbarkeit lebenswichtiger Arzneimittel zu verbessern und die Herstellungskosten zu senken, werden immer neue Syntheserouten und kontinuierlich optimierte Prozesse benötigt. Bei Dolutegravir handelt es sich um ein virostatisch wirksames Molekül, das zu der Gruppe der Integrase-Strangtransfer-Inhibitoren gehört und einer der vielversprechendsten Stoffe zur Behandlung einer HIV-Infektion der letzten Jahre ist. Der Wirkstoff wurde von der Weltgesundheitsorganisation für die Erstbehandlung von HIV empfohlen und wird pharmazeutisch in Form seines Natriumsalzes **137** oral verabreicht.[537]

In der Arbeitsgruppe Opatz soll unter Verwendung kosteneffizienter Reagenzien und Beachtung industrieller Aspekte eine Synthese für Dolutegravir-Natrium (**137**) entwickelt werden. Ausgehend von dem chiralen Baustein (3*R*)-Aminobutanol (**131**) sollen zunächst die Ringe B und C konstruiert werden. Nach Umsetzung mit Enolether **135** und anschließender Amidknüpfung sowie Salzbildung soll der Wirkstoff erhalten werden (Schema 6.6).

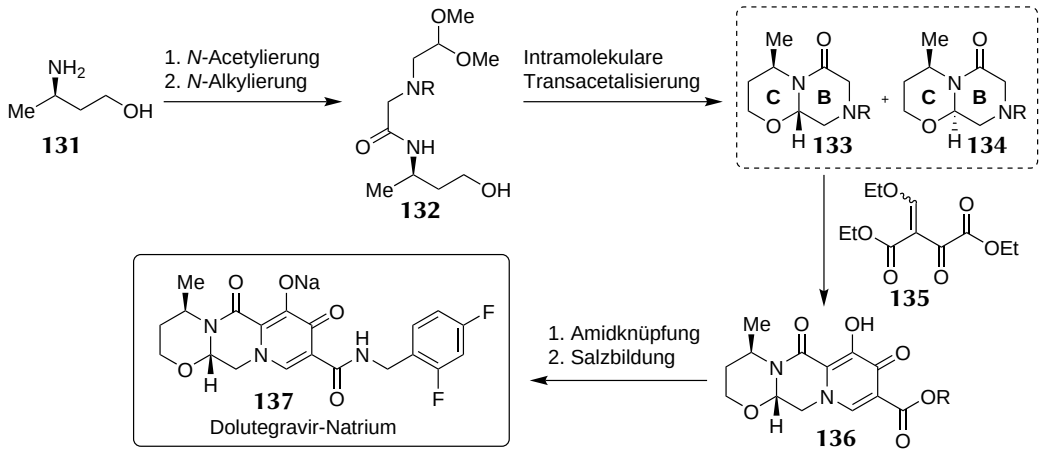

Schema 6.6: Geplante Syntheseroute für die Darstellung von Dolutegravir-Natrium (**137**).

Die Ringe B und C sollen mittels intramolekularer Transacetalisierungsreaktion aufgebaut werden, bei der zwei Diastereomere **133** und **134** entstehen können. Diese zwei möglichen Produkte **133** und **134** sollen durch Kombination von VCD-Spektroskopie mit DFT-Berechnungen unterschieden werden, um die Stereokonfiguration der erhaltenen Verbindungen eindeutig zu bestimmen.

6.2.3 Bestimmung der absoluten Konfiguration eines 13-Hydroxy-14-deoxyoxacyclododecindions

Im Jahr 2008 wurde im Rahmen einer Kooperation der Arbeitsgruppen um [redacted] und Prof. Till Opatz (Universität Hamburg) Oxacyclododecindion (**138**) als erster Naturstoff der Gruppe der Dihydroxyphenylessigsäurelactone aus dem Pilz *Exserohilum rostratum* isoliert (Abbildung 6.2).[538] Seitdem wurden im Arbeitskreis Opatz die Sekundärmetaboliten **139** und **140** aus diesem Pilz strukturell aufgeklärt, totalsynthetisch dargestellt und Derivate mit diesem Grundkörper synthetisiert.[539–542] Die hergestellten Substanzen zeichneten sich in verschiedenen biologischen Tests durch ihre hochwirksame entzündungshemmende und antifibrotische Aktivität aus.[538–545] Im Jahr 2018 wurde mit 13-Hydroxy-14-deoxyoxacyclododecindion **141** ein weiterer Naturstoff dieser Substanzklasse von Shang und Lin *et al.* isoliert, dessen Struktur und absolute Konfiguration durch eine Kombination von NMR- und ECD-Spektroskopie aufgeklärt wurde.[543]

Ziel ist es, die Verbindung **141** totalsynthetisch darzustellen und in Kooperation mit der Arbeitsgruppe [redacted] ausführlich auf die biologischen und pharmakologischen Eigenschaften zu testen.

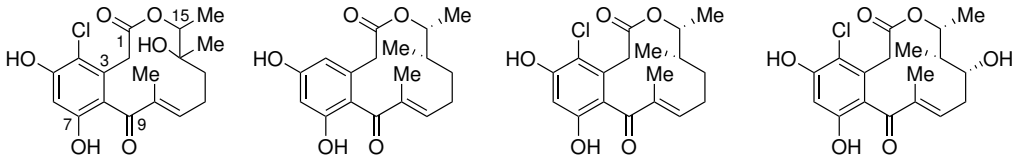

Abbildung 6.2: Bekannte Naturstoffe **138**–**141** aus der Gruppe der Dihydroxyphenylessigsäurelactone.[538,539,543]

Nach der erfolgreichen Synthese soll analog zu dem Vorgehen von Shang und Lin *et al.* die absolute Konfiguration des Naturstoffs **141** unter Verwendung von NMR- und ECD-Spektroskopie bestätigt werden.

6.3 Strukturaufklärung isolierter Naturstoffe mittels computergestützter Spektroskopie

Im Rahmen dieser Arbeit sollen computergestützte Methoden zur Aufklärung neu isolierter Naturstoffe aus Pflanzen und Pilzen genutzt werden. Der Fokus liegt hierbei auf der Anwendung verschiedener spektroskopischer Techniken in Kombination mit DFT-Berechnungen, um neu entdeckte Sekundärmetaboliten vollständig zu charakterisieren. Dies soll den stetigen Bedarf an neuen Wirkstoffen aufgrund der Identifikation neuer Targets oder auftretenden Resistenzbildungen adressieren.[546–550]

In Kooperation mit der Arbeitsgruppe um [redacted] sollen die Inhaltsstoffe eines Pilzes der Gattung *Alternaria* identifiziert und analysiert werden. Pilze dieser Gattung können verschiedene Nutzpflanzen, wie Trauben, Äpfel oder Getreide befallen und sowohl diverse Pflanzenkrankheiten hervorrufen als auch Mykotoxine bilden, die die Gesundheit von Menschen und Tieren gefährden.[551] Im Anschluss an die Strukturaufklärung mittels Massenspektrometrie und 2D-NMR-Spektroskopie soll die absolute Konfiguration der isolierten Substanzen unter Verwendung von ECD-Spektroskopie in Verbindung mit DFT-Berechnungen bestimmt werden. In einem weiteren Projekt sollen die aus einem Pilz der Gattung *Diaporthe* isolierten Naturstoffe untersucht und deren Struktur mittels NMR-Spektroskopie aufgeklärt werden. Auf unterschiedlichen Wirtspflanzen wurden Pilze dieser Gattung bereits als Pflanzenpathogene, nicht-pathogene Endophyten oder Saprophyten nachgewiesen.[552]

Ein weiteres Projekt zur Strukturaufklärung isolierter Naturstoffe befasst sich mit *Vernonia tufnelliae*, einer Pflanzenart der Gattung Scheinastern, die im westlichen Teil von Kamerun beheimatet ist und in dieser Region als traditionelle Heilpflanze zur Fieberbekämpfung verwendet wird.[553] Die Inhaltsstoffe dieser Pflanze sollen in Kooperation mit [redacted] und der Arbeitsgruppe um [redacted] extrahiert und isoliert, charakterisiert sowie auf ihre biologische Aktivität untersucht werden.

7 Resultate und Diskussion

7.1 *In silico* Betrachtung von Reaktionsmechanismen

7.1.1 Simulation des Reaktionspfads einer photokatalysierten [3+2]-Cycloaddition von Vinylcyclopropanen mit Acetylenen

Um die optimalen Reaktionsbedingungen für eine formale photochemische [3+2]-Cycloaddition von Vinylcylopropanen **114** mit Alkinen **115** zu bestimmen, wurden in der Arbeitsgruppe Opatz systematisch alle Reaktionsparameter variiert und verschiedene übergangsmetallbasierte sowie ein organischer Photokatalysator getestet. Die optimierte Methode wurde auf 13 Substrate angewendet, wobei Ausbeuten bis zu 85% erzielt wurden. Um ein besseres Verständnis des Reaktionsmechanismus zu erlangen, wurden die Grundzustände S_0 sowie die angeregten Zustände T_1 für die Reaktion von Vinylcyclopropan **114** (in der Publikation **4**) und Alkin **115** (in der Publikation **6a**) sowie des Produkts **116** auf DFT-Level berechnet, um daraus die adiabatische Energiedifferenz zu berechnen. Zur Visualisierung der elektronisch angeregten Zustände wurden die Spindichten graphisch dargestellt. Die Ergebnisse der quantenmechanischen Berechnungen sowie der spektroskopischen Untersuchungen belegen einen Triplett-Energietransfer des angeregten Ir(III)-Photokatalysators **142** (in der Publikation **PC I**) auf Vinylcyclopropan **114** (in der Publikation **4**). Infolgedessen kommt es zunächst zu einer Ringöffnung, die eine anschließende Addition an das Alkin **115** (in der Publikation **6a**) ermöglicht (Abbildung 7.1).[554]

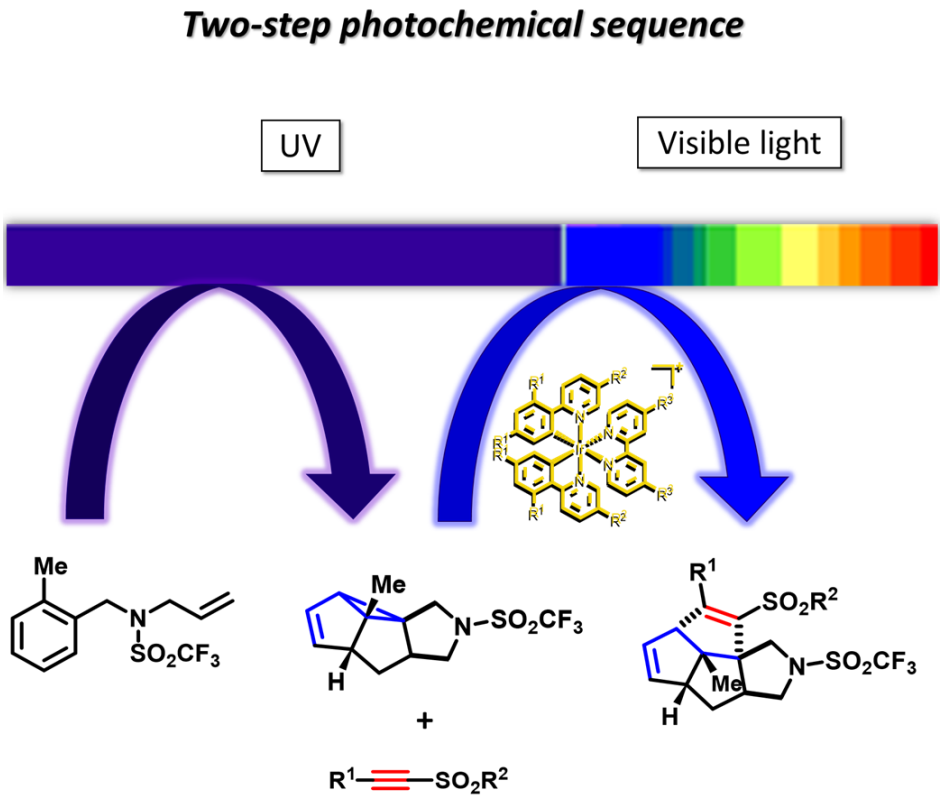

Abbildung 7.1: *Graphical abstract* der Publikation „Vinylcyclopropane [3+2]-Cycloaddition with Acetylenic Sulfones Based on Visible Light Photocatalysis“.[554]

Der Großteil der photochemischen Synthesen, die Isolierung und die Bestimmung der analytischen Daten wurde von [redacted] durchgeführt. Die Umsetzung zweier Vinylcyclopropane **143** und **144** (in der Publikation **8** und **11**) zu den entsprechenden Produkten **145** und **146** (in der Publikation **9** und **12**) sowie die selektive Desulfonierung von Tetrazyklus **147** (in der Publikation **7a**), die Isolierung und Charakterisierungen wurden von J. Groß durchgeführt. Darüber hinaus wurden alle DFT-Berechnungen von J. Groß durchgeführt. Die Laser-Blitzphotolyse-Studien wurden von [redacted] durchgeführt und das Manuskript von allen Autoren erstellt.[9]

[9] *Reprinted under the terms of the Creative Commons Attribution License CC BY-NC-ND 4.0. Copyright ©2022 A. Luque, J. Groß, T. Zähringer, C. Kerzig, T. Opatz, Chemistry 2022, 28, e202104329, Chemistry - A European Journal published by Wiley-VCH GmbH.*

Chemistry–A European Journal | Research Article
doi.org/10.1002/chem.202104329
Chemistry Europe
European Chemical Societies Publishing
www.chemeurj.org

Vinylcyclopropane [3+2] Cycloaddition with Acetylenic Sulfones Based on Visible Light Photocatalysis**

Adriana Luque,[a] Jonathan Groß,[a] Till J. B. Zähringer,[a] Christoph Kerzig,[a] and Till Opatz*[a]

Abstract: The first intermolecular visible light [3+2] cycloaddition reaction performed on a *meta* photocycloadduct employing acetylenic sulfones is described. The developed methodology exploits the advantages of combining UV and visible-light in a two-step sequence that provides a photogenerated cyclopropane which, through a strain-release process, generates a new cyclopentane ring while significantly increasing the molecular complexity. Mechanistic studies and DFT calculations indicate an energy transfer pathway for the visible light-driven reaction step. This strategy could be extended to simpler vinylcyclopropanes.

Introduction

Functionalized five-membered carbocyclic rings containing contiguous stereocenters are found in a wide array of natural products with diverse biological activities.[1] Therefore, simple and efficient methods to access highly substituted cyclopentanes and cyclopentenes within a polycyclic framework are particularly desirable in current organic and medicinal chemistry research.[2] One major general strategy to access them involves [3+2] cycloadditions, a powerful method that in a single step allows the formation of two new σ bonds and vicinal quaternary centers.[3] Vinylcyclopropanes (VCPs) represent an important class of reactive cyclopropane that can participate in this cycloaddition as three-carbon synthons, especially if they bear electron-withdrawing groups on the cyclopropane ring.[4] However, the use of non-activated VCP as a competent intermolecular cycloaddition partner is still limited. In particular, the use of Rh catalysts[5] is the most developed strategy for cycloadditions of non-activated VCPs and finding other catalyst systems and protocols that can exploit a wider range of VCP reactivity patterns remains a challenge. The merging of visible-light photocatalysis with the [3+2] cycloaddition involving VCPs already proved useful in strain-releasing fragmentation reactions in the assembly of larger-ring systems, but mainly used activated cyclopropanes as the substrates. Most reported examples are based on electron transfer (ET) photoredox processes,[6] while transformations proceeding through energy transfer (EnT) are underdeveloped.[7] The broad substrate scope, often relatively independent of the electronic nature, makes the energy transfer process attractive for a wide set of applications.

Considering the lack of examples of intermolecular transition metal-catalyzed visible light [3+2] cycloadditions involving nonactivated VCPs through EnT, we studied the scope of the same UV-driven strain-promoted/visible light strain-releasing sequence employed in our previous work on cyclopropyl ketones[8] by using *meta* photocycloadduct bearing a vinylcyclopropane substructure as substrates in a visible light-mediated intermolecular [3+2] cycloaddition (Scheme 1). This strategy which has gradually gained attention from the synthetic community,[9] uses the inherent ring-strain of the photogenerated intermediate as a thermodynamic driving force for the subsequent ring expansion. In other words, the first UV light induced transformation provides a complex fused ring skeleton that is otherwise difficult to obtain.[10] This *meta* photocycloadduct is prone to undergo an irreversible ring-opening due to the intrinsic strain of the three-membered ring.[11] This feature will be exploited in the second, visible light-induced transformation by reacting with an alkyne in a [3+2] cycloaddition reaction resulting in the formation of a new complex tetracycle.[12]

In general, non-activated alkynes display low reactivity in this type of cycloadditions, initial experiments using the *meta* photocycloadduct **4** and simple alkynes with different catalytic systems showed no reactions. After much optimization, we found the use of acetylenic sulfones to be an attractive

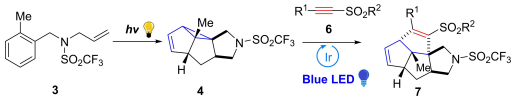

Scheme 1. UV and visible light activation sequence.

[a] *A. Luque, J. Groß, T. J. B. Zähringer, Prof. Dr. C. Kerzig, Prof. Dr. T. Opatz*
Johannes Gutenberg University
Department of Chemistry
Duesbergweg 10–14, 55128 Mainz (Germany)
E-mail: opatz@uni-mainz.de

[**] *A previous version of this manuscript has been deposited on a preprint server (https://doi.org/10.26434/chemrxiv-2021-k7k1w).*

Supporting information for this article is available on the WWW under https://doi.org/10.1002/chem.202104329

Chemistry–A European Journal | Research Article
doi.org/10.1002/chem.202104329
Chemistry Europe
European Chemical Societies Publishing

alternative. The sulfonyl group lowers the LUMO energy of the adjacent π-bond increasing their reactivity as dienophiles while providing the means for controlling the regiochemistry of the cycloaddition.[13] Furthermore, the sulfonyl group can be removed by different methods making the acetylenic sulfones useful reagents for a variety of cycloadditions.[14]

Results and Discussion

Our test of the new design started with the photo-induced intramolecular arene-olefin *meta*-cycloaddition of the *N*-allyl-1,1,1-trifluoro-*N*-(2-methylbenzyl)methanesulfonamide (**3**) which was synthesized in two steps: a reductive amination of 2-methyl-benzaldehyde (**1**) with allylamine, followed by the reaction with trifluoromethanesulfonic anhydride. The irradiation of **3** in anhydrous cyclohexane furnished two isomeric *meta*-photocycloadducts in 72% yield (ratio: 9:1), with the linear isomer **4** being favored over the angular isomer **5** (Scheme 2).

The acetylenic sulfones **6** as reaction partners were prepared in a two-step synthesis. The first step is the preparation of the intermediates β-iodovinyl sulfones using either the cerium(IV) ammonium nitrate (CAN) mediated reaction of aryl sulfinates and sodium iodide with alkynes[15] or the iodine-promoted reaction of the same substrates using water as solvent.[16] The second step was the dehydroiodination of the β-iodovinyl sulfones with potassium carbonate under reflux to afford the corresponding acetylenic sulfones in relatively good yields (see the Supporting Information).[15]

Reaction optimization

The screening of various photocatalysts for the [3+2] photocycloaddition with visible light was performed on *meta* photocycloadduct **4** and the acetylenic sulfone **6a** as the coupling partners (Supporting Information, Table S1). The desired product **7a** was obtained in appreciable yields (53% and 63%, respectively) when employing $[Ir(ppy)_2(dtbbpy)]PF_6$ (**PC I**, 2.5 mol%) and phenanthrene (**PC VI**, 100 mol%). In further optimization studies (Supporting Information, Tables S2, S3 and S4), the yield of **7a** could be increased to 85% when employing **PC I** with concomitant reduction of the catalyst loading to 2 mol% when using 2 equivalents of **6a**. Moreover, the cycloaddition proceeded with higher yields in polar solvents and at higher concentrations (0.15 M in CH_3OH).

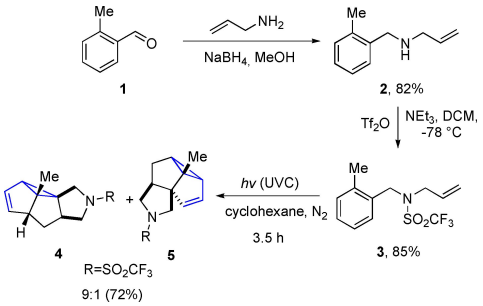

Scheme 2. Preparation of the *meta* photocycloadduct **4**.

Substrate scope

Having optimized the reaction conditions, the scope of the synthesized alkynyl sulfones **6** (Scheme 3) was explored next. Substrates bearing electron-neutral, electron-rich, and electron-withdrawing aromatic rings were found to be suitable substrates. Alkyl groups on the sulfone moiety also provided the desired product in moderate to good yields (**7i** and **7j**). However, aromatic groups at the triple bond were required for

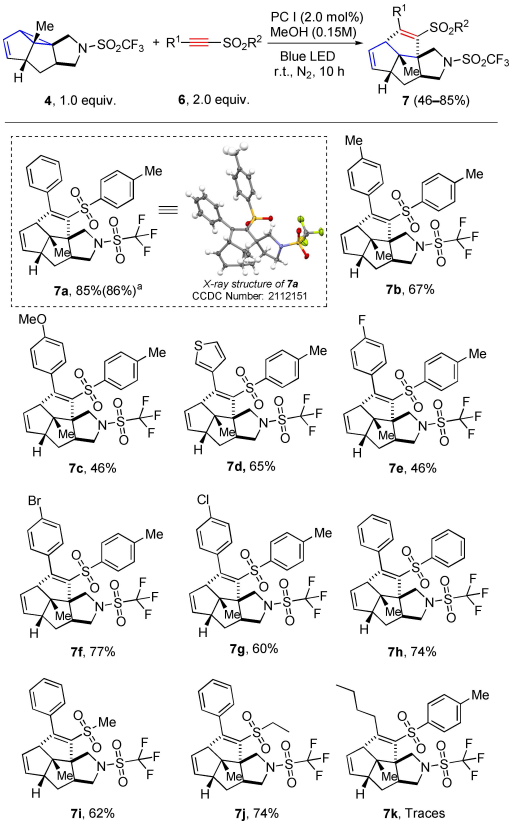

Scheme 3. Substrate scope of the formal [3+2] cycloaddition. All yields are those of isolated products.[a] **PC III** and Blue LED 440 nm was used (see Supporting Information for details).

Chemistry–A European Journal | Research Article doi.org/10.1002/chem.202104329 | Chemistry Europe European Chemical Societies Publishing

the reaction to proceed successfully; substrate **6k** featuring a butyl-substituted alkynyl sulfone gave no reaction.

At this point, the essential factors governing the catalyst reactivity used in this reaction were investigated by analyzing the results of the screening (Table 1). To distinguish the two possible mechanisms, ET or EnT, the redox potentials, and the calculated triplet energy of the *meta* photocycloadduct **4** were compared with those of the catalysts (Supporting Information, Table S7).

Table 1. Evaluation of photocatalysts in the [3+2] cycloaddition.

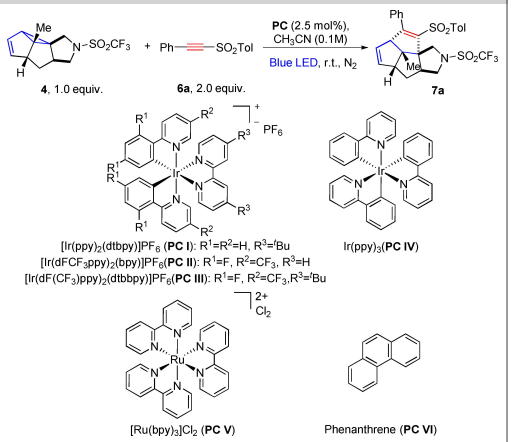

Entry	PC	$E_{1/2}(M^*/M^+)/E_{1/2}(M^*/M^-)$ (V vs. SCE)	E_T (kcal/mol)[a]	Yield (%)[b]
1	VI[c]	−2.10/+1.27	61.9	63
2	III	−0.89/+1.21	60.1	49
3	II	−1.00/+1.32	60.0	51
4	IV	−1.73/+0.31	55.2	49
5	I	−0.96/+0.66	49.2	53
6	V	−0.81/+0.77	46.0	traces

[a] 1 kcal mol^{-1} = 4.184 kJ mol^{-1}. [b] isolated yields. [c] 100 mol% of catalyst loading and UV/vis CFL bulb was used.

In the cyclic voltammograms of **4** (Supporting Information, Figure S7), oxidation and reduction features were observed with half-peak potentials of +1.96 V vs. SCE and −1.65/−1.34 V vs. SCE, respectively. Analyzing the reducing power of the catalyst **PC IV** (entry 4)[17] and **PC VI** (entry 1)[18] after excitation with that of **4** reveals that an oxidative quenching is feasible. However, the reduction potentials of the *meta* photocycloadduct are not sufficient to be reduced by the photoexcited states of the catalyst **PC V** (entry 6)[19] or the other iridium catalysts (entries 2–3, 5).[20] Likewise, reductive quenching could be ruled out based on the oxidation potentials of all the catalysts. On the other hand, there is no clear correlation between the triplet energies of the catalysts or photosensitizers and the reaction yield, making a Dexter energy transfer (sensitization)[21] also difficult. The Gibbs free energy of each reaction intermediate was predicted using density functional theory (DFT) as it has already be done in the literature for related reactions (Scheme 4).[22] While the reaction follows an overall exergonic pathway, releasing 48.9 kcal mol^{-1} of energy, the computed adiabatic triplet energy of **4** (59.1 kcal mol^{-1}) is considerably higher than those of **PC I** and **PC IV** (entries 4 and 5) but is low enough for the rest of iridium catalysts and **PC VI**. Although there is no compelling evidence for an energy transfer process based on these results, the direct excitation of the VCP moiety by UV irradiation of **4** also gives rise to **7a** in 27% yield (see the Supporting Information).[23]

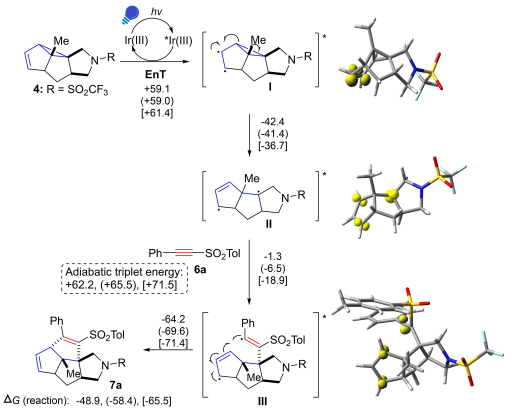

Scheme 4. Mechanistic proposal for the [3+2] photocycloaddition. The reported adiabatic energy differences obtained with different functionals are given in kcal mol^{-1} (no bracket: (U)B3LYP, parentheses: (U)CAM-B3LYP, square bracket: (U)M06-2X). The spin densities (yellow, isovalue = 0.04) were plotted for the triplet intermediates **I**–**III**.

Mechanistic studies

Several control experiments were performed to gain insight into the reaction mechanism. First, radical trapping using (2,2,6,6-tetramethylpiperidin-1-yl)oxyl (TEMPO) completely inhibits the reaction, indicating it may proceed through a radical pathway. To determine whether the reaction involves an efficient[24] radical chain mechanism, we performed a light on-off experiment showing no product formation in the dark phases (Figure 1). Initial intensity-based Stern-Volmer quenching experiments on **PC I** indicated that the phosphorescence of the catalyst could be quenched by **4**, suggesting an electron or energy transfer from the excited triplet state of the catalyst (see the Supporting Information). To get more reliable kinetic results, we turned to lifetime-based Stern–Volmer studies using laser flash photolysis (LFP). We selected **PC III** (the Ir catalyst with the highest triplet energy), which efficiently catalyzed our initial test reaction under optimized conditions (86% yield of **7a**) indicating the very same reaction mechanism as with **PC I**. Furthermore, **PC III** is well-suited for mechanistic investigations by LFP as it is known to possess clearly observable spectroscopic signatures in all states that might occur during photocatalytic cycles.[25] Linear Stern-Volmer plots were obtained clearly demonstrating that quenching by the *meta* photo-

Chemistry–A European Journal | Research Article doi.org/10.1002/chem.202104329 | Chemistry Europe European Chemical Societies Publishing

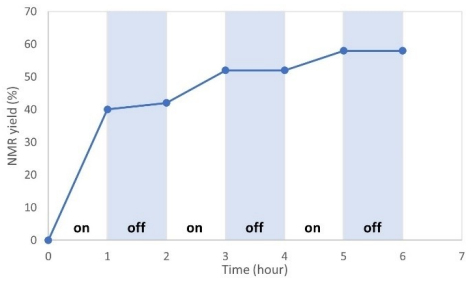

Figure 1. Visible light irradiation on/off experiment.

cycloadduct **4** is much faster than with the acetylenic sulfone **6a** (Figure 2, top). Despite the high triplet energy of **PC III** (Table 1), the quenching rate constant for the reaction between the excited catalyst and **4** ($4\times10^6\ M^{-1}s^{-1}$) is slower than the diffusion limit by almost 4 orders of magnitude. However, under typical conditions used for lab-scale photocatalysis with substrate concentrations on the order of 0.1 M, quenching can be quite efficient.

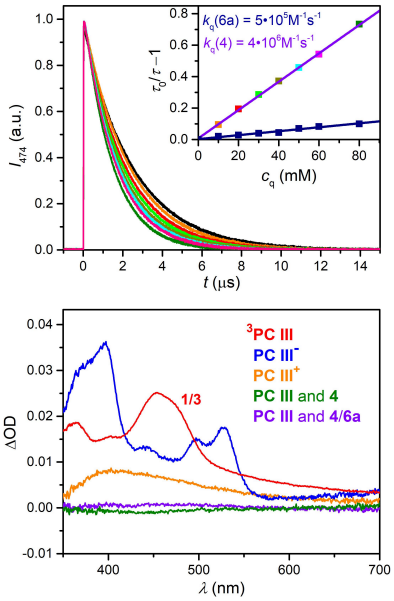

Figure 2. Mechanistic studies upon excitation with 355 nm laser pulses. Top: emission decay kinetics of excited **PC III** (32 µM) in the presence of varying concentrations of **4** in Ar-saturated MeCN. Inset: Stern-Volmer plots of **PC III** and **4** (purple fit, the colored symbols correspond to the same quencher concentration as in the main plot), and **PC III** combined with **6a** (dark blue). Bottom: transient absorption spectra of the triplet-excited state (^{3}**PC III**), the reduced species (**PC III**$^-$), the oxidized species (**PC III**$^+$), as well as in the presence of **4** and **4**/**6a** (80 mM) in Ar-saturated MeCN obtained by LFP. Apart from the triplet spectrum, all spectra have been recorded after the photoluminescence decay of **PC III** (see Supporting Information for details).

Next, we tried to directly identify the quenching product(s) by measuring transient absorption (TA) spectra with our LFP setup[26] upon selective excitation of **PC III**. Reference spectra (Figure 2, bottom; see Supporting Information for details) of the photocatalyst triplet, its one-electron-oxidized as well as its reduced species were recorded in the reaction medium (MeCN) prior to experiments with the substrates of this study. TA spectra with quencher (**4** and/or **6a**) concentrations ensuring about 50% ^{3}**PC III** quenching were measured. These spectra did not show any noticeable TA signals (green and purple spectra in Figure 2), but intense photocatalyst-derived bands in the transient spectra are expected for both oxidative and reductive quenching pathways, based on our reference measurements. Hence, our TA experiments summarized in Figure 2 (bottom) allow us to exclude quenching via ET.[27]

Accordingly, we propose a catalytic cycle as shown in Scheme 4 with an energy transfer as initial photochemical activation step. First, **PC I** (or **PC III**) acts as a sensitizer, transferring energy from its ^{3}MLCT state to the vinylcyclopropane moiety in **4**, generating the triplet state of the latter, which undergoes a rearrangement followed by a radical addition of the acetylenic sulfone to generate the intermediate **III**. A subsequent ring-closure reaction affords the final tetracycle **7**. The occurrence of radical intermediate **III** is supported by the finding that aromatic substituents at R^1 are required for the reaction to proceed. The absence of new signals in the TA spectra right after significant energy transfer quenching can be explained as follows: The catalyst triplet signals completely return to the baseline for EnT mechanisms and the substrate-derived intermediates **II** and **III** (compare, Scheme 4) are expected to absorb very weakly (and predominantly in the UV region), owing to the lack of π-conjugation and adjacent functional groups. The light absorbing properties of the triplet diradical intermediates **II** and **III** were predicted by means of time-dependent DFT. For the excitation of **II** and **III**, an energy of at least 3.67 eV (oscillator strength $f=0.0002$) and 2.71 eV ($f=0.0093$) is required for the first excited state. Local absorption maxima were predicted to be at 239 nm and 282 nm, respectively (see Supporting Information). Moreover, the exact factors governing the lifetimes of diradicals are not fully understood[28] and these species might be too short-lived for their efficient detection. Ring-opening of intermediate **I** in its triplet state is most likely faster by orders of magnitudes than for the well-known (doublet) alkyl cyclopropane radical clock (ring-opening rate constant, $1.3\times10^8\ s^{-1}$),[29] considering the accelerating effects of substituents and/or fused rings at the cyclopropane moiety.[30] We speculate that strain release and the associated substantial energy gain could potentially occur on a similar timescale as molecular collision and the actual Dexter energy transfer from the excited iridium complex. Such a concerted reaction mechanism (without the presence of intermediate **I**) could explain the observed quenching and energy transfer product when **PC I** is used, for which the generation of intermediate **I** via conventional mechanisms would be endergonic by about 10 kcal mol^{-1} (9.9 kcal mol^{-1}).

Chemistry–A European Journal | Research Article doi.org/10.1002/chem.202104329 | Chemistry Europe European Chemical Societies Publishing

This is clearly beyond the current limit for uphill energy transfer reactions,[31] rendering this stepwise pathway highly unlikely. Similar counter-thermodynamic reactions are well-established in the PCET community for concerted proton-coupled electron transfer reactions, but they seem underexplored for energy transfer catalysis. Moreover, concerted ring-opening to yield the low-energy triplet intermediate **II** would block back-EnT reaction channels, which frequently reduce the overall performance of uphill energy transfer reactions.

The mechanistic alternative of an EnT from the PC to the alkynylsulfone appears less likely as the triplet energy of the latter is higher (62.2 kcal mol^{-1}), no gain from a follow-up reaction such as the ring-opening of the VCP can occur and the reaction of the triplet alkynylsulfone to the VCP should occur at the distal carbon of the C=C double bond, which contradicts the observed regiochemistry. To further corroborate that only the vinylcyclopropane substructure of **4** is involved in the mechanism of this reaction, experiments with different substrates were performed. LFP experiments with photocatalyst **PC III** and (1-cyclopropylvinyl)benzene (**8**) as quencher gave a quenching rate constant of 5×10^8 M^{-1} s^{-1} (see Supporting Information), i.e. about two orders of magnitude faster than obtained with substrate **4** (Figure 2). We again excluded electron transfer quenching pathways by transient absorption measurements and the observed higher rate constant is consistent with the expectations for a Dexter-type energy transfer, given that the in silico triplet energy of **8** (49.3 kcal mol^{-1}) is lower than that of **4**. The preparative [3 + 2] cycloaddition with **8** and the *meta* photocycloadduct **11** (used as an inseparable mixture of isomers without further purification) yielded the expected products in 46 and 39% yield, respectively (Scheme 5). The procedure is thus likely applicable to other VCP-type products of intra- or intermolecular photocycloadditions and permits the construction of complex skeletons in only two consecutive photochemical transformations. Two further commercial and naturally ocurring VCPs, ethyl *trans*-chrysanthemate and (1*S*,3*R*)-*cis*-4-carene, could also successfully be reacted, albeit only in moderate yields, see the Supporting Information.

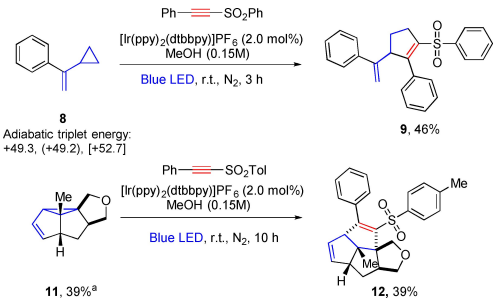

Scheme 5. Alternative substrates in the [3 + 2] photocycloaddition under standard conditions. The predicted energy differences are given in kcal mol^{-1} (no bracket: (U)B3LYP, parentheses: (U)CAM-B3LYP, square bracket: (U)M06-2X). [a] Inseparable mixture.

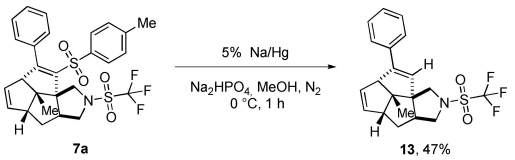

Scheme 6. Selective desulfonylation of tetracycle **7a**.

To extend the synthetic utility of the method, tetracyle **7a** was exemplarily subjected to a selective reductive desulfonylation, producing a styrene moiety suitable for further follow-up reactions (Scheme 6).

Conclusions

A visible light-mediated [3 + 2] cycloaddition of *meta*-photocycloadducts and acetylenic sulfones has been developed. Catalytic amounts of iridium complexes act as triplet sensitizers as indicated by DFT calculations and time-resolved optical spectroscopy, which allowed us to exclude photoinduced electron transfer reactions. The methodology highlights the power of a consecutive UV/visible light activation sequence involving the generation of a strained intermediate and subsequent catalytic strain release.

Crystallographic data

Deposition number 2112151 (for **7a**) contain the supplementary crystallographic data for this paper. These data are provided free of charge by the joint Cambridge Crystallographic Data Centre and Fachinformationszentrum Karlsruhe Access Structures service.

Acknowledgements

Financial support of the DFG (grants Op90/12-1 and Ke2313/3-1) is gratefully acknowledged. The authors also thank Leander Geske (Mainz) for assistance with preparative HPLC, Luca Großmann (Mainz) for assistance with cyclic voltammetry, Dr. Dieter Schollmeyer (Mainz) for crystallography, Dr. Johannes C. Liermann (Mainz) for NMR spectroscopy and Dr. Christopher Kampf (Mainz) for mass spectrometry. The authors gratefully acknowledge the computing time granted on the supercomputer Mogon at Johannes Gutenberg-University Mainz (hpc.uni-mainz.de). C.K. is grateful to the Chemical Industry Funds for a Liebig fellowship. Open Access funding enabled and organized by Projekt DEAL.

Chemistry–A European Journal | Research Article doi.org/10.1002/chem.202104329 | Chemistry Europe European Chemical Societies Publishing

Conflict of Interest

The authors declare no conflict of interest.

Data Availability Statement

The data that support the findings of this study are available in the supplementary material of this article.

Keywords: cycloaddition · density functional theory calculations · photochemistry · ring strain · strain release · vinylcyclopropane

[1] a) S. Aoki, Y. Watanabe, M. Sanagawa, A. Setiawan, N. Kotoku, M. Kobayashi, *J. Am. Chem. Soc.* **2006**, *128*, 3148–3149; b) C. M. Hasler, G. Acs, P. M. Blumberg, *Cancer Res.* **1992**, *52*, 202–208; c) C. Kiewert, V. Kumar, O. Hildmann, M. Rueda, J. Hartmann, R. S. Naik, J. Klein, *Brain Res.* **2007**, *1128*, 70–78; d) M. Kubo, C. Okada, J. M. Huang, K. Harada, H. Hioki, Y. Fukuyama, *Org. Lett.* **2009**, *11*, 5190–5193; e) S. M. Ogbourne, A. Suhrbier, B. Jones, S. J. Cozzi, G. M. Boyle, M. Morris, D. McAlpine, J. Johns, T. M. Scott, K. P. Sutherland, J. M. Gardner, T. T. Le, A. Lenarczyk, J. H. Aylward, P. G. Parsons, *Cancer Res.* **2004**, *64*, 2833–2839.

[2] a) M. Lautens, W. Klute, W. Tam, *Chem. Rev.* **1996**, *96*, 49–92; b) X. P. Zeng, Z. Y. Cao, Y. H. Wang, F. Zhou, J. Zhou, *Chem. Rev.* **2016**, *116*, 7330–7396.

[3] Z. Wang, J. Liu, Beilstein, *J. Org. Chem.* **2020**, *16*, 3015–3031.

[4] J. Wang, S. A. Blaszczyk, X. Li, W. Tang, *Chem. Rev.* **2021**, *121*, 110–139.

[5] a) L. Jiao, S. Ye, Z.-X. Yu, *J. Am. Chem. Soc.* **2008**, *130*, 7178–7179; b) P. Liu, P. H. Cheong, Z. X. Yu, P. A. Wender, K. N. Houk, *Angew. Chem. Int. Ed.* **2008**, *47*, 3939–3941; *Angew. Chem.* **2008**, *120*, 4003–4005; c) P. Liu, L. E. Sirois, P. H. Cheong, Z. X. Yu, I. V. Hartung, H. Rieck, P. A. Wender, K. N. Houk, *J. Am. Chem. Soc.* **2010**, *132*, 10127–10135; d) S. C. Wang, D. J. Tantillo, *J. Organomet. Chem.* **2006**, *691*, 4386–4392; e) Z. X. Yu, P. H. Cheong, P. Liu, C. Y. Legault, P. A. Wender, K. N. Houk, *J. Am. Chem. Soc.* **2008**, *130*, 2378–2379; f) Z.-X. Yu, P. A. Wender, K. N. Houk, *J. Am. Chem. Soc.* **2004**, *126*, 9154–9155.

[6] a) X. Gu, X. Li, Y. Qu, Q. Yang, P. Li, Y. Yao, *Chem. Eur. J.* **2013**, *19*, 11878–11882; b) B. S. Karki, L. Devi, A. Pokhriyal, R. Kant, N. Rastogi, *Chem. Asian J.* **2019**, *14*, 4793–4797; c) Z. Lu, M. Shen, T. P. Yoon, *J. Am. Chem. Soc.* **2011**, *133*, 1162–1164; d) S. Maity, M. Zhu, R. S. Shinabery, N. Zheng, *Angew. Chem. Int. Ed. Engl.* **2012**, *51*, 222–226; *Angew. Chem.* **2012**, *124*, 226–230; e) Y. Q. Zou, L. Q. Lu, L. Fu, N. J. Chang, J. Rong, J. R. Chen, W. J. Xiao, *Angew. Chem. Int. Ed. Engl.* **2011**, *50*, 7171–7175; *Angew. Chem.* **2011**, *58*, 1586–1604.

[7] D. F. Chen, C. H. Chrisman, G. M. Miyake, *ACS Catal.* **2020**, *10*, 2609–2614.

[8] J. Paternoga, J. Kühlborn, N. O. Rossdam, T. Opatz, *J. Org. Chem.* **2021**, *86*, 3232–3248.

[9] A. Luque, J. Paternoga, T. Opatz, *Chem. Eur. J.* **2021**, *27*, 4500–4516.

[10] a) D. C. Blakemore, A. Gilbert, *Tetrahedron Lett.* **1994**, *35*, 5267–5270; b) X.-C. Guo, Q.-Y. Chen, *J. Fluorine Chem.* **1999**, *97*, 149–156.

[11] a) R. D. Bach, O. Dmitrenko, *J. Am. Chem. Soc.* **2004**, *126*, 4444–4452; b) M. A. Cavitt, L. H. Phun, S. France, *Chem. Soc. Rev.* **2014**, *43*, 804–818; c) M. S. Gordon, *J. Am. Chem. Soc.* **1980**, *102*, 7419–7422.

[12] If not stated otherwise, products were always obtained as racemic mixtures.

[13] A. Gavezzotti in *The Chemistry of Sulphones and Sulphoxides* (Eds.: S., Patai, Z., Rappoport, C. J. M., Stirling), Wiley, New York, **1988**, p. 1–32.

[14] a) T. G. Back, *Tetrahedron* **2001**, *57*, 5263–5301; b) T. G. Back, K. N. Clary, D. Gao, *Chem. Rev.* **2010**, *110*, 4498–4553.

[15] V. Nair, A. Augustine, T. D. Suja, *Synthesis* **2002**, *2002*, 2259–2265.

[16] Y. Sun, A. Abdukader, D. Lu, H. Zhang, C. Liu, *Green Chem.* **2017**, *19*, 1255–1258.

[17] a) M. S. Lowry, J. I. Goldsmith, J. D. Slinker, R. Rohl, R. A. Pascal, G. G. Malliaras, S. Bernhard, *Chem. Mater.* **2005**, *17*, 5712–5719; b) J. D. Slinker, A. A. Gorodetsky, M. S. Lowry, J. Wang, S. Parker, R. Rohl, S. Bernhard, G. G. Malliaras, *J. Am. Chem. Soc.* **2004**, *126*, 2763–2767.

[18] a) G. J. Hoijtink, **1958**, *77*, 555–558; b) F. Wilkinson, A. Farmilo, *J. Chem. Soc. Faraday Trans. 2* **1984**, *80*, 1117–1124.

[19] a) C. R. Bock, J. A. Connor, A. R. Gutierrez, T. J. Meyer, D. G. Whitten, B. P. Sullivan, J. K. Nagle, *J. Am. Chem. Soc.* **1979**, *101*, 4815–4824; b) C. K. Prier, D. A. Rankic, D. W. C. MacMillan, *Chem. Rev.* **2013**, *113*, 5322–5363.

[20] T. Koike, M. Akita, *Inorg. Chem. Front.* **2014**, *1*, 562–576.

[21] F. Strieth-Kalthoff, M. J. James, M. Teders, L. Pitzer, F. Glorius, *Chem. Soc. Rev.* **2018**, *47*, 7190–7202.

[22] a) T. R. Blum, Z. D. Miller, D. M. Bates, I. A. Guzei, T. P. Yoon, *Science* **2016**, *354*, 1391–1395; b) M. J. James, J. L. Schwarz, F. Strieth-Kalthoff, B. Wibbeling, F. Glorius, *J. Am. Chem. Soc.* **2018**, *140*, 8624–8628; c) J. Zhao, J. L. Brosmer, Q. Tang, Z. Yang, K. N. Houk, P. L. Diaconescu, O. Kwon, *J. Am. Chem. Soc.* **2017**, *139*, 9807–9810.

[23] For an intramolecular cycloaddition of this general type, see: C. S. Penkett, J. A. Woolford, I. J. Day, M. P. Coles, *J. Am. Chem. Soc.* **2010**, *132*, 4–5.

[24] M. A. Cismesia, T. P. Yoon, *Chem. Sci.* **2015**, *6*, 5426–5434.

[25] a) Y. Qin, R. Sun, N. P. Gianoulis, D. G. Nocera, *J. Am. Chem. Soc.* **2021**, *143*, 2005–2015; b) B. Xu, L. Troian-Gautier, R. Dykstra, R. T. Martin, O. Gutierrez, U. K. Tambar, *J. Am. Chem. Soc.* **2020**, *142*, 6206–6215.

[26] a) M. S. Bertrams, C. Kerzig, *Chem. Commun.* **2021**, *57*, 6752–6755; b) T. J. B. Zähringer, M. S. Bertrams, C. Kerzig, *J. Mater. Chem. C.* **2022**. https://doi.org/10.1039/D1TC04782E

[27] F. M. Hormann, C. Kerzig, T. S. Chung, A. Bauer, O. S. Wenger, T. Bach, *Angew. Chem. Int. Ed.* **2020**, *59*, 9659–9668; *Angew. Chem.* **2020**, *132*, 9746–9755.

[28] L. J. Johnston, J. C. Scaiano, *Chem. Rev.* **1989**, *89*, 521–547.

[29] D. Griller, K. U. Ingold, *Acc. Chem. Res.* **1980**, *13*, 317–323.

[30] M. Newcomb, P. H. Toy, *Acc. Chem. Res.* **2000**, *33*, 449–455.

[31] F. Strieth-Kalthoff, C. Henkel, M. Teders, A. Kahnt, W. Knolle, A. Gómez-Suárez, K. Dirian, W. Alex, K. Bergander, C. G. Daniliuc, B. Abel, D. M. Guldi, F. Glorius, *Chem* **2019**, *5*, 2183–2194.

Manuscript received: December 3, 2021
Accepted manuscript online: February 8, 2022
Version of record online: March 4, 2022

7.1.2 Selektivitätsuntersuchung einer Diels-Alder-Reaktion eines β-Fluor-β-nitrostyrols mit Cyclopentadien

In Kooperation mit der Arbeitsgruppe [redacted] wurden in einer Diels-Alder-Reaktion β-Fluor-β-nitrostyrole **117** (in der Publikation **1a**–**l**) mit Cyclopentadien (**118**) oder Cyclohexadien zu den entsprechenden Norbornenen **119** (in der Publikation **2a**–**l**) und Bicyclooctenen **148** (in der Publikation **3a**–**d**) umgesetzt. Dabei verlief die Reaktion mit Cyclopentadien (**118**) deutlich schneller sowie mit höheren Ausbeuten und wurde an zwölf Substraten demonstriert. Es konnte gezeigt werden, dass sich bei Vorhandensein einer stark elektronenziehenden Gruppe im Styrol-Edukt **149** (in der Publikation **1h**) die Diastereoselektivität der Reaktion in Richtung des *endo*-Isomers **150** (in der Publikation **2h**) verschiebt. Neben den experimentell bestimmten kinetischen Parametern der Reaktion wurde der Reaktionspfad der Umsetzung mit Cyclopentadien (**118**) auf DFT-Level simuliert und die Geschwindigkeitskonstanten mittels der Eyring-Gleichung berechnet, um die auftretende Diastereoselektivität zwischen dem *exo*- und *endo*-Produkt **151** und **150** quantenchemisch zu bestimmen (Abbildung 7.2).[555]

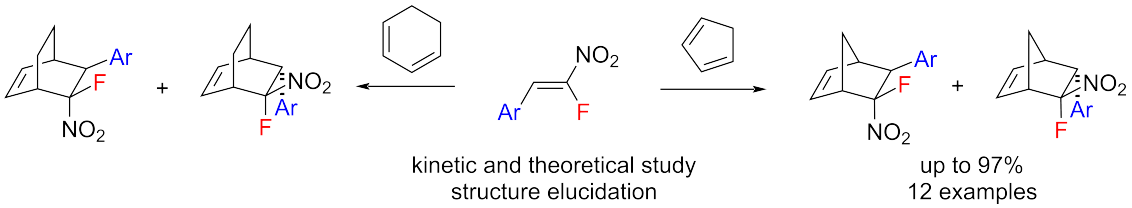

Abbildung 7.2: *Graphical abstract* der Publikation „Diels-Alder Reaction of β-Fluoro-β-nitrostyrenes with Cyclic Dienes“.[555]

Die synthetischen Arbeiten und die experimentelle Bestimmung der kinetischen Parameter wurden von [redacted], durchgeführt. Die Simulation des Reaktionspfades mittels DFT-Berechnungen wurde von J. Groß durchgeführt. J. Groß und T. Opatz haben zur Erstellung des Manuskripts beigetragen.[10]

[10] *Reprinted under the terms of the Creative Commons Attribution License CC BY 4.0. Copyright ©2021 S. Ponomarev, R. Larkovich, A. Aldoshin, A. Tabolin, S. Ioffe, J. Groß, T. Opatz, V. Nenajdenko, Beilstein J. Org. Chem., 2021, 17, 283–292, Beilstein-Institut.*

BEILSTEIN JOURNAL OF ORGANIC CHEMISTRY

Diels–Alder reaction of β-fluoro-β-nitrostyrenes with cyclic dienes

Savva A. Ponomarev[1], Roman V. Larkovich[1], Alexander S. Aldoshin[1], Andrey A. Tabolin[2], Sema L. Ioffe[2], Jonathan Groß[3], Till Opatz[3] and Valentine G. Nenajdenko[*1,§]

Full Research Paper

Open Access

Address:
[1]Department of Chemistry, Lomonosov Moscow State University, Leninskie gory 1, Moscow, 119991, Russian Federation, [2]N. D. Zelinsky Institute of Organic Chemistry, Russian Academy of Sciences Leninsky prosp. 47, Moscow 119991, Russian Federation and [3]Department of Chemistry Johannes Gutenberg-University, Duesbergweg 10–14, D-55128 Mainz, Germany

Email:
Valentine G. Nenajdenko[*] - nenajdenko@org.chem.msu.ru

* Corresponding author
§ Fax: (+)7-495-9328846

Keywords:
Diels–Alder reaction; fluorine; nitrostyrene; norbornene; stereochemistry

Beilstein J. Org. Chem. **2021,** *17,* 283–292.
https://doi.org/10.3762/bjoc.17.27

Received: 11 November 2020
Accepted: 13 January 2021
Published: 27 January 2021

This article is part of the thematic issue "Organo-fluorine chemistry V".

Guest Editor: D. O'Hagan

Abstract

The Diels–Alder reaction of β-fluoro-β-nitrostyrenes with cyclic 1,3-dienes was investigated. A series of novel monofluorinated norbornenes was prepared in up to 97% yield. The reaction with 1,3-cyclohexadiene permits the preparation of monofluorinated bicyclo[2.2.2]oct-2-enes. The kinetic data of the reactions with 1,3-cyclopentadiene and 1,3-cyclohexadiene were used to calculate activation parameters. Furthermore, the synthetic utility of the cycloadducts obtained was demonstrated.

Introduction

Organofluorine compounds play an exceptionally important role in various fields of science and technology. The incorporation of fluorine into molecules can significantly influence their pharmacokinetic and physicochemical properties and enhance their metabolic and chemical stability [1-5]. For instance, nearly a quarter of the currently manufactured agrochemical and pharmaceutical products contains at least one fluorine atom [6-8]. Fluorinated functional materials have also found wide application as durable ion exchange membranes, e.g., in fuel cells [9-11], as thermoplastic polymers [12-14], in electronic and optoelectronic technologies [15], and in liquid crystal display applications [16-21], etc [22]. The use of fluorinated building blocks is a very convenient approach and in many cases represents an indispensable alternative to late-stage fluorinations in the preparation of such unique materials [23].

The Diels–Alder reaction is considered a versatile and powerful tool for assembling a variety of fluorinated carbo- and

Beilstein J. Org. Chem. **2021,** *17,* 283–292.

heterocycles using either the diene [24-30] or the dienophile component [31-39] as fluorine-containing building blocks. The application of [4 + 2] cycloadditions for the preparation of fluorinated bicyclic compounds has attracted much attention [40-47]. In this regard, the development of new protocols to relevant monofluorinated bicyclic molecules involving novel versatile fluorine-containing building blocks is of key importance. Fluoroalkenes are recognized to be one of the most widely used fluorine-containing building blocks [48,49]. Recently, we have developed an efficient stereoselective synthesis of β-fluoro-β-nitrostyrenes **1** based on the radical nitration of 2-bromo-2-fluorostyrenes [50]. This process takes place with simultaneous elimination of bromine, and gives the target structures solely in the Z-isomeric form in high yields (up to 92%). These fluorine-containing olefins activated by a nitro group proved to be the appealing building blocks for the construction of numerous monofluorinated compounds [51-56]. This paper is devoted to a new synthetic approach to novel monofluorinated bicyclic compounds, namely norbornenes and bicyclo[2.2.2]oct-2-enes and their subsequent functionalization. The present study is our follow-up work on the Diels–Alder reaction involving β-fluoro-β-nitrostyrenes [57].

A recent review reported that by 2018, the total number of publications and patents related to the production and use of norbornene and norbornadiene derivatives had exceeded 30,000 [58]. Indeed, norbornene and its derivatives have found application in medicine, agriculture, microelectronics, and rocket technology as well as in production of polymeric materials, efficient gas separation membranes and solar energy converters [58]. Considering the high interest in such structures and the unique role of fluorine, we believe that novel norbornene derivatives obtained in the framework of this study can become relevant compounds in practical use.

Results and Discussion

Initially, we studied the Diels–Alder reaction of β-fluoro-β-nitrostyrenes **1** with 1,3-cyclopentadiene (CPD) to prepare a series of novel monofluorinated norbornenes. The starting nitrostyrenes were prepared and used in the *Z*-isomer form. The transformations were conducted in screw-top vials in *o*-xylene at 110 °C using a fivefold excess of the diene (Scheme 1). The reaction proceeded smoothly under these conditions to give the target cycloadducts **2** as a mixture of *exo* and *endo*-isomers in high isolated yield (up to 97%). It should be noted that in the present work we indicate an isomer as e*xo* or *endo* according to the stereo-position of the fluorine atom. Thus *exo*-**2** and *endo*-**2** means 5-*exo*-fluoro-5-*endo*-nitro-6-*exo*-arylnorbornene and 5-*endo*-fluoro-5-*exo*-nitro-6-*endo*-arylnorbornene, respectively (Figure 1). Both diastereomers are formed in a nearly 1:1 ratio for the majority of the substituents on the aryl group of the nitrostyrenes **1**. However, a higher diastereoselectivity towards the *endo*-isomer was observed when strong electron-withdrawing groups (EWGs) were present in the dienophile. For example, in the case of the 4-cyano and the 3-nitro-substituted derivative, the ratio of *endo*/*exo* was 2:1.

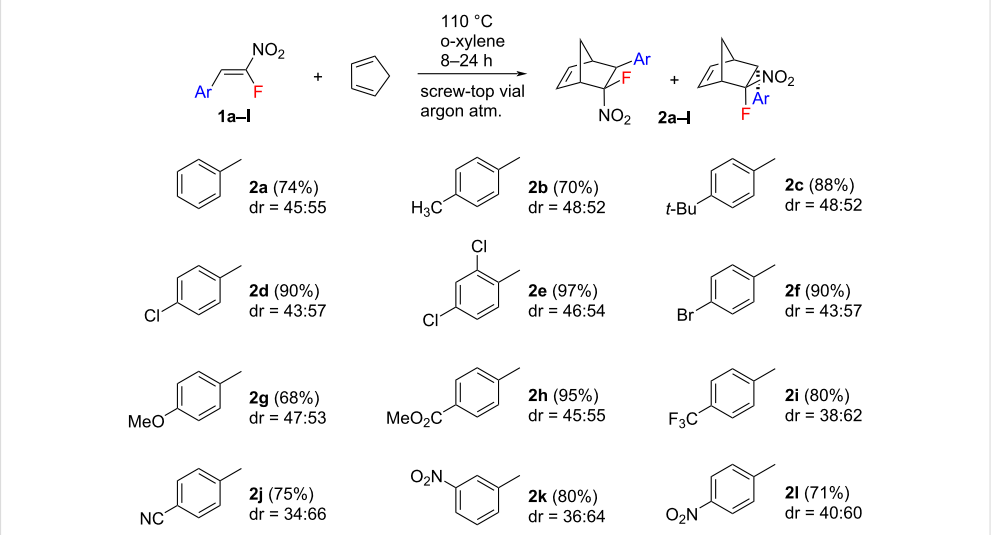

Scheme 1: Scope of the nitrostyrenes **1** in the Diels–Alder reaction with CPD (dr = *exo*:*endo*).

Beilstein J. Org. Chem. 2021, 17, 283–292.

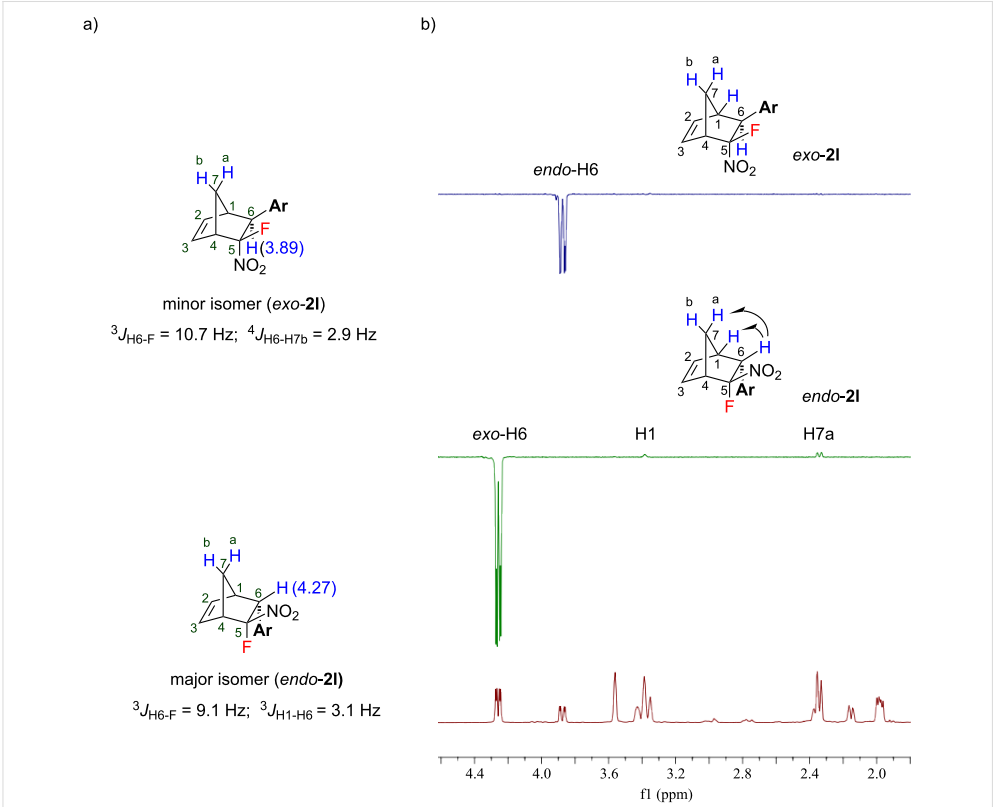

Figure 1: The structure assignment of norbornenes **2** by ^{1}H (a) and NOE (b) NMR spectroscopy.

The stereochemistry of the products **2a–l** can be unambiguously assigned using ^{1}H NMR spectroscopy. According to the literature data [59] the dienophile-derived proton at C6 resonates at lower field in the *exo*-form than the corresponding proton of the *endo*-isomer. For example, in the case of **2l**, the ^{1}H NMR spectrum shows a doublet of doublet signal for H6 at 3.89 ppm for the minor isomer and at 4.27 ppm for the major isomer (Figure 1a). A significant chemical shift difference is observed for the aryl proton signals of the *exo*- and *endo*-isomeric norbornenes **2**. Most probably such significant difference in the chemical shifts can be explained by the double bond anisotropy of the norbornene molecule [60]. The stereochemical assignments are in full accordance with the values of vicinal ($^3J_{H6-F}$ and $^3J_{H1-H6}$) and long-range coupling constants ($^4J_{H6-H7b}$). According to the literature data, the value of $^3J_{H1-H6}$ is larger than that of $^4J_{H6-H7b}$ [32,61-63]. For example, the ^{1}H NMR spectrum of the minor isomer of **2l** showed the coupling constants $^3J_{H6-F}$ = 10.7 Hz and $^4J_{H6-H7b}$ = 2.9 Hz consistent with an *exo*-geometry. In contrast, the major isomer having constants $^3J_{H6-F}$ = 9.1 Hz and $^3J_{H1-H6}$ = 3.1 Hz was ascribed to the *endo*-form (Figure 1). It should be noted that this observation applies for all cases investigated. The value of the coupling constant $^3J_{H6-F}$ between the *exo*-F and *endo*-H6 was always larger than the corresponding value between the *endo*-F and *exo*-H6. The stereochemical assignments were additionally confirmed by nuclear Overhauser effect spectroscopy (NOE). The peak of H6 was selected to be selectively excited for each isomer. As expected, in the case of *endo*-**2l** the NOE peaks resulted from the interaction of *exo*-H6 with H1 and H7a were observed. Whereas for *exo*-**2l** due to the opposite side position of *endo*-H6 there was no interaction observed. Thus, using these spectral data all the pairs of *exo*- and *endo*-isomers **2** obtained can be assigned unambiguously.

Moreover, the ^{13}C NMR spectra of the *exo* and *endo*-isomers exhibit a significant difference (approximately 3 ppm) in the

Beilstein J. Org. Chem. **2021,** *17,* 283–292.

chemical shifts for some carbon atoms (Figure 2). A considerable difference in the chemical shifts was observed for C-7 of the methylene bridge (46.1 for the *exo*- vs 48.9 ppm for the *endo*-isomer), C-6 (51.3 for the *exo* vs 53.4 for the *endo*-isomer), C-4 (52.4 for the *exo*- vs 55.3 ppm for the *endo*-isomer), and C-2 (139.7 for the *endo*- vs 143.0 ppm for the *exo*-isomer). The same pattern in the chemical shifts and coupling constants was observed for all structures **2** synthesized.

For further insights into the mechanistic background of the *endo*-*exo* selectivity, the Diels–Alder reaction of CPD with the model nitrostyrene **1h** was simulated in silico to predict the reaction pathway, the reaction rate constants, and the activation enthalpies. Density functional theory calculations were conducted for the reactants, products, and transition states using the B3LYP [64-66] and M062X [67] level of theory in combination with a Pople basis set and the IEFPCM [68] solvation model for *o*-xylene. Both functionals are already known in the literature for the investigation of cycloadditions [69-72]. For the computational details the reader is referred to Supporting Information File 1.

The predicted reaction pathways for the formation of the *exo*- and *endo*-isomeric norbornene **2h** using M062X are displayed in Figure 3. For each isomer one transition state *exo*-**TS** and *endo*-**TS** was identified. The former transition state is higher in energy and leads to the less exergonic product *exo*-**2h**. The *exo* and *endo*-isomers were predicted to have free energies of activation ($\Delta G^{\ddagger}_{383.15}$) of 120.62 and 119.64 kJ mol^{-1}, respectively. The corresponding predicted reaction free energies ($\Delta G_{383.15}$) are −39.66 and −42.07 kJ mol^{-1}. With the former values of $\Delta G^{\ddagger}$, the reaction rate coefficient k can be calculated using the Eyring equation (Equation 1) [73,74]:

$$k(T) = \frac{k_B T}{hc_0} e^{-\Delta G^{\ddagger}_{383.15K}/RT} \quad (1)$$

For T = 110 °C, the predicted ratio of k_{endo}/k_{exo} = 1.36 (1.68 for B3LYP) is in good accordance with the experimentally observed diastereomeric ratio of 1.22. The larger discrepancy in case of the B3LYP functional may be due to the fact that disper-

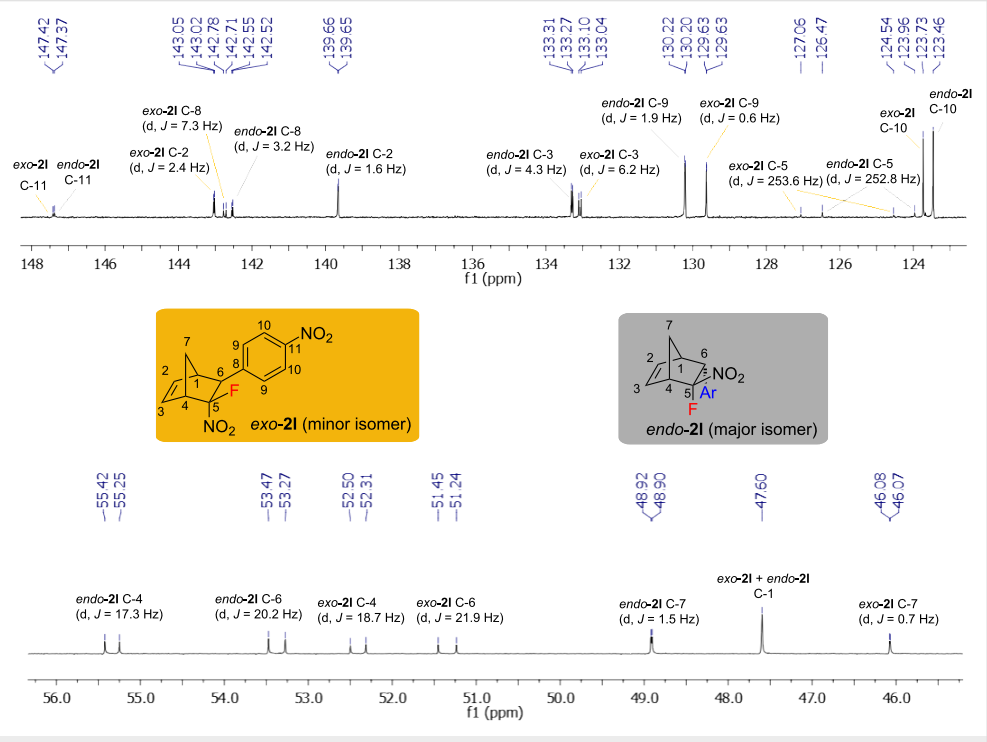

Figure 2: ^{13}C NMR spectrum of the mixture of *exo*- and *endo*-isomers of norbornene **2l**.

Beilstein J. Org. Chem. 2021, 17, 283–292.

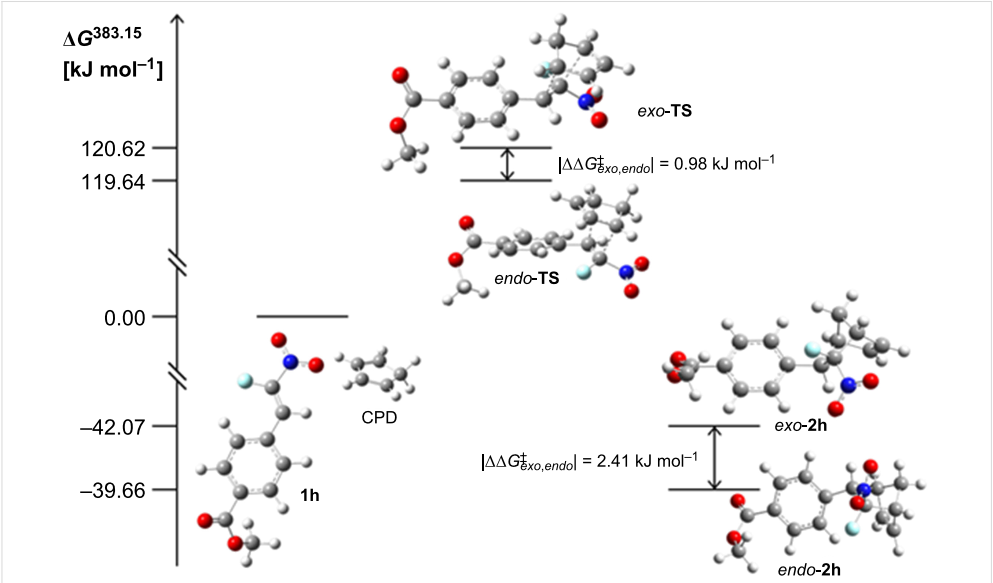

Figure 3: The predicted reaction pathway for the Diels–Alder reaction of nitrostyrene **1h** with CPD is displayed. The path leading to the *endo*-**2h** isomer has a lower lying transition state and is more exergonic than the path resulting in the *exo*-**2h** isomer. Energies are given in kJ mol^{-1} and were calculated with M062X/6-311+G(d,p) at 383.15 K in *o*-xylene (the corresponding B3LYP reaction pathway is not shown).

sion effects are not included, whereas M062X includes nonlocal effects of electronic dispersion [70,75].

We also demonstrate the preparation of norbornene structures substituted at the methylene bridge. The reaction of model nitrostyrene **1h** with spiro[2.4]hepta-4,6-diene was carried out (Scheme 2). As a result, the corresponding norbornene **2m** having a cyclopropane ring was obtained in moderate yield (44%). The cycloaddition proceeds much more slowly as a result of the high steric demand of the cyclopropyl ring of the spirodiene compared to the CH_2 group of cyclopentadiene. We believe that this is the reason of the lower yield in comparison to the reaction with CPD. The stereochemical assignment was performed using ^{1}H NMR spectroscopy (Scheme 2) to show similar peculiarities of the spectra. In contrast to the reaction with CPD, a slight prevalence in the formation of the *exo*-isomer (*exo*:*endo* = 56:44) was observed for the product **2m**.

Next, the reaction with 1,3-cyclohexadiene (CHD) was investigated. It was found that the reaction is very sensitive to the structure of starting diene and in the case of CHD proceeds much more slowly. Both thermal and microwave (MW) activation (Scheme 3) was investigated to accelerate the reaction with CHD. However, in all cases, the yields of the target cycloadducts **3** were below 35% despite the full conversion of the

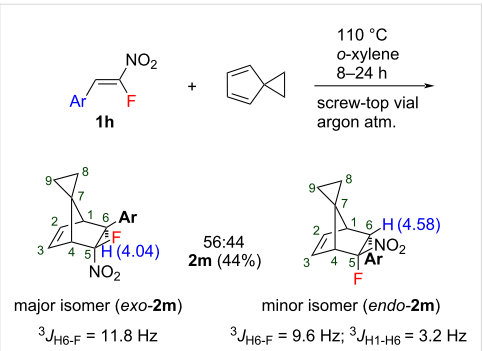

Scheme 2: The Diels–Alder reaction of nitrostyrene **1h** with spiro[2.4]hepta-4,6-diene.

nitrostyrenes **1** which is common for this type of dienophiles (Scheme 3). The stereochemical assignment was made similarly to the norbornene structures using ^{1}H NMR spectroscopy (Scheme 3). Larger values of $^3J_{H6\text{-}F}$ were observed for the *exo*-F isomers. The presence of a strong EWG on the aryl substituent led to higher stereoselectivity. For example, approximately a 2:1 ratio was observed for the nitro- and carboxymethyl-substituted products **3b**, **3c**, whereas in the absence of a

Beilstein J. Org. Chem. **2021,** *17,* 283–292.

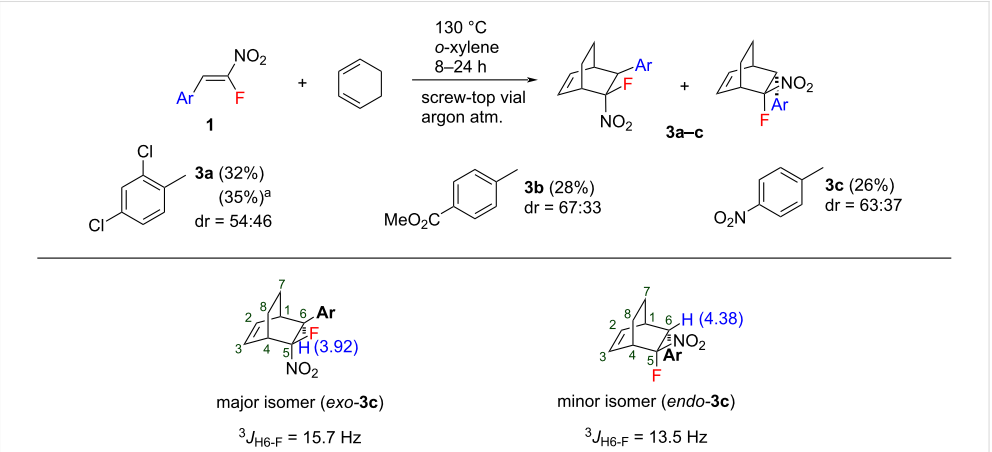

Scheme 3: Diels–Alder reaction of nitrostyrenes **1** with CHD (dr = *exo*:*endo*). (a) Reaction under microwave activation.

strong EWG, the ratio was about 1:1 (**3a**). However, in contrast to CPD derivatives, the major products formed in the reaction with CHD have *exo*-configuration.

To gain deeper insights into the reaction, we carried out some kinetic studies to evaluate and compare the reactivities of CHD and CPD in the reactions with model nitrostyrene **1h** (Scheme 4). All the kinetic runs were performed using a ≈43–49 molar excess of the diene in *o*-xylene (1:1) to provide pseudo-first order conditions. Conversions (F) of **1** were measured by ^{1}H NMR spectroscopy. The reactions were found to proceed under the kinetic control since the isomer ratio remained constant throughout the reaction course regardless of the temperature (Table 1).

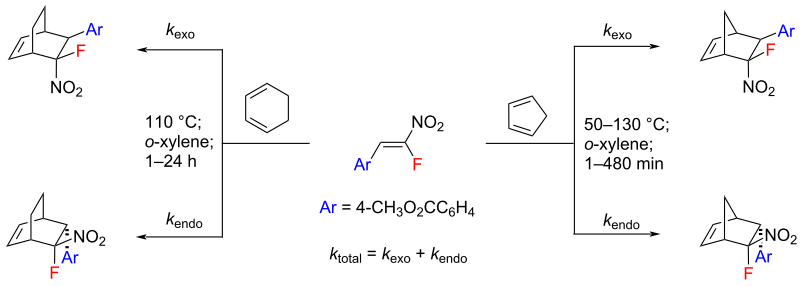

Scheme 4: Kinetic study of reactions of **1h** with CPD and CHD.

Table 1: Kinetic parameters for the reactions of **1h** with CPD and CHD.

entry	diene	T, °C	molar ratio *exo*/*endo*	$k^*\cdot10^4$, s^{-1}	$k_{total}\cdot10^5$, L/mol·s	$k_{exo}\cdot10^5$, L/mol·s	$k_{endo}\cdot10^5$, L/mol·s	R_{corr}
1	CPD	50	46:54	1.00	1.67	0.090	0.077	0.997
2	CPD	80	46:54	5.78	9.72	5.26	4.46	0.998
3	CPD	110	46:54	35.62	59.91	32.39	27.53	0.990
4	CPD	130	46:54	46.20	77.71	41.99	35.72	0.999
5	CHD	110	61:39	0.12	0.224	0.137	0.087	0.999

Beilstein J. Org. Chem. 2021, 17, 283–292.

The total effective pseudo-first order rate constants k^* were obtained by plotting the experimental values of $\ln(c_0/c)$ versus time with good correlations (Table 1). The overall second-order rate total constants k_{total} were calculated from the effective k^* and initial concentration of the diene (Table 1). The individual constants for the *endo* and *exo*-isomers (k_{endo} and k_{exo}) were evaluated by multiplication of k_{total} with the molar fractions of the isomers (Table 1). The data obtained demonstrated that the overall reaction rate for CHD is 267 times lower than that for CPD at 110 °C (Figure 4, Table 1). Such a large difference in the reactivity of CHD and CPD was described in the literature. For example, in model reactions with tetracyanoethene, the difference was 2600-fold at 20 °C [76]. The activation parameters were estimated for the reaction of **1h** with CPD by plotting $\ln(k/T)$ versus $1/T$ according to the Eyring equation (Equations 2–4) [77].

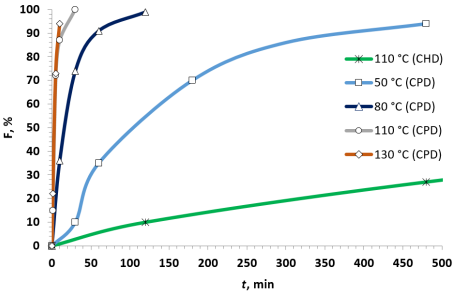

Figure 4: Kinetic curves for the reactions of nitrostyrene **1h** with CPD (50–130 °C) and CHD at 110 °C.

$$\ln(k/T) = \ln(k_b/\hbar) + \Delta S^{\neq}/R - \Delta H^{\neq}/RT \quad (2)$$

$$\ln(k_{endo}/T) = 1.89 - 6208/T \quad (R_{corr} = 0.989) \quad (3)$$

$$\ln(k_{exo}/T) = 1.72 - 6207/T \quad (R_{corr} = 0.989) \quad (4)$$

The activation enthalpies ($\Delta H^{\neq}$) for *exo*- and *endo*-**1h** were found to be identical for both reaction pathways (51.6 kJ mol^{-1}). Whereas the entropies of activation ($\Delta S^{\neq}$) were −181.8 and −183.1 J mol^{-1} K^{-1} for the formation of the *endo* and *exo*-isomers, respectively. The values obtained are typical for concerted [4 + 2]-cycloaddition reactions [60]. The free energies of activation ($\Delta G^{\ddagger}_{383.15}$) were calculated for 121.26 kJ mol^{-1} for *endo*-**1h** and 121.75 kJ mol^{-1} for *exo*-**1h** and were consistent with the predicted ones.

Next, the reaction with some other cyclic dienes was investigated. The reaction with the unsymmetrical 1-methoxy-1,3-cyclohexadiene (Scheme 5) led to the formation of a mixture of four products (regioisomers and stereoisomers, respectively) **3d** in 40% overall yield. Two pairs of regioisomers were partially separated by column chromatography with sufficiently slow elution and analyzed by ^{1}H NMR spectroscopy. The structure assignment was made as depicted in Scheme 5. The structures of two pairs of regioisomers were assigned by chemical shifts of the singlet of the methoxy group. The products having the MeO and NO_2 groups in the adjacent position have the signal of the methoxy protons shifted to a lower field. The assignment of the *exo*/*endo*-isomers was carried out by the position of the benzylic proton (H5 or H6) and its coupling constant to fluorine ($^3J_{H5\text{-}F}$ or $^3J_{H6\text{-}F}$).

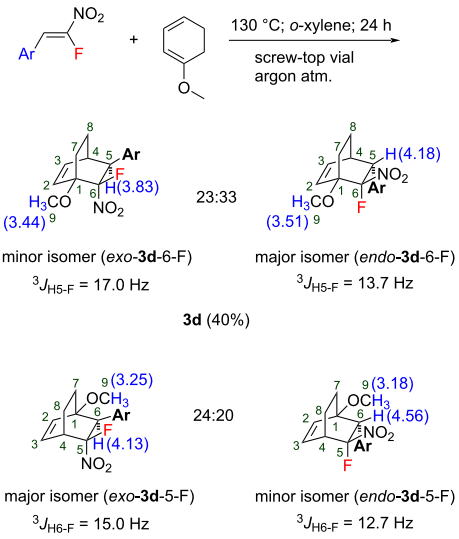

Scheme 5: The Diels–Alder reaction of the nitrostyrene **1h** with 1-methoxy-1,3-cyclohexadiene.

The reaction with 7- and 8-membered cyclic dienes (1,3-cycloheptadiene and 1,3-cyclooctadiene) did not result in the formation of the corresponding cycloadducts confirming that the reaction is very sensitive to the structure of the dienes. Moreover, it was found that furan did not react with nitrostyrenes **1**.

Furthermore, we performed some subsequent transformations of the fluorinated norbornenes prepared to investigate their chemical properties and to demonstrate their utility (Scheme 6). These reactions were carried out to involve either the double bond or the nitro group of the norbornene products. The treatment of cycloadducts **2** with *m*-chloroperbenzoic acid afforded a series of novel fluorinated epoxynorbornane derivatives **4** in high

Beilstein J. Org. Chem. **2021,** *17,* 283–292.

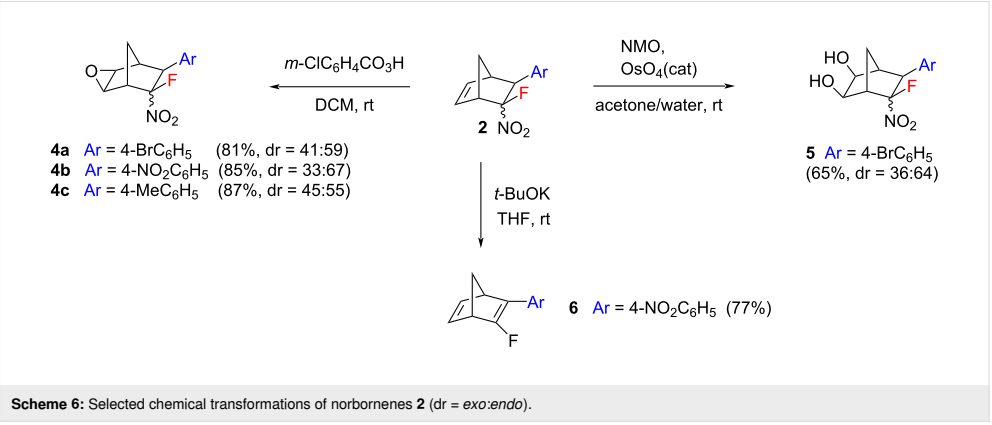

Scheme 6: Selected chemical transformations of norbornenes **2** (dr = *exo*:*endo*).

yields (up to 87%). In all cases, the formation of mixtures of only two products was observed in ratios similar to those of the starting mixture **2**. We believe that this is a result of an *exo*-epoxidation which is preferred in norbornene systems [78,79]. Such a functionalization is very attractive to produce new reactive building blocks bearing the norbornane scaffold. This approach can pave a straightforward way to numerous fluorine-containing bicyclic compounds not previously available. The *syn*-dihydroxylation of compound **2f** with the *N*-methylmorpholine-*N*-oxide (NMO)–OsO_4 system resulted in a mixture of the corresponding diols **5** in a 36:64 ratio in 65% yield. Again, *exo*-dihydroxylation is to be expected [80-82]. The treatment of norbornene **2l** with *t*-BuOK resulted in the selective elimination of nitrous acid to form the desired monofluorinated norbornadiene **6** in 77% yield. No competitive elimination of HF was observed. The Diels–Alder reaction–base-induced HNO_2 elimination sequence opens a straightforward way to novel fluorinated norbornadienes from β-fluoro-β-nitrostyrenes and CPD.

Conclusion

In summary, the Diels–Alder reaction of β-fluoro-β-nitrostyrenes with cyclic 1,3-dienes was investigated. A series of novel monofluorinated norbornenes was prepared in high yield up to 97%. A number of novel monofluorinated bicyclo[2.2.2]oct-2-enes was obtained in up to 40% yield. The reactivity of CPD and its homologues was evaluated and compared. The reaction rate for CHD proved to be 267 times lower than that for CPD in a model reaction, whereas 1,3-cycloheptadiene and 1,3-cyclooctadiene were found to be unable to react. The activation parameters of the reaction of nitrostyrene **1h** with CPD were estimated. In addition, the synthetic utility of the norbornenes obtained was demonstrated. All the structures obtained in this work were elucidated by NMR spectroscopy and elemental analysis or HRMS.

Supporting Information

Supporting Information File 1

Copies of spectra, experimental section, and computational details of DFT calculations.
[https://www.beilstein-journals.org/bjoc/content/supplementary/1860-5397-17-27-S1.pdf]

Acknowledgements

The authors acknowledge the partial support in measuring of NMR spectra from the M. V. Lomonosov Moscow State University Program of Development. We thank Jan Brauer and Paul Eckhardt for their assistance with the computational calculations and evaluations. Parts of this research were conducted using the supercomputer MOGON and/or advisory services offered by the Johannes Gutenberg University Mainz (hpc.uni-mainz.de), which is a member of the AHRP (Alliance for High Performance Computing in Rhineland Palatinate, http://www.ahrp.info) and the Gauss Alliance e.V. The authors gratefully acknowledge the computing time granted on the supercomputer MOGON at Johannes Gutenberg University Mainz.

Funding

This work was supported by RFBR, project number 20-33-70132.

ORCID® iDs

Savva A. Ponomarev - https://orcid.org/0000-0002-5667-4800
Alexander S. Aldoshin - https://orcid.org/0000-0003-3653-1439
Andrey A. Tabolin - https://orcid.org/0000-0003-3241-8279
Till Opatz - https://orcid.org/0000-0002-3266-4050
Valentine G. Nenajdenko - https://orcid.org/0000-0001-9162-5169

References

1. Purser, S.; Moore, P. R.; Swallow, S.; Gouverneur, V. *Chem. Soc. Rev.* **2008,** *37,* 320–330. doi:10.1039/b610213c
2. Shah, P.; Westwell, A. D. *J. Enzyme Inhib. Med. Chem.* **2007,** *22,* 527–540. doi:10.1080/14756360701425014
3. Wang, B.-C.; Wang, L.-J.; Jiang, B.; Wang, S.-Y.; Wu, N.; Li, X.-Q.; Shi, D.-Y. *Mini-Rev. Med. Chem.* **2017,** *17,* 683–692. doi:10.2174/1389557515666151016124957
4. Gillis, E. P.; Eastman, K. J.; Hill, M. D.; Donnelly, D. J.; Meanwell, N. A. *J. Med. Chem.* **2015,** *58,* 8315–8359. doi:10.1021/acs.jmedchem.5b00258
5. Meanwell, N. A. *J. Med. Chem.* **2018,** *61,* 5822–5880. doi:10.1021/acs.jmedchem.7b01788
6. Politanskaya, L. V.; Selivanova, G. A.; Panteleeva, E. V.; Tretyakov, E. V.; Platonov, V. E.; Nikul'shin, P. V.; Vinogradov, A. S.; Zonov, Y. V.; Karpov, V. M.; Mezhenkova, T. V.; Vasilyev, A. V.; Koldobskii, A. B.; Shilova, O. S.; Morozova, S. M.; Burgart, Y. V.; Shchegolkov, E. V.; Saloutin, V. I.; Sokolov, V. B.; Aksinenko, A. Y.; Nenajdenko, V. G.; Moskalik, M. Y.; Astakhova, V. V.; Shainyan, B. A.; Tabolin, A. A.; Ioffe, S. L.; Muzalevskiy, V. M.; Balenkova, E. S.; Shastin, A. V.; Tyutyunov, A. A.; Boiko, V. E.; Igumnov, S. M.; Dilman, A. D.; Adonin, N. Y.; Bardin, V. V.; Masoud, S. M.; Vorobyeva, D. V.; Osipov, S. N.; Nosova, E. V.; Lipunova, G. N.; Charushin, V. N.; Prima, D. O.; Makarov, A. G.; Zibarev, A. V.; Trofimov, B. A.; Sobenina, L. N.; Belyaeva, K. V.; Sosnovskikh, V. Y.; Obydennov, D. L.; Usachev, S. A. *Russ. Chem. Rev.* **2019,** *88,* 425–569. doi:10.1070/rcr4871
7. Inoue, M.; Sumii, Y.; Shibata, N. *ACS Omega* **2020,** *5,* 10633–10640. doi:10.1021/acsomega.0c00830
8. Han, J.; Remete, A. M.; Dobson, L. S.; Kiss, L.; Izawa, K.; Moriwaki, H.; Soloshonok, V. A.; O'Hagan, D. *J. Fluorine Chem.* **2020,** *239,* 109639. doi:10.1016/j.jfluchem.2020.109639
9. Mauritz, K. A.; Moore, R. B. *Chem. Rev.* **2004,** *104,* 4535–4586. doi:10.1021/cr0207123
10. Schmidt-Rohr, K.; Chen, Q. *Nat. Mater.* **2008,** *7,* 75–83. doi:10.1038/nmat2074
11. Kraytsberg, A.; Ein-Eli, Y. *Energy Fuels* **2014,** *28,* 7303–7330. doi:10.1021/ef501977k
12. Ferrari, M. C.; Galizia, M.; De Angelis, M. G.; Sarti, G. C. *Ind. Eng. Chem. Res.* **2010,** *49,* 11920–11935. doi:10.1021/ie100242q
13. Mastronardi, F.; Gutmann, B.; Kappe, C. O. *Org. Lett.* **2013,** *15,* 5590–5593. doi:10.1021/ol4027914
14. Kubota, T. *J. Synth. Org. Chem., Jpn.* **2013,** *71,* 196–206. doi:10.5059/yukigoseikyokaishi.71.196
15. Babudri, F.; Farinola, G. M.; Naso, F.; Ragni, R. *Chem. Commun.* **2007,** 1003–1022. doi:10.1039/b611336b
16. Hird, M. *Chem. Soc. Rev.* **2007,** *36,* 2070–2095. doi:10.1039/b610738a
17. Yokokoji, O.; Miyajima, T.; Irisawa, J.; Shimizu, T.; Inoue, S. *Liq. Cryst.* **2009,** *36,* 799–807. doi:10.1080/02678290903062986
18. Goodby, J. W.; Hindmarsh, P.; Hird, M.; Lewis, R. A.; Toyne, K. J. *Mol. Cryst. Liq. Cryst. Sci. Technol., Sect. A* **2001,** *364,* 889–898. doi:10.1080/10587250108025062
19. Ishigure, T.; Koike, Y. *Mol. Cryst. Liq. Cryst. Sci. Technol., Sect. A* **2000,** *353,* 451–469. doi:10.1080/10587250008025681
20. Kirsch, P. *J. Fluorine Chem.* **2015,** *177,* 29–36. doi:10.1016/j.jfluchem.2015.01.007
21. Al-Maharik, N.; Kirsch, P.; Slawin, A. M. Z.; Cordes, D. B.; O'Hagan, D. *Org. Biomol. Chem.* **2016,** *14,* 9974–9980. doi:10.1039/c6ob01986b
22. Pagliaro, M.; Ciriminna, R. *J. Mater. Chem.* **2005,** *15,* 4981–4991. doi:10.1039/b507583c
23. Kondratov, I. S.; Tolmachova, N. A.; Haufe, G. *Eur. J. Org. Chem.* **2018,** 3618–3647. doi:10.1002/ejoc.201800327
24. Hayashi, T.; Usuki, Y.; Wakamatsu, Y.; Iio, H. *Synlett* **2010,** 2843–2846. doi:10.1055/s-0030-1259013
25. Shi, G.-q.; Cottens, S.; Shiba, S. A.; Manfred, S. *Tetrahedron* **1992,** *48,* 10569–10574. doi:10.1016/s0040-4020(01)88354-x
26. Patrick, T. B.; Rogers, J.; Gorrell, K. *Org. Lett.* **2002,** *4,* 3155–3156. doi:10.1021/ol026512v
27. Patrick, T. B.; Gorrell, K.; Rogers, J. *J. Fluorine Chem.* **2007,** *128,* 710–713. doi:10.1016/j.jfluchem.2007.03.010
28. Jin, F.-q.; Xu, Y.-y.; Huang, W.-y. *J. Fluorine Chem.* **1995,** *71,* 1–4. doi:10.1016/0022-1139(94)03186-4
29. Shi, G.-q.; Schlosser, M. *Tetrahedron* **1993,** *49,* 1445–1456. doi:10.1016/s0040-4020(01)90196-6
30. Amii, H.; Kobayashi, T.; Terasawa, H.; Uneyama, K. *Org. Lett.* **2001,** *3,* 3103–3105. doi:10.1021/ol0163631
31. Hanamoto, T.; Korekoda, K.; Nakata, K.; Handa, K.; Koga, Y.; Kondo, M. *J. Fluorine Chem.* **2002,** *118,* 99–101. doi:10.1016/s0022-1139(02)00198-7
32. Sridhar, M.; Leela Krishna, K.; Madhusudana Rao, J. *Tetrahedron* **2000,** *56,* 3539–3545. doi:10.1016/s0040-4020(00)00242-8
33. de Meijere, A.; Teichmann, S.; Seyed-Mahdavi, F.; Kohlstruk, S. *Liebigs Ann.* **1996,** 1989–2000. doi:10.1002/jlac.199619961208
34. Ito, H.; Saito, A.; Taguchi, T. *Tetrahedron: Asymmetry* **1998,** *9,* 1979–1987. doi:10.1016/s0957-4166(98)00195-5
35. Arany, A.; Crowley, P. J.; Fawcett, J.; Hursthouse, M. B.; Kariuki, B. M.; Light, M. E.; Moralee, A. C.; Percy, J. M.; Salafia, V. *Org. Biomol. Chem.* **2004,** *2,* 455–465. doi:10.1039/b314314g
36. Crowley, P. J.; Percy, J. M.; Stansfield, K. *Tetrahedron Lett.* **1996,** *37,* 8237–8240. doi:10.1016/0040-4039(96)01877-1
37. Yamada, S.; Noma, M.; Konno, T.; Ishihara, T.; Yamanaka, H. *Org. Lett.* **2006,** *8,* 843–845. doi:10.1021/ol052897g
38. Yamada, S.; Hondo, K.; Konno, T.; Ishihara, T. *RSC Adv.* **2016,** *6,* 28458–28469. doi:10.1039/c6ra00569a
39. Shastin, A. V.; Nenajdenko, V. G.; Muzalevskiy, V. M.; Balenkova, E. S.; Fröhlich, R.; Haufe, G. *Tetrahedron* **2008,** *64,* 9725–9732. doi:10.1016/j.tet.2008.07.097
40. Crowley, P. J.; Percy, J. M.; Stansfield, K. *Tetrahedron Lett.* **1996,** *37,* 8233–8236. doi:10.1016/0040-4039(96)01876-x
41. Petrov, V.; Marchione, A. A.; Dooley, R. *Chem. Commun.* **2018,** *54,* 9298–9300. doi:10.1039/c8cc05075a
42. Chanteau, F.; Essers, M.; Plantier-Royon, R.; Haufe, G.; Portella, C. *Tetrahedron Lett.* **2002,** *43,* 1677–1680. doi:10.1016/s0040-4039(02)00107-7
43. Baum, K.; Archibald, T. G.; Tzeng, D.; Gilardi, R.; Flippen-Anderson, J. L.; George, C. *J. Org. Chem.* **1991,** *56,* 537–539. doi:10.1021/jo00002a011
44. Percy, J. M.; Stansfield, K.; Crowley, P. J.; Stansfield, K. *Chem. Commun.* **1997,** 2033–2034. doi:10.1039/a704717g
45. Petrov, V.; Dooley, R. J.; Marchione, A. A.; Diaz, E. L.; Clem, B. S. *J. Fluorine Chem.* **2019,** *225,* 1–10. doi:10.1016/j.jfluchem.2019.06.003
46. Ernet, T.; Maulitz, A. H.; Würthwein, E.-U.; Haufe, G. *J. Chem. Soc., Perkin Trans. 1* **2001,** 1929–1938. doi:10.1039/b102684b
47. Bogachev, A. A.; Kobrina, L. S.; Meyer, O. G. J.; Haufe, G. *J. Fluorine Chem.* **1999,** *97,* 135–143. doi:10.1016/s0022-1139(99)00040-8

Beilstein J. Org. Chem. **2021,** *17,* 283–292.

48. Konev, A. S.; Khlebnikov, A. F. *Collect. Czech. Chem. Commun.* **2008,** *73,* 1553–1611. doi:10.1135/cccc20081553
49. Yanai, H.; Taguchi, T. *Eur. J. Org. Chem.* **2011,** 5939–5954. doi:10.1002/ejoc.201100495
50. Motornov, V. A.; Muzalevskiy, V. M.; Tabolin, A. A.; Novikov, R. A.; Nelyubina, Y. V.; Nenajdenko, V. G.; Ioffe, S. L. *J. Org. Chem.* **2017,** *82,* 5274–5284. doi:10.1021/acs.joc.7b00578
51. Motornov, V. A.; Tabolin, A. A.; Novikov, R. A.; Nelyubina, Y. V.; Nenajdenko, V. G.; Ioffe, S. L. *Org. Chem. Front.* **2018,** *5,* 2588–2594. doi:10.1039/c8qo00623g
52. Motornov, V. A.; Tabolin, A. A.; Nelyubina, Y. V.; Nenajdenko, V. G.; Ioffe, S. L. *Org. Biomol. Chem.* **2019,** *17,* 1442–1454. doi:10.1039/c8ob03126f
53. Motornov, V. A.; Tabolin, A. A.; Nelyubina, Y. V.; Nenajdenko, V. G.; Ioffe, S. L. *Org. Biomol. Chem.* **2020,** *18,* 1436–1448. doi:10.1039/c9ob02668a
54. Aldoshin, A. S.; Tabolin, A. A.; Ioffe, S. L.; Nenajdenko, V. G. *Eur. J. Org. Chem.* **2018,** 3816–3825. doi:10.1002/ejoc.201800385
55. Motornov, V. A.; Tabolin, A. A.; Novikov, R. A.; Nelyubina, Y. V.; Ioffe, S. L.; Smolyar, I. V.; Nenajdenko, V. G. *Eur. J. Org. Chem.* **2017,** 6851–6860. doi:10.1002/ejoc.201701338
56. Aldoshin, A. S.; Tabolin, A. A.; Ioffe, S. L.; Nenajdenko, V. G. *Eur. J. Org. Chem.* **2019,** 4384–4396. doi:10.1002/ejoc.201900573
57. Larkovich, R. V.; Ponomarev, S. A.; Aldoshin, A. S.; Tabolin, A. A.; Ioffe, S. L.; Nenajdenko, V. G. *Eur. J. Org. Chem.* **2020,** 2479–2492. doi:10.1002/ejoc.202000054
58. Flid, V. R.; Gringolts, M. L.; Shamsiev, R. S.; Finkelshtein, E. S. *Russ. Chem. Rev.* **2018,** *87,* 1169–1205. doi:10.1070/rcr4834
59. Pretsch, E.; Bühlmann, P.; Badertscher, M. *Structure Determination of Organic Compounds, Tables of Spectral Data;* Springer-Verlag: Berlin, Heidelberg, 2009; p 174. doi:10.1007/978-3-540-93810-1
60. Jasiński, R.; Kwiatkowska, M.; Barański, A. *J. Phys. Org. Chem.* **2011,** *24,* 843–853. doi:10.1002/poc.1853
61. De Tollenaere, C.; Ghosez, L. *Tetrahedron* **1997,** *53,* 17127–17138. doi:10.1016/s0040-4020(97)10126-0
62. Sridhar, M.; Krishna, K. L.; Srinivas, K.; Rao, J. M. *Tetrahedron Lett.* **1998,** *39,* 6529–6532. doi:10.1016/s0040-4039(98)01357-4
63. Smart, B. E. *J. Org. Chem.* **1973,** *38,* 2027–2035. doi:10.1021/jo00951a013
64. Lee, C.; Yang, W.; Parr, R. G. *Phys. Rev. B* **1988,** *37,* 785–789. doi:10.1103/physrevb.37.785
65. Becke, A. D. *J. Chem. Phys.* **1993,** *98,* 5648–5652. doi:10.1063/1.464913
66. Vosko, S. H.; Wilk, L.; Nusair, M. *Can. J. Phys.* **1980,** *58,* 1200–1211. doi:10.1139/p80-159
67. Zhao, Y.; Truhlar, D. G. *Theor. Chem. Acc.* **2008,** *120,* 215–241. doi:10.1007/s00214-007-0310-x
68. Tomasi, J.; Mennucci, B.; Cancès, E. *J. Mol. Struct.: THEOCHEM* **1999,** *464,* 211–226. doi:10.1016/s0166-1280(98)00553-3
69. Pieniazek, S. N.; Clemente, F. R.; Houk, K. N. *Angew. Chem., Int. Ed.* **2008,** *47,* 7746–7749. doi:10.1002/anie.200801843
70. Mardirossian, N.; Head-Gordon, M. *Mol. Phys.* **2017,** *115,* 2315–2372. doi:10.1080/00268976.2017.1333644
71. Levandowski, B. J.; Houk, K. N. *J. Org. Chem.* **2015,** *80,* 3530–3537. doi:10.1021/acs.joc.5b00174
72. Opoku, E.; Tia, R.; Adei, E. *J. Phys. Org. Chem.* **2019,** *32,* e3992. doi:10.1002/poc.3992
73. McQuarrie, D. A.; Simon, J. D. *Physical chemistry: a molecular approach;* Sterling Publishing Company, Inc.: New York, NY, USA, 1997.
74. Eyring, H. *J. Chem. Phys.* **1935,** *3,* 107–115. doi:10.1063/1.1749604
75. Mardirossian, N.; Head-Gordon, M. *J. Chem. Theory Comput.* **2016,** *12,* 4303–4325. doi:10.1021/acs.jctc.6b00637
76. Fringuelli, F.; Taticchi, A. *Dienes in the Diels–Alder reaction;* John Wiley & Sons: Chichester, UK, 1990; p 179.
77. Chang, R. *Physical Chemistry for the Biosciences;* University Science Books: USA, 2005; pp 338–342.
78. Cadogan, J. I. G.; Cameron, D. K.; Gosney, I.; Millar, J. R. A.; Newlands, S. F.; Reed, D. *J. Chem. Soc., Perkin Trans. 2* **1996,** 2309–2317. doi:10.1039/p29960002309
79. Afarinkia, K.; Mahmood, F. *Tetrahedron Lett.* **2000,** *41,* 1287–1290. doi:10.1016/s0040-4039(99)02270-4
80. Lorenzo, J.; Delgado, A.; Montaña, Á. M.; Mesas, J. M.; Alegre, M.-T.; Rodríguez, M. d. C.; Avilés, F.-X. *Eur. J. Med. Chem.* **2014,** *83,* 374–388. doi:10.1016/j.ejmech.2014.06.042
81. Kiss, L.; Nonn, M.; Sillanpää, R.; Haukka, M.; Fustero, S.; Fülöp, F. *Chem. – Asian J.* **2016,** *11,* 3376–3381. doi:10.1002/asia.201601046
82. Das, M.; Du, Y.; Ribeiro, O.; Hariharan, P.; Mortensen, J. S.; Patra, D.; Skiniotis, G.; Loland, C. J.; Guan, L.; Kobilka, B. K.; Byrne, B.; Chae, P. S. *J. Am. Chem. Soc.* **2017,** *139,* 3072–3081. doi:10.1021/jacs.6b11997

7.1.3 Reaktivität verschiedener *N*-Carbonsäureanhydride in einer ringöffnenden Synthese von Polypeptiden

In Kooperation mit den Arbeitsgruppen [redacted] und [redacted] wurden α-substituierte und *N*-methylierte NCAs (αNNCAs) **120** synthetisch dargestellt und unter variierenden ringöffnenden Bedingungen polymerisiert. Es konnte eine Verringerung des Polymerisationsgrades bei der Verwendung von verzweigten Initiator-Molekülen im Vergleich zu linearen Strukturen festgestellt werden. Derselbe Effekt ist ersichtlich, wenn verzweigte Substituenten in α-Position verwendet werden, da die sterische Hinderung der Seitenkette einen starken Einfluss auf den Initiierungsschritt und die erreichbare Kettenlänge besitzt.

Darüber hinaus wurde die Polymerisation von *N*-methylierten und *N*-unsubstituierten NCAs auf Basis von α-Methionin verglichen. Um zu untersuchen, ob ein elektronischer Einfluss vorherrscht, wurden die entsprechenden HOMO-LUMO-Energien auf CC-Level berechnet. Aufgrund der unterschiedlichen Energieniveaus der Grenzorbitale wäre im Fall des *N*-methylierten NCAs **152** (in der Publikation NMMet-NCA) mit einem primären Amin **153** eine höhere Reaktivität zu erwarten. Dieser Trend steht jedoch im Widerspruch zu den beobachteten Reaktivitäten. Da die verringerte Reaktivität keine Folge der energetischen Eigenschaften zu sein scheint, ist die erhöhte sterische Hinderung aller Wahrscheinlichkeit nach der dominierende Effekt für die verringerte Polymerisationskinetik (Abbildung 7.3).[556]

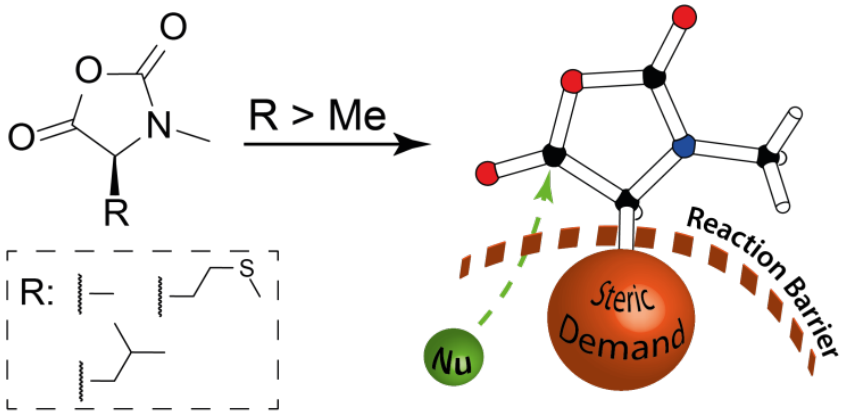

Abbildung 7.3: *Graphical abstract* der Publikation „An insight into the synthesis of *N*-methylated polypeptides“.[556]

Die Synthese der Monomere sowie die darauf aufbauenden Polymerisationsreaktionen wurden von [redacted] und [redacted] durchgeführt. Die quantenmechanischen Berechnungen wurden von J. Groß in Zusammenarbeit mit [redacted], im Rahmen seiner wissenschaftlichen Hilfstätigkeit, durchgeführt. An der Erstellung des Manuskripts waren [redacted], J. Groß, T. Opatz, [redacted] und [redacted] beteiligt.[11]

[11] *Reproduced from C. Muhl, L. Zengerling, J. Groß, P. Eckhardt, T. Opatz, P. Besenius, M. Barz, Polym. Chem., 2020, 11, 6919–6927, with permission from the Royal Society of Chemistry.*

Polymer Chemistry

ROYAL SOCIETY OF CHEMISTRY

PAPER

View Article Online
View Journal | View Issue

Cite this: *Polym. Chem.*, 2020, **11**, 6919

Insight into the synthesis of *N*-methylated polypeptides†

Christian Muhl,‡[a] Lydia Zengerling,‡[a] Jonathan Groß,[a] Paul Eckhardt,[a] Till Opatz,[a] Pol Besenius *[a] and Matthias Barz *[a,b]

Received 23rd July 2020,
Accepted 5th October 2020
DOI: 10.1039/d0py01055c
rsc.li/polymers

The ring-opening polymerization (ROP) of *N*-carboxy anhydrides (NCAs) is mostly divided into two classes: NCAs of α-substituted amino acids and *N*-methylated NCAs of α-unsubstituted glycine derivatives (NNCAs). The use of both monomer types offers different mechanistic features and results in a multitude of functional materials. To combine these properties, the synthesis and ROP of α-substituted and *N*-methylated NCAs (αNNCAs) of several amino acids were investigated. The current study provides insight into the influence of polymerization conditions and the limitations caused by the enhanced steric demand of the amino acid NCA monomers and their *N*-methylated derivatives. Namely, the effects of solvent polarity (DMF and DCM) and steric demand of the initiator by using neopentyl amine (NPA) and *n*-butyl amine (*n*Bu) were studied. Analysis by HFIP-GPC and MALDI-ToF MS reveals that the polymerization and the resulting polymers are tremendously affected by the steric demand of both the initiators and the monomers, while electronic effects seem to have only minor influences. The experimental results are further compared with computational studies, based on coupled cluster (CC) calculations, which underline that electronic effects are of lower importance than steric constraints for the ROP of αNNCAs. Moreover, poly(*N*-methyl-L-methionine) forms helical secondary structures in solution. Therefore, this work combines mechanistic studies of the ROP of αNNCAs with initial studies on the solution properties of these polypeptides.

Introduction

Amino acids and peptides can be modified synthetically in a versatile manner to fulfill a desired function. Besides the incorporation of D-amino acids, cyclic amino acids or dehydroamino acids, the *N*-alkylation of amino acids plays an important role in modulating the solubility, metabolic stability and biological activity.[1,2] The simplest form, *N*-methylation, prevents intramolecular hydrogen bonds and causes changes of conformation, polarity and steric demand. Furthermore, the lipophilicity,[3] membrane permeability[4] and metabolic stability[5] are increased and the proteolytic stability[6] is improved. All these properties make *N*-methylated amino acids interesting building blocks for the synthesis of polypeptides to obtain new biopolymers.

Currently, most of the ongoing research on polypeptides is either focused on the synthesis, characterization and polymerization of α-amino acids,[7,8] *N*-substituted glycine derivatives (polypeptoids)[9,10] and block copolymers thereof (polypept(o)ids),[11–15] but only a few publications have addressed the synthesis and properties of *N*-substituted α-amino acid containing polymers. An example for polypeptoids relies on the use of the naturally occurring *N*-methyl glycine, also known as sarcosine. The corresponding *N*-substituted *N*-carboxy anhydride (NNCA) can be polymerized by nucleophilic ring opening polymerization (ROP) for the synthesis of the highly water-soluble polysarcosine. Due to the absence of the acidic proton at the nitrogen, only the normal amine mechanism (NAM) can occur and thereby well-defined polymers with a low dispersity (D < 1.1) are obtained.[16] The polymerization of NNCAs with longer alkyl chains proceeds slowly (in the order Sar ≫ EtGly > PrGly > *n*BuGly > iBuGly).[10] The reason for lower polymerization rates is the steric hindrance for β-C branched NNCAs and the aggregation of the side chains for linear or γ-C branched NNCAs.[17]

One of the most studied α- and *N*-substituted polypeptides is poly(*N*-methyl-L-alanine), which was first synthesized by a ROP of the corresponding NNCA by Goodman and Fried in 1967.[18] Using conformational energy calculations, CD and NMR techniques, it was shown that this structure adopts a right-handed helix with all-*trans* peptide bonds.[19–21] This polymer could also be synthesized from an activated urethane derivate of *N*-methyl-L-alanine with *in situ* NCA formation by

[a]*Department of Chemistry, Johannes Gutenberg University Mainz, 55099 Mainz, Germany. E-mail: besenius@uni-mainz.de, barz@uni-mainz.de*
[b]*Leiden Academic Center for Drug Research (LACDR), Leiden University, Einsteinweg 55, 2333 CC Leiden, The Netherlands. E-mail: m.barz@lacdr.leidenuniv.nl*
†Electronic supplementary information (ESI) available. CCDC 1976455 and 1976456. For ESI and crystallographic data in CIF or other electronic format see DOI: 10.1039/d0py01055c
‡These authors contributed equally.

View Article Online
Paper Polymer Chemistry

heating in *N*,*N*-dimethylacetamide (DMAc) to 60 °C in the presence of the initiator *n*-butyl amine. The latter method is a phosgene-free synthesis and benefits from the absence of HCl to achieve control over molecular weights through the feed ratio of the monomer to the initiator.[22,23] Cosani *et al.* describe their unsuccessful attempts in the polymerization of *N*-benzylglycine, *N*-benzyl-L-alanine or *N*-methyl-L-phenylalanine NCAs. As an alternative route for the preparation of poly(*N*-methyl-γ-methyl-L-glutamate) and poly(*N*-methyl-γ-ethyl-L-glutamate), they tested different methylation methods on poly(γ-methyl-L-glutamate) or poly(γ-ethyl-L-glutamate).[24] Like poly(*N*-methyl-L-alanine), both polymers were found to form a right-handed helix in a TFE solution of remarkably high stability, which retained their conformation even in pure TFA as observed by CD (circular dichroism) measurements.[25] A special case is the amino acid proline, the only proteinogenic amino acid containing a secondary amine. Poly(L-proline) (PLP) can form a right-handed PLP I helix (*cis*) in aliphatic alcohols and a left-handed PLP II helix (*trans*) in water and organic acids.[26] The synthesis of well-defined PLP was challenging due to the impurity of the monomer and termination reactions in the polymerization. Highly pure NCA monomers can be synthesized from *N*-(Boc)-protected L-proline and were polymerized efficiently using dimethylamine as an initiator.[27]

In this work we describe the synthesis of different α-substituted and *N*-methylated NCAs (αNNCAs) with various side chains. Three synthetic strategies are widely used to prepare *N*-methylated amino acids: reductive amination, *N*-methylation by alkylation and a reductive ring opening of 5-oxazolidinones with a triethylsilane/TFA mixture.[28,29] The latter method introduced by Freidinger *et al.* proceeds without racemization and was therefore chosen to synthesize NMMet and NMLeu in the current work.[30] The polymerization of these αNNCAs strongly depends on the steric demand of the side chain and the resulting electronic structure of the applied monomers. Various conditions for the ROP of the prepared αNNCAs were investigated to study the influence of initiators with different steric demands and solvents with varying polarities. The resulting polymers were analyzed *via* GPC and MALDI-ToF measurements to obtain a deeper insight into the mechanistic pathway of the polymerization. Furthermore, the impact on secondary structure formation was investigated *via* CD spectroscopy and the results were compared with previous studies on these rarely described poly(*N*-alkylated α-substituted amino acids).

Experimental part

Schlenk techniques were used for the reactions with air- and moisture-sensitive reagents or intermediates, performed under an argon atmosphere, using laboratory glassware, and dried under high vacuum at 120 °C with a hot air gun. All the used solvents and reagents were purchased from ACROS Organics (Thermo Scientific GmbH, Nidderau), Alfer Aesar GmbH & Co. KG (Karlsruhe), Carbolution Chemicals GmbH (Saarbrücken), Iris Biotech GmbH (Markredwitz), Merck KGaA (Darmstadt), Sigma-Aldrich Chemie GmbH (Taufkirchen) and TCI Deutschland GmbH (Eschborn). Prior to use, water was demineralized, using PURELAB® flex by Elga. Solvents used for air- or moisture-sensitive reactions were bought anhydrous. DCM was dried using a solvent purification system. All the qualitative thin layer chromatography (TLC) analyses were carried out using silica coated aluminum sheets (60 Å, F_{254}) purchased from MACHEREY-NAGEL GmbH & Co. KG (Düren). The detection of the analytes was performed using UV light (λ = 254 nm) and the detection reagent ninhydrin or $KMnO_4$. Flash chromatography (FC) was performed by using silica gel with an average grain size of 15–40 μm, purchased from ACROS Organics™. Purification *via* medium pressure liquid chromatography (MPLC) was performed on a Sepacore® Easy Purification System (BÜCHI Labortechnik AG) equipped with a UV-Photometer C-640 (BÜCHI) and a Fraction Collector C-660 (BÜCHI). All runs were performed on a CHROMABOND Flash RS 120 C_{18} column (MACHEREY-NAGEL GmbH & Co. KG). Gel permeation chromatography (GPC) was performed with hexafluoroisopropanol (HFIP) containing 3 g L^{-1} potassium trifluoroacetate (KTFA) as an eluent at 40 °C. The column material was modified silica gel (PFG columns, particle size: 7 μm, porosity: 100 Å and 4000 Å), purchased from PSS Polymer Standards Service GmbH. For calibration, polymethyl methacrylate (PMMA, Polymer Standards Services GmbH) was used and toluene was used as the internal standard. A refractive index detector (G1362A RID) and a UV/VIS detector (at 230 nm, Jasco UV-2075 Plus) were used for polymer detection. All mass spectra were recorded on an electrospray ionization spectrometer (ESI) QT of Ultima. MALDI-ToF mass spectra were recorded using a Bruker rapifleX MALDI-ToF mass spectrometer equipped with a 337 nm N_2 laser. Acceleration of the ions was performed with pulsed ion extraction (PIE, Bruker) at a voltage of 20 kV. The analyzer was operated in the reflection mode and the ions were detected using a microchannel plate detector. The mass spectra were processed using the X-TOF 5.1.0 software (Bruker, Billerica, MA, USA). Sample preparation was performed using *trans*-2-[3-(4-*tert*-butylphenyl)-2-methyl-2-propenylidene] malononitrile (DCTB) as the matrix, sodium trifluoroacetate as the cationizing salt, and dichloromethane as the solvent. All NMR spectra were recorded on a BRUKER Avance II 400 spectrometer and the measurements were carried out in deuterated solvents ($CDCl_3$, DMSO-d_6, and D_2O). All the recorded NMR spectra were analyzed using MestReNova v12.0.0. CD spectroscopy was performed on a Jasco J-815 spectrometer at 20 °C. The spectra were analyzed using Spectra Manager 2.0. All spectra were recorded using a quartz cell with a path length of 1 mm at a concentration of c = 0.25 g L^{-1} polymer in HFIP. θ_{MR} was calculated from the following equation:

$$\theta_{MR} = \frac{\theta \cdot M_{\text{repeating unit}}}{10 c_M \cdot l} [^\circ \text{cm}^2 \text{dmol}^{-1}]$$

with $M_{\text{repeating unit}}$ = 147.1 g mol^{-1}, c_M = 0.25 g L^{-1} and l = 0.1 cm. All measurements of optical rotation were carried out

with a PerkinElmer 241 polarimeter at 589 nm. A quartz glass cuvette with a path length of 10 cm was used.

Synthesis of *N*-methyl-L-methionine NCA (NMMet-NCA)

For the synthesis of NMMet-NCA, 2.0 g (10.2 mmol, 1 eq.) of the corresponding amino acid was suspended in 150 mL of freshly distilled, anhydrous THF. Diphosgene (0.97 mL, 8 mmol, 0.8 eq.) was added at room temperature at once to the stirred suspension. After 15 min, the turbid solution became clear and was further stirred at room temperature for 30 min, before N_2 was bubbled through the solution for 10 min. The solution was cooled with an ice bath and dry TEA (7.1 mL, 51.1 mmol, 5.1 eq.) was added slowly while precipitation occurred (TEA·HCl). After filtration under a N_2 atmosphere, THF was removed under high vacuum and the residue was dissolved again in a minimum amount of dry ethyl acetate. The ethyl acetate solution was added to a mixture of dry *n*-hexane and diethyl ether (1 : 1) and stored at −20 °C overnight. This resulted in the crystallization of the corresponding NCA, which was filtered under a N_2 atmosphere and dried to yield 1.4 g (7.3 mmol, 72%). Crystal structure: CCDC 1976455;† ^{1}H-NMR (400 MHz, $CDCl_3$) δ [ppm] = 4.29 (dd, ^3J = 3.6, 3.2 Hz, 1H, –CH–), 3.00 (s, 3H, –NC$\underline{H}_3$), 2.67–2.51 (m, 2H, –C$\underline{H}_2$SCH$_3$), 2.32–2.23 (m, 1H, –C$\underline{H}_2$CH$_2$SCH$_3$), 2.18–2.13 (m, 1H, –C$\underline{H}_2$CH$_2$SCH$_3$), 2.11 (s, 3H, –SCH$_3$); ^{13}C-NMR (101 MHz, $CDCl_3$): δ [ppm] = 168.64 (–COO), 152.13 (–CNOO), 59.82 (–CHN–), 28.86 (–N$\underline{C}$H$_3$), 28.43 (–SCH$_2$), 27.94 (–SCH$_2$C$\underline{H}_2$–), 15.56 (–SCH$_3$).

Synthesis of *N*-methyl-DL-methionine NCA (DL-NMMet-NCA)

The synthesis of DL-NMMet-NCA is analogous to the synthesis of NMMet-NCA. After the crystallization of the NCA, the solution was decanted in order to separate the crystallized NCA from the residual solvent. The NCA could not be collected *via* filtration, since the melting point of the crystals was below room temperature (20 °C). After decanting, the crystals melted and the resulting colorless and clear oil (yield: 64 mg, 0.3 mmol, 67%) was dried under reduced pressure to remove trace solvents. The oil was then characterized and used for polymerization. ^{1}H-NMR (400 MHz, $CDCl_3$) δ [ppm] = 4.29 (dd, ^3J = 3.6, 3.2 Hz, 1H, –CH–), 3.00 (s, 3H, –NCH$_3$), 2.67–2.51 (m, 2H, –C$\underline{H}_2$SCH$_3$), 2.32–2.23 (m, 1H, –C$\underline{H}_2$CH$_2$SCH$_3$), 2.18–2.13 (m, 1H, –C$\underline{H}_2$CH$_2$SCH$_3$), 2.11 (s, 3H, –SCH$_3$).

Synthesis of *N*-methyl-DL-alanine NCA (NMAla-NCA)

N-Methyl-DL-alanine (1.70 g, 16.5 mmol, 1 eq.) was suspended in 100 mL of anhydrous THF. After the addition of diphosgene (1.59 mL, 13.2 mmol, 0.8 eq.), the suspension was stirred at room temperature for 1.5 hours until it became clear. N_2 was bubbled through the solution for 15 min and THF was removed *in vacuo*. The residue was dissolved again in 20 mL of anhydrous THF and added to 200 mL of *n*-hexane. After storage at −20 °C overnight, NMAla-NCA (1.10 g, 8.2 mmol, 51%) crystallized and was collected *via* filtration under a N_2 atmosphere and dried. Crystal structure: CCDC 1976456;† ^{1}H-NMR (400 MHz, $CDCl_3$) δ [ppm] = 4.19 (q, ^3J = 7.0 Hz, 1H, –CH–), 2.98 (s, 3H, –NCH$_3$), 1.54 (d, ^3J = 7.0 Hz, 3H, –CH$_3$); ^{13}C-NMR (101 MHz, $CDCl_3$): δ [ppm] = 169.42 (–COO), 151.73 (–CNOO), 57.00 (–CHN–), 28.37 (–N$\underline{C}$H$_3$), 15.19 (–CH$\underline{C}$H$_3$).

Synthesis of *N*-methyl-L-leucine NCA (NMLeu-NCA)

N-Methyl-L-leucine (0.60 g, 3.7 mmol, 1 eq.) was suspended in 75 mL of anhydrous THF. After the addition of 1.9 mL phosgene in toluene (20% phosgene in toluene, 4 mmol, 1.1 eq.), the suspension was stirred at room temperature for 15 min until it became clear. Due to the incomplete reaction (reaction control was performed *via* ^{1}H-NMR), TEA (1.1 mL, 8 mmol, 2 eq.) was added to the cooled solution in order to convert *N*-carbamoyl chloride to the corresponding NCA. The formed precipitate (TEA·HCl) was filtered under a N_2 atmosphere and THF was removed under reduced pressure from the clear, colorless solution. The residual oil could neither be crystallized nor precipitated and therefore the colorless oil was characterized and used for polymerization (NMLeu-NCA: 0.30 g, 1.7 mmol, 46%). ^{1}H-NMR (400 MHz, $CDCl_3$) δ [ppm] = 4.14 (t, ^3J = 5.6 Hz, 1H, –CH–), 2.99 (s, 3H, –NCH$_3$), 1.93 (dsep, ^3J = 6.6, 1.2 Hz, 1H, –C$\underline{H}$(CH$_3$)$_2$), 1.78 (dd, ^3J = 5.7, 2.2 Hz, 2H, –C$\underline{H}_2$CH(CH$_3$)$_2$), 0.98 (dd, ^3J = 6.7, 1.1 Hz, 6H, –CH(C$\underline{H}_3$)$_2$); ^{13}C-NMR (101 MHz, $CDCl_3$): δ [ppm] = 168.66 (–COO), 151.94 (–CNOO), 59.47 (–CHN–), 37.86 (–$\underline{C}$H$_2$CH(CH$_3$)$_2$), 28.56 (–N$\underline{C}$H$_3$), 24.00 (–CH$_2$$\underline{C}$H(CH$_3$)$_2$), 22.86 (–CH($\underline{C}H_3$)$_2$), 21.98 (–CH($\underline{C}H_3$)$_2$).

Ring-opening polymerization of αNNCAs

In the following, the procedure is described exemplarily for the polymerization of NMAla-NCA, but it can be extended to all other αNNCAs.

NMAla-NCA (78.9 mg, 0.61 mmol, 50 eq.) was transferred into a Schlenk tube under a dry nitrogen counter flow. Dry DMF (0.9 mL) and absolute *n*-butylamine (1.21 μL, 0.89 mg, 0.01 mmol, 1 eq.) in dry DMF were added using a stock solution. A steady flow of dry nitrogen was sustained during the polymerization, preventing any impurities from entering the Schlenk tube, while ensuring the escape of the produced CO_2. The progress of the polymerization was monitored *via* IR spectroscopy by the decreasing intensities of the NCA-associated carbonyl peaks at 1858 and 1788 cm^{-1}. Samples were taken using a nitrogen flushed syringe through a septum. If no conversion was observed after 16 h, equimolar amounts (relative to the initiator) of triethyl amine (TEA) in DMF were added, using a stock solution. The polymer precipitated after complete conversion in a mixture of cold diethyl ether and *n*-hexane (2 : 1). The suspension was centrifuged (3000 rpm, 10 min, 0–5 °C) and decanted. This procedure was repeated three times yielding poly(*N*-methyl-DL-alanine) (45 mg, 71%) as a colorless solid.

Results and discussion

The synthesis of αNNCAs starts with the synthesis of the corresponding amino acids. *N*-methyl-L-methionine and

N-methyl-L-leucine were prepared *via* a reductive ring-opening reaction using the corresponding Fmoc-protected 5-oxazolidinone according to literature procedures[30,31] and in the last step the Fmoc-protecing group was removed. *N*-Methyl-DL-alanine was synthesized starting from 2-bromopropanoic acid and methylamine.[32] The synthesis of α-substituted and *N*-methylated *N*-carboxy anhydrides (αNNCAs) was performed by suspending the corresponding *N*-methylated amino acids in dry THF and adding diphosgene at room temperature (Fig. 1A). After the suspension became clear, it was cooled down with an ice bath and anhydrous TEA was added slowly to precipitate the formed HCl, followed by filtration. In the case of *N*-methyl-L-leucine (NMLeu-NCA), addition of TEA was essential for ring closure, due to the reduced reactivity of the intermediate *N*-carbamoyl chloride.

THF was removed under reduced pressure and the crude product was dissolved in a minimum amount of dry ethyl acetate. Addition of an excess amount of the *n*-hexane/diethyl ether mixture (1 : 1 by volume) caused the precipitation of αNNCAs, which could be collected by filtration under an inert atmosphere. The dried αNNCAs were characterized *via* ^{1}H-NMR spectroscopy (Fig. 1B–D). In addition, a small amount of each αNNCA was crystallized for characterization by X-ray diffraction. Crystal structures were obtained for all samples except for the *N*-methyl-L-leucine NCA, for which we were unable to obtain suitable crystals. In the next step, the ring-opening polymerization of the prepared αNNCAs (Fig. 2A) was carried out under various conditions, which are presented in Table 1.

Monomer conversion could be monitored by FT-IR spectroscopy, since the intensities of the carbonyl vibration bands at 1786 and 1854 cm^{-1} are directly related to the remaining NCA concentration. Only the ROP of the *N*-methyl-DL-alanine NCA (NMAla-NCA) could be carried out to full conversion without the addition of a tertiary amine, whereas the polymerization of *N*-methyl-(D)L-methionine (NMMet-NCA, DL-NMMet-NCA) and NMLeu-NCA required equimolar amounts of a base (relative to the initiator) until initiation could be detected and reached full conversion after several days.

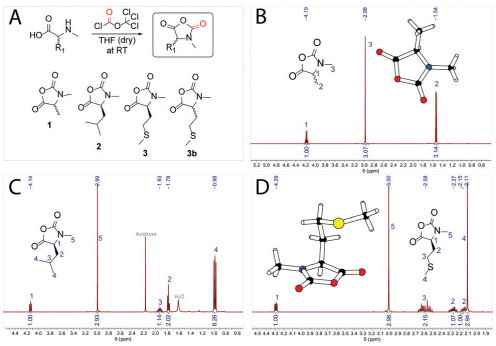

Fig. 1 Synthetic route for the preparation of α-substituted and *N*-methylated *N*-carboxy anhydrides (structures **1**, **2**, **3** and **3b**) using the Fuchs–Farthing method[33,34] (A). ^{1}H-NMR spectra of *N*-methyl-DL-alanine NCA (NMAla-NCA) (B), *N*-methyl-L-leucine NCA (NMLeu-NCA) (C) and *N*-methyl-L-methionine NCA (NMMet-NCA) (D) in $CDCl_3$. Crystal structures *via* X-ray diffraction of NMAla-NCA and NMMet-NCA are illustrated in the corresponding NMR spectra.

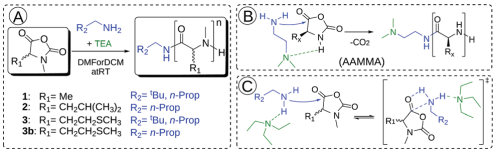

Fig. 2 Polymerization of αNNCAs **1**, **2**, **3** and **3b** in DMF (DCM) using different initiators (*n*-butyl amine and neopentyl amine) (A). Proposed accelerated amine mechanism through monomer activation (AAMMA) (B). Proposed mechanism for initiator activation caused by the added tertiary amine (TEA) (C).[35]

Table 1 Conditions for the ROP of αNNCAs. The used solvent, initiators and monomer to initiator ratios (M/I). In cases where no conversion was observed after 12 h (no detectable change of αNNCA related carbonyl peaks in the FT-IR spectrum), an anhydrous base (tertiary amine) was added in equimolar amounts relative to the initiator

Sample	Solvent	Initiator	M/I	Added base
NMAla-P1	DMF	NPA	25	—
NMAla-P2	DMF	NPA	50	—
NMAla-P3	DMF	*n*Bu	50	—
NMLeu-P1	DMF	*n*Bu	50	TEA
NMMet-P1	DMF	NPA	50	DIPEA
NMMet-P2	DMF	NPA + DABCO	25	—
NMMet-P3	DMF	*n*Bu	25	TEA
NMMet-P4	DCM	NPA	50	TEA
DL-NMMet-P1	DMF	*n*Bu	25	TEA

Complete conversion was confirmed by FT-IR spectroscopy and is exemplarily shown with NMAla-P1 in Fig. S1.† Due to this observation, the possible protonation of the initiator by residual HCl was tested by the reaction with silver nitrate solution ($AgNO_3$). Therefore, all the used monomers, initiators and solvents were treated separately in relevant concentrations with $AgNO_3$ solution. Since all samples showed no precipitation of AgCl, the residual HCl content could be neglected. Recently, Hadjichristidis and co-workers proposed the accelerated amine mechanism through monomer activation (AAMMA) for the ROP of NCAs, which is a combination of the normal amine mechanism (NAM) and the activated monomer mechanism (AMM) (Fig. 2B). They observed increased reaction kinetics by the use of initiators having primary and tertiary amines.[35] However, monomer activation like in AMM or AAMMA is not possible for αNNCAs, due to *N*-methylation. Therefore, it is most likely that addition of a tertiary amine enhances only the reactivity of the attacking nucleophile due to coordination effects (Fig. 2C).[36] In this regard, a possible reduced reactivity caused by the steric hindrance of the initiator was investigated in more detail. Both neopentyl

amine and the less bulky *n*-butyl amine showed no reaction with the *N*-methylated NCAs of D,L-methionine and L-leucine, unless equimolar amounts of TEA, DIPEA or DABCO were added to the polymerization system.

However, steric demand in general seems to be a critical factor for the ROP of αNNCAs, since NMAla-NCA could be initiated by both NPA and *n*Bu, without the need for tertiary amine addition. Therefore, polymerization was carried out under various conditions and the resulting polymers were analyzed *via* HFIP-GPC (Fig. 3). The HFIP-GPC traces of NMAla-P1 to P3 showed an overall elution volume that is higher than expected when compared to NPA initiated polysarcosine (pSar) with a degree of polymerization (DP) of 50. Due to the same monomer to initiator ratios (M/I = 50) used for the polymerizations of NMAla-NCA and Sar-NCA together with comparable solubility in HFIP, the elution volumes were expected to be similar. Therefore, the discrepancy between elugrams is caused by differences in the DP of the samples NMAla-P1 to P3.

This means that a methyl group in the α-position is already decreasing the polymerization efficiency if a methyl substituent on the N atom is also present. In addition, the use of the less bulky *n*-butyl amine as the initiator leads to an increased degree of polymerization compared to initiation by neopentyl amine, when using similar M/I ratios. However, the steric demand of the side chain in the α-position has a stronger impact on the polymerization compared to the initiator itself. The GPC analysis of NMLeu-P1 leads to the suggestion that the polymerization of NMLeu-NCA is tremendously hampered and only results in the production of low molecular weight oligomers. The multiple shoulders at lower elution volumes with decreasing intensities can be explained by the presence of different oligomers. The GPC results underline the reduced reactivity of the β-C branched NMLeu-NCA towards a nucleophilic attack of a primary amine. For further analysis, the samples NMAla-P1 and P3 were characterized *via* MALDI-ToF mass spectrometry (Fig. 4). The average DPs were determined relative to the most intensive peak and resulted in $X_{n,MALDI}$(NMAla-P1) = 16 and $X_{n,MALDI}$(NMAla-P3) = 29. Both spectra showed additional polymer distributions caused by water initiation, which is especially pronounced in the spectrum of NMAla-P1. In this case, initiation by traces of water seems to be more effective than initiation by neopentyl amine, given the higher intensity of water-initiation associated peaks compared to peaks resulting from NPA-initiation. If the less bulky *n*-butyl amine is used as an initiator, the H_2O-initiation related peaks decrease in intensity. These effects can also be observed in the NMR spectra of NMAla-P1 (Fig. S2†) and NMAla-P3 (Fig. S3†). The different amounts of the water initiated polymer lead to a higher discrepancy between the used M/I ratio and the DP determined *via* end group analysis by NMR at NMAla-P1 and a less pronounced discrepancy at NMAla-P3. The discrepancy is due to a reduction in the intensity for the initiator NMR signal compared to the polymer backbone NMR signal, caused by water initiation.

MALDI-ToF analysis thus clearly reveals that NMAla-NCA polymerization can be initiated by a primary amine, but the

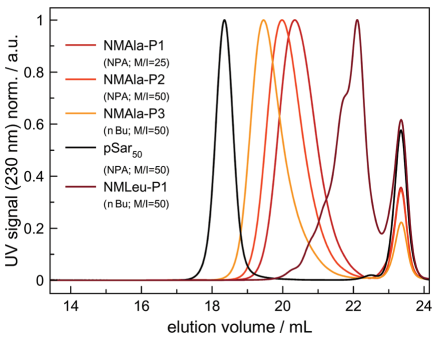

Fig. 3 HFIP-GPC elugrams of NMAla-P1 to P3, NMLeu-P1 and polysarcosine for reference. For all the samples, toluene was used as the internal standard (peak at 23.4 mL) and polymerizations were carried out in anhydrous DMF.

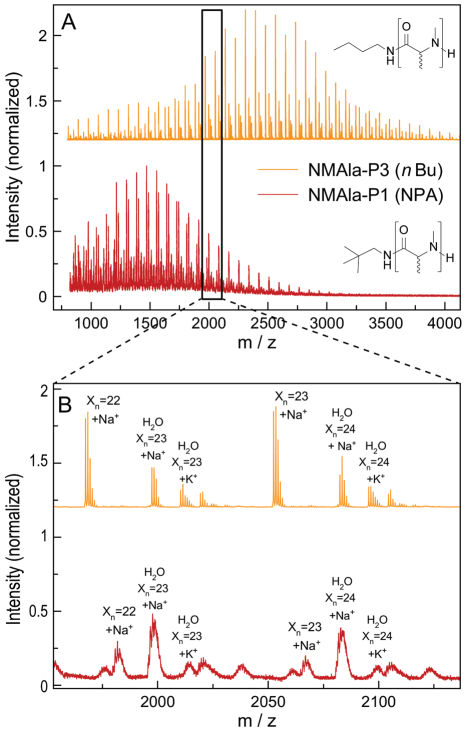

Fig. 4 Full MALDI-ToF spectra of NMAla-P1 (red) and NMAla-P3 (orange) (A) and the corresponding magnifications (B) with assignment of the individual peaks.

polymerization still suffers from the enhanced steric demand of the NCA monomer. The use of less bulky initiators helps to improve the initiation step, but does not seem to overcome the reduced reactivity towards a nucleophilic attack due to the high steric demand of the monomer. Our findings regarding the preparation of poly(*N*-methyl-DL-alanine) are in line with the results reported by Endo *et al.*[23] They also obtained polymers with lower DPs as calculated from the initiator to monomer ratio, although they used a different approach for the preparation of the polypeptoids. In their protocol, the NCA was formed *in situ*, which can also contribute to the observed reduced degrees of polymerization, because impurities are not removed and could thus interfere with the polymerization.

To get a deeper insight into how the side chain influences the polymerization rate, the ROP of NMMet-NCA was performed under various conditions. The resulting polymers were characterized by HFIP-GPC (see Fig. 5). In all cases, the HFIP-GPC elugrams show the same trend as already observed for the NMAla-based experiments. A comparison of the *N*-methylated derivatives with the unmethylated derivatives of poly-L-methionine reveals that all polymerizations resulted in lower molecular weights as expected based on the monomer to initiator ratio. In analogy to the ROP of NMAla-NCA, the use of the less bulky initiator *n*-butyl amine slightly improved the obtained degrees of polymerization, but in contrast the addition of a tertiary amine was needed for the efficient initiation of NMMet-NCA. Note that the polymerization of NMMet-NCA proceeds significantly better than the ROP of NMLeu-NCA (see Fig. 3, red-brown curve), even though the side chains at the α-position are of comparable steric demand.

Very recently, Ling and co-workers have shown in a detailed DFT study that linear and γ-C branched *N*-substituents lead to similar reaction barriers, regarding the calculated Gibbs free energies for nucleophile addition.[17] Given the observed differences in polymerization efficiency between NMLeu-NCA and NMMet-NCA, we conclude that branching in the side chains of α-substituted and *N*-methylated αNNCAs decreases the carbonyl reactivity much more compared to branching in the aliphatic side chains of *N*-alkylated and α-unsubstituted NCAs.

For additional insights, the samples NMMet-P1 to NMMet-P3 were analyzed by MALDI-ToF and the comparison of all three is shown in Fig. 6. In the mass spectra of NMMet-P1 and P2, most peaks are related to initiation by water. This trend could already be observed in the MALDI-ToF spectrum of NMAla-P1 (Fig. 4) and shows again that the steric demand of NPA presumably causes inefficient initiation. In comparison, initiation by the less bulky *n*-butyl amine yields polymers with a higher molecular mass, detectable by MALDI-ToF (Fig. 6) and HFIP-GPC (Fig. 5). The DP assignment of NMMet-P3 was performed using the most intense, initiator related peak and resulted in $X_{n,\mathrm{MALDI}}$ (NMMet-P3) = 8. This value has to be taken with caution though, since the mass spectrum is biased towards lower *m*/*z* ratios, due to a considerable mass discrimination effect.[37]

To further support our findings and validate our explanation, coupled cluster (CC) calculations of the LUMO (lowest unoccupied molecular orbital) energies at the DLPNO-CCSD(T) level of theory with the cc-pVDZ basis set were performed to check for a possible electronic influence of the *N*-methyl substituents but the results were inconclusive. The CC method was chosen over DFT because the former allows a comparison of the calculated single point energies of different molecules and also delivers highly accurate results.[38,39] In Fig. 7 the calculated frontier orbitals of NMMet-NCA, Met-NCA and ethylamine are illustrated and also the relative energy of the individual orbitals is provided.

Based on the Klopman–Salem theory, an interaction is favored if the related orbitals are similar in geometry and energy level.[40,41] Based on the differences in frontier orbital energy levels, a higher reactivity would be expected in the case of NMMet-NCA with a primary amine, since the LUMO of NMMet-NCA has a smaller energy difference to the HOMO of ethyl amine ($|\Delta E|$ = 14.10 eV) compared to the LUMO of Met-NCAQ7($|\Delta E|$ = 14.31 eV. However, this trend disagrees with the

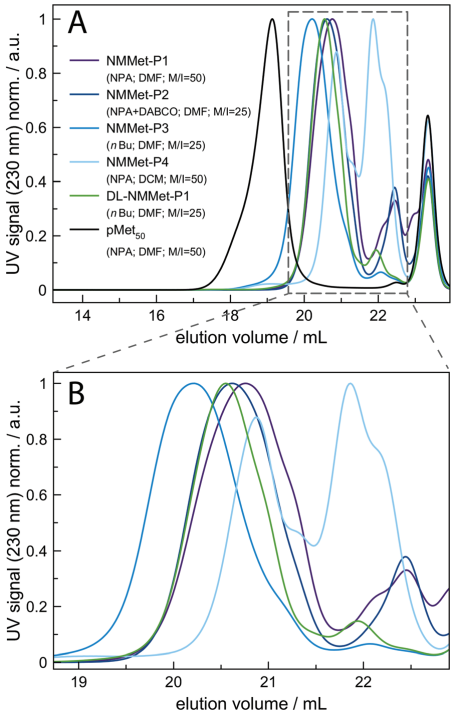

Fig. 5 HFIP-GPC elugrams of NMMet-P1 to P4, DL-NMMet-P1 and poly-L-methionine for reference (A). For a better overview of the NMMet samples, the elution volume between 19 and 23 mL is magnified (B). For all the samples, toluene was used as the internal standard (peak at 23.4 mL). Bottom: Full MALDI-ToF spectra of NMMet-P1 (lower, purple), NMMet-P2 (middle, dark blue) and NMMet-P3 (upper, light blue) (A) and the corresponding magnifications (B) with assignment of the individual peaks.

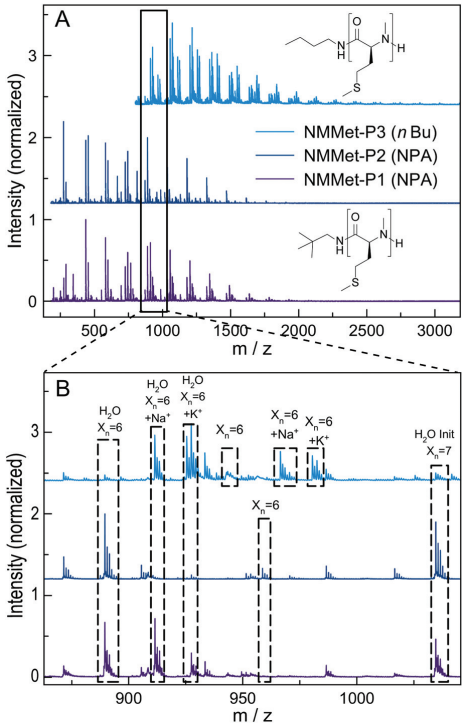

Fig. 6 Full MALDI-ToF spectra of NMMet-P1 (lower, purple), NMMet-P2 (middle, dark blue) and NMMet-P3 (upper, light blue) (A) and the corresponding magnifications (B) with assignment of the individual peaks.

observed reactivities of the NCAs. Since the reduced reactivity does not seem to be a consequence of energetic properties, we conclude that the increased steric hindrance dominates and is the decisive factor for the decreased polymerization kinetics upon the *N*-methylation of α-substituted NCAs. The results presented so far, generated by experimental observations and GPC and MALDI-ToF analyses, showed decreased polymerization efficiency and lower degrees of polymerizations with increasing steric demand of the initiator and the substituents in the α-position of the applied NCA monomer. The reduced reactivity is also reflected in the need for the addition of a base (TEA) in order to start and promote the polymerization. These findings can be related exclusively to an enhanced steric hindrance, since an energetic contribution could be excluded by the comparison of the involved frontier orbitals, which were calculated using CC.

Besides differences in the polymerization rates, we also expected differences in the solution properties between polypeptides and poly(*N*-methylated α-amino acids), because *N*-methylation is known to suppress the formation of secondary structures of polypeptides due to the lack of intramolecular hydrogen bonding. However, hydrophobic side chains are still

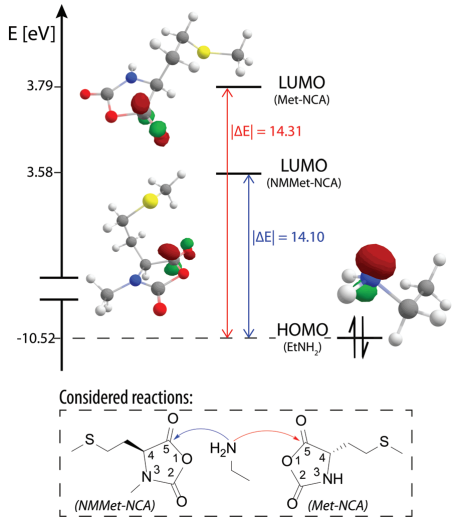

Fig. 7 Frontier orbitals of NMMet-NCA (LUMO), Met-NCA (LUMO) and ethylamine (HOMO) and the corresponding relative energies, calculated using coupled clusters (CC: DLPNO-CCSD(T)/cc-pVDZ).

present and can contribute to interactions of the individual chain segments and domains. The use of enantiopure monomers may therefore lead to secondary structure formation, which can be seen in the CD spectrum of NMMet-P3 (Fig. 8).

The CD pattern of NMMet-P3 in HFIP shows a broad symmetric negative band at 226 nm and a positive band at 195 nm. The results have strong similarities to previous studies by Cosani *et al.* where they observed similar values (min(θ_{MR}) = 228 nm; max(θ_{MR}) = 196 nm) for poly(*N*-methyl-γ-methyl-L-glutamate) and poly(*N*-methyl-γ-ethyl-L-glutamate) in TFE.[25] Along with conformational studies on poly(*N*-methyl-L-alanine), carried out by Goodman *et al.*, the authors proposed a right-handed helix as the secondary structure.[18] Despite a small blue shift of 1–2 nm for both bands (positive

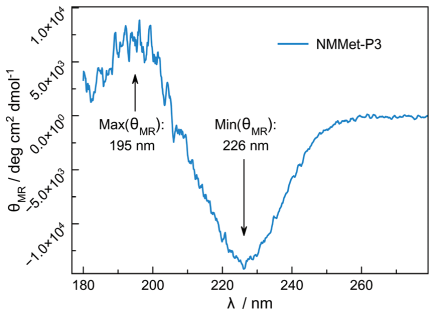

Fig. 8 CD spectrum of NMMet-P3 in HFIP (c = 0.25 g L^{-1}).

and negative), our observations match the results obtained by Cosani *et al.* Therefore, it is most likely that poly(*N*-methyl-L-methionine) also forms a helical secondary structure. Since *N*-methylation entails the loss of H-bond formation, the resulting structure has an increased hydrophobic character. The use of polar solvents, like DMF, could in consequence cause the formation of hydrophobic domains, due to insufficient solubilization of the polymer chains. In this regard, the polymerization of NMMet-NCA was further carried out in DCM to examine the influence of the solvent on the reaction properties. As can be seen in Fig. 4 (turquoise curve), the use of a less polar solvent, compared to DMF, has no benefit on the resulting polymerization and instead causes a bimodal distribution in HFIP-GPC.

Conclusions

In the present work, the influence of *N*-methylation on the polymerization properties of α-substituted *N*-carboxy anhydrides (NCAs) was investigated. To this end, different α-substituted and *N*-methylated NCAs (αNNCAs) were prepared and polymerized under various conditions. Next to the increasingly popular NCA polymerization of *N*-methylated glycine (sarcosine), and few reports using *N*-methylated alanine, we were intrigued that a strategy to polymerize αNNCAs had not been reported. We were able to demonstrate that the steric demand of both the initiator and side chain of the monomer has a major impact on the achievable degree of polymerization of the resulting polymer. The steric hindrance of the side chain in the α-position of the monomer is recognized as the major contribution to the low reactivity towards a nucleophilic attack by an amine. This strongly influences the initiation step of the polymerization and achievable chain lengths. Using the less bulky *n*-butyl amine compared to neopentyl amine resulted in more efficient initiation and propagation. Polymerization also benefitted from a heteroatom with free electron pairs in the side chain of the αNNCA, as shown with *N*-methyl-L-methionine. On the other hand, solvent polarity did not seem to influence the polymerization of αNNCAs. Moreover, the synthesized poly(*N*-methyl-α-amino acids) tend to form helical secondary structures in solution, which is in agreement with previously reported investigations using poly(*N*-methyl-L-alanine).

Conflicts of interest

There are no conflicts to declare.

Acknowledgements

We thank O. Stach for his help with the synthesis of *N*-methyl-L-methionine, Dr D. Schollmeyer for X-ray crystal structure analysis and S. Türk for MALDI-ToF MS measurements. Parts of this research were conducted using the supercomputer Mogon and/or advisory services offered by Johannes Gutenberg University Mainz (hpc.uni-mainz.de), which is a member of the AHRP (Alliance for High Performance Computing in Rhineland Palatinate, http://www.ahrp.info) and the Gauss Alliance e.V. The authors gratefully acknowledge the computing time granted on the supercomputer Mogon at Johannes Gutenberg University Mainz (hpc.uni-mainz.de). L. Z. acknowledges the financial support from the Evonik Foundation (Werner Schwarze Scholarship). C. M., P. B., T. O., and M. B. would like to thank the German Research Foundation (DFG) for financial support (CRC 1066-2).

Notes and references

1 J. Chatterjee, F. Rechenmacher and H. Kessler, *Angew. Chem., Int. Ed.*, 2013, **52**, 254–269.
2 A. Sharma, A. Kumar, S. A. H. Abdel Monaim, Y. E. Jad, A. El-Faham, B. G. de la Torre and F. Albericio, *Biopolymers*, 2018, **109**, e23110.
3 E. Biron, J. Chatterjee, O. Ovadia, D. Langenegger, J. Brueggen, D. Hoyer, H. A. Schmid, R. Jelinek, C. Gilon, A. Hoffman and H. Kessler, *Angew. Chem., Int. Ed.*, 2008, **47**, 2595–2599.
4 P. P. Bose, U. Chatterjee, I. Hubatsch, P. Artursson, T. Govender, H. G. Kruger, M. Bergh, J. Johansson and P. I. Arvidsson, *Bioorg. Med. Chem.*, 2010, **18**, 5896–5902.
5 Q. G. Dong, Y. Zhang, M. S. Wang, J. Feng, H. H. Zhang, Y. G. Wu, T. J. Gu, X. H. Yu, C. L. Jiang, Y. Chen, W. Li and W. Kong, *Amino Acids*, 2012, **43**, 2431–2441.
6 S. Sagan, P. Karoyan, O. Lequin, G. Chassaing and S. Lavielle, *Curr. Med. Chem.*, 2012, **11**, 2799–2822.
7 Z. Song, Z. Tan and J. Cheng, *Macromolecules*, 2019, **52**, 8521–8539.
8 A. Rasines Mazo, S. Allison-Logan, F. Karimi, N. J. A. Chan, W. Qiu, W. Duan, N. M. O'Brien-Simpson and G. G. Qiao, *Chem. Soc. Rev.*, 2020, **49**, 4737–4834.
9 B. A. Chan, S. Xuan, A. Li, J. M. Simpson, G. L. Sternhagen, T. Yu, O. A. Darvish, N. Jiang and D. Zhang, *Biopolymers*, 2017, 1–25.
10 C. Fetsch, A. Grossmann, L. Holz, J. F. Nawroth and R. Luxenhofer, *Macromolecules*, 2011, **44**, 6746–6758.
11 J. Sun and R. N. Zuckermann, *ACS Nano*, 2013, **7**, 4715–4732.
12 R. Luxenhofer, C. Fetsch and A. Grossmann, *J. Polym. Sci., Part A: Polym. Chem.*, 2013, **51**, 2731–2752.
13 K. Klinker and M. Barz, *Macromol. Rapid Commun.*, 2015, **36**, 1943–1957.
14 Z. Song, Z. Han, S. Lv, C. Chen, L. Chen, L. Yin and J. Cheng, *Chem. Soc. Rev.*, 2017, **46**, 6570–6599.
15 C. Bonduelle, *Polym. Chem.*, 2018, **9**, 1517–1529.
16 M. Sisido, Y. Imanishi and T. Higashimura, *Makromol. Chem.*, 1977, **178**, 3107–3114.
17 T. Bai and J. Ling, *Biopolymers*, 2019, **110**, e23261.
18 M. Goodman and M. Fried, *J. Am. Chem. Soc.*, 1967, **89**, 1264–1267.
19 J. E. Markt and M. Goodman, *Biopolymers*, 1967, **5**, 809–814.

20 M. Goodman, F. Chen and F. R. Prince, *Biopolymers*, 1973, **12**, 2549–2561.
21 A. M. Liquori and P. De Santis, *Biopolymers*, 1967, **5**, 815–820.
22 S. Yamada, K. Koga, A. Sudo, M. Goto and T. Endo, *J. Polym. Sci., Part A: Polym. Chem.*, 2013, **51**, 3726–3731.
23 Y. Shiraki, S. Yamada and T. Endo, *J. Polym. Sci., Part A: Polym. Chem.*, 2017, **55**, 1674–1679.
24 A. Cosani, M. Palumbo, M. Terbojevich and E. Peggion, *Macromolecules*, 1978, **11**, 1041–1045.
25 A. Cosani, M. Terbojevich, M. Palumbo, E. Peggion and M. Goodman, *Macromolecules*, 1979, **12**, 875–877.
26 I. Z. Steinberg, W. F. Harrington, A. Berger, M. Sela and E. Katchalski, *J. Am. Chem. Soc.*, 1960, **82**, 5263–5279.
27 M. Gkikas, H. Iatrou, N. S. Thomaidis, P. Alexandridis and N. Hadjichristidis, *Biomacromolecules*, 2011, **12**, 2396–2406.
28 L. Aurelio, R. T. C. Brownlee and A. B. Hughes, *Chem. Rev.*, 2004, **104**, 5823–5846.
29 M. L. Di Gioia, A. Leggio, F. Malagrinò, E. Romio, C. Siciliano and A. Liguori, *Mini-Rev. Med. Chem.*, 2016, **16**, 683–690.
30 R. M. Freidinger, J. S. Hinkle, D. S. Perlow and B. H. Arison, *J. Org. Chem.*, 1983, **48**, 77–81.
31 L. Aurelio, J. S. Box, R. T. C. Brownlee, A. B. Hughes and M. M. Sleebs, *J. Org. Chem.*, 2003, **68**, 2652–2667.
32 J. Etxabe, J. Izquierdo, A. Landa, M. Oiarbide and C. Palomo, *Angew. Chem., Int. Ed.*, 2015, **54**, 6883–6886.
33 A. C. Farthing, *J. Chem. Soc.*, 1950, 3213–3217.
34 C. J. Brown, D. Coleman and A. C. Farthing, *Nature*, 1949, **163**, 834–835.
35 W. Zhao, Y. Gnanou and N. Hadjichristidis, *Chem. Commun.*, 2015, **51**, 3663–3666.
36 J. Liu and J. Ling, *J. Phys. Chem. A*, 2015, **119**, 7070–7074.
37 K. Martin, J. Spickermann, H. J. Räder, K. Müllen and J. Grotemeyer, *Rapid Commun. Mass Spectrom.*, 1996, **10**, 1471–1474.
38 C. Riplinger, B. Sandhoefer, A. Hansen and F. Neese, *J. Chem. Phys.*, 2013, **139**, 134101.
39 D. G. Liakos, Y. Guo and F. Neese, *J. Phys. Chem. A*, 2020, **124**, 90–100.
40 L. Salem, *J. Am. Chem. Soc.*, 1968, **90**, 543–552.
41 T. Koopmans, *Physica*, 1934, **1**, 104–113.

7.1.4 Bestimmung des Substituenteneinflusses bei der photochemischen Dehydrierung von N-Heterozyklen

In der Arbeitsgruppe Opatz wurde eine Methode zur photochemischen Dehydrierung von N-Heterozyklen **123** (in der Publikation **1a**–**t**) untersucht und die optimierten Bedingungen erfolgreich auf 27 Substrate mit Ausbeuten von 17 bis zu 89% angewendet. Die entwickelte Methode kann sowohl für Pyridinon- und Chinolon-Strukturen (in der Publikation **2a**–**t**) verwendet werden als auch zur Darstellung von Azocinonen (in der Publikation **12a**–**e**) in einem Eintopf-Verfahren mit Acetylendiestern (in der Publikation **11a** und **b**). Durch die Verwendung von Sauerstoff als terminales Oxidationsmittel und sichtbarem Licht in Verbindung mit Rhodamin 6G als organischer Photokatalysator zeichnet sich die Reaktion durch eine hohe Umweltfreundlichkeit und eine hohe Kosteneffizienz aus.

Zur Untersuchung des Substituenteneinflusses am Stickstoffatom wurden Geometrieoptimierungen unterschiedlich substituierter Dihydropyridinone **154**, **155** und **156** (in der Publikation **2a**, **2w** und **2x**) auf DFT-Level durchgeführt. Im Gleichgewichtszustand wurde an *ortho*-substituierten Aryl-Gruppen eine Drehung des aromatischen Rings im Vergleich zu einem Phenylsubstituenten festgestellt. Aus dieser Rotation resultiert ein geringerer Orbitalüberlapp des π-Systems mit dem freien Elektronenpaar des Stickstoffatoms, wodurch die Oxidation mittels Einelektronentransfer (*single electron transfer*, SET) auf den Photokatalysator erschwert und somit die ausbleibende Reaktivität unter den gewählten Reaktionsbedingungen erklärt (Abbildung 7.4).[557]

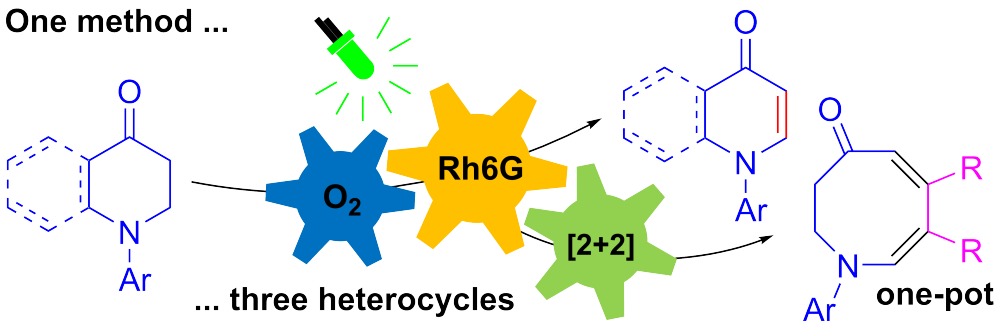

Abbildung 7.4: *Graphical abstract* der Publikation „Synthesis of 2,3-Dihydro-4-pyridones, 4-Quinolones, and 2,3-Dihydro-4-azocinones by Visible-Light Photocatalytic Aerobic Dehydrogenation“.[557]

Alle synthetischen Experimente wurden von [redacted] und [redacted] durchgeführt. Die DFT-Berechnungen wurden von J. Groß durchgeführt und das Manuskript von [redacted], J. Groß und T. Opatz erstellt.[12]

[12] *Reprinted with permission from A. Sevenich, P. S. Mark, T. Behrendt, J. Groß, T. Opatz, Eur. J. Org. Chem. 2020, 1505–1514, Copyright ©2019 WILEY-VCH Verlag GmbH & Co. KGaA, Weinheim,*

ChemPubSoc Europe
DOI: 10.1002/ejoc.201900584
EurJOC European Journal of Organic Chemistry
Full Paper
Check for updates

Photoredox Catalysis | *Very Important Paper* | SPECIAL ISSUE

VIP

Synthesis of 2,3-Dihydro-4-pyridones, 4-Quinolones, and 2,3-Dihydro-4-azocinones by Visible-Light Photocatalytic Aerobic Dehydrogenation

Adrian Sevenich,[a] Paulina Sophie Mark,[a] Torsten Behrendt,[a] Jonathan Groß,[a] and Till Opatz*[a]

Abstract: The synthesis of 2,3-dihydro-4-pyridones and 4-quinolones was realized by visible-light mediated photoredox-catalyzed aerobic dehydrogenation of 4-piperidones and 2,3-dihydro-4-quinolones. This method enables the synthesis of cyclic enaminones in up to 89 % yield under mild and eco-friendly conditions and with a high tolerance of functional groups using oxygen as an inexpensive terminal oxidant and rhodamine 6G as a readily available organic photocatalyst. The process can be extended to access 2,3-dihydro-4-azocinones in up to 62 % yield via a [2+2] cycloaddition/ring-expansion sequence in a telescoping one-pot reaction. Hence, a protocol for the synthesis of three different types of N-heterocycles was developed on the same general transformation.

Introduction

Owing to the vinylogous transposition of the reactivity of the amine nitrogen and the carbonyl group, enaminones show a versatile reactivity pattern.[1] Their simple cyclic representatives such as 2,3-dihydro-4-pyridines are attractive building blocks and can e.g. be used as precursors for piperidine-based target molecules.[2] Consequently, they have been applied as building blocks for drugs[3] or for alkaloid natural products such as indolizidines and quinolizidines.[1a,2a,2c,4] In addition, they represent key structures in drug candidates like peptidomimetic opioids,[5] flavivirus inhibitors[6] and antibacterial oxazolidinones.[7] Their benzo-fused relatives, the 4-quinolones, are one of the largest class of antimicrobial agents[8] and have recently attracted further attention due to their antitumor and anti-HIV activity.[8b,8c,9]

Dehydrogenation has been used as a direct strategy to access cyclic enaminones since preformed heterocycles can serve as the starting materials.[2c,3c,10] To this end, multistep procedures based on the Polonovski reaction[10a,10d,10g] or the Saegusa oxidation[7a,10m] have been used extensively. Among the one-step procedures, $Hg(OAc)_2$[10b,10f,10k] and DDQ[10e,10i,10n] have been applied by various groups. Nicolaou et al. found complexes of IBX and various amine *N*-oxides to enable the reaction under mild condition.[10h,10j,10r] However, these procedures generally suffer from lengthy sequences, the use of expensive or ecologically problematic reagents or catalysts and, most notably, stoichiometric amounts of oxidants being required to effect the dehydrogenation. First achievements to replace stoichiometric reagents by oxygen as terminal oxidant have been reported by Stahl et al. who proposed a $Pd(DMSO)_2(TFA)_2$ catalyst which enables the dehydrogenation of cyclic ketones (Scheme 1).[10l] The group of Mizuno found a heterogeneous catalyst system consisting of gold nanoparticles supported on manganese oxide to perform the aerobic dehydrogenation of β-heteroatom-substituted ketones.[10p] Recently, a photoredox catalyzed approach was reported by Jiang et al. using the non-commercial dicyanopyrazine chromophore (DPZ) as a photocatalyst in combination with oxygen to obtain 2,3-dihydro-4-pyridones and 4-quinolones on a limited scale.[10o]

Photoredox catalysis through organic dyes has proven to be a valuable and often eco-friendly tool for performing a large variety of selective transformations on amines under mild conditions,[11] which were also investigated in our labs.[12] It was therefore attempted to overcome the drawbacks of above-mentioned protocols for the synthesis of cyclic enaminones using an inexpensive commercially available organic dye as catalyst and oxygen as a sustainable, no-waste oxidant.

Partially saturated azocines have recently attracted attention due to their occurrence in natural products such as the manzamine alkaloids[13] and their various biological activities,[13a,14] for example against leishmaniasis.[13a] To access this interesting group of eight-membered N-heterocycles, ring-expansion has become a common strategy which can e.g. be initiated by [2+2] cycloaddition of acetylene esters and cyclic enamine containing structures.[14a,15] In this context, it appeared possible to combine the photocatalytic dehydrogenation step with a subsequent light-independent reaction like a [2+2] cycloaddition ultimately leading to ring-expansion. This would provide a direct access to eight-membered N-heterocycles from a completely

[a] *Institute of Organic Chemistry, Johannes Gutenberg University, Duesbergweg 10-14, 55128 Mainz, Germany*
E-mail: opatz@uni-mainz.de
https://ak-opatz.chemie.uni-mainz.de/
Supporting information and ORCID(s) from the author(s) for this article are available on the WWW under https://doi.org/10.1002/ejoc.201900584.

ChemPubSoc Europe
EurJOC European Journal of Organic Chemistry
Full Paper

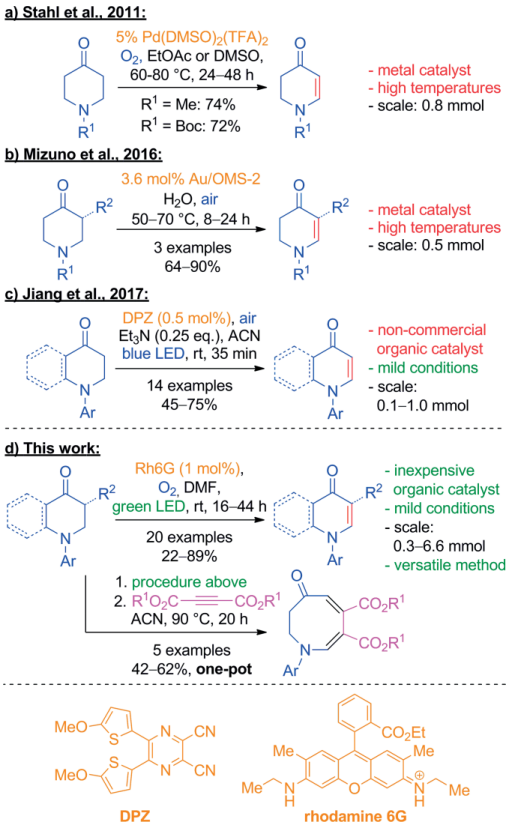

Scheme 1. Overview of catalytic one-step syntheses of cyclic enaminones by aerobic dehydrogenation.

saturated six-membered nitrogen containing precursor via the intermediate enaminone.

Here, we describe the synthesis of cyclic enaminones like 2,3-dihydro-4-pyridones and 4-quinolones by visible light-mediated aerobic dehydrogenation and exploited their reactivity to provide access to another class of N-heterocycles, namely 2,3-dihydro-4-azocinones in a one-pot reaction.

Results and Discussion

We started our optimization studies in terms of reaction yield by evaluating various xanthene dyes which have commonly been used for amine oxidations.[11b,11h,12a] Interestingly, the most frequently used catalysts rose bengal (RB, **5**) and eosin Y (EY, **4**) gave no clean reactions ,(Table 1, entries 2 and 3). Although the starting material was consumed very rapidly, the product yield remained always moderate, at both low and high conversion, indicating that **2** might not be stable under these conditions. Indeed, the C=C bond cleavage of enamines and enaminones under visible light catalyzed aerobic conditions using RB and EY is well documented.[16] Even though there have been debates as to whether or not singlet oxygen is involved in this reaction,[16c] it is obvious that these conditions are not suitable and overcoming this issue would be a key challenge for the outlined approach. The low yields of **2** observed using RB and EY are in agreement with the observations by Jiang and may have prompted them to use a non-commercial dye.[10o] Gratifyingly, fluorescein (**3**) and rhodamine 6G (**7**) gave the product **2** in satisfactory yields, with **7** being slightly superior (entry 5). Further evaluation of different solvents (entries 6 to 11) revealed DMF to be the best choice.

Table 1. Optimization studies for the photocatalytic dehydrogenation.[a]

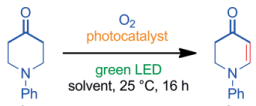

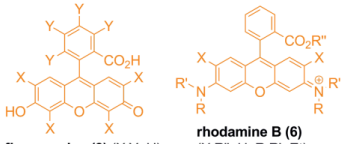

fluoresceine (3) (X,Y=H)
eosin Y (4) (X=Br, Y=H)
rose bengal (5) (X=I, Y=Cl)

rhodamine B (6) (X,R''=H, R,R'=Et)
rhodamine 6G (7) (X=Me, R'=H, R,R''=Et)

Entry	Cat. [mol-%]	Solvent	**1a** [%][b]	**2a** [%][b]
1	3 (5)	DMF	< 1	58[c]
2	5 (5)	DMF	< 1	36
3	4 (5)	DMF	< 1	49
4	6 (5)	DMF	13	53
5	7 (5)	DMF	15	61
6	7 (5)	DMSO	58	21
7	7 (5)	MeOH	96	2
8	7 (5)	DCM	42	35
9	7 (5)	PhMe	85	9
10	7 (5)	ACN	37	42
11	7 (5)	THF	15	49
12	7 (5)	DMF	65	24[d]
13	7 (10)	DMF	29	47
14	7 (2)	DMF	10	66
15	7 (1.5)	DMF	< 1	72
16	7 (1)	DMF	< 1	77 (70)[e]
17	7 (0.5)	DMF	4	68
18	7 (0.1)	DMF	7	59
19	–	DMF	96	0
20	7 (1)	DMF	98	0[f]
21	7 (1)	DMF	96	0[g]

[a] Reaction conditions: **1a** (0.3 mmol), 1 mL of dry solvent, RGB LED stripe (≈ 80 W) on green. [b] Yield determined by ^{1}H-NMR using 1,4-bis(trimethylsilyl)benzene as internal standard. [c] RGB LED stripe (≈ 80 W) on blue. [d] Air was used instead of oxygen. [e] Isolated yield in brackets. [f] In the dark. [g] Argon instead of oxygen atmosphere.

Replacement of oxygen by air led to reduced conversion showing that a fast catalyst quenching is vital for fast reaction kinetics. Variation of the catalyst loading (entries 13 to 18) showed a faster reaction at lower catalyst loading, with 1 mol-% as the optimum (entry 16). Most probably, at higher catalyst loading, light absorption is limited to a very small volume close to the surface of the vial and collision of excited catalyst with

ChemPubSoc Europe
EurJOC European Journal of Organic Chemistry
Full Paper

substrate molecules during the lifetime of the excited state is less likely. Further decreasing the catalyst loading resulted in a slightly decreased yield and conversion but a still satisfactory yield of 59 % was achieved with only 0.1 mol-% catalyst (entry 18), which is in good agreement with previous observations of organic dyes in part being highly efficient at even low catalyst loadings.[12a] In the absence of catalyst, light or oxygen the starting material remained untouched (entry 19 to 21). Various additives, light sources or variations of oxygen delivery were also taken into account in our studies but did not produce better results in terms of product yield or reaction time (see SI for further screenings).

With the improved reaction conditions, the scope of this reaction was evaluated (Scheme 2). A variety of functional groups were tolerated and moderate to high yields (**2b**, **2d**–**e**, **2j**–**l**, **2s**) could be achieved with electron donating and withdrawing

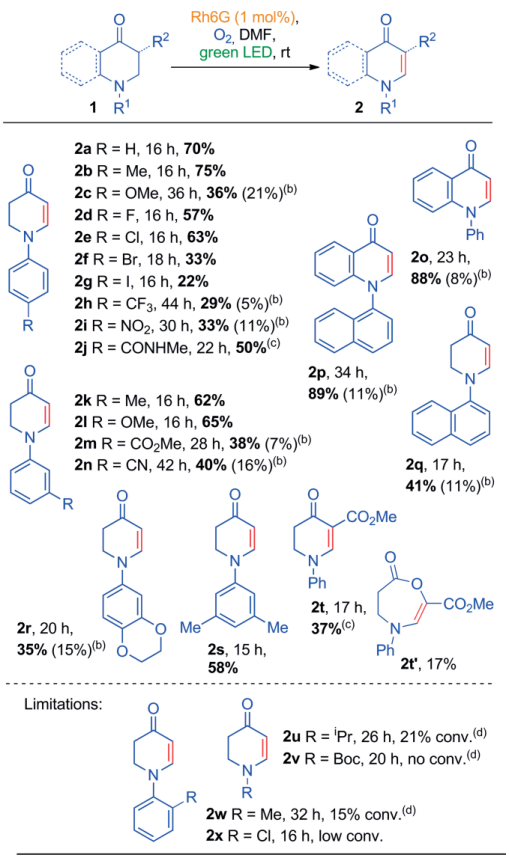

Scheme 2. Scope of cyclic enaminones by photocatalytic dehydrogenation. [a] Reaction conditions: **1** (0.3 mmol), 1 mL of dry solvent, **7** (1 mol-%), 1 atm O_2, RGB LED stripe (≈ 80 W) on green, 25 °C. [b] Yield of recovered starting material. [c] No extraction performed due to high polarity of product. [d] As judged by ^{1}H-NMR.

groups such as Me, OMe, F, Cl, or CONHMe. Strongly electron withdrawing groups like CF_3 and NO_2 led to increased reaction times and lower yields (**2h**, **2i**). Even Br- and I-substituents were tolerated, although partial halogen transfer with formation of dihalogenated species was observed (**2f**, **2g**). In the case of the 3-carboxy substituted starting material, product **2t** was formed as the sole regioisomer. The moderate yield can be partly explained by the formation of **2t′** as a by-product, most probably caused by a Bayer–Villiger reaction of **2t** with H_2O_2 generated in the course of the reaction. At prolonged reaction times, overoxidation to 4-pyridons and oxidative cleavage of the enaminone's C=C bond (vide supra) were frequently observed as side reactions of various substrates. The yields of 4-quinolones (**2o**, **2p**) were generally higher and in the range of 90 %, which can be explained by increased product stability and fewer possibilities of side reactions such as over-oxidation. In addition, they provide better stabilization of the intermediates **9** and **10** (Scheme 3) which seem to be crucial for a rapid and clean reaction. On the other hand, *N*-alkyl substituents devoid of any stabilizing effect (**2u**) gave only unsatisfactory conversions, presumably due to the lower HOMO energy of the unconjugated nitrogen lone pair. The same was observed with *ortho*-substituents (**2w**, **2x**) which force the aromatic ring out of conjugation with the lone pair, leading to decreased orbital overlap according to DFT calculations (see the supporting information). *N*-1-naphthyl substituents are however tolerated in the reaction (**2p**, **2q**).

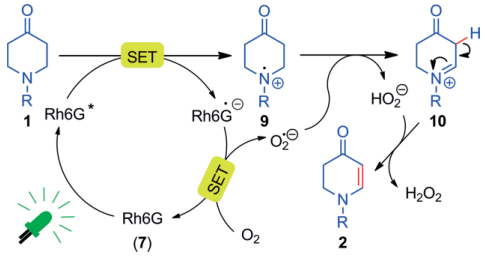

Scheme 3. Plausible reaction mechanism.

A plausible reaction mechanism is depicted in Scheme 3. After absorption of light, the catalyst **7** can react with substrate **1** to furnish the amine radical cation **9** by single electron transfer (SET). Upon reaction with molecular oxygen through a second SET step, the catalyst **7** is recycled leading to formation of a superoxide radical anion capable of abstracting a hydrogen atom from **9**.[17] By these means, the hydroperoxide anion and iminium ion **10** is formed, the latter undergoes rapid deprotonation to the more stable enaminone **2** furnishing hydrogen peroxide as a by-product.

To demonstrate the synthetic value of this protocol, the reaction was performed on a gram scale (Scheme 4). For this purpose, a steady stream of oxygen was slowly bubbled through the solution to ensure sufficient availability of the oxidant. Besides an increase in reaction time, the dehydrogenation of **1a** proceeded smoothly to give the enaminone **2a** in 60 % isolated yield.

ChemPubSoc Europe
EurJOC European Journal of Organic Chemistry
Full Paper

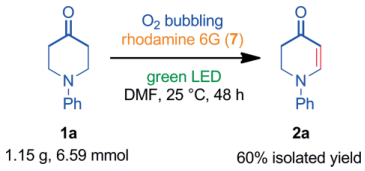

Scheme 4. Gram-scale synthesis of **2a**.

With ample amounts of the cyclic enaminone **2** in hand, the [2+2] cycloaddition/ring-expansion sequence was to be optimized and the applicability of the photoredox-catalyzed dehydrogenation to the synthesis of azocinone derivatives had to be demonstrated (Table 2). The studies were begun using a modified protocol of the microwave-assisted cycloaddition of DMAD (**11a**) reported by the Stanovnik laboratory.[15b] With the aim to develop a one-pot reaction, rhodamine 6G (**7**) and DMF were added to all screening reactions to imitate the conditions after the dehydrogenation step. Indeed, the cycloaddition went smoothly to yield directly the eight-membered heterocycle **12a**.

Table 2. Optimization studies for the photocatalytic dehydrogenation.[a]

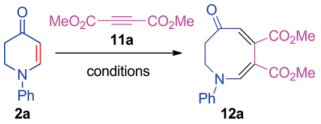

Entry	Co-solvent	Temp. [°C]	Time [h]	**2a** [%][b]	**12a** [%][b]
1	DMF	120	2	3	67
2	DCM	120	2	26	49
3	PhMe	120	2	25	53
4	ACN	120	2	4	74
5	ACN	150	1.5	3	68
6	ACN	105	6	12	79
7	ACN	90	17	7	88 (85)[c]
8	ACN	90	20	n.d.	(62)[c,d]

[a] Reaction conditions: **2a** (0.3 mmol), **7** (1 mol-%), 1 mL of DMF, 1 mL of co-solvent, **11a** (3.0 equiv.), sealed vessel, microwave irradiation. [b] Yield determined by ^{1}H-NMR using 1,4-bis(trimethylsilyl)benzene as internal standard, n.d. = not determined. [c] Isolated yields in brackets. Oil bath instead of microwave heating. [d] One-pot reaction starting from **1a**.

A short screening of co-solvents (entries 1 to 4) revealed acetonitrile to be the best choice of this group. Next, the reaction temperature was investigated. At higher temperature, the reaction was faster but a decrease in yield was observed (entry 5). Gradually decreasing the temperature led to longer reaction times but significantly increased yields. Finally, the best results were obtained when the reaction mixture was simply heated in an oil bath overnight (entry 7). In the end, a telescoped one-pot reaction starting from **1a** was performed proving the possibility to access eight-membered N-heterocycles **12** directly from piperidones **1** (entry 8).

The scope of the one-pot synthesis of azocinones **12** from piperidones **1** and acetylene dicarboxylates **11** is displayed in Scheme 5. The reaction gave a variety of 2,3-dihydro-4-azocinones in synthetically useful yields (**12a**–**e**). It appeared tempting to investigate simple acetylenic esters **11c** and **11d** in the one-pot reaction of **1a**, but no conversion took place even at 120 °C and the enaminone **2a** was the only product isolated in both cases. Apparently, only very electron deficient acetylenes do react with **2**. Furthermore, we wondered whether benzo[*b*]azocinone **12f** could be obtained by reacting **1o** with **11a** in this sequence but again, only the 4-quinolone **2o** could be isolated. This observation might be explained by the high stability and hence low reactivity of the 4-quinolone **2o** so that no cycloaddition takes place. A plausible mechanism of the cycloaddition/ring-expansion sequence is illustrated in Scheme 6. [2+2] cycloaddition of acetylene ester **11** and enaminone **2** furnish cyclobutene intermediate **13**. The cycloaddition can be either concerted (path a) or stepwise (path b).[15b] There had been some debate about the ring opening mechanism of *cis*-bicyclo[4.2.0]oct-7-ene-intermediates such as **13**.[18] The isolation of *cis*,*cis*-products in almost all cases has led to the assumption that ring opening may occur in a disrotatory fashion, which would violate the Woodward-Hoffmann rules. However, some studies have shown that *trans*,*cis*-products can be obtained under carefully controlled and mild reaction conditions.[18c,18d] Recent studies based on computational calculation revealed the conrotatory ring opening, followed by isomerization to be the most likely pathway.[18f] To determine the geometry of double bonds in **12a**, $^3J_{C\text{-}H}$ coupling constants between the methine protons and corresponding carbons were measured by CLIP-HSQMBC[19] and compared to literature values. Usually a *cis*-arrangement between C and H results in smaller values than in the case of a *trans*-arrangement (see Figure S2 in the SI).[20] From the measured values, the (2*E*,4*E*)-geometry was rationalized for **12a** which is consistent with the geometry of similar compounds.[15b,18e] Although none of the intermediates **14** have been observed, we assume the mechanism to proceed by

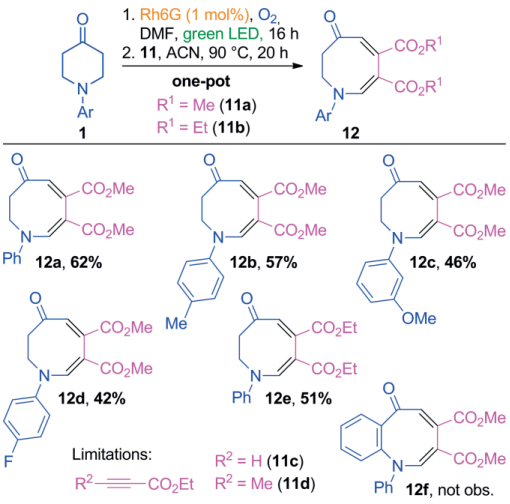

Scheme 5. Scope of the one-pot synthesis of azocine-derivatives from piperidones. Reaction conditions: **1** (0.3 mmol), 1 mL of dry DMF, **7** (1 mol-%), 1 atm O_2, RGB LED stripe (≈ 80 W) on green, 25 °C, then: 1 mL of co-solvent, **11** (3.0 equiv.), 90 °C, oil bath.

ChemPubSoc Europe

EurJOC European Journal of Organic Chemistry
Full Paper

a conrotatory electrocyclic ring opening of **13**. The isomerization to **12** in the cause of the reaction should be promoted by the push-pull character of intermediate **14**. The same geometry of **12** was obtained, when the reaction was performed either in a one-pot fashion starting from **1a** or from isolated **2a**, which shows that product geometry was not affected by any by-product from the previous dehydrogenation step, such as H_2O_2.

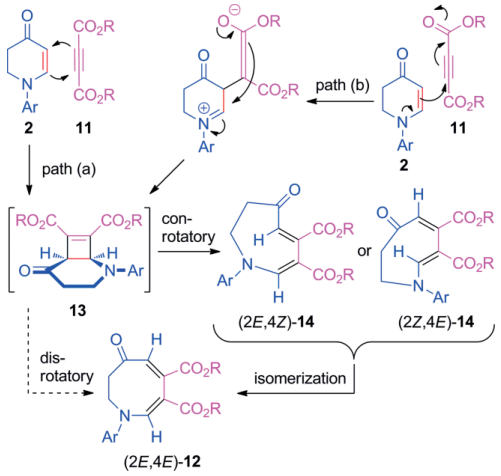

Scheme 6. Plausible mechanism of the cycloaddition/ring-expansion sequence.

Conclusions

In summary, a mild and environmentally benign protocol for the synthesis of 2,3-dihydro-4-pyridones and 4-quinolones by means of visible-light mediated dehydrogenation using oxygen as a terminal oxidant and inexpensive rhodamine 6G as photocatalyst was developed. To the best of our knowledge, there is currently no cheaper and more sustainable way to effect this transformation. The reported method tolerates a variety of functional groups and was successfully performed on a gram scale. In addition, it can be extended to access azocinones in a simple one-pot procedure. This versatile protocol could find application in the synthesis of natural products and drug precursors. Overcoming the necessity of *N*-aryl groups would make this method even more versatile and could eventually provide a general method to convert Mannich products into enaminones. Furthermore, better control of oxygen supply to increase efficiency and to avoid over-oxidation, potentially by means of flow chemistry, will remain a challenge for further investigations.

Experimental Section

General Information: All chemicals were obtained from commercial suppliers and used without purification unless stated otherwise. Anhydrous DCM was distilled from calcium hydride under nitrogen. Anhydrous toluene and THF were distilled from sodium/benzophenone under nitrogen. Extra dry DMF, ACN, MeOH and DMSO were purchased from Acros Organics (AcroSeal®). The eluents for column chromatography *c*Hex and EtOAc were purchased in technical grade and distilled prior to use. [D]Chloroform was stored over sodium sulfate and alumina (Brockmann activity I). Chromatographic purification was performed on silica gel (35–70 µm, Acros Organics). Automated flash chromatography was performed on an Isolera™ Flash Purification System (Biotage) with an integrated diode array detector using SNAP KP-Sil cartridges. TLC was carried out on silica plates (TLC Silica 60 F254 by Merck). NMR spectra were recorded on a Bruker Avance-III HD (^{1}H-NMR: 300 MHz, ^{13}C-NMR: 75.5 MHz), a Bruker Avance-II (^{1}H-NMR: 400 MHz, ^{13}C-NMR: 100.6 MHz) or a Bruker Avance-III (^{1}H-NMR: 600 MHz, ^{13}C-NMR: 151.1 MHz) spectrometer. Chemical shifts are referenced to residual solvent signals ($CDCl_3$: 7.26 ppm and 77.16 ppm, [D_6]DMSO: 2.50 ppm and 39.52 ppm for ^{1}H-NMR and ^{13}C-NMR respectively) and reported relative to TMS. IR spectra were recorded on a FTIR-spectrometer (Bruker Tensor 27) with a diamond ATR unit and are reported in terms of frequency of absorption $\tilde{\nu}$ [cm^{-1}]. ESI mass spectra were recorded on a 1200-series HPLC-system or a 1260-series Infinity II HPLC-system (Agilent-Technologies) with binary pump and integrated diode array detector coupled to a LC/MSD-Trap-XTC-mass spectrometer (Agilent-Technologies) or a LC/MSD Infinitylab LC/MSD (G6125B LC/MSD). HRMS spectra were recorded on a Micromass-Q-TOF-Ultima-3-mass spectrometer (Waters) with LockSpray-interface and a suitable external calibrant. Melting points were determined in open capillary tubes using a Krüss-Optronic KSP 1 N thermoelectric melting point meter. Reactions accelerated by microwave heating were performed in a Discover monomode apparatus from CEM in glass vials sealed with septa under constant temperature.

Compounds **1a–f**, **1h–i**, **1k–n**, **1q–s**,[21] **1i**,[22] **1o**,[23] **1p**,[23] and **1t**[24] were prepared by known procedures and their spectroscopic data are in accordance to those reported in the literature. Compounds **1u** and **1v** were obtained from commercial suppliers. Compound **1g**, **1j**, **1w** and **1x**[21] were prepared by known procedures but have not been characterized yet.

1-(4-Iodophenyl)piperidin-4-one (1g): Yield: 64.9 %, yellow solid; R_f = 0.39 (*c*Hex/EtOAc = 3:1); mp: 98.1–100.2 °C; ^{1}H-NMR, COSY (400 MHz, [D]Chloroform) δ = 7.57–7.52 (m, 2H, H3′, H5′), 6.75–6.71 (m, 2H, H2′, H6′), 3.58 (t, *J* = 6.1 Hz, 4H, H2, H6), 2.53 (t, *J* = 6.1 Hz, 4H, H3, H5); ^{13}C-NMR, HSQC, HMBC (101 MHz, [D]Chloroform) δ = 207.75 (C4), 148.80 (C1′), 138.24 (C3′, C5′), 117.89 (C2′, C6′), 81.47 (C4′), 48.40 (C2, C6), 40.59 (C3, C5). IR: $\tilde{\nu}$ = $\tilde{\nu}$ = 2824, 1716, 1583, 1490, 1381, 1357, 1315, 1221, 1086, 989, 808; ESI-MS: 302.1 (100 %) $[M + H]^+$; HRMS (ESI): *m/z* = 302.0034 ($[M + H]^+$, calcd. 302.0036).

***N*-Methyl-4-(4-oxopiperidin-1-yl)benzamide (1j):** Yield: 61.4 %, yellow solid; R_f = 0.25 (100 % EtOAc); mp: 134.6–137.6 °C; ^{1}H-NMR, COSY (400 MHz, [D]Chloroform) δ = 7.74–7.69 (m, 2H, H3′, H5′), 6.93–6.88 (m, 2H, H2′, H6′), 6.30–6.17 (m, 1H, N*H*), 3.69 (t, *J* = 6.1 Hz, 4H, H2, H6), 2.97 (d, *J* = 4.8 Hz, 3H, CH_3), 2.54 (t, *J* = 6.1 Hz, 4H, H3, H5); ^{13}C-NMR, HSQC, HMBC (101 MHz, [D]Chloroform) 207.65 (C4), 167.80 (CONH), 151.03 (C1′), 128.73 (C3′, C5′), 124.67 (C4′), 113.94 (C2′, C6′), 47.28 (C2, C6), 40.46 (C3, C5), 26.86 (CH_3). IR: $\tilde{\nu}$ = 3336, 2968, 2901, 1712, 1606, 1551, 1509, 1387, 1358, 1297, 1219, 768; ESI-MS: 233.2 (100 %) $[M + H]^+$, 255.2 (38.5 %) $[M + Na]^+$, 487.4 (20.9 %) $[2M + Na]^+$; HRMS (ESI): *m/z* = 233.1282 ($[M + H]^+$, calcd. 233.1285).

1-(*o*-Tolyl)piperidin-4-one (1w): Yield: 70.4 %, yellow solid; R_f = 0.21 (*c*Hex/EtOAc = 20:1); mp: 66.9–68.7 °C; ^{1}H-NMR, COSY

ChemPubSoc Europe

EurJOC European Journal of Organic Chemistry
Full Paper

(400 MHz, [D]Chloroform) δ = 7.25–7.21 (m, 1H, H3′), 7.21–7.16 (m, 1H, H5′), 7.06–7.01 (m, 2H, H4′, H6′), 3.22 (t, J = 6.1 Hz, 4H, H2, H6), 2.61 (t, J = 6.1 Hz, 4H, H3, H5), 2.40 (s, 3H, CH_3); ^{13}C-NMR, HSQC, HMBC (101 MHz, [D]Chloroform) δ = 208.75 (C4), 150.81 (C1′), 132.72 (C2′), 131.25 (C3′), 126.74 (C5′), 123.89 (C4′), 119.48 (C6′), 52.11 (C2, C6), 42.28 (C3, C5), 17.94 (CH_3); ESI-MS: 190.2 (100 %) [M + H]$^+$; HRMS (ESI): m/z = 190.1225 ([M + H]$^+$, calcd. 190.1226).

1-(2-Chlorophenyl)piperidin-4-one (1x): Yield: 31.7 %, colorless solid; R_f = 0.50 (*c*Hex/EtOAc = 3:1); mp: 83.1–83.5 °C; ^{1}H-NMR, COSY (400 MHz, [D]Chloroform) δ = 7.40 (dd, J = 7.9, 1.5 Hz, 1H, H3′), 7.23 (ddd, J = 8.0, 7.3, 1.5 Hz, 1H, H5′), 7.06 (dd, J = 8.0, 1.5 Hz, 1H, H6′), 7.04–6.99 (m, 1H, H4′), 3.34 (t, J = 6.1 Hz, 4H, H2, H6), 2.64 (t, J = 6.1 Hz, 4H, H3, H5); ^{13}C-NMR, HSQC, HMBC (101 MHz, [D]Chloroform) δ = 208.52 (C4), 148.66 (C1′), 130.79 (C3′), 129.06 (C2′), 127.74 (C5′), 124.38 (C4′), 120.90 (C6′), 51.49 (C2, C6), 42.02 (C3, C5). IR: $\tilde{\nu}$ = 2816, 1716, 1588, 1481, 1379, 1311, 1209, 1958, 1039, 756; ESI-MS: 210.1 (100 %) [M + H]$^+$, 212.1 (43.0 %) [M + H]$^+$; HRMS (ESI): m/z = 210.0680 ([M + H]$^+$, calcd. 210.0680).

General Procedure for the Photoredox-catalyzed Aerobic Dehydrogenation: A 10 mL glass vial was charged with the 4-piperidone or 2,3-dihydro-4-quinolone **1** (0.300 mmol, 1.00 equiv.), rhodamine 6G (**7**) (0.003 mmol, 1 mol-%) and anhydrous DMF (1.00 mL). The vial was sealed with a rubber septum and the mixture was stirred until rhodamine 6G was completely dissolved. The reaction vessel was flushed with oxygen for 2 minutes and placed inside a flask, covered with LED stripes (see SI for irradiation setup). The mixture was stirred under irradiation with green LED stripes, until the starting material **1** was almost consumed completely (as judged by TLC or LC-MS analysis). Water was added and the mixture was extracted with Et_2O to remove most of the DMF. For **2j** and **2t** the extraction step was skipped due to the high polarity of these compounds. The organic phases were combined and the solvent was removed in vacuo. The crude product was purified by automated flash column chromatography (SiO_2, *c*Hex/EtOAc).

1-Phenyl-2,3-dihydropyridin-4(1*H*)-one (2a): Yield: 36.4 mg, 0.210 mmol, 70 %, orange solid; R_f = 0.24 (*c*Hex/EtOAc = 2:3); mp: 89–90 °C; ^{1}H-NMR, COSY (400 MHz, [D]Chloroform) δ = 7.44 (d, J = 7.8 Hz, 1H, H6), 7.43–7.33 (m, 2H, H3′, H5′), 7.20–7.10 (m, 1H, H4′), 7.12–7.07 (m, 2H, H2′, H6′), 5.22 (d, J = 7.8 Hz, 1H, H5), 4.00 (t, J = 8.1 Hz, 2H, H2), 2.65 (t, J = 8.1 Hz, 2H, H3); ^{13}C-NMR, HSQC, HMBC (101 MHz, [D]Chloroform) δ = 192.04 (C4), 149.71 (C6), 145.23 (C1′), 129.74 (C3′, C5′), 124.47 (C4′), 118.29 (C2′, C6′), 102.17 (C5), 47.66 (C2), 36.05 (C3). IR: $\tilde{\nu}$ = 3058, 1645, 1572, 1494, 1315, 1219, 1178, 758, 694, 530; ESI-MS: 174.0 (100) [M + H]$^+$, 196.0 (20) [M + Na]$^+$. The analytical data are consistent with those reported in the literature.[2c]

1-(*p*-Tolyl)-2,3-dihydropyridin-4(1*H*)-one (2b): Yield: 42.0 mg, 0.224 mmol, 75 %, orange solid; R_f = 0.23 (*c*Hex/EtOAc = 2:3); mp: 69.5–71.4 °C; ^{1}H-NMR, COSY (400 MHz, [D]Chloroform) δ = 7.39 (d, J = 7.7 Hz, 1H, H2), 7.20–7.15 (m, 2H, H3′, H5′), 7.01–6.96 (m, 2H, H2′, H6′), 5.19 (d, J = 7.7 Hz, 1H, H3), 4.00–3.93 (m, 2H, H6), 2.66–2.60 (m, 2H, H5), 2.33 (s, 3H, CH_3); ^{13}C-NMR, HSQC, HMBC (101 MHz, [D]Chloroform) δ = 191.96 (C4), 150.01 (C2), 142.95 (C1′), 134.36 (C4′), 130.23 (C3′, C5′), 118.46 (C2′, C6′), 101.58 (C3), 47.88 (C6), 36.02 (C5), 20.81 (CH_3). IR: $\tilde{\nu}$ = 1644, 1573, 1513, 1304, 1272, 1215, 1176, 1105, 1027, 800; ESI-MS: 188.1 (100 %) [M + H]$^+$. The analytical data are consistent with those reported in the literature.[10o]

1-(4-Methoxyphenyl)-2,3-dihydropyridin-4(1*H*)-one (2c): Yield: 22.0 mg, 0.108 mmol, 36.1 %, yellow solid; R_f = 0.13 (*c*Hex/EtOAc = 2:3); mp: 102.2–102.9 °C; ^{1}H-NMR, COSY (400 MHz, [D]Chloroform) 7.34 (d, J = 7.7 Hz, 1H, H2), 7.06–7.02 (m, 2H, H2′, H6′), 6.93–6.88 (m, 2H, H3′, H5′), 5.17 (d, J = 7.7 Hz, 1H, H3), 3.95 (dd, J = 8.1, 7.2 Hz, 2H, H6), 3.81 (s, 3H, CH_3), 2.64 (dd, J = 8.1, 7.2 Hz, 2H, H5); ^{13}C-NMR, HSQC, HMBC (101 MHz, [D]Chloroform) δ = 191.85 (C4), 156.97 (C4′), 150.57 (C2), 139.03 (C1′), 120.51 (C3′, C5′), 114.90 (C2′, C6′), 101.16 (C3), 55.73 (CH_3), 48.48 (C6), 36.05 (C5). IR: $\tilde{\nu}$ = 1629, 1575, 1510, 1463, 1306, 1287, 1242, 1221, 1173, 1038, 806; ESI-MS: 204.1 (100 %) [M + H]$^+$, 226.1 (30.7 %) [M + Na]$^+$, 429.2 (35.7 %) [2M + Na]$^+$. The analytical data are consistent with those reported in the literature.[10o]

1-(4-Fluorophenyl)-2,3-dihydropyridin-4(1*H*)-one (2d): Yield: 32.4 mg, 0.169 mmol, 57 %, orange solid; R_f = 0.12 (*c*Hex/EtOAc = 2:3); mp: 110.2–113.4 °C; ^{1}H-NMR, COSY (400 MHz, [D]Chloroform) δ = 7.35 (d, J = 7.8 Hz, 1H, H2), 7.09–7.04 (m, 4H, H2′, H3′, H5′, H6′), 5.20 (d, J = 7.8 Hz, 1H, H3), 3.96 (dd, J = 8.1, 7.2 Hz, 2H, H6), 2.64 (dd, J = 8.1, 7.2 Hz, 2H, H5); ^{13}C-NMR, HSQC, HMBC (101 MHz, [D]Chloroform) δ = 191.90 (C4), 159.72 (d, J = 244.9 Hz, C4′), 150.02 (C2), 141.69 (d, J = 2.9 Hz, C1′), 120.31 (d, J = 8.1 Hz, C2′, C6′), 116.49 (d, J = 22.8 Hz, C3′, C5′), 102.05 (C3), 48.20 (C6), 35.98 (C5). IR: $\tilde{\nu}$ = 1632, 1577, 1508, 1316, 1306, 1276, 1214, 1181, 1164, 832, 818, 499; ESI-MS: 192.0 (100 %) [M + H]$^+$, 214.0 (12.1 %) [M + Na]$^+$. The analytical data are consistent with those reported in the literature.[10o]

1-(4-Chlorophenyl)-2,3-dihydropyridin-4(1*H*)-one (2e): Yield: 39.4 mg, 63 %, colorless solid; R_f = 0.27 (*c*Hex/EtOAc = 1:4); mp: 98.7–99.8 °C; ^{1}H-NMR, COSY (400 MHz, [D]Chloroform) δ = 7.37 (d, J = 7.8 Hz, 1H, H2), 7.35–7.30 (m, 2H, H3′, H5′), 7.04–6.99 (m, 2H, H2′, H6′), 5.22 (d, J = 7.8 Hz, 1H, H3), 3.99–3.92 (m, 2H, H6), 2.67–2.61 (m, 2H, H5); ^{13}C-NMR, HSQC, HMBC (101 MHz, [D]Chloroform) δ = 191.91 (C4), 149.18 (C2), 143.81 (C1′), 129.75 (C3′, C5′), 129.70 (C4′), 119.47 (C2′, C6′), 102.74 (C3), 47.71 (C6), 35.97 (C5). IR: $\tilde{\nu}$ = 3058, 2836, 1637, 1565, 1492, 1312, 1300, 1216, 1175, 1093, 798; ESI-MS: 208.0 (100 %) [M + H]$^+$, 209.9 (32.8 %) [M + H]$^+$; HRMS (APCI): m/z = 208.0525 ([M + H]$^+$, calcd. 208.0524).

1-(4-Bromophenyl)-2,3-dihydropyridin-4(1*H*)-one (2f): Yield: 24.8 mg, 33 %, yellow solid; R_f = 0.17 (*c*Hex/EtOAc = 2:3); mp: 122.6–124.5 °C; ^{1}H-NMR, COSY (400 MHz, [D]Chloroform) δ = 7.50–7.46 (m, 2H, H3′, H5′), 7.38 (d, J = 7.8 Hz, 1H, H2), 7.00–6.94 (m, 2H, H2′, H6′), 5.24 (d, J = 7.8 Hz, 1H, H3), 3.97 (dd, J = 8.0, 7.1 Hz, 2H, H6), 2.66 (dd, J = 8.0, 7.1 Hz, 2H, H5); ^{13}C-NMR, HSQC, HMBC (101 MHz, [D]Chloroform) δ = 191.93 (C4), 149.02 (C2), 144.30 (C1′), 132.72 (C3′, C5′), 119.77 (C2′, C6′), 117.22 (C4′), 102.93 (C3), 47.66 (C6), 36.02 (C5). IR: $\tilde{\nu}$ = 1644, 1596, 1567, 1491, 1311, 1266, 1217, 1177, 821, 800; ESI-MS: 252.2 (99.5 %), 254.0 (100 %) [M + H]$^+$, 274.0 (9.2 %), 276.0 (8.6 %) [M + Na]$^+$; HRMS (APCI): m/z = 252.0019 ([M + H]$^+$, calcd. 252.0019).

1-(4-Iodophenyl)-2,3-dihydropyridin-4(1*H*)-one (2g): Yield: 20.0 mg, 0.0669 mmol, 22 %, orange solid; R_f = 0.19 (*c*Hex/EtOAc = 2:3); mp: 158.5–161.6 °C; ^{1}H-NMR, COSY (400 MHz, [D]Chloroform) δ = 7.70–7.64 (m, 2H, H3′, H5′), 7.38 (d, J = 7.8 Hz, 1H, H2), 6.88–6.83 (m, 2H, H2′, H6′), 5.25 (d, J = 7.8 Hz, 1H, H3), 3.97 (dd, J = 8.0, 7.1 Hz, 2H, H6), 2.66 (dd, J = 8.0, 7.1 Hz, 2H, H5); ^{13}C-NMR, HSQC, HMBC (101 MHz, [D]Chloroform) δ = 191.94 (C4), 148.84 (C2), 144.97 (C1′), 138.67 (C3′, C5′), 120.05 (C2′, C6′), 103.10 (C3), 87.57 (C4′), 47.55 (C6), 36.04 (C5). IR: $\tilde{\nu}$ = 1649, 1594, 1572, 1488, 1312, 1299, 1264, 1247, 1218, 1177, 817; ESI-MS: 300.0 (100 %) [M + H]$^+$, 322.0 (9.9 %) [M + Na]$^+$; HRMS (APCI): m/z = 299.9878 ([M + H]$^+$, calcd. 299.9880).

1-[4-(Trifluoromethyl)phenyl]-2,3-dihydropyridin-4(1*H*)-one (2h): Yield: 20.7 mg, 0.0858 mmol, 29 %, yellow solid; R_f = 0.19 (*c*Hex/EtOAc = 2:3); mp: 119.2–121.8 °C; ^{1}H-NMR, COSY (400 MHz, [D]Chloroform) δ = 7.66–7.62 (m, 2H, H3′, H5′), 7.47 (d, J = 7.8 Hz, 1H, H2), 7.19–7.16 (m, 2H, H2′, H6′), 5.32 (d, J = 7.8 Hz, 1H, H3),

ChemPubSoc Europe

EurJOC European Journal of Organic Chemistry
Full Paper

4.07–4.01 (m, 2H, H6), 2.74–2.67 (m, 2H, H5); ^{13}C-NMR, HSQC, HMBC (101 MHz, [D]Chloroform) δ = 192.04 (C4), 148.27 (C2), 147.72 (C1′), 127.10 (q, J = 3.7 Hz, C3′, C5′), 125.97 (q, J = 33.1 Hz, C4′)*, 124.07 (q, J = 271.5 Hz, CF_3)*, 117.54 (C2′, C6′), 104.08 (C3), 47.35 (C6), 36.08 (C5); *Outer quartet signals can hardly be seen due to their low intensity. IR: $\tilde{\nu}$ = 1642, 1563, 1519, 1313, 1283, 1219, 1196, 1173, 1103, 1068; ESI-MS: 242.1 (100 %) [M + H]$^+$, 264.0 (5.6 %) [M + Na]$^+$; HRMS (APCI): m/z = 242.0793 ([M + H]$^+$, calcd. 242.0787).

1-(4-Nitrophenyl)-2,3-dihydropyridin-4(1*H*)-one (2i): Yield: 21.6 mg, 0.099 mmol, 33 %, yellow solid; R_f = 0.26 (*c*Hex/EtOAc = 1:4); mp: 125–135 °C; ^{1}H-NMR, COSY (400 MHz, [D]Chloroform) δ = 8.30–8.22 (m, 2H, H3′, H5′), 7.52 (d, J = 8.0 Hz, 1H, H2), 7.20–7.13 (m, 2H, H2′, H6′), 5.40 (d, J = 8.0 Hz, 1H, H3), 4.11–4.06 (m, 2H, H6), 2.76–2.69 (m, 2H, H5); ^{13}C-NMR, HSQC, HMBC (101 MHz, [D]Chloroform) δ = 191.96 (C4), 149.75 (C1′), 146.99 (C2), 143.19 (C4′), 125.86 (C3′, C5′), 116.84 (C2′, C6′), 105.71 (C3), 47.22 (C6), 36.04 (C5). IR: $\tilde{\nu}$ = 1655, 1573, 1501, 1310, 1284, 1221, 1181, 1113, 854, 751; ESI-MS: 219.1 (100 %) [M + H]$^+$. The analytical data are consistent with those reported in the literature.[25]

***N*-Methyl-4-[4-oxo-3,4-dihydropyridin-1(2*H*)-yl]benzamide (2j):** Yield: 34.6 mg, 0.150 mmol, 50 %, yellow solid; R_f = 0.19 (EtOAc/MeOH = 10:1); mp: 177.4–178.8 °C; ^{1}H-NMR, COSY (400 MHz, [D]Chloroform) δ = 7.85–7.79 (m, 2H, H3′, H5′), 7.46 (d, J = 7.8 Hz, 1H, H2), 7.12–7.07 (m, 2H, H2′, H6′), 6.58 (q, J = 4.8 Hz, 1H, N*H*), 5.25 (d, J = 7.8 Hz, 1H, H3), 4.03–3.98 (m, 2H, H6), 2.97 (d, J = 4.8 Hz, 3H, CH_3), 2.68–2.62 (m, 2H, H5); ^{13}C-NMR, HSQC, HMBC (101 MHz, [D]Chloroform) δ = 192.11 (C4), 167.15 (*C*O), 148.55 (C2), 147.22 (C1′), 129.96 (C4′), 128.73 (C3′, C5′), 117.26 (C2′, C6′), 103.44 (C3), 47.26 (C6), 35.99 (C5), 26.95 (CH_3). IR: $\tilde{\nu}$ = 1636, 1563, 1504, 1409, 1304, 1277, 1218, 1178, 767, 728; ESI-MS: 231.2 (100 %) [M + H]$^+$, 253.2 (47.5 %) [M + Na]$^+$, 483.1 (19.9 %) [M + Na]$^+$; HRMS (ESI): m/z = 231.1130 ([M + H]$^+$, calcd. 231.1128).

1-(*m*-Tolyl)-2,3-dihydropyridin-4(1*H*)-one (2k): Yield: 34.3 mg, 0.183 mmol, 62 %, yellow oil; R_f = 0.25 (*c*Hex/EtOAc = 2:3); ^{1}H-NMR, COSY (400 MHz, [D]Chloroform) δ = 7.43 (d, J = 7.8 Hz, 1H, H2), 7.25 (td, J = 7.6, 0.7 Hz, 1H, H5′), 6.94–6.98 (m, 1H, H6′), 6.92–6.87 (m, 2H, H2′, H4′), 5.20 (d, J = 7.8 Hz, 1H, H3), 4.03–3.94 (m, 2H, H6), 2.68–2.59 (m, 2H, H5), 2.37 (s, 3H, CH_3); ^{13}C-NMR, HSQC, HMBC (101 MHz, [D]Chloroform) δ = 192.11 (C4), 149.86 (C2), 145.23 (C1′), 139.79 (C3′), 129.53 (C5′), 125.31 (C6′), 119.07 (C4′), 115.42 (C2′), 101.89 (C3), 47.70 (C6), 36.03 (C5), 21.65 (CH_3). IR: $\tilde{\nu}$ = 1647, 1572, 1494, 1467, 1309, 1274, 1228, 1184, 778, 696; ESI-MS: 188.1 (100 %) [M + H]$^+$, 210.0.1 (8.4 %) [M + Na]$^+$, 397.1 (8.6 %) [2M + Na]$^+$; HRMS (APCI): m/z = 188.1071 ([M + H]$^+$, calcd. 188.1070).

1-(3-Methoxyphenyl)-2,3-dihydropyridin-4(1*H*)-one (2l): Yield: 39.8 mg, 0.196 mmol, 65 %, orange solid; R_f = 0.18 (*c*Hex/EtOAc = 2:3); mp: 67.3–68.8 °C; ^{1}H-NMR, COSY (400 MHz, [D]Chloroform) δ = 7.43 (d, J = 7.8 Hz, 1H, H2), 7.27 (t, J = 8.2 Hz, 1H, H5′), 6.69–6.65 (m, 2H, H4′, H6′), 6.60 (t, J = 2.3 Hz, 1H, H2′), 5.21 (d, J = 7.8 Hz, 1H, H3), 3.97 (dd, J = 8.1, 7.1 Hz, 2H, H6), 3.81 (s, 3H, CH_3), 2.64 (dd, J = 8.1, 7.1 Hz, 2H, H5); ^{13}C-NMR, HSQC, HMBC (101 MHz, [D]Chloroform) δ = 192.20 (C4), 160.71 (C3′), 149.66 (C2), 146.43 (C1′), 130.53 (C5), 110.56, 109.37 (C4′, C6′), 104.76 (C2′), 102.15 (C3), 55.52 (CH_3), 47.62 (C6), 35.99 (C5). IR: $\tilde{\nu}$ = 1646, 1572, 1497, 1310, 1280, 1251, 1237, 1202, 1173, 1051; ESI-MS: 204.1 (100 %) [M + H]$^+$, 226.1 (21.3 %) [M + Na]$^+$, 429.3 (20.1 %) [2M + Na]$^+$. The analytical data are consistent with those reported in the literature.[10o]

Methyl 3-[4-Oxo-3,4-dihydropyridin-1(2*H*)-yl]benzoate (2m): Yield: 26.3 mg, 0.114 mmol, 38 %, yellow oil; R_f = 0.14 (*c*Hex/EtOAc = 2:3); ^{1}H-NMR, COSY (400 MHz, [D]Chloroform) δ = 7.79 (dt, J = 8.0, 1.2 Hz, 1H, H4′), 7.75 (dd, J = 2.6, 1.2 Hz, 1H, H2′), 7.46 (d, J = 7.8, 1H, H2), 7.45 (t, J = 8.0, 1H, H5′), 7.28 (ddd, J = 8.0, 2.6, 1.2 Hz, 1H, H6′), 5.26 (d, J = 7.8 Hz, 1H, H3), 4.03 (dd, J = 8.1, 7.1 Hz, 2H, H6), 3.92 (s, 3H, CH_3), 2.67 (dd, J = 8.1, 7.1 Hz, 2H, H5); ^{13}C-NMR, HSQC, HMBC (101 MHz, [D]Chloroform) δ = 192.02 (C4), 166.38 (*C*OOMe), 149.08 (C2), 145.30 (C1′), 131.75 (C3′), 129.88 (C5′), 125.22 (C4′), 122.24 (C6′), 118.93 (C2′), 103.00 (C3), 52.54 (CH_3), 47.58 (C6), 36.02 (C5). IR: $\tilde{\nu}$ = 1718, 1648, 1570, 1306, 1262, 1242, 1219, 1177, 1108, 755; ESI-MS: 232.1 (100 %) [M + H]$^+$, 254.1 (30.2 %) [M + Na]$^+$, 485.1 (18.6 %) [2M + Na]$^+$; HRMS (ESI): m/z = 232.0971 ([M + H]$^+$, calcd. 232.0968).

3-[4-Oxo-3,4-dihydropyridin-1(2*H*)-yl]benzonitrile (2n): Yield: 23.7 mg, 0.120 mmol, 40 %, yellow solid; R_f = 0.11 (*c*Hex/EtOAc = 2:3); mp: 126.1–130.0 °C; ^{1}H-NMR, COSY (400 MHz, [D]Chloroform) δ = 7.54–7.45 (m, 1H, H5′), 7.42–7.38 (m, 2H, H2, H4′), 7.36–7.30 (m, 2H, H2′, H6′), 5.30 (d, J = 7.9 Hz, 1H, H3), 4.05–3.97 (m, 2H, H6), 2.72–2.66 (m, 2H, H5); ^{13}C-NMR, HSQC, HMBC (101 MHz, [D]Chloroform) δ = 191.82 (C4), 148.06 (C2), 145.70 (C1′), 130.76 (C5′), 127.34 (C4′), 122.01 (C6′), 120.91 (C2′), 118.16 (*C*N), 113.89 (C3′), 104.21 (C3), 47.38 (C6), 35.99 (C5). IR: $\tilde{\nu}$ = 2230, 1647, 1570, 1490, 1464, 1311, 1277, 1225, 1178, 1112, 796; ESI-MS: 199.1 (100 %) [M + H]$^+$, 221.0 (9.2 %) [M + Na]$^+$; HRMS (APCI): m/z = 199.0871 ([M + H]$^+$, calcd. 199.0866).

1-Phenylquinolin-4(1*H*)-one (2o): Yield: 58.4 mg, 0.264 mmol, 88 %, colorless solid; R_f = 0.07 (*c*Hex/EtOAc = 2:3); mp: 124.5–126.2 °C; ^{1}H-NMR, COSY (400 MHz, [D]Chloroform) δ = 8.43 (dd, J = 8.1, 1.6 Hz, 1H, H5), 7.61–7.51 (m, 4H, H2, H3′, H4′, H5′), 7.46 (ddd, J = 8.6, 7.0, 1.6 Hz, 1H, H7), 7.39–7.35 (m, 2H, H2′, H6′), 7.32 (ddd, J = 8.1, 7.0, 1.1 Hz, 1H, H6), 7.00–6.96 (m, 1H, H8), 6.33 (d, J = 7.8 Hz, 1H, H3); ^{13}C-NMR, HSQC, HMBC (101 MHz, [D]Chloroform) δ = 178.31 (C4), 142.80 (C2), 141.37, 141.35 (C8a, C1′), 131.90 (C7), 130.37 (C3′, C5′), 129.57 (C4′), 127.60 (C2′, C6′), 126.59 (C4a), 126.56 (C5), 123.92 (C6), 117.36 (C8), 110.22 (C3). IR: $\tilde{\nu}$ = 1626, 1589, 1550, 1493, 1479, 1465, 1365, 1290, 1237, 769, 704; ESI-MS: 222.1 (100 %) [M + H]$^+$, 465.2 (8.1 %) [2M + Na]$^+$. The analytical data are consistent with those reported in the literature.[26]

1-(Naphthalen-1-yl)quinolin-4(1*H*)-one (2p): Yield: 72.0 mg, 0.265 mmol, 89 %, yellow solid; R_f = 0.15 (*c*Hex/EtOAc = 2:3); mp: 174.2–178.3 °C; ^{1}H-NMR, COSY (400 MHz, [D]Chloroform) δ = 8.54–8.44 (m, 1H, H5), 8.07 (dt, J = 8.4, 1.0 Hz, 1H, H4′), 8.00 (dt, J = 8.2, 1.0 Hz, 1H, H5′), 7.64 (dd, J = 8.4, 7.3 Hz, 1H, H3′), 7.60 (d, J = 7.7 Hz, 1H, H2), 7.59–7.54 (m, 2H, H2′, H6′), 7.42 (ddd, J = 8.2, 6.8, 1.2 Hz, 1H, H7′), 7.37–7.27 (m, 3H, H6, H7, H8′), 6.70–6.64 (m, 1H, H8), 6.41 (d, J = 7.7 Hz, 1H, H3); ^{13}C-NMR, HSQC, HMBC (101 MHz, [D]Chloroform) δ = 178.48 (C4), 143.35 (C2), 141.96 (C8a), 137.45 (C1′), 134.64 (C4a′), 132.10 (C7), 130.41 (C4′), 130.09 (C8a′), 128.71 (C5′), 128.14 (C7′), 127.37 (C6′), 126.54 (C4a), 126.51 (C5), 126.14 (C2′), 125.83 (C3′), 123.95 (C6), 122.16 (C8′), 117.63 (C8), 110.41 (C3). IR: $\tilde{\nu}$ = 1624, 1606, 1590, 1551, 1478, 1395, 1365, 1289, 773, 729; ESI-MS: 272.1 (100 %) [M + H]$^+$, 565.3 (11.1 %) [2M + Na]$^+$; HRMS (ESI): m/z = 272.1073 ([M + H]$^+$, calcd. 272.1070).

1-(Naphthalen-1-yl)-2,3-dihydropyridin-4(1*H*)-one (2q): Yield: 27.5 mg, 0.123 mmol, 41 %, brown solid; R_f = 0.20 (*c*Hex/EtOAc = 2:3); mp: 90.0–98.9 °C; ^{1}H-NMR, COSY (400 MHz, [D]Chloroform) δ = 8.05–8.01 (m, 1H, H8′), 7.94–7.91 (m, 1H, H5′), 7.82 (dt, J = 8.4, 1.1 Hz, 1H, H2′), 7.65–7.52 (m, 2H, H6′, H7′), 7.48 (dd, J = 8.4, 7.3 Hz, 1H, H3′), 7.33 (d, J = 7.6 Hz, 1H, H2), 7.30 (dd, J = 7.3, 1.1 Hz, 1H, H4′), 5.27 (d, J = 7.6 Hz, 1H, H3), 3.99 (t, J = 7.6 Hz, 2H, H6), 2.92–2.63 (br m, 2H, H5); ^{13}C-NMR, HSQC, HMBC (101 MHz, [D]Chloroform) δ = 192.10 (C4), 153.81 (C2), 142.73 (C1′), 134.83 (C4a′), 128.97 (C8a′), 128.85 (C5′), 127.88 (C2′), 127.27, 126.89 (C6′, C7′), 125.73 (C3′), 122.45 (C8′), 121.77 (C4′), 101.26 (C3), 51.10 (C6), 36.57 (C5). IR: $\tilde{\nu}$ = 1644, 1585, 1570, 1395, 1300, 1221, 1173, 1111, 799, 774;

ChemPubSoc Europe

EurJOC European Journal of Organic Chemistry
Full Paper

ESI-MS: 224.1 (100 %) $[M + H]^+$, 246.1 (10.2 %) $[M + Na]^+$, 469.1 (12.5 %) $[2M + Na]^+$; HRMS (ESI): *m/z* = 224.1071 ($[M + H]^+$, calcd. 224.1070).

1-(2,3-Dihydrobenzo[*b*][1,4]dioxin-6-yl)-2,3-dihydropyridin-4(1*H*)-one (2r): Yield: 24.6 mg, 0.106 mmol, 35 %, orange needles; R_f = 0.24 (*c*Hex/EtOAc = 1:4); mp: 163.3–170.9 °C; ^{1}H-NMR, COSY (400 MHz, [D]Chloroform) δ = 7.33 (d, *J* = 7.7 Hz, 1H, H2), 6.85 (d, *J* = 8.7 Hz, 1H, H8′), 6.62 (d, *J* = 2.8 Hz, 1H, H5′), 6.59 (dd, *J* = 8.7, 2.8 Hz, 1H, H7′), 5.17 (d, *J* = 7.7 Hz, 1H, H3), 4.30–4.21 (m, 4H, H2′, H3′), 3.95–3.88 (m, 2H, H6), 2.67–2.58 (m, 2H, H5); ^{13}C-NMR, HSQC, HMBC (101 MHz, [D]Chloroform) δ = 191.96 (C4), 150.30 (C2), 144.12 (C4a′), 140.96 (C8a′), 139.63 (C6′), 118.03 (C8′), 112.09 (C7′), 108.31 (C5′), 101.39 (C3), 64.67, 64.40 (C2′, C3′), 48.27 (C6), 36.04 (C5). IR: $\tilde{\nu}$ = 1627, 1576, 1506, 1316, 1284, 1254, 1213, 1067, 894, 866; ESI-MS: 232.1 (100 %) $[M + H]^+$, 254.2 (26 %) $[M + Na]^+$, 485.2 (54 %) $[2M + Na]^+$; HRMS (ESI): *m/z* = 232.0970 ($[M + H]^+$, calcd. 232,0968).

1-(3,5-Dimethylphenyl)-2,3-dihydropyridin-4(1*H*)-one (2s): Yield: 35.2 mg, 0.175 mmol, 58 %, yellow oil; R_f = 0.18 (*c*Hex/EtOAc = 2:3); ^{1}H-NMR, COSY (400 MHz, [D]Chloroform) δ = 7.44 (d, *J* = 7.7 Hz, 1H, H2), 6.82–6.80 (m, 1H, H4′), 6.75–6.72 (m, 2H, H2′, H6′), 5.21 (d, *J* = 7.7 Hz, 1H, H3), 3.99 (dd, *J* = 8.1, 7.1 Hz, 2H, H6), 2.64 (dd, *J* = 8.1, 7.1 Hz, 2H, H5), 2.34 (s, 6H, 2 × CH_3); ^{13}C-NMR, HSQC, HMBC (101 MHz, [D]Chloroform) δ = 192.11 (C4), 149.94 (C2), 145.23 (C1′), 139.52 (C3′, C5′), 126.24 (C4′), 116.22 (C2′, C6′), 101.64 (C3), 47.72 (C6), 36.01 (C5), 21.51 (2 × CH_3). IR: $\tilde{\nu}$ = 1648, 1606, 1573, 1474, 1328, 1306, 1235, 1192, 1177, 840; ESI-MS: 202.1 (100 %) $[M + H]^+$. The analytical data are consistent with those reported in the literature.[10o]

Methyl 4-Oxo-1-phenyl-1,4,5,6-tetrahydropyridine-3-carboxylate (2t): Yield: 20.9 mg, 0.0904 mmol, 30 %, yellow oil; R_f = 0.14 (EtOAc = 100 %); ^{1}H-NMR, COSY (400 MHz, [D]Chloroform) δ = 8.51 (s, 1H, H2), 7.48–7.41 (m, 2H, H3′, H5′), 7.31–7.27 (m, 1H, H4′), 7.25–7.21 (m, 2H, H2′, H6′), 4.12–4.07 (m, 2H, H6), 3.80 (s, 3H, OCH_3), 2.76–2.70 (m, 2H, H5); ^{13}C-NMR, HSQC, HMBC (101 MHz, [D]Chloroform) δ = 186.93 (C4), 165.90 (COOMe), 156.60 (C1), 144.36 (C1′), 130.01 (C3′, C5′), 126.73 (C4′), 119.81 (C2′, C6′), 103.57 (C3), 51.70 (OCH_3), 48.27 (C6), 36.39 (C5). IR: $\tilde{\nu}$ = 1720, 1666, 1571, 1494, 1386, 1323, 1257, 1202, 1147, 1071, 762; ESI-MS: 232.1 (100 %) $[M + H]^+$, 254.1 (36.4 %) $[M + Na]^+$, 485.2 (68.1 %) $[2M + Na]^+$; HRMS (ESI): *m/z* = 232.0972 ($[M + H]^+$, calcd. 232.0968).

Methyl 7-Oxo-4-phenyl-4,5,6,7-tetrahydro-1,4-oxazepine-2-carboxylate (2t′): Yield: 12.5 mg, 0.0506 mmol, 17 %, yellow oil; R_f = 0.58 (*c*Hex/EtOAc = 2:3); ^{1}H-NMR, COSY (400 MHz, [D]Chloroform) δ = 7.62 (s, 1H, H3), 7.41–7.36 (m, 2H, H3′, H5′), 7.20–7.15 (m, 1H, H4′), 7.14–7.10 (m, 2H, H2′, H6′), 4.11–4.07 (m, 2H, H5), 3.81 (s, 3H, OCH_3), 3.12–3.09 (m, 2H, H6); ^{13}C-NMR, HSQC, HMBC (101 MHz, [D]Chloroform) 169.44 (C7), 164.38 (COOMe), 145.77 (C1′), 129.86 (C3′, C5′), 128.39 (C3), 125.00 (C4′), 119.82 (C2′, C6′), 119.69 (C2), 52.32 (OCH_3), 47.69 (C5), 35.41 (C6). IR: $\tilde{\nu}$ = 1756, 1709, 1645, 1595, 1495, 1266, 1242, 1216, 1145, 756; ESI-MS: 248.1 (100 %) $[M + H]^+$, 270.1 (28.0 %) $[M + Na]^+$, 517.2 (49.5 %) $[2M + Na]^+$; HRMS (ESI): *m/z* = 248.0920 ($[M + H]^+$, calcd. 248.0917).

Gram Scale Procedure for the Photoredox-catalyzed Aerobic Dehydrogenation: A 30 mL glass vial was charged with **1a** (1.15 g, 6.59 mmol, 1.00 equiv.), rhodamine 6G (**7**) (0.0659 mmol, 1 mol-%) and anhydrous DMF (22.0 mL). The mixture was stirred until rhodamine 6G was completely dissolved. A steady stream of oxygen was slowly bubbled through the solution (one bubble per second) using a disposable glass Pasteur pipette (see SI for irradiation setup). The mixture was stirred under irradiation with green LED stripes, until the starting material **1a** was almost consumed completely as judged by TLC and LC-MS analysis (careful monitoring the reaction progress is recommended to avoid over-oxidation). Water (50 mL) was added and the mixture was extracted with Et_2O (4 × 50 mL) to remove most of DMF. The organic phases were combined, dried with Na_2SO_4, filtered and the solvent was removed in vacuo. The crude product was purified by column chromatography (SiO_2, *c*Hex/EtOAc = 2:3) to yield **2a** (680.2 mg, 3.927 mmol, 60 %).

General Procedure for the One-pot Synthesis of Azocinones: The synthesis was performed according to the general procedure of the dehydrogenation, with the following exception: After irradiation the reaction vessel was flushed with argon for 2 minutes, followed by addition of anhydrous ACN (1.00 mL) and the respective acetylene ester **11** (0.900 mmol, 3.00 equiv.). The reaction mixture was heated at 90 °C in an oil bath for 20 h, followed by the usual work-up as described above.

Dimethyl (2*E*,4*E*)-6-Oxo-1-phenyl-1,6,7,8-tetrahydroazocine-3,4-dicarboxylate (12a): Yield: 58.2 mg, 0.185 mmol, 62 %, orange resin; R_f = 0.50 (*c*Hex/EtOAc = 2:3); ^{1}H-NMR, COSY (400 MHz, [D]Chloroform) δ = 7.63 (s, 1H, H2), 7.39–7.32 (m, 2H, H3′, H5′), 7.24–7.19 (m, 1H, H4′), 7.14–7.09 (m, 2H, H2′, H6′), 6.63 (s, 1H, H5), 4.35 (s, 2H, H8), 3.79 (s, 3H, 4-CO_2CH_3), 3.62 (s, 3H, 3-CO_2CH_3), 2.56 (s, 2H, H7); ^{13}C-NMR, HSQC, HMBC (101 MHz, [D]Chloroform) δ = 205.67 (C6), 168.61 (3-*C*O), 168.27 (4-*C*O), 146.49 (C1′), 144.79 (C2), 134.12 (C4), 132.64 (C5), 129.83 (C3′, C5′), 126.39 (C4′), 122.84 (C2′, C6′), 97.23 (C3), 52.71 (4-CO_2CH_3), 51.78 (3-CO_2CH_3), 47.35 (C8), 38.72 (C7). IR: $\tilde{\nu}$ = 1726, 1705, 1610, 1582, 1494, 1435, 1239, 1203, 1091, 1057; ESI-MS: 284.1 (39.5 %) $[M - OMe]^+$, 316.1 (100 %) $[M + H]^+$, 338.1 (44.8 %) $[M + Na]^+$, 653.3 (39.3 %) $[2M + Na]^+$; HRMS (ESI): *m/z* = 338.0994 ($[M + Na]^+$, calcd. 338.0999).

Dimethyl (2*E*,4*E*)-6-Oxo-1-(*p*-tolyl)-1,6,7,8-tetrahydroazocine-3,4-dicarboxylate (12b): Yield: 56.6 mg, 0.172 mmol, 57 %, orang resin; R_f = 0.57 (*c*Hex/EtOAc = 2:3); ^{1}H-NMR, COSY (400 MHz, [D]Chloroform) δ = 7.61 (s, 1H, H2), 7.18–7.15 (m, 2H, H3′, H5′), 7.03–6.98 (m, 2H, H2′, H6′), 6.62 (s, 1H, H5), 3.92–3.67 (br m, 2H, H8), 3.81 (s, 3H, OCH_3), 3.63 (s, 3H, OCH_3), 2.55 (br m, 2H, H7), 2.33 (s, 3H, $ArCH_3$); ^{13}C-NMR, HSQC, HMBC (101 MHz, [D]Chloroform) δ = 205.80 (C6), 168.72 (CO_2Me), 168.44 (CO_2Me), 145.18 (C2), 144.19 (C1′), 136.52 (C4′), 134.27 (C4), 132.43 (C5), 130.40 (C3′, C5′), 123.09 (C2′, C6′), 96.75 (C3), 52.75 (OCH_3), 51.79 (OCH_3), 47.58 (C8), 38.59 (C7), 20.95 ($ArCH_3$). IR: $\tilde{\nu}$ = 1726, 1704, 1581, 1511, 1434, 1305, 1238, 1202, 1090, 1057; ESI-MS: 298.1 (44.1 %) $[M - OMe]^+$, 330.2 (100 %) $[M + H]^+$, 352.2 (20.5 %) $[M + Na]^+$, 681.3 (46.7 %) $[2M + Na]^+$; HRMS (ESI): *m/z* = 352.1156 ($[M + Na]^+$, calcd. 352.1155).

Dimethyl (2*E*,4*E*)-1-(3-Methoxyphenyl)-6-oxo-1,6,7,8-tetrahydroazocine-3,4-dicarboxylate (12c): Yield: 47.9 mg, 0.139 mmol, 46 %, orange resin; R_f = 0.44 (cHex/EtOAc = 2:3); ^{1}H-NMR, COSY (400 MHz, [D]Chloroform) δ = 7.65 (s, 1H, H2), 7.27 (t, *J* = 8.2 Hz, 1H, H5′), 6.76 (ddd, *J* = 8.2, 2.3, 0.8 Hz, 1H, H4′), 6.71 (ddd, *J* = 8.2, 2.3, 0.8 Hz, 1H, H6′), 6.67–6.60 (m, 2H, H5, H2′), 4.34 (br m, 2H, H8), 3.81 (s, 3H, CO_2CH_3), 3.80 (s, 3H, $ArOCH_3$), 3.64 (s, 3H, CO_2CH_3), 2.57 (br m, 2H, H7); ^{13}C-NMR, HSQC, HMBC (101 MHz, [D]Chloroform) δ = 205.62 (C6), 168.63 (CO_2Me), 168.32 (CO_2Me), 160.70 (C3′), 147.71 (C1′), 144.67 (C2), 134.25 (C4), 132.65 (C5), 130.61 (C5′), 114.93 (C6′), 111.53 (C4′), 109.07 (C2′), 97.37 (C3), 55.61 ($ArOCH_3$), 52.77 (CO_2CH_3), 51.85 (CO_2CH_3), 47.36 (C8), 38.86 (C7). IR: $\tilde{\nu}$ = 1725, 1705, 1582, 1491, 1435, 1330, 1237, 1194, 1172, 1090, 1051, 777; ESI-MS: 314.1 (62.7 %) $[M - OMe]^+$, 346.2 (100 %) $[M + H]^+$, 368.1 (20.5 %) $[M + Na]^+$, 713.3 (26.8 %) $[2M + Na]^+$; HRMS (APPI): *m/z* = 346.1290 ($[M + H]^+$, calcd. 346.1285).

Dimethyl (2*E*,4*E*)-1-(4-Fluorophenyl)-6-oxo-1,6,7,8-tetrahydroazocine-3,4-dicarboxylate (12d): Yield: 42.4 mg, 0.127 mmol,

ChemPubSoc Europe

EurJOC European Journal of Organic Chemistry

Full Paper

42 %, orange resin; R_f = 0.51 (*c*Hex/EtOAc = 2:3); ^{1}H-NMR, COSY (400 MHz, [D]Chloroform) δ = 7.53 (s, 1H, H3), 7.13–7.03 (m, 4H, H2′, H3′, H5′, H6′), 6.65 (s, 1H, H5), 3.88–3.66 (br m, 2H, H8), 3.80 (s, 3H, CH_3), 3.63 (s, 3H, CH_3), 2.54 (br m, 2H, H7); ^{13}C-NMR, HSQC, HMBC (101 MHz, [D]Chloroform) δ = 205.58 (C6), 168.58 (CO_2Me), 168.22 (CO_2Me), 160.91 (d, *J* = 247.3 Hz, C4′), 144.97 (C2), 142.84 (d, *J* = 2.9 Hz, C1′), 133.97 (C4), 132.79 (C5), 125.34 (d, *J* = 8.2 Hz, C2′, C6′), 116.73 (d, *J* = 22.8 Hz, C3′, C5′), 97.33 (C3), 52.78 (CH_3), 51.87 (CH_3), 47.93 (C8), 38.49 (C7). IR: $\tilde{\nu}$ = 1702, 1609, 1585, 1506, 1434, 1230, 1201, 1158, 1090, 1057, 730; ESI-MS: 302.1 (41.1 %) [M – OMe]$^+$, 334.1 (100 %) [M + H]$^+$, 356.1 (61.4 %) [M + Na]$^+$, 689.3 (62.7 %) [2M + Na]$^+$; HRMS (ESI): *m/z* = 334.1086 ([M + H]$^+$, calcd. 334.1085).

Diethyl (2*E*,4*E*)-6-Oxo-1-phenyl-1,6,7,8-tetrahydroazocine-3,4-dicarboxylate (12e): Yield: 52.4 mg, 0.153 mmol, 51 %, orange resin; R_f = 0.59 (*c*Hex/EtOAc = 2:3); ^{1}H-NMR, COSY (400 MHz, [D]Chloroform) δ = 7.65 (s, 1H, H2), 7.40–7.34 (m, 2H, H3′, H5′), 7.25–7.20 (m, 1H, H4′), 7.15–7.11 (m, 2H, H2′, H6′), 6.63 (s, 1H, H5), 4.57–3.99 (m, 2H, H8), 4.27 (q, *J* = 7.1 Hz, 2H, OCH_2CH_3), 4.10 (q, *J* = 7.1 Hz, 2H, OCH_2CH_3), 2.58 (br m, 2H, H7), 1.32 (t, *J* = 7.1 Hz, 3H, OCH_2CH_3), 1.20 (t, *J* = 7.1 Hz, 3H, OCH_2CH_3); ^{13}C-NMR, HSQC, HMBC (101 MHz, [D]Chloroform) δ = 205.89 (C6), 168.32 (CO_2Et), 167.92 (CO_2Et), 146.60 (C1′), 144.65 (C2), 134.72 (C4), 132.26 (C5), 129.87 (C3′, C5′), 126.30 (C4′), 122.82 (C2′, C6′), 97.79 (C3), 61.70 (OCH_2CH_3), 60.62 (OCH_2CH_3), 47.37 (C8), 38.90 (C7), 14.35 (OCH_2CH_3), 14.29 (OCH_2CH_3). IR: $\tilde{\nu}$ = 1702, 1608, 1578, 1493, 1364, 1230, 1197, 1092, 1054, 1030, 757, 697; ESI-MS: 298.1 (45.7 %) [M – OEt]$^+$, 344.2 (100 %) [M + H]$^+$, 709.4 (44.8 %) [2M + Na]$^+$; HRMS (ESI): *m/z* = 344.1496 ([M + H]$^+$, calcd. 344.1492).

Acknowledgments

We thank Dr. Johannes C. Liermann (Mainz) for helpful discussions and measurements of NMR spectra, Dr. Christopher Kampf (Mainz) for mass spectrometry, and Prof. Jurij Svete (Ljubljana) for the helpful discussion. This work was supported by the LESSING initiative at JGU and by the Rhineland Palatinate Natural Products Research Center.

Keywords: Photocatalysis · Photooxidation · Sustainable chemistry · Nitrogen heterocycles · Ring expansion

[1] a) J. P. Michael, C. B. de Koning, D. Gravestock, G. D. Hosken, A. S. Howard, C. M. Jungmann, R. W. M. Krause, A. S. Parsons, S. C. Pelly, T. V. Stanbury, *Pure Appl. Chem.* **1999**, *71*, 979; b) G. Negri, C. Kascheres, A. J. Kascheres, *J. Heterocycl. Chem.* **2004**, *41*, 461–491; c) B. Stanovnik, J. Svete, *Chem. Rev.* **2004**, *104*, 2433–2480; d) J. V. Greenhill, *Chem. Soc. Rev.* **1977**, *6*, 277–294; e) A.-Z. A. Elassar, A. A. El-Khair, *Tetrahedron* **2003**, *59*, 8463–8480.

[2] a) D. L. Comins, *J. Heterocycl. Chem.* **1999**, *36*, 1491–1500; b) S. Joseph, D. L. Comins, *Curr. Opin. Drug Discov. Devel.* **2002**, *5*, 870–880; c) M. J. Niphakis, B. J. Turunen, G. I. Georg, *J. Org. Chem.* **2010**, *75*, 6793–6805; d) H. Seki, G. I. Georg, *Synlett* **2014**, *25*, 2536–2557; e) A. K. Chattopadhyay, S. Hanessian, *Chem. Commun.* **2015**, *51*, 16437–16449.

[3] a) P. S. Watson, B. Jiang, B. Scott, *Org. Lett.* **2000**, *2*, 3679–3681; b) C. A. Brooks, D. L. Comins, *Tetrahedron Lett.* **2000**, *41*, 3551–3553; c) X. M. Ye, A. W. Konradi, J. Smith, Y.-Z. Xu, D. Dressen, A. W. Garofalo, J. Marugg, H. L. Sham, A. P. Truong, J. Jagodzinski, M. Pleiss, H. Zhang, E. Goldbach, J.-M. Sauer, E. Brigham, M. Bova, G. S. Basi, *Bioorg. Med. Chem. Lett.* **2010**, *20*, 2195–2199.

[4] a) J. P. Michael, *Nat. Prod. Rep.* **2008**, *25*, 139–165; b) M. J. Niphakis, G. I. Georg, *Org. Lett.* **2011**, *13*, 196–199; c) S. V. Tsukanov, D. L. Comins, *Angew. Chem. Int. Ed.* **2011**, *50*, 8626–8628; *Angew. Chem.* **2011**, *123*, 8785–8787; d) M. F. Enamorado, C. M. Connelly, A. Deiters, D. L. Comins, *Tetrahedron Lett.* **2015**, *56*, 3683–3685; e) S. V. Tsukanov, D. L. Comins, *Angew. Chem. Int. Ed.* **2011**, *50*, 8626–8628; *Angew. Chem.* **2011**, *123*, 8785.

[5] C. J. Creighton, C. W. Zapf, J. H. Bu, M. Goodman, *Org. Lett.* **1999**, *1*, 1407–1409.

[6] A. Peduto, A. Massa, A. Di Mola, P. de Caprariis, P. La Colla, R. Loddo, S. Altamura, G. Maga, R. Filosa, *Chem. Biol. Drug Des.* **2011**, *77*, 441–449.

[7] a) M. F. Gordeev, Z. Y. Yuan, *J. Med. Chem.* **2014**, *57*, 4487–4497; b) C.-R. Li, Q.-Q. Zhai, X.-K. Wang, X.-X. Hu, G.-Q. Li, W.-X. Zhang, J. Pang, X. Lu, H. Yuan, M. F. Gordeev, L.-T. Chen, X.-Y. Yang, X.-F. You, *Antimicrob. Agents Chemother.* **2014**, *58*, 2418–2421.

[8] a) F. Van Bambeke, J. M. Michot, J. Van Eldere, P. M. Tulkens, *Clin. Microbiol. Infect.* **2005**, *11*, 256–280; b) C. Mugnaini, S. Pasquini, F. Corelli, *Curr. Med. Chem.* **2009**, *16*, 1746–1767; c) A. A. Boteva, O. P. Krasnykh, *Chem. Heterocycl. Compd.* **2009**, *45*, 757.

[9] V. Cecchetti, C. Parolin, S. Moro, T. Pecere, E. Filipponi, A. Calistri, O. Tabarrini, B. Gatto, M. Palumbo, A. Fravolini, *J. Med. Chem.* **2000**, *43*, 3799–3802.

[10] a) P. Stütz, P. A. Stadler, *Tetrahedron Lett.* **1973**, *14*, 5095–5098; b) M. Onda, Y. Sugama, R. Yabuki, *Heterocycles* **1985**, *23*, 111–116; c) H. Moehrle, M. Claas, *Pharmazie* **1988**, *43*, 749–753; d) M. E. Kuehne, R. S. Muth, *J. Org. Chem.* **1991**, *56*, 2701–2712; e) H. R. Pfaendler, W. Jenni, *Heterocycles* **1999**, *50*, 867–874; f) A. Guarna, F. Machetti, E. G. Occhiato, D. Scarpi, A. Comerci, G. Danza, R. Mancina, M. Serio, K. Hardy, *J. Med. Chem.* **2000**, *43*, 3718–3735; g) M. A. Ali, N. Bhogal, C. W. G. Fishwick, J. B. C. Findlay, *Bioorg. Med. Chem. Lett.* **2001**, *11*, 819–822; h) K. C. Nicolaou, T. Montagnon, P. S. Baran, *Angew. Chem. Int. Ed.* **2002**, *41*, 996–1000; *Angew. Chem.* **2002**, *114*, 1035–1038; i) Y. Asahina, I. Araya, K. Iwase, F. Iinuma, M. Hosaka, T. Ishizaki, *J. Med. Chem.* **2005**, *48*, 3443–3446; j) R. Šebesta, M. G. Pizzuti, A. J. Boersma, A. J. Minnaard, B. L. Feringa, *Chem. Commun.* **2005**, 1711–1713; k) A. C. Flick, A. Padwa, *Tetrahedron Lett.* **2008**, *49*, 5739–5741; l) T. Diao, S. S. Stahl, *J. Am. Chem. Soc.* **2011**, *133*, 14566–14569; m) K. Murakami, Y. Sasano, M. Tomizawa, M. Shibuya, E. Kwon, Y. Iwabuchi, *J. Am. Chem. Soc.* **2014**, *136*, 17591–17600; n) F. Mayr, R. Brimioulle, T. Bach, *J. Org. Chem.* **2016**, *81*, 6965–6971; o) J. Z. Shao Tianju, *Acta Chim. Sinica* **2017**, *75*, 70–73; p) D. Yoshii, X. Jin, T. Yatabe, J.-y. Hasegawa, K. Yamaguchi, N. Mizuno, *Chem. Commun.* **2016**, *52*, 14314–14317; q) T. S. Cameron, R. E. Cordes, B. M. Pinto, W. A. Szarek, *Can. J. Chem.* **1981**, *59*, 3136–3140; r) K. C. Nicolaou, T. Montagnon, P. S. Baran, *Angew. Chem. Int. Ed.* **2002**, *41*, 993–996; *Angew. Chem.* **2002**, *114*, 1035.

[11] a) D. Ravelli, D. Dondi, M. Fagnoni, A. Albini, *Chem. Soc. Rev.* **2009**, *38*, 1999–2011; b) D. A. Nicewicz, T. M. Nguyen, *ACS Catal.* **2014**, *4*, 355–360; c) N. A. Romero, D. A. Nicewicz, *Chem. Rev.* **2016**, *116*, 10075–10166; d) C.-S. Wang, P. H. Dixneuf, J.-F. Soulé, *Chem. Rev.* **2018**, *118*, 7532–7585; e) L. Shi, W. Xia, *Chem. Soc. Rev.* **2012**, *41*, 7687–7697; f) S. A. Morris, J. Wang, N. Zheng, *Acc. Chem. Res.* **2016**, *49*, 1957–1968; g) K. Nakajima, Y. Miyake, Y. Nishibayashi, *Acc. Chem. Res.* **2016**, *49*, 1946–1956; h) J. Hu, J. Wang, T. H. Nguyen, N. Zheng, *Beilstein J. Org. Chem.* **2013**, *9*, 1977–2001.

[12] a) J. C. Orejarena Pacheco, A. Lipp, A. M. Nauth, F. Acke, J.-P. Dietz, T. Opatz, *Chem. Eur. J.* **2016**, *22*, 5409–5415; b) A. M. Nauth, A. Lipp, B. Lipp, T. Opatz, *Eur. J. Org. Chem.* **2017**, *2017*, 2099–2103; c) A. M. Nauth, J. C. Orejarena Pacheco, S. Pusch, T. Opatz, *Eur. J. Org. Chem.* **2017**, *2017*, 6966–6974.

[13] a) P. Ashok, H. Lathiya, S. Murugesan, *Eur. J. Med. Chem.* **2015**, *97*, 928–936; b) R. K. Boeckman, H. Wang, K. W. Rugg, N. E. Genung, K. Chen, T. R. Ryder, *Org. Lett.* **2016**, *18*, 6136–6139; c) I. Yavari, L. Baoosi, M. R. Halvagar, *Synlett* **2018**, *29*, 635–639.

[14] a) M. Sutharchanadevi, R. Murugan, in *Comprehensive Heterocyclic Chemistry II* (Eds.: A. R. Katritzky, C. W. Rees, E. F. V. Scriven), Pergamon, Oxford, **1996**, pp. 403–428; b) G. Godin, E. Garnier, P. Compain, O. R. Martin, K. Ikeda, N. Asano, *Tetrahedron Lett.* **2004**, *45*, 579–581; c) S. A. Raw, R. J. K. Taylor, *Tetrahedron Lett.* **2004**, *45*, 8607–8610; d) Y. Shiono, K. Akiyama, H. Hayashi, *Biosci. Biotechnol. Biochem.* **2000**, *64*, 1519–1521.

[15] a) B. Stanovnik, *Org. Prep. Proced. Int.* **2014**, *46*, 24–65; b) J. Bezenšek, B. Prek, U. Grošelj, M. Počkaj, J. Svete, B. Stanovnik, *Tetrahedron* **2015**, *71*, 7209–7215; c) A. V. Listratova, L. G. Voskressensky, *Synthesis* **2017**, *49*, 3801–3834; d) P. A. Evans, B. Holmes, *Tetrahedron* **1991**, *47*, 9131–9166.

ChemPubSoc Europe

EurJOC European Journal of Organic Chemistry
Full Paper

[16] a) X. Cheng, B. Yang, X. Hu, Q. Xu, Z. Lu, *Chem. Eur. J.* **2016**, *22*, 17566–17570; b) S. Cao, S. Zhong, L. Xin, J.-P. Wan, C. Wen, *ChemCatChem* **2015**, *7*, 1478–1482; c) T. Ghosh, A. Das, B. König, *Org. Biomol. Chem.* **2017**, *15*, 2536–2540; d) H. H. Wasserman, J. L. Ives, *J. Org. Chem.* **1985**, *50*, 3573–3580.
[17] A. M. Nauth, E. Schechtel, R. Dören, W. Tremel, T. Opatz, *J. Am. Chem. Soc.* **2018**, *140*, 14169–14177.
[18] a) J. E. Baldwin, S. S. Gallagher, P. A. Leber, A. Raghavan, *Org. Lett.* **2004**, *6*, 1457–1460; b) J. E. Baldwin, S. S. Gallagher, P. A. Leber, A. S. Raghavan, R. Shukla, *J. Org. Chem.* **2004**, *69*, 7212–7219; c) D. N. Reinhoudt, W. Verboom, G. W. Visser, W. P. Trompenaars, S. Harkema, G. J. Van Hummel, *J. Am. Chem. Soc.* **1984**, *106*, 1341–1350; d) G. J. M. Vos, P. H. Benders, D. N. Reinhoudt, R. J. M. Egberink, S. Harkema, G. J. Van Hummel, *J. Org. Chem.* **1986**, *51*, 2004–2011; e) G. Maas, R. Reinhard, H.-G. Herz, *Z. Naturforsch. B* **2006**, *61*, 385; f) C. Silva López, O. Nieto Faza, Á. R. de Lera, *Chem. Eur. J.* **2007**, *13*, 5009–5017.
[19] J. Saurí, T. Parella, J. F. Espinosa, *Org. Biomol. Chem.* **2013**, *11*, 4473–4478.
[20] a) J. Bezenšek, T. Koleša, U. Grošelj, J. Wagger, K. Stare, A. Meden, J. Svete, B. Stanovnik, *Tetrahedron Lett.* **2010**, *51*, 3392–3397; b) J. Bezenšek, T. Koleša, U. Grošelj, A. Meden, K. Stare, J. Svete, B. Stanovnik, *Curr. Org. Chem.* **2011**, *15*, 2530–2539.
[21] D. R. Tortolani, M. A. Poss, *Org. Lett.* **1999**, *1*, 1261–1262.
[22] H. E. Katz, W. T. Lavell, *J. Org. Chem.* **1991**, *56*, 2282–2284.
[23] I. L. Baraznenok, V. G. Nenajdenko, E. S. Balenkova, *Chem. Heterocycl. Compd.* **1997**, *33*, 429–434.
[24] M. Sharma, V. Deekshith, A. Semwal, D. Sriram, P. Yogeeswari, *Bioorg. Chem.* **2014**, *52*, 69–76.
[25] R. C. Thomas, T.-J. Poel, M. R. Barbachyn, M. F. Gordeev, G. W. Luehr, A. Renslo, U. Singh, V. P. V. Josyula (Pfizer), US2004147760 (A1), **2004**.
[26] M. K. Mehra, M. P. Tantak, V. Arun, I. Kumar, D. Kumar, *Org. Biomol. Chem.* **2017**, *15*, 4956–4961.

Received: April 16, 2019

7.2 Computergestützte Strukturaufklärung kleiner organischer Moleküle

7.2.1 Benchmarkstudie über die Genauigkeit von DFT-Methoden in der VCD-Spektroskopie

Um die Anwendbarkeit verbreiteter DFT-Methoden in der Vorhersage von VCD-Spektren zu beurteilen, wurde innerhalb der Forschungsgruppe Opatz ein systematischer Vergleich durchgeführt. Dafür wurden die VCD-Spektren von sechs chiralen Verbindungen **125**–**130** (in der Publikation **1**–**6**) aufgenommen und mittels quantenmechanischer Methoden berechnet. Für jedes Molekül wurden insgesamt 480 Spektren simuliert, die sich aus den Kombinationen von 15 Funktionalen, 16 Basissätzen und zwei Solvatationsmodellen ergeben. Um die Übereinstimmung zwischen gemessenen und *in silico* generierten Spektren zu quantifizieren, wurde unter Verwendung der Software SpecDis der enantiomere Ähnlichkeitsfaktor (*enantiomeric similarity index*, ESI) bestimmt.[514,515] Anhand dieses Wertes wurde sowohl die Genauigkeit jeder Kombination für die Moleküle **125**–**130** bewertet als auch die Unterschiede der Funktionale, Basissätze und Solvatationsmodelle isoliert betrachtet. Abschließend wurden vielversprechende Varianten für chirale Moleküle mit unbekannter absoluter Konfiguration empfohlen (Abbildung 7.5).[558]

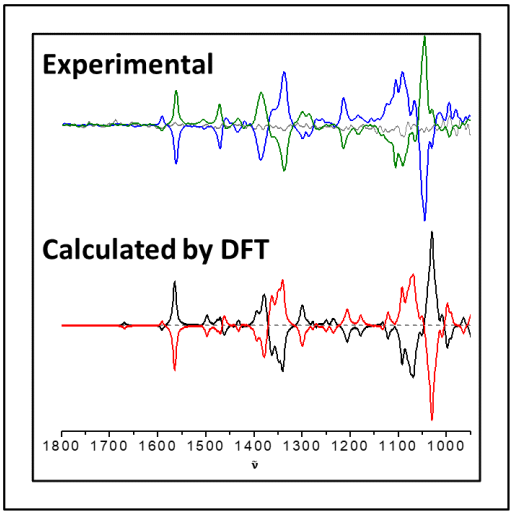

Abbildung 7.5: *Graphical abstract* der Publikation „Comparison of different density functional theory methods for the calculation of vibrational circular dichroism spectra“.[558]

Die VCD-Spektren von Thiocampher **130** (in der Publikation **6**) wurden von J. Groß gemessen und simuliert. Im Rahmen eines Forschungsmoduls wurde Sulfoxid **129** (in der Publikation **5**) von [redacted] dargestellt sowie die dazugehörigen VCD-Spektren aufgenommen. Die experimentelle Bestimmung sowie die *in silico* Vorhersage der VCD-Spektren der Verbindungen **125**–**128** (in der Publikation **1**–**4**) erfolgte durch [redacted], [redacted] und [redacted]. Die Datensätze aller Moleküle wurden von J. Groß, [redacted], [redacted] und [redacted] ausgewertet. [redacted] hat im Rahmen einer wissenschaftlichen Hilfstätigkeit erheblich zur Auswertung des Vergleichs simulierter und gemessener Spektren beigetragen und die VCD-Spektren von Sulfoxid **129** (in der Publikation **5**) simuliert. Das Manuskript wurde von J. Groß, [redacted], [redacted], [redacted], [redacted] und T. Opatz verfasst.[13]

[13] *Reprinted under the terms of the Creative Commons Attribution License CC BY 4.0. Copyright ©2023 J. Groß, J. Kühlborn, S. Pusch, C. Weber, L. Andernach, G. Renzer, P. Eckhardt, J. Brauer, T. Opatz, Chirality, 2023, 1–13, Chirality published by Wiley Periodicals LLC.*

Received: 30 January 2023 | Revised: 2 May 2023 | Accepted: 3 May 2023
DOI: 10.1002/chir.23580

RESEARCH ARTICLE

Chirality WILEY

Comparison of different density functional theory methods for the calculation of vibrational circular dichroism spectra

Jonathan Groß | Jonas Kühlborn | Stefan Pusch | Carina Weber | Lars Andernach | Galit Renzer | Paul Eckhardt | Jan Brauer | Till Opatz

Department of Chemistry, Johannes Gutenberg University, Mainz, Germany

Correspondence
Till Opatz, Department of Chemistry, Johannes Gutenberg University, Duesbergweg 10–14, 55128 Mainz, Germany.
Email: opatz@uni-mainz.de

Funding information
Alliance for High Performance Computing in Rhineland-Palatinate; Gauss Alliance e.V.

Abstract
The determination of the absolute configuration (AC) of an organic molecule is still a challenging task for which the combination of spectroscopic with quantum-mechanical methods has become a promising approach. In this study, we investigated the accuracy of DFT methods (480 overall combinations of 15 functionals, 16 basis sets, and 2 solvation models) to calculate the VCD spectra of six chiral organic molecules in order to benchmark their capability to facilitate the determination of the AC.

KEYWORDS
absolute configuration determination, basis set, benchmark, DFT, functional, solvation, VCD

1 | INTRODUCTION

In 1874, van't Hoff included the spatial configuration of aliphatic carbon atoms into organic structural formulae.[1] The first experiments to determine the absolute configuration (AC) of an organic molecule were reported by Bijvoet et al. not earlier than 1951. These authors used X-rays, more precisely zirconium K_α radiation, to assign the configuration of sodium rubidium tartrate using anomalous dispersion. Thereby, they confirmed Fischer's convention, who had previously ascribed the correct AC to L-(+)-tartaric acid.[2]

The correct determination of the AC of organic molecules is crucial to many areas such as asymmetric catalysis, natural product total synthesis, or pharmaceutical applications. Circular dichroism (CD) is one of the chirality-sensitive optical properties of molecules and can be exploited in combination with quantum-mechanical calculations for the assignment of the AC while no chemical derivatization or reference system is needed.[3,4] This phenomenon is based on the differential absorption of left- and right-circularly polarized light by a given molecule, resulting in mirror image CD spectra of a pair of enantiomers.[5] The visible–ultraviolet spectral region is used for electronic CD (ECD) as higher energy photons cause electronic excitations (e.g., $n \rightarrow \pi^*$ or $\pi \rightarrow \pi^*$) whereas irradiation in the infrared (IR) region leads to vibrational excitations, enabling the measurement of vibrational CD (VCD) spectra.[6]

An ECD spectrum in liquid phase was first recorded by Cotton in 1895, while it took almost a further century until the first VCD measurements were reported.[7,8] The latter was measured by Holzwarth et al. in 1974 and a year later was confirmed independently by Nafie et al.[9,10] For these measurements, crystallization of the sample and the presence of heavy atoms was not required

J. Groß and Dr. J. Kühlborn contributed equally.

anymore. VCD is normally measured for neat liquid or solution samples but can also be measured in the gas phase and in the solid phase.[6]

While the sensitivity of ECD is two orders of magnitude higher compared with VCD (resulting in a smaller amount of the sample being required), the compound of interest needs to have a chromophore close to a stereogenic center or another stereogenic element so that ECD spectroscopy can safely be applied. In contrast, VCD is even suitable for saturated hydrocarbons. In combination with Raman optical activity spectroscopy, these three chiroptical spectroscopies can usefully complement each other and offer specific advantages in the investigation of various stereochemical aspects.[3,6,11–16]

The simulation of VCD spectra requires suitable quantum-mechanical methods to calculate the vibrational rotational strengths. While the magnetic dipole transition moments contribute to them, the calculation is not possible within the Born–Oppenheimer (BO) approximation.[17] In the late 20th century, several ad hoc approaches were proposed (e.g., the fixed partial charge model,[18] a coupled oscillator model,[19] or a localized molecular orbital model[20]) but none of these proved to be generally useful.[21] Stephens reported in 1985 a solution for the calculation of magnetic dipole transition moments of vibrational transitions and subsequently, the first predicted VCD spectra at DFT level in 1994.[17,22] Until today, analytical derivative methods[23,24] in combination with gauge-invariant atomic orbital (GIAO) basis sets are applied for the prediction of vibrational rotational strengths by the calculation of the harmonic force field (HFF), the atomic polar tensors (APTs), and the atomic axial tensors (AATs) in a cost-efficient and accurate manner using DFT.[25–27]

Although visual comparison of measured and calculated VCD curves is often sufficient to decide on the correct AC, a quantitative comparison relies on the use of algorithms and computer programs.[28,29] In 2010, one of the first methods was published by Shen et al. (*Sim*VCD),[30] followed by the freely available software *CDSpecTech* by Covington and Polavarapu[29] and *SpecDis* by Bruhn et al.[3,31] The latter was developed initially for the comparison of experimental and calculated UV and ECD curves but was then extended to cover IR and VCD as well. The similarity factors f and f^* (enantiomeric f) were introduced to quantify the degree of matching of two curves (in this case experimental and calculated IR/VCD spectra) within a given range of wavelengths. Their values reach from 0 to 1, with 1 representing an ideal match. The absolute value of their difference ($|f - f^*|$) of the similarity factors of both enantiomers is called the Δ-value or enantiomeric similarity index (ESI), introduced by Bultinck et al.,[3,32–34] and serves as a useful measure to differentiate between two enantiomers.

The calculation of a sufficient number of excited states is necessary for ECD prediction of the whole range of the experimental spectrum,[3] for which the time-dependent density functional theory (TD-DFT) method may be very cost effective.[35] A computational flowchart was presented by Bruhn et al. for the AC determination by ECD including conformational analysis, optimization of the geometries, solvent effects and Boltzmann weighting.[36] This general procedure can also be adapted to VCD, where the DFT level of theory is sufficient for the calculation of vibrational rotational strengths to simulate the spectra (see the Supporting Information).[25] To achieve more accurate predictions and avoid arbitrary wavenumber shifts, anharmonic corrections at the second-order level of vibrational perturbation theory (VPT2)[37] can be applied, which have been successfully demonstrated for small molecules in recent years.[38,39] By applying the generalized VPT2 approach, Fusè et al. were able to compare experimental IR and VCD spectra with predicted spectra in the range of 900–9000 cm^{-1} including the fundamental and overtone CH-stretching regions and the mid-IR region.[40] Despite the increased computational costs, a perfect match has not yet been accomplished, and most AC determinations of flexible or larger molecules still rely on the calculation of harmonic spectra. Suitable programs for quantum-mechanical calculations are, among others, the Amsterdam Modeling Suite,[41] Dalton,[42] Gaussian,[43] and TURBOMOLE.[44]

The reader should bear in mind that AC determination is still not a black-box method and every computational method is prone to error.[45] For detailed information about the various methods of VCD spectra calculation, the quantum-mechanical theory behind them, MD simulations for the explicit description of solvent effects, and the transfer to machine learning methods, the reader shall be referred to the existing literature.[17,21,25,46–54]

2 | AIM OF THE CONDUCTED RESEARCH

The proposed procedure is analogous to that published by Pescitelli and Bruhn (summarized in Figure 1).[36]

1. A conformational search needs to be performed, ideally on a low-cost computational level (e.g., MMFF[55] or AM1[56]/PM6).[57] The main goal in this step is to obtain as many conformers as possible for a precise description of the conformational ensemble.

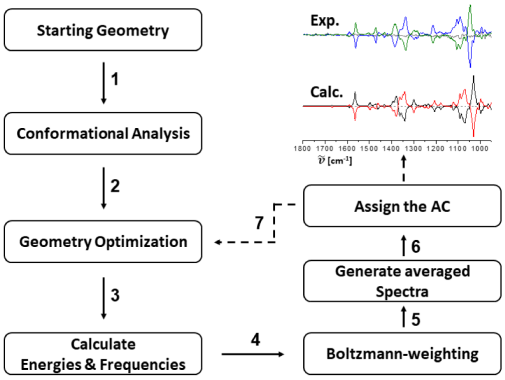

FIGURE 1 Flowchart for the general procedure to enable AC determination by VCD calculations.

2. A geometry optimization for each molecule from the obtained ensemble at DFT level with a given combination of *functional/basis set/solvation model* is the second step. Depending on the computational resources available, either a threshold can be applied to restrict the low-energy conformers, or every conformer can be kept until the Boltzmann weighting (Step 4).
3. Subsequently, an energy and frequency calculation must be performed for the optimized structures with the same method used for the geometry optimization. With the latter, true energy minima for each conformer can be confirmed by frequency analysis. Also, the desired vibrational rotational strengths for the prediction of the spectra are calculated in this step.
4. A Boltzmann weighting based on the calculated energies needs to be performed for the conformer ensemble. This can be either done manually or with suitable programs (e.g., *SpecDis*).
5. Now, the theoretical spectra can be plotted by converting the calculated vibrational frequencies, dipole strengths and rotational strengths into Lorentzian line shape functions.[11,58] Together with the previously obtained population-weighting factors, an averaged and Boltzmann-weighted IR and VCD spectrum can be generated.
6. In the last step, the obtained spectra are compared with the experimental spectra in a given wavelength region. For the best overlap, the scaling factor (to compensate a general frequency shift of the calculated spectra)[58,59] and the band width γ of the Lorentz curves need to be optimized. For both parameters, a range can be set to limit the employed cross-section algorithm (see the Supporting Information for the herein applied settings).[3] To prevent confirmation bias, as the AC is still unknown at this point, these values should be generated based on the comparison of IR-spectra alone and subsequently be applied to the predicted VCD spectrum to quantify the AC determination (e.g., using the ESI value).
7. If insufficient values are obtained, one should choose a different combination of functional and basis set and start over from Step 2 with a new geometry optimization.

In this benchmark analysis, calculations were solely conducted at the DFT level of theory. This approach has the advantage of low computational cost compared with more sophisticated post-HF ab initio approaches. Several classes of functionals, basis sets (Table 1) and two solvation models (IEFPCM[46,60,61] and SMD)[62] were compared to each other (see the Supporting Information for the respective xyz files). To cover a broad range of functionals, hybrid functionals, long-range-corrected functionals, and pure exchange–correlation functionals were taken into account, both with and without dispersion correction. These functionals were combined with several standard Dunning, Pople, and Karlsruhe basis sets (Table 1). For further insights, the reader is kindly referred to existing literature.[63–68]

With this paper, we intend to recommend a general approach on how to determine the AC of a chiral molecule by VCD using the free software *SpecDis* and without having to use too cost-intensive methods.

3 | THE APPROACH

The investigated molecules were selected to ensure clarity and comparability of the results. For the benchmarking analysis, fewer complex structures were chosen to keep the computational cost at a reasonable level. Furthermore, the molecules should have as few conformers as possible (ideally just a single one), contributing to cost-efficiency and reducing potential errors due to missing conformers in this benchmark approach. The solubility in carbon tetrachloride was the topmost criterion for the experimental spectroscopic part because it is a preferred solvent for VCD spectroscopy. Furthermore, carboxylic acids were excluded because they can form dimers in solution which are challenging to incorporate in the theoretical part.[107] Based on these criteria, we chose (1*R*,4*R*)-camphor (**1**), (2′*R*,3′*R*)-caripyrin (**2**), (*R*)-propylene oxide (**3**), (*S*)-1-phenethylamine (**4**), (*R*)-methyl *p*-tolyl sulfoxide (**5**), and (1*R*,4*R*)-thiocamphor (**6**) (Figure 2). Except for the sulfoxide **5**, which was prepared synthetically, all compounds were purchased from commercial sources.

TABLE 1 Chosen functionals and basis sets for the theoretical prediction of IR- and VCD spectra.

Functional		Basis set	
Hybrid	mPW1PW91[69–74]	6-31G[75]	Pople
	B3LYP[22,76–78]	6-31G(d)[75,79,80]	
	PW6B95[81]	6-31G(d,p)[75,79,80]	
	M06-2X[74]	6-31+G(d,p)[75,79,80,82]	
	PBE0[70,83,84]	6-31++G(d,p)[75,79,80,82]	
	B3P86[76,85]	6-311G[86,87]	
	B3PW91[71,72,74,76,88,89]	6-311G(d)[79,80,86,87]	
	TPSSh[89,90]	6-311G(d,p)[79,80,86,87]	
Long-range-corrected	CAM-B3LYP[91]	6-311+G(d,p)[79,80,82,86,87]	
	LC-ωPBE[71–73]	6-311++G(d,p)[79,80,82,86,87]	
	ωB97X-D[92,93]	def2-SVP[94–98]	Karlsruhe
Exchange–correlation (GGA and meta-GGA)	TPSS[99]	def2-TZVP[94–98]	
	PBE[83,84]	def2-TZVPP[94–98]	
	BP86[85]	cc-pVDZ[100,101]	Dunning
	B97-D3[102–105]	cc-pVTZ[100,101]	
		aug-cc-pVTZ[106]	

Note: Thus, a total number of 480 combinations were calculated and checked for similarity for each molecule.

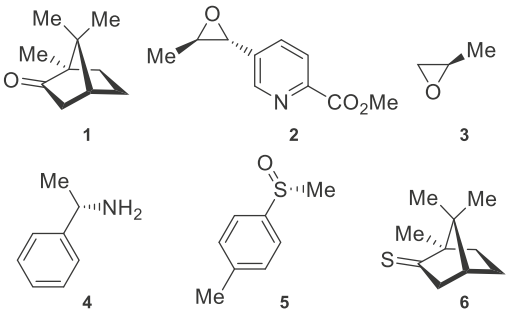

FIGURE 2 Molecular structures and absolute configurations of the examined compounds.

The results were evaluated including all compounds and additionally without the sulfur-containing compounds **5** and **6** because they were expected to behave differently due the presence of a polarizable third-row element. Technical, experimental, and computational details are specified in the Supporting Information, the coordinate files are in an additional zip file and the ESI value was used as the major evaluation criterion. The reader should keep in mind that a low ESI value does not necessarily correspond to a poor qualitative description of the experimental spectrum but can also result from poorly determined fitting parameters (see the Supporting Information). The quality of VCD spectra of flexible molecules also depends on the adequate description of the conformer ensemble in solution and another combination of *functional/basis set/solvation model* may be better suited for the correct description of equilibrium geometries and conformational populations.[14,15]

4 | RESULTS AND DISCUSSION

Sorting the respective levels of theory for the single molecules based on the ESI revealed that there are combinations that produce values higher than 80% for every molecule except for sulfoxide **5**. In those cases, the determination of the AC can be regarded as certain. For sulfoxide **5**, values of higher than 60% were obtained while values higher than 70% were not. This might be due to the aforementioned considerations regarding sulfur combined with the fact that the sulfur itself is the stereocenter of this compound.

5 | EVALUATION OF MEAN VALUES AND STANDARD DEVIATION

The calculation and plot of the mean values and standard deviations of the respective ESI values for every combination of *functional/basis set/solvation model* examined displays a common issue of DFT methods (Figure 3). About

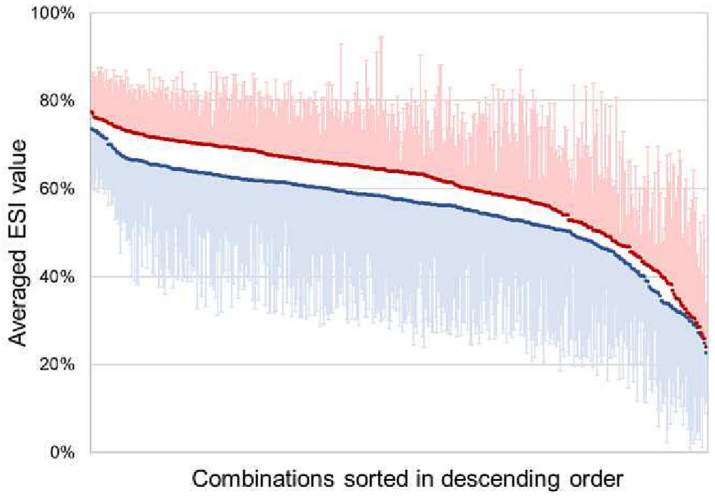

FIGURE 3 Averaged ESI values and standard deviations for all compounds (blue) and excluding the sulfur-containing compounds (red), sorted by mean values in descending order. For the sake of clarity, the standard deviation is only printed in one direction.

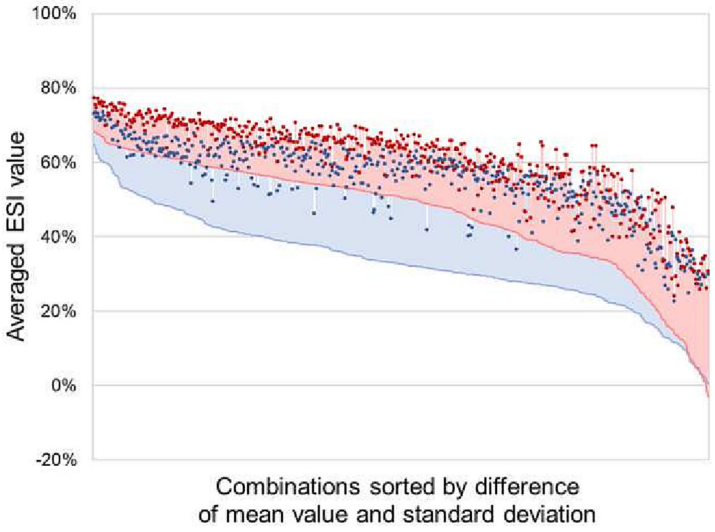

FIGURE 4 The averaged ESI values sorted by the difference of the mean value and the respective standard deviation in descending order, for all compounds (blue) and molecule **1**–**4**. The standard deviation is only printed in one direction to indicate the lower limitation.

50% of them produces quite high averaged ESI values of around 50% or higher but the deviation is also relatively high, especially in the case where all molecules were included (blue data set). An overall higher averaged ESI is achieved when only the molecules devoid of sulfur were evaluated (red data set), indicating a higher accuracy for light atom structures. The highest average values for a single combination reached in this work were above 70% (see the Supporting Information). In detail, there are 14 combinations that are above this threshold and it is striking that among these, the only basis sets represented are Dunning's correlation consistent (cc) triple zeta basis sets cc-pVTZ and aug-cc-pVTZ.[100,101,106] The most frequently occurring functionals were either hybrid (seven times) or long-range corrected functionals (six times), but there is no trend regarding the solvation model observable. When the sulfur-containing compounds **5** and **6** are not considered, the top 13 combinations reach averaged ESI values above 75%, this time including Pople, redefined Karlsruhe and Dunning basis sets, four, four, and five times, respectively. Among these 13, there is four times the B3LYP,[22,76–78] three times the Coulomb-

attenuated extended CAM-B3LYP,[91] and six times the ωB97X-D[92,93] functional. This supports the finding of the overall good performance of hybrid and long-range corrected functionals. A similar effect has been observed by Tsuneda and Hirao for the reproducibility of van der Waals bonds and the calculation of oscillator strengths in time-dependent DFT calculations using the latter class of functionals.[108]

When computing and plotting the difference between mean values and standard deviation (Figure 4), the lower limitations of the combinations are revealed (blue: all molecules, red: excluding sulfur). If the sulfur-containing molecules are excluded, a higher precision of the averaged ESI values is observable. In general, the plotted lower limitation lines show a relatively flat trend until reaching the negative spikes on the right edge of the graph. This again shows that DFT methods have a reasonable performance on average. Notably, those negative spikes (blue and red) almost exclusively contain the widely applicated Pople basis sets (without any additional polarization or diffuse functions)[75,86,87] which is also true for the graph in Figure 3, albeit to a lesser extent (see the Supporting Information).

It is noteworthy that one of the most frequently used combinations (B3LYP/6-311G(d,p)/SMD)[22,62,76–80,86,87] ranks second in this evaluation (just first and second row elements).

6 | EVALUATION OF THE 100 TOP AND BOTTOM COMBINATIONS

Extending this statistical approach to the top 100 and bottom 100 combinations sorted by the mean values of the ESI and the difference between them and the standard deviation (Figure 5) gives a more general trend of how these perform in VCD calculation (the bottom 100 combinations are displayed in the Supporting Information).

7 | FUNCTIONALS

Regarding the functionals (Figure 5, top), the first thing to notice is that they appear similarly often in the same plotted categories, regardless of whether sulfur is included or not. The combinations using B3P86,[76,85]

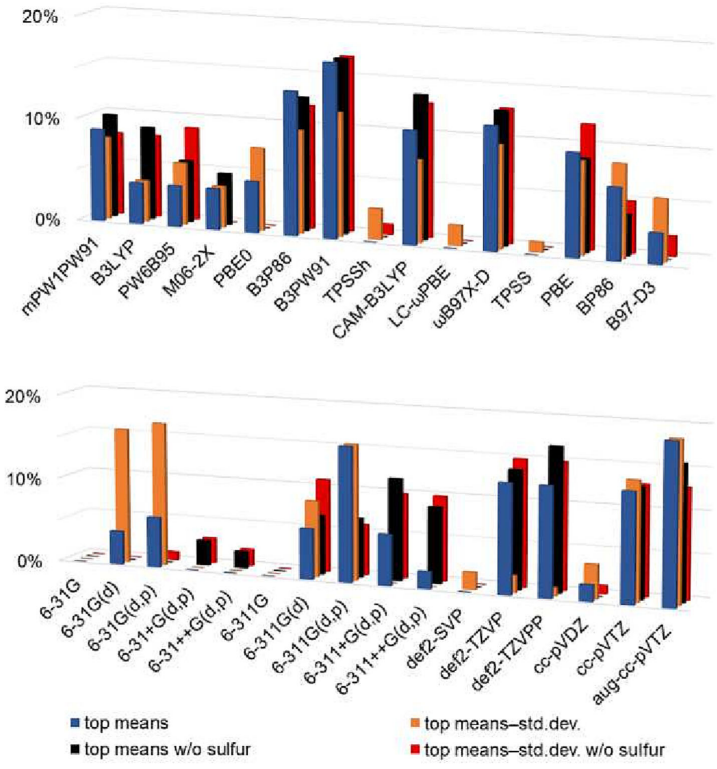

FIGURE 5 Occurrence of the respective examined functionals (top) and basis sets (bottom) among the top 100 combinations sorted by mean values and difference between mean value and standard deviation. The results were evaluated with and without the sulfur-containing compounds.

B3PW91,[71,72,74,76,88,89] and ωB97X-D[92,93] are the most frequent among the top 100 combinations and in the case where the difference between the mean value and the standard deviation is investigated (blue and orange bar). For the previous two functionals, this finding is in accordance with the studies of Ravichandran and Banik, who obtained similar results by benchmarking the potential of DFT methods to calculated vibrational frequencies (just IR), but it should be noted that the authors did not investigate the influence of different basis sets or a solvation model.[109] Barone et al. also reported on the good results that can be obtained with ωB97X-D functional in conjunction with double-ζ basis sets, after the authors benchmarked, among others, the equilibrium geometry and harmonic vibrational properties of 10 organic molecules of atmospheric and astrochemical relevance and compared the results with experimental values or high-level CCSD(T) computations.[110]

In the hybrid functional class, mPW1PW91[69–74] is the next most frequent among the top 100 combinations, while TPSSh[57,58] is the least. The other functionals are represented more or less equally in the top 100 and bottom 100 combinations. These results align with the extensive investigations of Goerigk and Grimme, who studied the performance of DFT methods regarding the calculation of thermochemistry, kinetics, and noncovalent interactions and came to the conclusion that hybrid functionals only had a medium performance.[111]

The range-separated functional CAM-B3LYP[91] performs quite well, whereas the remaining investigated functional from this class (LC-ωPBE[71–73]) is the most frequent among the bottom 100 combinations. Regarding the class of GGA and mGGA functionals, PBE[57,58] and BP86[85] appear quite often in the top 100, B97-D3[102–105] shows a balanced performance, and TPSS[99] appears the second most frequent among the bottom 100.

8 | BASIS SETS

In terms of the basis sets examined (Figure 5, bottom), the large Dunning basis sets perform quite well and occur the most amidst the top 100. The Karlsruhe basis sets (def2-TZVP and def2-TZVPP)[94–98] behave similarly. The smaller basis sets of the two previous classes, cc-pVDZ[74,75] and def2-SVP,[94–98] as well as the Pople basis sets 6-31G[75] and 6-311G[86,87] are found most often among the bottom 100 in both cases. This might be due to the fact that these basis sets consist of too few basis functions to describe the system sufficiently.

Regarding the other Pople basis sets, 6-311G(d,p)[79,80,86,87] performs quite well when all molecules are taken into account (blue bars). If sulfur is excluded, 6-311+G(d,p) and 6-311++G(d,p)[79,80,82,86,87] have the highest share among the top 100 combinations (black bars).

9 | SOLVATION MODELS

In terms of the solvation model, it does not seem to make a difference whether the model based on density (SMD)[62] or the integral equation formalism model polarizable continuum model (IEFPCM)[46,60,61] is used (see the Supporting Information).

10 | EVALUATION OF THE BEST PERFORMING COMBINATIONS FOR SINGLE COMPOUNDS

As already mentioned, there are several combinations that reached ESI values higher than 80% for every compound except for the sulfoxide (**5**). Only two combinations could exceed the aforementioned barrier for three molecules, each time using the ωB97X-D[92,93] functional and the SMD[62] solvation model, in conjunction with the 6-311+G(d,p)[79,80,82,86,87] and the aug-cc-pVTZ basis set.[106] The occurrence of a single combination (blue bars) and when a combination achieved for two molecules an ESI higher than 80% (orange bars), as well as the corresponding evaluation where the sulfur-containing compound **6** was excluded, were plotted (grey and yellow bars). Regarding the distribution of functionals and basis sets among these combinations (Figure 6), there are similarities and differences compared with the previous considerations.

11 | FUNCTIONALS

The functionals that reached >80% ESI for one compound (blue and grey bars) are more or less equally distributed (Figure 6, top), while mPW1PW91,[69–74] PBE0,[70,83,84] and ωB97X-D[92,93] being most frequent. Regarding the occurrence for two molecules, M06-2X,[74] B3P86,[76,85] and ωB97X-D[92,93] perform the best when all molecules are considered (orange bars), whereas B3LYP[22,76–78] and ωB97X-D[92,93] stand out when thiocamphor (**6**) is excluded (yellow bars). These findings are in accordance with the previously made observations that hybrid and long-range-corrected functionals can show a good performance, whereas the hybrid version (TPSSh[89,90]) and the meta-GGA functional TPSS[99] are again among the least frequent.

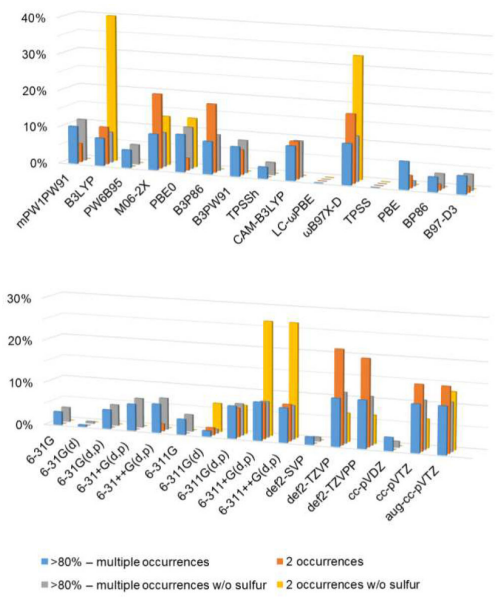

FIGURE 6 Occurrence of the respective examined functionals (top) and basis sets (bottom) among the combinations that reached over 80% ESI for at least one specific compound.

Nevertheless, the subpar performance of LC-ωPBE[71–73] on the other hand is rather surprising, but it was also among the less frequent functionals in the previous evaluation (vide supra).

12 | BASIS SETS

In terms of the basis sets (Figure 6, bottom), the occurrence in a single combination is almost independent on whether sulfur is included or not (blue and grey bars), comparable to the behavior of the functionals. Again, the Dunning (cc-pVTZ and aug-cc-pVTZ)[100,101,106] and Karlsruhe basis sets (def2-TZVP and def2-TZVPP)[94–98] are well represented but once more without cc-pVDZ[100,101] and def2-SVP.[94–98] The four basis sets mentioned foremost are also the most frequent amidst those combinations that reached at least 80% ESI for two compounds (orange bar). If sulfur is excluded, the Pople basis sets 6-311+G(d,p) and 6-311++G(d,p)[79,80,82,86,87] show the highest occurrence (yellow bar). The overall outstanding performance of the two triple zeta Dunning basis sets in combination with DFT functionals should be emphasized because these basis sets were originally developed using configuration interaction (CI) methods.[100] Nevertheless, this indicates that moving from double zeta (in the case of the Dunning basis sets) and split valence (in the case of the Ahlrichs basis sets) to the respective triple zeta basis sets gives a significant improvement of the results.

Regarding the Pople basis sets, there is a similar trend observable as previously, where smaller basis sets are less frequent among the high ESI values, especially when the occurrence for two molecules of the test set is investigated. In fact, it is clearly indicated that going from split valence double to triple zeta and adding diffuse functions gradually increases the accuracy because these basis sets become more frequent (blue and grey bars).

13 | SOLVATION MODELS

Again, the choice of the solvation model does not seem to make a crucial difference (a graphical representation can be found in the Supporting Information). Continuum models consider isotropic solvents, to which carbon tetrachloride approximately belongs, whereas SMD is a more universal solvation model and offers specifically parameterized radii to construct the solute cavity. Ultimately, both SMD[62] and IEFPCM[46,60,61] solve the Poisson–Boltzmann equation similarly.[62]

14 | EVALUATION BY SINGLE COMPOUNDS

Unsurprisingly, the methods that performed well for caripyrin (**2**) and propylene oxide (**3**) are very similar. Among these two, there is a high share of the B3LYP[22,76–78] functional with triple zeta basis sets (Pople, Karlsruhe, and Dunning equally distributed). Surprisingly, there is exclusively the SMD[62] solvation model being present.

The combinations that worked well on camphor (**1**) and thiocamphor (**6**) are almost identical but they differ completely from the ones of caripyrin (**2**) and propylene oxide (**3**). Interestingly, some of these methods (M06-2X,[74] PBE0,[70,83,84] and ωB97X-D[92,93]) in conjunction with larger Pople basis sets also performed well for phenethylamine (**4**), although these compounds differ significantly in their structure. In this case, almost only the IEFPCM[46,60,61] solvation model was present. Moreover, camphor (**1**), thiocamphor (**6**), and phenethylamine (**4**) were the only molecules where the two combinations already mentioned could achieve ESI values above 80% for all three molecules (vide supra).

After filtering these methods by their computational requirements to single out accurate but also cost-efficient methods which can also be applied to larger molecules,

we obtain the following list which could serve as starting point for the elucidation of the AC applying VCD spectroscopy:

- Chiral epoxides: B3LYP/6-311+G(d,p)/SMD.
- Bicyclic (thio)ketone or chiral amine: M06-2X/6-311+G(d,p)/IEFPCM, PBE0/6-311G(d)/IEFPCM, and ωB97X-D/6-311+G(d,p)/IEFPCM.

If sulfur-containing molecules give insufficient results, higher order polarization functions may be necessary, as described by Scholten et al.[112] The good performance of the PBE0 functional[70,83,84] is surprising because it is one of the few parameter-free functionals. Despite the overall good performance of the triple zeta Dunning and Ahlrichs basis sets, they are not included in the foregoing list due to their reduced cost-efficiency.

15 | CONCLUSION

The present work shows that there is no single combination to recommend in terms of the calculation of VCD spectra which is a common phenomenon of DFT methods. This leads to the outcome that there is no "one size fits all" multi-purpose method. However, based on the results of this study combined with our experience in successful calculation of VCD spectra and AC determination, some general advice can be given. In any case, it is always recommended to validate the results by simulating the VCD spectra with a different combination of *functional/basis set/solvation model* to exclude misassignments. Additional chiroptical methods, X-ray crystallography, or further measures, such as the confidence level, statistical robustness, or the vibrational dissymmetry factor, can also be applied to support the reliability of the AC assignment.[34,113,114]

- For the conformer distribution of larger molecules, force field, semi-empiric, or cost-efficient DFT methods are advised. Subsequent confinement of the conformer ensemble based on the relative energy might be useful.
- GGA and meta-GGA functionals are disadvantageous while hybrid and range-separated functionals are favored.
- Combinations worth trying are:
  - B3LYP/6-311G(d,p)/SMD
  - ωB97X-D/6-311+G(d,p)/SMD
  - M06-2X/6-311+G(d,p)/IEFPCM
  - PBE0/6-311G(d)/IEFPCM.

The Opatz group has particularly good experience with the hybrid density functionals B3LYP[22,76–78] and B3PW91[71,72,74,76,88,89] combined with the Pople basis set 6-311G(d,p)[79,80,86,87] and the IEFPCM[46,60,61] solvation model in the determination of the AC of natural products (e.g., dioxolanones,[115] hymenosetin,[116] caripyrin,[117] and oxalicumone C[118]), pesticides (imazalil),[119] synthetic cannabinoids (MDMB-CHMCZCA),[120] and synthetic products (e.g., 2,3-dihydro-1*H*,5*H*-pyrazolo[1,2-*a*]pyrazoles,[121] an oxazinone derivative,[122] and cyclopenta[*b*]benzofurans[123]).

ACKNOWLEDGMENTS

Parts of this research were conducted using the supercomputer MOGON 2 offered by Johannes Gutenberg-University Mainz (hpc.uni-mainz.de), which is a member of the Alliance for High Performance Computing in Rhineland-Palatinate (AHRP, www.ahrp.info) and the Gauss Alliance e.V. The authors gratefully acknowledge the computing time granted on the supercomputer MOGON 2 at Johannes Gutenberg-University Mainz (hpc.uni-mainz.de). Open Access funding enabled and organized by Projekt DEAL.

DATA AVAILABILITY STATEMENT

The data that support the findings of this study are available in the Supporting Information of this article.

ORCID

Till Opatz https://orcid.org/0000-0002-3266-4050

REFERENCES

1. van't Hoff JH. *La chimie dans l'espace*. Bazendijk; 1875.
2. Bijvoet JM, Peerdeman AF, van Bommel AJ. Determination of the absolute configuration of optically active compounds by means of X-rays. *Nature*. 1951;168(4268):271-272. doi:10.1038/168271a0
3. Bruhn T, Schaumlöffel A, Hemberger Y, Bringmann G. SpecDis: quantifying the comparison of calculated and experimental electronic circular dichroism spectra. *Chirality*. 2013;25(4):243-249. doi:10.1002/chir.22138
4. He Y, Bo W, Dukor RK, Nafie LA. Determination of absolute configuration of chiral molecules using vibrational optical activity: a review. *Appl Spectrosc*. 2011;65(7):699-723. doi:10.1366/11-06321
5. Stephens PJ, Devlin FJ, Pan J-J. The determination of the absolute configurations of chiral molecules using vibrational circular dichroism (VCD) spectroscopy. *Chirality*. 2008;20(5):643-663. doi:10.1002/chir.20477
6. Nafie LA. *Vibrational Optical Activity: Principles and Applications*. John Wiley & Sons; 2011.
7. Cotton A. Dispersion rotatoire anomale des corps absorbants. *Compt Rend*. 1895;120:1044.
8. Crabbé P. *Optical Rotatory Dispersion and Circular Dichroism in Organic Chemistry*. Holden-Day; 1965.
9. Holzwarth G, Hsu EC, Mosher HS, Faulkner TR, Moscowitz A. Infrared circular dichroism of carbon-hydrogen

and carbon-deuterium stretching modes. Observations. *J Am Chem Soc*. 1974;96(1):251-252. doi:10.1021/ja00808a042
10. Nafie LA, Cheng JC, Stephens PJ. Vibrational circular dichroism of 2,2,2-trifluoro-1-phenylethanol. *J Am Chem Soc*. 1975; 97(13):3842-3843. doi:10.1021/ja00846a061
11. Berova N, Polavarapu PL, Nakanishi K, Woody RW. *Comprehensive Chiroptical Spectroscopy: Instrumentation, Methodologies, and Theoretical Simulations*. John Wiley & Sons; 2011.
12. Berova N, Polavarapu PL, Nakanishi K, Woody RW. *Comprehensive Chiroptical Spectroscopy, Volume 2: Applications in Stereochemical Analysis of Synthetic Compounds, Natural Products, and Biomolecules*. John Wiley & Sons; 2012.
13. Polavarapu PL. Renaissance in chiroptical spectroscopic methods for molecular structure determination. *Chem Record*. 2007;7(2):125-136. doi:10.1002/tcr.20117
14. Batista JM Jr, Blanch EW, Bolzani VS. Recent advances in the use of vibrational chiroptical spectroscopic methods for stereochemical characterization of natural products. *Nat Prod Rep*. 2015;32(9):1280-1302. doi:10.1039/C5NP00027K
15. Polavarapu PL, Santoro E. Vibrational optical activity for structural characterization of natural products. *Nat Prod Rep*. 2020;37(12):1661-1699. doi:10.1039/D0NP00025F
16. Merten C, Golub TP, Kreienborg NM. Absolute configurations of synthetic molecular scaffolds from vibrational CD spectroscopy. *J Org Chem*. 2019;84(14):8797-8814. doi:10.1021/acs.joc.9b00466
17. Stephens PJ. Theory of vibrational circular dichroism. *J Phys Chem*. 1985;89(5):748-752. doi:10.1021/j100251a006
18. Schellman JA. Vibrational optical activity. *J Chem Phys*. 1973; 58(7):2882-2886. doi:10.1063/1.1679592
19. Holzwarth G, Chabay I. Optical activity of vibrational transitions: a coupled oscillator model. *J Chem Phys*. 1972;57(4): 1632-1635. doi:10.1063/1.1678447
20. Nafie LA, Walnut TH. Vibrational circular dichroism theory: a localized molecular orbital model. *Chem Phys Lett*. 1977; 49(3):441-446. doi:10.1016/0009-2614(77)87010-3
21. Stephens PJ, Lowe MA. Vibrational circular dichroism. *Annu Rev Phys Chem*. 1985;36(1):213-241. doi:10.1146/annurev.pc.36.100185.001241
22. Stephens PJ, Devlin FJ, Chabalowski CF, Frisch MJ. Ab initio calculation of vibrational absorption and circular dichroism spectra using density functional force fields. *J Phys Chem*. 1994;98(45):11623-11627. doi:10.1021/j100096a001
23. Amos RD. *Molecular property derivatives*. Ab Initio Methods in Quantum Chemistry, Volume 67, Part 1. Wiley; 2009:99.
24. Pulay P. Analytical derivative methods in quantum chemistry. *Adv Chem Phys*. 1987;69:241-286. doi:10.1002/9780470142943.ch4
25. Stephens PJ. Gauge dependence of vibrational magnetic dipole transition moments and rotational strengths. *J Phys Chem*. 1987;91(7):1712-1715. doi:10.1021/j100291a009
26. Cheeseman JR, Frisch MJ, Devlin FJ, Stephens PJ. Ab initio calculation of atomic axial tensors and vibrational rotational strengths using density functional theory. *Chem Phys Lett*. 1996;252(3):211-220. doi:10.1016/0009-2614(96)00154-6
27. Crawford TD. Ab initio calculation of molecular chiroptical properties. *Theor Chem Acc*. 2006;115(4):227-245. doi:10.1007/s00214-005-0001-4
28. Polavarapu PL, Covington CL. Comparison of experimental and calculated chiroptical spectra for chiral molecular structure determination. *Chirality*. 2014;26(9):539-552. doi:10.1002/chir.22316
29. Covington CL, Polavarapu PL. CDSpecTech: a single software suite for multiple chiroptical spectroscopic analyses. *Chirality*. 2017;29(5):178-192. doi:10.1002/chir.22691
30. Shen J, Zhu C, Reiling S, Vaz R. A novel computational method for comparing vibrational circular dichroism spectra. *Spectrochim Acta A Mol Biomol Spectrosc*. 2010;76(3):418-422. doi:10.1016/j.saa.2010.04.014
31. Bruhn T, Schaumlöffel A, Hemberger Y, Pescitelli G. *SpecDis, Version 1.71*; 2017. https://specdis-software.jimdofree.com/
32. Bruhn T, Schaumlöffel A, Hemberger Y, Bringmann G. *SpecDis Version 1.61*. University of Wuerzburg; 2013.
33. Kuppens T, Langenaeker W, Tollenaere JP, Bultinck P. Determination of the stereochemistry of 3-hydroxymethyl-2,-3-dihydro-[1,4]dioxino[2,3-*b*]-pyridine by vibrational circular dichroism and the effect of DFT integration grids. *J Phys Chem A*. 2003;107(4):542-553. doi:10.1021/jp021822g
34. Debie E, De Gussem E, Dukor RK, Herrebout W, Nafie LA, Bultinck P. A confidence level algorithm for the determination of absolute configuration using vibrational circular dichroism or Raman optical activity. *ChemPhysChem*. 2011; 12(8):1542-1549. doi:10.1002/cphc.201100050
35. Autschbach J, Nitsch-Velasquez L, Rudolph M. Time-dependent density functional response theory for electronic chiroptical properties of chiral molecules. In: Naaman R, Beratan DN, Waldeck D, eds. *Electronic and Magnetic Properties of Chiral Molecules and Supramolecular Architectures*. Springer; 2011:1-98.
36. Pescitelli G, Bruhn T. Good computational practice in the assignment of absolute configurations by TDDFT calculations of ECD spectra. *Chirality*. 2016;28(6):466-474. doi:10.1002/chir.22600
37. Bloino J, Barone V. A second-order perturbation theory route to vibrational averages and transition properties of molecules: general formulation and application to infrared and vibrational circular dichroism spectroscopies. *J Chem Phys*. 2012; 136(12):124108. doi:10.1063/1.3695210
38. Kreienborg NM, Bloino J, Osowski T, Pollok CH, Merten C. The vibrational CD spectra of propylene oxide in liquid xenon: a proof-of-principle CryoVCD study that challenges theory. *Phys Chem Chem Phys*. 2019;21(12):6582-6587. doi:10.1039/C9CP00537D
39. Paoloni L, Mazzeo G, Longhi G, et al. Toward fully unsupervised anharmonic computations complementing experiment for robust and reliable assignment and interpretation of IR and VCD spectra from mid-IR to NIR: the case of 2,3-butanediol and trans-1,2-cyclohexanediol. *J Phys Chem A*. 2020;124(5):1011-1024. doi:10.1021/acs.jpca.9b11025
40. Fusè M, Longhi G, Mazzeo G, et al. Anharmonic aspects in vibrational circular dichroism spectra from 900 to 9000 cm^{-1} for methyloxirane and methylthiirane. *J Phys Chem A*. 2022; 126(38):6719-6733. doi:10.1021/acs.jpca.2c05332
41. Koenis MAJ, Visser O, Visscher L, Buma WJ, Nicu VP. GUI implementation of VCDtools, a program to analyze computed vibrational circular dichroism spectra. *J Chem Inf Model*. 2020;60(1):259-267. doi:10.1021/acs.jcim.9b00956

42. Aidas K, Angeli C, Bak KL, et al. The Dalton quantum chemistry program system. *WIREs Comput Mol Sci*. 2014;4(3):269-284. doi:10.1002/wcms.1172
43. Frisch MJ, Trucks GW, Schlegel HB, et al. *Gaussian 16, Revision A.03*. Gaussian, Inc.; 2016.
44. TURBOMOLE V7.7. Germany: University of Karlsruhe and Forschungszentrum Karlsruhe GmbH, 1989-2007, TURBOMOLE GmbH, since 2007; 2022.
45. Polavarapu PL. Molecular structure determination using chiroptical spectroscopy: where we may go wrong? *Chirality*. 2012;24(11):909-920. doi:10.1002/chir.22015
46. Mennucci B, Cammi R. *Continuum Solvation Models in Chemical Physics: From Theory to Applications*. John Wiley & Sons; 2007. doi:10.1002/9780470515235
47. Sadlej J, Dobrowolski JC, Rode JE. VCD spectroscopy as a novel probe for chirality transfer in molecular interactions. *Chem Soc Rev*. 2010;39(5):1478-1488. doi:10.1039/B915178H
48. Bloino J, Biczysko M, Barone V. Anharmonic effects on vibrational spectra intensities: infrared, Raman, vibrational circular dichroism, and Raman optical activity. *J Phys Chem A*. 2015;119(49):11862-11874. doi:10.1021/acs.jpca.5b10067
49. Yang Q, Mendolicchio M, Barone V, Bloino J. Accuracy and reliability in the simulation of vibrational spectra: a comprehensive benchmark of energies and intensities issuing from generalized vibrational perturbation theory to second order (GVPT2). *Front Astron Space Sci*. 2021;8:665232. doi:10.3389/fspas.2021.665232
50. Vermeyen T, Brence J, Van Echelpoel R, et al. Exploring machine learning methods for absolute configuration determination with vibrational circular dichroism. *Phys Chem Chem Phys*. 2021;23(35):19781-19789. doi:10.1039/D1CP02428K
51. Merten C. Recent advances in the application of vibrational circular dichroism spectroscopy for the characterization of asymmetric catalysts. *Eur J Org Chem*. 2020;2020(37):5892-5900. doi:10.1002/ejoc.202000876
52. Ghidinelli S, Abbate S, Koshoubu J, Araki Y, Wada T, Longhi G. Solvent effects and aggregation phenomena studied by vibrational optical activity and molecular dynamics: the case of pantolactone. *J Phys Chem B*. 2020;124(22):4512-4526. doi:10.1021/acs.jpcb.0c01483
53. Le Barbu-Debus K, Bowles J, Jähnigen S, et al. Assessing cluster models of solvation for the description of vibrational circular dichroism spectra: synergy between static and dynamic approaches. *Phys Chem Chem Phys*. 2020;22(45):26047-26068. doi:10.1039/D0CP03869E
54. Keiderling TA. Instrumentation for vibrational circular dichroism spectroscopy: method comparison and newer developments. *Molecules*. 2018;23(9):2404. doi:10.3390/molecules23092404
55. Halgren TA. Merck molecular force field. I. Basis, form, scope, parameterization, and performance of MMFF94. *J Comput Chem*. 1996;17(5–6):490-519. doi:10.1002/(SICI)1096-987X(199604)17:5/63.0.CO;2-P
56. Dewar MJS, Zoebisch EG, Healy EF, Stewart JJP. Development and use of quantum mechanical molecular models. 76. AM1: a new general purpose quantum mechanical molecular model. *J Am Chem Soc*. 1985;107(13):3902-3909. doi:10.1021/ja00299a024
57. Stewart JJP. Optimization of parameters for semiempirical methods V: modification of NDDO approximations and application to 70 elements. *J Mol Model*. 2007;13(12):1173-1213. doi:10.1007/s00894-007-0233-4
58. Stephens PJ, Devlin FJ, Cheeseman JR. *VCD spectroscopy for organic chemists*. CRC Press; 2012. doi:10.1201/b12278
59. Merrick JP, Moran D, Radom L. An evaluation of harmonic vibrational frequency scale factors. *J Phys Chem A*. 2007;111(45):11683-11700. doi:10.1021/jp073974n
60. Mennucci B, Cancès E, Tomasi J. Evaluation of solvent effects in isotropic and anisotropic dielectrics and in ionic solutions with a unified integral equation method: theoretical bases, computational implementation, and numerical applications. *J Phys Chem B*. 1997;101(49):10506-10517. doi:10.1021/jp971959k
61. Tomasi J, Mennucci B, Cancès E. The IEF version of the PCM solvation method: an overview of a new method addressed to study molecular solutes at the QM ab initio level. *J Mol Struct (THEOCHEM)*. 1999;464(1–3):211-226. doi:10.1016/S0166-1280(98)00553-3
62. Marenich AV, Cramer CJ, Truhlar DG. Universal solvation model based on solute electron density and on a continuum model of the solvent defined by the bulk dielectric constant and atomic surface tensions. *J Phys Chem B*. 2009;113(18):6378-6396. doi:10.1021/jp810292n
63. Goerigk L, Grimme S. Double-hybrid density functionals. *WIREs Comput Mol Sci*. 2014;4(6):576-600. doi:10.1002/wcms.1193
64. Hill JG. Gaussian basis sets for molecular applications. *Int J Quantum Chem*. 2013;113(1):21-34. doi:10.1002/qua.24355
65. Jensen F. Atomic orbital basis sets. *WIREs Comput Mol Sci*. 2013;3(3):273-295. doi:10.1002/wcms.1123
66. Kryachko ES, Ludeña EV. Density functional theory: foundations reviewed. *Phys Rep*. 2014;544(2):123-239. doi:10.1016/j.physrep.2014.06.002
67. Laskowski R, Blaha P, Tran F. Assessment of DFT functionals with NMR chemical shifts. *Phys Rev B*. 2013;87(19):195130. doi:10.1103/PhysRevB.87.195130
68. Laurent AD, Jacquemin D. TD-DFT benchmarks: a review. *Int J Quantum Chem*. 2013;113(17):2019-2039. doi:10.1002/qua.24438
69. Adamo C, Barone V. Exchange functionals with improved long-range behavior and adiabatic connection methods without adjustable parameters: the mPW and mPW1PW models. *J Chem Phys*. 1998;108(2):664-675. doi:10.1063/1.475428
70. Adamo C, Barone V. Toward reliable density functional methods without adjustable parameters: the PBE0 model. *J Chem Phys*. 1999;110(13):6158-6170. doi:10.1063/1.478522
71. Vydrov OA, Heyd J, Krukau AV, Scuseria GE. Importance of short-range versus long-range Hartree-Fock exchange for the performance of hybrid density functionals. *J Chem Phys*. 2006;125(7):074106. doi:10.1063/1.2244560
72. Vydrov OA, Scuseria GE. Assessment of a long-range corrected hybrid functional. *J Chem Phys*. 2006;125(23):234109. doi:10.1063/1.2409292
73. Vydrov OA, Scuseria GE, Perdew JP. Tests of functionals for systems with fractional electron number. *J Chem Phys*. 2007;126(15):154109. doi:10.1063/1.2723119

74. Zhao Y, Truhlar DG. The M06 suite of density functionals for main group thermochemistry, thermochemical kinetics, noncovalent interactions, excited states, and transition elements: two new functionals and systematic testing of four M06-class functionals and 12 other functionals. *Theor Chem Acc*. 2008; 120(1):215-241. doi:10.1007/s00214-007-0310-x
75. Hehre WJ, Ditchfield R, Pople JA. Self-consistent molecular orbital methods. XII. Further extensions of Gaussian-type basis sets for use in molecular orbital studies of organic molecules. *J Chem Phys*. 1972;56(5):2257-2261. doi:10.1063/1.1677527
76. Becke AD. Density-functional thermochemistry. III. The role of exact exchange. *J Chem Phys*. 1993;98(7):5648-5652. doi:10.1063/1.464913
77. Lee C, Yang W, Parr RG. Development of the Colle-Salvetti correlation-energy formula into a functional of the electron density. *Phys Rev B*. 1988;37(2):785-789. doi:10.1103/PhysRevB.37.785
78. Vosko SH, Wilk L, Nusair M. Accurate spin-dependent electron liquid correlation energies for local spin density calculations: a critical analysis. *Can J Phys*. 1980;58(8):1200-1211. doi:10.1139/p80-159
79. Francl MM, Pietro WJ, Hehre WJ, et al. Self-consistent molecular orbital methods. XXIII. A polarization-type basis set for second-row elements. *J Chem Phys*. 1982;77(7):3654-3665. doi:10.1063/1.444267
80. Hariharan PC, Pople JA. The influence of polarization functions on molecular orbital hydrogenation energies. *Theor Chim Acta*. 1973;28(3):213-222. doi:10.1007/BF00533485
81. Zhao Y, Truhlar DG. Design of density functionals that are broadly accurate for thermochemistry, thermochemical kinetics, and nonbonded interactions. *J Phys Chem A*. 2005; 109(25):5656-5667. doi:10.1021/jp050536c
82. Clark T, Chandrasekhar J, Spitznagel GW, Schleyer PR. Efficient diffuse function-augmented basis sets for anion calculations. III. The 3-21+G basis set for first-row elements, Li–F. *J Comput Chem*. 1983;4(3):294-301. doi:10.1002/jcc.540040303
83. Perdew JP, Burke K, Ernzerhof M. Generalized gradient approximation made simple. *Phys Rev Lett*. 1996;77(18):3865-3868. doi:10.1103/PhysRevLett.77.3865
84. Perdew JP, Burke K, Ernzerhof M. Generalized gradient approximation made simple [Phys. Rev. Lett. 77, 3865 (1996)]. *Phys Rev Lett*. 1997;78(7):1396. doi:10.1103/PhysRevLett.78.1396
85. Perdew JP. Density-functional approximation for the correlation energy of the inhomogeneous electron gas. *Phys Rev B*. 1986;33(12):8822-8824. doi:10.1103/PhysRevB.33.8822
86. Krishnan R, Binkley JS, Seeger R, Pople JA. Self-consistent molecular orbital methods. XX. A basis set for correlated wave functions. *J Chem Phys*. 1980;72(1):650-654. doi:10.1063/1.438955
87. McLean AD, Chandler GS. Contracted Gaussian basis sets for molecular calculations. I. Second row atoms, Z=11–18. *J Chem Phys*. 1980;72(10):5639-5648. doi:10.1063/1.438980
88. Perdew JP, Wang Y. Accurate and simple analytic representation of the electron-gas correlation energy. *Phys Rev B*. 1992; 45(23):13244-13249. doi:10.1103/PhysRevB.45.13244
89. Staroverov VN, Scuseria GE, Tao J, Perdew JP. Comparative assessment of a new nonempirical density functional: molecules and hydrogen-bonded complexes. *J Chem Phys*. 2003; 119(23):12129-12137. doi:10.1063/1.1626543
90. Staroverov VN, Scuseria GE, Tao J, Perdew JP. Erratum: "Comparative assessment of a new nonempirical density functional: Molecules and hydrogen-bonded complexes" [J. Chem. Phys. 119, 12129 (2003)]. *J Chem Phys*. 2004;121(22):11507. doi:10.1063/1.1795692
91. Yanai T, Tew DP, Handy NC. A new hybrid exchange–correlation functional using the Coulomb-attenuating method (CAM-B3LYP). *Chem Phys Lett*. 2004;393(1–3):51-57. doi:10.1016/j.cplett.2004.06.011
92. Chai J-D, Head-Gordon M. Long-range corrected hybrid density functionals with damped atom-atom dispersion corrections. *Phys Chem Chem Phys*. 2008;10(44):6615-6620. doi:10.1039/b810189b
93. Chai J-D, Head-Gordon M. Systematic optimization of long-range corrected hybrid density functionals. *J Chem Phys*. 2008;128(8):084106. doi:10.1063/1.2834918
94. Schäfer A, Horn H, Ahlrichs R. Fully optimized contracted Gaussian basis sets for atoms Li to Kr. *J Chem Phys*. 1992; 97(4):2571-2577. doi:10.1063/1.463096
95. Schäfer A, Huber C, Ahlrichs R. Fully optimized contracted Gaussian basis sets of triple zeta valence quality for atoms Li to Kr. *J Chem Phys*. 1994;100(8):5829-5835. doi:10.1063/1.467146
96. Weigend F. Accurate Coulomb-fitting basis sets for H to Rn. *Phys Chem Chem Phys*. 2006;8(9):1057-1065. doi:10.1039/b515623h
97. Weigend F, Ahlrichs R. Balanced basis sets of split valence, triple zeta valence and quadruple zeta valence quality for H to Rn: design and assessment of accuracy. *Phys Chem Chem Phys*. 2005;7(18):3297-3305. doi:10.1039/b508541a
98. Zheng J, Xu X, Truhlar DG. Minimally augmented Karlsruhe basis sets. *Theor Chem Acc*. 2011;128(3):295-305. doi:10.1007/s00214-010-0846-z
99. Tao J, Perdew JP, Staroverov VN, Scuseria GE. Climbing the density functional ladder: nonempirical meta-generalized gradient approximation designed for molecules and solids. *Phys Rev Lett*. 2003;91(14):146401. doi:10.1103/PhysRevLett.91.146401
100. Dunning TH Jr. Gaussian basis sets for use in correlated molecular calculations. I. The atoms boron through neon and hydrogen. *J Chem Phys*. 1989;90(2):1007-1023. doi:10.1063/1.456153
101. Woon DE, Dunning TH Jr. Gaussian basis sets for use in correlated molecular calculations. III. The atoms aluminum through argon. *J Chem Phys*. 1993;98(2):1358-1371. doi:10.1063/1.464303
102. Becke AD. Density-functional thermochemistry. V. Systematic optimization of exchange-correlation functionals. *J Chem Phys*. 1997;107(20):8554-8560. doi:10.1063/1.475007
103. Grimme S. Semiempirical GGA-type density functional constructed with a long-range dispersion correction. *J Comput Chem*. 2006;27(15):1787-1799. doi:10.1002/jcc.20495
104. Grimme S, Ehrlich S, Goerigk L. Effect of the damping function in dispersion corrected density functional theory. *J Comput Chem*. 2011;32(7):1456-1465. doi:10.1002/jcc.21759

105. Schmider HL, Becke AD. Optimized density functionals from the extended G2 test set. *J Chem Phys*. 1998;108(23):9624-9631. doi:10.1063/1.476438
106. Kendall RA, Dunning TH Jr, Harrison RJ. Electron affinities of the first-row atoms revisited. Systematic basis sets and wave functions. *J Chem Phys*. 1992;96(9):6796-6806. doi:10.1063/1.462569
107. Polavarapu PL, Donahue EA, Hammer KC, et al. Chiroptical spectroscopy of natural products: avoiding the aggregation effects of chiral carboxylic acids. *J Nat Prod*. 2012;75(8):1441-1450. doi:10.1021/np300341z
108. Tsuneda T, Hirao K. Long-range correction for density functional theory. *WIREs Comput Mol Sci*. 2014;4(4):375-390. doi:10.1002/wcms.1178
109. Ravichandran L, Banik S. Performance of different density functionals for the calculation of vibrational frequencies with vibrational coupled cluster method in bosonic representation. *Theor Chem Acc*. 2017;137(1):1. doi:10.1007/s00214-017-2177-9
110. Barone V, Ceselin G, Fusè M, Tasinato N. Accuracy meets interpretability for computational spectroscopy by means of hybrid and double-hybrid functionals. *Front Chem*. 2020;8:8. doi:10.3389/fchem.2020.584203
111. Goerigk L, Grimme S. A thorough benchmark of density functional methods for general main group thermochemistry, kinetics, and noncovalent interactions. *Phys Chem Chem Phys*. 2011;13(14):6670-6688. doi:10.1039/c0cp02984j
112. Scholten K, Engelage E, Merten C. Basis set dependence of S═O stretching frequencies and its consequences for IR and VCD spectra predictions. *Phys Chem Chem Phys*. 2020;22(48):27979-27986. doi:10.1039/D0CP05420H
113. Vandenbussche J, Bultinck P, Przybył AK, Herrebout WA. Statistical validation of absolute configuration assignment in vibrational optical activity. *J Chem Theory Comput*. 2013;9(12):5504-5512. doi:10.1021/ct400843e
114. Covington CL, Polavarapu PL. Similarity in dissymmetry factor spectra: a quantitative measure of comparison between experimental and predicted vibrational circular dichroism. *J Phys Chem A*. 2013;117(16):3377-3386. doi:10.1021/jp401079s
115. Andernach L, Sandjo LP, Liermann JC, Buckel I, Thines E, Opatz T. Assignment of configuration in a series of dioxolanone-type secondary metabolites from *Guignardia bidwellii*—a comparison of VCD and ECD spectroscopy. *Eur J Org Chem*. 2013;2013(26):5946-5951. doi:10.1002/ejoc.201300530
116. Kauhl U, Andernach L, Weck S, et al. Total synthesis of (−)-hymenosetin. *J Org Chem*. 2016;81(1):215-228. doi:10.1021/acs.joc.5b02526
117. Andernach L, Opatz T. Assignment of the absolute configuration and total synthesis of (+)-caripyrin. *Eur J Org Chem*. 2014;2014(22):4780-4784. doi:10.1002/ejoc.201402540
118. Wink C, Andernach L, Opatz T, Waldvogel SR. Total synthesis of (±)-oxalicumone C and chiral resolution and elucidation of its absolute configuration. *Eur J Org Chem*. 2014;2014(35):7788-7792. doi:10.1002/ejoc.201403189
119. Casas ME, Kretschmann AC, Andernach L, Opatz T, Bester K. Separation, isolation and stereochemical assignment of imazalil enantiomers and their quantitation in an in vitro toxicity test. *J Chromatogr A*. 2016;1452:116-120. doi:10.1016/j.chroma.2016.05.008
120. Weber C, Pusch S, Schollmeyer D, Münster-Müller S, Pütz M, Opatz T. Characterization of the synthetic cannabinoid MDMB-CHMCZCA. *Beilstein J Org Chem*. 2016;12:2808-2815. doi:10.3762/bjoc.12.279
121. Pušavec Kirar E, Grošelj U, Golobič A, et al. Absolute configuration determination of 2,3-dihydro-1*H*,5*H*-pyrazolo[1,2-*a*]pyrazoles using chiroptical methods at different wavelengths. *J Org Chem*. 2016;81(23):11802-11812. doi:10.1021/acs.joc.6b02270
122. Dietz J-P, Lucas T, Groß J, et al. Six-step gram-scale synthesis of the human immunodeficiency virus integrase inhibitor dolutegravir sodium. *Org Process Res Dev*. 2021;25(8):1898-1910. doi:10.1021/acs.oprd.1c00139
123. Mirion M, Andernach L, Stobe C, et al. Synthesis and isolation of enantiomerically enriched cyclopenta[*b*]benzofurans based on products from anodic oxidation of 2,4-dimethylphenol. *Eur J Org Chem*. 2015;2015(22):4876-4882. doi:10.1002/ejoc.201500600

SUPPORTING INFORMATION

Additional supporting information can be found online in the Supporting Information section at the end of this article.

How to cite this article: Groß J, Kühlborn J, Pusch S, et al. Comparison of different density functional theory methods for the calculation of vibrational circular dichroism spectra. *Chirality*. 2023;35(10):753-765. doi:10.1002/chir.23580

7.2.2 Differenzierung von Diastereomeren in der Synthese eines HIV-Integrase-Inhibitors

In der Arbeitsgruppe Opatz wurde eine Syntheseroute zu Dolutegravir-Natrium (**137**, in der Publikation **15**) über sechs lineare Stufen entwickelt, die ohne chromatographische Reinigungsschritte auskommt. Dabei konnte nicht nur eine Gesamtausbeute von bis zu 51% erreicht, sondern auch die Umsetzbarkeit im Grammmaßstab demonstriert werden.

Bei der intramolekularen Transacetalisierung von **132** (in der Publikation **34**), dem entscheidenden Syntheseschritt bei der Konstruktion des B- und C-Rings, können zwei diastereomere Verbindungen **133** und **134** auftreten. Unter den gewählten Reaktionsbedingungen wurde ausschließlich ein Diastereomer isoliert und der Vergleich von gemessenen und simulierten VCD-Spektren ermöglichte die eindeutige Bestimmung der Konfiguration des gebildeten Oxazinons **133** (in der Publikation **35**) als C-4*R* und C-9a*S* (Abbildung 7.6).[559]

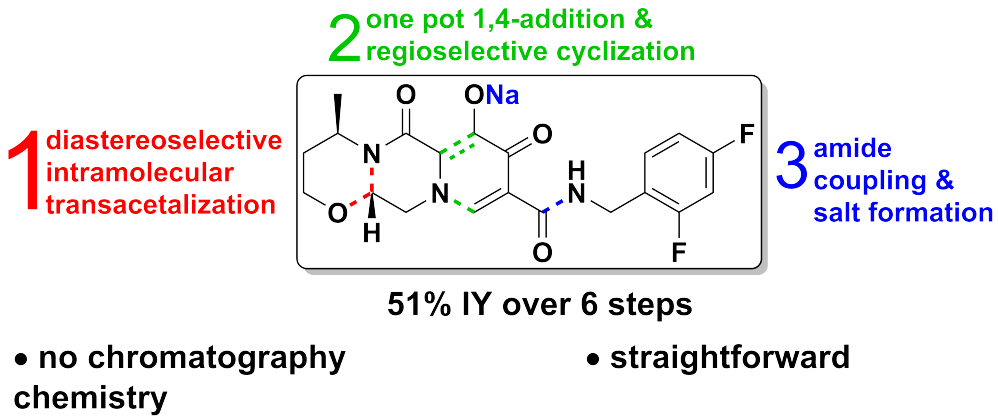

Abbildung 7.6: *Graphical abstract* der Publikation „Six-Step Gram Scale Synthesis of the HIV Integrase Inhibitor Dolutegravir Sodium“.[559]

Die Syntheseroute wurde von [redacted] entwickelt und optimiert sowie alternative Syntheserouten zusammen mit [redacted] untersucht. Die VCD-Spektren von Oxazinon **133** (in der Publikation **35**) wurden von [redacted] im Rahmen eines Forschungsmoduls aufgenommen und mittels DFT-Berechnungen simuliert. Die Spektren des anderen möglichen Diastereomers **134** wurden von J. Groß simuliert. Das Manuskript wurden von [redacted], J. Groß und T. Opatz erstellt.[14]

[14] *Reprinted with permission from J.-P. Dietz, T. Lucas, J. Groß, S. Seitel, J. Brauer, D. Ferenc, B. F. Gupton, T. Opatz, Org. Process Res. Dev. 2021, 25, 1898–1910. Copyright ©2021, American Chemical Society.*

ORGANIC PROCESS RESEARCH & DEVELOPMENT
OPR&D

pubs.acs.org/OPRD Article

Six-Step Gram-Scale Synthesis of the Human Immunodeficiency Virus Integrase Inhibitor Dolutegravir Sodium

Jule-Philipp Dietz, Tobias Lucas, Jonathan Groß, Sebastian Seitel, Jan Brauer, Dorota Ferenc, B. Frank Gupton, and Till Opatz*

Cite This: *Org. Process Res. Dev.* 2021, 25, 1898−1910 Read Online

ACCESS | Metrics & More | Article Recommendations | Supporting Information

ABSTRACT: A short and practical synthesis for preparing the active pharmaceutical ingredient dolutegravir sodium was developed. The convergent strategy starts from (*R*)-3-amino-1-butanol and establishes the BC ring system in a 76% isolated yield over four steps. Ring A was constructed by a one-pot 1,4-addition to diethyl-(2*E*/*Z*)-2-(ethoxymethylidene)-3-oxobutandioate and subsequent $MgBr_2 \cdot OEt_2$-mediated regioselective cyclization. Amide formation with 2,4-difluorobenzylamine was either performed from the free carboxylic acid or through aminolysis of the corresponding ethyl ester. Final salt formation afforded dolutegravir sodium in a 48−51% isolated yield (HPLC purity of 99.7−99.9%) over six linear steps.

KEYWORDS: *dolutegravir sodium, active pharmaceutical ingredient, antivirals, integrase inhibitors, carbamoyl pyridones*

INTRODUCTION

Infection with the human immunodeficiency virus (HIV) has become controllable in recent years due to enormous progress in development of highly active drugs, which are given for antiretroviral therapy (ART).[1] ART requires the administration of at least three different antiviral drugs to suppress the development of resistances.[2] Differentiated by the target enzyme, there are several classes of HIV-inhibiting drugs. The class of integrase strand transfer inhibitors (INSTIs) interferes with the HIV integrase enzyme and prevents it from inserting viral DNA into the human genome. INSTIs have been introduced in 2007 with the launch of raltegravir (**1**) followed by elvitegravir (**2**, 2012), dolutegravir (**3**, 2013), bictegravir (**4**, 2018), and cabotegravir (**5**, 2021)[3] (Scheme 1).[4]

The last three compounds exhibit a high similarity in their molecular structures, assigning them to the group of carbamoyl pyridine INSTIs. Dolutegravir (**3**), usually administered orally as its sodium salt, was recently recommended by the World Health Organization for first-line treatment of HIV initiating ART.[5] As a consequence, the demand of this important medication could further rise.

All synthetic approaches to **3** that have been published before 2019 have been carefully reviewed.[4,6] Since then, four more routes were disclosed.[7−10] Most of the published syntheses follow a similar strategy, which is represented here by the hitherto most efficient approach from Micro Labs (2016)[11] (Scheme 2). The highly functionalized pyridone **7** (ring A) is constructed first, which then undergoes cyclization with (*R*)-3-amino-1-butanol (**13**) to construct rings B and C. Deprotection of the usually protected enol and treatment with sodium hydroxide furnish dolutegravir sodium (**15**). The seven-step synthesis by Micro Labs afforded **15** in a 35% overall yield. This retained synthesis concept could be attributed to the late-stage introduction of the expensive amino alcohol **13**.

Since the discovery of dolutegravir and the emerging demand of (*R*)-3-amino-1-butanol (**13**), more efficient syntheses of this crucial building block have been developed with the consequence of a decreasing market price.[12] Thus, an earlier introduction of **13** could add additional value by bringing more diversification to the synthetic portfolio of dolutegravir. Extending the scope of industrially applicable synthetic routes should encourage generic manufacturing to ensure global supply of this important drug.

Here, a new synthetic route should be investigated by taking **13** as a starting material (Scheme 3). By using commodity chemicals, the ring system BC (**16**) should be constructed first. Next, **16** should be reacted with readily accessible diethyl-(2*E*/*Z*)-2-(ethoxymethylidene)-3-oxobutandioate (**17**) to install ring A. Amide coupling with 2,4-difluorobenzylamine and salt formation follow in the last step. All in all, an industrially feasible synthesis route was intended to be developed.

RESULTS AND DISCUSSION

Synthesis of the Ring System BC. The synthesis of amine **16** has already been described twice in the patent literature. Lerner et al. reported a five-step synthesis starting from ethyl bromoacetate (**19**) furnishing amine **16** in a 24% overall yield.[13] The crucial cyclization with amino alcohol **13** gave only a 55% yield under microwave conditions, and

Received: April 21, 2021
Published: July 12, 2021

https://doi.org/10.1021/acs.oprd.1c00139
Org. Process Res. Dev. 2021, 25, 1898−1910

Scheme 1. Structures of Raltegravir (1), Elvitegravir (2), Dolutegravir (3), Bictegravir (4), and Cabotegravir (5)

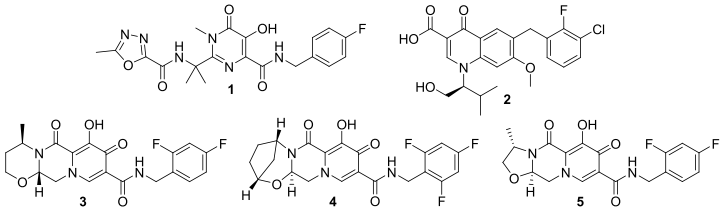

Scheme 2. Synthesis of Dolutegravir by Micro Labs (2016)

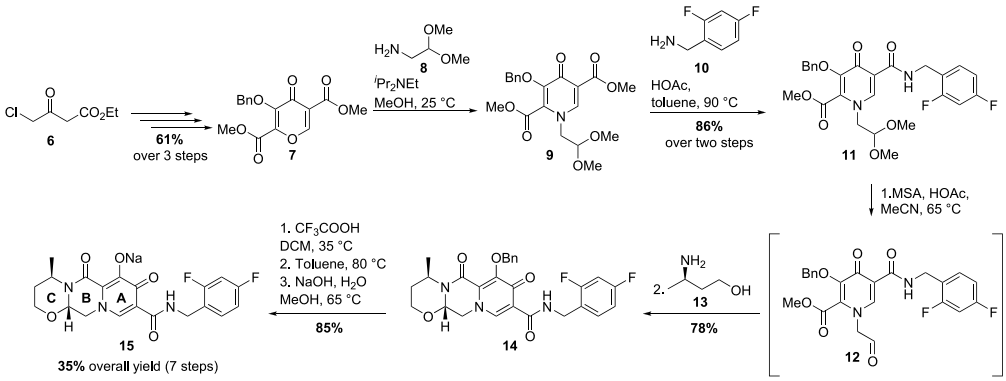

Scheme 3. Retrosynthetic Strategy toward Dolutegravir (15)

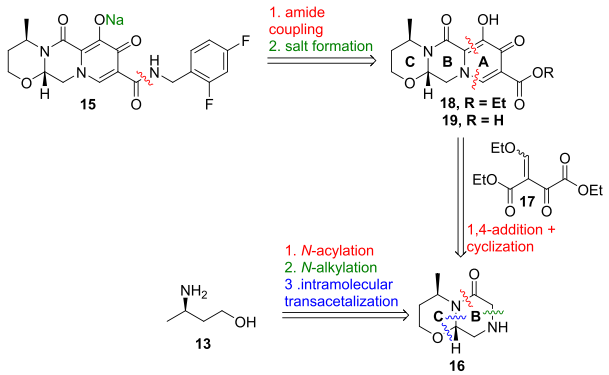

chromatographic steps were required. During our synthetic work, a patent from the Virginia Commonwealth University was disclosed, which describes a similar but more efficient approach toward **16**.[10] The methyl ester of intermediate **24** was prepared in three steps from methyl glycinate hydrochloride (**23**) in a 66% yield. The cyclization step was performed in a toluene/methanol/acetic acid mixture and achieved a 71% yield after column chromatography. Removing the Cbz group at higher hydrogen pressure gave slightly better results, and amine **16** was finally obtained in 44% over five steps. The synthesis was even performed on a multigram scale but required two chromatographic steps (Scheme 4).

A potentially shorter approach could be achieved by first *N*-acylating **13** with chloroacetyl chloride (**25**) (Scheme 5). Subsequent alkylation with aminoacetaldehyde dimethyl acetal (**8**) would furnish the acyclic precursor **27**. Acid-catalyzed intramolecular transacetalization would in turn afford the desired amine **16**.

When the acylation of **13** was performed under standard conditions (NEt_3, DCM, 0 °C), a mixture of desired **26** and *N*,*O*-bis-acylated compound **28** was obtained (Scheme 6).

https://doi.org/10.1021/acs.oprd.1c00139
Org. Process Res. Dev. 2021, 25, 1898−1910

Scheme 4. Known Syntheses of Amine 16

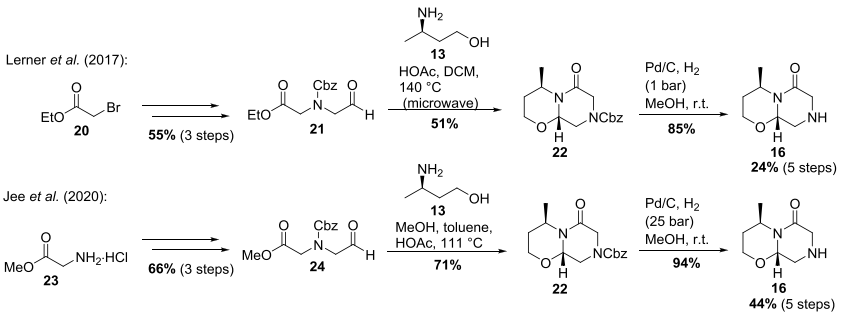

Scheme 5. Retrosynthetic Proposal toward Amine 16

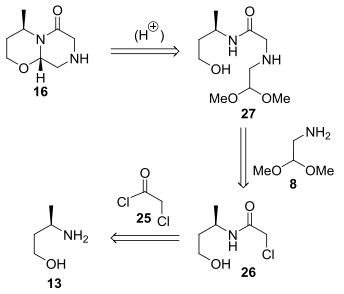

Nevertheless, **28** could be easily saponified to **26** by just adding an aqueous base to the crude reaction mixture. After extractive workup, only a 40% isolated yield of **26** was obtained. It turned out that large amounts of **26** had remained in the aqueous phase. When water was removed in vacuo and the salty residue was suspended in ethyl acetate, a further 40% of **26** could be isolated.

Due to the high polarity of **26**, the whole process was adjusted by using continuous extraction. After complete saponification of **28**, which was followed by GC−MS, the organic phase was separated and additionally extracted with water. The combined aqueous phases were neutralized with an acid, transferred into a Kutscher-Steudel apparatus, and continuously extracted for 72 h with ethyl acetate. This procedure enabled the isolation of **26** in a 91% isolated yield (Scheme 7). It should be noted that **26** showed high purity according to ^{1}H NMR and no further purification step was required. As an ambient-pressure distillation is involved in this continuous extraction, apparatus improvements can likely accelerate the procedure.

Scheme 7. *N*-Acylation of 13 with Chloroacetyl Chloride

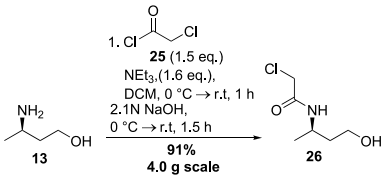

In the next step, **26** should be used for alkylating aminoacetaldehyde dimethyl acetal (**8**) to form the secondary amine **27**. The reaction was performed either by heating in toluene or by stirring at r.t. in DCM in the presence of sodium iodide (Scheme 8). After aqueous workup, only 33−45% of crude **27** could be isolated. As already reported for the previous reaction, a significant quantity of **27** remained in the aqueous phase, which could not be separated from excess amine **8**. Through LC−MS, one main impurity could be identified as the tertiary amine **29**. To circumvent its formation and to solve the water solubility issue, another strategy was chosen.

By converting primary amine **8** into a secondary and more lipophilic amine first, subsequent alkylation would lead to a tertiary and better extractable amine. Benzylation of **8** proved to be a good option as it can be easily reverted by hydrogenation. *N*-Benzyl-2,2-dimethoxyethylamine (**30**) was prepared in two different ways (Scheme 9). When heating chloroacetaldehyde-dimethylacetal (**31**) with an excess of benzylamine (**32**) in toluene, 77% of **30** was isolated after distillation. According to a procedure from Luu et al., **30** could also be prepared through reductive amination from stochiometric amounts of benzaldehyde (**33**) and aminoacetaldehyde dimethyl acetal (**8**).[14] The latter method furnished **30** in a 97% isolated yield.

Scheme 6. *N*-Acylation of 3-(*R*)-Amino-1-butanol (13)

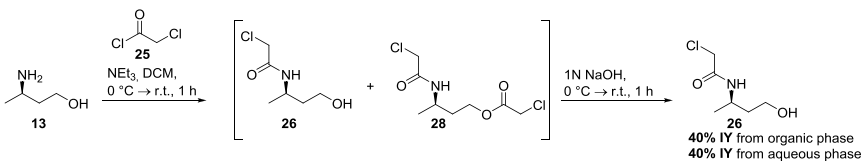

https://doi.org/10.1021/acs.oprd.1c00139
Org. Process Res. Dev. 2021, 25, 1898−1910

Scheme 8. *N*-Alkylation of Aminoacetaldehyde Dimethyl Acetal (8) with 26

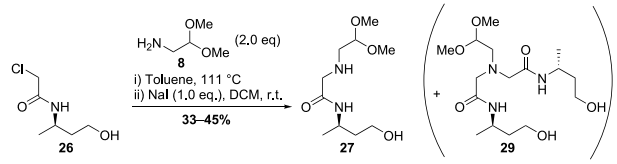

Scheme 9. Synthesis of *N*-Benzyl-2,2-dimethoxyethylamine (30) by *N*-Alkylation or Reductive Amination

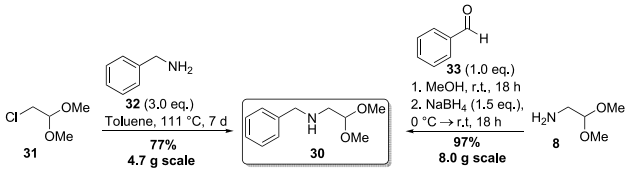

Using secondary amine **30** instead of primary amine **8** for the alkylation gave much better results (Scheme 10). The reaction was performed in acetonitrile (MeCN) in the presence of potassium iodide (KI) and potassium carbonate (K_2CO_3). Complete conversion of **26** was observed after 24 h at r.t. or after 3 h when heating to reflux. For workup, MeCN was removed and an extraction from water/ethyl acetate furnished **34** as a slightly brownish oil. Again, the reaction proceeded very cleanly, and no further purification of the product was necessary.

Scheme 10. Synthesis of Tertiary Amine 34 from 26 and 30 by Heating in MeCN in the Presence of KI and K_2CO_3

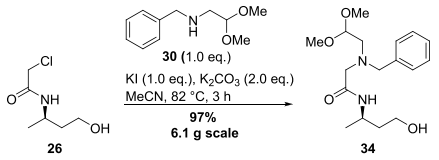

34 cyclized cleanly in aqueous hydrochloric acid to the desired diastereomer of oxazinone **35**. At least 6 N HCl was necessary to achieve complete conversion after 48 h at r.t. (Table 1). Only small amounts of byproducts were detected by LC–MS. As the undesired diastereomer with opposite configuration at the acetalic center was not isolated and characterized, diastereoselectivity can only be assumed based on the second largest HPLC peak to amount at least to 44:1 (for details, see the Supporting Information). When the reaction was performed on an 11.5 g scale, crude **35** was isolated in a 92% yield as a brown oil, which only contained slight impurities. For the workup, the reaction mixture was neutralized with sodium hydroxide and extracted with ethyl acetate. The stereoconfiguration of **35** was verified by VCD spectroscopy and comparison of the experimental data with calculations using density functional theory (for more details, see the Supporting Information). The enantiomeric excess was determined by chiral HPLC. Racemic **35** was prepared as a reference material in the same way starting from *rac*-3-amino-1-butanol (*rac*-**35**).

Table 1. Intramolecular Transacetalization of 34

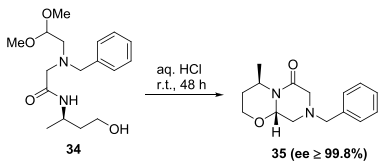

entry	solvent	conversion [%][a]	IY [%]
1	1 N HCl	4	-
2	3 N HCl	34	-
3[b]	6 N HCl	100	92

[a]Determined by LC–MS and UV absorption at 254 nm. [b]11.5 g scale.

The benzyl group was subsequently removed by hydrogenation (Scheme 11), and crude amine **16** was obtained in a 96% yield (78% IY over four steps) as a brown-orange oil, which solidified after a while to a beige and free-flowing solid. According to LC–MS and ^{1}H NMR, minor impurities could be detected in the crude material (see the corresponding spectra in the Supporting Information). Crude **16** was used for the next step, and no further purification efforts were investigated.

Scheme 11. Debenzylation of 35 by Hydrogenation

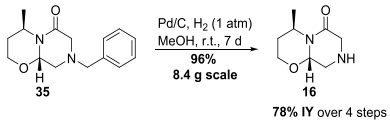

Construction of Ring A. Jee et al. also reported a synthesis route to dolutegravir starting from the ring system BC (**16**) (Scheme 12).[10] Intermediate **39**, which contains the crucial tricarbonyl moiety, was installed in two steps in a 89% yield. Ring A was constructed by regioselective cyclization using magnesium bromide ethyl etherate ($MgBr_2{\cdot}OEt_2$) and triethylamine (65% yield of **40**). Subsequent amide coupling afforded the desired dolutegravir **3** in a 67% yield. The route depicts the

https://doi.org/10.1021/acs.oprd.1c00139
Org. Process Res. Dev. 2021, 25, 1898–1910

Scheme 12. Synthesis of Dolutegravir (3) by Jee et al.

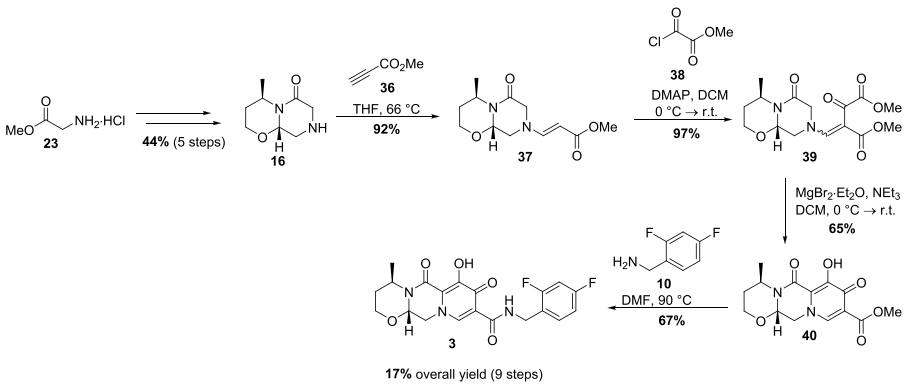

first one reported where the ring system AB was constructed first. The overall yield was only 17%, and five chromatographic steps were required.

Enaminone **39** should be also accessible in a single step by 1,4-addition from the corresponding enol ether **17**. According to a procedure of Jones,[15] **17** was prepared from the commercially available diethyl oxalacetate sodium salt (in two steps) (Scheme 13). The salt **41** had to be acidified first to obtain diethyl oxalacetate (**42**), which was then condensed with triethyl orthoformate (TEOF) in the presence of acetic anhydride (Ac_2O). The reaction could be performed in a distillation apparatus, and **17** was directly distilled out of the reaction mixture resulting in a 72% yield over two steps.

Scheme 13. Synthesis of Enol Ether 17 by Condensation of 42 with TEOF and Ac_2O

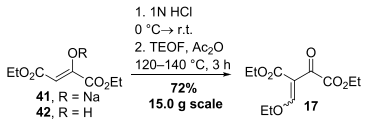

Amine **16** readily underwent 1,4-addition to **43** in several solvents (DCM, MeCN, EtOH, THF, and toluene). The formation of only one geometrical isomer of **43** could be detected by NMR and LC–MS (for more details, see the Supporting Information). Regarding the regioselective cyclization, it turned out that using strong bases like KO^{t}Bu, NaOEt, or NaH predominantly led to the formation of a product mixture. Applying the conditions of Jee et al., using a combination of magnesium bromide ethyl etherate ($MgBr_2$·OEt_2) and triethylamine (NEt_3) looked more promising, and predominant conversion to ester **18** (81 area % (254 nm), 35 area % (315 nm)) could be observed (entry 1, Table 2).[10] Nevertheless, there was still significant byproduct formation according to the HPLC trace at 315 nm and ^{1}H NMR. According to LC–MS data (m/z = 351), it is assumed that the main byproduct could be pyrrole **45** (Figure 1), which could form in an undesired 5-exo cyclization with the keto group adjacent to the ester group.

Furthermore, the reported workup method, which consisted of dissolving the crude reaction mixture in sat. $NaHCO_3$ solution followed by extraction, led to formation of barely soluble magnesium salts, which complicated the extraction.

Table 2. Screening Conditions for Building Up Ring A

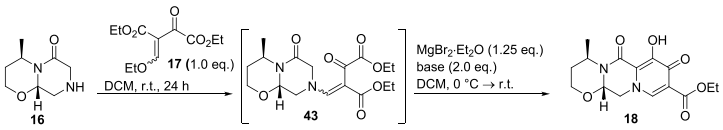

			area % **18**[a]	
entry	base	t [h]	254 nm	315 nm
1	NEt_3	2	81	35
2	DIPEA	2	91	44
3	2,6-lutidine	24	90	37
4	*N*,*N*-dimethylaniline	24	48	9
5	pyridine	2	67	22
		65	91	71
6	pyridine[b]	65	94	84

[a]Determined by LC–MS and UV absorption. [b]Three equivalents were used.

https://doi.org/10.1021/acs.oprd.1c00139
Org. Process Res. Dev. 2021, 25, 1898–1910

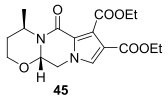

Figure 1. Proposed structure of byproduct **45**.

Additionally, ester **18** was partly saponified under these conditions.

For optimization, bases other than NEt_3 were investigated first. When diisopropylethylamine (DIPEA) was used, conversion slightly improved to 91 area % (254 nm) and 44 area % (315 nm) (entry 2, Table 2). Using 2,6-lutidine as a base resulted in a similar result to NEt_3 (entry 3, Table 2), while *N*,*N*-dimethylaniline gave only low conversion (entry 4, Table 2). With pyridine, the reaction proceeded much slower but also cleaner (91 area % (254 nm) and 71 area % (315 nm) conversion after 65 h) (entry 5, Table 2). Increasing the equivalents of pyridine (3.0) additionally improved the conversion (entry 6, Table 2).

For the workup, the reaction mixture was cooled, quenched with 1 N HCl, and extracted with DCM. When the reaction was performed on a 2 g scale, a 95% isolated yield of crude **18** was obtained. The orange-reddish solid showed purities of 94 area % (254 nm) and 87 area % (315 nm) (Scheme 14).

Crude **18** could be washed with ethyl acetate to remove impurities, but as some material was lost in this step, the crude material was used for the next step. As an alternative procedure for purification, it turned out that saponification furnished acid **19** in a pure form. A simple one-pot procedure was developed by adding aqueous 1 N NaOH to the DCM extract of ester **18**. After stirring the two-phase mixture overnight, **18** was completely saponified to acid **19**. Impurities stayed in the organic phase, and acid **19** precipitated out of the aqueous phase after acidification. Filtration and drying afterward afforded **19** as a colorless solid in a 72% yield over three steps (Scheme 15).

While investigating the regioselective cyclization, it was also considered to replace $MgBr_2 OEt_2$ by cheaper and more widely available $MgCl_2$. From all tested conditions, only heating in MeCN showed promising results (for more details, see the Supporting Information). Conversion to ester **18** was usually lower (85 area % (254 nm), 73 area % (315 nm)). As also partly saponification to acid **19** was observed, it appeared more reasonable to drive the reaction completely toward **18**. After removing MeCN, workup and saponification were performed as mentioned above to furnish a 53% isolated yield of **19** (Scheme 16).

Amide Coupling. Aminolysis of an ethyl ester moiety with 2,4-difluorobenzylamine by heating in toluene in the presence of acetic acid has already been reported in the literature for other dolutegravir building blocks.[11,16,17] The toluene/acetic acid conditions showed to be appropriate also for ester **18** and were thus optimized (for more details, see the Supporting Information). After heating overnight in the presence of an excess of amine and acetic acid (both 2.5 equiv), full conversion to dolutegravir (**3**) was detected by LC−MS. It turned out be more efficient when the aqueous workup was omitted. After complete conversion of ester **18**, all volatiles were removed in vacuo, and the residue was dissolved in hot EtOH and treated with sodium hydroxide (NaOH). After filtration and washing, the filtered salt was heated again in EtOH and hot-filtered to increase the purity. After drying, dolutegravir sodium (DTG-Na, **15**) was obtained in a 70% isolated yield (HPLC purity of 99.7% (254 nm)) (Scheme 17).

The amide coupling of acid **19** with amine **10** has been reported in the patent literature. By using the expensive coupling reagent HATU (1-[bis(dimethylamino)methylene]-1*H*-1,2,3-triazolo[4,5-b]pyridinium 3-oxide hexafluorophosphate), *N*-methylpyrrolidine, and DMF as the solvent, **15** was isolated in a 55% yield after purification by preparative HPLC.[18] The reaction has also been described for preparing bictegravir (**4**), but 1,1-carbonyldiimidazole (CDI) was used instead as a coupling reagent in this case.[19] Following this protocol, acid **19** was activated with CDI by stirring for 2 h in dimethyl carbonate (DMC) at 80 °C. Amine **10** was added at r.t., and clean conversion to **3** was detected by LC−MS after 2 h. Aqueous workup afforded crude dolutegravir (**3**), which was converted to the sodium salt as mentioned above giving **15** in a 94% isolated yield showing an HPLC purity of 99.9% (254 nm) (Scheme 18).

When only 1.7 equiv of CDI were used, incomplete conversion was observed. As a consequence, the final product contained more nonremovable traces of acid **19** or ester **18**. The reaction was once performed in a smaller scale (0.3 g) with skipping the aqueous workup the same as reported for aminolysis of ester **18**. A similar isolated yield (91%) was obtained, but **15** was slightly less pure (99.7%, 254 nm).

CONCLUSIONS

A practical synthesis route to dolutegravir sodium starting from (*R*)-3-amino-1-butanol (**13**) was introduced (Scheme 19). First, a new four-step and highly yielding synthesis to the ring system BC containing amine **16** was developed. It is noteworthy that the reaction sequence proceeded without significant byproduct formation and no cost-intensive purification steps had to be used. The regioselective cyclization to ring A was carefully optimized and significantly improved. Furthermore, efficient access to acid **19** was demonstrated. Ester **18** was isolated in a higher yield admittedly but showed a lower purity than acid **19**. Both compounds could be transformed to desired DTG-Na in similar overall yields. Conversion of ester **18** with 2,4-difluorobenzylamine required harsher conditions but less expensive reagents (toluene and

Scheme 14. Synthesis of Ester 18 by One-Pot 1,4-Addition of Amines 16 with 17 Followed by Regioselective Cyclization

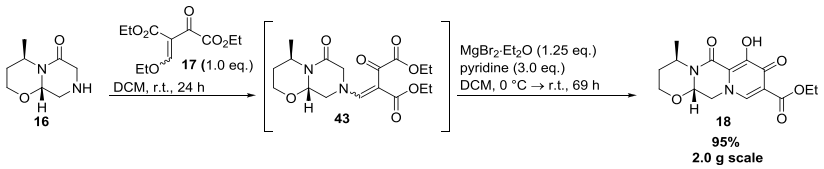

https://doi.org/10.1021/acs.oprd.1c00139
Org. Process Res. Dev. 2021, 25, 1898−1910

Scheme 15. Synthesis of Acid 19 by One-Pot 1,4-Addition of Amines 16 to 43 Followed by $MgBr_2$-Mediated Regioselective Cyclization and Saponification

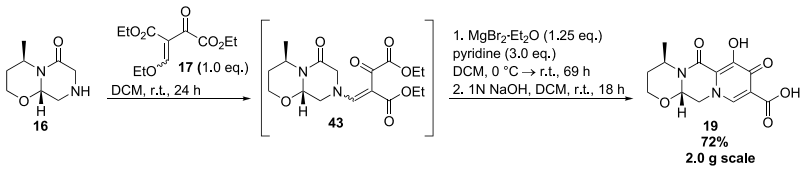

Scheme 16. Synthesis of Acid 19 by One-Pot 1,4-Addition of Amines 16 to 43 Followed by $MgCl_2$-Mediated Regioselective Cyclization and Saponification

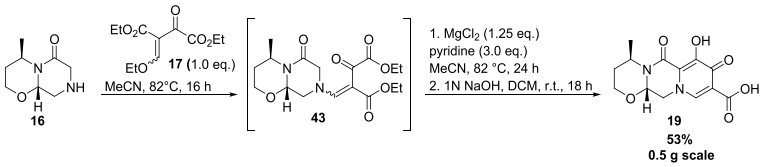

Scheme 17. Synthesis of DTG-Na (15) by Aminolysis of Crude Ester 18 and Subsequent Salt Formation

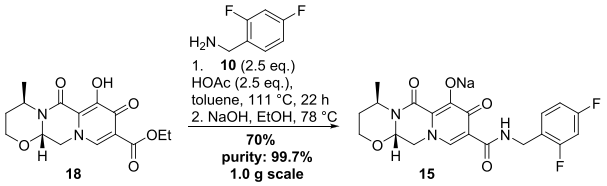

Scheme 18. Synthesis of DTG-Na (15) by Amide Coupling of Acid 19 and Subsequent Salt Formation

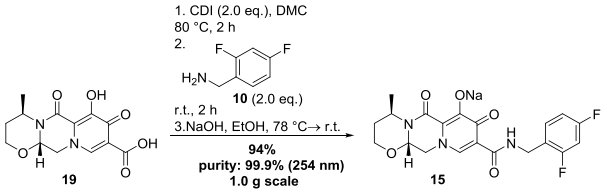

acetic acid), while acid **19** showed a cleaner conversion under milder conditions by using CDI as a coupling reagent. Ultimately, both transformations represent attractive routes and enable new synthetic access to DTG-Na.

■ EXPERIMENTAL SECTION

All employed chemicals were commercially available and used without prior purification except 2,4-difluorobenzylamine, which was distilled and stored over a nitrogen atmosphere. Anhydrous solvents were taken from a solvent purification system and under a nitrogen atmosphere. Oven-dried glassware was dried in an oven at 150 °C overnight, assembled while still hot, cooled to room temperature, and then purged with nitrogen. NMR spectra were recorded on a Bruker Avance-III HD instrument (^{1}H NMR, 300 MHz; ^{13}C NMR, 75 MHz) or a Bruker Avance-III HD instrument (^{1}H NMR, 400 MHz; ^{13}C NMR, 101 MHz; ^{19}F NMR, 377 MHz) with a 5 mm BBFO probe. The chemical shifts δ were expressed in ppm downfield from tetramethylsilane (^{1}H NMR and ^{13}C NMR). Deuterated solvents ($CDCl_3$ and DMSO-d_6) served as an internal reference. The reported signal splittings were abbreviated as follows: s_b = broad singlet, s = singlet, d = doublet, and t = triplet. Coupling constants J are reported in Hz. ESI-MS spectra were recorded on a 1260-series Infinity II HPLC system (Agilent Technologies) with a binary pump and an integrated diode array detector coupled to an LC/MSD Infinitylab LC/MSD (G6125B LC/MSD) mass spectrometer. For high-resolution (HR) mass spectra, an Agilent 6545 Q-TOF spectrometer and a suitable external calibrant were used. Analytical HPLC was carried out with an Agilent 1260 Infinity system equipped with a binary pump, a diode array detector, and an LC/MSD InfinityLab LC/MSD (G6125B LC/MSD) mass spectrometer. An Ascentis Express C18 column (2.7 μm, 2.1 mm × 30 mm, 40 °C) or an ACE C18 PFP column (3 μm, 4.6 mm × 150 mm, 40 °C) with gradient elution using acetonitrile/water (+0.1% formic acid) and a flow rate of 1.0

https://doi.org/10.1021/acs.oprd.1c00139
Org. Process Res. Dev. 2021, 25, 1898−1910

Scheme 19. Here Reported Synthesis of DTG-Na (15)

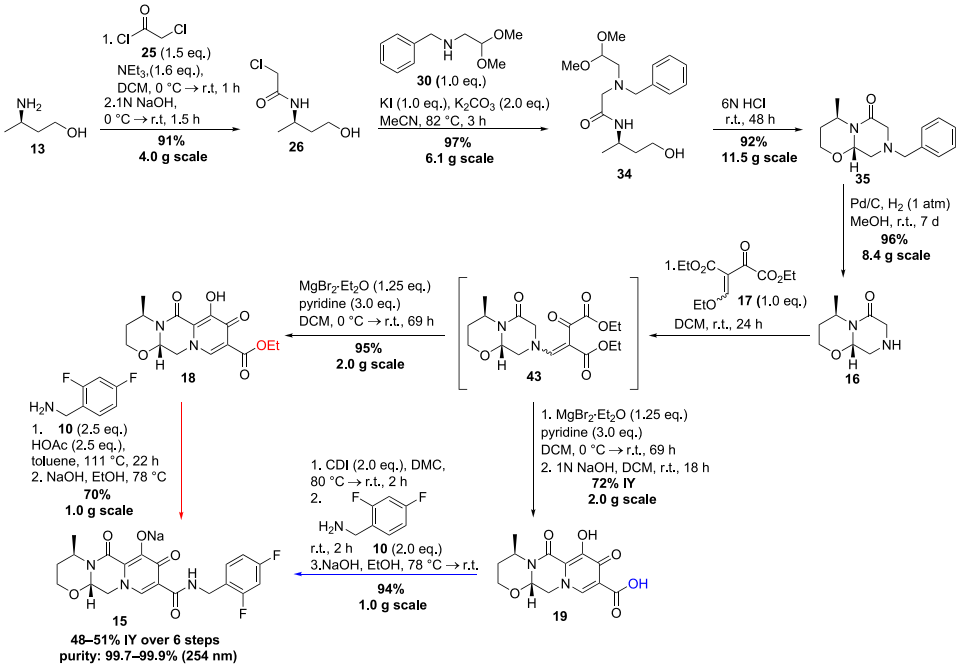

mL/min was used. Chiral HPLC was performed on a 1260-series Infinity II HPLC system (Agilent Technologies) in a normal phase and isocratic mode with EtOH/*n*-hexane as the mobile phase. A Daicel Chiralpak IF-3 column (3 μm, 4.6 mm × 250 mm, 40 °C) was used for enantiomeric excess determination. Gas chromatography was performed on an Agilent 8890 gas chromatograph equipped with a 5977 GC/MS detector. An Agilent Technologies HP 5MS UI column (30 m × 0.25 mm × 0.25 μm) as a stationary phase with helium as a carrier gas and a flow rate of 1.2 mL/min was used. The following parameters were used: an inlet temperature of 250 °C, a transfer line temperature of 250 °C, an ion source temperature of 230 °C, an MS-quadrupole temperature of 150 °C, and an initial oven temperature of 40 °C for 2 min with a temperature ramp of 50 °C/min to 320 °C over 5.6 min followed by 7.4 min holding. IR spectroscopy was conducted on a Bruker Tensor 27 FTIR spectrometer using a diamond ATR unit. Thin-layer chromatography was performed on Merck F_{254} silica gel plates. Spots were visualized with UV light (λ = 254 nm) or stained with appropriate reagents. Melting points are uncorrected and were taken by using a Krüss KSP1N digital melting point apparatus. Optical rotations were measured on a PerkinElmer 241 MC polarimeter.

4-Hydroxybutan-2-one Oxime, 44. According to a modified procedure by Budidet et al.,[20] a solution of 4-hydroxybutan-2-one (95%, 5.0 mL, 55 mmol, 1.0 equiv) in EtOH (60 mL) was cooled in an ice bath. Hydroxylamine hydrochloride (4.6 g, 66.0 mmol, 1.2 equiv) was added, and the pH was adjusted to 6 by slow addition of aq. sodium hydroxide solution (40 wt %). The colorless suspension was stirred for 4 h at r.t. (complete conversion detected by GC–MS) before it was filtered. The solvent was removed in vacuo at 40 °C, and the residue was suspended in EtOAc (50 mL). After drying over Na_2SO_4, all volatiles were removed in vacuo at 40 °C to obtain **44** as a mixture of anti/syn isomers (5.60 g, 54.3 mmol, 99%) as a colorless viscous oil. M ($C_4H_9NO_2$) = 103.12 g/mol. R_f (SiO_2) = 0.21 (EtOAc), stained with a ninhydrin reagent. IR (ATR): ν = 3249, 2889, 1660, 1427, 1370, 1261, 1050 cm^{-1}. ^{1}H NMR, COSY (400 MHz, DMSO-d_6): δ = 10.26/10.17 (s, 1H, –NOH), 4.62–4.56/4.55–4.48 (m, 1H, –OH), 3.59–3.50 (m, 2H, H-4), 2.41/2.25 (t, ^3J = 6.8 Hz, H-3), 1.78/1.73 (s, 3H, H-1) ppm. ^{13}C NMR, HSQC, HMBC (100 MHz, DMSO-d_6): δ = 154.1/153.8 (C-2), 58.4/57.3 (C-4), 38.8/32.1 (C-3), 20.2/13.5 (C-1) ppm. GC–MS: m/z = 58.1 (100%). ESI-HRMS: calcd for $[C_4H_9NO_2 + H]^+$, m/z = 104.0706; found, m/z = 104.0703.

***rac*-3-Aminobutan-1-ol, *rac*-13.** According to a modified procedure by Budidet et al.,[20] a suspension of 4-hydroxy-2-butanone oxime (**44**, 8.60 g, 83.4 mmol) and Raney nickel (10 wt %) in MeOH (70 mL) was hydrogenated in an autoclave for 28 h (10 bar H_2, 45 °C) (reaction control by TLC). The suspension was suction-filtered over celite, and the celite cake was washed several times with MeOH. All volatiles were removed in vacuo at 40 °C in order to obtain *rac*-**13** as a colorless oil (6.91 g, 77.6 mmol, 93%), which was used for the next step without further purification. M ($C_4H_{11}NO$) = 89.14 g/mol. T_b = 81–83 °C (22 mbar); lit. 95–97 °C (28 mbar).[21] R_f (SiO_2) = 0.19 (EtOAc:MeOH:NEt_3 = 2:1:1), stained with ninhydrin reagent. IR (ATR): ν = 3347, 3280, 3183, 2957, 2924, 2870, 1599, 1455, 1375, 1062 cm^{-1}. ^{1}H NMR, COSY

https://doi.org/10.1021/acs.oprd.1c00139
Org. Process Res. Dev. 2021, 25, 1898–1910

(400 MHz, $CDCl_3$): δ = 3.84−3.72 (m, 2H, H-1), 3.17−3.04 (m, 1H, H-3), 2.69 (s_B, 3H, −OH and $-NH_2$), 1.66−1.57 (m, 1H, H_a-2), 1.53−1.42 (m, 1H, H_b-2), 1.13 (d, ^3J = 6.4 Hz, 3H, H-4) ppm. ^{13}C NMR, HMBC, HSQC (101 MHz, $CDCl_3$): δ = 62.4 (C-1), 48.0 (C-3), 39.5 (C-2), 25.8 (C-4) ppm. ESI-HRMS: calcd for $[M + H]^+$, m/z = 90.0913; found, m/z = 90.0913. The spectrometric data are consistent with literature values.[22]

(*R*)-2-Chloro-*N*-(4-hydroxybutan-2-yl)acetamide, 26. In an oven-dried Schlenk flask, **13** (4.00 g, 44.9 mmol, 1.0 equiv) was dissolved in DCM (80 mL). NEt_3 (10.0 mL, 71.8 mmol, 1.6 equiv) was added, and the solution was cooled in an ice bath. Chloroacetyl chloride (**25**, 5.3 mL, 67 mmol, 1.5 equiv) was added dropwise over 10 min, cooling was removed, and the dark red-brown solution stirred for 1 h at r.t. (complete consumption of **13** detected by TLC). While cooling, first water (64 mL) and then 3 N NaOH (32 mL) were added to the reaction mixture. The cooling bath was removed, and the two-phasic mixture was stirred vigorously for 90 min at r.t. (complete saponification to **26** detected by GC−MS). The organic phase was separated and extracted with water (3 × 40 mL). The combined aqueous phases were cooled and adjusted to pH = 7−8 using conc. HCl. The solution was transferred into a Kutscher-Steudel apparatus and extracted continuously with EtOAc for 72 h. The orange organic phase was dried over Na_2SO_4 and filtered, and the solvent was removed in vacuo at 40 °C. **26** was obtained as an orange-brown viscous oil (6.73 g, 40.6 mmol, 91%) and used for the next step without any further purification. *M* ($C_6H_{12}ClNO_2$) = 165.63 g/mol. $[\alpha]_{589}^{20}$= −32.7 ($CHCl_3$, *c* = 10 mg/mL). R_f (SiO_2) = 0.30 (EtOAc), stained with ninhydrin reagent. IR (ATR): ν = 3280, 2936. 1651, 1543, 1056 cm^{-1}. ^{1}H NMR, COSY (300 MHz, $CDCl_3$): δ = 6.68 (s_B, 1H, -NH-), 4.27−4.12 (m, 1H, H-2′), 3.71−3.54 (m, 2H, H-4′), 3.01 (s_B, 1H, -OH), 1.93−1.80 (m, 1H, H_a-3′), 1.53−1.41 (m, 1H, H_b-3′), 1.26 (d, ^3J = 1.3 Hz, 3H, H-1′) ppm. ^{13}C NMR, HMBC, HSQC (75 MHz, $CDCl_3$): δ = 166.6 (C-1), 58.9 (C-4′), 43.2 (C-2′), 42.6 (C-2), 39.5 (C-3′), 20.9 (C-1′) ppm. GC−MS: m/z = 120.1 (100%). ESI-HRMS: calcd for $[M + H]^+$, m/z = 166.0629; found, m/z = 166.0633.

***N*-Benzyl-2,2-dimethoxyethylamine, 30.** For method 1, benzylamine (**32**, 12.2 g, 113 mmol, 3.0 equiv) and chloroacetaldehyde-dimethylacetal (**31**, 4.71 g, 38 mmol, 1.0 equiv) were dissolved in toluene (50 mL) and heated to reflux for seven days. The suspension was cooled in an ice bath and filtered, toluene was then removed in vacuo at 40 °C. The residue was distilled under vacuum to afford **30** as a colorless liquid (5.71 g, 29.2 mmol, 77%). For method 2, according to a modified procedure from Luu et al.,[14] to a solution of aminoacetaldehyde dimethyl acetal (**8**, 7.91 g, 75.2 mmol) in dry methanol (300 mL), prepared in an oven-dried Schlenk flask under a nitrogen atmosphere, was added freshly distilled benzaldehyde (**33**, 7.60 mL, 75.2 mmol, 1.0 equiv), and the solution was stirred for 18 h at r.t. While cooling in an ice bath, $NaBH_4$ (4.30 g, 114 mmol, 1.5 equiv) was added portion-wise over 3 min. The ice bath was removed, and the suspension was stirred at r.t. for 18 h. The reaction was quenched by adding sat. $NaHCO_3$ solution (30 mL), and the mixture was extracted with DCM (3 × 60 mL). The combined organic phases were washed once with brine (150 mL), dried over Na_2SO_4, and filtered. After removing all volatiles in vacuo at 40 °C, **30** was obtained as a clear colorless liquid (14.19 g, 72.7 mmol, 97%) and used for the next step without further purification. *M* ($C_{11}H_{17}NO_2$) = 195.26 g/mol. T_b = 130−138 °C (13 mbar); lit., 147−149 °C (18 mbar).[23] R_f (SiO_2) = 0.35 (EtOAc + 1% NEt_3). IR (ATR): ν = 2934, 2830, 1454, 1192, 1127, 1056 cm^{-1}. ^{1}H NMR, COSY (300 MHz, $CDCl_3$): δ = 7.34−7.20 (m, 5H, Ar-H), 4.49 (t, ^3J = 5.5 Hz, 1H, H-2), 3.81 (s, 2H, $-CH_2Ar$), 3.37 (s, 6H, 2× OCH_3), 2.75 (d, ^3J = 5.5 Hz, 2H, H-1), 1.54 (s_B, 1H, −NH−) ppm. ^{13}C NMR, HMBC, HSQC (75 MHz, $CDCl_3$): δ = 140.3 (Ar-C-1), 128.5 (Ar-C-3 and Ar-C-5), 128.3 (Ar-C-2 and Ar-C-6), 127.1 (Ar-C-4), 104.1 (C-2), 54.1 (2× $-OCH_3$), 54.0 ($-CH_2Ar$), 50.7 (C-1) ppm. ESI-MS: m/z = 196.1 (100%, $[M + H]^+$). The spectroscopic data are consistent with literature values.[14]

(*R*)-2-(Benzyl(2,2-dimethoxyethyl)amino)-*N*-(4-hydroxybutan-2-yl)acetamide, 34. To a solution of **30** (6.11 g, 36.9 mmol, 1 equiv) in MeCN (40 mL) were added K_2CO_3 (10.2 g, 73.8 mmol, 2.0 equiv) and KI (6.13 g, 36.9 mmol, 1.0 equiv) while stirring, followed by a solution of **26** (7.21 g, 36.9 mmol, 1.0 equiv) in MeCN (40 mL) and additional MeCN (130 mL). The suspension was heated to reflux for 3 h (full conversion detected by LC−MS, 254 nm). The solvent was removed in vacuo at 40 °C, and the salt-like residue was suspended in EtOAc (150 mL) and water (210 mL). The mixture was transferred into a separatory funnel, and the organic phase was separated. The aqueous phase was extracted with EtOAc (2 × 100 mL), and the combined organic phases were dried over Na_2SO_4. After removing all volatiles in vacuo at 40 °C, **34** was obtained as a brown oil (11.63 g, 35.8 mmol, 97%). *M* ($C_{17}H_{28}N_2O_4$) = 324.42 g/mol. $[\alpha]_{589}^{19}$= −29.6 ($CHCl_3$, *c* = 10 mg/mL). R_f (SiO_2) = 0.32 (EtOAc + 2% NEt_3). IR (ATR): ν = 3324, 2933, 2833, 1649, 1529, 1453, 1120, 1063 cm^{-1}. ^{1}H NMR, COSY (300 MHz, $CDCl_3$): δ = 7.59 (m, 1H, −NH−), 7.38−7.22 (m, 5H, Ar-H), 4.39 (t, ^3J = 5.3 Hz, H-2″), 4.20−4.04 (m, 1H, H-2′), 3.92−3.80 (m, 1H, −OH), 3.72 (s, 2H, $PhCH_2-$), 3.59−3.46 (m, 1H, H_a-4′), 3.35 (s, 3H, $-OCH_3$), 3.33 (s, 3H, $-OCH_3$), 3.33−3.30 (m, 1H, H_b-4′), 3.20 (d, ^4J = 1.8 Hz, 2H, H-2), 2.71 (dd, ^3J = 5.3 Hz, ^4J = 1.1 Hz, 2H, H-1″), 1.89−1.76 (m, 1H, H_a-3′), 1.33−1.24 (m, 1H, H_b-3′), 1.22 (d, ^3J = 6.7 Hz, 3H, H-1′) ppm. ^{13}C NMR, HMBC, HSQC (75 MHz, $CDCl_3$): δ = 172.0 (C═O), 138.0 (Ar-C), 129.0 (Ar-C), 128.7 (Ar-C), 127.8 (Ar-C), 102.9 (C-2″), 60.7 ($PhCH_2-$), 58.6 (C-4′), 58.6 (C-2), 57.3 (C-1″), 54.1 ($-OCH_3$), 53.9 ($-OCH_3$), 41.4 (C-2′), 40.5 (C-3′), 21.2 (C-1′) ppm. ESI-HRMS: calcd for $[M + H]^+$, m/z = 325.2122; found, m/z = 325.2130.

(4*R*,9a*S*)-8-Benzyl-4-methylhexahydro-2*H*,6*H*-pyrazino[2,1-b][1,3]oxazin-6-one, 35. Acetal **34** (11.53 g, 35.5 mmol) was suspended in water (160 mL) and cooled in an ice bath. Conc. HCl (160 mL) was added through a dropping funnel over 15 min while stirring. The cooling bath was removed, and the slightly yellow solution was stirred at r.t. for 48 h (complete conversion detected by LC−MS at 254 nm). The solution was cooled again in an ice bath, and sodium hydroxide pellets (75 g) were added in small portions over 2 h followed by sodium bicarbonate powder (4 g) in order to adjust the pH to 7−8. While approaching the desired pH, **35** started precipitating, resulting in a murky beige suspension. EtOAc (300 mL) was added while stirring, and the mixture was transferred into a separating funnel. The organic phase was separated, and the aqueous phase was extracted with EtOAc (2 × 200 mL). The combined organic phases were dried over Na_2SO_4 and filtered, and the solvent was removed in vacuo at 40 °C. Crude **35** was obtained as a thick orange-brown oil (8.49, 32.6 mmol, 92%, ≥99.8% ee according to chiral HPLC).

https://doi.org/10.1021/acs.oprd.1c00139
Org. Process Res. Dev. 2021, 25, 1898−1910

Racemic **35** was synthesized analogously from *rac*-**13**. *M* ($C_{15}H_{20}N_2O_2$) = 260.34 g/mol. $[\alpha]_{589}^{19}$ = −46.1 ($CHCl_3$, *c* = 10 mg/mL). R_f (SiO_2) = 0.32 (EtOAc). IR (ATR): ν = 2969, 2860, 1653, 1455, 1328, 1197, 1095, 1068 cm^{-1}. ^1H NMR, COSY (300 MHz, $CDCl_3$): δ = 7.36−7.23 (m, 5H, Ar-H), 4.97−4.86 (m, 2H, H-4 and H-9a), 3.93−3.81 (m, 2H, H-2), 3.57 (d, ^2J = 13.1 Hz, 1H, −NCH_aAr), 3.54 (d, ^2J = 13.1 Hz, 1H, −NCH_bAr), 3.24 (dd, ^2J = 16.0 Hz, ^4J = 1.9 Hz, 1H, H_a-7), 3.02 (dd, ^2J = 16.3 Hz, ^4J = 0.8 Hz, 1H, H_b-7), 2.97 (ddd, ^2J = 12.0 Hz, ^3J = 4.9 Hz, ^4J = 1.9 Hz, 1H, H_a-9), 2.44 (ddd, ^2J = 12.0 Hz, ^3J = 6.7 Hz, ^4J = 0.8 Hz, 1H, H_b-9), 2.19−2.04 (m, 1H, H_a-3), 1.43−1.34 (m, 1H, H_b-3), 1.27 (d, ^3J = 7.1 Hz, 4-CH_3) ppm. ^{13}C NMR, HSQC, HMBC (75 MHz, $CDCl_3$): δ = 166.3 (C-6), 136.3 (Ar-H), 129.4 (Ar-H), 128.6 (Ar-H), 127.7 (Ar-H), 79.3 (C-9a), 62.8 (C-2), 61.6 (−NCH_2Ar), 57.5 (C-7), 54.3 (C-9), 41.7 (C-4), 29.8 (C-3), 15.9 (−CH_3) ppm. ESI-HRMS: calcd for $[M + H]^+$, *m*/*z* = 261.1594; found, *m*/*z* = 261.1598.

(4*R*,9a*S*)-4-Methylhexahydro-2*H*,6*H*-pyrazino[2,1-b]-[1,3]oxazin-6-one, 16. A solution of oxazinone **35** (8.44 g, 324 mmol) in MeOH (120 mL) was degassed for 10 min by purging with nitrogen. Palladium (10% on carbon, 0.85 g) was added and the mixture was purged with hydrogen three times. The mixture stirred under hydrogen atmosphere for seven days (complete conversion detected by LC−MS and UV detection at 254 nm). After purging for 10 min with nitrogen, the mixture was suction-filtered over celite and washed several times with MeOH. All volatiles were removed in vacuo at 40 °C. Crude **16** was obtained as a viscous yellow-orange oil (5.31 g, 31.2 mmol, 96%), which solidified to a slight yellowish solid after a while. **16** was used for the next step without further purification. *M* ($C_8H_{14}N_2O_2$) = 170.21 g/mol. T_m = 56−61 °C; 79−83 °C (rac.). $[\alpha]_{589}^{19}$ = −103.1 ($CHCl_3$, *c* = 10 mg/mL). R_f (SiO_2) = 0.31 (EtOAc + 10% MeOH + 5% NEt_3), stained with ninhydrin reagent. IR (ATR): ν = 3307, 2968, 2865, 1643, 1451, 1324, 1193, 1080, 1064 cm^{-1}. ^1H NMR, COSY (300 MHz, $CDCl_3$): δ = 5.04−4.92 (m, 1H, H-4), 4.85−4.80 (m, 1H, H-9a), 4.00−3.85 (m, 1H, H-2), 3.48 (d, ^2J = 17.3 Hz, 1H, H_a-7), 3.38 (d, ^2J = 17.3 Hz, 1H, H_b-7), 3.14 (dd, ^2J = 13.6 Hz, ^3J = 3.8 Hz 1H, H_a-9), 2.97 (dd, ^2J = 13.6 Hz, ^3J = 4.3 Hz 1H, H_b-9), 2.16−2.01 (m, 1H, (H_a-3), 1.78 (s_B, 1H, −NH−), 1.41−1.32 (m, 1H, H_b-3), 1.26 (t, ^3J = 7.1 Hz, 3H, −CH_3) ppm. ^{13}C NMR, HSQC, HMBC (75 MHz, $CDCl_3$): δ = 167.8 (C-6), 78.8 (C-9a), 63.0 (C-2), 50.3 (C-7), 48.1 (C-9), 42.2 (C-4), 29.9 (C-3), 15.9 (−CH_3) ppm. ESI-MS: *m*/*z* = 171.1 (100%, $[M + H]^+$). The spectrometric data are consistent with literature values.[10]

Diethyl-(2*E*/*Z*)-2-(ethoxymethylidene)-3-oxobutandioate, 17. A diethyl oxalacetate sodium salt (**41**, 95%, 15.0 g, 67.8 mmol) was weighed into an Erlenmeyer flask and suspended in EtOAc (90 mL). The suspension was cooled in an ice bath, and 1 N HCl (86 mL) was added while stirring. After all of the salt was dissolved, the biphasic murky mixture was transferred into a separatory funnel. The organic phase was separated, and the aqueous phase was extracted with EtOAc (2 × 45 mL). The combined organic phases were dried over Na_2SO_4 and filtered, and the solvent was removed in vacuo at 30 °C. To the orange-brown oily residue (13.1 g) were added triethyl orthoformate (20.7 mL, 122 mmol, 1.8 equiv) and acetic anhydride (17.9 mL, 190 mmol, 2.8 equiv). The flask was equipped with a distillation apparatus, and the solution was heated for 1 h to 120 °C, for 1 h to 130 °C, and for 1 h to 140 °C, while a colorless clear liquid was distilled off. After cooling down, distillation under high vacuum afforded **17** as a yellow clear liquid (12.0 g, 49.2 mmol, 72%). *M* ($C_{11}H_{16}O_6$) = 244.24 g/mol. T_b = 116−120 °C (0.45 mbar); lit., 155−160 °C (1.3 mbar).[15] R_f (SiO_2) = 0.15 and 0.81 (EtOAc). IR (ATR): ν = 2987, 2937, 1359, 1256, 1177, 1019 cm^{-1}. ^1H NMR, COSY (300 MHz, $CDCl_3$): δ = 7.90 (s, 1H, =CH−), 7.88 (s, 1H, =CH′−), 4.40−4.32 (m, 2H, =CHOCH_2−), 4.40−4.32 (m, 2H, =CHOCH'_2−), 4.32−4.27 (m, 2H, O=C-4-OCH_2−), 4.32−4.27 (m, 2H, O=C-4′-OCH_2−), 4.27−4.18 (m, 2H, O=C-1-OCH_2−), 4.27−4.18 (m, 2H, O=C-1′-OCH_2−), 1.44 (t, ^3J = 7.2 Hz, 3H, =CHOCH$_2$CH_3), 1.43 (t, ^3J = 7.2 Hz, 3H=CHOCH$_2$CH'_3), 1.36 (t, ^3J = 7.2 Hz, 3H, O=C-4-OCH$_2$CH_3), 1.35 (t, ^3J = 7.2 Hz, 3H, O=C-4-OCH$_2$CH'_3), 1.28 (t, ^3J = 7.2 Hz, 3H, O=C-1-OCH$_2$CH_3), 1.27 (t, ^3J = 7.2 Hz, 3H, O=C-1-OCH$_2$CH'_3) ppm. ^{13}C NMR, HSQC, HMBC (75 MHz, $CDCl_3$): δ = 185.2 (C-3), 183.2 (C-3′), 170.1 (=CH−), 170.0 (=CH′−), 165.2 (C-1), 164.2 (C-4), 164.0 (C-4′), 163.5 (C-1′), 109.6 (C-2), 108.3 (C-2′), 74.7 (=CH−O−CH_2−), 74.6 (=CH−O−C′H_2−), 62.2 (O=C-1-OCH_2−), 62.0 (O=C-1′-OCH_2−), 61.1 (O=C-4-OCH_2−), 61.0 (O=C-4′-OCH_2−), 15.4 (=CHOCH$_2$CH_3), 15.4 (=CHOCH$_2$C′H_3), 14.3 (O=C-1-OCH$_2$CH_3), 14.2 (O=C-1′-OCH$_2$CH_3), 14.1 (O=C-4-OCH$_2$CH_3), 14.1 (O=C-4′-OCH$_2$CH_3) ppm. ESI-MS: *m*/*z* = 217.1 (100%, $[M\text{-}Et + H]^+$). Ethyl enol ether hydrolyzes during the LC−MS run to the free enol. The spectrometric data are consistent with literature values.[15]

Ethyl (4*R*,12a*S*)-7-Hydroxy-4-methyl-6,8-dioxo-3,4,6,8,12,12a-hexahydro-2*H*-pyrido[1′,2′:4,5]pyrazino-[2,1-b][1,3]oxazine-9-carboxylate, 18. Amine **16** (2.00 g, 11.8 mmol, 1.0 equiv) was added in a single portion to a solution of enol ether **17** (2.87 g, 11.8 mmol, 1.0 equiv) in dry DCM (80 mL), which was prepared in an oven-dried Schlenk flask under a nitrogen atmosphere. The yellow-greenish solution was stirred at r.t. for 24 h (full conversion of **17** detected by LC−MS and UV detection at 254/315 nm) before it was cooled in an ice bath. $MgBr_2{\cdot}OEt_2$ (3.79 g, 14.7 mmol, 1.25 equiv) was added all at once under a nitrogen reverse flow, and the suspension was stirred for 10 min before dry pyridine (2.8 mL, 35 mmol, 3.0 equiv) was dripped into the yellowish suspension within 2 min. A clear orange-red solution formed immediately, which was stirred at r.t. for three days (full conversion of **43** detected by LC−MS and UV detection at 254/315 nm). The suspension was cooled in an ice bath, and 1 N HCl (60 mL) was added while stirring. The mixture was transferred into a separatory funnel and vigorously shaken before the organic phase was separated. The aqueous phase was extracted with DCM (2 × 50 mL), combined organic phases were dried over Na_2SO_4 and filtered, and the solvent was removed in vacuo at 40 °C. Crude **18** was obtained as an orange fluffy solid (3.61 g, 11.2 mmol, 95%, HPLC purities of 94% (254 nm) and 87% (315 nm)) and used for the next step without further purification. To obtain a pure material, crude **18** was heated in EtOAc (0.1 g/2 mL) and cooled down to r.t. first then to −24 °C (freezer). The solid was filtered off, washed with ice-cold EtOAc, and dried in vacuo at 40 °C. *M* ($C_{15}H_{18}N_2O_6$) = 322.32 g/mol. T_m = 90−96 °C (sintering to an orange resin) and 104−106 °C (resin melts to a yellow-greenish liquid). $[\alpha]_{589}^{21}$= −35.6 ($CHCl_3$, *c* = 10 mg/mL). R_f (C_{18}-SiO_2) = 0.58 (EtOH:H_2O = 1:1 + 10% HOAc). IR (ATR): ν = 2979, 1725, 1632, 1452, 1282, 1262, 1181, 1090, 1048 cm^{-1}. ^1H NMR, COSY (300 MHz, $CDCl_3$): δ = 12.33 (s_B, 1H, −OH), 7.91 (s, 1H, H-10), 5.40−5.28 (m, 1H, H-

https://doi.org/10.1021/acs.oprd.1c00139
Org. Process Res. Dev. 2021, 25, 1898−1910

12a), 5.00−4.87 (m, 1H, H-4), 4.40−4.19 (m, 3H, H_a-12 and $-OCH_2-$), 4.12−3.91 (m 3H, H-2 and H_b-12), 2.29−2.11 (m, 1H, H_a-3), 1.60−1.49 (m, 1H, H_b-3), 1.43 (t, ^3J = 7.1 Hz, 3H, 4-CH_3), 1.33 (t, ^3J = 7.0 Hz, 3H, $-OCH_2CH_3$) ppm. ^{13}C NMR, HMBC, HSQC (75 MHz, $CDCl_3$): δ = 169.8 (C-8), 164.3 (−COOEt), 162.5 (C-6), 156.5 (C-7), 141.5 (C-10), 115.3 (C-6a), 114.8 (C-9), 76.4 (C-12a), 62.8 (C-2), 61.1 ($-OCH_2$), 52.6 (C-12), 44.8 (C-4), 29.5 (C-3), 15.7 (4-CH_3), 14.4 ($-OCH_2CH_3$) ppm. ESI-HRMS: calcd for $[M + H]^+$, m/z = 323.1238; found, m/z = 323.1227.

(4*R*)-7-Hydroxy-4-methyl-6,8-dioxo-3,4,6,8,12,12a-hexahydro-2*H*-pyrido[1′,2′:4,5]pyrazino[2,1-b][1,3]-oxazine-9-carboxylic Acid, 19. For method 1, a solution of enol ether **17** (2.87 g, 11.8 mmol, 1.0 equiv) in dry DCM (80 mL) was prepared in an oven-dried Schlenk flask under a nitrogen atmosphere. Amine **16** (2.00 g, 11.8 mmol, 1.0 equiv) was added all at once, and the yellow-greenish solution was stirred at r.t. for 24 h (full conversion of **17** detected by LC−MS and UV absorption at 254/315 nm) and then cooled in an ice bath. $MgBr_2{\cdot}OEt_2$ (3.79 g, 14.7 mmol, 1.25 equiv) was added all at once under a nitrogen reverse flow, and the suspension was stirred for 10 min before dry pyridine (2.8 mL, 35 mmol, 3.0 equiv) was dripped into the yellowish suspension within 2 min. A clear orange-red solution formed immediately, which was stirred at r.t. for three days (full conversion of **43** detected by LC−MS and UV detection at 254 nm). The solution suspension was cooled in an ice bath, and 1 N HCl (60 mL) was added while stirring. The mixture was transferred into a separating funnel and vigorously shaken, and the organic phase was separated. The aqueous phase was extracted with DCM (2 × 50 mL), and to the combined organic phases was added 1 N NaOH (60 mL). The two-phase mixture was stirred vigorously at r.t. for 24 h (complete saponification detected by LC−MS and UV detection at 254 nm). The aqueous phase was separated, extracted once with DCM (50 mL), and cooled in an ice bath. The pH was adjusted to 1−2 by slow addition of conc. HCl (5 mL) where a colorless suspension formed. The solid was vacuum-filtered and washed several times with cold water (5 × 3 mL). The colorless solid was dried in air first then at 70 °C in fine vacuum to obtain **19** (2.49 g, 8.46 mmol, 72%). For method 2, a solution of enol ether **17** (0.72 g, 2.94 mmol, 1.0 equiv) in dry MeCN (25 mL) was prepared in an oven-dried Schlenk flask under a nitrogen atmosphere. Amine **16** (0.5 g, 2.94 mmol, 1.0 equiv) was added in a single portion, and the yellow-greenish solution was heated to reflux for 16 h (full conversion of **17** detected by LC−MS and UV absorption at 254/315 nm). The orange solution was cooled to r.t. before anhydrous $MgCl_2$ (0.35 g, 3.67 mmol, 1.25 equiv) was added. The suspension was stirred for 10 min at r.t. before dry pyridine (0.71 mL, 8.81 mmol, 3.0 equiv) was added. The mixture was heated to reflux under a nitrogen atmosphere for 24 h (95% conversion of **43** as judged by LC−MS and UV detection 254 nm). MeCN was removed in vacuo at 40 °C, and to the brownish salty residue was added DCM (15 mL). The suspension was cooled in an ice bath, and 1 N HCl (15 mL) was added while stirring vigorously. The mixture was transferred into a separating funnel and shaken vigorously. The organic phase was separated, and the aqueous phase was extracted with DCM (2 × 10 mL). 1 N NaOH (15 mL) was added to the combined organic phases, and the mixture was stirred vigorously at r.t. for 24 h (complete saponification detected by LC−MS and UV detection at 254 nm). The aqueous phase was separated and extracted once with DCM (10 mL). The aqueous phase was cooled in an ice bath, and conc. HCl was slowly added for acidification to pH = 1−2. A colorless solid precipitated, which was vacuum-filtered and washed with water (4 × 2 mL). The solid was dried in air first then at 70 °C under high vacuum to obtain **19** (0.46 g, 1.56 mmol, 53%). M ($C_{13}H_{14}N_2O_6$) = 294.26 g/mol. T_m = 248−252 °C (decomposition). $[\alpha]_{589}^{21}$= −120.9 (MeCN, c = 10 mg/mL). R_f (C_{18}-SiO_2) = 0.65 (EtOH:H_2O = 2:1 + 20% HOAc). IR (ATR): ν = 1735, 1646, 1618, 1546, 1461, 1440, 1346, 1285, 1095, 1081 cm^{-1}. ^1H NMR, COSY (400 MHz, DMSO-d_6): δ = 15.39 (s_B, 1H, −COOH), 12.77 (s_B, 1H, −OH), 8.67 (s, 1H, H-10), 5.52−5.47 (m, 1H, H-12a), 4.84−4.75 (m, 1H, H-4), 4.65 (dd, ^2J = 13.9 Hz, ^3J = 4.6 Hz, 1H, H_a-12), 4.43 (dd, ^2J = 13.9 Hz, ^3J = 5.9 Hz, 1H, H_b-12), 4.09−3.99 (m, 1H, H_a-2), 3.95−3.87 (m, 1H, H_b-2), 2.09−1.97 (m, 1H, H_a-3), 1.60−1.53 (m, 1H, H_b-3), 1.34 (t, ^3J = 7.0 Hz, 3H, $-CH_3$) ppm. ^{13}C NMR, HMBC, HSQC (101 MHz, DMSO-d_6): δ = 172.2 (C-8), 165.4 (−COOH), 161.8 (C-6), 153.6 (C-7), 141.1 (C-10), 118.7 (C-6a), 113.0 (C-9), 76.0 (C-12a), 62.0 (C-2), 51.5 (C-12), 44.9 (C-4), 29.1 (C-3), 15.2 ($-CH_3$) ppm. ESI-HRMS: calcd for $[M + H]^+$, m/z = 295.0925; found, m/z = 295.0929.

Sodium (4*R*,12a*S*)-9-((2,4-Difluorobenzyl)carbamoyl)-4-methyl-6,8-dioxo-3,4,6,8,12,12a-hexahydro-2*H*-pyrido[1′,2′:4,5]pyrazino[2,1-b][1,3]oxazin-7-olate (Dolutegravir Sodium), 15. For method 1, an oven-dried Schlenk flask was charged with ester **18** (94%, 1.00 g, 2.92 mmol, 1.0 equiv), dry toluene (30 mL), acetic acid (0.42 mL, 7.29 mmol, 2.5 equiv), and 2,4-difluorobenzylamine (**10**, 0.87 mL, 7.29 mmol, 2.5 equiv) under a nitrogen atmosphere. The mixture was heated to reflux for 22 h (full conversion of **18** detected by LC−MS and UV detection at 254/315 nm). All volatiles were removed in vacuo at 40 °C, and the residue was dissolved in EtOH (30 mL) by heating to reflux. NaOH (0.13 g, 3.21 mmol, 1.1 equiv) was added, and the solution was heated again to reflux for 2 min during which a beige suspension formed. The mixture was stirred to r.t., filtered, and washed with EtOH (4 × 2 mL). The yellow filter cake was dried in air overnight and transferred into a new flask. EtOH (15 mL) was added, and the suspension was heated again to reflux, hot-filtered, and washed with hot ethanol (4 × 2 mL). The solid was dried in air overnight then for 2 h at 70 °C in fine vacuum to obtain **15** as a faint yellow solid (0.90 g, 2.04 mmol, 70%, purity of 99.7% (254 nm)). For method 2, an oven-dried flask was charged with acid **19** (1.00 g, 3.40 mmol, 1.0 equiv), carbonyl diimidazole (97%, 1.14 g, 6.80 mmol, 2.0 equiv), and dry dimethyl carbonate (30 mL) under a nitrogen atmosphere. The suspension was heated to 80 °C for 2 h during which a nearly clear orange solution formed. After cooling to r.t., 2,4-difluorobenzylamine (**10**, 0.81 mL, 6.80 mmol, 2.0 equiv) was added dropwise within 2 min, and the solution was stirred for 2 h at r.t. (full conversion of **19** detected by LC−MS and UV detection at 254/315 nm). The solvent was removed in vacuo at 40 °C, and the residue was redissolved in DCM (30 mL) and 1 N NaOH (30 mL). After stirring for 18 h at r.t., the colorless suspension was transferred into a separatory funnel. The organic phase was separated, and the aqueous phase was extracted twice with DCM (30 mL). The aqueous phase was cooled in an ice bath, acidified (pH = 1−2) with conc. HCl, and extracted with DCM (3 × 25 mL). The combined organic phases were dried over Na_2SO_4, and all volatiles were removed in vacuo at 40 °C. The colorless foamy residue was dissolved by heating in EtOH (30 mL). NaOH

https://doi.org/10.1021/acs.oprd.1c00139
Org. Process Res. Dev. 2021, 25, 1898−1910

(0.15 g, 3.74 mmol, 1.1 equiv) was added to the hot solution, and heating to reflux was continued for 2 min. The suspension was stirred to r.t., filtered, and washed with EtOH (5 × 3 mL). The solid was dried in air overnight then for 2 h at 70 °C under high vacuum to obtain **15** as a faint yellow solid (1.41 g, 3.19 mmol, 94%, purity of 99.9% (254 nm)). *M* ($C_{20}H_{18}F_2N_3NaO_5$) = 441.37 g/mol. T_m = 314 °C (decomposition); lit., 296 °C.[24] $[\alpha]_{589}^{21}$= −46.4 (DMSO-d_6, *c* = 10 mg/mL). IR (ATR): ν = 2975, 2913, 1641, 1537, 1504, 1424, 1321, 1274, 1258, 1106, 1093 cm^{-1}. ^{1}H NMR, COSY (400 MHz, DMSO-d_6): δ = 10.69 (t, ^3J = 6.0 Hz, 1H, −NH−), 7.89 (s, 1H, H-10), 7.39−7.27 (m, 1H, Ar-H-6), 7.25−7.14 (m, 1H, Ar-H-3), 7.06−6.93 (m, 1H, Ar-H-5), 5.22−5.10 (m, 1H, H-12a), 4.87−4.72 (m, 1H, H-4), 4.50 (d, ^3J = 6.0 Hz, 2H, −NHCH_2Ar), 4.36−4.24 (m, 1H, H_a-11), 4.21−4.08 (m, 1H, H_b-11), 4.04−3.87 (m, 1H, H_a-2), 3.86−3.73 (m, 1H, H_b-2), 1.96−1.76 (m, 1H, H_a-3), 1.45−1.29 (m, 1H, H_b-3), 1.23 (t, ^3J = 7.0 Hz, 3H, −CH_3) ppm. ^{13}C NMR, HMBC, HSQC (101 MHz, DMSO-d_6): δ = 177.9 (C-8), 167.0 (C-7), 166.0 (−CONH−), 162.0 (dd, ^1J = 247 Hz, ^3J = 12.3 Hz, Ar-C2), 161.2 (C-6), 158.8 (dd, ^1J = 249 Hz, ^3J = 12.3 Hz, Ar-C4), 134.4 (C-10), 130.5 (dd, ^3J = 9.2 Hz, ^3J = 6.2 Hz, Ar-C6), 115.0 (C-9), 111.3 (dd, ^2J = 20.9 Hz, ^4J = 3.6 Hz, Ar-C5), 108.9 (C-6a), 103.7 (t, ^2J = 25.7 Hz, Ar-C3), 75.6 (C-12a), 62.0 (C-2), 53.1 (C-11), 43.1 (C-4), 35.4 (^3J = 3.7 Hz, −NHCH_2Ar), 29.2 (C-3), 15.3 (-CH_3) ppm. ^{19}F NMR (377 MHz, DMSO-d_6): δ = −112.9, −115.2 ppm. ESI-MS: m/z = 418.2 (100%, $[M-Na]^-$). The spectroscopic data are consistent with literature values.[11]

■ ASSOCIATED CONTENT

Supporting Information

The Supporting Information is available free of charge at https://pubs.acs.org/doi/10.1021/acs.oprd.1c00139.

Optimization studies, chromatograms, VCD spectroscopy, computational details, and NMR spectra (PDF)

XYZ coordinates of benzyloxazinone **35** (ZIP)

■ AUTHOR INFORMATION

Corresponding Author

Till Opatz − *Department of Chemistry, Johannes Gutenberg University, 55128 Mainz, Germany;* orcid.org/0000-0002-3266-4050; Email: opatz@uni-mainz.de

Authors

Jule-Philipp Dietz − *Department of Chemistry, Johannes Gutenberg University, 55128 Mainz, Germany*

Tobias Lucas − *Department of Chemistry, Johannes Gutenberg University, 55128 Mainz, Germany*

Jonathan Groß − *Department of Chemistry, Johannes Gutenberg University, 55128 Mainz, Germany*

Sebastian Seitel − *Department of Chemistry, Johannes Gutenberg University, 55128 Mainz, Germany*

Jan Brauer − *Department of Chemistry, Johannes Gutenberg University, 55128 Mainz, Germany*

Dorota Ferenc − *Department of Chemistry, Johannes Gutenberg University, 55128 Mainz, Germany*

B. Frank Gupton − *Department of Chemical and Life Sciences Engineering, Virginia Commonwealth University, Richmond, Virginia 23284, United States;* orcid.org/0000-0002-8165-1088

Complete contact information is available at: https://pubs.acs.org/10.1021/acs.oprd.1c00139

Notes

The authors declare no competing financial interest.

■ ACKNOWLEDGMENTS

This work was supported by the Bill and Melinda Gates Foundation through the Medicines for All initiative. We thank Dr. J. C. Liermann (Mainz) for NMR spectroscopy and Dr. C. J. Kampf (Mainz) for mass spectrometry. Parts of this research were conducted using the supercomputer MOGON and/or advisory services offered by the Johannes Gutenberg University Mainz (hpc.uni-mainz.de), which is a member of the AHRP (Alliance for High Performance Computing in Rhineland Palatinate, www.ahrp.info) and the Gauss Alliance e.V. The authors gratefully acknowledge the computing time granted on the supercomputer MOGON at the Johannes Gutenberg University Mainz (hpc.uni-mainz.de).

■ REFERENCES

(1) *GLOBAL HIV AND AIDS STATISTICS*; 2019, https://www.avert.org/global-hiv-and-aids-statistics (accessed March 29, 2021).

(2) Cihlar, T.; Fordyce, M. Current status and prospects of HIV treatment. *Curr. Opin. Virol.* **2016**, *18*, 50−56.

(3) *FDA Approves First Extended-Release, Injectable Drug Regimen for Adults Living with HIV*; 2021, https://www.fda.gov/news-events/press-announcements/fda-approves-first-extended-release-injectable-drug-regimen-adults-living-hiv (accessed March 21, 2021).

(4) Hughes, D. L. Review of Synthetic Routes and Final Forms of Integrase Inhibitors Dolutegravir, Cabotegravir, and Bictegravir. *Org. Process Res. Dev.* **2019**, *23*, 716−729.

(5) *In 2020, our web migration project tackled over 180,000 pages of content and over 200,000 publications. Much of our content has been updated, made more dynamic and may no longer be found in the same place*; 2021, https://www.who.int/hiv/pub/arv/arv-update-2019-policy/en/ (accessed March 21, 2021).

(6) Topics in heterocyclic chemistry. *Synthesis of heterocycles in contemporary medicinal chemistry;* Časar, Z.; Barth, R., Eds.; *44*, Springer: Switzerland, 2016.

(7) Phull, M. S.; Shah, B.; Kadlag, M.; Rao, D. R.; Malhotra, G. Continues flow process for the preparation of active pharmaceutical ingredients - polycyclic carbamoyl pyridone derivatives and intermediates thereof. Patent WO 2019/159199 A1, August 22, 2019.

(8) Yasukata, T.; Masui, M.; Ikarashi, F.; Okamoto, K.; Kurita, T.; Nagai, M.; Sugata, Y.; Miyake, N.; Hara, S.; Adachi, Y.; et al. Practical Synthetic Method for the Preparation of Pyrone Diesters: An Efficient Synthetic Route for the Synthesis of Dolutegravir Sodium. *Org. Process Res. Dev.* **2019**, *23*, 565−570.

(9) Aoyama, Y.; Hakogi, T.; Fukui, Y.; Yamada, D.; Ooyama, T.; Nishino, Y.; Shinomoto, S.; Nagai, M.; Miyake, N.; Taoda, Y.; et al. Practical and Scalable Synthetic Method for Preparation of Dolutegravir Sodium: Improvement of a Synthetic Route for Large-Scale Synthesis. *Org. Process Res. Dev.* **2019**, *23*, 558−564.

(10) Jee, J.; Gade, N.; Roper, T. Novel pyrrole and pyridone derivatives and uses thereof. Patent WO 2020/081143 A1, April 23, 2020.

(11) Sankareswaran, S.; Mannam, M.; Chakka, V.; Mandapati, S. R.; Kumar, P. Identification and Control of Critical Process Impurities: An Improved Process for the Preparation of Dolutegravir Sodium. *Org. Process Res. Dev.* **2016**, *20*, 1461−1468.

(12) https://medicines4all.vcu.edu/our-portfolio/bmgf-projects/r-3-aminobutanol-batch-/ (accessed March 12, 2021).

(13) Lerner, C.; Krei, L.; Hilpert, H. Pyrimidone derivatives and their use in treatment, amelioration or prevention of a viral disease. Patent WO 2017/158151 A1, September 21, 2017.

(14) Luu, Q. H.; Guerra, J. D.; Castañeda, C. M.; Martinez, M. A.; Saunders, J.; Garcia, B. A.; Gonzales, B. V.; Aidunuthula, A. R.; Mito,

https://doi.org/10.1021/acs.oprd.1c00139
Org. Process Res. Dev. 2021, 25, 1898−1910

S. Ultrasound assisted one-pot synthesis of benzo-fused indole-4,9-dinones from 1,4-naphthoquinone and α-aminoacetals. *Tetrahedron Lett.* **2016**, *57*, 2253−2256.
(15) Jones, R. G. The Synthesis of Ethyl Ethoxymethyleneoxalacetate and Related Compounds. *J. Am. Chem. Soc.* **1951**, *73*, 3684−3686.
(16) Sumino, Y.; Masui, M.; Yamada, D.; Ikarashi, F.; Okamoto, K. Process fpr preparing compound having hiv integrase inhibitory activity. Patent US 2014/0011995 A1, January 09, 2014.
(17) Ziegler, R. E.; Desai, B. K.; Jee, J.-A.; Gupton, B. F.; Roper, T. D.; Jamison, T. F. 7-Step Flow Synthesis of the HIV Integrase Inhibitor Dolutegravir. *Angew. Chem., Int. Ed.* **2018**, *57*, 7181−7185.
(18) Sumino, Y.; Okamoto, K.; Masui, M.; Yamada, D.; Ikarashi, F. Process for preparing compund having HIV integrase activity. Patent EP 2602260 A1, June 12, 2013.
(19) Phull, M.; Rao, D.; Birari, D. A process for the preparation of bictegravir and intermediate thereof. Patent WO 2018/229798 A1, December 20, 2018.
(20) Budidet, S.; Dussa, N.; Kaki, G.; Yatcherla, S.; Sanapureddy, J.; Danda, S.; Katuroju, S.; Meenakshisunderam, S. An improved proecess for the preparation of dolutegravir. Patent WO 2014/128545 A2, August 24, 2014.
(21) Juhász, M.; Lázár, L.; Fülöp, F. Substituent effects in the ring-chain tautomerism of 4-alkyl-2-aryl substituted oxazolidines and tetrahydro-1,3-oxazines. *J. Heterocycl. Chem.* **2007**, *44*, 1465−1473.
(22) Gu, N.; Liu, M.; Wang, H.; Sun, S.; Zhou, Z.; Hu, W.; Yu, J.-T.; Cheng, J. Iridium-catalyzed annulation between 1,2-diarylethanone and 3-aminopropanol toward site-specific 2,3-diaryl pyridines. *Tetrahedron Lett.* **2017**, *58*, 3398−3400.
(23) Kaye, I. A.; Minsky, I. New Compounds. Preparation of N-Substituted Aminoacetals. *J. Am. Chem. Soc.* **1949**, *71*, 2272−2273.
(24) Hotter, A.; Thaler, A.; Lebar, A.; Jankovic, B.; Naversnik, K.; Klancar, U.; Abramovic, Z. Novel Hydrates of Dolutegravir Sodium. Patent WO 2016/016279 A1, February 16, 2016.

https://doi.org/10.1021/acs.oprd.1c00139
Org. Process Res. Dev. 2021, 25, 1898−1910

7.2.3 Bestimmung der absoluten Konfiguration eines 13-Hydroxy-14-deoxyoxacyclododecindions

Aufbauend auf der Isolierung eines Naturstoffs aus der Gruppe der Dihydroxyphenylessigsäurelactone von Shang und Lin *et al.*, wurde das vorgeschlagene 13-Hydroxy-14-deoxyoxacyclododecindion **141** (in der Publikation **4**) in der Arbeitsgruppe Opatz stereoselektiv über 15 lineare Stufen in einer Gesamtausbeute von 9% dargestellt und das Makrolacton **141** auf seine biologische Aktivität untersucht.[543] Dabei wurde von der Arbeitsgruppe [redacted] eine stark hemmende Wirkung auf die Interleukin-4 induzierten STAT6-abhängigen Signalwege mit einem IC_{50}-Wert von 56 nM nachgewiesen. Darüber hinaus wurde eine durch sichtbares Licht hervorgerufene *E*/*Z*-Isomerisierung der Doppelbindung des zwölfgliedrigen Rings **141** bei Raumtemperatur beobachtet.

Im Vergleich zu den veröffentlichten NMR-Daten des Naturstoffs, wiesen die gemessenen chemischen Verschiebungen des synthetischen Makrolactons **141** eine Diskrepanz auf.[543] Obwohl sich die experimentellen ECD-Spektren der synthetischen Verbindung **141** und des berichteten Naturstoffs sehr ähneln, kann es sich dennoch um diastereomere Verbindungen handeln. Trotz der Simulation aller möglichen Diastereomere von Verbindung **141** war weder eine Zuordnung der relativen noch der absoluten Konfiguration des Makrolactons **141** möglich.

Um die absolute Konfiguration der synthetischen Verbindung **141** zu bestimmen, wurden VCD-Spektren aufgenommen, die sich gegenüber ECD-Spektren durch eine deutlich höhere Informationsdichte auszeichnen und keinen Chromophor in der Nähe der Stereozentren benötigen. Der Vergleich der VCD-Spektren mit den simulierten Spektren aller Diastereomere von Verbindung **141** zeigte, dass die synthetische Verbindung **141** die Stereokonfiguration C-13*R*, C-14*S*, C-15*R* besitzt. Diese Zuordnung wurde durch eine zusätzliche Untersuchung mittels Röntgenkristallstrukturanalyse validiert. Diese Befunde implizieren eine Überarbeitung der vorgeschlagenen Struktur des von Shang und Lin *et al.* isolierten Naturstoffs (Abbildung 7.7).[543,560]

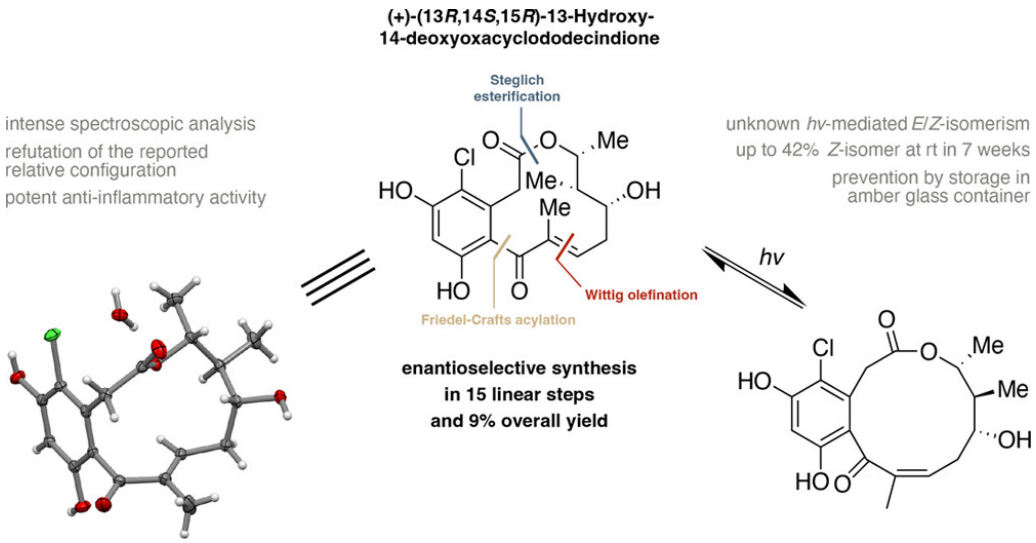

Abbildung 7.7: *Graphical abstract* der Publikation „Total Synthesis and Biological Evaluation of the Anti-Inflammatory (13*R*,14*S*,15*R*)-13-Hydroxy-14-deoxyoxacyclododecindione“.[560]

Die Synthese des Makrolactons **141** wurde von [redacted] durchgeführt. Die Aufnahme der ECD- und VCD-Spektren sowie deren Berechnung auf DFT-Level wurde von J. Groß ausgeführt. Die biologischen Eigenschaften von **141** wurden von [redacted] untersucht. Das Manuskript wurde von allen Autoren erstellt.[15]

[15] *Reprinted with permission from K. Seipp, J. Groß, A. M. Kiefer, G. Erkel, T. Opatz, J. Nat. Prod. 2023, 86, 924–938. Copyright ©2023, American Chemical Society.*

JOURNAL OF NATURAL PRODUCTS

pubs.acs.org/jnp Article

Total Synthesis and Biological Evaluation of the Anti-Inflammatory (13*R*,14*S*,15*R*)-13-Hydroxy-14-deoxyoxacyclododecindione

Kevin Seipp, Jonathan Groß, Anna Maria Kiefer, Gerhard Erkel, and Till Opatz*

Cite This: *J. Nat. Prod.* 2023, 86, 924−938 Read Online

ACCESS | Metrics & More | Article Recommendations | Supporting Information

ABSTRACT: The first total synthesis of the natural product (13*R*,14*S*,15*R*)-13-hydroxy-14-deoxyoxacyclododecindione, which was isolated in 2018 as a member of the oxacyclododecindione family, is reported. A synthetic strategy through intramolecular Friedel-Crafts acylation combined with the stereoselective synthesis of a new triol key fragment allowed the preparation of the macrolactone. Due to mismatching physical data of the synthetic product, a revision of the configuration of the natural product isolated in 2018 is required. Light-induced *E*/*Z*-isomerism of the macrolactone backbone is described for the first time in the class of oxacyclododecindione-type macrolactones. The hydroxylated macrolactone prepared herein was found to show highly promising IC_{50} values in biological assays addressing the inhibition of inflammatory responses.

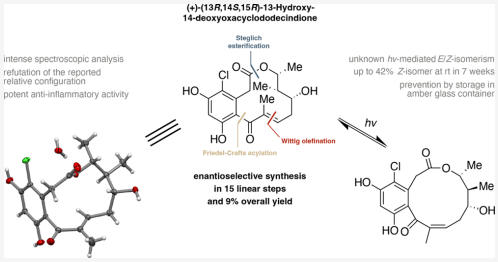

The family of the 12-membered oxacyclododecindione-type macrolactones currently consists of oxacyclododecindione (**1**),[1] 4-dechloro-14-deoxyoxacyclododecindione (**2**),[2] 14-deoxyoxacyclododecindione (**3**),[2] and the recently reported 13-hydroxy-14-deoxyoxacyclododecindione (**4**)[3] (Scheme 1). These secondary metabolites (**1**−**4**), isolated from the imperfect fungus *Exserohilum rostratum*, can be regarded as lead structures in the discovery of drugs against chronic inflammation and fibrotic diseases due to their highly potent anti-inflammatory and antifibrotic activity.[1−6]

Our contributions to the area of this macrolactone family include total syntheses, structure elucidation, and derivatizations and the establishment of initial structure−activity relationships through bioassays.[5,7−9] However, despite several attempts, it has not yet been possible to prepare a macrolactone possessing a hydroxylated aliphatic backbone, as found in natural products **1** and **4**. Fermentation of the producing strains provided only very small quantities of the hydroxylated derivatives oxacyclododecindione (**1**) and 13-hydroxy-14-deoxyoxacyclododecindione (**4**),[1,3] and the synthesis of the proposed natural product **4** reported herein is the first of its kind.

Compound **4** was first isolated from solid cultures of the fungus *E. rostratum*, an endophytic fungal strain in *Gymnadenia conopsea*. The structure was reported in 2018 by Shang and Lin et al., and its configuration was elucidated by NMR (modified Mosher's method) as well as electronic circular dichroism (ECD).[3]

Moreover, 13-hydroxy-14-deoxyoxacyclododecindione (**4**) can structurally be regarded as a synthetically more accessible constitutional isomer of oxacyclododecindione (**1**), the most potent anti-inflammatory oxacyclododecindione-type natural product known to date.[1,4,6] To investigate the biological effect of a hydroxy group in the backbone, 13-hydroxy-14-deoxyoxacyclododecindione (**4**) was synthesized according to a strategy related to that successfully used for the preparation of macrolactones **2** and **3**, respectively (Scheme 1).

RESULTS AND DISCUSSION

Although the class of oxacyclododecindiones so far only consists of four natural products, it has attracted considerable interest due to its superb anti-inflammatory potential.[3,4,10−12] To date, two natural products and 10 synthetic derivatives of the oxacyclododecindione series have been successfully synthesized.[5,9] All of the retrosynthetic approaches followed a strategy based on the key step of an intramolecular Friedel-Crafts acylation (IFCA) at low substrate concentration and low temperature.[5,9,11] Other approaches to the ring closure of the 12-membered lactone, such as carbonylative cross-coupling, hydroacylation, or metathesis reaction, have not proved fruitful.[7] The synthesis of 13-hydroxy-14-deoxyoxacyclododecindione (**4**) commenced with the preparation of the three building blocks **5**−**7** (Scheme 1), which were later coupled in a Steglich

Received: December 16, 2022
Published: March 31, 2023

https://doi.org/10.1021/acs.jnatprod.2c01145
J. Nat. Prod. 2023, 86, 924−938

Scheme 1. Structures of All Natural Representatives (1−4) of the Oxacyclododecindione Family and a General Retrosynthetic Approach

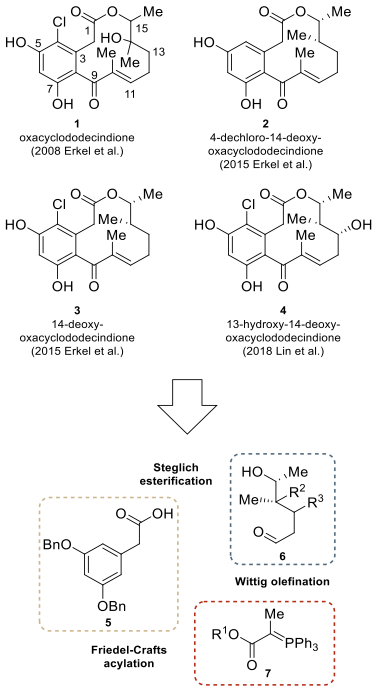

esterification and Wittig olefination, followed by the key IFCA.[13−15] Because the triol system was the only hitherto unknown building block in this approach, the total synthesis began with its stereoselective preparation (Scheme 2). Starting from 1,3-propanediol (**8**), monoprotection with TBDPS-Cl,[16] followed by oxidation with 1-hydroxy-1,2-benziodoxol-3(1*H*)-one-1-oxide (IBX),[17] produced a suitable precursor **9** for an asymmetric Evans *syn*-aldol reaction in two steps and 84% overall yield (for full stepwise details; see Supporting Information Scheme S1). Aldehyde **9** was then subjected to typical Evans aldol conditions using the chiral oxazolidinone **10**, which led to the formation of the *syn*-aldol product with an 88% yield.[18,19] To determine the stereochemical outcome of the aldol reaction, methyl ester **13** was prepared in the following three-step sequence and compared with its stereoisomeric congeners by NMR spectroscopy. The racemic methyl ester was synthesized according to known procedures (Scheme S1).[20,21] Upon treatment of the aldol product with catalytic amounts of TfOH and benzyl-2,2,2-trichloracetimidate, *O*-benzylation yielded the protected secondary alcohol **11** in 79%.[22,23] It is worth mentioning that the repeated addition of 0.1 equiv of TfOH and a maximum reaction temperature of 12 °C were of great importance to achieve complete conversion. Higher reaction temperatures led to the degradation of the oxazolidinone and to a deterioration of the yield. In the next step, the Evans auxiliary was cleaved by $LiOH/H_2O_2$ to furnish carboxylic acid **12**,[18] followed by methylation with MeI, generating methyl ester **13** with a yield of 70% over two steps.[24] NMR spectroscopic comparison of *syn*-product **13** with a racemic mixture of *syn*- and *anti*-congeners revealed a diastereomeric ratio (dr) of >40:1. The further route to the triol fragment **17** involved $LiBH_4$-mediated reduction of the oxazolidinone **11** to the primary alcohol,[25] which was then oxidized to aldehyde **14** in two steps and 63% combined yield using the IBX procedure mentioned earlier.[17] The desired final step included 1,3-asymmetric induction during the nucleophilic addition of MeMgBr toward aldehyde **14** according to the cyclic Cram−Reetz model.[26−28] Unfortunately, this reaction gave a diastereomeric mixture of 2.3:1 in favor of the undesired alcohol **16**. Nevertheless, to our delight, the separation of both diastereomers **16** and **17** by flash chromatography was successful. Alternatively, stronger coordinating reagents like $MeTiCl_3$ are conceivable to reverse the ratio in favor of the desired isomer. However, this approach was not pursued, as another pathway developed in parallel was more promising. Based on the previously synthesized carboxylic acid **12**, conversion to the Weinreb amide and treatment with MeMgBr[26,29] produced ketone **15** in two steps and 83% yield.

In the next step, according to the Felkin−Anh model, the nonperpendicular attack of the nucleophilic bulky hydride reagent L-selectride proceeded along the Bürgi−Dunitz trajectory across the smallest substituent.[30−32] This provided the appropriate alcohol **17** in a dr of 95:5. After column chromatography, building-block **17** was isolated in 77% yield with a dr of >99:1.[33] To investigate the relative configurations of **16** and **17**, their acetonides were prepared in a short sequence combining hydrogenolytic debenzylation and subsequent acetonide formation with camphorsulfonic acid in 2,2-dimethoxypropane.[34] The *syn*-(**18**) and *anti*-acetonide (**19**) were obtained in 54% and 51% yield, respectively. ^{13}C chemical shifts and NOE contacts of the two isomers **18** and **19** clearly revealed the identity of the respective isomer (Scheme 2).[34,35]

With the synthon **17** in hand, the synthesis was continued by a Steglich esterification of secondary alcohol **17** with 3,5-bis(benzyloxy)phenylacetic acid (**5**) (Scheme 3),[9] which was synthesized according to a known five-step procedure.[36−39] The obtained ester was converted into aldehyde **20** by desilylation with TBAF and subsequent IBX oxidation of the primary alcohol, resulting in a combined yield of 71% over three steps (Scheme S2).[17,40] Following the work of Chen et al.,[11] in addition to the Wittig ylide **21**, available in three steps as demonstrated earlier,[41] the phosphoranylidene **23** served as another building block for a new Friedel-Crafts precursor **26**. Its synthesis was achieved in a two-step sequence, commencing with the reaction of *tert*-butyl 2-bromopropanoate (**22**) and triphenylphosphine to form the phosphonium salt, which, after deprotonation with aqueous NaOH solution, produced ylide **23** with an overall yield of 70% (Scheme S2). Compared to the literature procedure, yield and purity could be significantly increased by a longer reaction time and a modified workup.[41] Wittig olefination was carried out with both ylides, **21** and **23**, obtaining the allyl ester **24** as well as the *tert*-butyl ester **26** in 90% yield, respectively. While compound **26** served as a direct precursor of an IFCA, the allyl ester **24** first had to be converted into the carboxylic acid **25**, an established precursor for the IFCA, in a Pd^0-catalyzed deallylation.[42]

The construction of the 12-membered lactone ring proved to be one of the most challenging steps in the total synthesis of the oxacyclododecindione members. Therefore, the IFCA conditions were initially adopted from previous published studies

https://doi.org/10.1021/acs.jnatprod.2c01145
J. Nat. Prod. 2023, 86, 924−938

Scheme 2. Stereoselective Synthesis of the Triol Fragment 17, Key Building Block in the Total Synthesis of (13*R*,14*S*,15*R*)-13-Hydroxy-14-deoxyoxacyclododecindione (4); Preparation of *syn*- and *anti*-Acetonides (18 and 19) Unambiguously Confirmed Their Relative Configurations

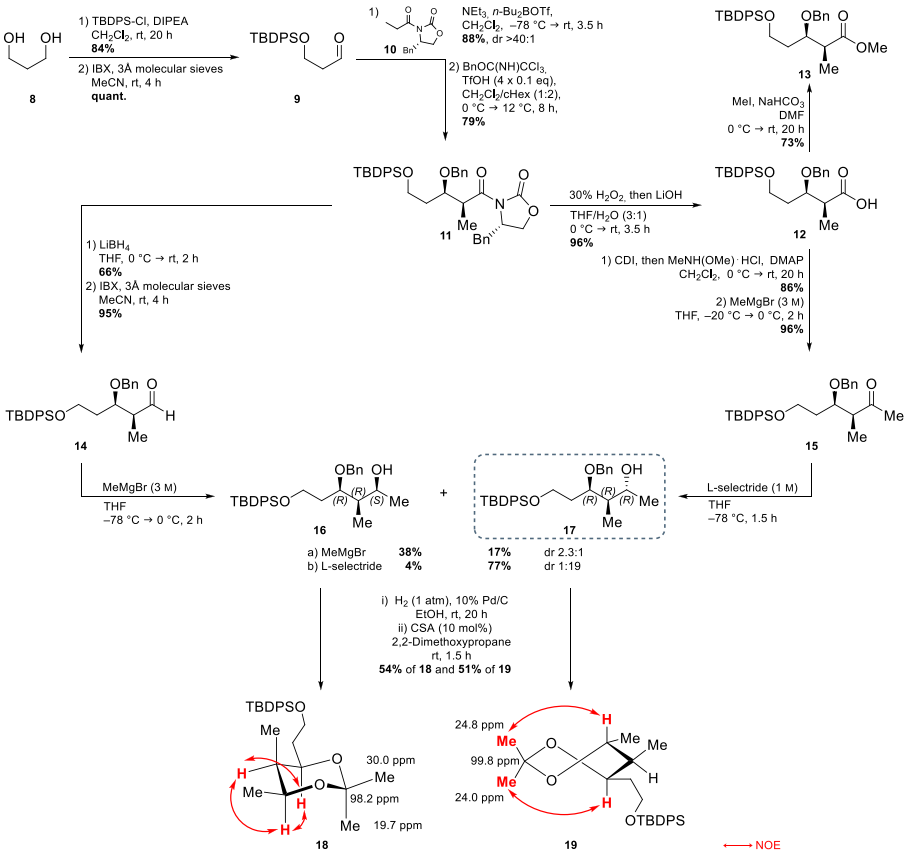

(Table 1), starting with the free carboxylic acid **25** (entry 1).[5,9] Extending the reaction time from 2 to 3 d led to a slight increase of the yield (entry 2). Since some unidentifiable byproducts were observed in addition to the moderate yield of 25% (2 d) and 40% (3 d) of the desired product **28**, the amount of TFA/TFAA was halved in the next step and the reaction medium was warmed up to room temperature and stirred for 4 d (entry 3). This resulted in a 52% yield, whereas longer reaction times under the same conditions led to an increase in byproducts at the expense of product formation. Neither the extension to 7 d, combined with the stepwise addition of TFA over that period, nor the reaction without TFA addition led to an improvement of the yield (entries 4 + 5). The application of the optimized procedure for cyclization of the carboxylic acid **25** was applied to *tert*-butyl ester **26**, whereby an increased yield of up to 48% and 63% was achieved in both cases (entries 6 + 7). The optimized conditions (entry 7) also furnished 14-membered macrolactone **27** in 6% yield, resulting from the debenzylation of one of the two benzyl ethers in the 5- or 7-position and subsequent esterification in acidic medium.

To conclude the stereoselective synthesis of 13-hydroxy-14-deoxyoxacyclododecindione (**4**), a reaction sequence of BCl_3-mediated debenzylation and electrophilic aromatic chlorination with *N*-chlorosuccinimide was performed.[9] Because the isolation of the dechloro derivative **30** could only be carried out in moderate yield due to the high polarity of the compound and resulting problems in the purification step, the reaction sequence was reversed. Chlorination and final deprotection furnished the proposed macrolactone **4** in 15 linear steps with an overall yield of 9%. The target compound was extensively characterized by both spectroscopic methods and X-ray crystallography (see next section).

During this characterization, a light-induced *E*/*Z*-isomerization, hitherto unknown in the oxacyclododecindione family, occurred. Within 42 days, isomerization to a maximum of 42% of the *Z*-isomer was observed in an NMR sample in DMSO-d_6 at room temperature (Figure S81). Although the isolation of the pure *Z*-isomer **34** failed, its presence could be confirmed by 2D NMR spectroscopy. In particular, the NOE contacts of the backbone (H-11 to H-15) showed deviations from the

https://doi.org/10.1021/acs.jnatprod.2c01145
J. Nat. Prod. 2023, 86, 924−938

Scheme 3. Assembly of All Three Synthons into Ring Closure Precursor 25 and 26, Followed by IFCA under Optimized Conditions, Resulted in a 12-Membered Macrolactone 28 and Its 14-Membered Congener 27

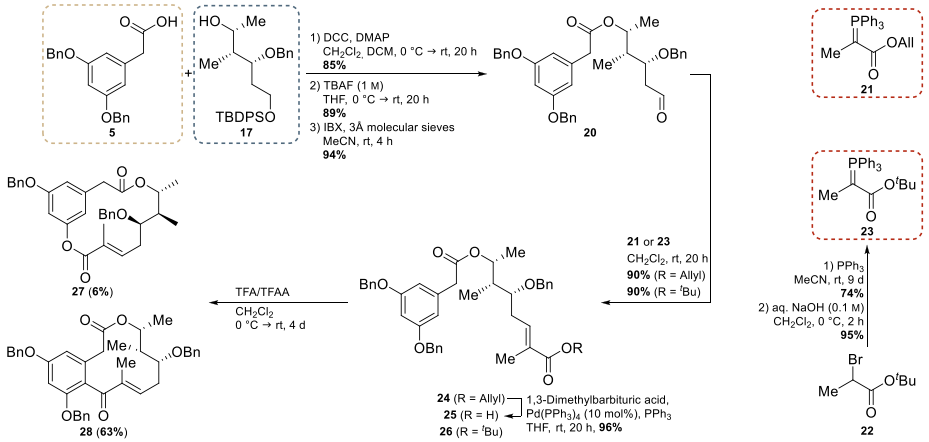

Table 1. Optimization Conditions of the Intramolecular Friedel-Crafts Acylation[a]

entry	TFA [μM]	TFAA [μM]	ratio (v/v)	T [°C]	t [d]	R =	yield [%]
1	882	253	2/1	−8 °C	2	H	25[b]
2	824	236	2/1	−8 °C	3	H	40[b]
3	418	118	2/1	−8 °C to rt	4	H	52[b]
4	68.0/day	231		−8 °C to rt	7	H	32[b]
5		231		−8 °C to rt	7	H	3[c]
6	424	119	2/1	−8 °C to rt	3	tBu	48[b]
7	406	114	2/1	−8 °C to rt	4	tBu	63[b]

[a]All reactions were performed at 0.68 mM substrate concentration. [b]After flash chromatography. [c]Monitored by UV-DAD detection (254.4 nm) with an Agilent Technologies 1260 Infinity II system.

synthesized *E*-isomer **4**, with the change in NOE from H-11−H_2-12, H-14 to H-11−H_3-16, H-13 confirming our hypothesis. These findings were observed for all other macrolactones **28**−**30** synthesized in this study. Both chloro- and dechloro- as well as benzyl-protected and unprotected derivatives showed similar behavior in isomerization tendency (ca. 20% *Z*-isomer after 14 days), yielding **31**−**34** (Scheme 4). Measurements in deuterated MeOH and MeCN showed the isomerization process to be largely solvent independent. The undesired isomerization, presumably due to the high strain of the 12-membered macrolactone, was suppressed by storage in amber glassware. For all four 12-membered macrolactones **4** and **28**−**30**, no isomerization was detected even after 6 weeks of storage in an amber glass vial at room temperature.

STRUCTURE ELUCIDATION OF SYNTHETIC AND NATURAL MACROLACTONES

Following the successful synthesis of (13*R*,14*S*,15*R*)-13-hydroxy-14-deoxyoxacyclododecindione (**4**), an extensive analytical characterization was carried out, due to mismatching

Scheme 4. Final Chlorination and Deprotection Led to 4-Dechloro-13-hydroxy-14-deoxyoxacyclododecindione (30) and the Supposed Natural Product 13-Hydroxy-14-deoxyoxacyclododecindione (4); In Addition, Light-Mediated *E*/*Z*-Isomerism Was Detected within All Macrocyclic Compounds 4 and 28−34

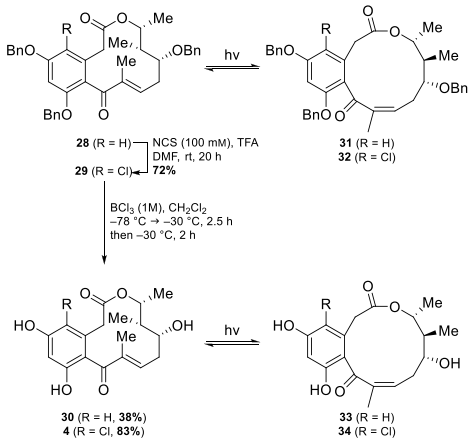

NMR data between synthetic **4** and natural macrolactone isolated by Shang and Lin et al.[3] Comparing the ^{1}H and ^{13}C NMR data of both macrolactones (Table 2), the strong deviation of the proton shifts in the backbone region from H-13−H-15 was particularly striking. In addition, the authors reported a coupling constant of 4.8 Hz between H-14 and H-15,[3] which contrasts with synthetic derivatives **2**−**4** having an *erythro*-arrangement of the methyl groups and exhibiting coupling constants in the range of 8.5−9.6 Hz.[5,9]

More importantly for the overall typical 3D structure of the oxacyclododecindione family, the triangular NOE contacts between H-11, H-12b, and H-14 indicate the characteristic L-

https://doi.org/10.1021/acs.jnatprod.2c01145
J. Nat. Prod. 2023, 86, 924−938

Table 2. ^{1}H and ^{13}C NMR Data Comparison of the Natural Product[3] Isolated in 2018 and the Macrolactone 4 Synthesized in Our Study[a]

	natural product		synthetic product **4**	
position	δ_C[b]	δ_H[c,d] (J in Hz)	δ_C[b]	δ_H[c,d] (J in Hz)
1	167.7		167.8	
2a	37.6	3.41, d (16.2)	37.5	3.50, d (17.3)
2b		3.02, d (16.2)		2.97, d (17.3)
3	130.5		130.8	
4	121.1		121.0	
5	153.1		153.7	
6	102.3	6.50, s	102.4	6.49, s
7	153.1		153.3	
8	110.9		111.5	
9	197.6		197.9	
10	135.8		137.5	
11	148.3	6.37, dd (5.4, 1.6)	147.0	6.43, dd (10.4, 5.1)
12a	35.4	2.50−2.52, m	38.6	2.48−2.43, m
12b		2.25−2.27, m		2.17, ddd (14.0, 10.0, 5.1)
13	68.9	3.93−3.95, m	71.8	3.17−3.07, m
14	43.8	1.75−1.77, m	43.6	1.57, dqd, (9.6, 7.3, 3.8)
15	71.6	4.84, dt (4.8, 6.0)	75.1	4.56, dq (9.6, 6.3)
16	10.1	1.77, s	10.3	1.79, s
17	13.9	0.77, d (7.2)	11.5	0.78, d (7.3)
18	18.1	1.05, d (7.2)	18.4	1.01, d (6.3)
OH-5		9.66, s		9.71, s
OH-7		10.22, s_{br}		10.24, s
OH-13		4.71, d (4.2)		4.89, d (4.9)

[a]Compounds were measured in DMSO-d_6. [b]Recorded at 151 MHz. [c]Recorded at 600 MHz. [d]Deshielded signals of methylenes were labeled as "a" and shielded signals as "b".

shaped molecular structure. These contacts were lacking in the published spectra of the natural product, whereas the atypical NOE signals between H_2-12−H_3-17 and H-13−H_3-18 were conspicuous in the published spectra of the isolated natural product and could give an indication of the actual structure and configuration (Figure 1).[3]

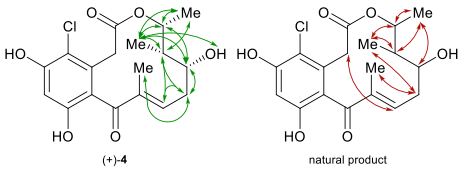

Figure 1. Key NOESY correlations observed in the synthetic macrolactone **4** (green) and reported in the natural product[3] (red).

The published ECD spectra provide another point of comparison to the isolated natural product. The authors described the experimental spectrum in combination with the predicted spectra for (13*R*,14*S*,15*R*) and its antipode.[3] Although the experimental spectrum of the synthetic macrolactone **4** was in good agreement with the literature, our calculated ECD spectra prevented any conclusion regarding the configuration of the natural product. As the calculated ECD spectra of all four possible diastereomers showed great similarity, it became apparent that ECD is not an appropriate method to elucidate the absolute configuration of the macrocyclic natural product (Figure S89). Therefore, a vibrational circular dichroism (VCD) spectroscopic investigation was carried out to further elucidate the absolute configuration of the synthesized compound **4**. This method proved to be an additional pillar for the elucidation of the absolute configuration of 13-hydroxy-14-deoxyoxacyclododecindione (**4**), because there were a larger number of useful signals that could be used for absolute structure elucidation.[43] In terms of the similarity factor, a metric developed by Bringmann et al. for such application to quantify the degree of matching spectra,[44] the calculated spectrum for the (13*R*,14*S*,15*R*)-diastereomer **4** exhibited a sufficiently high similarity factor (73%) with the experimental spectrum, while all other stereoisomers showed low to moderate similarity factors (50−15%, Figure S91). Compared to the calculated ECD spectra, the characteristic signals of the theoretical VCD spectra for each stereoisomer can be considered an additional advantage of this method. Therefore, the measurement of a VCD spectrum of the isolated natural product would be of further importance for the elucidation of its absolute configuration. To our delight, following the spectroscopic analyses, we were able to obtain an X-ray crystal structure (Flack parameter of −0.02(2)) of the synthetic target compound **4**, which unambiguously confirmed the (13*R*,14*S*,15*R*) configuration. In analogy to previously published crystal structures of this class,[5,9] an L-shaped conformation with a (*Z*)-configured ester unit in combination with a perpendicular arrangement of the enone and the aromatic ring could be observed (Figure 2). These three structural features were also consistent with the NMR data of the synthesized derivative **4** and might play a significant role for the biological activity of the oxacyclododecindione family (see the Biological Evaluation).

Taken together, these observations suggest that the compound isolated by Shang and Lin et al. indeed belongs to the oxacyclododecindione family but apparently has a different

https://doi.org/10.1021/acs.jnatprod.2c01145
J. Nat. Prod. 2023, 86, 924−938

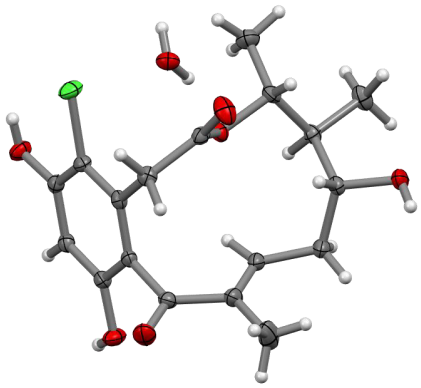

Figure 2. X-ray crystal structure of (+)-**4** as ORTEP ellipsoids. C: gray, H: white, O: red, Cl: green.

relative configuration compared to lactone **4** synthesized here.[3] As a presumed alternative to the configuration reported in 2018,[3] the (13*R*,14*S*,15*S*) arrangement could be consistent with the observed NOE contacts and the smaller coupling constant. Another, biosynthetically more likely possibility, maintaining the classical *erythro*-arrangement of the methyl groups, would be the inversion of the hydroxy group to (13*S*,14*S*,15*R*), which could result in a twisted backbone due to an intramolecular hydrogen bond between COH-13 and CO-1 and might explain the atypical coupling constants and NOE contacts. Further studies to clarify the relative configuration of the natural product are currently under investigation in our group.

BIOLOGICAL EVALUATION

Macrolactones of the oxacyclododecindione series **1**−**3** represent potent inhibitors of TGF-β and IL-4 signaling pathways in mammalian cells.[1,2,5,6,9] To classify the bioactivity of the hydroxylated compound **4** in the same way as done for the natural products and synthetic derivatives studied earlier, its inhibitory effect on IL-4-inducible STAT6-dependent and TGF-β-inducible Smad2/3-dependent transcriptional luciferase reporters in transiently transfected HepG2 cells (Table 3) was investigated. Oxacyclododecindione (**1**), the first member of this natural class, is still the most active representative, with IC_{50} values of 68 nM (STAT6) and 136 nM (Smad2/3), respectively.[1] It was not until the accomplished synthesis of (14*S*,15*R*)-14-deoxyoxacyclododecindione (**3**) in 2015 that the most potent representative in the IL-4 reporter gene expression was found with an IC_{50} value of 20 nM, while a higher but still appreciable IC_{50} value of 90 nM was achieved in the TGF-β reporter assay.[5] The structure−activity relationship study conducted in 2020 revealed that the racemic 14-deoxy-14-methyloxacyclododecindione was the most active substance in the TGF-β-inducible Smad2/3-dependent pathway at an IC_{50} of 30 nM, whereas in the IL-4-inducible STAT6-dependent pathway an IC_{50} value of 79 nM was achieved.[9] The (13*R*,14*S*,15*R*)-13-hydroxy-14-deoxyoxacyclododecindione (**4**) synthesized in this study showed excellent inhibitory activity on IL-4-induced STAT6 signaling. With an IC_{50} value of 56 nM, the compound ranked second among all derivatives tested so far. Moderate activity was observed in the TGF-β-induced Smad(2/3)-dependent signaling pathway with an IC_{50} value of 236 nM. In addition, this value underlined the assumption that the double methyl effect at C-14 further increases the activity in the TGF-β reporter assay. A comparison of the two hydroxylated macrolactones **1** and **4** showed the same tendency of activity, with the latter showing remarkable inhibition, particularly in the STAT6 signaling pathway.

Table 3. Effects of Natural and Synthetic 12-Membered Macrolactones in Two Relevant Reporter Gene Assays[a]

	pGL3-TK-7xN_4 (STAT6) IC_{50} (nM)	$(CAGA)_{9x}$-MLP-Luc (Smad2/3) IC_{50} (nM)
oxacyclododecindione (isolated) (**1**)	68 ± 5	137 ± 14
(14*S*,15*R*)-14-deoxyoxacyclododecindione (synthetic) (**3**)	20 ± 1	90 ± 10
14-deoxy-14-methyloxacyclododecindione (synthetic)	79 ± 27	30 ± 11
(13*R*,14*S*,15*R*)-13-hydroxy-14-deoxyoxacyclododecindione (synthetic) (**4**)	56 ± 13	236 ± 28

[a]As internal normalization control and to exclude cytotoxic effects, the EF1α promoter in front of a renilla luciferase was co-electroporated into the HepG2 cells. All values are described as mean from three independent replicates ± SEM.

CONCLUSION

In summary, the first stereoselective synthesis of the potent anti-inflammatory (13*R*,14*S*,15*R*)-13-hydroxy-14-deoxyoxacyclododecindione (**4**, 9% yield over 15 steps) was accomplished. An extensive analytical study (NMR, ECD, VCD spectroscopy, X-ray crystallography) of the synthesized derivative **4** disproved the configuration of the natural product reported in 2018. This comprehensive analytical study, including detailed 3D analysis based on previous crystal structures and NOE data, underlines their importance for a correct assignment of the configuration within this compound class. Therefore, our study is intended to facilitate further structure elucidation of oxacyclododecindione-type macrolactones. Circular dichroism measurements can be helpful in the structure elucidation, yet the theoretical spectra of all possible stereoisomers need to be considered. In general, it was also found that the L-shaped conformation, the (*Z*)-configured ester, and the enone unit almost perpendicular to the aromatic moiety are distinct features of the current oxacyclododecindione members, which also exhibit an *erythro*-arrangement of the C-14 and C-15 methyl groups. Moreover, a light-mediated *E*/*Z*-isomerism was observed in all synthetic macrolactones **4** and **28**−**34**, which was previously unknown for the oxacyclododecindione series, and could be prevented by storage in amber glassware. Nevertheless, the question arises whether this isomerization can be associated with other natural products of the 12-membered macrolides (e.g., *cis*-dehydrocurvularin), or is it just an isolated case. In addition, the synthesized derivative **4** was shown to be a potent inhibitor of TGF-β-dependent Smad2/3 and IL-4-dependent STAT6 signaling pathways with IC_{50} values in the nanomolar range.

EXPERIMENTAL SECTION

General Experimental Procedures. Optical rotation measurements were accomplished with a PerkinElmer 241MC polarimeter at 546 and 578 nm. The data obtained were extrapolated to a wavelength of λ = 589 nm using the Drude equation.[46] Electronic circular dichroism

https://doi.org/10.1021/acs.jnatprod.2c01145
J. Nat. Prod. 2023, 86, 924−938

spectra of **4** (c = 0.02 mmol/L in MeOH) were recorded on a JASCO J-815 spectrometer equipped with a JASCO PTC-423S/15 temperature controller. The measurement was repeated five times and averaged using a scanning speed of 50 nm/min at 20 °C. The solvent background was recorded applying the same parameters and was subtracted from the sample measurement. The so-obtained experimental spectrum was compared to the Boltzmann-averaged simulated spectra using the software SpecDis 1.71.[44] The infrared and vibrational circular dichroism spectra of **4** were measured with a Tensor 27 FTIR spectrometer equipped with a photoelastic modulator optimized for 1400 cm^{-1} using a 100 μm BaF_2 sample cell. A solution of **4** in CD_3CN (0.23 mol/L) was prepared, and the IR data were recorded in the spectral range of 4000−800 cm^{-1} with 16 scans. The spectrum was baseline-corrected by subtraction of a solvent spectrum recorded with the same parameters. Using the same solution of **4**, the VCD spectra were measured with an accumulation time of 360 min with a resolution of 4 cm^{-1} in the spectral range of 1800−800 cm^{-1}, and the baseline was subtracted, in the same manner as above. The experimental noise was obtained by subtraction of two measured solvent spectra from each other. Infrared spectroscopy was performed on a Bruker Tensor 27 FT-IR spectrometer including a diamond ATR unit. Measured NMR spectra were, unless otherwise mentioned, recorded at 296 K on a 300 MHz Bruker Avance-III HD 300, a 400 MHz Bruker Avance-II HD 400, or a 600 MHz Bruker Avance-III 600 spectrometer. All chemical shifts (δ) are referenced to the residual solvent signal ($CDCl_3$: 7.26 and 77.16 ppm; DMSO-d_6: 2.50 and 39.52 ppm; CD_3OD: 3.31 and 49.00 ppm; CD_3CN: 1.94 and 1.32 ppm for ^1H NMR and ^{13}C NMR, respectively) and are expressed relative to tetramethylsilane (TMS).[47] Low-resolution electrospray ionization (ESI) mass spectra were measured on an InfinityLab LC/MSD (G6125B) spectrometer. HRMS was conducted on an Agilent G6545A Q-ToF with ESI, APCI, or APPI source coupled with an Agilent 1260 Infinity II HPLC system. If not described otherwise, spectra were recorded using a positive ionization mode. For reaction control by analytical thin-layer chromatography (TLC), 0.25 mm silica plates ($60F_{254}$) from Merck were used, and the detection was reached by fluorescence quenching under UV light (λ = 254 nm) or by staining with potassium permanganate reagent (solution of $KMnO_4$ (3 g), K_2CO_3 (20 g), 5% NaOH (5 mL), and H_2O (300 mL)) followed by heating at 400 °C. Preparative column chromatography was performed on silica gel (35−70 μm, Acros Organics) using an overpressure of 0.5−0.6 bar nitrogen. The composition of the mobile phase was given as v/v. For analytical HPLC separation, an Agilent Technologies 1260 Infinity II system including an ACE3-C_{18}-PFP-column (particle size: 3 μm, length: 150 mm, diameter: 4.6 mm, column temperature: 40 °C, flow rate: 1 mL/min^{-1}) with UV-DAD detection was used. Preparative HPLC was performed on an Agilent Technologies 1290 Infinity II system with two high-pressure gradient K-1800 pumps and an S-260-UV-DAD detector. The separation took place on ACE 5 C_{18}-PFP (particle size: 5 μm, length: 150 mm, diameter: 30 mm, flow rate: 42.5 mL/min^{-1}) or Macherey-Nagel Nucleodur C_{18}-HTEC (particle size: 5 μm, length: 150 mm, diameter: 32 mm, flow rate: 42.5 mL/min^{-1}) columns. For both analytical and preparative HPLC, the eluent mixtures of solvents A: H_2O (LCMS grade and Milli-Q) + 0.1% TFA (LCMS grade) and B: MeCN (HPLC and LCMS grade) were given in the v/v ratio. X-ray crystallographic measurements were performed on a Stoe IPDS-2T with Mo Kα radiation (graphite monochromator). Unless otherwise stated, all chemicals and solvents were obtained from commercial sources and used without prior purification. Chloroform, CH_2Cl_2, and triethylamine were distilled over $CaCl_2$ before use. Anhydrous cyclohexane, diethyl ether, and tetrahydrofuran (THF) were obtained by distillation over sodium/benzophenone. Dimethyl sulfoxide, *N*,*N*-dimethylformamide, MeOH, and EtOH were purchased from commercial suppliers as extra dry solvents stored over 3 Å molecular sieves and used without additional purification. IBX was prepared according to the literature-known synthesis of Henderson et al.[45] Allyl 2-(triphenylphoshoranylidine)propanoate (**21**) was prepared in three steps starting from 2-bromopropionic acid according to Opatz et al.[5] All reactions were performed under an argon atmosphere using flame-dried glassware at ambient pressure. Reaction temperatures of −78 °C were achieved using a dry ice/acetone cooling bath. When a temperature gradient in the range of −78 °C to room temperature was required, a cryostat (Julabo FT902) was used.

*3-((tert-Butyldiphenylsilyl)oxy)propan-1-ol (**35**).* According to a previously published procedure,[16] *tert*-butylchlorodiphenylsilane (3.00 mL, 11.5 mmol, 1.00 equiv) and *N*,*N*-diisopropylethylamine (7.26 mL, 42.7 mmol, 3.70 equiv) were added in a sequential fashion to a solution of 1,3-propanediol (**8**, 2.63 g, 34.6 mmol, 3.00 equiv) in CH_2Cl_2 (25 mL), and the reaction was stirred overnight. After the TLC showed full conversion of the starting material, the reaction mixture was washed with H_2O (30 mL) and extracted with EtOAc (3 × 100 mL), and the combined organic layers were washed with brine and dried over $MgSO_4$. The solvent was removed under reduced pressure, and the crude mixture was purified by column chromatography (cyclohexane/EtOAc, 3:1), furnishing TBDPS-ether **35** as a white solid (3.06 g, 9.73 mmol, 84%). R_f 0.33 (cyclohexane/EtOAc, 3:1); IR (ATR) $\tilde{\nu}$ [cm^{-1}] 3342, 3071, 2931, 2857, 1472, 1427, 1390, 1361, 1189, 1109, 965, 823, 736, 701, 613, 504, 433; ^1H NMR, COSY (400 MHz, $CDCl_3$) δ_H 7.74−7.63 (m, 4H, CH_{arom}), 7.49−7.35 (m, 6H, CH_{arom}), 3.85 (ptd, J = 5.6, 2.1 Hz, 4H, 1-CH_2, 3-CH_2), 2.30 (s, 1H, OH), 1.82 (quintet, J = 5.7 Hz, 2H, 2-CH_2), 1.06 (s, 9H, C(CH_3)$_3$); ^{13}C NMR, HSQC, HMBC (101 MHz, $CDCl_3$) δ_C 135.7 (4C, 4 × *o*-CH), 133.4 (2C, 2 × *ipso*-C), 129.9 (2C, 2 × *p*-CH), 127.9 (4C, 4 × *m*-CH), 63.4 (3-CH_2), 62.1 (1-CH_2), 34.4 (2-CH_2), 27.0 (3C, SiC(CH_3)$_3$), 19.2 (SiC(CH_3)$_3$); HRESIMS m/z 315.1778 [M + H]$^+$ (calcd for $C_{19}H_{26}O_2Si$, 315.1775). The analytical data are in accordance with the literature.[48]

*3-((tert-Butyldiphenylsilyl)oxy)propanal (**9**).* Using a modified procedure of Pannecoucke et al.,[17] monoprotected alcohol **35** (4.00 g, 12.7 mmol, 1.00 equiv) was dissolved in dry MeCN (260 mL), IBX (8.90 g, 31.8 mmol, 2.50 equiv) was added, and the reaction mixture was stirred over preactivated 3 Å molecular sieves (5.08 g). After 4 h, the solvent was removed under reduced pressure at room temperature (rt) and the residue was taken up in EtOAc (100 mL). The mixture was filtered through a pad of Celite, and the solvent was removed under reduced pressure, furnishing the aldehyde **9** (3.96 g, 12.7 mmol, 100%) as a yellowish-green oil, which was used immediately for the next reaction. R_f 0.61 (cyclohexane/EtOAc, 3:1); IR (ATR) $\tilde{\nu}$ [cm^{-1}] 3071, 3050, 2958, 2931, 2888, 2858, 2731, 1728, 1472, 1427, 1390, 1109, 823, 741, 702, 613, 505, 490; ^1H NMR, COSY (300 MHz, $CDCl_3$) δ_H 9.82 (t, J = 2.2 Hz, 1H, 1-CHO), 7.70−7.61 (m, 4H, CH_{arom}), 7.50−7.33 (m, 6H, CH_{arom}), 4.03 (t, J = 6.0 Hz, 2H, 3-CH_2), 2.61 (td, J = 6.0, 2.2 Hz, 2H, 2-CH_2), 1.04 (s, 9H, C(CH_3)$_3$); ^{13}C NMR, HSQC, HMBC (75.5 MHz, $CDCl_3$) δ_C 202.1 (1-CHO), 135.7 (4C, 4 × *o*-CH), 133.4 (2C, 2 × *ipso*-C), 130.0 (2C, 2 × *p*-CH), 127.9 (4C, 4 × *m*-CH), 58.4 (3-CH_2), 46.5 (2-CH_2), 26.9 (3C, SiC(CH_3)$_3$), 19.3 (SiC(CH_3)$_3$); HRESIMS m/z 335.1433 [M + Na]$^+$ (calcd for $C_{19}H_{24}O_2Si$, 335.1438). The analytical data are in accordance with the literature.[17]

*(S)-4-Benzyl-3-((2S,3R)-5-((tert-butyldiphenylsilyl)oxy)-3-hydroxy-2-methylpentanoyl) oxazolidin-2-one (**36**).* The Evans aldol reaction was performed according to a procedure by Hermann et al.[18] To a solution of (*S*)-4-benzyl-3-propionyloxazolidin-2-one **10** (2.02 g, 8.64 mmol, 0.90 equiv) in CH_2Cl_2 (45 mL) was added *n*-Bu_2BOTf (1 M in CH_2Cl_2, 10.1 mL, 10.1 mmol, 1.05 equiv) dropwise at 0 °C over a period of 10 min. Triethylamine (1.52 mL, 11.0 mmol, 1.14 equiv) was then added to the solution. The reaction mixture was stirred for an additional 45 min and cooled to −78 °C before the previously prepared aldehyde **9** (3.00 g, 9.60 mmol, 1.00 equiv) in CH_2Cl_2 (12 mL + 2 mL rinse) was slowly added. The resulting reaction mixture was stirred at −78 °C for 2 h and at 0 °C for another 1.5 h before quenching it with phosphate buffer (pH 7, 40 mL). Afterward, the aqueous layer was extracted three times with CH_2Cl_2 (50 mL), and the combined organic extracts were dried ($MgSO_4$), filtered, and concentrated in vacuo. The residue was dissolved in MeOH (45 mL), and a 35% H_2O_2 solution (23 mL) was added at 0 °C. After 1 h at 0 °C, the excess peroxide was quenched by slow addition of 10% aqueous $NaHSO_4$ (30 mL), and the solution was extracted with EtOAc (3 × 100 mL). The combined organic extracts were washed with saturated aqueous $NaHCO_3$ (20 mL) and brine (20 mL), filtered, dried ($MgSO_4$), and concentrated under reduced pressure. The crude product was first rinsed through a short filter column (cyclohexane/EtOAc, 2:1) to remove boron species.

https://doi.org/10.1021/acs.jnatprod.2c01145
J. Nat. Prod. 2023, 86, 924−938

Finally, purification by flash chromatography (toluene/EtOAc, 95:5) yielded the desired secondary alcohol **36** (4.16 g, 7.63 mmol, 88%) as a colorless oil. $[\alpha]_D^{23}$ +31.8 (*c* 1.02, $CHCl_3$); R_f 0.18 (toluene/EtOAc, 95:5); IR (ATR) $\tilde{\nu}$ [cm^{-1}] 3510, 3070, 2931, 2858, 1781, 1697, 1456, 1428, 1387, 1209, 1110, 739, 703, 505; ^{1}H NMR, COSY (400 MHz, $CDCl_3$) δ_H 7.71−7.64 (m, 4H, CH_{arom}), 7.46−7.18 (m, 11H, CH_{arom}), 4.75−4.65 (m, 1H, 4′-C*H*), 4.29−4.15 (m, 3H, 3-C*H*, 5′-CH_2), 3.93−3.78 (m, 3H, 2-C*H*, 5-CH_2), 3.46 (s_{br}, 1H, O*H*), 3.28 (dd, *J* = 13.4, 3.3 Hz, 1H, $CH_{2\text{-A Bn-Evans}}$), 2.79 (dd, *J* = 13.4, 9.6 Hz, 1H, $CH_{2\text{-B Bn-Evans}}$), 1.88−1.76 (m, 1H, 4-$CH_{2\text{-A}}$), 1.72−1.62 (m, 1H, 4-$CH_{2\text{-B}}$), 1.29 (d, *J* = 7.0 Hz, 3H, 2-CH_3), 1.05 (s, 9H, C(CH_3)$_3$); ^{13}C NMR, HSQC, HMBC (101 MHz, $CDCl_3$) δ_C 176.6 (1-CON), 153.2 (2′-NCO_2), 135.7 (2C, 2 × *o*-CH_{TBDPS}), 135.7 (2C, 2 × *o*-CH_{TBDPS}), 153.3 (*ipso*-C_{Evans}), 133.4 (*ipso*-C_{TBDPS}), 133.3 (*ipso*-C_{TBDPS}), 129.9 (2C, 2 × *p*-CH_{TBDPS}), 129.6 (2C, 2 × *o*-CH_{Evans}), 129.1 (2C, 2 × *m*-CH_{Evans}), 127.9 (4C, 4 × *m*-CH_{TBDPS}), 127.5 (*p*-CH_{Evans}), 70.9 (3-CH), 66.3 (5′-CH_2), 62.7 (5-CH_2), 55.4 (4′-CH), 42.9 (2-CH), 37.9 ($CH_{2\ Bn\text{-}Evans}$), 36.1 (4-CH_2), 27.0 (3C, SiC(CH_3)$_3$), 19.2 (SiC(CH_3)$_3$), 11.4 (2-CH_3); HRESIMS *m*/*z* 568.2492 [M + Na]$^+$ (calcd for $C_{32}H_{39}NO_5Si$, 568.2489). The analytical data are in accordance with the literature.[18,19]

*(S)-4-Benzyl-3-((2S,3R)-3-(benzyloxy)-5-((tert-butyldiphenylsilyl)-oxy)-2-methylpentanoyl) oxazolidin-2-one (**11**).* Following a modified procedure of Guindon et al.,[23] to an ice-cooled solution of secondary alcohol **36** (2.32 g, 4.24 mmol, 1.00 equiv) in CH_2Cl_2/cyclohexane (42 mL, 1:2) was added benzyl 2,2,2-trichloracetimidate (1.21 mL, 6.37 mmol, 1.50 equiv) and catalytic amounts of triflic acid (38.0 μL, 0.42 mmol, 0.10 equiv). The reaction mixture was stirred 2 h while slowly warming up to a maximum cooling bath temperature of 12 °C. The solution was then cooled back to 0 °C, triflic acid (38.0 μL, 0.42 mmol, 0.10 equiv) added again, and the mixture was warmed up to a maximum of 12 °C in 2 h (this cycle was repeated twice more, four times in total). After complete consumption of the starting material, as detected by TLC, the reaction mixture was quenched by the addition of 50 mL of saturated $NaHCO_3$(aq). The residue was taken up in ether and the aqueous layer was extracted three times (100 mL). The combined organic layers were washed with a saturated aqueous solution of $NaHCO_3$ (20 mL) and brine (20 mL), dried over $MgSO_4$, and filtered, and the solvent was removed in vacuo. Purification of the crude product by flash chromatography (cyclohexane/EtOAc, 12:1) yielded the protected benzyl ether **11** (2.12 g, 3.33 mmol, 79% (82% purity, determined by UV-DAD detection at 254 nm)) as a colorless oil. For analytical purposes, a small amount was further purified by preparative HPLC (C_{18}-PFP, isocratic 80% MeCN in H_2O, 20 min). $[\alpha]_D^{23}$ +59.2 (*c* 0.99, $CHCl_3$); R_f 0.50 (cyclohexane/EtOAc, 3:1); t_R (HPLC) 15.92 min (C_{18}-PFP, isocratic 80% MeCN in H_2O); IR (ATR): $\tilde{\nu}$ [cm^{-1}] 2957, 2931, 2857, 1778, 1698, 1555, 1428, 1384, 1350, 1236, 1208, 1108, 823, 738, 700, 614, 505; ^{1}H NMR, COSY (400 MHz, $CDCl_3$) δ_H 7.71−7.61 (m, 4H, CH_{arom}), 7.46−7.16 (m, 16H, CH_{arom}), 4.56 (d, *J* = 11.2 Hz, 1H, $CH_{2\text{-A Bn}}$), 4.52−4.45 (m, 1H, 4′-C*H*), 4.45 (d, *J* = 11.2 Hz, 1H, $CH_{2\text{-B Bn}}$), 4.22 (qd, *J* = 6.9, 4.9 Hz, 1H, 2-C*H*), 4.07 (dd, *J* = 9.0, 2.1 Hz, 1H, 5′-$CH_{2\text{-A}}$), 3.97−3.89 (m, 2H, 3-C*H*, 5′-$CH_{2\text{-B}}$), 3.86−3.73 (m, 2H, 5-CH_2), 3.28 (dd, *J* = 13.3, 3.3 Hz, 1H, $CH_{2\text{-A Bn-Evans}}$), 2.74 (dd, *J* = 13.3, 9.7 Hz, 1H, $CH_{2\text{-B Bn-Evans}}$), 1.97−1.85 (m, 1H, 4-$CH_{2\text{-A}}$), 1.81−1.70 (m, 1H, 4-$CH_{2\text{-B}}$), 1.26 (d, *J* = 6.9 Hz, 3H, 2-CH_3), 1.06 (s, 9H, C(CH_3)$_3$); ^{13}C NMR, HSQC, HMBC (101 MHz, $CDCl_3$) δ_C 175.2 (1-CON), 153.3 (2′-NCO_2), 138.5 (*ipso*-C_{Bn}), 135.8 (2C, 2 × *o*-CH_{TBDPS}), 135.7 (2C, 2 × *o*-CH_{TBDPS}), 135.6 (*ipso*-C_{Evans}), 134.0 (*ipso*-C_{TBDPS}), 133.9 (*ipso*-C_{TBDPS}), 129.7 (2C, 2 × *p*-CH_{TBDPS}), 129.6 (2C, 2 × *o*-CH_{Evans}), 129.1 (2C, 2 × *m*-CH_{Evans}), 128.4 (2C, 2 × *m*-CH_{Bn}), 128.3 (2C, 2 × *o*-CH_{Bn}), 127.8 (2C, 2 × *m*-CH_{TBDPS}), 127.8 (2C, 2 × *m*-CH_{TBDPS}), 127.7 (*p*-CH_{Bn}), 127.4 (*p*-CH_{Evans}), 77.6 (3-CH), 72.7 ($CH_{2\ Bn}$), 66.1 (5′-CH_2), 60.5 (5-CH_2), 55.9 (4′-CH), 40.9 (2-CH), 37.9 ($CH_{2\ Bn\text{-}Evans}$), 35.1 (4-CH_2), 27.0 (3C, SiC(CH_3)$_3$), 19.3 (SiC(CH_3)$_3$), 12.9 (2-CH_3); HRESIMS *m*/*z* 658.2955 [M + Na]$^+$ (calcd for $C_{39}H_{45}NO_5Si$, 658.2959).

*(2S,3R)-3-(Benzyloxy)-5-((tert-butyldiphenylsilyl)oxy)-2-methylpentanoic Acid (**12**).* Based on a literature procedure by Hermann et al.,[18] to oxazolidin-2-one **11** (4.45 g, 6.99 mmol, 1.00 equiv) in THF/H_2O (140 mL, 3:1) were slowly added a 35% H_2O_2 solution (3.01 mL, 35.0 mmol, 5.00 equiv) and 1 M LiOH (14 mL, 14.0 mmol, 2.00 equiv) sequentially at 0 °C. At the same temperature, the resultant solution was stirred for 1 h, then for 2.5 h at rt, and the excess H_2O_2 was quenched by the addition of 778 mM Na_2SO_3 solution (45 mL, 35 mmol, 5.00 equiv). The remaining THF was removed by rotary evaporation at a maximum bath temperature of 25 °C, and the residue was adjusted to pH 2 at 0 °C with aqueous 1 M HCl. The resulting cloudy solution was extracted with diethyl ether (5 × 120 mL), the combined organic layers were dried over $MgSO_4$, filtered, and concentrated, and the crude product was purified by flash chromatography (cyclohexane/EtOAc, 12:1, 1% AcOH). The carboxylic acid **12** (3.21 g, 6.73 mmol, 96%) was obtained as a colorless oil. $[\alpha]_D^{23}$ +20.7 (*c* 1.01, $CHCl_3$); R_f 0.32 (cyclohexane/EtOAc, 3:1, 1% AcOH); IR (ATR) $\tilde{\nu}$ [cm^{-1}] 3070, 2931, 2858, 1704, 1461, 1427, 1235, 1107, 1091, 1028, 939, 823, 735, 699, 613, 504, 489; ^{1}H NMR, COSY (400 MHz, $CDCl_3$) δ_H 10.62 (s_{br}, 1H, 1-COO*H*), 7.70−7.59 (m, 4H, CH_{arom}), 7.46−7.19 (m, 11H, CH_{arom}), 4.61 (d, *J* = 11.2 Hz, 1H, $CH_{2\text{-A Bn}}$), 4.51 (d, *J* = 11.2 Hz, 1H, $CH_{2\text{-B Bn}}$), 4.05 (dt, *J* = 8.7, 4.5 Hz, 1H, 3-C*H*), 3.86−3.71 (m, 2H, 5-CH_2), 2.82 (qd, *J* = 7.1, 4.5 Hz, 1H, 2-C*H*), 1.87−1.70 (m, 2H, 4-CH_2), 1.20 (d, *J* = 7.1 Hz, 3H, 2-CH_3), 1.06 (s, 9H, C(CH_3)$_3$); ^{13}C NMR, HSQC, HMBC (101 MHz, $CDCl_3$) δ_C 178.1 (1-COOH), 137.8 (*ipso*-C_{Bn}), 135.7 (4C, 4 × *o*-CH_{TBDPS}), 133.8 (*ipso*-C_{TBDPS}), 133.7 (*ipso*-C_{TBDPS}), 129.9 (*p*-CH_{TBDPS}), 129.8 (*p*-CH_{TBDPS}), 128.6 (2C, 2 × *m*-CH_{Bn}), 128.0 (2C, 2 × *o*-CH_{Bn}), 127.9 (5C, 4 × *m*-CH_{TBDPS}, *p*-CH_{Bn}), 77.4 (3-CH), 72.7 ($CH_{2\ Bn}$), 60.3 (5-CH_2), 42.6 (2-CH), 34.4 (4-CH_2), 27.0 (3C, SiC(CH_3)$_3$), 19.3 (SiC(CH_3)$_3$), 11.9 (2-CH_3); HRESIMS *m*/*z* 499.2270 [M + Na]$^+$ (calcd for $C_{29}H_{36}O_4Si$, 499.2275).

*Methyl (2S,3R)-3-(Benzyloxy)-5-((tert-butyldiphenylsilyl)oxy)-2-methylpentanoate (**13**).* According to a procedure from Xu and Ye et al.,[24] MeI (16.3 μL, 262 μmol, 2.50 equiv) and $NaHCO_3$ (44.1 mg, 524 μmol, 5.00 equiv) were added to a solution of pentanoic acid **12** (50.0 mg, 105 μmol, 1.00 equiv) in DMF (0.50 mL) at 0 °C. The solution was warmed to rt overnight and diluted with EtOAc (4 mL), and the organic layer was washed with H_2O, saturated NH_4Cl(aq), and brine (10 mL each). The organic extract was dried ($MgSO_4$) and filtered, and the crude product was purified by flash chromatography (cyclohexane/EtOAc, 6:1). The methyl ester **13** (37.5 mg, 76.4 μmol, 73%) was obtained as a colorless oil. $[\alpha]_D^{23}$ +20.4 (*c* 0.98, $CHCl_3$); R_f 0.59 (cyclohexane/EtOAc, 3:1); IR (ATR) $\tilde{\nu}$ [cm^{-1}] 3070, 2931, 2858, 1737, 1472, 1457, 1428, 1257, 1197, 1111, 823, 737, 702, 614, 505; ^{1}H NMR, COSY (400 MHz, $CDCl_3$) δ_H 7.69−7.62 (m, 4H, CH_{arom}), 7.46−7.22 (m, 11H, CH_{arom}), 4.53 (d, *J* = 11.3 Hz, 1H, $CH_{2\text{-A Bn}}$), 4.46 (d, *J* = 11.3 Hz, 1H, $CH_{2\text{-B Bn}}$), 4.04 (ddd, *J* = 7.0, 5.8, 4.9 Hz, 1H, 3-C*H*), 3.85−3.69 (m, 2H, 5-CH_2), 3.66 (s, 3H, 1-$COOCH_3$), 2.73 (qd, *J* = 7.1, 4.9 Hz, 1H, 2-C*H*), 1.84−1.75 (m, 2H, 4-CH_2), 1.20 (d, *J* = 7.1 Hz, 3H, 2-CH_3), 1.06 (s, 9H, C(CH_3)$_3$); ^{13}C NMR, HSQC, HMBC (101 MHz, $CDCl_3$) δ_C 175.4 (1-$COOCH_3$), 138.6 (*ipso*-C_{Bn}), 135.7 (4C, 4 × *o*-CH_{TBDPS}), 133.9 (*ipso*-C_{TBDPS}), 133.8 (*ipso*-C_{TBDPS}), 129.8 (2C, 2 × *p*-CH_{TBDPS}), 128.4 (2C, 2 × *m*-CH_{Bn}), 127.9 (2C, 2 × *o*-CH_{Bn}), 127.8 (4C, 4 × *m*-CH_{TBDPS}), 127.7 (*p*-CH_{Bn}), 77.3 (3-CH), 72.5 ($CH_{2\ Bn}$), 60.5 (5-CH_2), 51.8 (1-$COOCH_3$), 43.4 (2-CH), 35.3 (4-CH_2), 27.0 (3C, SiC(CH_3)$_3$), 19.3 (SiC(CH_3)$_3$), 11.9 (2-CH_3); HRESIMS *m*/*z* 513.2440 [M + Na]$^+$ (calcd for $C_{30}H_{38}O_4Si$, 513.2431).

*Methyl 5-((tert-Butyldiphenylsilyl)oxy)-3-hydroxy-2-methylpentanoate (**37**).* The pentanoate **37** was prepared using a modified procedure reported by Jarvo and Hong et al.[21] To a solution of LDA (1 M in THF/hexane, 2.16 mL, 2.16 mmol, 1.70 equiv) at −78 °C was added methyl propionate (222 μL, 2.29 mmol, 1.80 equiv), and the mixture was stirred for 1.75 h. The aldehyde **9** (397 mg, 1.27 mmol, 1.00 equiv) was added dropwise in THF (2 mL), and the reaction mixture was stirred for an additional 2.25 h. After quenching with saturated NH_4Cl solution (20 mL) and extraction with EtOAc (3 × 30 mL), the combined organic layers were dried ($MgSO_4$) and concentrated under reduced pressure. The crude product was purified by flash chromatography (cyclohexane/EtOAc, 3:1) to afford the β-hydroxy ester **37** (0.29 g, 0.72 mmol, 57%) as a colorless oil. R_f 0.38 (cyclohexane/EtOAc, 3:1); IR (ATR) $\tilde{\nu}$ [cm^{-1}] 3508, 3071, 2953, 2932, 2858, 1736, 1461, 1428, 1257, 1197, 1172, 1110, 823, 738, 703, 614, 505; ^{1}H NMR, COSY (400 MHz, $CDCl_3$) δ_H 7.71−7.62 (m, 4H, CH_{arom}), 7.48−7.35 (m, 6H, CH_{arom}), 4.19−4.11 (m, 1H, 3-CH_{anti}), 4.06−3.98 (m, 1H, 3-CH_{syn}), 3.94−3.78 (m, 2H, 5-CH_2), 3.71 (s, 3H,

https://doi.org/10.1021/acs.jnatprod.2c01145
J. Nat. Prod. 2023, 86, 924−938

1-COOC$H_{3\ syn}$), 3.70 (s, 3H, 1-COOC$H_{3\ anti}$), 3.38 (s_{br}, 1H, OH_{syn}), 3.35 (s_{br}, 1H, OH_{anti}), 2.66−2.52 (m, 1H, 2-CH), 1.81−1.58 (m, 2H, 4-CH_2), 1.23 (d, J = 7.1 Hz, 3H, 2-C$H_{3\ anti}$), 1.18 (d, J = 7.1 Hz, 3H, 2-C$H_{3\ syn}$), 1.05 (s, 9H, C(CH_3)$_3$); ^{13}C NMR, HSQC, HMBC (101 MHz, $CDCl_3$) δ_C 176.1 (1-COOCH$_{3\ syn}$), 176.0 (1-COOCH$_{3\ anti}$), 135.7 (4C, 4 × o-CH$_{TBDPS\ syn}$), 135.7 (4C, 4 × o-CH$_{TBDPS\ anti}$), 133.3 (*ipso*-C$_{TBDPS\ syn}$), 133.2 (*ipso*-C$_{TBDPS\ anti}$), 133.2 (*ipso*-C$_{TBDPS\ syn}$), 133.1 (*ipso*-C$_{TBDPS\ anti}$), 129.9 (2C, 2 × p-CH$_{TBDPS}$), 127.9 (4C, 4 × m-CH$_{TBDPS}$), 72.8 (3-CH$_{syn}$), 71.7 (3-CH$_{anti}$), 62.9 (5-CH$_{2\ anti}$), 62.7 (5-CH$_{2\ syn}$), 51.9 (1-COOCH$_{3\ anti}$), 51.8 (1-COOCH$_{3\ syn}$), 45.7 (2-CH$_{syn}$), 45.2 (2-CH$_{anti}$), 36.0 (4-CH$_{2\ anti}$), 35.9 (4-CH$_{2\ syn}$), 26.9 (3C, SiC(CH$_3$)$_3$), 19.2 (SiC(CH$_3$)$_3$), 13.8 (2-CH$_{3\ syn}$), 11.9 (2-CH$_{3\ anti}$); HRESIMS m/z 423.1970 [M + Na]$^+$ (calcd for $C_{23}H_{32}O_4Si$, 423.1962). The analytical data are in accordance with the literature.[49]

*Methyl 3-(Benzyloxy)-5-((tert-butyldiphenylsilyl)oxy)-2-methylpentanoate (**38**).* According to Guindon et al.,[23] the benzyl protection of pentanoate **37** followed the same procedure as the synthesis of oxazolidin-2-one **11**. To an ice-cooled solution of secondary alcohol **37** (289 mg, 721 μmol, 1.00 equiv) in CH_2Cl_2/cyclohexane (6.9 mL, 1:2) was added benzyl 2,2,2-trichloracetimidate (205 μL, 1.08 mmol, 1.50 equiv) and catalytic amounts of triflic acid (6.46 μL, 72.1 μmol, 0.10 equiv). The reaction mixture was stirred 2 h while slowly warming up to a maximum cooling bath temperature of 20 °C. The solution was then cooled back to 0 °C, triflic acid (6.46 μL, 72.1 μmol, 0.10 equiv) added again, and the solution warmed up to a maximum of 20 °C in 2 h (this cycle was repeated another two times, four times in sum). After complete consumption of the starting material, as detected by TLC, the reaction mixture was quenched by addition of 20 mL of saturated $NaHCO_3$(aq). The residue was taken up in ether, and the aqueous layer was extracted three times (30 mL). The combined organic layers were washed with a saturated aqueous solution of $NaHCO_3$ and brine, dried over $MgSO_4$, and filtered, and the solvent was removed in vacuo. Purification of the crude product by flash chromatography (cyclohexane/EtOAc, 10:1) yielded the protected benzyl ether **38** (0.25 g, 0.50 mmol, 69%) as a colorless oil. R_f 0.59 (cyclohexane/EtOAc, 3:1); IR (ATR) $\tilde{\nu}$ [cm^{-1}] 3070, 2951, 2932, 2858, 1736, 1471, 1456, 1428, 1257, 1197, 1174, 1107, 1091, 1065, 823, 736, 700, 613, 504, 490; ^{1}H NMR, COSY (400 MHz, $CDCl_3$) δ_H 7.69−7.61 (m, 4H, CH_{arom}), 7.46−7.20 (m, 11H, CH_{arom}), 4.53 (d, J = 11.3 Hz, 1H, C$H_{2\text{-A Bn syn}}$), 4.50 (d, J = 11.3 Hz, 1H, C$H_{2\text{-A Bn anti}}$), 4.46 (d, J = 11.3 Hz, 1H, C$H_{2\text{-B Bn syn}}$), 4.45 (d, J = 11.3 Hz, 1H, C$H_{2\text{-B Bn anti}}$), 4.07−3.95 (m, 1H, 3-CH), 3.87−3.69 (m, 2H, 5-CH_2), 3.66 (s, 3H, 1-COOC$H_{3\ syn}$), 3.65 (s, 3H, 1-COOC$H_{3\ anti}$), 2.85 (pq, J = 7.0 Hz, 1H, 2-CH_{anti}), 2.72 (qd, J = 7.1, 4.9 Hz, 1H, 2-CH_{syn}), 1.84−1.65 (m, 2H, 4-CH_2), 1.20 (d, J = 7.1 Hz, 3H, 2-C$H_{3\ syn}$), 1.12 (d, J = 7.0 Hz, 3H, 2-C$H_{3\ anti}$), 1.05 (s, 9H, C(CH_3)$_3$); ^{13}C NMR, HSQC, HMBC (101 MHz, $CDCl_3$) δ_C 175.4 (1-COOCH$_3$), 138.6 (*ipso*-C$_{Bn\ syn}$), 138.6 (*ipso*-C$_{Bn\ anti}$), 135.7 (4C, 4 × o-CH$_{TBDPS}$), 133.9 (*ipso*-C$_{TBDPS}$), 133.9 (*ipso*-C$_{TBDPS}$), 129.8 (2C, 2 × p-CH$_{TBDPS}$), 128.4 (2C, 2 × m-CH$_{Bn}$), 127.9 (2C, 2 × o-CH$_{Bn}$), 127.8 (4C, 4 × m-CH$_{TBDPS}$), 127.7 (p-CH$_{Bn}$), 77.6 (3-CH$_{anti}$), 77.3 (3-CH$_{syn}$), 72.5 (CH$_{2\ Bn\ syn}$), 72.4 (CH$_{2\ Bn\ anti}$), 60.5 (5-CH$_{2\ syn}$), 60.1 (5-CH$_{2\ anti}$), 51.8 (1-COOCH$_{3\ anti}$), 51.8 (1-COOCH$_{3\ syn}$), 43.4 (2-CH$_{syn}$), 43.3 (2-CH$_{anti}$), 35.3 (4-CH$_{2\ syn}$), 34.1 (4-CH$_{2\ anti}$), 27.0 (3C, SiC(CH$_3$)$_3$), 19.3 (SiC(CH$_3$)$_3$), 12.1 (2-CH$_{3\ anti}$), 11.9 (2-CH$_{3\ syn}$). HRESIMS m/z 513.2440 [M + Na]$^+$ (calcd for $C_{30}H_{38}O_4Si$, 513.2431).

*(2R,3R)-3-(Benzyloxy)-5-((tert-butyldiphenylsilyl)oxy)-2-methylpentan-1-ol (**39**).* According to Williams et al.,[25] MeOH (0.1 mL) was added to a solution of oxazolidin-2-one **11** (504 mg, 0.79 mmol, 1.00 equiv) in THF (6.0 mL), and the solution was cooled to 0 °C. $LiBH_4$ (36.3 mg, 1.59 mmol, 2.00 equiv) was added in small portions, and the reaction mixture was stirred at 0 °C for 1.5 h. After the addition of further $LiBH_4$ (18.2 mg, 0.79 mmol, 1.00 equiv), the reaction mixture was allowed to warm to rt within 1.5 h before being quenched by the addition of saturated Rochelle salt (30 mL). The aqueous layer was extracted with EtOAc (3 × 50 mL), dried ($MgSO_4$), filtered, and concentrated in vacuo. Flash chromatography (cyclohexane/EtOAc, 6:1) afforded the primary alcohol **39** (243 mg, 0.53 mmol, 66%) as a colorless oil. $[\alpha]_D^{23}$ +7.7 (c 0.99, $CHCl_3$); R_f 0.27 (cyclohexane/EtOAc, 3:1); IR (ATR) $\tilde{\nu}$ [cm^{-1}] 3422, 3070, 2958, 2931, 2857, 1472, 1428, 1110, 1089, 823, 736, 701, 614, 505; ^{1}H NMR, COSY (400 MHz, DMSO-d_6) δ_H 7.64−7.56 (m, 4H, CH_{arom}), 7.50−7.36 (m, 6H, CH_{arom}), 7.32−7.18 (m, 5H, CH_{arom}), 4.47 (d, J = 11.7 Hz, 1H, C$H_{2\text{-A Bn}}$), 4.43 (t, J = 5.1 Hz, 1H, OH), 4.41 (d, J = 11.7 Hz, 1H, C$H_{2\text{-B Bn}}$), 3.75−3.64 (m, 3H, 3-CH, 5-CH_2), 3.44 (ddd, J = 10.3, 6.2, 5.1 Hz, 1H, 1-C$H_{2\text{-A}}$), 3.27 (ddd, J = 10.3, 6.8, 5.1 Hz, 1H, 1-C$H_{2\text{-B}}$), 1.80−1.66 (m, 3H, 4-CH_2, 2-CH), 0.99 (s, 9H, C(CH_3)$_3$), 0.82 (d, J = 6.9 Hz, 3H, 2-CH_3); ^{13}C NMR, HSQC, HMBC (101 MHz, DMSO-d_6) δ_C 139.1 (*ipso*-C$_{Bn}$), 135.0 (4C, 4 × o-CH$_{TBDPS}$), 133.2 (*ipso*-C$_{TBDPS}$), 133.2 (*ipso*-C$_{TBDPS}$), 129.8 (2C, 2 × p-CH$_{TBDPS}$), 128.1 (2C, 2 × m-CH$_{Bn}$), 127.9 (4C, 4 × m-CH$_{TBDPS}$), 127.3 (2C, 2 × o-CH$_{Bn}$), 127.2 (p-CH$_{Bn}$), 76.3 (3-CH), 71.3 (CH$_{2\ Bn}$), 63.1 (1-CH$_2$), 60.7 (5-CH$_2$), 38.9 (2-CH), 34.1 (4-CH$_2$), 26.7 (3C, SiC(CH$_3$)$_3$), 18.7 (SiC(CH$_3$)$_3$), 11.9 (2-CH$_3$); HRESIMS m/z 485.2477 [M + Na]$^+$ (calcd for $C_{29}H_{38}O_3Si$, 485.2482).

*(2S,3R)-3-(Benzyloxy)-5-((tert-butyldiphenylsilyl)oxy)-2-methylpentanal (**14**).* Using a modified procedure of Pannecoucke et al.,[17] primary alcohol **39** (151 mg, 326 μmol, 1.00 equiv) was dissolved in dry MeCN (6.50 mL), IBX (229 mg, 816 μmol, 2.50 equiv) was added, and the reaction mixture was stirred over preactivated 3 Å molecular sieves (0.15 g). After 4 h, the solvent was removed under reduced pressure at rt and the residue was taken up in EtOAc (30 mL). The mixture was filtered through a pad of Celite, and the solvent was removed under reduced pressure, furnishing the aldehyde **14** (143 mg, 309 μmol, 95%) as a yellow oil, which was used immediately for the next reaction. $[\alpha]_D^{23}$ +32.0 (c 0.99, $CHCl_3$); R_f 0.58 (cyclohexane/EtOAc, 3:1); IR (ATR) $\tilde{\nu}$ [cm^{-1}] 3070, 2955, 2931, 2857, 1724, 1472, 1428, 1107, 1088, 1065, 938, 823, 736, 700, 614, 504; ^{1}H NMR, COSY (400 MHz, $CDCl_3$) δ_H 9.73 (m, 1H, 1-CHO), 7.68−7.62 (m, 4H, CH_{arom}), 7.45−7.34 (m, 6H, CH_{arom}), 7.33−7.22 (m, 5H, CH_{arom}), 4.50 (d, J = 12.0 Hz, 1H, C$H_{2\text{-A Bn}}$), 4.48 (d, J = 12.0 Hz, 1H, C$H_{2\text{-B Bn}}$), 4.13 (ddd, J = 7.9, 5.4, 3.6 Hz, 1H, 3-CH), 3.85−3.79 (m, 1H, 5-C$H_{2\text{-A}}$), 3.76−3.71 (m, 1H, 5-C$H_{2\text{-B}}$), 2.61−2.54 (m, 1H, 2-CH), 1.89−1.82 (m, 1H, 4-C$H_{2\text{-A}}$), 1.80−1.73 (m, 1H, 4-C$H_{2\text{-B}}$), 1.10 (d, J = 7.1 Hz, 3H, 2-CH_3), 1.06 (s, 9H, C(CH_3)$_3$); ^{13}C NMR, HSQC, HMBC (101 MHz, $CDCl_3$) δ_C 204.8 (1-CHO), 138.3 (*ipso*-C$_{Bn}$), 135.7 (2C, 2 × o-CH$_{TBDPS}$), 135.7 (2C, 2 × o-CH$_{TBDPS}$), 133.7 (*ipso*-C$_{TBDPS}$), 133.7 (*ipso*-C$_{TBDPS}$), 129.9 (p-CH$_{TBDPS}$), 129.9 (p-CH$_{TBDPS}$), 128.5 (2C, 2 × m-CH$_{Bn}$), 127.9 (4C, 4 × m-CH$_{TBDPS}$), 127.8 (2C, 2 × o-CH$_{Bn}$), 127.8 (p-CH$_{Bn}$), 75.6 (3-CH), 72.1 (CH$_{2\ Bn}$), 60.5 (5-CH$_2$), 49.9 (2-CH), 34.6 (4-CH$_2$), 27.0 (3C, SiC(CH$_3$)$_3$), 19.3 (SiC(CH$_3$)$_3$), 8.3 (2-CH$_3$); HRESIMS m/z 483.2323 [M + Na]$^+$ (calcd for $C_{29}H_{36}O_3Si$, 483.2326).

*(2S,3R,4R)-4-(Benzyloxy)-6-((tert-butyldiphenylsilyl)oxy)-3-methylhexan-2-ol (**16**).* According to Dalby et al.,[26] to a precooled solution of aldehyde **14** (205 mg, 445 μmol, 1.00 equiv) in THF (5 mL) was added dropwise MeMgBr (3 M in DEE, 297 μL, 890 μmol, 2.00 equiv) at −78 °C within 5 min, and the reaction mixture was stirred for 1.5 h at −78 °C. After the reaction mixture was quenched by the addition of 10 mL of saturated NH_4Cl(aq), the organic layer was removed in vacuo, the aqueous layer was extracted with EtOAc (3 × 30 mL), dried ($MgSO_4$), and filtered, and the solvent was removed in vacuo. This provided a 70:30 mixture of diastereomeric alcohols, which were separated by means of flash chromatography (cyclohexane/EtOAc, 13:1), to yield the mismatched alcohol **16** (80.5 mg, 169 μmol, 38%) and its matched diastereomer **17** (35.3 mg, 74.0 μmol, 17%) as colorless oils. $[\alpha]_D^{23}$ −22.0 (c 1.02, $CHCl_3$); R_f 0.35 (cyclohexane/EtOAc, 3:1); IR (ATR) $\tilde{\nu}$ [cm^{-1}] 3444, 3070, 2690, 2931, 2857, 1471, 1455, 1428, 1390, 1360, 1110, 1088, 1066, 1058, 1008, 940, 902, 823, 737, 701, 614, 543, 505, 490; ^{1}H NMR, COSY (400 MHz, DMSO-d_6) δ_H 7.64−7.58 (m, 4H, CH_{arom}), 7.50−7.36 (m, 6H, CH_{arom}), 7.33−7.19 (m, 5H, CH_{arom}), 4.41 (d, J = 11.8 Hz, 1H, C$H_{2\text{-A Bn}}$), 4.38 (d, J = 11.8 Hz, 1H, C$H_{2\text{-B Bn}}$), 4.24 (d, J = 5.0 Hz, 1H, OH), 3.77−3.55 (m, 4H, 4-CH, 6-CH_2, 2-CH), 1.88−1.74 (m, 2H, 5-CH_2), 1.51 (dqd, J = 9.8, 6.9, 5.0 Hz, 1H, 3-CH), 1.03 (d, J = 6.3 Hz, 3H, 1-CH_3), 0.99 (s, 9H, C(CH_3)$_3$), 0.86 (d, J = 6.9 Hz, 3H, 3-CH_3); ^{13}C NMR, HSQC, HMBC (101 MHz, DMSO-d_6) δ_C 139.0 (*ipso*-C$_{Bn}$), 135.0 (4C, 4 × o-CH$_{TBDPS}$), 133.2 (*ipso*-C$_{TBDPS}$), 133.2 (*ipso*-C$_{TBDPS}$), 129.8 (2C, 2 × p-CH$_{TBDPS}$), 128.1 (2C, 2 × m-CH$_{Bn}$), 127.9 (4C, 4 × m-CH$_{TBDPS}$), 127.4 (2C, 2 × o-CH$_{Bn}$), 127.2 (p-CH$_{Bn}$), 77.5 (4-CH), 70.6 (CH$_{2\ Bn}$), 66.4 (2-CH), 60.6 (6-CH$_2$), 42.5 (3-CH), 33.8 (5-CH$_2$), 26.6 (3C, SiC(CH$_3$)$_3$), 22.0 (1-CH$_3$), 18.7 (SiC(CH$_3$)$_3$), 9.9 (3-CH$_3$); HRESIMS m/z 499.2638 [M +

https://doi.org/10.1021/acs.jnatprod.2c01145
J. Nat. Prod. 2023, 86, 924−938

Na]$^+$ (calcd for $C_{30}H_{40}O_3Si$, 499.2639). The analytical data of the mismatched alcohol **16** are reported herein, while the analytical data of the matched secondary alcohol **17** were given in the step of the L-selectride reduction.

*tert-Butyldiphenyl(2-((4R,5R,6S)-2,2,5,6-tetramethyl-1,3-dioxan-4-yl)ethoxy)silane (**18**).* Following a modified procedure of Olsson et al.,[34] secondary alcohol **16** (22.9 mg, 48.0 μmol, 1.00 equiv) was dissolved in degassed EtOH (1 mL), and 10% Pd/C (7.67 mg, 7.21 μmol, 0.15 equiv) was added. The suspension was stirred under a hydrogen atmosphere (10 bar) at rt until complete consumption of the starting material by TLC was detected. The reaction mixture was filtered through a pad of Celite, and the solvent was removed under reduced pressure. The resulting diol was taken up in 2,2-dimethoxypropane (1 mL) and treated with camphor-10-sulfonic acid (1.12 mg, 4.80 mmol, 0.10 equiv). After 1.5 h the reaction mixture was diluted with EtOAc (5 mL) and washed with saturated aqueous $NaHCO_3$ (5 mL) and brine (5 mL). The organic layer was dried ($MgSO_4$) and filtered, and the crude product was purified by preparative HPLC (C_{18}-PFP, isocratic 75% MeCN in H_2O, 20 min). The *cis*-1,3-diol-acetonide **18** (10.0 mg, 25.9 mmol, 54%) was obtained as a colorless oil. R_f 0.67 (cyclohexane/EtOAc, 3:1); t_R (HPLC) 18.16 min (C_{18}-PFP, isocratic 75% MeCN in H_2O); IR (ATR) $\tilde{\nu}$ [cm^{-1}] 3071, 2958, 2932, 2887, 2858, 1472, 1460, 1428, 1378, 1265, 1198, 1178, 1111, 1019, 961, 823, 702, 614, 505; ^{1}H NMR, COSY, NOESY (600 MHz, DMSO-d_6) δ_H 7.63−7.58 (m, 4H, CH_{arom}), 7.49−7.40 (m, 6H, CH_{arom}), 4.13 (ddd, J = 8.3, 4.8, 2.2 Hz, 1H, 4-CH), 4.03 (qd, J = 6.3, 2.2 Hz, 1H, 6-CH), 3.72 (ddd, J = 10.1, 8.2, 5.3 Hz, 1H, 8-C$H_{2\text{-}A}$), 3.64 (pdt, J = 10.1, 5.5 Hz, 1H, 8-C$H_{2\text{-}B}$), 1.66−1.52 (m, 2H, 7-CH_2), 1.33 (s, 3H, 2-C$H_{3\ ax}$), 1.22 (s, 3H, 2-C$H_{3\ eq}$), 1.19 (pqt, J = 6.9, 2.2 Hz, 1H, 5-CH), 0.99 (d, J = 6.3 Hz, 3H, 6-CH_3), 0.98 (s, 9H, C(CH_3)$_3$), 0.71 (d, J = 6.9 Hz, 3H, 5-CH_3); ^{13}C NMR, HSQC, HMBC (151 MHz, DMSO-d_6) δ_C 135.1 (4C, 4 × *o*-CH_{TBDPS}), 133.2 (2C, 2 × *ipso*-C$_{TBDPS}$), 129.9 (2C, 2 × *p*-CH_{TBDPS}), 128.0 (2C, 2 × *m*-CH_{TBDPS}), 127.9 (2C, 2 × *m*-CH_{TBDPS}), 98.2 (2-C$_q$), 69.0 (4-CH), 68.3 (6-CH), 59.9 (8-CH$_2$), 35.4 (7-CH$_2$), 35.2 (5-CH), 30.0 (2-CH$_{3\ eq}$), 26.7 (3C, SiC(CH$_3$)$_3$), 19.7 (2-CH$_{3\ ax}$), 18.8 (SiC(CH$_3$)$_3$), 18.7 (6-CH$_3$), 4.6 (5-CH$_3$); HRESIMS m/z 449.2477 [M + Na]$^+$ (calcd for $C_{26}H_{38}O_3Si$, 449.2482).

*(2S,3R)-3-(Benzyloxy)-5-((tert-butyldiphenylsilyl)oxy)-N-methoxy-N,2-dimethylpentanamide (**40**).* Following a previously published procedure,[29] carboxylic acid **12** (1.35 g, 2.83 mmol, 1.00 equiv) was dissolved in CH_2Cl_2 (57 mL) and cooled to 0 °C, and 1,1′-carbonyldiimidazole (0.62 g, 3.68 mmol, 1.30 equiv) was added. After 30 min at 0 °C, *N*,*O*-dimethylhydroxylamine hydrochloride (0.71 g, 7.08 mmol, 2.50 equiv) and 4-(dimethylamino)pyridine (34.6 mg, 0.28 mmol, 0.10 equiv) were added, and the reaction was stirred overnight at rt. The reaction mixture was diluted with CH_2Cl_2 (50 mL) and washed with H_2O (40 mL). The organic layer was dried ($MgSO_4$), filtered, and purified by flash chromatography (cyclohexane/EtOAc, 3:1). The Weinreb amide **40** (1.27 g, 2.43 mmol, 86%) was obtained as a colorless oil. $[\alpha]_D^{23}$ +11.9 (*c* 0.94, $CHCl_3$); R_f 0.23 (cyclohexane/EtOAc, 3:1); IR (ATR) $\tilde{\nu}$ [cm^{-1}] 3070, 2932, 2857, 1659, 1470, 1427, 1384, 1108, 1027, 996, 938, 822, 737, 700, 614, 505; ^{1}H NMR, COSY (400 MHz, $CDCl_3$) δ_H 7.70−7.60 (m, 4H, CH_{arom}), 7.45−7.21 (m, 11H, CH_{arom}), 4.56 (d, J = 11.0 Hz, 1H, C$H_{2\text{-}A\ Bn}$), 4.49 (d, J = 11.0 Hz, 1H, C$H_{2\text{-}B\ Bn}$), 3.92−3.71 (m, 3H, 3-CH, 5-CH_2), 3.59 (s, 3H, NOCH_3), 3.16 (s, 3H, NCH_3), 3.16−3.03 (m, 1H, 2-CH), 1.95−1.83 (m, 1H, 4-C$H_{2\text{-}A}$), 1.81−1.70 (m, 1H, 4-C$H_{2\text{-}B}$), 1.23 (d, J = 7.0 Hz, 3H, 2-CH_3), 1.05 (s, 9H, C(CH_3)$_3$); ^{13}C NMR, HSQC, HMBC (101 MHz, $CDCl_3$) δ_C 176.2 (1-CON), 138.6 (*ipso*-C$_{Bn}$), 135.8 (2C, 2 × *o*-CH_{TBDPS}), 135.7 (2C, 2 × *o*-CH_{TBDPS}), 134.1 (*ipso*-C$_{TBDPS}$), 134.0 (*ipso*-C$_{TBDPS}$), 129.7 (2C, 2 × *p*-CH_{TBDPS}), 128.5 (2C, 2 × *m*-CH_{Bn}), 128.1 (2C, 2 × *o*-CH_{Bn}), 127.8 (2C, 2 × *m*-CH_{TBDPS}), 127.7 (2C, 2 × *m*-CH_{TBDPS}), 127.7 (*p*-CH_{Bn}), 78.1 (3-CH), 73.3 (C$H_{2\ Bn}$), 61.5 (NOCH_3), 60.7 (5-CH$_2$), 40.2 (2-CH), 36.3 (4-CH$_2$), 32.3 (NCH$_3$), 27.0 (3C, SiC(CH_3)$_3$), 19.3 (SiC(CH$_3$)$_3$), 14.1 (2-CH$_3$); HRESIMS m/z 542.2687 [M + Na]$^+$ (calcd for $C_{31}H_{41}NO_4Si$, 542.2697).

*(3S,4R)-4-(Benzyloxy)-6-((tert-butyldiphenylsilyl)oxy)-3-methylhexan-2-one (**15**).* Based on a literature-known procedure by Marco et al.,[29] to a solution of Weinreb amide **40** (2.65 g, 5.09 mmol, 1.00 equiv) in THF (63 mL) was added MeMgBr (3 M in DEE, 6.62 mL, 19.9 mmol, 3.90 equiv) dropwise at −20 °C. After 40 min at −20 °C, the stirring was continued 1 h at 0 °C. The reaction mixture was quenched by the addition of 50 mL of saturated NH_4Cl(aq) and taken up in 50 mL of H_2O and diethyl ether, and the aqueous layer was extracted three times with 100 mL. Drying ($MgSO_4$), filtration, and flash chromatography (cyclohexane/EtOAc, 10:1) of the crude product gave ketone **15** (2.33 g, 4.91 mmol, 96%) as a colorless oil. $[\alpha]_D^{23}$ +36.8 (*c* 1.01, $CHCl_3$); R_f 0.53 (cyclohexane/EtOAc, 3:1); IR (ATR) $\tilde{\nu}$ [cm^{-1}] 3070, 2931, 2858, 1711, 1471, 1428, 1360, 1179, 1109, 1090, 938, 823, 737, 701, 614, 505; ^{1}H NMR, COSY (400 MHz, DMSO-d_6) δ_H 7.64−7.55 (m, 4H, CH_{arom}), 7.50−7.36 (m, 6H, CH_{arom}), 7.33−7.17 (m, 5H, CH_{arom}), 4.51 (d, J = 11.6 Hz, 1H, C$H_{2\text{-}A\ Bn}$), 4.40 (d, J = 11.6 Hz, 1H, C$H_{2\text{-}B\ Bn}$), 3.92 (dt, J = 7.5, 4.4 Hz, 1H, 4-CH), 3.77−3.65 (m, 2H, 6-CH_2), 2.88 (qd, J = 7.0, 4.4 Hz, 1H, 3-CH), 2.09 (s, 3H, 1-CH_3), 1.73−1.58 (m, 2H, 5-CH_2), 0.99 (s, 9H, C(CH_3)$_3$), 0.96 (d, J = 7.0 Hz, 3H, 3-CH_3); ^{13}C NMR, HSQC, HMBC (101 MHz, DMSO-d_6) δ_C 210.1 (2-CO), 138.4 (*ipso*-C$_{Bn}$), 135.0 (4C, 4 × *o*-CH_{TBDPS}), 133.1 (*ipso*-C$_{TBDPS}$), 133.1 (*ipso*-C$_{TBDPS}$), 129.9 (2C, 2 × *p*-CH_{TBDPS}), 128.2 (2C, 2 × *m*-CH_{Bn}), 127.9 (4C, 4 × *m*-CH_{TBDPS}), 127.5 (2C, 2 × *o*-CH_{Bn}), 127.4 (*p*-CH_{Bn}), 76.3 (4-CH), 70.8 (C$H_{2\ Bn}$), 60.3 (6-CH$_2$), 48.9 (3-CH), 34.1 (5-CH$_2$), 29.5 (1-CH$_3$), 26.6 (3C, SiC(CH_3)$_3$), 18.7 (SiC(CH$_3$)$_3$), 11.0 (3-CH$_3$); HRESIMS m/z 497.2492 [M + Na]$^+$ (calcd for $C_{30}H_{38}O_3Si$, 497.2482).

*(2R,3R,4R)-4-(Benzyloxy)-6-((tert-butyldiphenylsilyl)oxy)-3-methylhexan-2-ol (**17**).* Based on a literature-known procedure by McGarvey et al.,[33] to a precooled solution of ketone **15** (1.17 g, 2.46 mmol, 1.00 equiv) in THF (90 mL) was added dropwise L-selectride (1 M in THF, 6.15 mL, 6.15 mmol, 2.50 equiv) at −78 °C within 5 min, and the reaction mixture was stirred for 1.5 h. After the reaction mixture was quenched by the addition of 30 mL of saturated NH_4Cl(aq), the aqueous layer was extracted with EtOAc (3 × 80 mL), dried ($MgSO_4$), and filtered, and the solvent was removed in vacuo. This provided a 95:5 mixture of diastereomeric alcohols, which were separated by means of flash chromatography (cyclohexane/EtOAc, 13:1), to yield the matched alcohol **17** (0.91 g, 1.90 mmol, 77%) and its diastereomer **16** (48.0 mg, 0.10 mmol, 4%) as colorless oils. $[\alpha]_D^{23}$ +15.5 (*c* 1.01, $CHCl_3$); R_f 0.41 (cyclohexane/EtOAc, 3:1); IR (ATR) $\tilde{\nu}$ [cm^{-1}] 3477, 3070, 2960, 2930, 2883, 2858, 1471, 1455, 1428, 1389, 1360, 1110, 1086, 1028, 938, 823, 736, 701, 614, 505, 490; ^{1}H NMR, COSY (400 MHz, DMSO-d_6) δ_H 7.65−7.57 (m, 4H, CH_{arom}), 7.50−7.36 (m, 6H, CH_{arom}), 7.33−7.18 (m, 5H, CH_{arom}), 4.51 (d, J = 11.6 Hz, 1H, C$H_{2\text{-}A\ Bn}$), 4.45 (d, J = 11.6 Hz, 1H, C$H_{2\text{-}B\ Bn}$), 4.41 (d, J = 4.8 Hz, 1H, OH), 3.98 (ddd, J = 8.0, 5.4, 2.9 Hz, 1H, 4-CH), 3.75−3.64 (m, 2H, 6-CH_2), 3.63−3.53 (m, 1H, 2-CH), 1.84−1.72 (m, 1H, 5-C$H_{2\text{-}A}$), 1.71−1.59 (m, 1H, 5-C$H_{2\text{-}B}$), 1.48−1.38 (m, 1H, 3-CH), 1.05 (d, J = 6.2 Hz, 3H, 1-CH_3), 0.99 (s, 9H, C(CH_3)$_3$), 0.75 (d, J = 6.9 Hz, 3H, 3-CH_3); ^{13}C NMR, HSQC, HMBC (101 MHz, DMSO-d_6) δ_C 139.3 (*ipso*-C$_{Bn}$), 135.1 (4C, 4 × *o*-CH_{TBDPS}), 133.2 (*ipso*-C$_{TBDPS}$), 133.2 (*ipso*-C$_{TBDPS}$), 129.8 (2C, 2 × *p*-CH_{TBDPS}), 128.1 (2C, 2 × *m*-CH_{Bn}), 127.9 (4C, 4 × *m*-CH_{TBDPS}), 127.2 (2C, 2 × *o*-CH_{Bn}), 127.1 (*p*-CH_{Bn}), 75.6 (4-CH), 71.7 (C$H_{2\ Bn}$), 67.2 (2-CH), 60.8 (6-CH$_2$), 44.2 (3-CH), 35.1 (5-CH$_2$), 26.7 (3C, SiC(CH_3)$_3$), 21.5 (1-CH$_3$), 18.7 (SiC(CH$_3$)$_3$), 9.9 (3-CH$_3$); HRESIMS m/z 499.2639 [M + Na]$^+$ (calcd for $C_{30}H_{40}O_3Si$, 499.2639). The analytical data of the matched alcohol **17** are reported here, while the analytical data of the undesired diastereomer **16** were previously given in the step of the methyl Grignard reduction.

*tert-Butyldiphenyl(2-((4R,5R,6R)-2,2,5,6-tetramethyl-1,3-dioxan-4-yl)ethoxy)silane (**19**).* Following a modified procedure of Olsson et al.,[34] secondary alcohol **17** (28.2 mg, 59.2 μmol, 1.00 equiv) was dissolved in degassed EtOH (1.2 mL), and 10% Pd/C (9.44 mg, 8.87 μmol, 0.15 equiv) was added. The suspension was stirred under a hydrogen atmosphere (10 bar) at rt until complete consumption of the starting material by TLC was detected. The reaction mixture was filtered through a pad of Celite, and the solvent was removed under reduced pressure. The resulting diol was taken up in 2,2-dimethoxypropane (1 mL) and treated with camphorsulfonic acid (1.37 mg, 5.92 μmol, 0.10 equiv). After 1.5 h the reaction mixture was diluted with EtOAc (5 mL) and washed with saturated aqueous $NaHCO_3$ (5 mL) and brine. The organic layer was dried ($MgSO_4$), and filtered, and the crude product was purified by preparative HPLC (C_{18}-

https://doi.org/10.1021/acs.jnatprod.2c01145
J. Nat. Prod. 2023, 86, 924−938

PFP, isocratic 75% MeCN in H_2O, 20 min). The *anti*-1,3-diol-acetonide **19** (11.7 mg, 30.3 mmol, 51%) was obtained as a colorless oil. R_f 0.67 (cyclohexane/EtOAc, 3:1); t_R (HPLC) 18.83 min (C_{18}-PFP, isocratic 75% MeCN in H_2O); IR (ATR) $\tilde{\nu}$ [cm^{-1}] 3071, 2959, 2932, 2888, 2858, 1472, 1461, 1428, 1379, 1230, 1220, 1180, 1148, 1111, 1073, 823, 737, 702, 614, 505; ^{1}H NMR, COSY, NOESY (600 MHz, DMSO-d_6) δ_H 7.65−7.57 (m, 4H, CH_{arom}), 7.49−7.40 (m, 6H, CH_{arom}), 4.06 (ddd, J = 9.4, 5.2, 4.1 Hz, 1H, 4-C*H*), 3.71 (ddd, J = 10.1, 8.6, 5.2 Hz, 1H, 8-C$H_{2\text{-}A}$), 3.64 (ddd, J = 10.1, 6.0, 4.5 Hz, 1H, 8-C$H_{2\text{-}B}$), 3.34−3.29 (m, 1H, 6-C*H*), 1.62−1.43 (m, 3H, 7-CH_2, 5-C*H*), 1.21 (s, 3H, 2-CH_3), 1.20 (s, 3H, 2-CH_3), 1.12 (d, J = 6.2 Hz, 3H, 6-CH_3), 0.98 (s, 9H, C(CH_3)$_3$), 0.73 (d, J = 6.8 Hz, 3H, 5-CH_3); ^{13}C NMR, HSQC, HMBC (151 MHz, DMSO-d_6) δ_C 135.1 (4C, 4 × *o*-CH_{TBDPS}), 133.2 (*ipso*-C_{TBDPS}), 133.2 (*ipso*-C_{TBDPS}), 129.9 (2C, 2 × *p*-CH_{TBDPS}), 127.9 (4C, 4 × *m*-CH_{TBDPS}), 99.8 (2-C_q), 70.3 (6-CH), 64.6 (4-CH), 60.2 (8-CH_2), 41.1 (5-CH), 33.2 (7-CH_2), 26.7 (3C, SiC(CH_3)$_3$), 24.8 (2-CH_3), 24.0 (2-CH_3), 20.2 (6-CH_3), 18.8 (SiC(CH_3)$_3$), 11.7 (5-CH_3); HRESIMS m/z 449.2475 [M + Na]$^+$ (calcd for $C_{26}H_{38}O_3Si$, 449.2482).

*(2R,3R,4R)-4-(Benzyloxy)-6-((tert-butyldiphenylsilyl)oxy)-3-methylhexan-2-yl 2-[3,5-bis(benzyloxy)phenyl]acetate (**41**).* According to procedures from Opatz et al.,[5,9] a solution of *N*,*N*′-dicyclohexylcarbodiimide (211 mg, 1.02 mmol, 1.20 equiv) in CH_2Cl_2 (4.3 mL) was added dropwise to an ice-cooled solution of hexan-2-ol **17** (407 mg, 853 μmol, 1.00 equiv), (3,5-bis(benzyloxy)-phenyl)acetic acid (**5**, 303 mg, 870 μmol, 1.02 equiv), and 4-(dimethylamino)pyridine (20.8 mg, 171 μmol, 0.20 equiv) in CH_2Cl_2 (28 mL). The reaction mixture was stirred at 0 °C for 3 h until another portion of *N*,*N*′-dicyclohexylcarbodiimide (35.2 mg, 171 μmol, 0.20 equiv) in CH_2Cl_2 (0.7 mL) was added, and the solution was then warmed to rt overnight. After the addition of 20 mL of saturated NH_4Cl(aq) the aqueous layer was washed with CH_2Cl_2 (3 × 25 mL), dried ($MgSO_4$), and filtered. The crude product was purified by flash chromatography (cyclohexane/EtOAc, 15:1), yielding ester **41** (586 mg, 726 μmol, 85%) as a colorless oil. $[\alpha]_D^{19}$ −9.3 (*c* 1.00, $CHCl_3$); R_f 0.52 (cyclohexane/EtOAc, 10:1); IR (ATR) $\tilde{\nu}$ [cm^{-1}] 3068, 3032, 2931, 2858, 1728, 1594, 1497, 1454, 1428, 1378, 1291, 1250, 1160, 1111, 1084, 1062, 941, 824, 736, 700, 614, 505; ^{1}H NMR, COSY (400 MHz, $CDCl_3$) δ_H 7.71−7.64 (m, 4H, CH_{arom}), 7.46−7.18 (m, 21H, CH_{arom}), 6.57−6.48 (m, 3H, 2″-C*H*, 4″-C*H*, 6″-C*H*), 5.08−4.89 (m, 1H, 2-C*H*), 4.95 (s, 4H, 3″-C$H_{2\ Bn}$, 5″-C$H_{2\ Bn}$), 4.38 (d, J = 11.3 Hz, 1H, 4-C$H_{2\text{-}A\ Bn}$), 4.29 (d, J = 11.3 Hz, 1H, 4-C$H_{2\text{-}B\ Bn}$), 3.82−3.65 (m, 3H, 4-C*H*, 6-CH_2), 3.48 (d, J = 16.6 Hz, 1H, 2′-C$H_{2\text{-}A}$), 3.45 (d, J = 16.6 Hz, 1H, 2′-C$H_{2\text{-}B}$), 1.93−1.77 (m, 2H, 3-C*H*, 5-C$H_{2\text{-}A}$), 1.77−1.64 (m, 1H, 5-C$H_{2\text{-}B}$), 1.20 (d, J = 6.4 Hz, 3H, 1-CH_3), 1.07 (s, 9H, C(CH_3)$_3$), 0.89 (d, J = 7.0 Hz, 3H, 3-CH_3); ^{13}C NMR, HSQC, HMBC (101 MHz, $CDCl_3$) δ_C 170.8 (1′-COO), 160.1 (2C, 3″-, 5″-*C*), 139.0 (*ipso*-4-C_{Bn}), 136.9 (2C, ipso-3″, ipso-5″-C_{Bn}), 136.5 (*ipso*-1″-*C*), 135.7 (2C, 2 × *o*-CH_{TBDPS}), 135.7 (2C, 2 × *o*-CH_{TBDPS}), 133.9 (*ipso*-C_{TBDPS}), 133.8 (*ipso*-C_{TBDPS}), 129.8 (2C, 2 × *p*-CH_{TBDPS}), 128.7 (4C, 2 × *m*-3″, 2 × *m*-5″-CH_{Bn}), 128.4 (2C, 3″-, 5″-*p*-CH_{Bn}), 128.1 (2C, 2 × *m*-4-CH_{Bn}), 127.8 (2C, 2 × *m*-CH_{TBDPS}), 127.8 (2C, 2 × *m*-CH_{TBDPS}), 127.8 (2C, 2 × *o*-4-CH_{Bn}), 127.7 (4C, 2 × *o*-3″, 2 × *o*-5″-CH_{Bn}), 127.5 (*p*-4-CH_{Bn}), 108.5 (2C, 2″-, 6″-CH), 100.9 (4″-*C*), 75.8 (4-CH), 72.9 (2-CH), 72.4 (4-$CH_{2\ Bn}$), 70.1 (2C, 3″-, 5″- $CH_{2\ Bn}$), 61.0 (6-CH_2), 42.1 (2′-CH_2), 41.6 (3-CH), 34.9 (5-CH_2), 27.0 (3C, SiC(CH_3)$_3$), 19.3 (Si*C*(CH$_3$)$_3$), 18.0 (1-CH_3), 9.9 (3-CH_3); HRESIMS m/z 829.3883 [M + Na]$^+$ (calcd for $C_{52}H_{58}O_6Si$, 829.3895).

*(2R,3R,4R)-4-(Benzyloxy)-6-hydroxy-3-methylhexan-2-yl 2-[3,5-Bis(benzyloxy)phenyl]acetate (**42**).* Following a previously published procedure,[40] silyl ether **41** (550 mg, 681 μmol, 1.00 equiv) was dissolved in THF (5 mL), and TBAF (1M in THF, 886 μL, 886 μmol, 1.30 equiv) was added dropwise at 0 °C. The reaction mixture was stirred overnight at ambient temperature before it was quenched with 30 mL of saturated NH_4Cl(aq). The aqueous layer was washed with EtOAc (50 mL), dried ($MgSO_4$), and filtered. After flash chromatography (cyclohexane/EtOAc, 3:1) the primary alcohol **42** (347 mg, 609 μmol, 89%) could be obtained as a colorless oil. $[\alpha]_D^{19}$ −28.3 (*c* 1.00, $CHCl_3$); R_f 0.09 (cyclohexane/EtOAc, 3:1); IR (ATR) $\tilde{\nu}$ [cm^{-1}] 3499, 2979, 2933, 2878, 1724, 1569, 1497, 1452, 1378, 1346, 1290, 1250, 1214, 1156, 1057, 950, 834, 737, 670; ^{1}H NMR, COSY (400 MHz, DMSO-d_6) δ_H 7.43−7.17 (m, 15H, CH_{arom}), 6.59−6.50 (m, 3H, 2″-C*H*, 4″-C*H*, 6″-C*H*), 5.01 (s, 4H, 3″-C$H_{2\ Bn}$, 5″-C$H_{2\ Bn}$), 4.82 (dq, J = 8.4, 6.3 Hz, 1H, 2-C*H*), 4.46 (t, J = 5.0 Hz, 1H, 6-O*H*), 4.33 (d, J = 11.3 Hz, 1H, 4-C$H_{2\text{-}A\ Bn}$), 4.11 (d, J = 11.3 Hz, 1H, 4-C$H_{2\text{-}B\ Bn}$), 3.59−3.49 (m, 3H, 4-C*H*, 2′-CH_2), 3.48−3.39 (m, 2H, 6-CH_2), 1.80−1.68 (m, 2H, 3-C*H*, 5-C$H_{2\text{-}A}$), 1.60−1.50 (m, 1H, 5-C$H_{2\text{-}B}$), 1.15 (d, J = 6.3 Hz, 3H, 1-CH_3), 0.82 (d, J = 7.0 Hz, 3H, 3-CH_3); ^{13}C NMR, HSQC, HMBC (101 MHz, DMSO-d_6) δ_C 170.3 (1′-COO), 159.5 (2C, 3″-, 5″-*C*), 139.0 (*ipso*-4-C_{Bn}), 136.9 (2C, ipso-3″, ipso-5″-C_{Bn}), 136.6 (*ipso*-1″-*C*), 128.4 (4C, 2 × *m*-3″, 2 × *m*-5″-CH_{Bn}), 128.1 (2C, 2 × *m*-4-CH_{Bn}), 127.8 (2C, 3″-, 5″-*p*-CH_{Bn}), 127.7 (4C, 2 × *o*-3″, 2 × *o*-5″-CH_{Bn}), 127.3 (2C, 2 × *o*-4-CH_{Bn}), 127.2 (*p*-4-CH_{Bn}), 108.4 (2C, 2″-, 6″-CH), 100.2 (4″-*C*), 75.5 (4-CH), 71.9 (2-CH), 71.3 (4-$CH_{2\ Bn}$), 69.3 (2C, 3″-, 5″- $CH_{2\ Bn}$), 57.9 (6-CH_2), 41.1 (2′-CH_2), 41.0 (3-CH), 34.8 (5-CH_2), 17.8 (1-CH_3), 9.5 (3-CH_3); HRESIMS m/z 591.2719 [M + Na]$^+$ (calcd for $C_{36}H_{40}O_6$, 591.2717).

*(2R,3R,4R)-4-(Benzyloxy)-3-methyl-6-oxohexan-2-yl 2-[3,5-Bis-(benzyloxy)phenyl]acetate (**20**).* Using a modified procedure of Pannecoucke et al.,[17] primary alcohol **42** (347 mg, 610 μmol, 1.00 equiv) was dissolved in dry MeCN (16 mL), IBX (427 mg, 1.53 mmol, 2.50 equiv) was added, and the reaction mixture was stirred over preactivated 3 Å molecular sieves (0.25 g). After 2 h, another portion of IBX (34.2 mg, 122 μmol, 0.20 equiv) was added, and the reaction mixture was stirred for another 2 h until the solvent was removed under reduced pressure at rt and the residue was taken up in EtOAc (50 mL). The mixture was filtered through a pad of Celite, and the solvent was removed under reduced pressure, furnishing the aldehyde **20** (326 mg, 575 μmol, 94%) as a yellowish-green oil, which was used immediately for the next reaction. $[\alpha]_D^{22}$ −32.2 (*c* 1.01, $CHCl_3$); R_f 0.65 (cyclohexane/EtOAc, 3:1); IR (ATR) $\tilde{\nu}$ [cm^{-1}] 3033, 2981, 2940, 2877, 2728, 1723, 1594, 1497, 1453, 1378, 1291, 1250, 1160, 1060, 1029, 953, 834, 738, 698; ^{1}H NMR, COSY (400 MHz, DMSO-d_6) δ_H 9.65 (pt, J = 2.0 Hz, 1H, 6-C*H*O), 7.44−7.14 (m, 15H, CH_{arom}), 6.61−6.49 (m, 3H, 2″-C*H*, 4″-C*H*, 6″-C*H*), 5.01 (s, 4H, 3″-C$H_{2\ Bn}$, 5″-C$H_{2\ Bn}$), 4.81 (dq, J = 8.6, 6.3 Hz, 1H, 2-C*H*), 4.30 (d, J = 11.2 Hz, 1H, 4-C$H_{2\text{-}A\ Bn}$), 4.09 (d, J = 11.2 Hz, 1H, 4-C$H_{2\text{-}B\ Bn}$), 4.02 (ddd, J = 6.9, 5.6, 2.7 Hz, 1H, 4-C*H*), 3.58 (d, J = 17.4 Hz, 1H, 2′-C$H_{2\text{-}A}$), 3.54 (d, J = 17.4 Hz, 1H, 2′-C$H_{2\text{-}B}$), 2.72 (ddd, J = 16.6, 6.9, 2.5 Hz, 1H, 5-C$H_{2\text{-}A}$), 2.59 (ddd, J = 16.6, 5.6, 1.7 Hz, 1H, 5-C$H_{2\text{-}B}$), 1.83−1.71 (m, 1H, 3-C*H*), 1.16 (d, J = 6.3 Hz, 3H, 1-CH_3), 0.83 (d, J = 7.0 Hz, 3H, 3-CH_3); ^{13}C NMR, HSQC, HMBC (101 MHz, DMSO-d_6) δ_C 202.1 (6-CHO), 170.2 (1′-COO), 159.5 (2C, 3″-, 5″-*C*), 138.4 (*ipso*-4-C_{Bn}), 136.9 (2C, ipso-3″, ipso-5″-C_{Bn}), 136.6 (*ipso*-1″-*C*), 128.4 (4C, 2 × *m*-3″, 2 × *m*-5″-CH_{Bn}), 128.2 (2C, 2 × *m*-4-CH_{Bn}), 127.9 (2C, 3″-, 5″-*p*-CH_{Bn}), 127.7 (4C, 2 × *o*-3″, 2 × *o*-5″-CH_{Bn}), 127.4 (2C, 2 × *o*-4-CH_{Bn}), 127.4 (*p*-4-CH_{Bn}), 108.4 (2C, 2″-, 6″-CH), 100.2 (4″-*C*), 72.9 (4-CH), 71.7 (2-CH), 71.2 (4-$CH_{2\ Bn}$), 69.3 (2C, 3″-, 5″- $CH_{2\ Bn}$), 46.2 (5-CH_2), 41.6 (3-CH), 41.1 (2′-CH_2), 17.9 (1-CH_3), 9.6 (3-CH_3); HRESIMS m/z 589.2560 [M + Na]$^+$ (calcd for $C_{36}H_{38}O_6$, 589.2560).

*Allyl (5R,6R,7R,E)-5-(Benzyloxy)-7-(2-(3,5-bis(benzyloxy)phenyl)-acetoxy)-2,6-dimethyloct-2-enoate (**24**).* According to procedures from Opatz et al.,[5,9] phosphonium ylide **21** (214 mg, 572 μmol, 1.20 equiv) was added to a solution of aldehyde **20** (270 mg, 476 μmol, 1.00 equiv) in CH_2Cl_2 (27 mL) at ambient temperature. After 3 h, another portion of phosphonium ylide **21** (17.8 mg, 47.9 μmol, 0.10 equiv) was added, and the solution was stirred overnight. The solvent was removed under reduced pressure, and the residue was purified by flash chromatography (toluene/EtOAc, 99:1), yielding the unsaturated allyl ester **24** (285 mg, 429 μmol, 90%) as a colorless oil in an *E*/*Z* ratio of 95:5. $[\alpha]_D^{22}$ −4.1 (*c* 0.95, $CHCl_3$); R_f 0.43 (toluene/EtOAc, 95:5); IR (ATR) $\tilde{\nu}$ [cm^{-1}] 3032, 2981, 2935, 2877, 1713, 1649, 1594, 1498, 1453, 1378, 1290, 1249, 1215, 1160, 1060, 1028, 948, 833, 738; ^{1}H NMR, COSY (600 MHz, CD_3CN) δ_H 7.41−7.19 (m, 15H, CH_{arom}), 6.74 (ddt, J = 7.2, 5.6, 1.5 Hz, 1H, 3-C*H*), 6.55−6.49 (m, 3H, 2″-C*H*, 4″-C*H*, 6″-C*H*), 5.95 (ddt, J = 17.2, 10.6, 5.4 Hz, 1H, OCH$_2$C*H*═CH$_2$), 5.30 (dq, J = 17.2, 1.6 Hz, 1H, OCH$_2$CH═CH_2^E), 5.19 (dq, J = 10.6, 1.6 Hz, 1H, OCH$_2$CH═CH_2^Z), 4.99 (s, 4H, 3″-C$H_{2\ Bn}$, 5″-C$H_{2\ Bn}$), 4.84 (dq, J = 9.0, 6.3 Hz, 1H, 7-C*H*), 4.59 (m, 2H, OCH_2CH═CH$_2$), 4.32 (d, J = 11.1 Hz, 1H, 5-C$H_{2\text{-}A\ Bn}$), 4.07 (d, J = 11.1 Hz, 1H, 5-C$H_{2\text{-}B\ Bn}$), 3.56

https://doi.org/10.1021/acs.jnatprod.2c01145
J. Nat. Prod. 2023, 86, 924−938

(td, J = 6.9, 2.5 Hz, 1H, 5-C*H*), 3.53 (d, J = 18.7 Hz, 1H, 2′-C$H_{2\text{-A}}$), 3.50 (d, J = 18.7 Hz, 1H, 2′-C$H_{2\text{-B}}$), 2.59−2.48 (m, 1H, 4-C$H_{2\text{-A}}$), 2.35−2.27 (m, 1H, 4-C$H_{2\text{-B}}$), 1.83−1.79 (m, 3H, 2-CH_3), 1.68 (dqd, J = 9.0, 7.0, 2.5 Hz, 1H, 6-C*H*), 1.18 (d, J = 6.3 Hz, 3H, 8-CH_3), 0.87 (d, J = 7.0 Hz, 3H, 6-CH_3); ^{13}C NMR, HSQC, HMBC (151 MHz, CD_3CN) δ_C 171.4 (1′-COO), 168.0 (1-COO), 161.0 (2C, 3″-, 5″-*C*), 139.9 (*ipso*-5-C_{Bn}), 139.5 (3-CH), 138.1 (2C, ipso-3″, ipso-5″-C_{Bn}), 138.0 (*ipso*-1″-*C*), 133.9 ($OCH_2CH{=}CH_2$), 130.0 (2-C), 129.5 (4C, 2 × *m*-3″, 2 × *m*-5″-CH_{Bn}), 129.2 (2C, 2 × *m*-5-CH_{Bn}), 128.9 (2C, 3″-, 5″-*p*-CH_{Bn}), 128.7 (2C, 2 × *o*-5-CH_{Bn}), 128.7 (4C, 2 × *o*-3″, 2 × *o*-5″-CH_{Bn}), 128.4 (*p*-5-CH_{Bn}), 117.9 ($OCH_2CH{=}CH_2$), 109.5 (2C, 2″-, 6″-CH), 101.3 (4″-*C*), 78.3 (5-CH), 73.1 (7-CH), 72.9 (5-$CH_{2\ Bn}$), 70.7 (2C, 3″-, 5″-$CH_{2\ Bn}$), 65.7 ($OCH_2CH{=}CH_2$), 42.7 (6-CH), 42.6 (2′-CH_2), 32.0 (4-CH_2), 18.4 (8-CH_3), 12.9 (2-CH_3), 9.8 (6-CH_3); HRESIMS m/z 663.3308 $[M + H]^+$ (calcd for $C_{42}H_{46}O_7$, 663.3317).

*(5R,6R,7R,E)-5-(Benzyloxy)-7-(2-(3,5-bis(benzyloxy)phenyl)-acetoxy)-2,6-dimethyloct-2-enoic Acid (**25**).* Using a modified procedure of Kunz et al.,[42] allyl ester **24** (90.0 mg, 136 μmol, 1.00 equiv), 1,3-dimethylbarbituric acid (25.4 mg, 163 μmol, 1.20 equiv), $Pd(PPh_3)_4$ (15.7 mg, 13.6 μmol, 0.10 equiv), and PPh_3 (39.2 mg, 149 μmol, 1.10 equiv) were dissolved in THF (7.7 mL) and stirred overnight at rt. After complete conversion of the starting material, the solvent was removed under reduced pressure and the crude product was purified by flash chromatography (cyclohexane/EtOAc, 5:1, 1% AcOH), yielding the free carboxylic acid **25** (81.4 mg, 131 μmol, 96%) as a colorless oil. $[\alpha]_D^{22}$ −6.4 (c 1.02, $CHCl_3$); R_f 0.24 (cyclohexane/EtOAc, 3:1, 1% AcOH); IR (ATR) $\tilde{\nu}$ [cm^{-1}] 3032, 2980, 2931, 2885, 1724, 1685, 1642, 1594, 1497, 1453, 1377, 1347, 1290, 1250, 1213, 1156, 1059, 1028, 950, 910, 834, 735, 697; ^{1}H NMR, COSY (400 MHz, $CDCl_3$) δ_H 10.78 (s_{br}, 1H, 1-COO*H*), 7.40−7.18 (m, 15H, CH_{arom}), 6.83 (ddd, J = 8.3, 6.9, 1.6 Hz, 1H, 3-C*H*), 6.58−6.50 (m, 3H, 2″-C*H*, 4″-C*H*, 6″-C*H*), 5.00−4.88 (m, 5H, 3″-C$H_{2\ Bn}$, 5″-C$H_{2\ Bn}$, 7-C*H*), 4.31 (d, J = 11.2 Hz, 1H, 5-C$H_{2\text{-A Bn}}$), 4.13 (d, J = 11.2 Hz, 1H, 5-C$H_{2\text{-B Bn}}$), 3.56−3.44 (m, 3H, 5-C*H*, 2′-CH_2), 2.57−2.46 (m, 1H, 4-C$H_{2\text{-A}}$), 2.37−2.25 (m, 1H, 4-C$H_{2\text{-B}}$), 1.85−1.79 (m, 3H, 2-CH_3), 1.68 (dqd, J = 8.9, 7.0, 2.3 Hz, 1H, 6-C*H*), 1.21 (d, J = 6.3 Hz, 3H, 8-CH_3), 0.90 (d, J = 7.0 Hz, 3H, 6-CH_3); ^{13}C NMR, HSQC, HMBC (101 MHz, $CDCl_3$) δ_C 172.2 (1-COOH), 170.7 (1′-COO), 160.2 (2C, 3″-, 5″-*C*), 141.0 (3-CH), 138.5 (*ipso*-5-C_{Bn}), 136.9 (2C, ipso-3″, ipso-5″-C_{Bn}), 136.5 (*ipso*-1″-*C*), 128.7 (4C, 2 × *m*-3″, 2 × *m*-5″-CH_{Bn}), 128.6 (2-C), 128.5 (2C, 2 × *m*-5-CH_{Bn}), 128.1 (2C, 3″-, 5″-*p*-CH_{Bn}), 127.8 (2C, 2 × *o*-5-CH_{Bn}), 127.7 (*p*-5-CH_{Bn}), 127.6 (4C, 2 × *o*-3″, 2 × *o*-5″-CH_{Bn}), 108.6 (2C, 2″-, 6″-CH), 100.9 (4″-*C*), 77.3 (5-CH), 72.7 (7-CH), 72.4 (5-$CH_{2\ Bn}$), 70.1 (2C, 3″-, 5″- $CH_{2\ Bn}$), 42.4 (2′-CH_2), 42.1 (6-CH), 31.9 (4-CH_2), 18.2 (8-CH_3), 12.5 (2-CH_3), 9.6 (6-CH_3); HRESIMS m/z 621.2842 $[M - H]^-$ (calcd for $C_{39}H_{42}O_7$, 621.2858).

*(1-(tert-Butoxy)-1-oxopropan-2-yl)triphenylphosphonium Bromide (**43**).* Based on a literature-known procedure by Jacobsen and Lokey et al.,[41] *tert*-butyl 2-bromopropionate **22** (1.00 g, 4.64 mmol, 1.00 equiv) was added dropwise to a solution of PPh_3 (1.70 g 6.50 mmol, 1.40 equiv) in MeCN (23 mL). The resulting solution was stirred at rt for 9 d, after which it was diluted with toluene (20 mL) until a white, sticky solid precipitated. The solvent was decanted off, and the separated solid was washed twice with toluene (10 mL) and hexane using an ultrasonic bath. The sticky residue was taken up in MeCN/H_2O (1:1) and lyophilized, yielding the pure phosphonium salt **43** (1.61 g, 3.41 mmol, 74%) as a colorless, fluffy foam. IR (ATR) $\tilde{\nu}$ [cm^{-1}] 3411, 3055, 2981, 2934, 2775, 1731, 1618, 1587, 1485, 1438, 1371, 1292, 1249, 1150, 1110, 997, 898, 839, 752, 724, 672, 521; ^{1}H NMR, COSY (400 MHz, DMSO-d_6) δ_H 8.03−7.66 (m, 15H, CH_{arom}), 5.55 (dq, J = 16.0, 7.2 Hz, 1H, 2-C*H*), 1.51 (dd, J = 18.3, 7.2 Hz, 3H, 3-CH_3), 1.11 (s, 9H, OC(CH_3)$_3$); ^{13}C NMR, HSQC, HMBC (101 MHz, DMSO-d_6) δ_C 166.1 (1-COO^{t}Bu), 135.1 (d, ^4J = 2.9 Hz, 3C, 3 × *p*-CH), 134.1 (d, ^3J = 10.0 Hz, 6C, 6 × *m*-CH), 130.2 (d, ^2J = 12.7 Hz, 6C, 6 × *o*-CH), 117.6 (d, ^1J = 86.1 Hz, 3C, 3 × *ipso*-CH), 84.4 (OC(CH_3)$_3$), 35.5 (d, J = 48.7 Hz, 2-CH), 26.9 (3C, OC(CH_3)$_3$), 12.6 (d, J = 2.5 Hz, 3-CH_3); HRESIMS m/z 391.1850 $[M]^+$ (calcd for $C_{25}H_{28}O_2P$, 391.1822).

*tert-Butyl 2-(Triphenylphosphoranylidene)propanoate (**23**).* Based on a literature known procedure by Jacobsen and Lokey et al.,[41] to a solution of phosphonium bromide **43** (228 mg, 484 μmol, 1.00 equiv) in CH_2Cl_2 (15 mL) was added a NaOH solution (0.1 M in H_2O, 15 mL, 1.50 mmol, 3.10 equiv) at 0 °C, and the reaction mixture was vigorously stirred for 2 h. The aqueous solution was extracted with CH_2Cl_2 (3 × 30 mL), the combined organic layers were dried ($MgSO_4$) and filtered, and the solvent was removed under reduced pressure, to afford the pure phosphonium ylide **23** (180 mg, 461 μmol, 95%) as a yellow solid. IR (ATR) $\tilde{\nu}$ [cm^{-1}] 3057, 2971, 2925, 2856, 1731, 1619, 1483, 1437, 1385, 1361, 1312, 1250, 1180, 1100, 1088, 1028, 998, 956, 926, 863, 785, 749, 715, 694, 642, 619, 583, 540, 517, 504. ^{1}H NMR, COSY (400 MHz, $CDCl_3$) δ_H 7.73−7.35 (m, 15H, CH_{arom}), 1.57 (d, J = 14.5 Hz, 3H, 3-CH_3), 1.01 (s, 9H, OC(CH_3)$_3$); ^{13}C NMR, HSQC, HMBC (101 MHz, $CDCl_3$) δ_C 170.3 (1-COO^{t}Bu), 133.9−133.6 (m, 3C, 3 × *o*-CH), 132.2−131.8 (m, 6C, 6 × *p*-CH), 128.7−128.4 (m, 9C, 3 × *ipso*-CH, 6 × *m*-CH), 80.0 (OC(CH_3)$_3$), 32.8 (d, J = 110.3 Hz, 2-*C*), 28.6 (3C, OC(CH_3)$_3$), 12.8 (d, J = 11.3 Hz, 3-CH_3); HRESIMS m/z 391.1823 $[M + H]^+$ (calcd for $C_{25}H_{27}O_2P$, 391.1822).

*tert-Butyl (5R,6R,7R,E)-5-(Benzyloxy)-7-(2-(3,5-bis(benzyloxy)-phenyl)acetoxy)-2,6-dimethyloct-2-enoate (**26**).* According to procedures from Opatz et al.,[5,9] phosphonium ylide **23** (44.8 mg, 115 μmol, 1.30 equiv) was added to a solution of aldehyde **20** (50.0 mg, 88.2 μmol, 1.00 equiv) in CH_2Cl_2 (4 mL) at ambient temperature. After 3 h, another portion of phosphonium ylide **23** (3.40 mg, 8.82 μmol, 0.10 equiv) was added, and the solution was stirred overnight. The solvent was removed under reduced pressure, and the residue was purified by flash chromatography (cyclohexane/EtOAc, 12:1), yielding the unsaturated *tert*-butyl ester **26** (53.6 mg, 79.0 μmol, 90%) as a colorless oil in an E/Z ratio of 95:5. $[\alpha]_D^{22}$ −2.6 (c 1.03, $CHCl_3$); R_f 0.18 (cyclohexane/EtOAc, 10:1); IR (ATR) $\tilde{\nu}$ [cm^{-1}] 3064, 3033, 2978, 2931, 1727, 1702, 1653, 1647, 1594, 1497, 1497, 1454, 1368, 1349, 1290, 1251, 1216, 1160, 1083, 1060, 1029, 993, 952, 910, 848, 737, 698, 633; ^{1}H NMR, COSY (400 MHz, CD_3CN) δ_H 7.42−7.19 (m, 15H, CH_{arom}), 6.63 (ddq, J = 8.4, 7.00, 1.5 Hz, 1H, 3-C*H*), 6.56−6.49 (m, 3H, 2″-C*H*, 4″-C*H*, 6″-C*H*), 4.99 (s, 4H, 3″-C$H_{2\ Bn}$, 5″-C$H_{2\ Bn}$), 4.84 (dq, J = 9.0, 6.3 Hz, 1H, 7-C*H*), 4.33 (d, J = 11.1 Hz, 1H, 5-C$H_{2\text{-A Bn}}$), 4.07 (d, J = 11.1 Hz, 1H, 5-C$H_{2\text{-B Bn}}$), 3.55 (td, J = 7.0, 2.5 Hz, 1H, 5-C*H*), 3.54−3.46 (m, 2H, 2′-CH_2), 2.55−2.45 (m, 1H, 4-C$H_{2\text{-A}}$), 2.34−2.23 (m, 1H, 4-C$H_{2\text{-B}}$), 1.79−1.74 (m, 3H, 2-CH_3), 1.68 (dqd, J = 9.0, 7.0, 2.5 Hz, 1H, 6-C*H*), 1.44 (s, 9H, OC(CH_3)$_3$), 1.18 (d, J = 6.3 Hz, 3H, 8-CH_3), 0.86 (d, J = 7.0 Hz, 3H, 6-CH_3); ^{13}C NMR, HSQC, HMBC (101 MHz, CD_3CN) δ_C 171.5 (1′-COO), 167.9 (1-COO^{t}Bu), 161.0 (2C, 3″-, 5″-*C*), 139.9 (*ipso*-5-C_{Bn}), 138.2 (3-CH), 138.0 (3C, *ipso*-1″-*C*, ipso-3″, ipso-5″-C_{Bn}), 131.6 (2-*C*), 129.5 (4C, 2 × *m*-3″, 2 × *m*-5″-CH_{Bn}), 129.2 (2C, 2 × *m*-5-CH_{Bn}), 128.9 (2C, 3″-, 5″-*p*-CH_{Bn}), 128.7 (2C, 2 × *o*-5-CH_{Bn}), 128.7 (4C, 2 × *o*-3″, 2 × *o*-5″-CH_{Bn}), 128.4 (*p*-5-CH_{Bn}), 109.6 (2C, 2″-, 6″-CH), 101.4 (4″-*C*), 80.7 (OC(CH_3)$_3$), 78.4 (5-CH), 73.2 (7-CH), 72.9 (5-$CH_{2\ Bn}$), 70.7 (2C, 3″-, 5″-$CH_{2\ Bn}$), 42.6 (2′-CH_2), 42.6 (6-CH), 32.0 (4-CH_2), 28.3 (3C, OC(CH_3)$_3$), 18.4 (8-CH_3), 13.0 (2-CH_3), 9.8 (6-CH_3); HRESIMS m/z 701.3458 $[M + Na]^+$ (calcd for $C_{43}H_{50}O_7$, 701.3449).

*(13R,14R,15R)-5,7,13-Tris(benzyloxy)-4-dechloro-14-deoxyoxacyclododecindione (**28**).* Following modified procedures of Roberts et al.[15] and Opatz et al.,[5] a solution of CH_2Cl_2 (138 mL), trifluoroacetic acid (4.68 mL), and trifluoroacetic anhydride (2.34 mL) was precooled to −8 °C, and (5*R*,6*R*,7*R*,*E*)-5-(benzyloxy)-7-(2-(3,5-bis(benzyloxy)-phenyl)acetoxy)-2,6-dimethyloct-2-enoic acid (**25**) (60.0 mg, 96.4 μmol, 1.00 equiv) in CH_2Cl_2 (2.50 mL) was added dropwise. The reaction mixture was left to stand at −8 °C for 2 d and then gradually warmed to 0 °C and rt to stir for another 2 d. The reaction mixture was neutralized by careful addition of saturated $NaHCO_3$(aq) and washing of the organic layer (3 × 80 mL). The organic residue was dried ($MgSO_4$) and filtered, and the solvent was removed under reduced pressure. After purification by flash chromatography (cyclohexane/EtOAc, 15:1, 1% AcOH) the 12-membered macrolactone **28** (30.3 mg, 50.1 μmol, 52%) was obtained as a colorless oil. Starting from *tert*-butyl (5*R*,6*R*,7*R*,*E*)-5-(benzyloxy)-7-(2-(3,5-bis(benzyloxy)phenyl)-acetoxy)-2,6-dimethyloct-2-enoate (**26**) (60.0 mg, 88.5 μmol, 1.00 equiv), the 12-membered macrolactone **28** (33.9 mg, 56.1 μmol, 63%)

https://doi.org/10.1021/acs.jnatprod.2c01145
J. Nat. Prod. 2023, 86, 924−938

was obtained by applying the same procedure as a colorless oil. $[\alpha]_D^{22}$ +47.0 (*c* 0.23, CH_2Cl_2); R_f 0.05 (cyclohexane/EtOAc, 15:1, 1% AcOH); IR (ATR) $\tilde{\nu}$ [cm^{-1}] 3067, 3032, 2978, 2925, 1723, 1656, 1604, 1584, 1498, 1455, 1434, 1380, 1332, 1306, 1292, 1256, 1210, 1147, 1113, 1085, 1068, 1029, 1005, 738, 698; ^{1}H NMR, COSY (600 MHz, CD_3CN) δ_H 7.48−7.22 (m, 15H, CH_{arom}), 6.62 (d, *J* = 2.0 Hz, 1H, 6-C*H*), 6.55−6.47 (m, 1H, 4-C*H*), 6.47−6.34 (m, 1H, 11-C*H*), 5.12−5.00 (m, 4H, 5-$CH_{2\ Bn}$, 7-$CH_{2\ Bn}$), 4.70−4.60 (m, 1H, 15-C*H*), 4.54 (d, *J* = 11.7 Hz, 1H, 13-$CH_{2\text{-}A\ Bn}$), 4.40 (d, *J* = 11.7 Hz, 1H, 13-$CH_{2\text{-}B\ Bn}$), 3.45−3.28 (m, 1H, 2-$CH_{2\text{-}A}$), 3.22 (ddd, *J* = 9.4, 4.0, 2.0 Hz, 1H, 13-C*H*), 3.16 (d, *J* = 15.9 Hz, 1H, 2-$CH_{2\text{-}B}$), 2.69−2.55 (m, 1H, 12-$CH_{2\text{-}A}$), 2.46−2.33 (m, 1H, 12-$CH_{2\text{-}B}$), 1.83 (s, 3H, 10-CH_3), 1.74−1.66 (m, 1H, 14-C*H*), 1.06 (d, *J* = 6.3 Hz, 3H, 15-CH_3), 0.91 (d, *J* = 7.4 Hz, 3H, 14-CH_3); ^{13}C NMR, HSQC, HMBC (151 MHz, CD_3CN) δ_C 199.5 (9-CO), 170.1 (1-COO), 160.6 (5-*C*), 157.3 (7-*C*), 148.2 (11-CH), 139.8 (*ipso*-13-C_{Bn}), 139.2 (10-*C*), 138.0 (*ipso*-7-C_{Bn}), 137.9 (*ipso*-5-C_{Bn}), 134.5 (3-C), 129.5 (2C, 2 × *m*-CH_{Bn}), 129.5 (2C, 2 × *m*-CH_{Bn}), 129.2 (2C, 2 × *m*-CH_{Bn}), 129.0 (*p*-CH_{Bn}), 128.9 (*p*-CH_{Bn}), 128.7 (2C, 2 × *o*-CH_{Bn}), 128.6 (2C, 2 × *o*-CH_{Bn}), 128.4 (*p*-CH_{Bn}), 128.3 (2C, 2 × *o*-CH_{Bn}), 124.9 (8-*C*), 109.5 (4-CH), 100.7 (6-CH), 81.5 (13-CH), 76.4 (15-CH), 72.5 (13-$CH_{2\ Bn}$), 71.0 (7-$CH_{2\ Bn}$), 70.8 (5-$CH_{2\ Bn}$), 44.7 (14-CH), 40.1 (2-CH_2), 34.0 (12-CH_2), 19.1 (15-CH_3), 12.9 (14-CH_3), 10.5 (10-CH_3); HRESIMS *m*/*z* 605.2892 [M + H]$^+$ (calcd for $C_{39}H_{40}O_6$, 605.2989).

*(7R,8R,9R,E)-1^5,7-Bis(benzyloxy)-4,8,9-trimethyl-2,10-dioxa-1-(1,3)-benzenacyclododecaphan-4-ene-3,11-dione (**27**).* The 14-membered macrolactone **27** was obtained as a minor byproduct of the previously mentioned ring-closing procedure after flash chromatography (cyclohexane/EtOAc, 15:1, 1% AcOH) and preparative HPLC (C_{18}-HTEC, isocratic 75% MeCN in H_2O, 20 min). The byproduct **27** (2.60 mg, 5.05 μmol, 6%) was obtained as a colorless oil. $[\alpha]_D^{22}$ −71.7 (*c* 0.38, CH_2Cl_2); R_f 0.32 (cyclohexane/EtOAc, 5:1, 1% AcOH); t_R (HPLC) 15.49 min (C_{18}-HTEC, isocratic 75% MeCN in H_2O); IR (ATR) $\tilde{\nu}$ [cm^{-1}] 3064, 3032, 2979, 2944, 2885, 1727, 1599, 1588, 1529, 1497, 1453, 1382, 1331, 1286, 1246, 1198, 1141, 1058, 1028, 998, 956, 910, 844,815, 784, 739, 699, 681, 634, 482, 465; ^{1}H NMR, COSY (600 MHz, DMSO-d_6) δ_H 7.42−7.22 (m, 8H, CH_{arom}), 7.17−7.13 (m, 2H, CH_{arom}), 6.84−6.81 (m, 1H, 1^4-CH_{arom}), 6.77 (pt, *J* = 2.2 Hz, 1H, 1^6-CH_{arom}), 6.65−6.62 (m, 1H, 1^2-CH_{arom}), 5.99 (ddd, *J* = 9.6, 6.5, 1.7 Hz, 1H, 5-C*H*), 5.11 (s, 2H, 1^5-$CH_{2\ Bn}$), 4.70 (dq, *J* = 9.6, 6.4 Hz, 1H, 9-C*H*), 4.31 (d, *J* = 11.6 Hz, 1H, 7-$CH_{2\text{-}A\ Bn}$), 3.96 (d, *J* = 11.6 Hz, 1H, 7-$CH_{2\text{-}B\ Bn}$), 3.66 (d, *J* = 13.0 Hz, 1H, 12-$CH_{2\text{-}A}$), 3.38 (d, *J* = 13.0 Hz, 1H, 12-$CH_{2\text{-}B}$), 2.56 (dd, *J* = 10.0, 1.5 Hz, 1H, 7-C*H*), 2.23−2.16 (m, 1H, 6-$CH_{2\text{-}A}$), 2.15−2.06 (m, 1H, 6-$CH_{2\text{-}B}$), 1.60 (dq, *J* = 9.6, 7.1 Hz, 1H, 8-C*H*), 1.47 (d, *J* = 1.7 Hz, 3H, 4-CH_3), 1.17 (d, *J* = 6.4 Hz, 3H, 9-CH_3), 0.81 (d, *J* = 7.1 Hz, 3H, 8-CH_3). ^{13}C NMR, HSQC, HMBC (151 MHz, DMSO-d_6) δ_C 169.4 (11-COO), 168.5 (3-COO), 159.3 (1^5-*C*), 154.3 (1-*C*), 138.3 (*ipso*-7-C_{Bn}), 138.1 (5-CH), 137.0 (1^3-*C*), 136.6 (*ipso*-1^5-C_{Bn}), 128.5 (2C, 2 × *m*-CH_{Bn}), 128.5 (4-*C*), 128.3 (2C, 2 × *m*-CH_{Bn}), 128.0 (*p*-CH_{Bn}), 127.7 (2C, 2 × *o*-CH_{Bn}), 127.6 (2C, 2 × *o*-CH_{Bn}), 127.5 (*p*-CH_{Bn}), 114.4 (1^2-C*H*), 113.4 (1^4-C*H*), 105.6 (1^6-C*H*), 77.1 (7-CH), 71.9 (9-CH), 70.9 (7-$CH_{2\ Bn}$), 69.5 (1^5-$CH_{2\ Bn}$), 42.0 (12-CH_2), 41.6 (8-CH), 29.0 (6-CH_2), 18.3 (9-CH_3), 13.5 (4-CH_3), 8.8 (8-CH_3); HRESIMS *m*/*z* 537.2252 [M + Na]$^+$ (calcd for $C_{32}H_{34}O_6$, 537.2247).

*(13R,14R,15R)-5,7,13-Tris(benzyloxy)-14-deoxyoxacyclododecindione (**29**).* Following modified procedures of Opatz et al.,[5,9] a solution of macrolactone **28** (73.8 mg, 122 μmol, 1.00 equiv) in *N*,*N*-dimethylformamide was treated with trifluoroacetic acid (14.1 μL, 183 μmol, 1.50 equiv), and a freshly prepared solution of *N*-chlorosuccinimide (100 mM in DMF, 488 μL, 48.8 μmol, 0.40 equiv) was added slowly in 3 min at rt. After further addition of *N*-chlorosuccinimide on day 2 (100 mM in DMF, 488 μL, 48.8 μmol, 0.40 equiv) and day 3 (100 mM in DMF, 292 μL, 29.2 μmol, 0.24 equiv), the reaction mixture was quenched by the addition of H_2O (10 mL) after complete conversion of the starting material on day 4. The aqueous phase was extracted with diethyl ether (3 × 30 mL), the combined organic layers were dried ($MgSO_4$) and filtered, and the solvent was removed under reduced pressure. The residue was purified by flash chromatography (cyclohexane/EtOAc, 15:1, 1%AcOH) to yield the 14-deoxyoxacyclododecindione **29** (56.3 mg, 88.1 μmol, 72%) as a colorless oil. $[\alpha]_D^{22}$ +87.9 (*c* 0.31, CH_2Cl_2); R_f 0.50 (cyclohexane/EtOAc, 3:1, 1% AcOH); IR (ATR) $\tilde{\nu}$ [cm^{-1}] 3062, 3032, 2979, 2937, 2872, 1728, 1656, 1636, 1593, 1575, 1498, 1454, 1412, 1383, 1334, 1298, 1284, 1252, 1203, 1187, 1168, 1088, 1067, 1028, 967, 644, 909, 869, 814, 738, 697, 664, 621, 563, 472; ^{1}H NMR, COSY (600 MHz, CD_3CN) δ_H 7.48−7.24 (m, 15H, CH_{arom}), 6.86 (s, 1H, 6-C*H*), 6.47−6.37 (m, 1H, 11-C*H*), 5.21 (d, *J* = 11.9 Hz, 1H, 5-$CH_{2\text{-}A\ Bn}$), 5.17 (d, *J* = 11.9 Hz, 1H, 5-$CH_{2\text{-}B\ Bn}$), 5.09 (d, *J* = 12.2 Hz, 1H, 7-$CH_{2\text{-}A\ Bn}$), 5.06 (d, *J* = 12.2 Hz, 1H, 7-$CH_{2\text{-}B\ Bn}$), 4.66−4.57 (m, 1H, 15-C*H*), 4.57 (d, *J* = 11.8 Hz, 1H, 13-$CH_{2\text{-}A\ Bn}$), 4.43 (d, *J* = 11.8 Hz, 1H, 13-$CH_{2\text{-}B\ Bn}$), 3.62 (d, *J* = 17.1 Hz, 1H, 2-$CH_{2\text{-}A}$), 3.11 (d, *J* = 17.1 Hz, 1H, 2-$CH_{2\text{-}B}$), 3.08−2.97 (m, 1H, 13-C*H*), 2.71 (t, *J* = 11.8 Hz, 1H, 12-$CH_{2\text{-}A}$), 2.26−2.18 (m, 1H, 12-$CH_{2\text{-}B}$), 1.84 (s, 3H, 10-CH_3), 1.69−1.61 (m, 1H, 14-C*H*), 1.06 (d, *J* = 6.2 Hz, 3H, 15-CH_3), 0.90 (d, *J* = 7.4 Hz, 3H, 14-CH_3); ^{13}C NMR, HSQC, HMBC (151 MHz, CD_3CN) δ_C 198.3 (9-CO), 168.7 (1-COO), 155.6 (5-*C*), 155.3 (7-*C*), 148.6 (11-CH), 139.8 (*ipso*-13-C_{Bn}), 139.0 (10-*C*), 137.5 (*ipso*-7-C_{Bn}), 137.4 (*ipso*-5-C_{Bn}), 132.7 (3-*C*), 129.6 (2C, 2 × *m*-CH_{Bn}), 129.5 (2C, 2 × *m*-CH_{Bn}), 129.2 (2C, 2 × *m*-CH_{Bn}), 129.2 (*p*-CH_{Bn}), 129.1 (*p*-CH_{Bn}), 128.7 (2C, 2 × *o*-CH_{Bn}), 128.6 (2C, 2 × *o*-CH_{Bn}), 128.5 (2C, 2 × *o*-CH_{Bn}), 128.4 (*p*-CH_{Bn}), 125.7 (8-*C*), 116.7 (4-CCl), 100.6 (6-CH), 81.4 (13-CH), 76.8 (15-CH), 72.8 (13-$CH_{2\ Bn}$), 71.9 (5-$CH_{2\ Bn}$), 71.6 (7-$CH_{2\ Bn}$), 44.8 (14-CH), 38.4 (2-CH_2), 35.2 (12-CH_2), 18.8 (15-CH_3), 11.9 (14-CH_3), 10.5 (10-CH_3); HRESIMS *m*/*z* 639.2488 [M + H]$^+$ (calcd for $C_{39}H_{39}ClO_6$, 639.2508).

*(13R,14S,15R)-4-Dechloro-13-hydroxy-14-deoxyoxacyclododecindione (**30**).* Following a modified procedure of Opatz et al.,[5,9] boron trichloride (1 M in heptane, 450 μL, 450 μmol, 9.00 equiv) was added to a solution of benzyl-protected macrolactone **28** (30.2 mg, 50.0 μmol, 1.00 equiv) in CH_2Cl_2 (9 mL) at −78 °C. Within 2.5 h, the deep orange solution was gradually warmed to −30 °C and stirred for another 2 h at the same temperature. After complete conversion of the starting material, the reaction mixture was quenched by the addition of saturated aqueous $NaHCO_3$ (10 mL) while warming to rt. The aqueous layer was extracted with CH_2Cl_2 (7 × 30 mL), dried ($MgSO_4$), and filtered, and the solvent was removed under reduced pressure. The crude product was purified by preparative HPLC (C_{18}-HTEC, isocratic 23% MeCN in H_2O, 20 min), and (13*R*,14*S*,15*R*)-4-dechloro-13-hydroxy-14-deoxyoxacyclododecindione (**30**) (6.39 mg, 19.1 μmol, 38%) was obtained as a colorless oil. $[\alpha]_D^{22}$ +94.4 (*c* 0.21, MeOH); R_f 0.32 (cyclohexane/EtOAc, 1:1, 1% AcOH); t_R (HPLC) 10.04 min (C_{18}-HTEC, isocratic 23% MeCN in H_2O); IR (ATR) $\tilde{\nu}$ [cm^{-1}] 3360, 2982, 2936, 1705, 1620, 1462, 1381, 1343, 1260, 1148, 1107, 1026, 999, 950, 871, 847, 596, 573, 534, 420; ^{1}H NMR, COSY (600 MHz, DMSO-d_6) δ_H 9.48 (s, 1H, 5-CO*H*), 9.44 (s, 1H, 7-CO*H*), 6.38−6.27 (m, 1H, 11-C*H*), 6.22 (d, *J* = 2.1 Hz, 1H, 6-C*H*), 6.16−6.08 (m, 1H, 4-C*H*), 4.85 (d, *J* = 4.7 Hz, 1H, 13-O*H*), 4.61 (dq, *J* = 8.6, 6.3 Hz, 1H, 15-C*H*), 3.32−3.21 (m, 2H, 13-C*H*, 2-$CH_{2\text{-}A}$), 2.99 (d, *J* = 15.5 Hz, 1H, 2-$CH_{2\text{-}B}$), 2.43−2.34 (m, 1H, 12-$CH_{2\text{-}A}$), 2.33−2.23 (m, 1H, 12-$CH_{2\text{-}B}$), 1.75 (s, 3H, 10-CH_3), 1.58−1.50 (m, 1H, 14-C*H*), 1.04 (d, *J* = 6.3 Hz, 3H, 15-CH_3), 0.80 (d, *J* = 7.3 Hz, 3H, 14-CH_3). ^{13}C NMR, HSQC, HMBC (151 MHz, DMSO-d_6) δ_C 199.2 (9-CO), 169.3 (1-COO), 158.0 (5-*C*), 155.3 (7-*C*), 146.4 (11-*C*H), 137.7 (10-*C*), 132.9 (3-*C*), 119.9 (8-*C*), 108.5 (4-CH), 101.3 (6-CH), 74.7 (15-CH), 71.9 (13-CH), 43.9 (14-CH), 39.0 (2-CH_2), 38.0 (12-CH_2), 18.7 (15-CH_3), 12.4 (14-CH_3), 10.5 (10-CH_3); HRESIMS *m*/*z* 335.1485 [M + H]$^+$ (calcd for $C_{18}H_{22}O_6$, 335.1489).

*(13R,14S,15R)-13-Hydroxy-14-deoxyoxacyclododecindione (**4**).* Following a modified procedure of Opatz et al.,[5,9] boron trichloride (1 M in heptane, 4.92 mL, 4.92 mmol, 9.00 equiv) was added to a solution of benzyl-protected macrolactone **29** (349 mg, 547 mmol, 1.00 equiv) in CH_2Cl_2 (100 mL) at −78 °C. Within 2.5 h, the deep orange solution was gradually warmed to −30 °C and stirred for another 2 h at the same temperature. After complete conversion of the starting material, the reaction mixture was quenched by the addition of saturated aqueous $NaHCO_3$ (50 mL) while warming to rt. The aqueous layer was extracted with CH_2Cl_2 (7 × 50 mL), dried ($MgSO_4$), and filtered, and the solvent was removed under reduced pressure. The crude product was purified by preparative HPLC (C_{18}-HTEC, isocratic

https://doi.org/10.1021/acs.jnatprod.2c01145
J. Nat. Prod. 2023, 86, 924−938

24% MeCN in H_2O, 20 min), and (13*R*,14*S*,15*R*)-13-hydroxy-14-deoxyoxacyclododecindione (**4**) (166 mg, 451 mmol, 83%) was obtained as a colorless oil. $[\alpha]_D^{24}$ +81.3 (*c* 0.19, MeOH); R_f 0.40 (cyclohexane/EtOAc, 1:1, 1% AcOH); t_R (HPLC) 13.78 min (C_{18}-HTEC, isocratic 24% MeCN in H_2O); IR (ATR) $\tilde{\nu}$ [cm^{-1}] 3404, 2982, 2932, 1707, 1608, 1439, 1340, 1245, 1203, 1167, 1114, 1069, 1001, 947, 856, 652, 585; ^1H NMR, COSY (600 MHz, DMSO-d_6) δ_H 10.24 (s, 1H, 7-CO*H*), 9.71 (s, 1H, 5-CO*H*), 6.49 (s, 1H, 6-C*H*), 6.43 (dd, *J* = 10.4, 5.1 Hz, 1H, 11-C*H*), 4.89 (d, *J* = 4.9 Hz, 1H, 13-O*H*), 4.56 (dq, *J* = 9.6, 6.3 Hz, 1H, 15-C*H*), 3.50 (d, *J* = 17.3 Hz, 1H, 2-$CH_{2\text{-A}}$), 3.17−3.07 (m, 1H, 13-C*H*), 2.97 (d, *J* = 17.3 Hz, 1H, 2-$CH_{2\text{-B}}$), 2.48−2.43 (m, 1H, 12-$CH_{2\text{-A}}$), 2.17 (ddd, *J* = 14.0, 10.0, 5.1 Hz, 1H, 12-$CH_{2\text{-B}}$), 1.79 (s, 3H, 10-CH_3), 1.57 (dqd, *J* = 9.6, 7.3, 3.8 Hz, 1H, 14-C*H*), 1.01 (d, *J* = 6.3 Hz, 3H, 15-CH_3), 0.78 (d, *J* = 7.3 Hz, 3H, 14-CH_3); ^{13}C NMR, HSQC, HMBC (151 MHz, DMSO-d_6) δ_C 197.9 (9-CO), 167.8 (1-COO), 153.7 (5-*C*), 153.3 (7-*C*), 147.0 (11-CH), 137.5 (10-C), 130.8 (3-*C*), 121.0 (4-CCl), 111.5 (8-*C*), 102.4 (6-CH), 75.1 (15-CH), 71.8 (13-CH), 43.6 (14-CH), 38.6 (12-CH_2), 37.5 (2-CH_2), 18.4 (15-CH_3), 11.5 (14-CH_3), 10.3 (10-CH_3). HRESIMS *m*/*z* 369.1096 $[M + H]^+$ (calcd for $C_{18}H_{21}ClO_6$, 369.1100).

*(13R,14S,15R)-13-Hydroxy-14-deoxyoxacyclododecindione (Z-Isomer) (**34**).* The *Z*-isomer **34** results from a light-induced isomerization of the previously described pure natural product (*E*-isomer) **4**. While the sample was stored in an NMR tube (solvent DMSO-d_6), a maximum isomeric ratio of 58:42 (*E*-isomer/*Z*-isomer) was detected within a period of 42 days. The analytical data reported are from an 18-day-old NMR sample with an isomerization ratio of 80:20. Because isolation of pure *Z*-isomer **34** could not be achieved by preparative HPLC, a complete analysis of the unusual macrolactone **34** was not possible. ^1H NMR, COSY (600 MHz, DMSO-d_6) δ_H 10.54 (s, 1H, 7-CO*H*), 9.91 (s, 1H, 5-CO*H*), 6.48 (s, 1H, 6-C*H*), 6.08 (dd, *J* = 9.9, 6.8 Hz, 1H, 11-C*H*), 4.67 (d, *J* = 5.8 Hz, 1H, 13-O*H*), 4.32 (dq, *J* = 9.4, 6.1 Hz, 1H, 15-C*H*), 3.91 (d, *J* = 16.6 Hz, 1H, 2-$CH_{2\text{-A}}$), 3.71 (d, *J* = 16.6 Hz, 1H, 2-$CH_{2\text{-B}}$), 2.95−2.85 (m, 1H, 13-C*H*), 2.54−2.44 (m, 2H, 12-CH_2), 1.87 (s, 3H, 10-CH_3), 1.42−1.31 (m, 1H, 14-C*H*), 1.09 (d, *J* = 6.1 Hz, 3H, 15-CH_3), 0.78 (d, *J* = 7.0 Hz, 3H, 14-CH_3); ^{13}C NMR, HSQC, HMBC (151 MHz, DMSO-d_6) δ_C 198.9 (9-CO), 167.9 (1-COO), 155.1 (5-*C*), 155.0 (7-*C*), 137.3 (10-*C*), 135.3 (11-CH), 130.8 (3-*C*), 122.9 (4-CCl), 112.7 (8-C), 102.5 (6-CH), 75.3 (15-CH), 73.2 (13-CH), 43.6 (14-CH), 38.6 (12-CH_2), 35.2 (2-CH_2), 20.9 (10-CH_3), 19.3 (15-CH_3), 13.9 (14-CH_3).

Biological Assays. HepG2 cells (DSMZ ACC 180) were maintained in DMEM supplemented with 10% fetal calf serum (FCS) and antibiotics (65 μg/mL penicillin G, 100 μg/mL streptomycin sulfate) at 37 °C and 5% CO_2. The cells were transfected with the indicated plasmids by electroporation. For this, they were suspended in DMEM at 1×10^7 cells/mL and electroporated with 50 μg of plasmid DNA at 220 V in a 4 mm gap cuvette (Nepagene, Nepa21). HepG2 were then seeded at 2×10^5 cells/mL in 24-well plates. After 24 h of incubation at 37 °C and 5% CO_2 the culture medium was replaced by DMEM (containing 0.5% FCS and antibiotics) with 5 ng/mL of either IL-4 or TGF-β and the test compound. Untreated cells and cells treated with the respective cytokine were used as control. After 24 h the medium was removed, and the luciferase levels detected using the luciferase assay system (Promega) according to the manufacturer's instruction. The plasmids used were pGL3-TK-7xN4 and TOPO-Stat6[1] to test for inhibition of IL-4 signaling and $(CAGA)_{9x}$-MLP-Luc to test for inhibition of TGF-β-induced signaling as described in Opatz et al.[9] As an internal normalization control and to exclude cytotoxic effects, the constitutively active pRL-EF1α construct (Promega) was co-electroporated into the HepG2 cells. The $(CAGA)_{9x}$-MLP-Luc plasmid was kindly provided by Prof. S. Dooley (University of Mannheim, Germany).

■ ASSOCIATED CONTENT

Supporting Information

The Supporting Information is available free of charge at https://pubs.acs.org/doi/10.1021/acs.jnatprod.2c01145.

Overview of the detailed synthetic route to macrolactone **4**, additional ^1H, $^{13}C\{^1H\}$, and 2D (COSY, HSQC, HMBC, NOESY) spectra of compounds, *E*/*Z*-isomerization studies, X-ray crystallographic analysis, ECD and VCD analysis, ECD results, VCD results, and references (PDF)

Calculated geometries (in Cartesian coordinates) of each stereoisomer (**4a**−**4d**) for ECD and VCD analysis (ZIP)

Crystallographic Information file of compound **4** (CIF)

■ AUTHOR INFORMATION

Corresponding Author

Till Opatz − *Department of Chemistry, Johannes Gutenberg-University, 55128 Mainz, Germany;* orcid.org/0000-0002-3266-4050; Email: opatz@uni-mainz.de

Authors

Kevin Seipp − *Department of Chemistry, Johannes Gutenberg-University, 55128 Mainz, Germany*

Jonathan Groß − *Department of Chemistry, Johannes Gutenberg-University, 55128 Mainz, Germany*

Anna Maria Kiefer − *Department of Molecular Biotechnology & Systems Biology, University of Kaiserslautern, 67663 Kaiserslautern, Germany*

Gerhard Erkel − *Department of Molecular Biotechnology & Systems Biology, University of Kaiserslautern, 67663 Kaiserslautern, Germany*

Complete contact information is available at: https://pubs.acs.org/10.1021/acs.jnatprod.2c01145

Notes

The authors declare no competing financial interest.

■ ACKNOWLEDGMENTS

Financial support from the MWG Rhineland-Palatinate (NeurodegX Forschungskolleg) is gratefully acknowledged. We thank Dr. J. C. Liermann and P. Eckhardt for NMR spectroscopy, Dr. C. J. Kampf for high-resolution mass spectrometry, Dr. D. Schollmeyer for X-ray crystal structure analysis, and Prof. S. Seiffert for granting access to the CD spectrometer (all JGU Mainz). Parts of this research were conducted using the supercomputer MOGON 2 offered by Johannes Gutenberg-University Mainz (hpc.unimainz.de), which is a member of the AHRP (Alliance for High Performance Computing in Rhineland-Palatinate, www.ahrp.info) and the Gauss Alliance e.V.

■ REFERENCES

(1) Erkel, G.; Belahmer, H.; Serwe, A.; Anke, T.; Kunz, H.; Kolshorn, H.; Liermann, J.; Opatz, T. *J. Antibiot.* **2008**, *61*, 285−290.

(2) Richter, J.; Sandjo, L. P.; Liermann, J. C.; Opatz, T.; Erkel, G. *Bioorg. Med. Chem.* **2015**, *23*, 556−563.

(3) Lin, P.-C.; Wu, Y.-Z.; Bao, T.-W.; Wang, Y.-N.; Shang, X.-Y.; Lin, S. *J. Asian Nat. Prod. Res.* **2018**, *20*, 1093−1100.

(4) Henke, J.; Erkel, G.; Brochhausen, C.; Kleinert, H.; Schwarting, A.; Menke, J.; Pautz, A. *Kidney Int.* **2014**, *86*, 780−789.

(5) Tauber, J.; Rohr, M.; Walter, T.; Erkel, G.; Opatz, T. *Org. Biomol. Chem.* **2015**, *13*, 7813−7821.

(6) Rudolph, K.; Serwe, A.; Erkel, G. *Cytokine* **2013**, *61*, 285−296.

(7) Tauber, J.; Rudolph, K.; Rohr, M.; Erkel, G.; Opatz, T. *Eur. J. Org. Chem.* **2015**, *2015*, 3587−3608.

(8) Tauber, J.; Rohr, M.; Walter, T.; Schollmeyer, D.; Rahn-Hotze, K.; Erkel, G.; Opatz, T. *Org. Biomol. Chem.* **2016**, *14*, 3695−3698.

(9) Weber, C.; Vierengel, N.; Walter, T.; Behrendt, T.; Lucas, T.; Erkel, G.; Opatz, T. *Org. Biomol. Chem.* **2020**, *18*, 5906−5917.

https://doi.org/10.1021/acs.jnatprod.2c01145
J. Nat. Prod. 2023, 86, 924−938

(10) Brzozowski, R. S.; Wuest, W. M. *Chem. Biol. Drug Des.* **2017**, *89*, 169−191.
(11) Liu, X.; Nie, H.; Yao, L.; Jiang, R.; Chen, W. *RSC Adv.* **2020**, *10*, 16882−16885.
(12) Saurin, S.; Meineck, M.; Erkel, G.; Opatz, T.; Weinmann-Menke, J.; Pautz, A. *Pharmaceuticals* **2022**, *15*, 503.
(13) Neises, B.; Steglich, W. *Angew. Chem., Int. Ed.* **1978**, *17*, 522−524.
(14) Wittig, G.; Schöllkopf, U. *Chem. Ber.* **1954**, *87*, 1318−1330.
(15) Baker, P. M.; Bycroft, B. W.; Roberts, J. C. *J. Chem. Soc.* **1967**, 1913−1915.
(16) Kuntiyong, P.; Lee, T. H.; Kranemann, C. L.; White, J. D. *Org. Biomol. Chem.* **2012**, *10*, 7884−7899.
(17) Pierry, C.; Cahard, D.; Couve-Bonnaire, S.; Pannecoucke, X. *Org. Biomol. Chem.* **2011**, *9*, 2378−2386.
(18) Hermann, C.; Pais, G. C. G.; Geyer, A.; Kühnert, S. M.; Maier, M. E. *Tetrahedron* **2000**, *56*, 8461−8471.
(19) Smith, A. B.; Minbiole, K. P.; Verhoest, P. R.; Schelhaas, M. *J. Am. Chem. Soc.* **2001**, *123*, 10942−10953.
(20) Heathcock, C. H. *Science* **1981**, *214*, 395−400.
(21) Sanford, A. B.; Thane, T. A.; McGinnis, T. M.; Chen, P.-P.; Hong, X.; Jarvo, E. R. *J. Am. Chem. Soc.* **2020**, *142*, 5017−5023.
(22) Wessel, H.-P.; Iversen, T.; Bundle, D. R. *J. Chem. Soc., Perkin Trans. 1* **1985**, 2247−2250.
(23) Brazeau, J.-F.; Mochirian, P.; Prévost, M.; Guindon, Y. *J. Org. Chem.* **2009**, *74*, 64−74.
(24) Long, B.; Tang, S.; Chen, L.; Qu, S.; Chen, B.; Liu, J.; Maguire, A. R.; Wang, Z.; Liu, Y.; Zhang, H.; Xu, Z.; Ye, T. *Chem. Commun. (Cambridge, U. K.)* **2013**, *49*, 2977−2979.
(25) Liu, K.; Kim, H.; Ghosh, P.; Akhmedov, N. G.; Williams, L. J. *J. Am. Chem. Soc.* **2011**, *133*, 14968−14971.
(26) Paterson, I.; Paquet, T.; Dalby, S. M. *Org. Lett.* **2011**, *13*, 4398−4401.
(27) Leitereg, T. J.; Cram, D. J. *J. Am. Chem. Soc.* **1968**, *90*, 4011−4018.
(28) Reetz, M. T.; Kesseler, K.; Jung, A. *Tetrahedron Lett.* **1984**, *25*, 729−732.
(29) García-Fortanet, J.; Murga, J.; Carda, M.; Marco, J. A. *Org. Lett.* **2006**, *8*, 2695−2698.
(30) Chérest, M.; Felkin, H.; Prudent, N. *Tetrahedron Lett.* **1968**, *9*, 2199−2204.
(31) Anh, N. T.; E, O. *Nouv. J. Chim.* **1977**, *1*, 61−70.
(32) Nguyen Trong, A.; Eisenstein, O.; Lefour, J. M.; Tran Huu Dau, M. E. *J. Am. Chem. Soc.* **1973**, *95*, 6146−6147.
(33) McGarvey, G. J.; Williams, J. M.; Hiner, R. N.; Matsubara, Y.; Oh, T. *J. Am. Chem. Soc.* **1986**, *108*, 4943−4952.
(34) Olsson, R.; Berg, U.; Frejd, T. *Tetrahedron* **1998**, *54*, 3935−3954.
(35) Evans, D. A.; Rieger, D. L.; Gage, J. R. *Tetrahedron Lett.* **1990**, *31*, 7099−7100.
(36) Elzner, S.; Schmidt, D.; Schollmeyer, D.; Erkel, G.; Anke, T.; Kleinert, H.; Förstermann, U.; Kunz, H. *ChemMedChem.* **2008**, *3*, 924−939.
(37) Bycroft, B. W.; Roberts, J. C.; Kopple, K. D.; Thursack, R. A.; Eden, C.; Feilchenfeld, H.; Jones, J. R.; Waters, W. A.; Squire, J. M.; Ayad, K. N.; McCall, E. B.; Neale, A. J.; Jackman, L. M.; Beattie, I. R.; McQuillan, G.; Gabali, E. N.; Abou-Zeid, Y. M.; Danby, C. J.; Gobbett, E.; Linnett, J. W.; Grundon, M. F.; McGarvey, J. E. B.; Colton, R.; Abraham, R. J.; Freeman, R.; Hall, L. D.; McLauchlan, K. A.; McKinnell, J. P.; Percival, E.; Boulton, A. J.; Katritzky, A. R. *J. Chem. Soc.* **1962**, 2063−2084.
(38) Rachele, J. R. *J. Org. Chem.* **1963**, *28*, 2898−2898.
(39) Theilacker, W.; Wendtland, G. *Liebigs Ann.* **1950**, *570*, 33−53.
(40) Radha Krishna, P.; Rao, T. J. *Org. Biomol. Chem.* **2010**, *8*, 3130−3132.
(41) Bockus, A. T.; Lexa, K. W.; Pye, C. R.; Kalgutkar, A. S.; Gardner, J. W.; Hund, K. C. R.; Hewitt, W. M.; Schwochert, J. A.; Glassey, E.; Price, D. A.; Mathiowetz, A. M.; Liras, S.; Jacobson, M. P.; Lokey, R. S. *J. Med. Chem.* **2015**, *58*, 4581−4589.
(42) Kunz, H.; März, J. *Angew. Chem., Int. Ed.* **1988**, *27*, 1375−1377.
(43) Nafie, L. A. In *Encyclopedia of Spectroscopy and Spectrometry*, 3rd ed.; Lindon, J. C., Tranter, G. E., Koppenaal, D. W., Eds.; Academic Press: Oxford, 2017; pp 524−533.
(44) Bruhn, T.; Schaumlöffel, A.; Hemberger, Y.; Bringmann, G. *Chirality* **2013**, *25*, 243−249.
(45) Henderson, K. W.; Kerr, W. J.; Moir, J. H. *Tetrahedron* **2002**, *58*, 4573−4587.
(46) Lippke, G.; Thaler, H. *Starch - Stärke* **1970**, *22*, 344−351.
(47) Fulmer, G. R.; Miller, A. J. M.; Sherden, N. H.; Gottlieb, H. E.; Nudelman, A.; Stoltz, B. M.; Bercaw, J. E.; Goldberg, K. I. *Organometallics* **2010**, *29*, 2176−2179.
(48) Druais, V.; Hall, M. J.; Corsi, C.; Wendeborn, S. V.; Meyer, C.; Cossy, J. *Org. Lett.* **2009**, *11*, 935−938.
(49) Godin, F.; Prévost, M.; Gorelsky, S. I.; Mochirian, P.; Nguyen, M.; Viens, F.; Guindon, Y. *Chem.—Eur. J.* **2013**, *19*, 9308−9318.

https://doi.org/10.1021/acs.jnatprod.2c01145
J. Nat. Prod. 2023, 86, 924−938

7.3 Strukturaufklärung isolierter Naturstoffe mittels computergestützter Spektroskopie

7.3.1 Bestimmung der absoluten Konfiguration von Perylenchinonen

Perylenchinone sind natürlich auftretende aromatische Polyketide mit einem oxidierten pentacyclischen Kern, die vor allem in Pilzen und Pflanzen vorkommen. Viele Vertreter dieses Strukturtyps können aus der Gattung *Alternaria* isoliert werden, die äußerst vielfältige Schimmelpilze umfasst.[561] Aufgrund der weiten Verbreitung des Pilzes und des häufigen Befalls von Lebensmitteln, werden *Alternaria*-Toxine als kritische Kontaminationen von Lebens- und Futtermitteln angesehen (Abbildung 7.8).[562]

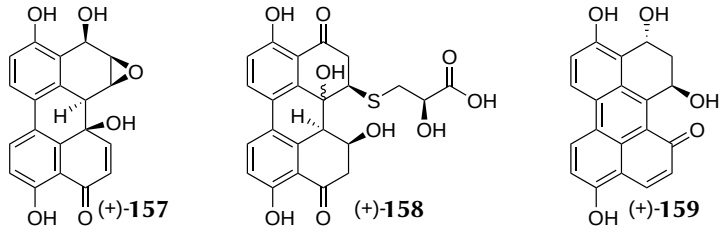

Abbildung 7.8: Isolierte Perylenchinone **157**, **158** und **159** aus Pilzen der Gattung *Alternaria*.[563]

In Kooperation mit der Arbeitsgruppe [redacted] wurden drei neuartige Perylenchinone **157**, **158** und **159** (in der Publikation **1**, **2** und **3**) isoliert und deren chemische Struktur aufgeklärt (Abbildung 7.8). Bei zwei Verbindungen **157** und **159** (in der Publikation **1** und **3**) konnte mittels 2D-NMR-Spektroskopie die relative Konfiguration bestimmt werden, sodass durch einen Vergleich der gemessenen ECD-Spektren mit simulierten Spektren die Bestimmung der absoluten Konfiguration dieser Moleküle möglich war. Für Perylenchinon **158** zeigten die NMR-Daten, dass dieser Naturstoff dasselbe Grundgerüst wie die bekannten Altertoxine besitzt, allerdings war es auf Grundlage der Spektren nicht möglich, die relative Konfiguration vollständig aufzuklären.[564]

Im Rahmen biologischer Untersuchungen, die in der Zelllinie BEAS-2B durchgeführt wurden, konnten für Naturstoff **157** (in der Publikation **1**) sowohl eine stark zytotoxische

Wirkung, ausgeprägte oxidative Eigenschaften als auch eine erhöhte Expression der Häm-Oxygenase 1 auf mRNA- und Proteinebene nachgewiesen werden. Von Verbindung **158** konnten nur so geringe Mengen isoliert werden, dass neben der Strukturaufklärung keine biologischen Tests möglich waren. Perylenchinon **159** (in der Publikation **3**) zeigte weder zytotoxische noch oxidative Eigenschaften und zeichnete sich durch eine starke Reduktion der Nrf2/ARE-abhängigen *sod3* mRNA-Level in oxidativ gestressten Zellen aus.[563]

Die Naturstoffe wurden im Arbeitskreis [redacted] extrahiert und isoliert. Die Strukturaufklärung mittels Massenspektrometrie und NMR-Spektroskopie wurde von [redacted] und [redacted] durchgeführt. Die Aufnahme der ECD-Spektren sowie die Simulation der entsprechenden Spektren mittels TD-DFT wurde von J. Groß durchgeführt. Das Manuskript wurde von [redacted], [redacted], J. Groß, [redacted], T. Opatz und [redacted] erstellt.[16]

[16] *Reprinted under the terms of the Creative Commons Attribution License CC BY 4.0. Copyright ©2023 A. Kiefer, M. Arnholdt, V. Grimm, L. Geske, J. Groß, N. Vierengel, T. Opatz, G. Erkel, Mycotoxin Res., 2023, 39, 303–316, Springer Nature.*

Mycotoxin Research (2023) 39:303–316
https://doi.org/10.1007/s12550-023-00495-1

ORIGINAL ARTICLE

Structure elucidation and biological activities of perylenequinones from an *Alternaria* species

Anna Kiefer[1] · Marcel Arnholdt[1] · Viktoria Grimm[1] · Leander Geske[2] · Jonathan Groß[2] · Nina Vierengel[2] · Till Opatz[2] · Gerhard Erkel[1]

Received: 27 March 2023 / Revised: 9 June 2023 / Accepted: 11 June 2023 / Published online: 23 June 2023

Abstract
The KEAP1-Nrf2/ARE pathway is a pivotal cytoprotective regulator against oxidative stress which plays an important role in the development of many inflammatory diseases and cancer. Activation of the Nrf2 transcription factor by oxidative stress or electrophiles regulates antioxidant response element (ARE)-dependent transcription of antioxidative, detoxifying, and anti-inflammatory proteins. Therefore, modulators of the KEAP1-Nrf2/ARE pathway have received considerable interest as therapeutics to protect against diseases where oxidative stress constitutes the underlying pathophysiology. In a search for fungal secondary metabolites affecting the Nrf2/ARE-dependent expression of a luciferase reporter gene in BEAS-2B cells, three new perylenequinones, compounds **1**, **2**, and **3**, together with altertoxin-I (ATX-I), were isolated from fermentations of an *Alternaria* species. The structures of the compounds were elucidated by a combination of one- and two-dimensional NMR spectroscopy and mass spectrometry. Compound **1** and ATX-I exhibited strong cytotoxic effects with LC_{50}-values of 3.8 µM and 6.43 µM, respectively, whereas compound **3** showed no cytotoxic effects up to 100 µM on BEAS-2B cells. ATX-I induced ARE-dependent luciferase expression approximately fivefold and compound **1** approximately 2.6-fold at a concentration of 3 µM in transiently transfected BEAS-2B cells. In addition, compound **1** and ATX-I exhibited strong oxidative effects, whereas compound **3** did not show significant oxidative properties. For compound **1** and ATX-I, a strong upregulation of heme oxygenase-1 could be observed on mRNA and protein level in treated BEAS-2B cells. Moreover, compound **3** significantly decreased *sod3* mRNA levels after induction of oxidative stress with benzoquinone.

Keywords Altertoxins · *Alternaria* · Perylenequinones · Oxidative stress

Abbreviations

ATX	Altertoxin
PDT	Photodynamic therapy
Nrf2	Nuclear factor erythroid-derived 2
KEAP1	Kelch-like ECH-associated protein 1
ARE	Antioxidant response element
ROS	Reactive oxygen species
NF-κB	Nuclear factor κ-light-chain enhancer of activated B cells
ITS	Internal transcribed spacer
DMEM	Dulbecco's modified eagle medium
FCS	Fetal calf serum
DCFH-DA	Dichlorodihydrofluorescein diacetate

✉ Till Opatz
opatz@uni-mainz.de

✉ Gerhard Erkel
erkel@bio.uni-kl.de

[1] Molecular Biotechnology & Systems Biology, RPTU, Paul-Ehrlich-Straße 23, D-67663 Kaiserslautern, Germany

[2] Department of Chemistry, Johannes Gutenberg-University, Duesbergweg 10-14, D-55128 Mainz, Germany

Introduction

Perylenequinones are naturally occurring aromatic polyketides with an oxidized pentacyclic core, mostly found in various fungi but also in aphids, crinoids, and plants. Many of them have been isolated from *Alternaria* species, a highly diverse genus of molds (Khiralla et al. 2022). According to Weiss et al., natural perylenequinones can be categorized into three classes: Class A contains the simple perylenequinones without carbon substituents including altertoxin I (ATX-I), which are commonly produced by *Alternaria* species (Fig. 1). Class B consists of structures like cercosporin or phleichrome which all contain carbon substituents. Class C includes non-fungal pherylenequinones like rhodoaphin isolated from aphids (Weiss et al. 1987). *Alternaria* is a

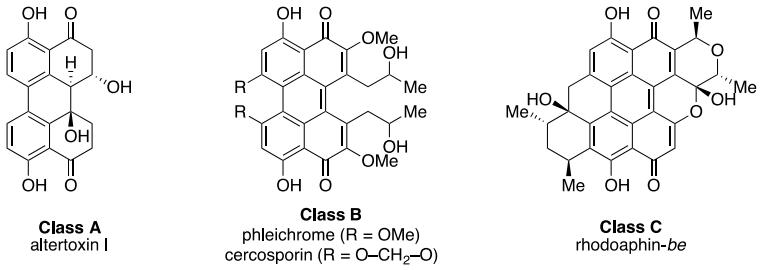

Fig. 1 Classes A–C of perylenequinones: (A) without carbon substituents; (B) with carbon-containing substituents; (C) non-fungal perylenequinones

common genus of saprophytic or pathogenic fungi. They can be found on a variety of crop plants like cereals, fruits, and vegetables and are known to produce various mycotoxins like altertoxin I-III, tenuazonic acid, alternariol, and alternariol monomethyl ether (Lee et al. 2015). Due to the wide distribution of the fungus and the frequent infestation of food crops, alternaria toxins are considered as critical contaminants of food and feed (Arcella et al. 2016).

Whereas several successful total syntheses of members with an intact perylenequinone framework, like cercosporin (Morgan et al. 2009) or phleichrome (Morgan et al. 2010, 2009), have been achieved, only few attempts were made to synthesize altertoxins and related compounds ex vivo as they are not stable against elimination of water with formation of fully aromatic compounds. This and their tendency towards aggregation resulting in solubility problems make these structure a very challenging and a rarely tackled target for total synthesis (Geiseler et al. 2013; Pfaff et al. 2017).

For some perylenequinones and their precursors, especially those isolated from *Alternaria* sp., toxic effects have been described (Aichinger et al. 2021). For ATX-I, a mutagenic effect was confirmed with the Ames test in *Salmonella typhimurium* (Stack and Prival 1986). In addition, ATX-I inhibits topoisomerase II, which plays an essential role in maintaining the correct DNA topology (Jarolim et al. 2017a). Nevertheless, the exact mechanism of action of ATX-I genotoxicity has not yet been clarified.

Due to their photochemical activities, perylenequinones are discussed as possible drugs in photodynamic therapy (PDT) of cancer (Mulrooey et al. 2012). PDT is used to specifically induce cell death in cancer cells through photosensitizing compounds that generate reactive oxygen species upon irradiation (Agostinis et al. 2011; Fayter et al. 2010; Gao et al. 2010). Some perylenequinones like hypocrellin A and hypocrellin B showed beneficial properties for application in photodynamic therapy as they trigger cell death or decrease migration in cancer cell lines after irradiation (Qi et al. 2019; Jiang et al. 2014).

Nrf2/ARE signaling pathway

Reactive oxygen species (ROS) are an unavoidable side effect of aerobic life. While elevated levels of ROS are toxic to cells and organisms, ROS also are an essential part of many cellular defense signaling pathways. Under physiological conditions, a constant regulation between formation and removal of ROS takes place, preventing the emergence of oxidative stress (Sies et al. 2017). Exposure to excessive oxidative stress drives inflammation, tumor growth, or even cell death (Sies and Jones 2020). One important coping mechanism for oxidative stress is the (nuclear factor erythroid-derived 2)-like 2/antioxidant response element (Nrf2/ARE) pathway. Under quiescent conditions, the transcription factor Nrf2 is located in the cytoplasm and is rapidly degraded. Proteolytic degradation is mediated by Kelch-like ECH-associated protein 1 (KEAP1), which catalyzes ubiquitination of Nrf2. In response to oxidative stress, degradation is inhibited, allowing Nrf2 to translocate into the nucleus, where it binds to ARE. Genes induced by Nrf2 encode proteins which stimulate NADPH synthesis, catalyze ROS degradation, accelerate toxin export, and inhibit cytokine-mediated inflammation (Hayes and McMahon 2009). There is a crosstalk between Nrf2 and other transcription factors, amongst them the nuclear factor κ-light-chain enhancer of activated B cells NF-κB transcription factor (Wakabayashi et al. 2010). NF-κB is an important regulator of immune response, cell proliferation, and cell death. It also plays a critical role in the promotion of inflammation and is deregulated in various diseases like cancer (Dolcet et al. 2005), asthma (Janssen-Heininger et al. 2009), and atherosclerosis (Pamukcu et al. 2011). Because of its essential regulatory role not only in redox household but also in inflammation, maintenance of metabolic and protein homeostasis, the NRF2/ARE pathway is a potential drug target (Cuadrado et al. 2019). For the class A perylenequinone ATX-II, an activation of the Nrf2/ARE pathway through the oxidative properties of the compound was observed in CHO and HT29 cells by Jarolim et al. (Jarolim et al. 2017b). However, this could not be shown for ATX-I.

Materials and methods

Culturing and isolation of metabolites

Alternaria sp. was isolated from *Actaea spicata* (baneberry) plant material. The fungus was cultivated on standard growth medium (yeast extract 4 g/L, glucose 4 g/L, malt extract 10 g/L, 2% agar for solid media). Fungal DNA was isolated from the mycelium according to (Liu et al. 2000). Assignment to the genus *Alternaria* was made both morphologically by the typical cylindrical spore shape enlarging gradually to the end (Fig. 2) and by sequencing of the ITS1-5.8S rDNA-ITS2 region of nuclear DNA. Sequencing of the ITS region with ITS4 and ITS5 primers (White et al. 1990) revealed 99–100% similarity to different *Alternaria* species (mainly to *Alternaria rosae* and *Alternaria triticina*). Sporulation was induced by exposure to UV-A radiation (340 nm) (Wei et al. 1985).

Slices of well grown agar plates were used to inoculate 1 L liquid cultures in standard growth medium. The fungus was fermented in 2 L flasks with four baffles at room temperature and shaking (120 rpm). The fermentation was ended after 7 days of growth, and culture fluid was separated from the mycelium by filtration. Culture fluid was extracted twice with an equal volume of ethyl acetate. Phases were separated, and the organic phase was dried with Na_2SO_4, then concentrated in a rotary evaporator yielding 184 mg crude extract. The crude extract was purified by isocratic preparative HPLC (Agilent ZORBAX XDB-C8, 21.2 × 150 mm, 5 µm, flow 21.24 mL/min) with H_2O + 0.1% HCO_2H:MeCN 27:73 to yield 5.3 mg compound **1** (t_R: 11 min), 30.7 mg ATX-1 (t_R: 16 min), 7.3 mg compound **3** (t_R: 25 min), and 1.2 mg compound **2** (t_R: 28 min). The purity of the compounds was estimated to be > 95% as determined by HPLC with diode array detector and mass spectrometry (see supporting information).

Fig. 2 Spores of the fungus producing the compounds **1**–**3**. The cylindrical, club-shaped spores are highly segmented vertically and horizontally as it is typical for *Alternaria* sp. Sporulation was induced through exposure to UV-A radiation (Wei et al. 1985). Bar = 10 µM

Cell culture

BEAS-2B (ATCC CRL-9609) cells were cultivated in DMEM supplemented with 10% FCS, 65 µg/mL penicillin G, and 100 µg/mL streptomycin at 37 °C and 5% CO_2. Benzoquinone was purchased from Sigma-Aldrich (B10358).

Cytotoxicity

Cytotoxic effects of the compounds on BEAS-2B cells were assessed after 24 h via XTT cell viability assay (Roehm et al. 1991). Briefly, 5×10^4 cells/mL were seeded into 24-well plates and incubated 24 h at standard culture conditions. The medium was then removed and replaced by medium with or without the compounds. After 24 h incubation at 37 °C, 5% CO_2, 0.5 mL of the medium was removed and replaced by 0.25 mL of prewarmed medium containing 25 µM phenazine methosulfate and 1 mg/mL XTT. Absorbance at 480 nm was measured after 3 h.

Reporter gene assay

A triple human ARE sequence was synthesized (Sigma Aldrich) with compatible restriction enzyme sites for Sac1 and Nhe1 and cloned into a pTA-Luc backbone (Clontech) (forward 5′CATGCAGTCACAGTGACTCAGCAGAATCTGATGCAGTCACAGTGACTCAGCAGAATCTGATGCAGTCACAGTGACTCAGCAGAATCTGG 3′, reverse 5′CTAGCCAGATTCTGCTGAGTCACTGTGACTGCATCAGATTCTGCTGAGTCACTGTGACTGCATCAGATTCTGCTGAGTCACTGTGACTGCATGAGCT 3′). Plasmid DNA (50 µg) was transfected in 3.5×10^7 cells/mL by electroporation (Nepagene, Nepa 21) in 400 µL of DMEM as described in the supporting information. The cells were then suspended in DMEM supplemented with 10% FCS and antibiotics at 1×10^6 cells/mL and seeded into plates. After 24 h of incubation, the medium was replaced by DMEM with 10% FCS and antibiotics with and without compounds. After further incubation for 24 h, the luciferase expression was analyzed using Dual-Glo luciferase assay system (Promega) in a plate luminometer (BMG Labtech). The CXCL10 promoter (−875 to +97 relative to the transcriptional start site) reporter plasmid has been described previously (Rohr et al. 2017). BEAS-2B cells were electroporated as described above, and luciferase expression was induced with 10 ng/mL TNF-α, 10 ng/mL IFN-γ, and 5 ng/mL IL-1β.

Dichlorodihydrofluorescein diacetate assay

A dichlorodihydrofluorescein diacetate assay was performed to detect the changes in redox status of the cells caused by the compounds. BEAS-2B cells were seeded in black 96-well plates (5000 cells/well) and incubated for 24 h under standard conditions. 2,7-Dichlorodihydrofluorescein diacetate (Cayman Chemical) was diluted in serum-free cell culture medium without phenol red (Panserin 293S, PAN-Biotech) at a final concentration of 100 µM and applied to the cells. After 30 min at 37 °C, 5% CO_2, the medium was replaced by Panserin 293S with or without test compounds. After 60 min incubation at 37 °C, 5% CO_2, the fluorescence was measured (excitation 485 nm, emission 530 nm).

Comet assay

Comet assay was performed as previously described by Olive and Banáth with slight changes (Olive and Banáth 2006). BEAS-2B were seeded into a 6-well plate and incubated with the respective compound for 3 h. Cells were then detached mechanically with a cell scraper. After centrifugation (1000 × g, 10 min, 4 °C), cells were resuspended in cold PBS to a density of 2×10^4 cells/mL. Microscope slides were prepared by pre-coating them with 1% agarose in ddH_2O (Agarose LE, Genaxxon bioscience). The cell suspension (400 µL) was mixed with 1.4 mL of 1% agarose (40 °C) and pipetted on the microscopic slide. Cell lysis was performed under alkaline conditions in a buffer containing 1.2 M NaCl, 100 mM EDTA, 1% Triton-X 100, and 300 mM NaOH for 18–20 h at 4 °C. Before electrophoresis, slides were washed with electrophoresis buffer (30 mM NaOH, 2 mM Na_2EDTA) three times for 20 min to remove residual salts. Electrophoresis was performed at 0.6 V/cm for 30 min. Slides were rinsed with ddH_2O before staining with 2.5 µg/mL propidium iodide. Imaging was done with an Olympus BX53 system with MC50 Microscope Camera (Zeiss). Analysis was performed with CometScore (TriTek).

Quantitative real-time PCR

To test for alterations in expression of selected antioxidative genes, BEAS-2B cells were seeded in plates and grown to 70% confluence. The medium was then replaced by fresh DMEM containing 10% FCS and antibiotics with and without test compounds. After incubation for 8 or 16 h, the medium was removed. Cells were washed with PBS and scraped off the plate. RNA extraction was performed using the GenUP™ Total RNA Kit (Biotechrabbit) according to manufacturer's instructions. First-strand cDNA was generated using M-MLV Reverse Transcriptase (Promega) according to the manual. Relative mRNA levels were detected using 5 × HOT FIREPol® EvaGreen® qPCR Supermix (Solis Biodyne) and specific primers (see supporting information) using StepOnePlus real-time PCR System (Thermo Fisher Scientific). The following protocol was used for quantitative amplification: initial inactivation for 12 min at 95 °C; 15 s at 95 °C, 30 s at 56 °C, 30 s at 72 °C for 40 cycles. Relative mRNA levels were calculated using ΔΔCt (Livak and Schmittgen 2001).

To test for antioxidative properties, BEAS-2B cells were seeded in plates and grown to 70% confluence. The medium was then replaced with medium containing 30 µM benzoquinone to induce oxidative stress, and compounds were added additionally, if applicable. Cells without benzoquinone and test compounds were used as control. After 16 h, RNA isolation and quantitative real-time PCR was performed as described before.

Western blot analysis

BEAS-2B cells were seeded into 100 mm dishes and incubated until they reached 70% confluence. The medium was then removed and replaced by medium with or without test substances. After 16 h, the medium was removed. The cells were then washed with PBS and lysed in ice cold RIPA buffer (150 mM NaCl, 50 mM Tris pH 7.4, 1% Nonidet P-40, 0.1% SDS, 0.5% sodium deoxycholate, 5 mM EDTA) supplemented with 1 × protease inhibitor cocktail (completeTM EDTA free Protease Inhibitor Cocktail, Roche). Cell debris was removed by centrifugation (8000 × g, 10 min, 4 °C) and protein content determined using the PierceTM BCA Protein Assay kit (Thermo Fisher Scientific) according to the manual. Lysates were then mixed with equal amounts of 50 mM DTT, 50 mM Na_2CO_3, 2.5% (w/v) SDS, and 15% (w/v) sucrose and boiled for 5 min at 95 °C. Equal amounts of protein were then separated on a 10% SDS–polyacrylamide gel and subsequently transferred to a nitrocellulose membrane. Primary antibodies used to detect protein of interest were anti-Nrf2 (MABC1556, Sigma-Aldrich, 1:2,000), anti-HMOX1 (ZRB1609, Sigma-Aldrich, 1:2,000), anti-TrxR1 (sc-28321, Santa Cruz Biotechnology, 1:500), anti-NQO1 (sc-32793, Santa Cruz Biotechnology, 1:500), anti-GAPDH (sc-47724, Santa Cruz Biotechnology, 1:1,000). Secondary antibodies used were anti-mouse (sc-516102, Santa Cruz Biotechnology, 1:10,000) and anti-rabbit HRP (A9169, Sigma-Aldrich, 1:60,000).

Statistical analysis

Significance of quantitative real-time PCR, dichlorodihydrofluorescein diacetate (DCF-DA), and reporter gene assay results was evaluated via one sample two-sided *t*-test. Multiple testing correction was performed according to Benjamini and Hochberg (1995). Significance of comet assay was evaluated using Welch's *t*-test after transforming the data

using the logit-function. Analyses were performed using OriginPro 2021 (OriginLab Corporation) and Microsoft Excel (Microsoft Corporation).

NMR spectroscopy

NMR spectra were recorded on a Bruker Avance-III (^{1}H NMR: 600 MHz, ^{13}C NMR: 151 MHz) spectrometer. All chemical shifts are referenced to the signal of the residual solvent (CD_3OD: 3.35 ppm and 49.3 ppm for ^{1}H NMR and ^{13}C NMR, respectively) and reported in parts per million (ppm) relative to tetramethylsilane (TMS). For multiplicities of NMR signals, the following abbreviations were used: s = singlet, d = doublet, t = triplet, q = quartet, m = multiplet, and combinations thereof. Spectra were processed with the software MestReNova from MestrelabResearch.

Mass spectrometry

Electrospray ionization (ESI) mass spectra were measured on an Agilent Infinity II 1200. Mixtures of water (containing 0.1% formic acid) and acetonitrile at a flow rate of 1.0 mL/min were used as eluent. An Ascentis Express C18 column from Supelco (2.7 µm particle size, 3 cm column length, 2.1 mm diameter) was used at a temperature of 40 °C. High-resolution electrospray ionization (HR-ESI) spectra were recorded on an Agilent 6545 QTOF-LC/MS with a suitable external calibrant.

Infrared spectra

Infrared (IR) spectra were recorded on a FT-IR spectrometer (Bruker Tensor 27) with a diamond ATR unit and are reported in terms of frequency of absorption $\tilde{\nu}$ (cm^{-1}).

Optical activity

The optical activity of chiral compounds was determined using a Perkin-Elmer 241 MS polarimeter.

The electronic circular dichroism (ECD) spectra of compounds (+)-**1** and (+)-**3** were recorded on a JASCO J-815 spectrometer equipped with a JASCO PTC-423S/15 temperature controller at 20 °C. Each compound was measured using a scanning speed of 50 nm/min. Each measurement was repeated five times, and the five replicates were averaged. Applying the same parameters, the solvent background was recorded and subtracted from the sample measurement.

For the simulation of compound **1** and **3**, a conformational analysis was first performed (Spartan'10; Wavefunction, Inc., Irvine, CA, USA, 2009), followed by geometry refinement at DFT level. Even though both compounds are fairly rigid, several conformers in the range of 4.5 kcal/mol above the energetically lowest conformer were identified from the respective set of the conformer distribution. After calculation of the electronic excitations using time-dependent DFT and Boltzmann weighting, the ECD spectra were simulated and compared to the experimental spectra (see supporting information for computational details). All quantum mechanical calculations were performed with Gaussian 16 (Frisch et al. 2019), while the spectra comparison was conducted using SpecDis (Bruhn et al 2017).

Results and discussion

Structure elucidation

Four major compounds were isolated from the crude extract by preparative HPLC. The largest fraction proved to mainly consist of well-known altertoxin I (Stinson et al. 1982) with all analytical data matching the literature. Additionally, three further compounds (+)-**1**–(+)-**3** were isolated (Table 1; Fig. 3). The structure of (+)-**1** appears to be a reduced form of the previously described stemphyltoxin III (Arnone et al. 1986). Compounds (+)-**2** and (+)-**3** have also not been described before in literature to the best of our knowledge. Unfortunately, all attempts to crystallize compounds **1**–**3** from various solvents were unsuccessful.

Compound (+)-**1** was isolated as an amorphous yellow solid. Its molecular formula was determined to be $C_{20}H_{14}O_6$ by HR-ESI–MS (calc. for $[C_{20}H_{14}O6–H]^-$: $m/z = 349.0717$, found: 349.0715), and ^{1}H-,^{13}C-, and 2D-NMR spectroscopy enabled the complete assignment of all carbon and proton signals. The ^{13}C-, HSQC-, and HMBC-NMR spectra showed 20 carbon signals assigned to 12 aromatic carbons of which four are protonated, and one conjugated ketone carbonyl.

The COSY correlations of H-5/H-6 (6.85 ppm and 7.66 ppm) and H-7/H-8 (8.02 ppm and 7.02 ppm) along with their appearance as four doublets possessing coupling constants of 8.4 Hz and 8.8 Hz, respectively, revealed the presence of two 1,2,3,4-tetrasubstituted benzene moieties. The HMBC correlations from H-6 (7.66 ppm) to C-6b (126.7 ppm) and from H-7 (8.02 ppm) to C-6a (125.6 ppm) suggested the presence of a C-6a/C-6b linkage. Moreover, the observed HMBC correlations from H-6 (7.66 ppm) to C-4 (158.2 ppm) and from H-7 (8.02 ppm) to C-9 (162.0 ppm) revealed the presence of a 4,4′-dihydroxybiphenylic system. The COSY correlations of H-11/H-12 (6.51 ppm and 7.68 ppm) with the downfield-shifted carbon C-12 (148.7 ppm) suggests another double bond being attached to a carbonyl C-10 (191.6 ppm). The HMBC contacts from H-11 (6.51 ppm) and H-8 (7.02 ppm) to carbon C-9a (114.0 ppm) show that this conjugated ketone is attached to carbon C-9a (114.0 ppm) via the carbonyl group. Further HMBC contacts from H-11 (6.51 ppm) to the oxygenated quaternary carbon C-12a (67.1 ppm) and

Table 1 Structural formulars of compounds (+)-**1**–(+)-**3** and assignment of ^{1}H (600 MHz) and ^{13}C 150 MHz) signals measured in methanol-*d4* at 294 K

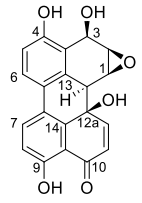

(+)-**1**

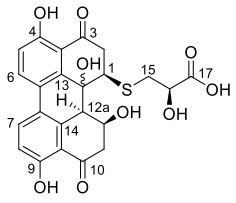

(+)-**2**

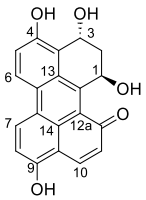

(+)-**3**

(+)-**1**			(+)-**2**			(+)-**3**		
#	H	C	#	H	C	#	H	C
1	3.99 (d, *J* = 3.7 Hz)	51.0	1	4.70 (t, *J* = 3.3 Hz)	52.0	1	5.96 (t, *J* = 3.4 Hz)	64.1
2	3.59–3.57 (m)	57.0	2	3.73 (dd, *J* = 17.3, 3.3 Hz) + 3.11 (dd, *J* = 17.3, 3.3 Hz)	41.6	2	2.75 (ddd, *J* = 13.0, 5.0, 3.4 Hz, $H_{ax.}$) + 2.20 (ddd, *J* = 13.0, 11.2, 3.4 Hz, Heq.)	40.4
3	5.18 (t, *J* = 1.5 Hz)	62.7	3		205.2	3	5.68 (dd, *J* = 11.2, 5.0 Hz)	66.3
3a		123.4	3a		115.7	3a		120.8
4		158.2	4		163.2	4		155.8
5	6.85 (d, *J* = 8.4 Hz)	115.4	5	7.03 (d, *J* = 8.8 Hz)	120.2	5	7.42 (d, *J* = 9.2 Hz)	122.8
6	7.66 (d, *J* = 8.4 Hz)	125.3	6	8.01 (d, *J* = 8.8 Hz)	133.2	6	8.72 (d, *J* = 9.2 Hz)	124.6
6a		125.6	6a		125.6	6a		128.1
6b		126.7	6b		125.3	6b		123.5
7	8.02 (d, *J* = 8.8 Hz)	133.1	7	7.97 (d, *J* = 8.8 Hz)	133.4	7	9.07 (d, *J* = 9.3 Hz)	134.4
8	7.03 (d, *J* = 8.8 Hz)	119.1	8	6.93 (d, *J* = 8.8 Hz)	117.3	8	7.41 (d, *J* = 9.3 Hz)	120.0
9		162.0	9		163.1	9		167.8
9a		114.0	9a		118.1	9a		112.8
10		191.6	10		205.2	10	8.74 (d, *J* = 10.0 Hz)	140.8
11	6.51 (d, *J* = 10.3 Hz)	129.6	11	3.05–2.95 (m)	48.7	11	6.98 (d, *J* = 10.0 Hz)	127.9
12	7.68 (d, *J* = 10.3 Hz)	148.7	12	4.68–4.63 (m)	67.3	12		190.0
12a		67.1	12a	4.15 (d, *J* = 8.3 Hz)	48.7	12a		123.9
12b	3.38–3.35 (m)	43.7	12b		73.1	12b		141.0
13		128.0	13		138.0	13		127.7
14		140.2	14		139.0	14		126.1
			15	3.22–3.15 (m) + 3.05–2.95 (m)	38.0			
			16	4.32 (dd, *J* = 6.9, 4.3 Hz)	72.2			
			17		176.8			

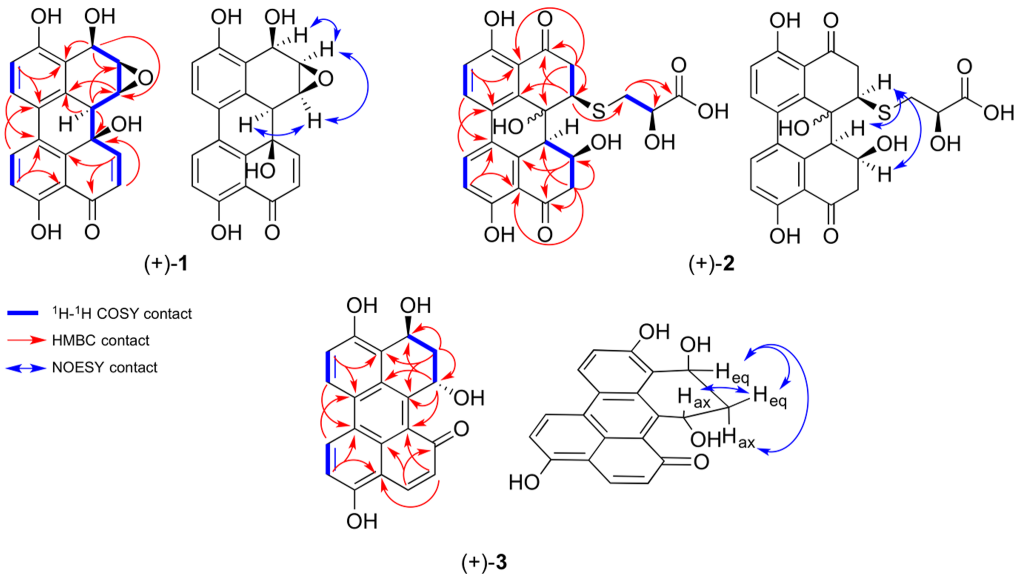

Fig. 3 Graphic display of key ^{1}H–^{1}H COSY, HMBC, and NOESY contacts of compounds (+)-**1**–(+)-**3**. COSY contacts: bold blue, HMBC contacts: single headed red arrows, NOESY-contacts: double headed blue arrows

from H-12 (7.68 ppm) to the quaternary aromatic carbon C-14 (140.2 ppm) lead to the conclusion that one aromatic core is annealed with a cyclohexenone moiety, suggesting this compound to be also structurally related to the altertoxin family members.

The remaining signals belong to a tertiary hydrogen H-12b (3.38–3.35 ppm) and to three secondary hydrogens H-1–H-3 (3.99 ppm, 3.59–3.57 ppm, and 5.18 ppm) attached to the oxygenated carbons C-1–C-3 (51.0 ppm, 57.0 ppm, and 62.7 ppm). However, the molecular formula has only two more oxygen atoms, thereby indicating the presence of an epoxide functionality. The HMBC contacts from H-12b (3.38–3.35 ppm) and H-1 (3.99 ppm) to quaternary aromatic carbon C-13 (128.0 ppm) together with the HMBC contacts from H-3 (5.18 ppm) to quaternary aromatic carbon C-3a (123.4) and oxygenated carbons C-2 and C-3 (57.0 ppm and 62.7 ppm) led to the complete assignment of structure (+)-**1**.

The relative stereochemistry was deduced by NOESY-NMR spectroscopy. NOESY contacts from H-12b (3.38–3.35 ppm) to H-1 (3.99 ppm), from H-1 (3.99 ppm) to H-2 (3.59–3.57 ppm), and from H-2 (3.59–3.57 ppm) to H-3 (5.18 ppm) indicate that protons H-1–H-3 (3.99 ppm, 3.59–3.57 ppm and 5.18 ppm) and H-12b (3.38–3.35 ppm) share the same side of the molecule. The absolute configuration of compound (+)-**1** was tentatively determined to (1*S*,2*R*,3*R*,12a*R*,12b*S*) by comparing measured and calculated electronic circular dichroism (ECD) spectra (see supporting information for detailed results).

Compound (+)-**2** was isolated as an amorphous yellow solid. Its molecular formula was determined to be $C_{23}H_{20}O_9S$ by HR-ESI–MS (calc. for $[C_{23}H_{20}O_9S–H]^-$: $m/z = 471.0755$, found: 471.0739), and ^{1}H-, ^{13}C-, and 2D-NMR spectroscopy enabled the complete assignment of all carbon and proton signals. The ^{13}C-, HSQC-, and HMBC-NMR spectra showed 23 carbon signals assigned to three methylenes, 12 aromatic carbons of which four are protonated, two conjugated ketone carbonyls, and one carboxyl carbon.

The COSY correlations of H-5/H-6 (7.03 ppm and 8.01 ppm) and H-7/H-8 (7.97 ppm and 6.93 ppm) along with their appearance as four doublets possessing a coupling constant of 8.8 Hz revealed the presence of two 1,2,3,4-tetrasubstituted benzene moieties. The HMBC correlations from H-6 (8.01 ppm) to C-6b (125.3 ppm) and from H-7 (7.97 ppm) to C-6a (125.6 ppm) suggested that there is a C-6a/C-6b linkage. Moreover, the observed HMBC correlations from H-6 (8.01 ppm) to C-4 (163.2 ppm) and from H-7 (7.97 ppm) to C-9 (163.1 ppm) revealed the presence of a 4,4′-dihydroxybiphenylic system. The observed HMBC correlations from H-2 (3.73 ppm and 3.09 ppm) to C-1 (52.0 ppm), C-12b (73.1 ppm), C-3a (115.7 ppm) and carbonyl C-3 (205.2 ppm) alongside the HMBC correlations from H-11 (3.05–3.01 ppm) to C-12a

(48.6 ppm), C-12 (67.3 ppm), C-9a (118.1 ppm), and carbonyl C-10 (205.1 ppm) lead to the conclusion that the core structure of compound **2** is also similar to that of the altertoxin natural products.

The chemical shifts of C-12 (67.3 ppm) and C-12b (73.1) furthermore indicate hydroxyl groups at this position. The observed chemical shift of C-1 (52.0 ppm) together with the HRMS experiment and the HMBC correlation of H15 (3.18 ppm and 3.02–2.98 ppm) to C-1 (52.0) suggests that the remaining part of the molecule is linked via a thioether bridge at C-1 (52.0 ppm). The COSY correlation between H-15 (3.18 ppm and 3.02–2.98 ppm) and H-16 (4.32 ppm) alongside their HMBC contacts to the carboxyl C-17 (176.8 ppm) unambiguously shows the presence of a 3-mercaptolactate moiety.

The relative stereochemistry was partly deduced by NOESY-NMR spectroscopy. Strong NOESY contacts from H-1 (4.70 ppm) to H-12 (4.69–4.62 ppm) and H-12a (4.15 ppm) indicate that these protons show to the same side of the molecule (see supporting information for detailed results). As compound (+)-**2** was isolated from a fungus, we assumed the stereogenic center at C-16 (72.2 ppm) to possess a *R*-configuration, as lower fungi predominantly produce D-3-mercaptolactate (Meng et al. 2013). A related compound was isolated in 2020 in the Rychlik group from *Alternaria alternata*; however, the orientation of the hydroxy group was not determined here either (Gotthardt 2020). With the protons of the 1-, 12-, and 12a-position showing to the same side of the molecule but the orientation of the hydroxyl group at the 12b-position remaining unclear, the absolute configuration of (+)-**2** could not unequivocally be determined.

Compound (+)-**3** was isolated as an amorphous orange-red solid. Its molecular formula was determined to be $C_{20}H_{14}O_5$ by HR-ESI–MS (calc. for $[C_{20}H_{14}O_5–H]^-$: $m/z = 333.0768$, found: 333.0763) and intensive ^{1}H-, ^{13}C-, and 2D-NMR spectroscopy enabled the complete assignment of all carbon and proton signals. The ^{13}C-, HSQC-, and HMBC-NMR spectra showed 20 carbon signals assigned to one methylene, 14 aromatic carbons of which four are protonated, and one conjugated ketone carbonyl.

The COSY correlations of H-5/H-6 (7.42 ppm and 8.72 ppm) and H-7/H-8 (9.07 ppm and 7.41 ppm) along with their appearance as four doublets possessing coupling constant of 9.2 Hz and 9.3 Hz, respectively, revealed the presence of two 1,2,3,4-tetrasubstituted benzene moieties. The HMBC correlations from H-6 (8.72 ppm) to C-6b (123.5 ppm) and from H-7 (9.07 ppm) to C-6a (128.1 ppm) suggested that there is a C-6a/C-6b linkage. Moreover, the observed HMBC correlations from H-6 (8.72 ppm) to C-4 (155.8 ppm) and from H-7 (9.07 ppm) to C-9 (167.8 ppm) revealed the presence of a 4,4′-dihydroxybiphenylic system. The observed HMBC correlations from H-2 (2.75 ppm and 2.20 ppm) and H-3 (5.68 ppm) to C-3a (115.7 ppm) and the downfield shifted carbons C-1 (64.1 ppm) and C-3 (66.3 ppm), alongside the COSY correlations from H-2 (2.75 ppm and 2.20 ppm) to both, H-1 (5.96 ppm) and H-3 (5.68 ppm), lead to the conclusion that a 1,3-propanediol chain can only be attached to carbon C-3a (115.7 ppm) via carbon C-3 (66.3 ppm).

The COSY correlation of H-10/H-11 (8.74 ppm and 6.98 ppm) and the HMBC contacts from H-10 (8.74 ppm) to C-12 (190.0 ppm) and C-14 (126.1 ppm), alongside the downfield shift of C-10 (140.8), unambiguously show the presence of an α,β-unsaturated ketone attached to carbon C-9a (112.8 ppm) via carbon C-10 (140.8 ppm). Four further HMBC contacts from H-11 (6.98 ppm) to aromatic carbon C-12a (123.9) and from H-1 (5.96 ppm) to aromatic carbons C-12a (123.9 ppm), C-12b (141.0 ppm), and C-13 (127.6 ppm) indicated that compound (+)-**3** share a partially saturated perylenone core structure.

The relative stereochemistry was deduced by the coupling constants of H-1 (5.96 ppm) and H-3 (5.68 ppm). While H-1 (5.96 ppm) appears as a pseudo-triplet with a coupling constant of 3.4 Hz and therefore likely occupies an equatorial position, H-3 (5.68 ppm) forms a clean doublet of doublets with coupling constants of 11.2 Hz and 5.0 Hz, thereby indicating an axial position of H-3. Consequently, the hydroxyl groups at C-1 (64.1 ppm) and C-3 (66.3 ppm) take up a *trans* relationship. The absolute configuration of (+)-**3** was tentatively determined as (1*R*,3*R*) by means of ECD and quantum mechanical calculations as previously described (see the supporting information for detailed results).

Biological activities

During a screening for biologically active compounds, we found that the crude extracts and extract fractions of *Alternaria* spec. showed effects on an ARE-transcriptional reporter carrying a triple ARE. The reporter plasmid was transiently transfected into BEAS-2B cells. As positive control, *p*-benzoquinone was applied to the cells which induces reactive oxygen species formation. Subjecting BEAS-2B to benzoquinone has been previously shown to induce Nrf2 expression and ARE reporter activity leading to elevated levels of Nrf2-dependent proteins (Rubio et al. 2011). After activity guided purification of three compounds, the same reporter was used to confirm the activity observed in the crude extract and its fractions. The fungus produced several perylene quinones; however, compound (+)-**2** was only obtained in minute amounts and could therefore not be subjected to further biological testing.

The cytotoxicity of the isolated compounds was assessed through an XTT cell viability assay for BEAS-2B cells. The strongest effect was observed after application of compound (+)-**1** ($LC_{50} = 3.8 \pm 0.13$ µM), ATX-I also showed strong

cytotoxic effects (LC_{50} = 6.43 ± 0.86 µM), while compound (+)-**3** had no effects on the viability of the cells (Fig. 4). The effect of higher concentrations could not be analyzed because of the limited solubility of the compounds in the cell culture medium.

Compound (+)-**1**, ATX-I, and compound (+)-**3** showed modulation of the ARE reporter activity albeit with different specificity. As a control 30 µM benzoquinone was applied to induce the ARE reporter. Benzoquinone mediates the release of Nrf2 from KEAP and subsequently the induction of ARE-dependent gene expression in BEAS-2B cells (Rubio et al. 2011). Upon treatment with benzoquinone, the luciferase levels increased to 2.8 ± 0.4-fold compared to the untreated control (Fig. 5). ATX-I and (+)-**1** displayed concentration-dependent activation of the triple ARE transcriptional reporter. ATX-I exhibited the strongest effect to the ARE reporter with an induction of 5.0 ± 0.15-fold at 3 µM, while (+)-**1** induced to levels of 2.6 ± 0.19-fold at the same concentration. Application of higher concentrations of ATX-I and (+)-**1** led to a massive drop of luciferase activity, presumably due to cytotoxic effects. Induction of ARE by ATX-I was previously tested in reporter gene assays by Jarolim et al. (2017a) in CHO cells, where application of up to 5 µM did not lead to significant induction of luciferase levels (Jarolim et al. 2017b). In contrast, we observed a significant induction of Nrf2/ARE-dependent luciferase expression after application of 3 µM ATX-I in the bronchial epithelial cell line BEAS-2B which may be due to a higher sensitivity to the compound and/or differences in the expression and activation of NRF2 in various normal and transformed cell lines (Kitamura and Motohashi 2018).

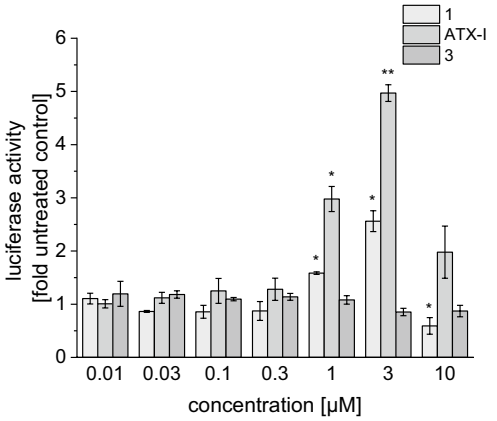

Fig. 5 Effect of compounds **1**, ATX-I, and **3** on ARE reporter gene activity in BEAS-2B cells. Cells were transiently transfected with an ARE dependent luciferase reporter construct by electroporation. BEAS-2B treated with 30 µM benzoquinone and untreated cells were used as control. Data are shown as mean ± SEM from three independent replicates

Interestingly compound (+)-**3** showed no significant induction of NRF2/ARE mediated luciferase expression in the reporter gene assay but strongly inhibited ARE-dependent reporter activity in BEAS-2B cells after induction of the antioxidative response with 30 µM benzoquinone (Fig. 6). The benzoquinone-induced luciferase expression was reduced by 70% compared to the untreated control at a concentration of 1 µM of compound (+)-**3**. Various synthetic and natural activators of the NRF2/ARE pathway

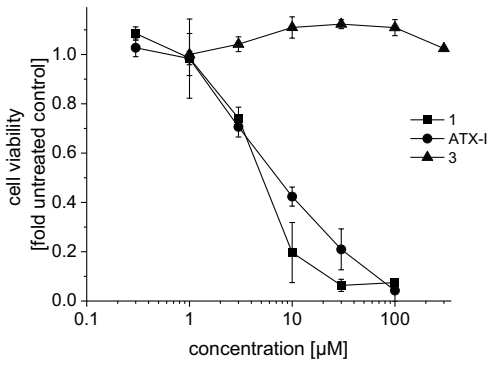

Fig. 4 Cytotoxic effects of compounds **1**, ATX-I, and **3** on BEAS-2B cells. Cytotoxicity was analyzed by XTT cell viability assay. Cells were incubated with compounds for 24 h. Untreated BEAS-2B cells were used as control. Data are shown as mean ± SEM from three independent replicates

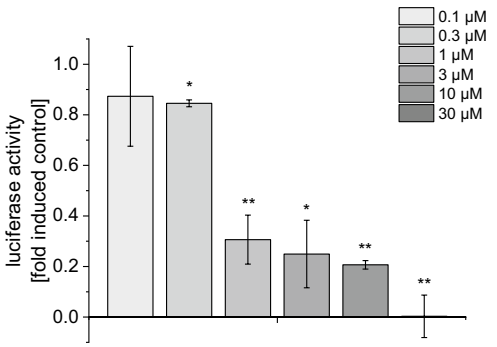

Fig. 6 Effect of compound **3** on ARE reporter activity after induction of oxidative stress with 30 µM benzoquinone. BEAS-2B cells treated with 30 µM benzoquinone were used as control. Untreated cells were used to determine basal activity of ARE construct. Data are shown as mean ± SEM from three independent replicates

including altertoxin II have been found to suppress production of pro-inflammatory cytokines by interfering with NF-κB and interferon signaling (Cuadrado et al. 2019; Del Favero et al. 2020; Ryan et al. 2022). We therefore investigated the effect of the isolated compounds on the TNF-α/IL-1β/IFN-γ inducible CXCL10 transcriptional reporter as a pro-inflammatory marker gene in transiently transfected BEAS-2B cells. The inducible expression of luciferase therefore reflects the cooperative induction of *cxcl10* mRNA expression by Stat1, NF-κB, and IRF3 transcription factors (Tamassia et al. 2007). Stimulation of transfected cells with 10 ng/mL TNF-α, 5 ng/mL IL-1β, and 10 ng/mL IFN-γ increased the luciferase activity sixfold compared to the uninduced control. None of the isolated compounds significantly affected the inducible expression of the CXCL10 promoter activity up to the highest concentrations tested (0.3 µM for ATX-I and (+)-**1**, 3 µM for (+)-**3**), indicating that the compounds do not display anti-inflammatory properties (see supplementary information). To investigate the oxidative properties of the compounds, we used a dichlorodihydrofluorescein diacetate assay as described in the "Materials and methods" section. The fluorescence measurement was performed after 60 min. As positive control 30 µM *p*-benzoquinone was applied to the BEAS-2B cells which led to significantly elevated fluorescence levels compared to the untreated control. Compound (+)-**1**, ATX-I, and (+)-**3** were applied in concentrations of 3 µM, 10 µM, and 30 µM (Fig. 7A). Application of compound (+)-**1** and ATX-I led to a strong increase of fluorescence in a concentration dependent manner, whereas application of (+)-**3** only slightly affected fluorescence levels in comparison to the untreated control. We assume that the rather small increase in fluorescence after application of up to 30 µM of (+)-**3** may be caused by the reaction of the compound with the DCF radical which is generated during the reaction of DCFH-DA to the fluorescent DCF and can lead to self-propagating redox cycling (Kalyanaraman et al. 2012). Also, with this assay, only the total redox state of the cells can be detected. DCFH-DA reacts with a variety of reactive species like hydroxyl radicals, hypochlorous acid, and nitrogen dioxide leading to a rather low specificity (Kalyanaraman et al. 2012). However, regardless of these limitations, it can be assumed that compound (+)-**1** and ATX-I cause a significant shift in the redox state in BEAS-2B cells.

The induction of oxidative stress by various *Alternaria* perylenquinones such altertoxin II and stemphyltoxin III has been implicated in the DNA-damaging properties of these compounds (Aichinger et al. 2021). To analyze possible DNA damage caused by application of the isolated compounds, a comet assay was conducted. The percentage of DNA in head and in tail is visualized in Fig. 7B. Application of 60 µM benzoquinone and either 10 µM compound (+)-**1**, ATX-I, and compound (+)-**3** resulted in a significant increase in tail DNA (BQ: 75 ± 5%, (+)-**1**: 77.8 ± 9.2%, ATX-I: 84.6 ± 4.2%, (+)-**3**: 73.2 ± 11.9%), indicating increased rates of double and single strand breaks.

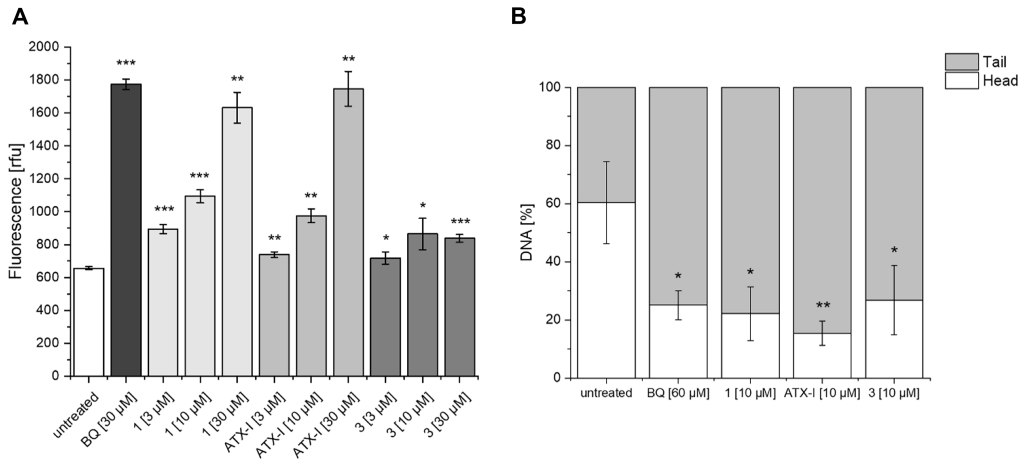

Fig. 7 Influence of **1**, ATX-I, and **3** on redox state of BEAS-2B cells. **A** 2,7-Dichlorodihydrofluorescein diacetate was applied to the cells; after 30 min, it was replaced by serum-free medium with and without test compounds. After 60 min, the fluorescence was measured. Data are shown as mean ± SEM from three independent replicates. $*p < 0.05$, $**p < 0.01$, $***p < 0.001$. **B** BEAS-2B cells were treated with the indicated compounds for 3 h. After cell lysis, alkaline comet assay was performed. Percentage of DNA in head and tail was analyzed using CometScore. Data are shown as mean ± SEM from three independent replicates. * < 0.05, ** < 0.01

Since all three tested compounds affected the triple ARE transcriptional reporter, we investigated their effect on the expression levels of selected NRF2/ARE-induced genes via quantitative real-time PCR (Ma 2013). Relative mRNA amounts were calculated in relation to expression of a housekeeping gene (*gapdh*) and compared to the untreated control. As shown in Fig. 8A–B, benzoquinone, compound (+)-**1**, and ATX-I strongly upregulated the mRNA levels of heme oxygenase-1 (*hmox1*), regardless of the incubation time. After 16 h, a slight upregulation of mRNA levels for NAD(P)H dehydrogenase (quinone) 1 (*nqo1*) could be observed. Application of compound (+)-**3** had almost no effect on the selected mRNA levels. After 16 h incubation with 3 µM of (+)-**3**, *sod3* mRNA levels were slightly elevated: To assess whether compound (+)-**3** inhibits NRF2/ARE mediated mRNA transcription, real-time PCR analyses were performed with cells co-treated for 16 h with compound (+)-**3** and 30 µM benzoquinone to induce oxidative stress. Compared to the untreated control, benzoquinone slightly induced the levels of all tested mRNAs. Application of compound (+)-**3** decreased the expression of all mRNAs analyzed starting at 1 µM with the strongest suppression of superoxide dismutase 3 (*sod3*) gene expression (Fig. 8C), an extracellular antioxidant enzyme which plays an essential role in the pathogenesis of inflammatory diseases and cancer (Nguyen et al. 2020; O´Leary et al. 2021).

To analyze the effect of the isolated compounds on levels of selected proteins involved in antioxidative response, cells were treated with compound (+)-**1**, ATX-I, and compound (+)-**3** for 16 h in comparison with benzoquinone. Cells were lysed, and protein extracts were then subjected to SDS-PAGE and western blotting. While there was no significant change in Nrf2 and Nqo1 levels, a strong upregulation of HMOX1 protein levels after treatment with 3 µM of compound (+)-**1** and ATX-I (Fig. 8D) could be detected. Accordingly, the upregulation of the *hmox1* mRNA levels observed during quantitative real-time PCR was also confirmed at the protein level. HMOX1 is a highly inducible enzyme which primarily functions in in heme catabolism, where it catalyzes the breakdown of heme into iron, biliverdin, and CO. Besides, it is involved in anti-oxidative and anti-inflammatory responses and is known to be upregulated by most cells in reaction to various stress conditions (Campbell et al. 2021). Strong upregulation of HMOX1 was also observed in many human cancers such as lung and gastric cancer where it plays an important role in cancer progression and resistance to anti-tumor therapy (Degese et al. 2012; Yin et al. 2012). In case of the compounds (+)-**1** and ATX-I, the induction of HMOX1 expression presumably is a coping mechanism due to the generation of oxidative stress.

In summary, we identified three new perylenequinones compounds (+)-**1**–**3** along with the previously isolated alternariol (ATX-1) from fermentations of an *Alternaria* species. The minor metabolite compound (+)-**2** contains an esterified

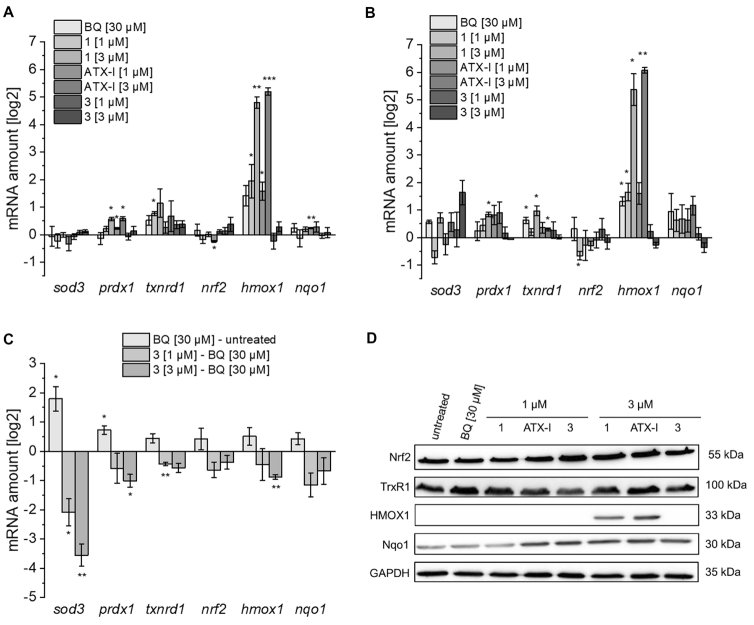

Fig. 8 Effects of compounds **1**, ATX-I, and **3** on mRNA expression and protein levels of selected ARE dependent genes in BEAS-2B cells. The cells were incubated with the compounds for 8 h (**A**) and 16 h (**B**), respectively. **C** Effect of compound **3** on mRNA expression levels of selected ARE dependent genes in BEAS-2B cells after induction of oxidative stress with benzoquinone. The cells were incubated with the compound for 16 h. All mRNA levels refer to *gapdh* as housekeeping control. Data are shown as mean ± standard deviation from three independent replicates. Asterisks indicate *q*-values of * < 0.05, and ** < 0.01. **D** Western blot analyses of selected anti-oxidative proteins. BEAS-2B cells were treated with indicated compounds for 16 h. GAPDH was detected as a housekeeping control

3-mercaptolactate group. Several sulfur-containing polyketides from fungi have been described so far which include pandangolide 3 (also bearing a mercaptolactate moiety) and pandangolide 4, where a sulfide bridge connects two macrocyclic polyketides, isolated from *Cladosporium herbarum* and the related thiocladospolides A-D from *Cladosporium cladosporoides* (Jadulco et al. 2001; Zhang et al. 2019). Also, the sulfur-containing curvularin derivatives sumalarins A-C, previously isolated from fermentations of *Penicillium sumatrense*, contain the same mercaptolactone moity (Meng et al. 2013). Recently, it has been shown that the spontaneous condensation of 10,11-dehydrocurvularin with 3-mercaptopyruvate originating from L-cysteine to cyclothiocurvularin followed by further oxidation to cyclosulfoxicurvularin may be a detoxification reaction under stress conditions (Castro et al. 2016). Therefore, it seems conceivable that the production of the mercaptolactate-containing compound (+)-**2** also represents a detoxification process by the fungus to reduce toxicity of the altertoxins. Compound (+)-**1** and altertoxin I display cyctotoxic effects, oxidative properties, induce DNA damage, activate the NRF2/ARE pathway, and strongly upregulate heme oxygenase 1 expression on mRNA and protein level in BEAS-2B cells. Although the DNA-damaging properties of some altertoxins such as altertoxin II or stemphyltoxin III has been attributed to the occurrence the reactive epoxy moiety forming DNA-adducts (Soukup et al. 2020), we observed similar DNA-damaging properties of compound (+)-**1**, bearing an epoxy group, and altertoxin I in BEAS-2B cells. In contrast to compound (+)-**1** and altertoxin I, compound (+)-**3** exhibited no significant cytotoxicity and antagonized benzoquinone induced NRF2/ARE-dependent luciferase expression in BEAS-2B cells. In addition, compound (+)-**3** strongly inhibited ARE/NRF2 dependent *sod3* mRNA levels in benzoquinone induced BEAS-2B cells. These results indicate that compound (+)-**3** acts as a transcriptional inhibitor of NRF2/ARE signaling but the exact mode of action still has to be determined. In contrast to earlier reports for ATX II from Del Favero et al. (2020), no anti-inflammatory activity was observed after treatment with the tested Alternaria toxins in BEAS-2B cells using a CXCL-10 promoter dependent transcriptional reporter (see supplementary information).

Supplementary Information The online version contains supplementary material available at https://doi.org/10.1007/s12550-023-00495-1.

Acknowledgements We thank Anja Meffert for the kind support with the HPLC measurements. Parts of this research were conducted using the supercomputer Mogon offered by Johannes Gutenberg University Mainz (hpc.uni-mainz.de), which is a member of the AHRP (Alliance for High Performance Computing in Rhineland Palatinate, www.ahrp.info) and the Gauss Alliance e.V. The authors gratefully acknowledge the computing time granted.

Funding Open Access funding enabled and organized by Projekt DEAL. This work was supported by a grant from the Rhineland Palatinate Ministry for Science and Health (Forschungskolleg NeurodegX).

Declarations

Conflict of interest The authors declare no competing interests.

References

Agostinis P, Berg K, Cengel KA, Foster TH, Girotti AW, Gollnick SO et al (2011) Photodynamic therapy of cancer: an update. CA Cancer J Clin 61:250–281. https://doi.org/10.3322/caac.20114

Aichinger G, Del Favero G, Warth B, Marko D (2021) Alternaria toxins-still emerging? Compr Rev Food Sci Food Saf 20:4390–4406. https://doi.org/10.1111/1541-4337.12803

Arcella D, Eskola M, Gómez R, Jose A (2016) Dietary exposure assessment to Alternaria toxins in the European population. EFSA J 14:4654. https://doi.org/10.2903/j.efsa.2016.4654

Arnone A, Nasini G, Merlini L, Assante G (1986) Secondary mould metabolites. Part 16. Stemphyltoxins, new reduced perylenequinone metabolites from Stemphylium botryosum var. Lactucum. J Chem Soc, Perkin Trans 1:525–530. https://doi.org/10.1039/P19860000525

Benjamini Y, Hochberg Y (1995) Controlling the false discovery rate: a practical and powerful approach to multiple testing. J R Statist Soc B 57:289–300. https://doi.org/10.1111/j.2517-6161.1995.tb02031.x

Bruhn T, Schaumlöffel A, Hemberger Y, Pecitelli G (2017) SpecDis version 1.71, Berlin, Germany. https://specdis-software.jimdo.com

Campbell NK, Fitzgerald HK, Dunne A (2021) Regulation of inflammation by the antioxidant haem oxygenase 1. Nat Rev Immunol 21:411–425. https://doi.org/10.1038/s41577-020-00491-x

Cuadrado A, Rojo AI, Wells G, Hayes JD, Cousin SP, Rumsey WL et al (2019) Therapeutic targeting of the NRF2 and KEAP1 partnership in chronic diseases. Nat Rev Drug Discov 18:295–317. https://doi.org/10.1038/s41573-018-0008-x

de Castro MV, Ióca LP, Williams DE, Costa BZ, Mizuno CM, Santos MFC et al (2016) Condensation of macrocyclic polyketides produced by Penicillium sp. DRF2 with mercaptopyruvate represents a new fungal detoxification pathway. J Nat Prod 79:1668–1678. https://doi.org/10.1021/acs.jnatprod.6b00295

Degese MS, Mendizabal JE, Gandini NA, Gutkind JS, Molinolo A, Hewitt SM, Curino AC, Coso OA, Facchinetti MM (2012) Expression of heme oxygenase-1 in non-small cell lung cancer (NSCLC) and its correlation with clinical data. Lung Cancer 77:168–175. https://doi.org/10.1016/j.lungcan.2012.02.016

Del Favero G, Hohenbichler J, Mayer RM, Rychlik M, Marko D (2020) Mycotoxin Altertoxin II induces lipid peroxidation connecting mitochondrial stress response to NF-κB inhibition in THP-1 macrophages. Chem Res Toxicol 33:492–504. https://doi.org/10.1021/acs.chemrestox.9b00378

Dolcet X, Llobet D, Pallares J, Matias-Guiu X (2005) NF-kB in development and progression of human cancer. Virchows Arch 446:475–482. https://doi.org/10.1007/s00428-005-1264-964-9
Fayter D, Corbett M, Heirs M, Fox D, Eastwood A (2010) A systematic review of photodynamic therapy in the treatment of pre-cancerous skin conditions, Barrett's oesophagus and cancers of the biliary tract, brain, head and neck, lung, oesophagus and skin. Health Technol Assess 14:1–288. https://doi.org/10.3310/hta14370
Frisch MJ, Trucks GW, Schlegel HB, Scuseria GE, Robb MA, Cheeseman JR et al (2019) Gaussian 16, Revision C.01, Wallingford, CT
Gao F, Bai Y, Ma SR, Liu F, Li ZS (2010) Systematic review: photodynamic therapy for unresectable cholangiocarcinoma. J Hepatobiliary Pancreat Sci 17:125–131. https://doi.org/10.1007/s00534-009-0109-3
Geiseler O, Müller M, Podlech J (2013) Synthesis of the altertoxin III framework. Tetrahedron 69:3683–3689. https://doi.org/10.1016/j.tet.2013.03.013
Gotthardt M (2020) Targeted and non-targeted studies on Alternaria alternata metabolites. With assistance of Michael Rychlik. München: Universitätsbibliothek der TU München
Hayes JD, McMahon M (2009) NRF2 and KEAP1 mutations: permanent activation of an adaptive response in cancer. Trends Biochem Sci 34:176–188. https://doi.org/10.1016/j.tibs.2008.12.008
Jadulco R, Proksch P, Wray VS, Berg A, Gräfe U (2001) New macrolides and furan carboxylic acid derivative from the sponge-derived fungus Cladosporium herbarum. J Nat Prod 64:527–530. https://doi.org/10.1021/np000401s
Janssen-Heininger YMW, Poynter ME, Aesif SW, Pantano C, Ather JL, Reynaert IL et al (2009) Nuclear factor kappaB, airway epithelium, and asthma: avenues for redox control. Proc Am Thorac Soc 6:249–255. https://doi.org/10.1513/pats.200806-054rm
Jarolim K, Del Favero G, Ellmer D, Stark TD, Hofmann T, Sulyok M, Humpf HU, Marko D (2017) Dual effectiveness of Alternaria but not Fusarium mycotoxins against human topoisomerase II and bacterial gyrase. Arch Toxicol 91:2007–2016. https://doi.org/10.1007/s00204-016-1855-z
Jarolim K, Del Favero G, Pahlke G, Dostal V, Zimmermann K, Heiss E, Ellmer D, Stark TD, Hofmann T, Marko D (2017b) Activation of the Nrf2-ARE pathway by the Alternaria alternata mycotoxins altertoxin I and II. Arch Toxicol 91:203–216. https://doi.org/10.1007/s00204-016-1726-7
Jiang Y, Leung AW, Wang X, Zhang H, Xu Ch (2014) Effect of photodynamic therapy with hypocrellin B on apoptosis, adhesion, and migration of cancer cells. Int J Radiat Biol 90:575–579. https://doi.org/10.3109/09553002.2014.906765
Kalyanaraman B, Darley-Usmar V, Davies KJA, Dennery PA, Forman HJ, Grisham MB, Mann GE, Moore K, Roberts LJ, Ischiropoulos H (2012) Measuring reactive oxygen and nitrogen species with fluorescent probes: challenges and limitations. Free Radic Biol Med 52:1–6. https://doi.org/10.1016/j.freeradbiomed.2011.09.030
Khiralla A, Mohammed AO, Yagi S (2022) Fungal Perylenequinones Mycol Progress 21:38. https://doi.org/10.1007/s11557-022-01790-4
Kitamura H, Motohashi H (2018) NRF2 addiction in cancer cells. Cancer Sci 109:900–911. https://doi.org/10.1111/cas.13537
Lee HB, Patriarca A, Magan N (2015) Alternaria in food: ecophysiology, mycotoxin production and toxicology. Mycobiology 43:93–106. https://doi.org/10.5941/MYCO.2015.43.2.93
Liu D, Coloe S, Baird R, Pederson J (2000) Rapid mini-preparation of fungal DNA for PCR. J Clin Microbiol 38:471. https://doi.org/10.1128/JCM.38.1.471-471.2000
Livak KJ, Schmittgen TD (2001) Analysis of relative gene expression data using real-time quantitative PCR and the 2(-Delta Delta C(T)) method. Methods 25:402–408. https://doi.org/10.1006/meth.2001.1262
Ma Q (2013) Role of nrf2 in oxidative stress and toxicity. Ann Rev Pharmacol Toxicol 53:401–426. https://doi.org/10.1146/annurev-pharmtox-011112-140320
Meng LH, Li XM, Lv CT, Li CS, Xu GM, Huang CG, Wang BG (2013) Sulfur-containing cytotoxic curvularin macrolides from Penicillium sumatrense MA-92, a fungus obtained from the rhizosphere of the mangrove Lumnitzera racemosa. J Nat Prod 76:2145–2149. https://doi.org/10.1021/np400614f
Morgan BJ, Dey S, Johnson SW, Kozlowski MC (2009) Design, synthesis, and investigation of protein kinase C inhibitors: total syntheses of (+)-calphostin D, (+)-phleichrome, cercosporin, and new photoactive perylenequinones. J Am Chem Soc 131:9413–9425. https://doi.org/10.1021/ja902324j
Morgan BJ, Mulrooney CA, O'Brien EM, Kozlowski MC (2010) Perylenequinone natural products: total syntheses of the diastereomers (+)-phleichrome and (+)-calphostin D by assembly of centro-chiral and axial chiral fragments. J Org Chem 75:30–43. https://doi.org/10.1021/jo901384h
Mulrooey CA, O'Brien EM, Morgan BJ, Kozlowski MC (2012) Perylenequinones: isolation, synthesis, and biological activity. Eur J Org Chem 3887–3904. https://doi.org/10.1002/ejoc.201200184
Nguyen NH, Tran GB, Nguyen CT (2020) Anti-oxidative effects of superoxide dismutase 3 on inflammatory diseases. J Mol Med 98:59–69. https://doi.org/10.1007/s00109-019-01845-2
O´Leary BR, Caroll RS, Steers GJ, Hrabe J, Domann FE, Cullen JJ, (2021) Impact of EcSOD perturbations in cancer progression. Antioxidants 10:1219. https://doi.org/10.3390/antiox10081219
Olive PL, Banáth JP (2006) The comet assay: a method to measure DNA damage in individual cells. Nat Protoc 1:23–29. https://doi.org/10.1038/nprot.2006.5
Pamukcu B, Lip GYH, Shantsila E (2011) The nuclear factor-kappa B pathway in atherosclerosis: a potential therapeutic target for atherothrombotic vascular disease. Thromb Res 128:117–123. https://doi.org/10.1016/j.thromres.2011.03.025
Pfaff D, Bestgen S, Podlech J (2017) Synthesis of cis- and trans-configured octahydroperylenes. Eur J Org Chem 37:5666–5670. https://doi.org/10.1002/ejoc.201701218
Qi S, Guo L, Yan S, Lee RJ, Yu S, Chen S (2019) Hypocrellin A-based photodynamic action induces apoptosis in A549 cells through ROS-mediated mitochondrial signaling pathway. Acta Pharm Sin B 9:279–293. https://doi.org/10.1016/j.apsb.2018.12.004
Roehm NW, Rodgers GH, Hatfield SM, Glasebrook AL (1991) An improved colorimetric assay for cell proliferation and viability utilizing the tetrazolium salt XTT. J Immunol Methods 142:257–265. https://doi.org/10.1016/0022-1759(91)90114-U
Rohr M, Oleinikov K, Jung M, Sandjo LP, Opatz T, Erkel G (2017) Anti-inflammatory tetraquinane diterpenoids from a *Crinipellis* species. Bioorg Med Chem 25:514–522. https://doi.org/10.1016/j.bmc.2016.11.016
Rubio V, Zhang J, Valverde M, Rojas E, Shi ZZ (2011) Essential role of Nrf2 in protection against hydroquinone- and benzoquinone-induced cytotoxicity. Toxicol in Vitro 25:521–529. https://doi.org/10.1016/j.tiv.2010.10.021
Ryan DG, Knatko EV, Casey AM, Hukelmann JL, Naidu SD, Brenes AJ et al (2022) Nrf2 activation reprograms macrophage intermediary metabolism and suppresses the type I interferon response. IScience 25:103827. https://doi.org/10.1016/j.isci.2022.103827
Sies H, Berndt C, Jones DP (2017) Oxidative stress. Annu Rev Biochem 86:715–748. https://doi.org/10.1146/annurev-biochem-061516-045037
Sies H, Jones DP (2020) Reactive oxygen species (ROS) as pleiotropic physiological signalling agents. Nat Rev Mol Cell Biol 21:363–383. https://doi.org/10.1038/s41580-020-0230-3
Soukup ST, Fleck SC, Pfeiffer E, Podlech J, Kulling SE, Metzler M (2020) DNA reactivity of altertoxin II: identification of two covalent guanine adducts formed under cell-free conditions. Toxicol Lett 331:75–81. https://doi.org/10.1016/j.toxlet.2020.05.018
Stack ME, Prival MJ (1986) Mutagenicity of the Alternaria metabolites altertoxins I, II, and III. Appl Environ Microbiol 52:718–722. https://doi.org/10.1128/aem.52.4.718-722.1986

Stinson EE, Osman SF, Pfeffer PE (1982) Structure of Altertoxin I, a mycotoxin from Alternaria. J Org Chem 47:4110–4113. https://doi.org/10.1021/jo00142a020

Tamassia N, Calzetti F, Ear T, Cloutier A, Gasperini S, Bazzoni F, McDonald PP, Cassatella MA (2007) Molecular mechanisms underlying the synergistic induction of CXCL10 by LPS and IFN-γ in human neutophils. Eur J Immunol 37:2627–2634. https://doi.org/10.1002/eji.200737340

Wakabayashi N, Slocum SL, Skoko JJ, Shin S, Kensler TW (2010) When NRF2 talks, who's listening? Antioxid Redox Signal 13:1649–1663. https://doi.org/10.1089/ars.2010.3216

Wei CI, Swartz DD, Cornell JA (1985) Effects of culture media, exposure time and temperature on near-ultraviolet-induced sporulation of Alternariaalternata. J Food Prot 48:316–319. https://doi.org/10.4315/0362-028X-48.4.316

Weiss U, Merlini L, Nasini G (1987) Naturally occurring perylenequinones. In: Progress in the chemistry of organic natural products. Springer, Vol 52:1–71. https://doi.org/10.1007/978-3-7091-8906-1_1

White TJ, Bruns T, Lee S, Taylor J (1990) Amplification and direct sequencing of fungal ribosomal RNA genes for phylogenetics. In: Innis MA, Gelfand DH, Sninsky JJ, White TJ (eds) PCR protocols: a guide to methods and applications. Academic Press, New York, 315–322. https://doi.org/10.1016/B978-0-12-372180-8.50042-1

Yin Y, Liu Q, Wang B, Chen G, Xu L, Zhou H (2012) Expression and function of heme oxygenase-1 in human gastric cancer. Exp Biol Med 237:362–371. https://doi.org/10.1258/ebm.2011.011193

Zhang FZ, Li XM, Yang SQ, Meng LH, Wang BG (2019) Thiocladospolides A-D, 12-membered macrolides from the mangrove-derived endophytic fungus Cladosporium cladosporioides MA-299 and structure revision of Pandangolide 3. J Nat Prod 82:1535–1541. https://doi.org/10.1021/acs.jnatprod.8b01091

7.3.2 Bestimmung der absoluten Konfiguration eines Dihydroxanthons

In Kooperation mit der Arbeitsgruppe [redacted] wurde neben dem bekannten Dihydroxanthon AGI-B4 (**160**, in der Publikation **1**) ein strukturell sehr ähnlicher Naturstoff **161** (in der Publikation **2**) mit demselben Grundgerüst aus einem Pilz der Gattung *Diaporthe* isoliert (Abbildung 7.9). Beide isolierten Verbindungen **160** und **161** zeigten entzündungshemmende Eigenschaften bei Verwendung der menschlichen MonoMac6-Zelllinie, indem sie in den JAK/Stat1- und den NFκB-Signalweg eingreifen und die dadurch induzierte Transkription von entzündungsfördernden Genen blockieren (Abbildung 7.9).

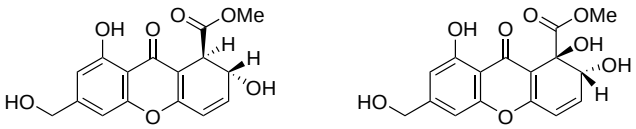

Abbildung 7.9: Isolierte Xanthone **160** und **161** aus Pilzen der Gattung *Diaporthe*.[565]

Da die relative Konfiguration des Dihydroxanthons **161** (in der Publikation **2**) nicht mittels 2D-NMR-Spektroskopie bestimmbar war, wurden die $\mathcal{J}$-DP4- und die DP4+-Methode von Sarotti *et al.* angewendet, um die relative Konfiguration der chiralen Kohlenstoff-Atome zu bestimmen.[458,469] Im Anschluss wurde die absolute Konfiguration auf Grundlage einer Benchmarkstudie von Stephens *et al.* mit einer Wahrscheinlichkeit >95% zugeordnet.[566] Dabei wurde der spezifische Drehwinkel mittels zeitabhängiger DFT berechnet und mit dem experimentellen Wert verglichen.[565]

Die Isolation der Naturstoffe sowie die biologischen Tests wurden von [redacted] und [redacted] durchgeführt. Die Strukturaufklärung mittels NMR-Spektroskopie wurde von [redacted] ausgeführt. Die Berechnung der chemischen Verschiebungskonstanten, die Anwendung der $\mathcal{J}$-DP4- und der DP4+-Methode sowie die Berechnung des spezifischen Drehwinkels erfolgte durch J. Groß. Das Manuskript wurde von allen Autoren erstellt.[17]

[17] *Reprinted with permission from M. Rohr, A. M. Kiefer, U. Kauhl, J. Gross, T. Opatz, G. Erkel, Biol. Chem. 2022, 403, 89–101. Copyright ©2022, De Gruyter.*

DE GRUYTER Biol. Chem. 2021; aop

Markus Rohr, Anna Maria Kiefer, Ulrich Kauhl, Jonathan Groß, Till Opatz* and Gerhard Erkel*

Anti-inflammatory dihydroxanthones from a *Diaporthe* species

https://doi.org/10.1515/hsz-2021-0192
Received March 12, 2021; accepted July 9, 2021;
published online August 2, 2021

Abstract: In a search for anti-inflammatory compounds from fungi inhibiting the promoter activity of the small chemokine CXCL10 (Interferon-inducible protein 10, IP-10) as a pro-inflammatory marker gene, the new dihydroxanthone methyl (1*R*, 2*R*)-1,2,8-trihydroxy-6-(hydroxymethyl)-9-oxo-2,9-dihydro-1*H*-xanthene-1-carboxylate (**2**) and the previously described dihydroxanthone AGI-B4 (**1**) were isolated from fermentations of a *Diaporthe* species. The structures of the compounds were elucidated by a combination of one- and two-dimensional NMR spectroscopy, mass spectrometry, and calculations using density functional theory (DFT). Compounds **1** and **2** inhibited the LPS/IFNγ induced CXCL10 promoter activity in transiently transfected human MonoMac6 cells in a dose-dependent manner with IC_{50} values of 4.1 μM (±0.2 μM) and 1.0 μM (±0.06 μM) respectively. Moreover, compounds **1** and **2** reduced mRNA levels and synthesis of pro-inflammatory mediators such as cytokines and chemokines in LPS/IFNγ stimulated MonoMac6 cells by interfering with the Stat1 and NFκB pathway.

Keywords: CXCL10; dihydroxanthones; inflammation; inhibitor.

Introduction

Xanthones are frequently occurring polyphenolic secondary metabolites produced by plants, bacteria, fungi, and lichens (El-Seedi et al. 2009). This class of compounds has gained attraction for medicinal chemists due to their remarkable pharmacological and biochemical activities, depending on the nature and position of the substituents on the tricyclic xanthone scaffold (Masters and Bräse 2012; Shagufta 2016). Numerous natural and synthetic xanthones have been described to possess antimicrobial, antiviral, anti-cancer, anti-inflammatory, anti-diabetic and enzyme-inhibitory activities in different *in vitro* and *in vivo* models (Fotie and Bohle 2006). Several prenylated xanthones like α-mangostin, isolated from the pericarp of *Garcinia mangostana*, are under evaluation as potential therapeutics for obesity and concomitant diseases (Liu et al. 2015; Mohan et al. 2018). In our ongoing search for anti-inflammatory compounds from fungi inhibiting a LPS/IFNγ inducible CXCL10 transcriptional reporter as a marker gene, we found that cultures of a *Diaporthe* species produced the new dihydroxanthone methyl (1*R*,2*R*)-1,2,8-trihydroxy-6-(hydroxymethyl)-9-oxo-2,9-dihydro-1*H*-xanthene-1-carboxylate (**2**) and the known dihydroxanthone AGI-B4 (**1**). The genus *Diaporthe* (asexual state: *Phomopsis*) are frequently occurring endophytic, saprobic and plant pathogenic fungi, which produce a variety of biologically active secondary metabolites (Chepkirui and Stadler 2017). Both compounds inhibit CXCL10 promoter activity, CXCL10 expression and production in MonoMac6 cells. The small inducible chemokine CXCL10 (IP10) is involved in the pathology of many inflammatory and autoimmune diseases through the recruitment and activation of T-cells, neutrophils and monocytes. CXCL10 expression is increased in autoimmune disorders like psoriasis, type-I diabetes, rheumatoid arthritis, systemic sclerosis, systemic lupus erythematosus, idiopathic pulmonary fibrosis and allograft rejection (Griffith et al. 2014; Lee et al. 2009). The up-regulation of *cxcl10* mRNA levels during these processes is mainly regulated by the activation of the NFκB, Stat1 and IRF-3 transcription factors after cytokine induction and engagement of the Toll-like receptors (TLRs) by LPS (Spurrel et al. 2005; Tamassia et al. 2007). Blocking the JAK-STAT or the NFκB pathway by pharmacological inhibitors not only has been shown to reduce CXCL10 expression but also the expression of many pro-inflammatory mediators (e.g. cytokines, enzymes) in various inflammatory disease models (Fenwick et al. 2015; Gupta et al. 2010; Jamilloux et al. 2019). Therefore, blocking CXCL10 expression may represent an attractive target for

***Corresponding authors: Till Opatz**, Department of Chemistry, University of Mainz, Duesbergweg 10-14, D-55128 Mainz, Germany, E-mail: opatz@uni-mainz.de; and **Gerhard Erkel**, Department of Molecular Biotechnology and Systems Biology, University of Kaiserslautern, Paul-Ehrlich-Strasse 23, D-67663 Kaiserslautern, Germany, E-mail: erkel@bio.uni-kl.de
Markus Rohr and Anna Maria Kiefer, Department of Molecular Biotechnology and Systems Biology, University of Kaiserslautern, Paul-Ehrlich-Strasse 23, D-67663 Kaiserslautern, Germany
Ulrich Kauhl and Jonathan Groß, Department of Chemistry, University of Mainz, Duesbergweg 10-14, D-55128 Mainz, Germany

the development of new therapeutics against various chronic inflammatory and autoimmune diseases.

Results and discussion

Structure elucidation

Compounds **1** and **2** (Figure 1) were obtained by a bioactivity guided isolation procedure as described in the materials and methods section.

Compound **2** was isolated as a yellow amorphous powder. Its positive-ion mode ESI-MS spectrum exhibited a $[M+H]^+$ adduct at *m/z* 335.0, indicating a molecular mass of 334 a.m.u., compatible with the molecular formula of $C_{16}H_{14}O_8$.

The ^{13}C NMR spectrum of compound **2** (Table 1) showed nine quaternary carbons, five methine carbons, one methylene- as well as one methyl carbon. The ^1H NMR spectrum (in DMSO-d_6) suggested the presence of a 2,3,5-trisubstituted phenol, in which a sharp signal at δ = 12.39 ppm pointed towards a keto group (C-9) in ortho position to the OH-group. One of the meta carbons had to bear an oxygen substituent due to its chemical shift of δ = 154.9 ppm (C-10a), while HMBC contacts of both aromatic protons (δ = 7.01/104.2 ppm H-5, δ = 6.76/108.4 ppm, H-7) to the methylene group (δ = 4.57/62.2 ppm) as well as the downfield shift of the latter suggested the presence of a hydroxymethylene group at the other meta position of the phenol group.

Furthermore, the HMBC spectrum revealed two contacts of an olefinic proton (δ = 6.50/119.8 ppm, H-4) to a carbonyl group (δ = 180.4 ppm, C-9) and one quaternary carbon (δ = 114.6 ppm, C-9a). Based on COSY contacts, the former proton is neighboured by a second olefinic proton (δ = 6.62/141.0 ppm, H-3). The olefinic protons form an allylic system with a hydroxylated methine group (δ = 4.26/71.5 ppm, H-2). HMBC contacts of the olefinic proton H-3 to two oxygenated, quaternary carbons (δ = 74.9 ppm, C-1 and δ = 159.8 ppm, C-4a) gave the scaffold of a xanthone. Additionally, an HMBC contact of H-2 to the carbonyl carbon of the ester group (δ = 171.8 ppm $\underline{C}O_2Me$) completed the substitution pattern (Figure 2). The flat structure was first elucidated in the Opatz lab in 2017 (Kauhl 2017), yet the relative configuration of the asymmetric carbons in compound **2** could not be unequivocally determined by the usual 2D NMR methods. A chiral HPLC analysis was performed to investigate the optical purity of compound **2** (see the SI for details) but due to decomposition under normal phase conditions, the results were inconclusive and do not affect the determination of the absolute configuration (vide infra).

In addition to the new xanthone derivative **2**, the previously known, related compound AGI-B4 **1** was also isolated and identified by comparison of its spectroscopic data with literature values (Kim et al. 2002).

Table 1: ^1H (600 MHz) and ^{13}C (151 MHz) NMR data of compound **2** in CD_3OD and DMSO-d_6 (δ in ppm and *J* in Hz).

Position	CD_3OD		DMSO-d_6	
	^1H	^{13}C	^1H	^{13}C
1		77.8		74.9
1–OH			5.76 (*s*, 1 H)	
2	4.55 (*dd*, 3.8, 1.7, 1 H)	74.0	4.26 (*ddd*, 8.5, 4.3, 1.2, 1 H)	71.5
2–OH			5.86 (*d*, 8.5, 1 H)	
3	6.59 (*dd*, 10.1, 3.8, 1 H)	141.8	6.62 (*dd*, 10.0, 4.3, 1 H)	141.0
4	6.46 (*dd*, 10.1, 1.7, 1H)	121.4	6.50 (*dd*, 10.0, 1.2, 1H)	119.8
4a		161.6		159.8
5	7.01 (*d*, 1.2, 1 H)	105.6	7.01 (*d*, 1.3, 1 H)	104.2
6		152.9		152.5
7	6.78 (*d*, 1.2, 1 H)	109.9	6.76 (*d*, 1.3, 1 H)	108.4
8		161.6		159.5
8–OH			12.39 (*s*, 1 H)	
8a		110.7		108.8
9		182.6		180.4
9a		115.6		114.6
10a		157.1		154.9
$\underline{CH_2}OH$	4.66 (*s*, 2 H)	64.2	4.57 (*d*, 5.9, 2 H)	62.2
$CH_2\underline{O}H$			5.52 (*t*, 5.9, 1 H)	
$\underline{C}OOMe$		173.6		171.8
$COO\underline{Me}$	3.72 (*s*, 3 H)	52.9	3.59 (*s*, 3 H)	51.8

Experimental data

Methyl (1*R*,2*R*)-1,2,8-trihydroxy-6-(hydroxymethyl)-9-oxo-2,9-dihydro-1*H*-xanthene-1-carboxylate **2**: yellow amorphous

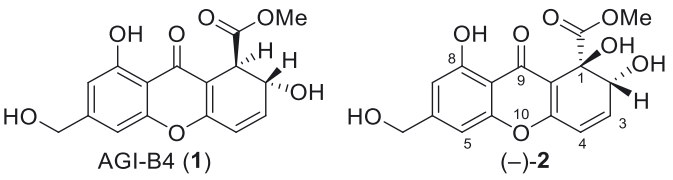

Figure 1: Chemical structure of compound **1** (AGI-B4) and compound (–)-**2** (methyl (1*R*,2*R*)-1,2,8-trihydroxy-6-(hydroxymethyl)-9-oxo-2,9-dihydro-1H-xanthene-1-carboxylate).

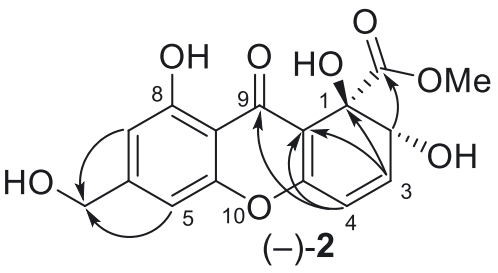

Figure 2: Important HMBC (H → C) correlations of compound (–)-**2**.

powder; ^{1}H NMR data, see Table 1; ^{13}C NMR data, see Table 1; $[\alpha]_D^{29}$ −72.6 (*c* = 0.2, MeOH); ESIMS *m/z* 335.0 $[M+H]^+$ ($C_{16}H_{15}O_8$), HRESIMS *m/z* 317.0654 $[M-OH]^+$ (calcd. for $C_{16}H_{13}O_7$: 317.0656,); IR (BaF_2) *ν* = 1751, 1738, 1658, 1599, 1500, 1450, 1319, 1199, 1059, 1037, 833 cm^{-1}.

Methyl 2,8-dihydroxy-6-(hydroxymethyl)-9-oxo-2,9-dihydro-1*H*-xanthene-1-carboxylate (**1**): ^{1}H NMR, COSY (600 MHz, pyridine-d_5): 13.11 (1H, *s*, OH-8), 7.94 (1H, *d*, *J* = 7.3 Hz, OH-2), 7.38 (1H, *s*, $CH_2O\underline{H}$-6), 7.18–7.17 (1H, *m*, H-5), 7.15–7.13 (1H, *m*, H-7), 6.88 (1H, *dd*, *J* = 9.9, 4.6 Hz, H-3), 6.48 (1H, *dd*, *J* = 9.9, 0.9 Hz, H-4), 5.27–5.24 (1H, *m*, H-2), 5.00–4.97 (2H, *m*, $C\underline{H}_2$OH-6), 4.76 (1H, *d*, *J* = 4.4 Hz, H-1), 3.67 (3H, *s*, $CO_2C\underline{H}_3$-1) ppm; ^{13}C NMR, HSQC, HMBC (151 MHz, Pyr-d_5): 182.2 (C-9), 172.5 ($\underline{C}O_2CH_3$-1), 161.5 (C-8), 160.3 (C-4a), 156.7 (C-10a), 153.6 (C-6), 142.1 (C-3), 122.2 (C-4), 111.8 (C-9a), 110.2 (C-8a), 109.3 (C-7), 105.1 (C-5), 66.0 (C-2), 63.9 ($\underline{C}H_2$OH-6), 52.9 ($CO_2\underline{C}H_3$-1), 46.9 (C-1) ppm; ESIMS *m/z* 319 $[M+H]^+$ ($C_{16}H_{15}O_7$).

Quantum mechanical-assisted structure elucidation

To determine the relative configuration of compound **2**, DFT-based quantum mechanical calculations were conducted and a *J*-DP4- as well as a DP4+-probability analysis were performed (see the SI for the detailed results) (Grimblat et al. 2015, 2019). Both methods are further developments of the probability measure DP4 originally developed by Smith and Goodman in 2010, which was successfully applied for the stereochemical and structural assignment of experimental NMR spectra by comparison with simulated spectra of several possible isomers. For a set of 117 organic molecules, this method shows that the errors between the experimental and calculated proton- and carbon shifts can be approximated by a Student *t* distribution. The probability for one possible isomer can then be calculated with the mean value, the standard deviation and the degrees of freedom obtained from this *t* distribution as well as the use of Bayes' theorem, (Riley et al. 2006; Smith and Goodman 2010). Conformational analysis for the *RR*- and the *RS*-diastereomer were performed using the MMFF (Halgren 1996) level of theory. For the DP4+-method, the geometry of each conformer was reoptimized [B3LYP/6-31G(d)] (Becke 1988, 1993; Hariharan and Pople 1973; Hehre et al. 1972; Lee et al. 1988; Vosko et al. 1980) and the structure was confirmed as a local minimum by frequency analysis (N_{imag} = 0). Subsequently, the NMR shielding tensors were calculated [mPW1PW91/6-311+G(d,p)] (Adamo and Barone 1998; Clark et al. 1983; Frisch et al. 1984; Krishnan et al. 1980) with the IEFPCM solvation model (Tomasi et al. 1999) for methanol as well as with the use of the gauge-independent atomic orbital (GIAO) method (Ditchfield 1974). For the *J*-DP4-method, all geometries of the free conformational analysis were used directly for the calculation of the shielding tensors as well as the coupling constants [B3LYP/6-31G(d,p)]. The corresponding DP4+- and *J*-DP4-probabilities were calculated after Boltzmann weighting of the obtained results.

The DP4+-probability suggested the *RR*/*SS* enantiomeric pair as the correct relative configuration (*RR* = 99.99% vs. *RS* = 0.01%) whereas the *J*-DP4-method proposed the *RS*/*SR* pair (*RR* = 0.02% vs. *RS* = 99.98%). In our opinion, the DP4+-method has the higher predictivity for the relative configuration of compound **2** for several reasons. The DP4+-probability was developed to improve the performance of the original DP4-method by the use of more sophisticated starting geometries and the differentiation of the hybridization of carbon atoms. Furthermore, higher levels of theory with larger basis sets were applied for the NMR calculations and the unscaled data were also evaluated. Moreover, the DP4-method has been reported to lead to stereochemical misassignments or afforded inconsistent and unreliable results (Grimblat et al. 2015; Nazarski et al. 2011; Smith and Goodman 2010; Willwacher et al. 2015). The *J*-DP4-method improves the DP4-method only by taking the $^{3}J_{HH}$ couplings into account to achieve a more accurate but still fast assignment at low computational cost, without any solvation model (Grimblat et al. 2019). This is accomplished by the absence of any geometry optimization at DFT level, even though these additional calculations are recommended in the literature to improve the predictivity of the calculated NMR shifts (Ermanis et al. 2019; Kim et al. 2020). In addition, the *J*-DP4 probability can be analysed by its individual contributions (SI, Table S2). The (H+C) component equals the original DP4--probability and is in favour of the *RS*/*SR* enantiomeric pair. In contrast, if only the *J* contribution is considered for the analysis of compound **2**, the probability points also in the

direction of the *RR*/*SS* enantiomeric pair (*RR* = 62.20% vs. *RS* = 37.80%), although no scalar H,H-coupling in **2** directly depends on the relative configuration so that the predictivity of this subset is also low.

Stephens et al. (2005) determined the absolute configuration (AC) of a rigid molecule from a set of 65 molecules based on its specific rotation ($[\alpha]_D$) compared to the calculated $[\alpha]_D$. To achieve an assignment with 95% confidence, the calculated $[\alpha]_D$ value for one, but not both, of the possible ACs must lie within the error margin of 57.8 of the experimental $[\alpha]_D$ value (Stephens et al. 2005). In analogy to this methodology, all geometries of the free conformational analysis of the *RR* enantiomer were reoptimized [B3LYP/6-31G(d)] and were confirmed as local minima by frequency analysis (N_{imag} = 0). The specific rotation was then calculated for a wavelength of 589.3 nm at 29 °C in methanol [B3LYP/aug-cc-pVTZ/IEFPCM]. The obtained results were Boltzmann weighted and a calculated value of $[\alpha]_D^{29}$ – 46.3 (*c* = 0.2, MeOH) was received. The difference of the experimental $[\alpha]_D$ of compound **2** ($[\alpha]_D^{29}$ – 72.6 (*c* = 0.2, MeOH)) and the calculated value of the *RR* enantiomer lies within Stephens' error margin of 57.8 (–46.3 – –72.6 = 26.3), whereas the difference with its antipode is >57.8 (+46.3 – –72.6 = 118.9). With the above discussed results, the AC of compound **2** was assigned with >95% confidence.

Biological activities

For identification and characterization of active compounds, we used a human CXCL10 promoter dependent transcriptional reporter in transiently transfected monocytic MonoMac6 cells. The LPS/IFNγ inducible expression of luciferase therefore reflects the cooperative induction of *cxcl10* mRNA expression by Stat1, NFκB and IRF3 transcription factors (Tamassia et al. 2007). Stimulation of transfected cells with 10 ng/mL IFNγ and 1 µg/mL LPS increased the luciferase activity 6–8 fold compared to the uninduced control. Screening of fungal cultures for the inhibition of CXCL10 promoter activity resulted in the isolation of two dihydroxanthones methyl (1*R*,2*R*)-1,2,8-trihydroxy-6-(hydroxymethyl)-9-oxo-2,9-dihydro-1*H*-xanthene-1-carboxylate (**2**) and 7,8-dihydroxanthenone-8-carboxylic acid methyl ester (AGI-B4; **1**) from fermentations of a *Diaporthe* species. Although AGI-B4 has been previously isolated from fermentations of an *Aspergillus* species as an inhibitor of VEGF-induced proliferation of human umbilical vein endothelial cells (HUVECs) (Kim et al. 2002) and also inhibited superoxide anion and elastase release in fMLP-induced human neutrophils (Chung et al. 2013), it has not been reported to interfere with inducible pro-inflammatory gene expression. As shown in Figure 3, treatment of MonoMac6 cells with different concentrations of compound **1** or **2** dose-dependently reduced the LPS/IFNγ inducible CXCL10 promoter activity with IC_{50} values of 4.1 µM (±0.2 µM) and 1.0 µM (±0.06 µM), respectively, as calculated by a dose response fitting. The constitutive activity of the EF1α-promoter was only slightly affected by the test compounds up to the highest concentrations tested, indicating that the compounds do not interfere with transcription in a general manner.

Binding of LPS to Toll-like receptors and stimulation of cells by IFNγ synergistically activate NFκB, Stats and interferon regulatory factors (IRFs) members which are key transcriptions factors involved in the inducible transcription of many pro-inflammatory cytokines and chemokines such as CXCL10 or interleukin-8 (De Nardo 2015; Kopitar-Jerala 2017).

We therefore investigated the effect of compounds **1** and **2** on NFκB driven expression of the reporter gene luciferase in LPS/IFNγ stimulated MonoMac6 cells. As shown in Table 2, both compounds inhibited the inducible NFκB-dependent luciferase expression in MonoMac6 cells with similar IC_{50}- and IC_{90} values in a concentration range of 6–9 µM. We also determined the influence of the compounds on an interleukin-8 (IL-8/CXCL8) transcriptional reporter in LPS/IFNγ-stimulated MonoMac6 cells. IL-8 is a pro-angiogenic and pro-inflammatory CXC chemokine, which also plays critical roles in cancer cell survival, invasion and metastasis (Waugh and Wilson 2008). In addition, it functions as a chemo-attractant for the recruitment of granulocytes in innate immune reactions and inflammatory diseases (Russo et al. 2014). As shown in Table 2, compound **1** and **2** inhibited the inducible IL-8 promoter activity with IC_{50}-values of 5.57 µM (±0.06 µM) and 3.5 µM (±0.03 µM) respectively.

The transcriptional activation of the CXCL10 promoter also largely depends on three distal interferon stimulated response elements (ISRE) and two Stat1 recognition sites (GAS) which bind activated Stat1/2 and Stat1 dimers (Spurrel et al. 2005). We therefore investigated the effect of **1** and **2** on ISRE (Stat1/2) and GAS- (Stat1) driven expression of the reporter gene luciferase in either IFNα- or IFNγ--stimulated MonoMac6 cells. Interestingly the IFNα induced ISRE-dependent expression of the reporter gene was only inhibited by compound **2** with an IC_{50} of 0.124 µM. Compound **1** which differs from compound **2** by the lack of the hydroxyl group at C-1 did not significantly affect the IFNα-induced Stat1/2 pathway up to the highest concentration tested (10 µM). The IFNγ-induced Stat1-dependent transcriptional reporter was inhibited in a dose dependent

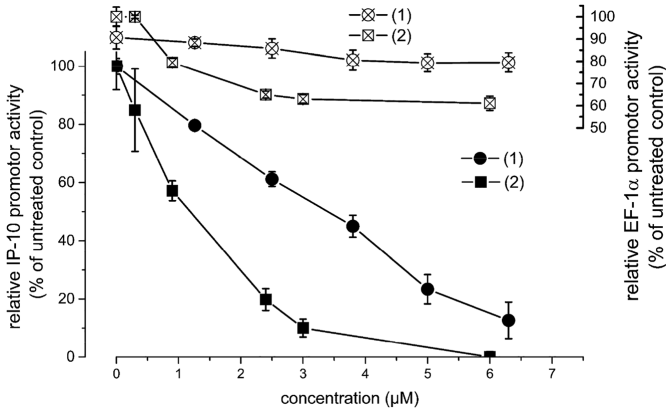

Figure 3: Effect of compounds **1** and **2** on CXCL10- and EF-1α-promoter activity in MonoMac6 cells.
MonoMac6 cells were transiently transfected with a human CXCL10- and EF-1α-promoter dependent reporter plasmid by electroporation and stimulated with LPS/IFNγ for 4 h with and without test compounds. Control (100%): stimulation only. Data represent the mean ± SEM of at least three independent experiments.

Table 2: Effect of **1** and **2** on LPS/IFNγ induced GAS-, IL-8 promoter, NFκB- and IFNα induced ISRE driven luciferase activity.

Comp	pGAS (µM)		pISRE (µM)		hIL-8 (µM)		NFκB (µM)	
	IC_{50}	IC_{90}	IC_{50}	IC_{90}	IC_{50}	IC_{90}	IC_{50}	IC_{90}
1	4.4 (±0.05)***	7 (±0.3)***	–	–	5.57 (±0.06)**	9.2 (±0.25)**	5.97 (±0.1)***	8.5 (±0.33)***
2	1.79 (±0.09)***	5.4 (±0.6)***	0.124 (±0.35) ***	0.658 (±0.117) ***	3.5 (±0.03)***	5.0 (±0.03)***	5.92 (±0.117)*	7.74 (±0.28)*

The values represent the mean of at least three independent biological replicates. ±SEM. The IC_{50}- and IC_{90} values were calculated using a pharmacological dose response fitting function as described in the material and methods section (*$p < 0.05$; **$p < 0.01$; ***$p < 0.001$).

manner with IC_{50}-values of 4.4 µM for compound **1** and 1.79 µM for compound **2** (Table 2).

The transcription factor Stat1 is a major regulatory factor for IP10 expression (Ohmori and Hamilton 2001). Binding of IFNγ to the receptor leads to tyrosine 701 phosphorylation of Stat1 which promotes dimerization, nuclear translocation and DNA binding of Stat1 dimers to GAS elements (Wen et al. 1995). In addition, serine 727 phosphorylation in the transactivating domain of Stat1 is required for full transcriptional potency (Decker and Kovarik 2000). To address whether the inhibitory effect of both xanthones on the IFNγ-inducible Jak/Stat pathway is due to an inhibition of the Stat1 tyrosine or serine phosphorylation, we performed Western blots for total and phosphorylated forms of Stat1. As shown in Figure 4A, stimulation of MonoMac6 cells with 10 ng/mL IFNγ for 30 min resulted in a strong induction of either tyrosine or serine phosphorylation of Stat1. Both compounds showed no inhibition of tyrosine or serine phosphorylation of the Stat1 transcription factor up to the highest concentration tested, as analyzed by densiometry. Since both xanthones do not interfere with the activation of Stat1, we examined whether they interfere with nuclear translocation. Western blots of nuclear and cytosolic fractions of MonoMac6 cells showed a quick translocation of Stat1 to the nucleus upon IFNγ stimulation which was not significantly affected by both test compounds (Figure 4B). Also, the levels of α-tubulin and histone 3 as internal controls for cytosolic and nuclear fractions were unchanged, indicating successful fractionation and equal sample loading.

We further characterized the mechanism involved in the inhibition of IFNγ signaling by analyzing the influence of the compounds on DNA binding of the activated (phosphorylated) Stat1 transcription factor to its specific DNA binding sequence. As shown in Figure 4C, treatment of MonoMac6 cells with 10 ng/mL IFNγ for 45 min resulted in an induction of Stat1 DNA binding. Compound **1** inhibited the binding significantly at a concentration of 12.52 µM whereas compound **2** did not show any significant inhibition at the concentrations tested.

Other major regulators of *cxcl10* transcription are the NFκB family of transcription factors. This protein family consists of five NFκB/Rel proteins which associate to form homo or heterodimers which can be either activators (e.g. p65/p50 complexes) or repressors (e.g. p50 homodimers) of transcription (Oeckinghaus and Ghosh 2009). In

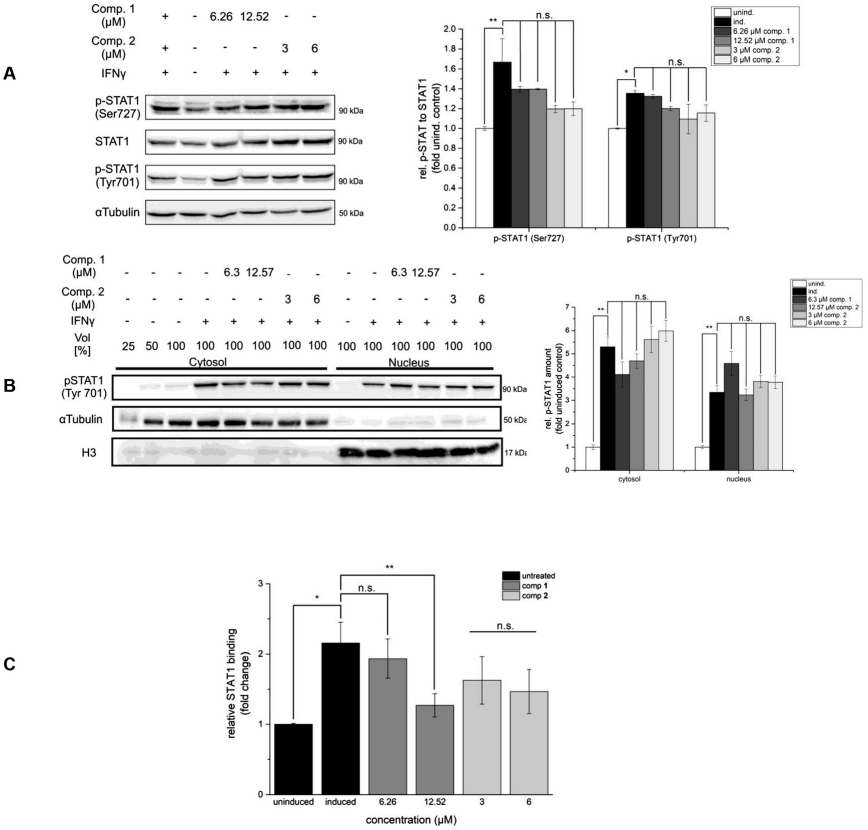

Figure 4: Effect of compounds **1** and **2** on Stat1 phosphorylation, nuclear translocation and DNA binding.
(A) Effect of compounds **1** and **2** on serine and tyrosine phosphorylation of Stat1. Representative experiments of Western blotting and densiometric analysis for phospho(ser727)-, phospho(tyr701)- and total Stat1 in whole cell lysates of IFNγ induced (30 min) and (B) phosphoStat1 in cytoplasmatic and nuclear extracts of MonoMac6 cells. α-tubulin and histone 3 served as internal controls for cytosolic and nuclear fractions. (C) Analysis of Stat1 binding to its specific DNA sequence. MonoMac6 cells were pretreated for 1 h with different concentrations of compound **1** and **2** and stimulated with 10 ng/mL IFNγ (45 min). Twenty microgram of nuclear protein was analyzed using the TransAM STAT family kit from Active Motif. The results represent the means of three independent biological replicates. ±SEM (*: $p < 0.05$; **: $p < 0.01$; n.s.: not significant).

unstimulated cells these dimers are bound to the inhibitor protein IκB. Upon stimulation, IκB becomes phosphorylated by IκB kinase proteins (IKK) which leads to IκB degradation by the ubiquitin-proteasomal pathway. The released NF-κB dimers (the most common form is the p50/p65 dimer) then translocate to the nucleus, bind to the promoters of responsive genes and activate transcription (Wan and Lenardo 2009).

In order to characterize the influence of both xanthones on NFκB activation, Western blots of cytoplasmatic and nuclear extracts against IκB, p65 and p50 of IFNγ/LPS-induced MonoMac6 cells were performed. As controls for nuclear fractions we used antibodies against nuclear lamin B1 and histone 3 and α-tubulin for cytosolic fractions (Figure 5A). Upon stimulation with IFNγ and LPS, IκB becomes degraded and p50 and p65 are released to translocate to the nucleus. Treatment with both compounds significantly reduced IκB degradation which prevented p50 and p65 from entering the nucleus (Figure 5B–D).

We further investigated the effect of the two xanthones on the expression of selected LPS/IFNγ-induced pro-inflammatory and anti-apoptotic marker genes, which are

regulated at the transcriptional level by NFκB- and Stat transcription factors by real-time PCR experiments as described in the materials and methods section. Values are expressed as relative mRNA content of induced versus uninduced cells (100%), and induced and compound treated versus induced and untreated cells, each corrected for the constitutive expressed housekeeping gene *gapdh* as reference determined in the same sample in parallel. As shown in Figure 6, stimulation of MonoMac6 cells with LPS/IFNγ caused a strong up-regulation of mRNA levels for the cytokines *tnfα and il6*, the chemokines *ccl2* and *cxcl10* and the pro-inflammatory enzyme cyclooxygenase 2 (*cox-2*), which are important mediators in the pathogenesis of inflammatory diseases (Clària and Romano 2005; Lee et al. 2013). Since several natural xanthones such as the structurally closely related globosuxanthone A exhibit anti-tumor and apoptosis-inducing properties (Su et al. 2011), we also investigated the mRNA levels of the anti-apoptotic genes *xiap* and *survivin* and the cell cycle regulator protein cyclin D1 (Martinez-Garcia et al. 2019; Tashiro et al. 2007). Compound **1** significantly reduced the expression of all analyzed mRNAs starting at 3.13 µM. Interestingly, compound **1** completely inhibited the expression of the genes *xiap* and *cyclin d1* (Figure 6A). In contrast, compound **2** showed no significant inhibition of *cox2-*, *survivin-*, and *xiap* expression but suppressed expression of *ccl2*, *cyclin d1* and *cxcl10* in a concentration dependent manner (Figure 6B). Both compounds **1** and **2** seem to have similar effects on pro-inflammatory gene expression whereas compound **1** additionally affects genes responsible for cell proliferation. The measured mRNA values for *gapdh* did not vary significantly upon treatment of the cells with LPS/IFNγ or test compounds (data not shown).

In order to confirm the qRT-PCR experiments on protein level, we examined the influence of the isolated xanthones on the inducible synthesis and secretion of the

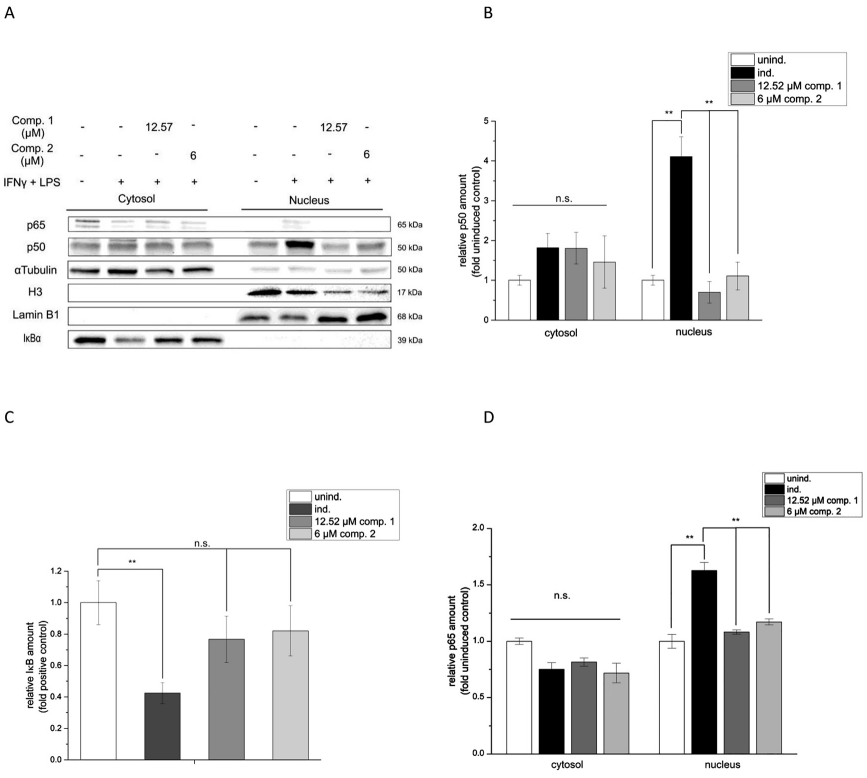

Figure 5: Effect of compound **1** and **2** on p65, p50 nuclear translocation and IκB degradation.
MonoMac6 cells were treated with test compounds and stimulated with LPS/IFNγ for 30 min. p65, p50 and IκB content in nuclear and cytosolic extracts were analyzed by Western blot analysis (A) and densiometry (B, C, D). Results are a representative experiment repeated three times with essentially similar findings (**: $p < 0.01$, *: $p < 0.05$; n.s.: not significant).

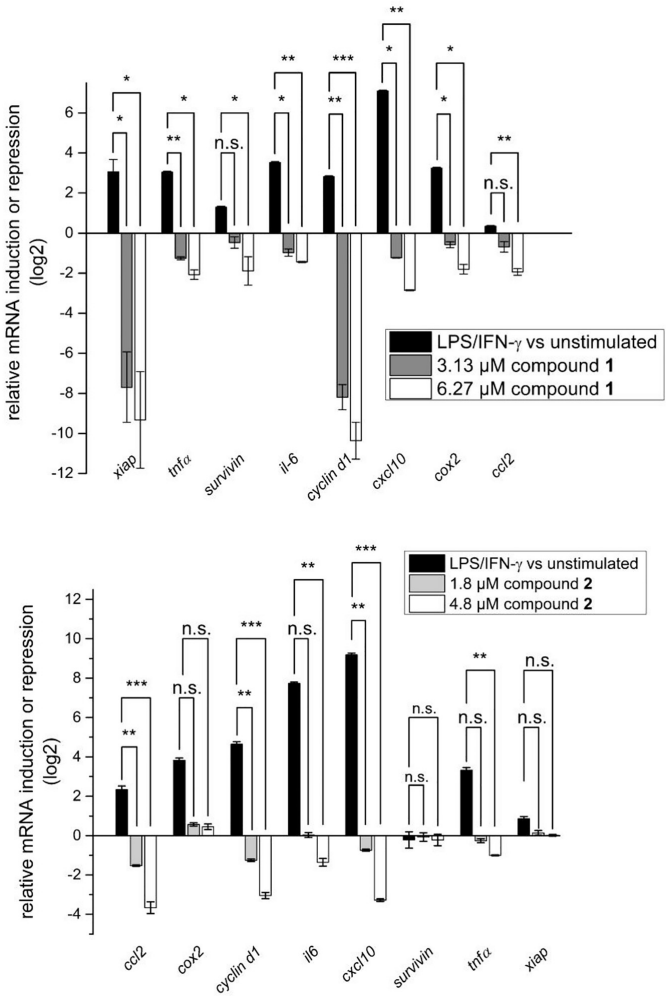

Figure 6: Effect of compound **1** and **2** on mRNA levels of selected LPS/IFNγ inducible genes in MonoMac6 cells.
Values are expressed as ratios (log2) of relative mRNA levels of stimulated (6 h IFNγ/LPS) versus un-stimulated cells as control and compound pre-treated and stimulated versus untreated, stimulated cells, corrected for gapdh as reference determined in the same sample in parallel. Data are shown as mean values ± SEM of three independent experiments (***$p < 0.001$; **$p < 0.01$; *$p < 0.05$; n.s. not significant vs. stimulated cells).

cytokine TNFα and the chemokines CXCL10 and CCL2 by Western blotting. As shown in Figure 7, stimulation of MonoMac6 cells with LPS/IFNγ resulted in a strong synthesis of the investigated pro-inflammatory mediators TNFα, CXCL10 and CCL2. Treatment of LPS/IFNγ-stimulated cells with 12.52 µM compound **1** and 6 µM compound **2** almost completely inhibited the synthesis of the investigated pro-inflammatory mediators which are responsible for the activation and recruitment of immune cells to the site of inflammation (Turner at al. 2014).

These results indicate that the isolated xanthones exert their inhibitory activity on the transcriptional level and thus inhibiting LPS/IFNγ-induced protein expression of pro-inflammatory genes.

Since both compounds interfere with the expression the cell cycle regulator cyclin D1 and compound **1** in addition significantly reduced mRNA levels of survivin and the anti-apoptotic gene *xiap*, we assessed the apoptosis-inducing activity by flow cytometry and Annexin V-Cy5/PI staining. Treatment of MonoMac6 cells with up to 12.54 µM of compound **1** or 6 µM of compound **2** for 24 h did not induce an apoptotic response and did not result in an increase of necrotic cells (see Supplementary Material). We also performed an analysis of the cell cycle with propidium iodide

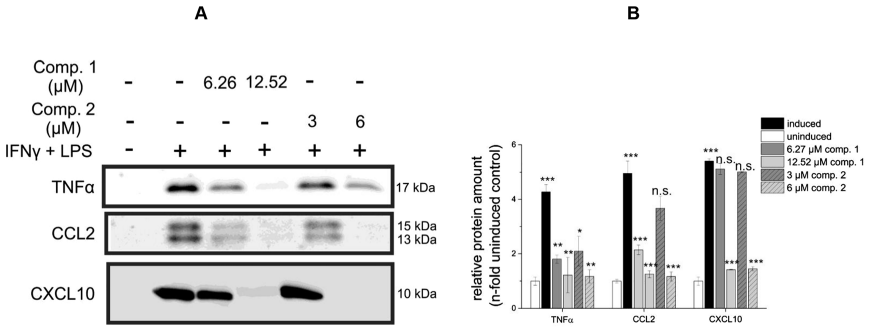

Figure 7: Compounds **1** and **2** reduce production of the proinflammatory cytokine TNFα and the chemokines CXCL10, CCL2 in LPS/IFNγ stimulated MonoMac6-cells.
MonoMac6 cells were pretreated for 1 h with compound **1** or **2** and stimulated with IFNγ/LPS for 24 h. Cytokine and chemokine production in the cell culture supernatant were analyzed by Western blotting and densiometry. (A) Representative western blot of three individual experiments. (B) Densiometric analysis. ±SEM (***: $p < 0.001$; **: $p < 0.01$; *: $p < 0.05$; n.s.: not significant).

DNA staining and flow cytometry to assess the influence of the isolated compounds on cell cycle progression. Both compounds did not show any effect on the progression of the cells to the different phases of the cell cycle up to the highest concentration tested (see Supplementary Material).

In addition, cytotoxic properties of the compounds were evaluated against MonoMac6 cells by measuring the reduction of 2,3-bis(2-methoxy-4-nitro-5-sulfophenyl)-2*H*-tetrazolium-5-carboxanilide sodium (XTT) into a coloured formazan. No significant cytotoxic activities against MonoMac6 cells could be observed for compounds **1** and **2** up to the highest concentrations used in the CXCL10-promoter dependent reporter assays during a 24 h incubation period (data not shown).

Materials and methods

Chiral HPLC was carried out on a 1260-series Infinity II HPLC-system (Agilent-Technologies) in normal phase and isocratic mode with ethanol/*n*-hexane. A list of the used columns for enantiomer analysis can be found in the Supplementary Material.

General procedures

^{1}H NMR (400 MHz) and ^{13}C NMR (100.6 MHz) spectra were recorded on a Bruker Avance-II spectrometer equipped with a 5 mm BBO probe head. ^{1}H NMR (600 MHz) and ^{13}C NMR (150.9 MHz) spectra were recorded on a Bruker Avance-III spectrometer equipped with a 5 mm TCI cryoprobe. The spectra were measured in pyridine-d_5, CD_3OD and DMSO-d_6 and the chemical shifts were referenced to the residual solvent signal (pyridine-d_5: δ_H = 8.74 ppm, δ_C = 150.35 ppm; CD_3OD: δ_H = 3.31 ppm, δ_C = 49.00 ppm; DMSO-d_6: δ_H = 2.50 ppm, δ_C = 39.52 ppm) (Budavari et al. 1989; Gottlieb et al. 1997). Standard pulse sequences were used for 2D NMR experiments. ESI-HRMS data were measured from a solution of the analyte in acetonitrile with a Waters Q-TOF-Ultima 3 equipped with a LockSpray interface (tri-*n*-octylamine as external reference). IR spectra were measured with a Bruker Tensor 27 FTIR spectrometer. The optical rotation was measured on a Perkin-Elmer 241 polarimeter at 578 and 546 nm and extrapolated to 589 nm using Drude's equation (Lippke and Thaler 1970).

Culturing and isolation of metabolites

Diaporthe sp. strain IBWF E99390 was obtained from the culture collection of the Institute of Biotechnology and Drug Research (IBWF), Kaiserslautern, Germany. ITS sequence analysis of the ITS1-5.8S rDNA-ITS2 region of nuclear DNA (White et al. 1990) showed a high similarity of 98–99% to different *Diaporthe* (asexual state: *Phomopsis*) isolates and therefore the species could not be unequivocally determined.

For maintenance, the fungus was grown on malt agar slants (malt extract 20 g/L, for solid media 2% of agar was added). The fermentation was done using 5 L shaking flasks at room temperature and constant agitation (120 rpm). Slices of well grown agar plates were used to inoculate 2.5 L of potato glucose medium (glucose 20 g/L, potato extract 4 g/L, pH 5.5). The production of compound **1** and **2** was followed by the inhibitory effect of various concentrations of a crude extract of the culture fluid on LPS/IFNγ-inducible CXCL10 promoter-dependent reporter gene assay as described below. The compounds were isolated from the culture fluid by bioactivity-guided fractionation using the CXCL10 transcriptional reporter in MonoMac6 cells. As control 2 µM of the fungal Stat and NF-κB inhibitor galiellalactone was used which reduced LPS/IFN-γ induced CXCL10 promoter activity 90% compared to untreated cells (Péres et al. 2014; Weidler et al. 2000).

The fermentation was stopped after 288 h when the inhibition of the CXCL10 promoter activity reached a maximum. The culture fluid (10 L) was separated from the mycelia by filtration and extracted twice with an equal volume of ethyl acetate (EtOAc). The organic phase was separated from the aqueous phase, dried over Na_2SO_4 and concentrated *in vacuo*.

After concentration *in vacuo*, the crude extract (2.9 g) was fractionated by subsequent chromatography on silica gel (Merck 60). Elution with cyclohexane-EtOAc (40:60) resulted in fraction A (530 mg) and elution with cyclohexane-EtOAc (20:80) yielded fraction B (360 mg). Both fractions were precleared by binding the fraction to a solid phase extraction column (CHROMABOND C18, 15 mL, 2000 mg, Macherey- Nagel, Düren, Germany) and eluting them with 100% methanol. The resulting enriched fraction A (270 mg) and fraction B (175 mg) were further purified by isocratic preparative HPLC (Macherey & Nagel, Nucleosil RP18; column 250 × 21 mm, flow 25 mL/min) with H_2O–MeCN. Compound **1** (AGI–B4) was isolated from fraction A with H_2O–MeCN 68:32 (t_R: 4 min) to yield 16 mg and compound **2** from fraction B with H_2O–MeCN 75:25 (t_R: 18 min) to yield 10 mg respectively. The purity of the compounds was greater than 98.5% as determined by HPLC equipped with diode-array detection and mass spectrometry analysis (see Supplementary Material).

Cell culture

MonoMac6 (DSMZ ACC124) cells were cultured in RPMI 1640 medium containing 25 mM HEPES, 2 mM L-Glutamine, supplemented with 10% FCS, 100 units/mL Penicillin G and 10 µg/mL streptomycin at 37 °C and 5% CO_2.

IFNγ and IFNα were purchased from ImmunoTools, Germany. LPS O111:B4 (L3012) was purchased from Sigma-Aldrich.

Cytotoxicity and cell cycle analysis

The cytotoxicity of the isolated compounds against MonoMac6 cells, treated for 24 and 48 h, was determined in an XTT based cell viability assay (Roehm et al. 1991).

The influence of the two isolated compounds on induction of apoptosis and necrosis was determined via flow cytometric analysis after treatment of MonoMac6 cells with the test substances for 24 h. For the measurement, cells were dual stained with the Annexin V-Cy5 Apoptosis detection Kit (Abcam, Cambridge, UK) and propidium iodide according to manufacturer's instruction. Cells subjected to cell cycle analysis were labelled using the FxCycle™PI/RNase Staining Solution (Thermo Fisher Scientific, Waltham, USA). Measurement of the stained samples was performed using an Attune NxT Flow Cytometer (Thermo Fisher Scientific, Waltham, USA).

Reporter gene assays

The CXCL10 promoter (–875 to +97 relative to the transcriptional start site) reporter plasmid has been described previously (Rohr et al. 2017). The plasmid pRL-EF1α for normalizing transfection efficiency was obtained from Promega (Mannheim, Germany). The NFκB-, Stat1- and IRF-driven reporter plasmids pNFκB-Luc, pGAS-Luc and pISRE-Luc were obtained from Clontech (Saint-Germain-en-Laye, France). Transient transfections of MonoMac6 cells were performed by electroporating (BioRad, Gen Pulser) 3×10^7 cells/mL in 0.4 mL RPMI 1640 medium containing 25 mM HEPES buffer together with 40 µg of the indicated plasmids at 200 V and 975 µF. After electroporation, the cells were seeded at 1×10^6 cells/mL RPMI 1640 medium containing 10% FCS in a 24 well plate with and without test compounds and luciferase expression was induced with 1 µg/mL LPS and 10 ng/mL IFNγ. Luciferase activity was measured 4 h after induction using the Dual-Glo luciferase assay system (Promega, Mannheim, Germany) according to the manufacturer's instructions with a luminometer (BMG Labtech, Ortenberg, Germany).

Western immunoblotting

MonoMac6 cells were starved in RPMI1640 Medium containing 0.5% FCS for 24 h. The cells were then seeded in petri dishes with a diameter of 10 cm with a density of 1×10^6 cells/mL, pretreated for 1 h with or without different concentrations of test compounds and induced with 10 ng/mL IFNγ and 1 µg/mL LPS as indicated. Total cell extracts were obtained by washing the cells two times in ice cold PBS and resuspending the cell pellet in 200 µL ice cold RIPA buffer (150 mM NaCl, 5 mM EDTA (pH 8.0), 50 mM Tris (pH 8.0), 1.0% V/V NP-40, 0.5% V/V sodium deoxycholate, 0.1% SDS, 5 mM sodium orthovanadate, 10 mM sodium fluoride). The protein content was determined using the Pierce™ BCA Protein assay kit (Thermo Fisher Scientific, Waltham, USA).

For separation of cytosolic and nuclear extracts, the cells were resuspended in 5 mL lysis buffer (10 mM HEPES (pH 7.9), 1.5 mM $MgCl_2$, 10 mM KCl, 0.5 mM DTT, 1:50) complete protease-inhibitor cocktail (Roche Diagnostics, Mannheim, Germany) and incubated on ice for 5 min. The cell membranes were lysed using 20 strokes of an ice cold dounce homogenizer with a tight pestle. The released nuclei were collected by centrifugation at 1000 × g for 5 min at 4 °C. The supernatant was collected as cytoplasmatic fraction and precipitated with TCA and washed with acetone. The nuclear pellet was resuspended in 3 mL buffer S1 (250 mM sucrose, 10 mM $MgCl_2$, Protease Inhibitor), layered over a 3 mL cushion of buffer S2 (880 mM sucrose, 0.5 mM $MgCl_2$, Protease Inhibitor) and centrifuged at 2800 × g for 10 min at 4 °C. The nuclei were resuspended in RIPA buffer. The determination of protein concentrations was done using the Pierce™ BCA Protein assay according to manufacturer's instructions.

For the analysis of secreted proteins, serum starved MonoMac6 cells were pretreated with or without the compounds for 1 h and stimulated with 10 ng/mL IFNγ and 1 µg/mL LPS as indicated. The cell culture supernatant was collected, centrifuged at 5000 × g for 10 min at 4 °C to remove cellular debris and precipitated with 10% V/V TCA at –20 °C. The samples were thawed on ice, centrifuged at 12,000 × g at 4 °C for 30 min and washed with 9 vol ice cold acetone. After centrifugation at max speed and 4 °C the pellet was resuspended in a buffer containing 1% w/v SDS, 60 mM Tris-HCL, pH 6.8.

For western blotting same amounts of protein (50–100 µg) were separated by 10% SDS-PAGE, transferred to nitrocellulose membranes and subjected to immunoblotting. The membranes were probed with specific antibodies against serine phosphorylated, tyrosine phosphorylated, total Stat1 protein (New England Biolabs, Frankfurt, Germany); specific antibodies against IκB, p50, p65, CXCL10, CCL2, TNF-α and lamin B1 (Santa Cruz Biotechnology, Dallas, USA). Specific antibodies against α-tubulin and histone 3 (New England Biolabs, Frankfurt, Germany) served as an endogenous control. For detection appropriate secondary antibodies conjugated with horseradish peroxidase were used and signals were visualized by the enhanced chemoluminescence detection system (New England Biolabs GmbH, Frankfurt, Germany). Stripping of probed membranes was done using the harsh stripping protocol according to Abcam (Cambridge, UK).

Binding of activated transcription factors to DNA

The binding of activated Stat1 proteins to the respective DNA sequence was analyzed using the TransAM® STAT family Kit (Active Motif, Carlsbad, USA). The nuclei were isolated using the Active Motif nuclear extraction Kit (Active Motif, Carlsbad, USA) according to the manufacturer's instructions.

Real time quantitative PCR

For qRT-PCR analysis, MonoMac6 cells were starved for 24 h in RPMI 1640 medium with 0.5% FCS. Afterwards, the cells were plated into six well plates at a density of 1×10^6 cells per well. After treatment with test compounds for 1 h, the cells were induced with 1 µg/mL lipopolysaccharide (LPS) and 10 ng/mL IFNγ for 7 h. Following stimulation, the cells were lysed with 1 mL TRIzol reagent (Thermo Fisher Scientific, Waltham, USA) and total RNA was prepared according to manufacturer's instructions. First strand cDNA was generated using the RevertAid H Minus First Strand cDNA Synthesis Kit (Fermentas, St. Leon-Roth, Germany). Gene expression was quantified from 300 ng cDNA using the 5x HOT FIREPoly® EvaGreen® qPCR Supermix (Solis Biodyne, Tartu, Estonia) according to manufacturer's suggestions with the following gene-specific primers (Table 3).

Measurements were done using the StepOnePlus real-time PCR System (Thermo Fisher Scientific, Waltham, USA) with the following protocol: initial activation of HotStar Taq DNA polymerase at 95 °C for 12 min, 40 cycles of 95 °C for 15 s, annealing at 56 °C for 30 s, extension/detection at 72 °C for 30 s. Relative mRNA amounts were determined using the mathematical model for relative quantification in real-time PCR proposed by Pfaffl (2001).

Table 3: qRT-PCR primer.

CLL2 (Genbank Accession NM002982)	
Sense	ATCAATGCCCCAGTCACC
Antisense	AGTCTTCGGAGTTTGGG
COX-2 (Genbank Accession NM000963)	
Sense	TTCAAATGAGATTGTGGGAAAATTGCT
Antisense	AGATCATCTCTGCCTGAGTATCTT
CXCL10 (Genbank Accession NM001565)	
Sense	TGAGCCTACAGCAGAGGAA
Antisense	TACTCCTTGAATGCCACTTAGA
Cyclin D1 (Genbank Accession NM053056.2)	
Sense	CTGGCCATGAACTACCTGGA
Antisense	GTCACA CTTGATCACTCTGG
GAPDH (Genbank Accession NM001357944.1)	
Sense	CCTCCGGGAAACTGTGG
Antisense	AGTGGGGACACGGAAG
IL-6 (Genbank Accession NM000600)	
Sense	TCTCCACAAGCGCCTTCG
Antisense	CTCAGGGCTGAGATGCCG
Survivin (Genbank Accession NM001012271)	
Sense	ACCAGGTGAGAAGTGAGGGA
Antisense	AACAGTAGAGGAGCCAGGGA
TNF-α (Genbank Accession NM000594.3)	
Sense	TCTTCTGCCTGCTGCACTTTGG
Antisense	ATCTCTCAGCTCCACGCCATTG
XIAP (Genbank Accession NM001167.3)	
Sense	CCGTGCGGTGCTTTAGTTGT
Antisense	TTCCTCGGGTATATGGTGTCTGAT

Statistical analysis

Data represent means ± SEM. Statistical differences were determined by one-way ANOVA testing combined with a Tukey post-hoc analysis. The pharmacological fitting was done using a dose response function with the Levenberg-Marquardt algorithm. Analyses were performed using OriginPro 9.1 (OriginLab Corporation, Northampton, USA).

Conclusion

In summary, we identified a new dihydroxanthone (**2**) along with the previously isolated AGI-B4 (**1**) from fermentations of a *Diaporthe* species. Both compounds display anti-inflammatory properties by interfering with the JAK/Stat1- and the NFκB pathway and thus blocking the inducible transcription of pro-inflammatory genes. Inhibition of the production of pro-inflammatory cytokines, enzymes like iNOS or COX-2 and chemokines in different *in vivo* and *in vitro* models by blocking JNK, ERK, p38 MAP kinase signaling as well as NFκB signaling have been described for various simple oxygenated xanthones, xanthone glycosides, prenylated xanthones and xanthonolignoids (Feng et al. 2020). Interfering with the Jak/Stat pathway may also account for the previously described inhibition of VEGF-induced HUVEC proliferation by AGI-B4 since it was shown that activation of Sat1 by VEGF promotes endothelial cell growth and survival (Bartoli et al. 2000). In contrast to the structurally closely related fungal dihydroxanthones nidulalins and globosuxanthone A which have been isolated due to their antitumor activities, compounds **1** and **2** neither exhibit significant cytotoxicity nor induce apoptosis or interfere with cell cycle progression.

Acknowledgments: We thank L. Geske (Mainz) for assistance with chiral HPLC analysis, Dr. J. C. Liermann (Mainz) for NMR spectroscopy, Dr. N. Hanold (Mainz), Dr. C. Kampf (Mainz) for high resolution mass spectrometry as well as Prof. Z. Storchova (Kaiserslautern) for FACS analyses. Parts of this research were conducted using the supercomputer Mogon and/or advisory services offered by Johannes Gutenberg University Mainz (hpc.uni-mainz.de), which is a member of the AHRP (Alliance for High Performance Computing in Rhineland Palatinate, www.ahrp.info) and the Gauss Alliance e.V. The authors gratefully acknowledge the computing

time granted on the supercomputer Mogon at Johannes Gutenberg University Mainz (hpc.uni-mainz.de).

Author contributions: All the authors have accepted responsibility for the entire content of this submitted manuscript and approved submission.

Research funding: This work was supported by a grant from the Stiftung Rheinland-Pfalz für Innovation and by the Rhineland Palatinate Natural Products Research Center.

Conflict of interest statement: The authors declare no conflict of interest.

Supplementary Information

Computational details and FACS analyses associated with this paper can be found in the online version of the article.

References

Adamo, C. and Barone, V. (1998). Exchange functionals with improved long-range behavior and adiabatic connection methods without adjustable parameters: the *m*PW and *m*PW1PW models. J. Chem. Phys. 108: 664–675.

Bartoli, M., Gu, X., Tsai, N.T., Venema, R.C., Brooks, S.E., Marrero, M.B., and Caldwell, R.B. (2000). Vascular endothelial growth factor activates stat proteins in aortic endothelial cells. J. Biol. Chem. 275: 33189–33192.

Becke, A.D. (1988). Density-functional exchange-energy approximation with correct asymptotic behavior. Phys. Rev. A 38: 3098–3100.

Becke, A.D. (1993). Density-functional thermochemistry. III. The role of exact exchange. J. Chem. Phys. 98: 5648–5652.

Budavari, S., O'Neil, M.J., Smith, A., and Heckelman, P.E. (1989). *The Merck index, an encyclopedia of chemicals, drugs, and biologicals*, 11th ed. Rahway: Merck Co., Inc.

Chepkirui, C. and Stadler, M. (2017). The genus *Diaporthe*: a rich source of diverse bioactive metabolites. Mycol. Prog. 16: 477–494.

Chung, Y.M., Wei, C.K., Chuang, D.W., El-Shazly, M., Hsieh, C.T., Asai, T., Oshima, Y., Hsieh, T.J., Hwang, T.L., Wu, Y.C., et al. (2013). An epigenetic modifier enhances the production of anti-diabetic and anti-inflammatory sesquiterpenoids from *Aspergillus sydowii*. Bioorg. Med. Chem. 21: 3866–3872.

Clària, J. and Romano, M. (2005). Pharmacological intervention of cyclooxygenase-2 and 5-lipoxygenase pathways. Impact on inflammation and cancer. Curr. Pharmaceut. Des. 11: 3431–3447.

Clark, T., Chandrasekhar, J., Spitznagel, G.W., and Schleyer, P.V.R. (1983). Efficient diffuse function-augmented basis sets for anion calculations. III. The 3-21+G basis set for first-row elements, Li-F. J. Comput. Chem. 4: 294–301.

De Nardo, D. (2015). Toll-like receptors: activation, signaling and transcriptional modulation. Cytokine 74: 181–189.

Decker, T. and Kovarik, P. (2000). Serine phosphorylation of STATs. Oncogene 19: 2628–2637.

Ditchfield, R. (1974). Self-consistent perturbation theory of diamagnetism. Mol. Phys. 27: 789–807.

El-Seedi, H.R., El-Ghorab, D.M.H., El-Barbary, M.A., Zayed, M.F., Göransson, U., Larsson, S., and Verpoorte, R. (2009). Naturally occurring xanthones; latest investigations: isolation, structure elucidation and chemosystematic significance. Curr. Med. Chem. 16: 2581–2626.

Ermanis, K., Parkes, K.E.B., Agback, T., and Goodman, J.M. (2019). The optimal DFT approach in DP4 NMR structure analysis – pushing the limits of relative configuration elucidation. Org. Biomol. Chem. 17: 5886–5890.

Feng, Z., Lu, X., Gan, L., Zhang, Q., and Lin, L. (2020). Xanthones, a promising anti-inflammatory scaffold: structure, activity, and drug likeness analysis. Molecules 25: 598.

Fenwick, P.S., Macedo, P., Kilty, I.C., Barnes, P.J., and Donnelly, L.E. (2015). Effect of JAK inhibitors on release of CXCL9, CXCL10 and CXCL11 from human airway epithelial cells. PloS One 10: e0128757.

Fotie, J. and Bohle, D.S. (2006). Pharmacological and biological activities of xanthones. Anti-Infect. Agents Med. Chem. 5: 15–31.

Frisch, M.J., Pople, J.A., and Binkley, J.S. (1984). Self-consistent molecular orbital methods 25. Supplementary functions for Gaussian basis sets. J. Chem. Phys. 80: 3265–3269.

Gottlieb, H.E., Kotlyar, V., and Nudelman, A. (1997). NMR chemical shifts of common laboratory solvents as trace impurities. J. Org. Chem. 62: 7512–7515.

Griffith, J.W., Sokol, C.L., and Luster, A.D. (2014). Chemokines and chemokine receptors: positioning cells for host defense and immunity. Annu. Rev. Immunol. 32: 659–702.

Grimblat, N., Gavín, J.A., Hernández Daranas, A., and Sarotti, A.M. (2019). Combining the power of *J* coupling and DP4 analysis on stereochemical assignments: The *J*-DP4 methods. Org. Lett. 21: 4003–4007.

Grimblat, N., Zanardi, M.M., and Sarotti, A.M. (2015). Beyond DP4: an improved probability for the stereochemical assignment of isomeric compounds using quantum chemical calculations of NMR shifts. J. Org. Chem. 80: 12526–12534.

Gupta, S.C., Sundaram, C., Reuter, S., and Aggarwal, B.B. (2010). Inhibiting NF-kappaB activation by small molecules as a therapeutic strategy. Biochim. Biophys. Acta 1799: 775–787.

Halgren, T.A. (1996). Merck molecular force field. I. Basis, form, scope, parameterization, and performance of MMFF94. J. Comput. Chem. 17: 490–519.

Hariharan, P.C. and Pople, J.A. (1973). The influence of polarization functions on molecular orbital hydrogenation energies. Theor. Chim. Acta 28: 213–222.

Hehre, W.J., Ditchfield, R., and Pople, J.A. (1972). Self-consistent molecular orbital methods. XII. Further extensions of Gaussian-type basis sets for use in molecular orbital studies of organic molecules. J. Chem. Phys. 56: 2257–2261.

Jamilloux, Y., El Jammal, T., Vuitton, L., Gerfaud-Valentin, M., Kerever, S., and Sève, P. (2019). JAK inhibitors for the treatment of autoimmune and inflammatory diseases. Autoimmun. Rev. 18: 102390.

Kauhl, U. (2017). *Dissertation*. Johannes Gutenberg-Universität, Mainz.

Kim, C.S., Oh, J., and Lee, T.H. (2020). Structure elucidation of small organic molecules by contemporary computational chemistry methods. Arch. Pharm. Res. 43: 1114–1127.

Kim, H.S., Park, I.Y., Park, Y.J., Lee, J.H., Hong, Y.S., and Lee, J.J. (2002). A novel dihydroxanthenone, AGI-B4 with inhibition of VEGF-induced endothelial cell Growth. J. Antibiot. 55: 669–672.

Kopitar-Jerala, N. (2017). The role of interferons in inflammation and inflammasome activation. Front. Immunol. 8: 873.
Krishnan, R., Binkley, J.S., Seeger, R., and Pople, J.A. (1980). Self-consistent molecular orbital methods. XX. A basis set for correlated wave functions. J. Chem. Phys. 72: 650–654.
Lee, C., Yang, W., and Parr, R.G. (1988). Development of the Colle-Salvetti correlation-energy formula into a functional of the electron density. Phys. Rev. B 37: 785–789.
Lee, E.Y., Lee, Z.H., and Song, Y.W. (2009). CXCL10 and autoimmune diseases. Autoimmun. Rev. 8: 379–383.
Lee, E.Y., Lee, Z.H., and Song, Y.W. (2013). The interaction between CXCL10 and cytokines in chronic inflammatory arthritis. Autoimmun. Rev. 12: 554–557.
Lippke, G. and Thaler, H. (1970). The specific rotation of sorbitol and of the sorbitol molybdate complex. Starch 22: 344–351.
Liu, Q.Y., Wang, Y.T., and Lin, L.G. (2015). New insights into the anti-obesity activity of xanthones from *Garcinia mangostana*. Food Funct. 6: 383–393.
Martínez-García, D., Manero-Rupérez, N., Quesada, R., Korrodi-Gregório, L., and Soto-Cerrato, V. (2019). Therapeutic strategies involving survivin inhibition in cancer. Med. Res. Rev. 39: 887–909.
Masters, K.-S. and Bräse, S. (2012). Xanthones from fungi, lichens, and bacteria: the natural products and their synthesis. Chem. Rev. 112: 3717–3776.
Mohan, S., Syam, S., Abdelwahab, S.I., and Thangavel, N. (2018). An anti-inflammatory molecular mechanism of action of α-mangostin, the major xanthone from the pericarp of *Garcinia mangostana*: an *in silico, in vitro* and *in vivo* approach. Food Funct. 9: 3860–3871.
Nazarski, R.B., Pasternak, B., and Leśniak, S. (2011). Three-component conformational equilibria of some flexible pyrrolidin-2-(thi)ones in solution by NMR data (δC, δH, and nJHH) and their DFT predictions: a confrontation of different approaches. Tetrahedron 67: 6901–6916.
Oeckinghaus, A. and Ghosh, S. (2009). The NF-kappaB family of transcription factors and its regulation. Cold Spring Harb. Perspect. Biol. 1: a000034.
Ohmori, Y. and Hamilton, T.A. (2001). Requirement for STAT1 in LPS-induced gene expression in macrophages. J. Leukoc. Biol. 69: 598–604.
Pérez, M., Soler-Torronteras, R., Collado, J.A., Limones, C.G., Hellsten, R., Johansson, M., Sterner, O., Bjartell, A., Calzado, M.A., and Muños, E. (2014). The fungal metabolite galiellalactone interferes with the nuclear import of NF-κB and inhibits HIV-1 replication. Chem. Biol. Interact. 214: 69–76.
Pfaffl, M.W. (2001). A new mathematical model for relative quantification in real-time RT-PCR. Nucleic Acids Res. 29: 45e.
Riley, K.F., Hobson, M.P., and Bence, S.J. (2006). *Mathematical methods for physics and engineering*, 3rd ed. Cambridge: Cambridge University Press.
Roehm, N.W., Rodgers, H., Hatfield, S.M., and Glasebrook, A.L. (1991). An improved colorimetric assay for cell proliferation and viability utilizing the tetrazolium salt XTT. J. Immunol. Methods 142: 257–265.
Rohr, M., Oleinikov, K., Jung, M., Sandjo, L.P., Opatz, T., and Erkel, G. (2017). Anti-inflammatory tetraquinane diterpenoids from a *Crinipellis species*. Bioorg. Med. Chem. 25: 514–522.
Russo, R.C., Garcia, C.C., Teixeira, M.M., and Amaral, F.A. (2014). The CXCL8/IL-8 chemokine family and its receptors in inflammatory diseases. Expet Rev. Clin. Immunol. 10: 593–619.
Shagufta, I.A. (2016). Recent insight into the biological activities of synthetic xanthone derivatives. Eur. J. Med. Chem. 116: 267–280.
Smith, S.G. and Goodman, J.M. (2010). Assigning stereochemistry to single diastereoisomers by GIAO NMR calculation: the DP4 probability. J. Am. Chem. Soc. 132: 12946–12959.
Spurrell, J.C., Wiehler, S., Zaheer, R.S., Sanders, S.P., and Proud, D. (2005). Human airway epithelial cells produce IP-10 (CXCL10) *in vitro* and *in vivo* upon rhinovirus infection. Am. J. Physiol. Lung Cell Mol. Physiol. 289: L85–L95.
Stephens, P.J., McCann, D.M., Cheeseman, J.R., and Frisch, M.J. (2005). Determination of absolute configurations of chiral molecules using ab initio time-dependent density functional theory calculations of optical rotation: how reliable are absolute configurations obtained for molecules with small rotations. Chirality 17: S52–S64.
Su, Q.G., Liu, Y., Cai, Y.C., Sun, Y.L., Wang, B., and Xian, L.J. (2011). Anti-tumour effects of xanthone derivatives and the possible mechanisms of action. Invest. N. Drugs 29: 1230–1240.
Tamassia, N., Calzetti, F., Ear, T., Cloutier, A., Gasperini, S., Bazzoni, F., McDonald, P.P., and Cassatella, M.A. (2007). Molecular mechanisms underlying the synergistic induction of CXCL10 by LPS and IFN-γ in human neutrophils. Eur. J. Immunol. 37: 2627–2634.
Tashiro, E., Tsuchiya, A., and Imoto, M. (2007). Functions of cyclin D1 as an oncogene and regulation of cyclin D1 expression. Canc. Sci. 98: 629–635.
Tomasi, J., Mennucci, B., and Cancès, E. (1999). The IEF version of the PCM solvation method: an overview of a new method addressed to study molecular solutes at the QM ab initio level. J. Mol. Struct. THEOCHEM 464: 211–226.
Turner, M.D., Nedjai, B., Hurst, T., and Pennington, D.J. (2014). Cytokines and chemokines: at the crossroads of cell signalling and inflammatory disease. Biochim. Biophys. Acta 1843: 2563–2582.
Vosko, S.H., Wilk, L., and Nusair, M. (1980). Accurate spin-dependent electron liquid correlation energies for local spin density calculations: a critical analysis. Can. J. Phys. 58: 1200–1211.
Wan, F. and Lenardo, M.J. (2009). Specification of DNA binding activity of NF-kB proteins. Cold Spring Harb. Perspect. Biol. 1: a000067.
Waugh, D.J.J. and Wilson, C. (2008). The interleukin-8 pathway in cancer. Clin. Canc. Res. 14: 6735–6741.
Weidler, M., Rether, J., Anke, T., and Erkel, G. (2000). Inhibition of interleukin-6 signaling by galiellalactone. FEBS Lett. 484: 1–6.
Wen, Z., Zhong, Z., and Darnell, J.E. (1995). Maximal activation of transcription by Stat1 and Stat3 requires both tyrosine and serine phosphorylation. Cell 82: 241–250.
White, T.J., Bruns, T., Lee, S., and Taylor, J. (1990). Amplification and direct sequencing of fungal ribosomal RNA genes for phylogenetics. In: Innis, M.A., Gelfand, D.H., Sninsky, J.J., and White, T.J. (Eds.), *PCR protocols: a guide to methods and applications*. Academic Press, San Diego, pp. 315–322.
Willwacher, J., Heggen, B., Wirtz, C., Thiel, W., and Fürstner, A. (2015). Total synthesis, stereochemical revision, and biological reassessment of mandelalide A: chemical mimicry of intrafamily relationships. Chem. Eur J. 21: 10416–10430.

Supplementary Material: The online version of this article offers supplementary material (https://doi.org/10.1515/hsz-2021-0192).

7.3.3 Bestimmung der relativen Konfiguration eines Sesquiterpenlactons

In Kooperation mit der Arbeitsgruppe [redacted] wurden neben zehn bekannten Naturstoffen fünf neuartige Naturstoffe **162**–**166** (in der Publikation **1**–**5**) mit germacranoliden Strukturelementen aus einer Pflanze der Gattung *Vernonia* isoliert und deren Struktur aufgeklärt (Abbildung 7.10).

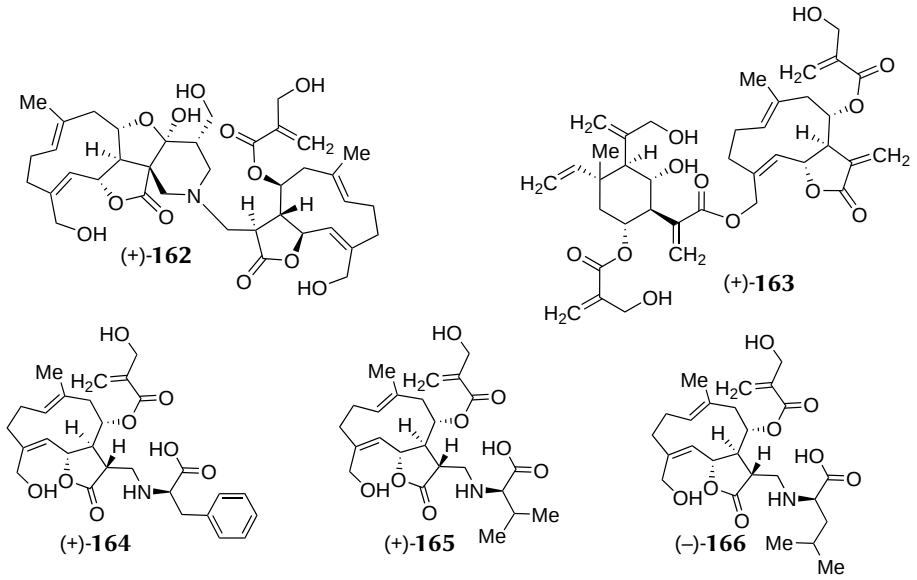

Abbildung 7.10: Neu isolierte Naturstoffe **162**–**166** mit germacranolidem Grundgerüst aus der Pflanzenart *Vernonia tufnelliae*.[567]

Die Strukturaufklärung der isolierten Naturstoffe ergab für Verbindung **162** ein bisher unbeschriebenes 10/5/5/6-tetrazyklisches Grundgerüst und für Verbindung **163** eine Grundstruktur, die aus einer verknüpften Eleman- und Germacranolid-Einheit bestand. Bei den Naturstoffen **164**–**166** handelt es sich um Derivate der Germacranolid-Struktur, die auf unterschiedlichen Aminosäuren basieren. Da es mittels 2D-NMR-Spektroskopie nicht möglich war, die relative Struktur von Sesquiterpenlacton **162** (in der Publikation **1**) aufzuklären, wurde auf Grundlage des DP4+-Modells von Sarotti *et al.* und dem Vergleich von gemessenen und simulierten ECD-Spektren die absolute Konfiguration vorhergesagt.[469] Darüber hinaus wurde für dieses Alkaloid (**162**, in der Publikation **1**) sowohl ein möglicher Weg der Biosynthese als auch der Trivialname Tufnelacton A vorgeschlagen.

Die Rohextrakte sowie die isolierten Naturstoffe **162**–**166** (in der Publikation **1**–**5**, **7**–**10** und **12**–**15**) wurden auf ihre inhibitorische Wirkung auf das Wachstum von menschlichen Krebszellen der HeLaS3-Zelllinie, verschiedenen Pilzen und Bakterien getestet, wobei sich alle Verbindungen mit einem IC_{50} > 10 µM als inaktiv erwiesen (Abbildung 7.11).[567]

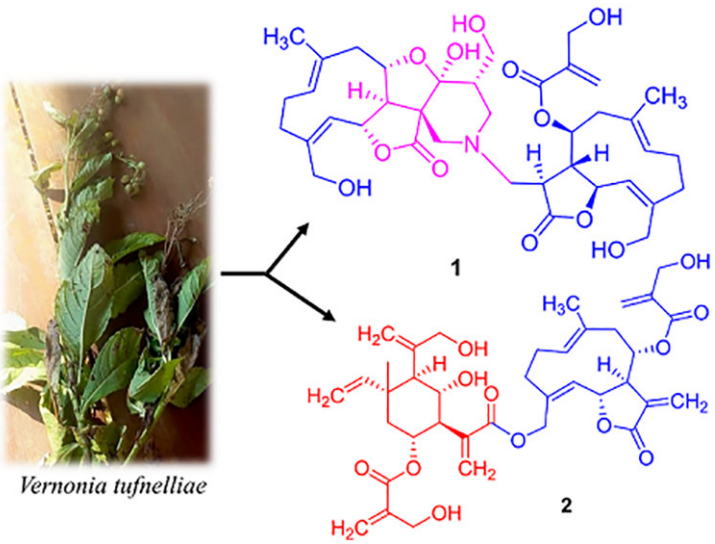

Abbildung 7.11: *Graphical abstract* der Publikation „Sesquiterpene Lactones from *Vernonia tufnelliae*: Structural Features, Stereochemistry, and Biological Evaluation“.[567]

Die Naturstoffe wurden von [redacted] isoliert und in ihrer Struktur aufgeklärt sowie von [redacted] auf ihre biologische Aktivität untersucht. Die Berechnung der chemischen Verschiebungskonstanten auf DFT-Level und die Anwendung des DP4+-Modells sowie die Messung der ECD-Spektren in Kombination mit zeitabhängigen DFT-Berechnungen für Tufnelacton A (**162**, in der Publikation **1**) wurden von J. Groß durchgeführt. Das Manuskript wurde von allen Autoren erstellt.[18]

[18] *Reprinted with permission from G. Bitchagno, A. Schueffler, J. Gross, M. Krumb, P. Tané, T. Opatz, J. Nat. Prod., 2022, 85, 1681–1690. Copyright ©2022, American Chemical Society.*

JOURNAL OF NATURAL PRODUCTS

pubs.acs.org/jnp Article

Sesquiterpene Lactones from *Vernonia tufnelliae*: Structural Characterization and Biological Evaluation

Gabin Thierry M. Bitchagno,* Anja Schüffler, Jonathan Gross, Matthias Krumb, Pierre Tane,# and Till Opatz*

Cite This: *J. Nat. Prod.* 2022, 85, 1681−1690 Read Online

ACCESS | Metrics & More | Article Recommendations | Supporting Information

ABSTRACT: The genus *Vernonia* is an extremely rich source of biologically active sesquiterpene lactones. The present report describes the spectroscopic structure elucidation and the cytotoxic and antimicrobial properties of five hitherto unknown germacranolide-like sesquiterpenoids and several known compounds. These new derivatives include a compound (**1**) with an unprecedented 10/5/5/6 tetracyclic framework featuring a hexahydro-1*H*,3*H*,7*H*-furo[3′,4′:3,4]furo[3,2-*c*]pyridin-1-one core resulting from an intramolecular cyclization cascade involving a methacrylate substituent and a low molecular weight amine. Furthermore, an elemane−germacranolide hybrid (**2**) and three amino acid-derived lactones (**3**−**5**) were characterized. A plausible biosynthetic pathway to the key alkaloid is presented, while shielding tensor calculations using DFT in combination with the DP4+ method were applied to elucidate its stereostructure. The newly characterized compounds along with ten known sesquiterpene lactones and phenolic compounds have been isolated from *Vernonia tufnelliae*, a medicinal plant from the western region of Cameroon. Their structures were consistent with spectroscopic and spectrometric data recorded. The present report is the first investigation of the chemistry and biology of *V. tufnelliae*.

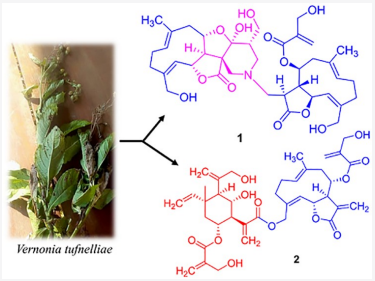

Terpenoid alkaloids are constituted by isoprene-like units with, in general, one nitrogen atom being incorporated in the terpene skeleton. They are known as pseudo- or cryptoalkaloids, referring to their "false" biosynthetic origins, being built from prenyl units rather than from amino acids like "true" alkaloids.[1] Although the sources of nitrogen are not yet well established, β-aminoethanol, ethylamine, or methylamine have been found to be involved in the biosynthesis of these compounds.[2] In this process, the incorporation of nitrogen can occur before or after the cyclase phase.[1] Terpenoid alkaloids (including *C*-dihydrotoxiferine, *C*-curarine, and *C*-calebassine) have been used since ancient times as poisons for hunting or in homicides and have served for many years as ingredients in traditional medicines around the world.[3] They are not widespread in Nature but often exhibit interesting or even unprecedented structures.

The genus *Vernonia* comprises roughly 350 species of flowering herbaceous shrubs distributed in tropical regions around the world. *V. tufnelliae* S. Moore (Asteraceae) is a flowering medicinal shrub reported to occur in the western region of Cameroon, Congo, Equatorial Guinea (Rio Muni), Uganda, and Tanganyika.[4] The local population in West Cameroon, where the plant was collected for the present investigation, uses the leaves of *V. tufnelliae* to relieve fever. The chemical and biological properties of *V. tufnelliae* have not been investigated previously, but the genus is represented chemically by sesquiterpene lactones and polyoxygenated stigmastane derivatives belonging to the germacranolide, eudesmanolide, and guaianolide classes.[5] These compounds are responsible not only for the bitter taste of species from this genus[5] but also for their well-known cytotoxic and anti-inflammatory properties.[6−10] The present report reveals sesquiterpene lactone hybrids with unprecedented scaffolds that incorporate germacranolide, elemane, and amino acid subunits. Compound **1** contains an unprecedented 10/5/5/6 tetracyclic moiety featuring a hexahydro-1*H*,3*H*,7*H*-furo-[3′,4′:3,4]furo[3,2-*c*]pyridin-1-one unit linked to a typical cyclodecane ring of germacrene, while compound **2** is the first elemane−germacranolide heterodimer ever to have been found in Nature. The present report is part of an ongoing research initiative on bioactive metabolites from Cameroonian folk medicine.[11−15]

RESULTS AND DISCUSSION

A total of 15 compounds (Figure 1) were isolated, their spectroscopic features interpreted, and their structures

Received: January 16, 2022
Published: June 15, 2022

https://doi.org/10.1021/acs.jnatprod.2c00055
J. Nat. Prod. 2022, 85, 1681−1690

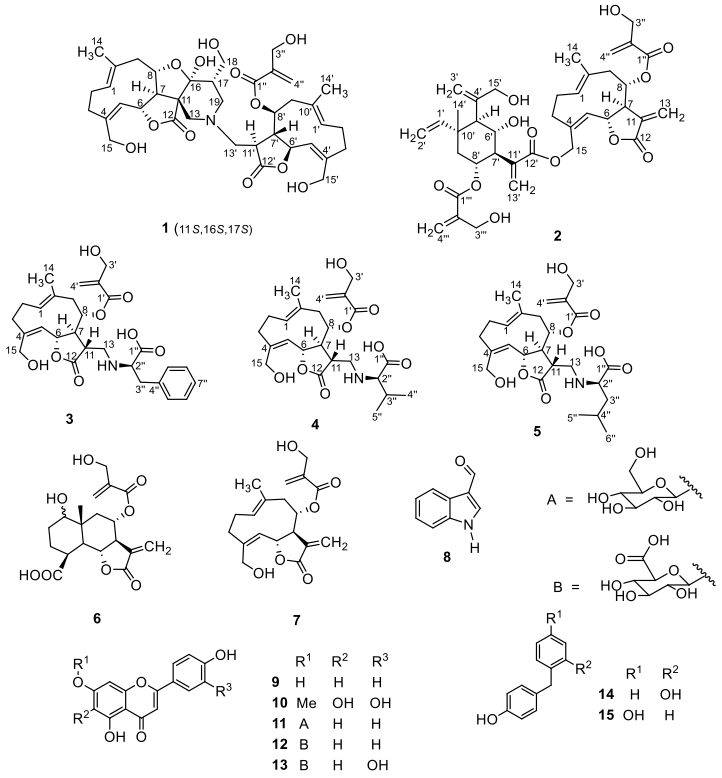

Figure 1. Structures of compounds **1**−**15** from *Vernonia tufnelliae*.

elucidated on this basis. Five structures were unprecedented in Nature, including a germacranolide−alkaloid dimer (**1**), an elemane−germacranolide dimer (**2**), and three amino acid-containing germacranolide derivatives (**3**−**5**). Spectroscopy (NMR, IR, UV), mass spectrometry, and spectral simulation were used for compound structure elucidation.

Compound **1** was obtained as a colorless powder from hexane with an $[\alpha]^{22}_{D}$ of +11.2 (*c* 0.8, acetone). Its positive-mode HRESIMS exhibited a protonated molecular ion peak $[M + H]^+$ at *m*/*z* 714.3471, corresponding to the molecular formula $C_{38}H_{52}NO_{12}^+$ (calcd for $C_{38}H_{52}NO_{12}^+$ 714.3484). Compound **1** showed a UV absorption maximum at 200 nm together with a shoulder at 216 nm in acetonitrile, and its infrared spectrum exhibited a broad band at 3306 cm^{-1} attributable to a hydroxy group, while a sharp band occurred at 1764 cm^{-1}, characteristic of a γ-lactone group paired with a band at 1714 cm^{-1} for the carbonyl group of esters. The ^1H and ^{13}C NMR spectra of compound **1** showed resonances of an α,β-unsaturated carbonyl at δ_C 165.3 (C-1″), a tertiary olefinic carbon at δ_C 141.6 (C-2″), an *exo*-methylene group at δ_H 6.20 (br d, *J* = 1.6 Hz, H_1-4″), 5.95 (br d, *J* = 1.6 Hz, H_2-4″), and δ_C 123.3 (C-4″), and a hydroxymethylene carbon at δ_H 4.33 (brs, H-3″) and δ_C 60.6 (C-3″) ascribed to a hydroxymethacrylate moiety. A spin system inferred from $^1H-^1H$ COSY correlations (Figure 2), between H-1′/H-2′/H-3′ and H-6′/H-7′/H-8′/H-9′/H-11′/H-13′, together with HMBC correlations (Figure 2), from H-15′ (δ_H 4.28 and 4.06) to carbons C-3′ (δ_C 33.9), C-4′ (δ_C 142.3), and C-5′ (δ_C 129.7), from H-7′ (δ_H 3.63) to carbons C-5′, C-6′ (δ_C 77.1), C-8′ (δ_C 73.6), C-9′ (δ_C 48.6), C-11′ (δ_C 44.3), and C-13′ (δ_C 54.3), from H-11′ (δ_H 2.67) to carbons C-12′ (δ_C 177.6) and C-13′, and from H-14′ (δ_H 1.59) to carbons C-1′ (δ_C 129.4), C-9′ (δ_C 48.6), and C-10′ (δ_C 131.9), revealed a germacranolide moiety in the structure of compound **1**.[16−19] The hydroxymethacrylate group could be attached to the cyclodecane backbone according to the HMBC cross-peak from H-8′ (δ_H 5.15) to the carbonyl C-1″. In addition, a similar set of signals was observed in the NMR spectrum of compound **1** (Tables 1 and 2) and suggested the presence of a second germacranolide-like moiety as part of this molecule. However, unlike the former, the latter did not contain a hydroxymethacrylate group, although this unit is represented in almost all sesquiterpene lactones reported in the genus *Vernonia*.[20−22] In contrast, new resonances appeared that included three deshielded methylenes at δ_H 2.75/2.13 (2H, m, H-13), 3.95/3.73 (2H, m, H-18), and 2.79/2.06 (2H, m, H-19) and an aliphatic methine at δ_H 2.58 (1H, m, H-17) as part of a new spin system deduced from the $^1H-^1H$ COSY correlations (Figure 2) between H-17/H-18/H-19. The nature of this unit was established by HMBC correlations (Figure 2) from H-13 to carbons C-11 (δ_C 58.3), C-12 (δ_C 174.6), C-15 (δ_C 59.0), and C-16 (δ_C 104.6) and from H-18 to carbons C-

https://doi.org/10.1021/acs.jnatprod.2c00055
J. Nat. Prod. 2022, 85, 1681−1690

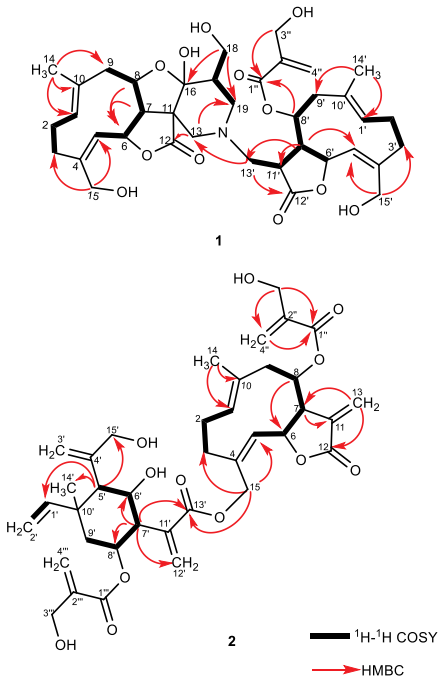

Figure 2. HMBC (red arrows) and ^{1}H, ^{1}H COSY (bold lines) interactions in compounds **1** and **2**.

16, C-17, and C-19 (δ_C 59.1), suggesting a hexahydro-1*H*,3*H*,7*H*-furo[3′,4′:3,4]furo[3,2-*c*]pyridin-1-one moiety fused to the germacrene moiety.

Thus, compound **1** bears a new nitrogen-containing 10/5/5/6 tetracyclic scaffold where both germacranolide-like fragments of compound **1** are linked through a tertiary nitrogen, as supported by the HMBC cross-peaks from H-13′ (δ_H 2.90) to carbon C-13 (δ_C 54.0) and the odd molecular mass obtained for **1**. A ^{1}H,^{15}N-HMBC spectrum was recorded but turned out to be featureless due to a too low signal/noise ratio. Thus, compound **1** is a member of the sesquiterpenoid alkaloid group, with the origin of nitrogen as well as its biosynthesis not fully understood. Nevertheless, a possible biosynthetic scheme from which compound **1** with its unprecedented ring system could be obtained was proposed (Scheme 1).

The reactive sesquiterpene lactone onopordopicrin (**7**), abundant in the plant, could undergo Michael addition through its α-methylene-γ-butyrolactone group with a source of nitrogen followed by an intramolecular Claisen condensation (5-*exo*-*trig* and therefore preferred according to the Baldwin classification), releasing the alcoholate at C-8, which gets protonated. The *N*-alkylation process of the already bonded nitrogen could continue by bond formation to the *exo*-methylene of the hydroxymethacrylate group, affording a piperidine ring through a 6-*endo*-*trig* cyclization. The enolate obtained could be rearranged to the carbanion and then to the alcoholate at C-8 followed by another proton exchange. The hydroxy group at C-8 could further attack the carbonyl of the piperidine ring, leading to a new five-membered ring (5-*exo*-*trig* cyclization) that undergoes a second proton shift to afford a fused tetracyclic ring system including a lactone. Subsequent cleavage of the substituent on nitrogen and alkylation of the piperidine (or an inverse sequence of the latter two steps) would give a dimerization with a second molecule of onopordopicrin (**7**) through its activated α-methylene-γ-butyrolactone, resulting in compound **1** (Scheme 1). The compound **1** thus obtained may be taken as the precursor of a new subclass of sesquiterpenoid alkaloid secondary metabolites with four fused rings including a lactone. Brocksom and collaborators identified only three subclasses of sesquiterpenoid alkaloids in their seminal review of 2017, including the most abundant dendrobines and guaipyridines, as well as the rotundines, which were represented by just three members.[23]

The relative configuration of the stereocenters of each germacranolide moiety of compound **1** is similar to that of related compounds in the literature: the butyrolactone is *trans*-fused; the proton H-7 is on one side; the protons H-6 and H-8 are on the opposite side of the ring system. The latter protons are also in proximity to the methyl (C-14) and the hydroxymethylene (C-15) groups.[17−19,24] This arrangement was supported by NOESY cross-peaks (Figure 3) from H-6 to H-8; H-8 to H-14; and H-14 to H-15 then from H-6′ to H-8′; H-8′ to H-14′/H-11′; and H-14′ to H-15′. The double bonds C-1/C10 and C-4/C-5 in both cyclodecyl rings are *trans*- and *cis*-configured, respectively, as indicated by NOESY interactions from H-14 to H-2 (δ_H 2.53) and H-8; H-14′ to H-2′ (δ_H 2.33) and H-8′; and H-5′ to H-3′ (δ_H 1.98) and H-7′. However, the configuration of the newly generated stereocenters C-11 and C-16 could not be deduced directly from the NOESY spectrum (Figure 3). Moreover, H-17 showed no nontrivial cross-peaks. Therefore, a conformational analysis [Spartan'10 (MMFF level of theory)][25] was performed alongside geometry optimization [B3LYP[26−29] functional in combination with the Pople basis set 6-31G(d)][30,31] and density functional theory (DFT) calculation (Gaussian 16, rev. C.01)[32] of the shielding tensors [mPW1PW91/6-31+G-(d,p)][33−35] for every conformer of all eight diastereomers related to these three stereocenters (C-11, C-16, and C-17), using the DP4+ method developed by Sarotti et al. The comparison of the calculated and Boltzmann-weighted shielding tensors with the experimental NMR shifts allowed no unequivocal stereochemical assignment. Nevertheless, the 11*R*,16*R*,17*R*- and the 11*S*,16*S*,17*S*-configurations provide the best match with the measured values (see the Supporting Information). Furthermore, the electronic circular dichroism (ECD) spectrum of compound **1** was recorded and compared to the simulated spectra of the two remaining possible diastereomeric configurations 11*R*,16*R*,17*R* and 11*S*,16*S*,17*S*. Both these calculated data as well as compound **1** feature the same excitation energies in the detected area of the spectrum with a strong positive Cotton effect with a maximum at 220 nm, inconclusive in the assignment of the relative but supportive of the overall absolute configuration of **1**. Analysis of the corresponding molecular orbitals (MOs) revealed that the recorded excitations are most likely due to $\pi-\pi^*$ transitions in the onopordopicrin portion of compound **1**. This can be expected since the latter part possesses the same configuration in both possible diastereomers. Significant differences for the diastereomers could only be indicated in the spectral region beyond the solvent cutoff and therefore were not detectable. A comparison of the experimental specific

https://doi.org/10.1021/acs.jnatprod.2c00055
J. Nat. Prod. 2022, 85, 1681−1690

Table 1. ^{1}H (600 MHz) NMR Spectroscopic Data for Compounds 1−5 (δ in ppm, J in Hz)

position	1[a]	2[a]	3[b]	4[b]	5[c]
1	5.19, m	5.16, m	4.88, m	4.96, m	5.10, m
2	2.15, m; 2.53, m	2.36, m; 2.23, m	2.14, m; 2.08, m	2.17, m; 2.08, m	2.31, m; 2.24, m
3	2.61, m; 2.41, m	2.59, m; 2.07, m	2.48, m; 1.82, m	2.49, m; 1.82, m	2.60, m; 2.01, m
4					
5	5.22, m	5.18, m	4.55, d (10.0)	4.74, d (10.0)	4.93, d (10.0)
6	5.21, m	5.23, m	5.09, t (9.5)	5.14, t (9.4)	5.43, m
7	2.52, m	3.39[d]	2.56, m	2.63, m	2.73, m
8	4.09, m	5.26, m	5.04, m	5.08, m	5.34, td (9.7, 2.5)
9	2.58, m; 2.27, m	2.63, m; 2.58, m	2.29, m	2.42, m; 2.31, d (11.9)	2.53, m
10					
11			2.65, m	2.71, m	3.23, m
12					
13	2.13, m; 2.75, m	6.16, br d (3.6); 5.84, br d (3.6)	2.89, m	2.93, d (12.0, 6.5); 2.76, m	3.48, m; 3.38, m
14	1.73, s	1.59, s	1.43, s	1.45, s	1.59, s
15	4.26, d (13.5); 3.91, d (13.5)	4.82, m	4.03, dd (13.7, 4.5); 3.82, dd (13.7, 5.8)	4.06, dd (13.6, 4.0); 3.84, dd (13.6, 5.3)	4.27, d (13.6); 4.07, d (13.6)
16					
17	2.58, m				
18	3.95, m; 3.73, m				
19	2.79;[d] 2.06, m				
1′	5.29, m	5.82, m			
2′	2.16, m; 2.33, m	4.94[d]			
3′	2.61, m; 1.98, m	5.36, s; 4.98, s	4.13, m	4.13, br s	4.33, m
4′			6.10, d (1.7); 5.82, d (1.7)	6.13, d (2.0); 5.86, d (2.0)	6.31, d (1.6); 6.01, d (1.6)
5′	5.06, d (10.1)	2.02, m			
6′	5.20, m	4.29, m			
7′	3.63, m	2.79, m			
8′	5.15, m	5.43, m			
9′	2.70, m; 2.36, m	1.84, dd (12.3, 4.4); 1.67, m			
10′					
11′	2.67, m				
12′					
13′	2.90[d]	6.32, s; 5.86, s			
14′	1.59, s	1.22, s			
15′	4.28, d (13.5); 4.06, d (13.5)	4.03, m; 3.91, m			
1″					
2″			3.28, t (7.0)	2.77, d (6.1)	3.39, m
3″	4.33, br s	4.32, br s	2.86, d (6.3); 2.78, dd (13.6, 7.6)	1.81, m	1.67, m; 1.40, m
4″	6.20, br d (1.6); 5.95, br d (1.6)	6.29, br s; 6.02, s		0.87, d (6.2)	1.94, m
5″			7.23, m	0.88, d (6.2)	1.05, d (7.4)
6″			7.27, m		1.03, d (7.4)
7″			7.21, m		
8″			7.27, m		
9″			7.23, m		
1‴					
2‴					
3‴		4.23, br s			
4‴		6.14, d (1.8); 5.86, br s			

[a]Data measured in acetone-d_6. [b]Data measured in DMSO-d_6. [c]DMSO-d_6/MeOH-d_4 (1:4) was used, and spectra were calibrated with the residual signal of MeOH-d_4. [d]Signal identified from the HSQC spectrum due to overlap.

rotation value with the simulated values was inconclusive as well (see the Supporting Information for further details and example figures). As a result, compound **1** was characterized as an N-containing germacranolide heterodimer for which the trivial name tufnelactone A is proposed.

Compound **2** was obtained as a colorless powder from hexane with an $[\alpha]^{22}_{D}$ of +29.1 (c 0.55, acetone). Its positive-mode HRESIMS exhibited a sodium adduct ion peak $[M + Na]^+$ at m/z 719.3038, corresponding to the molecular formula, $C_{38}H_{48}O_{12}Na^+$ (calcd 719.3038 for $C_{38}H_{48}O_{12}Na^+$).

https://doi.org/10.1021/acs.jnatprod.2c00055
J. Nat. Prod. 2022, 85, 1681−1690

Table 2. ^{13}C (150 MHz) NMR Spectroscopic Data for Compounds 1−5 (δ in ppm)

position	1[a]	2[a]	3[b]	4[b]	5[c]
1	128.4, CH	129.4, CH	129.4, CH	129.5, C	129.6, CH
2	25.2, CH_2	25.9, CH_2	25.9, CH_2	25.9, CH_2	25.7, CH_2
3	33.4, CH_2	34.4, CH_2	34.2, CH_2	34.2, CH_2	34.2, CH_2
4	144.5, C	138.9, C	143.5, C	143.7, C	144.3, C
5	128.6, CH	131.3, CH	128.9, CH	128.9, CH	128.05, CH
6	78.8, CH	76.2, CH	76.5, CH	76.6, CH	77.6, CH
7	63.3, CH	52.3, CH	50.7, CH	51.4, CH	52.6, CH
8	79.9, CH	72.8, CH	73.6, CH	73.7, CH	73.2, CH
9	44.1, CH_2	48.3, CH_2	48.5, CH_2	48.5, CH_2	48.3, CH_2
10	129.9, C	132.7, C	132.6, C	132.6, C	132.6, C
11	58.3, C	136.4, C	46.0, CH	46.1, CH	42.2, CH
12	174.6, C	169.5, C	177.9, C	178.0, C	177.6, C
13	54.0, CH_2	123.8, CH_2	46.8, CH_2	48.4, CH_2	48.2, CH_2
14	16.9, CH_3	16.5, CH_3	16.8, CH_3	16.8, CH_3	16.1, CH_3
15	59.0, CH_2	61.7, CH_2	59.2, CH_2	59.3, CH_2	59.6, CH_2
16	104.6, C				
17	43.8, CH				
18	61.1, CH_2				
19	59.1, CH_2				
1′	129.4, CH	147.5, CH	165.1, C	165.1, C	165.0, C
2′	25.5, CH_2	110.6, CH_2	141.4, C	141.4, C	141.0, C
3′	33.9, CH_2	111.8, CH_2	60.0, CH_2	60.0, CH_2	60.5, CH_2
4′	142.3, C	147.5, C	124.3, CH_2	124.2, CH	125.3, CH_2
5′	129.7, CH	55.7, CH			
6′	77.1, CH	70.7, CH			
7′	48.4, CH	55.0, CH			
8′	73.6, CH	70.9, CH			
9′	48.6, CH_2	43.6, CH_2			
10′	131.9, C	40.2, C			
11′	44.3, CH	139.2, C			
12′	177.6, C	166.2, C			
13′	54.3, CH_2	127.6, CH_2			
14′	16.0, CH_3	18.3, CH_3			
15′	59.7, CH_2	66.5, CH_2			
1″	165.3, C	164.8, C	175.6, C	176.0, C	177.6, C
2″	141.6, C	141.1, C	63.4, CH	68.4, CH	67.5, CH
3″	60.6, CH_2	60.4, CH_2	39.1, CH_2	31.2, CH_2	25.6, CH_2
4″	123.3, CH_2	124.0, CH_2	138.7, C	18.9, CH_3	36.5, CH_2
5″			129.7, C	19.9, CH_3	14.8, CH_3
6″			128.6, C		11.5, CH_3
7″			126.7, C		
8″			128.6, C		
9″			129.7, C		
1‴		164.8, C			
2‴		141.2, C			
3‴		60.3, CH_2			
4‴		122.8, CH_2			

[a]Data measured in acetone-d_6. [b]Data measured in DMSO-d_6. [c]DMSO-d_6/MeOH-d_4 (1:4) was used, and spectra were calibrated with the residual solvent signal of MeOH-d_4.

Compound **2** showed only weak shoulders in its UV spectrum at 275 and 340 nm in acetonitrile, and its IR spectrum exhibited a broad band at 3381 cm^{-1} attributable to a hydroxy group, along with a sharp band at 1762 cm^{-1} characteristic for a γ-lactone paired with a band at 1713 cm^{-1} for the carbonyl group of esters. Compound **2** showed two sets of signals, of which one was similar to those of onopordopicrin (**7**), which are listed for compound **1** in Tables 1 and 2. The ^1H and ^{13}C NMR spectra of the second set displayed three exomethylenes at δ_H 6.32 (s, H_1-13′), 5.86 (s, H_2-13′), 5.36 (s, H_1-3′), 4.98 (s, H_2-3′), and 4.94 (m, H_1-2′) and at δ_C 127.6 (C-13′), 111.8 (C-3′), and 110.6 (C-2′), an olefinic methine at δ_H 5.82 (s, H-1′) and δ_C 147.5 (C-1′), a hydroxymethylene at δ_H 4.03 (m, H_1-15′), 3.91 (m, H_2-15′) and δ_C 66.5 (C-15′), and a methyl at δ_H 1.22 (s, H-14′) and δ_C 18.3 (C-14′). A spin system inferred from the ^1H, ^1H COSY spectrum (Figure 2) by connectivities between H-5′/H-6′/H-7′/H-8′/H-9′ revealed a cyclohexane ring in the structure of compound **2**. The positions of the methyl, vinyl, 3-hydroxypropen-2-yl, and 2-propenoyl substituents were defined by HMBC cross-peaks

https://doi.org/10.1021/acs.jnatprod.2c00055
J. Nat. Prod. 2022, 85, 1681−1690

Scheme 1. Proposed Biosynthetic Route to the Piperidine Ring Formation in Compound 1

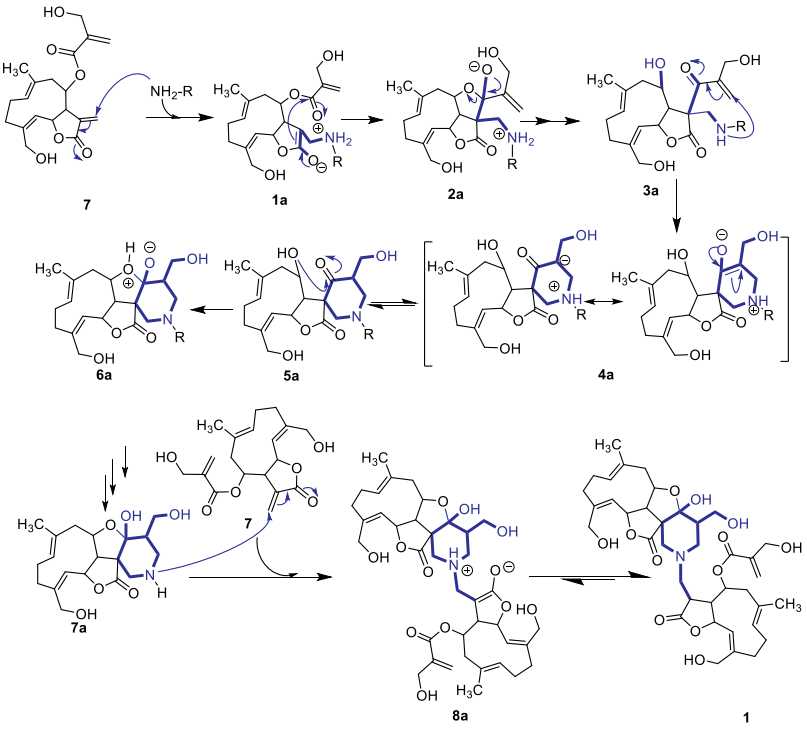

from H-5′ (δ_H 2.02) to carbons C-14′, C-1′, and C-15′ and from H-7′ (δ_H 2.79) to carbons C-6′ (δ_C 70.7), C-8′ (δ_C 70.9), C-12′, and C-13′. This moiety of compound **2** so determined belongs to the elemane type of sequiterpenes, with a ring-opened C-6/C-12 γ-lactone, a structural motif widespread in the family Asteraceae.[17−19,24] Its biosynthetic origin is likely a [3,3]-sigmatropic rearrangement (Cope rearrangement) of a germacranolide-type sesquiterpenoid.[36,37] The point of attachment of the elemane moiety to the germacranolide was located based on HMBC cross-peaks (Figure 2) from H-15 (δ_H 4.82) to carbon C-12′ (δ_C 166.2). The configuration of the germacranolide-type part of the molecule was similar to that of compound **1** and onopordopicrin (**7**): NOESY cross-peaks (Figure 4) from H-6 to H-8, H-8 to H-14, H-14 to H-15 and H-2 (δ_H 2.36), H-1 to H-9 (δ_H 2.63), and H-5 to H-3 (δ_H 2.07) and H-7. Moreover, the large vicinal coupling constant between H-5′ and H-6′ ($J_{5',6'}$ = 10.4 Hz) was suggestive of an antiperiplanar orientation. The NOESY cross-peaks (Figure 4) between H-6′/H-8′/H-14′ and between H-5′/H-9′/H-7′/H-1′ supported the configuration of **2** as being similar to that of related compounds in the literature.[17−19,24] Thus, compound **2** was characterized as the first ever reported elemane−germacranolide heterodimer in Nature, for which the trivial name tufnelactone B is being proposed.

Compounds **3**−**5** were found to share the same core skeleton, which was identified as 11,13-dihydroonopordopicrin and is similar to the structure of compound **1**. Compound **3** was obtained as a white powder from MeOH with an $[\alpha]^{22}_D$ of +13.3 (*c* 0.45, DMSO). Its molecular formula, $C_{28}H_{35}NO_8$, was deduced from its positive-mode HRESIMS, which showed a protonated molecular ion peak $[M + H]^+$ at *m*/*z* 514.2445 (calcd for $C_{28}H_{36}NO_8^+$, 514.2435). Compound **3** displayed a UV absorption maximum at 203 nm in acetonitrile, and its IR spectrum exhibited absorption bands at 3364 cm^{-1} for a hydroxy group, 1754 and 1708 cm^{-1} for carbonyl groups, and 1657 and 1632 cm^{-1} for aromatic and olefinic double bonds. The NMR data were supportive of the occurrence of a germacranolide moiety (Tables 1 and 2), as described for compound **1**. The ^1H and ^{13}C NMR spectra of compound **3** gave signals for an *N*-methine at δ_H 3.28 (t, *J* = 7.0 Hz, H-2″) and δ_C 63.4 (C-2″) and a benzylic methylene at δ_H 2.86 (br d, *J* = 6.3 Hz, H_1-3″), 2.78 (dd, *J* = 13.6 and 7.6 Hz, H_2-3″), and δ_C 39.1 (C-3″). A monosubstituted benzene ring substructure of the molecule was also evident from signals at δ_H 7.27 (m, H-6″/8″), 7.23 (m, H-5″/9″), 7.21 (m, H-7″) and δ_C 138.7 (C-4″), 129.7 (C-5″/C-9″), 128.6 (C-6″/C-8″), and 126.7 (C-7″). Analysis of these signals gave evidence of **3** containing a phenylalanine unit, which was bonded to the germacranolide fragment, as judged by the HMBC cross-peak (Figure 5) from H-2″ to C-13 (δ_C 46.8).

Compound **4** was also obtained as a white powder from MeOH with an $[\alpha]^{22}_D$ of +16.0 (*c* 1.0, DMSO). Its molecular formula, $C_{24}H_{35}NO_8$, was deduced from its positive-mode HRESIMS, which showed a protonated molecular ion peak $[M + H]^+$ at *m*/*z* 466.2436 (calcd for $C_{24}H_{36}NO_8^+$, 466.2435). Its UV spectrum presented a maximum at 204 nm in methanol,

https://doi.org/10.1021/acs.jnatprod.2c00055
J. Nat. Prod. 2022, 85, 1681−1690

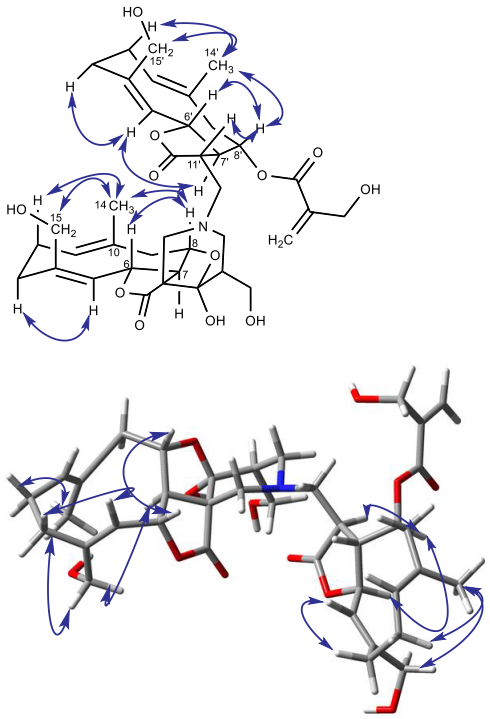

Figure 3. NOESY interactions in compound **1** (11*S*,16*S*,17*S*).

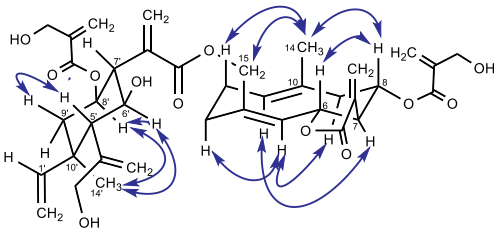

Figure 4. NOESY correlations of compound **2**.

and its IR spectrum exhibited a broad band at 3392 cm^{-1} attributable to a hydroxy group and a broad band at 1655 cm^{-1} for the presence of a carbonyl and olefinic double bonds. As for compound **3**, the NMR data revealed the presence of a germacranolide moiety (Tables 1 and 2), as described for compound **1**. Evidence in the ^{1}H and ^{13}C NMR spectra was presented for compound **4** containing an *N*-methine at δ_H 2.77 (d, J = 6.1 Hz, H-2″) and δ_C 68.4 (C-2″) and an isopropyl group at δ_H 1.81 (m, H-3″), 0.87 (d, J = 6.2 Hz, H-4″), 0.88 (d, J = 6.2 Hz, H-5″) and δ_C 31.2 (C-3″), 18.9 (C-4″), and 19.9 (C-5″). Hence, **4** was determined to contain a valine unit, linked to the germacranolide moiety, as judged by the HMBC cross-peak (Figure 5) between H-2″ and C-13 (δ_C 48.4).

Finally, compound **5** was obtained as a white powder from MeOH with an $[\alpha]^{22}_{D}$ of −2.5 (*c* 0.8, DMSO). Its molecular formula, $C_{25}H_{37}NO_8$, was deduced from its positive-mode

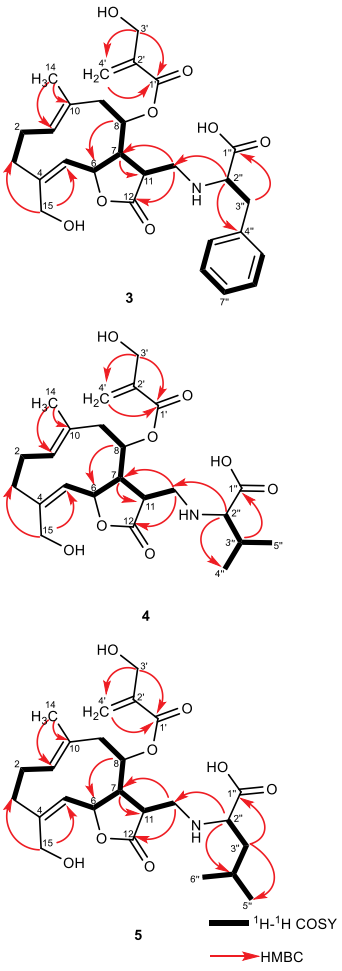

Figure 5. HMBC and $^{1}H-^{1}H$ COSY interactions in compounds **3**−**5**.

HRESIMS, which showed a sodium adduct ion peak [M + Na]$^+$ at m/z 502.2419 (calcd for $C_{25}H_{37}NO_8Na^+$, 502.2411). Its UV spectrum presented a maximum at 204 nm in methanol, and its IR spectrum exhibited bands at 3402 cm^{-1} attributable to a hydroxy group, at 1754 and 1709 cm^{-1} for carbonyl groups, and at 1628 and 1565 cm^{-1} for olefinic double bonds. On the basis of the NMR data and in accordance with the previous observations, compound **5** was also assigned with a germacranolide moiety as described for compound **1** (Tables 1 and 2). The ^{1}H and ^{13}C NMR spectra of compound **5** gave evidence for an *N*-methine at δ_H 3.39 (m, H-2″) and δ_C 67.5 (C-2″) and an isobutyl group at δ_H 1.94 (m, H-4″), 1.67/1.40 (m, H-3″), 1.05 (d, J = 7.4 Hz, H-5″), 1.03 (d, J = 7.4 Hz, H-6″) and δ_C 36.5 (C-4″), 25.6 (C-3‴), 14.8 (C-5″), and 11.5 (C-6″). Hence, **5** was assigned with a leucine present, which was connected to the germacranolide moiety in the same manner as in its congeners **3** and **4**.

https://doi.org/10.1021/acs.jnatprod.2c00055
J. Nat. Prod. 2022, 85, 1681−1690

This is the first report of amino acid-containing sesquiterpenoids from the genus *Vernonia*. These sesquiterpenoid−amino acid hybrid molecules impressively demonstrate the strong electrophilic reactivity of the α-methylene-γ-butyrolactone group in sesquiterpene lactones. Some instances have been reported in *Anvillea garcinii*, a member of the Asteraceae family.[38] Once biosynthesized, the sesquiterpene lactones can undergo rapid and spontaneous nonenzymatic condensation with a nitrogen nucleophile as in the formation of isoindolinone analogues (e.g., azacoccone, rinacerin, and stachyflim derivatives)[39−41] presumed to be produced in an abiotic conjugation of phthalic aldehyde-type double electrophiles with ammonia, amines, or amino acids.[41]

The configuration of the amino acid portions was tentatively assigned to be L, as the vinylogous addition is most likely a noncatalyzed process and the relative abundance of the respective nucleophile in the cell or cellular compartment will be decisive. This clearly favors the L- over the D-series. Thus, compounds **3**−**5** were characterized as amino acids containing germacranolide-like sesquiterpenoids for which the trivial names tufnelactones C−E are being proposed.

The known compounds 8α-[4′-hydroxymethacryloyloxy]-sonchucarpolide (**6**),[42] onopordopicrin (**7**),[43] 1*H*-indole-3-carbaldehyde (**8**),[43] apigenin (**9**), pedalitin (**10**),[44] apigenin 7-*O*-β-glucopyranoside (**11**), apigenin 7-*O*-β-glucuronide (**12**), luteolin 7-*O*-β-glucuronide (**13**),[45] 2,4′-methylenebisphenol (**14**), and bisphenol F (**15**)[46] were identified by comparison of their spectroscopic data with those reported in the literature.

The crude extract and compounds **1**−**5**, **7**−**10**, and **12**−**15** were evaluated against a cancer cell line (HeLaS3, a human cell line) at successive concentrations of 2.5, 5, 10, 25, and 50 μg/mL and against a panel of bacterial and fungal strains (except for compounds **6** and **11**, which were not isolated in sufficient quantities to allow biological tests). The choice of these bioactivities is based on a solid background of sesquiterpene lactones inducing apoptosis in cells.[6−10] Against bacteria and fungi, no activity was observed at 25 and 50 μg/mL. However, the crude extract exhibited 100% cytotoxicity at 25 μg/mL and 25% cytotoxicity at 10 μg/mL. The new compounds **1**−**5** and the known compounds tested were all deemed inactive (IC_{50} > 10 μM).

EXPERIMENTAL SECTION

General Experimental Procedures. Optical rotations were measured with a PerkinElmer 241 MC polarimeter (using the sodium D line and a quartz cuvette with a 10 cm path length and 0.5 or 1.0 mL volume). UV−vis spectra were recorded on an Evolution 201 UV−visible spectrophotometer using 10 mm quartz cuvettes. Infrared (IR) spectra were recorded on an FT-IR spectrometer (Bruker Tensor 27) equipped with a diamond ATR unit and are reported in terms of frequency of absorptions in cm^{-1}. NMR spectra were recorded on a Bruker Avance-III (^1H NMR, 600 MHz; ^{13}C NMR, 151.1 MHz) spectrometer equipped with a 5 mm TCl cryoprobe. Chemical shifts were referenced to residual solvent signals and reported in parts per million (ppm) relative to tetramethylsilane (TMS). Electrospray ionization (ESI) mass spectra were recorded on a 1200-series HPLC system or a 1260-series Infinity II HPLC system (Agilent Technologies) with a binary pump and integrated diode array detector coupled to an LC/MSD-Trap-XTC mass spectrometer (Agilent Technologies) or an LC/MSD Infinity Lab LC/MSD (G6125B LC/MSD). High-resolution mass spectra were recorded on an Agilent 6545 QTOF-MS spectrometer (Waters) with a LockSpray interface and a suitable external calibrant. Circular dichroism spectra were recorded on a JASCO J-815 spectrometer equipped with a JASCO PTC-423S/15 temperature controller. The measurement of compound **1** (c = 0.1 mM in MeOH) was repeated five times and averaged using a scanning speed of 50 nm/min at 20 °C. The solvent background was recorded applying the same parameters and was subtracted from the sample measurement. The Boltzmann averaged CD spectra were created with SpecDis v1.71.[47]

Chromatographic purification of compounds was performed on silica gel (35−70 μm, Acros Organics). Thin-layer chromatography (TLC) was carried out on silica plates (TLC silica 60 F_{254}, Merck), and zones were detected by spraying with 20% H_2SO_4 followed by charring at 100 °C. Analytical HPLC analysis was performed on an Agilent Technologies 1260 Infinity II system equipped with a binary pump and a diode array detector. An ACE C_{18} PFP column (150 mm × 4.6 mm, 3 μm, 40 °C) with a flow rate of 1 mL/min was used. Preparative reversed-phase separation was carried out on a Smartline HPLC system (Knauer) with mixtures of acetonitrile (HPLC grade) and water (HPLC grade) as eluents on an ACE 5 C_{18} PFP 150 mm × 30 mm column, at a flow rate of 37.5 mL/min. The eluents were degassed prior to use by means of ultrasonication for 30 min. Two Smartline K 1800 pumps (pump head size: 100 mL each, high-pressure gradient; Knauer) and an S2600 diode array detector (Knauer) were used.

Plant Material. The whole plants of *Vernonia tufnelliae* were collected on the slope of the Bamboutos Mountain in the western region of Cameroon in December 2017. The identification was performed at the Cameroon National Herbarium (Yaoundé) by comparison with a voucher specimen maintained under the accession number 58856/HCN.

Extraction and Isolation. The dried whole plants of *V. tufnelliae* (1.0 kg) were ground and extracted with ethanol (3 × 5 L, 72 h each) at room temperature to yield a crude extract (40.0 g) after evaporation under reduced pressure. A portion (35.0 g) of this extract was purified by flash chromatography on a silica gel column with gradients of cyclohexane−EtOAc and EtOAc−MeOH. Altogether, 76 fractions of 200 mL each were collected and combined on the basis of their TLC profiles (using mixtures of cyclohexane−EtOAc, 85:15, 70:30, 30:70) into five main fractions, coded A−E (A: 1−6; B: 7−25; C: 26−50; D: 51−65; E: 66−76). Fraction A (3.8 g) contained mostly lipids and was not further investigated. Successive silica gel chromatography columns of fraction B (1.5 g) were not followed up. Fraction C (2.1 g) was dissolved in EtOAc for purification by silica gel column chromatography and afforded compound **9** (20 mg) by simple filtration. Further open column chromatography over silica gel of fraction C using a gradient of cyclohexane−EtOAc (100:0, 95:5, 90:10, 85:15, 80:20, 75:25, and 70:30) afforded three subfractions (C1−C3). Fraction C1 (50 mg) was purified by RP-HPLC eluting with 25% CH_3CN−H_2O (isocratic) to afford compound **8** (3 mg). Fraction D (10.8 g) was also purified by flash chromatography with a gradient of cyclohexane−acetone (100:0, 95:5, 90:10, 85:15, 80:20, 75:25, and 70:30), affording six fractions (D1−D6). Subfraction D6 (1.8 g) was further fractionated on an open silica gel column with a gradient of cyclohexane−acetone prior to purification of resulting fractions by RP-HPLC (25% CH_3CN−H_2O) to give compounds **7** (3.1 mg), **14** (2.4 mg), and **15** (2.1 mg). Subfraction D4 (3.2 g) was treated in the same way as D6 to afford **1** (4.2 mg), **2** (5.1 mg), **6** (1.4 mg), and **10** (13.2 mg). Subfraction D5 (1.7 g) was also subfractionated by open silica gel column chromatography with a gradient of cyclohexane−acetone, affording compound **11** (17.0 mg). Compounds **3** (1.8 mg), **4** (2.0 mg), **5** (1.2 mg), **12** (2.6 mg), and **13** (2.7 mg) were obtained from fraction E (15.0 g) through purification by silica gel open-column chromatography using a gradient of EtOAc−MeOH to yield a green powder, which was subsequently purified by RP-HPLC eluting with a gradient of CH_3CN−H_2O.

Tufnelactone A (1): white amorphous powder; $[\alpha]^{22}_D$ +11.2 (c 0.8, acetone); λ_{max} (log ε, acetonitrile) 216 (sh, 4.5) nm; IR (ATR) ν_{max} 3306, 2928, 1764, 1714, 1660, 1454, 1007, 565 cm^{-1}; ^1H NMR (acetone-d_6) and ^{13}C NMR (acetone-d_6), see Tables 1 and 2; (+)-HRESIMS m/z 714.3471 $[M + H]^+$ (calcd for $C_{38}H_{52}NO_{12}^+$, 714.3484).

https://doi.org/10.1021/acs.jnatprod.2c00055
J. Nat. Prod. 2022, 85, 1681−1690

*Tufnelactone B (**2**):* white amorphous powder; $[\alpha]^{22}_{D}$ +29.1 (*c* 0.55, acetone); λ_{max} (log ε, acetonitrile) 275 (sh, 3.1), 340 (sh, 2.8) nm; IR (ATR) ν_{max} 3381, 2929, 1762, 1713, 1633, 1412, 1263, 1009, 599, 556 cm^{-1}; ^1H NMR (acetone-d_6) and ^{13}C NMR (acetone-d_6), see Tables 1 and 2; (+)-HRESIMS *m*/*z* 719.3038 $[M + Na]^+$ (calcd for $C_{38}H_{48}NaO_{12}^+$, 719.3038).

*Tufnelactone C (**3**):* white amorphous powder; $[\alpha]^{22}_{D}$ +13.3 (*c* 0.45, DMSO); λ_{max} (log ε, acetonitrile) 203 (3.6) nm; IR (ATR) ν_{max} 3364, 2920, 1754, 1708, 1657, 1631, 1406, 1289, 1139, 1017, 950 cm^{-1}; ^1H NMR (DMSO-d_6) and ^{13}C NMR (DMSO-d_6), see Tables 1 and 2; (+)-HRESIMS *m*/*z* 514.2445 $[M + H]^+$ (calcd for $C_{28}H_{36}NO_8^+$, 514.2435).

*Tufnelactone D (**4**):* white amorphous powder; $[\alpha]^{22}_{D}$ +16.0 (*c* 1.0, DMSO); λ_{max} (log ε, methanol) 204 (3.9) nm; IR (ATR) ν_{max} 3392, 1655, 1494, 1436, 1014, 951 cm^{-1}; ^1H NMR (DMSO-d_6) and ^{13}C NMR (DMSO-d_6), see Tables 1 and 2; (+)-HRESIMS *m*/*z* 466.2436 $[M + H]^+$ (calcd for $C_{24}H_{36}NO_8^+$, 466.2435).

*Tufnelactone E (**5**):* white amorphous powder; $[\alpha]^{22}_{D}$ −2.5 (*c* 0.8, DMSO); λ_{max} (log ε, methanol) 204 (4.4) nm; IR (ATR) ν_{max} 3402, 1754, 1709, 1628, 1565, 1165, 1021, 1002, 823, 761 cm^{-1}; ^1H NMR [DMSO-d_6 + methanol-d_4 (1:4)] and ^{13}C NMR [DMSO-d_6 + methanol-d_4 (1:4)], see Tables 1 and 2; (+)-HRESIMS *m*/*z* 502.2419 $[M + Na]^+$ (calcd for $C_{25}H_{37}NO_8Na^+$, 502.2411).

Bioactivity. Bioactivity was tested as described previously.[48] In brief, the HeLa-S3 human cervical cells (DSMZ ACC 161) were grown in DMEM medium (Gibco, Thermo Fisher Scientific Inc.). The medium was supplemented with 10% inactivated fetal calf serum (Gibco, Thermo Fisher Scientific Inc.), 65 μg/mL of penicillin G, and 100 μg/mL of streptomycin sulfate (Gibco). A humidified atmosphere containing 5% CO_2 at 37 °C was used to incubate the cultures. The assays were carried out in 96-well plates containing 5 × 10^4 cells/mL, and HeLa-S3 cells were seeded for 24 h before the test compounds were added. The test compounds (at a concentration of 2.5, 5, 10, 25, and 50 μg/mL) were transferred to a new 96-well plate, with the solvent evaporated, and subsequently the compounds were dissolved in the appropriate volume of cell culture medium followed by shaking for 15 min. The medium in the 96-well plate with HeLa-S3 cells was replaced by either medium with test compound, or medium alone (negative control) or medium with camptothecin (IC_{50} 0.29 μM; positive control). All tests were conducted in triplicate. The cell viability was evaluated by microscopy, and 48 h after the addition of the test compounds or control the approximate value of cytotoxicity was given in terms of % of dead cells.

Antibacterial and antifungal assays (serial dilution assays) against *Aneurinibacillus migulans* (ATCC 9999, 37 °C), *Staphylococcus aureus* subsp. *aureus* (ATCC 11632, 37 °C), *Pseudomonas aeruginosa* (ATCC 15442, 37 °C), *Rhizomucor miehei* (Tü 284, 37 °C), *Penicillium chrysogenum* (IBWF strain, 27 °C), *Paecilomyces variotii* (ETH 114646, 37 °C), *Phytophthora infestans* (CBS 430.90, 18 °C), and *Candida albicans* (ATCC 90028, 37 °C) as well as germination assays with *Pyricularia oryzae* (70−15) and *Botrytis cinerea* were performed in accordance with methods described before.[49,50] All methods follow techniques described by Anke et al.[51]

■ ASSOCIATED CONTENT

Supporting Information

The Supporting Information is available free of charge at https://pubs.acs.org/doi/10.1021/acs.jnatprod.2c00055.

NMR, UV, IR, and HR-ESIMS data for compounds **1**−**5**; shielding tensor values of conformers from compound **1** (PDF)

■ AUTHOR INFORMATION

Corresponding Authors

Gabin Thierry M. Bitchagno − *Department of Chemistry, Johannes Gutenberg-University of Mainz, D-55128 Mainz, Germany; Department of Chemistry, University of Dschang, Dschang, Cameroon*; Email: bmgt198716@ymail.com

Till Opatz − *Department of Chemistry, Johannes Gutenberg-University of Mainz, D-55128 Mainz, Germany*; orcid.org/0000-0002-3266-4050; Email: opatz@uni-mainz.de

Authors

Anja Schüffler − *Institut für Biotechnologie und Wirkstoff-Forschung gGmbH (IBWF), 55128 Mainz, Germany*

Jonathan Gross − *Department of Chemistry, Johannes Gutenberg-University of Mainz, D-55128 Mainz, Germany*

Matthias Krumb − *Department of Chemistry, Johannes Gutenberg-University of Mainz, D-55128 Mainz, Germany*

Pierre Tane − *Department of Chemistry, University of Dschang, Dschang, Cameroon*

Complete contact information is available at: https://pubs.acs.org/10.1021/acs.jnatprod.2c00055

Author Contributions

[#]Deceased July 29, 2019.

Notes

The authors declare no competing financial interest.

■ ACKNOWLEDGMENTS

G.T.M.B. is grateful to the German Academic Exchange Service (DAAD) (57381410) and the Rhineland Palatinate Natural Products Research Center for financial support. Parts of this research were conducted using the supercomputer MOGON and/or advisory services offered by Johannes Gutenberg University Mainz (hpc.unimainz.de), which is a member of the AHRP (Alliance for High Performance Computing in Rhineland Palatinate, www.ahrp.info) and the Gauss Alliance e.V. The authors gratefully acknowledge the computing time granted on the supercomputer MOGON at Johannes Gutenberg University Mainz (hpc.unimainz.de). The authors thank Prof. Sebastian Seiffert (Mainz) for granting access to the CD spectrometer.

■ REFERENCES

(1) Wang, F. P.; Liang, X. T. In *Alkaloids: Chemistry and Biology*; Cordell, G. A., Ed.; Elsevier Science: Amsterdam, 2002; Vol. *59*; Chapter 20, pp 1−280.

(2) Cherney, E. C.; Baran, P. S. *Isr. J. Chem.* **2011**, *51*, 391−405.

(3) Wang, F. P.; Chen, Q. H.; Liu, X. Y. *Nat. Prod. Rep* **2010**, *27*, 529−570.

(4) Jeffrey, C. *Kew Bull.* **1988**, *43*, 195−277.

(5) Chaturvedi, D. In *Opportunity, Challanges and Scope of Natural Products in Medicinal Chemistry*; Tiwari, V. K., Mishra, B. B., Eds.; Research Signpost: Trivandrum, 2011; Vol. *1*; pp 313−334.

(6) Zunino, S. J.; Ducore, J. M.; Storms, D. H. *Cancer Lett.* **2007**, *254*, 119−127.

(7) Sobota, R.; Szwed, M.; Kasza, A.; Bugno, M.; Kordula, T. *Biochem. Biophys. Res. Commun.* **2000**, *267*, 329−333.

(8) Kwok, B. H. B.; Koh, B.; Ndubuisi, M. I.; Elofsson, M.; Crews, C. M. *Chem. Biol.* **2001**, *8*, 759−766.

(9) García-Piñeres, A. J.; Castro, V.; Mora, G.; Schmidt, T. J.; Strunck, E.; Pahl, H. L.; Merfort, I. *J. Biol. Chem.* **2001**, *276*, 39713−39720.

(10) Ghantous, A.; Gali-Muhtasib, H.; Vuorela, H.; Saliba, N. A.; Darwiche, N. *Drug Discovery Today* **2010**, *15*, 668−678.

(11) Nganou, B. K.; Simo Konga, I.; Fankam, A. G.; Bitchagno, G. T. M.; Sonfack, G.; Nayim, P.; Celik, I.; Koyutürk, S.; Kuete, V.; Tane, P. *Nat. Prod. Res.* **2019**, *33*, 2638−2646.

(12) Tchinda, C. F.; Sonfack, G.; Simo, I. K.; Çelik, I.; Voukeng, I. K.; Nganou, B. K.; Bitchagno, G. T. M.; Ekti, S. F.; Tene, M.; Tane, P.; Beng, V. P.; Kuete, V. *BMC Complement. Altern. Med.* **2019**, *19*, 120.
(13) Damen, F.; Demgne, O. M. F.; Bitchagno, G. T. M.; Celik, I.; Mpetga, J. D. S.; Tankeo, S. B.; Opatz, T.; Kuete, V.; Tane, P. *Nat. Prod. Res.* **2021**, *35*, 2381−2387.
(14) Mbaveng, A. T.; Damen, F.; Guefack, M. G. F.; Tankeo, S. B.; Abdelfatah, S.; Bitchagno, G. T. M.; Çelik, İ.; Kuete, V.; Efferth, T. *Phytomedicine* **2020**, *70*, 153215.
(15) Koagne, R. R.; Bitchagno, G. T. M.; Fobofou, S. A. T.; Konga, I. S.; Tamokou, J. D. D.; Wessjohann, L. A.; Tane, P. *Nat. Prod. Commun.* **2017**, *12*, 1435−1436.
(16) Lonergan, G.; Routsi, E.; Georgladis, T.; Ageus, G.; Hondrelis, J.; Matsoukas, J.; Larsen, L. K.; Capean, F. R. *J. Nat. Prod* **1992**, *55*, 225−228.
(17) Rosselli, S.; Maggio, A. M.; Canzoneri, M.; Simmonds, M. S. J.; Bruno, M. *Nat. Prod. Commun.* **2012**, *7*, 1131−1132.
(18) Skaltsa, H.; Lazari, D.; Garcia, B.; Pedro, J. R.; Sokovic, M.; Constantinidis, T. *Z. Naturforsch. C* **2000**, *55*, 534−539.
(19) Formisano, C.; Sanna, C.; Ballero, M.; Chianese, G.; Sirignano, C.; Rigano, D.; Millán, E.; Muñoz, E.; Taglialatela-Scafati, O. *Fitoterapia* **2017**, *116*, 61−65.
(20) Youn, U. J.; Wongwiwatthananukit, S.; Songsak, T.; Chang, L. C. *Chem. Nat. Compd.* **2018**, *54*, 235−237.
(21) Kimani, N. M.; Matasyoh, J. C.; Kaiser, M.; Brun, R.; Schmidt, T. J. *Molecules* **2018**, *23*, 248.
(22) Kupchan, S. M.; Hemingway, R. J.; Karim, A.; Werner, D. *J. Org. Chem.* **1969**, *34*, 3908−3911.
(23) Brocksom, T. J.; De Oliveira, K. T.; Desiderá, A. L. *J. Braz. Chem. Soc.* **2017**, 933−942.
(24) Demir, S.; Karaalp, C.; Bedir, E. *Phytochem. Lett.* **2016**, *15*, 245−250.
(25) Halgren, T. A. *J. Comput. Chem.* **1996**, *17*, 490−519.
(26) Vosko, S. H.; Wilk, L.; Nusair, M. *Can. J. Phys.* **1980**, *58*, 1200−1211.
(27) Lee, C.; Yang, W.; Parr, R. G. *Phys. Rev. B* **1988**, *37*, 785−789.
(28) Becke, A. D. *J. Chem. Phys.* **1993**, *98*, 5648−5652.
(29) Becke, A. D. *Phys. Rev. A* **1988**, *38*, 3098−3100.
(30) Hariharan, P. C.; Pople, J. A. *Theor. Chim. Acta* **1973**, *28*, 213−222.
(31) Hehre, W. J.; Ditchfield, K.; Pople, J. A. *J. Chem. Phys.* **1972**, *56*, 2257−2261.
(32) Frisch, M. J.; Trucks, G. W.; Schlegel, H. B.; Scuseria, G. E.; Robb, M. A.; Cheeseman, J. R.; Scalmani, G.; Barone, V.; Petersson, G. A.; Nakatsuji, H.; Li, X.; Caricato, M.; Marenich, A. V.; Bloino, J.; Janesko, B. G.; Gomperts, R.; Mennucci, B.; Hratchian, H. P.; Ortiz, J. V.; Izmaylov, A. F.; Sonnenberg, J. L.; Williams-Young, D.; Ding, F.; Lipparini, F.; Egidi, F.; Goings, J.; Peng, B.; Petrone, A.; Henderson, T.; Ranasinghe, D.; Zakrzewski, V. G.; Gao, J.; Rega, N.; Zheng, G.; Liang, W.; Hada, M.; Ehara, M.; Toyota, K.; Fukuda, R.; Hasegawa, J.; Ishida, M.; Nakajima, T.; Honda, Y.; Kitao, O.; Nakai, H.; Vreven, T.; Throssell, K.; Montgomery, J. A., Jr.; Peralta, J. E.; Ogliaro, F.; Bearpark, M. J.; Heyd, J. J.; Brothers, E. N.; Kudin, K. N.; Staroverov, V. N.; Keith, T. A.; Kobayashi, R.; Normand, J.; Raghavachari, K.; Rendell, A. P.; Burant, J. C.; Iyengar, S. S.; Tomasi, J.; Cossi, M.; Millam, J. M.; Klene, M.; Adamo, C.; Cammi, R.; Ochterski, J. W.; Martin, R. L.; Morokuma, K.; Farkas, O.; Foresman, J. B.; Fox, D. J. *Gaussian 09*, Revision A.02; Gaussian Inc., 2016.
(33) Adamo, C.; Barone, V. *J. Chem. Phys.* **1998**, *108*, 664−675.
(34) Frisch, M. J.; Pople, J. A.; Binkley, J. S. *J. Chem. Phys.* **1984**, *80*, 3265−3269.
(35) Clark, T.; Chandrasekhar, J.; Spitznagel, G. W.; Schleyer, P. V. R. *J. Comput. Chem.* **1983**, *4*, 294−301.
(36) Jain, T. C.; Banks, C. M.; McCloskey, J. E. *Tetrahedron Lett.* **1970**, *11*, 841−844.
(37) Gopalan, A.; Magnus, P. *J. Org. Chem.* **1984**, *49*, 2317−2321.
(38) Perveen, S.; Al-Taweel, A. M.; Yusufoglu, H. S.; Fawzy, G. A.; Foudah, A.; Abdel-Kader, M. S. *J. Nat. Med.* **2018**, *72*, 106−117.
(39) Wang, K.; Bao, L.; Qi, Q.; Zhao, F.; Ma, K.; Pei, Y.; Liu, H. *J. Nat. Prod* **2015**, *78*, 146−154.
(40) Minagawa, K.; Kouzuki, S.; Tani, H.; Ishii, K.; Tanimoto, T.; Terui, Y.; Kamigauchi, T. *J. Antibiot.* **2002**, *55*, 239−248.
(41) Harwoko, H.; Lee, J.; Hartmann, R.; Mándi, A.; Kurtán, T.; Müller, W. E. G.; Feldbrügge, M.; Kalscheuer, R.; Ancheeva, E.; Daletos, G.; Frank, M.; Liu, Z.; Proksch, P. *Fitoterapia* **2020**, *146*, 104698.
(42) Miski, M.; Meriçli, A. H.; Mabry, T. J. *Phytochemistry* **1988**, *27*, 1417−1420.
(43) Ashour, M. A.; Elkhayat, E. S.; Ebel, R.; Edrada, R.; Proksch, P. *Arkivoc* **2007**, *2007*, 225−231.
(44) Fuji, Y.; Uchida, A.; Fukahori, K.; Chino, M.; Ohtsuki, T.; Matsufuji, H. *PLoS One* **2018**, *13*, No. e0194449.
(45) Iwashina, T.; Kokubugata, G. *Bull. Natl. Museum Nat. Sci. Ser. B Bot* **2010**, *36*, 117−125.
(46) Fisher, T. H.; Chao, P.; Upton, C. G.; Day, A. J. *Magn. Reson. Chem.* **1995**, *33*, 717−723.
(47) Bruhn, T.; Schaumlöffel, A.; Hemberger, Y.; Bringmann, G. *Chirality* **2013**, *25*, 243−249.
(48) Bitchagno, G. T. M.; Schüffler, A.; Simo, I. K.; Krumb, M.; Tane, P.; Opatz, T. *Nat. Prod. Res.* **2021**, *35*, 3210−3219.
(49) Togue, T. A. M.; Ndontsa, B. L.; Bitchagno, G. T. M.; Schüffler, A.; Opatz, T.; Tane, P.; Tene, M. *Planta Med.* **2020**, *86*, 1298−1303.
(50) Ombito, J. O.; Majinda, R. R. T.; Masesane, I. B.; Bojase, G.; Schüffler, A.; Opatz, T. *Phytochem. Lett.* **2018**, *26*, 110−114.
(51) Anke, H.; Bergendorff, O.; Sterner, O. *Food Chem. Toxicol.* **1989**, *27*, 393−397.

https://doi.org/10.1021/acs.jnatprod.2c00055
J. Nat. Prod. 2022, 85, 1681−1690

8 Zusammenfassung

8.1 *In silico* Betrachtung von Reaktionsmechanismen

8.1.1 Simulation des Reaktionspfads einer photokatalysierten [3+2]-Cycloaddition von Vinylcyclopropanen mit Acetylenen

Im Rahmen dieser Doktorarbeit wurde mittels DFT-Berechnungen der Reaktionsmechanismus der von [redacted] entwickelten Iridium-katalysierten formalen [3+2]-Cycloaddition von Vinylcyclopropan **114** mit Acetylensulfon **167** simuliert (Schema 8.1).

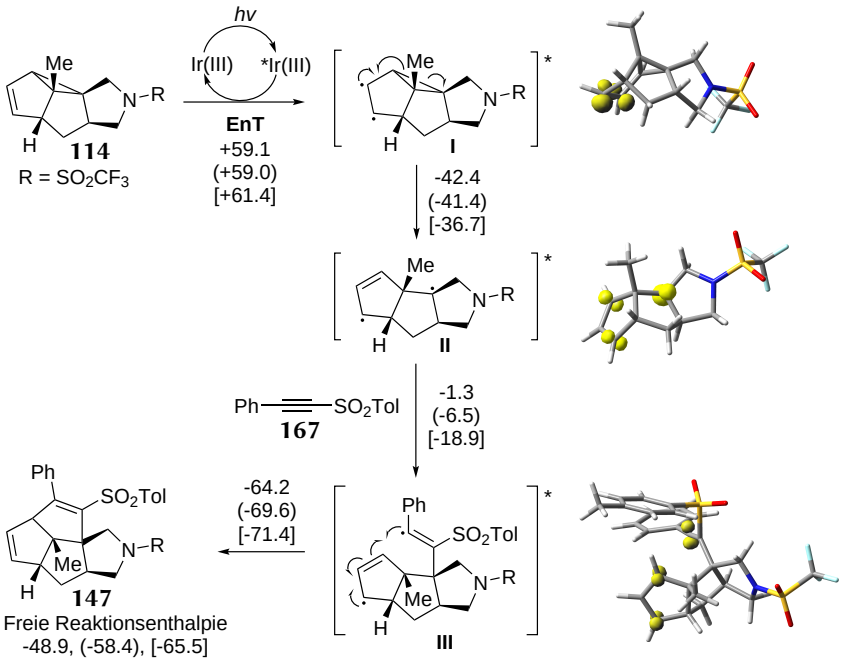

Schema 8.1: Die adiabatischen Energiedifferenzen der formalen [3+2]-Cycloaddition wurden mit verschiedenen DFT-Funktionalen für die einzelnen Reaktionsschritte berechnet (B3LYP, (CAM-B3LYP) und [M06-2X]/6-311+G(2d,p)/IEFPCM(Methanol) in kcal mol^{-1}).

Für die untersuchte durch sichtbares Licht induzierte C–C-Aktivierungvon von nicht aktivierten Vinylcyclopropanen **114** konnte ein Energietransfermechanismus mittels spektroskopischer Laser-Blitzphotolyse-Messungen und DFT-Berechnungen nachgewiesen werden. Dafür wurden die S_0- und T_1-Zustände der Edukte **114** und **167**, des Produkts **147** und der angeregten Zustände **I**–**III** berechnet. Die während des Reaktionsmechanismus auftretenden ungepaarten Elektronen wurden in Form der entsprechenden Spindichten abgebildet.[554]

8.1.2 Selektivitätsuntersuchung einer Diels-Alder-Reaktion eines β-Fluor-β-nitrostyrols mit Cyclopentadien

Bei der von [redacted] und seinen Mitarbeitern entwickelten Diels-Alder-Reaktion von β-Fluor-β-nitrostyrolen **117** mit Cyclopentadien (**118**) konnte die beobachtete *endo*-Selektivität bei aromatischen Verbindungen mit elektronenziehender Gruppe durch quantenmechanische Berechnungen erklärt werden (Abbildung 8.1).

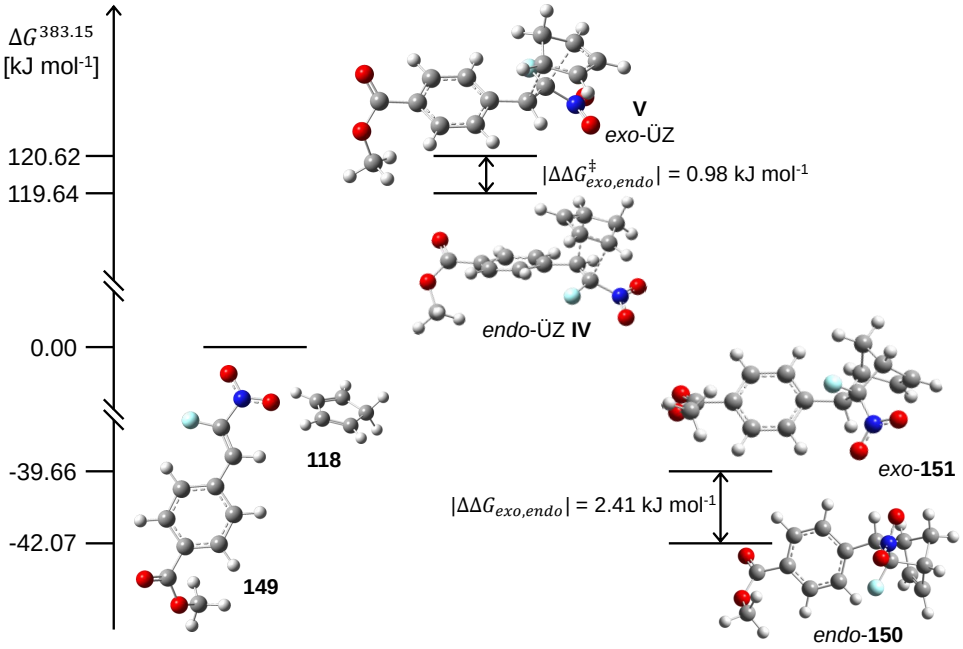

Abbildung 8.1: Energetische Lage der Edukte **118** und **149**, der verschiedenen Übergangszustände **IV** und **V**, die zu den entsprechenden *endo*- und *exo*-Produkten **150** und **151** führen. Der Reaktionspfad wurde mittels M06-2X/6-311+G(d,p)/IEFPCM(*o*-Xylol) bei 383.15 K berechnet.[555]

Eine Berechnung der energetischen Lage von Cyclopentadien (**118**) und *p*-substituiertem Fluornitrostyrol **149**, der Übergangszustände **IV** und **V** sowie der möglichen *endo*- und *exo*-Produkte **150** und **151** ermöglichte es, unter Verwendung der Eyring-Gleichung die Geschwindigkeitskonstanten k vorherzusagen. Das simulierte Verhältnis k_{endo}/k_{exo} = 1.36 ist in guter Übereinstimmung mit dem experimentell bestimmten Diastereomerenverhältnis *dr* = 1.22 unter den gewählten Reaktionsbedingungen.[555]

8.1.3 Reaktivität verschiedener *N*-Carbonsäureanhydride in einer ringöffnenden Synthese von Polypeptiden

In einem Kooperationsprojekt mit den Arbeitsgruppen [redacted] und [redacted] wurde mittels CC-Methoden untersucht, ob die beobachteten Polymerisationskinetiken auf die elektronischen Umgebungen der verwendeten *N*-alkylierten beziehungsweise *N*-unsubstituierten NCAs **152** und **168** zurückzuführen sind (Abbildung 8.2).

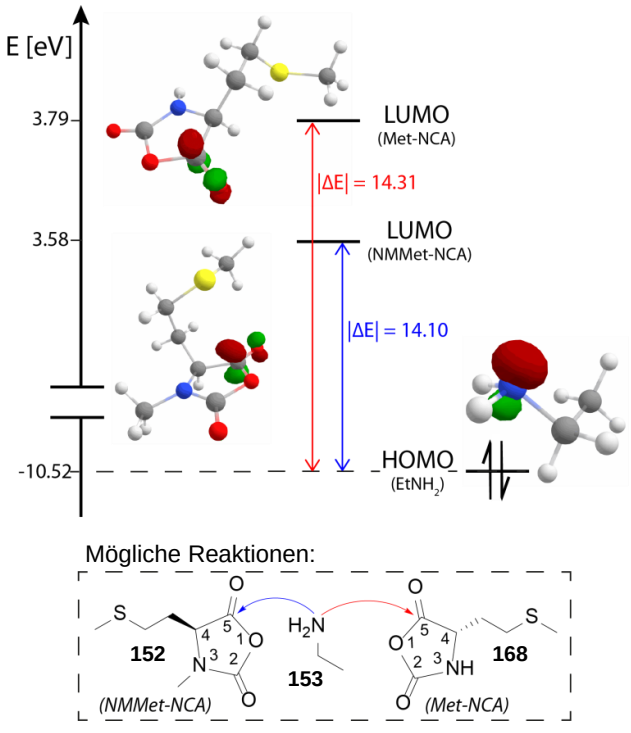

Abbildung 8.2: Die berechneten energetischen Lagen der relevanten Grenzorbitale von NMMet-NCA **152**, Ethylamin (**153**) und Met-NCA **168**, visualisiert als NBOs (DLPNO-CCSD(T)/cc-pVDZ//B3LYP/6-311G(d,p)).

Die Anwendung der Klopman-Salem-Gleichung auf die energetischen Lagen der berechneten NBOs in der Gasphase deuten darauf hin, dass bei NMMet-NCA **152** eine höhere Reaktivität mit einem primären Amin **153** zu erwarten ist, da die Energiedifferenz geringer ist im Vergleich zu Met-NCA **168**. Die experimentellen Befunde spiegelten diese *in silico* Vorhersage jedoch nicht wider, sodass gefolgert wurde, dass der sterische Einfluss des Stickstoff-Substituenten für das verringerte Polymerisationsverhalten verantwortlich ist.[535,556]

8.1.4 Bestimmung des Substituenteneinflusses bei der photochemischen Dehydrierung von N-Heterozyklen

In der von [redacted] entwickelten photochemischen Dehydrierung von N-Heterozyklen **123** zeigte sich bei den Verbindungen **155** und **156**, die *ortho*-substituierte Aromaten am Stickstoff tragen, ein verringerter bis ganz ausbleibender Umsatz unter den gewählten Reaktionsbedingungen. Die Simulation der optimalen Geometrie mittels DFT verdeutlichte eine Drehung des aromatischen Rings derartig substituierter Verbindungen im Vergleich zu einem Phenylsubstituenten. Der daraus resultierende verringerte Orbitalüberlapp erklärt die geringeren Ausbeuten für die Substrate **155** und **156** im Vergleich zu dem Phenylsubstituierten Piperidon **154** (Abbildung 8.3).[557]

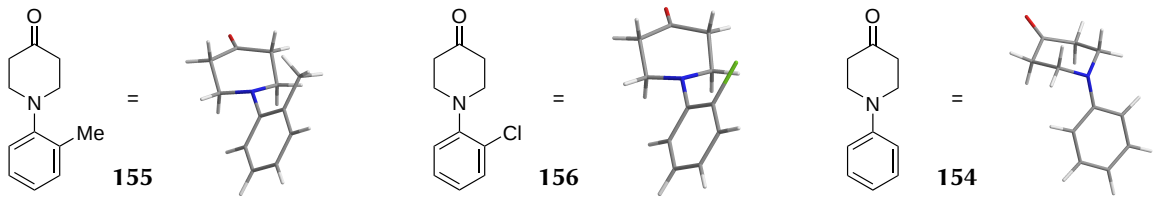

Abbildung 8.3: Die unterschiedliche Ausrichtung verschiedener N-Substituenten der Piperidone **154**, **155** und **156** nach einer Geometrieoptimierung auf DFT-Level (B3LYP/6-311+G(d,p)/IEFPCM(DMF).[557]

8.2 Computergestützte Strukturaufklärung kleiner organischer Moleküle

8.2.1 Benchmarkstudie über die Genauigkeit von DFT-Methoden in der VCD-Spektroskopie

In der durchgeführten Benchmarkstudie wurden diverse Kombinationen aus DFT-Funktionalen, Basissätzen und Solvatationsmodellen im Bezug auf die Verlässlichkeit und Güte ihrer Vorhersage von VCD-Spektren systematisch untersucht. Die berechneten harmonischen Rotationsstärken von sechs organischen Verbindungen wurden unter Verwendung der Software SpecDis in Lorentzkurven übersetzt, der spektrale Überlapp mit den entsprechenden experimentellen Spektren bestimmt und durch den *enantiomeric similarity index* quantifiziert. Auf Grundlage der Ergebnisse konnten folgende Empfehlungen ausgesprochen werden, die sich für die Strukturaufklärung mit dieser spektroskopischen Methode eignen:

- B3LYP/6-311G(d,p)/SMD
- ωB97X-D/6-311+G(d,p)/SMD
- M06-2X/6-311+G(d,p)/IEFPCM
- PBE0/6-311G(d)/IEFPCM.

Die breiteste Anwendbarkeit wiesen die Kombinationen bestehend aus dem ωB97X-D Funktional und dem SMD Solvatationsmodell in Verbindung mit dem 6-311+G(d,p)- oder dem aug-cc-pVTZ-Basissatz auf. Diese zwei Kombinationen erreichten für Campher **125**, Phenethlyamin **128** und Thiocampher **130** ESI-Werte >80%.

8.2.2 Differenzierung von Diastereomeren in der Synthese eines HIV-Integrase-Inhibitors

In der von [redacted] entwickelten Syntheseroute zu Dolutegravir-Natrium (**137**) können bei der Transacetalisierung von Verbindung (–)-**169** zwei Diastereomere **170** und **171** auftreten, deren Differenzierung mittels NMR-Spektroskopie nicht möglich war. Das ausschließ-

lich gebildete Produkt (–)-**170** sowie dessen absolute Konfiguration konnte durch den Vergleich der aufgenommen VCD-Spektren mit den *in silico* Simulationen der Vibrationsspektren beider möglichen Diastereomere bestimmt werden (B3LYP/6-31G(d,p)/IEFPCM(CCl_4)). Das berechnete Oxazinon **170** mit der gewünschten *S*-Konfiguration an C-9a besitzt einen Ähnlichkeitsfaktor von 76% zu dem experimentellen Spektrum, wohingegen Isomer **171** mit *R*-Konfiguration an C-9a lediglich einen Ähnlichkeitsfaktor von 25% besitzt (Schema 8.2).[559]

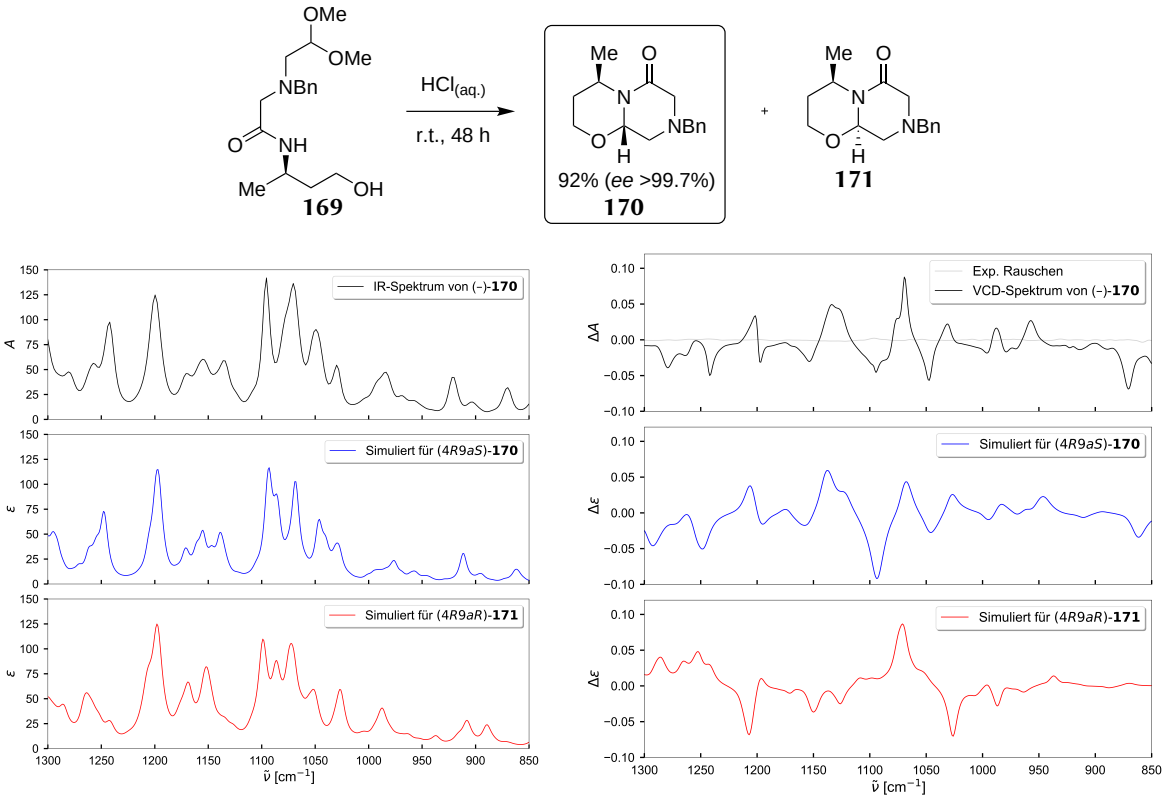

Schema 8.2: Das in der Umsetzung von Verbindung (–)-**169** gebildete Produkt (–)-**170** sowie dessen absolute Konfiguration wurde durch den Vergleich von aufgenommenen VCD-Spektren mit simulierten Spektren identifiziert.[559]

8.2.3 Bestimmung der absoluten Konfiguration eines 13-Hydroxy-14-deoxyoxacyclododecindions

Die NMR-spektroskopischen Daten des von [redacted] hergestellten 13-Hydroxy-14-deoxyoxacyclododecindions (+)-**141** wiesen eine deutliche Diskrepanz zu den NMR-Daten eines

Naturstoffs, für den dieselbe chemische Struktur vorgeschlagen wurde, auf. Infolgedessen wurde analog zu der Veröffentlichung von Shang und Lin *et al.* die ECD-Spektroskopie für die Bestimmung der absoluten Konfiguration herangezogen.[543] Obwohl gewisse Ähnlichkeiten in den Spektren der synthetischen Verbindung (+)-**141** und des Naturstoffs festgestellt werden konnten, stellte sich diese Methode in dieser Anwendung als nicht aussagekräftig heraus, da die simulierten Spektren aller möglichen Diastereomere des Makrozyklus **141** eine zu hohe Ähnlichkeit im untersuchten Wellenlängenbereich aufwiesen (Abbildung 8.4).[543]

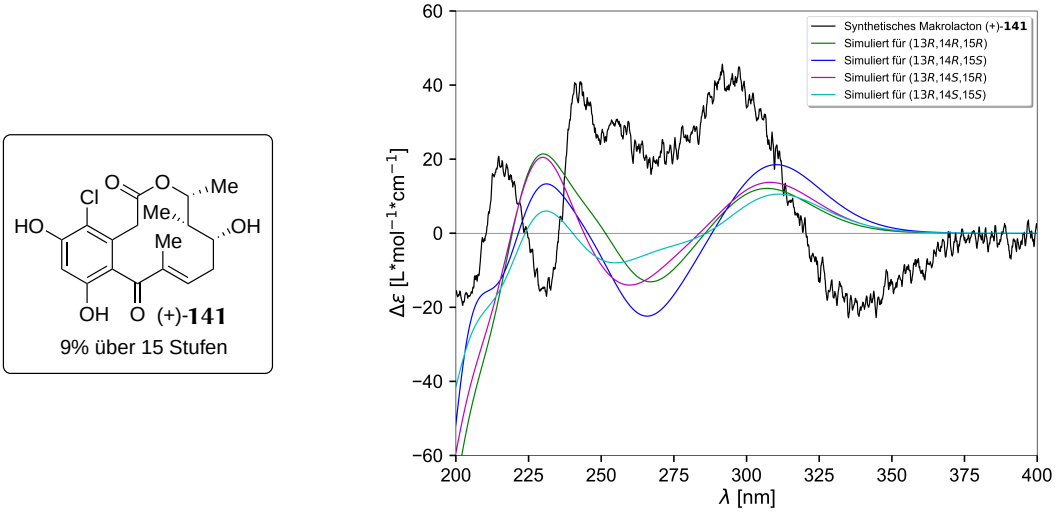

Abbildung 8.4: Simulierte ECD-Spektren aller möglichen Diastereomere des Makrolactons **141** im Vergleich zu dem experimentellen Spektrum.

Aus diesem Grund wurde der synthetische Makrozyklus (+)-**141** zusätzlich mittels VCD-Spektroskopie in Verbindung mit DFT-Berechnungen untersucht. Durch die Bestimmung des spektralen Überlapps im mittleren IR-Bereich konnten alle möglichen Diastereomere unterschieden und eine eindeutige Zuordnung der absoluten Konfiguration des Makrolactons (+)-**141** vorgenommen werden. Im Vergleich mit den experimentell aufgenommen Spektren wies das Oxacyclododecindion **141** mit (13*R*,14*S*,15*R*)-Konfiguration sowohl den größten Ähnlichkeitsfaktor mit 73%, als auch den höchsten ESI mit 71% auf (Abbildung 8.5). Eine anschließende Röntgenkristallstruktur-Analyse konnte die so bestimmte absolute Konfiguration bestätigen.

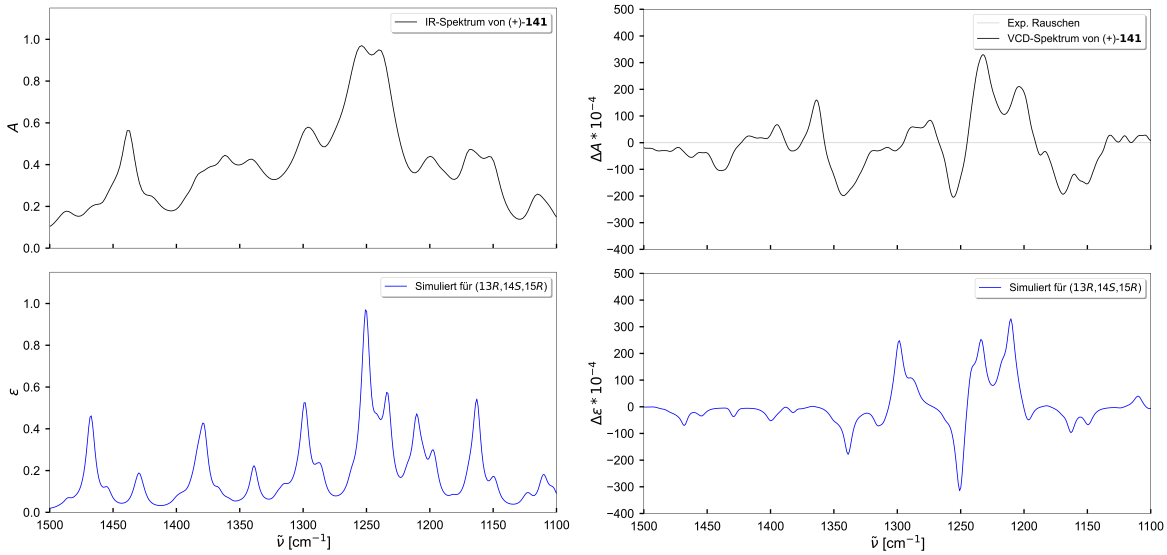

Abbildung 8.5: Experimentell aufgenommenen IR- und VCD-Spektren (oben) sowie die simulierten Spektrum (unten) des synthetischen Makrolactons (+)-**141**.

8.3 Strukturaufklärung isolierter Naturstoffe mittels computergestützter Spektroskopie

Im Rahmen diverser Kooperationsprojekte wurden die Inhaltsstoffe verschiedener Pilze und Pflanzen untersucht, wobei nicht nur bekannte Verbindungen detektiert, sondern auch die Strukturen mehrerer neuartiger Sekundärmetaboliten aufgeklärt werden konnten (Abbildung 8.6).

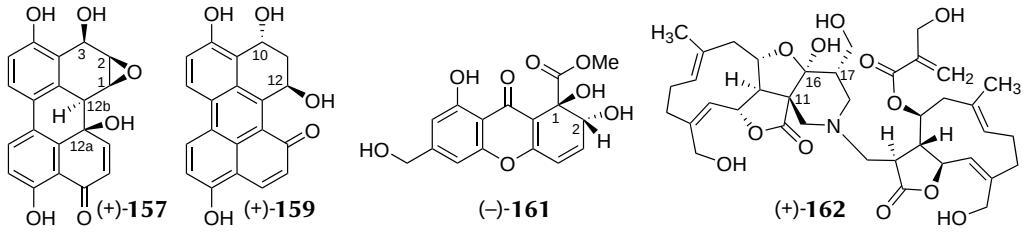

Abbildung 8.6: Neuartige Naturstoffe **157**, **159**, **161** und **162**, deren Struktur mittels computergestützter Spektroskopie aufgeklärt werden konnte.

In einem Kooperationsprojekt mit der Arbeitsgruppe [redacted] ermöglichte der Vergleich von simulierten und gemessenen ECD-Spektren die Bestimmung der absoluten Konfigura-

tion zweier Perylenchinone (+)-**157** und (+)-**159**, die aus einem Pilz der Gattung *Alternaria* isoliert wurden (Abbildung 8.7). Die elektronischen Anregungen wurden mittels TD-DFT berechnet, die erhaltenen Linienspektren mit der Software SpecDis in Gaußkurven übersetzt und anschließend der spektrale Überlapp mit den experimentellen Spektren bestimmt. Für Perylenchinon (1*S*,2*R*,3*R*,12a*R*,12b*S*)-**157** wurde ein ESI von 83% erhalten, während Perylenchinon (10*R*,12*R*)-**159** einen Wert von 52% ergab. Aufgrund zu geringer Substanzmengen war es allerdings nicht möglich, die Konfiguration des ebenfalls isolierten Perylenchinons **158** vollständig aufzuklären oder biologische Tests durchzuführen.

In Zelltests zeigte der Naturstoff (+)-**157** eine zytotoxische Wirkung, die Induktion von DNA-Schäden sowie die Aktivierung des Nrf2/ARE-Signalwegs und die Erhöhung des mRNA-Spiegels der Häm-Oxygenase 1. Erste Tests mit Perylenchinon (+)-**159** deuteten zwar auf eine Transkriptionsinhibition der Nrf2/ARE-Signalübertragung hin, der genaue Wirkmechanismus muss jedoch in zukünftigen Studien genauer untersucht werden.[563]

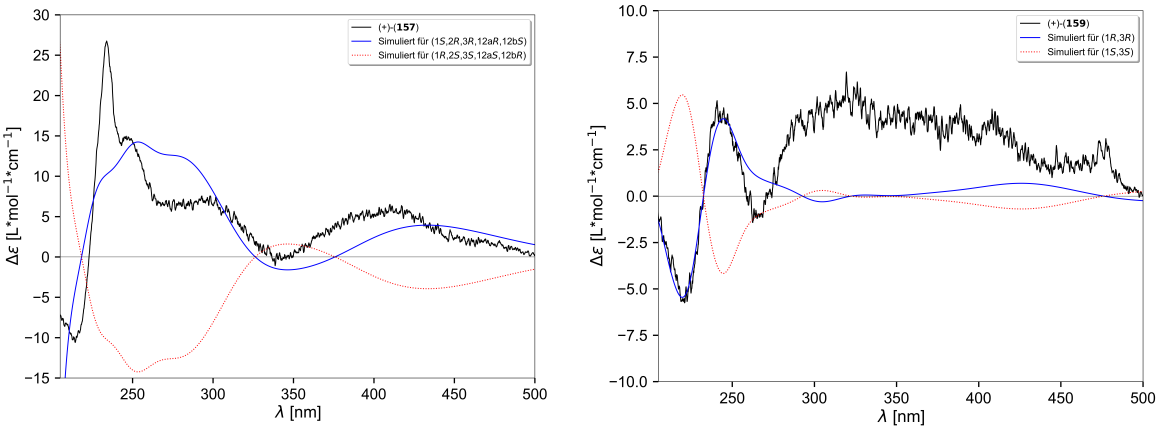

Abbildung 8.7: Vergleich der aufgenommenen ECD-Spektren der Perylenchinone (+)-**157** und (+)-**159** mit simulierten Spektren, die mittels TD-DFT (B3LYP/6-311+G(2d,p)/IEFPCM(Methanol)) für die 60 energetisch tiefliegendsten, elektronisch angeregten Zustände berechnet wurden.[563]

In einem weiteren Kooperationsprojekt mit der Arbeitsgruppe [redacted] konnte für Dihydroxanthon **161** durch Kombination von NMR-Spektroskopie und Polarimetrie in Verbindung mit (zeitabhängigen) DFT-Berechnungen ein Vorschlag für die absolute Konfiguration C-1*R*, C-2*R* ausgearbeitet werden. Dieser Naturstoff **161** wurde von der Arbeitsgruppe [redacted] aus einem Pilz der Gattung *Diaporthe* isoliert und wies in biologischen Tests mit menschlichen Zellen eine entzündungshemmende Wirkung auf.

In Kooperation mit der Arbeitsgruppe [redacted] wurde aus *Vernonia tufnelliae* ein neuartiges Sesquiterpenlacton (+)-**162** isoliert. Da auf Basis der durchgeführten NMR-Spektroskopie keine vollständige Aufklärung der Konfiguration von C-11, C-16 und C-17 des Naturstoffs (+)-**162** möglich war, wurde das wahrscheinlichste Diastereomer aus acht möglichen Diastereomeren durch die Anwendung des DP4+-Modells bestimmt. Dieser Ansatz zur Aufklärung der absoluten Konfiguration des Naturstoffs wurde allerdings durch die sehr ähnlichen Wahrscheinlichkeiten von 57 gegenüber 43% für die Kandidaten (6*R*,7*R*,8*S*,11*R*,16*R*,17*R*,6'*R*,7'*R*,8'*S*,11'*R*)-**162** und (6*R*,7*R*,8*S*,11*S*,16*S*,17*S*,6'*R*,7'*R*,8'*S*,11'*R*)-**162** erschwert. Obwohl die ECD-Spektren für beide Kandidatenstrukturen simuliert und mit dem von der Substanz aufgenommenen Spektrum verglichen wurden, konnte die absolute Konfiguration von Tufnelacton A ((+)-**162**) nicht eindeutig nachgewiesen werden, da die elektronischen Anregungen mit signifikanten Unterschieden außerhalb des experimentell zugänglichen Bereichs lagen (< 200 nm) (Abbildung 8.8).[567]

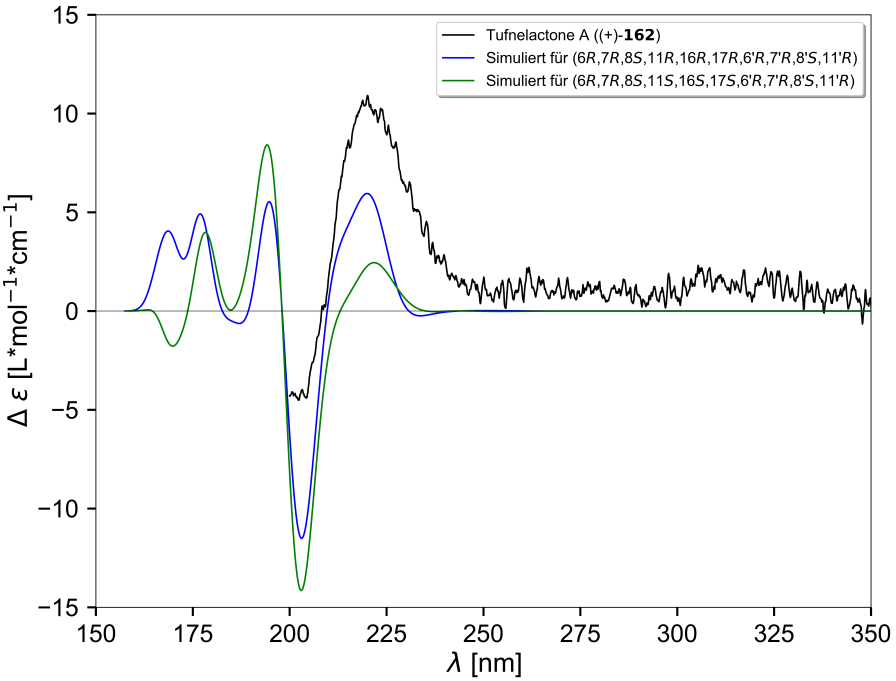

Abbildung 8.8: Vergleich des experimentellen ECD-Spektrums von Tufnelacton A ((+)-**162**) mit den simulierten Spektren der auf Grundlage des DP4+-Modells wahrscheinlichsten Diastereomere. Die elektronischen Anregungen für die 50 energetisch tiefliegendsten, angeregten Zustände wurden mittels TD-DFT (CAM-B3LYP/6-311+G(2d,p)/IEFPCM(Methanol)) berechnet.[567]

Literaturverzeichnis

[1] G. H. Brundtland, *Environ. Conserv.* **1987**, *14*, 291–294.

[2] United Nations Framework Convention on Climate Change (UNFCCC), Kyoto, **1997**.

[3] Conference of the Parties to the United Nations Framework Convention on Climate Change, Paris, **2015**.

[4] The European Commission, The European Green Deal, Brüssel, **2019**.

[5] V. Masson-Delmotte, P. Zhai, H.-O. Pörtner, D. Roberts, J. Skea, P. R. Shukla, *Global warming of 1.5 °C: An IPCC Special Report on the impacts of global warming of 1.5°C above pre-industrial levels and related global greenhouse gas emission pathways, in the context of strengthening the global response to the threat of climate change, sustainable development, and efforts to eradicate poverty*, IPCC, **2018**.

[6] I. T. Horváth, P. T. Anastas, *Chem. Rev.* **2007**, *107*, 2167–2168.

[7] C.-J. Li, P. T. Anastas, *Chem. Soc. Rev.* **2012**, *41*, 1413–1414.

[8] I. T. Horváth, P. T. Anastas, *Chem. Rev.* **2007**, *107*, 2169–2173.

[9] C. Capello, U. Fischer, K. Hungerbühler, *Green Chem.* **2007**, *9*, 927–934.

[10] R. A. Sheldon, *Green Chem.* **2014**, *16*, 950–963.

[11] P. T. Anastas, J. C. Warner, *Principles of Green Chemistry*, Oxford University Press, Oxford, UK, **1998**.

[12] J. B. Zimmerman, P. T. Anastas, H. C. Erythropel, W. Leitner, *Science* **2020**, *367*, 397–400.

[13] J. Martínez, J. F. Cortés, R. Miranda, *Processes* **2022**, *10*, 1274.

[14] B. M. Trost, *Science* **1991**, *254*, 1471–1477.

[15] R. A. Sheldon, *Chem. Ind.* **1992**, *23*, 903–906.

[16] R. A. Sheldon, *Green Chem.* **2007**, *9*, 1273–1283.

[17] R. A. Sheldon, *Green Chem.* **2017**, *19*, 18–43.

[18] R. A. Sheldon, *Green Chem.* **2023**, *25*, 1704–1728.

[19] R. A. Sheldon, *Green Chem.* **2005**, *7*, 267.

[20] C. J. Clarke, W.-C. Tu, O. Levers, A. Bröhl, J. P. Hallett, *Chem. Rev.* **2018**, *118*, 747–800.

[21] K. Alfonsi, J. Colberg, P. J. Dunn, T. Fevig, S. Jennings, T. A. Johnson, H. P. Kleine, C. Knight, M. A. Nagy, D. A. Perry, *Green Chem.* **2008**, *10*, 31–36.

[22] D. Prat, O. Pardigon, H.-W. Flemming, S. Letestu, V. Ducandas, P. Isnard, E. Guntrum, T. Senac, S. Ruisseau, P. Cruciani *et al.*, *Org. Process Res. Dev.* **2013**, *17*, 1517–1525.

[23] C. M. Alder, J. D. Hayler, R. K. Henderson, A. M. Redman, L. Shukla, L. E. Shuster, H. F. Sneddon, *Green Chem.* **2016**, *18*, 3879–3890.

[24] D. Prat, A. Wells, J. Hayler, H. Sneddon, C. R. McElroy, S. Abou-Shehada, P. J. Dunn, *Green Chem.* **2016**, *18*, 288–296.

[25] J. P. Adams, C. M. Alder, I. Andrews, A. M. Bullion, M. Campbell-Crawford, M. G. Darcy, J. D. Hayler, R. K. Henderson, C. A. Oare, I. Pendrak *et al.*, *Green Chem.* **2013**, *15*, 1542.

[26] H. Olivier-Bourbigou, L. Magna, D. Morvan, *Appl. Catal. A: Gen.* **2010**, *373*, 1–56.

[27] M. Moniruzzaman, K. Nakashima, N. Kamiya, M. Goto, *Biochem. Eng. J.* **2010**, *48*, 295–314.

[28] R. M. de Almeida, J. Li, C. Nederlof, P. O'Connor, M. Makkee, J. A. Moulijn, *ChemSusChem* **2010**, *3*, 325–328.

[29] X. Han, M. Poliakoff, *Chem. Soc. Rev.* **2012**, *41*, 1428–1436.

[30] M. J. Muldoon, *Dalton Trans.* **2010**, *2*, 337–348.

[31] J.-P. Lange, *ChemSusChem* **2009**, *2*, 587–592.

[32] P. Gallezot, *Chem. Soc. Rev.* **2012**, *41*, 1538–1558.

[33] N. Yan, X. Chen, *Nature* **2015**, *524*, 155–157.

[34] I. Parmar, H. P. V. Rupasinghe, *Bioresour. Technol.* **2013**, *130*, 613–620.

[35] R. Liguori, C. Soccol, L. Porto de Souza Vandenberghe, A. Woiciechowski, V. Faraco, *Energies* **2015**, *8*, 2575–2586.

[36] R. A. Verlinden, D. J. Hill, M. A. Kenward, C. D. Williams, Z. Piotrowska-Seget, I. K. Radecka, *AMB Express* **2011**, *1*, 11.

[37] A. J. Arduengo III, T. Opatz, https://xylochemistry.com/portal/ (aufgerufen am 12.09.2023).

[38] D. Stubba, G. Lahm, M. Geffe, J. W. Runyon, A. J. Arduengo III, T. Opatz, *Angew. Chem. Int. Ed.* **2015**, *54*, 14187–14189.

[39] J. Kühlborn, A.-K. Danner, H. Frey, R. Iyer, A. J. Arduengo, T. Opatz, *Green Chem.* **2017**, *19*, 3780–3786.

[40] A. Lipp, D. Ferenc, C. Gütz, M. Geffe, N. Vierengel, D. Schollmeyer, H. J. Schäfer, S. R. Waldvogel, T. Opatz, *Angew. Chem. Int. Ed.* **2018**, *57*, 11055–11059.

[41] A. Lipp, M. Selt, D. Ferenc, D. Schollmeyer, S. R. Waldvogel, T. Opatz, *Org. Lett.* **2019**, *21*, 1828–1831.

[42] R. Klintworth, C. B. de Koning, T. Opatz, J. P. Michael, *J. Org. Chem.* **2019**, *84*, 11025–11031.

[43] J. Kühlborn, M. Konhäuser, J. Groß, P. R. Wich, T. Opatz, *ACS Sustain. Chem. Eng.* **2019**, *7*, 4414–4419.

[44] K. J. Ngwira, J. Kühlborn, Q. A. Mgani, C. B. de Koning, T. Opatz, *Eur. J. Org. Chem.* **2019**, *2019*, 4778–4790.

[45] L. Geske, U. Kauhl, M. E. M. Saeed, A. Schüffler, E. Thines, T. Efferth, T. Opatz, *Molecules* **2021**, *26*, 3224.

[46] J. Groß, J. Kühlborn, T. Opatz, *Green Chem.* **2020**, *22*, 4411–4425.

[47] J. Groß, C. Grundke, J. Rocker, A. J. Arduengo, T. Opatz, *ChemComm.* **2021**, *57*, 9979–9994.

[48] D. Graham-Rowe, *Nature* **2011**, *474*, 6–8.

[49] A. Ajanovic, *Energy J.* **2011**, *36*, 2070–2076.

[50] S. Prasad, A. P. Ingle in *Sustainable Bioenergy*, Elsevier, Amsterdam, NL, **2019**, S. 327–346.

[51] C. O. Tuck, E. Pérez, I. T. Horváth, R. A. Sheldon, M. Poliakoff, *Science* **2012**, *337*, 695.

[52] L. T. Mika, E. Csefalvay, A. Nemeth, *Chem. Rev.* **2018**, *118*, 505–613.

[53] A. M. Ruppert, K. Weinberg, R. Palkovits, *Angew. Chem. Int. Ed.* **2012**, *51*, 2564–2601.

[54] R. A. Sheldon, *ACS Sustain. Chem. Eng.* **2018**, *6*, 4464–4480.

[55] J. J. Bozell, L. Moens, D. Elliott, Y. Wang, G. Neuenscwander, S. Fitzpatrick, R. Bilski, J. Jarnefeld, *Resour. Conserv. Recycl.* **2000**, *28*, 227–239.

[56] M. Zirbes, D. Schmitt, N. Beiser, D. Pitton, T. Hoffmann, S. R. Waldvogel, *ChemElectroChem* **2019**, *6*, 155–161.

[57] M. Zirbes, L. L. Quadri, M. Breiner, A. Stenglein, A. Bomm, W. Schade, S. R. Waldvogel, *ACS Sustain. Chem. Eng.* **2020**, *8*, 7300–7307.

[58] B. H. Nguyen, R. J. Perkins, J. A. Smith, K. D. Moeller, *J. Org. Chem.* **2015**, *80*, 11953–11962.

[59] D. Montané, *Biomass Bioenergy* **2002**, *22*, 295–304.

[60] A. A. Rosatella, S. P. Simeonov, R. F. M. Frade, C. A. M. Afonso, *Green Chem.* **2011**, *13*, 754–793.

[61] A. K. Biswas, A. B. Roy, *Nature* **1958**, *182*, 1299–1300.

[62] G. Mele, G. Vasapollo, *Mini-Rev. Org. Chem.* **2008**, *5*, 243–253.

[63] L. A. Pfaltzgraff, M. de bruyn, E. C. Cooper, V. Budarin, J. H. Clark, *Green Chem.* **2013**, *15*, 307.

[64] G. A. Burdock, *Fenaroli's Handbook of Flavor Ingredients*, 6th ed., Taylor and Francis, Hoboken, NJ, USA, **2009**.

[65] M. Kabbour, R. Luque in *Biomass, Biofuels, Biochemicals*, Elsevier, **2020**, S. 283–297.

[66] H. Pringsheim, H. Noth, *Chem. Ber.* **1920**, *53*, 114–118.

[67] H. Mehdi, V. Fábos, R. Tuba, A. Bodor, L. T. Mika, I. T. Horváth, *Top. Catal.* **2008**, *48*, 49–54.

[68] J. Sherwood, A. Constantinou, L. Moity, C. R. McElroy, T. J. Farmer, T. Duncan, W. Raverty, A. J. Hunt, J. H. Clark, *ChemComm.* **2014**, *50*, 9650–9652.

[69] J. E. Camp, *ChemSusChem* **2018**, *11*, 3048–3055.

[70] M. Geffe, T. Opatz, *Org. Lett.* **2014**, *16*, 5282–5285.

[71] J. Saska, Z. Li, A. L. Otsuki, J. Wei, J. C. Fettinger, M. Mascal, *Angew. Chem. Int. Ed.* **2019**, *58*, 17293–17296.

[72] S. Inoue, H. Koinuma, T. Tsuruta, *Makromol. Chem.* **1969**, *130*, 210–220.

[73] O. Dechy-Cabaret, B. Martin-Vaca, D. Bourissou, *Chem. Rev.* **2004**, *104*, 6147–6176.

[74] C. M. Byrne, S. D. Allen, E. B. Lobkovsky, G. W. Coates, *J. Am. Chem. Soc.* **2004**, *126*, 11404–11405.

[75] C. M. Thomas, *Chem. Soc. Rev.* **2010**, *39*, 165–173.

[76] G. Fiorani, M. Stuck, C. Martín, M. M. Belmonte, E. Martin, E. C. Escudero-Adán, A. W. Kleij, *ChemSusChem* **2016**, *9*, 1304–1311.

[77] N. Kindermann, À. Cristòfol, A. W. Kleij, *ACS Catal.* **2017**, *7*, 3860–3863.

[78] L. E. Manzer, *Appl. Catal. A: Gen.* **2004**, *272*, 249–256.

[79] A. D. Sadiq, X. Chen, N. Yan, J. Sperry, *ChemSusChem* **2018**, *11*, 532–535.

[80] T. T. Pham, G. Gözaydın, T. Söhnel, N. Yan, J. Sperry, *Eur. J. Org. Chem.* **2019**, *2019*, 1355–1360.

[81] T. T. Pham, X. Chen, T. Söhnel, N. Yan, J. Sperry, *Green Chem.* **2020**, *22*, 1978–1984.

[82] V. Bragoni, R. K. Rit, R. Kirchmann, A. S. Trita, L. J. Gooßen, *Green Chem.* **2018**, *20*, 3210–3213.

[83] P. H. Gedam, P. S. Sampathkumaran, *Prog. Org. Coat.* **1986**, *14*, 115–157.

[84] A. H. Tullo, *Chem. Eng. News* **2008**, *86*, 26–27.

[85] S. Lavoie, J. Legault, F. Simard, É. Chiasson, A. Pichette, *Tetrahedron Lett.* **2013**, *54*, 1631–1633.

[86] F. Simard, J. Legault, S. Lavoie, A. Pichette, *Phytochem.* **2014**, *100*, 141–149.

[87] F. Simard, C. Gauthier, É. Chiasson, S. Lavoie, V. Mshvildadze, J. Legault, A. Pichette, *J. Nat. Prod.* **2015**, *78*, 1147–1153.

[88] J. Alsarraf, J.-F. Bilodeau, J. Legault, F. Simard, A. Pichette, *ACS Sustain. Chem. Eng.* **2020**, *8*, 6194–6199.

[89] L. Geske, J. Baier, J. C. Boulos, T. Efferth, T. Opatz, *J. Nat. Prod.* **2023**, *86*, 131–137.

[90] V. Gold, *The IUPAC Compendium of Chemical Terminology*, International Union of Pure and Applied Chemistry (IUPAC), Research Triangle Park, NC, **2019**.

[91] E. Hoffmann, *Evolution der Erde und des Lebens: Von der Urzelle zum Homo Sapiens*, 1th ed., UTB GmbH, Norderstedt, DE, **2015**.

[92] A. J. Lynch, *The History of Grinding*, Society for Mining Metallurgy and Exploration Inc, Littleton, Colorado, US, **2005**.

[93] L. Takacs, *Chem. Soc. Rev.* **2013**, *42*, 7649–7659.

[94] S. L. James, C. J. Adams, C. Bolm, D. Braga, P. Collier, T. Friščić, F. Grepioni, K. D. M. Harris, G. Hyett, W. Jones *et al.*, *Chem. Soc. Rev.* **2012**, *41*, 413–447.

[95] P. Baláž, *Mechanochemistry in Nanoscience and Minerals Engineering*, Springer, Berlin und Heidelberg, DE, **2008**.

[96] W. Ostwald, *Lehrbuch der allgemeinen Chemie*, *Bd. 1*, W. Engelmann, **1910**.

[97] https://scifinder-n.cas.org/, (aufgerufen am 17.03.2023).

[98] A. Bruckmann, A. Krebs, C. Bolm, *Green Chem.* **2008**, *10*, 1131.

[99] A. Stolle, T. Szuppa, S. E. S. Leonhardt, B. Ondruschka, *Chem. Soc. Rev.* **2011**, *40*, 2317–2329.

[100] A. Stolle, *Ball Milling Towards Green Synthesis: Applications, Projects, Challenges*, 1st ed., Royal society of chemistry, Cambridge, UK, **2015**.

[101] R. R. A. Bolt, J. A. Leitch, A. C. Jones, W. I. Nicholson, D. L. Browne, *Chem. Soc. Rev.* **2022**, *51*, 4243–4260.

[102] L. Gonnet, C. B. Lennox, J.-L. Do, I. Malvestiti, S. G. Koenig, K. Nagapudi, T. Friščić, *Angew. Chem. Int. Ed.* **2022**, *61*, e202115030.

[103] K. Kubota, R. Takahashi, H. Ito, *Chem. Sci.* **2019**, *10*, 5837–5842.

[104] J. L. Howard, M. C. Brand, D. L. Browne, *Angew. Chem. Int. Ed.* **2018**, *57*, 16104–16108.

[105] S. Hwang, S. Grätz, L. Borchardt, *ChemComm.* **2022**, *58*, 1661–1671.

[106] F. Gomollón-Bel, *Chem. Int.* **2019**, *41*, 12–17.

[107] K. J. Ardila-Fierro, J. G. Hernández, *ChemSusChem* **2021**, *14*, 2145–2162.

[108] J. G. Hernández, C. Bolm, *J. Org. Chem.* **2017**, *82*, 4007–4019.

[109] J. G. Hernández, *Chem. Eur. J.* **2017**, *23*, 17157–17165.

[110] G. Gorrasi, A. Sorrentino, *Green Chem.* **2015**, *17*, 2610–2625.

[111] C. Lu, Q. Wang, *J. Mater. Process. Technol.* **2004**, *145*, 336–344.

[112] C. Bolm, J. G. Hernández, *Angew. Chem. Int. Ed.* **2019**, *58*, 3285–3299.

[113] C. C. Piras, S. Fernández-Prieto, W. M. de Borggraeve, *Nanoscale Adv.* **2019**, *1*, 937–947.

[114] A. V. Trask, W. Jones in *Organic Solid State Reactions*, (Hrsg.: F. Toda), Topics in Current Chemistry, Springer, Berlin und Heidelberg, DE, **2005**, S. 41–70.

[115] P. Vishweshwar, J. A. McMahon, J. A. Bis, M. J. Zaworotko, *J. Pharm. Sci.* **2006**, *95*, 499–516.

[116] M. Kumar, X. Xiong, Z. Wan, Y. Sun, D. C. W. Tsang, J. Gupta, B. Gao, X. Cao, J. Tang, Y. S. Ok, *Bioresour. Technol.* **2020**, *312*, 123613.

[117] E. Colacino, G. Ennas, I. Halasz, A. Porcheddu, A. Scano, *Mechanochemistry*, De Gruyter, Berlin, DE, **2020**.

[118] S. Reichle, M. Felderhoff, F. Schüth, *Angew. Chem. Int. Ed.* **2021**, *60*, 26385–26389.

[119] P. Baláž, M. Achimovičová, M. Baláž, P. Billik, Z. Cherkezova-Zheleva, J. M. Criado, F. Delogu, E. Dutková, E. Gaffet, F. J. Gotor *et al.*, *Chem. Soc. Rev.* **2013**, *42*, 7571–7637.

[120] A. Pichon, A. Lazuen-Garay, S. L. James, *CrystEngComm* **2006**, *8*, 211.

[121] T. Stolar, K. Užarević, *CrystEngComm* **2020**, *22*, 4511–4525.

[122] A. N. Swinburne, J. W. Steed, *CrystEngComm* **2009**, *11*, 433.

[123] I. N. Egorov, S. Santra, D. S. Kopchuk, I. S. Kovalev, G. V. Zyryanov, A. Majee, B. C. Ranu, V. L. Rusinov, O. N. Chupakhin, *Green Chem.* **2020**, *22*, 302–315.

[124] G. S. Lee, H. W. Lee, H. S. Lee, T. Do, J.-L. Do, J. Lim, G. I. Peterson, T. Friščić, J. G. Kim, *Chem. Sci.* **2022**, *13*, 11496–11505.

[125] A. Krusenbaum, S. Grätz, G. T. Tigineh, L. Borchardt, J. G. Kim, *Chem. Soc. Rev.* **2022**, *51*, 2873–2905.

[126] Y. Zheng, Z. Li, P. Deng, Y. Yu, *Polym. Chem.* **2023**, *14*, 324–329.

[127] B. Mishra, *Int. J. Miner. Process.* **2003**, *71*, 73–93.

[128] B. Mishra, *Int. J. Miner. Process.* **2003**, *71*, 95–112.

[129] C. F. Burmeister, A. Kwade, *Chem. Soc. Rev.* **2013**, *42*, 7660–7667.

[130] K. Kubota, H. Ito, *Trends Chem.* **2020**, *2*, 1066–1081.

[131] T. Seo, N. Toyoshima, K. Kubota, H. Ito, *J. Am. Chem. Soc.* **2021**, *143*, 6165–6175.

[132] D. A. Fulmer, W. C. Shearouse, S. T. Medonza, J. Mack, *Green Chem.* **2009**, *11*, 1821.

[133] F. Schneider, B. Ondruschka, *ChemSusChem* **2008**, *1*, 622–625.

[134] Q. Cao, J. L. Howard, E. Wheatley, D. L. Browne, *Angew. Chem. Int. Ed.* **2018**, *130*, 11509–11513.

[135] E. Tullberg, D. Peters, T. Frejd, *J. Organomet. Chem.* **2004**, *689*, 3778–3781.

[136] G.-W. Wang, *Chem. Soc. Rev.* **2013**, *42*, 7668–7700.

[137] T. H. El-Sayed, A. Aboelnaga, M. A. El-Atawy, M. Hagar, *Molecules* **2018**, *23*, 1348.

[138] K. J. Ardila-Fierro, C. Bolm, J. G. Hernández, *Angew. Chem. Int. Ed.* **2019**, *58*, 12945–12949.

[139] K. Kubota, Y. Pang, A. Miura, H. Ito, *Science* **2019**, *366*, 1500–1504.

[140] L. Chen, D. Leslie, M. G. Coleman, J. Mack, *Chem. Sci.* **2018**, *9*, 4650–4661.

[141] A. Biswas, A. Bhunia, S. K. Mandal, *Chem. Sci.* **2023**, *14*, 2606–2615.

[142] K. S. Rodygin, Y. A. Vikenteva, V. P. Ananikov, *ChemSusChem* **2019**, *12*, 1483–1516.

[143] W. Pickhardt, S. Grätz, L. Borchardt, *Chem. Eur. J.* **2020**, *26*, 12903–12911.

[144] T. Castanheiro, J. Suffert, M. Donnard, M. Gulea, *Chem. Soc. Rev.* **2016**, *45*, 494–505.

[145] A. W. Erian, S. M. Sherif, *Tetrahedron* **1999**, *55*, 7957–8024.

[146] M. Gao, M. Vuagnat, M.-Y. Chen, X. Pannecoucke, P. Jubault, T. Besset, *Chem. Eur. J.* **2021**, *27*, 6145–6160.

[147] F. Wang, X. Yu, Z. Qi, X. Li, *Chem. Eur. J.* **2016**, *22*, 511–516.

[148] N. Muniraj, J. Dhineshkumar, K. R. Prabhu, *ChemistrySelect* **2016**, *1*, 1033–1038.

[149] K. Nikoofar, S. Gorji, *J. Sulphur Chem.* **2016**, *37*, 80–88.

[150] J. S. Yadav, B. V. Reddy, M. K. Gupta, *Synth.* **2004**, *2004*, 1983–1986.

[151] J. Jiao, L. X. Nguyen, D. R. Patterson, R. A. Flowers, *Org. Lett.* **2007**, *9*, 1323–1326.

[152] W. Fan, Q. Yang, F. Xu, P. Li, *J. Org. Chem.* **2014**, *79*, 10588–10592.

[153] H. Yang, X.-H. Duan, J.-F. Zhao, L.-N. Guo, *Org. Lett.* **2015**, *17*, 1998–2001.

[154] J. Ruiz, R. Quesada, V. Riera, M. Vivanco, S. García-Granda, M. R. Díaz, *Angew. Chem. Int. Ed.* **2003**, *115*, 2494–2497.

[155] Di Wu, J. Qiu, P. G. Karmaker, H. Yin, F.-X. Chen, *J. Org. Chem.* **2018**, *83*, 1576–1583.

[156] K. Jouvin, C. Matheis, L. J. Goossen, *Chem. Eur. J.* **2015**, *21*, 14324–14327.

[157] S. Kadam, A. Ambhore, M. Hebade, R. Kamble, S. Hese, M. Gaikwad, P. Gavhane, B. Dawane, *Synlett* **2018**, *29*, 1902–1908.

[158] K. Yamaguchi, K. Sakagami, Y. Miyamoto, X. Jin, N. Mizuno, *Org. Biomol. Chem.* **2014**, *12*, 9200–9206.

[159] F. Teng, J.-T. Yu, H. Yang, Y. Jiang, J. Cheng, *ChemComm.* **2014**, *50*, 12139–12141.

[160] V. Merz, W. Weith, *Chem. Ber.* **1877**, *10*, 746–765.

[161] D. D. Kuhn, T. C. Young, *Chemosphere* **2005**, *60*, 1222–1230.

[162] C. Bolm, R. Mocci, C. Schumacher, M. Turberg, F. Puccetti, J. G. Hernández, *Angew. Chem. Int. Ed.* **2018**, *57*, 2423–2426.

[163] C. Jiang, Y. Zhu, H. Li, P. Liu, P. Sun, *J. Org. Chem.* **2022**, *87*, 10026–10033.

[164] D. Zhu, D. Chang, L. Shi, *ChemComm.* **2015**, *51*, 7180–7183.

[165] R. Frei, T. Courant, M. D. Wodrich, J. Waser, *Chem. Eur. J.* **2015**, *21*, 2662–2668.

[166] L. C. D. de Rezende, S. M. G. de Melo, S. Boodts, B. Verbelen, W. Dehaen, F. da Silva Emery, *Org. Biomol. Chem.* **2015**, *13*, 6031–6038.

[167] L. C. Rezende, S. M. Melo, S. Boodts, B. Verbelen, F. S. Emery, W. Dehaen, *Dyes Pigm.* **2018**, *154*, 155–163.

[168] D. F. Murphy, C. H. Peet, *J. Econ. Entomol.* **1932**, *25*, 123–129.

[169] J. S. Mchargue, R. K. Calfee, *J. Ind. Eng. Chem.* **1937**, *29*, 1232–1233.

[170] N. Bakry, R. L. Metcalf, T. R. Fukuto, *J. Econ. Entomol.* **1968**, *61*, 1303–1309.

[171] P.-Y. Renard, H. Schwebel, P. Vayron, L. Josien, A. Valleix, C. Mioskowski, *Chem. Eur. J.* **2002**, *8*, 2910.

[172] J. Gonda, M. Martinková, J. Raschmanová, E. Balentová, *Tetrahedron Asymmetry* **2006**, *17*, 1875–1882.

[173] X. Lu, H. Wang, R. Gao, D. Sun, X. Bi, *RSC Adv.* **2014**, *4*, 28794–28797.

[174] S. Majedi, L. Sreerama, E. Vessally, F. Behmagham, *J. Chem. Lett.* **2020**, *1*, 25–31.

[175] J. A. Varela, L. Castedo, C. Saá, *J. Org. Chem.* **2003**, *68*, 8595–8598.

[176] Z. P. Demko, K. B. Sharpless, *Org. Lett.* **2001**, *3*, 4091–4094.

[177] M. Gulea, F. Hammerschmidt, P. Marchand, S. Masson, V. Pisljagic, F. Wuggenig, *Tetrahedron Asymmetry* **2003**, *14*, 1829–1836.

[178] L. Melzig, C. B. Rauhut, N. Naredi-Rainer, P. Knochel, *Chem. Eur. J.* **2011**, *17*, 5362–5372.

[179] F. Wang, C. Chen, G. Deng, C. Xi, *J. Org. Chem.* **2012**, *77*, 4148–4151.

[180] S. Potash, S. Rozen, *J. Fluor. Chem.* **2014**, *168*, 173–176.

[181] G. K. S. Prakash, P. V. Jog, P. T. D. Batamack, G. A. Olah, *Science* **2012**, *338*, 1324–1327.

[182] W. Han, Y. Li, H. Tang, H. Liu, *J. Fluor. Chem.* **2012**, *140*, 7–16.

[183] C. Hansch, A. Leo, R. W. Taft, *Chem. Rev.* **1991**, *91*, 165–195.

[184] M. J. Garson, J. S. Simpson, A. E. Flowers, E. J. Dumdei in *Bioactive Natural Products (Part B)*, Studies in Natural Products Chemistry, Elsevier, Amsterdam, NL, **2000**, S. 329–372.

[185] V. A. Kokorekin, A. O. Terent'ev, G. V. Ramenskaya, N. É. Grammatikova, G. M. Rodionova, A. I. Ilovaiskii, *Pharm. Chem. J.* **2013**, *47*, 422–425.

[186] M. P. Fortes, P. B. N. Da Silva, T. G. Da Silva, T. S. Kaufman, G. C. G. Militão, C. C. Silveira, *Eur. J. Med. Chem.* **2016**, *118*, 21–26.

[187] S. M. Weinreb, *Chem. Rev.* **2006**, *106*, 2531–2549.

[188] P. Ahmad, C. A. Fyfe, A. Mellors, *Biochem. Pharmacol.* **1975**, *24*, 1103–1109.

[189] G. E. G. Linares, E. L. Ravaschino, J. B. Rodriguez, *Curr. Med. Chem.* **2006**, *13*, 335–360.

[190] F.-Y. Lin, Y.-L. Liu, K. Li, R. Cao, W. Zhu, J. Axelson, R. Pang, E. Oldfield, *J. Med. Chem.* **2012**, *55*, 4367–4372.

[191] R. J. Capon, C. Skene, E. H.-T. Liu, E. Lacey, J. H. Gill, K. Heiland, T. Friedel, *J. Org. Chem.* **2001**, *66*, 7765–7769.

[192] R. J. Capon, C. Skene, E. H.-T. Liu, E. Lacey, J. H. Gill, K. Heiland, T. Friedel, *J. Nat. Prod.* **2004**, *67*, 1277–1282.

[193] A. T. Pham, T. Ichiba, W. Y. Yoshida, P. J. Scheuer, T. Uchida, J.-i. Tanaka, T. Higa, *Tetrahedron Lett.* **1991**, *32*, 4843–4846.

[194] H. Y. He, J. Salva, R. F. Catalos, D. J. Faulkner, *J. Org. Chem.* **1992**, *57*, 3191–3194.

[195] N. Fusetani, H. J. Wolstenholme, K. Shinoda, N. Asai, S. Matsunaga, H. Onuki, H. Hirota, *Tetrahedron Lett.* **1992**, *33*, 6823–6826.

[196] M. J. Garson, J. S. Simpson, *Nat. Prod. Rep.* **2004**, *21*, 164–179.

[197] A. Srikrishna, S. J. Gharpure, *Tetrahedron Lett.* **1999**, *40*, 1035–1038.

[198] A. Srikrishna, S. J. Gharpure, *J. Chem. Soc. Perkin Trans.* **2000**, 3191–3193.

[199] C. Jiménez, P. Crews, *Tetrahedron* **1991**, *47*, 2097–2102.

[200] I. C. Piña, J. T. Gautschi, G.-Y.-S. Wang, M. L. Sanders, F. J. Schmitz, D. France, S. Cornell-Kennon, L. C. Sambucetti, S. W. Remiszewski, L. B. Perez *et al.*, *J. Org. Chem.* **2003**, *68*, 3866–3873.

[201] C. P. Li, A. J. Blackman, *Aust. J. Chem.* **1994**, *47*, 1355–1361.

[202] C. P. Li, A. J. Blackman, *Aust. J. Chem.* **1995**, *48*, 955–965.

[203] H. Abe, S. Aoyagi, C. Kibayashi, *J. Am. Chem. Soc.* **2000**, *122*, 4583–4592.

[204] J.-H. Maeng, R. L. Funk, *Org. Lett.* **2002**, *4*, 331–333.

[205] J. O. Egekeze, F. W. Oehme, *Vet. Q.* **1980**, *2*, 104–114.

[206] International Cyanide Management Institute, The Cyanide Code - Use in mining, **2022**.

[207] Z. P. Demko, K. B. Sharpless, *J. Org. Chem.* **2001**, *66*, 7945–7950.

[208] C. Grundke, T. Opatz, *Green Chem.* **2019**, *21*, 2362–2366.

[209] C. Grundke, C. Kong, C. J. Kampf, B. F. Gupton, D. T. McQuade, T. Opatz, *J. Org. Chem.* **2021**, *86*, 10320–10329.

[210] C. Grundke, J. Groß, N. Vierengel, J. Sirleaf, M. Schmitz, L. Krieger, T. Opatz, *Org. Biomol. Chem.* **2022**, *21*, 644–650.

[211] Q.-W. Zhang, L.-G. Lin, W.-C. Ye, *Chin. Med.* **2018**, *13*, 20.

[212] L. Bohlin, U. Göransson, C. Alsmark, C. Wedén, A. Backlund, *Phytochem. Rev.* **2010**, *9*, 279–301.

[213] M. Sorokina, C. Steinbeck, *J. Cheminform.* **2020**, *12*, 20.

[214] P. Nuhn, *Naturstoffchemie: Mikrobielle, pflanzliche und tierische Naturstoffe*, 4. neu bearb. Aufl., Hirzel, Stuttgart, DE, **2006**.

[215] G. Habermehl, P. E. Hammann, H. C. Krebs, Ternes W., *Naturstoffchemie: Eine Einführung*, 3. vollst. überarb. und erw. Aufl., Springer, Berlin und Heidelberg, **2008**.

[216] R. S. Solecki, *Science* **1975**, *190*, 880–881.

[217] J. Lietava, *J. Ethnopharmacol.* **1992**, *35*, 263–266.

[218] J. Frackenpohl, *Chem. Unserer Zeit* **2000**, *34*, 99–112.

[219] F. W. Sertürner, *Apotheker und Chemisten* **1806**, *14*, 47–93.

[220] M. L. Grayson, G. M. Eliopoulos, C. B. Wennersten, K. L. Ruoff, P. C. de Girolami, M. J. Ferraro, R. C. Moellering, *Antimicrob. Agents Chemother.* **1991**, *35*, 2180–2184.

[221] I. M. Tleyjeh, H. M. Tlaygeh, R. Hejal, V. M. Montori, L. M. Baddour, *Clin. Infect. Dis.* **2006**, *42*, 788–797.

[222] R. L. Bunch, J. M. Mcguire, US2653899A, US, **1953**.

[223] V.-M. Platon, B. Dragoi, L. Marin, *Pharmaceutics* **2022**, *14*, 2180.

[224] D. J. Newman, G. M. Cragg, K. M. Snader, *Nat. Prod. Rep.* **2000**, *17*, 215–234.

[225] G. Szakács, J. K. Paterson, J. A. Ludwig, C. Booth-Genthe, M. M. Gottesman, *Nat. Rev. Drug Discov.* **2006**, *5*, 219–234.

[226] H. Nikaido, *Annu. Rev. Biochem.* **2009**, *78*, 119–146.

[227] J. Tanwar, S. Das, Z. Fatima, S. Hameed, M. Lanzafame, *Interdiscip. Perspect. Infect. Dis.* **2014**, *2014*, 541340.

[228] M. C. Wani, H. L. Taylor, M. E. Wall, P. Coggon, A. T. McPhail, *J. Am. Chem. Soc.* **1971**, *93*, 2325–2327.

[229] B. A. Weaver, *Mol. Biol. Cell.* **2014**, *25*, 2677–2681.

[230] L. Zhu, L. Chen, *Cell. Mol. Biol. Lett.* **2019**, *24*, 40.

[231] F. Barré-Sinoussi, J. C. Chermann, F. Rey, M. T. Nugeyre, S. Chamaret, J. Gruest, C. Dauguet, C. Axler-Blin, F. Vézinet-Brun, C. Rouzioux *et al.*, *Science* **1983**, *220*, 868–871.

[232] K. Stadler, V. Masignani, M. Eickmann, S. Becker, S. Abrignani, H.-D. Klenk, R. Rappuoli, *Nat. Rev. Microbiol.* **2003**, *1*, 209–218.

[233] A. B. Bhatti, M. Usman, V. Kandi, *Cureus* **2016**, *8*, e515.

[234] C. P. Austin, C. M. Cutillo, L. P. L. Lau, A. H. Jonker, A. Rath, D. Julkowska, D. Thomson, S. F. Terry, B. de Montleau, D. Ardigò *et al.*, *Clin. Transl. Sci.* **2018**, *11*, 21–27.

[235] N. N. Chathappady House, S. Palissery, H. Sebastian, *Microbiol. Insights* **2021**, *14*, 11786361211002481.

[236] A. G. Atanasov, B. Waltenberger, E.-M. Pferschy-Wenzig, T. Linder, C. Wawrosch, P. Uhrin, V. Temml, L. Wang, S. Schwaiger, E. H. Heiss *et al.*, *Biotechnol. Adv.* **2015**, *33*, 1582–1614.

[237] D. J. Newman, G. M. Cragg, *J. Nat. Prod.* **2016**, *79*, 629–661.

[238] S. A. M. Khalifa, N. Elias, M. A. Farag, L. Chen, A. Saeed, M.-E. F. Hegazy, M. S. Moustafa, A. Abd El-Wahed, S. M. Al-Mousawi, S. G. Musharraf *et al.*, *Mar. Drugs* **2019**, *17*, 491.

[239] L. D. Edwards, A. W. Fox, P. D. Stonier, *Principles and Practice of Pharmaceutical Medicine*, Chichester, UK, **2002**.

[240] B. David, J.-L. Wolfender, D. A. Dias, *Phytochem. Rev.* **2015**, *14*, 299–315.

[241] M. A. Sierra, M. C. de la Torre, *Angew. Chem.* **2000**, *112*, 1628–1650.

[242] J. J. Li, E. J. Corey, *Total synthesis of natural products: At the frontiers of organic chemistry*, Springer, Berlin, Heidelberg, DE, **2012**.

[243] J. M. Bijvoet, A. F. Peerdeman, A. J. van Bommel, *Nature* **1951**, *168*, 271–272.

[244] L.-Y. Kong, P. Wang, *Chin. J. Nat. Med.* **2013**, *11*, 193–198.

[245] A. Mándi, T. Kurtán, *Nat. Prod. Rep.* **2019**, *36*, 889–918.

[246] M. O. Marcarino, M. A. M. Zanardi, S. Cicetti, A. M. Sarotti, *Acc. Chem. Res* **2020**, *53*, 1922–1932.

[247] K. C. Nicolaou, S. A. Snyder, *Angew. Chem. Int. Ed.* **2005**, *44*, 1012–1044.

[248] M. E. Maier, *Nat. Prod. Rep.* **2009**, *26*, 1105–1124.

[249] T. L. Suyama, W. H. Gerwick, K. L. McPhail, *Bioorg. Med. Chem.* **2011**, *19*, 6675–6701.

[250] K. C. Nicolaou, C. R. H. Hale, C. Nilewski, H. A. Ioannidou, A. ElMarrouni, L. G. Nilewski, K. Beabout, T. T. Wang, Y. Shamoo, *J. Am. Chem. Soc.* **2014**, *136*, 12137–12160.

[251] Q. Xiao, K. Young, A. Zakarian, *J. Am. Chem. Soc.* **2015**, *137*, 5907–5910.

[252] L. Zhu, Y. Liu, R. Ma, R. Tong, *Angew. Chem. Int. Ed.* **2015**, *54*, 627–632.

[253] K. C. Nicolaou, A. A. Shah, H. Korman, T. Khan, L. Shi, W. Worawalai, E. A. Theodorakis, *Angew. Chem. Int. Ed.* **2015**, *127*, 9335–9340.

[254] L. Grauso, R. Teta, G. Esposito, M. Menna, A. Mangoni, *Nat. Prod. Rep.* **2019**, *36*, 1005–1030.

[255] S. Superchi, P. Scafato, M. Gorecki, G. Pescitelli, *Curr. Med. Chem.* **2018**, *25*, 287–320.

[256] https://www.olcf.ornl.gov/frontier/, aufgerufen am 30.06.2023.

[257] M. A. J. Koenis, O. Visser, L. Visscher, W. J. Buma, V. P. Nicu, *J. Chem. Inf. Model.* **2020**, *60*, 259–267.

[258] D. A. Matthews, L. Cheng, M. E. Harding, F. Lipparini, S. Stopkowicz, T.-C. Jagau, P. G. Szalay, J. Gauss, J. F. Stanton, *J. Chem. Phys.* **2020**, *152*, 214108.

[259] K. Aidas, C. Angeli, K. L. Bak, V. Bakken, R. Bast, L. Boman, O. Christiansen, R. Cimiraglia, S. Coriani, P. Dahle *et al.*, *Wiley Interdiscip. Rev. Comput. Mol. Sci.* **2014**, *4*, 269–284.

[260] M. J. Frisch, G. W. Trucks, H. B. Schlegel, G. E. Scuseria, M. A. Robb, J. R. Cheeseman, G. Scalmani, V. Barone, G. A. Petersson, H. Nakatsuji *et al.*, Gaussian 16, Revision C.01, Wallingford, CT, **2019**.

[261] F. Neese, *Wiley Interdiscip. Rev. Comput. Mol. Sci.* **2022**, *12*, e1606.

[262] E. Epifanovsky, A. T. B. Gilbert, X. Feng, J. Lee, Y. Mao, N. Mardirossian, P. Pokhilko, A. F. White, M. P. Coons, A. L. Dempwolff *et al.*, *J. Chem. Phys.* **2021**, *155*, 084801.

[263] Spartan'10, Irvine, CA und USA, **2009**.

[264] S. G. Balasubramani, G. P. Chen, S. Coriani, M. Diedenhofen, M. S. Frank, Y. J. Franzke, F. Furche, R. Grotjahn, M. E. Harding, C. Hättig *et al.*, *J. Chem. Phys.* **2020**, *152*, 184107.

[265] M. Born, R. Oppenheimer, *Ann. Phys.* **1927**, *389*, 457–484.

[266] J. C. Slater, *Phys. Rev.* **1929**, *34*, 1293–1322.

[267] J. C. Slater, *Phys. Rev.* **1951**, *81*, 385–390.

[268] P. A. M. Dirac, *Proc. R. Soc. Lond. A* **1926**, *112*, 661–677.

[269] D. R. Hartree, *Math. Proc. Camb. Phil. Soc.* **1928**, *24*, 89–110.

[270] D. R. Hartree, *Math. Proc. Camb. Phil. Soc.* **1928**, *24*, 111–132.

[271] V. Fock, *Z. Physik* **1930**, *61*, 126–148.

[272] L. Pauling, *Chem. Rev.* **1928**, *5*, 173–213.

[273] F. Bloch, *Z. Physik* **1929**, *52*, 555–600.

[274] J. E. Lennard-Jones, *Trans. Faraday Soc.* **1929**, *25*, 668–686.

[275] W. J. Hehre, R. Ditchfield, J. A. Pople, *J. Chem. Phys.* **1972**, *56*, 2257–2261.

[276] A. Schäfer, H. Horn, R. Ahlrichs, *J. Chem. Phys.* **1992**, *97*, 2571–2577.

[277] T. H. Dunning, *Int. J. Chem. Phys.* **1989**, *90*, 1007–1023.

[278] C. C. J. Roothaan, *Rev. Mod. Phys.* **1951**, *23*, 69–89.

[279] G. G. Hall, *Proc. R. Soc. Lond. A* **1951**, *205*, 541–552.

[280] N. L. Allinger in *Advances in Physical Organic Chemistry Volume 13*, Advances in Physical Organic Chemistry, Elsevier, Amsterdam, NL, **1976**, S. 1–82.

[281] A. D. MacKerell, N. Banavali, N. Foloppe, *Biopolymers* **2000**, *56*, 257–265.

[282] J. A. Lemkul, J. Huang, B. Roux, A. D. MacKerell, *Chem. Rev.* **2016**, *116*, 4983–5013.

[283] P. Xu, E. B. Guidez, C. Bertoni, M. S. Gordon, *Int. J. Chem. Phys.* **2018**, *148*, 090901.

[284] E. Hückel, *Z. Physik* **1931**, *70*, 204–286.

[285] R. Hoffmann, *Int. J. Chem. Phys.* **1963**, *39*, 1397–1412.

[286] J. J. P. Stewart, *J. Comput. Chem.* **1989**, *10*, 221–264.

[287] W. Thiel, *Modern Methods and Algorithms of Quantum Chemistry: Winterschool, 21 - 25 February 2000, Forschungszentrum Jülich, Germany*, **2000**.

[288] W. Thiel, *Wiley Interdiscip. Rev. Comput. Mol. Sci.* **2014**, *4*, 145–157.

[289] J. M. Foster, S. F. Boys, *Rev. Mod. Phys.* **1960**, *32*, 300–302.

[290] W. Duch, *Comput. Theor. Chem.* **1991**, *234*, 27–49.

[291] C. David Sherrill, H. F. Schaefer, *Adv. Quantum Chem.* **1999**, *34*, 143–269.

[292] J. J. Eriksen, J. Gauss, *Wiley Interdiscip. Rev. Comput. Mol. Sci.* **2021**, *11*, e1525.

[293] R. J. Bartlett, *Annu. Rev. Phys. Chem.* **1981**, *32*, 359–401.

[294] R. J. Bartlett, M. Musiał, *Rev. Mod. Phys.* **2007**, *79*, 291–352.

[295] R. J. Bartlett, *Wiley Interdiscip. Rev. Comput. Mol. Sci.* **2012**, *2*, 126–138.

[296] C. Møller, M. S. Plesset, *Phys. Rev.* **1934**, *46*, 618–622.

[297] D. Cremer, *Wiley Interdiscip. Rev. Comput. Mol. Sci.* **2011**, *1*, 509–530.

[298] J. A. Keith, V. Vassilev-Galindo, B. Cheng, S. Chmiela, M. Gastegger, K.-R. Müller, A. Tkatchenko, *Chem. Rev.* **2021**, *121*, 9816–9872.

[299] T. Hansson, C. Oostenbrink, W. van Gunsteren, *Curr. Opin. Struct. Biol.* **2002**, *12*, 190–196.

[300] M. P. Allen, *Computational Soft Matter: From Synthetic Polymers to Proteins; Winter School, 29 February - 6 March 2004, Gustav-Stresemann-Institut, Bonn, Germany*, NIC, Jülich, **2004**.

[301] K. Binder, J. Horbach, W. Kob, W. Paul, F. Varnik, *J. Phys.: Condens. Matter* **2004**, *16*, S429–S453.

[302] S. A. Hollingsworth, R. O. Dror, *Neuron* **2018**, *99*, 1129–1143.

[303] A. Görling, *Phys. Rev. A* **1999**, *59*, 3359–3374.

[304] W. Koch, M. C. Holthausen, *A Chemist's Guide to Density Functional Theory*, 2nd ed., Wiley-VCH, Weinheim, DE, **2001**.

[305] E. S. Kryachko, E. V. Ludeña, *Phys. Rep.* **2014**, *544*, 123–239.

[306] R. G. Parr, *Density-Functional Theory of Atoms and Molecules*, Oxford University Press, Oxford, UK, **2015**.

[307] M. Orio, D. A. Pantazis, F. Neese, *Photosynth. Res.* **2009**, *102*, 443–453.

[308] M. Bursch, J.-M. Mewes, A. Hansen, S. Grimme, *Angew. Chem. Int. Ed.* **2022**, *61*, e202205735.

[309] P. Hohenberg, W. Kohn, *Phys. Rev.* **1964**, *136*, B864–B871.

[310] W. Kohn, L. J. Sham, *Phys. Rev.* **1965**, *140*, A1133–A1138.

[311] J. P. Perdew, *AIP Conf. Proc.* **2001**, *577*, 1–20.

[312] U. von Barth, L. Hedin, *J. Phys. C: Solid State Phys.* **1972**, *5*, 1629–1642.

[313] D. C. Langreth, M. J. Mehl, *Phys. Rev. B* **1983**, *28*, 1809–1834.

[314] A. D. Becke, *Phys. Rev. A* **1988**, *38*, 3098.

[315] J. P. Perdew, K. Burke, M. Ernzerhof, *Phys. Rev. Lett.* **1996**, *77*, 3865–3868.

[316] A. D. Becke, *Int. J. Chem. Phys.* **1998**, *109*, 2092–2098.

[317] J. P. Perdew, S. Kurth, A. Zupan, P. Blaha, *Phys. Rev. Lett.* **1999**, *82*, 2544–2547.

[318] J. Tao, J. P. Perdew, V. N. Staroverov, G. E. Scuseria, *Phys. Rev. Lett.* **2003**, *91*, 146401.

[319] J. P. Perdew, A. Ruzsinszky, G. I. Csonka, L. A. Constantin, J. Sun, *Phys. Rev. Lett.* **2009**, *103*, 026403.

[320] J. Sun, B. Xiao, A. Ruzsinszky, *J. Chem. Phys.* **2012**, *137*, 051101.

[321] J. Sun, R. Haunschild, B. Xiao, I. W. Bulik, G. E. Scuseria, J. P. Perdew, *J. Chem. Phys.* **2013**, *138*, 044113.

[322] A. D. Becke, *Int. J. Chem. Phys.* **1993**, *98*, 5648–5652.

[323] J. P. Perdew, M. Ernzerhof, K. Burke, *Int. J. Chem. Phys.* **1996**, *105*, 9982–9985.

[324] M. Ernzerhof, G. E. Scuseria, *J. Chem. Phys.* **1999**, *110*, 5029–5036.

[325] S. Grimme, *J. Comput. Chem.* **2006**, *27*, 1787–1799.

[326] S. Grimme, *Int. J. Chem. Phys.* **2006**, *124*, 034108.

[327] F. Neese, T. Schwabe, S. Grimme, *Int. J. Chem. Phys.* **2007**, *126*, 124115.

[328] D. Bohm, D. Pines, *Phys. Rev.* **1951**, *82*, 625–634.

[329] D. C. Langreth, J. P. Perdew, *Phys. Rev. B* **1977**, *15*, 2884–2901.

[330] D. C. Langreth, J. P. Perdew, *Solid State Commun.* **1979**, *31*, 567–571.

[331] F. Furche, *Phys. Rev. B* **2001**, *64*, 195120.

[332] L. González, R. Lindh, *Quantum Chemistry and Dynamics of Excited States: Methods and Applications*, John Wiley & Sons, Chichester, UK, **2020**.

[333] P.-F. Loos, A. Scemama, D. Jacquemin, *J. Phys. Chem. Lett.* **2020**, *11*, 2374–2383.

[334] I. Prigogine, S. A. Rice, *Advances in Chemical Physics*, John Wiley & Sons, Inc, Hoboken, NJ, USA, **1996**.

[335] M. R. Silva-Junior, W. Thiel, *J. Chem. Theory Comput.* **2010**, *6*, 1546–1564.

[336] J. E. Del Bene, R. Ditchfield, J. A. Pople, *Int. J. Chem. Phys.* **1971**, *55*, 2236–2241.

[337] M. Head-Gordon, R. J. Rico, M. Oumi, T. J. Lee, *Chem. Phys. Lett.* **1994**, *219*, 21–29.

[338] N. Ishikawa, M. Head-Gordon, *Int. J. Quantum Chem.* **1995**, *56*, 421–427.

[339] J. A. McCleverty, *Comprehensive Coordination Chemistry II: From biology to nanotechnology*, Elsevier, Oxford, UK, **2003**.

[340] B. O. Roos, P. R. Taylor, P. E. M. Sigbahn, *Chem. Phys.* **1980**, *48*, 157–173.

[341] K. Andersson, P. A. Malmqvist, B. O. Roos, A. J. Sadlej, K. Wolinski, *J. Phys. Chem.* **1990**, *94*, 5483–5488.

[342] K. Andersson, P.-Å. Malmqvist, B. O. Roos, *Int. J. Chem. Phys.* **1992**, *96*, 1218–1226.

[343] P. Celani, H.-J. Werner, *Int. J. Chem. Phys.* **2003**, *119*, 5044–5057.

[344] C. Angeli, R. Cimiraglia, S. Evangelisti, T. Leininger, J.-P. Malrieu, *Int. J. Chem. Phys.* **2001**, *114*, 10252–10264.

[345] F. Neese, *Int. J. Chem. Phys.* **2003**, *119*, 9428–9443.

[346] G. H. Booth, A. J. W. Thom, A. Alavi, *J. Chem. Phys.* **2009**, *131*, 054106.

[347] A. A. Holmes, N. M. Tubman, C. J. Umrigar, *J. Chem. Theory Comput.* **2016**, *12*, 3674–3680.

[348] J. J. Eriksen, F. Lipparini, J. Gauss, *J. Phys. Chem. Lett.* **2017**, *8*, 4633–4639.

[349] A. Baiardi, M. Reiher, *J. Chem. Phys.* **2020**, *152*, 040903.

[350] E. Runge, E. K. U. Gross, *Phys. Rev. Lett.* **1984**, *52*, 997–1000.

[351] M. E. Casida, *Comput. Theor. Chem.* **2009**, *914*, 3–18.

[352] S. Hirata, M. Head-Gordon, *Chem. Phys. Lett.* **1999**, *314*, 291–299.

[353] M. E. Casida, M. Huix-Rotllant, *Annu. Rev. Phys. Chem.* **2012**, *63*, 287–323.

[354] C. van Caillie, R. D. Amos, *Chem. Phys. Lett.* **1999**, *308*, 249–255.

[355] C. van Caillie, R. D. Amos, *Chem. Phys. Lett.* **2000**, *317*, 159–164.

[356] F. Furche, R. Ahlrichs, *Int. J. Chem. Phys.* **2002**, *117*, 7433–7447.

[357] G. Scalmani, M. J. Frisch, B. Mennucci, J. Tomasi, R. Cammi, V. Barone, *Int. J. Chem. Phys.* **2006**, *124*, 94107.

[358] J. Liu, W. Liang, *J. Chem. Phys.* **2011**, *135*, 014113.

[359] J. Liu, W. Liang, *J. Chem. Phys.* **2011**, *135*, 184111.

[360] E. Brémond, M. Savarese, C. Adamo, D. Jacquemin, *J. Chem. Theory Comput.* **2018**, *14*, 3715–3727.

[361] D. J. Tozer, R. D. Amos, N. C. Handy, B. O. Roos, L. Serrano-Andrés, *Mol. Phys.* **1999**, *97*, 859–868.

[362] A. Dreuw, M. Head-Gordon, *J. Am. Chem. Soc.* **2004**, *126*, 4007–4016.

[363] D. J. Tozer, N. C. Handy, *Int. J. Chem. Phys.* **1998**, *109*, 10180–10189.

[364] M. E. Casida, C. Jamorski, K. C. Casida, D. R. Salahub, *Int. J. Chem. Phys.* **1998**, *108*, 4439–4449.

[365] N. T. Maitra, F. Zhang, R. J. Cave, K. Burke, *Int. J. Chem. Phys.* **2004**, *120*, 5932–5937.

[366] B. G. Levine, C. Ko, J. Quenneville, T. J. MartÍnez, *Mol. Phys.* **2006**, *104*, 1039–1051.

[367] P. Elliott, S. Goldson, C. Canahui, N. T. Maitra, *Chem. Phys.* **2011**, *391*, 110–119.

[368] Y. Shao, M. Head-Gordon, A. I. Krylov, *Int. J. Chem. Phys.* **2003**, *118*, 4807–4818.

[369] F. Wang, T. Ziegler, *Int. J. Chem. Phys.* **2004**, *121*, 12191–12196.

[370] D. Casanova, A. I. Krylov, *Phys. Chem. Chem. Phys.* **2020**, *22*, 4326–4342.

[371] S. Lee, W. Park, H. Nakata, M. Filatov, C. H. Choi, *Bulletin Korean Chem. Soc.* **2022**, *43*, 17–34.

[372] A. Savin in *Recent Developments and Applications of Modern Density Functional Theory*, Theoretical and computational chemistry, Elsevier, Amsterdam, NL, **1996**, S. 327–357.

[373] H. Iikura, T. Tsuneda, T. Yanai, K. Hirao, *Int. J. Chem. Phys.* **2001**, *115*, 3540–3544.

[374] T. Yanai, D. P. Tew, N. C. Handy, *Chem. Phys. Lett.* **2004**, *393*, 51–57.

[375] O. A. Vydrov, G. E. Scuseria, *J. Chem. Phys.* **2006**, *125*, 234109.

[376] L. Goerigk, S. Grimme, *Int. J. Chem. Phys.* **2010**, *132*, 184103.

[377] E. Brémond, I. Ciofini, J. C. Sancho-García, C. Adamo, *Acc. Chem. Res* **2016**, *49*, 1503–1513.

[378] T. Schwabe, L. Goerigk, *J. Chem. Theory Comput.* **2017**, *13*, 4307–4323.

[379] A. D. Laurent, D. Jacquemin, *Int. J. Quantum Chem.* **2013**, *113*, 2019–2039.

[380] A. J. Cohen, P. Mori-Sánchez, W. Yang, *Science* **2008**, *321*, 792–794.

[381] J. Autschbach, M. Srebro, *Acc. Chem. Res* **2014**, *47*, 2592–2602.

[382] D. Hait, M. Head-Gordon, *J. Phys. Chem. Lett.* **2018**, *9*, 6280–6288.

[383] K. R. Bryenton, A. A. Adeleke, S. G. Dale, E. R. Johnson, *Wiley Interdiscip. Rev. Comput. Mol. Sci.* **2023**, *13*, e1631.

[384] H. Koch, P. Jørgensen, *Int. J. Chem. Phys.* **1990**, *93*, 3333–3344.

[385] J. F. Stanton, R. J. Bartlett, *Int. J. Chem. Phys.* **1993**, *98*, 7029–7039.

[386] J. F. Stanton, J. Gauss, *Theor. Chim. Acta* **1995**, *91*, 267.

[387] S. A. Kucharski, M. Włoch, M. Musiał, R. J. Bartlett, *Int. J. Chem. Phys.* **2001**, *115*, 8263–8266.

[388] O. Christiansen, H. Koch, P. Jørgensen, *Chem. Phys. Lett.* **1995**, *243*, 409–418.

[389] O. Christiansen, H. Koch, P. Jørgensen, *Int. J. Chem. Phys.* **1995**, *103*, 7429–7441.

[390] C. Adamo, D. Jacquemin, *Chem. Soc. Rev.* **2013**, *42*, 845–856.

[391] A. D. Laurent, C. Adamo, D. Jacquemin, *Phys. Chem. Chem. Phys.* **2014**, *16*, 14334–14356.

[392] M. Schreiber, M. R. Silva-Junior, S. P. A. Sauer, W. Thiel, *Int. J. Chem. Phys.* **2008**, *128*, 134110.

[393] M. R. Silva-Junior, M. Schreiber, S. P. A. Sauer, W. Thiel, *J. Chem. Phys.* **2010**, *133*, 174318.

[394] C. Fang, B. Oruganti, B. Durbeej, *J. Phys. Chem. A* **2014**, *118*, 4157–4171.

[395] P.-F. Loos, A. Scemama, A. Blondel, Y. Garniron, M. Caffarel, D. Jacquemin, *J. Chem. Theory Comput.* **2018**, *14*, 4360–4379.

[396] P.-F. Loos, M. Boggio-Pasqua, A. Scemama, M. Caffarel, D. Jacquemin, *J. Chem. Theory Comput.* **2019**, *15*, 1939–1956.

[397] P.-F. Loos, F. Lipparini, M. Boggio-Pasqua, A. Scemama, D. Jacquemin, *J. Chem. Theory Comput.* **2020**, *16*, 1711–1741.

[398] M. Dierksen, S. Grimme, *J. Phys. Chem. A* **2004**, *108*, 10225–10237.

[399] P.-F. Loos, D. Jacquemin, *ChemPhotoChem* **2019**, *3*, 684–696.

[400] A. Klamt, G. Schüürmann, *J. Chem. Soc. Perkin Trans. 2* **1993**, 799–805.

[401] B. Mennucci, E. Cancès, J. Tomasi, *J. Phys. Chem. B* **1997**, *101*, 10506–10517.

[402] J. Tomasi, B. Mennucci, E. Cancès, *Comput. Theor. Chem.* **1999**, *464*, 211–226.

[403] B. Mennucci, R. Cammi, *Continuum Solvation Models in Chemical Physics: From Theory to Applications*, John Wiley & Sons, Chichester, UK, **2008**.

[404] A. V. Marenich, C. J. Cramer, D. G. Truhlar, *J. Phys. Chem. B* **2009**, *113*, 6378–6396.

[405] M. Stahn, S. Ehlert, S. Grimme, *J. Phys. Chem. A* **2023**, *127*, 7036–7043.

[406] J. B. Foresman, A. Frisch, *Exploring Chemistry with Electronic Structure Methods*, Third edition, Gaussian Inc, Wallingford, CT USA, **2015**.

[407] V. Barone, S. Alessandrini, M. Biczysko, J. R. Cheeseman, D. C. Clary, A. B. McCoy, R. J. DiRisio, F. Neese, M. Melosso, C. Puzzarini, *Nat. Rev. Methods Primers* **2021**, *1*, 38.

[408] H. P. Hratchian, X. Li, *J. Chem. Theory Comput.* **2012**, *8*, 4853–4855.

[409] H. B. Schlegel, *Wiley Interdiscip. Rev. Comput. Mol. Sci.* **2011**, *1*, 790–809.

[410] J. U. Reveles, A. M. Köster, *J. Comput. Chem.* **2004**, *25*, 1109–1116.

[411] P. E. Gill, W. Murray, M. H. Wright, *Practical Optimization*, Academic Press, London, **1981**.

[412] L. E. Scales, *Introduction to Non-Linear Optimization*, Macmillan, London, **1985**.

[413] R. Fletcher, *Practical Methods of Optimization*, 2. ed., Wiley, Chichester, UK, **1987**.

[414] J. E. Dennis, R. B. Schnabel, *Numerical Methods for Unconstrained Optimization and Nonlinear Equations*, SIAM, Philadelphia, US, **1996**.

[415] C. Broyden, *IMA J. Appl. Math.* **1970**, *6*, 76–90.

[416] R. Fletcher, *Comput. J.* **1970**, *13*, 317–322.

[417] D. Goldfarb, *Math. Comp.* **1970**, *24*, 23–26.

[418] D. F. Shanno, *Math. Comp.* **1970**, *24*, 647–656.

[419] H. B. Schlegel, *J. Comput. Chem.* **1982**, *3*, 214–218.

[420] F. Eckert, P. Pulay, H.-J. Werner, *J. Comput. Chem.* **1997**, *18*, 1473–1483.

[421] G. Zheng, M. Lundberg, J. Jakowski, T. Vreven, M. J. Frisch, K. Morokuma, *Int. J. Quantum Chem.* **2009**, *109*, 1841–1854.

[422] D. J. Wales, *Energy Landscapes: With Applications to Clusters, Biomolecules and Glasses*, Cambridge Univ. Press, Cambridge, UK, **2003**.

[423] J. M. Bofill, *J. Comput. Chem.* **1994**, *15*, 1–11.

[424] Ö. Farkas, H. B. Schlegel, *Int. J. Chem. Phys.* **1999**, *111*, 10806–10814.

[425] J. M. Bofill, *Int. J. Quantum Chem.* **2003**, *94*, 324–332.

[426] T. A. Halgren, W. N. Lipscomb, *Chem. Phys. Lett.* **1977**, *49*, 225–232.

[427] C. Peng, H. Bernhard Schlegel, *Isr. J. Chem.* **1993**, *33*, 449–454.

[428] P. Császár, P. Pulay, *J. Mol. Struct.* **1984**, *114*, 31–34.

[429] Ö. Farkas, H. B. Schlegel, *Phys. Chem. Chem. Phys.* **2002**, *4*, 11–15.

[430] X. Li, M. J. Frisch, *J. Chem. Theory Comput.* **2006**, *2*, 835–839.

[431] B. C. Garrett, M. J. Redmon, R. Steckler, D. G. Truhlar, K. K. Baldridge, D. Bartol, M. W. Schmidt, M. S. Gordon, *J. Phys. Chem.* **1988**, *92*, 1476–1488.

[432] B. J. Berne, G. Ciccotti, D. F. Coker, *Classical and Quantum Dynamics in Condensed Phase Simulations*, World Scientific, Singapore, SG, **1998**.

[433] G. Henkelman, H. Jónsson, *Int. J. Chem. Phys.* **2000**, *113*, 9978–9985.

[434] G. Henkelman, B. P. Uberuaga, H. Jónsson, *Int. J. Chem. Phys.* **2000**, *113*, 9901–9904.

[435] P. Y. Ayala, H. B. Schlegel, *Int. J. Chem. Phys.* **1997**, *107*, 375–384.

[436] W. E, W. Ren, E. Vanden-Eijnden, *Phys. Rev. B* **2002**, *66*, 052301.

[437] B. Peters, A. Heyden, A. T. Bell, A. Chakraborty, *Int. J. Chem. Phys.* **2004**, *120*, 7877–7886.

[438] W. E, W. Ren, E. Vanden-Eijnden, *Int. J. Chem. Phys.* **2007**, *126*, 164103.

[439] A. Goodrow, A. T. Bell, M. Head-Gordon, *J. Chem. Phys.* **2009**, *130*, 244108.

[440] H. P. Hratchian, H. B. Schlegel, *Int. J. Chem. Phys.* **2004**, *120*, 9918–9924.

[441] H. P. Hratchian, H. B. Schlegel, *J. Chem. Theory Comput.* **2005**, *1*, 61–69.

[442] E. B. Wilson, J. C. Decius, P. C. Cross, *Molecular Vibrations: The Theory of Infrared and Raman Vibrational Spectra*, Dover Publications, New York, NY, **1980**.

[443] L. A. Nafie, *Vibrational Optical Activity: Principles and Applications*, John Wiley & Sons, Chichester, UK, **2011**.

[444] M. Hesse, H. Meier, B. Zeeh, *Spektroskopische Methoden in der organischen Chemie: 102 Tabellen*, Thieme, Stuttgart, DE, **2005**.

[445] P. Zeeman, *London Edinburgh Dublin Philos. Mag. J. Sci.* **1897**, *43*, 226–239.

[446] J.-B. Biot, F. Savart, *Ann. Chem. Phys.* **1820**, *15*, 222.

[447] F. London, *J. Phys. Radium* **1937**, *8*, 397–409.

[448] R. Ditchfield, *Mol. Phys.* **1974**, *27*, 789–807.

[449] K. Wolinski, J. F. Hinton, P. Pulay, *J. Am. Chem. Soc.* **1990**, *112*, 8251–8260.

[450] G. Barone, L. Gomez-Paloma, D. Duca, A. Silvestri, R. Riccio, G. Bifulco, *Chem. Eur. J.* **2002**, *8*, 3233.

[451] G. Barone, D. Duca, A. Silvestri, L. Gomez-Paloma, R. Riccio, G. Bifulco, *Chem. Eur. J.* **2002**, *8*, 3240.

[452] S. G. Smith, J. M. Goodman, *J. Org. Chem.* **2009**, *74*, 4597–4607.

[453] D. C. Braddock, H. S. Rzepa, *J. Nat. Prod.* **2008**, *71*, 728–730.

[454] C. Timmons, P. Wipf, *J. Org. Chem.* **2008**, *73*, 9168–9170.

[455] A. Aiello, E. Fattorusso, P. Luciano, A. Mangoni, M. Menna, *Eur. J. Org. Chem.* **2005**, *2005*, 5024–5030.

[456] S. D. Rychnovsky, *Org. Lett.* **2006**, *8*, 2895–2898.

[457] S. G. Smith, J. M. Goodman, *J. Am. Chem. Soc.* **2010**, *132*, 12946–12959.

[458] N. Grimblat, J. A. Gavín, A. Hernández Daranas, A. M. Sarotti, *Org. Lett.* **2019**, *21*, 4003–4007.

[459] R. B. Nazarski, B. Pasternak, S. Leśniak, *Tetrahedron* **2011**, *67*, 6901–6916.

[460] D. J. Shepherd, P. A. Broadwith, B. S. Dyson, R. S. Paton, J. W. Burton, *Chem. Eur. J.* **2013**, *19*, 12644–12648.

[461] J. Willwacher, B. Heggen, C. Wirtz, W. Thiel, A. Fürstner, *Chem. Eur. J.* **2015**, *21*, 10416–10430.

[462] G. Bifulco, P. Dambruoso, L. Gomez-Paloma, R. Riccio, *Chem. Rev.* **2007**, *107*, 3744–3779.

[463] M. W. Lodewyk, M. R. Siebert, D. J. Tantillo, *Chem. Rev.* **2012**, *112*, 1839–1862.

[464] M. M. Zanardi, A. M. Sarotti, *J. Org. Chem.* **2015**, *80*, 9371–9378.

[465] G. K. Pierens, *J. Comput. Chem.* **2014**, *35*, 1388–1394.

[466] G. Saielli, K. C. Nicolaou, A. Ortiz, H. Zhang, A. Bagno, *J. Am. Chem. Soc.* **2011**, *133*, 6072–6077.

[467] Y. Li, *RSC Adv.* **2015**, *5*, 36858–36864.

[468] K. G. Andrews, A. C. Spivey, *J. Org. Chem.* **2013**, *78*, 11302–11317.

[469] N. Grimblat, M. M. Zanardi, A. M. Sarotti, *J. Org. Chem.* **2015**, *80*, 12526–12534.

[470] A. Navarro-Vázquez, R. R. Gil, K. Blinov, *J. Nat. Prod.* **2018**, *81*, 203–210.

[471] C. Cobas, *Magn. Reson. Chem.* **2020**, *58*, 512–519.

[472] A. M. Sarotti, *Magn. Reson. Chem.* **2020**, *58*, 477.

[473] Y. Guan, S. V. Shree Sowndarya, L. C. Gallegos, P. C. St John, R. S. Paton, *Chem. Sci.* **2021**, *12*, 12012–12026.

[474] Z. Yang, M. Chakraborty, A. D. White, *Chem. Sci.* **2021**, *12*, 10802–10809.

[475] Y.-H. Tsai, M. Amichetti, M. M. Zanardi, R. Grimson, A. H. Daranas, A. M. Sarotti, *Org. Lett.* **2022**, *24*, 7487–7491.

[476] I. M. Novitskiy, A. G. Kutateladze, *Nat. Prod. Rep.* **2022**, *39*, 2003–2007.

[477] I. Cortés, C. Cuadrado, A. Hernández Daranas, A. M. Sarotti, *Front. Nat. Prod.* **2023**, *2*, 1122426.

[478] A. Howarth, K. Ermanis, J. M. Goodman, *Chem. Sci.* **2020**, *11*, 4351–4359.

[479] J. B. Kleine Büning, S. Grimme, *J. Chem. Theory Comput.* **2023**, *19*, 3601–3615.

[480] P. L. Polavarapu, *Chiroptical Spectroscopy: Fundamentals and Applications*, CRC press, Boca Raton, US, **2016**.

[481] P. L. Polavarapu, E. Santoro, *Nat. Prod. Rep.* **2020**, *37*, 1661–1699.

[482] S. Zhu, M. Sun, *Appl. Spectrosc. Rev.* **2021**, *56*, 553–587.

[483] A. Cotton, *Compt. Rend.* **1895**, *120*, 1044.

[484] J. M. Batista, E. W. Blanch, V. S. Da Bolzani, *Nat. Prod. Rep.* **2015**, *32*, 1280–1302.

[485] C. Merten, T. P. Golub, N. M. Kreienborg, *J. Org. Chem.* **2019**, *84*, 8797–8814.

[486] G. Holzwarth, E. C. Hsu, H. S. Mosher, T. R. Faulkner, A. Moscowitz, *J. Am. Chem. Soc.* **1974**, *96*, 251–252.

[487] La Nafie, J. C. Cheng, P. J. Stephens, *J. Am. Chem. Soc.* **1975**, *97*, 3842–3843.

[488] P. A. M. Dirac, *Math. Proc. Camb. Phil. Soc.* **1929**, *25*, 62–66.

[489] P. J. Stephens, F. J. Devlin, J. R. Cheeseman, *VCD Spectroscopy for Organic Chemists*, CRC press, Boca Raton, US, **2012**.

[490] P. J. Stephens, *J. Phys. Chem.* **1985**, *89*, 748–752.

[491] L. Rosenfeld, *Z. Physik* **1929**, *52*, 161–174.

[492] R. D. Amos, *Molecular Property Derivatives: Ab Initio Methods in Quantum Chemistry Part I, Bd. 67*, John Wiley & Sons, Ltd, Chichester, UK, **1987**.

[493] K. P. Lawley, *Advances in Chemical Physics, Volume 69, Part 2: Ab Initio Methods in Quantum Chemistry*, Wiley, Chichester, US, **1987**.

[494] P. J. Stephens, *J. Phys. Chem.* **1987**, *91*, 1712–1715.

[495] J. R. Cheeseman, M. J. Frisch, F. J. Devlin, P. J. Stephens, *Chem. Phys. Lett.* **1996**, *252*, 211–220.

[496] T. D. Crawford, *Theor. Chim. Acta* **2006**, *115*, 227–245.

[497] J. Bloino, M. Biczysko, V. Barone, *J. Phys. Chem. A* **2015**, *119*, 11862–11874.

[498] J. Bloino, V. Barone, *J. Chem. Phys.* **2012**, *136*, 124108.

[499] N. M. Kreienborg, J. Bloino, T. Osowski, C. H. Pollok, C. Merten, *Phys. Chem. Chem. Phys.* **2019**, *21*, 6582–6587.

[500] L. Paoloni, G. Mazzeo, G. Longhi, S. Abbate, M. Fusè, J. Bloino, V. Barone, *J. Phys. Chem. A* **2020**, *124*, 1011–1024.

[501] S. Ghidinelli, S. Abbate, J. Koshoubu, Y. Araki, T. Wada, G. Longhi, *J. Phys. Chem. B* **2020**, *124*, 4512–4526.

[502] T. Vermeyen, J. Brence, R. van Echelpoel, R. Aerts, G. Acke, P. Bultinck, W. Herrebout, *Phys. Chem. Chem. Phys.* **2021**, *23*, 19781–19789.

[503] P. L. Polavarapu, *Chem. Rec.* **2007**, *7*, 125–136.

[504] G. Pescitelli, T. Kurtán, U. Flörke, K. Krohn, *Chirality* **2009**, *21*, 181–201.

[505] P. J. Stephens, N. Harada, *Chirality* **2010**, *22*, 229–233.

[506] N. Berova, P. L. Polavarapu, K. Nakanishi, R. W. Woody, *Comprehensive Chiroptical Spectroscopy: Instrumentation, Methodologies, and Theoretical Simulations*, John Wiley & Sons, Hoboken, US, **2011**.

[507] N. Berova, P. L. Polavarapu, K. Nakanishi, R. W. Woody, *Comprehensive Chiroptical Spectroscopy, Volume 2: Applications in Stereochemical Analysis of Synthetic Compounds, Natural Products, and Biomolecules*, *Bd. 2*, John Wiley & Sons, Hoboken, US, **2012**.

[508] M. Olivucci, *Computational Photochemistry*, Elsevier, Amsterdam, NL, **2005**.

[509] R. Beig, W. Beiglböck, W. Domcke, B.-G. Englert, U. Frisch, P. Hänggi, G. Hasinger, K. Hepp, W. Hillebrandt, D. Imboden *et al.*, *Time-Dependent Density Functional Theory*, *Bd. 706*, Springer Berlin Heidelberg, Berlin, Heidelberg, DE, **2006**.

[510] T. D. Crawford, M. C. Tam, M. L. Abrams, *J. Phys. Chem. A* **2007**, *111*, 12057–12068.

[511] P. L. Polavarapu, C. L. Covington, *Chirality* **2014**, *26*, 539–552.

[512] C. L. Covington, P. L. Polavarapu, *Chirality* **2017**, *29*, 178–192.

[513] J. Shen, C. Zhu, S. Reiling, R. Vaz, *Spectrochim. Acta A Mol. Biomol. Spectrosc.* **2010**, *76*, 418–422.

[514] T. Bruhn, A. Schaumlöffel, Y. Hemberger, G. Bringmann, *Chirality* **2013**, *25*, 243–249.

[515] T. Bruhn, A. Schaumlöffel, Y. Hemberger, G. Pescitelli, SpecDis, Version 1.71, Berlin, DE, **2017**.

[516] T. Kuppens, W. Langenaeker, J. P. Tollenaere, P. Bultinck, *J. Phys. Chem. A* **2003**, *107*, 542–553.

[517] E. Debie, E. de Gussem, R. K. Dukor, W. Herrebout, L. A. Nafie, P. Bultinck, *ChemPhysChem* **2011**, *12*, 1542–1549.

[518] T. Bruhn, A. Schaumlöffel, Y. Hemberger, G. Bringmann, SpecDis version 1.61, Würzburg, DE, **2013**.

[519] E. R. Kellenbach, R. K. Dukor, L. A. Nafie, *Spectrosc. Eur.* **2007**, *19*, 14–18.

[520] J. Paternoga, J. Kühlborn, N. O. Rossdam, T. Opatz, *J. Org. Chem.* **2021**, *86*, 3232–3248.

[521] S. Purser, P. R. Moore, S. Swallow, V. Gouverneur, *Chem. Soc. Rev.* **2008**, *37*, 320–330.

[522] E. P. Gillis, K. J. Eastman, M. D. Hill, D. J. Donnelly, N. A. Meanwell, *J. Med. Chem.* **2015**, *58*, 8315–8359.

[523] N. A. Meanwell, *J. Med. Chem.* **2018**, *61*, 5822–5880.

[524] M. Inoue, Y. Sumii, N. Shibata, *ACS Omega* **2020**, *5*, 10633–10640.

[525] J. Han, A. M. Remete, L. S. Dobson, L. Kiss, K. Izawa, H. Moriwaki, V. A. Soloshonok, D. O'Hagan, *J. Fluor. Chem.* **2020**, *239*, 109639.

[526] I. S. Kondratov, N. A. Tolmachova, G. Haufe, *Eur. J. Org. Chem.* **2018**, *2018*, 3618–3647.

[527] V. A. Motornov, V. M. Muzalevskiy, A. A. Tabolin, R. A. Novikov, Y. V. Nelyubina, V. G. Nenajdenko, S. L. Ioffe, *J. Org. Chem.* **2017**, *82*, 5274–5284.

[528] G. Chelucci, *Chem. Rev.* **2012**, *112*, 1344–1462.

[529] D. J. Burton, Z.-Y. Yang, W. Qiu, *Chem. Rev.* **1996**, *96*, 1641–1716.

[530] C. Fetsch, A. Grossmann, L. Holz, J. F. Nawroth, R. Luxenhofer, *Macromol.* **2011**, *44*, 6746–6758.

[531] E. Biron, J. Chatterjee, O. Ovadia, D. Langenegger, J. Brueggen, D. Hoyer, H. A. Schmid, R. Jelinek, C. Gilon, A. Hoffman *et al.*, *Angew. Chem. Int. Ed.* **2008**, *47*, 2595–2599.

[532] P. P. Bose, U. Chatterjee, I. Hubatsch, P. Artursson, T. Govender, H. G. Kruger, M. Bergh, J. Johansson, P. I. Arvidsson, *Bioorg. Med. Chem.* **2010**, *18*, 5896–5902.

[533] Q.-G. Dong, Y. Zhang, M.-S. Wang, J. Feng, H.-H. Zhang, Y.-G. Wu, T.-J. Gu, X.-H. Yu, C.-L. Jiang, Y. Chen *et al.*, *Amino Acids* **2012**, *43*, 2431–2441.

[534] A. Rasines Mazo, S. Allison-Logan, F. Karimi, N. J.-A. Chan, W. Qiu, W. Duan, N. M. O'Brien-Simpson, G. G. Qiao, *Chem. Soc. Rev.* **2020**, *49*, 4737–4834.

[535] L. Salem, *J. Am. Chem. Soc.* **1968**, *90*, 543–552.

[536] G. Klopman, *J. Am. Chem. Soc.* **1968**, *90*, 223–234.

[537] S. Kanters, M. Vitoria, M. Zoratti, M. Doherty, M. Penazzato, A. Rangaraj, N. Ford, K. Thorlund, A. H. Anis, M. E. Karim *et al.*, *EClinicalMedicine* **2020**, *28*, 100573.

[538] G. Erkel, H. Belahmer, A. Serwe, T. Anke, H. Kunz, H. Kolshorn, J. Liermann, T. Opatz, *J. Antibiot.* **2008**, *61*, 285–290.

[539] J. Richter, L. P. Sandjo, J. C. Liermann, T. Opatz, G. Erkel, *Bioorg. Med. Chem.* **2015**, *23*, 556–563.

[540] J. Tauber, M. Rohr, T. Walter, G. Erkel, T. Opatz, *Org. Biomol. Chem.* **2015**, *13*, 7813–7821.

[541] J. Tauber, K. Rudolph, M. Rohr, G. Erkel, T. Opatz, *Eur. J. Org. Chem.* **2015**, *2015*, 3587–3608.

[542] C. Weber, N. Vierengel, T. Walter, T. Behrendt, T. Lucas, G. Erkel, T. Opatz, *Org. Biomol. Chem.* **2020**, *18*, 5906–5917.

[543] P.-C. Lin, Y.-Z. Wu, T.-W. Bao, Y.-N. Wang, X.-Y. Shang, S. Lin, *J. Asian Nat. Prod. Res.* **2018**, *20*, 1093–1100.

[544] J. Henke, G. Erkel, C. Brochhausen, H. Kleinert, A. Schwarting, J. Menke, A. Pautz, *Kidney Int.* **2014**, *86*, 780–789.

[545] K. Rudolph, A. Serwe, G. Erkel, *Cytokine* **2013**, *61*, 285–296.

[546] D. C. Ngnokam Jouogo, P. Eckhardt, J.-D.-D. Tamokou, G. Matsuete Takongmo, L. Voutquenne-Nazabadioko, T. Opatz, L. A. Tapondjou, D. Ngnokam, R. B. Teponno, *Nat. Prod. Res.* **2023**, 1–11.

[547] R. V. Kepdieu Tchebou, P. Eckhardt, B. M. Kemkuignou, R. Tchuenguem, R. T. Fouedjou, B. K. Ponou, J. P. Dzoyem, R. B. Teponno, L. Barboni, T. Opatz *et al.*, *Phytochem. Lett.* **2022**, *48*, 62–67.

[548] B. Tsakem, P. Eckhardt, R. T. Tchuenguem, B. K. Ponou, J. P. Dzoyem, R. B. Teponno, T. Opatz, L. Barboni, L. A. Tapondjou, *Biochem. Syst. Ecol.* **2022**, *101*, 104397.

[549] C. F. Kenmogne, B. K. Ponou, B. M. Kemkuignou, J. Kühlborn, R. T. Tchuenguem, R. B. Teponno, J. P. Dzoyem, T. Opatz, L. A. Tapondjou, *Nat. Prod. Res.* **2023**, *37*, 1356–1364.

[550] P. Sinda, R. T. Tchuenguem, B. K. Ponou, J. Kühlborn, B. Y. Kianfé, J. P. Dzoyem, R. B. Teponno, T. Opatz, L. Barboni, L. A. Tapondjou, *S. Afr. J. Bot.* **2022**, *147*, 937–941.

[551] V. Ostry, *World Mycotoxin J.* **2008**, *1*, 175–188.

[552] R. R. Gomes, C. Glienke, S. I. R. Videira, L. Lombard, J. Z. Groenewald, P. W. Crous, *Persoonia* **2013**, *31*, 1–41.

[553] C. Jeffrey, *Kew Bull.* **1988**, *43*, 195.

[554] A. Luque, J. Groß, T. J. B. Zähringer, C. Kerzig, T. Opatz, *Chemistry* **2022**, *28*, e202104329.

[555] S. A. Ponomarev, R. V. Larkovich, A. S. Aldoshin, A. A. Tabolin, S. L. Ioffe, J. Groß, T. Opatz, V. G. Nenajdenko, *Beilstein J. Org. Chem.* **2021**, *17*, 283–292.

[556] C. Muhl, L. Zengerling, J. Groß, P. Eckhardt, T. Opatz, P. Besenius, M. Barz, *Polym. Chem.* **2020**, *11*, 6919–6927.

[557] A. Sevenich, P. S. Mark, T. Behrendt, J. Groß, T. Opatz, *Eur. J. Org. Chem.* **2020**, *2020*, 1505–1514.

[558] J. Groß, J. Kühlborn, S. Pusch, C. Weber, L. Andernach, G. Renzer, P. Eckhardt, J. Brauer, T. Opatz, *Chirality* **2023**, *35*, 753–765.

[559] J.-P. Dietz, T. Lucas, J. Groß, S. Seitel, J. Brauer, D. Ferenc, B. F. Gupton, T. Opatz, *Org. Process Res. Dev.* **2021**, *25*, 1898–1910.

[560] K. Seipp, J. Groß, A. M. Kiefer, G. Erkel, T. Opatz, *J. Nat. Prod.* **2023**, *86*, 924–938.

[561] A. Khiralla, A. O. Mohammed, S. Yagi, *Mycol. Prog.* **2022**, *21*, 38.

[562] D. Arcella, M. Eskola, J. A. Gómez Ruiz, *EfSA Journal* **2016**, *14*, e04654.

[563] A. Kiefer, M. Arnholdt, V. Grimm, L. Geske, J. Groß, N. Vierengel, T. Opatz, G. Erkel, *Mycotoxin Res.* **2023**, *39*, 303–316.

[564] H. B. Lee, A. Patriarca, N. Magan, *Mycobiology* **2015**, *43*, 93–106.

[565] M. Rohr, A. M. Kiefer, U. Kauhl, J. Groß, T. Opatz, G. Erkel, *Biol. Chem.* **2022**, *403*, 89–101.

[566] P. J. Stephens, D. M. McCann, J. R. Cheeseman, M. J. Frisch, *Chirality* **2005**, *17*, S52–S64.

[567] G. T. M. Bitchagno, A. Schüffler, J. Gross, M. Krumb, P. Tane, T. Opatz, *J. Nat. Prod.* **2022**, *85*, 1681–1690.

Teil III

Anhang

A Grüne Chemie

A.1 Zusatzmaterial der Publikation zur Darstellung organischer Thiocyanate unter grünen Reaktionsbedingungen

Im folgenden ist die *supporting information* der Publikation „Complementary Mechanochemical and Biphasic Approaches for the Synthesis of Organic Thiocyanates using Hexacyanoferrates as Non-Toxic Cyanide Sources“ abgedruckt.[210]

Electronic Supplementary Material (ESI) for Organic & Biomolecular Chemistry.

Complementary Mechanochemical and Biphasic Approach for the Synthesis of Organic Thiocyanates using Hexacyanoferrates as Non-Toxic Cyanide Sources

*Caroline Grundke, Jonathan Groß, Nina Vierengel, Jason Sirleaf, Matthias Schmitz, Leonie Krieger and Till Opatz**

Department of Chemistry, Johannes Gutenberg University, Duesbergweg 10−14, 55128 Mainz, Germany

Supporting Information

*Email: opatz@uni-mainz.de

Table of Contents

Experimental Section

General Experimental Information

Unless stated otherwise, all commercially available solvents and reagents were used as provided without further purification. Two of the eluents that were used for column chromatography (ethyl acetate (EtOAc) and cyclohexane (^{c}Hex)) were purchased in technical grade and distilled prior to use. Deuterated solvents were purchased from *Deutero GmbH* (Kastellaun). Solvents were evaporated under reduced pressure at 40 °C (water bath temperature).

Flash column chromatography was performed on 35–70 µm silica gel. For automatic flash column chromatography, an automatic flash chromatography system (*Isolera One*™) with UV-diode array detector was used together with silica gel filled cartridges (10 g or 25 g) as solid phases. Analytical thin layer chromatography (TLC) was performed on silica gel 60 F_{245}, visualized by irradiation with UV light (λ = 254 nm and λ = 365 nm) or TLC staining reagents. R_f values are referred to the corresponding eluents.

^{1}H-NMR and ^{13}C-NMR spectra were recorded on a *Bruker* Avance III HD 300, Avance II 400 or Avance III 600 spectrometer. Chemical shifts were referred to the corresponding deuterated solvents (for ^{1}H-NMR: δ($CDCl_3$) = 7.26 ppm, δ(MeOH-d_4) = 3.31 ppm and δ(DMSO-d_6) = 2.50 ppm; for ^{13}C-NMR: δ($CDCl_3$) = 77.16 ppm, δ(MeOH-d_4) = 49.00 and δ(DMSO-d_6) = 39.52 ppm) and reported in parts per million (ppm, δ) relative to tetramethylsilane (δ(TMS) = 0.00 ppm).[1] Coupling constants (J) were reported in Hz and the following abbreviations for NMR signal multiplicities were used: s (singlet), bs (broad singlet), d (doublet), t (triplet), q (quartet), m (multiplet) and combinations of these. Structural assignments were made with additional information from gCOSY, gHSQC, and gHMBC experiments.

Electrospray Ionization (ESI) masses were recorded by LC-MS on a 1260- series Infinity II HPLC-system using a binary pump system, a C18 column (2.7 μm, 30x2.1 mm) at 40 °C and an integrated diode array detector coupled to a LC/MSD Infinitylab LC/MSD (G6125B LC/MSD). High resolution mass spectrometry was performed on a G6545AQ-ToF with electrospray ionization (ESI). Sample inlet was performed via a 1260 Infinity II HPLC system with a G7111B 1260 quaternary pump, a G7129A 1260 vial sampler, and a G7116A 1260 multicolumn thermostat. Mass calibration was performed on the day of measurement using a suitable external calibrant. The mass accuracy of the measurement results is better than 5 ppm. Preparative HPLC separations were performed on an Infinity II 1260 system using a high-pressure gradient mixture together with a DAD and a fraction collector. As eluents, acetonitrile and water were used at a flowrate of 42.5 mL/min. An Macherey-Nagel Nucleodur C18 HTec (150 mm x 40 mm, 5 µm) column was used for sample separation with an MeCN content of the solvent mixture at either 15%, 29%, 40%, 50% or 80%. Chiral HPLC analysis (normal phase, isocratic mode with ethanol:*n*-hexane = 10:90) was performed using a CHIRALPAK IF-3 column (Daicel Corporation) on a 1260-series Infinity II HPLC system (Agilent Technologies).

Gas chromatographic measurements were performed on an 8890 GC system coupled to a 5977 GC/MS detector. As solid phase a HP 5MS UI GC column (30 m x 0.25 mm x 0.25 µm) was used and helium was applied as carrier gas with a flowrate of 1.2 mL/min. The injection temperature was 250 °C, the transfer line temperature was 250 °C, the MS-source temperature was 230 °C and the MS-quadrupole temperature was 150 °C. The column stove temperature was adjusted to 40 °C for 2 minutes followed by a temperature gradient of 50 °C/min over 5.6 minutes to 320 °C. This temperature was kept for 7.4 minutes.

All mechanochemical reactions were carried out in a "Pulverisette 7 Premium Line" planetary micro mill from FRITSCH GmbH (Idar-Oberstein, Germany). The grinding bowls and balls were made of inert

ZrO_2. The grinding was carried out with 18 balls each (diameter 10 mm). The ball mill with the respective charged milling jars can be seen in Figure F1.
Melting points are uncorrected and were measured on a *KRÜSS Optronic KPS I N* melting point meter or on a Mettler Toledo MP30 melting point system in open capillary tubes.
Infrared spectra were recorded as FT-IR spectra on a *Tensor 27* spectrometer (*Bruker Corporation*) using a diamond ATR unit and are reported in terms of frequency of absorption ($\tilde{\nu}$, cm^{-1}).
The optical rotation was measured on a Perkin-Elmer 241 polarimeter at 589 nm and extrapolated using Drude's equation.[2]

Figure F1: *Pulverisette 7 Premium Line* with the respective milling jars.

Optimization in Batch

Based on a previously published biphasic reaction system for the synthesis of α-aminonitriles with hexacyanoferrates as non-toxic cyanide source developed by the Opatz group,[3] the same reaction conditions (EtOAc:H_2O as the solvent system and a mixture of $K_3[Fe(CN)_6]$ and $K_4[Fe(CN)_6]$ as the cyanide source) were initially applied for the synthesis of thiocyanates using diphenyl disulfide **13** as the substrate (see Table T1, entry 1).

Table T1: Initial experiments and successive linear optimization for the synthesis of thiocyanates.

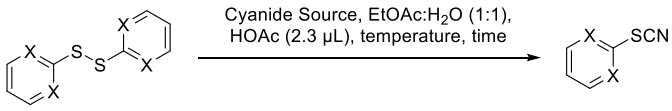

Substrate	Entry	Cyanide Source	Eq.	Time [h]	T [°C]	Yield* [%]
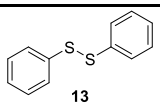 **13**	1	$K_3[Fe(CN)_6]$:$K_4[Fe(CN)_6]$ (3:4)	1.0	70	80	—[a]
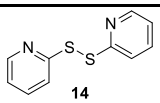 **14**	2	$K_3[Fe(CN)_6]$:$K_4[Fe(CN)_6]$ (3:4)	1.0	70	80	31[a]
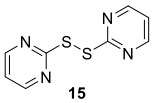 **15**	3	$K_3[Fe(CN)_6]$:$K_4[Fe(CN)_6]$ (3:4)	1.0	25	80	22[a]
	4	$K_3[Fe(CN)_6]$:$K_4[Fe(CN)_6]$ (3:4)	1.0	14	80	53
	5	$K_3[Fe(CN)_6]$	1.0	14	80	57
	6	$K_4[Fe(CN)_6]$	1.0	14	80	25
	7	$K_3[Fe(CN)_6]$	1.5	14	80	62
	8	$K_3[Fe(CN)_6]$	2.0	14	80	71
	9	$K_3[Fe(CN)_6]$	2.5	14	80	65
	10	$K_3[Fe(CN)_6]$	3.0	14	80	59
 **16**	11	$K_3[Fe(CN)_6]$	0.16	14	80	5
	12	$K_3[Fe(CN)_6]$	1.0	14	80	72
	13	$K_3[Fe(CN)_6]$	1.5	14	80	83
	14	**$K_3[Fe(CN)_6]$**	**2.0**	**14**	**80**	**95**
	15	$K_3[Fe(CN)_6]$	2.5	14	80	77
	16	**$K_3[Fe(CN)_6]$**	**3.0**	**14**	**80**	**100**
	17	$K_3[Fe(CN)_6]$	3.5	14	80	85
	18	$K_3[Fe(CN)_6]$	4.0	14	80	78
	19	$K_3[Fe(CN)_6]$+I_2 (1 mol%)	1.0	14	80	72
	20	$K_3[Fe(CN)_6]$	2.0	2	80	28
	21	$K_3[Fe(CN)_6]$	2.0	4	80	48
	22	$K_3[Fe(CN)_6]$	2.0	8	80	86
	23	$K_3[Fe(CN)_6]$	2.0	12	80	90
	24	$K_3[Fe(CN)_6]$	2.0	14	r.t.	27[b]
	25	$K_3[Fe(CN)_6]$	2.0	14	40	44[b]
	26	$K_3[Fe(CN)_6]$	2.0	14	60	31; 27[b]
	27	$K_3[Fe(CN)_6]$+H_2O (without EtOAc)	3.0	14	80	81
	28	$K_3[Fe(CN)_6]$+MeCN:H_2O (1:1)	3.0	14	80	61
	29	$K_3[Fe(CN)_6]$+MeOH	3.0	14	80	14
	30	$K_3[Fe(CN)_6]$	3.0	16	80	49[c]

*Isolated Yields. [a] Vial was opened during reaction for monitoring via TLC. [b] Disulfide as product. [c] Reaction was performed in gram scale.

As described in entry 1, no product formation could be observed after 70 h of heating the reaction mixture to 80 °C. The substrate was changed to 1,2-di(pyridin-2-yl)disulfide **14**, as the S–S bond should be more reactive towards oxidation due to the electron withdrawing effect of the ring nitrogen (entry 2). Product formation could be observed in 31% yield, but the reaction vial was opened for TLC and LCMS monitoring, so gaseous HCN might have been released and the reaction and the conversion of substrate **14** was therefore limited. To increase the electron withdrawing effects, 1,2-di(pyrimidin-2-yl)disulfide **15** was applied as another benchmark substrate which furnished the desired pyrimidine thiocyanate **16a** in 22% yield after opening the reaction vial for reaction monitoring. This yield could be increased to 53% by leaving the reaction vessel closed during the reaction (entries 3+4). Next, the cyanide source was investigated. When applying exclusively $K_3[Fe(CN)_6]$ in the protocol, the desired product could be obtained in 57% yield, whereas the application of only $K_4[Fe(CN)_6]$ decreases the yield to 25%. As can be seen in entries 5–10, no $K_4[Fe(CN)_6]$ is needed in the reaction mixture for increasing yields, and therefore, all further optimization was performed with only $K_3[Fe(CN)_6]$ as the cyanide source. Afterwards, the cyanide equivalents were investigated and it was found that increasing the equivalents from 1.0 to 3.0 equiv. does not lead to significant increases in yield, but 2.0 equiv. showed the highest yield (71%) when applying the respective disulfide **15** as starting material. As $K_3[Fe(CN)_6]$ itself is a known oxidizing agent, it was investigated if a direct application of thiols instead of disulfides can also be successful in this reaction setup. When applying pyrimidine-2-thiol **16** to the reaction conditions, 72% of the desired product **16a** could be obtained, which could be increased to 95% and even quantitative yield by increasing the cyanide equivalents (entries 12-18). By decreasing the cyanide amount to 0.16 eq., corresponding to the minimum possible amount of cyanide release to convert one equivalent of thiol, yield significantly decreased to only 5% (entry 11). The addition of 1 mol% of iodine as a catalyst for faster *in-situ* formation of the corresponding disulfide did not lead to higher yields (entry 19). In the next step, the reaction time was investigated (entries 20-23), and as can be seen, shorter reaction times of less than 12–14 h lead to significantly decreasing product yields, so 14 h were chosen as the optimum. In the last step, the reaction temperature was investigated (entries 24-26). At lower reaction temperatures, only disulfide formation or significantly lower product formation could be observed, so heating the reaction mixture up to 80 °C in presence of an acid (2.3 µL) as confirmed by various literature reports is assumed to be crucial for the reaction to proceed.[4-6] To investigate solvent effects on the reaction outcome, a 1:1 mixture of acetonitrile and water was applied yielding the respective product in a decreased yield of 61% (entry 28) compared to the initial solvent mixture. Using solely methanol led to a significant yield decline down to 14%, while application of exclusively water as the solvent for the reaction furnished the corresponding thiocyanate **16a** in 81% yield (entry 27). The developed procedure might be adapted to solvents with different polarity, but as solubility issues could be a problem for less polar substrates in such reaction settings the biphasic system ethyl acetate and water in a 1:1 mixture was chosen to be the most suitable solvent system for the formation of thiocyanates in general. To conclude, the optimized reaction conditions can be found in Scheme S1.

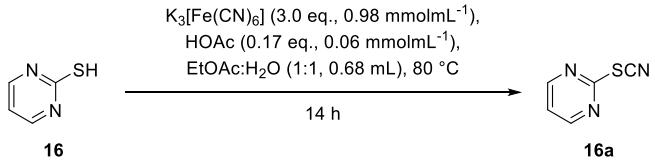

16 **16a**

Scheme S1: Optimized reaction conditions for the formation of thiocyanates.

Optimization in Ball Mill

As an initial experiment (Table T2, entry 1), the developed batch protocol was successfully transferred to the ball mill with the addition of silica as grinding auxiliary[7] affording the desired product **16a** in 12% ^{1}H-NMR yield after 10 min of milling. Initial work-up of the slurry reaction mixture included neutralization of acetic acid with an aqueous sodium bicarbonate solution, followed by extraction with ethyl acetate. As can be seen in entry 2, no additional acetic acid was needed for the cyanide release from ferricyanide, as pure silica also furnished the desired product **16a** (47%), while no disulfide **15** was detected. Based on this result, the optimized work-up emerged as transfer of the solid reaction mixture and the milling balls to an Erlenmeyer flask with the addition of acetone (50 mL) followed by ultrasonication for 10 min and filtration of the solid residues. Next, the equivalents of ferricyanide were kept on a constant level and the milling time was investigated (entries 3–7). With shorter reaction times (entry 7), **15** was still detected as a byproduct, whereas longer milling (entry 2) led to a decrease in product yield. The highest yield was obtained after 6 min of reaction time and the equivalents of the cyanide source were investigated subsequently (entries 8–12). With the optimized conditions (6 min, 1.0 eq.), an isolated yield of 72% of the desired product **16a** was obtained. Furthermore, additional grinding auxiliaries as quartz or the acidic $KHSO_4$ were tested as well as dividing the milling time into smaller fractions (entries 13–15).

Table T2: Optimization of mechanochemical parameters.

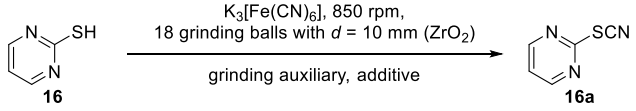

Entry	Grinding Auxiliary	Time [min]	Eq.	Analysis of Byproducts via ESI-LCMS (DAD)/^{1}H-NMR	SCN Yield [%]
1	SiO_2[b)]	10	1.5	**15** as a byproduct	12
2	SiO_2	10	1.5	–	47
3	**SiO_2**	**6**	**1.5**	–	**63**
4	SiO_2	5	1.5	–	54
5	SiO_2	4	1.5	**15** as a byproduct	51
6	SiO_2	3	1.5	**15** as a byproduct	38
7	SiO_2	2	1.5	**15** as the major product	16
8	SiO_2	6	1.3	–	50
9	**SiO_2**	**6**	**1.0**	**–**	**72**[a)]
10	SiO_2	6	0.8	–	53
11	SiO_2	6	0.5	**15** as a byproduct	37
12	SiO_2	6	0.3	**15** as the major product	27
13	$KHSO_4$[c)]	10	1.5	Exclusive formation of **15**	–
14	Quartz[c)]	10	1.5	Traces of **15** and **16**	51
15	SiO_2[b)]	6 x 1 min	1.5	Exclusive formation of **15**	–
16	SiO_2	90 min overall	1.0	**15** as a byproduct	15[a,d)]

Unless stated otherwise, all optimization reactions were performed on a 75 mg scale of 2-thiopyrimidine **16** with 1.5 g of grinding auxiliary and full conversion of **16** was observed via ESI-LCMS (DAD) or ^{1}H-NMR. Furthermore, all yields are based on ^{1}H-NMR analysis using dimethylsulfoxide as the internal standard. [a)] Isolated yield. [b)] 0.7 g of grinding auxiliary was applied together with 0.9 mL of acetic acid as additive. [c)] 1.0 g of grinding auxiliary was applied. [d)] Reaction was performed in gram scale.

General Batch Procedure A

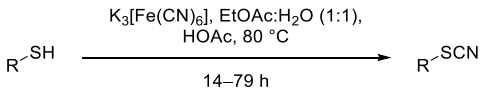

To a 10 mL reaction vial sealed with a rubber septum were added the corresponding thiol (0.23 mmol, 1.0 eq.) and $K_3[Fe(CN)_6]$ (222.2 mg, 0.67 mmol, 3.0 eq.). Both were dissolved in a biphasic solvent mixture of ethyl acetate and water (1:1, 0.68 mL). Acetic acid (2.3 µL) was added and the tightly sealed reaction vessel was heated to 80 °C. After the reaction was completed (14-79 h, followed via TLC and GC/LCMS), the reaction mixture was poured into a saturated $NaHCO_3$ solution (10 mL) and extracted with ethyl acetate (3x15 mL). The combined organic layers were washed with a saturated NaCl solution (10 mL), dried over Na_2SO_4, filtered and the solvent was removed under reduced pressure. The crude product was purified by column chromatography using SiO_2 as the stationary phase. Considering the sustainability of the developed procedure, distillation, continuous extraction of the aqueous phase using a Kutscher-Steudel apparatus or crystallization could also be applied as alternative purifications of the crude products instead of column chromatography. This was exemplarily demonstrated on selected compounds, but for comparison reasons, column chromatography was used as the standard purification method.

General Ball Mill Procedure B

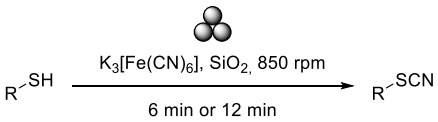

Each grinding bowl was placed in the heating oven at 80 °C for several hours prior to use and, after cooling to ambient temperature, was subsequently charged with 18 grinding balls, $K_3[Fe(CN)_6]$ (0.669 mmol, 1.0 eq.), the respective thiol (0.669 mmol, 1.0 eq.) as well as silica gel (to act as acidic grinding auxiliary, 1.5 g). The grinding bowl was accelerated for 6 min to 850 rpm. After cooling down to ambient temperature, the respective powder and the balls were sinked in acetone, sonicated in an ultrasonic bath for 10 min* and then filtered over silica. The solvent was removed under reduced pressure and the crude product was subjected to further suitable purification. Column chromatography using SiO_2 as the stationary phase was applied as standard method for comparison reasons.

* Sonification for 30 min of the starting materials without milling did not lead to any product formation.

Substrate Scope in Batch and Ball Mill

1,2-Di(pyrimidin-2-yl)disulfide (15)

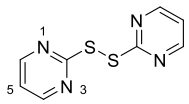

According to a modified procedure of *B. Zeynizadeh*.[8]
A 50 mL round bottom flask was charged with 2-mercaptopyrimidine **16** (500 mg, 4.46 mmol, 1.0 eq.) and suspended in a mixture of acetonitrile and water (5:1, 14 mL). Iodine (567 mg, 2.23 mmol, 0.5 eq.) was added and after 30 min (reaction followed by TLC), the reaction mixture was quenched by a 1% solution of thiosulfate (10 mL). After extraction with ethyl acetate (3x20 mL), the combined organic layers were dried over Na_2SO_4, filtered and the solvent was removed under reduced pressure. The crude product was purified by flash column chromatography (SiO_2, *Isolera One*™ 0%-100% EtOAc), furnishing the product as a slightly yellow solid.

Yield: 433.8 mg (1.95 mmol, 44%).

R_f = 0.12 (^{c}Hex:EtOAc = 1:1).

ESI-LCMS: *m/z* = 223.0 ($[M+H]^+$).

GC-MS: *m* = 222.0 [M].

Mp: 136.2–138.7 °C (Lit.:[9] 132–135 °C)

IR (ATR): $\tilde{\nu}$ [cm^{-1}] = 3070, 1549, 1372, 1195, 1166, 821, 767, 744, 628, 448.

^{1}H-NMR, COSY (300 MHz, $CDCl_3$): δ [ppm] = 8.57 (d, *J* = 4.8 Hz, 4H, 4-H, 6-H), 7.08 (t, *J* = 4.8 Hz, 2H, 5-H).

^{13}C-NMR, HSQC, HMBC (75 MHz, $CDCl_3$): δ [ppm] = 169.7 (2-C), 157.9 (4-C, 6-C), 118.2 (5-C).

The obtained data are in accordance with the literature.[9]

Pyrimidine-2-ylthiocyanate (16a)

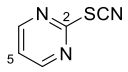

Following the general procedure A using 2-mercaptopyrimidine **16** (25.2 mg, 0.23 mmol, 1.0 eq.). After 14 h, column chromatography (SiO_2, *Isolera One*™ 20%–80% EtOAc) afforded the title compound as a colorless solid. General procedure B was alternatively applied. Alternatively, purification could be achieved via crystallization from DMSO.

Yield: 31.7 mg (0.23 mmol, 100%, procedure A), 65.6 mg (0.48 mmol, 72%, procedure B).

R_f = 0.51 (^{c}Hex:EtOAc = 1:1).

ESI-LCMS: *m/z* = 138.1 $[M+H]^+$.

Mp: 110.2–110.6 °C (Lit.:[10] 112.6–113.0 °C)

IR (ATR): $\tilde{\nu}$ [cm^{-1}] = 2174, 1561, 1378, 1278, 1180, 814, 767, 742, 627.

^{1}H-NMR, COSY (300 MHz, $CDCl_3$): δ [ppm] = 8.69 (d, *J* = 4.9 Hz, 2H, 4-H, 6-H), 7.28 (t, *J* = 4.9 Hz, 1H, 5-H).

^{13}C-NMR, HSQC, HMBC (75 MHz, $CDCl_3$): δ [ppm] = 164.4 (2-C), 159.1 (4-C, 6-C), 119.9 (5-C), 107.5 (S*C*N).

The obtained data are in accordance with the literature.[10]

Pyridine-2-ylthiocyanate (17a)

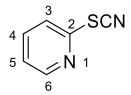

Following the general batch procedure using 2-mercaptopyridine **17** (25.0 mg, 0.23 mmol, 1.0 eq.). After 14 h, purification by column chromatography (SiO_2, *Isolera One*™ 20%–80% EtOAc) afforded the product as a colorless oil.

Yield: 21.9 mg (0.16 mmol, 72%).

R_f = 0.54 (^{c}Hex:EtOAc = 2:1).

ESI-LCMS: *m/z* = 137.0 $[M+H]^+$.

GC-MS: *m* = 136.1 [M], 78.1[M−SCN].

IR (ATR): $\tilde{\nu}$ [cm^{-1}] = 2162, 1573, 1563, 1450, 1420, 1119, 989, 760, 716, 615.

^{1}H-NMR, COSY (300 MHz, $CDCl_3$): δ [ppm] = 8.51 (ddd, *J* = 4.8, 1.9, 0.9 Hz, 1H, 6-H), 7.76 (td, *J* = 7.8, 1.9 Hz, 1H, 4-H), 7.59 (dt, *J* = 8.1, 1.0 Hz, 1H, 3-H), 7.27 (ddd, *J* = 7.5, 4.8, 1.0 Hz, 1H, 5-H).

^{13}C-NMR, HSQC, HMBC (75 MHz, $CDCl_3$): δ [ppm] = 150.6 (6-C), 150.0 (2-C), 138.6 (4-C), 122.9 (5-C), 122.1 (3-C), 109.1 (S*C*N).

The obtained data are in accordance with the literature.[11]

Pyridine-4-ylthiocyanate (18a)

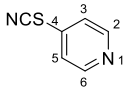

Following the general batch procedure using 4-mercaptopyridine **18** (55.6 mg, 0.50 mmol, 1 eq.) and $K_3[FeCN_6]$ (494 mg, 0.50 mmol, 3.0 eq.) in 1.36 mL solvent mixture. After 16 h, purification by column chromatography (SiO_2, *Isolera One*™ 0%–80% EtOAc) afforded the product as a colorless solid.

Yield: 36.1 mg (0.27 mmol, 53%).

R_f = 0.19 (^{c}Hex:EtOAc = 2:1).

Mp: 54.7–55.7 °C (Lit.:[12] 54–56 °C).

ESI-LCMS: *m/z* = 137.0 $[M+H]^+$.

IR (ATR): $\tilde{\nu}$ [cm^{-1}] = 3033, 2164, 1571, 1544, 1482, 1407, 1222, 1067, 811, 802, 696.

^{1}H-NMR, COSY (300 MHz, $CDCl_3$): δ [ppm] = 8.69–8.52 (m, 2H, 2-H, 6-H), 7.44–7.31 (m, 2H, 3-H, 5-H).

^{13}C-NMR, HSQC, HMBC (75 MHz, $CDCl_3$): δ [ppm] = 150.8 (2-C, 6-C), 136.8 (4-C), 121.6 (3-C, 5-C), 107.4 (S*C*N).

The obtained data are in accordance with the literature.[13]

2-Thiocyanatopyridine-*N*-oxide (19a)

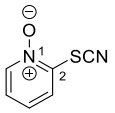

Following the general procedure A using 2-mercaptopyridine-*N*-oxide **19** (28.6 mg, 0.23 mmol, 1.0 eq.). After 14 h, purification by column chromatography (SiO_2, *Isolera One*™ 20%–80% EtOAc) afforded the title compound as a colorless solid.

Yield: 17.1 mg (0.13 mmol, 50%).

R_f = 0.35 (EtOAc).

ESI-LCMS: *m/z* = 153.0 $[M+H]^+$.

ESI-HRMS ($C_6H_4N_2OS$ $[M]^+$): calculated: *m/z* = 152.0044

found: *m/z* = 152.0045.

Mp: 154.2–155.1 °C (Lit.:[14] 158–160 °C).

IR (ATR): $\tilde{\nu}$ [cm^{-1}] = 3097, 2168, 1468, 1421, 1253, 1225, 1140, 841, 760, 705, 529.

^{1}H-NMR, COSY (300 MHz, $CDCl_3$): δ [ppm] = 8.28 (dd, *J* = 6.3, 1.2 Hz, 1H, 6-H), 7.80 (dd, *J* = 8.3, 1.7 Hz, 1H, 3-H), 7.46 (t, 1H, 4-H), 7.34 (m, 1H, 5-H).

^{13}C-NMR, HSQC, HMBC (75 MHz, $CDCl_3$): δ [ppm] = 143.9 (2-C), 138.1 (6-C), 127.3 (4-C), 124.2 (5-C), 123.2 (3-C), 109.5 (S*C*N).

No spectroscopic data available in the literature.

1-Methyl-1*H*-imidazole-2-yl thiocyanate (20a)

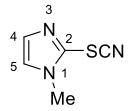

Following the general batch procedure using 2-mercapto-1-methylimidazole **20** (25.7 mg, 0.23 mmol, 1.0 eq.). After 14 h, column chromatography (SiO_2, *Isolera One*™ 0%–80% EtOAc) afforded the title compound as a colorless oil. General procedure B was alternatively applied with a reaction time of either 6 min or 12 min.

Yield: 25.0 mg (0.18 mmol, 80%, procedure A), no conversion of **20** with procedure B.

R_f = 0.93 (^{c}Hex:EtOAc = 2:1).

GC-MS: *m* = 138.9 [M].

IR (ATR): $\tilde{\nu}$ [cm^{-1}] = 3115, 2162, 1506, 1462, 1413, 1279, 1124, 915, 766, 684, 515.

^{1}H-NMR, COSY (300 MHz, $CDCl_3$): δ [ppm] = 7.19 (d, *J* = 1.3 Hz, 1H, 4-H), 7.17 (d, *J* = 1.3 Hz, 1H, 5-H), 3.86 (s, 3H, CH_3).

^{13}C-NMR, HSQC, HMBC (75 MHz, $CDCl_3$): δ [ppm] = 131.8 (4-C), 126.6 (2-C), 126.2 (5-C), 107.5 (S*C*N), 34.59 (*C*H_3).

The obtained data are in accordance with the literature.[15]

4-Nitrophenylthiocyanate (21a)

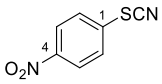

Following the general procedure A using 4-nitrothiophenol **21** (34.8 mg, 0.23 mmol, 1.0 eq.). After 14 h, column chromatography (SiO_2, *Isolera One*™ 10%–80% EtOAc) yielded the title compound as a colorless solid. General procedure B was alternatively applied with a reaction time of 12 min.

Yield: 24.5 mg (0.14 mmol, 61%, procedure A), 80.7 mg (0.45 mmol, 67%, procedure B).

R_f = 0.51 (^{c}Hex:EtOAc = 2:1).

ESI-LCMS: *m/z* = 181.0 $[M+H]^+$.

Mp: 129.9–130.8 °C. (Lit.:[16] 127–129 °C).

IR (ATR): $\tilde{\nu}$ [cm^{-1}] = 2164, 1603, 1578, 1517, 1318, 1342, 1121, 855, 843, 737.

^{1}H-NMR, COSY (300 MHz, $CDCl_3$): δ [ppm] = 8.37–8.26 (m, 2H, 3-H, 5-H), 7.73–7.63 (m, 2H, 2-H, 6-H).

^{13}C-NMR, HSQC, HMBC (75 MHz, $CDCl_3$): δ [ppm] = 148.0 (4-C), 133.4 (1-C), 128.7 (2-C, 6-C), 125.1 (3-C, 5-C), 108.1 (S*C*N).

The obtained data are in accordance with the literature.[16]

1-Chloro-4-thiocyanatobenzene (22a)

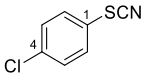

Following the general procedure A using 4-chlorothiophenol **22** (72.0 mg, 0.50 mmol, 1.0 eq.) and $K_3[FeCN_6]$ (444.5 mg, 1.50 mmol, 3.0 eq.) in 1.36 mL solvent mixture. After 18 h, column chromatography (SiO_2, *Isolera One*™ 0%–80% EtOAc) afforded the title compound as a colorless oil. General procedure B was alternatively applied with a reaction time of 12 min.

Yield: 17.0 mg (0.10 mmol, 20%, procedure A), 58.2 mg (0.34 mmol, 51%, procedure B).

R_f = 0.62 (^{c}Hex:EtOAc = 10:1).

GC-MS: *m* = 169.0 [M].

IR (ATR): $\tilde{\nu}$ [cm^{-1}] = 3085, 2925, 2853, 2159, 1582, 1476, 1391, 1090, 1011, 817, 742, 701, 548, 501.

^{1}H-NMR, COSY (400 MHz, $CDCl_3$): δ [ppm] = 7.50–7.45 (m, 2H, 2-H, 6-H), 7.44–7.40 (m, 2H, 3-H, 5-H).

^{13}C-NMR, HSQC, HMBC (101 MHz, $CDCl_3$): δ [ppm] = 136.3(4-C), 131.6 (2-C, 6-C), 130.6 (3-C, 5-C), 122.9 (1-C), 110.1 (S*C*N).

The obtained data match to those reported in the literature.[16]

1-Methoxy-4-thiocyanatobenzene (23a) and 1,2-Bis(4-methoxyphenyl)disulfide (23b)

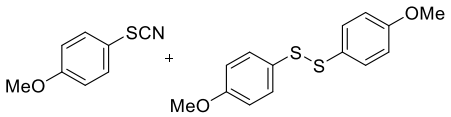

Following the general procedure B using 4-methoxythiophenol **23** (93.8 mg, 0.67 mmol, 1.0 eq.) as reagent with a milling time of 12 min. Separation of the desired product **23a** from the respective disulfide **23b** was not feasible by column chromatography (SiO_2, *Isolera One*™ 0%–80% EtOAc). Therefore, the yield was determined by ^{1}H-NMR using dimethylsulfone as the internal standard. Following the general procedure A using **23** (70.1 mg, 0.50 mmol, 1.0 eq.) and $K_3[FeCN_6]$ (494 mg, 1.50 mmol, 3.0 eq.) in 1.36 mL solvent mixture, column chromatography (SiO_2, *Isolera One*™ 0%–80% EtOAc) afforded exclusively **23b** as a yellow oil, after 16 h of reaction time.

Procedure B:

^{1}H-NMR yield of 23a: 0.21 mmol, 32%.

^{1}H-NMR yield of 23b: 0.21 mmol, 58%.

NMR data of 23a:

^{1}H-NMR, COSY (400 MHz, DMSO-d_6): δ [ppm] = 7.63–7.59 (m, 2H, 2-H, 6-H), 7.09–7.05 (m, 2H, 3-H, 5-H), 3.79 (s, 3H, CH_3).

^{13}C-NMR, HSQC, HMBC (101 MHz, DMSO-d_6): δ [ppm] =160.8 (4-C), 133.8 (2-C, 6-C), 116.0 (3-C, 5-C), 113.7 (1-C), 112.3 (S*C*N), 55.5 (*C*H_3).

The obtained data match to those reported in the literature.[17]

NMR data of 23b:

^{1}H-NMR, COSY (400 MHz, DMSO-d_6): δ [ppm] = 7.43–7.38 (m, 4H, 2-H, 6-H), 6.96–6.92 (m, 4H, 3-H, 5-H), 3.75 (s, 6H, CH_3).

^{13}C-NMR, HSQC, HMBC (101 MHz, DMSO-d_6): δ [ppm] =159.6 (4-C), 132.0 (2-C, 6-C), 126.9 (1-C), 114.9 (3-C, 5-C), 55.2 (*C*H_3).

The obtained data match to those reported in the literature.[18]

Procedure A:

Yield: 45.8 mg (0.17 mmol, 66%).

R_f = 0.26 (^{c}Hex:EtOAc = 50:1).

ESI-LCMS: *m/z* = 279.0 $[M+H]^+$.

IR (ATR): $\tilde{\nu}$ [cm^{-1}] = 3003, 2938, 2835, 1589, 1489, 1461, 1288, 1243, 1171, 1029, 824.

^{1}H-NMR, COSY (300 MHz, $CDCl_3$): δ [ppm] = 7.45–7.36 (m, 4H, 2 H, 6-H), 6.89–6.77 (m, 4H, 3-H, 5-H), 3.80 (s, 6H, OCH_3).

^{13}C-NMR, HSQC, HMBC (75 MHz, $CDCl_3$): δ [ppm] = 160.0 (4-C), 132.8 (2-C, 6-C), 128.5 (1-C), 114.7 (3-C, 5-C), 55.5 (O*C*H_3).

The obtained data are in accordance with the literature.[19]

4-Aminophenylthiocyanate (25a)

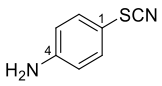

Following the general procedure A using 4-mercaptoaniline **25** (56.3 mg, 0.50 mmol, 1.0 eq.) and $K_3[FeCN_6]$ (444.5 mg, 1.50 mmol, 3.0 eq.) in 1.36 mL solvent mixture. After 30 h, an additional

equivalent of $K_3[FeCN_6]$ and acetic acid was added, and the reaction was heated for another 24 h. After work-up of the reaction mixture according to the general procedure, column chromatography (SiO_2, *Isolera One*™ 0%–80% EtOAc) furnished the title compound as a brown oil. General procedure B was alternatively applied.

Yield: 9.30 mg (0.06 mmol, 14%, procedure A), 37.0 mg (0.25 mmol, 37%, procedure B).

R_f = 0.63 (^{c}Hex:EtOAc = 1:1).

ESI-LCMS: *m/z* = 151.1 $[M+H]^+$.

IR (ATR): $\tilde{\nu}$ [cm^{-1}] = 3474, 3375, 2152, 1625, 1595, 1496, 1302, 824, 522.

^{1}H-NMR, COSY (300 MHz, $CDCl_3$): δ [ppm] = 7.42–7.30 (m, 2H, 2-H, 6-H), 6.73–6.62 (m, 2H, 3-H, 5-H), 3.96 (bs, 2H, NH_2).

^{13}C-NMR, HSQC, HMBC (75 MHz, $CDCl_3$): δ [ppm] = 148.7 (4-C), 134.5 (2-C, 6-C), 116.1 (3-C, 5-C), 112.3 (S*C*N), 109.7 (1-C).

The obtained data are in accordance with the literature.[20]

Benzo[*d*]thiazol-2-amine (26a)

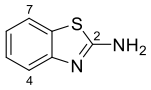

Following the general procedure A using 2-aminothiophenol **26** (56.3 mg, 0.45 mmol, 1.0 eq.) and $K_3[FeCN_6]$ (444.5 mg, 1.50 mmol, 3.0 eq.) in 1.36 mL solvent mixture. After 15 h, column chromatography (SiO_2, *Isolera One*™ 20%–80% EtOAc) furnished the product as a colorless solid.

Yield: 27.2 mg (0.18 mmol, 40%).

R_f = 0.13 (^{c}Hex:EtOAc = 2:1).

ESI-LCMS: *m/z* = 151.1 $[M+H]^+$.

Mp: 107.9–108.7 °C (Lit.:[21] 112–113 °C).

IR (ATR): $\tilde{\nu}$ [cm^{-1}] = 3397, 3056, 1642, 1527, 1446, 1285, 1067, 845, 741, 720.

^{1}H-NMR, COSY (300 MHz, $CDCl_3$): δ [ppm] = 7.61–7.53 (m, 1H, 7-H), 7.58–7.51 (m, 1H, 4-H), 7.30 (td, *J* = 7.7, 1.3 Hz, 1H, 5-H), 7.12 (td, *J* = 7.7, 1.3 Hz, 1H, 6-H), 5.82 (bs, 2H, NH_2).

^{13}C-NMR, HSQC, HMBC (75 MHz, $CDCl_3$): δ [ppm] = 166.4 (2-C), 152.1 (3a-C), 131.5 (7a-C), 126.1 (5-C), 122.3 (6-C), 121.0 (7-C), 119.1 (4-C).

The obtained data are in accordance with the literature.[22]

5-Chlorobenzo[*d*]thiazol-2-amine (27a)

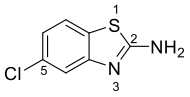

Following the general procedure A using 2-amino-4-chlorothiophenol **27** (71.6 mg, 0.50 mmol, 1.0 eq.) and $K_3[FeCN_6]$ (444.5 mg, 1.50 mmol, 3.0 eq.) in 1.36 mL solvent mixture. After 15 h, column chromatography (SiO_2, *Isolera One*™ 0%–80% EtOAc) afforded the title compound as a colorless solid.

Yield: 34.5 mg (0.19 mmol, 42%).

R_f = 0.29 (^{c}Hex:EtOAc = 2:1).

ESI-LCMS: *m/z* = 185.0 $[M+H]^+$.

ESI-HRMS ($C_7H_6ClN_2S$ $[M+H]^+$): calculated: *m/z* = 184.9935;

found: *m/z* = 184.9928.

Mp: 198.1–200.4 °C (Lit.:[23] 201–202 °C).

IR (ATR): $\tilde{\nu}$ [cm^{-1}] = 2498, 2282, 1598, 1551, 1449, 1417,1073, 855, 790, 739.

^{1}H-NMR, COSY (300 MHz, MeOH-*d*$_4$): δ [ppm] = 7.51 (d, *J* = 8.4 Hz, 1H, 7-H), 7.34 (d, *J* = 2.1 Hz, 1H, 4-H), 7.03 (dd, *J* = 8.4, 2.1 Hz, 1H, 6-H).

^{13}C-NMR, HSQC, HMBC (75 MHz, MeOH-*d*$_4$): δ [ppm] = 169.1 (2-C), 152.2 (3a-C), 130.6 (5-C), 128.4 (7a-C), 120.6 (7-C), 120.5 (6-C), 116.4 (4-C).

The spectroscopic data match to those reported in the literature.[24]

Benzylthiocyanate (28a)

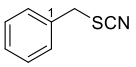

Following the general batch procedure using benzylmercaptane **28** (62.1 mg, 0.50 mmol, 1.0 eq.) and $K_3[FeCN_6]$ (444.5 mg, 1.50 mmol, 3.0 eq.) in 1.36 mL solvent mixture. After 18 h, column chromatography (SiO_2, *Isolera One*™ 0%–80% EtOAc) afforded the title compound as a colorless oil. General procedure B was alternatively applied with a reaction time of 12 min.

Yield: 28.5 mg (0.19 mmol, 38%, procedure A), 10.4 mg (0.07 mmol, 10%, procedure B).

R_f = 0.37 (^{c}Hex:EtOAc = 10:1).

GC-MS: *m* = 149.0 [M].

IR (ATR): $\tilde{\nu}$ [cm^{-1}] = 3064, 3032, 2153, 1495, 1455, 1245, 1203, 1074, 766, 698, 646.

^{1}H-NMR, COSY (400 MHz, $CDCl_3$): δ [ppm] = 7.42–7.34 (m, 5H, Ar-H), 4.17 (s, 2H, CH_2).

^{13}C-NMR, HSQC, HMBC (101 MHz, $CDCl_3$): δ [ppm] = 134.3 (1-C), 129.2 (2-C, 6-C), 129.0 (3-C), 128.9 (4-C), 112.0 (S*C*N), 38.4 (*C*H_2).

The obtained data are in accordance with the literature.[25]

2-Phenylethylthiocyanate (29a)

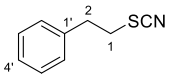

Following the general batch procedure using 2-phenylethan-1-thiol **29** (200.0 µL, 1.50 mmol, 1.0 eq.), $K_3[Fe(CN)_6]$ (1.48 g, 4.50 mmol, 3.0 eq.), H_2O (2 mL), EtOAc (2.0 mL) and HOAc (15.0 µL). After 79 h, column chromatography (SiO_2, *Isolera One*™ 0%–80% EtOAc) afforded the title compound as a colorless oil. General procedure B was alternatively applied with a reaction time of 12 min.

Yield: 165.0 mg (1.01 mmol, 67%, procedure A), 38.2 mg (0.23 mmol, 35%, procedure B).

***R*$_f$** = 0.39 (^{c}Hex:EtOAc = 10:1).

GC-MS: *m* = 163.1 [M].

IR (ATR): $\tilde{\nu}$ [cm^{-1}] = 3029, 2153, 1603, 1497, 1454, 1283, 1232, 752, 701, 565, 491.

^{1}H-NMR, COSY (400 MHz, $CDCl_3$): δ [ppm] = 7.41–7.34 (m, 2H, 2'-H, 6'-H), 7.33–7.28 (m, 1H, 4'-H), 7.27–7.22 (m, 2H, 3'-H, 5'-H), 3.24–3.18 (m, 2H, 1-C*H*$_2$), 3.17–3.12 (m, 2H, 2-C*H*$_2$).

^{13}C-NMR, HSQC, HMBC (101 MHz, $CDCl_3$): δ [ppm] = 137.7 (1'-C), 128.9 (2'-C, 6'-C), 128.7 (3'-C, 5'-C), 127.3 (4'-C), 112.1 (S*C*N), 36.1 (2-C), 35.2 (1-C).

The obtained data are in accordance with the literature.[16]

1*H*-Benzimidazol-2-ylthiocyanat (32a)

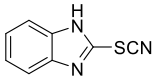

Following the general procedure A using 2-mercaptobenzimidazole **32** (67.5 mg, 0.50 mmol, 1.0 eq.) and $K_3[FeCN_6]$ (444.5 mg, 1.50 mmol, 3.0 eq.) in 1.36 mL solvent mixture. After 18 h, purification by column chromatography (SiO_2, *Isolera One*™ 0%–80% EtOAc) afforded the title compound as a colorless solid. General procedure B was alternatively applied with a reaction time of 12 min but no product formation could be observed.

Yield: 24.6 mg (0.14 mmol, 31%, procedure A).

***R*$_f$** = 0.75 (^{c}Hex:EtOAc = 1:1).

ESI-LCMS: *m/z* = 176.0 $[M+H]^+$.

Mp: 149.9–150.6 °C (EtOAc). (Lit.:[26] 163 °C).

IR (ATR): $\tilde{\nu}$ [cm^{-1}] = 3069, 2962, 2167, 1689, 1424, 1270, 1222, 1008, 979, 744.

^{1}H-NMR, COSY (400 MHz, MeOH-d_4): δ [ppm] = 7.63–7.57 (m, 2H, 5-H,6-H), 7.35–7.30 (m, 2H, 4-H,7-H).

^{13}C-NMR, HSQC, HMBC (101 MHz, MeOH-d_4): δ [ppm] = 135.4 (3a-C, 7a-C), 122.9 (4,5,6,7-C), 114.2 (br, 2-C), 106.1 (S*C*N).

The obtained data are in accordance with the literature.[27]

2,4-Dichlorthiocyanatobenzene (33a)

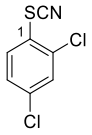

Following the general procedure B using 2,4-dichlorthiophenol **33** (119.8 mg, 0.67 mmol, 1.0 eq.) as the reagent with a milling time of 10 min. Column chromatography (SiO_2, *Isolera One*™ 0%–80% EtOAc) afforded the title compound as a colorless solid.

Yield: 67.5 mg (0.33 mmol, 49%).

R_f = 0.48 (^{c}Hex:EtOAc = 20:1).

ESI-LCMS: *m/z* = 205.1 $[M+H]^+$.

IR (ATR): $\tilde{\nu}$ [cm^{-1}] = 3088, 2165, 1569, 1452, 1375, 1136, 1101, 858, 814.

Mp: 70.1–71.1 °C, H_2O. (Lit.:[28] 72°C, H_2O).

^{1}H-NMR, COSY (300 MHz, $CDCl_3$): δ [ppm] = 7.64 (d, *J* = 8.6 Hz, 1H, 6-H), 7.49 (d, *J* = 2.2 Hz, 1H, 3-H), 7.38 (dd, *J* = 8.6, 2.2 Hz, 1H, 5-H).

^{13}C-NMR, HSQC, HMBC (75 MHz, $CDCl_3$): δ [ppm] = 136.0 (2-C), 133.6 (4-C), 130.7 (6-C), 130.3 (3-C), 128.8 (5-C), 123.3 (1-C), 108.8 (S*C*N).

The analytical data match those reported in the literature.[16]

Cyclopentylthiocyanate (34a)

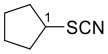

Following the general procedure A using cyclopentanethiol **34** (51.1 mg, 0.50 mmol, 1.0 eq.) and $K_3[FeCN_6]$ (444.5 mg, 1.50 mmol, 3.0 eq.) in 1.36 mL solvent mixture. After 18 h, column chromatography (SiO_2, ^{c}Hex:EtOAc 10:1) afforded the title compound as a colorless oil. General procedure B was alternatively applied with a reaction time of either 6 or 12 min but no product formation could be observed.

Yield: 23.4 mg (0.18 mmol, 37%, procedure A).

R_f = 0.41 (^{c}Hex:EtOAc = 10:1).

GC-MS: *m* = 127.0 [M], 69.10 [M−SCN].

IR (ATR): $\tilde{\nu}$ [cm^{-1}] = 2957, 2924, 2853, 2153, 1725, 1452, 1377, 1321, 1243.

^{1}H-NMR, COSY (300 MHz, $CDCl_3$): δ [ppm] = 3.66 (qd, *J* = 7.4, 5.2 Hz, 1H, 1-H), 2.13 (ddt, *J* = 11.0, 7.5, 5.2 Hz, 2H, 2-H$_a$, 5-H$_a$), 1.90–1.60 (m, 6H, 2-H$_b$, 3-H, 4-H, 5-H$_b$).

^{13}C-NMR, HSQC, HMBC (75 MHz, $CDCl_3$): δ [ppm] = 112.5 (*S*CN), 47.7 (1-C), 33.9 (2-C, 5-C), 24.4 (3-C, 4-C).

The obtained data are in accordance with the literature.[29]

Cyclohexylthiocyanate (35a)

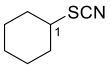

Following the general procedure A using cyclohexanethiol **35** (58.1 mg, 0.50 mmol, 1.0 eq.) and $K_3[FeCN_6]$ (444.5 mg, 1.50 mmol, 3.0 eq.) in 1.36 mL solvent mixture. After 18 h, column chromatography (SiO_2, Cy:EtOAc 10:1) afforded the title compound as a colorless oil. Alternatively, distillation of the crude reaction mixture was performed, furnishing the title compound in comparable 5% product yield. General procedure B was alternatively applied with a reaction time of either 6 or 12 min but no product formation could be observed.

Yield: 5.0 mg (0.04 mmol, 7%, procedure A).

R_f = 0.53 (^{c}Hex:EtOAc = 10:1).

GC-MS: *m* = 141.0 [M], 83.08 [M−SCN].

IR (ATR): $\tilde{\nu}$ [cm^{-1}] = 2935, 2857, 2152, 1450, 1343, 1264, 1206, 1183, 995, 889, 716.

^{1}H-NMR, COSY (400 MHz, $CDCl_3$): δ [ppm] = 3.24 (tt, *J*= 10.9, 3.8 Hz, 1H, 1-H), 2.33–2.02 (m, 2H, 2-H$_a$', 6-H$_a$'), 1.84 (m, 2H, 3-H$_a$, 5-H$_a$), 1.70–1.60 (m, 2H, 4-H$_a$), 1.60–1.52 (m, 2H, 2-H$_b$, 6-H$_b$), 1.48–1.32 (m, 2H, 3-H$_b$, 5-H$_b$), 1.31–1.19 (m, 1H, 4-H$_b$).

^{13}C-NMR, HSQC, HMBC (101 MHz, $CDCl_3$): δ [ppm] = 111.8 (*S*CN), 48.1 (1-C), 33.8 (2-C, 6-C), 26.0 (3-C, 5-C), 25.0 (4-C).

The obtained data are in accordance with the literature.[30]

1-Thiocyanatoadamantane (36a)

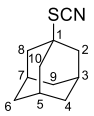

Following the general procedure A using adamantane-1-thiol **36** (75.6 mg, 0.50 mmol, 1.0 eq.) and $K_3[FeCN_6]$ (444.5 mg, 1.50 mmol, 3.0 eq.) in 1.36 mL solvent mixture. After 15 h, column chromatography (SiO_2, ^{c}Hex:EtOAc = 20:1) afforded the title compound as a colorless oil. General procedure B was applied with a reaction time of 12 min but no product formation could be observed.

Yield: 14.5 mg (0.08 mmol, 17%, procedure A).

R_f = 0.44 (^{c}Hex:EtOAc = 20:1).

GCMS: m = 193.1 [M]; 135.1 [M-SCN].

IR (ATR): $\tilde{\nu}$ [cm^{-1}] = 2913, 2854, 2144, 1453, 1343, 1301, 1035, 684.

^{1}H-NMR, COSY (300 MHz, $CDCl_3$): δ [ppm] = 2.22–2.12 (m, 3H, 3-H, 5-H, 7-H), 2.07 (d, *J* = 2.9 Hz, 6H, 2-H, 8-H, 10-H), 1.72 (t, *J* = 2.3 Hz, 6H, 4-H, 6-H, 9-H).

^{13}C-NMR, HSQC, HMBC (75 MHz, $CDCl_3$): δ [ppm] = 111.0 (S*C*N), 54.1 (1-C), 43.7 (2-C, 8-C, 10-C), 35.5 (4-C, 6-C, 9-C), 30.4 (3-C, 5-C, 7-C).

The obtained data are in accordance with the literature.[10]

4,5-Dihydrothiazol-2-amine (37a)

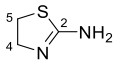

Following the general batch procedure using cysteamine **37** (34.7 mg, 0.50 mmol, 1.0 eq.) and $K_3[FeCN_6]$ (444.5 mg, 1.50 mmol, 3.0 eq.) in 1.36 mL solvent mixture. After 26 h, continuous extraction of the aqueous phase with ethyl acetate (4 days) afforded the title compound as a light-brown oil. For proper yield determination, the product yield was determined via ^{1}H-NMR using phenanthrene as the internal standard. General procedure B was alternatively applied with a reaction time of 12 min.

^{1}H-NMR yield: 0.42 mmol, 92%, procedure A; 0.07 mmol, 11%, procedure B.

R_f = 0.86 (acetone:^{i}PrOH = 4:1).

ESI-LCMS: *m/z* = 103.1 $[M+H]^+$.

ESI-HRMS ($C_3H_7N_2S$ $[M+H]^+$): calculated: *m/z* = 103.0325;

found: *m/z* = 103.0326.

Characteristic ^{1}H-NMR signal (300 MHz, $CDCl_3$): δ [ppm] = 3.89 (t, 2H, 4-H).

The obtained data are in accordance with the literature.[31]

22-Thiocyanato-2,5,8,11,14,17,20-heptaoxadocosane (38a) and
2,5,8,11,14,17,20,27,30,33,36,39,42,45-tetradecaoxa-23,24-dithiahexatetracontane (38b)

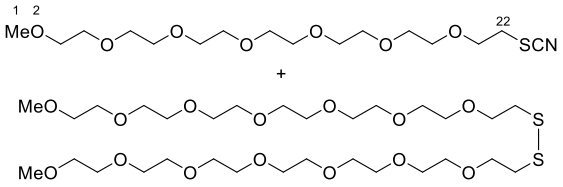

Following the general procedure A using 2,5,8,11,14,17,20-heptaoxadocosane-22-thiol **38** (160.3 mg, 0.50 mmol, 1.0 eq.) and $K_3[FeCN_6]$ (444.5 mg, 1.50 mmol, 3.0 eq.) in 1.36 mL solvent mixture. After 24 h, work up according to the general procedure afforded the title compound together with **62** as an inseparable mixture as a colorless oil. General procedure B was alternatively applied with a reaction time of 12 min yielding exclusively **38a** using 2,5,8,11,14,17,20-heptaoxadocosane-22-thiol **38** (22.6 mg, 0.07 mmol, 1.0 eq.) and $K_3[FeCN_6]$ (20.9 mg, 0.07 mmol, 1.0 eq.).

Yield: overall 102.1 mg, **38a**: 55.05 mg (0.14 mmol, 29%); **38b**: 47.05 mg (0.07 mmol, 7%) based on ^{1}H-NMR ratio of 22-H (**38a**): 22-H (**38b**), procedure A.

^{1}H-NMR yield 38a: 0.02 mmol, 29%, procedure B.

R_f = 0.71 (on AlO_x, EtOAc:MeOH = 20:1).

IR (ATR): $\tilde{\nu}$ [cm^{-1}] = 2868, 2153, 1455, 1350, 1295, 1248, 1199, 1099, 1038, 947, 850.

NMR data of 38a:

ESI-LCMS: *m/z* = 404.2 $[M+Na]^+$.

ESI-HRMS ($C_{16}H_{31}NO_7S$ $[M+Na]^+$): calculated: *m/z* = 404.1713;

found: *m/z* = 404.1711.

^{1}H-NMR, COSY (400 MHz, $CDCl_3$): δ [ppm] = 3.81 (t, *J* = 5.9 Hz, 2H, 21-H), 3.67–3.59 (m, 22H, 4,6,7,9,10,12,13,15,16,18,19-H), 3.53–3.51 (m, 2H, 3-H), 3.35 (s, 3H, 1-H), 3.14 (t, *J* = 5.9 Hz, 2H, 22-H).

^{13}C-NMR, HSQC, HMBC (101 MHz, $CDCl_3$): δ [ppm] = 112.2 (S*C*N), 71.9 (3-C), 70.8–70.4 (11C, 4,6,7,9,10,12,13,15,16,18,19-C), 68.9 (21-C), 59.0 (1-C), 33.9 (22-C).

NMR data of 38b:

ESI-LCMS: *m/z* = 733.3 $[M+Na]^+$.

ESI-HRMS ($C_{30}H_{62}O_{14}S_2$ $[M+Na]^+$): calculated: *m/z* = 733.3454;

found: *m/z* = 733.3460.

^{1}H-NMR, COSY (400 MHz, $CDCl_3$): δ [ppm] = 3.70 (t, *J* = 6.7 Hz, 2H, 21-H), 3.67–3.59 (m, 22H, 4,6,7,9,10,12,13,15,16,18,19-H), 3.53–3.51 (m, 2H, 3-H), 3.35 (s, 3H, 1-H), 2.86 (t, *J* = 6.7 Hz, 2H, 22-H).

^{13}C-NMR, HSQC, HMBC (101 MHz, $CDCl_3$): δ [ppm] = 71.9 (3-C), 69.6 (21-C), 70.8–70.4 (11C, 4,6,7,9,10,12,13,15,16,18,19-C), 59.0 (1-C), 38.3 (22-C).

No spectroscopic data available in the literature.

2-Amino-4,5-dihydrothiazol-4-carboxylic acid (39a)

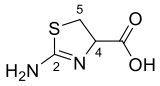

Following the general procedure A using L-cystine **39** (108.1 mg, 0.50 mmol, 1.0 eq.) and $K_3[FeCN_6]$ (444.5 mg, 1.50 mmol, 3.0 eq.) in 1.36 mL solvent mixture. After 22.5 h, continuous extraction of the aqueous phase with ethyl acetate (2 days) afforded the title compound as a colorless solid. For proper yield determination, the product yield was determined via ^{1}H-NMR using phenanthrene as the internal standard as signals of acetic acid were still present after extraction. General procedure B was applied with a reaction time of 12 min but no product formation could be observed.

^{1}H-NMR yield: 0.09 mmol, 21%.

***R*$_f$** = 0.91 (EtOAc).

ESI-LCMS: *m/z* = 146.9 $[M+H]^+$.

ESI-HRMS ($C_4H_7N_2O_2S$ $[M+H]^+$): calculated: *m/z* = 147.0223;

found: *m/z* = 147.0228.

^{1}H-NMR, COSY (300 MHz, MeOH-*d*$_4$): δ [ppm] = 4.66 (t, *J* = 7.9 Hz, 1H, 4-H), 3.81–3.62 (m, 2H, 5-H).

^{13}C-NMR, HSQC, HMBC (75 MHz, MeOH-*d*$_4$): δ [ppm] = 173.1 (*C*OO^-), 171.9 (2-C), 64.3 (4-C), 33.3 (5-C).

The obtained data are in accordance with the literature.[32]

Methyl-*N*-acetyl-S-cyano-L-cysteinate (40a)

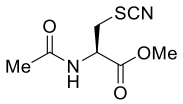

Following the general procedure B using *N*-acetyl-L-cysteine methyl ester **40** (118.5 mg, 0.67 mmol, 1.0 eq.) as the reagent with a milling time of 6 min. Column chromatography (SiO_2, ^{c}Hex:EtOAc = 1:1) afforded the title compound as yellow oil.*

Yield: 18.9 mg (0.09 mmol, 13%).

***R*$_f$** = 0.29 (^{c}Hex:EtOAc = 1:1).

IR = 3297, 2956, 2160, 1744, 1662, 1537, 1438, 1374.

Optical rotation: $[\alpha]_D^{21}$ = +50.3 (0.1, $CHCl_3$).

ESI-LCMS: *m/z* = 203.0 $[M+H]^+$.

^{1}H-NMR, COSY (300 MHz, $CDCl_3$): δ [ppm] = 6.55 (d, *J* = 6.4 Hz, 1H, N*H*), 4.96 (dt, *J* = 6.4, 4.2 Hz, 1H, C*H*), 3.86 (s, 3H, OCH_3), 3.62 (dd, *J* = 14.2, 4.2 Hz, 1H, CH_{2a}), 3.43 (dd, *J* = 14.2, 3.8 Hz, 1H, CH_{2b}), 2.09 (s, 3H, CH_3).

^{13}C-NMR, HSQC, HMBC (75 MHz, $CDCl_3$): δ [ppm] = 170.4 (*C*OCH_3), 169.2 (*C*O_2CH_3), 111.4 (S*C*N), 53.4 (O*C*H_3), 52.4 (*C*H), 35.5 (*C*H_2), 23.0 (*C*H_3).

2-Thiocyanatoethan-1-ol (41a)

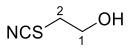

Following the general procedure A using 2-mercaptoethan-1-ol **41** (35.1 mg, 0.50 mmol, 1.0 eq.) and $K_3[FeCN_6]$ (444.5 mg, 1.50 mmol, 3.0 eq.) in 1.36 mL solvent mixture. After 14 h of heating, work-up of the crude reaction mixture was performed according to the general procedure and the yield was determined via ^{1}H-NMR using phenanthrene as the internal standard. General procedure B was alternatively applied with a reaction time of either 6 or 12 min but no product formation was observed.

^{1}H-NMR yield: 0.16 mmol, 35%, procedure A.

***R*$_f$** = 0.48 (EtOAc).

GC-MS: *m* = 102.9 [M].

ESI-HRMS (C_3H_6NOS $[M+H]^+$): calculated: *m/z* = 104.0165;

found: *m/z* = 104.0164.

Characteristic ^{1}H-NMR Signal (300 MHz, $CDCl_3$): δ [ppm] = 2.87 (t, *J* = 5.8 Hz, 2H, CH_2SCN).

No spectroscopic data available in the literature.

2-((1*H*-Tetrazol-5-yl)thio)pyrimidine (60)

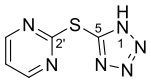

According to a modified procedure of *L. Myznikov et al*.[33]
In a 10 mL reaction vial pyrimidine-2-ylthiocyanate **16a** (61.7 mg, 0.45 mmol, 1.0 eq.), sodium azide (35.1 mg, 0.54 mmol, 1.2 eq.) and zinc(II)chloride (61.3 mg, 0.45 mmol, 1.0 eq.) were dissolved in isopropanol (1.5 mL) and the reaction mixture was heated to 50 °C. After the reaction was finished (3 h, reaction followed by TLC and LCMS), the solvent was evaporated under reduced pressure, 5% NaOH solution (3 mL) was added to the residue and the mixture was stirred for further 20 min until a suspension had formed. This mixture was filtrated and the remaining solid was washed with 5% NaOH solution (3 mL). The filtrate was adjusted to pH = 1 using concentrated HCl, which was accompanied by a color change from colorless to yellow. After extraction with ethyl acetate (3x15 mL), the combined

organic layers were washed with saturated NaCl solution, dried over Na_2SO_4, filtered and the solvent was removed under reduced pressure. The title compound was obtained as a colorless solid.

Yield: 67.8 mg (0.38 mmol, 84%).

R_f = 0.81 (H_2O:MeCN = 90:10).

ESI-LCMS: *m/z* = 181.0 $[M+H]^+$.

ESI-HRMS ($C_5H_4N_6S$ $[M+H]^+$): calculated: *m/z* = 181.0291;

found: *m/z* = 181.0288.

Mp: 143.5–146.3 °C. There is no melting point reported in the literature.

IR (ATR): $\tilde{\nu}$ [cm^{-1}] = 3075, 2155, 1558, 1445, 1384, 1208, 1012, 827, 767, 635.

^{1}H-NMR, COSY (300 MHz, DMSO-d_6): δ [ppm] = 8.68 (d, *J* = 4.9 Hz, 2H, 4'-H, 6'-H), 7.40 (t, *J* = 4.9 Hz, 1H, 5'-H).

^{13}C-NMR, HSQC, HMBC (75 MHz, DMSO-d_6): δ [ppm] = 192.6 (5-C), 167.1 (2'-C), 158.8 (4'C, 6'-C), 119.2 (5'-C).

No spectroscopic data available in the literature.

Synthesis of Psammaplins A and B

Psammaplin A (55)

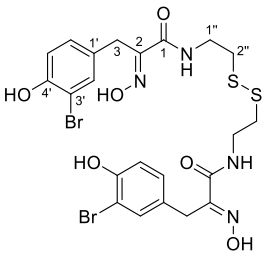

According to a modified procedure of *J. R. Sufrin et al*.[34]
To a stirred solution of **57** (135 mg, 0.49 mmol, 1.0 eq.), *N*-hydroxysuccinimide (85 mg, 0.74 mmol, 1.5 eq.) and DCC (152 mg, 0.74 mmol, 1.5 eq.) in dry DMF (10 mL), cysteamine (**37**, 55 mg, 0.25 mmol, 0.5 eq.) and TEA (136 µL, 0.98 mmol, 2.0 eq.) were added and the reaction was stirred for 16 h at room temperature. The solvent was removed under reduced pressure and the crude product was purified via preparative HPLC (40% MeCN, Machery Nagel Nucleodur C18 HTec column). The title compound was obtained as a colorless oil.

Yield: 78.1 g (0.12 mmol, 24%).

R_f = 0.37 (H_2O:MeCN = 50:50).

ESI-LCMS: *m/z* = 662.9 $[M+H]^+$.

ESI-LCMS: *m/z* = 661.0 $[M-H]^-$.

ESI-HRMS ($C_{22}H_{24}Br_2N_4O_6S_2Na$ $[M+Na]^+$): calculated: *m/z* = 684.9396;

found: *m/z* = 684.9396.

IR (ATR): $\tilde{\nu}$ [cm^{-1}] = 3357, 2930, 2853, 1659, 1625, 1534, 1494, 1255, 1211, 1015.

^{1}H NMR (300 MHz, MeOH-d_4) δ [ppm] = 7.37 (d, *J* = 2.1 Hz, 2H, H-2'), 7.07 (dd, *J* = 8.3, 2.1 Hz, 2H, H-6'), 6.76 (d, *J* = 8.3 Hz, 2H, H-5'), 3.79 (s, 4H, H-3), 3.51 (t, *J* = 6.7 Hz, 4H, H-1''), 2.79 (t, *J* = 6.7 Hz, 4H, H-2'').

^{13}C NMR (75 MHz, MeOH-d_4) δ [ppm] = 165.8 (C-1), 153.6 (C-4'), 153.0 (C-2), 134.4 (C-2), 130.5 (C-1'), 130.3 (C-6'), 117.0 (C-5'), 110.4 (C-3'), 39.5 (C-1''), 38.4 (C-2''), 28.6 (C-3).

The analytical data are in accordance with the literature.[34]

(*E*/*Z*)-2-(Hydroxyimino)-3-(4-hydroxyphenyl)propanoic acid (56)

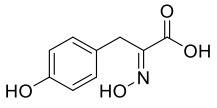

According to a modified procedure of *J. R. Sufrin et al*.[34]

A solution of hydroxyphenylpyruvic acid **54** (1.10 g, 6.12 mmol, 1.0 eq.) and hydroxylamine hydrochloride (638 mg, 9.18 mmol, 1.5 eq.) in dry pyridine (20 mL) was stirred for 5 h at room temperature. The solvent was removed under reduced pressure yielding the pyridinium salt. The salt was dissolved in 2 M HCl (50 mL) and the aqueous phase was extracted with ethyl acetate (3x50 mL). The combined organic layers were dried over $MgSO_4$ and the solvents were removed under reduced pressure to yield the title compound as a beige oil.

Yield: 750 mg (3.84 mmol, 63%).

R_f = 0.59 (H_2O:MeCN = 50:50).

ESI-LCMS: *m/z* = 196.0 $[M+H]^+$.

ESI-LCMS: *m/z* = 194.1 $[M-H]^-$.

^{1}H-NMR, COSY (300 MHz, MeOH-d_4): δ [ppm] = 7.09 (d, *J* = 8.5 Hz, 2H), 6.66 (d, *J* = 8.5 Hz, 2H), 3.80 (s, 2H).

The obtained data are in accordance with the literature.[34]

(*E*/*Z*)-3-(3-Bromo-4-hydroxyphenyl)-2-(hydroxyimino)propanoic acid (57)

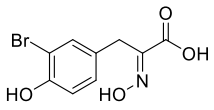

According to a modified procedure of *J. R. Sufrin et al*.[34]
A solution of **56** (248 mg, 1.27 mmol, 1.0 eq.) and *N*-bromosuccinimide (180 mg, 1.02 mmol, 0.8 eq.) in methanol (5 mL) was stirred for 16 h at room temperature. The solvent was removed under reduced pressure and the crude product was purified by flash column chromatography (C_{18}, H_2O:MeCN = 90:10 to MeCN) yielding the title compound **57** in the first fraction as a brown solid. As a side product, (*E*/*Z*)-3-(3,5-dibromo-4-hydroxyphenyl)-2-(hydroxy-imino)propanoic acid **58** was obtained in a second fraction as a lyophilisate.

(*E*/*Z*)-3-(3-bromo-4-hydroxyphenyl)-2-(hydroxyimino)propanoic acid (**57**):
Yield: 135 mg (0.49 mmol, 39%).

R_f = 0.69 (H_2O:MeCN = 50:50).

ESI-LCMS: *m/z* = 274.0 $[M+H]^+$.

ESI-LCMS: *m/z* = 271.9 $[M-H]^-$.

^{1}H-NMR, COSY (300 MHz, MeOH-d_4): δ [ppm] = 7.37 (d, *J* = 2.2 Hz, 1H), 7.08 (dd, *J* = 8.3, 2.2 Hz, 1H), 6.78 (d, *J* = 8.3 Hz, 1H), 3.80 (s, 2H).

The analytical data are in accordance with the literature.[34]

(*E*/*Z*)-3-(3,5-dibromo-4-hydroxyphenyl)-2-(hydroxy-imino)propanoic acid (**58**):

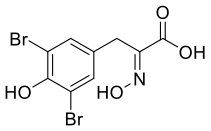

Yield: 45 mg (0.13 mmol, 10%).

R_f = 0.76 (H_2O:MeCN = 50:50).

ESI-LCMS: *m/z* = 349.9 $[M+H]^+$.

ESI-LCMS: *m/z* = 351.9 $[M-H]^-$.

^{1}H-NMR, COSY (300 MHz, MeOH-d_4): δ [ppm] =7.40 (s, 2H), 3.80 (s, 2H).

The analytical data match to those reported in the literature.[34]

5,5'-Dibromopsammaplin A (59)

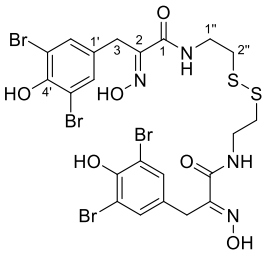

According to a modified procedure of *J. R. Sufrin et al*.[34]
To a stirred solution of **58** (48 mg, 0.14 mmol, 1.0 eq.), *N*-hydroxysuccinimide (24 mg, 0.20 mmol, 1.5 eq.) and DCC (42 mg, 0.20 mmol, 1.5 eq.) in dry DMF (5 mL), cysteamine (15 mg, 0.07 mmol, 0.5 eq.) and TEA (38 µL, 0.27 mmol, 2.0 eq.) were added and the reaction was stirred for 16 h at room temperature. The solvent was removed under reduced pressure and the crude product was purified via preparative HPLC (50% MeCN, Machery Nagel Nucleodur C18 HTec column). The title compound was obtained as a colorless oil.

Yield: 21.1 mg (0.026 mmol, 13%).

R_f = 0.19 (H_2O:MeCN = 50:50).

ESI-LCMS: *m/z* = 818.8 $[M+H]^+$.

ESI-LCMS: *m/z* = 816.8 $[M-H^+]^-$.

ESI-HRMS ($C_{22}H_{22}Br_4N_4O_6S_2Na$ $[M+Na]^+$): calculated: *m/z* = 840.7606;

found: *m/z* = 840.7597.

IR (ATR): $\tilde{\nu}$ [cm^{-1}] = 3222, 2872, 1656, 1556, 1474, 1408, 1317, 1258, 997.

^{1}H NMR (300 MHz, MeOH-d_4) δ [ppm] = 7.39 (s, 4H, H-2', H-6'), 3.79 (s, 4H, H-3), 3.53 (t, J = 6.7 Hz, 4H, H-1''), 2.82 (t, J = 6.7 Hz, 4H, H-2'').

^{13}C NMR (75 MHz, MeOH-d_4) δ [ppm] = 165.6 (C-1), 152.5 (C-2), 150.7 (C-4'), 133.9 (C-2', C-6'), 132.2 (C-1'), 111.9 (C-3', C-5'), 39.6 (C-1''), 38.6 (C-2''), 28.4 (C-3).

The analytical data are in accordance with the literature.[34]

Psammaplin B (1)

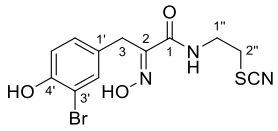

Following the general procedure, Psammaplin A **55** (24.0 mg, 0.04 mmol, 1.0 eq.) was used together with $K_3[FeCN_6]$ (35.7 mg, 0.11 mmol, 3.0 eq.) in 108 µL solvent mixture. The reaction was monitored via LCMS, and after 7 h, additional $K_3[FeCN_6]$ (3 eq.) was added to the reaction mixture. After 23 h, another 1.5 eq. of $K_3[FeCN_6]$ were added, so that in total 7.5 eq. of $K_3[FeCN_6]$ were applied. The reaction was quenched with saturated $NaHCO_3$ solution after 72 h, and the following work-up was performed according to the general procedure. The title compound **1** was obtained as colorless lyophilisate after purification of the crude product via preparative HPLC (29% MeCN, Machery Nagel Nucleodur C18 HTec column).

Yield: 3.405 mg (9.51 nmol, 26%).

R_f = 0.50 (H_2O:MeCN = 50:50).

ESI-LCMS: m/z = 358.0 $[M+H]^+$.

ESI-HRMS ($C_{12}H_{12}BrN_3O_3SNa$ $[M+Na]^+$):	calculated:	m/z = 379.9675;
	found:	m/z = 379.9668.
ESI-HRMS ($C_{12}H_{12}BrN_3O_3SK$ $[M+K]^+$):	calculated:	m/z = 395.9415;
	found:	m/z = 395.9404.

IR (ATR): $\tilde{\nu}$ [cm^{-1}] = 3325, 2928, 2514, 2158, 1657, 1493, 1466, 1421, 1206, 996.

^{1}H NMR (600 MHz, MeOH-d_4) δ [ppm] = 7.37 (d, J = 2.2 Hz, 1H, H-2'), 7.07 (dd, J = 8.3, 2.2 Hz, 1H, H-6'), 6.76 (d, J = 8.3 Hz, 1H, H5'), 3.79 (s, 2H, H-3), 3.62 (t, J = 6.4 Hz, 2H, H-1''), 3.14 (t, J = 6.4 Hz, 2H, H-2'').

^{13}C NMR (151 MHz, MeOH-d_4) δ [ppm] = 166.2 (C-1), 153.7 (C-4'), 152.8 (C-2), 134.5 (C-2'), 130.5 (C-1'), 130.4 (C-6'), 116.9 (C-5'), 113.3 (S*C*N), 110.4 (C-3'), 40.1 (C-1''), 34.1 (C-2''), 28.6 (C-3).

No spectroscopic data available.

Isolated Side Products

Disulfides

Diphenyl disulfide (13)

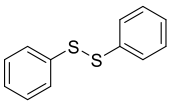

Following the general procedure A using thiophenol **46** (55.1 mg, 0.50 mmol, 1 eq.) and $K_3[FeCN_6]$ (494 mg, 1.50 mmol, 3.0 eq.) in 1.36 mL solvent mixture. After 36 h, column chromatography (SiO_2, *Isolera One*™ 0%–80% EtOAc) afforded the title compound as a colorless solid.

Yield: 47.1 mg (0.22 mmol, 86%).

R_f = 0.24 (^{c}Hex).

GC-MS: *m* = 218.1 [M].

Mp: 57.6–58.7 °C. (Lit.:[35] 58–60 °C).

IR (ATR): $\tilde{\nu}$ [cm^{-1}] = 3071, 1576, 1475, 1437, 1072, 1022, 739, 688, 473, 464.

^{1}H-NMR, COSY (300 MHz, $CDCl_3$): δ [ppm] = 7.62–7.47 (m, 4H, 2-H, 6-H), 7.43–7.30 (m, 4H, 3-H, 5-H), 7.29–7.20 (m, 2H, 4-H, 4'-H).

^{13}C-NMR, HSQC, HMBC (75 MHz, $CDCl_3$): δ [ppm] = 137.2 (1-C), 129.2 (3-C, 5-C), 127.6 (2-C, 6-C), 127.3 (4-C).

The obtained data are in accordance with the literature.[35]

1,2-Bis(4-chlorophenyl)disulfide (22b)

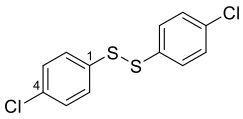

Following the general procedure A using 4-chlorothiophenol **22** (32.4 mg, 0.23 mmol, 1 eq.). After 14 h, column chromatography (SiO_2, *Isolera One*™ 0%–80% EtOAc) afforded the title compound as a colorless solid.

Yield: 14.3 mg (0.05 mmol, 22%).

R_f = 0.20 (^{c}Hex).

GC-MS: *m* = 285.9 [M].

Mp: 66.5–69.6 °C (Lit.:[36] 68–70 °C).

IR (ATR): $\tilde{\nu}$ [cm^{-1}] = 3078, 1473, 1387, 1090, 1010, 812, 741, 536, 483, 1633.

^{1}H-NMR, COSY (300 MHz, $CDCl_3$): δ [ppm] = 7.43–7.37 (m, 4H, 2-H, 6-H), 7.31–7.25 (m, 4H, 3-H, 5-H).

^{13}C-NMR, HSQC, HMBC (75 MHz, $CDCl_3$): δ [ppm] = 135.1 (1-C), 133.6 (4-C), 129.3 (2-C, 3-C, 5-C, 6-C).

The obtained data are in accordance with the literature.[36]

Bis(4-tolyl)disulfide (24b)

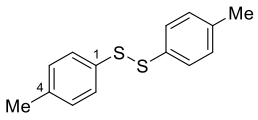

Following the general procedure A using 4-mercaptotoluene **24** (62.1 mg, 0.50 mmol, 1 eq.) and $K_3[FeCN_6]$ (494 mg, 1.50 mmol, 3.0 eq.) in 1.36 mL solvent mixture. After 15 h, column chromatography (SiO_2, *Isolera One*™ 0%–80% EtOAc) afforded the title compound as a colorless oil. General procedure B was alternatively applied with a reaction time of 6 min.

Yield: 18.0 mg (0.07 mmol, 29%, procedure A), 40.1 mg (0.16 mmol, 49%, procedure B).

R_f = 0.24 (^{c}Hex).

GC-MS: *m* = 246.1 [M].

IR (ATR): $\tilde{\nu}$ [cm^{-1}] = 3919, 2920, 2863, 1489, 1338, 1397, 1210, 1116, 1016, 803, 486.

^{1}H-NMR, COSY (300 MHz, $CDCl_3$): δ [ppm] = 7.41–7.38 (m, 4H, 2-H, 6-H), 7.13–7.10 (m, 4H, 3-H, 5-H), 2.33 (s, 6H, CH_3).

^{13}C-NMR, HSQC, HMBC (75 MHz, $CDCl_3$): δ [ppm] = 137.6 (4-C), 134.0 (1-C), 129.9 (3-C, 5-C), 128.7 (2-C, 6-C), 21.2 (CH_3).

The obtained data are in accordance with the literature.[37]

Bis(4-aminophenyl)disulfide (25b)

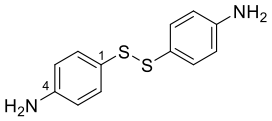

Following the general procedure A using 4-aminothiophenol **25** (62.6 mg, 0.50 mmol, 1 eq.) and $K_3[FeCN_6]$ (494 mg, 1.50 mmol, 3.0 eq.) in 1.36 mL solvent mixture. After 59 h, column chromatography (SiO_2, *Isolera One*™ 0%–80% EtOAc) afforded the title compound as a brown oil.

Yield: 4.4 mg (0.02 mmol, 7%).

R_f = 0.52 (^{c}Hex:EtOAc = 1:1).

ESI-LCMS: *m/z* = 249.0 $[M+H]^+$.

IR (ATR): $\tilde{\nu}$ [cm^{-1}] = 3473, 3376, 3035, 2922, 2852, 2152, 1625, 1595, 1496, 1304, 825.

^{1}H-NMR, COSY (300 MHz, $CDCl_3$): δ [ppm] = 7.44–7.30 (m, 4H, 2-H, 6-H), 6.82–6.56 (m, 4H, 3-H, 5-H), 3.96 (s, 4H, NH_2).

^{13}C-NMR, HSQC, HMBC (75 MHz, $CDCl_3$): δ [ppm] = 148.9 (4-C), 134.7 (3-C, 5-C), 116.2 (2-C, 6-C), 109.8 (1-C).

The obtained data are in accordance with the literature.[38]

2,2'-Disulfidediyldianiline (26b)

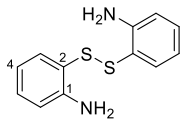

Following the general batch procedure using 2-aminothiophenol **26** (28.1 mg, 0.23 mmol, 1 eq.). After 14 h, column chromatography (SiO_2, *Isolera One*™ 0%–80% EtOAc) afforded the title compound as a yellow oil.

Yield: 22.1 mg (0.09 mmol, 40%).

R_f = 0.49 (^{c}Hex:EtOAc = 2:1).

ESI-LCMS: *m/z* = 249.0 $[M+H]^+$.

IR (ATR): $\tilde{\nu}$ [cm^{-1}] = 3464, 3364, 1605, 1562, 1475, 1445, 1308, 1250, 1158, 747.

^{1}H-NMR, COSY (300 MHz, $CDCl_3$): δ [ppm] = 7.22–7.10 (m, 4H, 3-H, 3'-H, 5-H, 5'-H), 6.77–6.68 (m, 2H, 6-H, 6'-H), 6.59 (td, *J* = 7.5, 1.3 Hz, 2H, 4-H, 4'-H), 4.33 (bs, 4H, NH_2).

^{13}C-NMR, HSQC, HMBC (75 MHz, $CDCl_3$): δ [ppm] = 148.7 (1-C, 1'-C), 136.9 (3-C, 3'-C), 131.7 (5-C, 5'-C), 118.8 (2-C, 2'-C), 118.3 (4-C, 4'-C), 115.31 (6-C, 6'-C).

The obtained data are in accordance with the literature.[39]

Di(benzothiazole-2yl)disulfide (30b)

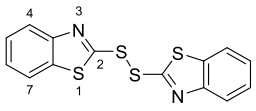

Following the general procedure A using 2-mercaptobenzothiazole **30** (37.6 mg, 0.23 mmol, 1.0 eq.). After 14 h, column chromatography (SiO_2, *Isolera One*™ 0%–80% EtOAc) afforded the title compound as a slightly yellow solid.

Yield: 31.4 mg (0.01 mmol, 42%).

R_f = 0.78 (^{c}Hex:EtOAc = 2:1).

ESI-LCMS: *m/z* = 332.9 $[M+H]^+$.

Mp: 101.3–102.1 °C. (Lit.:[40] 102–106 °C).

IR (ATR): $\tilde{\nu}$ [cm^{-1}] = 3060, 1455, 1417, 1312, 1237, 1079, 1008, 991, 755, 726.

^{1}H-NMR, COSY (300 MHz, DMSO-d_6): δ [ppm] = 8.14 (ddd, *J* = 7.9, 1.5, 0.7 Hz, 2H, 7-H), 8.05 (ddd, *J* = 8.1, 1.4, 0.7 Hz, 2H, 4-H), 7.61–7.54 (m, 2H, 5-H), 7.50 (ddd, *J* = 8.5, 7.3, 1.3 Hz, 2H, 6-H).

^{13}C-NMR, HSQC, HMBC (75 MHz, DMSO-d_6): δ [ppm] = 159.7 (2-C), 152.2 (3a-C), 136.0 (7a-C), 126.9 (5-C), 125.9 (6-C), 122.4 (4-C), 122.2 (7-C).

The obtained data are in accordance with the literature.[41, 42]

1,2-Bis(2,4-dichlorophenyl)disulfide (33b)

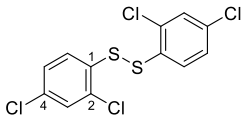

Following the general procedure A using 2,4-dichlorobenzenethiol **33** (42.5 mg, 0.23 mmol, 1 eq.). After 22 h, the title compound could be obtained as a colorless solid.

Yield: 46.8 mg (0.13 mmol, 55%).

R_f = 0.85 (^{c}Hex:EtOAc = 9:1).

ESI-LCMS: *m/z* = 354.8 ($[M+H]^+$).

Mp: 78.7–80.5 ° (Lit.:[43] 82–84 °C).

IR (ATR): $\tilde{\nu}$ [cm^{-1}] =2923, 1568, 1551, 1448, 1371, 1095, 1028, 865, 807, 550.

^{1}H-NMR, COSY (300 MHz, $CDCl_3$): δ [ppm] = 7.46 (d, *J* = 8.6 Hz, 2H, 6-H, 6'-H), 7.39 (d, *J* = 2.2 Hz, 2H, 3-H, 3'-H), 7.20 (dd, *J* = 8.6, 2.2 Hz, 2H, 5-H 5'-H).

^{13}C-NMR, HSQC, HMBC (75 MHz, $CDCl_3$): δ [ppm] = 133.5 (2-C, 2'-C), 132.8 (4-C, 4'-C), 132.7 (1-C, 1'-C), 129.6 (3-C, 3'-C), 128.5 (6-C, 6'-C), 128.0 (5-C, 5'-C).

The obtained data are in accordance with the literature.[44]

Dimethyl 2,2'-disulfidediyldiacetate (43b)

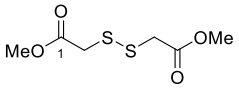

Following the general procedure A using thioglycolic acid methyl ester **43** (47.7 mg, 0.50 mmol, 1 eq.) and $K_3[FeCN_6]$ (494 mg, 1.50 mmol, 3.0 eq.) in 1.36 mL solvent mixture. After 16 h, column chromatography (SiO_2, ^{c}Hex:EtOAc = 2:1) afforded the title compound as a colorless oil.

Yield: 11.1 mg (0.05 mmol, 12%).

$\boldsymbol{R_f}$ = 0.46 (^{c}Hex:EtOAc = 2:1).

ESI-LCMS: *m/z* = 210.9 ($[M+H]^+$); *m/z* = 232.9 $[M+Na]^+$.

ESI-HRMS ($C_6H_{11}O_4S_2$ $[M+H]^+$): calculated: *m/z* = 211.0094;

found: *m/z* = 211.0095.

IR (ATR): $\tilde{\nu}$ [cm^{-1}] = 2954, 1732, 1435, 1273, 1155, 1126, 1007.

^{1}H-NMR, COSY (300 MHz, $CDCl_3$): δ [ppm] = 3.76 (s, 6H, OCH_3), 3.59 (s, 4H, CH_2).

^{13}C-NMR, HSQC, HMBC (75 MHz, $CDCl_3$): δ [ppm] = 169.9 (*C*O), 52.8 (O*C*H_3), 41.3 (*C*H_2).

The obtained data are in accordance with the literature.[45]

Dimethyl-3,3'-disulfidediyldipropionate (44b)

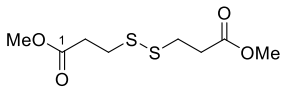

Following the general procedure A using 3-mercaptopropioic acid methyl ester **44** (54.0 mg, 0.50 mmol, 1 eq.) and $K_3[FeCN_6]$ (494 mg, 1.50 mmol, 3.0 eq.) in 1.36 mL solvent mixture. After 18 h, column chromatography (SiO_2, ^{c}Hex:EtOAc = 2:1) afforded the title compound as a colorless oil.

Yield: 38.2 mg (0.16 mmol, 36%).

$\boldsymbol{R_f}$ = 0.52 (^{c}Hex:EtOAc = 2:1).

ESI-LCMS: *m/z* = 239.0 $[M+H]^+$; 261.0 $[M+Na]^+$.

IR (ATR): $\tilde{\nu}$ [cm^{-1}] = 2953, 1731, 1564, 1436, 1356, 1239, 1171, 1141, 1048, 1016, 824.

^{1}H-NMR, COSY (300 MHz, $CDCl_3$): δ [ppm] = 3.69 (s, 6H, OCH_3), 2.91 (td, *J* = 7.1, 0.9 Hz, 4H, 3-H, 3'-H), 2.72 (td, *J* = 7.1, 0.9 Hz, 4H, 2-H, 2'-H).

^{13}C-NMR, HSQC, HMBC (75 MHz, $CDCl_3$): δ [ppm] = 172.2 (*C*OCH_3), 52.0 (COO*C*H_3), 33.9 (2-C, 2'-C), 33.1 (3-C, 3'-C).

The obtained data are in accordance with the literature.[46]

1,2-Bis(4-methoxybenzyl)disulfide (45b)

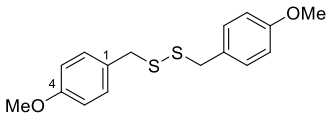

Following the general procedure A using (4-methoxyphenyl)methanethiol **45** (69.3 mg, 0.50 mmol, 1 eq.) and $K_3[FeCN_6]$ (494 mg, 1.50 mmol, 3.0 eq.) in 1.36 mL solvent mixture. After 42 h, column chromatography (SiO_2, *Isolera One*™ 0%–80% EtOAc) afforded the title compound as a colorless oil. General procedure B was alternatively applied with a reaction time of 6 min.

Yield: 8.1 mg (0.03 mmol, 6%, Procedure A), 15.9 mg (0.05 mmol, 16%, procedure B).

R_f = 0.47 (^{c}Hex:EtOAc = 10:1).

ESI-LCMS (pos. found for $C_8H_9O^+$)**:** *m/z* = 121.1 [M-$C_8H_9OS_2$].

ESI-HRMS ($C_{16}H_{18}O_2S_2Na$ [M+Na]$^+$): calculated: *m/z* = 329.0640;

found: *m/z* = 329.0609.

IR (ATR): $\tilde{\nu}$ [cm^{-1}] = 2834, 1609, 1510, 1463, 1301, 1248, 1175, 1033, 832.

^{1}H-NMR, COSY (300 MHz, $CDCl_3$): δ [ppm] = 7.21–7.15 (m, 4H, 2-H, 6-H), 6.89–6.82 (m, 4H, 3-H, 5-H), 3.80 (s, 6H, O*C*H$_3$), 3.59 (s, 4H, C*H*$_2$).

^{13}C-NMR, HSQC, HMBC (75 MHz, $CDCl_3$): δ [ppm] = 159.1 (4-C), 130.6 (2-C, 6-C), 129.5 (1-C), 114.0 (3-C, 5-C), 55.4 (O*C*H$_3$), 42.9 (*C*H$_2$).

The obtained data are in accordance with the literature.[35]

Didecyldisulfide (53b)

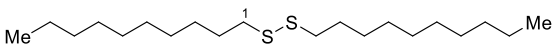

Following the general procedure B using decanthiol **53** (116.6 mg, 0.669 mmol, 1.0 eq.) with a milling time of either 6 or 12 min. Column chromatography (SiO_2, *Isolera One*™ 10%–80% EtOAc) afforded the title compound as a colorless oil.

Yield: 66.9 mg (0.19 mmol, 58%, Procedure B).

R_f = 0.60 (^{c}Hex).

ESI-LCMS: *m/z* = 369.0 [M+Na]$^+$.

IR (ATR): $\tilde{\nu}$ [cm^{-1}] = 2922, 2852, 1463, 1377, 721.

^{1}H-NMR, COSY (300 MHz, $CDCl_3$): δ [ppm] = 2.69–2.66 (m, 4H, CH_2S), 1.69–1.64 (m, 4H, 2-H), 1.42–1.35 (m, 4H), 1.32–1.24 (m, 24H), 0.88 (t, J = 7.0 Hz, 6H, 10-H)

^{13}C-NMR, HSQC, HMBC (151 MHz, $CDCl_3$): δ [ppm] = 39.3 (CH_2S), 32.0, 29.7, 29.7, 29.5, 29.4, 29.4, 28.7, 22.8, 14.3 (CH_3).

Further Side Products

Bis(benzothiazol-2-yl)sulfide (30c)

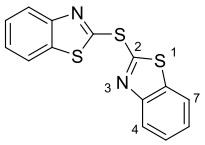

Following the general procedure A using 2-mercaptobenzothiazole **30** (37.6 mg, 0.23 mmol, 1.0 eq.). After 14 h, column chromatography (SiO_2, *Isolera One*™ 0%–80% EtOAc) afforded the title compound as a slightly yellow solid.

Yield: 40.2 mg (0.01 mmol, 54%).

R_f = 0.60 (^{c}Hex:EtOAc= 3:1).

ESI-LCMS: *m/z*= 301.0 $[M+H]^+$.

Mp: 99.0–99.8 °C (Lit.:[42]101–102 °C).

IR (ATR): $\tilde{\nu}$ [cm^{-1}] = 3061, 1471, 1450, 1427, 1410, 1238, 1026, 1010, 990, 754, 727.

^{1}H-NMR, COSY (300 MHz, $CDCl_3$): δ [ppm] = 8.08–8.02 (m, 2H, 4-H), 7.88–7.81 (m, 2H, 7-H), 7.52 (ddd, *J* = 8.3, 7.3, 1.3 Hz, 2H, 5-H), 7.42 (ddd, *J* = 8.4, 7.3, 1.3 Hz, 2H, 6-H).

^{13}C-NMR, HSQC, HMBC (75 MHz, $CDCl_3$): δ [ppm] = 160.0 (2-C), 152.9 (3a-C), 136.6 (7a-C), 126.6 (5-C), 125.7 (6-C), 123.0 (4-C), 121.2 (7-C).

The obtained data are in accordance with the literature.[41, 42]

Benzo[d]oxazol-2-amine (31b)

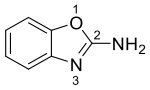

Following the general procedure A using 2-mercaptobenzoxazol **31** (34.0 mg, 0.23 mmol, 1 eq.). After 14 h, column chromatography (SiO_2, *Isolera One*™ 10%–80% EtOAc) afforded the title compound as a colorless oil.

Yield: 5.2 mg (0.04 mmol, 17%).

R_f = 0.10 (^{c}Hex:EtOAc = 2:1).

ESI-LCMS: *m/z* = 135.1 $[M+H]^+$.

^{1}H-NMR, COSY (300 MHz, $CDCl_3$): δ [ppm] = 7.39–7.33 (m, 1H, 7-H), 7.31–7.27 (m, 1H, 4-H), 7.20 (td, *J* = 7.7, 1.2 Hz, 1H, 6-H), 7.10 (td, *J* = 7.7, 1.3 Hz, 1H, 5-H), 4.87 (bs, 2H, NH_2).

^{13}C-NMR, HSQC, HMBC (75 MHz, $CDCl_3$): δ [ppm] = 161.2 (*C*NH_2), 148.0 (3a-C), 139.8 (7a-C), 124.7 (6-C), 122.2 (5-C), 116.0 (7-C), 109.5 (4-C).

The obtained data are in accordance with the literature.[47]

Bis(benzoxazol-2-yl)sulfide (31c)

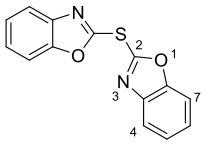

Following the general procedure A using 2-mercaptobenzoxazole **31** (67.9 mg, 0.5 mmol, 1.0 eq.) and $K_3[FeCN_6]$ (444.5 mg, 1.50 mmol, 3.0 eq.) in 1.36 mL solvent mixture. After 18 h, column chromatography (SiO_2, *Isolera One*™ 0%–80% EtOAc) afforded the title compound as a colorless solid. General procedure B was alternatively applied with a reaction time of 6 min.

Yield: 18.2 mg (0.07 mmol,15%, procedure A), 29.7 mg (0.11 mmol, 33%, procedure B).

R_f = 0.70 (^{c}Hex:EtOAc = 1:1).

ESI-LCMS: *m/z* = 269.0 $[M+H]^+$.

Mp: 121.3–124.6 °C (Lit.:[48] 132–133 °C).

IR (ATR): $\tilde{\nu}$ [cm^{-1}] = 1815, 1496, 1447, 1321, 1239, 1119, 1089, 929, 803, 742.

^{1}H-NMR, COSY (300 MHz, $CDCl_3$): δ [ppm] = 7.81–7.69 (m, 2H, 4-H), 7.59–7.49 (m, 2H, 7-H), 7.45–7.33 (m, 4H, 5-H, 6-H).

^{13}C-NMR, HSQC, HMBC (75 MHz, $CDCl_3$): δ [ppm] = 155.4 (2-C), 152.5 (7a-C), 141.8 (3a-C), 126.0 (6-C), 125.1 (5-C), 120.3 (4-C), 110.9 (7-C).

The obtained data are in accordance with the literature.[48]

Methyl-2-acetamidoacrylate (40b)

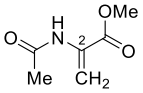

Following the general procedure A using *N*-acetyl-L-cysteine methyl ester **40** (40.7 mg, 0.23 mmol, 1.0 eq.). After 20 h, column chromatography (SiO_2, ^{c}Hex:EtOAc = 1:1) afforded the title compound as a colorless solid.

Yield: 3.1 mg (0.02 mmol, 10%).

R_f = 0.48 (^{c}Hex:EtOAc = 1:1).

ESI-LCMS: *m/z* = 144.1 $[M+H]^+$.

ESI-HRMS ($C_6H_{10}NO_3$ $[M+H]^+$): calculated: *m/z* = 144.0659;

found: *m/z* = 144.0655.

IR (ATR): $\tilde{\nu}$ [cm^{-1}] = 3364, 1728, 1676, 1635, 1515, 1440, 1371, 1324, 1202, 1171, 995, 902.

^{1}H-NMR, COSY (300 MHz, $CDCl_3$): δ [ppm] = 7.72 (bs, 1H, N*H*), 6.60 (s_{app}, 1H, C$H_{2,a}$), 5.88 (d, *J* = 1.5 Hz, 1H, C$H_{2,b}$), 3.85 (s, 3H, OCH_3), 2.13 (s, 3H, CH_3).

^{13}C-NMR, HSQC, HMBC (75 MHz, $CDCl_3$): δ [ppm] = 168.8 (CH_3*C*ONH), 164.6 (*C*OOCH_3), 130.8 (2-C), 108.7 (*C*H_2), 53.0 (COO*C*H_3), 24.7 (*C*H_3CONH).

The obtained data are in accordance with the literature.[49]

***p*-Anisyl alcohol (45c)**

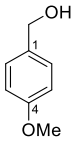

Following the general procedure A using (4-methoxyphenyl)methanethiol **45** (69.3 mg, 0.50 mmol, 1.0 eq.) and $K_3[FeCN_6]$ (494 mg, 1.50 mmol, 3.0 eq.) in 1.36 mL solvent mixture. After 42 h, column chromatography (SiO_2, *Isolera One*™ 0%–80% EtOAc) afforded the title compound as a colorless oil.

Yield: 16.9 mg (0.12 mmol, 27%).

***R*$_f$** = 0.08 (^{c}Hex:EtOAc = 10:1).

GC-MS: *m* = 138.0 [M].

IR (ATR): $\tilde{\nu}$ [cm^{-1}] = 3343, 1612, 1512, 1463, 1302, 1245, 1174, 1032, 816, 572.

^{1}H-NMR, COSY (300 MHz, $CDCl_3$): δ [ppm] = 7.32–7.26 (m, 2H, 2-H, 6-H), 6.92–6.85 (m, 2H, 3-H, 5-H), 4.60 (s, 2H, CH_2), 3.81 (s, 3H, OCH_3).

^{13}C-NMR, HSQC, HMBC (75 MHz, $CDCl_3$): δ [ppm] = 159.2 (4-C), 133.1 (1-C), 128.7 (2-C, 6-C), 113.9 (3-C, 5-C), 65.0 (*C*H_2), 55.3 (O*C*H_3).

The obtained data are in accordance with the literature.[50]

Crystallographic Data

For psammaplin B (**1**), an X-ray molecular structure was obtained. Supplementary crystallographic data for this publication is contained in CCDC 2206744. These data are provided free of charge by The Cambridge Crystallographic Data Centre.

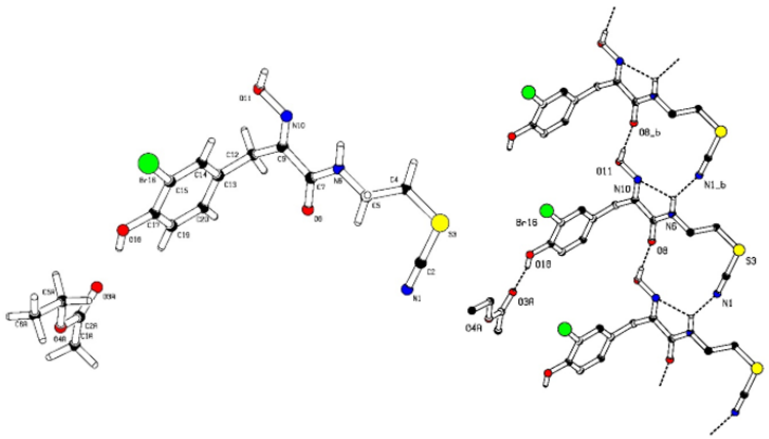

Figure F2: Molecular crystallographic structure of compound **1** at 120 K (C: black, O: red, N: blue, S: yellow, Br: green).

Table 3: Crystal structure determination of compound **1**.

Crystal data:

Sum formular	$C_{16}H_{20}BrN_3O_5S$
Molecular formular	$C_{12}H_{12}BrN_3O_3S$, $C_4H_8O_2$
Molar mass	446.32 g mol^{-1}
Temperature	120 K
Wavelength	0.71073Å, MoKα
Diffractometer	STOE IPDS 2T
Crystal system	Monoclinic
Space group	P $2_1/c$
Habitus	Colorless plate
Crystal size	0.030 x 0.230 x 0.570 mm^3
Lattice constants (from 13589 reflections with 2.70° <=Θ<= 28.31°)	*a* = 19.9760(12), α = 90°
	b = 6.7233(3) Å, β = 100.337(5)°
	c = 14.7489(10) Å, γ = 90°
	V = 1948.7(2) $Å^3$
	F(000) = 912
Density (calculated)	1.521 Mg/m^3
Absorption coefficient	2.248 mm^{-1}

Data collection:

Wavelength, radiation	0.71073Å, MoKα
Diffractometer	STOE IPDS 2T
Scan width	2.813–28.017°.
Scan range	−19<=*h*<=26,
	−8<=*k*<=8,
	−19<=*l*<=19
Measured reflections	9405
Independent reflections	4610 [R_{int} = 0.0253]
Observed reflections	3789 [I>2σ(I)]
Integrity at Θ_{max}= 25.2°	99.2%

Data correction, structure solution and refinement:

Absorption correction	Integration
Refinement	Full-matrix least-squares on F^2
Reflexes/Restraints/Parameters	4610/0/286
Goodness on fit for F^2	1.134
Final R values [I>2σ(I)]	R1 = 0.0437, *w*R_2 = 0.0869
R value (all data)	R_1 = 0.0619, *w*R_2 = 0.0966
Fourier synthesis	0.646 and -0.439 eÅ^{-3}
Annotation	H-Atoms partly isotropically refined

References

1. H. E. Gottlieb, V. Kotlyar and A. Nudelman, *J. Org. Chem.*, 1997, **62**, 7512-7515.
2. G. Lippke and H. Thaler, *Starch-Stärke*, 1970, **22**, 344-351.
3. C. Grundke and T. Opatz, *Green Chem.*, 2019, **21**, 2362-2366.
4. V. Merz and W. Weith, *Ber. Dtsch. Chem. Ges.*, 1877, **10**, 746-765.
5. A. M. Nauth, T. Konrad, Z. Papadopulu, N. Vierengel, B. Lipp and T. Opatz, *Green Chem.*, 2018, **20**, 4217-4223.
6. S. Pechenyuk, D. Domonov, A. Shimkin and Y. V. Ivanov, *Russ. Chem. Bull.*, 2015, **64**, 322-328.
7. C. Bolm, R. Mocci, C. Schumacher, M. Turberg, F. Puccetti and J. G. Hernández, *Angew. Chem.*, 2018, **130**, 2447-2450.
8. B. Zeynizadeh, *J. Chem. Res.*, 2002, **2002**, 564-566.
9. F. Rajabi, T. Kakeshpour and M. R. Saidi, *Catal. Commun.*, 2013, **40**, 13-17.
10. R. Frei, T. Courant, M. D. Wodrich and J. Waser, *Chem. Eur. J.*, 2015, **21**, 2662-2668.
11. P. Zhou, C. Chen and S. Li, *J. Chem. Res.*, 2020, **44**, 376-380.
12. F. Friedrich and R. Pohloudek-Fabini, *Arch. Pharm. Ber. Dtsch. Pharm. Ges.*, 1965, **298**, 162-175.
13. F. Teng, J.-T. Yu, H. Yang, Y. Jiang and J. Cheng, *Chem. Commun. (Cambridge, U. K.)*, 2014, **50**, 12139-12141.
14. F. Leonard and A. Wajngurt, *J. Org. Chem.*, 1956, **21**, 1077-1081.
15. R. E. Koeppe and J. L. Wood, *J. Am. Chem. Soc.*, 1953, **75**, 4655-4657.
16. W. Guo, W. Tan, M. Zhao, L. Zheng, K. Tao, D. Chen and X. Fan, *J. Org. Chem.*, 2018, **83**, 6580-6588.
17. M. Hosseini-Sarvari and M. Tavakolian, *J. Chem. Res.*, 2008, **2008**, 318-321.
18. F. Zhu, E. Miller, S.-q. Zhang, D. Yi, S. O'Neill, X. Hong and M. A. Walczak, *J. Am. Chem. Soc.*, 2018, **140**, 18140-18150.
19. X.-B. Li, Z.-J. Li, Y.-J. Gao, Q.-Y. Meng, S. Yu, R. G. Weiss, C.-H. Tung and L.-Z. Wu, *Angew. Chem. Int. Ed.*, 2014, **53**, 2085-2089.
20. H. Jiang, W. Yu, X. Tang, J. Li and W. Wu, *J. Org. Chem.*, 2017, **82**, 9312-9320.
21. P. Sharma, A. Kumar, P. Kumari, J. Singh and M. P. Kaushik, *Med. Chem. Res.*, 2012, **21**, 1136-1148.
22. M. Singh, L. Dhar S. Yadav and R. Krishna Pal Singh, *Tetrahedron Lett.*, 2020, **61**, 151700.
23. F. Jackson and A. T. Peters, *J. Chem. Soc. C Org.*, 1969, 268-272.
24. M. Karle, W. Knecht and Y. Xue, *Bioorg. Med. Chem. Lett.*, 2012, **22**, 4839-4843.
25. Y. Chen, H. Qi, N. Chen, D. Ren, J. Xu and Z. Yang, *J. Org. Chem.*, 2019, **84**, 9044-9050.
26. *DPMA, Germany Pat.*, 1963.
27. A. Miyashita, I. Nagasaki, A. Kawano, Y. Suzuki, K.-i. Iwamoto and T. Higashino, *Heterocycles*, 1997, **4**, 745-755.
28. K. Pilgram and D. D. Phillips, *J. Org. Chem.*, 1965, **30**, 2388-2392.
29. L. A. Spurlock, R. K. Porter and W. G. Cox, *J. Org. Chem.*, 1972, **37**, 1162-1168.
30. H. Meshram, P. B. Thakur, B. M. Babu and V. M. Bangade, *Tetrahedron Lett.*, 2012, **53**, 1780-1785.
31. L. KumaráPandey and V. Malladi, *Green Chem.*, 2011, **13**, 1648-1651.
32. R. Xuan, W. Hu and Z. Yang, *Synth. Commun.*, 2003, **33**, 1109-1112.
33. S. Vorona, T. Artamonova, Y. Zevatskii and L. Myznikov, *Synthesis*, 2014, **46**, 781-786.
34. A. M. Godert, N. Angelino, A. Woloszynska-Read, S. R. Morey, S. R. James, A. R. Karpf and J. R. Sufrin, *Bioorg. Med. Chem. Lett.*, 2006, **16**, 3330-3333.
35. N. Spiliopoulou and C. G. Kokotos, *Green Chem.*, 2021, **23**, 546-551.
36. X. Li, J. Du, Y. Zhang, H. Chang, W. Gao and W. Wei, *Org. Biomol. Chem.*, 2019, **17**, 3048-3055.
37. R. Rahaman and P. Barman, *Eur. J. Org. Chem.*, 2017, **2017**, 6327-6334.

38. Y. Dou, X. Huang, H. Wang, L. Yang, H. Li, B. Yuan and G. Yang, *Green Chem.*, 2017, **19**, 2491-2495.
39. J. Zhang, L. Hu, Y. Liu, Y. Zhang, X. Chen, Y. Luo, Y. Peng, S. Han and B. Pan, *J. Org. Chem.*, 2021, **86**, 14485-14492.
40. M. Zohrevandi, R. Mozafari and M. Ghadermazi, *RSC Adv.*, 2021, **11**, 14717-14729.
41. P. J. Chai, Y. S. Li and C. X. Tan, *Chin. Chem. Lett.*, 2011, **22**, 1403-1406.
42. B. V. Varun and K. R. Prabhu, *J. Org. Chem.*, 2014, **79**, 9655-9668.
43. L. D. Small, *J. Pharm. Sci.*, 1976, **65**, 1692-1694.
44. L. Liu, B. Luo and C. Wang, *Eur. J. Org. Chem.*, 2021, **2021**, 5880-5883.
45. X. Lei, Y. Wang, E. Fan and Z. Sun, *Org. Lett.*, 2019, **21**, 1484-1487.
46. M. Oka, R. Kozako and H. Iida, *Synlett*, 2021, **32**, 1227-1230.
47. U. Kloeckner, N. M. Weckenmann and B. J. Nachtsheim, *Synlett*, 2012, **2012**, 97-100.
48. J. J. D'Amico and R. H. Campbell, *J. Org. Chem.*, 1967, **32**, 3196-3197.
49. Y. A. Lin, O. Boutureira, L. Lercher, B. Bhushan, R. S. Paton and B. G. Davis, *J. Am. Chem. Soc.*, 2013, **135**, 12156-12159.
50. G. Zhang, B. L. Scott and S. K. Hanson, *Angew. Chem. Int. Ed.*, 2012, **51**, 12102-12106.

^{1}H– and ^{13}C–NMR Spectra of Compounds

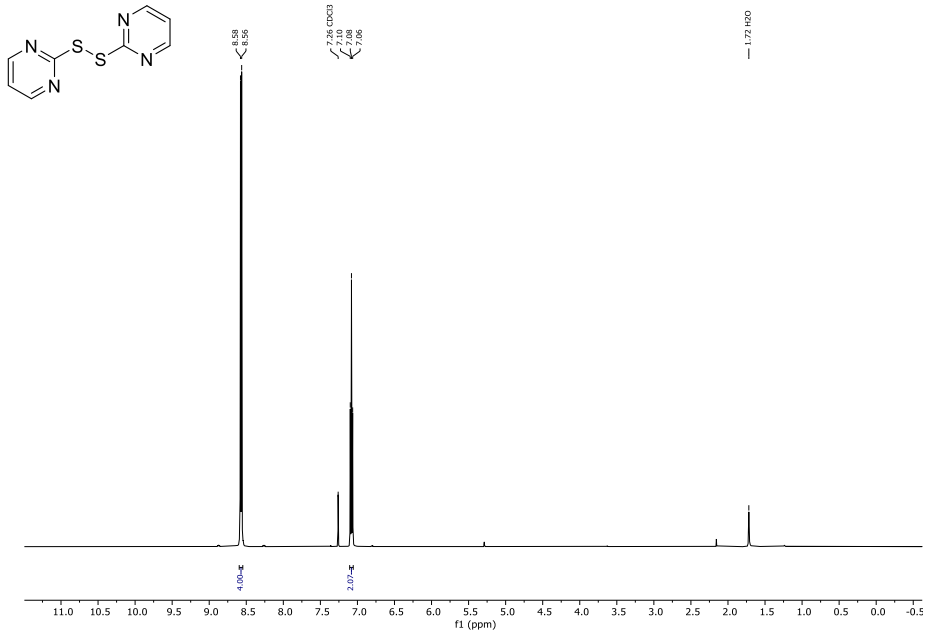

Figure F3: ^{1}H-NMR ($CDCl_3$, 300 MHz) of compound **15**.

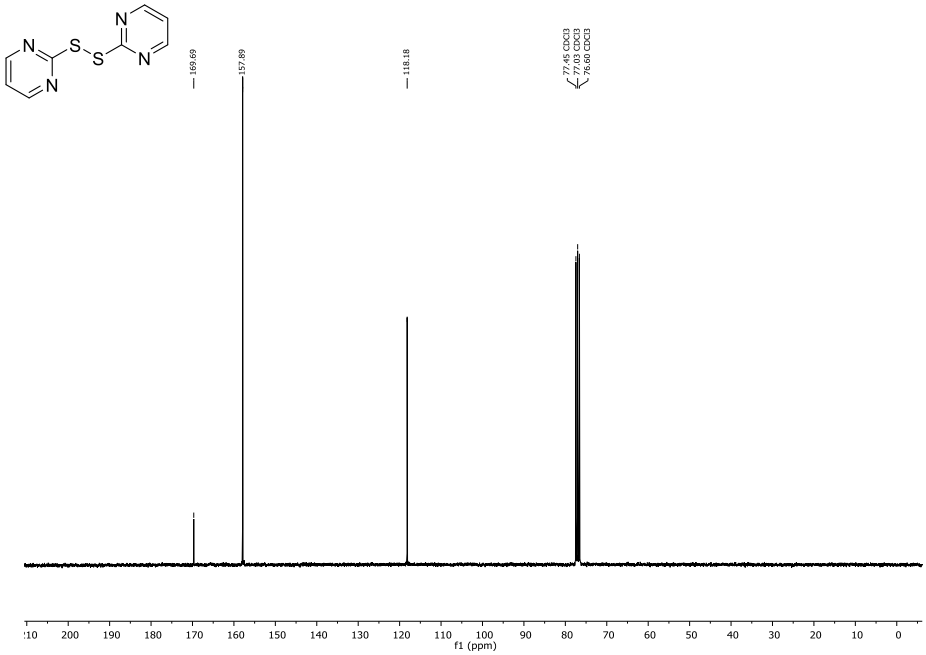

Figure F4: ^{13}C-NMR ($CDCl_3$, 75 MHz) of compound **15**.

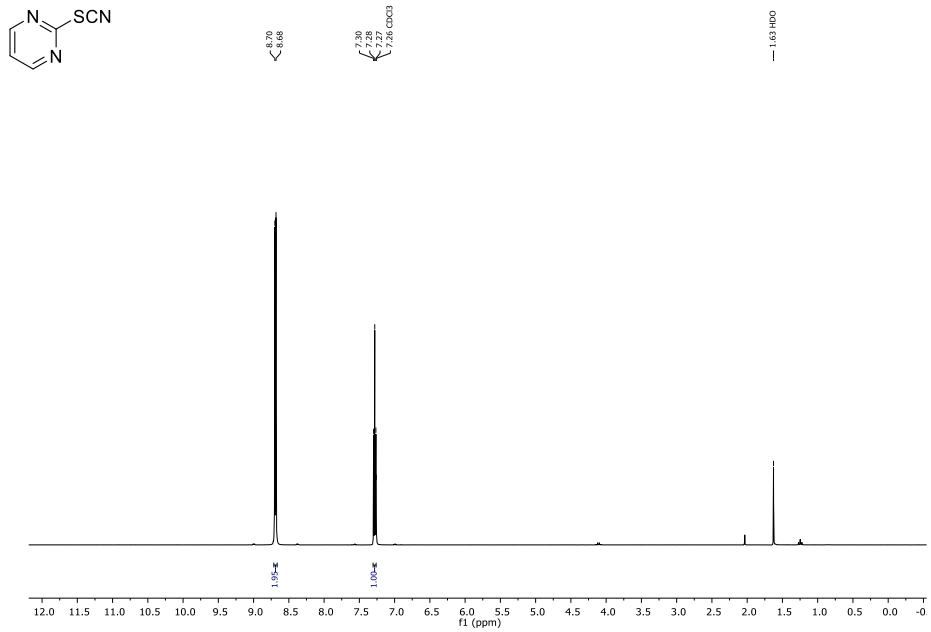

Figure F5: ^{1}H-NMR ($CDCl_3$, 300 MHz) of compound **16a**.

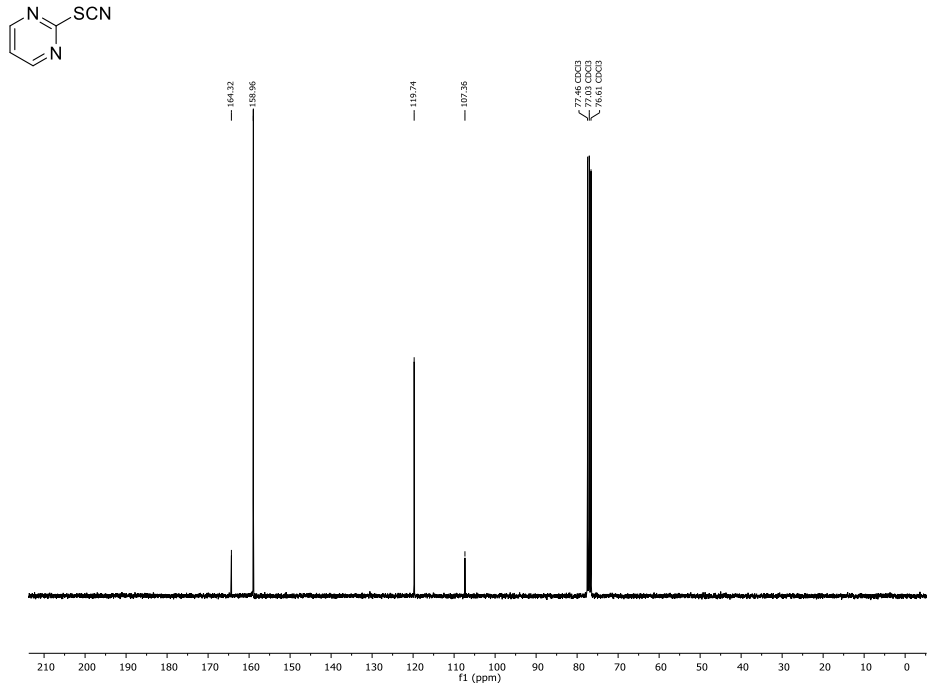

Figure F6: ^{13}C-NMR ($CDCl_3$, 75 MHz) of compound **16a**.

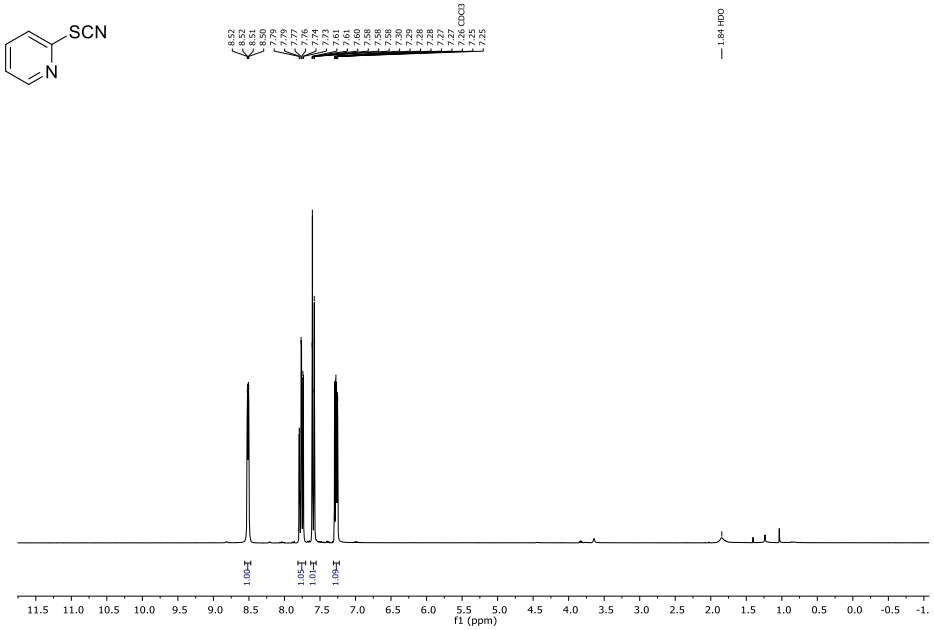

Figure F7: ^{1}H-NMR ($CDCl_3$, 300 MHz) of compound **17a**.

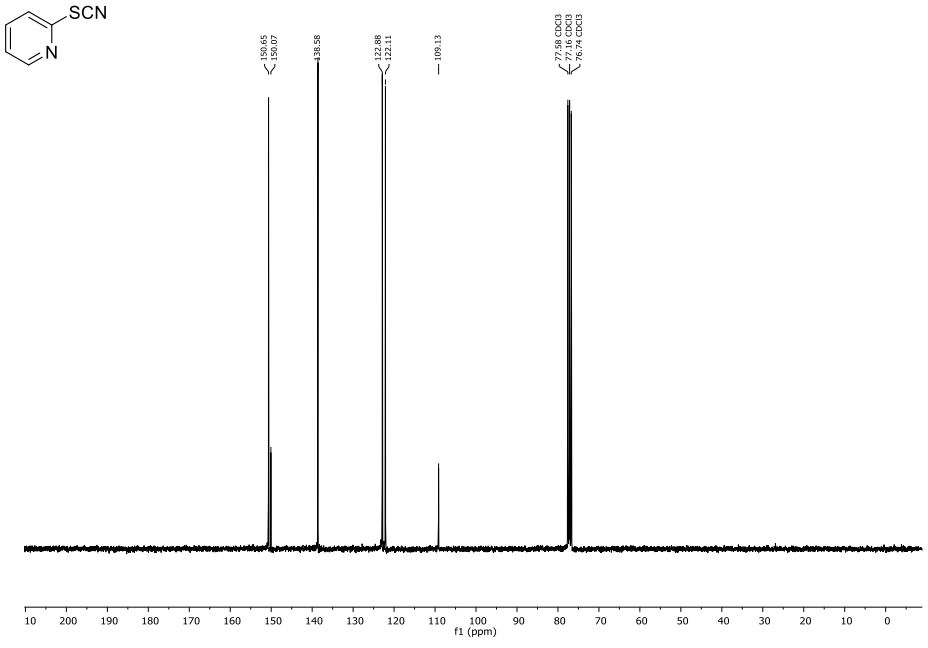

Figure F8: ^{13}C-NMR ($CDCl_3$, 75 MHz) of compound **17a**.

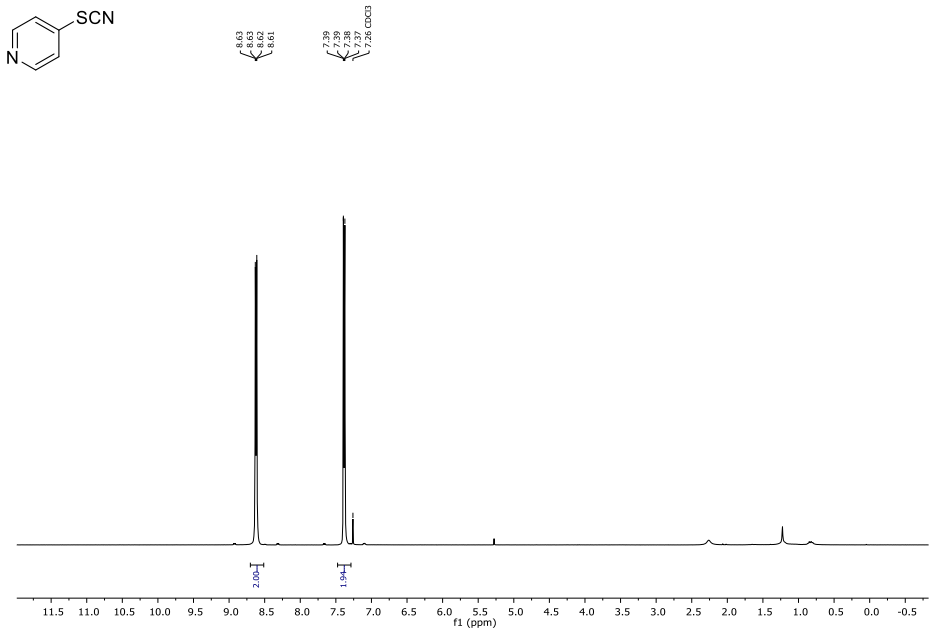

Figure F9: ^{1}H-NMR ($CDCl_3$, 300 MHz) of compound **18a**.

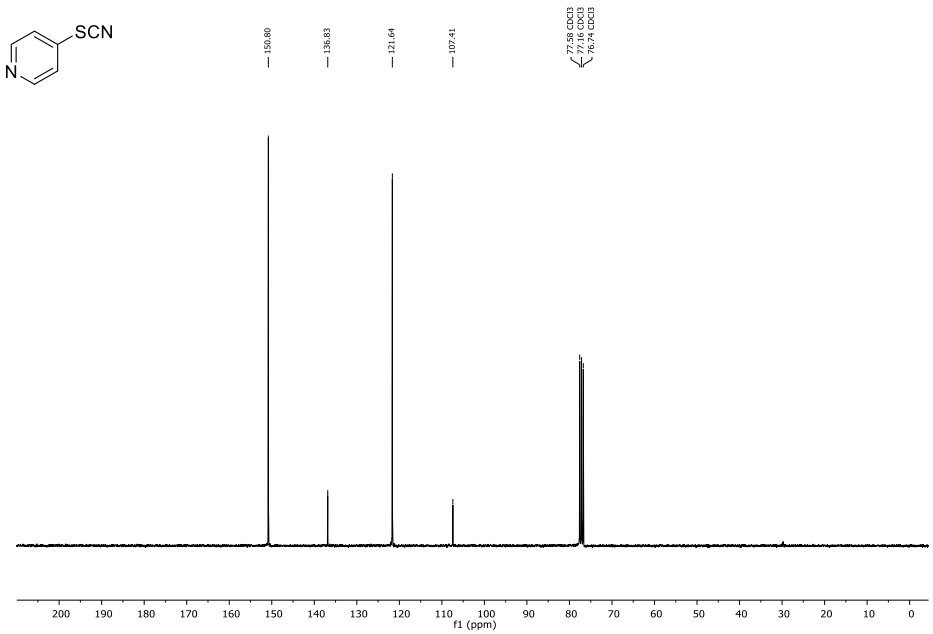

Figure F10: ^{13}C-NMR ($CDCl_3$, 75 MHz) of compound **18a**.

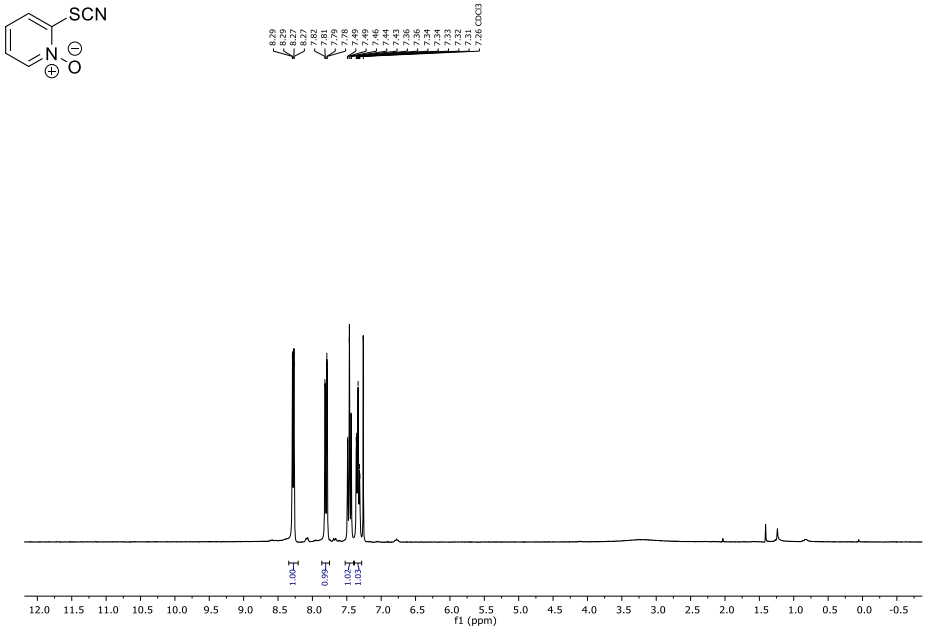

Figure F11: ^{1}H-NMR ($CDCl_3$, 300 MHz) of compound **19a**.

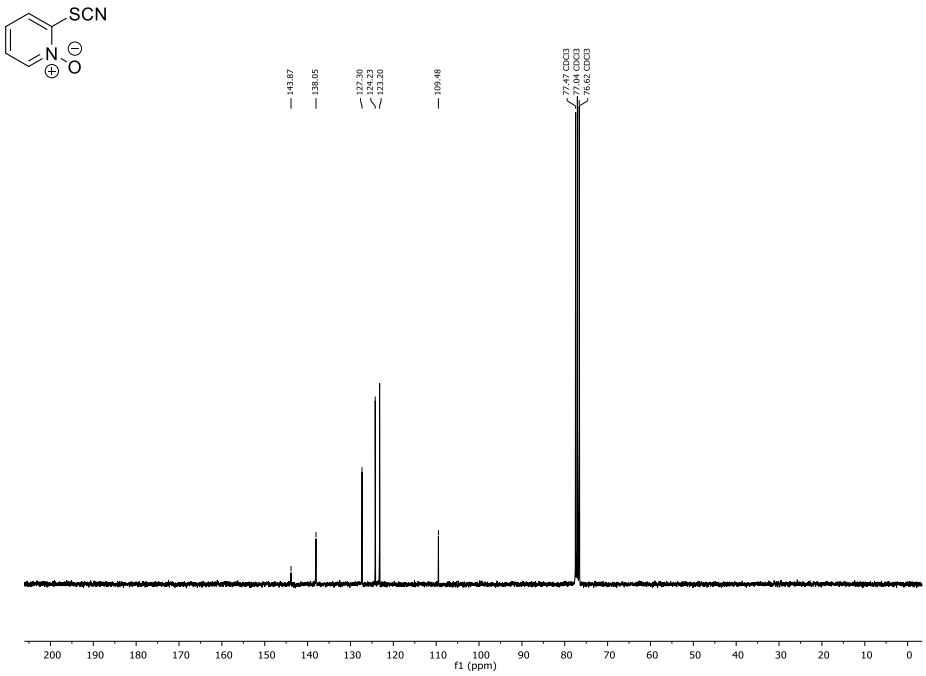

Figure F12: ^{13}C-NMR ($CDCl_3$, 75 MHz) of compound **19a**.

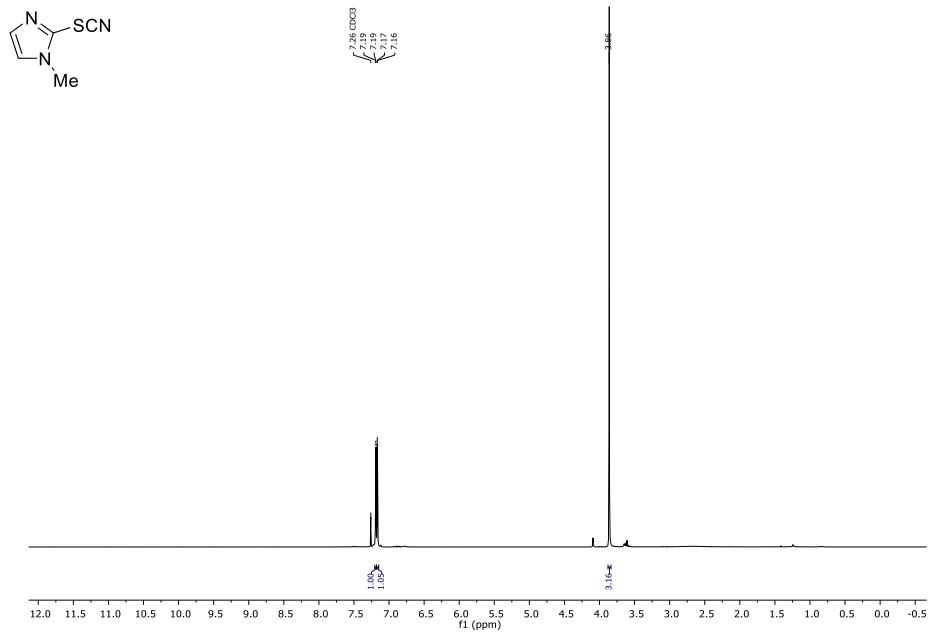

Figure F13: ^{1}H-NMR ($CDCl_3$, 300 MHz) of compound **20a**.

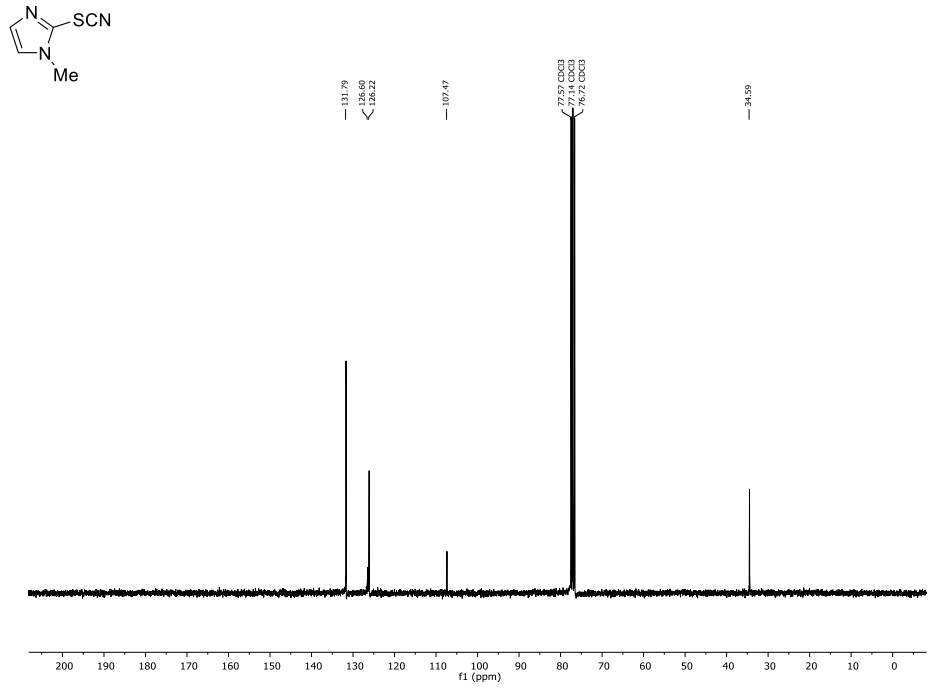

Figure F14: ^{13}C-NMR ($CDCl_3$, 75 MHz) of compound **20a**.

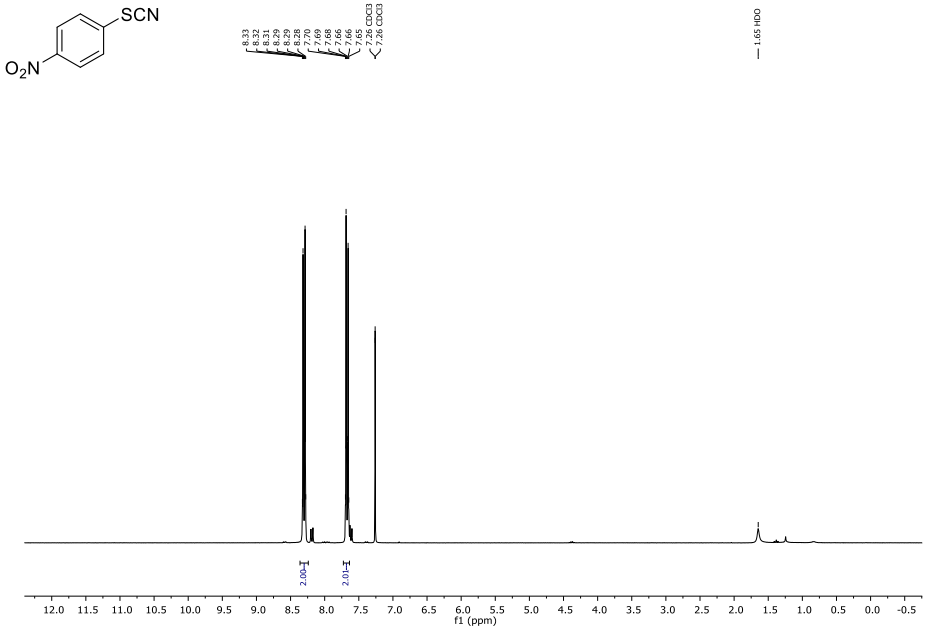

Figure F15: ^{1}H-NMR ($CDCl_3$, 300 MHz) of compound **21a**.

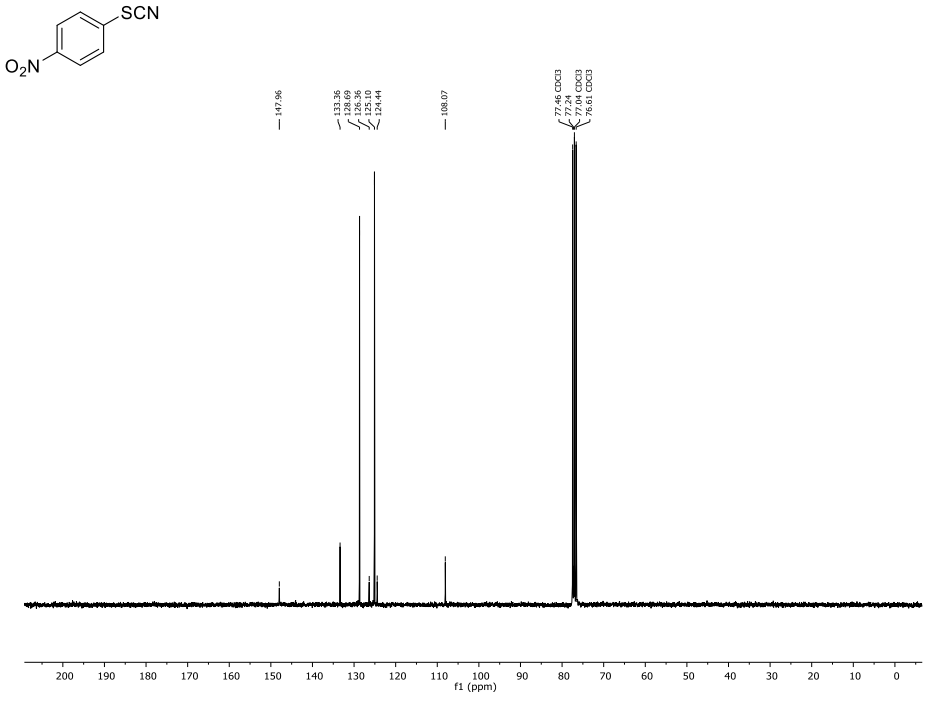

Figure F16: ^{13}C-NMR ($CDCl_3$, 75 MHz) of compound **21a**.

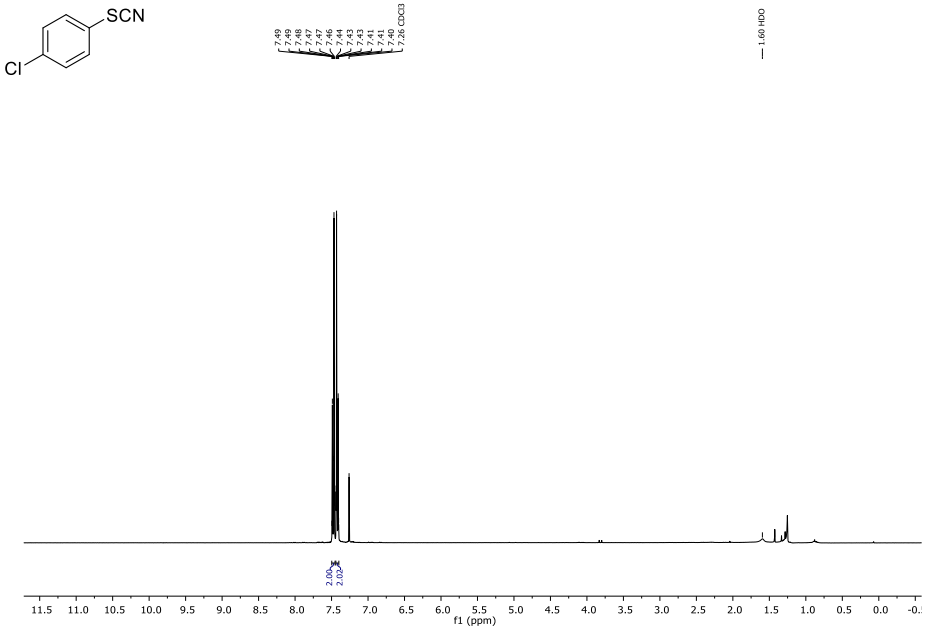

Figure F17: ^{1}H-NMR ($CDCl_3$, 400 MHz) of compound **22a**.

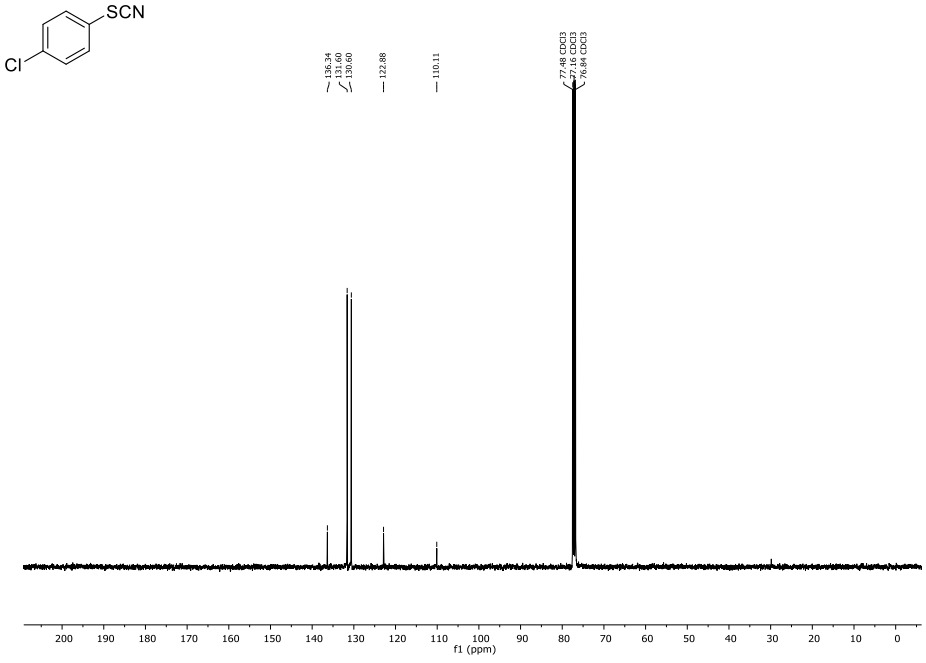

Figure F18: ^{13}C-NMR ($CDCl_3$, 101 MHz) of compound **22a**.

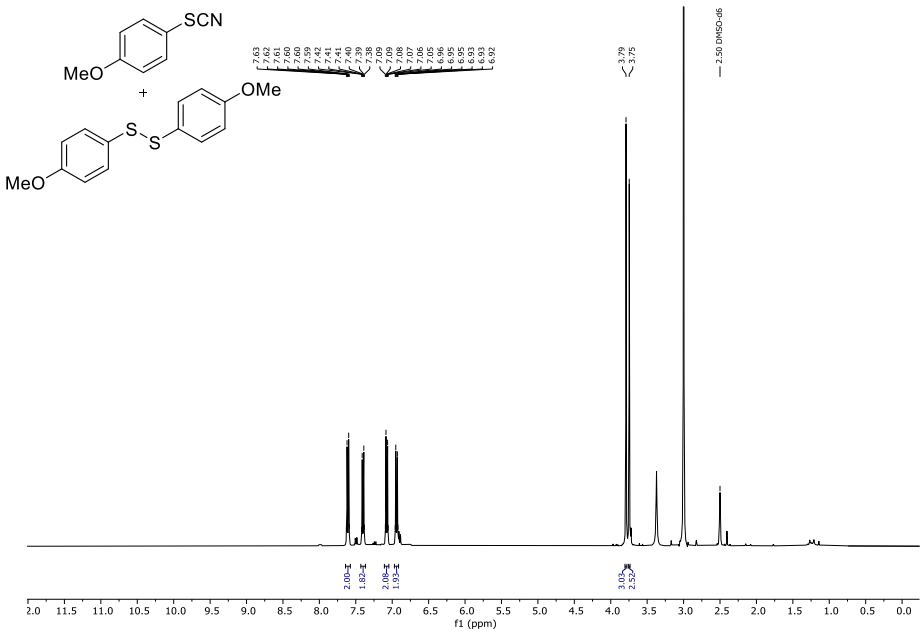

Figure F19: ^{1}H-NMR (DMSO-d_6, 300 MHz) of compound **23a**+**23b** with dimethylsulfone as internal standard.

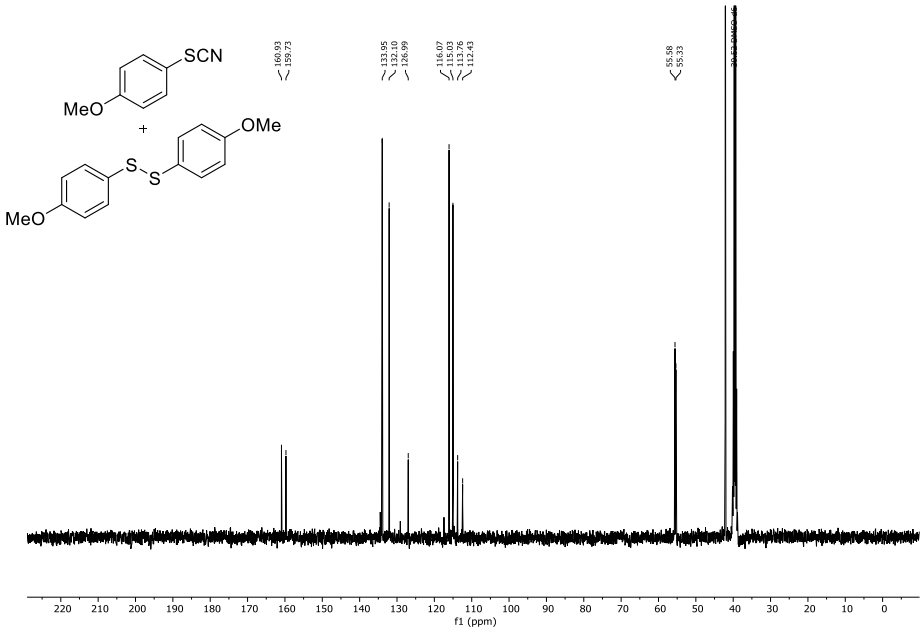

Figure F20: ^{13}C-NMR (DMSO-d_6, 75 MHz) of compound **23a**+**23b** with dimethylsulfone as internal standard.

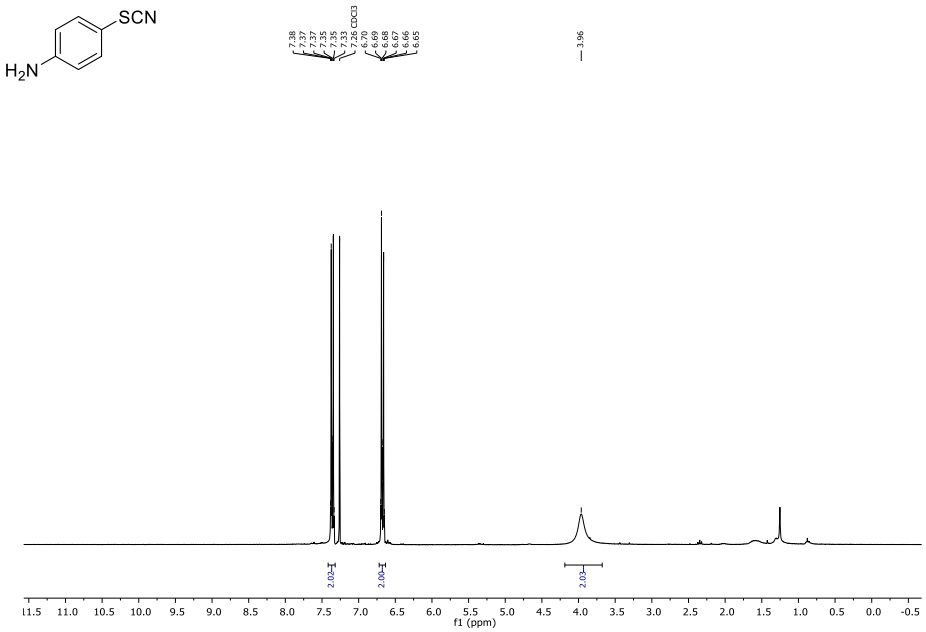

Figure F21: ^{1}H-NMR ($CDCl_3$, 300 MHz) of compound **25a**.

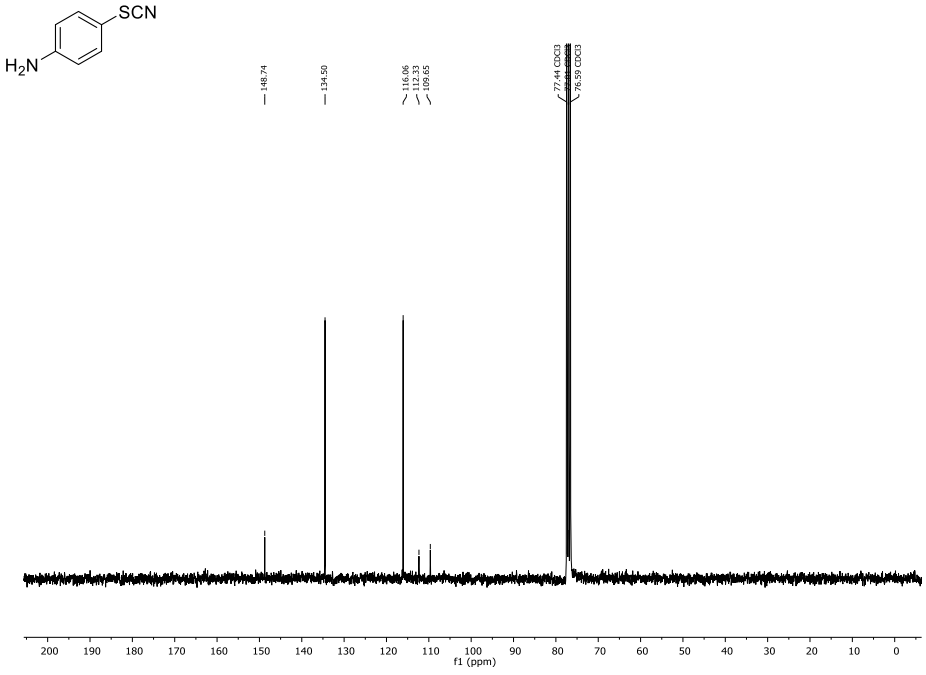

Figure F22: ^{13}C-NMR ($CDCl_3$, 75 MHz) of compound **25a**.

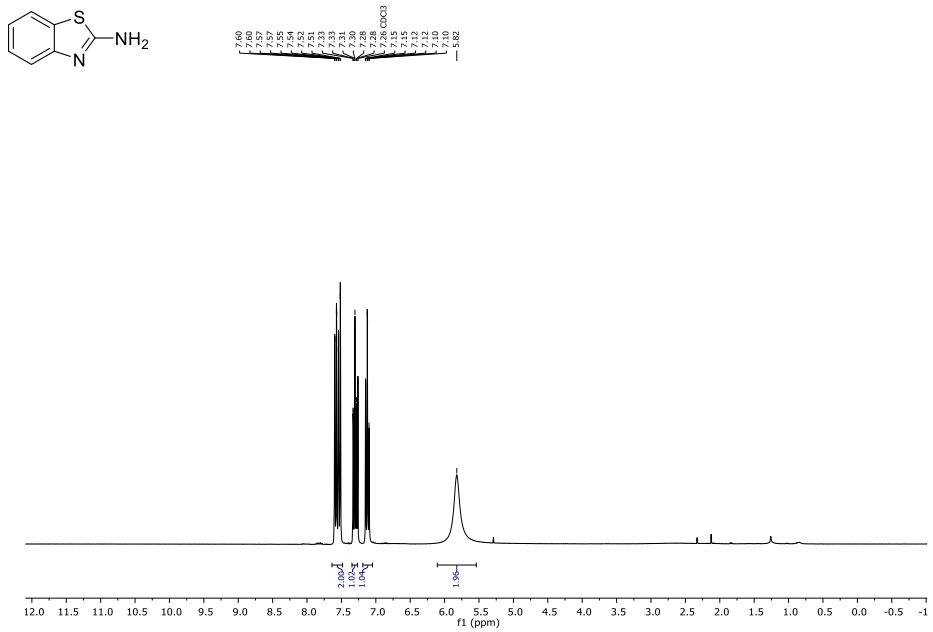

Figure F23: ^{1}H-NMR ($CDCl_3$, 300 MHz) of compound **26a**.

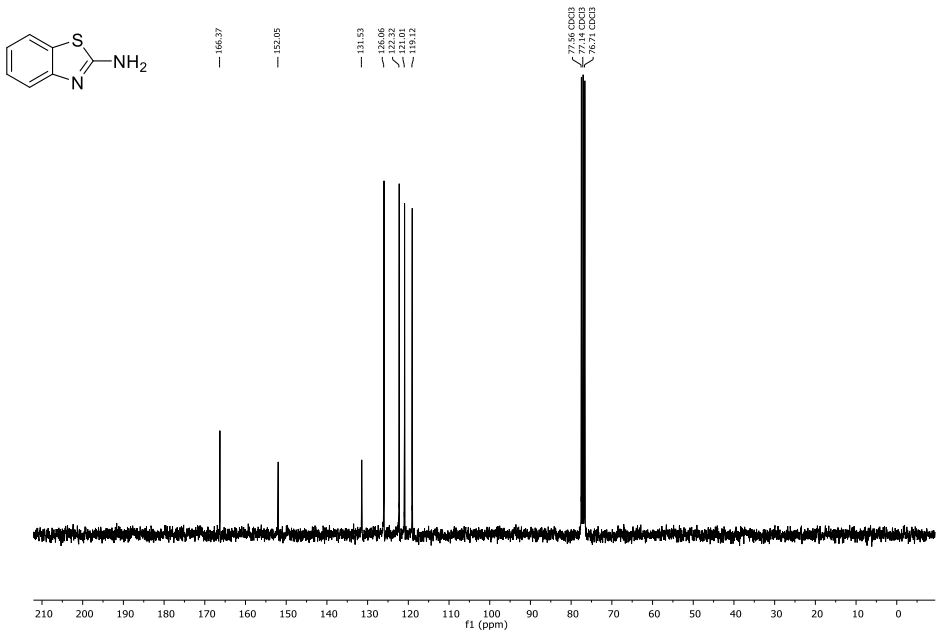

Figure F24: ^{13}C-NMR ($CDCl_3$, 75 MHz) of compound **26a**.

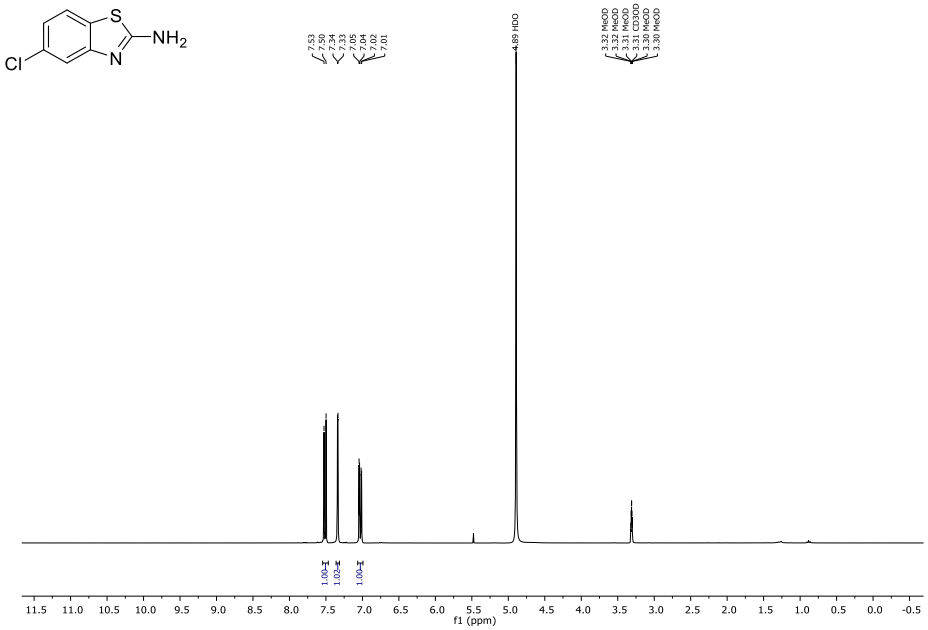

Figure F25: ^{1}H-NMR (MeOH-d_4, 300 MHz) of compound **27a**.

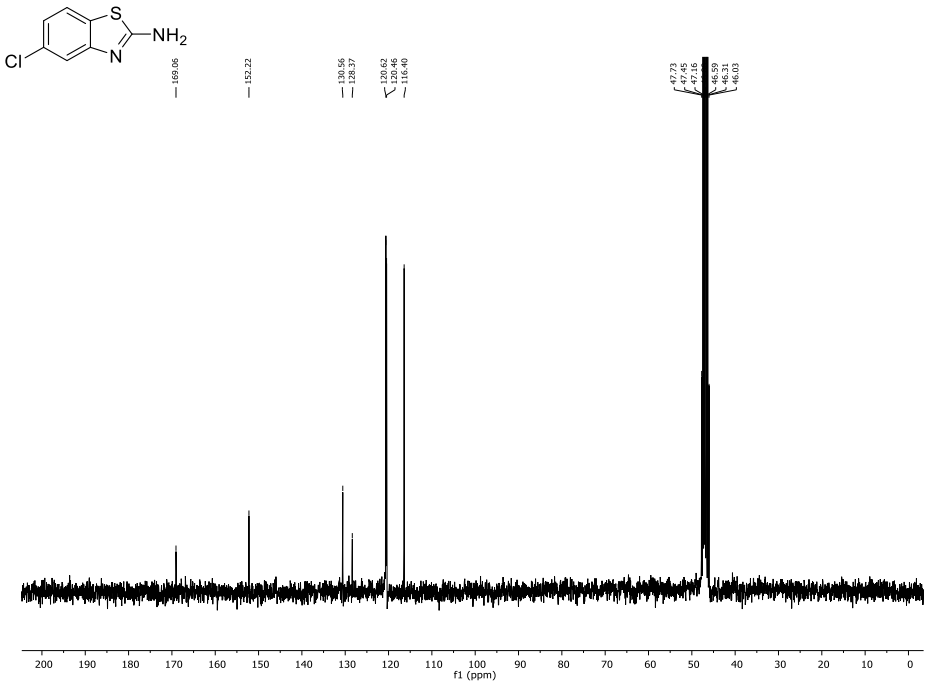

Figure F26: ^{13}C-NMR (MeOH-d_4, 75 MHz) of compound **27a**.

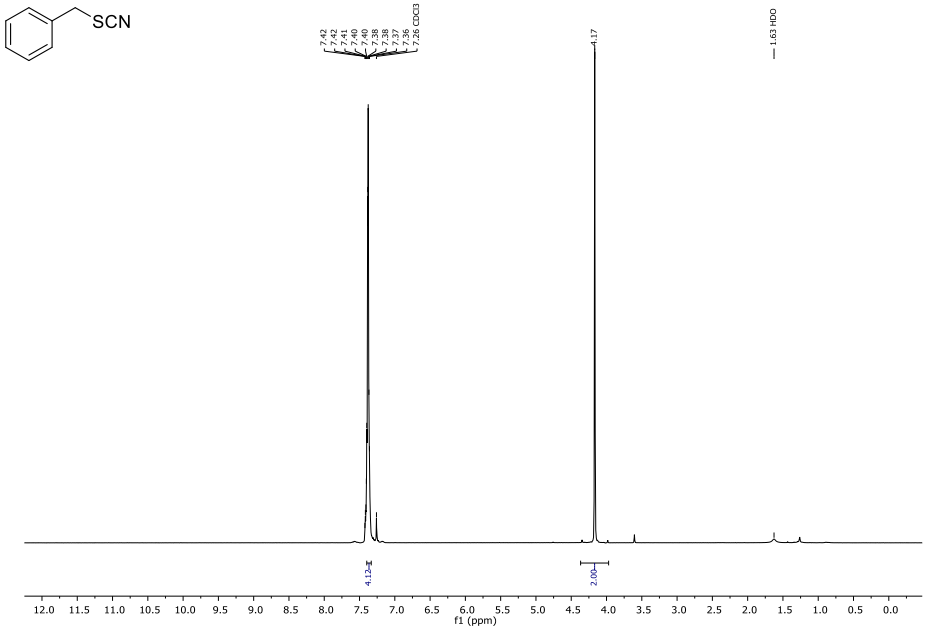

Figure F27: ^{1}H-NMR ($CDCl_3$, 400 MHz) of compound **28a**.

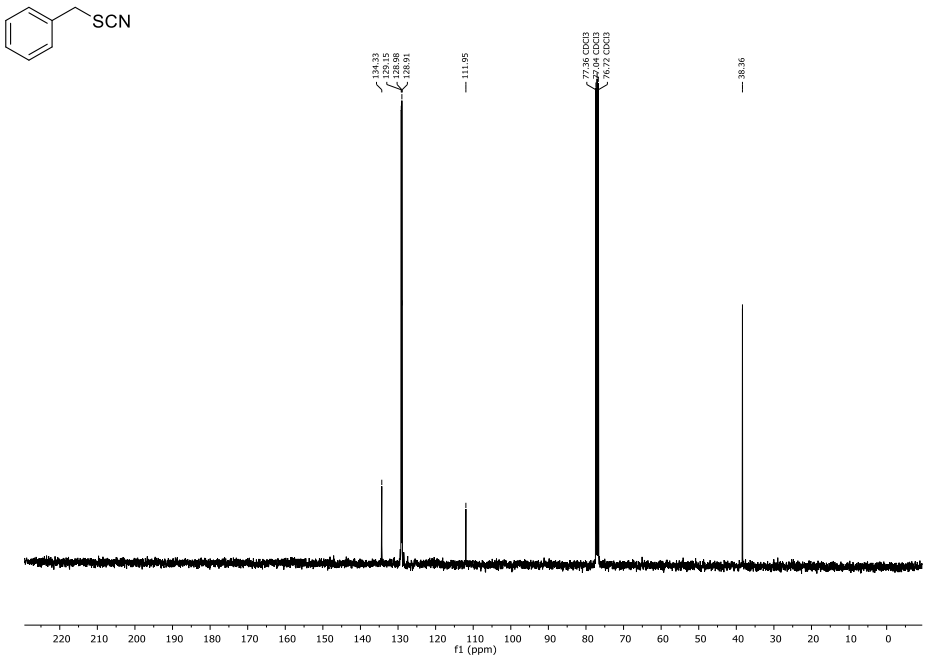

Figure F28: ^{13}C-NMR ($CDCl_3$, 101 MHz) of compound **28a**.

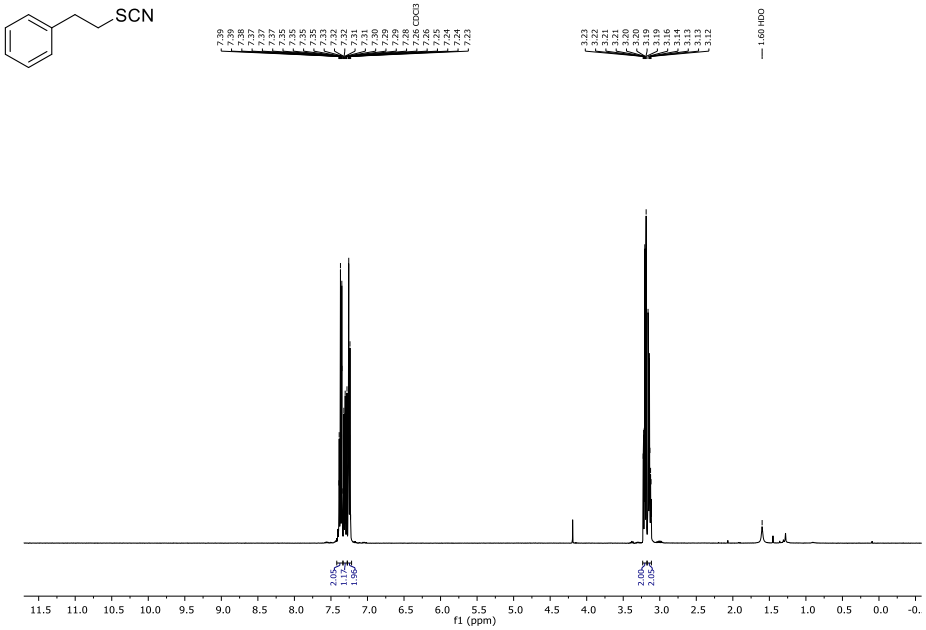

Figure F29: ^{1}H-NMR ($CDCl_3$, 400 MHz) of compound **29a**.

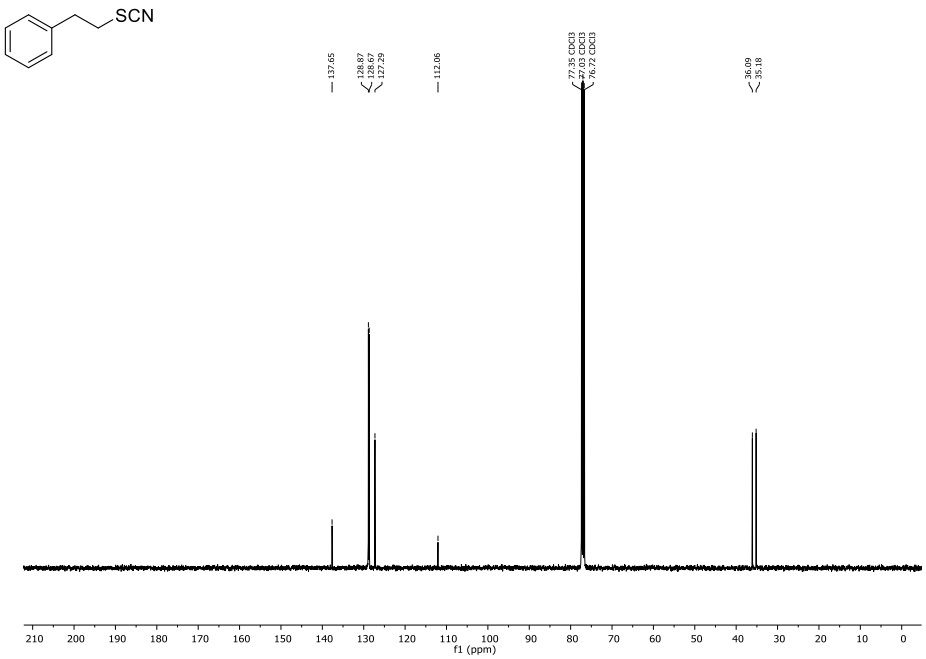

Figure F30: ^{13}C-NMR ($CDCl_3$, 101 MHz) of compound **29a**.

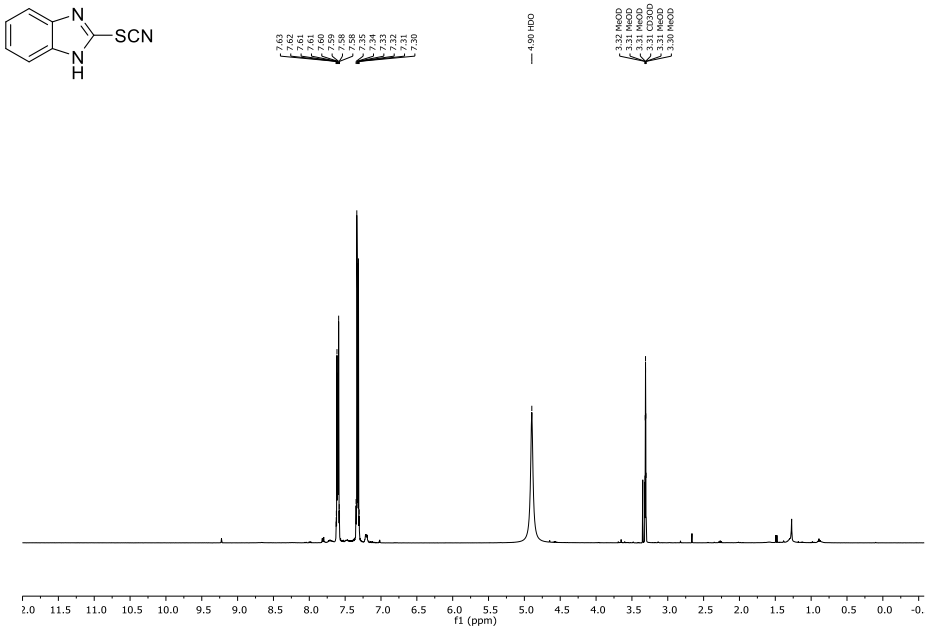

Figure F31: ^{1}H-NMR (MeOH-d_4, 400 MHz) of compound **32a**.

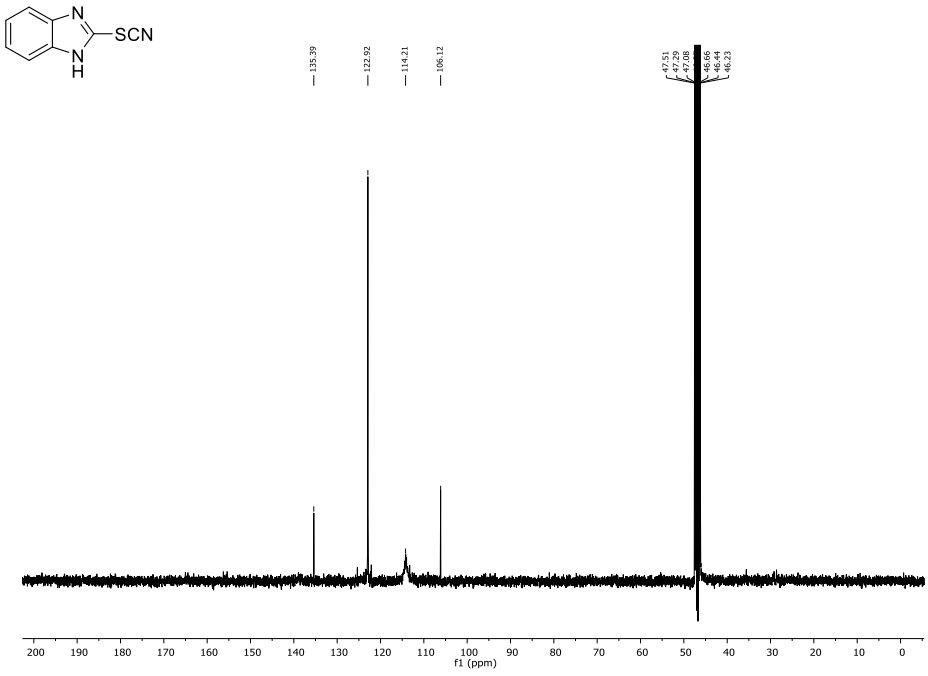

Figure F32: ^{13}C-NMR (MeOH-d_4, 101 MHz) of compound **32a**.

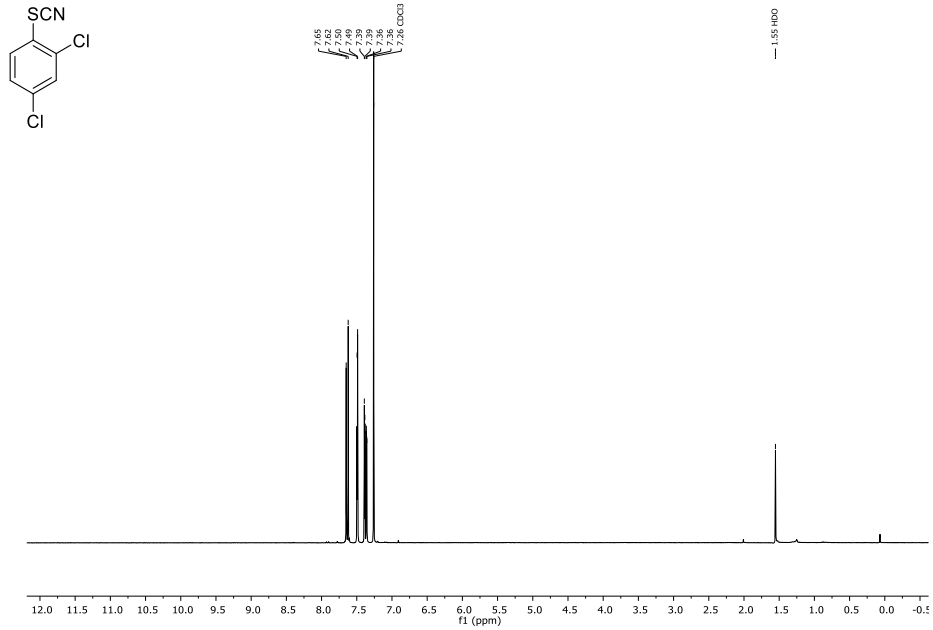

Figure F33: ^{1}H-NMR ($CDCl_3$, 300 MHz) of compound **33a**.

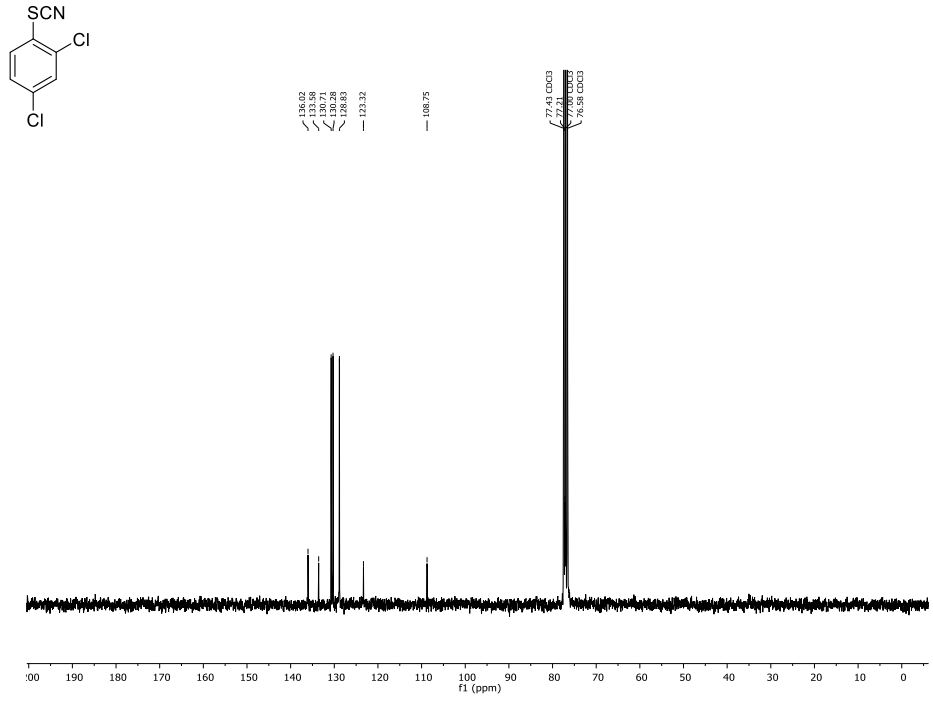

Figure F34: ^{13}C-NMR ($CDCl_3$, 75 MHz) of compound **33a**.

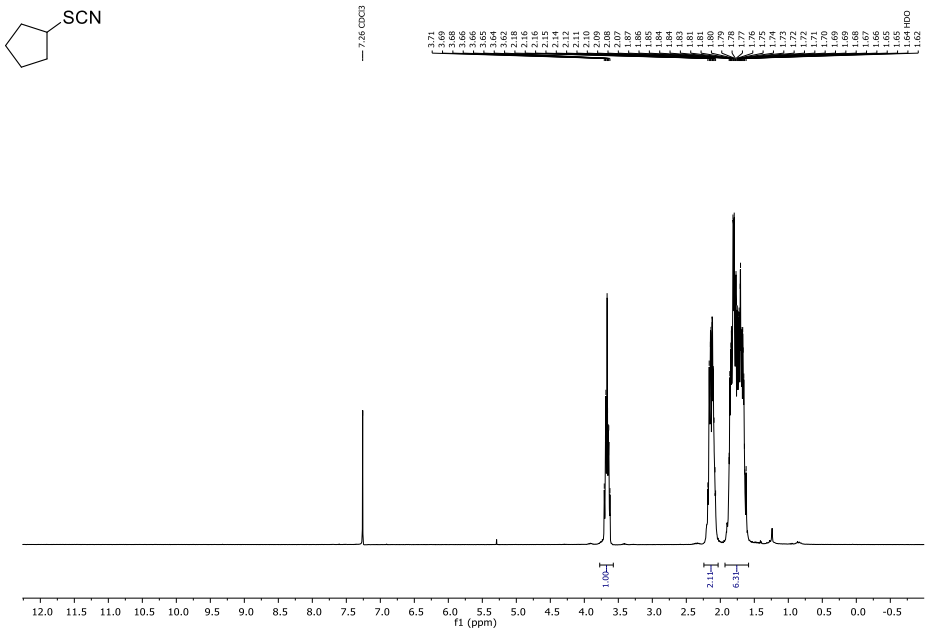

Figure F35: ^{1}H-NMR ($CDCl_3$, 300 MHz) of compound **34a**.

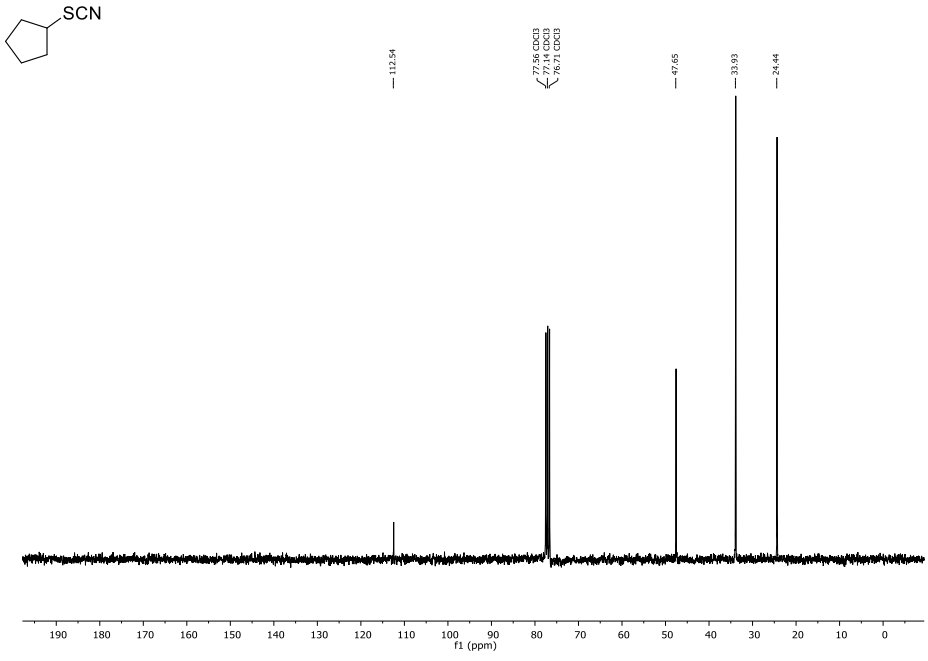

Figure F36: ^{13}C-NMR ($CDCl_3$, 75 MHz) of compound **34a**.

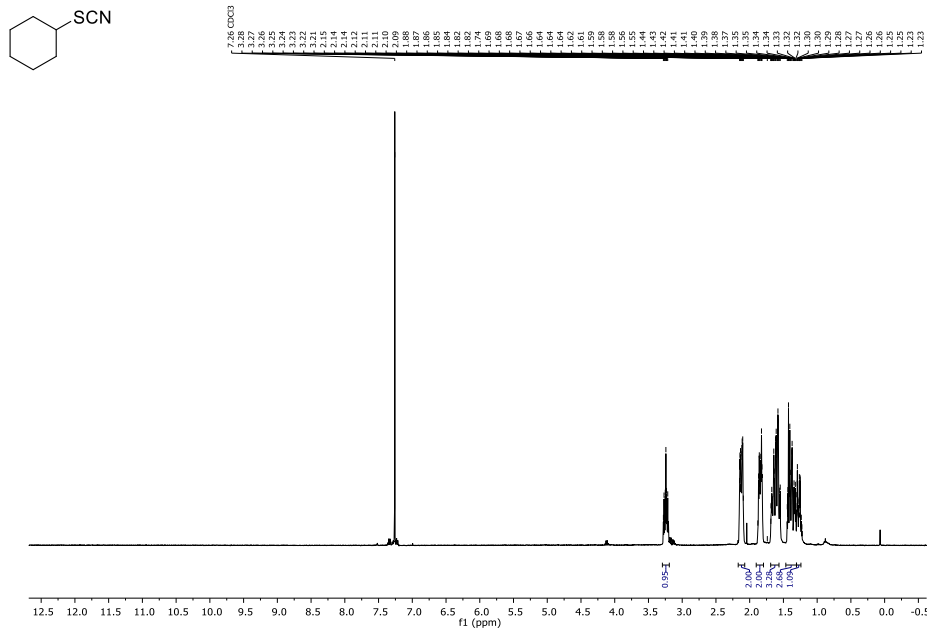

Figure F37: ^{1}H-NMR ($CDCl_3$, 400 MHz) of compound **35a**.

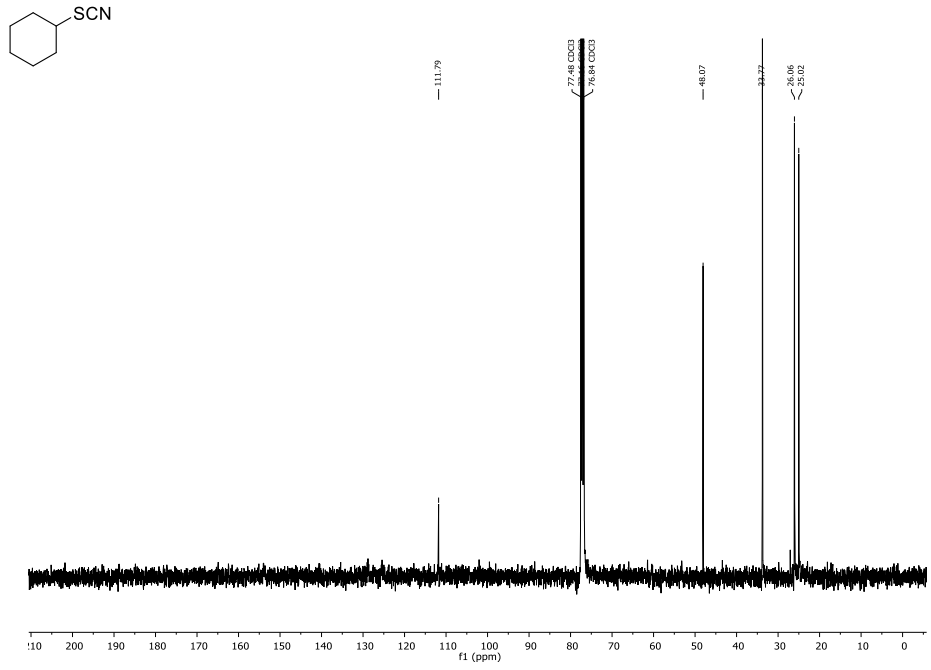

Figure F38: ^{13}C-NMR ($CDCl_3$, 101 MHz) of compound **35a**.

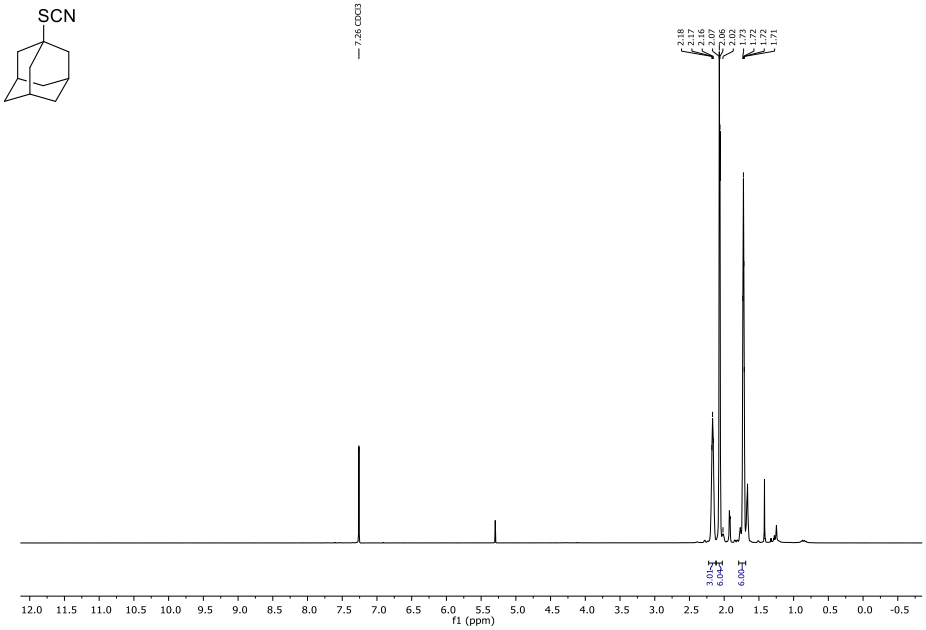

Figure F39: ^{1}H-NMR ($CDCl_3$, 300 MHz) of compound **36a**.

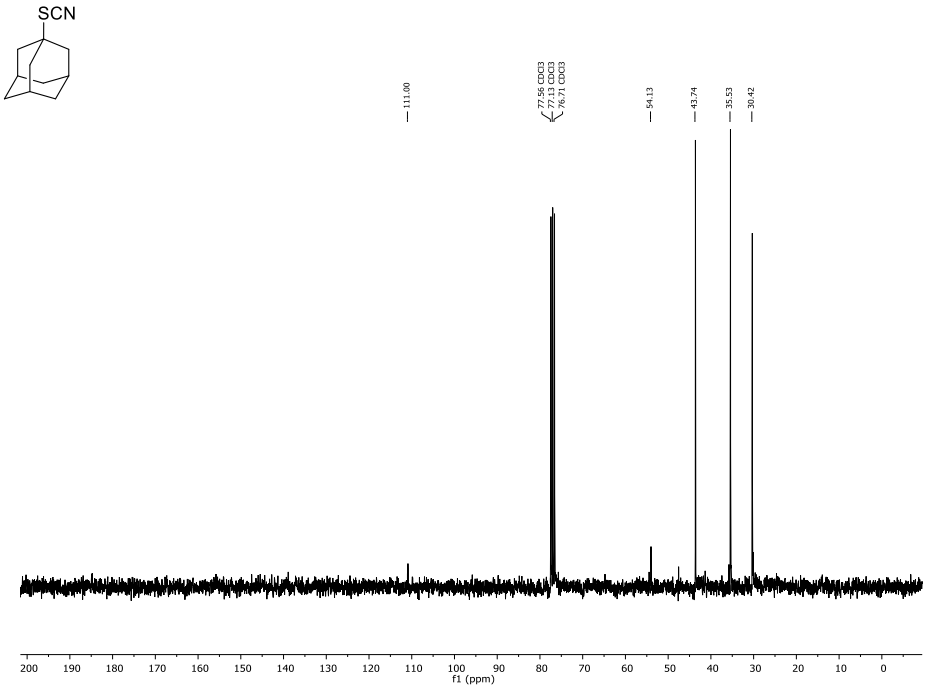

Figure F40: ^{13}C-NMR ($CDCl_3$, 75 MHz) of compound **36a**.

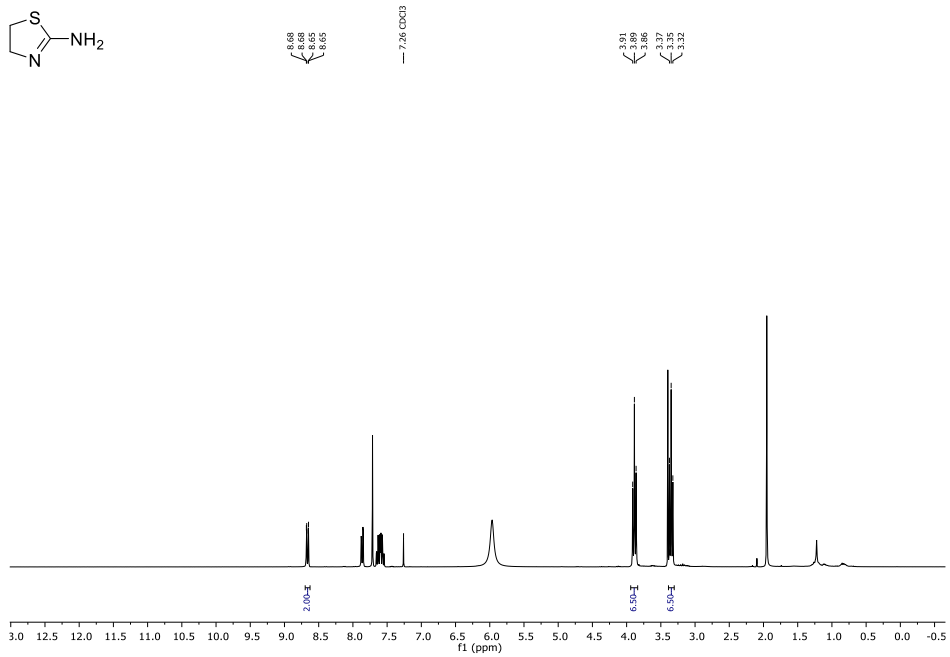

Figure F41*:* ^{1}H-NMR ($CDCl_3$, 300 MHz) of compound **37a** with internal standard phenanthrene.

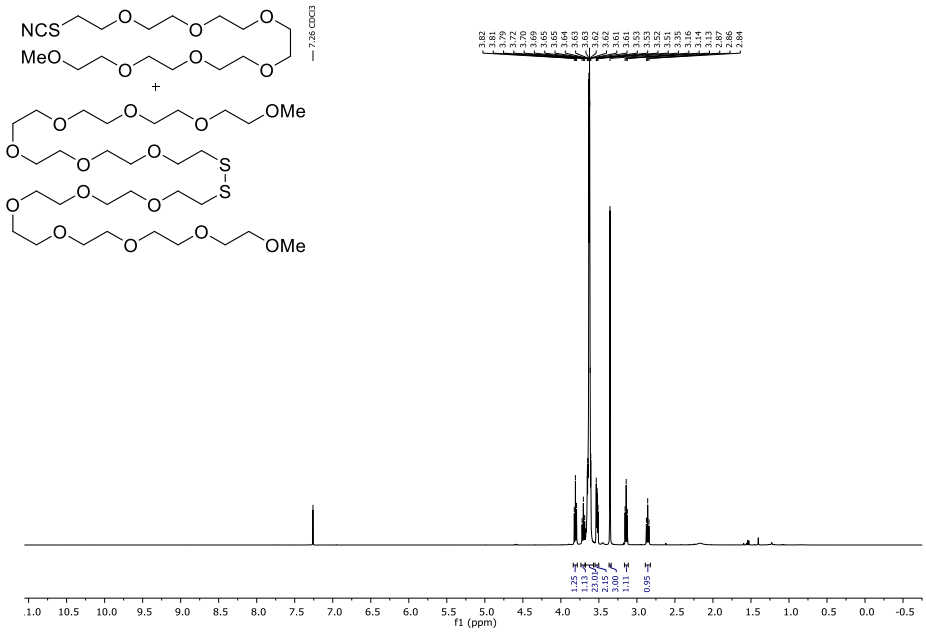

Figure F42: ^{1}H-NMR ($CDCl_3$, 400 MHz) of compound **38a**+**38b**.

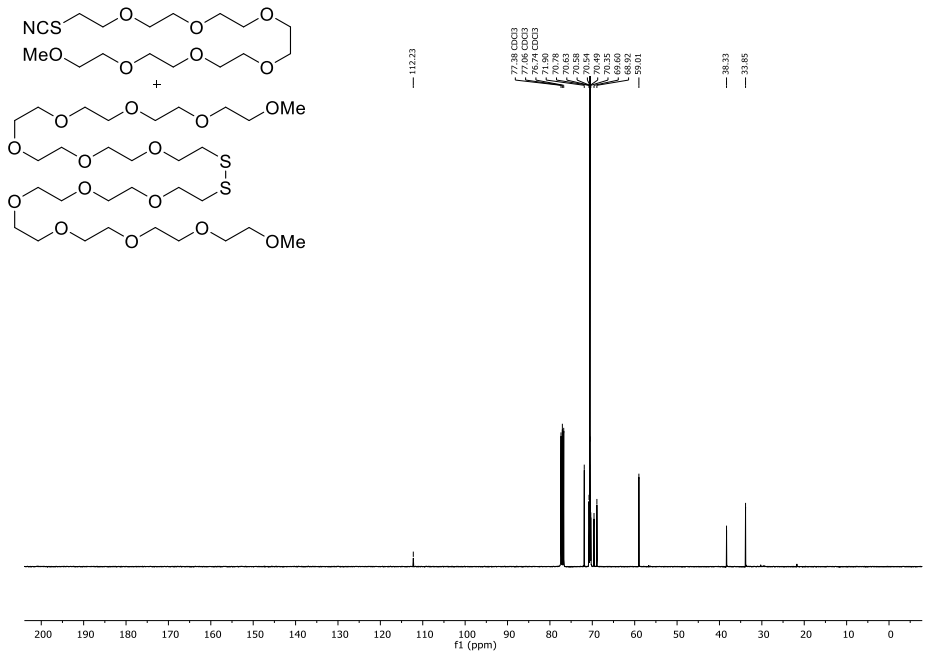

Figure F43: ^{13}C-NMR ($CDCl_3$, 101 MHz) of compound **38a**+**38b**.

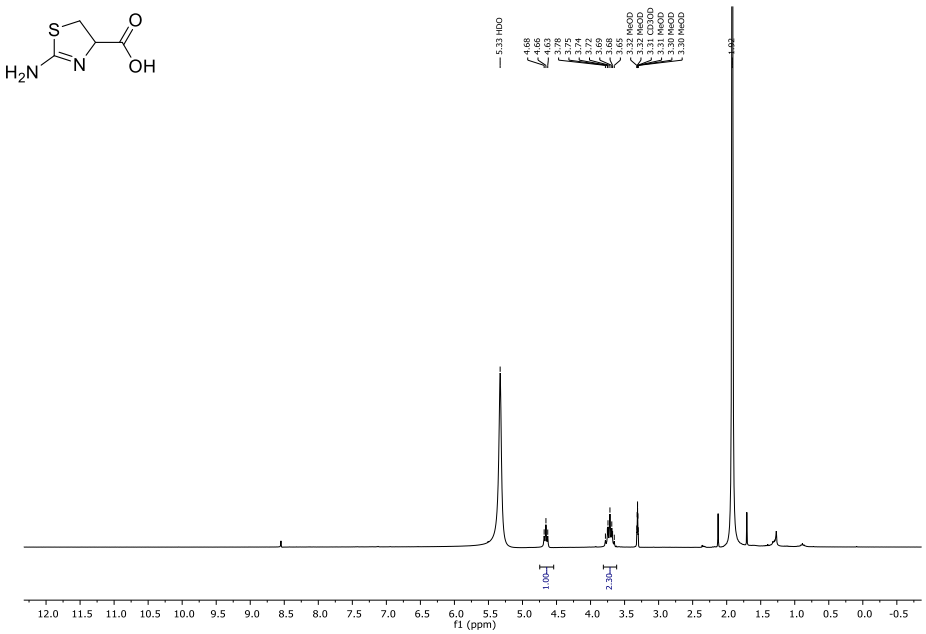

Figure F44: ^{1}H-NMR (MeOH-d_4, 300 MHz) of compound **39a** with HOAc as impurity after continuous extraction with EtOAc.

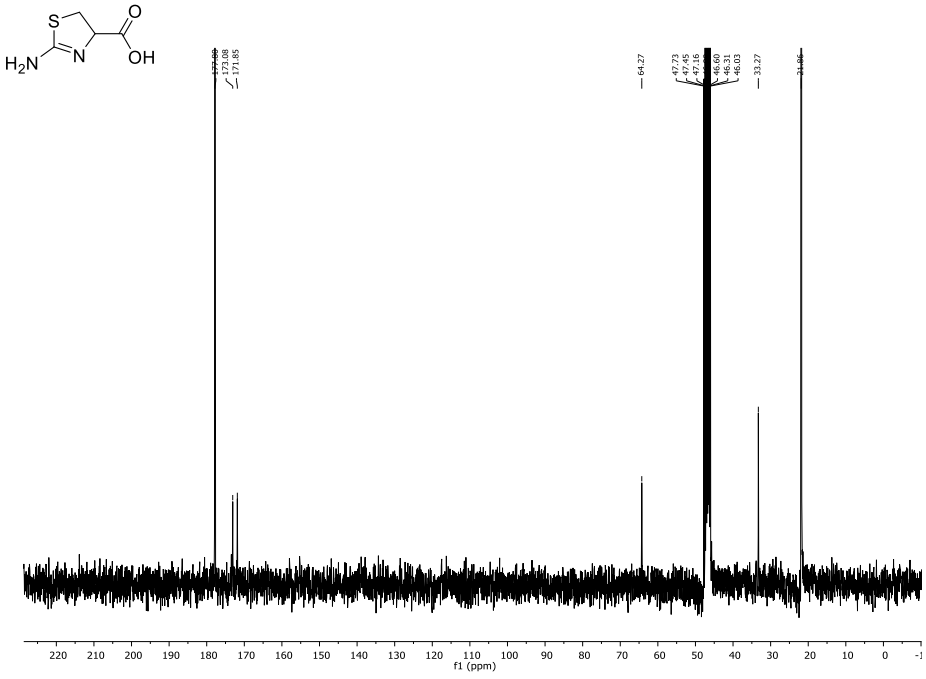

Figure F45: ^{13}C-NMR (MeOH-d_4, 75 MHz) of compound **39a** with HOAc as impurity after continuous extraction with EtOAc.

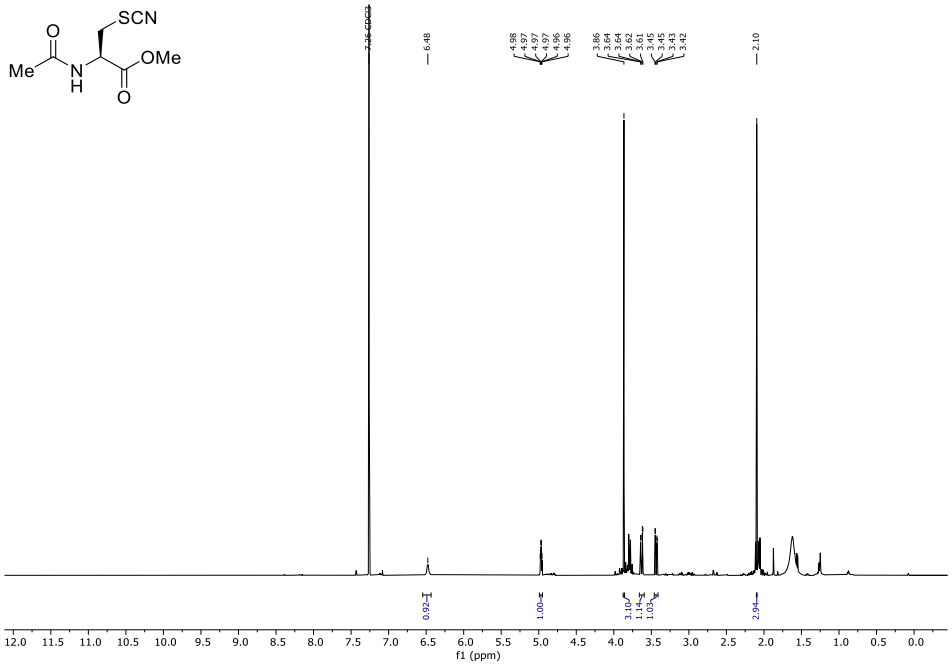

Figure F46: ^{1}H-NMR ($CDCl_3$, 600 MHz) of compound **40a.**

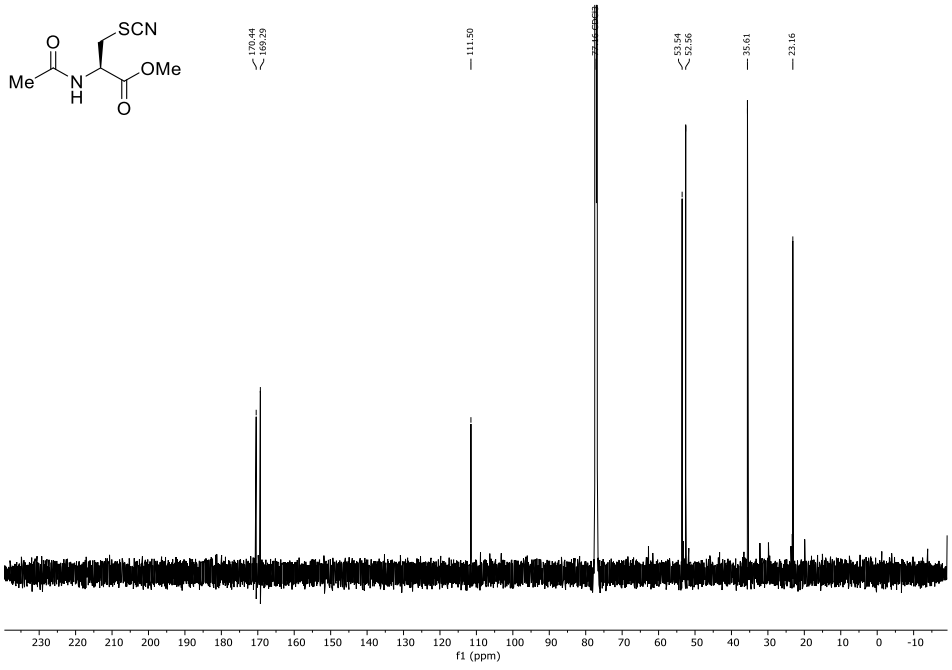

Figure F47: ^{13}C-NMR ($CDCl_3$, 151 MHz) of compound **40a**.

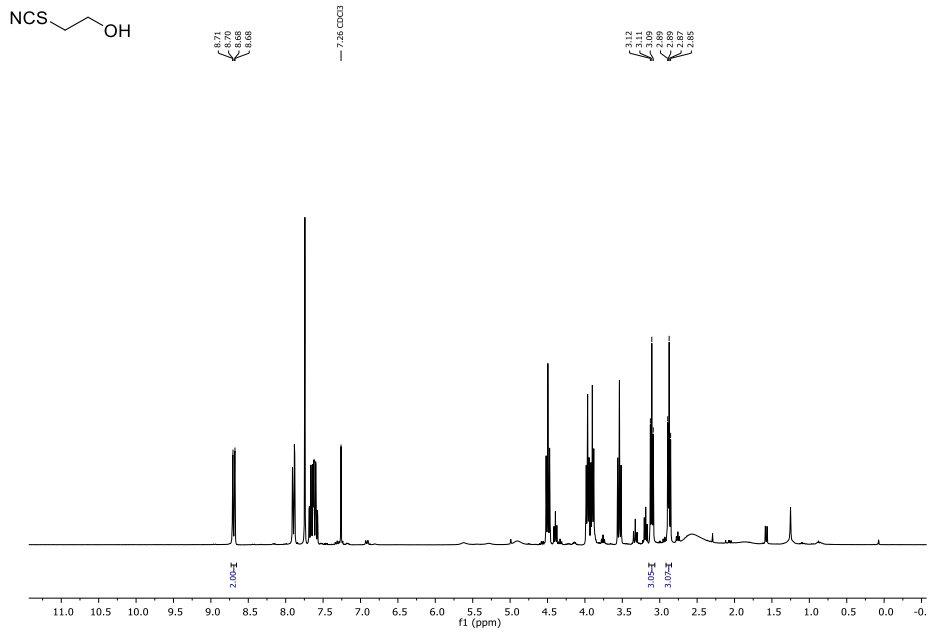

Figure F48: ^{1}H-NMR ($CDCl_3$, 300 MHz) of compound **41a** with internal standard phenanthrene.

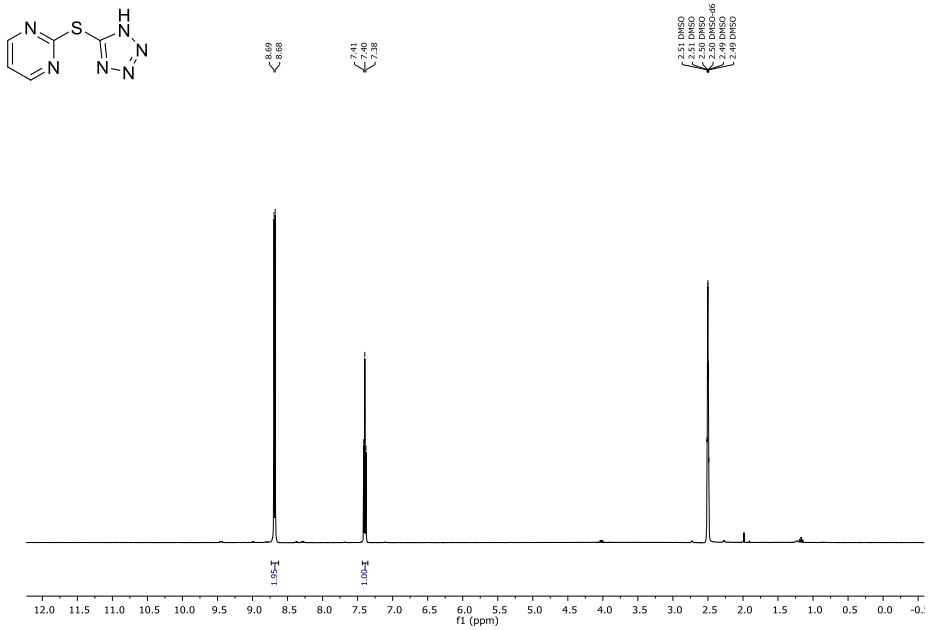

Figure F49: ^{1}H-NMR (DMSO-d_6, 300 MHz) of compound **60**.

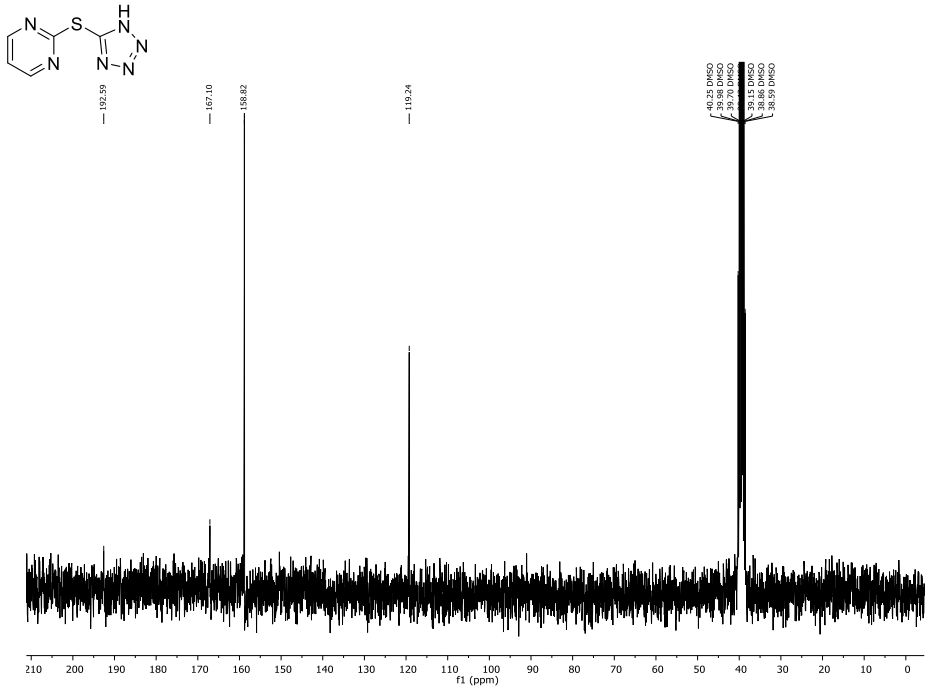

Figure F50: ^{13}C-NMR (DMSO-d_6, 75 MHz) of compound **60**.

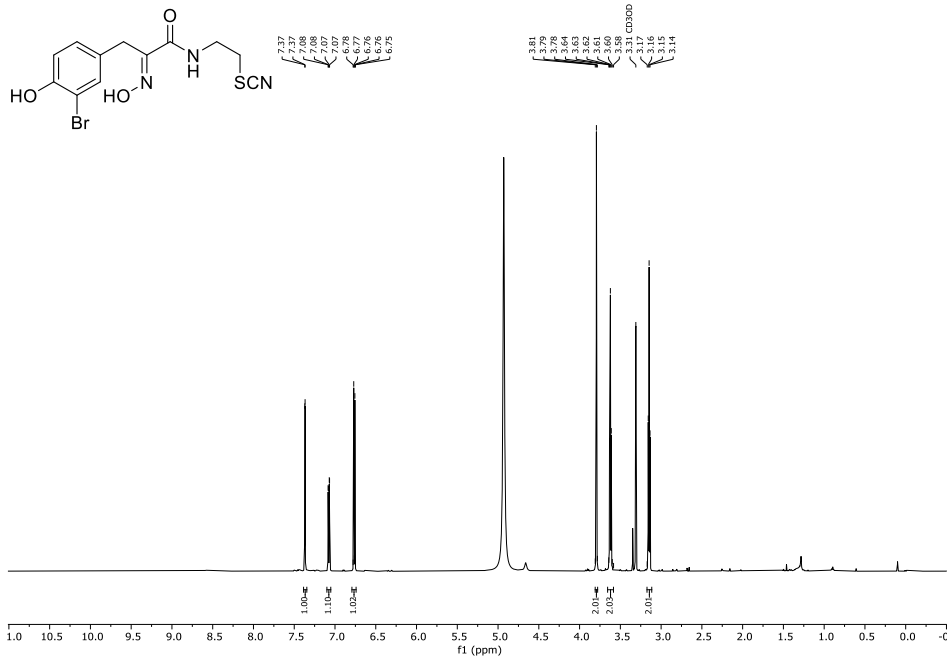

Figure F51: ^{1}H-NMR (MeOH-d_4, 600 MHz) of Psammaplin B (**1**).

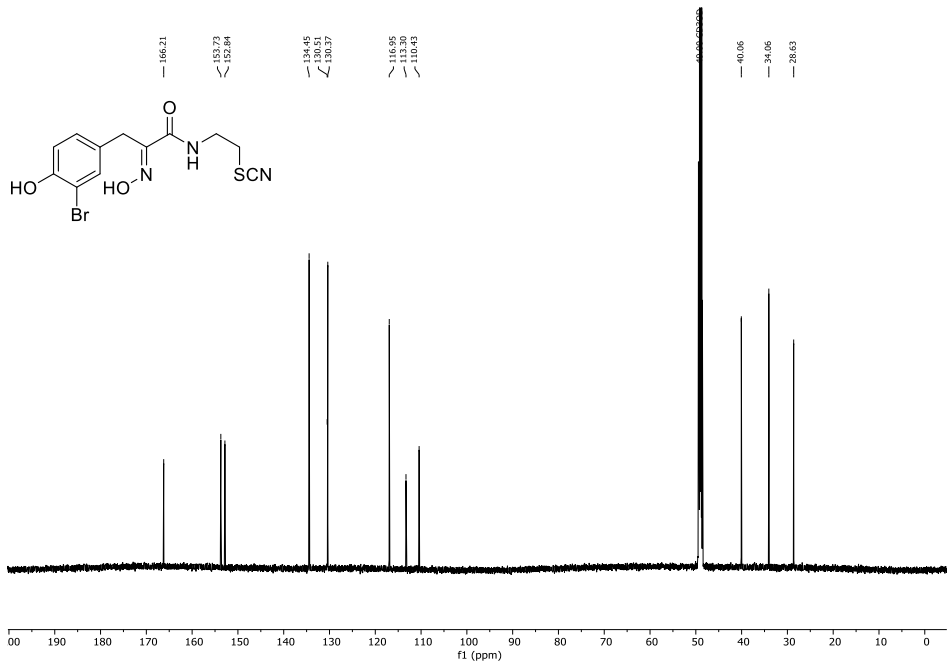

Figure F52: ^{13}C-NMR (MeOH-d_4, 151 MHz) of Psammaplin B (**1**).

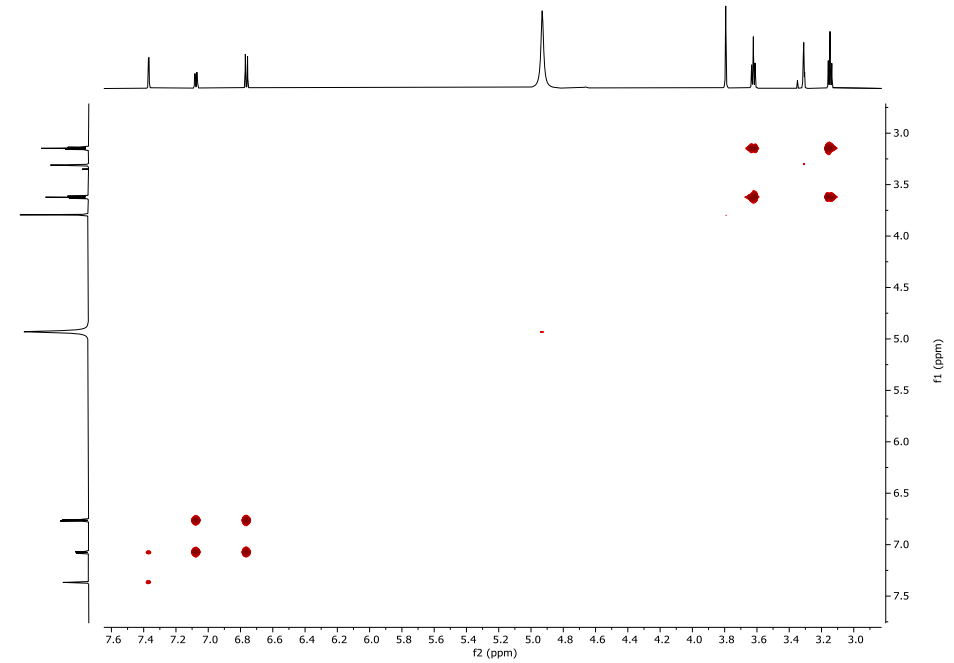

Figure F53: ^{1}H–^{1}H-COSY (MeOH-d_4) of Psammaplin B (**1**).

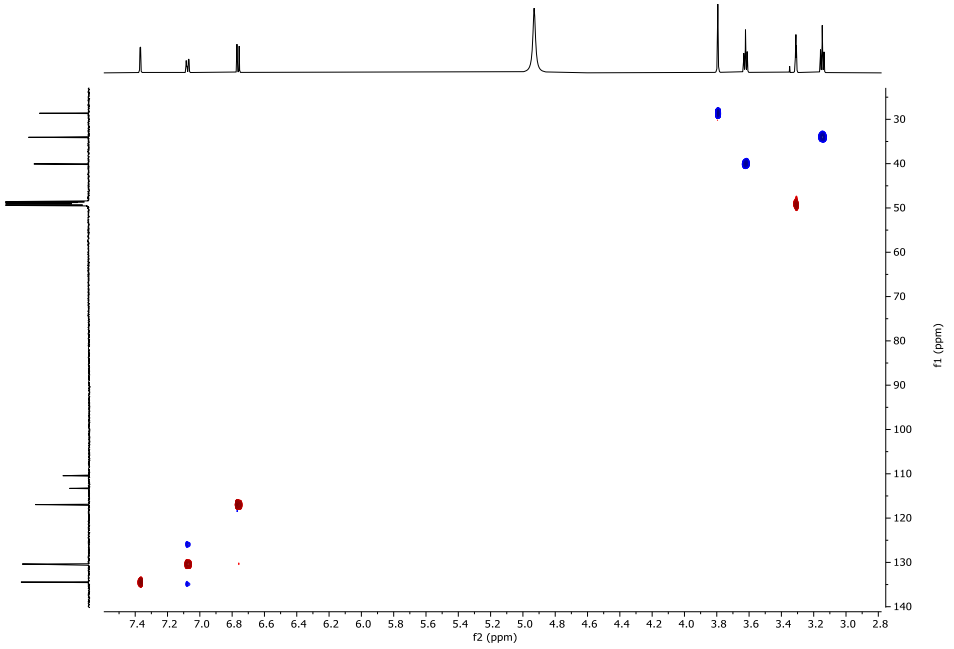

Figure F54: ^{1}H–^{13}C-HSQC (MeOH-d_4) of Psammaplin B (**1**).

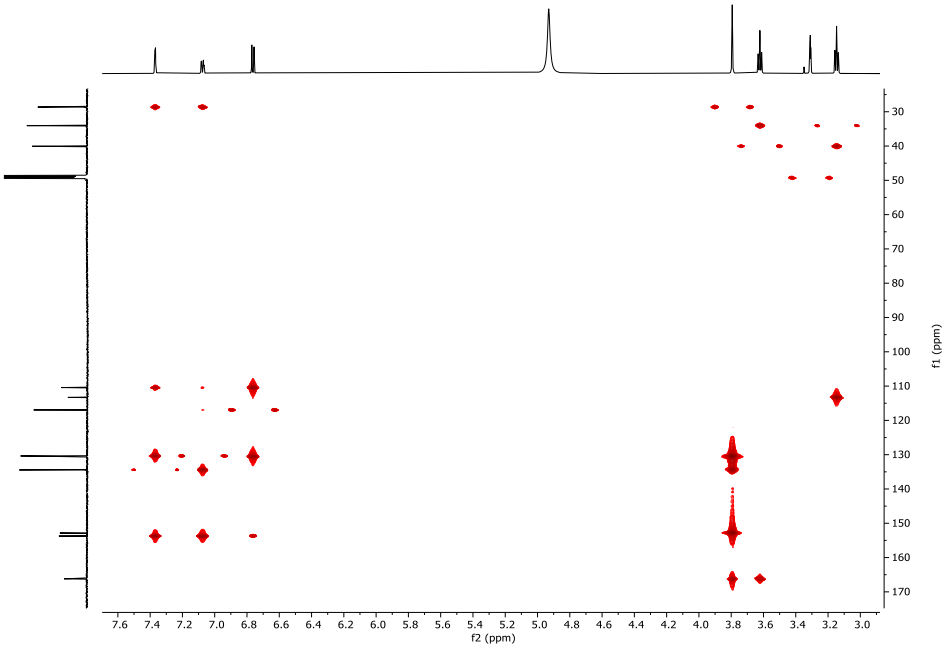

Figure F55: ^{1}H–^{13}C-HMBC (MeOH-d_4) of Psammaplin B (**1**).

Spectra of Isolated Side Products

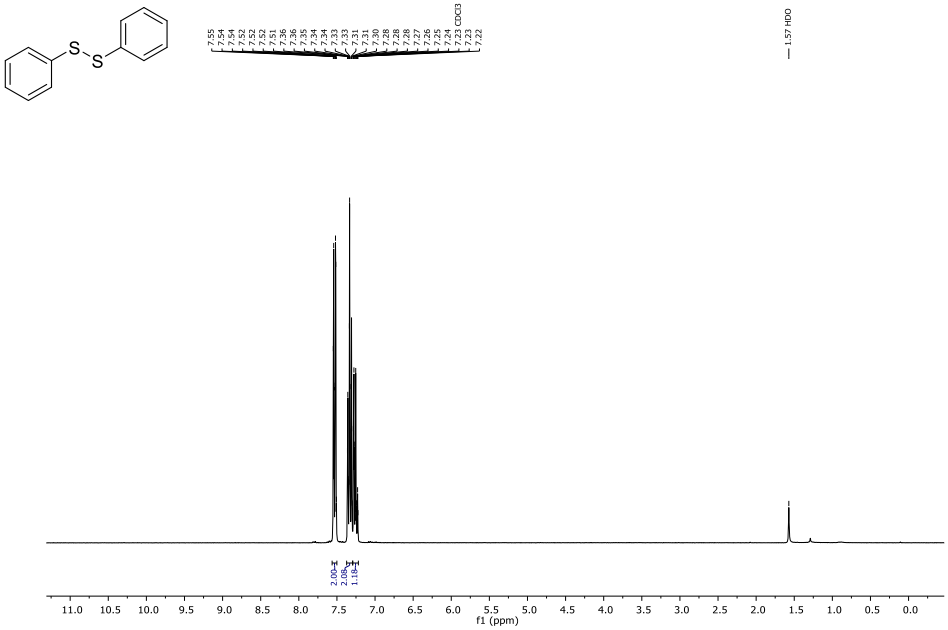

Figure F56: ^{1}H-NMR ($CDCl_3$, 300 MHz) of compound **13**.

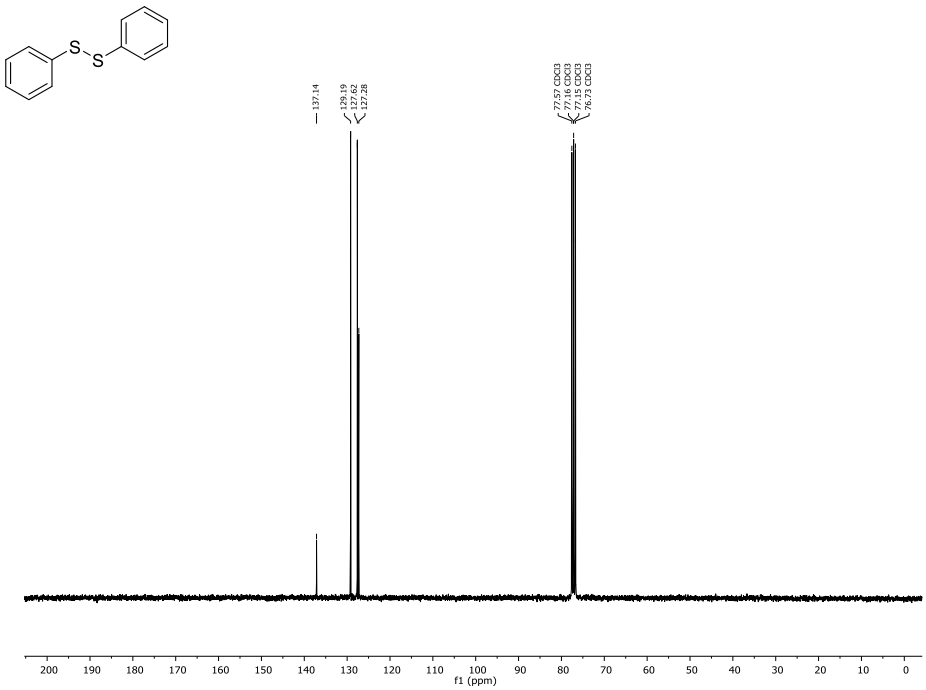

Figure F57: ^{13}C-NMR ($CDCl_3$, 75 MHz) of compound **13**.

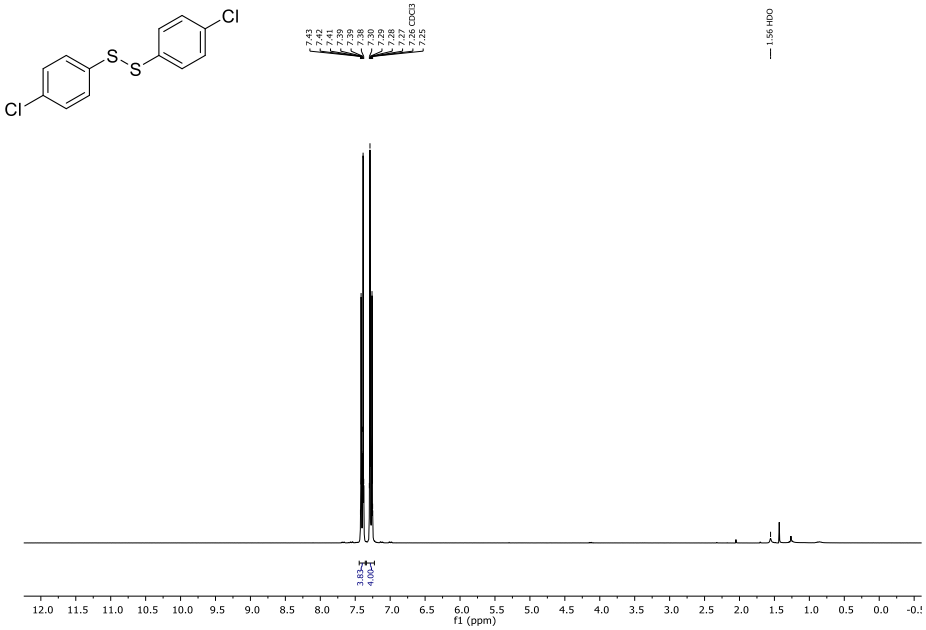

Figure F58: ^{1}H-NMR ($CDCl_3$, 300 MHz) of compound **22b**.

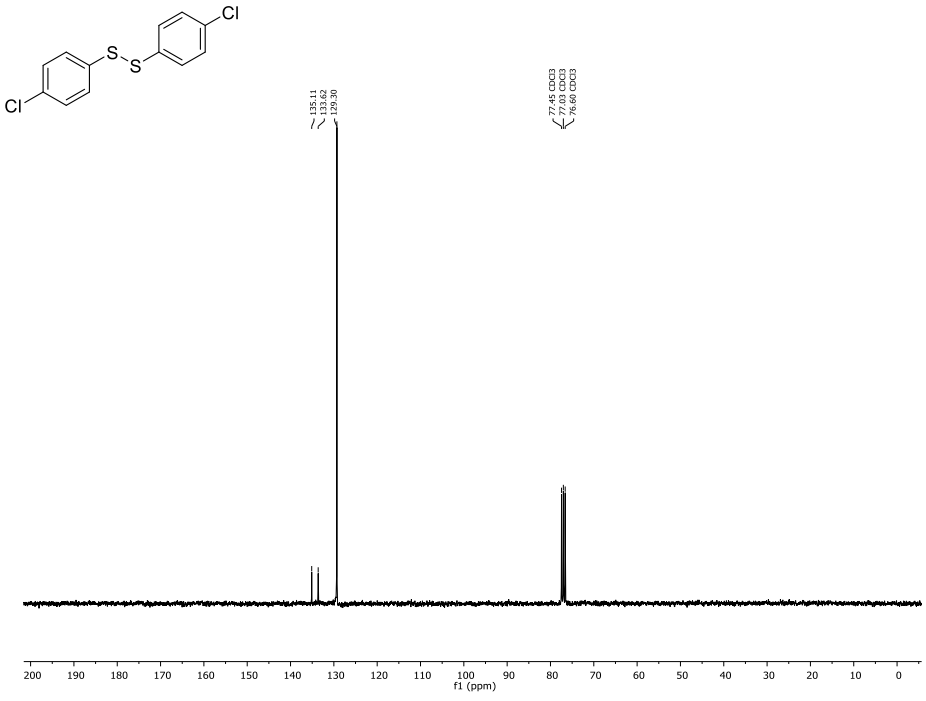

Figure F59*:* ^{13}C-NMR ($CDCl_3$, 75 MHz) of compound **22b**.

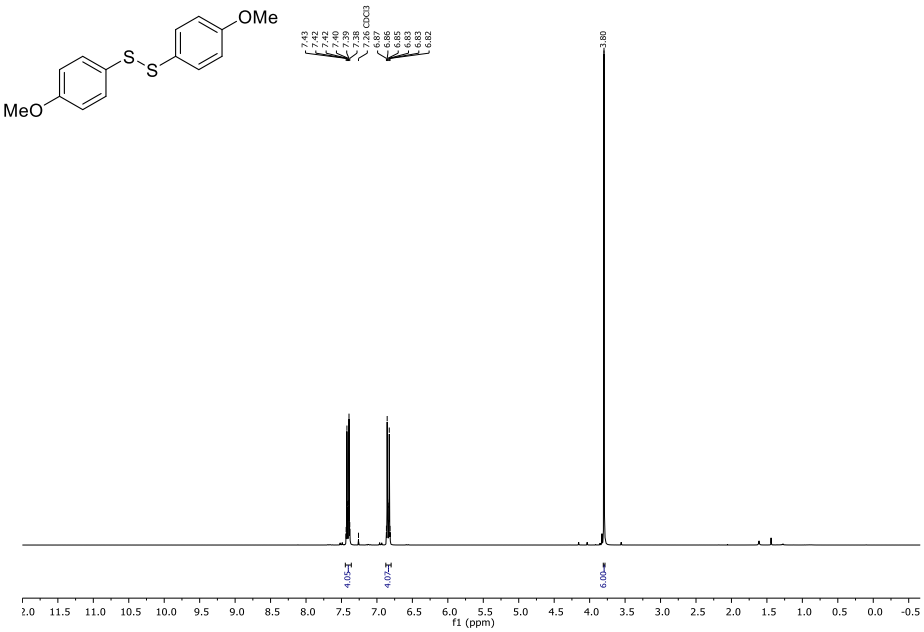

Figure F60: ^{1}H-NMR ($CDCl_3$, 300 MHz) of compound **23b**.

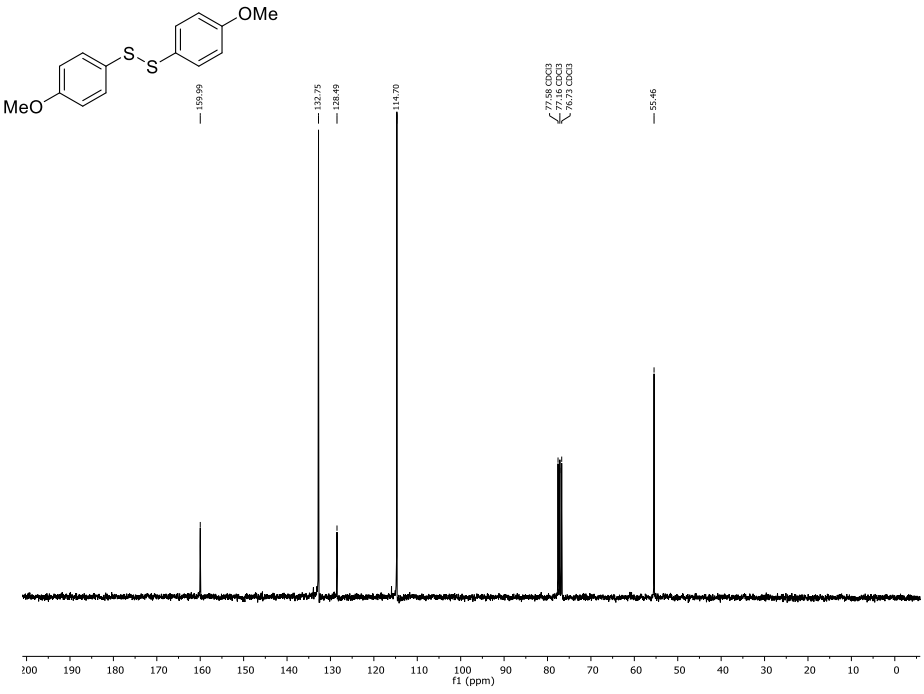

Figure F61: ^{13}C-NMR ($CDCl_3$, 75 MHz) of compound **23b**.

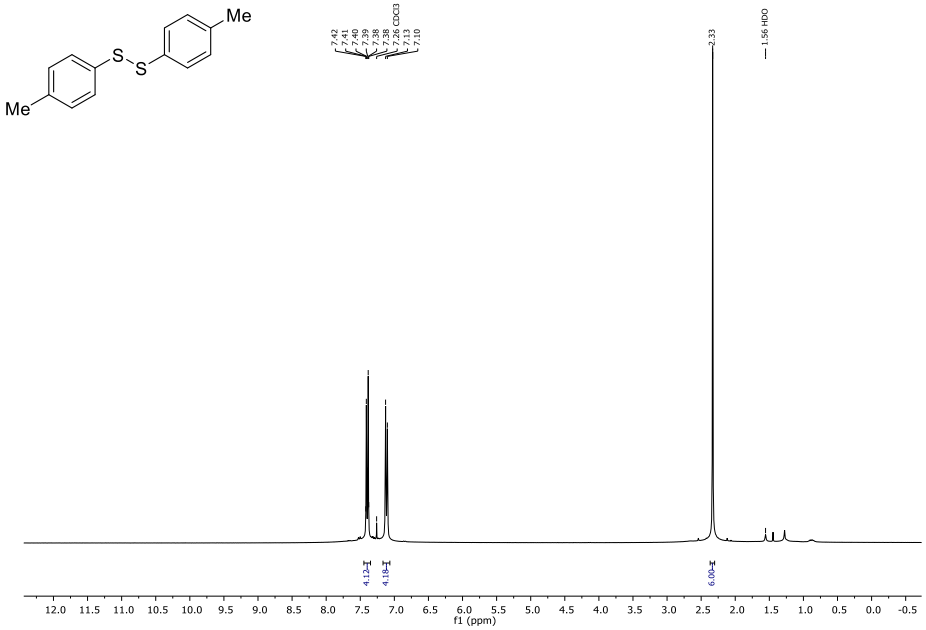

Figure F62: ^{1}H-NMR ($CDCl_3$, 300 MHz) of compound **24b**.

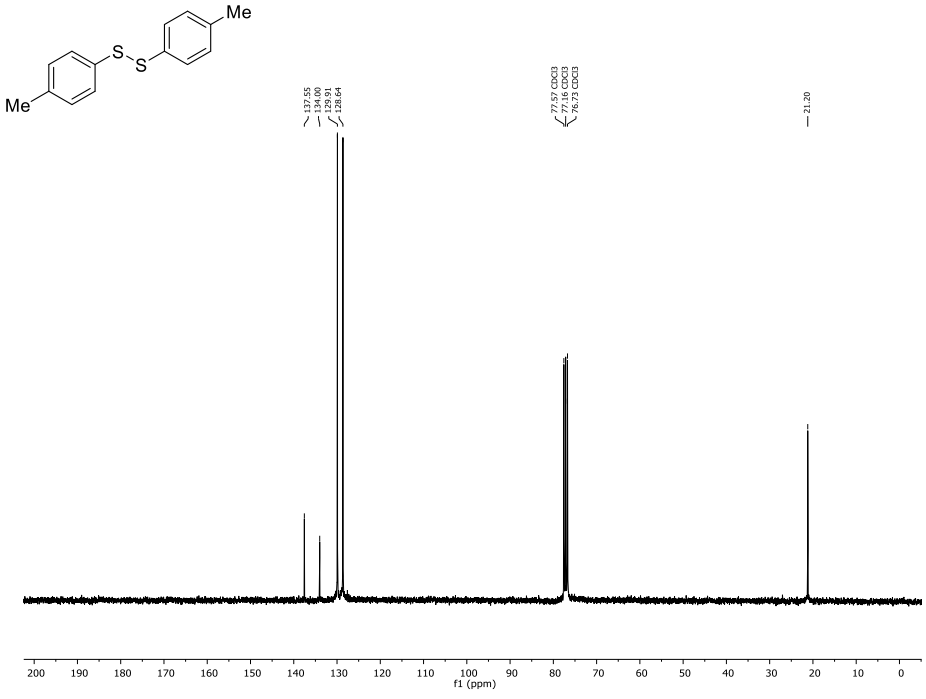

Figure F63: ^{13}C-NMR ($CDCl_3$, 75 MHz) of compound **24b**.

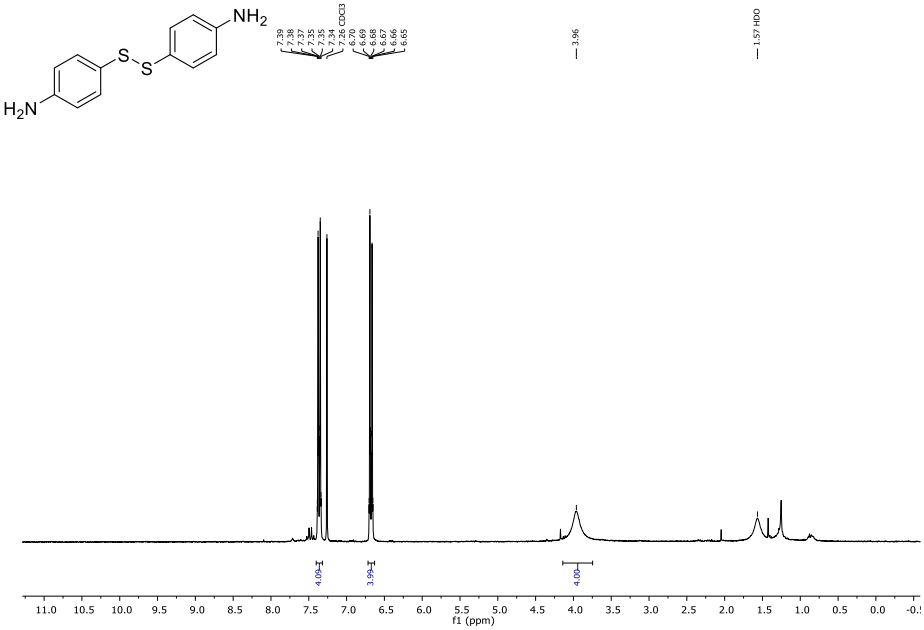

Figure F64: ^{1}H-NMR ($CDCl_3$, 300 MHz) of compound **25b**.

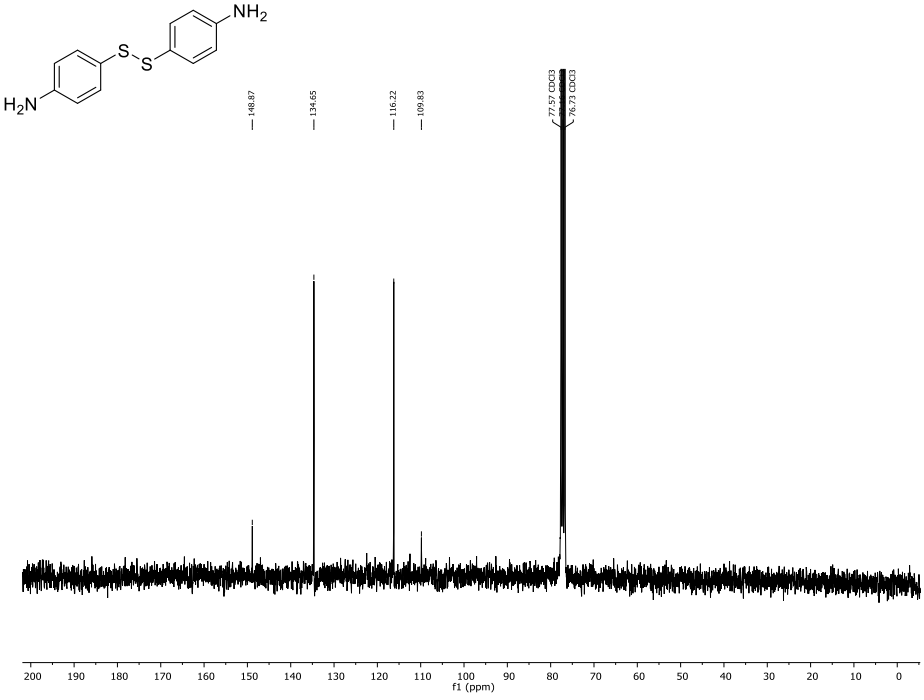

Figure F65: ^{13}C-NMR ($CDCl_3$, 75 MHz) of compound **25b**.

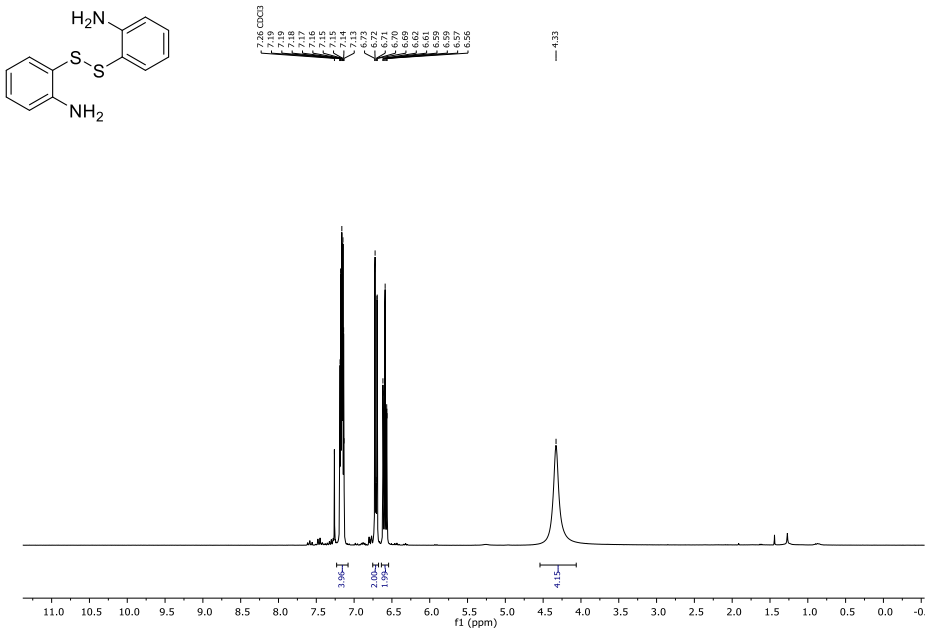

Figure F66: ^{1}H-NMR ($CDCl_3$, 300 MHz) of compound **26b**.

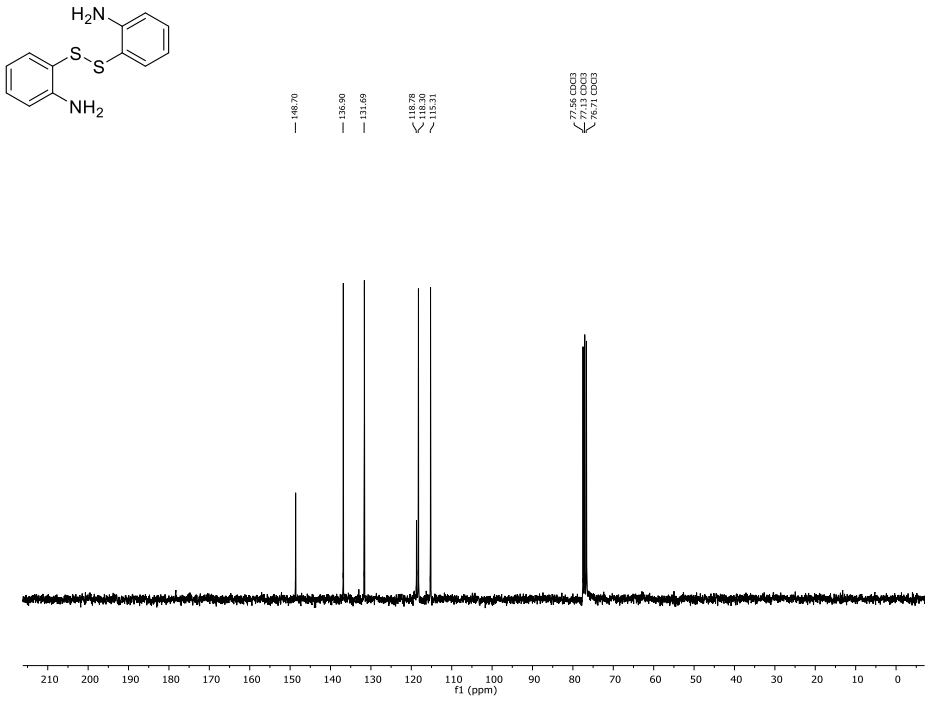

Figure F67: ^{13}C-NMR ($CDCl_3$, 75 MHz) of compound **26b**.

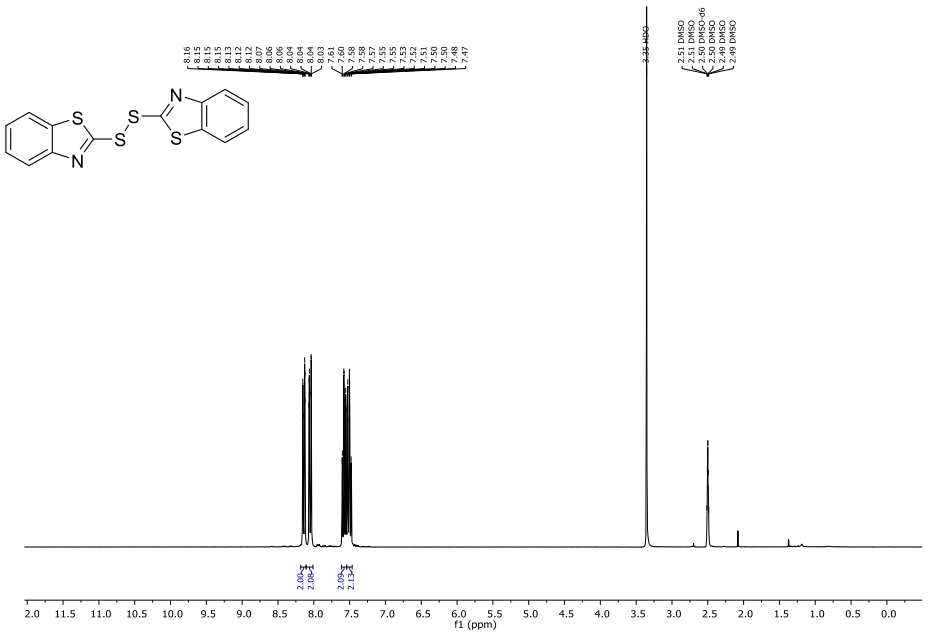

Figure F68: ^{1}H-NMR (DMSO-d_6, 300 MHz) of compound **30b**.

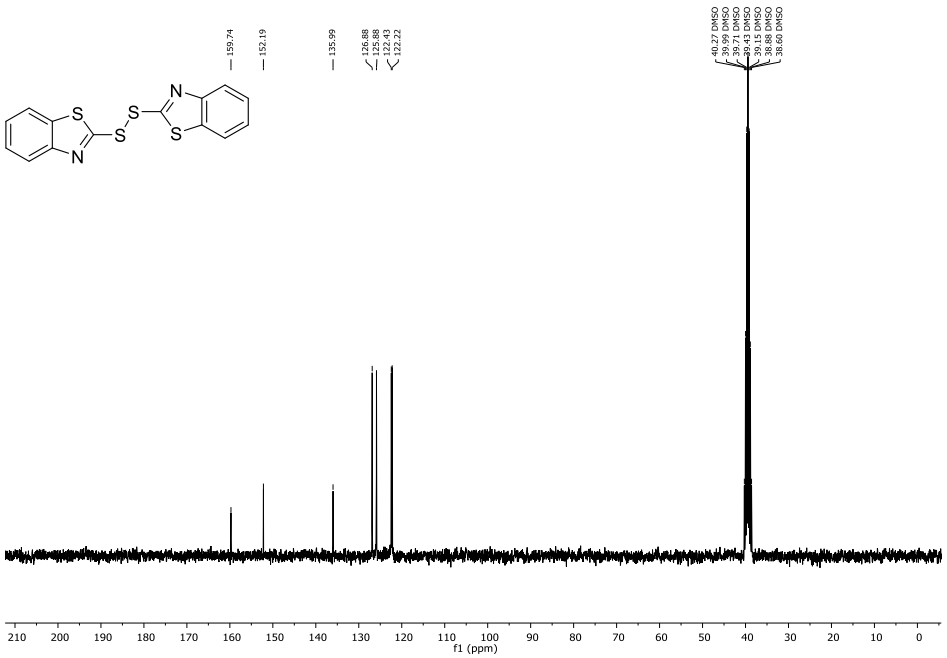

Figure F69: ^{13}C-NMR (DMSO-d_6, 75 MHz) of compound **30b**.

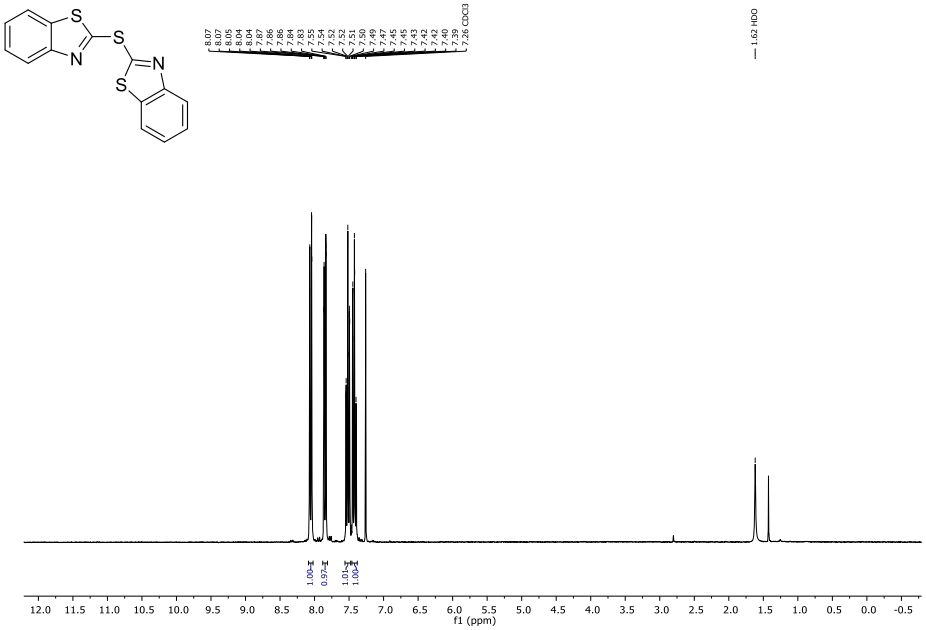

Figure F70: ^{1}H-NMR ($CDCl_3$, 300 MHz) of compound **30c**.

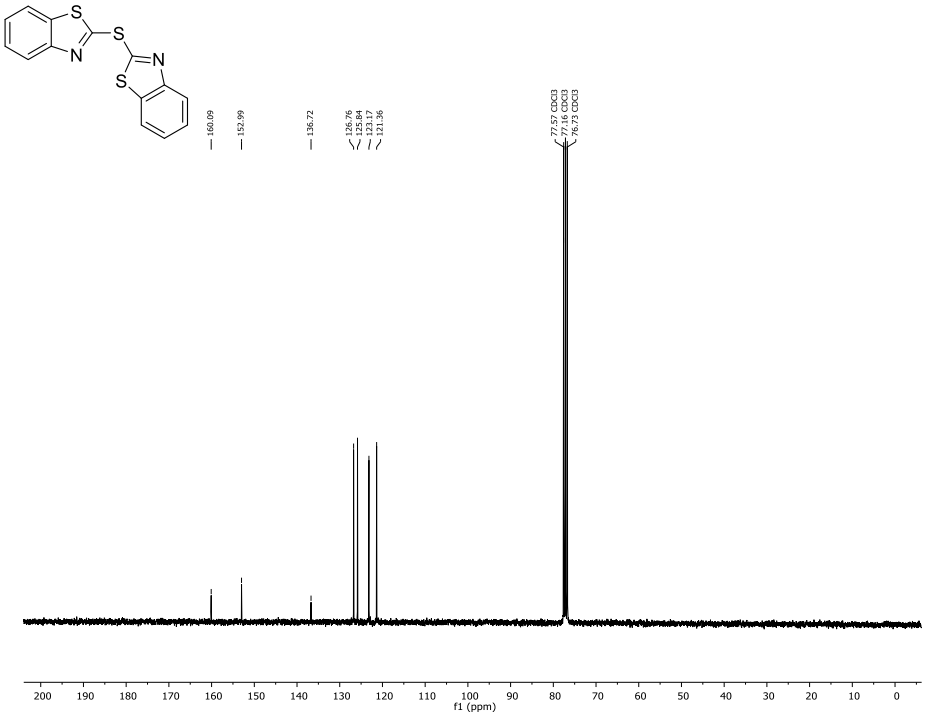

Figure F71: ^{13}C-NMR ($CDCl_3$, 75 MHz) of compound **30c**.

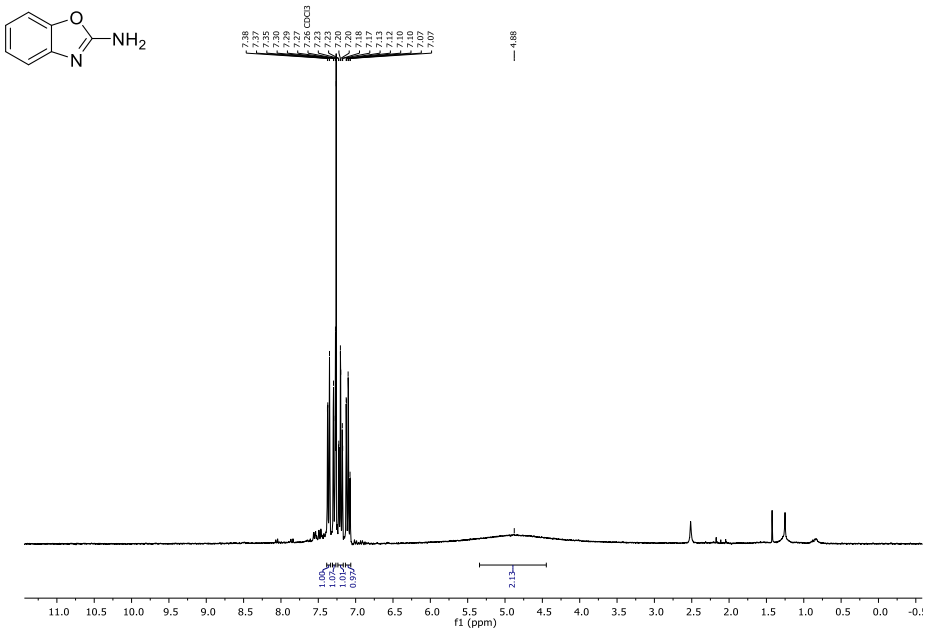

Figure F72: ^{1}H-NMR ($CDCl_3$, 300 MHz) of compound **31b**.

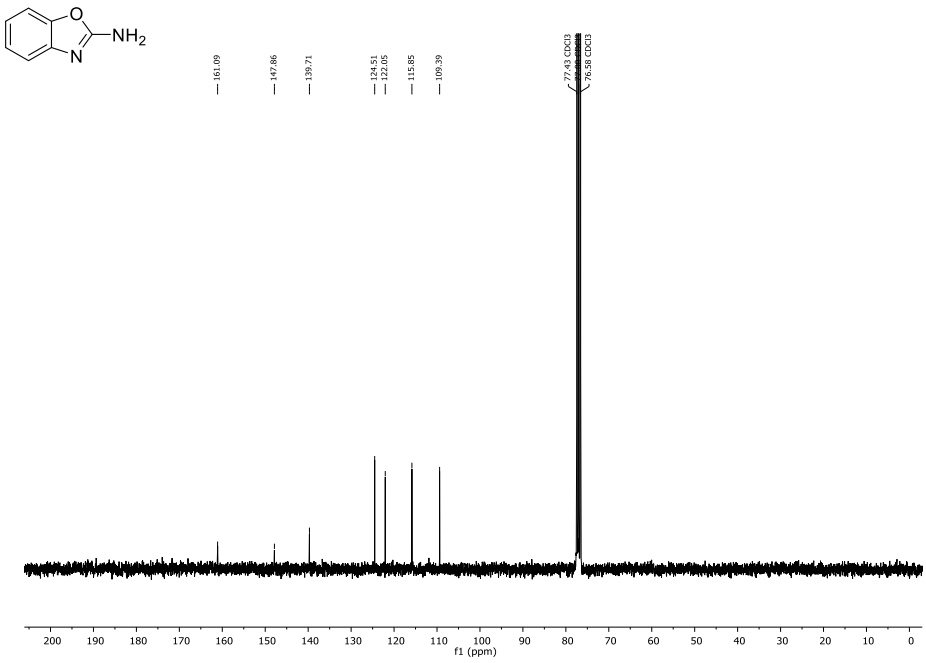

Figure F73: ^{13}C-NMR ($CDCl_3$, 75 MHz) of compound **31b**.

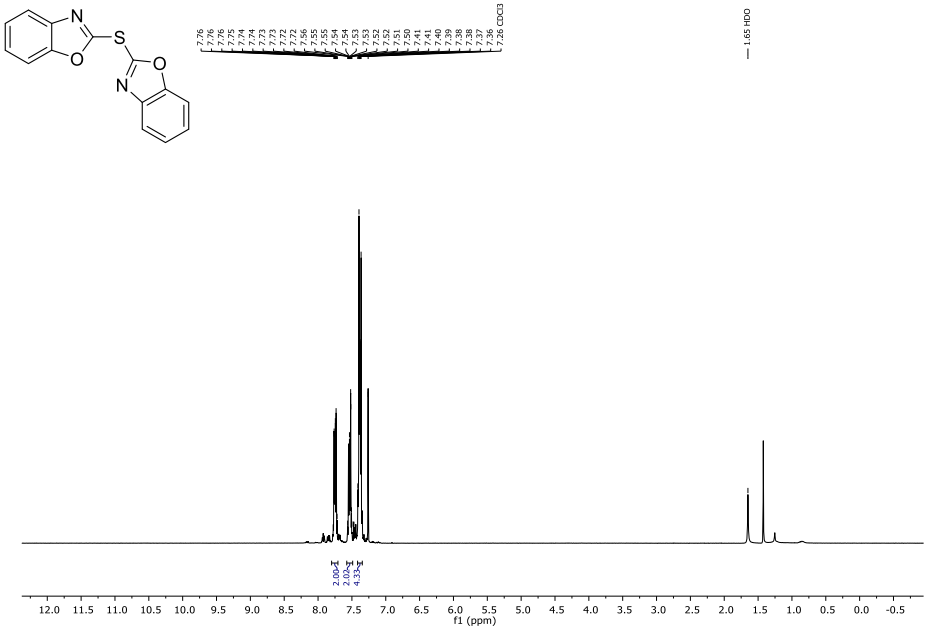

Figure F74: ^{1}H-NMR ($CDCl_3$, 300 MHz) of compound **31c**.

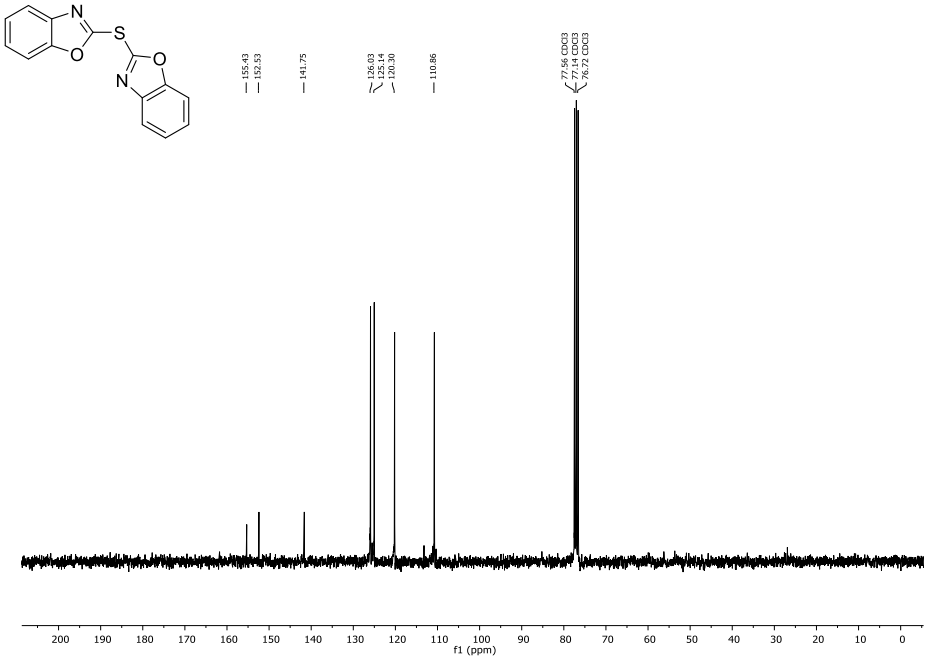

Figure F75: ^{13}C-NMR ($CDCl_3$, 75 MHz) of compound **31c**.

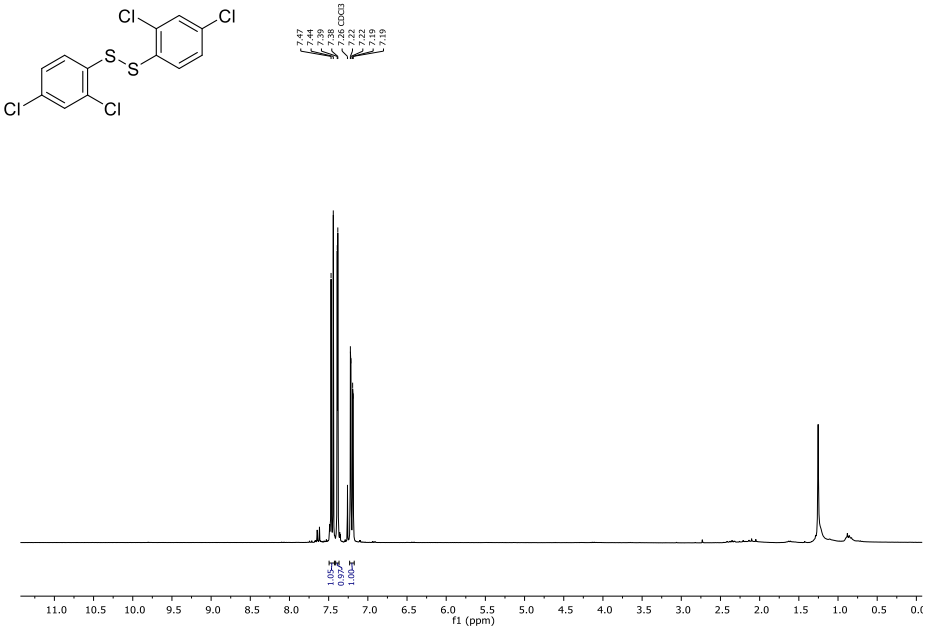

Figure F76: ^{1}H-NMR ($CDCl_3$, 300 MHz) of compound **33b**.

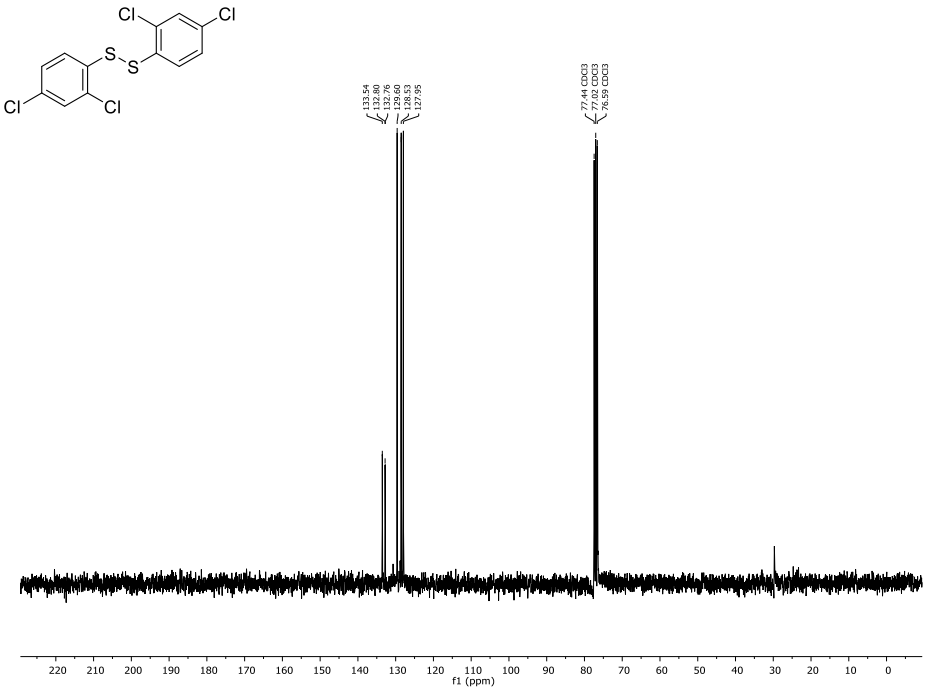

Figure F77: ^{13}C-NMR ($CDCl_3$, 75 MHz) of compound **33b**.

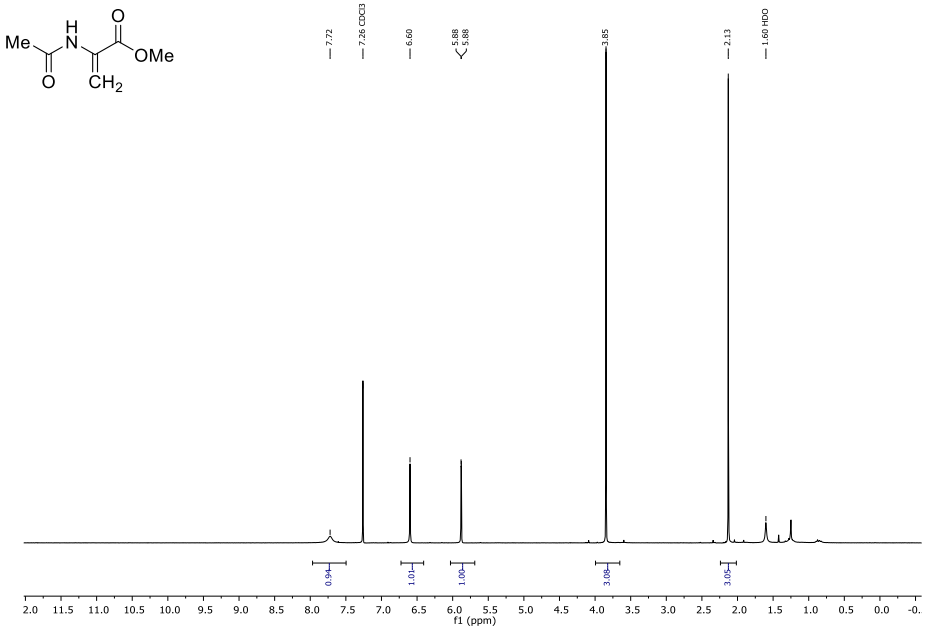

Figure F78: ^{1}H-NMR ($CDCl_3$, 300 MHz) of compound **40b**.

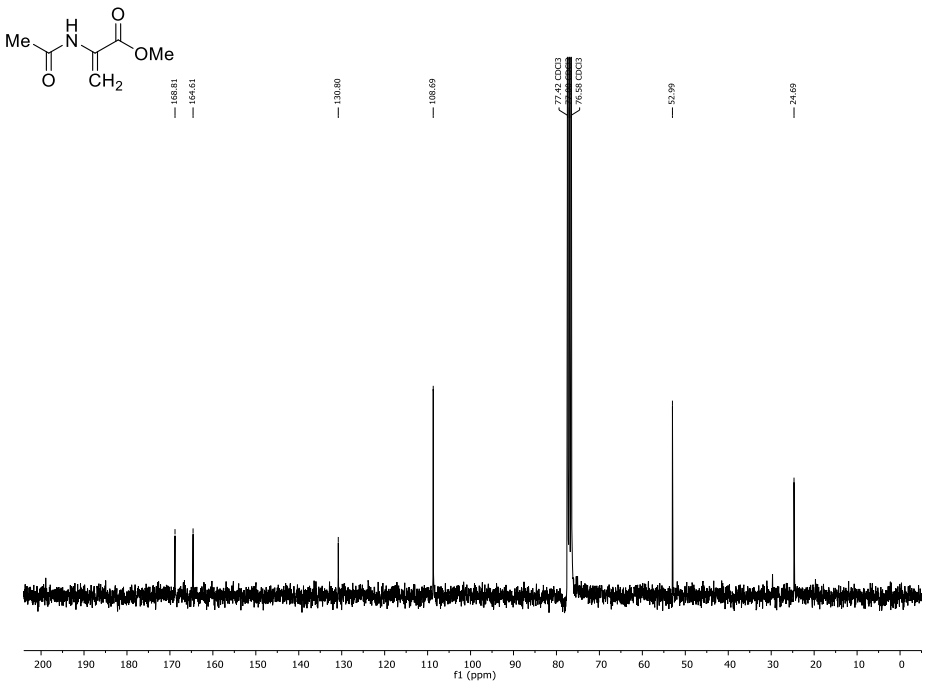

Figure F79: ^{13}C-NMR ($CDCl_3$, 75 MHz) of compound **40b**.

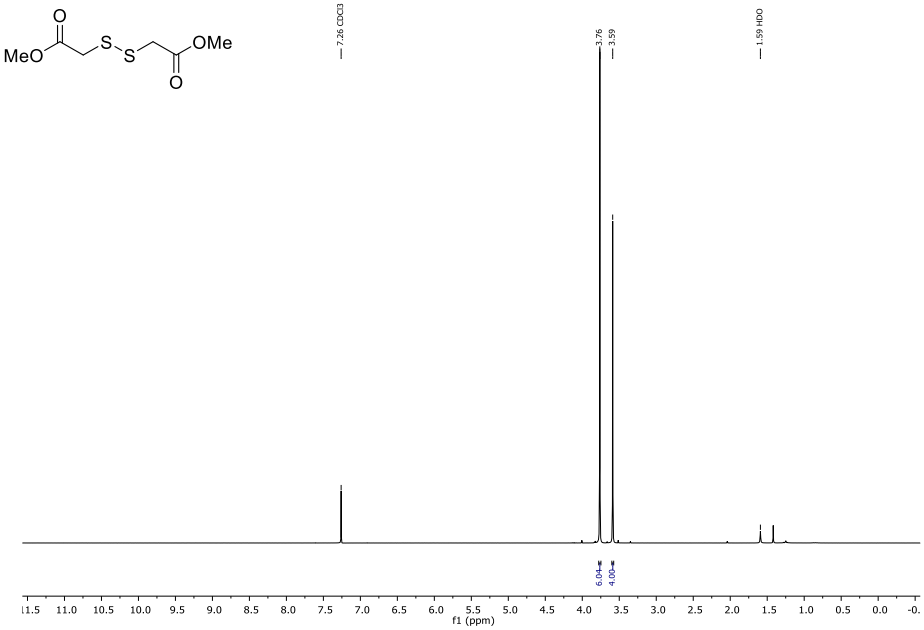

Figure F80: ^{1}H-NMR ($CDCl_3$, 300 MHz) of compound **43b**.

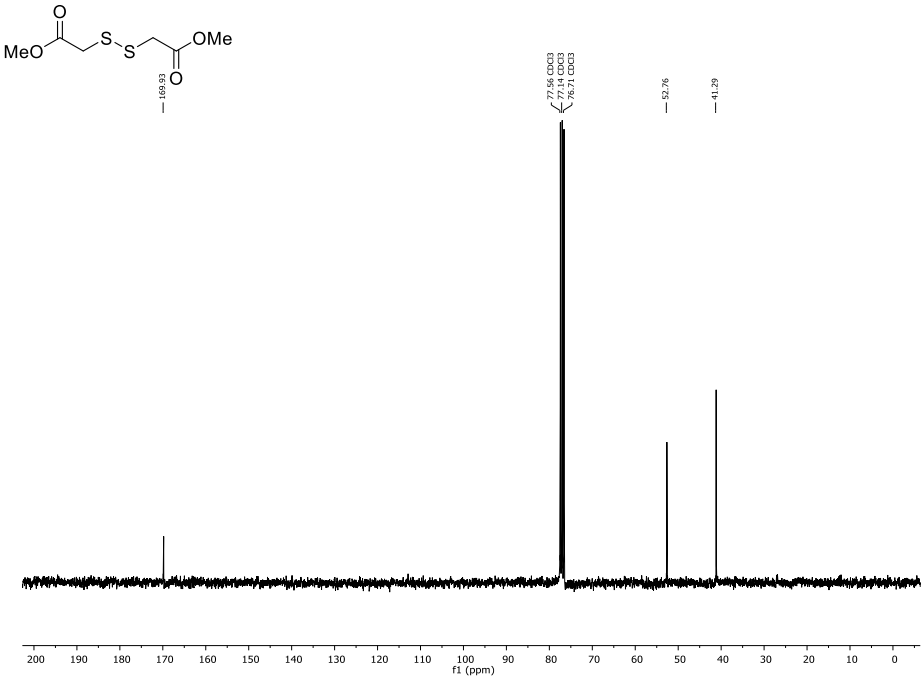

Figure F81: ^{13}C-NMR ($CDCl_3$, 75 MHz) of compound **43b**.

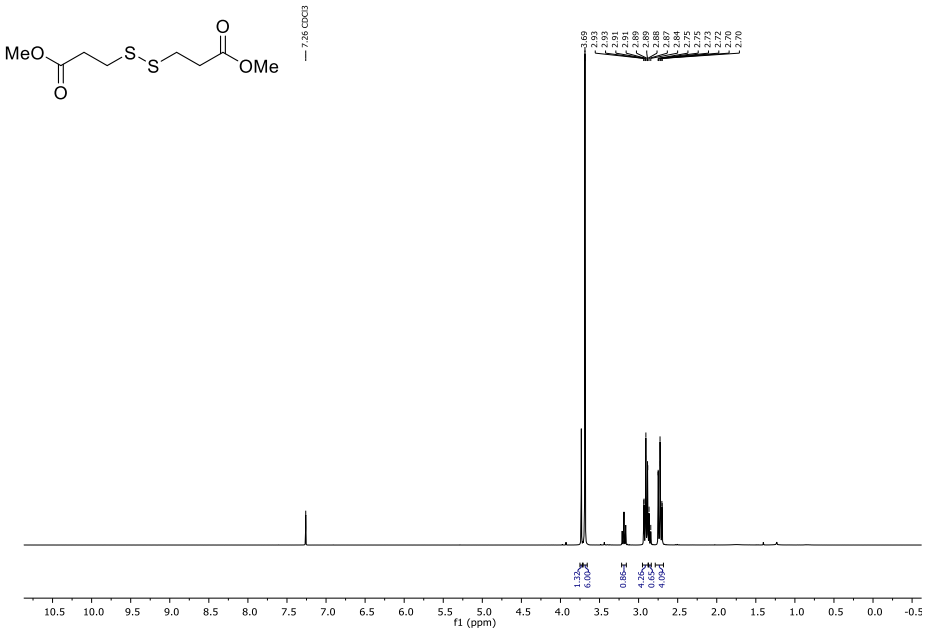

Figure F82: ^{1}H-NMR ($CDCl_3$, 300 MHz) of compound **44b**.

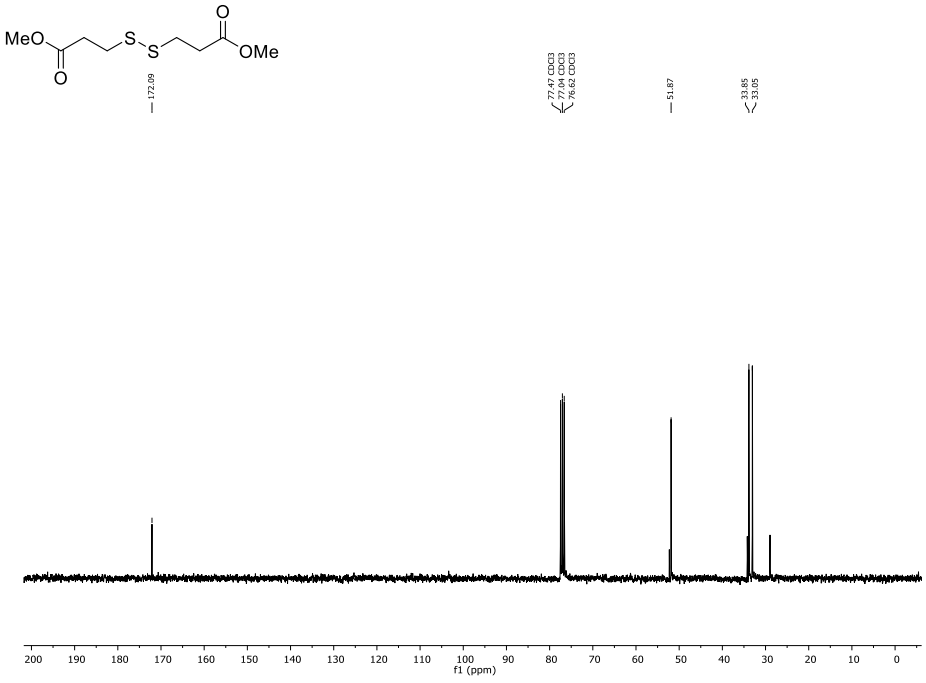

Figure F83: ^{13}C-NMR ($CDCl_3$, 75 MHz) of compound **44b**.

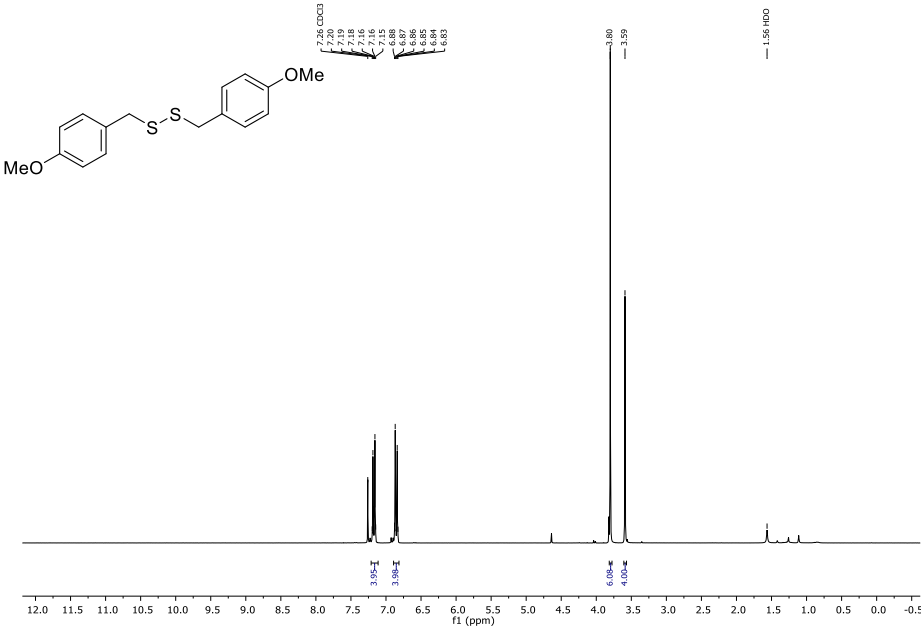

Figure F84: ^{1}H-NMR ($CDCl_3$, 300 MHz) of compound **45b**.

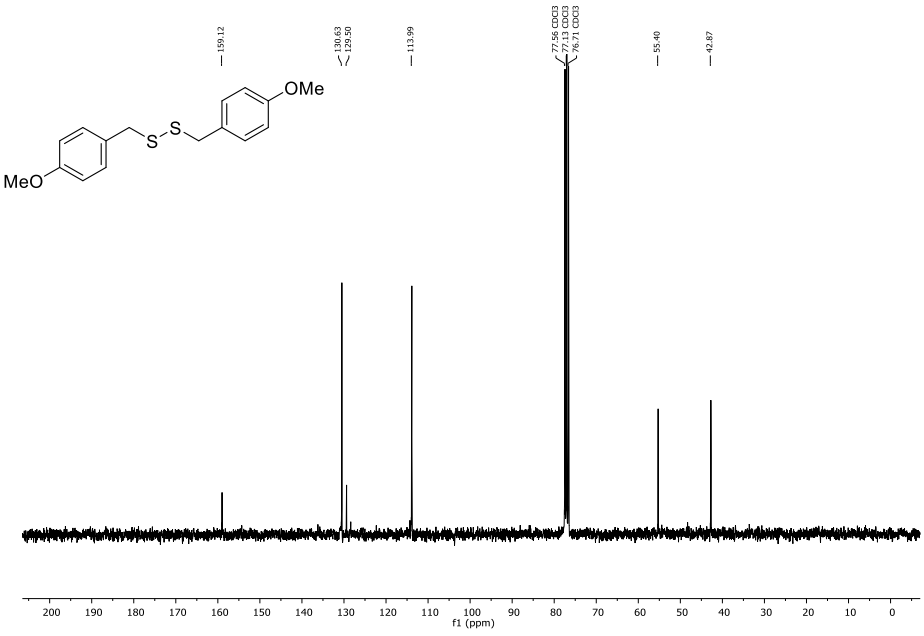

Figure F85: ^{13}C-NMR ($CDCl_3$, 75 MHz) of compound **45b**.

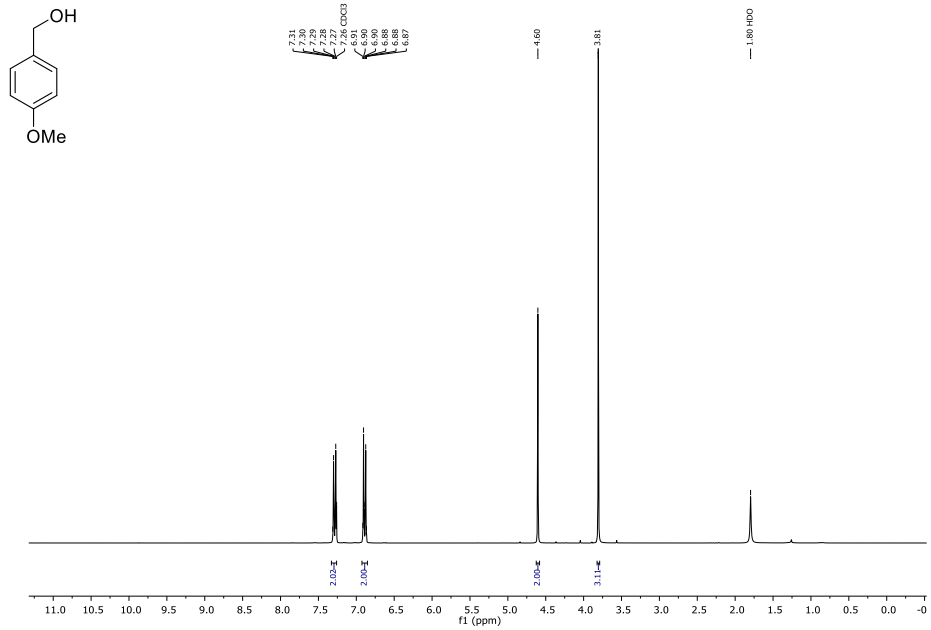

Figure F86: ^{1}H-NMR ($CDCl_3$, 300 MHz) of compound **45c**.

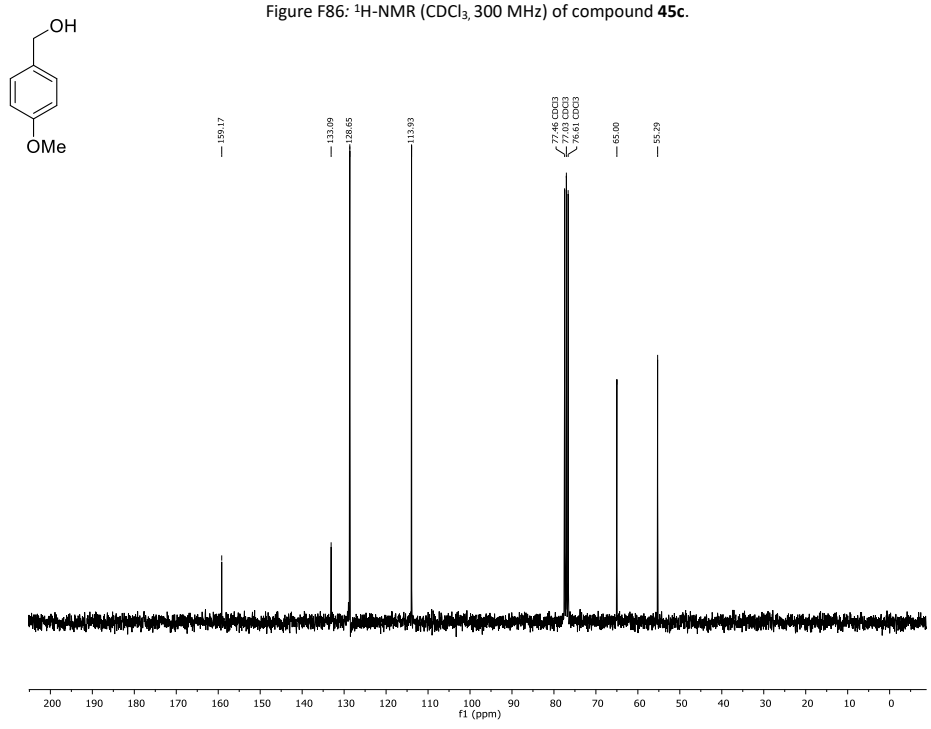

Figure F87: ^{13}C-NMR ($CDCl_3$, 75 MHz) of compound **45c**.

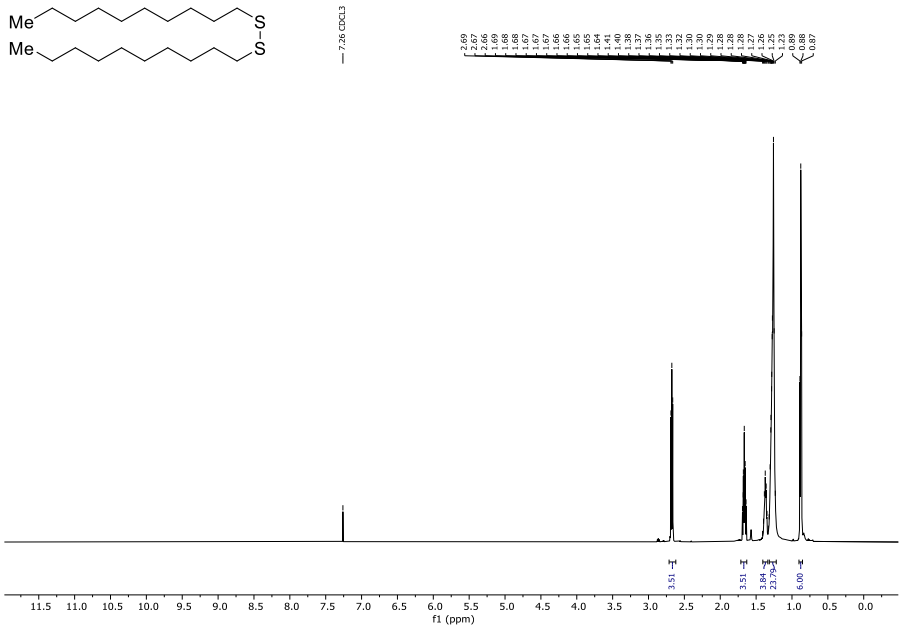

Figure F88: ^{1}H-NMR ($CDCl_3$, 600 MHz) of compound **53b**.

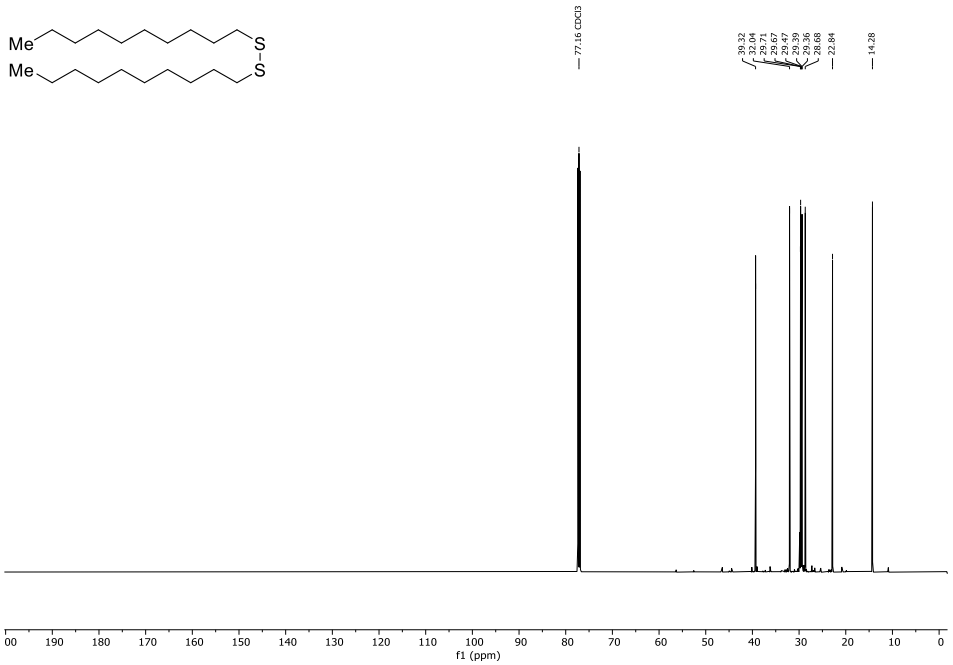

Figure F89: ^{13}C-NMR ($CDCl_3$, 151 MHz) of compound **53b.**

B Computerchemie und Spektroskopie

Die zugehörigen experimentellen Daten und Spektren zu den einzelnen Publikationen sind in Form der jeweiligen *supporting information* abgebildet. Die Molekülgeometrien, die für die quantenmechanischen Berechnungen verwendet wurden, sind bei einer geringen Anzahl an untersuchten Molekülen in der entsprechenden *supporting information* abgedruckt. Andernfalls werden die Koordinaten als zip-Datei von den entsprechenden Journalen in elektronischer Form bereitgestellt.

B.1 Zusatzmaterial zur *in silico* Betrachtung von Reaktionsmechanismen

B.1.1 Zusatzmaterial der Publikation zur Simulation des Reaktionspfads einer photokatalysierten [3+2]-Cycloaddition von Vinylcyclopropanen mit Acetylenen

Im Folgenden ist die *supporting information* der Publikation „Vinylcyclopropane [3+2]-Cycloaddition with Acetylenic Sulfones Based on Visible Light Photocatalysis“ abgedruckt.[554]

Chemistry—A European Journal

Supporting Information

Vinylcyclopropane [3+2] Cycloaddition with Acetylenic Sulfones Based on Visible Light Photocatalysis

Adriana Luque, Jonathan Groß, Till J. B. Zähringer, Christoph Kerzig, and Till Opatz*

Table of Contents

1. LIGHT SOURCES AND REACTION SETUP

1.1 Light sources

All photoreactions using UV-light were performed in a Rayonet photoreactor (RPR 100, SOUTHERN NEW ENGLAND ULTRAVIOLET COMPANY) with 16 circular arranged Philips TUV 8W G8T5 lamps and equipped with a magnetic stirrer and an internal cooling fan. The reactions were performed under inert gas atmosphere in 50 mL quartz tubes (diameter: 2 cm, length: 27 cm) under vigorous stirring. All photoreactions using blue LEDs were performed with Kessil lamp (KSPR, 50 W, 160L-456 nm) and (KSPR, 45 W, 160L-440 nm). The emission spectra of the lamps can be found on the manufacturer's homepage: https://www.kessil.com/science/PR160L.php.

1.2 Irradiation setup

The irradiation setup for each of the wavelengths is shown in figures S1 and S2.

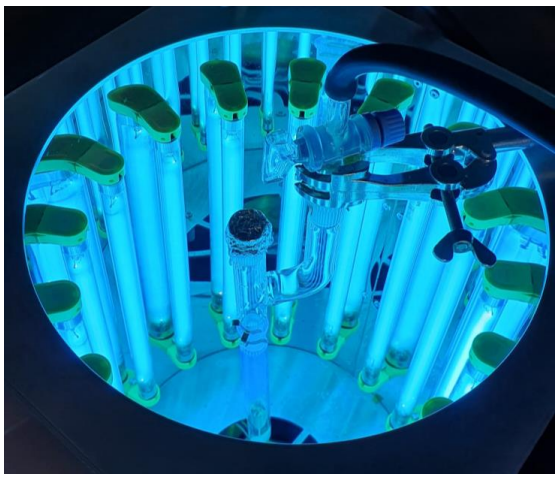

Figure S1. Setup for the irradiation of the allylation product with UVC-light in a Rayonet photoreactor.

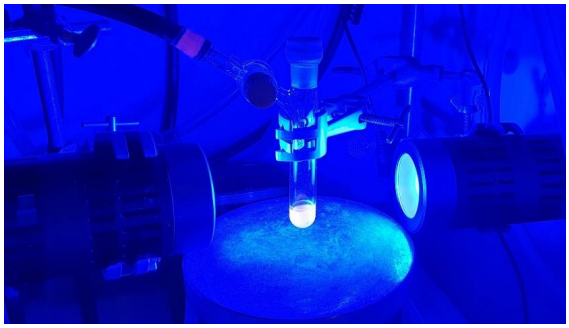

Figure S2. Setup for the irradiation of *meta* photoadducts with the blue LED (distance: 5 cm).

2. OPTIMIZATION STUDIES

2.1. General procedure for screening reactions

An oven-dried Schlenk tube (10 mL) was charged with the *meta* photocycloadduct **4**, the alkynyl sulfone **6** and the respective photocatalyst. The flask was set under an atmosphere of argon by three cycles of vacuum and backfill, followed by the addition of the respective solvent mixture via syringe. All solvents had been degassed beforehand by argon sparging for 20 min in an ultrasonic bath. After the reaction mixture was irradiated for 10 h with the respective light, the solvent was removed under reduce pressure and the residue purified by flash column chromatography.

Table S1. Catalyst screening.

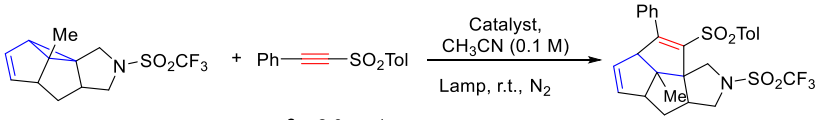

4, 1.0 equiv. **6a**, 2.0 equiv. **7a**

Entry	Catalyst (2.5 mol %) [a]	Yield (%) [c]
1	$[Ir(ppy)_2(dtbbpy)]PF_6$	53
2	phenanthrene (100 mol%) [b]	63
3	$Ir(ppy)_3$	49
4	$[Ru(bpy)_3]Cl_2$	traces [d]
5	$[Ir(dFCF_3ppy)_2(bpy)]PF_6$	51
6	$[Ir(dF(CF_3)ppy)_2(dtbbpy)]PF_6$	49

Procedure: The reactions were performed according to the general procedure for screening reactions using the *meta* photoadduct (**4**, 35.0 mg, 0.12 mmol, 1.00 equiv), alkynyl sulfone (**6a**, 61.2 mg, 0.24 mmol, 2.00 equiv), the respective catalyst and CH_3CN (1.1 mL, c = 0.10 M). [a] A 40 W blue LED 456 nm module was used for irradiation. [b] A UV/vis CFL bulb was used for irradiation. [c] All yields are those of isolated products. [d] Not isolated.

As can be seen in Table S1, among the photoredox catalyst the highest yield of the desired tetracycle **7a** is obtained when using $[Ir(ppy)_2(dtbbpy)]PF_6$ and phenanthrene. The optimization process with these two catalysts (Table S2) showed that decreasing the catalyst loading to 2 mol% in the case of the iridium catalyst increases the yield while variations in the case of phenanthrene did not lead to a higher yield. The screening with different solvents (Table S3) indicated that in the case of the iridium catalyst by increasing the polarity of the solvent the yield was also increasing being methanol the best option (entry 6), but similar variations in the case of the phenanthene were not so effective and further optimization of the reaction conditions was carried out using only $[Ir(ppy)_2(dtbbpy)]PF_6$ as the catalyst.

Finally, variations on the equivalents of the acetylenic sulfone **6a** and the concentration of the *meta* photoadduct **4** (Table S4) showed that the best conditions are 2 equivalents of **6a** and a concentration of 0.15 M of **4** (entry 4).

Table S2. Catalyst loading.

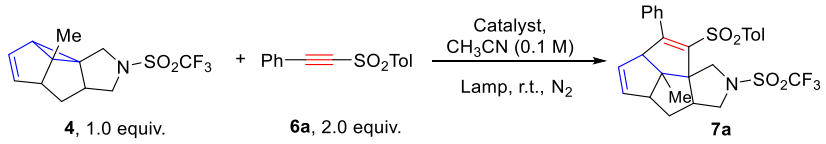

4, 1.0 equiv. **6a**, 2.0 equiv. **7a**

Entry	Catalyst (mol %) [a]	Yield (%) [c]
1	$[Ir(ppy)_2(dtbbpy)]PF_6$ (1.0)	55
2	$[Ir(ppy)_2(dtbbpy)]PF_6$ (1.5)	56
3	$[Ir(ppy)_2(dtbbpy)]PF_6$ (2.0)	58
4	$[Ir(ppy)_2(dtbbpy)]PF_6$ (2.5)	53
5	phenanthrene (50) [b]	55
6	phenanthrene (100) [b]	63
7	phenanthrene (150) [b]	63

Procedure: The reactions were performed according to the general procedure for screening reactions using the *meta* photoadduct (**4**, 35.0 mg, 0.12 mmol, 1.00 equiv), alkynyl sulfone (**6a**, 61.2 mg, 0.24 mmol, 2.00 equiv), the respective catalyst and CH_3CN (1.1 mL, c = 0.10 M). [a] A 40 W blue LED λ= 456 nm module was used for irradiation. [b] A UV/vis CFL bulb was used for irradiation. [c] All yields are those of isolated products.

Table S3. Solvent screening.

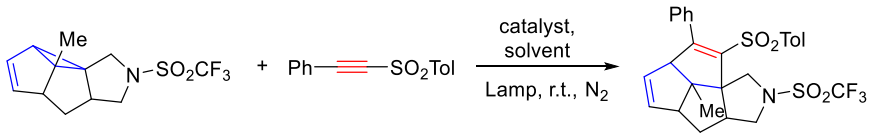

4, 1.0 equiv. **6a**, 2.0 equiv. **7a**

Entry	Catalyst (mol%) [a]	Solvent	Yield (%) [c]
1	$[Ir(ppy)_2(dtbbpy)]PF_6$ (2 mol%)	DCM	49
2	$[Ir(ppy)_2(dtbbpy)]PF_6$ (2 mol%)	DMF	60
3	$[Ir(ppy)_2(dtbbpy)]PF_6$ (2 mol%)	DMSO	53
4	$[Ir(ppy)_2(dtbbpy)]PF_6$ (2 mol%)	CH_3CN	58
5	$[Ir(ppy)_2(dtbbpy)]PF_6$ (2 mol%)	$CH_3CN:H_2O$ (9:1)	68
6	$[Ir(ppy)_2(dtbbpy)]PF_6$ (2 mol%)	CH_3OH	80
7	phenanthrene (100 mol%) [b]	CH_3CN	63
8	phenanthrene (100 mol%) [b]	$CH_3CN:H_2O$ (9:1)	58
9	phenanthrene (100 mol%) [b]	CH_3CN: CH_3OH (8:2)	58

Procedure: The reactions were performed according to the general procedure for screening reactions using the *meta* photoadduct (**4**, 35.0 mg, 0.12 mmol, 1.00 equiv), alkynyl sulfone (**6a**, 61.2 mg, 0.24 mmol, 2.00 equiv), the respective catalyst and solvent (1.1 mL, c = 0.10 M). [a] A 40 W blue LED λ= 456 nm module was used for irradiation. [b] A UV/vis CFL bulb was used for irradiation. [c] All yields are those of isolated products.

Table S4. Screening of reaction stoichiometry and concentration.

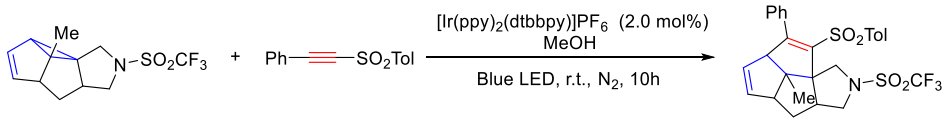

4, 1.0 equiv. **6a**, 1.0-4.0 equiv. **7a**

Entry	Equiv of 6a	Concentration of 4 (M)	Yield (%) [a]
1	1.0	0.10	63
2	2.0	0.10	80
3	4.0	0.10	85
4	2.0	0.15	85
5	2.0	0.20	78

Procedure: The reactions were performed according to the general procedure for screening reactions using the *meta* photoadduct (**4**, 35.0 mg, 0.12 mmol, 1.00 equiv), $[Ir(ppy)_2(dtbbpy)]PF_6$ (2.2 mg, 2.4 µmol, 0.02 equiv) and varying amounts of alkynyl sulfone (**6a**), and solvent (10-20 mM). [a] All yields are those of isolated products.

3. MECHANISTIC CONSIDERATIONS

3.1. Control experiments

Table S5 Control experiments**.**

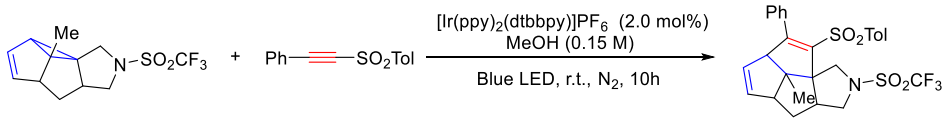

4, 1.0 equiv. **6a**, 2.0 equiv. **7a**

Entry	conditions	Yield (%) [a]
1	optimized	85
2	no light	0
3	with air	0
4	No $[Ir(ppy)_2(dtbbpy)]PF_6$	0

TEMPO coupling product detected by HRMS and NMR

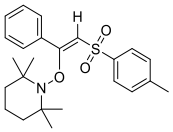

Procedure: The reactions were performed according to the general procedure for screening reactions using the *meta* photoadduct (**4**, 35 mg, 0.12 mmol, 1.00 equiv), 1-methyl-4-(phenylethynylsulfonyl)benzene (**2a**, 61.2 mg, 0.24 mmol, 2.00 equiv), $[Ir(ppy)_2(dtbbpy)]PF_6$ (2.2 mg, 2.4 µmol, 0.02 equiv) and 0.8 mL of degassed solvent (15 mM). [a] All yields are those of isolated products.

Initial control experiments (Table S4) proved the reaction to be light and catalyst dependent (entries 2 and 4). Additionally, the presence of air suppresses the product formation. A radical trapping experiment was set up using TEMPO as a radical scavenger. No desired product was obtained, but instead the TEMPO trapping product was determined by ESI-HRMS and NMR. To check whether the product is formed through a radical-chain mechanism, a light-dark cycle experiment was performed (Table S6).

3.2. UV-Vis studies.

Since the reaction did not proceed without light, the UV/Vis absorption spectra of all reactants and a combination thereof were recorded. The spectra are compiled in Figure S3. No new absorption maxima was detected pointing towards no ground state charge-transfer-complex formation. Considering the emission spectrum of the blue LED Kessil lamp (λmax ≈ 456 nm), the absorption spectra clearly indicate that the catalyst is the only compound absorbing light. Thus, it is reasonable to assume that the developed cycloaddition is indeed initiated by the excited ^{3}MLCT-state of the catalyst.

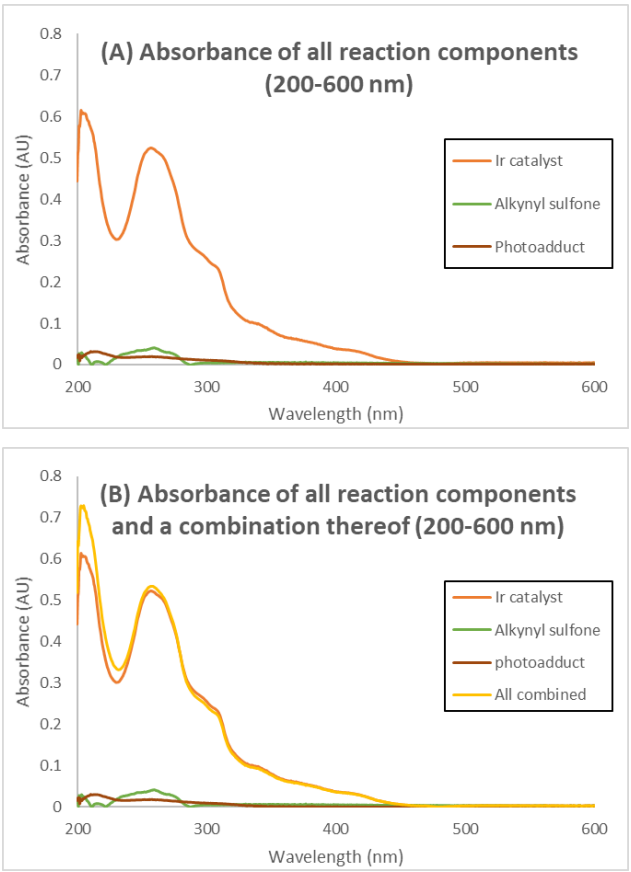

Figure S3. UV/vis spectra of all reaction components (A) and a combination thereof (B). All spectra were measured in MeOH with a concentration of 1×10^{-5} M for all compounds. The sample "All combined" contained equimolar amounts of all reaction components with a concentration of 1×10^{-5} M each. The spectra were collected on a Thermo Fisher Scientific UV/Vis spectrometer (Model: Evolution 201).

3.3. Light ON-OFF experiments.

The *meta* photoadduct **4** (50.0 mg, 0.17 mmol, 1.00 equiv), alkynyl sulfone **6a** (87.4 mg, 0.34 mmol, 2.00 equiv), $Ir(ppy)_2(dtbbpy)PF_6$ (3.12 mg, 0.003 mmol, 2.00 mol-%), 1,4-bis(trimehtylsilyl)benzene (18.0 mg, 0.09 mmol, 0.50 equiv), and methanol-d_4 (1.1 mL, c = 0.15 M) were loaded in an oven-dried Schlenk tube (10 mL) under nitrogen atmosphere, and the mixture was degassed and then placed in front of two blue LEDs at a distance of 5 cm. The reaction vessel was irradiated discontinuously and after each light-phase and each dark phase, an aliquot of 0.1 mL was taken via syringe, diluted with methanol-d_4 and analyzed by ^{1}H NMR spectroscopy.

Table S6. Results of the light-dark cycle experiment for the formation of product **7a**.

Time (h)	Yield of 7a (%)
0	0
1	40
2	42
3	52
4	52
5	58
6	58

The Table S6 shows that no efficient self-sustained radical-chain mechanism occurs. No product formation was observed in the absence of light and the small differences in yield are within the margin of error.

3.4. Initial luminescence quenching studies

Emission spectra were recorded on a JASCO FP–8300 spectrofluorometer with 1 cm quartz cuvettes in degassed methanol exciting with a wavelength of λ = 460 nm. All samples were degassed by bubbling argon through the analytical sample for 10 minutes. The Stern-Volmer plots were constructed by the general equation $(I_0/I) = K_{SV}[Q]$(Figure S4–S5).

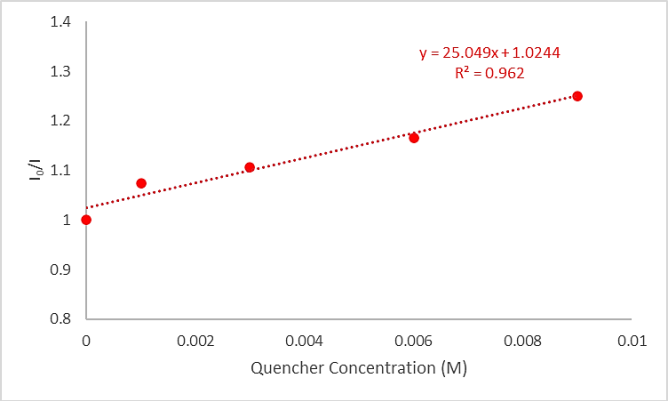

Figure S4. Stern-Volmer plot for the fluorescence quenching of the $[Ir(ppy)_2(dtbbpy)]PF_6$ (1×10^{-5} M in degassed methanol) with the *meta* photoadduct **4**.

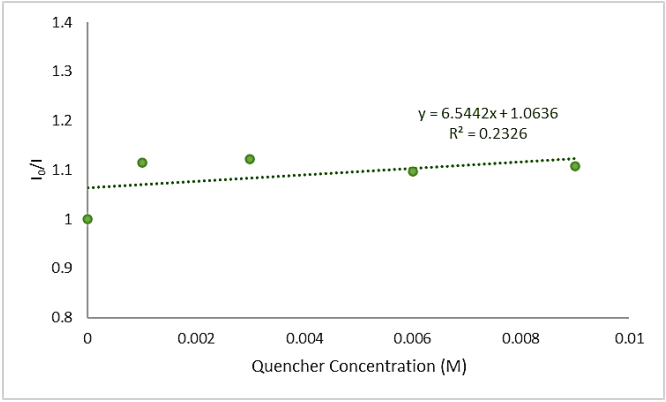

Figure S5. Stern-Volmer plot for the fluorescence quenching of the $[Ir(ppy)_2(dtbbpy)]PF_6$ (1×10^{-5} M in degassed methanol) with the acetylenic sulfone **6a**.

These initial quenching experiments indicate that an electron or energy transfer from the excited triplet state of the catalyst to *meta* photoadduct **4** occurs. However, to confirm the mechanism described in Scheme 4 (main paper), a more detailed and thorough study was carried out as described in in Sections 3.5 and 3.6.

3.5. Reduction potential measurements

The *meta* photoadduct **4** and alkynyl sulfone **6a** were analyzed using cyclic voltammetry (Figure S6). The cyclic voltammograms were recorded at room temperature with solution of the substrate (5.0 mM) in acetonitrile with Bu_4NBF_6 (0.1 M) as electrolyte. The potentials were expressed against the Ag/AgCl in 3M KCl reference electrode and here was converted against SCE by subtracting 45 mV. The potentials of the *meta* photoadduct were determined to be E_{red} = –1.69 V vs Ag/AgCl = –1.65 V vs SCE; E_{red} = –1.38 V vs Ag/AgCl = –1.34 V vs SCE E_{ox} = +2.00 V vs Ag/AgCl = +1.96 V vs SCE. The potentials of the alkynyl sulfone were determined to be E_{red} = –1.76 V vs Ag/AgCl = –1.72 V vs SCE; E_{red} = –1.48 V vs Ag/AgCl = –1.44 V vs SCE.

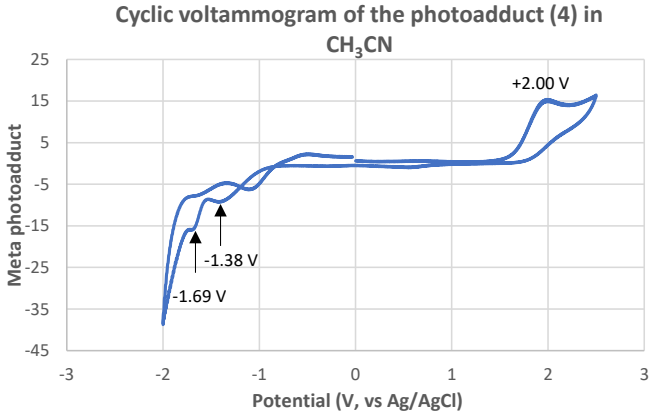

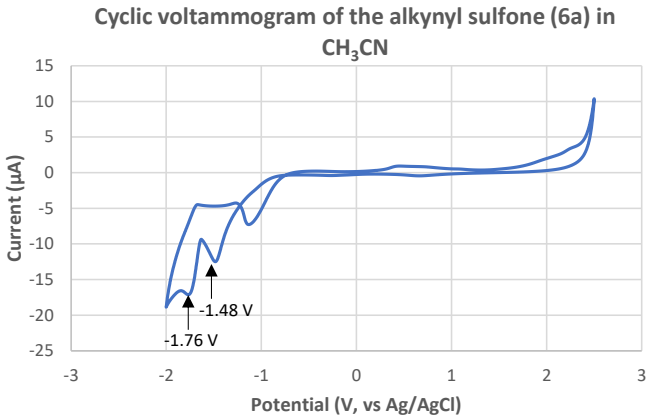

Figure S6. Cyclic voltammograms of **4** and **6a** at room temperature (22 °C) using an *Autolab PGSTAT 204* potentiostat from Metrohm. Conditions: 5 mM substrate in acetonitrile (10 mL) with 0.1 M Bu_4NBF_6. WE: platinum tip (d = 2 mm); CE: glassy carbon rod; RE: Ag/AgCl in 3 M KCl; Scan rate: 100 mV/s.

The thermodynamic feasibility of single electron transfer (SET) steps, which could occur during the reaction were evaluated by comparing the Gibbs free energies of the single SET steps. These Gibbs free energies were calculated as described in the literature and can be summarized in the Table S7.[1] However, the Gibbs free energies provided are rather estimations, considering the fact that the literature redox potentials might fluctuate due to the variation in conditions.

Table S7. Redox potentials and Gibbs free energies for relevant SET steps.

Entry	Catalyst $E_{1/2}^{red}$/ $E_{1/2}^{oxd}$ (V vs SCE)	Electron acceptor	Electron donor	Gibbs free energy (kcal/mol)	Comment
1	-2.10	*meta* photoadduct **4**	[Phenanthrene]*	-10.377 -17.526	Oxidative quenching
	+1.27	[Phenanthrene]*	*meta* photoadduct **4**	+15.912	Reductive quenching
2	-0.89	*meta* photoadduct **4**	$[Ir(dF(CF_3)ppy)_2(dtbbpy)]^{+*}$	+17.526 +10.377	Oxidative quenching
	+1.21	$[Ir(dF(CF_3)ppy)_2(dtbbpy)]^{+*}$	*meta* photoadduct **4**	+17.296	Reductive quenching
3	-1.00	*meta* photoadduct **4**	$[Ir(dFCF_3ppy)_2(bpy)]^{+*}$	+14.990 +7.841	Oxidative quenching
	+1.32	$[Ir(dFCF_3ppy)_2(bpy)]^{+*}$	*meta* photoadduct **4**	+14.759	Reductive quenching
4	-1.73	*meta* photoadduct **4**	[*fac*-Ir(ppy)$_3$]*	-1.845 -8.994	Oxidative quenching
	+0.31	[*fac*-Ir(ppy)$_3$]*	*meta* photoadduct **4**	+38.051	Reductive quenching
5	-0.96	*meta* photoadduct **4**	$[Ir(ppy)_2(dtbbpy)]^{+*}$	+15.912 +8.763	Oxidative quenching
	+0.66	$[Ir(ppy)_2(dtbbpy)]^{+*}$	*meta* photoadduct **4**	+29.97	Reductive quenching
6	−0.81	*meta* photoadduct **4**	$[Ru(bpy)_3]^{+2*}$	+19.371 +12.222	Oxidative quenching
	+0.77	$[Ru(bpy)_3]^{+2*}$	*meta* photoadduct **4**	+27.443	Reductive quenching

From the data compiled in Table S7 can be inferred that a SET steps are possible when using phenanthrene or *fac*-Ir(ppy)$_3$ but only in an oxidative quenching process, where electron transfer from these catalyst to the *meta* photoadduct **4** is exergonic. The possibility of SET with the rest of the listed catalysts can be excluded as the quenching process, both oxidation and reduction are endergonic being probably thermodynamically unfavorable. Since the tetracycle **7a** could be isolated in moderate yields (Table S1) by using almost every of these catalysts except for [Ru(bpy)$_3$]Cl$_2$, it can be assumed that a photo-initiated electron transfer is less likely to be involved and led us to propose that an energy transfer pathway could instead be in operation for this cycloaddition reaction.

3.6. Laser flash photolysis studies

Laser flash photolysis (LFP) studies with absorption and emission detection of transient species using a frequency tripled Nd:YAG laser (355 nm, ~5 ns pulse duration) combined with an LP980KS spectrometer from Edinburgh Instruments were performed to further investigate the underlying mechanism. A more detailed description of the setup can be found in Section 5.

3.6.1 Stern-Volmer experiments

Initial luminescence quenching experiments showed that [Ir(ppy)$_2$(dtbbpy)]PF$_6$ is predominantly quenched by the *meta* photoadduct **4**. Lifetime-based quenching experiments with selected photosensitizers (Ir(ppy)$_3$, [Ir(dF(CF$_3$)ppy)$_2$(dtbbpy)]PF$_6$ and [Ir(ppy)$_2$(dtbbpy)]PF$_6$) showed that [Ir(dF(CF$_3$)ppy)$_2$(dtbbpy)]PF$_6$ is most effectively quenched by the *meta* photoadduct **4**, in line with its highest triplet energy. High quenching efficiencies are pivotal for obtaining reliable results. Hence, all further LFP experiments were conducted with [Ir(dF(CF$_3$)ppy)$_2$(dtbbpy)]PF$_6$ as sensitizer. Lifetime-based Stern-Volmer experiments of [Ir(dF(CF$_3$)ppy)$_2$(dtbbpy)]PF$_6$ (32 µM) with varying concentrations of *meta* photoadduct **4** and sulfone **6a** yielded quenching rates k_q of $4 \cdot 10^6$ M^{-1} s^{-1} and $5 \cdot 10^5$ M^{-1} s^{-1}, respectively (Figure S7).

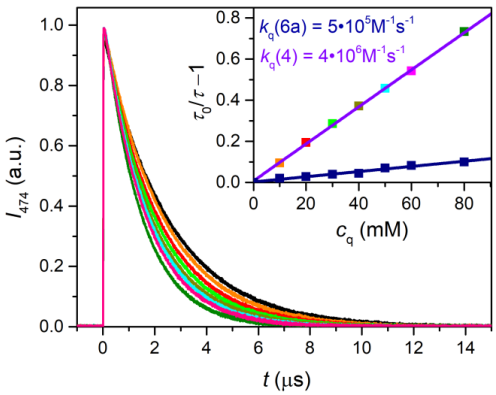

Figure S7. Emission decay kinetics of excited [Ir(dF(CF$_3$)ppy)$_2$(dtbbpy)]PF$_6$ (32 µM) in the presence of varying concentrations of **4** in Ar-saturated MeCN. Inset: Stern-Volmer plots of [Ir(dF(CF$_3$)ppy)$_2$(dtbbpy)]PF$_6$ and **4** (purple fit, the colored symbols correspond to the same quencher

concentration as in the main plot), and [Ir(dF(CF$_3$)ppy)$_2$(dtbbpy)]PF$_6$ and **6a** (dark blue). Detection occurred at 474 nm.

3.6.2 Transient absorption studies

Subsequently, it was explored whether the sensitizer quenching proceeds via energy or electron transfer. Transient absorption (TA) studies were performed to monitor the quenching products. Three solutions of 32 µM [Ir(dF(CF$_3$)ppy)$_2$(dtbbpy)]PF$_6$ in the absence of any substrate, in the presence of 80 mM of **4**, and 80 mM of both **4** and **6a**, were prepared in Ar-saturated MeCN. After excitation, the iridium sensitizer efficiently populates the triplet-excited state with a lifetime of 2.5 µs in MeCN (Equation 1). The transient absorption spectrum of the triplet-excited state of [Ir(dF(CF$_3$)ppy)$_2$(dtbbpy)]$^+$ is shown in Figure S8, Panel B (recorded 10 ns after the laser pulse and time-integrated over 100 ns).

$$[\mathrm{Ir(dF(CF_3)ppy)_2(dtbbpy)}]^+ \underset{\tau_0 = 2.5\ \mu s}{\overset{h\nu,\ \mathrm{ISC}}{\rightleftharpoons}} {}^3[\mathrm{Ir(dF(CF_3)ppy)_2(dtbbpy)}]^+ \qquad \text{(Equation 1)}$$

The emission lifetime of [Ir(dF(CF$_3$)ppy)$_2$(dtbbpy)]$^+$ is reduced in the presence of 80 mM **4** and 80 mM of **6a** (Figure S8, Panel A) in agreement with the lifetime-based Stern-Volmer experiments. However, for either solution, once the initial triplet-excited ^{3}[Ir(dF(CF$_3$)ppy)$_2$(dtbbpy)]$^+$ had decayed completely (after about 10 µs), no reaction intermediate(s) could be observed (i.e., baseline-like spectra were obtained).

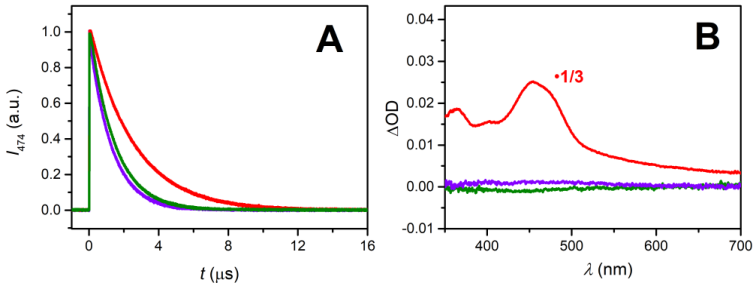

Figure S8: LFP experiments after excitation with 355 nm laser pulses with a solution of 32 µM [Ir(dF(CF$_3$)ppy)$_2$(dtbbpy)]PF$_6$ and 80 mM of **4** (green), and 80 mM of both **4** and **6a** (purple) in Ar-saturated MeCN. Panel A: Time-resolved emission monitored at 474 nm in the absence (red) and presence of quenchers. Panel B: Transient absorption spectrum of the triplet-excited ^{3}[Ir(dF(CF$_3$)ppy)$_2$(dtbbpy)]$^+$ (red, delay 10 ns) and spectra recorded right after the initial sensitizer triplet decay (delay 10 µs).

In order to provide further evidence that an electron transfer reaction between the sensitizer and one of the substrates can be excluded, transient absorption spectra of the reduced and oxidized catalyst were recorded with other reductive or oxidative quenchers.

A solution of 32 µM [Ir(dF(CF$_3$)ppy)$_2$(dtbbpy)]PF$_6$ and 5 mM of the well-known reductive quencher triethanolamine (TEOA), whose radical cation is essentially transparent in the resulting TA spectra, was prepared to investigate the reductive quenching of the excited catalyst (Figure S9). Time-resolved emission spectroscopy showed that the lifetime of the sensitizer emission is strongly reduced by the addition of TEOA (Panel A). A transient absorption spectrum was recorded once the excited sensitizer

was fully quenched, 6 µs after excitation (Panel B). As opposed to the transient absorption spectra recorded for [Ir(dF(CF$_3$)ppy)$_2$(dtbbpy)]PF$_6$ in combination with **4** and **6a**, a new absorbing species is formed. This novel species decays on a much longer timescale as time-resolved transient spectroscopy at a detection wavelength of 452 nm revealed (Panel C).

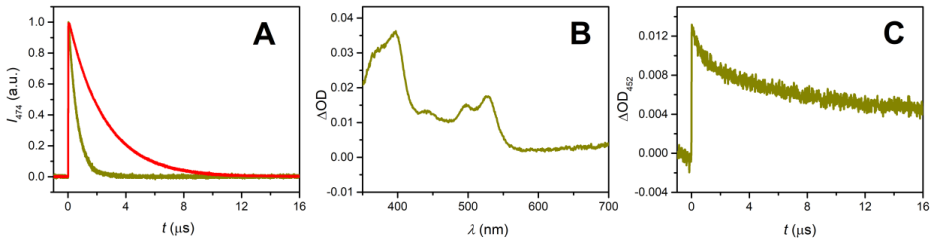

Figure S9: Identification of the reduced [Ir(dF(CF$_3$)ppy)$_2$(dtbbpy)] species by LFP experiments after excitation with 355 nm laser pulses of a solution containing 32 µM [Ir(dF(CF$_3$)ppy)$_2$(dtbbpy)]PF$_6$ and 5 mM TEOA in Ar-saturated MeCN. Panel A: Time-resolved emission monitored at 474 nm in the absence (red) and presence of TEOA (dark yellow). Panel B: Transient absorption spectrum of the quenching product (delay 6 µs, integration over 100 ns). Panel C: Transient absorption traces monitored at 452 nm.

TEOA has been widely used as a reductive quencher before, with an oxidation potential of 0.57-0.82 V vs SCE (aqueous solution).[2] This is low enough to be oxidized by the triplet-excited catalyst (Ir^{3+*}/Ir^{2+} = 1.21 V vs SCE) (Equation 2). The reaction generates the reduced species, [Ir(dF(CF$_3$)ppy)$_2$(dtbbpy)], and the radical cation, $N(EtOH)_3^{\cdot+}$. Radical cations of aliphatic amines are essentially transparent in our detection range;[3] hence we assign the TA spectrum in Figure S9 to the reduced catalyst. Similar absorption spectra of the reduced catalyst [Ir(dF(CF$_3$)ppy)$_2$(dtbbpy)] have been reported in the literature.[4]

$$^3[Ir(dF(CF_3)ppy)_2(dtbbpy)]^+ + N(EtOH)_3 \longrightarrow [Ir(dF(CF_3)ppy)_2(dtbbpy)] + N(EtOH)_3^{\cdot+} \qquad \text{(Equation 2)}$$

A solution of 32 µM [Ir(dF(CF$_3$)ppy)$_2$(dtbbpy)]PF$_6$ and 2 M tetrachloromethane was prepared to investigate the oxidative quenching of the excited catalyst. Tetrachloromethane was selected as the quencher as the excited state oxidation potential of [Ir(dF(CF$_3$)ppy)$_2$(dtbbpy)]PF$_6$ (Ir^{4+}/Ir^{3+*} = -0.89 V vs SCE) should be sufficient to reduce CCl_4 (-0.78 V vs SCE)[5] and the fragments $CCl_3\cdot$ and Cl^- upon reduction are not expected to absorb in the selected detection range (350-700 nm) (Equation 3).[6] The related lab-scale reaction with the very same iridium complex has also been reported in the literature.[7] We tried methyl viologen dihexafluorophosphate as an oxidative quencher as well. However, the reduced quencher strongly absorbs in the visible region, making it difficult to obtain a clean spectrum of the oxidized sensitizer.

$$^3[Ir(dF(CF_3)ppy)_2(dtbbpy)]^+ + CCl_4 \longrightarrow [Ir(dF(CF_3)ppy)_2(dtbbpy)]^{2+} + CCl_3^{\cdot} + Cl^- \qquad \text{(Equation 3)}$$

Time-resolved emission spectroscopy showed that the lifetime of the sensitizer emission is reduced by the addition of CCl_4 (Figure S10, Panel A). After the luminescence has fully returned to baseline a transient absorption spectrum was recorded (10.5 µs delay) (Panel B). A new absorbing species is observed with a maximum at 410 nm. This newly formed species decays on a longer timescale (detection

wavelength of 400 nm) compared to the sensitizer emission (Panels A and C). Since no other compound apart from the oxidized sensitizer should absorb in the range, the new absorbing species is assigned to $[Ir(dF(CF_3)ppy)_2(dtbbpy)]^{2+}$.

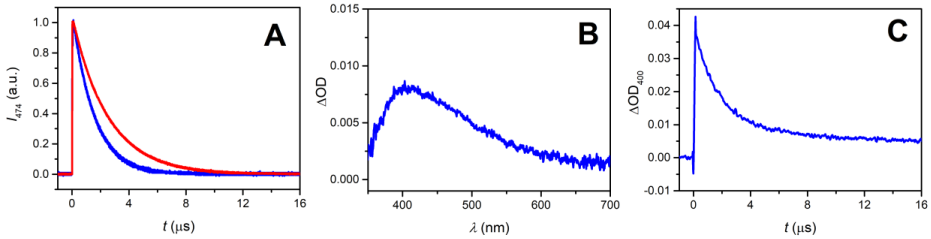

Figure S10: Identification of the oxidized $[Ir(dF(CF_3)ppy)_2(dtbbpy)]^{2+}$ species by LFP experiments after excitation with 355 nm laser pulses of a solution containing 32 µM $[Ir(dF(CF_3)ppy)_2(dtbbpy)]PF_6$ and 2 M CCl_4 in Ar-saturated MeCN. Panel A: Time-resolved emission monitored at 474 nm in the absence (red) and presence of CCl_4 (blue). Panel B: Transient absorption spectrum of the quenching product (delay 10.5 µs). Panel C: Transient absorption traces monitored at 400 nm.

Additional Stern-Volmer experiments of $[Ir(dF(CF_3)ppy)_2(dtbbpy)]PF_6$ were performed with varying concentrations of (1-cyclopropylvinyl)benzene (**8**). Because of the extended π-system, we presumed that compound **8** has a lower triplet energy (ca. 10 kcal mol^{-1}) than compound **4**. Hence, a higher quenching rate constant is expected for **8**. We obtained a k_q value of $5 \cdot 10^{8} M^{-1} s^{-1}$ from the Stern-Volmer plot (Figure S11, Panel A), confirming the assumptions. After the sensitizer's emission has been fully quenched and at high quenching efficiencies above 95% (40 mM of **8**) no new absorbing species was observed (Panel B). If oxidative or reductive quenching were to occur, pronounced spectroscopic signatures of the reduced or oxidized sensitizer would have been observed in the transient absorption spectrum (compare, Figures S9 and S10).

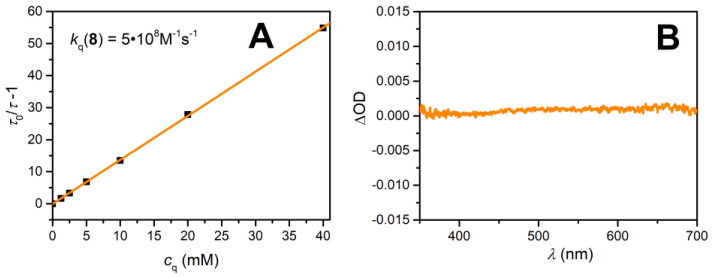

Figure S11: LFP experiments after excitation with 355 nm laser pulses of a solution containing 32 µM $[Ir(dF(CF_3)ppy)_2(dtbbpy)]PF_6$ and (1-cyclopropylvinyl)benzene (**8**) in Ar-saturated MeCN. Panel A: Lifetime-based Stern-Volmer plot with varying concentrations of **8**. Panel B: Transient absorption spectrum of the quenching product of 32 µM $[Ir(dF(CF_3)ppy)_2(dtbbpy)]PF_6$ and 40 mM of **8** (delay 0.4 µs).

4. COMPUTATIONAL STUDIES

All structures were optimized applying the functionals B3LYP,[8] CAM-B3LYP[9] as well as M062X[10] in conjunction with the Pople basis-set 6-311+G(2d,p)[11] with the IEFPCM solvation model[12] for methanol. The adiabatic S_0–T_1 energy gaps were determined as difference between the electronically excited states (T_1) and the respective ground states (S_0). To predict the vertical excitation energies and the UV/vis-spectra, the time-dependent DFT method[13] was used with the respective optimized ground state structures at the same level of theory.[14] Frequency analysis was performed to obtain the Gibbs free energies of each molecule and to confirm every structure as local minima (N_{imag} = 0). All calculations were performed using the software Gaussian 16, rev. C.01.[15] Spin densities were visualized using GaussView 6.[16]

Input Lines

Geometry Optimization

#p opt=tight freq $FUNC 6-311+g(2d,p) scrf=(iefpcm,solvent=methanol)

Vertical Excitation Energy

#p td=(triplets,root=1) $FUNC 6-311+g(2d,p) scrf=(iefpcm,solvent=methanol)

UV/vis-spectra

#p td=(triplets,nstates=100) ub3lyp 6-311+g(2d,p) scrf=(iefpcm,solvent=acetonitrile)

Coordinates and Energies

Ground States

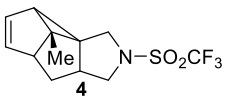

4

6c-Methyl-2-[(trifluoromethyl)sulfonyl]-1,2,3,3a,4,4a,6a,6c-octahydrocyclopropa[1,6]pentaleno[1,2-*c*]pyrrole (4)

B3LYP

Sum of electronic and thermal Free Energies: -1368.617594 Hartree

Vertical excitation energy to the first triplet state: 3.5325 eV

Coordinates of S_0:

C	-2.45882	1.97718	-0.39336
C	-3.49812	1.41538	-1.00656
C	-3.66687	-0.02346	-0.54780
C	-2.91460	-0.06803	0.84136
C	-1.93908	1.07724	0.67208
C	-2.83331	-0.88594	-1.56314
C	-1.48746	-1.13899	-0.85961
C	-1.50810	-0.39546	0.45940
C	-0.08863	-0.82971	-1.38393
N	0.66466	-0.91224	-0.08038
C	-0.24044	-0.85743	1.13390
S	2.26014	-0.83542	0.02413
O	2.85834	-1.30969	-1.20283
C	2.69193	0.99583	0.05049
O	2.68463	-1.30855	1.32214
F	4.01361	1.15485	0.15431
F	2.10316	1.59522	1.09132
F	2.27364	1.58582	-1.07403
C	-3.64526	-0.41735	2.10946
H	-2.03214	2.94709	-0.61665
H	-4.03710	1.82335	-1.85316
H	-4.70327	-0.35712	-0.48164
H	-1.47734	1.51202	1.55288
H	-3.32438	-1.83773	-1.77067
H	-2.73063	-0.36550	-2.51545
H	-1.46077	-2.19989	-0.58188
H	0.31111	-1.56076	-2.08199
H	-0.01591	0.17220	-1.81005
H	0.15382	-0.17174	1.87868
H	-0.31198	-1.85870	1.56266

H	-4.48283	0.26513	2.27934
H	-4.04715	-1.43398	2.06757
H	-2.98109	-0.35470	2.97424

CAM-B3LYP

Sum of electronic and thermal Free Energies: -1368.223829 Hartree

Vertical excitation energy to the first triplet state: 3.5481 eV

Coordinates of S_0:

C	-2.39079	1.95057	-0.43700
C	-3.43488	1.39488	-1.03293
C	-3.62934	-0.02428	-0.54006
C	-2.88033	-0.04961	0.84031
C	-1.88915	1.06822	0.64800
C	-2.81657	-0.91592	-1.53259
C	-1.47303	-1.16162	-0.83635
C	-1.48580	-0.40292	0.46638
C	-0.08076	-0.85948	-1.36450
N	0.66971	-0.92626	-0.06840
C	-0.22481	-0.86678	1.14078
S	2.25099	-0.82224	0.03009
O	2.85077	-1.28885	-1.18769
C	2.62943	0.99409	0.04189
O	2.68621	-1.27314	1.32178
F	3.93879	1.18990	0.14046
F	2.02810	1.57943	1.07461
F	2.19255	1.55938	-1.08001
C	-3.61015	-0.35709	2.11337
H	-1.94747	2.90606	-0.68462
H	-3.96760	1.79194	-1.88773
H	-4.67095	-0.33564	-0.46494
H	-1.42482	1.51521	1.52014
H	-3.31600	-1.86795	-1.71050
H	-2.71773	-0.42304	-2.49890
H	-1.44559	-2.21711	-0.54422
H	0.31749	-1.59640	-2.05595
H	-0.01097	0.13755	-1.80062
H	0.17222	-0.17976	1.88196
H	-0.30203	-1.86461	1.57326
H	-4.43344	0.34351	2.27009
H	-4.02926	-1.36586	2.09454
H	-2.94152	-0.28704	2.97269

M062X

Sum of electronic and thermal Free Energies: -1368.232195 Hartree

Vertical excitation energy to the first triplet state: 4.0289 eV

Coordinates of S_0:

C	-1.98620	1.81143	-0.70837
C	-3.09625	1.31260	-1.23972
C	-3.48692	0.02485	-0.53794
C	-2.74353	0.10143	0.84259
C	-1.61324	1.04785	0.51250
C	-2.80635	-1.10559	-1.37263
C	-1.46631	-1.37114	-0.66803
C	-1.40419	-0.47344	0.54518
C	-0.06597	-1.19249	-1.23941
N	0.70659	-1.17085	0.05258
C	-0.17641	-0.96620	1.26073
S	2.25114	-0.78510	0.08327
O	2.87899	-1.23415	-1.12618
C	2.31507	1.05906	-0.03863
O	2.79302	-1.06035	1.38312
F	3.57370	1.47030	-0.03271
F	1.67805	1.60453	0.99097
F	1.73303	1.46425	-1.16047
C	-3.49950	0.08164	2.13917
H	-1.41329	2.64670	-1.08952
H	-3.56269	1.63428	-2.16258
H	-4.56149	-0.12564	-0.43429
H	-1.10037	1.55102	1.32477
H	-3.40447	-2.01633	-1.36023
H	-2.69543	-0.80476	-2.41418
H	-1.49219	-2.39226	-0.27196
H	0.29148	-2.01289	-1.85575
H	0.03524	-0.24508	-1.77086
H	0.27171	-0.25775	1.95228
H	-0.31072	-1.92888	1.75464
H	-4.21594	0.90491	2.17996
H	-4.05129	-0.85359	2.25611
H	-2.81528	0.18219	2.98320

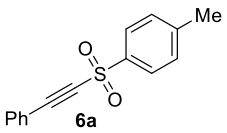

6a

1-Methyl-4-(phenylethynesulfonyl)benzene (6a)

B3LYP

Sum of electronic and thermal Free Energies: -1127.428415 Hartree

Coordinates of S_0:

C	5.50027	-1.37166	-0.00000
C	4.87969	-1.05842	1.20736
C	3.64111	-0.43327	1.21380
C	3.01079	-0.11576	0.00000
C	3.64113	-0.43324	-1.21380
C	4.87970	-1.05838	-1.20737
C	1.74061	0.52370	0.00000
C	0.66205	1.06668	0.00000
S	-0.87148	1.83415	0.00001
C	-2.02973	0.48920	0.00000
C	-2.47280	-0.03247	-1.21262
C	-3.37355	-1.08786	-1.20217
C	-3.83874	-1.63135	-0.00001
C	-3.37355	-1.08786	1.20216

C	-2.47280	-0.03248	1.21262
O	-0.99296	2.55999	1.25479
O	-0.99296	2.56000	-1.25477
C	-4.83789	-2.75662	-0.00001
H	6.46723	-1.85964	-0.00000
H	5.36221	-1.30172	2.14575
H	3.15471	-0.18753	2.14897
H	3.15474	-0.18747	-2.14897
H	5.36223	-1.30166	-2.14575
H	-2.12321	0.38478	-2.14737
H	-3.72148	-1.49564	-2.14396
H	-3.72148	-1.49565	2.14394
H	-2.12321	0.38477	2.14737
H	-4.73007	-3.38335	-0.88616
H	-4.73007	-3.38336	0.88613
H	-5.85835	-2.36116	-0.00001

CAM-B3LYP

Sum of electronic and thermal Free Energies: -1127.033037 Hartree

Coordinates of S_0:

C	5.48081	-1.36043	0.00000
C	4.86284	-1.04970	1.20252
C	3.62770	-0.42878	1.20794
C	3.00296	-0.11532	-0.00000
C	3.62770	-0.42879	-1.20794
C	4.86283	-1.04971	-1.20252
C	1.72870	0.52384	-0.00000
C	0.65638	1.06095	-0.00000
S	-0.87545	1.82411	-0.00000
C	-2.02199	0.48824	-0.00000
C	-2.46182	-0.03075	-1.20770
C	-3.35626	-1.08401	-1.19777
C	-3.81711	-1.62481	0.00000
C	-3.35626	-1.08401	1.19778
C	-2.46182	-0.03075	1.20770
O	-0.99560	2.54376	1.24710
O	-0.99560	2.54376	-1.24711
C	-4.81093	-2.74874	0.00000
H	6.44798	-1.84659	0.00001
H	5.34556	-1.29211	2.14020
H	3.14033	-0.18350	2.14214
H	3.14033	-0.18352	-2.14215
H	5.34556	-1.29213	-2.14020
H	-2.11274	0.38933	-2.14091
H	-3.70411	-1.49366	-2.13796
H	-3.70411	-1.49365	2.13797
H	-2.11274	0.38933	2.14091
H	-4.70086	-3.37425	-0.88524
H	-4.70088	-3.37422	0.88527
H	-5.82990	-2.35428	-0.00002

M062X

Sum of electronic and thermal Free Energies: -1127.087274 Hartree

Coordinates of S_0:

C	5.46131	-1.36479	0.00124
C	4.84381	-1.05061	1.20703
C	3.60917	-0.42168	1.21278
C	2.98818	-0.10568	0.00057
C	3.60999	-0.42136	-1.21130
C	4.84462	-1.05029	-1.20488
C	1.71444	0.54206	0.00018
C	0.64299	1.08843	-0.00023
S	-0.89768	1.84745	-0.00124
C	-2.02059	0.49281	-0.00018
C	-2.44226	-0.03674	-1.21273
C	-3.31557	-1.11178	-1.20115
C	-3.76773	-1.65841	0.00134
C	-3.32245	-1.10491	1.20268
C	-2.44875	-0.02952	1.21271
O	-1.02468	2.56325	1.24614
O	-1.02403	2.56064	-1.25019
C	-4.73918	-2.80459	0.00020
H	6.42607	-1.85584	0.00150
H	5.32538	-1.29593	2.14456
H	3.11984	-0.17227	2.14526
H	3.12129	-0.17170	-2.14403
H	5.32683	-1.29537	-2.14215
H	-2.09573	0.39181	-2.14413
H	-3.65375	-1.53400	-2.13979
H	-3.66568	-1.52136	2.14198
H	-2.10729	0.40435	2.14350
H	-4.58259	-3.45026	-0.86330
H	-4.64627	-3.39947	0.90792
H	-5.76355	-2.42784	-0.04867

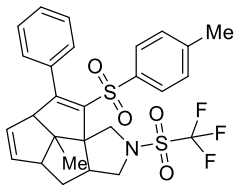

7a

8b-Methyl-8-[(4-methylphenyl)sulfonyl]-7-phenyl-2-[(trifluoromethyl)sulfonyl]-1,2,3,3a,4,4a,6a,8b-octahydrocyclopenta[3,4]pentaleno[1,6a-*c*]-pyrrole (7a)

B3LYP

Sum of electronic and thermal Free Energies: -2496.123889 Hartree

Coordinates of S_0:

C	-1.32560	-3.97156	0.16681
C	-0.14925	-4.53785	-0.08007
C	1.00926	-3.79623	0.53473
C	0.35037	-2.52889	1.17306
C	-1.18489	-2.69877	0.97483
C	2.06801	-3.28363	-0.45065
C	1.53862	-1.94057	-0.97667

C	0.75396	-1.30873	0.23366
C	2.64488	-0.95317	-1.33803
N	2.94718	-0.35307	-0.02077
C	1.75078	-0.28725	0.85412
S	4.34601	0.33451	0.35508
O	5.40087	-0.22515	-0.45817
C	4.23127	2.11870	-0.22983
O	4.46067	0.44697	1.79129
F	3.23695	2.74989	0.40064
F	4.00221	2.15825	-1.54538
F	5.37701	2.75593	0.02759
C	-0.60667	-0.72923	-0.16285
C	-1.65299	-1.47597	0.21576
S	-0.77200	0.73432	-1.19937
C	-3.10476	-1.30770	-0.02803
C	-3.95845	-1.07770	1.05813
C	-5.33183	-0.98253	0.86933
C	-5.87551	-1.14288	-0.40277
C	-5.03648	-1.39323	-1.48377
C	-3.65924	-1.47159	-1.30079
C	-1.91517	1.83824	-0.38018
C	-1.53344	2.46921	0.80305
C	-2.40188	3.36718	1.40194
C	-3.64920	3.65854	0.83346
C	-4.00110	3.01923	-0.35576
C	-3.14490	2.10726	-0.96475
C	-4.57688	4.64160	1.49638
O	0.53353	1.39399	-1.22094
O	-1.35496	0.34991	-2.48185
C	0.69461	-2.37693	2.65373
H	-2.28726	-4.34699	-0.16016
H	-0.01169	-5.45428	-0.64347
H	1.48370	-4.42434	1.29555
H	-1.73025	-2.77709	1.92207
H	3.00975	-3.12128	0.08173
H	2.27160	-3.98648	-1.26132
H	0.87571	-2.09898	-1.82676
H	2.29913	-0.18906	-2.03342
H	3.53215	-1.43823	-1.73804
H	1.33899	0.71741	0.85897
H	2.04331	-0.54780	1.86411
H	-3.54427	-0.95950	2.05253
H	-5.97784	-0.78785	1.71695
H	-6.94698	-1.07679	-0.54869
H	-5.45259	-1.52678	-2.47521
H	-3.01111	-1.65906	-2.14578
H	-0.56783	2.27270	1.25043
H	-2.10546	3.85696	2.32240
H	-4.95907	3.23207	-0.81535
H	-3.42666	1.61382	-1.88416
H	-5.50524	4.75366	0.93637
H	-4.82643	4.31912	2.51050
H	-4.10746	5.62530	1.57886
H	1.77227	-2.37432	2.83057
H	0.27182	-1.46418	3.08186
H	0.27987	-3.22349	3.20607

CAM-B3LYP

Sum of electronic and thermal Free Energies: -2495.349947 Hartree

Coordinates of S_0:

C	-1.29343	-3.97054	0.11081
C	-0.11681	-4.53907	-0.09509
C	1.01704	-3.81647	0.57709
C	0.34202	-2.55810	1.19488
C	-1.17864	-2.71945	0.94681
C	2.10320	-3.29545	-0.36267
C	1.55722	-1.98000	-0.91761
C	0.77744	-1.34684	0.27833
C	2.63632	-0.98312	-1.30464
N	2.93689	-0.35296	-0.00924
C	1.78629	-0.36218	0.91626
S	4.29265	0.41131	0.31209
O	5.34229	-0.07662	-0.53701
C	4.03755	2.15722	-0.25981
O	4.45425	0.53307	1.73371
F	3.04295	2.72196	0.41521
F	3.74653	2.17465	-1.55577
F	5.14645	2.86311	-0.05938
C	-0.56016	-0.74204	-0.13265
C	-1.61420	-1.48402	0.20283
S	-0.68138	0.73002	-1.12887
C	-3.05253	-1.29080	-0.08019
C	-3.92855	-1.05281	0.97675
C	-5.28672	-0.92130	0.74589
C	-5.78942	-1.05146	-0.54039
C	-4.92628	-1.30977	-1.59275
C	-3.56366	-1.42561	-1.36646
C	-1.85079	1.79870	-0.33642
C	-1.51835	2.39574	0.87223
C	-2.41380	3.26186	1.46388
C	-3.63880	3.55291	0.86186
C	-3.94158	2.94897	-0.35143
C	-3.05650	2.06908	-0.95387
C	-4.59739	4.50293	1.51851
O	0.61649	1.38151	-1.07465
O	-1.20538	0.37992	-2.43572
C	0.63629	-2.40705	2.67988
H	-2.24191	-4.33335	-0.26367
H	0.03812	-5.44465	-0.66991
H	1.45686	-4.45488	1.34782
H	-1.75332	-2.81593	1.87323
H	3.01596	-3.10033	0.20672
H	2.35887	-4.00105	-1.15447
H	0.89073	-2.17058	-1.75733
H	2.27174	-0.24041	-2.01219
H	3.52819	-1.46015	-1.70261
H	1.36709	0.63393	1.01629
H	2.12760	-0.69286	1.88945
H	-3.54266	-0.95726	1.98441
H	-5.95532	-0.72089	1.57348
H	-6.85275	-0.95541	-0.72022
H	-5.31311	-1.41951	-2.59805
H	-2.89113	-1.61589	-2.19118
H	-0.56607	2.19478	1.34485
H	-2.15785	3.72845	2.40744
H	-4.88572	3.16499	-0.83580
H	-3.29840	1.59745	-1.89533
H	-5.51117	4.61117	0.93627
H	-4.86699	4.15385	2.51687

H	-4.14659	5.49050	1.63263
H	1.70565	-2.42856	2.89389
H	0.22082	-1.48234	3.08678
H	0.18361	-3.24014	3.22036

M062X

Sum of electronic and thermal Free Energies: -2495.423874 Hartree

Coordinates of S_0:

C	-3.36895	-2.75746	0.18568
C	-2.52544	-3.71654	-0.17400
C	-1.14504	-3.53792	0.40137
C	-1.21666	-2.15534	1.11094
C	-2.69762	-1.70933	1.04616
C	-0.02417	-3.41804	-0.63200
C	-0.08734	-1.96985	-1.12219
C	-0.44732	-1.15227	0.15918
C	1.25952	-1.44113	-1.59672
N	1.91288	-1.06674	-0.32570
C	0.92632	-0.67100	0.70142
S	3.37216	-1.58427	0.08304
O	3.89852	-2.44993	-0.93313
C	4.39272	-0.05587	-0.03578
O	3.42847	-1.92769	1.47604
F	3.96831	0.83387	0.85061
F	4.29541	0.46090	-1.25211
F	5.66203	-0.34242	0.21257
C	-1.48478	-0.06033	-0.09145
C	-2.70101	-0.35851	0.37350
S	-1.21710	1.33276	-1.16254
C	-3.99621	0.34875	0.25327
C	-4.50272	1.04855	1.34531
C	-5.74684	1.66180	1.26414
C	-6.50045	1.55883	0.10158
C	-6.00589	0.84113	-0.98181
C	-4.75847	0.23756	-0.90753
C	0.12862	2.24616	-0.47122
C	1.34747	2.28145	-1.12998
C	2.39008	3.00447	-0.56784
C	2.23237	3.66526	0.64854
C	0.98842	3.61808	1.28472
C	-0.06860	2.91827	0.72940
C	3.38580	4.39126	1.28070
O	-0.78094	0.80754	-2.44541
O	-2.38308	2.18983	-1.12359
C	-0.72571	-2.21324	2.55099
H	-4.41413	-2.69724	-0.09121
H	-2.78467	-4.56505	-0.79681
H	-0.93003	-4.34296	1.10984
H	-3.17466	-1.63556	2.02959
H	0.93902	-3.59380	-0.14012
H	-0.11233	-4.13532	-1.44946
H	-0.84991	-1.84539	-1.89034
H	1.15217	-0.55933	-2.22465
H	1.85342	-2.18917	-2.11573
H	0.96037	0.40431	0.85593
H	1.18915	-1.14749	1.63866
H	-3.91577	1.12364	2.25363
H	-6.12796	2.21744	2.11170
H	-7.47157	2.03348	0.04048
H	-6.59089	0.75511	-1.88887
H	-4.36431	-0.31177	-1.75479
H	1.47219	1.76202	-2.07144
H	3.34512	3.04607	-1.07739
H	0.84947	4.14068	2.22362
H	-1.03367	2.88651	1.22159
H	3.04357	5.25909	1.84378
H	3.90736	3.72914	1.97629
H	4.10418	4.71781	0.52980
H	0.26534	-2.66524	2.62746
H	-0.69602	-1.22060	3.00827
H	-1.41063	-2.83281	3.13289

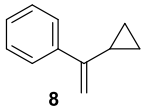

8

(1-cyclopropylvinyl)benzene (8)

B3LYP

Sum of electronic and thermal Free Energies: –426.312414 Hartree

Coordinates of S_0:

C	-3.20534	-0.53425	0.01231
C	-2.19298	-1.47473	-0.15136
C	-0.85901	-1.07913	-0.14655
C	-0.50465	0.26822	0.00896
C	-1.53701	1.20085	0.18662
C	-2.86953	0.80654	0.18501
C	0.92432	0.69110	-0.00610
C	1.91006	-0.30021	0.52299
C	1.28731	1.88907	-0.47941
C	2.66656	-1.22670	-0.41542
C	3.39837	-0.15952	0.35182
H	-4.24400	-0.84262	0.01463
H	-2.44053	-2.52158	-0.28351
H	-0.08486	-1.82363	-0.28013
H	-1.29209	2.24334	0.34855
H	-3.64766	1.54677	0.33065
H	1.59582	-0.77165	1.44853
H	2.31740	2.21979	-0.46129
H	0.56718	2.57181	-0.91235
H	2.78986	-2.26089	-0.11931
H	2.52709	-1.06868	-1.47749
H	3.78226	0.68485	-0.20444
H	4.02093	-0.46501	1.18296

CAM-B3LYP

Sum of electronic and thermal Free Energies: –426.119335 Hartree

Coordinates of S_0:

C	3.16832	-0.42996	0.15872

C	2.29027	-1.32609	-0.42911
C	0.95397	-0.99413	-0.58785
C	0.46740	0.24624	-0.17694
C	1.36174	1.13244	0.42451
C	2.69571	0.80091	0.58903
C	-0.96156	0.61313	-0.37238
C	-1.95805	-0.49840	-0.32224
C	-1.32963	1.87061	-0.59828
C	-2.39046	-1.06692	1.00047
C	-3.35901	-0.28570	0.15705
H	4.21097	-0.69119	0.28889
H	2.64510	-2.29237	-0.76575
H	0.28741	-1.71110	-1.04814
H	1.00412	2.08792	0.78606
H	3.36781	1.50437	1.06483
H	-1.85078	-1.22950	-1.11546
H	-2.36989	2.13231	-0.73875
H	-0.60868	2.67517	-0.66256
H	-2.51938	-2.13768	1.08206
H	-2.01110	-0.58578	1.89263
H	-3.63689	0.70043	0.50238
H	-4.15097	-0.82554	-0.34407

M062X

Sum of electronic and thermal Free Energies: –426.050586 Hartree

Coordinates of S_0:

C	-3.18340	-0.53913	-0.00269
C	-2.16663	-1.47604	-0.13524
C	-0.83685	-1.07400	-0.11624
C	-0.49771	0.27463	0.02291
C	-1.53110	1.20491	0.17066
C	-2.85907	0.80403	0.15470
C	0.92888	0.70188	0.02176
C	1.90690	-0.29801	0.53798
C	1.29226	1.89841	-0.44136
C	2.59805	-1.22935	-0.43168
C	3.38181	-0.18027	0.30220
H	-4.21971	-0.85262	-0.01197
H	-2.40764	-2.52526	-0.25345
H	-0.05309	-1.81341	-0.22309
H	-1.29077	2.25008	0.32202
H	-3.64333	1.54087	0.27678
H	1.61429	-0.76160	1.47345
H	2.32243	2.22746	-0.41314
H	0.57043	2.57980	-0.87355
H	2.71933	-2.26420	-0.14253
H	2.40661	-1.05779	-1.48269
H	3.74883	0.65912	-0.27046
H	4.03376	-0.50475	1.10071

Excited States

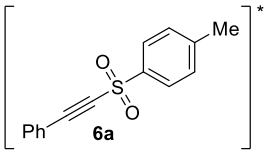

B3LYP

Sum of electronic and thermal Free Energies: –1127.329337 Hartree

Coordinates of T_1:

C	-4.71379	-1.21923	0.00000
C	-4.13677	-0.80428	-1.22673
C	-3.03243	-0.00735	-1.25098
C	-2.42609	0.44768	-0.00000
C	-3.03243	-0.00735	1.25098
C	-4.13677	-0.80429	1.22673
C	-1.36258	1.26999	-0.00000
C	-0.38296	2.07907	0.00000
S	1.37193	2.04341	0.00000
C	1.80096	0.32303	0.00000
C	1.93478	-0.35211	1.21416
C	2.23029	-1.70601	1.20369
C	2.38462	-2.40521	-0.00000
C	2.23029	-1.70601	-1.20369
C	1.93478	-0.35211	-1.21416
O	1.81277	2.64483	-1.25299
O	1.81277	2.64483	1.25299
C	2.73149	-3.86820	-0.00000
H	-5.58849	-1.85545	0.00000
H	-4.58204	-1.12995	-2.15896
H	-2.58671	0.30922	-2.18421
H	-2.58671	0.30921	2.18421
H	-4.58203	-1.12995	2.15896
H	1.82099	0.18103	2.14844
H	2.34391	-2.23097	2.14488
H	2.34391	-2.23096	-2.14488
H	1.82099	0.18104	-2.14844
H	2.34133	-4.36959	0.88659
H	2.34132	-4.36959	-0.88659
H	3.81808	-4.00154	-0.00001

CAM-B3LYP

Sum of electronic and thermal Free Energies: –1126.928617 Hartree

Coordinates of T_1:

C	-4.67763	-1.19313	-0.00000
C	-4.10141	-0.78098	-1.22507
C	-3.00321	0.00978	-1.25227
C	-2.39604	0.46665	0.00000
C	-3.00320	0.00976	1.25227
C	-4.10140	-0.78100	1.22507
C	-1.34327	1.28143	0.00001
C	-0.35974	2.07857	0.00001
S	1.38074	2.02763	0.00000

C	1.77836	0.31203	-0.00000
C	1.90862	-0.35797	1.20815
C	2.18889	-1.71046	1.19829
C	2.33484	-2.40612	-0.00001
C	2.18889	-1.71046	-1.19830
C	1.90863	-0.35796	-1.20816
O	1.82776	2.61643	-1.24504
O	1.82777	2.61643	1.24504
C	2.66703	-3.86884	-0.00000
H	-5.55310	-1.82709	-0.00000
H	-4.54779	-1.10804	-2.15547
H	-2.55589	0.32538	-2.18432
H	-2.55587	0.32534	2.18432
H	-4.54777	-1.10808	2.15547
H	1.80123	0.17803	2.14113
H	2.29694	-2.23733	2.13829
H	2.29695	-2.23732	-2.13831
H	1.80124	0.17804	-2.14113
H	2.27052	-4.36501	0.88526
H	2.27088	-4.36494	-0.88546
H	3.75043	-4.01163	0.00021

M062X

Sum of electronic and thermal Free Energies: –1126.973357 Hartree

Coordinates of T_1:

C	3.25389	1.36067	0.03202
C	2.48911	2.10954	0.93526
C	1.15838	2.34360	0.69033
C	0.54583	1.81798	-0.48591
C	1.34264	1.06681	-1.39958
C	2.67291	0.84748	-1.13229
C	-0.78675	2.07634	-0.75841
C	-1.99622	1.60777	-0.63162
S	-2.57452	0.07923	0.09830
C	-1.11644	-0.90073	0.20727
C	-0.75074	-1.68889	-0.87454
C	0.47880	-2.32980	-0.84820
C	1.34658	-2.17036	0.23176
C	0.94127	-1.38554	1.31542
C	-0.28531	-0.74716	1.31130
O	-3.06063	0.37152	1.43227
O	-3.48615	-0.51136	-0.86139
C	2.71206	-2.79428	0.22864
H	4.30081	1.17762	0.23637
H	2.94835	2.50076	1.83372
H	0.55351	2.91402	1.38324
H	0.87725	0.66460	-2.29015
H	3.27091	0.26459	-1.82131
H	-1.41591	-1.78846	-1.72279
H	0.77650	-2.94817	-1.68642
H	1.60515	-1.26468	2.16370
H	-0.59299	-0.12184	2.14019
H	3.47153	-2.01975	0.08932
H	2.91918	-3.28588	1.17979
H	2.81628	-3.52216	-0.57432

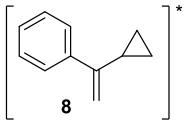

B3LYP

Sum of electronic and thermal Free Energies: –426.233887 Hartree

Coordinates of T_1:

C	-3.32319	-0.37405	-0.00000
C	-2.40950	-1.43077	-0.00001
C	-1.04580	-1.19349	-0.00001
C	-0.52283	0.13068	-0.00000
C	-1.47905	1.18606	0.00000
C	-2.83948	0.93671	0.00000
C	0.87725	0.42694	0.00000
C	1.90458	-0.63236	-0.00000
C	1.32896	1.82347	0.00001
C	3.22622	-0.46131	-0.74708
C	3.22622	-0.46132	0.74708
H	-4.38869	-0.56823	-0.00000
H	-2.76902	-2.45363	-0.00001
H	-0.37752	-2.04337	-0.00001
H	-1.12559	2.21020	0.00001
H	-3.53408	1.76919	0.00000
H	1.53440	-1.64706	-0.00001
H	1.50235	2.36458	0.92518
H	1.50235	2.36458	-0.92516
H	3.60619	-1.33124	-1.26727
H	3.39153	0.48146	-1.25176
H	3.39153	0.48145	1.25177
H	3.60619	-1.33125	1.26726

CAM-B3LYP

Sum of electronic and thermal Free Energies: –426.035404 Hartree

Coordinates of T_1:

C	3.30940	-0.36889	-0.00002
C	2.40200	-1.42339	-0.00003
C	1.04284	-1.18926	-0.00003
C	0.52178	0.12812	-0.00000
C	1.46985	1.18143	0.00002
C	2.82597	0.93573	0.00001
C	-0.87394	0.42036	0.00001
C	-1.89995	-0.63723	-0.00001
C	-1.32757	1.81353	0.00004
C	-3.20875	-0.45637	0.74487
C	-3.20876	-0.45633	-0.74486
H	4.37459	-0.56095	-0.00002
H	2.76345	-2.44470	-0.00005
H	0.37589	-2.03915	-0.00004
H	1.11400	2.20393	0.00003
H	3.51867	1.76872	0.00002
H	-1.53158	-1.65149	-0.00004

H	-1.49963	2.35226	-0.92539
H	-1.49963	2.35222	0.92549
H	-3.60033	-1.32114	1.26285
H	-3.36612	0.48751	1.24822
H	-3.36615	0.48758	-1.24816
H	-3.60036	-1.32107	-1.26288

M062X

Sum of electronic and thermal Free Energies: –425.972155 Hartree

Coordinates of T_1:

C	3.31647	-0.36082	0.00000
C	2.41207	-1.42128	0.00000
C	1.04858	-1.19281	0.00000
C	0.52276	0.12424	0.00000
C	1.46549	1.18466	-0.00000
C	2.82595	0.94391	-0.00000
C	-0.87903	0.40921	-0.00000
C	-1.90135	-0.65009	0.00000
C	-1.34248	1.80183	-0.00000
C	-3.21040	-0.44863	0.74540
C	-3.21040	-0.44863	-0.74540
H	4.38241	-0.54795	0.00000
H	2.77772	-2.44110	0.00000
H	0.38555	-2.04632	0.00000
H	1.10711	2.20686	-0.00000
H	3.51454	1.78030	-0.00000
H	-1.54501	-1.66854	0.00000
H	-1.49567	2.34379	-0.92592
H	-1.49567	2.34379	0.92591
H	-3.61216	-1.30986	1.26004
H	-3.34629	0.49967	1.24671
H	-3.34629	0.49967	-1.24671
H	-3.61216	-1.30986	-1.26004

Diradical Intermediates

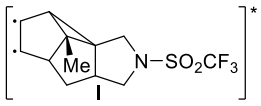

B3LYP

Sum of electronic and thermal Free Energies: -1368.523469 Hartree

Coordinates of T_1:

C	-2.59137	1.92597	-0.46732
C	-3.90491	1.30865	-0.82193
C	-3.70950	-0.15745	-0.55840
C	-2.90799	-0.12484	0.81488
C	-2.01798	1.10812	0.58510
C	-2.73908	-0.74465	-1.65224
C	-1.45836	-1.12134	-0.90640
C	-1.51750	-0.40354	0.41697
C	-0.04204	-0.82008	-1.38684
N	0.68513	-0.86266	-0.07186
C	-0.23620	-0.76821	1.11999
S	2.28046	-0.82413	0.06137
O	2.88899	-1.35685	-1.13587
C	2.75664	0.99570	0.03100
O	2.66598	-1.26137	1.38375
F	4.07937	1.12625	0.15650
F	2.16202	1.64590	1.03725
F	2.37530	1.55362	-1.12242
C	-3.60120	-0.46581	2.10682
H	-2.15773	2.82598	-0.87840
H	-4.83216	1.78888	-0.50225
H	-4.63673	-0.72231	-0.47298
H	-1.49672	1.56197	1.42258
H	-3.18329	-1.60763	-2.14777
H	-2.55076	0.00915	-2.41849
H	-1.49346	-2.19231	-0.66829
H	0.37789	-1.56175	-2.06109
H	0.03016	0.17274	-1.83528
H	0.11675	-0.02580	1.83144
H	-0.28110	-1.74255	1.61077
H	-4.50101	0.14080	2.23770
H	-3.89950	-1.51800	2.12475
H	-2.94863	-0.28575	2.96358

CAM-B3LYP

Sum of electronic and thermal Free Energies: -1368.129807 Hartree

Coordinates of T_1:

C	-2.54591	1.89561	-0.51049
C	-3.87262	1.29533	-0.82376
C	-3.68186	-0.16638	-0.54588
C	-2.88261	-0.11386	0.81494
C	-1.97849	1.09121	0.56368
C	-2.72093	-0.75958	-1.63157
C	-1.44314	-1.12719	-0.89002
C	-1.49483	-0.39338	0.41884
C	-0.03379	-0.83249	-1.37449
N	0.69043	-0.86548	-0.06716
C	-0.22127	-0.77193	1.11993
S	2.27257	-0.81207	0.06089
O	2.88063	-1.33154	-1.13087
C	2.70699	0.99102	0.03047
O	2.66548	-1.24058	1.37347
F	4.01974	1.14949	0.14718
F	2.10611	1.62209	1.03607
F	2.30670	1.53745	-1.11401
C	-3.56465	-0.43107	2.11206
H	-2.06824	2.72928	-1.00297
H	-4.77978	1.78615	-0.46936
H	-4.60982	-0.72689	-0.45157
H	-1.47468	1.56638	1.39930
H	-3.16472	-1.62567	-2.11956
H	-2.53505	-0.01285	-2.40408
H	-1.47706	-2.19287	-0.63610
H	0.38399	-1.57762	-2.04503
H	0.03705	0.15692	-1.82889
H	0.13747	-0.03432	1.83230

H	-0.27579	-1.74621	1.60662
H	-4.45786	0.18337	2.24204
H	-3.86965	-1.47929	2.14828
H	-2.90313	-0.24284	2.95878

M062X

Sum of electronic and thermal Free Energies: -1368.134285 Hartree

Coordinates of T_1:

C	-2.13945	1.75290	-0.75205
C	-3.54460	1.31568	-0.99533
C	-3.55073	-0.11566	-0.53168
C	-2.75297	0.00197	0.82456
C	-1.69223	1.03846	0.44401
C	-2.67584	-0.95588	-1.52322
C	-1.42363	-1.35221	-0.74331
C	-1.40654	-0.49319	0.49187
C	-0.00037	-1.18040	-1.25691
N	0.73942	-1.13641	0.04811
C	-0.16923	-0.92372	1.22791
S	2.28642	-0.76588	0.11515
O	2.94609	-1.25171	-1.06238
C	2.37010	1.07366	-0.05205
O	2.78362	-1.01267	1.43827
F	3.62914	1.47850	0.00909
F	1.68320	1.64863	0.92854
F	1.84998	1.45152	-1.21289
C	-3.47044	-0.04602	2.14190
H	-1.56513	2.47183	-1.31557
H	-4.35980	1.96575	-0.67527
H	-4.54520	-0.53190	-0.38086
H	-1.15019	1.55440	1.23035
H	-3.21535	-1.83305	-1.87541
H	-2.42848	-0.34978	-2.39665
H	-1.52464	-2.38659	-0.39579
H	0.37681	-2.00334	-1.85773
H	0.10689	-0.23713	-1.79651
H	0.24041	-0.18400	1.91111
H	-0.28924	-1.87451	1.74868
H	-4.26683	0.70081	2.17091
H	-3.91839	-1.02825	2.30613
H	-2.78237	0.15856	2.96350

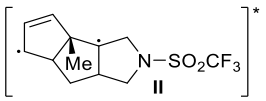

B3LYP

Sum of electronic and thermal Free Energies: -1368.591107 Hartree

Coordinates of T_1:

C	-4.75587	0.10215	-1.17107
C	-4.59043	-0.90046	-0.22652
C	-3.45076	-0.57981	0.69939
C	-2.84085	0.76311	0.10621
C	-3.79991	1.09030	-1.02907
C	-2.29912	-1.61565	0.72688
C	-1.35885	-1.18422	-0.42016
C	-1.48403	0.31447	-0.39414
C	0.14179	-1.47762	-0.25510
N	0.68574	-0.18127	0.23481
C	-0.15453	0.96718	-0.22256
S	2.18029	-0.01024	0.79943
O	2.59663	-1.23507	1.44247
C	3.31600	0.12292	-0.69701
O	2.30513	1.27674	1.44364
F	4.58223	0.26432	-0.30028
F	2.97525	1.18064	-1.44059
F	3.21889	-0.97816	-1.44930
C	-2.76933	1.91145	1.12699
H	-5.53225	0.10840	-1.92701
H	-5.20000	-1.79011	-0.13760
H	-3.82378	-0.41536	1.71617
H	-3.70343	1.97815	-1.64009
H	-1.76397	-1.54426	1.67790
H	-2.65517	-2.64219	0.62209
H	-1.71036	-1.61615	-1.36356
H	0.59730	-1.74566	-1.21006
H	0.35200	-2.25953	0.47064
H	-0.13679	1.75953	0.52376
H	0.23876	1.37525	-1.16282
H	-2.14347	1.64378	1.98221
H	-2.36112	2.81855	0.67473
H	-3.76875	2.14494	1.49862

CAM-B3LYP

Sum of electronic and thermal Free Energies: -1368.195732 Hartree

Coordinates of T_1:

C	-4.74318	0.08091	-1.12782
C	-4.54828	-0.90965	-0.18338
C	-3.39882	-0.56833	0.71653
C	-2.81714	0.76479	0.10294
C	-3.79831	1.07610	-1.00919
C	-2.24452	-1.58830	0.72636
C	-1.35036	-1.17070	-0.45172
C	-1.47208	0.32453	-0.42379
C	0.14578	-1.46317	-0.32622
N	0.68916	-0.18864	0.19271
C	-0.14324	0.96653	-0.22672
S	2.15740	-0.03823	0.78952
O	2.56396	-1.27636	1.39026
C	3.28501	0.14323	-0.67278
O	2.27216	1.21813	1.47334
F	4.54346	0.26688	-0.27116
F	2.94752	1.22166	-1.37470
F	3.18508	-0.92509	-1.45895
C	-2.72974	1.91385	1.10889
H	-5.53336	0.07406	-1.86806
H	-5.14456	-1.80546	-0.07608
H	-3.75624	-0.39838	1.73651
H	-3.72337	1.96176	-1.62543

H	-1.67797	-1.49320	1.65608
H	-2.59303	-2.61911	0.65361
H	-1.73491	-1.60398	-1.37933
H	0.58493	-1.69496	-1.29739
H	0.37198	-2.26862	0.36711
H	-0.12951	1.73396	0.54399
H	0.25139	1.40417	-1.15115
H	-2.08991	1.65245	1.95429
H	-2.33024	2.81738	0.64424
H	-3.72184	2.14813	1.49619

M062X

Sum of electronic and thermal Free Energies: -1368.192716 Hartree

Coordinates of T_1:

C	-4.72749	0.01941	-1.10581
C	-4.49466	-0.94883	-0.14145
C	-3.35530	-0.54846	0.74991
C	-2.80511	0.77465	0.08941
C	-3.81133	1.04719	-1.01026
C	-2.17691	-1.54023	0.77757
C	-1.34437	-1.16872	-0.46135
C	-1.46895	0.33367	-0.47167
C	0.15715	-1.44770	-0.36788
N	0.67075	-0.18834	0.21479
C	-0.13395	0.97082	-0.24859
S	2.14717	-0.03901	0.79766
O	2.55616	-1.27809	1.39309
C	3.24684	0.13887	-0.67453
O	2.26531	1.21808	1.47829
F	4.50744	0.26943	-0.29382
F	2.89046	1.21002	-1.37240
F	3.13511	-0.93299	-1.44886
C	-2.69520	1.94484	1.06805
H	-5.52128	-0.02627	-1.84036
H	-5.05990	-1.86151	-0.01272
H	-3.71450	-0.35251	1.76540
H	-3.76269	1.92382	-1.64205
H	-1.57111	-1.36665	1.67211
H	-2.50054	-2.58183	0.78040
H	-1.76666	-1.63530	-1.35532
H	0.58971	-1.61346	-1.35646
H	0.40610	-2.28186	0.28403
H	-0.13019	1.75100	0.51054
H	0.28733	1.38110	-1.17382
H	-2.04032	1.69168	1.90562
H	-2.29823	2.83457	0.57439
H	-3.68091	2.18849	1.46651

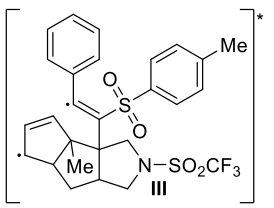

III

B3LYP

Sum of electronic and thermal Free Energies: -2496.021638 Hartree

Coordinates of T_1:

C	1.91889	-0.16276	3.29423
C	0.88325	0.48938	3.94369
C	-0.30117	0.58486	3.02750
C	0.02574	-0.41804	1.85753
C	1.51440	-0.63251	2.05623
C	-0.43567	1.96869	2.35648
C	-1.04930	1.68170	0.99013
C	-0.41570	0.32232	0.49660
C	-2.57941	1.46399	1.04856
N	-2.77080	0.10061	0.50618
C	-1.58880	-0.33703	-0.26214
S	-4.22322	-0.57690	0.34748
O	-5.09126	-0.07676	1.38737
C	-4.97086	0.10234	-1.24300
O	-4.07152	-1.98791	0.08147
F	-6.18290	-0.42088	-1.43466
F	-4.19400	-0.20974	-2.28457
F	-5.07996	1.43282	-1.17224
C	0.77498	0.61505	-0.43420
C	1.51627	1.67168	-0.39792
S	1.28368	-0.54139	-1.83512
C	2.38720	2.73203	-0.47949
C	3.58520	2.75325	0.29348
C	4.44383	3.83154	0.21576
C	4.15319	4.91693	-0.61678
C	2.98140	4.91287	-1.38042
C	2.10547	3.84761	-1.32143
C	2.28127	-1.86444	-1.16694
C	3.63243	-1.63901	-0.90734
C	4.40581	-2.67553	-0.40911
C	3.85495	-3.94089	-0.16686
C	2.50055	-4.13911	-0.44194
C	1.70850	-3.10981	-0.93903
C	4.71433	-5.05842	0.36050
O	0.08324	-1.14527	-2.41127
O	2.15025	0.25326	-2.70017
C	-0.66739	-1.77787	2.08612
H	2.91409	-0.29646	3.70064
H	0.92950	0.94133	4.92510
H	-1.23921	0.31998	3.52399
H	2.13084	-1.20739	1.38250
H	-1.03388	2.66668	2.94528
H	0.55322	2.41336	2.22932
H	-0.83962	2.47805	0.27884
H	-3.09791	2.20835	0.44342
H	-2.97175	1.50633	2.06231
H	-1.55206	-1.41917	-0.30585
H	-1.63638	0.04768	-1.27954
H	3.80953	1.91491	0.93992
H	5.35155	3.83311	0.80711
H	4.83313	5.75779	-0.67013
H	2.75612	5.75238	-2.02701
H	1.19980	3.84484	-1.91391
H	4.07278	-0.66988	-1.10036
H	5.45685	-2.50241	-0.20827

H	2.05545	-5.11172	-0.26852
H	0.66366	-3.27795	-1.16148
H	5.28426	-4.73620	1.23476
H	4.11444	-5.92438	0.64027
H	5.43742	-5.37868	-0.39498
H	-1.75400	-1.69611	2.06067
H	-0.35535	-2.51865	1.34769
H	-0.38444	-2.15651	3.07006

CAM-B3LYP

Sum of electronic and thermal Free Energies: -2495.239068 Hartree

Coordinates of T_1:

C	1.81929	-0.30204	3.27214
C	0.75488	0.29236	3.92087
C	-0.38485	0.44380	2.96319
C	-0.01806	-0.49683	1.76879
C	1.46558	-0.69342	1.99730
C	-0.45779	1.84933	2.34968
C	-1.04864	1.63147	0.96777
C	-0.43853	0.28386	0.44133
C	-2.57728	1.44335	0.99694
N	-2.77884	0.08936	0.45877
C	-1.61627	-0.33837	-0.32784
S	-4.21509	-0.59682	0.34922
O	-5.05330	-0.10562	1.40454
C	-4.98942	0.07414	-1.19869
O	-4.06144	-1.99730	0.08016
F	-6.19476	-0.45234	-1.37025
F	-4.23230	-0.22499	-2.24979
F	-5.10281	1.39660	-1.11603
C	0.75114	0.57979	-0.48055
C	1.48782	1.63702	-0.41542
S	1.25806	-0.53969	-1.85031
C	2.33996	2.71015	-0.43996
C	3.51390	2.71916	0.35807
C	4.35424	3.80776	0.33864
C	4.06634	4.91314	-0.45896
C	2.91733	4.91946	-1.24709
C	2.06027	3.84395	-1.24651
C	2.34672	-1.76765	-1.18668
C	3.67537	-1.44254	-0.95013
C	4.52160	-2.40540	-0.43946
C	4.06468	-3.69489	-0.16579
C	2.73151	-3.99493	-0.41905
C	1.86769	-3.03908	-0.92753
C	5.00496	-4.73501	0.36862
O	0.08377	-1.22553	-2.35710
O	2.03847	0.27615	-2.76012
C	-0.68544	-1.87100	1.92555
H	2.80070	-0.44977	3.70413
H	0.75825	0.68119	4.92922
H	-1.34888	0.17321	3.40090
H	2.11465	-1.21360	1.31087
H	-1.04303	2.54625	2.95051
H	0.54921	2.25954	2.25921
H	-0.81099	2.44998	0.29275
H	-3.07174	2.19068	0.37654
H	-2.98735	1.49932	2.00201
H	-1.59101	-1.41772	-0.40709
H	-1.66823	0.07886	-1.33216
H	3.73506	1.86163	0.97944
H	5.24722	3.80239	0.95065
H	4.73359	5.76490	-0.46653
H	2.69443	5.77776	-1.86805
H	1.16888	3.84811	-1.85936
H	4.04238	-0.44884	-1.16843
H	5.55884	-2.15564	-0.25205
H	2.35958	-4.99170	-0.21734
H	0.83377	-3.28094	-1.13091
H	5.61805	-4.33172	1.17522
H	4.46541	-5.60308	0.74439
H	5.68418	-5.07535	-0.41620
H	-1.77166	-1.80887	1.88270
H	-0.34715	-2.57307	1.16246
H	-0.41311	-2.28526	2.89683

M062X

Sum of electronic and thermal Free Energies: -2495.310111 Hartree

Coordinates of T_1:

C	1.69857	-0.50336	3.22226
C	0.61711	0.04976	3.88468
C	-0.46809	0.33980	2.89326
C	-0.08681	-0.51584	1.64349
C	1.38896	-0.75660	1.89693
C	-0.41304	1.79123	2.38549
C	-1.00230	1.71554	0.98512
C	-0.46336	0.37025	0.37173
C	-2.54178	1.60121	0.99428
N	-2.78702	0.25125	0.45974
C	-1.67801	-0.14965	-0.41545
S	-4.24539	-0.39386	0.37296
O	-5.04250	0.10376	1.45590
C	-5.01538	0.32798	-1.14213
O	-4.13338	-1.79248	0.07723
F	-6.23997	-0.14551	-1.30364
F	-4.28306	0.01549	-2.20308
F	-5.06966	1.64891	-1.03169
C	0.74209	0.66001	-0.51828
C	1.61126	1.59356	-0.30305
S	1.16160	-0.37231	-1.97456
C	2.71040	2.43171	-0.30463
C	3.85442	2.09367	0.46256
C	4.94648	2.93685	0.47829
C	4.93383	4.12582	-0.25127
C	3.81078	4.47068	-1.00417
C	2.70644	3.64464	-1.03636
C	2.13169	-1.69598	-1.32550
C	3.46684	-1.45713	-1.01505
C	4.20345	-2.46669	-0.42356
C	3.62581	-3.70987	-0.14034
C	2.29161	-3.92294	-0.47754
C	1.53553	-2.91935	-1.07106

C	4.44799	-4.79143	0.50144	H	5.81785	2.67102	1.06307
O	-0.05287	-0.93562	-2.53396	H	5.79469	4.78113	-0.23257
O	2.02053	0.43628	-2.81609	H	3.80342	5.39313	-1.57066
C	-0.77566	-1.88996	1.68449	H	1.83323	3.90564	-1.62000
H	2.65790	-0.71695	3.67519	H	3.91218	-0.49332	-1.23161
H	0.58355	0.33588	4.92596	H	5.24390	-2.29433	-0.17395
H	-1.47242	0.09845	3.25346	H	1.83488	-4.88367	-0.27312
H	2.05298	-1.22738	1.18694	H	0.49911	-3.08334	-1.33784
H	-0.94652	2.49076	3.02987	H	4.92690	-4.42273	1.40960
H	0.63080	2.11008	2.32789	H	3.83628	-5.65530	0.75561
H	-0.71091	2.56443	0.36964	H	5.24003	-5.11802	-0.17534
H	-2.99302	2.36120	0.35501	H	-1.86042	-1.81021	1.61614
H	-2.96470	1.67782	1.99384	H	-0.41767	-2.53842	0.88295
H	-1.69459	-1.22129	-0.58620	H	-0.53073	-2.36909	2.63407
H	-1.75128	0.36360	-1.37562				
H	3.85144	1.17206	1.03249				

5. EXPERIMENTAL PROCEDURES

Materials and Methods

Cyclohexane was distilled under nitrogen atmosphere from metallic sodium (Na) and benzophenone. Acetone was distilled from anhydrous calcium sulfate under a nitrogen atmosphere. Acetonitrile, dichloromethane and THF were dried over activated alumina columns on MBraun Solvent Purification System (SPS-800). All other reagent grade chemicals procured from commercial suppliers were used directly without further purification unless otherwise indicated. Yields refer to chromatographically and spectroscopically (^{1}H-NMR) homogeneous material unless otherwise stated. Solvents were degassed using freeze–pump–thaw cycles or by bubbling argon through the liquid in an ultrasonic bath. Deuterochloroform was stored over basic alumina. All reagents were purchased from commercial suppliers and used without further purification. Water- or oxygen-sensitive reactions were performed under an atmosphere of nitrogen in oven-dried glassware using standard Schlenk techniques. Photochemical reactions using UV light were performed in quartz tubes using a photochemical reactor equipped with a circular array of 16 UV lamps (Philips TUV 8W G8T5), a magnetic stirrer, and a cooling fan. Visible light photochemical reactions were performed using blue LEDs (Kessil KSPR, 40 W, λ≈ 160-456 nm) that were placed approximately 5 cm from the reaction mixture in a 10 mL Schlenk tube. Thin-layer chromatography (TLC) was carried out on silica plates (TLC Silica 60 F254 by Merck). Visualization of the compounds was accomplished by projecting UV-light onto the developed plates and with the Dragendorff reagent or using potassium permanganate solution. Chromatographic purification of products was performed as flash column chromatography on silica gel (35–70 µm, Acros Organics) according to the procedure of Still or with the automatic purification system Isolera One from Biotage. Melting points were determined in open capillary tubes and are not corrected. NMR spectra were recorded on a 300, 400, or 600 MHz instrument at 23 °C using standard pulse sequences. The ^{1}H and ^{13}C{H} chemical shifts (δ) were referenced to the residual solvent signal as an internal standard ($CDCl_3$: 7.26 ppm and 77.16 ppm, acetone d_6: 2.05 ppm and 206.26/29.84 ppm for ^{1}H-NMR and ^{13}C-NMR respectively) and reported in parts per million (ppm) relative to tetramethylsilane (TMS). Structural assignments were made with additional information from gCOSY, gHSQC, gNOESY, and gHMBC experiments. FT-IR spectra (given in cm^{-1}) were recorded using a diamond ATR unit. HPLC/ESI-MS

spectra were recorded using an HPLC system with a UV diode array detector coupled with an LC/MSD ion trap. Mixtures of water (with 0.1% formic acid) and acetonitrile were used as an eluent at a total flow rate of 1.0 mL/min. High-resolution masses (APCI-MS and ESI-MS) were recorded using a Q-ToF instrument with dual source and suitable external calibrant. An LP980KS setup from Edinburgh Instruments equipped with an Nd:YAG laser from Litron (Nano LG 300-10) was employed for laser flash photolysis. The frequency-tripled laser output with a wavelength of 355 nm served as excitation source. The laser pulse duration was ~5 ns and the pulse frequency 10 Hz. The typical pulse energy used for transient absorption and emission studies was 15 mJ. Detection of transient absorption spectra occurred on an iCCD camera from Andor. Single-wavelength kinetics were recorded using a photomultiplier tube. The spectroscopic experiments were performed at 293 K using a cuvette holder that allows temperature control. If not stated otherwise the TA spectra were integrated over 100 ns. All samples were prepared in 1 cm quartz cuvettes and degassed by bubbling argon through the analytical sample for 10 minutes.

Preparation of *N*-(2-methylbenzyl)prop-2-en-1-amine (2)

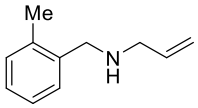

2

To a solution of the allylamine (0.62 mL, 8.32 mmol, 1.00 equiv) in methanol (16 mL) at 0 °C, was added the 2-methylbenzaldehyde (0.96 mL, 8.32 mmol, 1.00 equiv). After stirring at 0 °C until full consumption of the amine and formation of the corresponding imine, $NaBH_4$ (1.20 equiv) was added portionwise at 0 °C and the reaction mixture was stirred at 0 °C for 30 min. The mixture was concentrated under reduced pressure to remove the methanol then was diluted with ethyl acetate and washed with water. The aqueous layer was extracted three times with ethyl acetate (3 x 50 mL). The residue was purified by flash chromatography (SiO_2, eluent: cyclohexane/ethyl acetate, 20:0 → 5:1) to isolate **2** (1.10 g, 6.82 mmol, 82%) as a colorless oil. R_f = 0.23 (3:1 cyclohexane/ethyl acetate). IR/cm^{-1} (ATR): 3015, 2976, 2975, 1643, 1492, 1457, 1097, 1049, 993, 916 cm^{-1}. ^{1}H NMR, COSY (400 MHz, $CDCl_3$) δ 7.33 – 7.29 (m, 1H, H-6), 7.21 – 7.15 (m, 3H, H-3, 4, 5), 5.97 (ddt, *J* = 17.2, 10.2, 6.0 Hz, 1H, -CH=), 5.24 (dq, *J* = 17.2, 1.7 Hz, 1H, =C**H**$_{trans}$), 5.14 (dq, *J* = 10.2, 1.4 Hz, 1H, =C**H**$_{cis}$), 3.79 (s, 2H, -CH_2-), 3.34 (dt, *J* = 6.0, 1.4 Hz, 2H, -C**H$_2$**-CH=), 2.37 (s, 3H, -CH_3). ^{13}C{H} NMR, HSQC, HMBC (101 MHz, $CDCl_3$) δ 138.3 (C-1), 137.0 (-CH=), 136.4 (C-2), 130.4 (C_{Ar}H), 128.5 (C-6), 127.1 (C_{Ar}H), 126.0 (C_{Ar}H), 116.2 (=CH_2), 52.3 (-**C**H_2-CH=), 50.9 (-CH_2-),19.1 (-CH_3). MS (EI): m/z = 161.1 $[M]^+$.

Preparation of *N*-allyl-1,1,1-trifluoro-*N*-(2-methylbenzyl)methanesulfonamide (3)

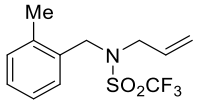

3

To a solution of the amine **2** (5.27 g, 32.7 mmol, 1.00 equiv) in dry CH_2Cl_2 (19 mL) at -78 °C and under N_2 was added triethylamine (6.84 mL, 49.0 mmol, 1.50 equiv) followed by the addition dropwise of trifluoromethansulfonic anhydride (10.14 mL, 36.0 mmol, 1.10 equiv). After 1 h the mixture was allowed to warm to room temperature and stirred for 12 h. The reaction was quenched with water (30 mL), and the organic layer was separated. The aqueous was extracted twice with CH_2Cl_2 (3 x 60 mL). The combined organic phase was dried over $NaSO_4$, filtered, and concentrated under reduced pressure. The residue was purified by flash chromatography (SiO_2, eluent: cyclohexane/ethyl acetate, 100:0 → 98:1) to give **3** (8.15 g, 27.8 mmol, 85%) as a slightly yellow oil. R_f = 0.54 (10:1 cyclohexane/ethyl acetate). IR/cm^{-1} (ATR): 3026, 2933, 1494, 1389, 1226, 1187, 1140, 1060, 912, 610 cm^{-1}.^{1}H NMR, COSY (400 MHz, $CDCl_3$) δ 7.31 – 7.27 (m, 1H, H-6), 7.26 – 7.22 (m, 2H, H-4, 5), 7.20 – 7.16 (m, 1H, H-3), 5.71 (ddt, *J* = 17.0, 10.2, 6.7 Hz, 1 H, -CH=), 5.24 (dq, *J* = 10.2, 1.4 Hz, 1H, =C**H**$_{cis}$), 5.07 (dq, *J* = 17.0, 1.4 Hz, 1H, =C**H**$_{trans}$), 4.57 (s, 2H, -CH_2-), 3.89 (s, 2H, -C**H**$_2$-CH=), 2.32 (s, 3H, -CH_3). ^{13}C{H} NMR, HSQC, HMBC (101 MHz, $CDCl_3$) δ 136.8 (C-1), 131.7 (C-2), 131.1 (-CH=), 131.0 (C-3), 128.5 (C-6), 128.4 (C-4), 126.4 (C-5), 122.0 (=CH_2), 120.1 (q, CF_3, *J* = 323.2 Hz), 50.2 (-**C**H_2-CH=), 48.9 (-CH_2-), 19.3(-CH_3). ^{19}F NMR (376 MHz, $CDCl_3$) δ −76.8 (s, CF_3). MS (ESI): *m/z* = 316.1 [M + Na]$^+$. HRMS (ESI-ToF) *m/z*: [M + Na]$^+$ calcd for $C_{12}H_{14}F_3NO_2SNa$: 316.0589, found: 316.0596.

***meta* photoadduct synthesis**

In an oven-dried quartz tube under nitrogen atmosphere was charged 100.0 mg of the allylation product and 10 mL of anhydrous cyclohexane. The solution was degassed for 15 min and placed in a Rayonet photoreactor. The vessel was irradiated (λ_{max} = 254 nm, 16 × 8 W) at room temperature for 3.5-4.0 h. After removal of the solvent under reduced pressure, the crude isomeric mixture was separated by flash chromatography.

Preparation of (*3aS,4aR,6cR*)-6c-Methyl-2-[(trifluoromethyl)sulfonyl]-1,2,3,3a,4,4a,6a,6c-octahydrocyclopropa[1,6]pentaleno[1,2-*c*]pyrrole (4)

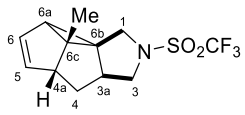

4

Following the general procedure, a mixture of allyl benzyl amine **3** (100.0 mg, 0.34 mmol) and 10 mL of anhydrous cyclohexane was irradiated for 3.5 h. After column chromatography (SiO_2, eluent: cyclohexane/ethyl acetate, 100:0 → 98:1) a 9:1 colorless oily mixture of two isomeric *meta*-photocycloadducts was isolated (72.0 mg, 0.25 mmol, 72%). R_f = 0.50 [$KMnO_4$] (10:1 cyclohexane/ethyl acetate). IR/cm^{-1} (ATR): 3056, 2931, 1479, 1451, 1388, 1226, 1184, 1152, 1023, 729 cm^{-1}. Spectroscopic data are those of the major isomer: ^{1}H NMR, COSY, NOESY (400 MHz, $CDCl_3$) δ 5.64 (dd, *J* = 5.5, 2.2 Hz, 1H, H-6), 5.49 (ddd, *J* = 5.5, 2.3, 0.8 Hz, 1H, H-5), 3.73 (t, *J* = 9.5 Hz, 1H, H-3$_a$), 3.51 (d, *J* = 4.1 Hz, 2H, H-1$_{a,b}$), 3.42 (dd, *J* = 10.6, 3.6 Hz, 1H, H-3$_b$), 3.01 (dd, *J* = 5.3, 2.3 Hz, 1H, H-4a), 2.52 (dtd, *J* = 9.5, 6.2, 3.2 Hz, 1H, H-3a), 1.92 (dt, *J* = 6.2, 1.0 Hz, 1H, H-4$_b$), 1.83 (dd, *J* = 5.1, 2.2 Hz, 1H, H-4$_a$), 1.75 – 1.72 (m, 1H, H-6a), 1.32 (s, 3H, CH_3–C-6b). ^{13}C{H} NMR, HSQC, HMBC (101

MHz, $CDCl_3$) δ 133.6 (C-5), 128.2 (C-6), 120.4 (q, CF_3, J = 323.8 Hz), 57.2 (C-4a), 54.2 (C-3), 48.9 (C-1), 48.1 (C-6b), 47.3 (C-6b), 46.0 (C-4), 41.3 (C-3a), 39.4 (C-6a), 13.7 (**C**H_3–C-6b). ^{19}F NMR (376 MHz, $CDCl_3$) δ −76.2 (s, CF_3). MS (EI): *m/z* = 293.1 $[M]^+$. HRMS (API) *m/z*: $[M]^+$ calcd. for $C_{12}H_{14}F_3NO_2S$: 293.0697, found: 293.0696.

General procedure for the synthesis of alkynyl sulfones (6)

Method A

A solution of ceric ammonium nitrate (2.50 equiv) in CH_3CN (c = 0.25 mmol/mL) was added dropwise to a stirred mixture of the corresponding alkyne (1.00 equiv), the sodium sulfinate (1.20 equiv) and sodium iodide (1.20 equiv) in the same solvent (c=0.20 mmol/mL) under nitrogen atmosphere. After approximately 1 h, the solvent was removed, and the residue was re-dissolved in ethyl acetate and washed with $Na_2S_2O_3$(aq) (3×50 mL) followed by brine (50 mL) and dried over Na_2SO_4. The solvent was removed, and the crude product was refluxed with K_2CO_3 (2.00 equiv) in anhydrous acetone (c= 0.4 mmol/mL) until TLC or HPLC/ESI-MS indicated full consumption of the starting material. The reaction mixture was washed with H_2O (50 mL) and extracted with CH_2Cl_2 (3×20 mL). The combined organic extracts were washed with brine and dried over anhydrous Na_2SO_4. The solvent was removed *in vacuo* and the residue was purified by flash column chromatography (SiO_2, eluent: cyclohexane/ethyl acetate, 97:3) to afford the expected acetylenic sulfone.

Method B

A mixture of the corresponding sodium sulfinate (2.00 equiv), alkyne (1.00 equiv), and iodine (1.50 equiv) in water (c=0.15 mmol/mL) was stirred at room temperature for 2h. After the reaction was completed, the mixture was quenched with $Na_2S_2O_3$(aq) (10 mL). Further stirring was followed by extraction with ethyl acetate (3 × 30 mL). The organic layer was dried with anhydrous Na_2SO_4 and concentrated in vacuo. The residue was refluxed with K_2CO_3 (2.00 equiv) in anhydrous acetone (c= 0.4 mmol/mL) until TLC or HPLC/ESI-MS indicated full consumption of the starting material. the reaction mixture was washed with H_2O (50 mL) and extracted with CH_2Cl_2 (3×20 mL). The combined organic extracts were washed with brine and dried over anhydrous Na_2SO_4. The solvent was removed *in vacuo* and the residue was purified by flash column chromatography (SiO_2, eluent: cyclohexane/ethyl acetate, 97:3) to afford the expected acetylenic sulfone.

1-Methyl-4-(phenylethynesulfonyl)benzene (6a)

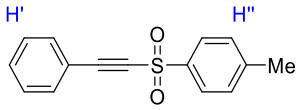

6a

Following general procedure A with phenylacetylene (1.00 g, 9.8 mmol, 1.00 equiv) and sodium *p*-toluenesulfinate (2.10 g, 11.8 mmol, 1.20 equiv) the title compound (1.70 g, 6.63 mmol, 68%) was isolated as a colorless solid. R_f = 0.52 (3:1 cyclohexane/ethyl acetate). Mp: 77−78 °C (cyclohexane-ethyl acetate) Lit.:[17] 78–79 °C. IR/cm^{-1} (ATR): 2988, 2179, 1593, 1486, 1443, 1322, 1291, 1180, 1080,

679 cm^{-1}. ^{1}H NMR, COSY (400 MHz, $CDCl_3$) δ 7.96 (d, *J* = 8.4 Hz, AA‘ part of AA‘BB‘ system, 2H, H-2“,6“), 7.54 – 7.50 (m, 2H, H-2’,6’), 7.49 – 7.44 (m, 1H, H-4’), 7.41 – 7.33 (m, 4H, H-3’,5’/ H-3“,5“), 2.47 (s, 3H, –CH_3). ^{13}C{H} NMR, HSQC, HMBC (101 MHz, $CDCl_3$) δ 145.5 (C-4”), 139.1 (C-1”), 132.9 (C-2‘,6‘), 131.6 (C-4’), 130.2 (C-3”,5”), 128.8 (C-3‘,5‘), 127,8 (C-2”,6”), 118.2 (C-1’), 93.1 (–**C**≡C-SO_2), 85.8 (–C≡**C**-SO_2), 21.9 (–CH_3). MS (ESI): *m/z* = 257.0 $[M + H]^+$. The spectroscopic data are in accordance with the literature.[17-18]

1-Methyl-4-[(4-methylbenzene-1-sulfonyl)ethynyl]benzene (6b)

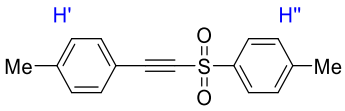

6b

Following general procedure A with 4-ethynyltoluene (0.50 g, 4.30 mmol, 1.00 equiv) and sodium *p*-toluenesulfinate (2.10 g, 5.17 mmol, 1.20 equiv) the title compound (0.81 g, 3.00 mmol, 70%) was isolated as a colorless solid. R_f = 0.52 (3:1 cyclohexane/ethyl acetate). Mp:103 − 104 °C (cyclohexane-ethyl acetate) Lit.:[17] 103–105 °C. IR/cm^{-1} (ATR): 2988, 2177, 1594, 1486, 1441, 1328, 1155, 1085, 859, 606 cm^{-1}. ^{1}H NMR, COSY (400 MHz, $CDCl_3$) δ 7.95 (d, *J* = 8.3 Hz, AA‘ part of AA‘BB‘ system, 2H, H-2“,6“), 7.41 (d, *J* = 8.2 Hz, AA‘ part of AA‘BB‘ system, 2H, H-2’,6’), 7.38 (d, *J* = 8.3 Hz, BB‘ part of AA‘BB‘ system, 2H, H-3“,5“), 7.17 (d, *J* = 8.2 Hz, BB‘ part of AA‘BB‘ system, 2H, H-3’,5’), 2.47 (s, 3H, –CH_3“), 2.37 (s, 3H, –CH_3‘). ^{13}C{H} NMR, HSQC, HMBC (101 MHz, $CDCl_3$) δ 145.4 (C-4”), 142.4 (C-4’), 139.2 (C-1”), 132.8 (C-2‘,6‘), 130.1 (C-3”,5”), 129.6 (C-3‘,5‘), 127,8 (C-2”,6”), 115.0 (C-1’), 93.8 (–**C**≡C-SO_2), 85.3 (–C≡**C**-SO_2), 21.9 (–CH_3‘), 21.8 (–CH_3”). MS (ESI): 271.0 *m/z* = $[M + H]^+$. The spectroscopic data are in accordance with the literature.[17-18]

1-Methoxy-4-[(4-methylbenzene-1-sulfonyl)ethynyl]benzene (6c)

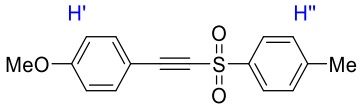

6c

Following general procedure A with 1-ethynyl-4-methoxybenzene (0.60 g, 4.54 mmol, 1.00 equiv) and sodium *p*-toluenesulfinate (0.97 g, 5.45 mmol, 1.20 equiv) the title compound (0.65 g, 6.63 mmol, 50%) was isolated as a yellow solid. R_f = 0.34 (3:1 cyclohexane/ethyl acetate). Mp: 123–124 °C (cyclohexane-ethyl acetate) Lit.:[17]123–124 °C. IR/cm^{-1} (ATR): 2173, 1602, 1509, 1442, 1328, 1258, 1173, 1085, 861, 670 cm^{-1}. ^{1}H NMR, COSY (400 MHz, $CDCl_3$) δ 7.95 (d, *J* = 8.4 Hz, AA‘ part of AA‘BB‘ system, 2H, H-2“,6“), 7.46 (d, *J* = 8.9 Hz, AA‘ part of AA‘BB‘ system, 2H, H-2’,6’), 7.38 (d, *J* = 8.4 Hz, BB‘ part of AA‘BB‘ system, 2H, H-3“,5“), 6.86 (d, *J* = 8.9 Hz, BB‘ part of AA‘BB‘ system, 2H, H-3’,5’), 3.82 (s, 3H, –OCH_3), 2.46 (s, 3H, –CH_3). ^{13}C{H} NMR, HSQC, HMBC (101 MHz, $CDCl_3$) δ 162.2 (C-4’), 145.3 (C-4”), 139.4 (C-1”), 134.8 (C-2‘,6‘), 130.1 (C-3”,5”), 127,5 (C-2”,6”), 114.5 (C-3‘,5‘), 109.8 (C-1’), 94.2 (–**C**≡C-SO_2),

85.0 (–C≡**C**-SO_2), 25.6 (–OCH_3), 21.9 (–CH_3). MS (ESI):287.0 *m/z* = $[M + H]^+$. The spectroscopic data are in accordance with the literature.[17]

3-[(4-Methylbenzene-1-sulfonyl)ethynyl]thiophene (6d)

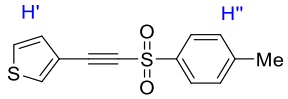

6d

Following general procedure A with 3-ethynylthiophene (0.30 g, 2.77 mmol, 1.00 equiv) and sodium *p*-toluenesulfinate (0.59 g, 3.33 mmol, 1.20 equiv) the title compound (0.44 g, 1.67 mmol, 60%) was isolated as a colorless solid. R_f = 0.34 (3:1 cyclohexane/ethyl acetate). Mp: 98−99 °C (cyclohexane-ethyl acetate) Lit.:[18] 74.2−75.3 °C. IR/cm^{-1} (ATR): 2171, 2166, 1593, 1359, 1152, 1083, 950, 875, 838, 741 cm^{-1}. ^{1}H NMR, COSY (400 MHz, $CDCl_3$) δ 7.95 (d, *J* = 8.4 Hz, AA‘ part of AA‘BB‘ system, 2H, H-2”,6“), 7.74 (dd, *J* = 3.0, 1.2 Hz, 1H, H-5‘), 7.39 (d, *J* = 8.4 Hz, BB‘ part of AA‘BB‘ system, 2H, H-3“,5“), 7.32 (dd, *J* = 5.0, 1.3 Hz, 1H, H-4‘), 7.03 (d, *J* = 8.3 Hz, BB‘ part of AA‘BB‘ system, 2H, H-3”,5”), 7.17 (dd, *J* = 5.0, 1.2 Hz, 1H, H-2‘), 2.47 (s, 3H, –CH_3). ^{13}C{H} NMR, HSQC, HMBC (101 MHz, $CDCl_3$) δ 145.5 (C-4”), 139.1 (C-1”), 134.7 (C-5‘), 130.1 (C-3”,5”), 130.0 (C-2’), 127,7 (C-2”,6”), 126.6 (C-4‘), 117.4 (C-3’), 88.7 (–**C**≡C-SO_2), 85.7 (–C≡**C**-SO_2), 21.9 (–CH_3). MS (ESI):263.0 *m/z* = $[M + H]^+$. The spectroscopic data are in accordance with the literature.[18]

1-Fluoro-4-[(4-methylbenzene-1-sulfonyl)ethynyl]benzene (6e)

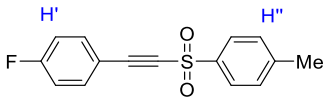

6e

Following general procedure A with 1-ethynyl-4-fluorobenzene (0.50 g, 4.16 mmol, 1.00 equiv) and sodium *p*-toluenesulfinate (0.89 g, 5.00 mmol, 1.20 equiv) the title compound (0.46 g, 1.68 mmol, 40%) was isolated as a colorless solid. R_f = 0.43 (3:1 cyclohexane/ethyl acetate). Mp: 85−87 °C (cyclohexane-ethyl acetate) Lit.:[19] 86.0−87.0 °C. IR/cm^{-1} (ATR): 2183, 1598, 1506, 1402, 1332, 1239, 1158, 1087, 863, 669 cm^{-1}. ^{1}H NMR, COSY (400 MHz, $CDCl_3$) δ 7.95 (d, *J* = 8.4 Hz, AA‘ part of AA‘BB‘ system, 2H, H-2“,6“), 7.56 – 7.50 (m, AA‘ part of AA‘BB‘ system, 2H, H-2’,6’), 7.39 (d, *J* = 8.4 Hz, BB‘ part of AA‘BB‘ system, 2H, H-3“,5“), 7.11 – 7.02 (m, BB‘ part of AA‘BB‘ system, 2H, H-3’,5’), 2.47 (s, 3H, –CH_3). ^{13}C{H} NMR, HSQC, HMBC (101 MHz, $CDCl_3$) δ 162.5 (d, J_{CF} = 255.2 Hz, C-4’), 145.6 (C-4”), 138.9 (C-1”), 135.3 (d, J_{CF} = 9.0 Hz, C-2‘,6‘), 130.2 (C-3”,5”), 127,7 (C-2”,6”), 116.5 (d, J_{CF} = 22.4 Hz,C-3‘,5‘), 114.3 (C-1’), 92.0 (–**C**≡C-SO_2), 85.7 (–C≡**C**-SO_2), 21.9 (–CH_3). ^{19}F NMR (376 MHz, $CDCl_3$) δ -105.77 (tt, *J* = 9.2, 5.2 Hz, 1F, F–C-4’). MS (ESI): 275.0 *m/z* = $[M + H]^+$. The spectroscopic data are in accordance with the literature.[18-19]

1-Bromo-4-[(4-methylbenzene-1-sulfonyl)ethynyl]benzene (6f)

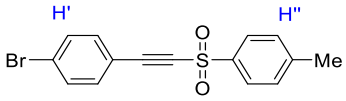

6f

Following general procedure A with 1-bromo-4-ethynylbenzene (0.50 g, 2.76 mmol, 1.00 equiv) and sodium *p*-toluenesulfinate (0.59 g, 3.31 mmol, 1.20 equiv) the title compound (0.73 g, 2.18 mmol, 78%) was isolated as a colorless solid. R_f = 0.43 (3:1 cyclohexane/ethyl acetate). Mp: 105−106 °C (cyclohexane-ethyl acetate) Lit.:[19] 106.7−107.7 °C. IR/cm^{-1} (ATR): 2183, 1583, 1485, 1395, 1332, 1185, 1159, 1086, 851, 652 cm^{-1}. ^{1}H NMR, COSY (400 MHz, $CDCl_3$) δ 7.95 (d, *J* = 8.4 Hz, AA‘ part of AA‘BB‘ system, 2H, H-2“,6“), 7.52 (d, *J* = 8.6 Hz, AA‘ part of AA‘BB‘ system, 2H, H-2’,6’), 7.39 (d, *J* = 8.4 Hz, BB‘ part of AA‘BB‘ system, 2H, H-3“,5“), 7.36 (d, *J* = 8.6 Hz, BB‘ part of AA‘BB‘ system, 2H, H-3’,5’), 2.47 (s, 3H, –CH_3). ^{13}C{H} NMR, HSQC, HMBC (101 MHz, $CDCl_3$) δ 145.7 (C-4”), 138.8 (C-1”), 134.1 (C-3‘,5‘), 132.3 (C-2‘,6‘), 130.2 (C-3”,5”), 127,7 (C-2”,6”), 126.6 (C-4’), 117.1 (C-1’), 91.7 (–**C**≡C-SO_2), 86.7 (–C≡**C**-SO_2), 21.9 (–CH_3). MS (ESI): 275.0 *m/z* =335.0 [M + H]$^+$. The spectroscopic data are in accordance with the literature.[19]

1-Chloro-4-[(4-methylbenzene-1-sulfonyl)ethynyl]benzene (6g)

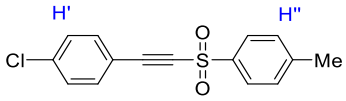

6g

Following general procedure A with 1-chloro-4-ethynylbenzene (0.60 g, 4.39 mmol, 1.00 equiv) and sodium *p*-toluenesulfinate (0.94 g, 5.27 mmol, 1.20 equiv) the title compound (0.66 g, 2.28 mmol, 52%) was isolated as a colorless solid. R_f = 0.51 (3:1 cyclohexane/ethyl acetate). Mp: 98−100 °C (cyclohexane-ethyl acetate) Lit.:[19] 98.7−99.2°C. IR/cm^{-1} (ATR): 2182, 1592, 1488, 1400, 1331, 1185, 1159, 1087, 852, 659 cm^{-1}. ^{1}H NMR, COSY (400 MHz, $CDCl_3$) δ 7.95 (d, *J* = 8.4 Hz, AA‘ part of AA‘BB‘ system, 2H, H-2“,6“), 7.44 (d, *J* = 8.6 Hz, AA‘ part of AA‘BB‘ system, 2H, H-2’,6’), 7.39 (d, *J* = 8.4 Hz, BB‘ part of AA‘BB‘ system, 2H, H-3“,5“), 7.35 (d, *J* = 8.6 Hz, BB‘ part of AA‘BB‘ system, 2H, H-3’,5’), 2.47 (s, 3H, –CH_3). ^{13}C{H} NMR, HSQC, HMBC (101 MHz, $CDCl_3$) δ 145.7 (C-4”), 138.8 (C-1”), 138.1 (C-4’), 134.0 (C-2‘,6‘), 130.2 (C-3”,5”), 129.3 (C-3‘,5‘), 127,7 (C-2”,6”), 116.6 (C-1’), 91.6 (–**C**≡C-SO_2), 86.6 (–C≡**C**-SO_2), 21.9 (–CH_3). MS (ESI): 275.0 *m/z* =291.0 [M + H]$^+$. The spectroscopic data are in accordance with the literature.[18-19]

[(Benzenesulfonyl)ethynyl]benzene (6h)

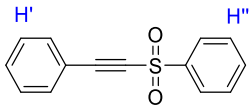

6h

Following general procedure A with phenylacetylene (0.80 g, 7.83 mmol, 1.00 equiv) and sodium benzenesulfinate (1.54 g, 9.40 mmol, 1.20 equiv) the title compound (1.21 g, 5.01 mmol, 64%) was isolated as a colorless solid. R_f = 0.41 (3:1 cyclohexane/ethyl acetate). Mp: 67−69 °C (cyclohexane-ethyl acetate) Lit.:[18] 55.4−55.1°C. IR/cm^{-1} (ATR): 2988, 2179, 1328, 1159, 1086, 850, 756, 727, 685, 657 cm^{-1}. ^{1}H NMR, COSY (400 MHz, $CDCl_3$) δ 8.11 – 8.06 (m, 2H, H-2“,6“), 7.72 – 7.66 (m, 1H, H-4“), 7.63 – 7.57 (m, 2H, H-3“,5“), 7.54 – 7.50 (m, 2H, H-2’,6’), 7.50 – 7.44 (m, 1H, H-4’), 7.40 – 7.33 (m, 2H, H-3’,5’).^{13}C{H} NMR, HSQC, HMBC (101 MHz, $CDCl_3$) δ 141.8 (C-1”), 134.3 (C-4”), 132.9 (C-2‘,6‘), 131.7 (C-4’), 129.5 (C-3”,5”), 128.8 (C-3‘,5‘), 127,5 (C-2”,6”), 117.9 (C-1’), 93.6 (–**C**≡C-SO_2), 85.4 (–C≡**C**-SO_2). MS (ESI): *m/z* = 243.0 [M + H]$^+$. The spectroscopic data are in accordance with the literature.[18]

[(Methanesulfonyl)ethynyl]benzene (6i)

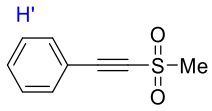

6i

Following general procedure B with phenylacetylene (0.25 g, 2.45 mmol, 1.00 equiv) and sodium methanesulfinate (0.50 g, 5.00 mmol, 2.00 equiv) the title compound (0.28 g, 1.57 mmol, 64%) was isolated as a yellow solid. R_f = 0.28 (3:1 cyclohexane/ethyl acetate). Mp: 58−59 °C (cyclohexane-ethyl acetate) Lit.:[20] 57−58 °C. IR/cm^{-1} (ATR): 2988, 2928, 2184, 1489, 1322, 1149, 1066, 965, 847, 765 cm^{-1}. ^{1}H NMR, COSY (400 MHz, $CDCl_3$) δ 7.65 – 7.58 (m, 2H, H-2’,6’), 7.58 – 7.52 (m, 1H, H-4’), 7.48 – 7.41 (m, 2H, H-3’,5’), 3.33 (s, 3H, –SO_2CH_3). ^{13}C{H} NMR, HSQC, HMBC (101 MHz, $CDCl_3$) δ 133.0 (C-2‘,6‘), 131.9 (C-4’), 129.0 (C-3‘,5‘), 117.6 (C-1’), 91.7 (–**C**≡C-SO_2), 84.5 (–C≡**C**-SO_2), 47.0 (–SO_2CH_3). MS (ESI): *m/z* = 203.0 [M + Na]$^+$. The spectroscopic data are in accordance with the literature.[20]

[(Ethanesulfonyl)ethynyl]benzene (6j)

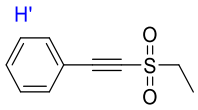

6j

Following general procedure B with phenylacetylene (0.30 g, 2.94 mmol, 1.00 equiv) and sodium ethanesulfinate (0.62 g, 5.87 mmol, 2.00 equiv) the title compound (0.11 g, 0.57 mmol, 20%) was isolated as a yellow oil. R_f = 0.35 (3:1 cyclohexane/ethyl acetate). IR/cm^{-1} (ATR): 2984, 2184, 1492, 1324, 1141, 1047, 849, 760, 733, 690 cm^{-1}. ^{1}H NMR, COSY (400 MHz, $CDCl_3$) δ 7.63 – 7.56 (m, 2H, H-2’,6’), 7.56 – 7.48 (m, 1H, H-4’), 7.46 – 7.37 (m, 2H, H-3’,5’), 3.30 (q, *J* = 7.4 Hz, 2H, SO_2CH_2–), 1.54 (t, *J* = 7.4 Hz, 3H, –CH_3). ^{13}C{H} NMR, HSQC, HMBC (101 MHz, $CDCl_3$) δ 133.0 (C-2‘,6‘), 131.9 (C-4’), 129.0 (C-3‘,5‘), 117.8 (C-1’), 92.7 (–**C**≡C-SO_2), 82.8 (–C≡**C**-SO_2), 52.9 (SO_2CH_2–), 7.9 (–CH_3). MS (ESI): *m/z* = 217.0 [M + Na]$^+$. The spectroscopic data are in accordance with the literature.[20]

[(Butane-1-sulfonyl)ethynyl]benzene (6k)

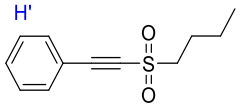

6k

Following general procedure B with 1-hexyne (0.60 g, 7.30 mmol, 1.00 equiv) and sodium *p*-toluenesulfinate (2.60 g, 14.6 mmol, 2.00 equiv) the title compound (1.04 g, 4.68 mmol, 64%) was isolated as a colorless oil. R_f = 0.50 (3:1 cyclohexane/ethyl acetate). IR/cm^{-1} (ATR): 2960, 2200, 1596, 1329, 1185, 1090, 814, 706, 678, 620 cm^{-1}. ^{1}H NMR, COSY (400 MHz, $CDCl_3$) δ 7.85 (d, *J* = 8.4 Hz, AA‘ part of AA‘BB‘ system, 2H, H-2“,6“), 7.34 (d, *J* = 8.4 Hz, BB‘ part of AA‘BB‘ system, 2H, H-3“,5“), 2.44 (s, 3H, –CH_3), 2.33 (t, *J* = 7.1 Hz, 2H, H-1’), 1.55 – 1.45 (m, 2H, H-2’), 1.40 – 1.28 (m, 2H, H-3’), 0.86 (t, *J* = 7.3 Hz, 3H, H-4’). ^{13}C{H} NMR, HSQC, HMBC (101 MHz, $CDCl_3$) δ 145.2 (C-4”), 139.2 (C-1”), 129.9 (C-3”,5”), 127,3 (C-2”,6”), 97.4 (–**C**≡C-SO_2), 78.4 (–C≡**C**-SO_2), 133.0 (C-2‘), 21.9 (C-3’), 21.8 (–CH_3), 18.7 (C-1‘), 13.4 (C-4‘). MS (ESI): 275.0 *m/z* =237.1 [M + H]$^+$. The spectroscopic data are in accordance with the literature.[20]

General procedure for tetracycle (7) synthesis

The *meta* photoadduct **4** (35.0 mg, 0.12 mmol, 1.00 equiv), alkynyl sulfone **6** (0.24 mmol, 2.00 equiv), $Ir(ppy)_2(dtbbpy)PF_6$ (2.2 mg, 0.002 mmol, 0.02 equiv) and methanol (0.8 mL, c = 0.15 M) were loaded in an oven-dried Schlenk tube (10 mL) under nitrogen atmosphere, and the mixture was degassed and then placed in front of two blue LEDs 456 nm (see the materials section) at a distance of 5 cm. The vessel was irradiated until TLC or HPLC/ESI-MS indicated full consumption of the starting material (approx. 10-14 h). The resultant solution was concentrated and purified by flash column chromatography on silica gel (cyclohexane/ethyl acetate) or reversed-phase column chromatography (SiO_2-C_{18}, water/acetonitrile) to give the corresponding product **7** as a racemic mixture.

8b-Methyl-8-[(4-methylphenyl)sulfonyl]-7-phenyl-2-[(trifluoromethyl)sulfonyl]-1,2,3,3a,4,4a,6a,8b-octahydrocyclopenta[3,4]pentaleno[1,6a-*c*]pyrrole (7a)

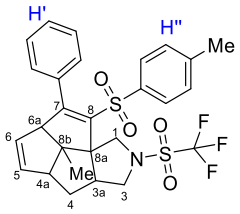

7a

Following the general procedure using 1-methyl-4-(phenylethynesulfonyl)benzene (61.2 mg, 0.24 mmol, 2.00 equiv) after 10 h, column chromatography (SiO_2, eluent: cyclohexane/ethyl acetate, 95:1 → 20:1) afforded the title compound (54.5 mg, 0.10 mmol, 85%) as a colorless solid. R_f = 0.52 (3:1 cyclohexane/ethyl acetate). Mp: 140−142 °C (ethanol). IR/cm^{-1} (ATR): 3056, 2956, 2871, 1595, 1259,

1225, 1189, 1144, 720, 619 cm^{-1}. ^{1}H NMR, COSY, NOESY (400 MHz, $CDCl_3$) δ 7.26 – 7.23 (m, 1H, H-4'), 7.16 (t, *J* = 7.5 Hz, 2H, H-3', 5'), 7.05 (d, *J* = 8.4 Hz, AA' part of AA'BB' system, 2H, H-2",6"), 6.95 (d, *J* = 8.4 Hz, BB' part of AA'BB' system, 2H, H-3",5"), 6.85 – 6.73 (m, 2H, H-2',6'), 5.81 (dt, *J* = 5.6, 2.2 Hz, 1H, H-5), 5.29 (ddd, *J* = 5.6, 2.7, 1.4 Hz, 1H, H-6), 4.59 (d, *J* = 10.2 Hz, 1H, H-1_a), 4.03 (t, *J* = 9.4 Hz, 1H, H-3_a), 3.98 (d, *J* = 10.2 Hz, 1H, H-1_b), 3.79 (tdd, *J* = 8.6, 5.9, 2.4 Hz, 1H, H-3a), 3.38 (t, *J* = 9.4 Hz, 1H, H-3_b), 3.35 (dd, *J* = 2.7, 1.9 Hz, 1H, H-6a), 2.98 (t, *J* = 8.4 Hz, 1H, H-4a), 2.31 (s, 3H, CH_3–C4"), 2.06 (ddd, *J*= 13.6, 8.1, 2.5 Hz, 1H, H-4_b), 1.68 (ddd, *J*= 13.6, 8.7, 2.5 Hz, 1H, H-4_a), 1.36 (s, 3H, CH_3–C-8b). $^{13}C\{H\}$ NMR, HSQC, HMBC (101 MHz, $CDCl_3$) δ 159.6 (C-8), 143.8 (C-4"), 138.3 (C-1"), 137.7 (C-7), 136.1 (C-5), 133.9 (C-1'), 129.1 (C-3",5"), 128.2 (C-6), 128.1 (C-4'), 127.9 (C-3',5'), 127.7 (C-2',6'), 127,5 (C-2",6"), 120.4 (q, *J* = 323.4 Hz, CF_3), 71.0 (C-6a), 70.4 (C-8a), 61.3 (C-8b), 58.7 (C-4a), 52.7 (C-3a), 52.4 (C-3), 52.2 (C-1), 34.4 (C-4), 23.8 (**C**H_3–C-8b), 21.6 (**C**H_3–C4"). ^{19}F NMR (376 MHz, $CDCl_3$) δ −76.3 (s, CF_3). MS (ESI): *m/z* = 550.1 $[M + H]^+$. HRMS (ESI-ToF) *m/z*: $[M + Na]^+$ calcd for $C_{27}H_{26}F_3NO_4S_2Na$: 572.1147, found: 572.1161.

8b-Methyl-7-(4-methylphenyl)-8-[(4-methylphenyl)sulfonyl]-2-[(trifluoromethyl)sulfonyl]-1,2,3,3a,4,4a,6a,8b-octahydrocyclopenta[3,4]pentaleno[1,6a-*c*]pyrrole (7b)

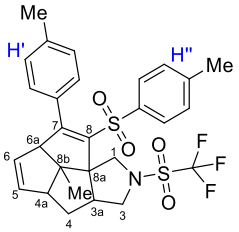

7b

Following the general procedure using 1-methyl-4-[(4-methylbenzene-1-sulfonyl)ethynyl]benzene (64.5 mg, 0.24 mmol, 2.00 equiv) after 10 h, column chromatography (SiO_2, eluent: cyclohexane/ethyl acetate, 95:1 → 20:1) afforded the title compound (45 mg, 0.08 mmol, 67%) as a colorless solid. R_f = 0.53 (3:1 cyclohexane/ethyl acetate). Mp: 143−145 °C (ethanol). IR/cm^{-1} (ATR): 3051, 2927, 2871, 1597, 1259, 1225, 1189, 1144, 813, 616 cm^{-1}. ^{1}H NMR, COSY, NOESY (400 MHz, $CDCl_3$) δ 7.07 (d, *J* = 8.1 Hz, AA' part of AA'BB' system, 2H, H-2",6"), 6.98 (d, *J* = 8.1 Hz, BB' part of AA'BB' system, 2H, H-3',5'), 6.96 (d, *J* = 8.1 Hz, BB' part of AA'BB' system, 2H, H-3",5"), 6.71 (d, *J* = 8.1 Hz, AA' part of AA'BB' system, 2H, H-2',6'), 5.80 (dt, *J* = 5.6, 2.2 Hz, 1H, H-5), 5.30 (ddd, *J* = 5.7, 2.7, 1.4 Hz, 1H, H-6), 4.57 (d, *J* = 10.3 Hz, 1H, H-1_a), 4.02 (t, *J* = 9.4 Hz, 1H, H-3_a), 3.95 (d, *J* = 10.3 Hz, 1H, H-1_b), 3.77 (tdd, *J* = 8.6, 5.9, 2.5 Hz, 1H, H-3a), 3.36 (t, *J* = 9.4 Hz, 1H, H-3_b), 3.33 (dd, *J* = 2.7, 1.9 Hz, 1H, H-6a), 2.96 (t, *J* = 8.5 Hz, 1H, H-4a), 2.34 (s, 3H, CH_3–C4'), 2.32 (s, 3H, CH_3–C4"), 2.04 (ddd, *J*= 13.6, 8.1, 2.5 Hz, 1H, H-4_b), 1.66 (ddd, *J*= 13.6, 8.7, 6.0 Hz, 1H, H-4_a), 1.35 (s, 3H, CH_3–C-8b). $^{13}C\{H\}$ NMR, HSQC, HMBC (101 MHz, $CDCl_3$) δ 159.9 (C-8), 143.8 (C-4"), 138.5 (C-4'), 138.2 (C-1"), 137.5 (C-7), 136.0 (C-5), 131.0 (C-1'), 129.0 (C-3",5"), 128.6 (C-3',5'), 128.4 (C-6), 127.7 (C-2',6'), 127.6 (C-2",6"), 120.4 (q, *J* = 323.9 Hz, CF_3), 71.2 (C-6a), 70.3 (C-8a), 61.2 (C-8b), 58.8 (C-4a), 52.7 (C-3a), 52.4 (C-3), 52.2 (C-1), 34.4 (C-4), 23.8 (**C**H_3–C-8b), 21.7 (**C**H_3–C4"), 21.4 (**C**H_3–C4'). ^{19}F NMR (376 MHz, $CDCl_3$) δ −76.3 (s, CF_3). MS

(ESI): *m/z* = 564.2 [M + H]$^+$. HRMS (APCI-ToF) *m/z*: [M]$^+$ calcd for $C_{28}H_{28}F_3NO_4S_2$: 563.1412, found: 563.1407.

7-(4-Methoxyphenyl)-8b-methyl-8-[(4-methylphenyl)sulfonyl]-2-[(trifluoromethyl)sulfonyl]-1,2,3,3a,4,4a,6a,8b-octahydrocyclopenta[3,4]pentaleno[1,6a-*c*]pyrrole (7c)

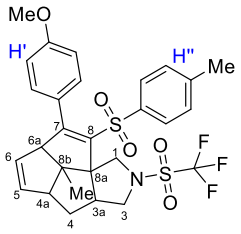

7c

Following the general procedure using 1-methoxy-4-[(4-methylbenzene-1-sulfonyl)ethynyl]benzene (68.3 mg, 0.24 mmol, 2.00 equiv) after 10 h, column chromatography (SiO_2, eluent: cyclohexane/ethyl acetate, 95:1 → 20:1) afforded the title compound (32 mg, 0.05 mmol, 46%) as a colorless solid. R_f = 0.37 (3:1 cyclohexane/ethyl acetate). Mp: 145−146 °C (ethanol). IR/cm^{-1} (ATR): 2957, 2902, 2840, 1602, 1387, 1226, 1183, 1144, 813, 615 cm^{-1}. ^{1}H NMR, COSY, NOESY (400 MHz, $CDCl_3$) δ 7.08 (d, *J* = 8.1 Hz, AA‘ part of AA‘BB‘ system, 2H, H-2”,6”), 6.98 (d, *J* = 8.1 Hz, BB‘ part of AA‘BB‘ system, 2H, H-3”,5”), 6.78 (d, *J* = 8.8 Hz, AA‘ part of AA‘BB‘ system, 2H, H-2‘,6’), 6.71 (d, *J* = 8.8 Hz, BB‘ part of AA‘BB‘ system, 2H, H-3‘,5’), 5.80 (dt, *J* = 5.7, 2.2 Hz, 1H, H-5), 5.29 (ddd, *J* = 5.7, 2.7, 1.5 Hz, 1H, H-6), 4.57 (d, *J* = 10.3 Hz, 1H, H-1$_a$), 4.02 (t, *J* = 9.4 Hz, 1H, H-3$_a$), 3.95 (d, *J* = 10.3 Hz, 1H, H-1$_b$), 3.81 (s, 3H, CH_3O–C4’), 3.78 (m, 1H, H-3a), 3.36 (t, *J* = 9.4 Hz, 1H, H-3$_b$), 3.33 (dd, *J* = 2.6, 1.9 Hz, 1H, H-6a), 2.96 (t, *J* = 8.3 Hz, 1H, H-4a), 2.32 (s, 3H, CH_3–C4”), 2.05 (ddd, *J*= 13.6, 8.0, 2.5 Hz, 1H, H-4$_b$), 1.66 (ddd, *J*= 13.6, 8.7, 6.0 Hz, 1H, H-4$_a$), 1.35 (s, 3H, CH_3–C-8b). ^{13}C{H} NMR, HSQC, HMBC (101 MHz, $CDCl_3$) δ 159.8 (C4’), 159.7 (C-8), 143.7 (C-4”), 138.5 (C-1”), 137.5 (C-7), 136.1 (C-5), 129.2 (C-2‘,6‘), 129.1 (C-3”,5”), 128.4 (C-6), 127.5 (C-2”,6”), 126.1 (C-1’), 113.4 (C-3‘,5‘), 120.4 (q, *J* = 323.6 Hz, CF_3), 71.1 (C-6a), 70.3 (C-8a), 61.1 (C-8b), 58.8 (C-4a), 55.5 (**C**H$_3$O–C4’), 52.8 (C-3a), 52.4 (C-3), 52.2 (C-1), 34.4 (C-4), 23.8 (**C**H$_3$–C-8b), 21.7 (**C**H$_3$–C4”). ^{19}F NMR (376 MHz, $CDCl_3$) δ −76.3 (s, CF_3). MS (ESI): *m/z* = 580.2 [M + H]$^+$. HRMS (APCI-ToF) *m/z*: [M]$^+$ calcd for $C_{28}H_{28}F_3NO_5S_2$: 579,1361, found: 579.1362.

8b-Methyl-8-[(4-methylphenyl)sulfonyl]-7-(thiophen-3-yl)-2-[(trifluoromethyl)sulfonyl]-1,2,3,3a,4,4a,6a,8b-octahydrocyclopenta[3,4]pentaleno[1,6a-*c*]pyrrole (7d)

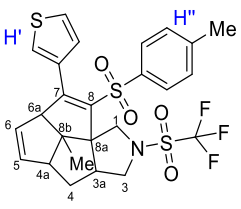

7d

Following the general procedure using 3-[(4-methylbenzene-1-sulfonyl)ethynyl]thiophene (62.6 mg, 0.24 mmol, 2.00 equiv) after 13 h, column chromatography (SiO_2, eluent: cyclohexane/ethyl acetate, 95:1 → 20:1) afforded the title compound (43.0 mg, 0.08 mmol, 65%) as a colorless solid. R_f = 0.50 (3:1 cyclohexane/ethyl acetate). Mp: 150−152 °C (ethanol). IR/cm^{-1} (ATR): 3058, 2954, 2871, 1597, 1387, 1226, 1188, 1144, 706, 621 cm^{-1}. ^{1}H NMR, COSY, NOESY (400 MHz, $CDCl_3$) δ 7.19 (dd, *J* = 3.0, 1.3 Hz, 1H, H-2‘), 7.16 (d, *J* = 8.3 Hz, AA‘ part of AA‘BB‘ system, 2H, H-2”,6“), 7.15 – 7.13 (m, 1H, H-5‘), 7.03 (d, *J* = 8.3 Hz, BB‘ part of AA‘BB‘ system, 2H, H-3”,5”), 6.66 (dd, *J* = 5.0, 1.3 Hz, 1H, H-4‘), 5.80 (ddd, *J* = 5.7, 2.7, 1.9 Hz, 1H, H-5), 5.33 (ddd, *J* = 5.7, 2.7, 1.4 Hz, 1H, H-6), 4.57 (d, *J* = 10.3 Hz, 1H, H-1$_a$), 4.02 (t, *J* = 9.4 Hz, 1H, H-3$_a$), 3.96 (d, *J* = 10.3 Hz, 1H, H-1$_b$), 3.78 (tdd, *J* = 8.7, 5.9, 2.5 Hz, 1H, H-3a), 3.37 (dd, *J* = 2.7, 1.9 Hz, 1H, H-6a), 3.36 (t, *J* = 9.4 Hz, 1H, H-3$_b$), 2.97 (t, *J* = 8.3 Hz, 1H, H-4a), 2.33 (s, 3H, **C**H$_3$–C4”), 2.04 (ddd, *J*= 13.6, 8.1, 2.5 Hz, 1H, H-4$_b$), 1.65 (ddd, *J*= 13.6, 8.6, 5.9 Hz, 1H, H-4$_a$), 1.36 (s, 3H, **C**H$_3$–C-8b).^{13}C{H} NMR, HSQC, HMBC (101 MHz, $CDCl_3$) δ 155.1 (C-8), 143.9 (C-4”), 138.3 (C-1”), 137.9 (C-7), 136.3 (C-5), 133.3 (C-3’), 129.2 (C-3”,5”), 128.5 (C-6), 127.4 (C-4‘), 127.2 (C-2”,6”), 126.0 (C-2’), 125.4 (C-5’), 120.42 (q, *J* = 323.1 Hz, CF_3), 70.5 (C-6a), 70.4 (C-8a), 61.1 (C-8b), 58.8 (C-4a), 52.8 (C-3a), 52.5 (C-3), 52.2 (C-1), 34.5 (C-4), 23.9 (**C**H$_3$–C-8b), 21.7 (**C**H$_3$–C4”).^{19}F NMR (376 MHz, $CDCl_3$) δ −76.1 (s, CF_3). MS (ESI): *m/z* = 556.1 [M + H]$^+$. HRMS (APCI-ToF) *m/z*: [M]$^+$ calcd for $C_{25}H_{24}F_3NO_4S_3$: 555.082, found: 555.0817.

7-(4-Fluorophenyl)-8b-methyl-8-[(4-methylphenyl)sulfonyl]-2-[(trifluoromethyl)sulfonyl]-1,2,3,3a,4,4a,6a,8b-octahydrocyclopenta[3,4]pentaleno[1,6a-*c*]pyrrole (7e)

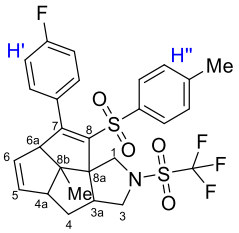

7e

Following the general procedure using 1-fluoro-4-[(4-methylbenzene-1-sulfonyl)ethynyl]benzene (65.5 mg, 0.24 mmol, 2.00 equiv) after 12 h, column chromatography (SiO_2, eluent: cyclohexane/ethyl acetate, 95:1 → 20:1) afforded the title compound (31.0 mg, 0.05 mmol, 65%) as a colorless solid. R_f = 0.53 (3:1 cyclohexane/ethyl acetate). Mp: 141−142 °C (ethanol). IR/cm^{-1} (ATR): 3048, 2954, 1598, 1387,1506, 1225, 1189, 1144, 736, 615 cm^{-1}. ^{1}H NMR, COSY, NOESY (400 MHz, $CDCl_3$) δ 7.08 (d, *J* = 8.3 Hz, AA‘ part of AA‘BB‘ system, 2H, H-2”,6”), 7.01 (d, *J* = 8.3 Hz, BB‘ part of AA‘BB‘ system, 2H, H-3”,5“), 6.92 – 6.82 (m, BB‘ part of AA‘BB‘ system, 2H, H-3‘,5’), 6.84 – 6.74 (m, AA‘ part of AA‘BB‘ system, 2H, H-2‘,6’), 5.83 (ddd, *J* = 5.7, 2.7, 1.9 Hz, 1H, H-5), 5.27 (ddd, *J* = 5.7, 2.7, 1.4 Hz, 1H, H-6), 4.58 (d, *J* = 10.4 Hz, 1H, H-1$_a$), 4.02 (t, *J* = 9.4 Hz, 1H, H-3$_a$), 3.97 (d, *J* = 10.4 Hz, 1H, H-1$_b$), 3.78 (tdd, *J* = 8.7, 5.7, 2.1 Hz, 1H, H-3a), 3.36 (t, *J* = 9.4 Hz, 1H, H-3$_b$), 3.32 (dd, *J* = 2.7, 1.9 Hz, 1H, H-6a), 2.98 (t, *J* = 8.3 Hz, 1H, H-4a), 2.34 (s, 3H, CH$_3$–C4’), 2.07 (ddd, *J*= 13.6, 8.3, 2.5 Hz, 1H, H-4$_b$), 1.66 (ddd, *J*= 13.6, 8.7, 6.0 Hz, 1H, H-4$_a$), 1.36 (s, 3H, CH$_3$–C-8b).^{13}C{H} NMR, HSQC, HMBC (101 MHz, $CDCl_3$) δ 162.7 (d, J_{CF} = 248.5 Hz, C-4’), 158.5 (C-8), 144.1 (C-4”), 138.5 (C-7), 138.3 (C-1”), 136.5 (C-5), 129.8 (d, J_{CF} = 3.3 Hz, C-

1'), 129.7 (d, J_{CF} = 8.3 Hz, C-2',6'), 129.2 (C-3",5"), 128.0 (C-6), 127.4 (C-2",6"), 120.4 (q, *J* = 323.6 Hz, CF_3), 115.1 (d, J_{CF} = 21.5 Hz, C-3',5'), 71.0 (C-6a), 70.4 (C-8a), 61.3 (C-8b), 58.8 (C-4a), 52.8 (C-3a), 52.4 (C-3), 52.2 (C-1), 34.4 (C-4), 23.8 (**C**H_3–C-8b), 21.7 (**C**H_3–C4"). ^{19}F NMR (376 MHz, $CDCl_3$) δ −76.3 (s, CF_3), -113.9 – (-114.0) (m, F–C-4'). MS (ESI): *m/z* = 568.2 $[M + H]^+$. HRMS (APCI-ToF) *m/z*: $[M]^+$ calcd for $C_{27}H_{25}F_4NO_4S_2$: 567.1161, found: 567.1158.

7-(4-Bromophenyl)-8b-methyl-8-[(4-methylphenyl)sulfonyl]-2-[(trifluoromethyl)sulfonyl]-1,2,3,3a,4,4a,6a,8b-octahydrocyclopenta[3,4]pentaleno[1,6a-*c*]pyrrole (7f)

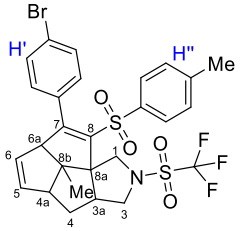

7f

Following the general procedure using 1-bromo-4-[(4-methylbenzene-1-sulfonyl)ethynyl]benzene (80.0 mg, 0.24 mmol, 2.00 equiv) after 10 h, column chromatography (SiO_2, eluent: cyclohexane/ethyl acetate, 95:1 → 20:1) afforded the title compound (32 mg, 0.05 mmol, 46%) as a colorless solid. R_f = 0.55 (3:1 cyclohexane/ethyl acetate). Mp: 150−152 °C (methanol). IR/cm^{-1} (ATR): 3057, 2954, 2871, 1597, 1387, 1301, 1259, 1188, 1144, 813, 615 cm^{-1}. ^{1}H NMR, COSY, NOESY (400 MHz, $CDCl_3$) δ 7.29 (d, *J* = 8.4 Hz, BB' part of AA'BB' system, 2H, H-3',5'), 7.09 (d, *J* = 8.4 Hz, AA' part of AA'BB' system, 2H, H-2",6"), 7.03 (d, *J* = 8.4 Hz, BB' part of AA'BB' system, 2H, H-3",5"), 6.67 (d, *J* = 8.4 Hz, AA' part of AA'BB' system, 2H, H-2',6'), 5.83 (ddd, *J* = 5.7, 2.7, 1.9 Hz, 1H, H-5), 5.27 (ddd, *J* = 5.7, 2.7, 1.4 Hz, 1H, H-6), 4.57 (d, *J* = 10.2 Hz, 1H, H-1_a), 4.02 (t, *J* = 9.4 Hz, 1H, H-3_a), 3.96 (d, *J* = 10.2 Hz, 1H, H-1_b), 3.78 (tdd, *J* = 8.6, 5.9, 2.3 Hz, 1H, H-3a), 3.36 (t, *J* = 9.4 Hz, 1H, H-3_b), 3.32 (dd, *J* = 2.7, 1.9 Hz, 1H, H-6a), 2.98 (t, *J* = 8.4 Hz, 1H, H-4a), 2.35 (s, 3H, CH_3–C4"), 2.06 (ddd, *J*= 13.6, 8.1, 2.5 Hz, 1H, H-4_b), 1.65 (ddd, *J*= 13.6, 8.7, 6.0 Hz, 1H, H-4_a), 1.35 (s, 3H, CH_3–C-8b). ^{13}C{H} NMR, HSQC, HMBC (101 MHz, $CDCl_3$) δ 158.0 (C-8), 144.3 (C-4"), 138.6 (C-7), 138.1 (C-1"), 136.6 (C-5), 132.9 (C-1'), 131.2 (C-3',5'), 129.4 (C-2',6'), 129.3 (C-3",5"), 127.9 (C-6), 127.5 (C-2",6"), 122.6 (C4'), 118.8 (q, *J* = 323.2 Hz, CF_3), 70.8 (C-6a), 70.4 (C-8a), 61.4 (C-8b), 58.8 (C-4a), 52.7 (C-3a), 52.4 (C-3), 52.1 (C-1), 34.4 (C-4), 23.8 (**C**H_3–C-8b), 21.7 (**C**H_3–C4"). ^{19}F NMR (376 MHz, $CDCl_3$) δ −76.3 (s, CF_3).MS (ESI): *m/z* = 628.1 $[M + H]^+$. HRMS (APCI-ToF) *m/z*: $[M]^+$ calcd for $C_{27}H_{25}BrF_3NO_4S_2$: 627.0360, found: 627.0349.

7-(4-Chlorophenyl)-8b-methyl-8-[(4-methylphenyl)sulfonyl]-2-[(trifluoromethyl)sulfonyl]-1,2,3,3a,4,4a,6a,8b-octahydrocyclopenta[3,4]pentaleno[1,6a-*c*]pyrrole (7g)

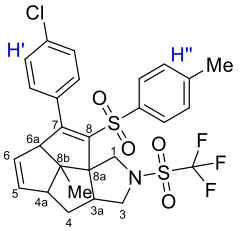

7g

Following the general procedure using 1-chloro-4-[(4-methylbenzene-1-sulfonyl)ethynyl]benzene (69.4 mg, 0.24 mmol, 2.00 equiv) after 10 h, column chromatography (SiO_2, eluent: cyclohexane/ethyl acetate, 95:1 → 20:1) afforded the title compound (42 mg, 0.07 mmol, 60%) as a colorless solid. R_f = 0.53 (3:1 cyclohexane/ethyl acetate). Mp: 148−149 °C (ethanol). IR/cm^{-1} (ATR): 3056, 2954, 2872, 1596, 1387, 1302, 1259, 1190, 1144, 813, 615 cm^{-1}. ^{1}H NMR, COSY, NOESY (400 MHz, $CDCl_3$) δ 7.14 (d, *J* = 8.5 Hz, BB‘ part of AA‘BB‘ system, 2H, H-3‘,5’), 7.10 (d, *J* = 8.3 Hz, AA‘ part of AA‘BB‘ system, 2H, H-2”,6”), 7.02 (d, *J* = 8.3 Hz, BB‘ part of AA‘BB‘ system, 2H, H-3“,5“),6.74 (d, *J* = 8.5 Hz, AA‘ part of AA‘BB‘ system, 2H, H-2‘,6’), 5.83 (ddd, *J* = 5.7, 2.7, 1.9 Hz, 1H, H-5), 5.27 (ddd, *J* = 5.7, 2.7, 1.4 Hz, 1H, H-6), 4.57 (d, *J* = 10.3 Hz, 1H, H-1$_a$), 4.02 (t, *J* = 9.4 Hz, 1H, H-3$_a$), 3.96 (d, *J* = 10.3 Hz, 1H, H-1$_b$), 3.78 (tdd, *J* = 8.5, 5.7, 2.3 Hz, 1H, H-3a), 3.36 (t, *J* = 9.4 Hz, 1H, H-3$_b$), 3.32 (dd, *J* = 2.7, 1.9 Hz, 1H, H-6a), 2.98 (t, *J* = 8.4 Hz, 1H, H-4a), 2.35 (s, 3H, CH_3–C4”), 2.06 (ddd, *J*= 13.7, 8.1, 2.5 Hz, 1H, H-4$_b$), 1.66 (ddd, *J*= 13.7, 8.7, 6.0 Hz, 1H, H-4$_a$), 1.36 (s, 3H, CH_3–C-8b). ^{13}C{H} NMR, HSQC, HMBC (101 MHz, $CDCl_3$) δ 158.1 (C-8), 144.2 (C-4”), 138.6 (C-7), 138.2 (C-1”), 136.6 (C-5), 134.5 (C4’), 132.4 (C-1’), 129.2(C-3”,5”), 129.2 (C-2‘,6‘), 128.2 (C-3‘,5‘), 127.9 (C-6), 127.5 (C-2”,6”), 118.8 (q, *J* = 320.5 Hz, CF_3), 70.9 (C-6a), 70.4 (C-8a), 61.4 (C-8b), 58.8 (C-4a), 52.7 (C-3a), 52.4 (C-3), 52.1 (C-1), 34.4 (C-4), 23.8 (**C**H$_3$–C-8b), 21.7 (**C**H$_3$–C4”). ^{19}F NMR (376 MHz, $CDCl_3$) δ −76.3 (s, CF_3).MS (ESI): *m/z* = 584.1 $[M + H]^+$. HRMS (ESI-ToF) *m/z*: $[M]^+$ calcd for $C_{27}H_{25}ClF_3NO_4S_2$: 583.0866, found: 583.0879.

8b-Methyl-7-phenyl-8-(phenylsulfonyl)-2-[(trifluoromethyl)sulfonyl]-1,2,3,3a,4,4a,6a,8b-octahydrocyclopenta[3,4]pentaleno[1,6a-*c*]pyrrole (7h)

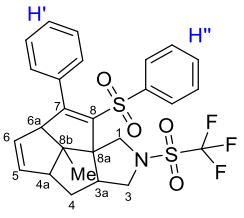

7h

Following the general procedure using [(benzenesulfonyl)ethynyl]benzene (57.8 mg, 0.24 mmol, 2.00 equiv) after 10 h, column chromatography (SiO_2, eluent: cyclohexane/ethyl acetate, 95:1 → 20:1)

afforded the title compound (47.0 mg, 0.09 mmol, 74%) as a colorless solid. R_f = 0.44 (3:1 cyclohexane/ethyl acetate). Mp: 154−156 °C (methanol). IR/cm^{-1} (ATR): 3059, 2953, 2872, 1593, 1259, 1225, 1190, 1145, 726, 619 cm^{-1}. ^{1}H NMR, COSY, NOESY (400 MHz, $CDCl_3$) δ 7.38 – 7.34 (m, 1H, H-4“), 7.25 – 7.20 (m, 1H, H_{Ar}), 7.19 – 7.12 (m, 6H, H_{Ar}), 6.79 – 6.76 (m, 2H, H-2’,6’), 5.82 (dt, *J* = 5.7, 2.3 Hz, 1H, H-5), 5.29 (ddd, *J* = 5.7, 2.7, 1.4 Hz, 1H, H-6), 4.61 (d, *J* = 10.2 Hz, 1H, H-1$_a$), 4.04 (t, *J* = 9.3 Hz, 1H, H-3$_a$), 4.00 (d, *J* = 10.2 Hz, 1H, H-1$_b$), 3.80 (tdd, *J* = 8.6, 5.9, 2.4 Hz, 1H, H-3a), 3.38 (t, *J* = 9.4 Hz, 1H, H-3$_b$), 3.36(dd, *J* = 2.7, 1.9 Hz, 1H, H-6a), 2.99 (td, *J* = 8.5,4.5 Hz, 1H, H-4a), 2.08 (ddd, *J*= 13.6, 8.1, 2.5 Hz, 1H, H-4$_b$), 1.69 (ddd, *J*= 13.6, 8.7, 6.0 Hz, 1H, H-4$_a$), 1.37 (s, 3H, CH_3–C-8b). ^{13}C{H} NMR, HSQC, HMBC (101 MHz, $CDCl_3$) δ 160.0 (C-8), 141.1 (C-1“), 137.6 (C-7), 136.2 (C-5), 133.8 (C-1’), 132.8 (C-4”), 128.5 (2C, C_{Ar}H), 128.3 (C-4’), 128.2 (C-6), 128.1(2C, C_{Ar}H), 127.7 (C-2‘,6‘), 127.4 (2C, C_{Ar}H), 120.4 (q, *J* = 324.0 Hz, CF_3), 71.2 (C-6a), 70.4 (C-8a), 61.3 (C-8b), 58.8 (C-4a), 52.7 (C-3a), 52.4 (C-3), 52.2 (C-1), 34.4 (C-4), 23.8 (**C**H_3–C-8b). ^{19}F NMR (376 MHz, $CDCl_3$) δ −76.3 (s, CF_3). MS (ESI): *m/z* = 536.1 $[M + H]^+$. HRMS (ESI-ToF) *m/z*: $[M + Na]^+$ calcd for $C_{26}H_{24}F_3NO_4S_2Na$: 535.1099, found: 535.1111.

8b-Methyl-8-(methylsulfonyl)-7-phenyl-2-[(trifluoromethyl)sulfonyl]-1,2,3,3a,4,4a,6a,8b-octahydrocyclopenta[3,4]pentaleno[1,6a-*c*]pyrrole (7i)

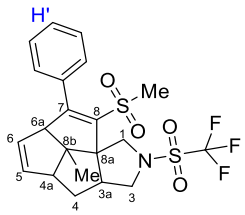

7i

Following the general procedure using [(methanesulfonyl)ethynyl]benzene (43.0 mg, 0.24 mmol, 2.00 equiv) after 10 h, reversed-phase column chromatography (SiO_2-C_{18}, eluent: water/acetonitrile, 99:1 → 80:20) afforded the title compound (35.0 mg, 0.07 mmol, 62%) as a colorless solid. R_f = 0.34 (3:1 cyclohexane/ethyl acetate). Mp: 182−184 °C (cyclohexane-chloroform). IR/cm^{-1} (ATR): 3056, 2956, 2873, 1594, 1259, 1225, 1189, 1134, 737, 619 cm^{-1}. ^{1}H NMR, COSY, NOESY (400 MHz, $CDCl_3$) δ 7.47 – 7.37 (m, 3H, H-3‘, 4‘, 5‘), 7.31 – 7.27 (m, 2H, H-2’,6’), 5.84 (ddd, *J* = 5.7, 2.6, 1.9 Hz, 1H, H-5), 5.37 (ddd, *J* = 5.7, 2.7, 1.5 Hz, 1H, H-6), 4.43 (d, *J* = 10.2 Hz, 1H, H-1$_a$), 3.95 (t, *J* = 9.4 Hz, 1H, H-3$_a$), 3.93 (d, *J* = 10.2 Hz, 1H, H-1$_b$), 3.58 (ddd, *J* = 5.7, 2.7, 1.5 Hz, 1H, H-3a), 3.56 – 3.53 (m, 1H, H-6a), 3.33 (t, *J* = 9.4 Hz, 1H, H-3$_b$), 3.02 – 2.96 (m, 1H, H-4a), 2.50 (s, 3H, SO_2CH_3), 2.03 (ddd, *J*= 13.6, 8.1, 2.7 Hz, 1H, H-4$_b$), 1.67 (ddd, *J*= 13.6, 8.5, 6.1 Hz, 1H, H-4$_a$), 1.39 (s, 3H, CH_3–C-8b). ^{13}C{H} NMR, HSQC, HMBC (101 MHz, $CDCl_3$) δ 158.7 (C-8), 136.7 (C-7), 136.4 (C-5), 134.0 (C-1’), 129.3 (C-4’), 128.8 (C-3‘,5‘), 128.2 (C-6), 127.7 (C-2‘,6‘), 120.4 (q, *J* = 323.5 Hz, CF_3), 71.1 (C-6a), 70.4 (C-8a), 61.3 (C-8b), 58.8 (C-4a), 52.8 (C-3a), 52.3 (C-3), 52.0 (C-1), 44.9 (SO_2**C**H_3), 34.4 (C-4), 23.8 (**C**H_3–C-8b). ^{19}F NMR (376 MHz, $CDCl_3$) δ −76.4 (s, CF_3). MS (ESI): *m/z* = 474.1 $[M + H]^+$. HRMS (ESI-ToF) *m/z*: $[M + H]^+$ calcd for $C_{21}H_{22}F_3NO_4S_2$: 474.1021, found: 474.1006.

8-(Ethylsulfonyl)-8b-methyl-7-phenyl-2-[(trifluoromethyl)sulfonyl]-1,2,3,3a,4,4a,6a,8b-octahydrocyclopenta[3,4]pentaleno[1,6a-*c*]pyrrole (7j)

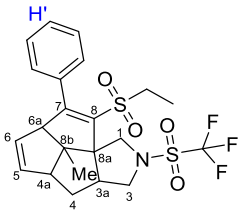

7j

Following the general procedure using [(ethanesulfonyl)ethynyl]benzene (46.4 mg, 0.24 mmol, 2.00 equiv) after 10 h, reversed-phase column chromatography (SiO_2-C_{18}, eluent: water/acetonitrile, 99:1 → 80:20) afforded the title compound (43.0 mg, 0.09 mmol, 74%) as a colorless solid. R_f = 0.39 (3:1 cyclohexane/ethyl acetate). Mp: 152−153 °C (cyclohexane-chloroform). IR/cm^{-1} (ATR): 3057, 2945, 2901, 1594, 1260, 1225, 1189, 1047, 728, 619 cm^{-1}. ^{1}H NMR, COSY, NOESY (400 MHz, $CDCl_3$) δ 7.45 – 7.38 (m, 3H, H-3‘, 4‘, 5‘), 7.32 – 7.28 (m, 2H, H-2’,6’), 5.85 (ddd, *J* = 5.7, 2.7, 1.8 Hz, 1H, H-5), 5.39 (ddd, *J* = 5.7, 2.7, 1.4 Hz, 1H, H-6), 4.39 (d, *J* = 10.3 Hz, 1H, H-1$_a$), 3.95 (t, *J* = 9.4 Hz, 1H, H-3$_a$), 3.90 (d, *J* = 10.3 Hz, 1H, H-1$_b$), 3.58 (ddt, *J* = 8.8, 5.4, 2.7 Hz, 1H, H-3a), 3.55 (dd, *J* = 2.7, 1.8 Hz, 1H, H-6a), 3.33 (t, *J* = 9.4 Hz, 1H, H-3$_b$), 3.07 – 2.94 (m, 1H, H-4a), 2.41 (qd, *J* = 7.4, 3.5 Hz, 1H, $SO_2C\mathbf{H_2}CH_3$), 2.03 (ddd, *J*= 13.6, 8.1, 2.7 Hz, 1H, H-4$_b$), 1.68 (ddd, *J*= 13.6, 8.5, 6.0 Hz, 1H, H-4$_a$), 1.39 (s, 3H, CH_3–C-8b), 2.50 (t, *J* = 7.4 Hz, 1H, $SO_2CH_2C\mathbf{H_3}$). ^{13}C{H} NMR, HSQC, HMBC (101 MHz, $CDCl_3$) δ 158.5 (C-8), 136.4 (C-5), 134.8 (C-7), 134.0 (C-1’), 129.3 (C-4’), 128.8 (C-3‘,5‘), 128.2 (C-6), 127.6 (C-2‘,6‘), 120.4 (q, *J* = 323.7 Hz, CF_3), 71.2 (C-6a), 70.3 (C-8a), 61.3 (C-8b), 58.8 (C-4a), 52.7 (C-3a), 52.3 (C-3), 52.1 (C-1), 49.6 (SO_2 **C**H_2CH_3), 34.4 (C-4), 23.9 (**C**H_3–C-8b), 7.1 (SO_2 CH_2**C**H_3). ^{19}F NMR (376 MHz, $CDCl_3$) δ −76.3 (s, CF_3). MS (ESI): *m/z* = 488.1 [M + H]$^+$. HRMS (ESI-ToF) *m/z*: [M]$^+$ calcd for $C_{22}H_{24}F_3NO_4S_2$: 487.1099, found: 487.1091.

Preparation of 8b-methyl-7-phenyl-2-[(trifluoromethyl)sulfonyl]-1,2,3,3a,4,4a,6a,8b-octahydrocyclopenta[3,4]pentaleno[1,6a-*c*]pyrrole (13)

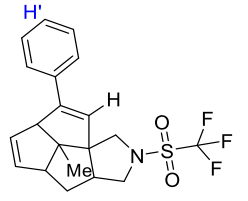

13

Following a procedure published by Tam et al,[21] 5% sodium amalgam (149.5 mg, 0.325 mmol, 9.0 equiv) was added to a solution of 8b-methyl-8-[(4-methylphenyl)sulfonyl]-7-phenyl-2-[(trifluoromethyl)sulfonyl]-1,2,3,3a,4,4a,6a,8b-octahydrocyclopenta[3,4]pentaleno[1,6a-*c*]pyrrole (**7a**) (19.9 mg, 0.036 mmol, 1.0 equiv) and sodium hydrogen phosphate (30.7 mg, 0.216 mmol, 6.0 equiv) in

methanol (4 mL) at 0 °C under nitrogen atmosphere. After 1 h, TLC indicated full consumption of **7a** and the reaction mixture was filtrated over silica. The solvent was removed under reduced pressure and the residue purified by flash column chromatography (SiO_2, eluent: cyclohexane/ethyl acetate, 98:2) to afford the desired product (6.9 mg, 0.017 mmol, 47%) as colorless solid. R_f = 0.65 (4:1 cyclohexane/ethyl acetate). Mp: 118 − 119 °C (chloroform). IR/cm^{-1} (ATR): 3051, 2952, 2896, 1385, 1226, 1182, 1005, 730, 626, 583 cm^{-1}. ^{1}H NMR, COSY, NOESY (600 MHz, $CDCl_3$) δ 7.47 – 7.45 (m, 2H, H-2‘, 6‘), 7.35 (dd, *J* = 8.5, 7.0 Hz, 2H, H-3’, 5’), 7.30 – 7.27 (m, 1H, H-4’), 5.81 (dt, *J* = 5.8, 2.1 Hz, 1H, H-6), 5.74 (d, *J* = 1.6 Hz, 1H, H-8), 5.63 (dt, *J* = 5.8, 2.2 Hz, 1H, H-5), 3.83 (d, *J* = 10.6 Hz, 1H, H-1$_b$), 3.82 (d, *J* = 9.0 Hz, 1H, H-3$_a$), 3.72 (d, *J* = 2.1 Hz, 1H, H-6a), 3.56 (d, *J* = 10.6 Hz, 1H, H-1$_a$), 3.37 – 3.34 (m, 1H, H-3$_b$), 2.91 (ddd, *J* = 8.4, 6.3, 2.2 Hz, 1H, H-4a), 2.77 (ddd, *J* = 13.3, 7.7, 5.5 Hz ,1H, H-3a), 1.90 (ddd, *J* = 13.0, 7.7, 4.9 Hz 1H, H-4$_b$), 1.60 (dt, *J* = 13.0, 6.3 Hz, 1H, H-4$_a$), 1.34 (s, 3H, CH_3–C-8b). ^{13}C{H} NMR, HSQC, HMBC (151 MHz, $CDCl_3$) δ 146.2 (C-7), 134.7 (C-1’), 134.0 (C-5), 130.7 (C-6), 128.7 (C-3’,5’), 128.1 (C-4‘), 126.3 (C-8), 126.2 (C-2‘,6‘), 120.5 (q, *J* = 323.8 Hz, CF_3), 68.1 (C-8a), 66.4 (C-6a), 61.4 (C-8b), 58.1 (C-4a), 53.6 (C-1), 52.9 (C-3a), 52.6 (C-3), 35.3 (C-4), 23.6 (**C**H$_3$–C-8b). ^{19}F NMR (377 MHz, $CDCl_3$) δ −76.2 (s, CF_3). MS (ESI): *m/z* = 396.1 [M + H]$^+$. HRMS (APCI) *m/z*: [M]$^{\bullet+}$ calcd for $C_{20}H_{20}F_3NO_2S$: 395.1162, found: 395.1153.

Synthesis of (1-Cyclopropylvinyl)benzene (8)

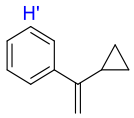

8

To a solution cooled to -78 °C of methyltriphenylphosphonium bromide (1.79 g, 5.0 mmol, 2.00 equiv) in dry THF (15 mL) nBuLi (2.0 mL, 2.5M, 5 mmol, 2.00 equiv) was added dropwise, after which the cooling was removed. To this mixture cyclopropyl phenyl ketone (0.37 g, 2.5 mmol, 1.00 equiv) dissolved in dry THF (1.5 mL) was added dropwise and the reaction was left to stir for 3 hours. After this time, brine was added and the phases were separated. The aqueous phase was extracted with pentane (3x 10 mL), and the combined organic phases were dried over Na_2SO_4, filtered onto celite and concentrated under reduce pressure. The residue was purified by flash chromatography (SiO_2, eluent: cyclohexane/ethyl acetate, 100:0 → 98:1) and **8** was isolated as a colorless liquid (0.30 g, 2.1 mmol, 87%). R_f = 0.69 (50:1 cyclohexane/ethyl acetate). ^{1}H NMR, COSY (400 MHz, $CDCl_3$): δ 7.61 (d, *J* = 7.3 Hz, 2H, H-2’,6’), 7.39 – 7.32 (m, 2H, H-3‘, 5‘), 7.32 – 7.27 (m, 1H, H-4‘), 5.29 (s, 1H, -C=C**H$_a$**H), 4.95 (s, 1H, -C=C**H$_b$**H), 1.67 (dddd, *J* = 8.3, 6.8, 5.3, 4.0 Hz, 1H, H-1), 0.91 – 0.81 (m, 2H, H-2), 0.63-0.59 (m, 2H, H-3). ^{13}C NMR, HSQC, HMBC (101 MHz, $CDCl_3$): δ 149.5 (-**C**=CH$_2$), 141.8 (C-1’), 128.3 (C-3‘,5‘), 127.6 (C-4‘), 126.3 (C-2‘,6‘), 109.2(-C=**C**H$_2$), 15.8 (C-1), 6.8 (C-1,2). MS (EI): m/z = 144.1 [M]$^+$. These data are consistent with those previously reported.[22]

Synthesis of ((2-Phenyl-3-(1-phenylvinyl)cyclopent-1-en-1-yl)sulfonyl)benzene (9)

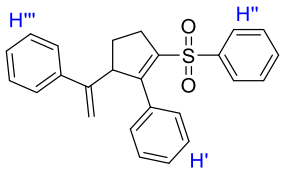

9

Following the general procedure for the preparation of **7** a mixture of (1-cyclopropylvinyl)benzene **8** (35.0 mg, 0.24 mmol, 1.00 equiv) and ((phenylethynyl)sulfonyl)benzene (117.6 mg, 0.49 mmol, 2.00 equiv) was irradiated for 2.5 h. After column chromatography (SiO_2, eluent: cyclohexane/ethyl acetate, 95:1 → 20:1), the title compound (38.0 mg, 0.01 mmol, 41%) was isolated as a colorless oil. R_f = 0.55 (3:1 cyclohexane/ethyl acetate). IR/cm^{-1} (ATR): 3058, 2965, 2861, 1378, 1445, 1319, 1305, 1149, 1082, 904 cm^{-1}. ^{1}H NMR, COSY, NOESY (400 MHz, acetone-d_6) δ 7.72 – 7.68 (m, 2H, H-2”,6”), 7.67 – 7.64 (m, 1H, H-4”), 7.56 – 7.51 (m, 2H, H-3”,5”), 7.32 – 7.22 (m, 10H, H-2’,3’,4’,5’,6’/ H-2”,3”,4”,5”,6”), 5.28 (s, 1H, -C=C**H$_a$**H), 5.01 (s, 1H, -C=C**H$_b$**H), 4.38 (ddt, *J* = 9.1, 4.4, 2.0 Hz, 1H, H-3), 2.87 – 2.83 (m, 2H, H-5$_{ab}$), 2.44 (dtd, *J* = 13.0, 9.1, 7.1 Hz, 1H, H-4$_a$), 1.88 (ddt, *J* = 13.0, 8.4, 4.9 Hz, 1H).^{13}C{H} NMR, HSQC, HMBC (101 MHz, acetone-d_6) δ 156.2 (C-1), 149.6 (-**C**=CH$_2$), 142.2 (C-1”), 141.8 (C-1”’), 140.7 (C-2), 135.3 (C-1’), 134.2 (C-4”), 129.9 (C-3”,5”), 129.7 (2C, C$_{Ar}$H), 129.2 (2C, C$_{Ar}$H), 129.0 (1C, C$_{Ar}$H), 128.5 (1C, C$_{Ar}$H), 128.(C-2”,6”), 128.3 (2C, C$_{Ar}$H), 127.2 (2C, C$_{Ar}$H), 115.0 (-C=**C**H$_2$), 58.7 (C-3), 30.6 (C-5), 30.4 (C-4). MS (ESI): *m/z* = 387.1 [M + H]$^+$. HRMS (ESI-ToF) *m/z*: [M]$^+$ calcd for $C_{25}H_{22}O_2S$: 386.1341, found: 386.1354.

Preparation of 1-((Allyloxy)methyl)-2-methylbenzene (10)

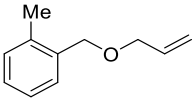

10

To a suspension of sodium hydride (0.11 g, 4.50 mmol, 1.10 equiv) in dry THF (5.31 mL) was added a solution of benzyl alcohol (0.50 g, 4.09 mmol, 1.00 equiv) in dry THF (0.8 mL). After the reaction was stirred at room temperature for two hours under an inert atmosphere, allyl bromide (0.39 mL, 4.50 mmol, 1.10 equiv) was added dropwise and the resulting suspension was stirred overnight at room temperature. The solvent was partially removed in vacuo and saturated ammonium chloride solution (5 mL) was added. The aqueous phase was extracted with ethyl acetate (3 x 50 mL) and the combined organic extracts were dried over Na_2SO_4, filtered, and concentrated under reduced pressure. The residue was purified by flash chromatography (SiO_2, eluent: cyclohexane/ethyl acetate, 100:0 → 95:1) to give **10** as a colorless oil (0.59 g, 3.64 mmol, 89%). R_f = 0.56 (10:1 cyclohexane/ethyl acetate). IR/cm^{-1} (ATR): 3021, 2856, 1460, 1356, 1123, 1080, 989, 923, 764, 743 cm^{-1}. 1H NMR, COSY (400 MHz, $CDCl_3$) δ 7.36 – 7.34 (m, 1H, H-6), 7.25 – 7.14 (m, 3H, H-3, 4, 5), 5.99 (ddt, *J* = 17.2, 10.4, 5.6 Hz, 1H, -CH=), 5.34 (dq, *J* = 17.2, 1.7 Hz, 1H, =C**H$_{trans}$**), 5.23 (dq, *J* = 10.4, 1.4 Hz, 1H, =C**H$_{cis}$**), 4.54 (s,

2H, -CH_2-), 4.06 (dt, *J* = 5.6, 1.4 Hz, 2H, -C**H**$_2$-CH=), 2.32 (s, 3H, -CH_3). ^{13}C{H} NMR, HSQC, HMBC (101 MHz, $CDCl_3$) δ 136.8 (C-1), 136.3 (C-2), 135.0 (-CH=), 130.3 ($C_{Ar}H$), 128.7 (C-6), 127.9 ($C_{Ar}H$), 125.9 ($C_{Ar}H$), 117.2 (=CH_2), 71.4 (-**C**H_2-CH=), 70.6 (-CH_2-), 18.9(-CH_3). MS (EI): m/z = 162.1 $[M]^+$. These data are consistent with those previously reported.[23]

Preparation of 6c-methyl-3,3a,4,4a,6a,6c-hexahydrocyclopropa[1,6]pentaleno[1,2-*c*]furan (11)

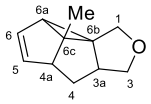

11

Following the general procedure for the *meta* photoadduct synthesis, a mixture of 1-((allyloxy)methyl)-2-methylbenzene **10** (100 mg, 0.62 mmol) and 10 mL of anhydrous cyclohexane was irradiated for 4 h. After column chromatography (SiO_2, eluent: cyclohexane/ethyl acetate, 100:0 → 50:1), a 7:1 colorless oil mixture of two isomeric *meta*-photocycloadducts was isolated (38.5 mg, 0.24 mmol, 39%).[24] R_f = 0.38 [$KMnO_4$] (10:1 cyclohexane/ethyl acetate). IR/cm^{-1} (ATR): 2922, 2851, 1448, 1378, 1360, 1065, 1016, 914, 795, 735 cm^{-1}. Spectroscopic data are those of the major isomer: ^{1}H NMR, COSY, NOESY (400 MHz, $CDCl_3$) δ 5.67 (dd, *J* = 5.5, 2.3 Hz, 1H, H-6), 5.45 (ddd, *J* = 5.5, 2.4, 0.8 Hz, 1H, H-5), 3,88 (t, *J* = 9.0 Hz, 1H, H-3$_a$), 3.67 – 3.65 (m, 1H, H-3$_b$), 3.64 – 3.62 (m, 2H, H-1$_{a,b}$), 2,98 (dd, *J* = 4.1, 1.9 Hz, 1H, H-4a), 2.40 – 2.32 (m, 1H, H-3a), 1.86 – 1.79 (m, 2H, H-4$_{ab}$), 1.70 – 1.63 (m, 1H, H-6a), 1.29 (s, 3H, CH_3–C-6b). ^{13}C{H} NMR, HSQC, HMBC (101 MHz, $CDCl_3$) δ 133.3 (C-5), 129.1 (C-6), 73.7 (C-3), 67.5 (C-1), 57.9 (C-4a), 51.1 (C-6b), 46.0 (C-6b), 45.5 (C-4), 42.9 (C-3a), 38.2 (C-6a), 13.8 (**C**H_3–C-6b). MS (EI): *m/z* = 162.1 $[M]^+$. HRMS (API) *m/z*: $[M]^+$ calcd. for $C_{11}H_{14}O$: 162.1045, found: 162.1041. These data are consistent with those previously reported.[24]

8b-methyl-8-[(4-methylphenyl)sulfonyl]-7-phenyl-3,3a,4,4a,6a,8b-hexahydrocyclopenta[3,4]pentaleno[1,6a-*c*]furan (12)

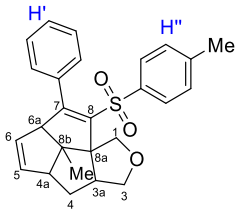

12

Following the general procedure for the preparation of **7** a mixture of the *meta* photoadduct **11** (25.0 mg, 0.15 mmol, 1.00 equiv) and 1-methyl-4-(phenylethynylsulfonyl)benzene (79.0 mg, 0.31 mmol, 2.00 equiv) was irradiated for 10 h. After column chromatography (SiO_2, eluent: cyclohexane/ethyl acetate, 99:1 → 93:1), the title compound (22.3 mg, 0.05 mmol, 39%) was isolated as a colorless solid. R_f = 0.40 (3:1 cyclohexane/ethyl acetate). Mp: 180−182 °C (cyclohexane-ethyl acetate). IR/cm^{-1} (ATR): 3056, 2924, 2867, 1594, 1311, 1144, 1086, 920, 720, 581 cm^{-1}. ^{1}H NMR, COSY, NOESY (400 MHz, $CDCl_3$) δ 7.25 – 7.20 (m, 1H, H-4'), 7.18 – 7.12 (m, *J* = 7.5 Hz, 2H, H-3', 5'), 7.09 (d, *J* = 8.4 Hz, AA' part of

AA‘BB‘ system, 2H, H-2“,6“), 6.96 (d, *J* = 8.4 Hz, BB‘ part of AA‘BB‘ system, 2H, H-3“,5“), 6.85 – 6.77 (m, 2H, H-2’,6’), 5.79 (dt, *J* = 5.7, 2.3 Hz, 1H, H-5), 5.32 (ddd, *J* = 5.7, 2.7, 1.5 Hz, 1H, H-6), 4.65 (d, *J* = 8.9 Hz, 1H, H-1_a), 4.26 (t, *J* = 8.1 Hz, 1H, H-3_a), 4.16 (d, *J* = 8.9 Hz, 1H, H-1_b), 3.68 (tdd, *J* = 7.8, 7.3, 2.4 Hz, 1H, H-3a), 3.62 (t, *J* = 8.1 Hz, 1H, H-3_b), 3.30 (t, *J* = 2.3 Hz, 1H, H-6a), 2.93 (m, 1H, H-4a), 2.31 (s, 3H, CH_3–C4”), 2.03 (ddd, *J*= 13.5, 8.4, 2.5 Hz, 1H, H-4_b), 1.67 (ddd, *J*= 13.5, 8.2, 6.5 Hz, 1H, H-4_a), 1.33 (s, 3H, CH_3–C-8b). ^{13}C{H} NMR, HSQC, HMBC (101 MHz, $CDCl_3$) δ 159.6 (C-8), 143.3 (C-4”), 139.0 (C-1”), 138.5 (C-7), 136.8(C-5), 134.8 (C-1’), 129.0 (C-3”,5”), 128.0 (C-6), 127.8 (C-3‘,4’,5‘),127.8 (C-2‘,6‘), 127,5 (C-2”,6”), 73.0 (C-3), 72.3 (C-8a), 71.5 (C-6a), 71.3 (C-1), 61.3 (C-8b), 59.5 (C-4a), 54.1 (C-3a), 35.2 (C-4), 23.8 (**C**H_3–C-8b), 21.6 (**C**H_3–C4”). MS (ESI): *m/z* = 419.1 $[M + H]^+$. HRMS (ESI-ToF) *m/z*: $[M]^+$ calcd for $C_{26}H_{26}O_3S$: 418.1603, found: 418.1600.

Preparation of ethyl 5,5-dimethyl-2-[(4-methylphenyl)sulfonyl]-4-(2-methylprop-1-en-1-yl)-3-phenylcyclopent-2-ene-1-carboxylate (14)

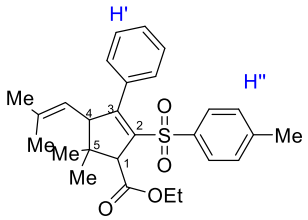

14

Following the general procedure for the preparation of **7**, a mixture of ethyl 2,2-dimethyl-3-(2-methyl-1-propenyl)cyclopropane-1-carboxylate (120.0 mg, 0.611 mmol, 1.0 equiv), 1-methyl-4-(phenylethynylsulfonyl)benzene (313.2 mg, 1.222 mmol, 2.0 equiv) and $[Ir(ppy)_2(dtbbpy)]PF_6$ (11.0 mg, 0.01 mmol, 0.02 equiv) in methanol (4.1 mL, c = 0.15 M) was irradiated overnight. The full consumption of the starting material was confirmed via TLC and HPLC/ESI-MS. The crude product was dissolved in 1 mL of acetonitrile and 0.2 mL of this solution purified via preparative HPLC (Macherey-Nagel NUCLEODUR C18 HTec, oven temperature: 40 °C, eluent: water (+0.1% formic acid)/acetonitrile, 30:70) yielding the title compound (6.7 mg, 0.015 mmol, 12%) as a mixture of diastereomers (*cis*/*trans*, 2:3, based on ^{1}H NMR) as a colorless oil. Based on the 2D NMR data, the signal sets are denoted individually.

R_f = 0.36 (10:1 cyclohexane/ethyl acetate). IR/cm^{-1} (ATR): 2969, 2930, 1729, 1444, 1313, 1302, 1146, 768, 700, 583 cm^{-1}. ^{1}H NMR, COSY, NOESY (600 MHz, $CDCl_3$, *trans*-**14**) δ 7.19 – 7.16 (m, 2H, H-2‘‘, 6‘‘), 7.09 – 7.06 (m, 3H, H-3’,4’,5’), 6.93 (d, *J* = 8.0 Hz, 2H, H-3‘’,5‘’), 6.80 (d, *J* = 7.0 Hz, 2H, H-2’,6’), 4.62 – 4.60 (m, 1H, $(CH_3)_2$C=C**H**), 4.27 – 4.23 (m, 1H, H-4), 4.22 – 4.12 (m, 2H, O–C$\mathbf{H}_2$), 2.72 (d, *J* = 9.4 Hz, 1H, H-1), 2.29 (s, 3H, C4‘’-C$\mathbf{H}_3$), 1.78 (s, 3H, C5-$C_a\mathbf{H}_3$), 1.46 (s, 3H, C5-$C_b\mathbf{H}_3$), 1.42 (d, *J* = 1.4 Hz, 3H, C=C($C_a\mathbf{H}_3C_bH_3$)), 1.38 (d, *J* = 1.4 Hz, 3H, C=C($C_aH_3C_b\mathbf{H}_3$)), 1.34 – 1.29 (m, 3H, OCH_2–C$\mathbf{H}_3$). ^{13}C{H} NMR, HSQC, HMBC (151 MHz, $CDCl_3$, *trans*-**14**) δ 171.9 (**C**$O_2CH_2CH_3$), 155.3 (C-2), 144.8 (C-3), 143.1 (C-4‘’), 139.0 (C-1‘’), 136.3 ($(CH_3)_2$**C**=CH), 128.8 (C-3‘’,5‘’), 128.1 (C-2‘,5’), 127.5 (C-2‘’,6‘’), 127.4 (C-3’,4’,5’), 123.3 (C4–**C**H), 61.9 (C–1), 61.0 (CO_2-**C**H_2), 51.1 (C-5), 49.9 (C-4), 28.2 (C5–**C**$_aH_3$), 25.8 (C=C(**C**$_aH_3C_bH_3$)), 22.6 (C5–**C**$_bH_3$), 21.6 (C4‘’–**C**H_3), 18.1 (C=C(C_aH_3**C**$_bH_3$)), 14.5 (OCH_2–**C**H_3). ^{1}H

NMR, COSY, NOESY (600 MHz, $CDCl_3$, *cis*-**14**) δ 7.38 – 7.36 (m, 2H, H-2'',6''), 7.15 – 7.12 (m, 3H, H-3',4',5'), 6.97 – 6.96 (m, 2H, H-2',6'), 6.96 (d, *J* = 9.1 Hz, 2H, H-3'',5''), 4.71 (dp, *J* = 10.8, 1.4 Hz, 1H, $(CH_3)_2C$=C**H**), 4.22 – 4.12 (m, 2H, O–C$\mathbf{H}_2$), 3.97 (dd, *J* = 10.8, 1.7 Hz, 1H, H-4), 3.75 (d, *J* = 1.7 Hz, 1H, H-1), 2.28 (s, 3H, C4''-C$\mathbf{H}_3$), 1.52 (d, *J* = 1.4 Hz, 3H, C=C($C_aH_3C_b\mathbf{H}_3$)), 1.50 (d, *J* = 1.4 Hz, 3H, C=C($C_aH_3C_b\mathbf{H}_3$)), 1.34 – 1.29 (m, 3H, OCH_2–C$\mathbf{H}_3$), 1.11 (s, 3H, C5-$C_a\mathbf{H}_3$), 1.07 (s, 3H, C5-$C_b\mathbf{H}_3$). $^{13}C\{H\}$ NMR, HSQC, HMBC (151 MHz, $CDCl_3$, *cis*-**14**) δ 171.9 (**C**$O_2CH_2CH_3$), 159.3 (C-2), 143.5 (C-3), 143.1 (C-4''), 137.8 (C-2), 137.4 (C-1''), 137.4 ($(CH_3)_2$**C**=CH), 128.8 (C-3'',5''), 128.2 (C-2'',5''), 128.1 (C-2'',6''), 127.5 (C-3',4',5'), 61.0 (CO_2-**C**H_2), 62.3 (C-1), 57.9 (C-4), 46.6 (C-5), 26.1 (C=C(**C**$_aH_3C_bH_3$)), 25.2 (C5–**C**$_aH_3$), 23.4 (C5–**C**$_bH_3$), 18.0 (C=C(C_aH_3**C**$_bH_3$)), 14.5 (OCH_2–**C**H_3). MS (ESI): *m/z* = 453.2 $[M + H]^+$. HRMS (ESI) *m/z*: $[M+Na]^+$ calcd for $C_{27}H_{32}NaO_4S$: 475.1913, found: 475.1908.

Preparation of (*3aR,6R,7aS*)-1,1,6-trimethyl-3-phenyl-2-tosyl-3a,6,7,7a-tetrahydro-1*H*-indene (15)

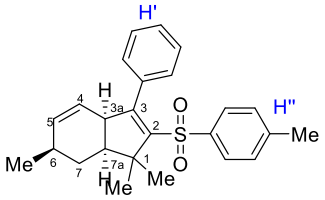

15

Following the general procedure for the preparation of **7** a mixture of (1*S*,3*R*)-*cis*-4-carene (120.0 mg, 0.881 mmol, 1.0 equiv), 1-methyl-4-(phenylethynylsulfonyl)benzene (451.6 mg, 1.762 mmol, 2.0 equiv) and $[Ir(ppy)_2(dtbbpy)]PF_6$ (16.5 mg, 0.018 mmol, 0.02 equiv) in methanol (5.8 mL, c = 0.15 M) was irradiated overnight. The full consumption of the starting material was confirmed via TLC and HPLC/ESI-MS. The crude product was dissolved in 1 mL of acetonitrile and 0.2 mL of this solution was purified via preparative HPLC (ACE C18-PFP, oven temperature: 40 °C, eluent: water (+0.1% formic acid)/acetonitrile, 35:65) yielding the title compound (18.4 mg, 0.047 mmol, 27%) as a colorless solid.

R_f = 0.43 (10:1 cyclohexane/ethyl acetate). Mp: 116 − 117 °C (chloroform). IR/cm^{-1} (ATR): 3022, 2955, 1311, 1300, 1142, 1087, 812, 698, 665, 591 cm^{-1}. ^1H NMR, COSY, NOESY (600 MHz, $CDCl_3$) δ 7.29 – 7.28 (m, 2H, H-2'',6''), 7.25 – 7.23 (m, 1H, H-4'), 7.20 – 7.18 (m, 2H, H-3',5'), 7.16 – 7.14 (t, *J* = 7.4 Hz, 2H, H-2',6'), 6.98 (d, *J* = 8.1 Hz, 2H, H-3'',5''), 5.52 –5.50 (m, 1H, H-5), 5.09 (ddd, *J* = 10.0, 4.7, 2.7 Hz, 1H, H-4), 3.57 (ddt, *J* = 6.9, 4.7, 2.6 Hz, 1H, H-3a), 2.31 (s, 3H, C4''–C$\mathbf{H}_3$), 2.08 – 2.04 (m, 1H, H-7a), 2.04 – 2.00 (m, 1H, H-6), 1.73 (m, 1H, H-7_a), 1.50 (s, 3H, C1–$C_b\mathbf{H}_3$), 1.45 (s, 3H, C1–$C_a\mathbf{H}_3$), 0.96 (d, *J* = 7.1 Hz, 3H, C6–$C_a\mathbf{H}_3$), 0.94 (d, *J* = 11.9 Hz, 1H, H-7_b). $^{13}C\{H\}$ NMR, HSQC, HMBC (151 MHz, $CDCl_3$) δ 155.2 (C-3), 143.9 (C-2), 143.0 (C-4''), 139.4 (C-1''), 136.5 (C-5), 134.7 (C-1'), 128.9 (C-3'',5''), 127.7 (C-2',4',6'), 127.6 (C-2'',6''), 124.0 (C-4), 50.3 (C-1), 49.3 (C-7a), 48.1 (C-3a), 31.1 (C-7), 30.0 (C-6), 27.2 (C1-**C**$_aH_3$), 22.1 (C1-**C**$_bH_3$), 21.8 (C6-**C**H_3), 21.3 (C4''–**C**H_3). MS (ESI): *m/z* = 393.3 $[M + H]^+$. HRMS (ESI) *m/z*: $[M+Na]^+$ calcd for $C_{25}H_{28}O_2S$: 415.1702, found: 415.1695. $[\alpha]_D^{20}$ = –17.8 (*c* = 1.84, ethyl acetate).

Non-catalyzed cycloaddition (sensitization protocol). Preparation of the tetracycle 7a.

In an oven-dried quartz tube under nitrogen atmosphere was charged the *meta* photoadduct **4** (35.0 mg, 0.12 mmol, 1.00 equiv), 1-methyl-4-(phenylethynylsulfonyl)benzene (61.2 mg, 0.24 mmol, 2.00 equiv), and methanol (0.8 mL, c = 0.15 M). The solution was degassed for 15 min and placed in a Rayonet photoreactor. The vessel was irradiated (λ_{max} = 254 nm, 16 × 8 W) at room temperature for 14 h. After removal of the solvent under reduced pressure, column chromatography (SiO_2, eluent: cyclohexane/ethyl acetate, 95:1 → 20:1) afforded the title compound (17.7 mg, 0.03 mmol, 27%) as a colorless solid.

Synthesis of the tetracycle 7a using PC III

The *meta* photoadduct **4** (35.0 mg, 0.12 mmol, 1.00 equiv), alkynyl sulfone **6** (61.2 mg, 0.24 mmol, 2.00 equiv), $[Ir(dF(CF_3)ppy)_2(dtbbpy)]PF_6$ (2.7 mg, 0.002 mmol, 0.02 equiv) and methanol (0.8 mL, c = 0.15 M) were loaded in an oven-dried Schlenk tube (10 mL) under nitrogen atmosphere, and the mixture was degassed and then placed in front of two blue LEDs 440 nm (see the materials section) at a distance of 5 cm. After 10 h, the resultant solution was concentrated and purified by flash column chromatography (SiO_2, eluent: cyclohexane/ethyl acetate, 95:1 → 20:1) to afford **7a** (56.5 mg, 0.10 mmol, 86%) as a colorless solid.

5. X-RAY CRYSTAL STRUCTURE DETERMINATION

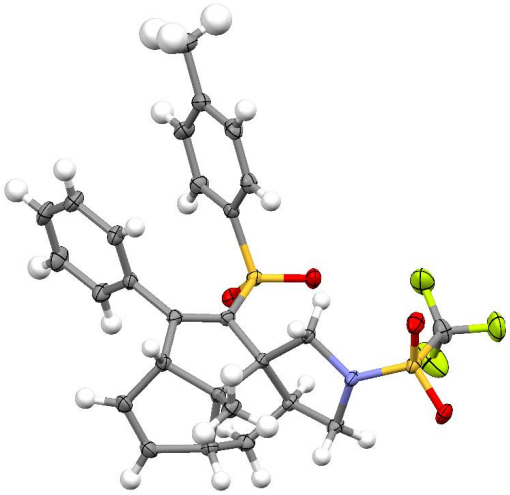

Figure S7. Molecular structure of compound **7a** in the solid state (ORTEP-ellipsoids, C: black, H: gray, N: blue, O: red, S: yellow, F: green). **CCDC Number: 2112151**.

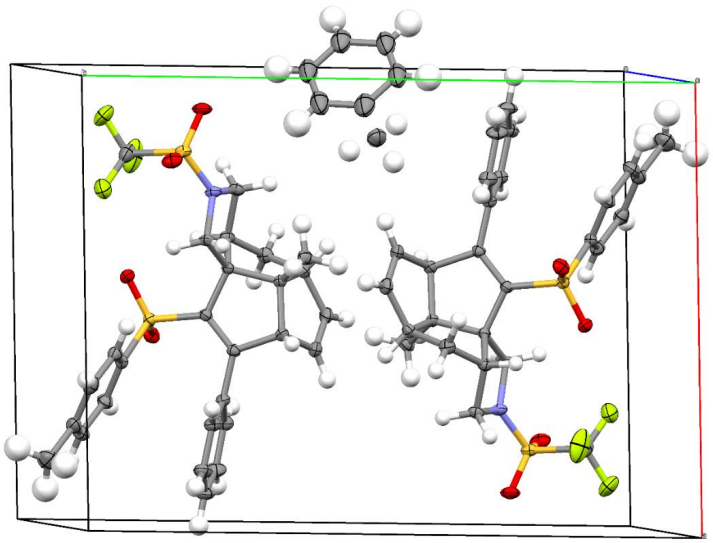

Figure S8. Cell unit of tetracycle **7a**.

Table S8. Crystal structure determination of compound **7a**.

Empirical formula	$C_{61}H_{60}F_6N_2O_8S_4$	
moiety formula	$2(C_{27}H_{26}F_3NO_4S_2)$, C_7H_8	
Formula weight	1191.35	
Temperature	120(2) K	
Wavelength, radiation type	0.71073Å, MoKα	
Diffractometer	STOE IPDS 2T	
Crystal system	Monoclinic	
Space group name, number	P 21/c, (14)	
Unit cell dimensions	a = 13.4345(4) Å	α = 90°
	b = 18.1709(8) Å	β = 100.182(3)°
	c = 11.7583(4) Å	γ = 90°
Volume	2825.19(18) $Å^3$	
Number of reflections	18469	
and range used for lattice parameters	2.72° <=θ<= 28.39°	
Z	2	
Density (calculated)	1.400 Mg/m^3	
Absorption coefficient	0.246 mm^{-1}	
Absorption correction	Integration	
Max. and min. transmission	0.9795 and 0.8638	

F(000)	1244
Crystal size, colour and form	0.080 x 0.400 x 0.650 mm^3, colourless plate
Theta range for data collection	2.720 to 27.942°.
Index ranges	-17<=h<=17, -23<=k<=22, -15<=l<=15
Number of reflections:	
collected	13943
independent	6713 [R(int) = 0.0211]
observed [I>2sigma(I)]	5478
Completeness to theta = 25.2°	99.9 %
Refinement method	Full-matrix least-squares on F^2
Data / restraints / parameters	6713 / 0 / 373
Goodness-of-fit on F^2	1.037
Final R indices [I>2sigma(I)]	R1 = 0.0416, wR2 = 0.0937
R indices (all data)	R1 = 0.0554, wR2 = 0.1017
Largest diff. peak and hole	0.432 and -0.353 $eÅ^{-3}$
remark	Toluene is located around a centre of inversion

7. REFERENCES

[1] a) D. Cyr and P. Das, *Res. Chem. Intermed.* **2015**, *41*, 8603-8623; b) B. Lipp, L. M. Kammer, M. Kucukdisli, A. Luque, J. Kuhlborn, S. Pusch, G. Matuleviciute, D. Schollmeyer, A. Sackus and T. Opatz, *Chem. Eur. J.* **2019**, *25*, 8965-8969; c) H. G. Roth, N. A. Romero and D. A. Nicewicz, *Synlett* **2016**, *27*, 714-723.

[2] Y. Pellegrin and F. Odobel, *Cr Chim* **2017**, *20*, 283-295.

[3] A. M. Halpern, D. A. Forsyth and M. Nosowitz, *J. Phys. Chem.* **1986**, *90*, 2677-2679.

[4] B. Xu, L. Troian-Gautier, R. Dykstra, R. T. Martin, O. Gutierrez and U. K. Tambar, *J. Am. Chem. Soc.* **2020**, *142*, 6206-6215.

[5] M. Mitani, T. Kiriyama and T. Kuratate, *J. Org. Chem.* **1994**, *59*, 1279-1282.

[6] P. Herr, C. Kerzig, C. B. Larsen, D. Haussinger and O. S. Wenger, *Nat Chem* **2021**, *13*, 956-+.

[7] C. J. Wallentin, J. D. Nguyen, P. Finkbeiner and C. R. J. Stephenson, *J. Am. Chem. Soc.* **2012**, *134*, 8875-8884.

[8] a) C. Lee, W. Yang and R. G. Parr, *Phys. Rev. B* **1988**, *37*, 785-789; b) A. D. Becke, *J. Chem. Phys.* **1993**, *98*, 5648-5652; c) S. H. Vosko, L. Wilk and M. Nusair, *Can. J. Phys.* **1980**, *58*, 1200-1211.

[9] T. Yanai, D. P. Tew and N. C. Handy, *Chem. Phys. Lett.* **2004**, *393*, 51-57.

[10] Y. Zhao and D. G. Truhlar, *Theor. Chem. Acc.* **2008**, *120*, 215-241.

[11] a) R. Krishnan, J. S. Binkley, R. Seeger and J. A. Pople, *J. Chem. Phys.* **1980**, *72*, 650-654; b) M. J. Frisch, J. A. Pople and J. S. Binkley, *J. Chem. Phys.* **1984**, *80*, 3265-3269.

[12] J. Tomasi, B. Mennucci and E. Cancès, *J. Mol. Struct.* **1999**, *464*, 211-226.

[13] E. Runge and E. K. U. Gross, *Phys. Rev. Lett.* **1984**, *52*, 997-1000.

[14] C. Adamo and D. Jacquemin, *Chem. Soc. Rev.* **2013**, *42*, 845-856.

[15] M. J. Frisch, G. W. Trucks, H. B. Schlegel, G. E. Scuseria, M. A. Robb, J. R. Cheeseman, G. Scalmani, V. Barone, G. A. Petersson, H. Nakatsuji, X. Li, M. Caricato, A. V. Marenich, J. Bloino, B. G. Janesko, R. Gomperts, B. Mennucci, H. P. Hratchian, J. V. Ortiz, A. F. Izmaylov, J. L. Sonnenberg, Williams, F. Ding, F. Lipparini, F. Egidi, J. Goings, B. Peng, A. Petrone, T. Henderson, D. Ranasinghe, V. G.

Zakrzewski, J. Gao, N. Rega, G. Zheng, W. Liang, M. Hada, M. Ehara, K. Toyota, R. Fukuda, J. Hasegawa, M. Ishida, T. Nakajima, Y. Honda, O. Kitao, H. Nakai, T. Vreven, K. Throssell, J. A. Montgomery Jr., J. E. Peralta, F. Ogliaro, M. J. Bearpark, J. J. Heyd, E. N. Brothers, K. N. Kudin, V. N. Staroverov, T. A. Keith, R. Kobayashi, J. Normand, K. Raghavachari, A. P. Rendell, J. C. Burant, S. S. Iyengar, J. Tomasi, M. Cossi, J. M. Millam, M. Klene, C. Adamo, R. Cammi, J. W. Ochterski, R. L. Martin, K. Morokuma, O. Farkas, J. B. Foresman and D. J. Fox in *Gaussian 16, Revision C.01*, *Vol.* Wallingford, CT, **2019**.

[16] Dennington R., Keith T.A. and Millam J. M., *GaussView, Version 6.* **2016**, *Semichem Inc.:Shawnee Mission, KS, USA*.

[17] V. Nair, A. Augustine and T. D. Suja, *Synthesis* **2002**, 2259-2265.

[18] L. L. Wang, W. Wei, D. S. Yang, H. H. Cui, H. L. Yue and H. Wang, *Tetrahedron Lett.* **2017**, *58*, 4799-4802.

[19] Z. Y. Mo, Y. Z. Zhang, G. B. Huang, X. Y. Wang, Y. M. Pan and H. T. Tang, *Adv. Synth. Catal.* **2020**, *362*, 2160-2167.

[20] Z. Wu, Y. H. Xu, H. H. Zhang, X. X. Wu and C. Zhu, *Chem. Commun.* **2021**, *57*, 6066-6069.

[21] N. Riddell and W. Tam, *J. Org. Chem.* **2006**, *71*, 1934-1937.

[22] S. K. Kristensen, S. L. R. Laursen, E. Taarning and T. Skrydstrup, *Angew. Chem. Int. Edit.* **2018**, *57*, 13887-13891; *Angew. Chem. Int. Edit.* **2018**, *130*, 14083-14087.

[23] S. Doobary, A. T. Sedikides, H. P. Caldora, D. L. Poole and A. J. J. Lennox, *Angew. Chem. Int. Edit.* **2020**, *59*, 1155-1160; *Angew. Chem.* **2020**, *132*, 1171-1176.

[24] D. C. Blakemore and A. Gilbert, *J. Chem. Soc. Perk T. 1* **1992**, 2265-2270.

NMR SPECTRA

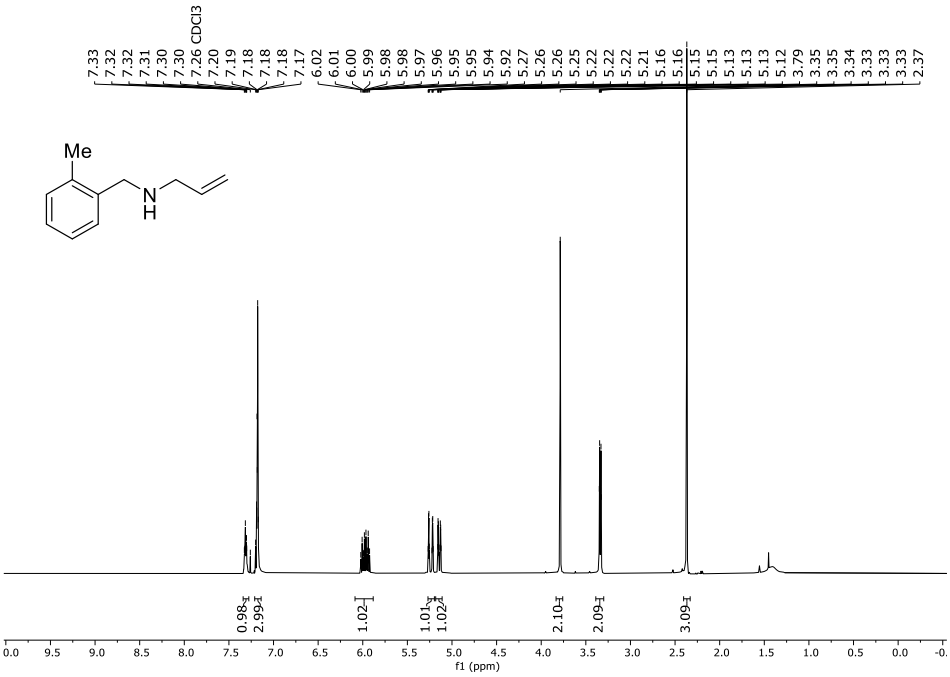

^{1}H NMR (400 MHz, $CDCl_3$) spectrum of **2**

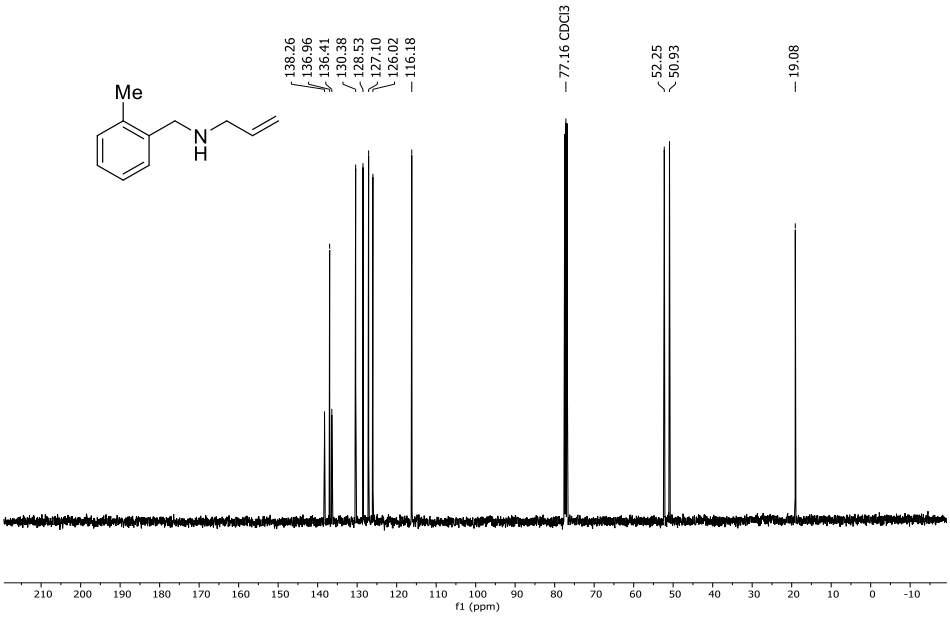

^{13}C NMR (101 MHz, $CDCl_3$) spectrum of **2**

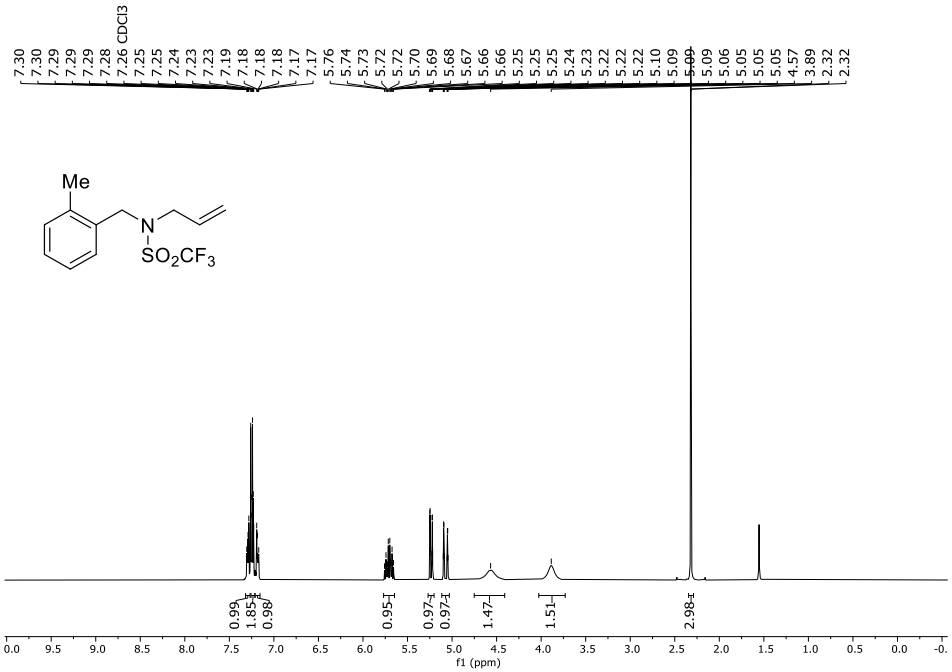

^{1}H NMR (400 MHz, $CDCl_3$) spectrum of **3**

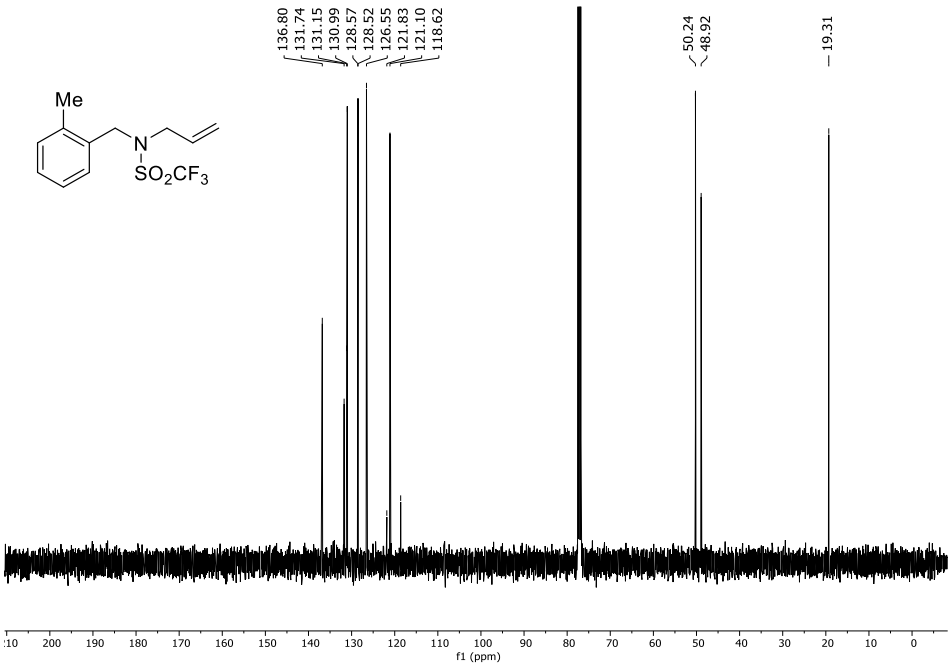

^{13}C NMR (101 MHz, $CDCl_3$) spectrum of **3**

S51

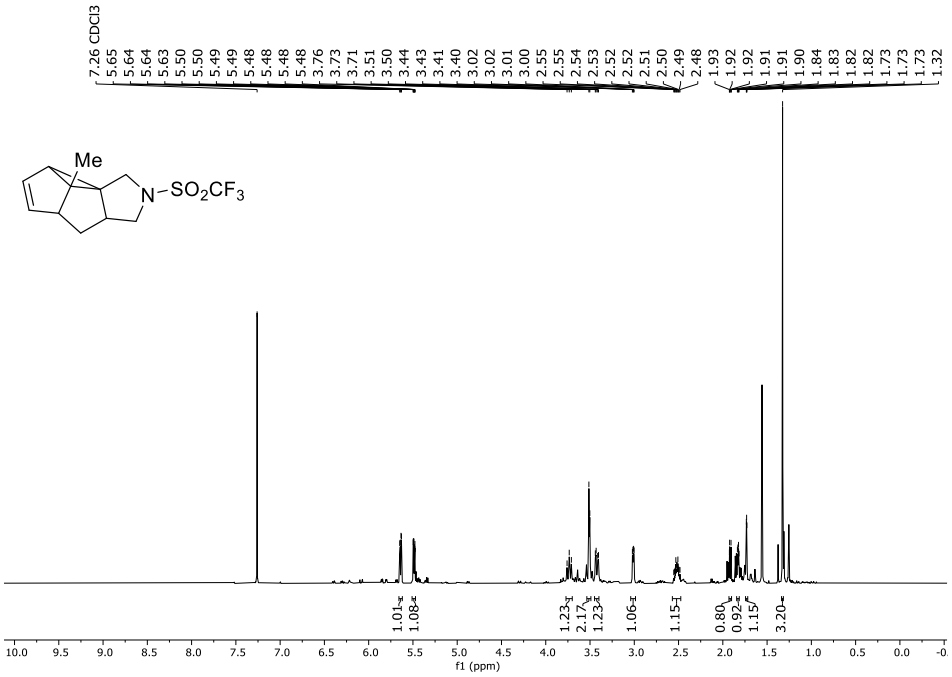

^{1}H NMR (400 MHz, $CDCl_3$) spectrum of **4**

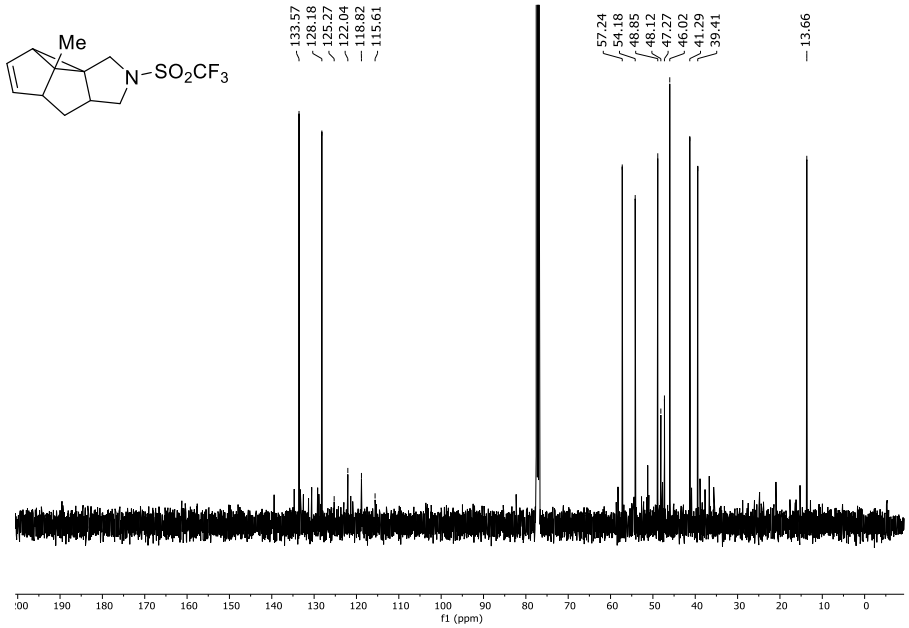

^{13}C NMR (101 MHz, $CDCl_3$) spectrum of **4**

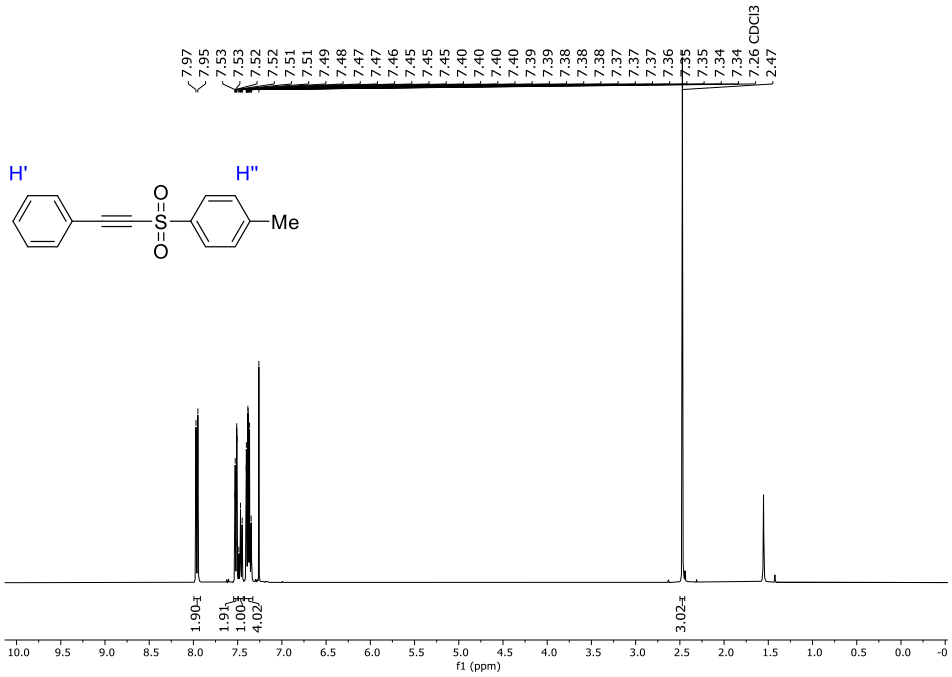

^{1}H NMR (400 MHz, $CDCl_3$) spectrum of **6a**

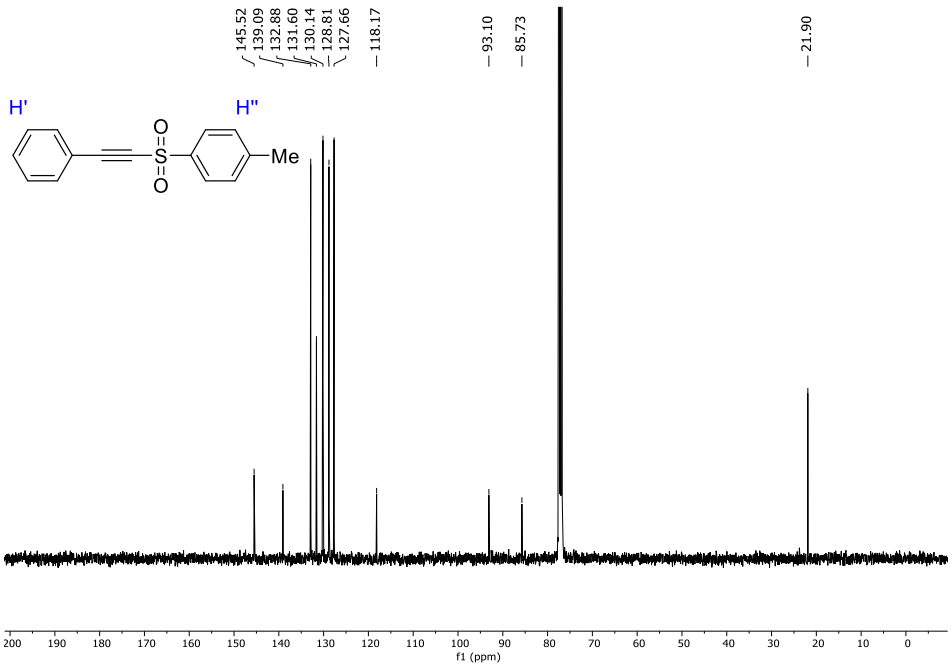

^{13}C NMR (101 MHz, $CDCl_3$) spectrum of **6a**

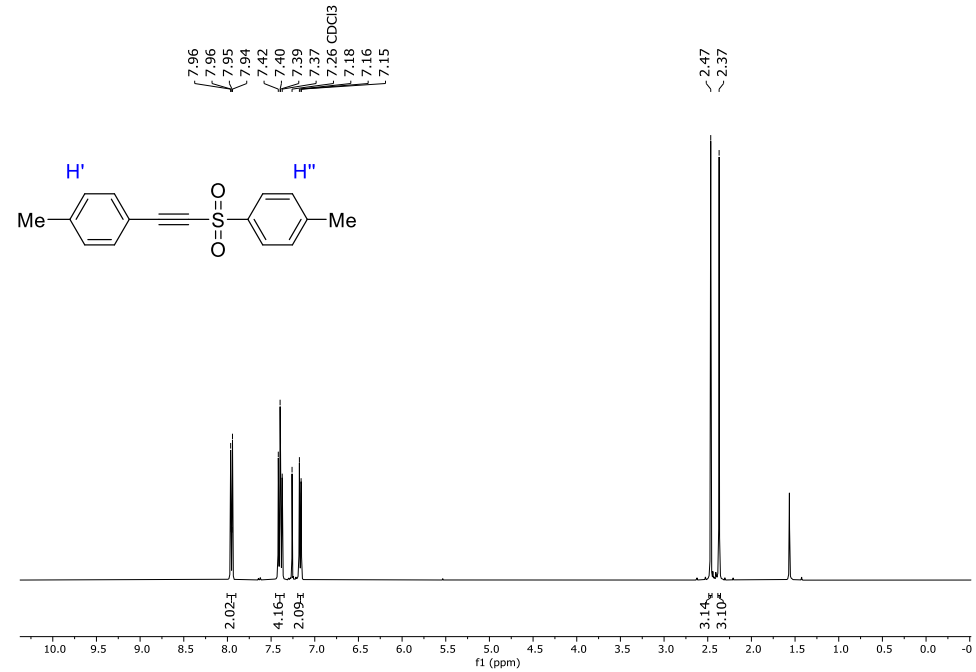

^{1}H NMR (400 MHz, $CDCl_3$) spectrum of **6b**

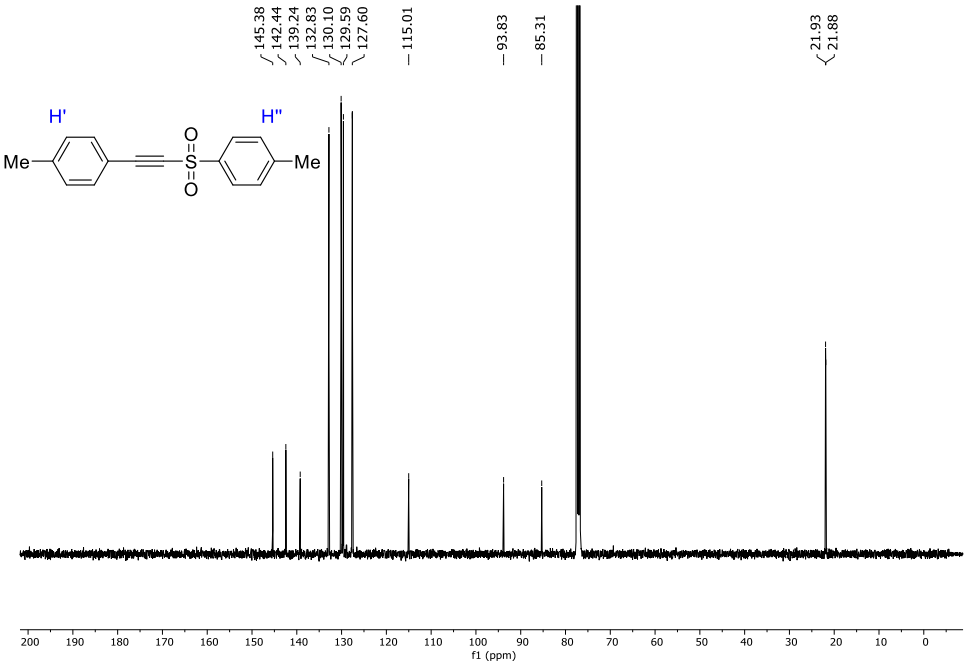

^{13}C NMR (101 MHz, $CDCl_3$) spectrum of **6b**

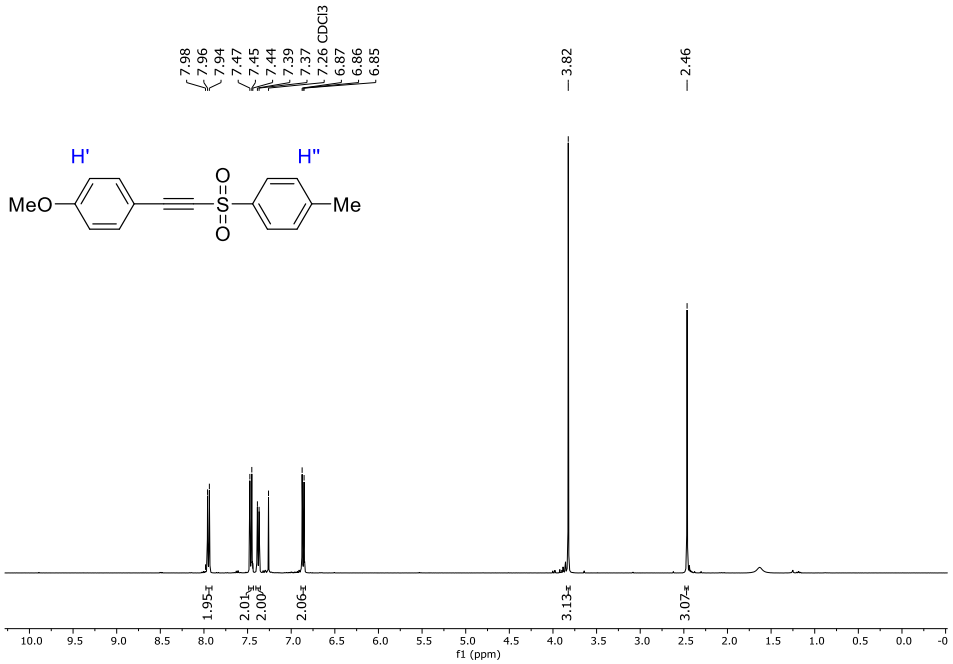

^{1}H NMR (400 MHz, $CDCl_3$) spectrum of **6c**

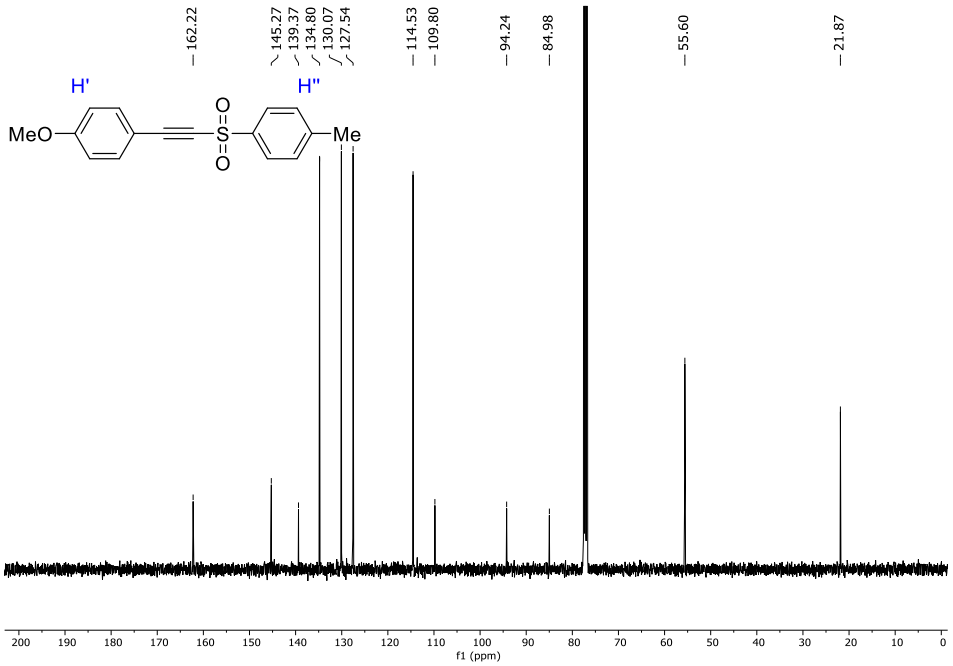

^{13}C NMR (101 MHz, $CDCl_3$) spectrum of **6c**

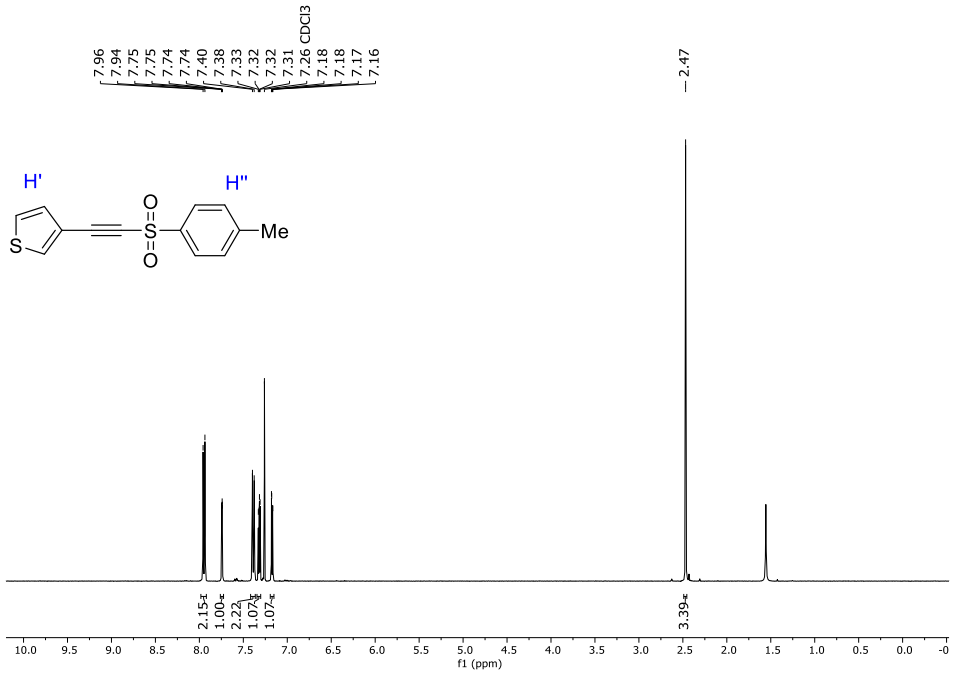

^{1}H NMR (400 MHz, $CDCl_3$) spectrum of **6d**

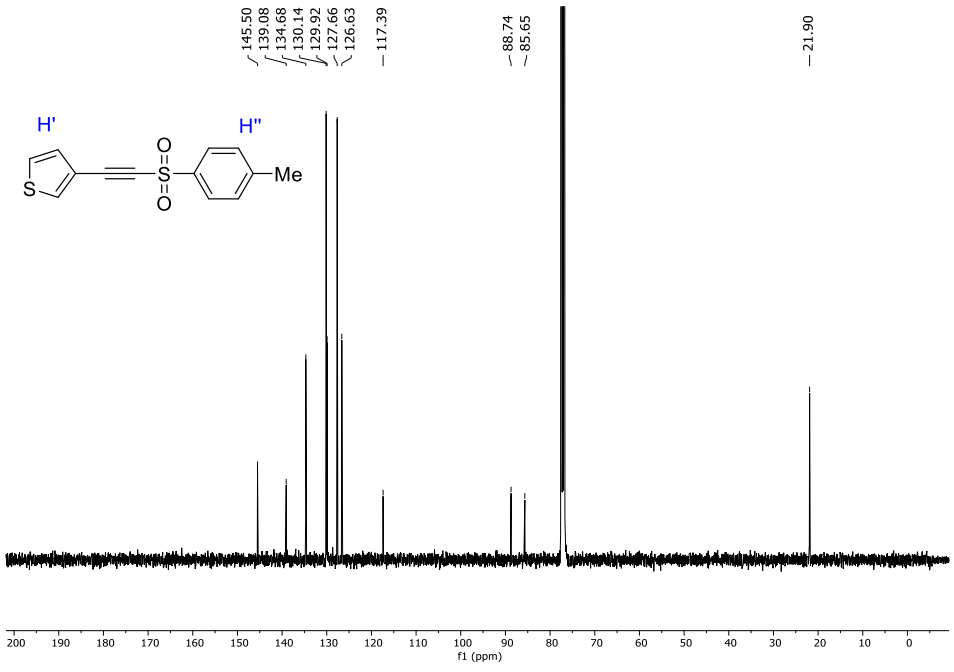

^{13}C NMR (101 MHz, $CDCl_3$) spectrum of **6d**

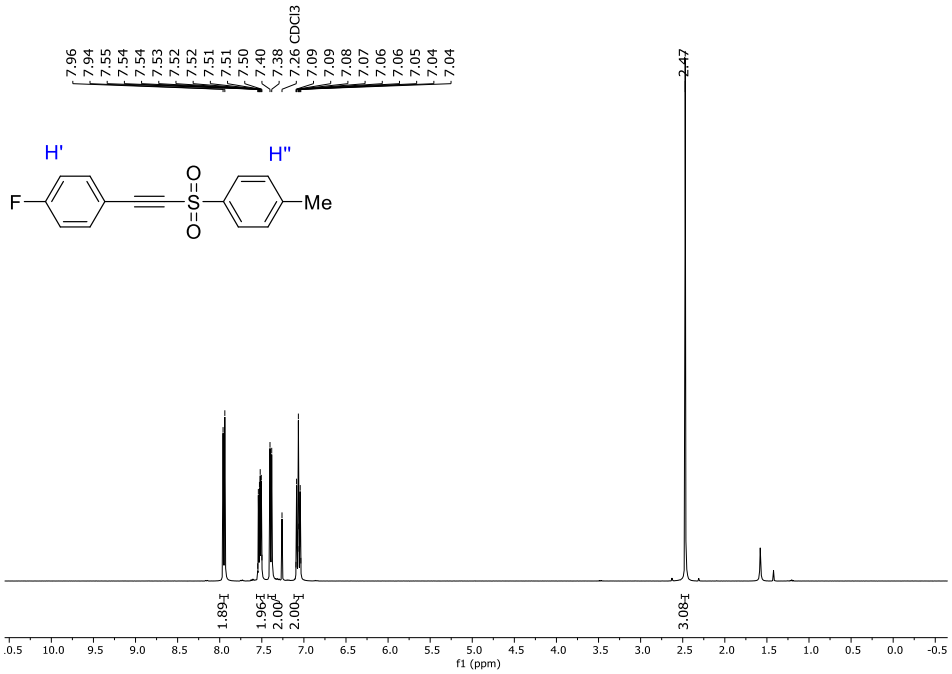

^{1}H NMR (400 MHz, $CDCl_3$) spectrum of **6e**

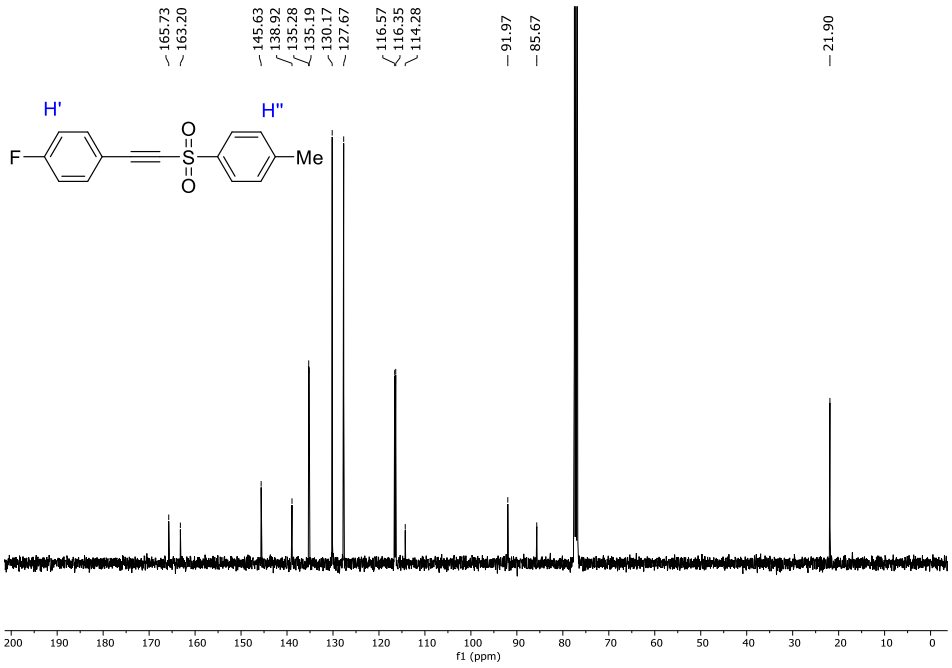

^{13}C NMR (101 MHz, $CDCl_3$) spectrum of **6e**

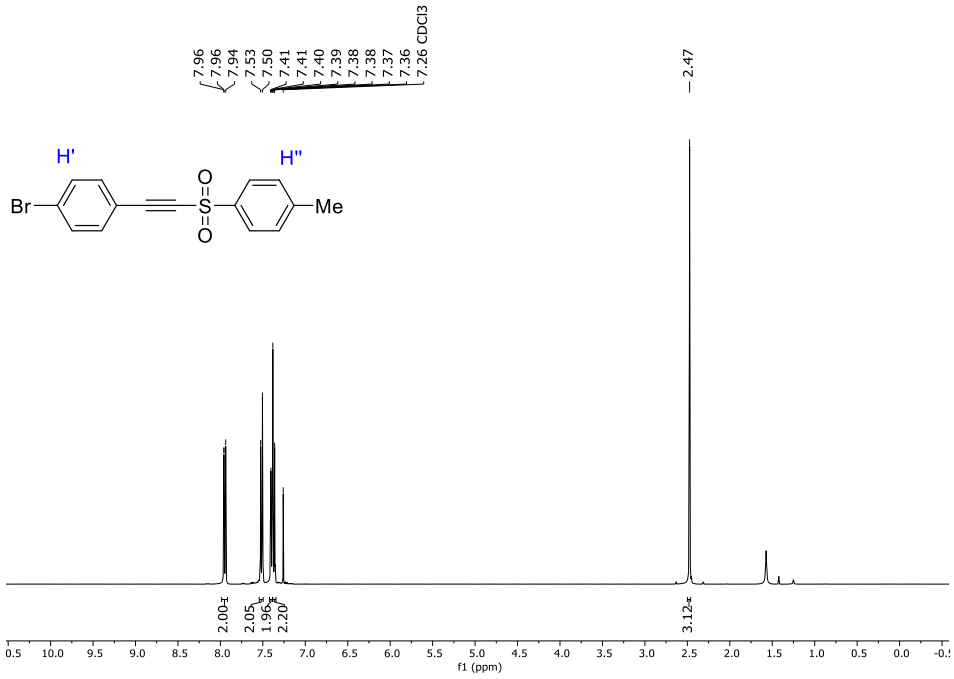

^{1}H NMR (400 MHz, $CDCl_3$) spectrum of **6f**

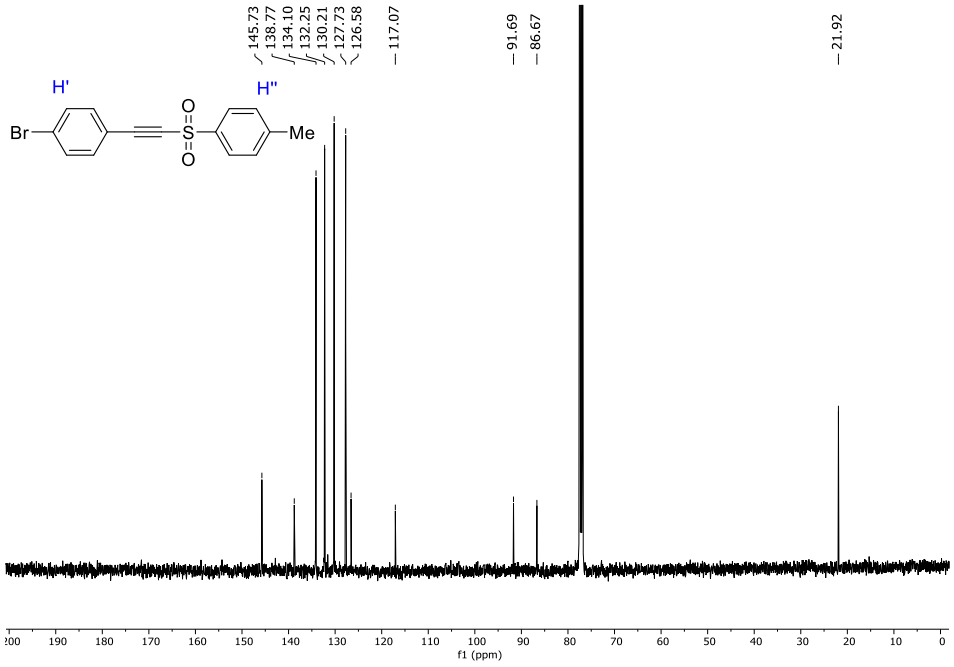

^{13}C NMR (101 MHz, $CDCl_3$) spectrum of **6f**

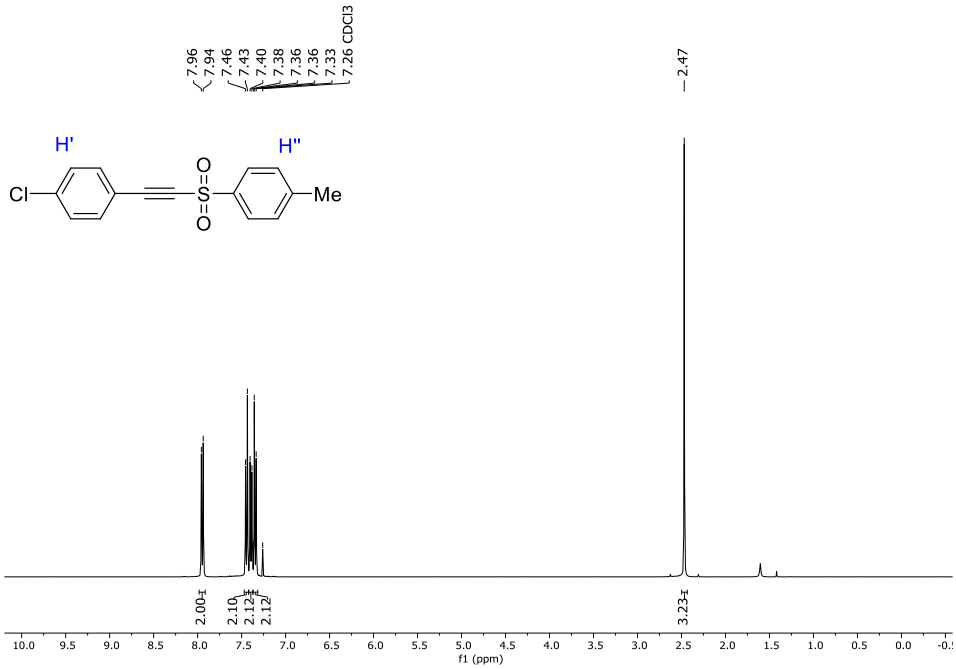

^{1}H NMR (400 MHz, $CDCl_3$) spectrum of **6g**

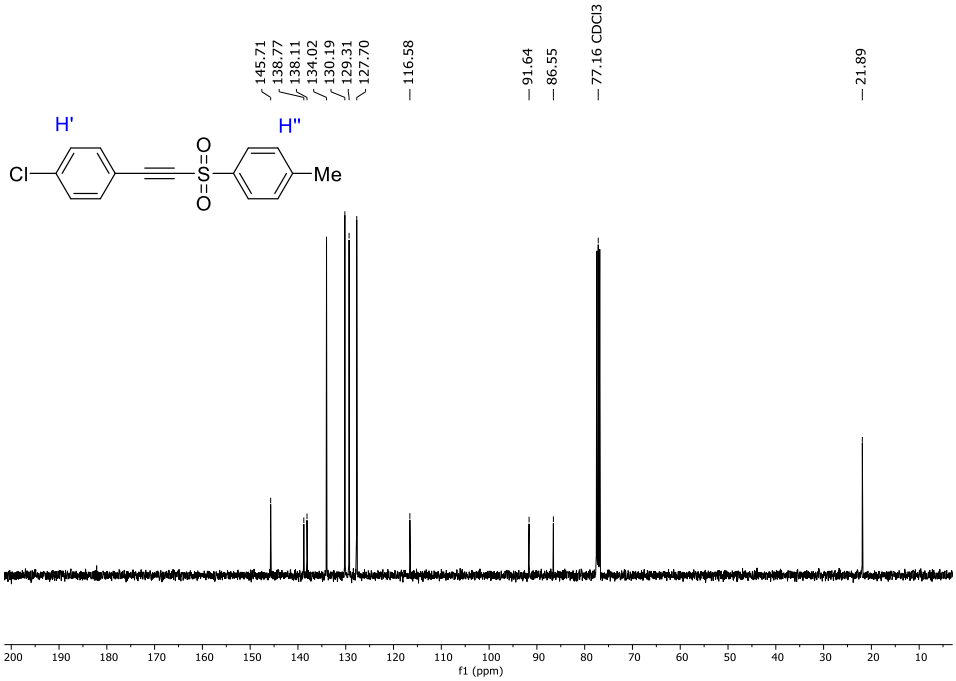

^{13}C NMR (101 MHz, $CDCl_3$) spectrum of **6g**

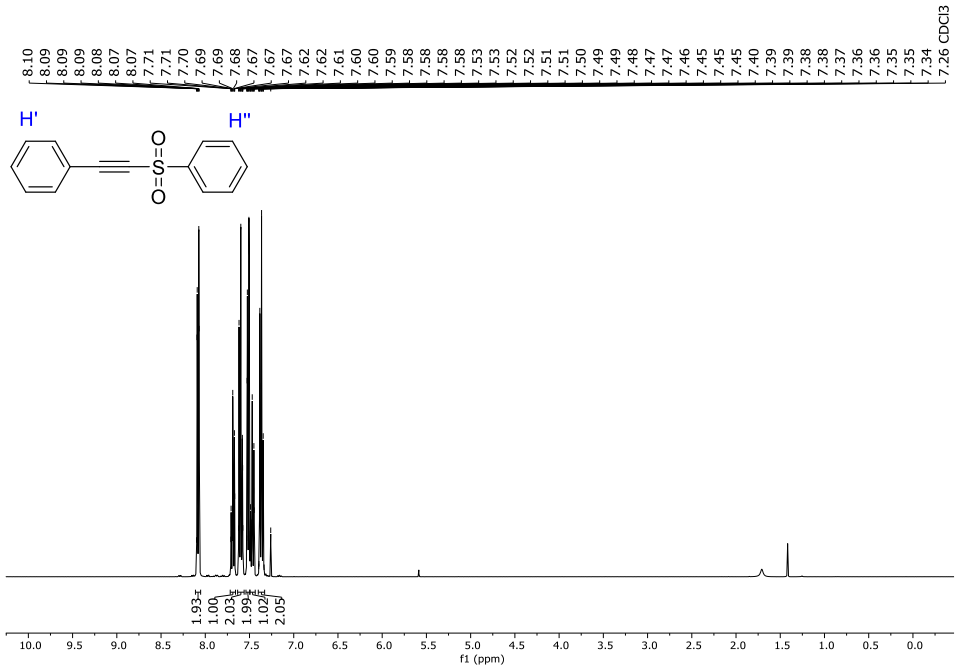

^{1}H NMR (400 MHz, $CDCl_3$) spectrum of **6h**

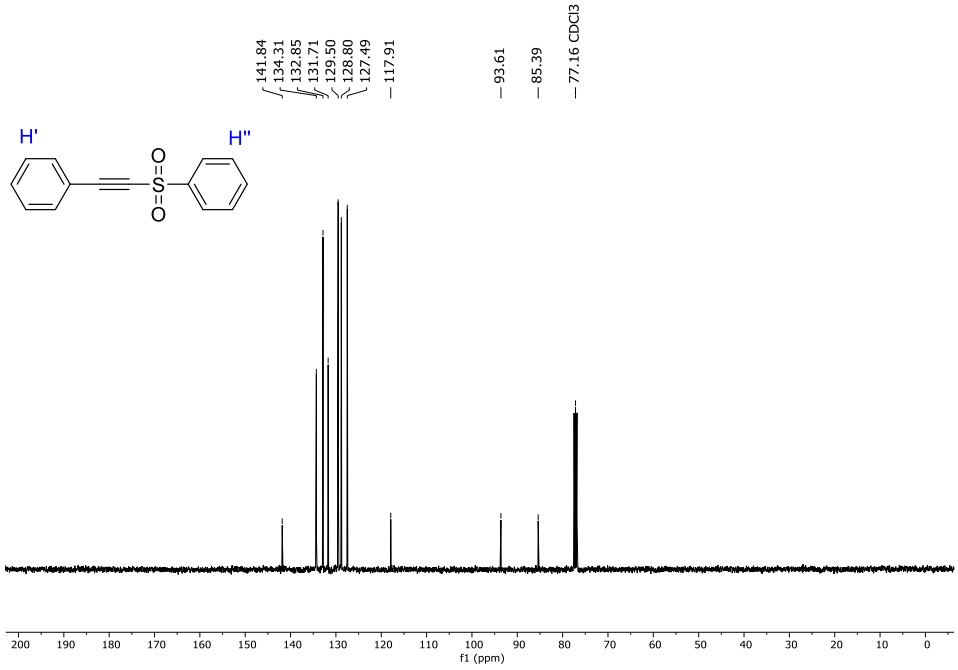

^{13}C NMR (101 MHz, $CDCl_3$) spectrum of **6h**

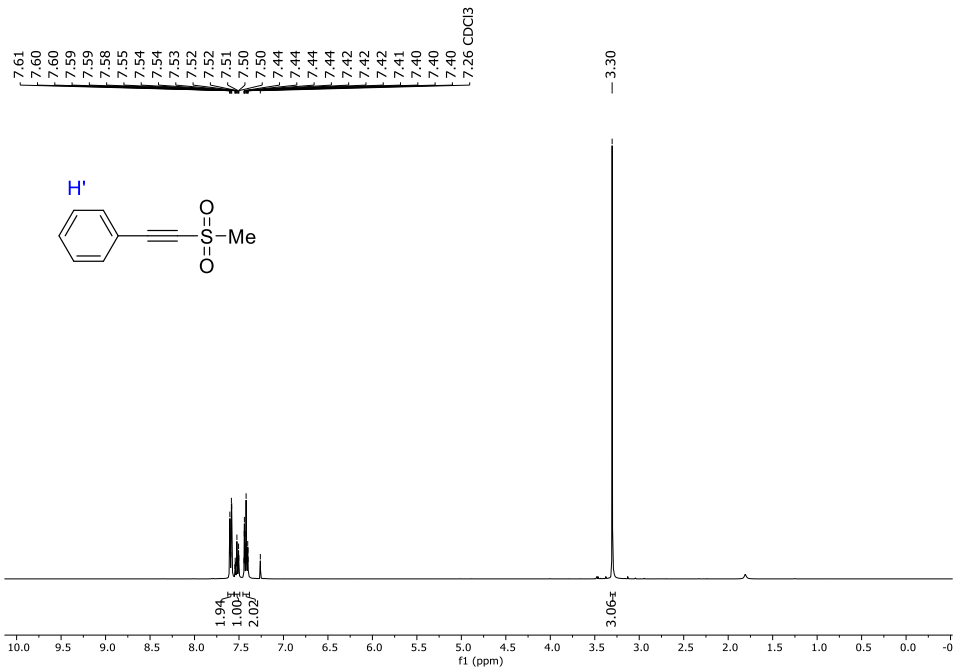

^{1}H NMR (400 MHz, $CDCl_3$) spectrum of **6i**

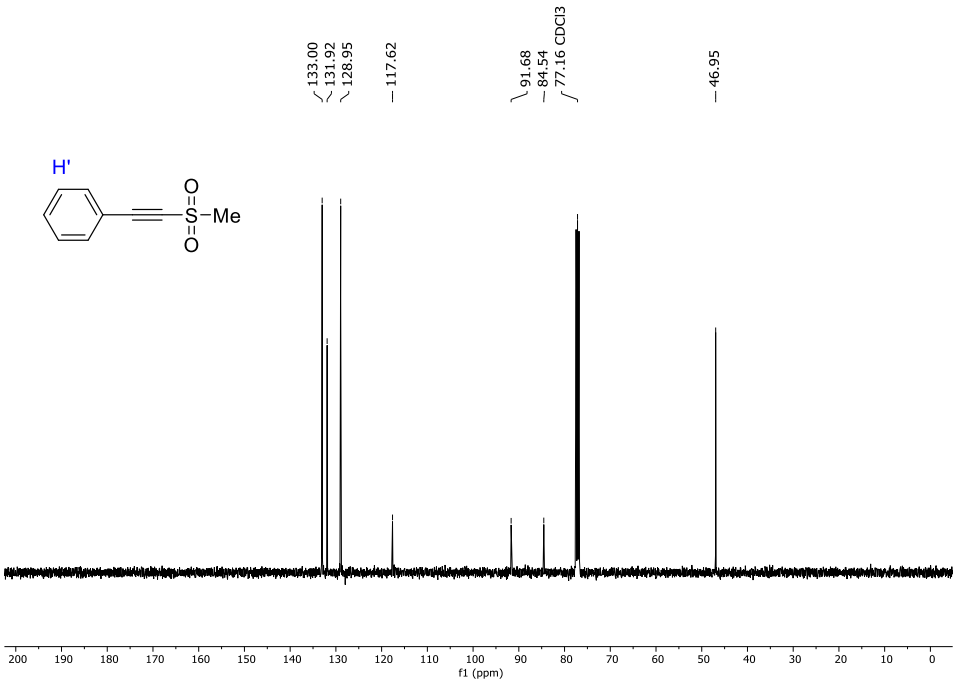

^{13}C NMR (101 MHz, $CDCl_3$) spectrum of **6i**

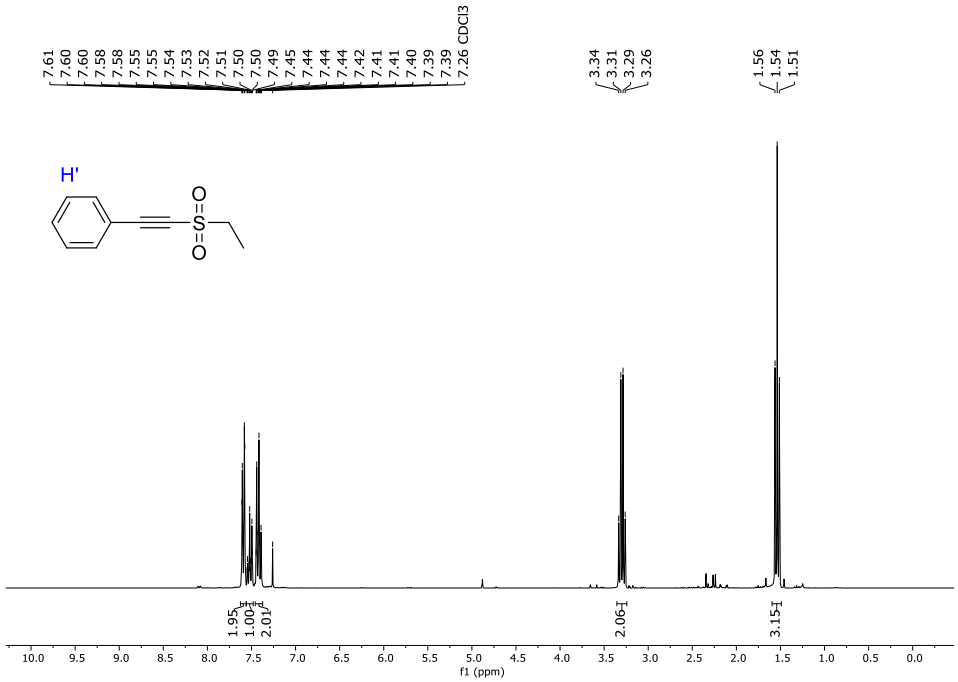

^{1}H NMR (400 MHz, $CDCl_3$) spectrum of **6j**

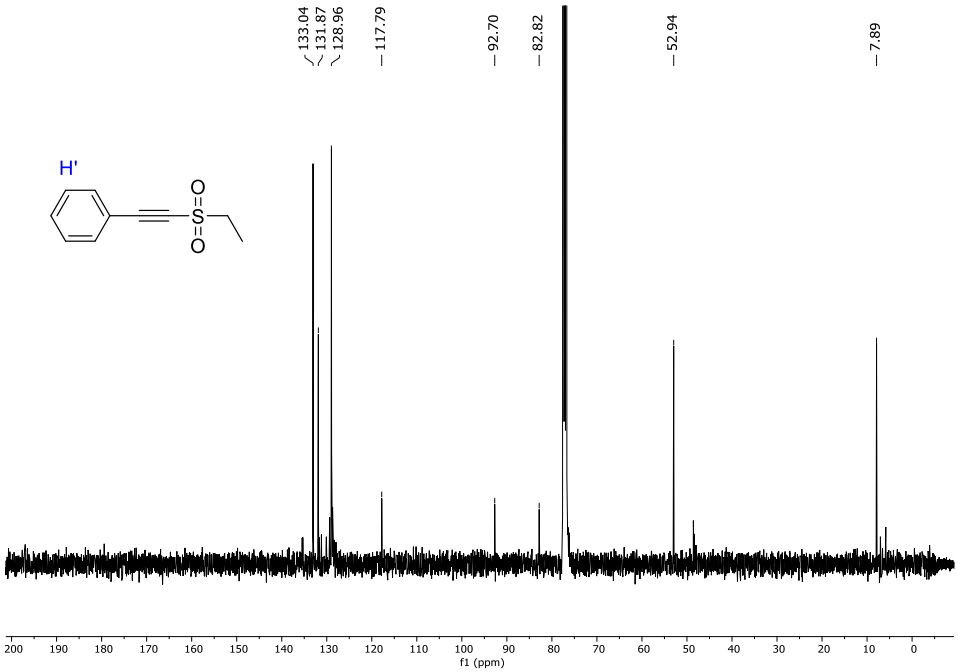

^{13}C NMR (101 MHz, $CDCl_3$) spectrum of **6j**

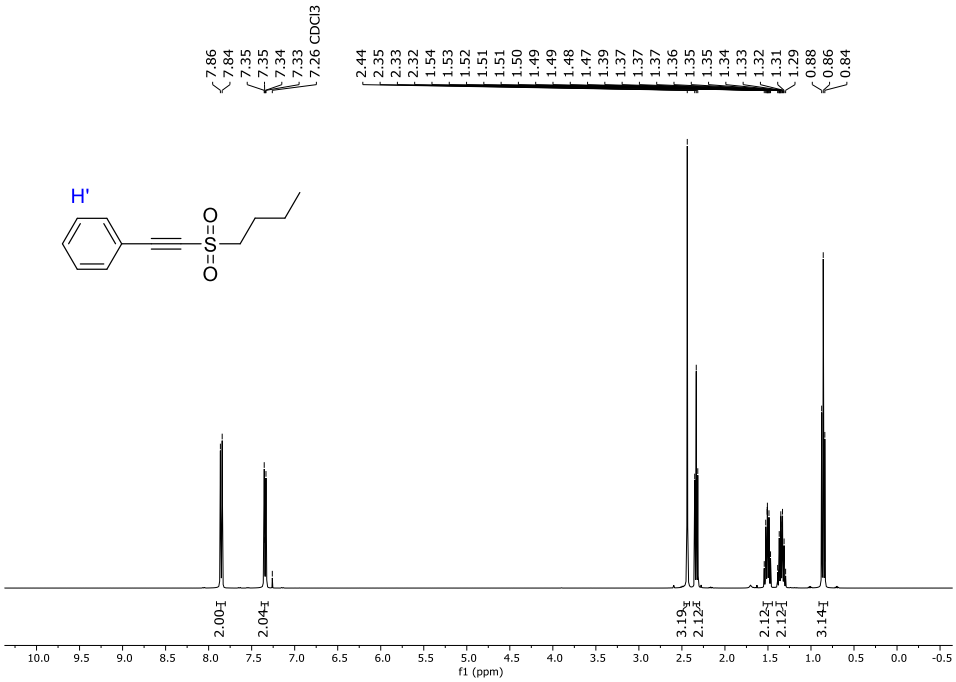

^{1}H NMR (400 MHz, $CDCl_3$) spectrum of **6k**

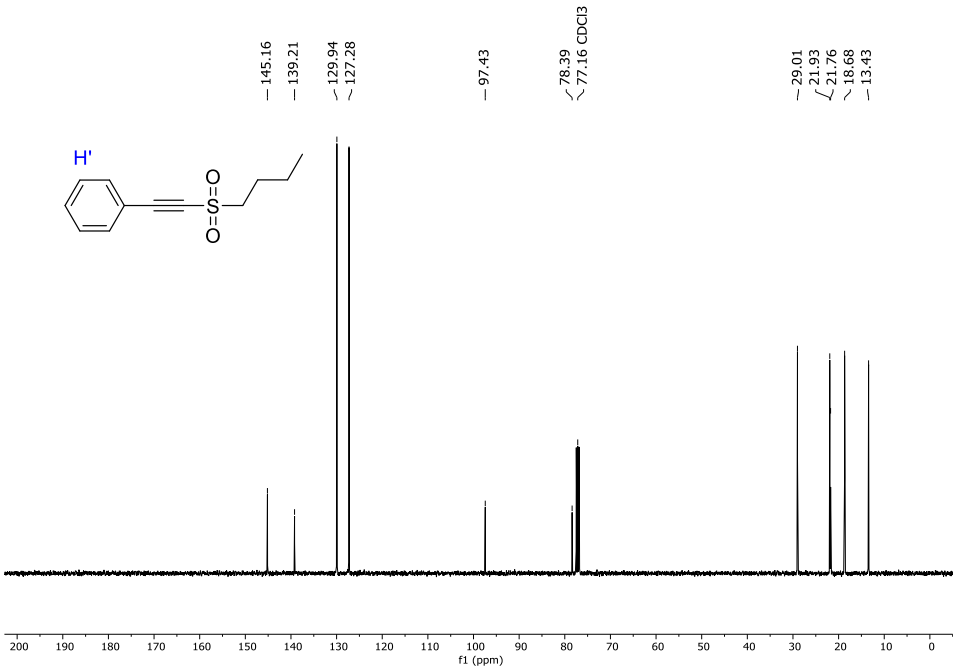

^{13}C NMR (101 MHz, $CDCl_3$) spectrum of **6k**

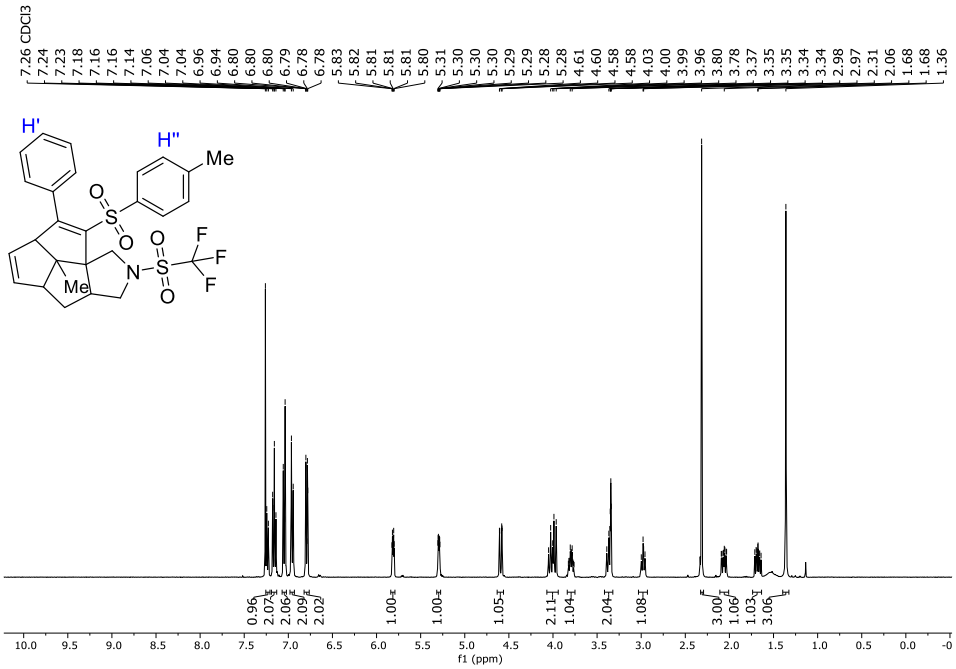

^{1}H NMR (400 MHz, $CDCl_3$) spectrum of **7a**

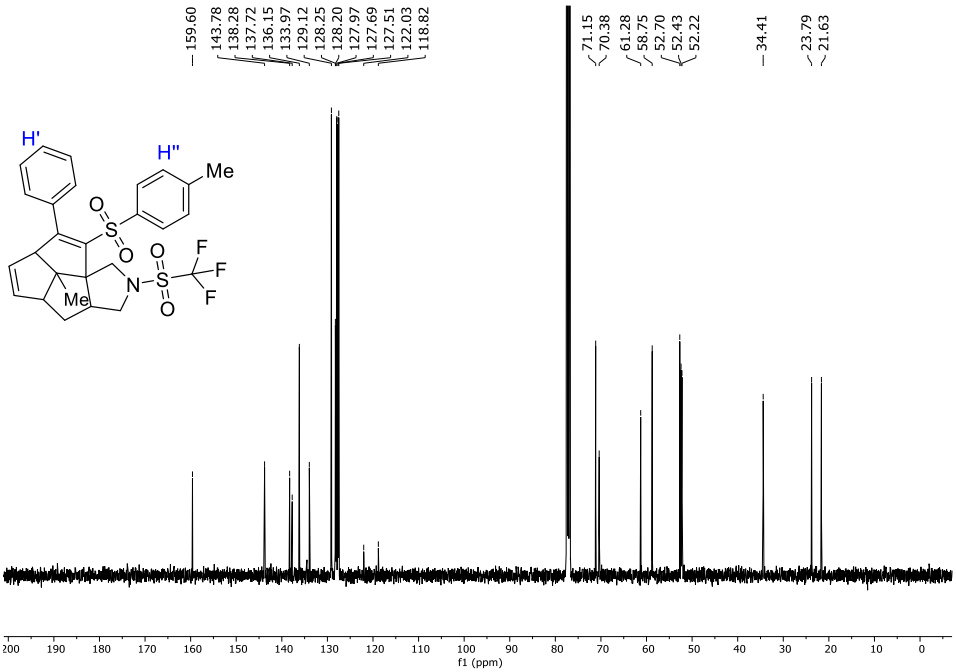

^{13}C NMR (101 MHz, $CDCl_3$) spectrum of **7a**

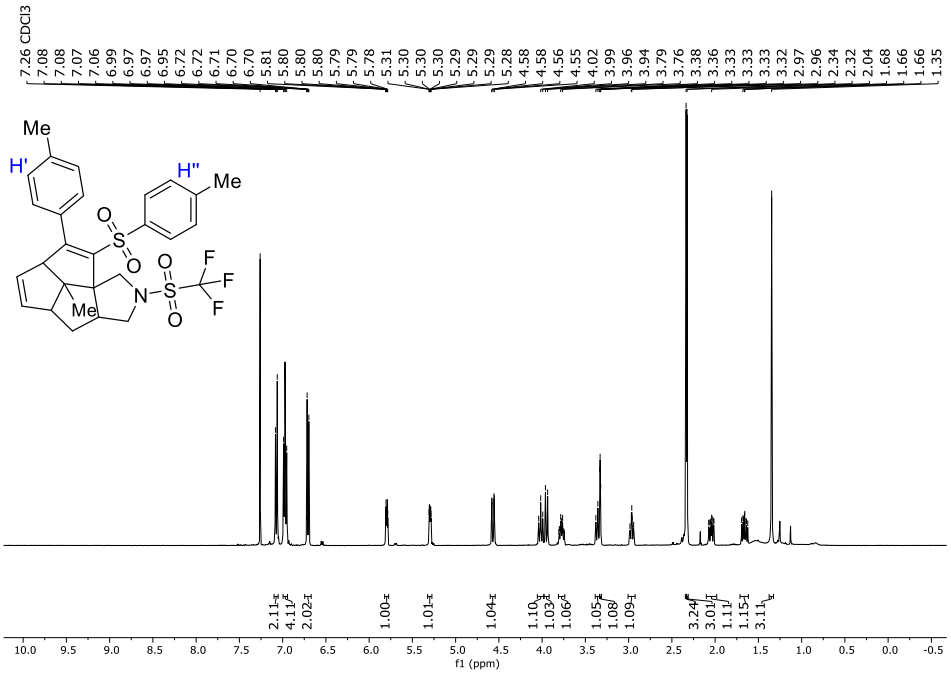

^{1}H NMR (400 MHz, $CDCl_3$) spectrum of **7b**

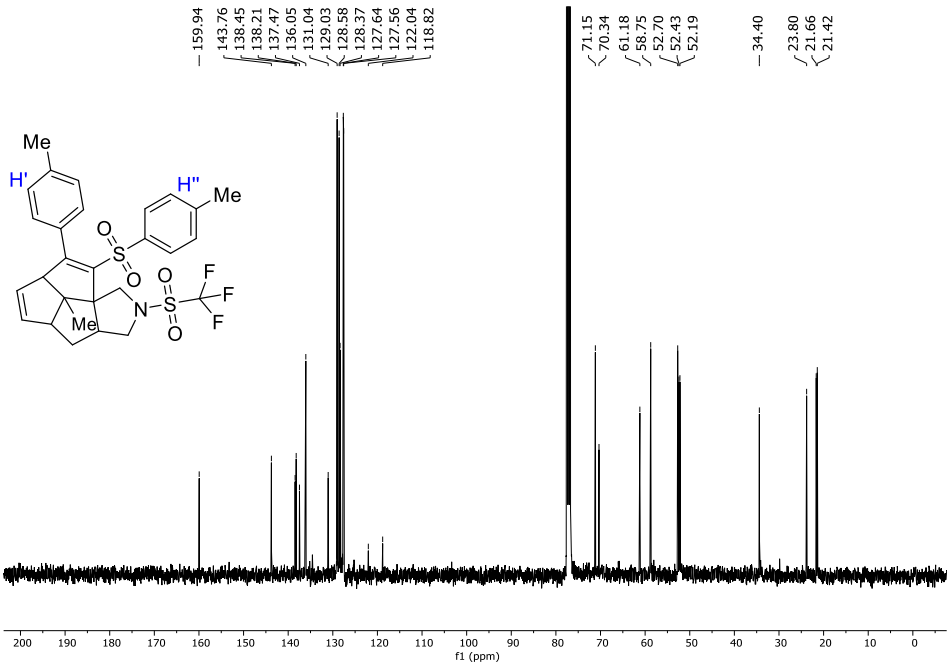

^{13}C NMR (101 MHz, $CDCl_3$) spectrum of **7b**

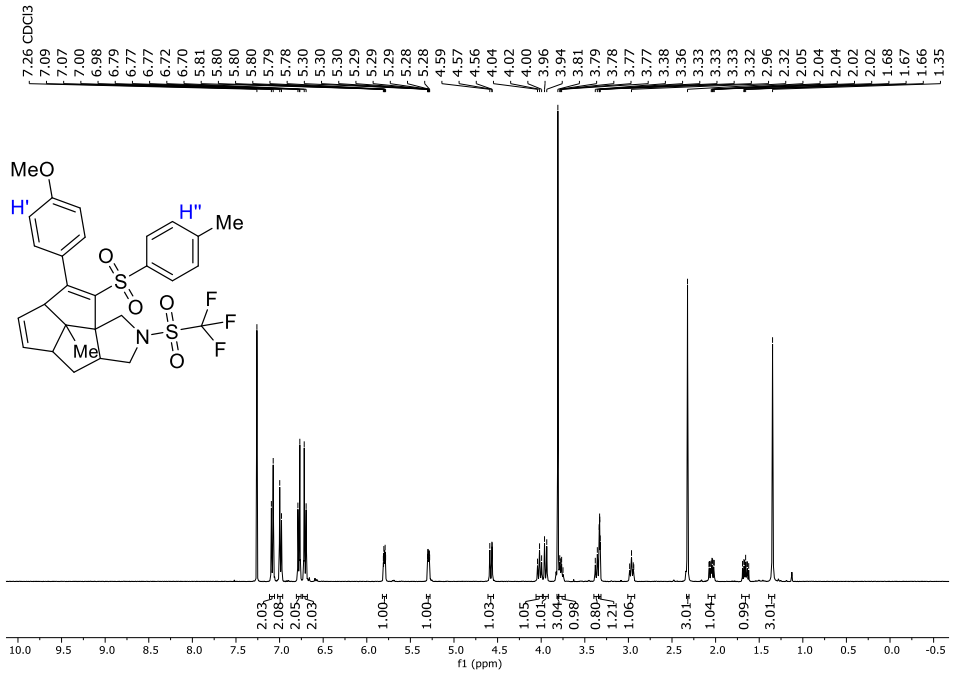

^{1}H NMR (400 MHz, $CDCl_3$) spectrum of **7c**

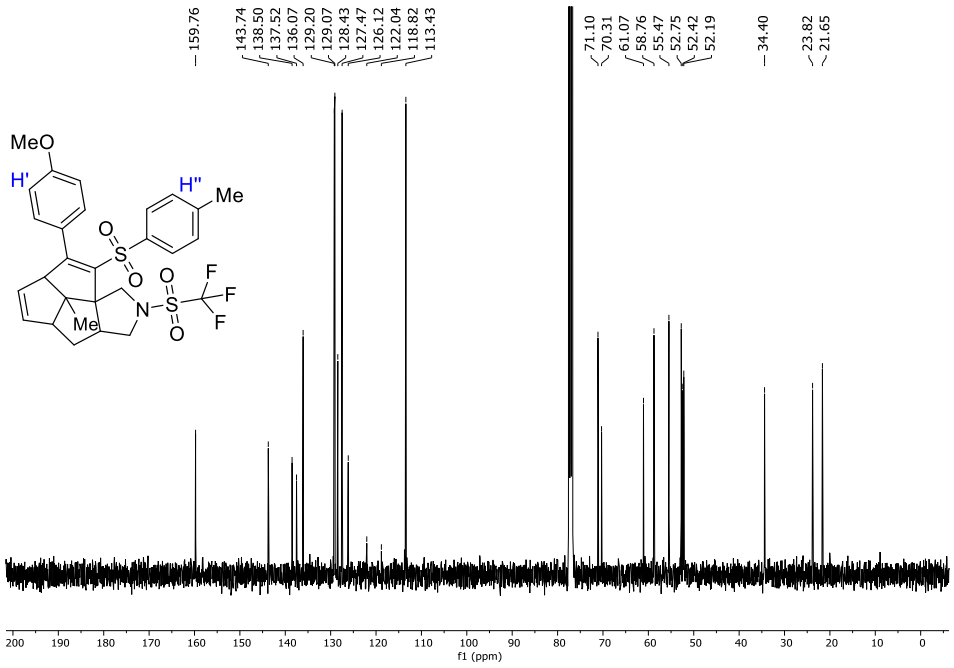

^{13}C NMR (101 MHz, $CDCl_3$) spectrum of **7c**

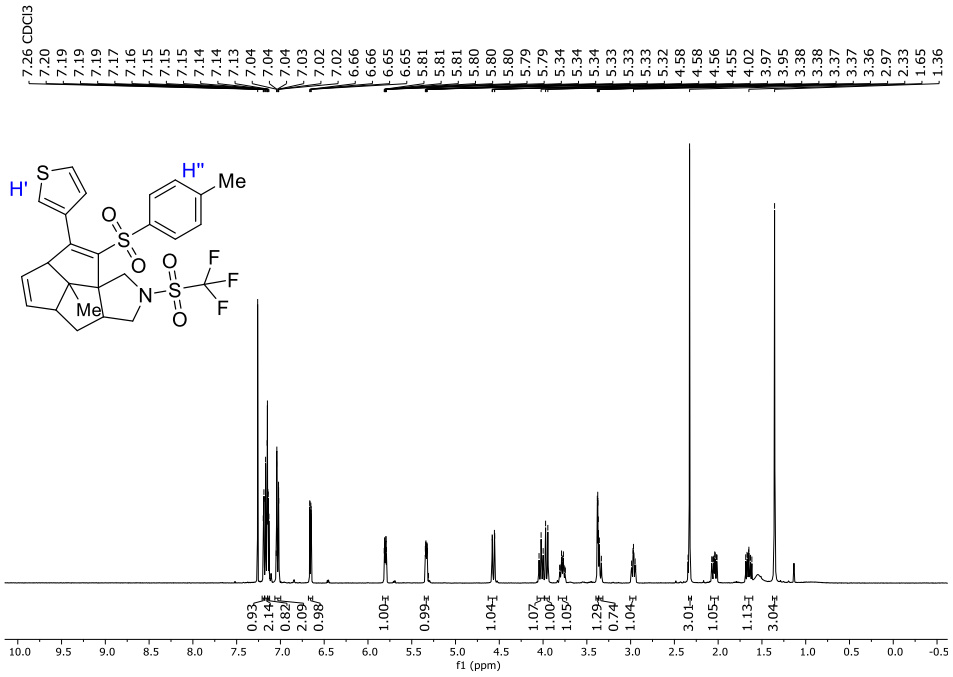

^{1}H NMR (400 MHz, $CDCl_3$) spectrum of **7d**

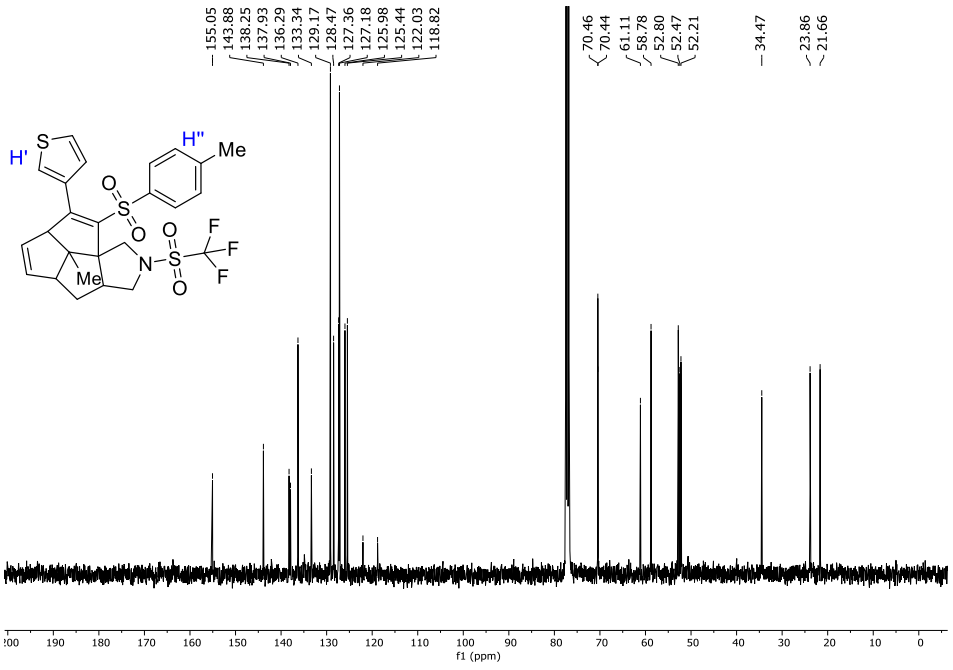

^{13}C NMR (101 MHz, $CDCl_3$) spectrum of **7d**

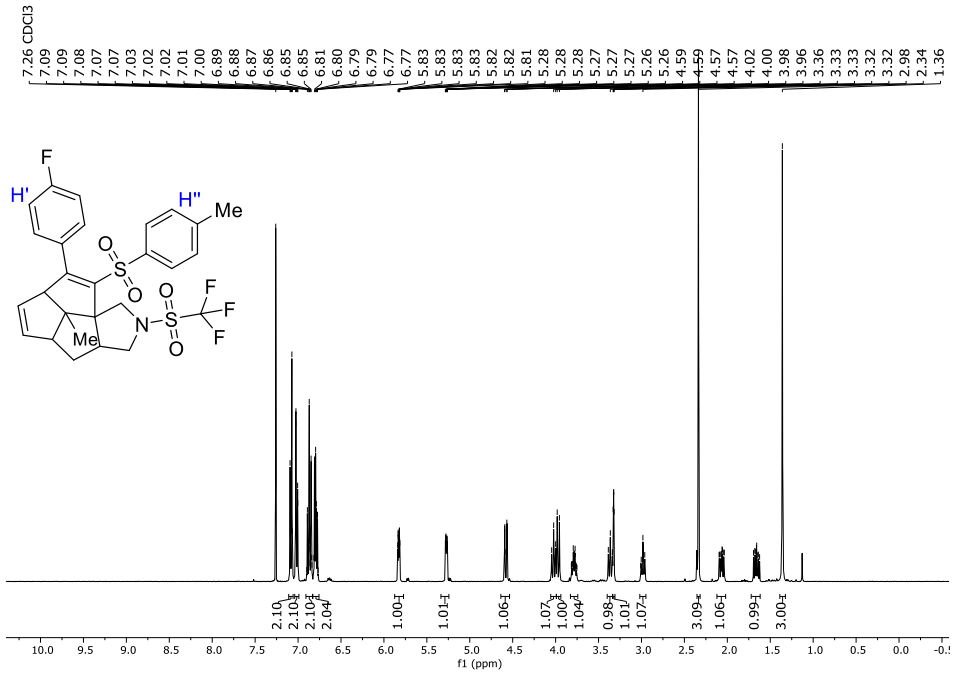

^{1}H NMR (400 MHz, $CDCl_3$) spectrum of **7e**

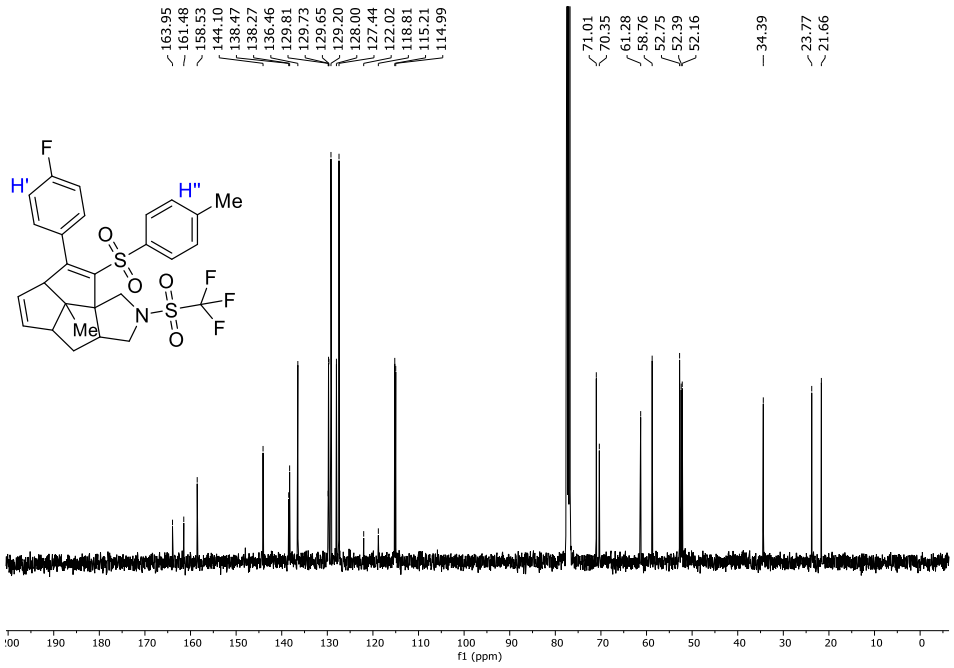

^{13}C NMR (101 MHz, $CDCl_3$) spectrum of **7e**

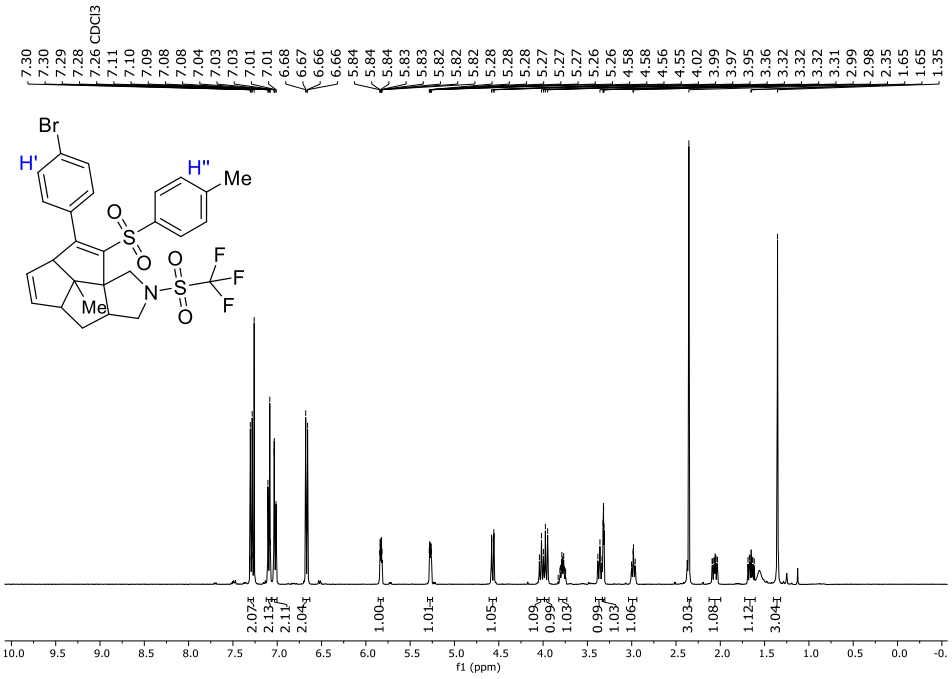

^{1}H NMR (400 MHz, $CDCl_3$) spectrum of **7f**

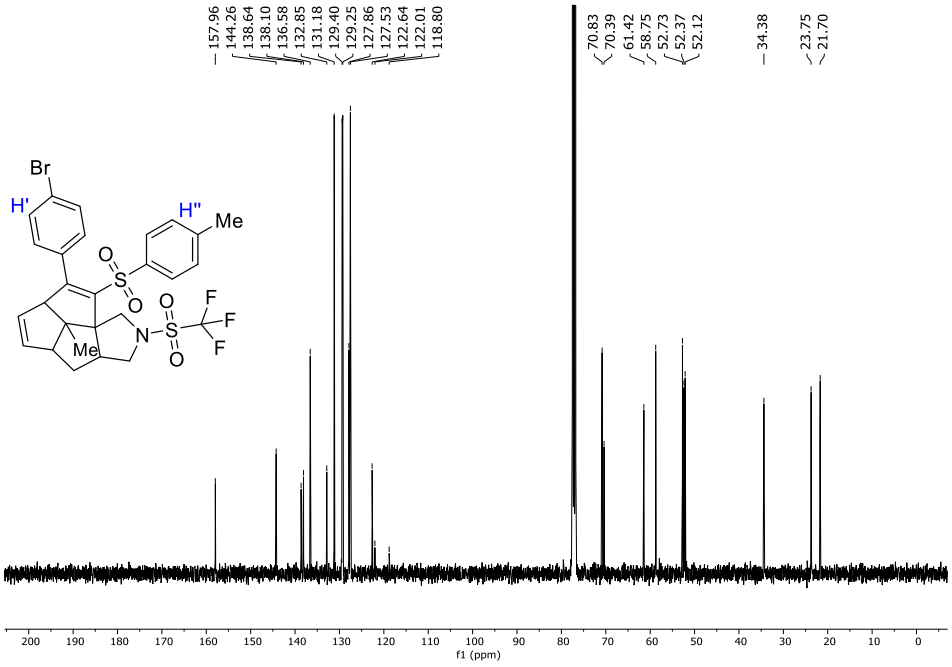

^{13}C NMR (101 MHz, $CDCl_3$) spectrum of **7f**

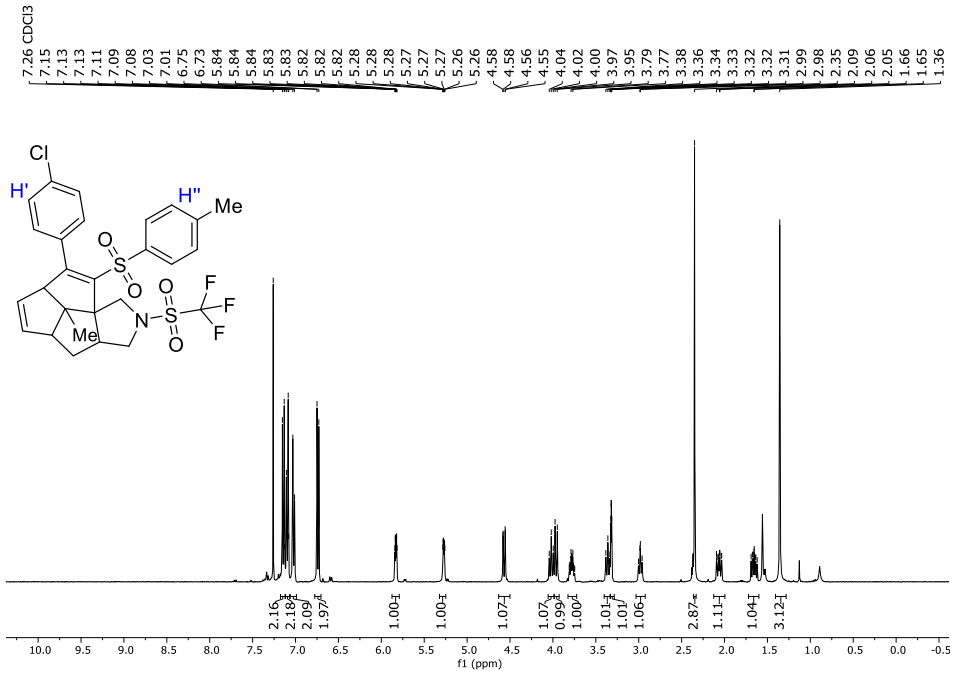

^{1}H NMR (400 MHz, $CDCl_3$) spectrum of **7g**

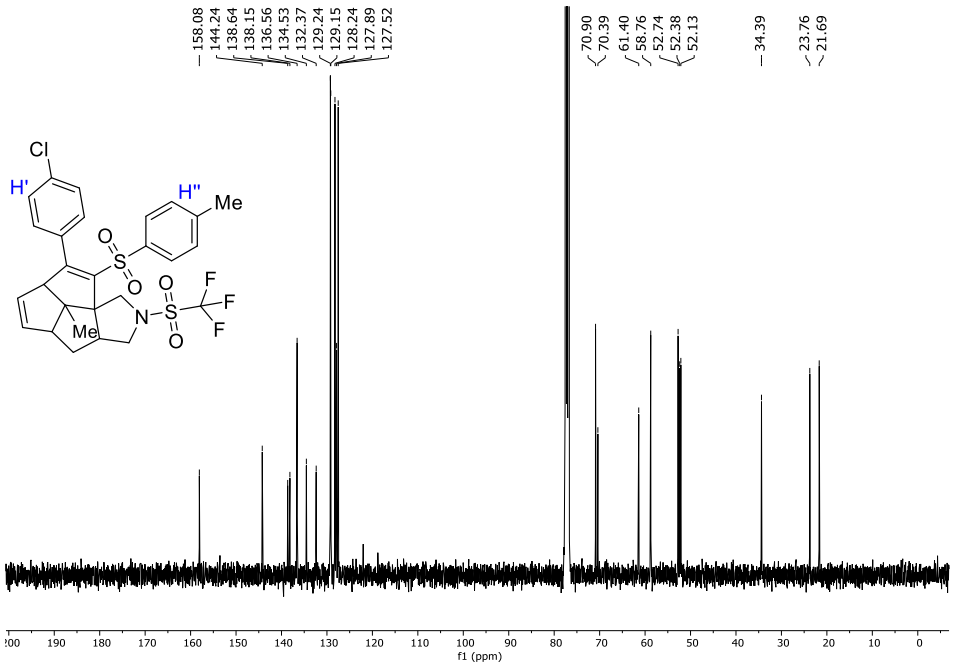

^{13}C NMR (101 MHz, $CDCl_3$) spectrum of **7g**

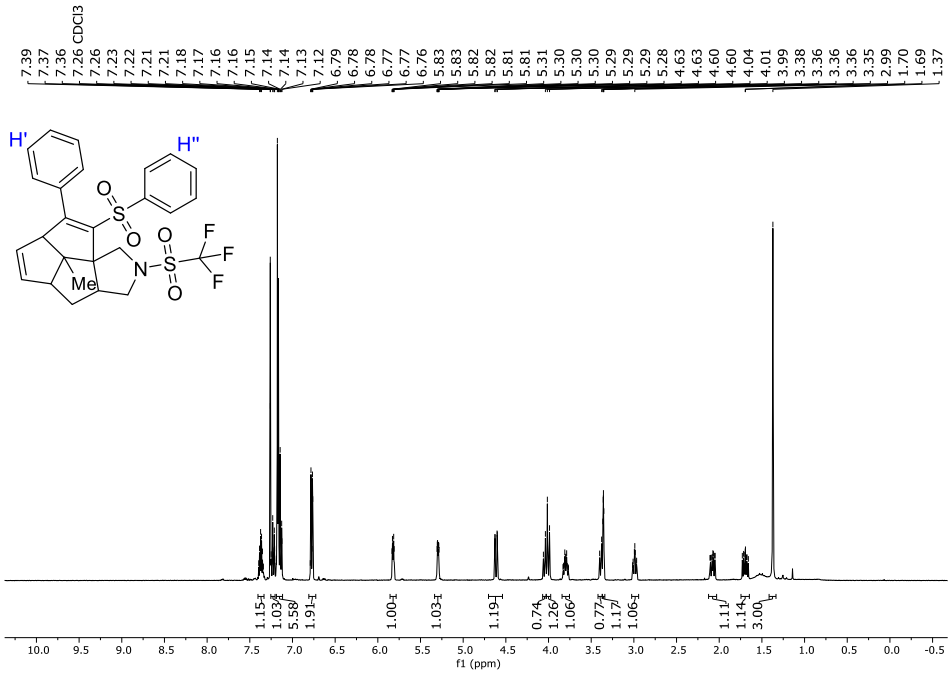

^{1}H NMR (400 MHz, $CDCl_3$) spectrum of **7h**

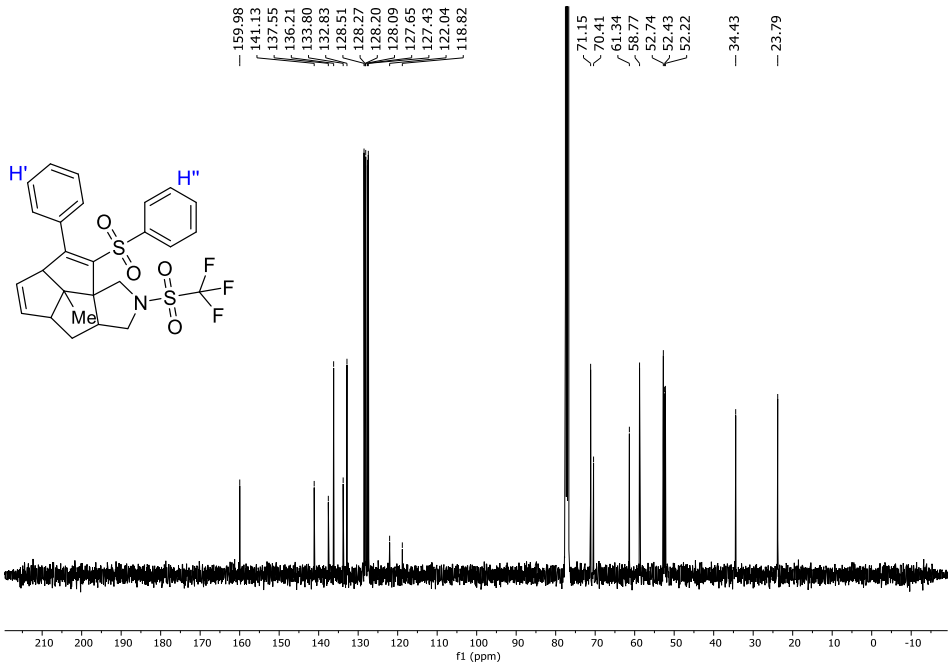

^{13}C NMR (101 MHz, $CDCl_3$) spectrum of **7h**

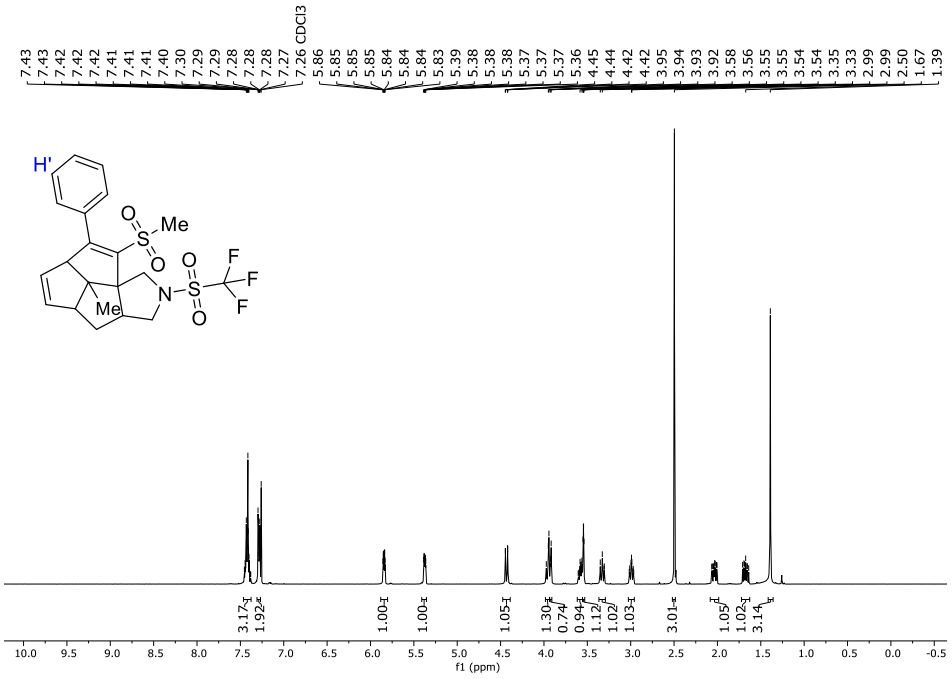

^{1}H NMR (400 MHz, $CDCl_3$) spectrum of **7i**

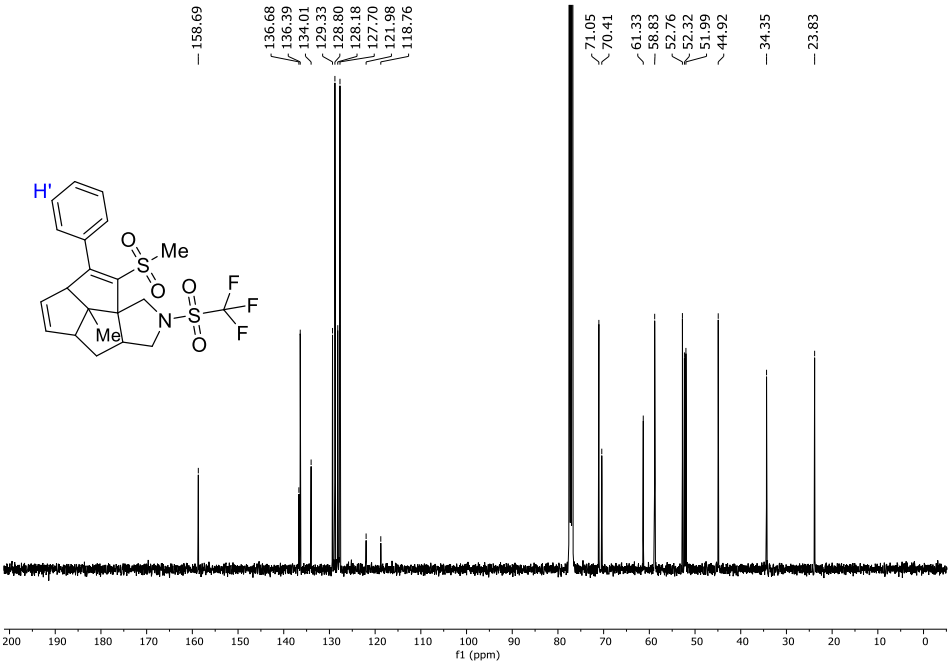

^{13}C NMR (101 MHz, $CDCl_3$) spectrum of **7i**

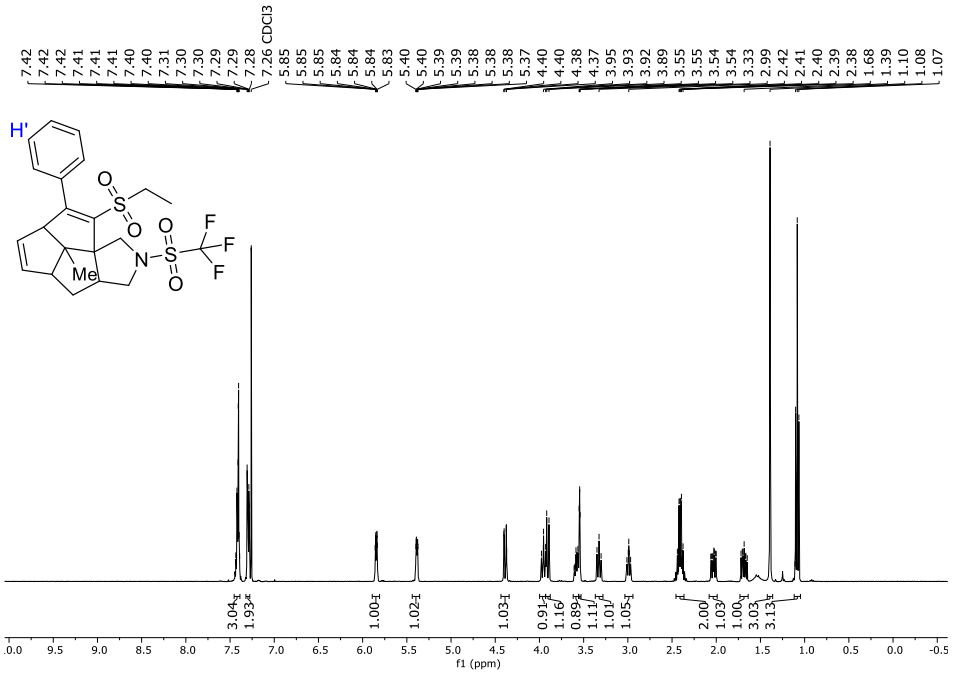

^{1}H NMR (400 MHz, $CDCl_3$) spectrum of **7j**

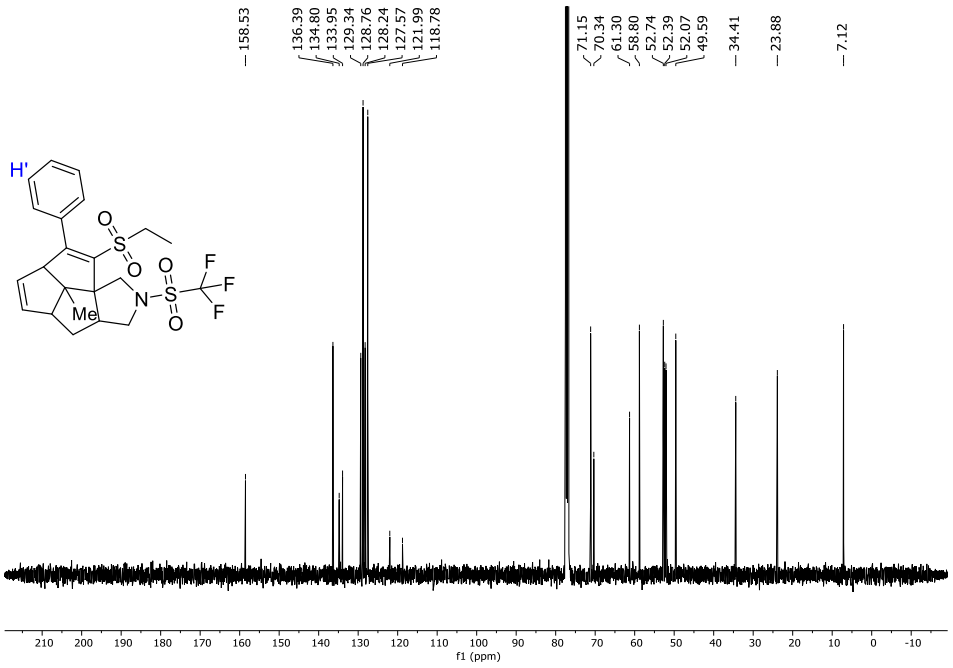

^{13}C NMR (101 MHz, $CDCl_3$) spectrum of **7j**

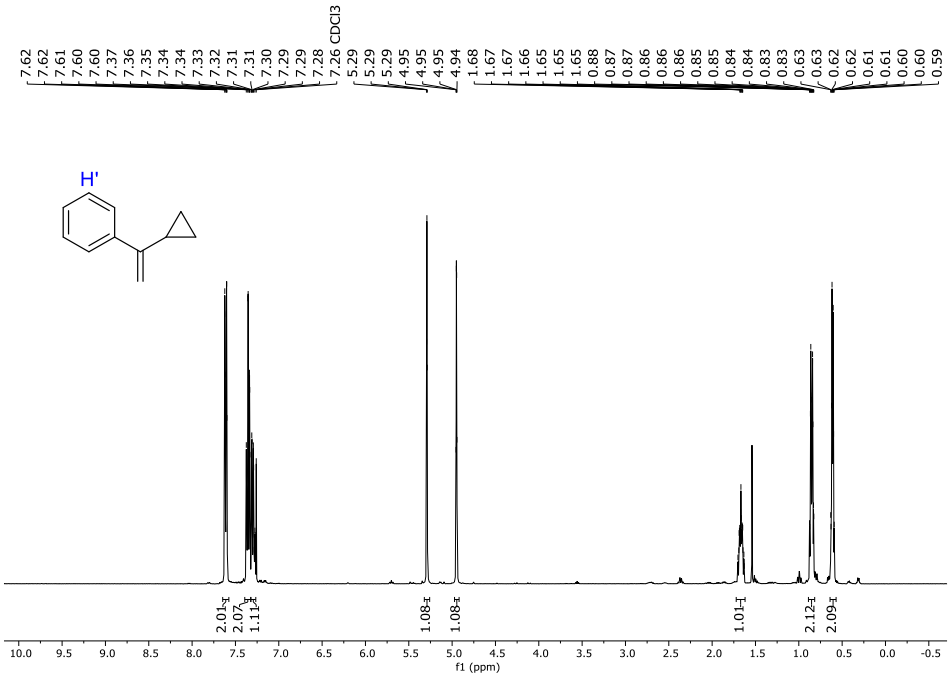

^{1}H NMR (400 MHz, $CDCl_3$) spectrum of **8**

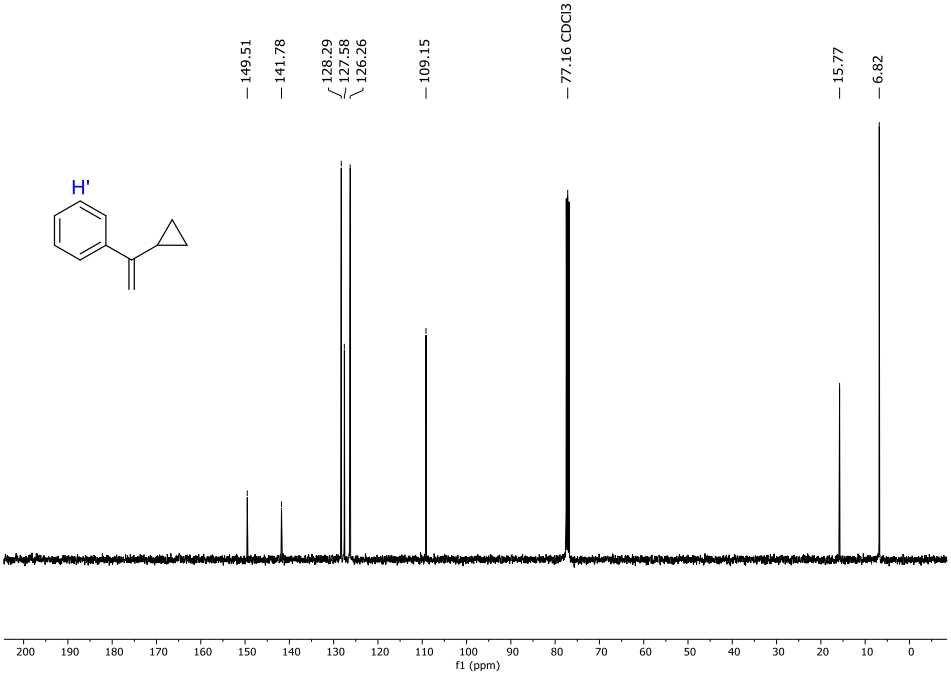

^{13}C NMR (101 MHz, $CDCl_3$) spectrum of **8**

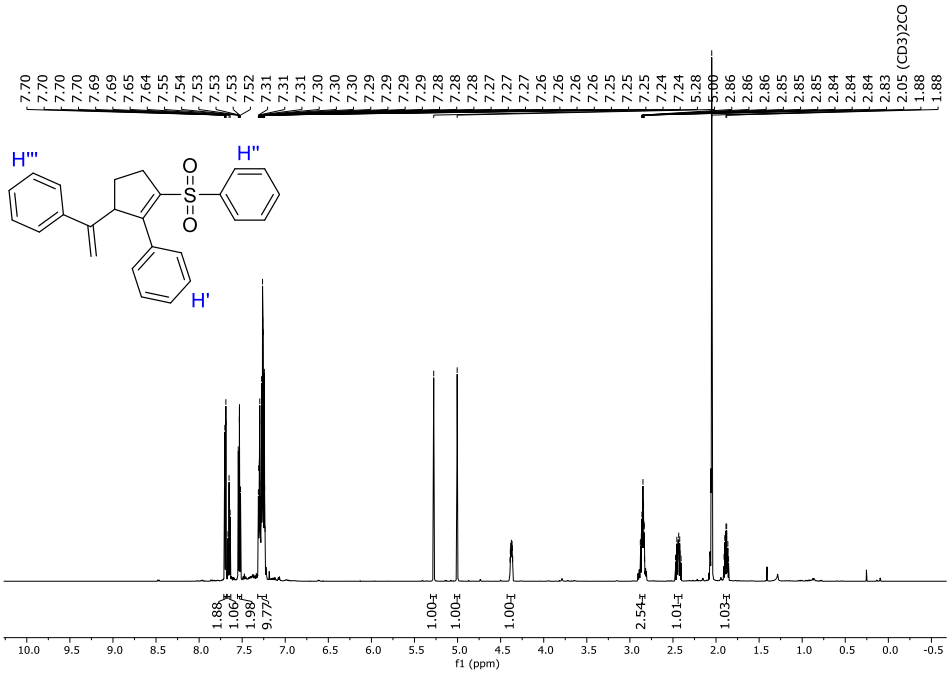

^{1}H NMR (400 MHz, acetone-d$_6$) spectrum of **9**

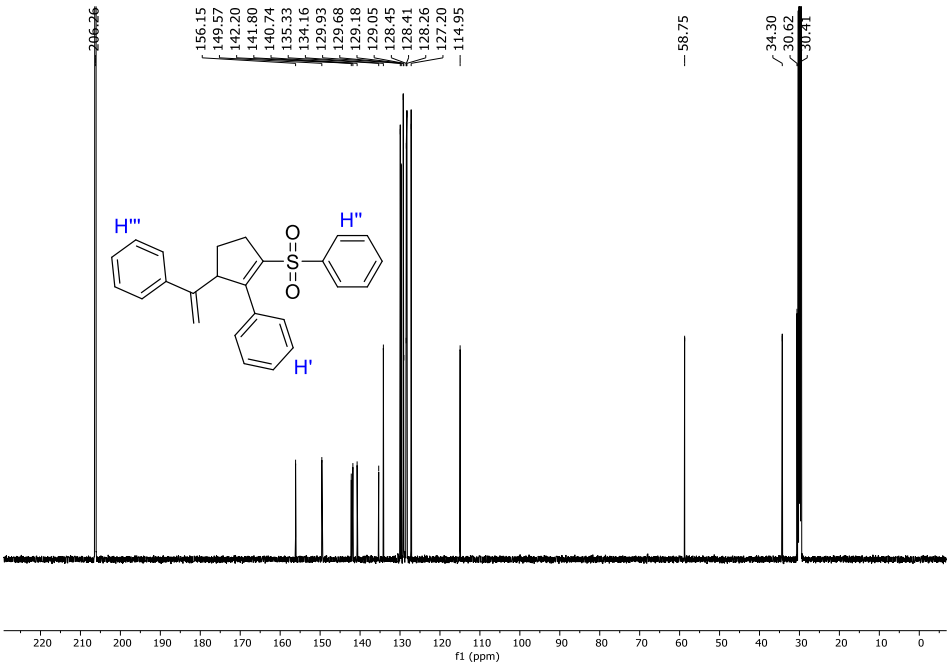

^{13}C NMR (101 MHz, acetone-d$_6$) spectrum of **8**

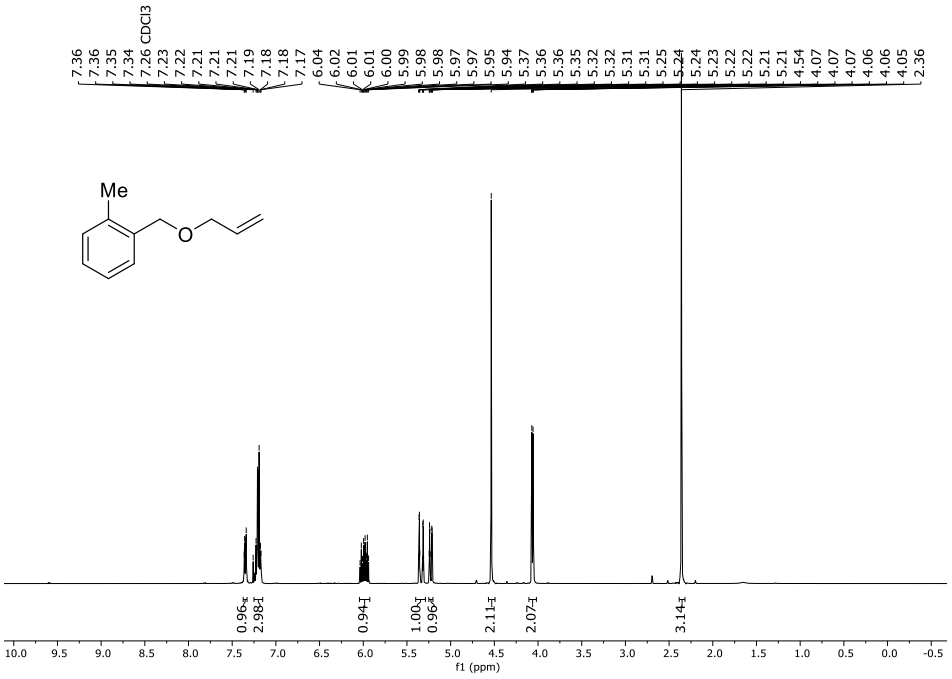

^{1}H NMR (400 MHz, $CDCl_3$) spectrum of **10**

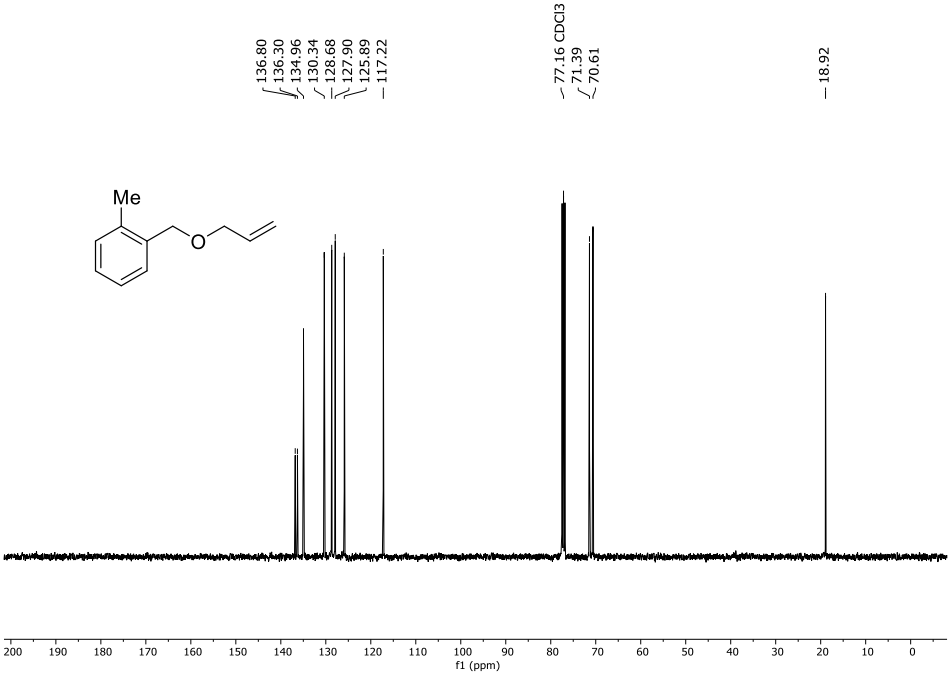

^{13}C NMR (101 MHz, $CDCl_3$) spectrum of **10**

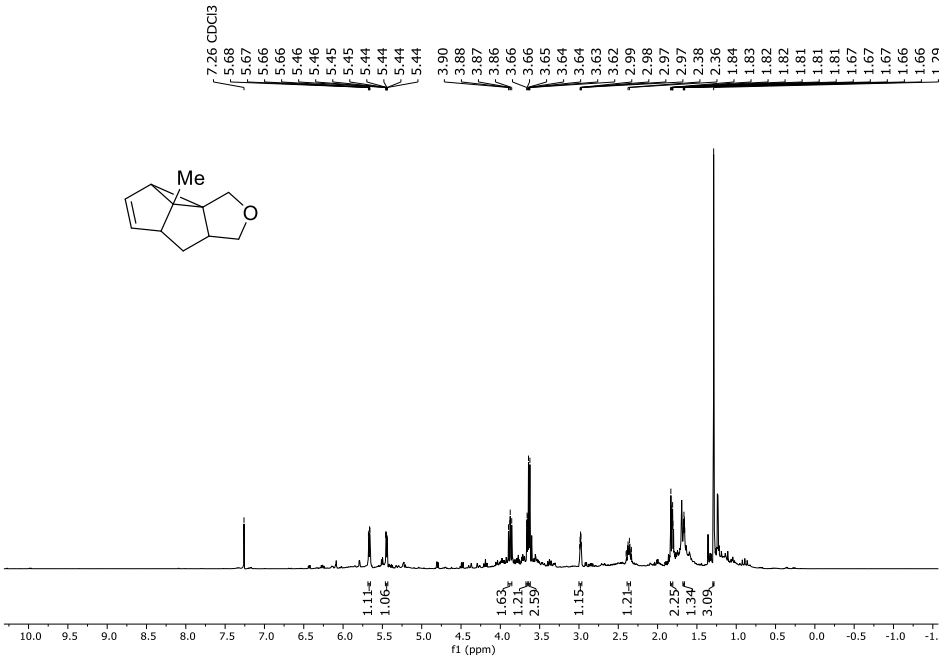

^{1}H NMR (400 MHz, $CDCl_3$) spectrum of **11** (inseparable product mixture – used without further purification for the next step)

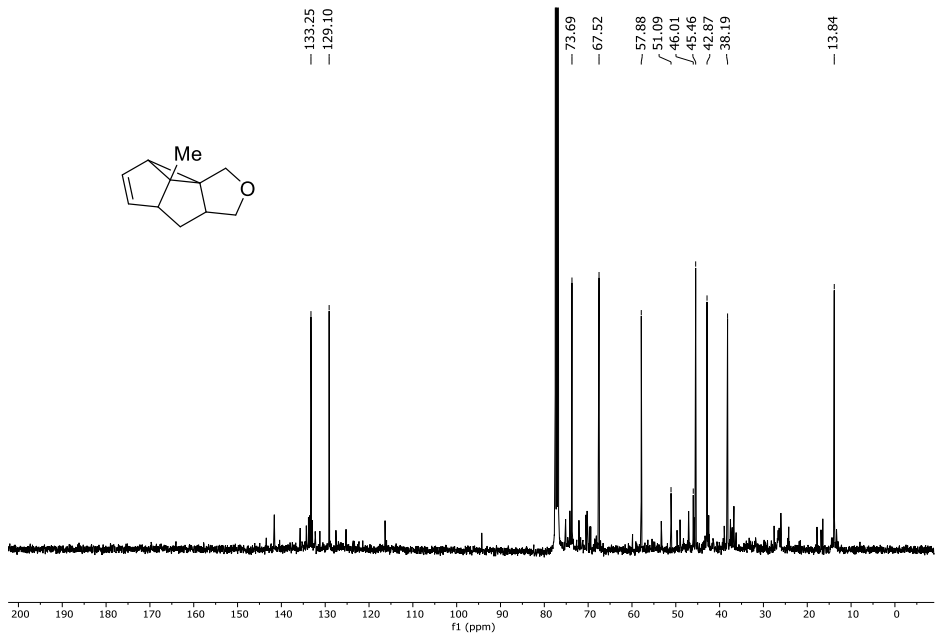

^{13}C NMR (101 MHz, $CDCl_3$) spectrum of **11** (inseparable product mixture – used without further purification for the next step)

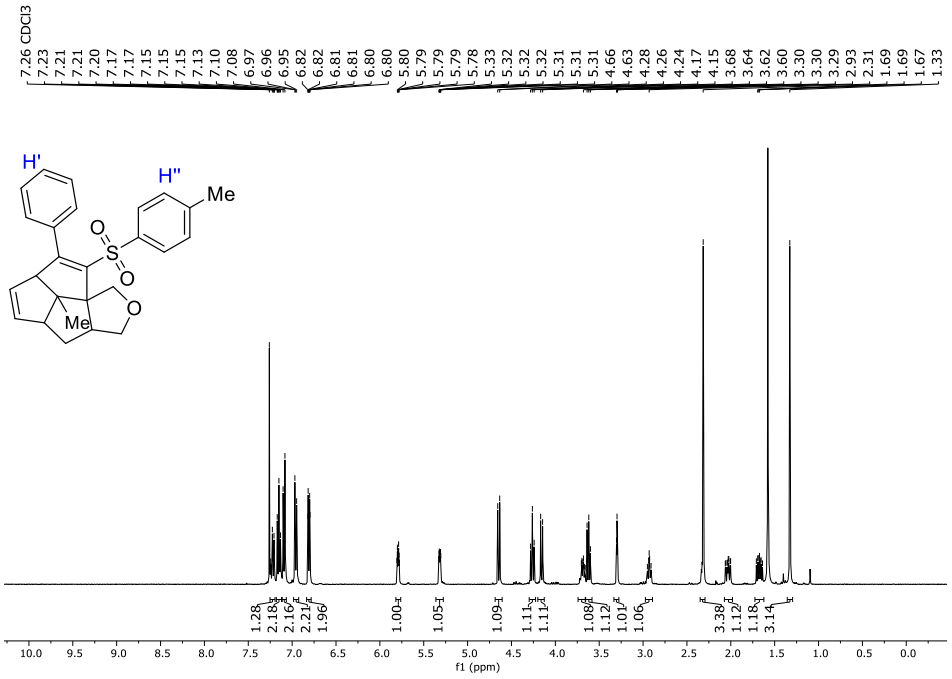

^{1}H NMR (400 MHz, $CDCl_3$) spectrum of **12**

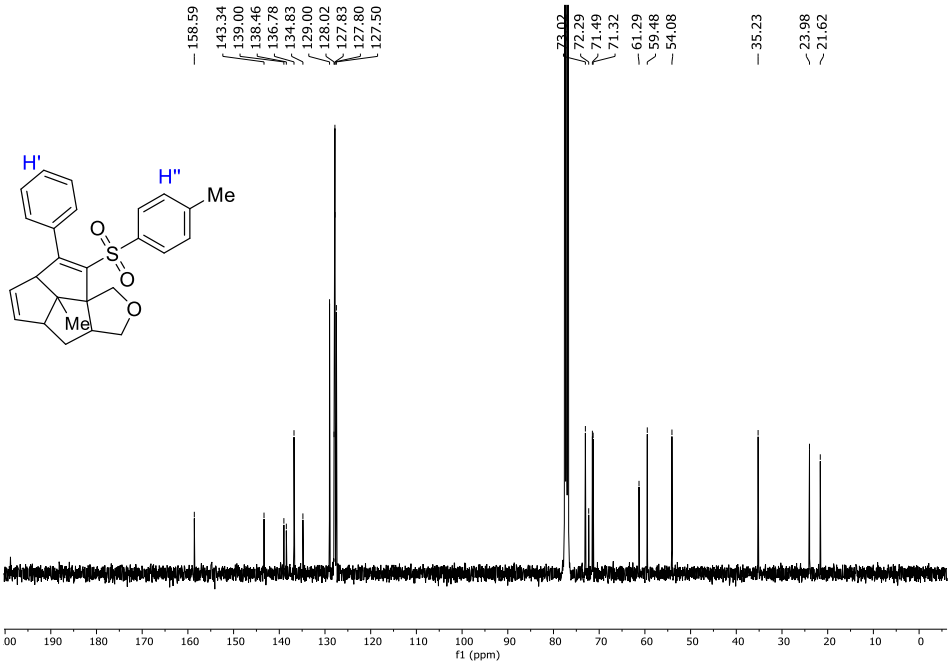

^{13}C NMR (101 MHz, $CDCl_3$) spectrum of **12**

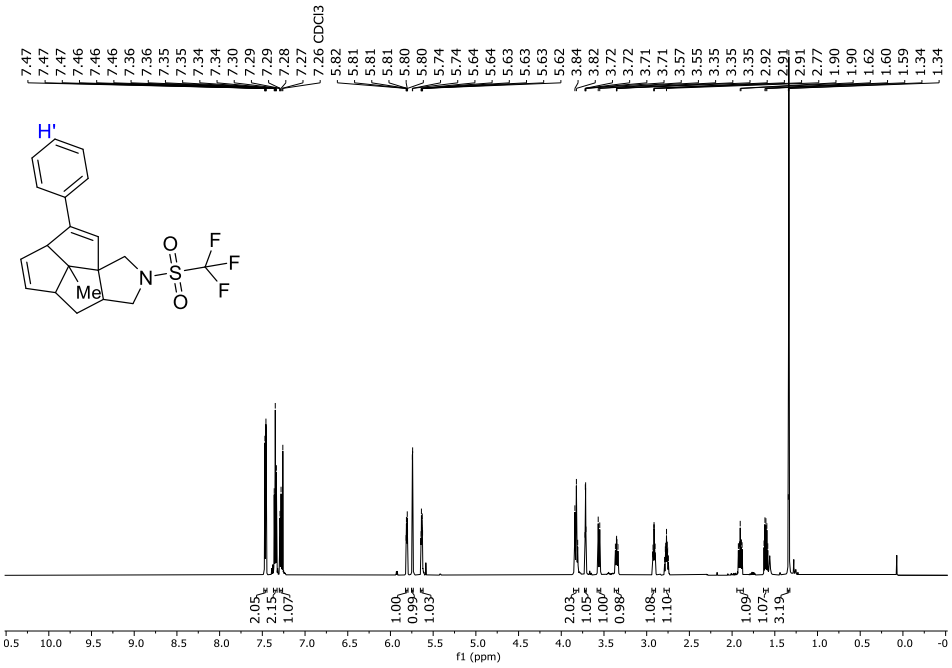

^{1}H NMR (600 MHz, $CDCl_3$) spectrum of **13**

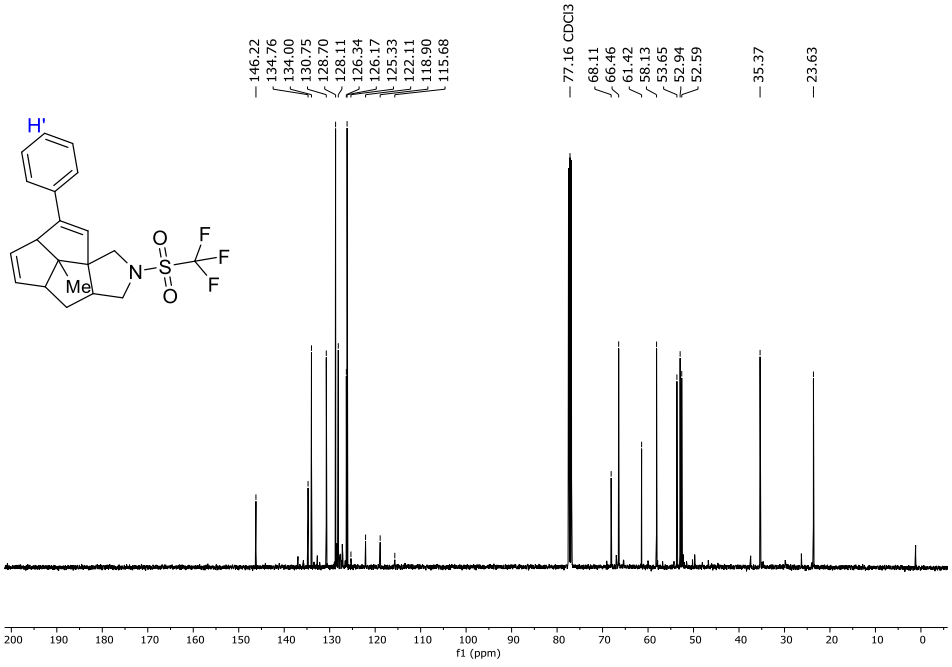

^{13}C NMR (151 MHz, $CDCl_3$) spectrum of **13**

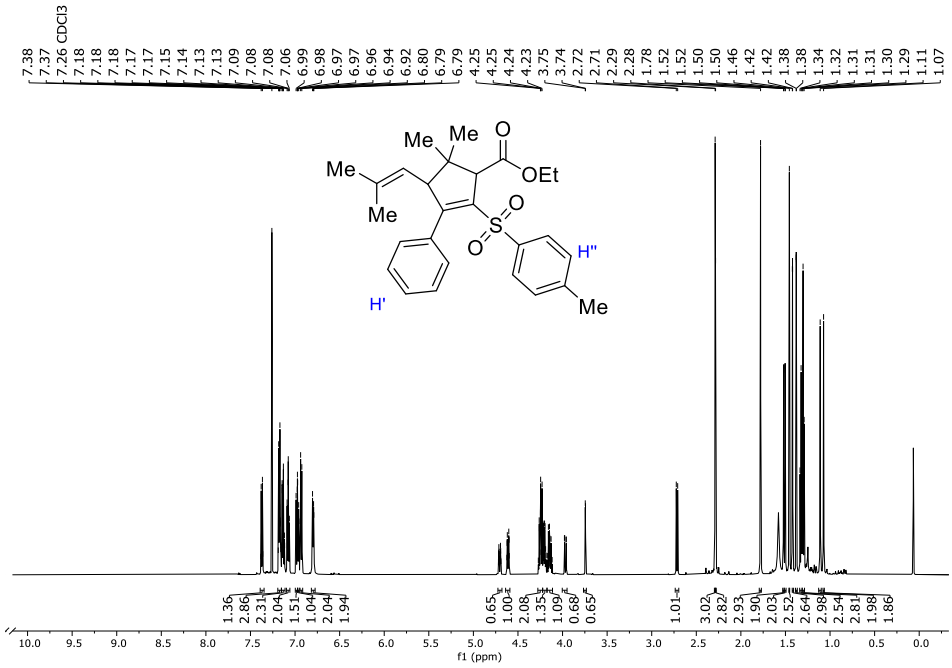

^{1}H NMR (600 MHz, $CDCl_3$) spectrum of **14**

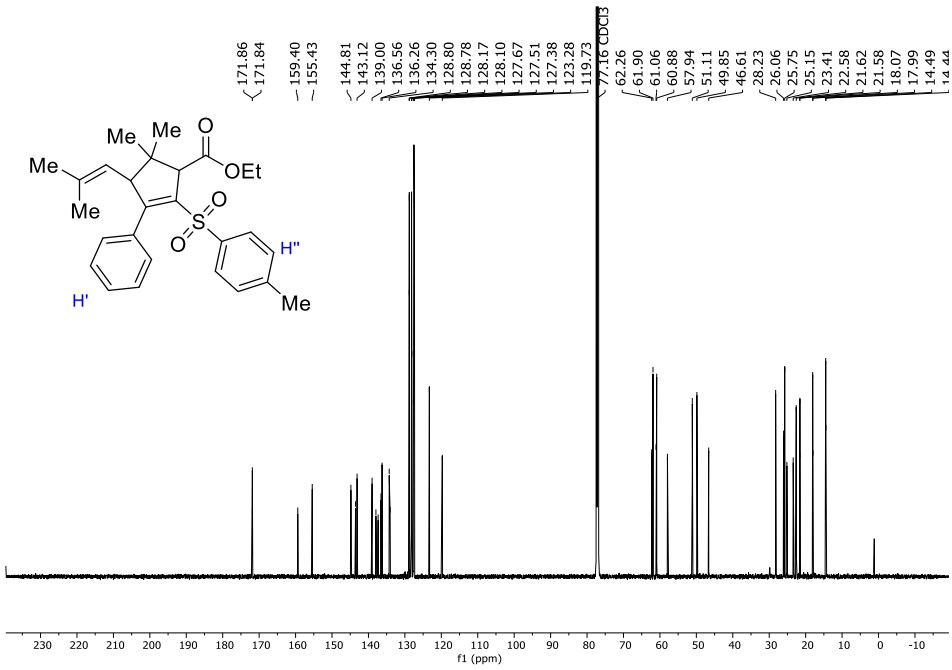

^{13}C NMR (151 MHz, $CDCl_3$) spectrum of **14**

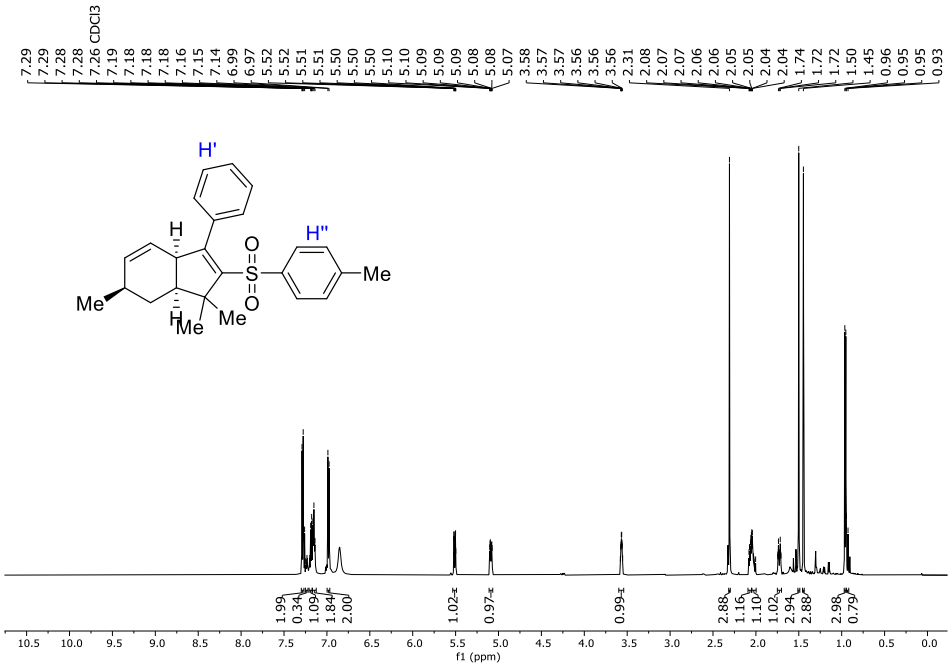

^{1}H NMR (600 MHz, $CDCl_3$) spectrum of **15**

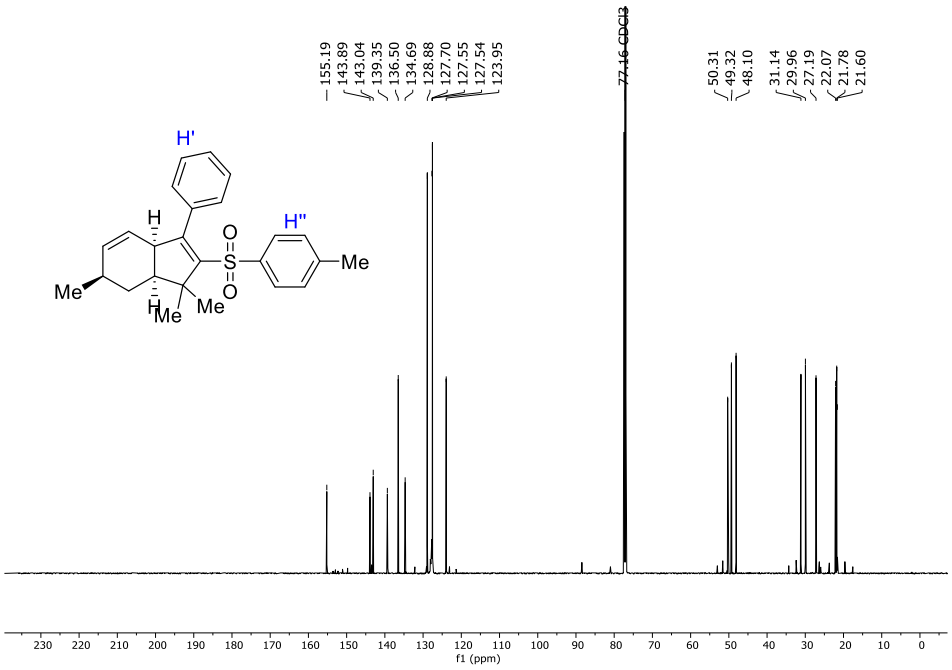

^{13}C NMR (151 MHz, $CDCl_3$) spectrum of **15**

B.1.2 Zusatzmaterial der Publikation zur Selektivitätsuntersuchung einer Diels-Alder-Reaktion eines β-Fluor-β-nitrostyrols mit Cyclopentadien

Im Folgenden ist die *supporting information* der Publikation „Diels-Alder Reaction of β-Fluoro-β-nitrostyrenes with Cyclic Dienes“ abgedruckt.[555]

BEILSTEIN JOURNAL OF ORGANIC CHEMISTRY

Supporting Information

for

Diels–Alder reaction of β-fluoro-β-nitrostyrenes with cyclic dienes

Savva A. Ponomarev, Roman V. Larkovich, Alexander S. Aldoshin, Andrey A. Tabolin, Sema L. Ioffe, Jonathan Groß, Till Opatz and Valentine G. Nenajdenko

Beilstein J. Org. Chem. **2021,** *17,* 283–292. doi:10.3762/bjoc.17.27

Copies of spectra, experimental section, and computational details of DFT calculations

Table of contents

1. NMR spectra

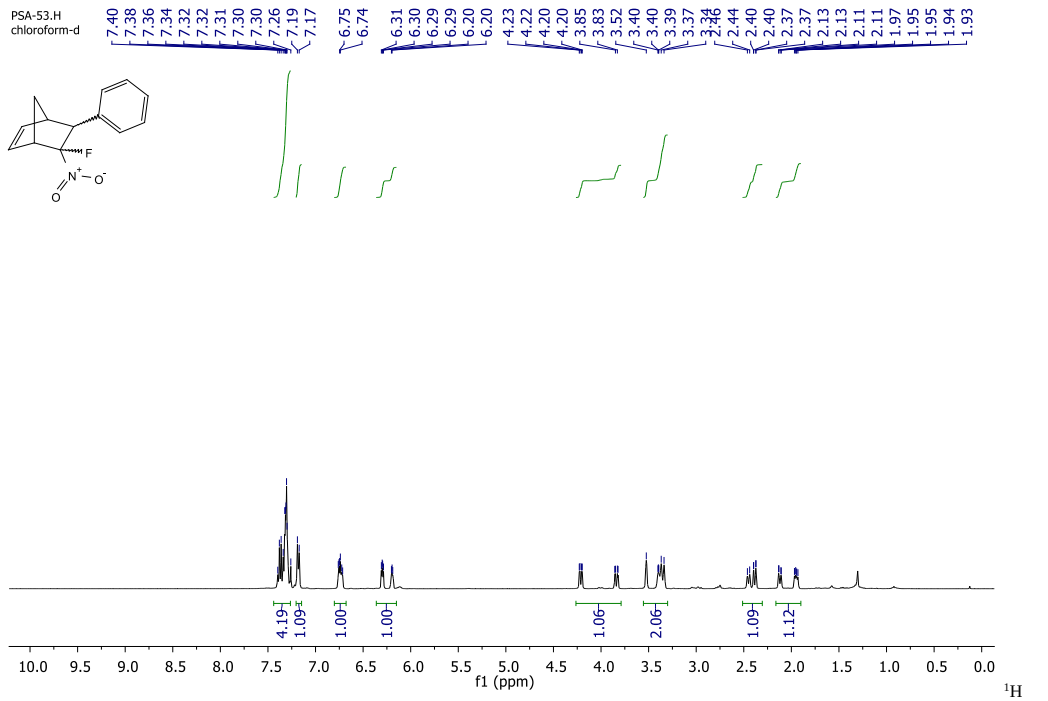

NMR spectrum of 5-fluoro-5-nitro-6-phenylbicyclo[2.2.1]hept-2-ene (**2a**)

S2

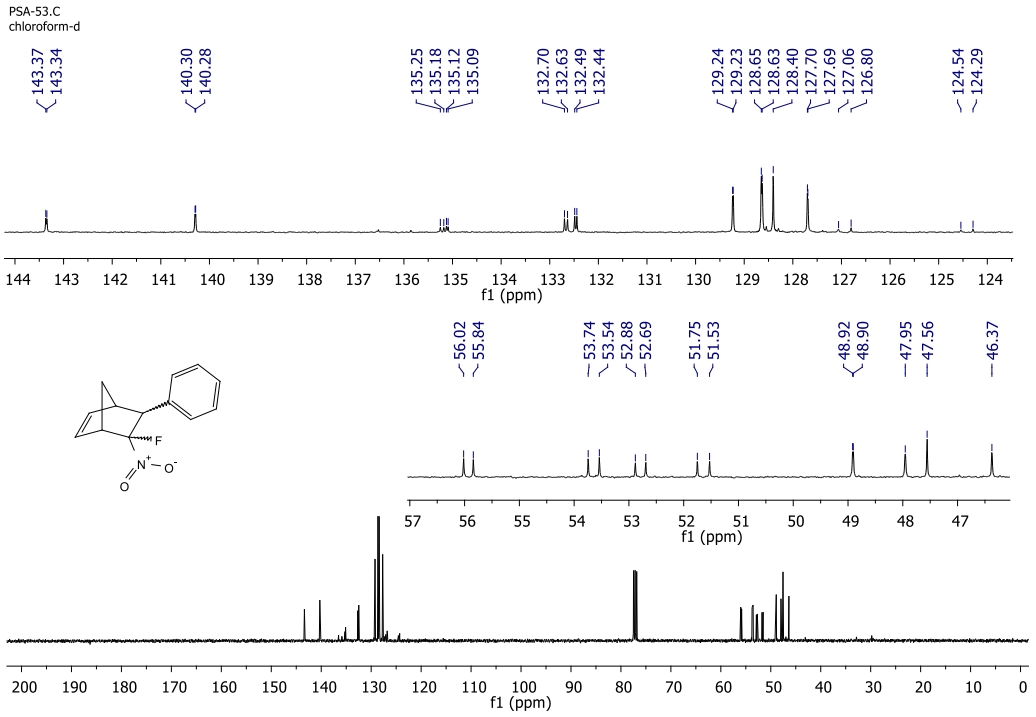

^{13}C NMR spectrum of 5-fluoro-5-nitro-6-phenylbicyclo[2.2.1]hept-2-ene (**2a**)

S3

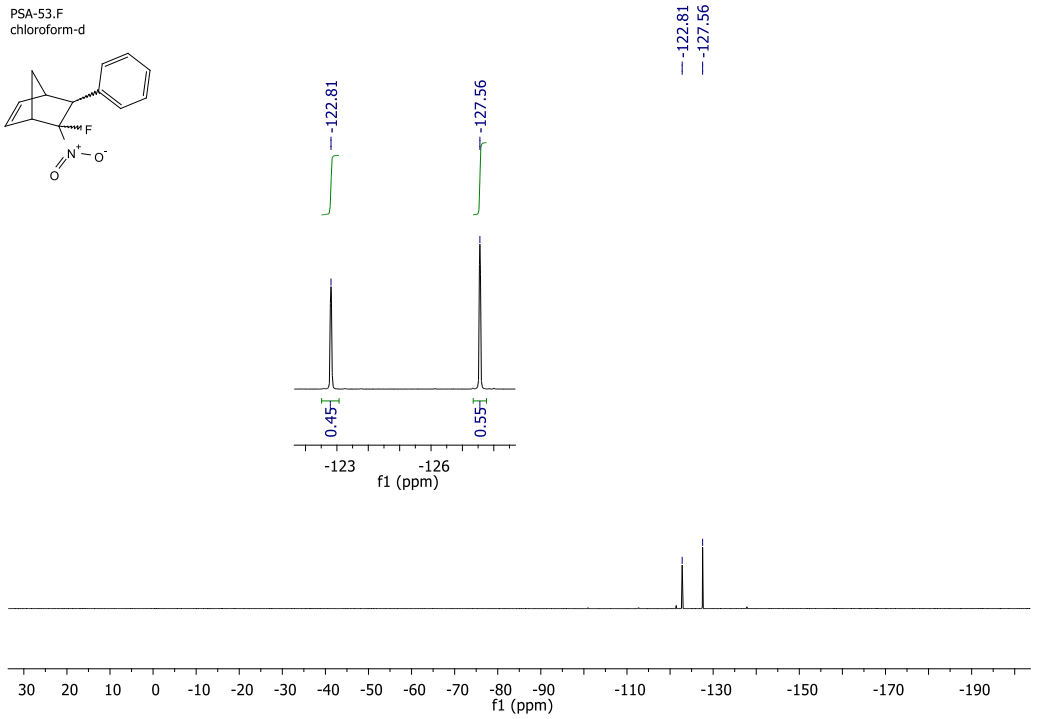

^{19}F NMR spectrum of 5-fluoro-5-nitro-6-phenylbicyclo[2.2.1]hept-2-ene (**2a**)

S4

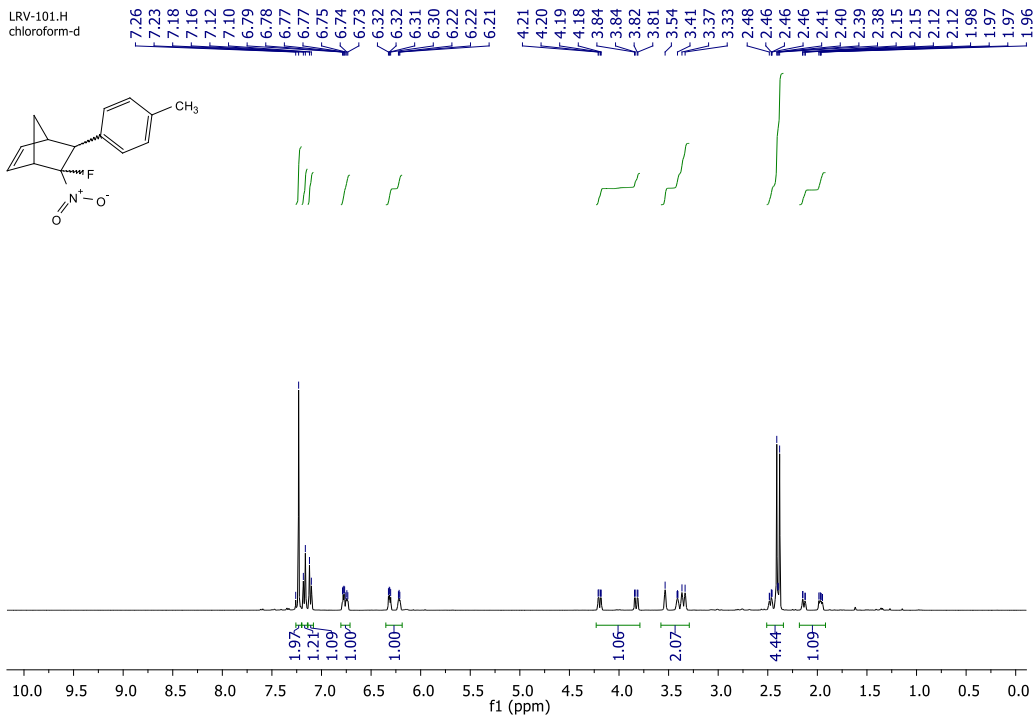

^{1}H NMR spectrum of 5-fluoro-5-nitro-6-(p-tolyl)bicyclo[2.2.1]hept-2-ene (**2b**)

S5

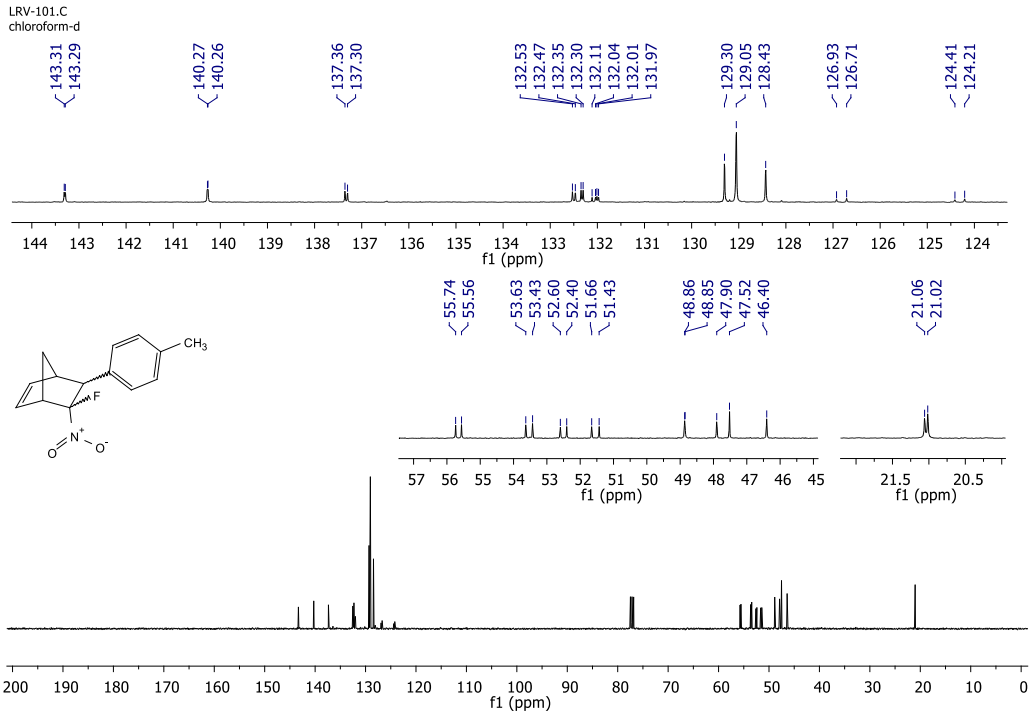

^{13}C NMR spectrum of 5-fluoro-5-nitro-6-(p-tolyl)bicyclo[2.2.1]hept-2-ene (**2b**)

S6

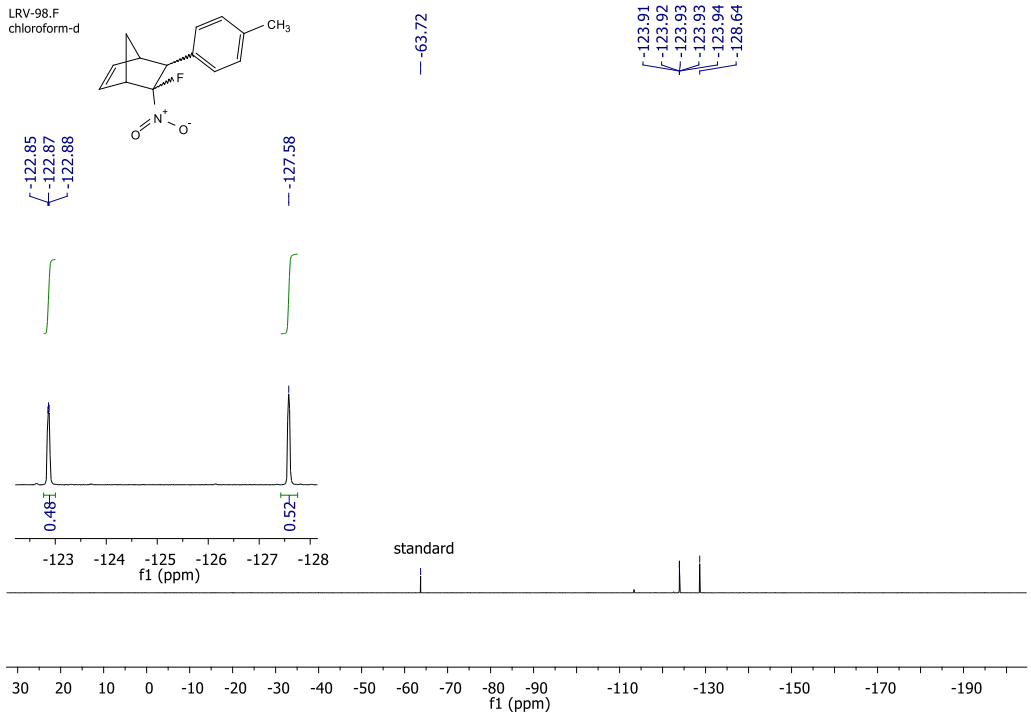

^{19}F NMR spectrum of 5-fluoro-5-nitro-6-(p-tolyl)bicyclo[2.2.1]hept-2-ene (**2b**)

S7

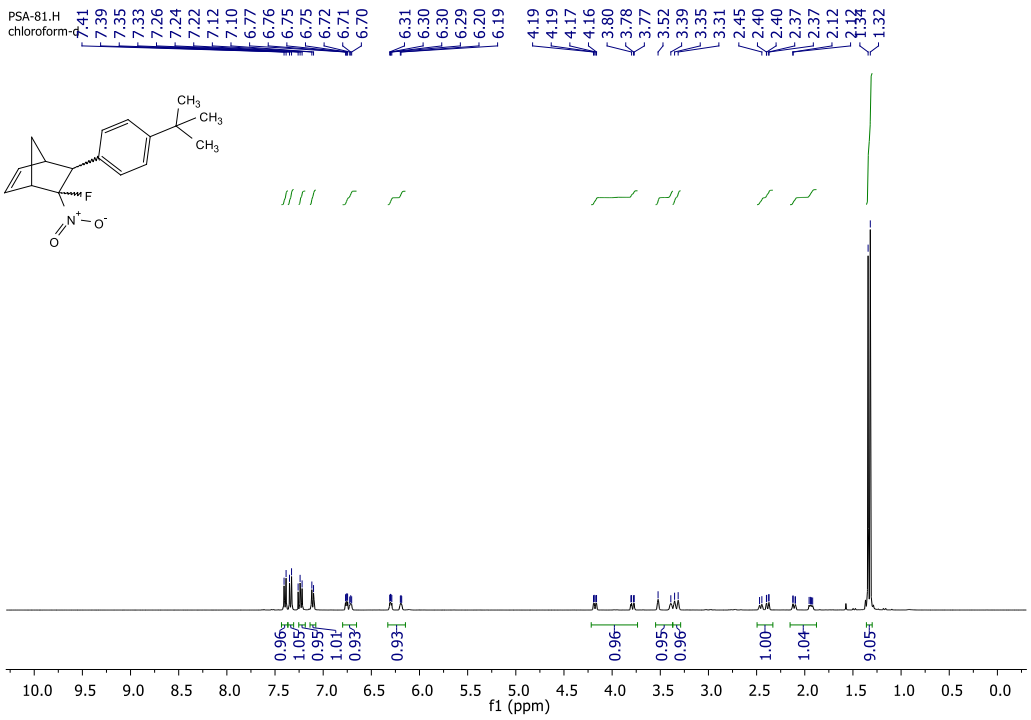

^{1}H NMR spectrum of 6-(4-(tert-butyl)phenyl)-5-fluoro-5-nitrobicyclo[2.2.1]hept-2-ene (**2c**)

S8

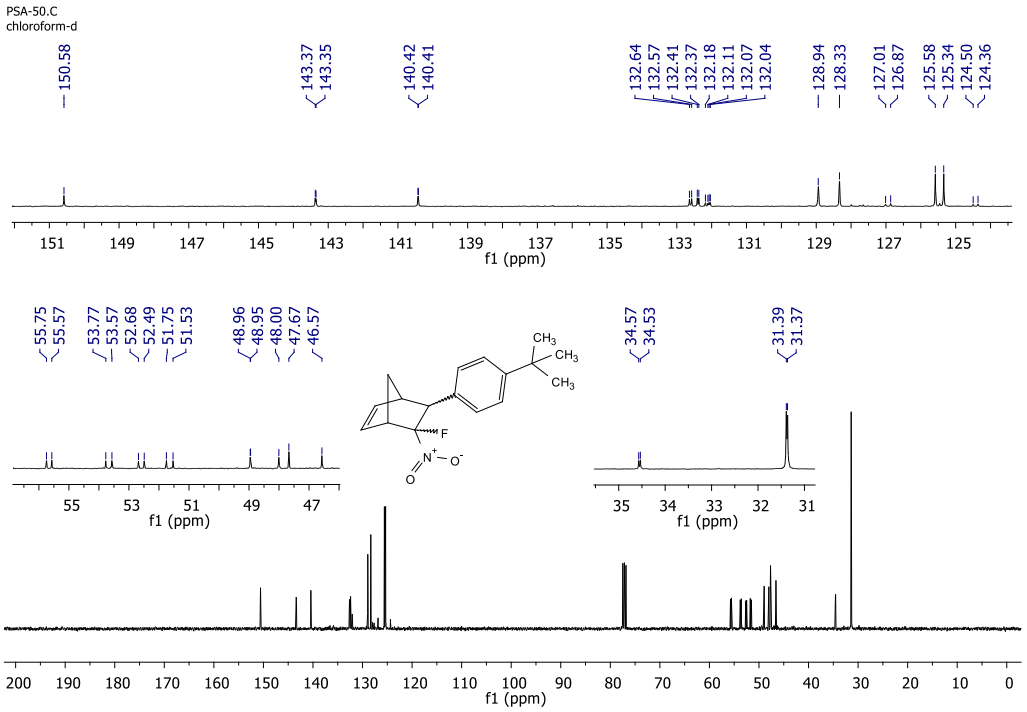

^{13}C NMR spectrum of 6-(4-(tert-butyl)phenyl)-5-fluoro-5-nitrobicyclo[2.2.1]hept-2-ene (**2c**)

S9

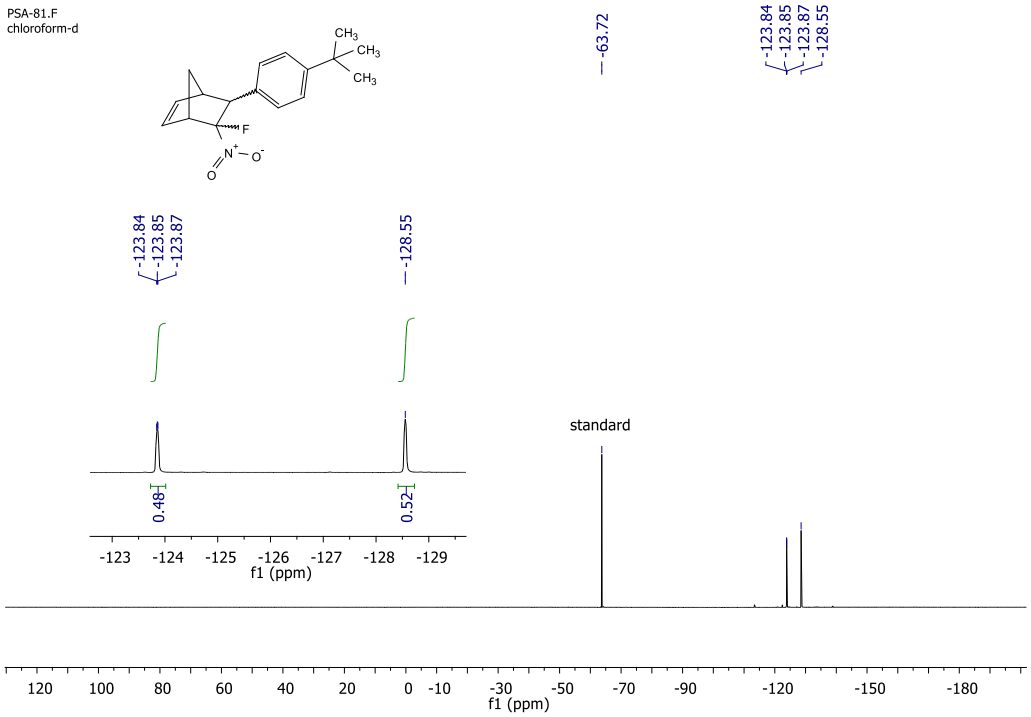

^{19}F NMR spectrum of 6-(4-(tert-butyl)phenyl)-5-fluoro-5-nitrobicyclo[2.2.1]hept-2-ene (**2c**)

S10

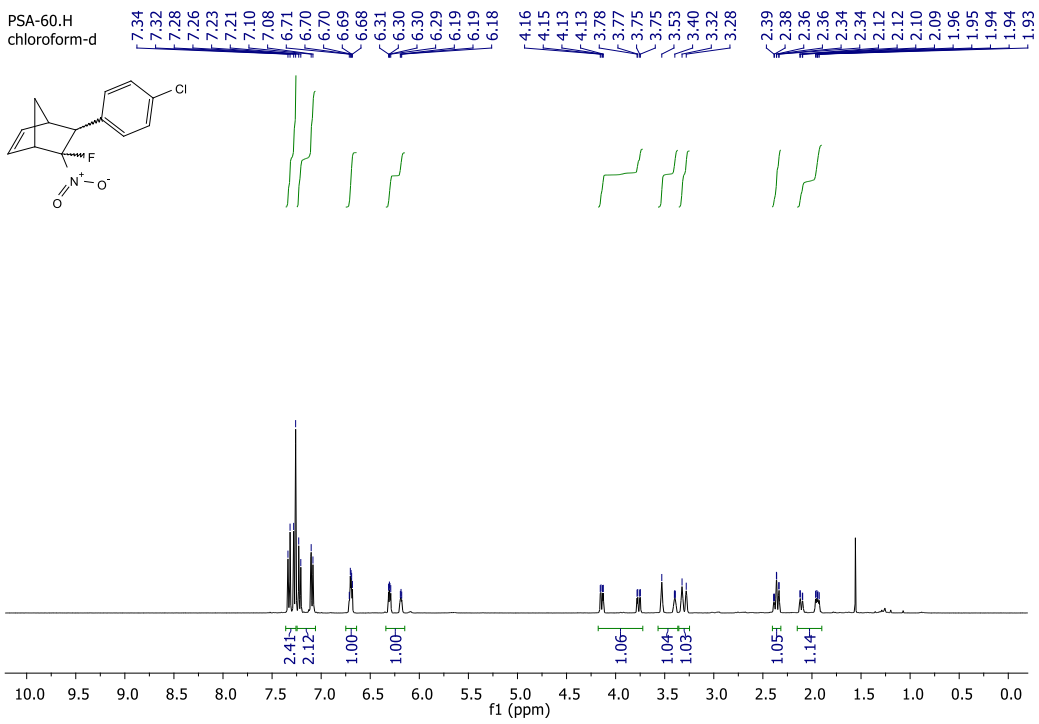

^{1}H NMR spectrum of 6-(4-chlorophenyl)-5-fluoro-5-nitrobicyclo[2.2.1]hept-2-ene (**2d**)

S11

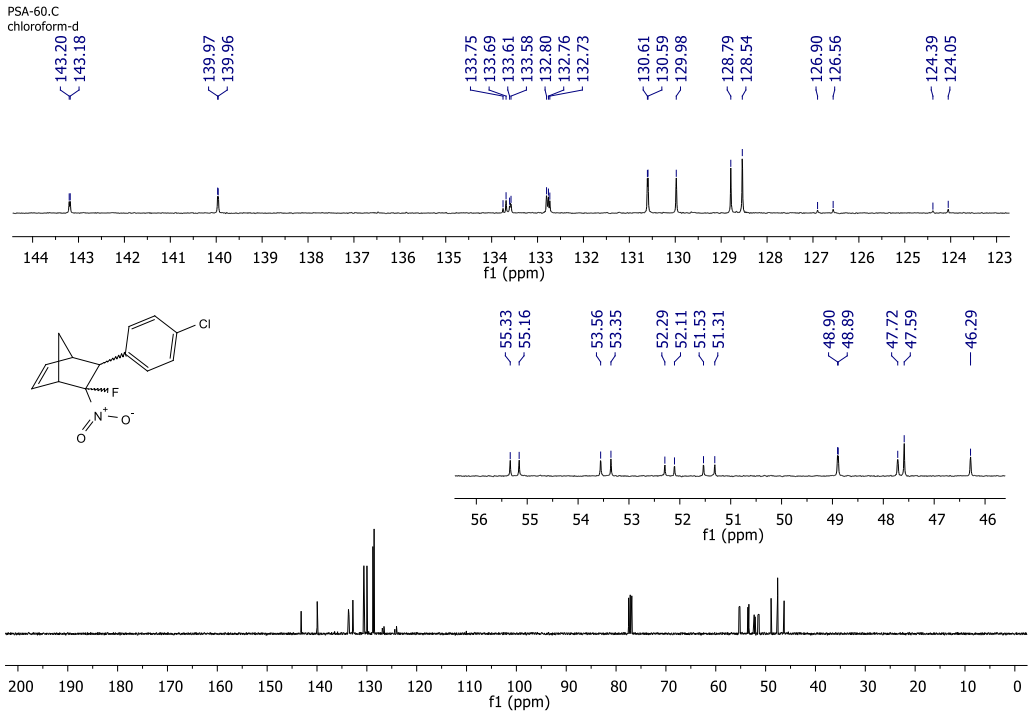

^{13}C NMR spectrum of 6-(4-chlorophenyl)-5-fluoro-5-nitrobicyclo[2.2.1]hept-2-ene (**2d**)

S12

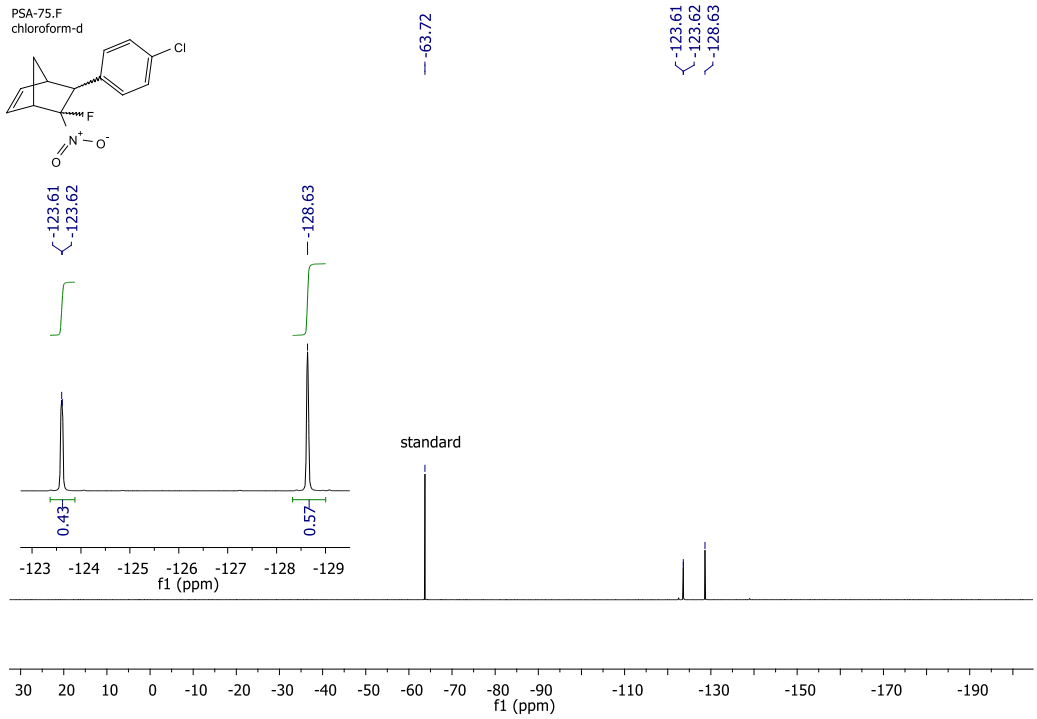

^{19}F NMR spectrum of 6-(4-chlorophenyl)-5-fluoro-5-nitrobicyclo[2.2.1]hept-2-ene (**2d**)

S13

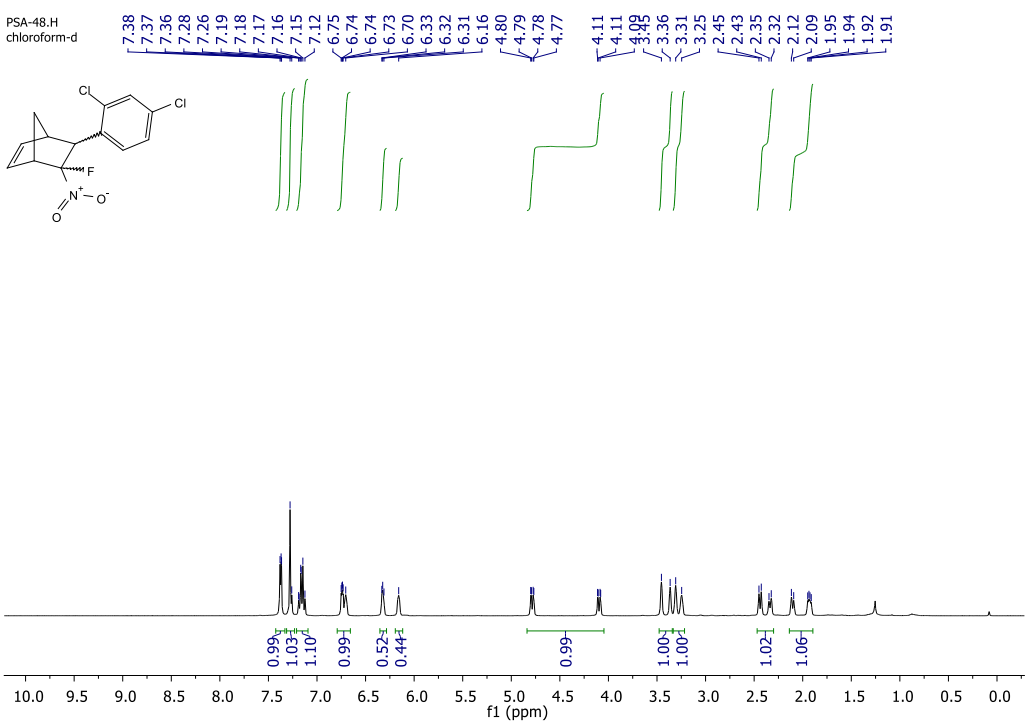

^{1}H NMR spectrum of 6-(2,4-dichlorophenyl)-5-fluoro-5-nitrobicyclo[2.2.1]hept-2-ene (**2e**)

S14

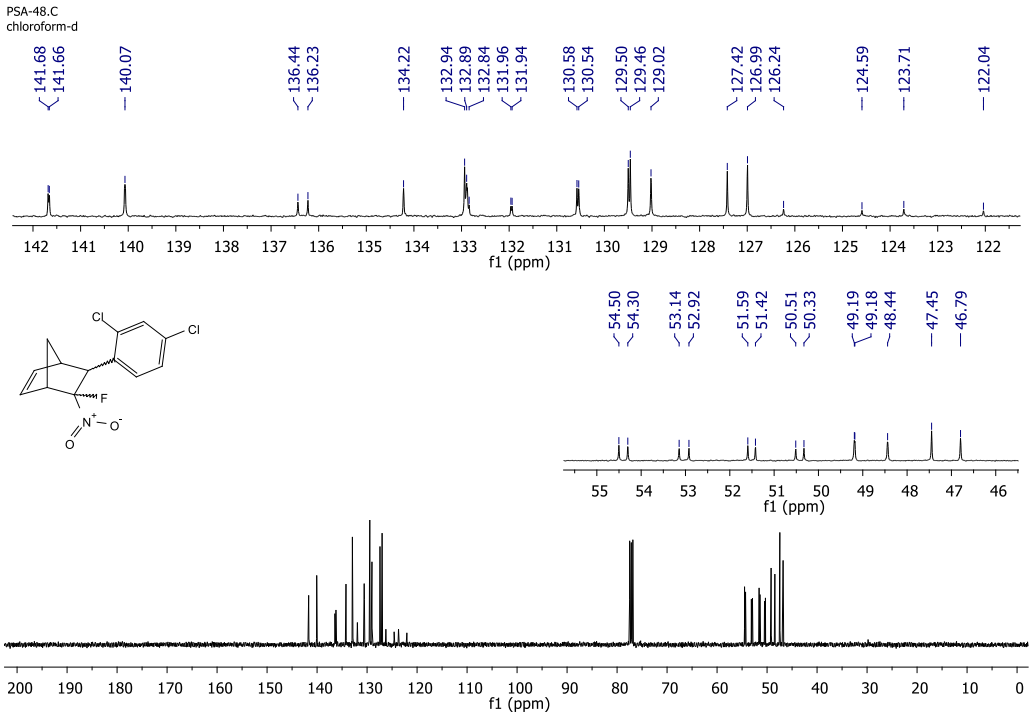

^{13}C NMR spectrum of 6-(2,4-dichlorophenyl)-5-fluoro-5-nitrobicyclo[2.2.1]hept-2-ene (**2e**)

S15

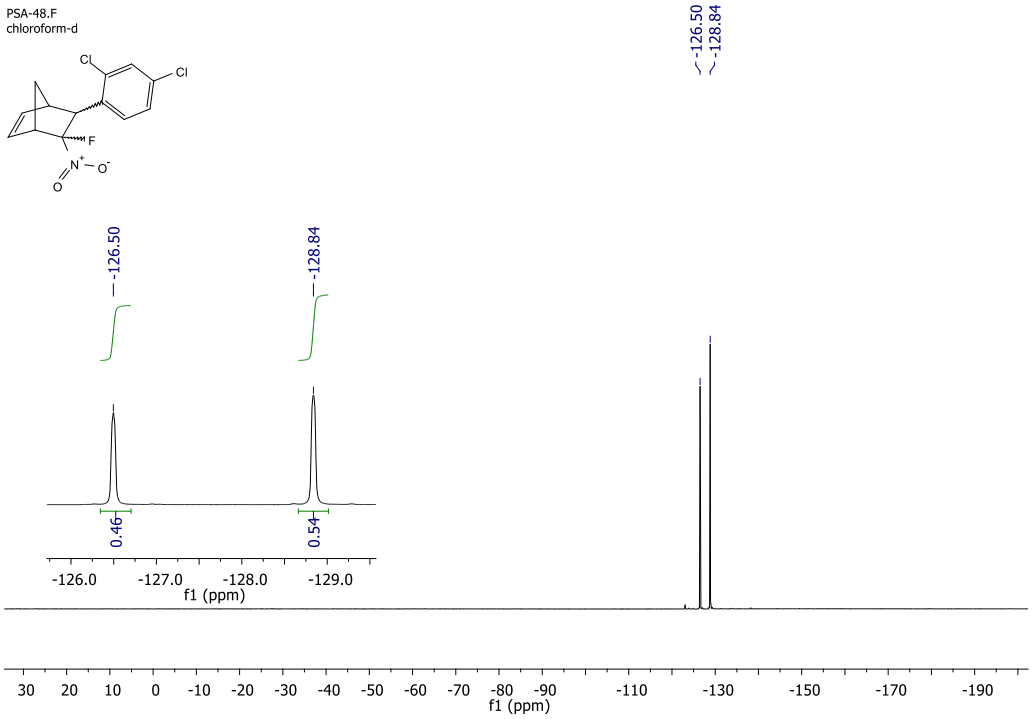

^{19}F NMR spectrum of 6-(2,4-dichlorophenyl)-5-fluoro-5-nitrobicyclo[2.2.1]hept-2-ene (**2e**)

S16

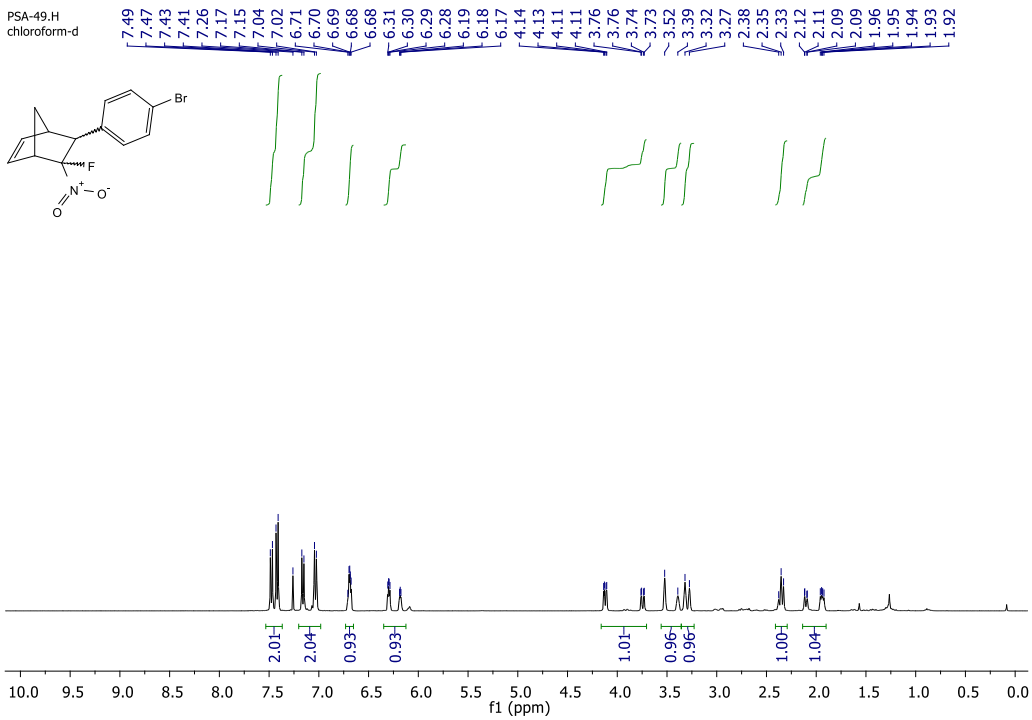

^{1}H NMR spectrum of 6-(4-bromophenyl)-5-fluoro-5-nitrobicyclo[2.2.1]hept-2-ene (**2f**)

S17

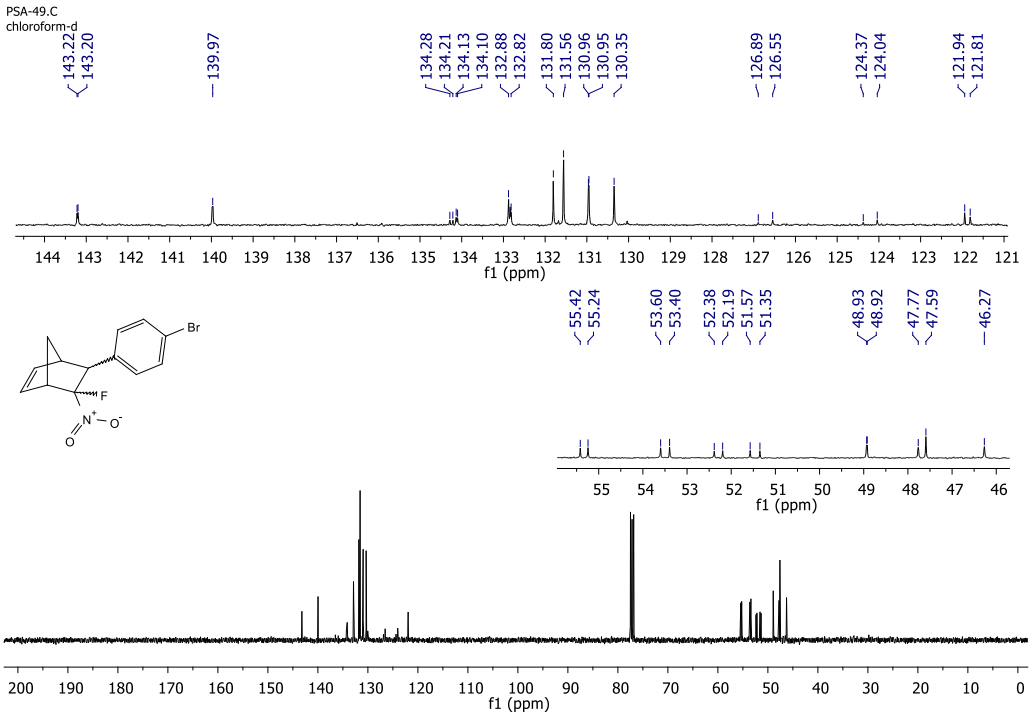

^{13}C NMR spectrum of 6-(4-bromophenyl)-5-fluoro-5-nitrobicyclo[2.2.1]hept-2-ene (**2f**)

S18

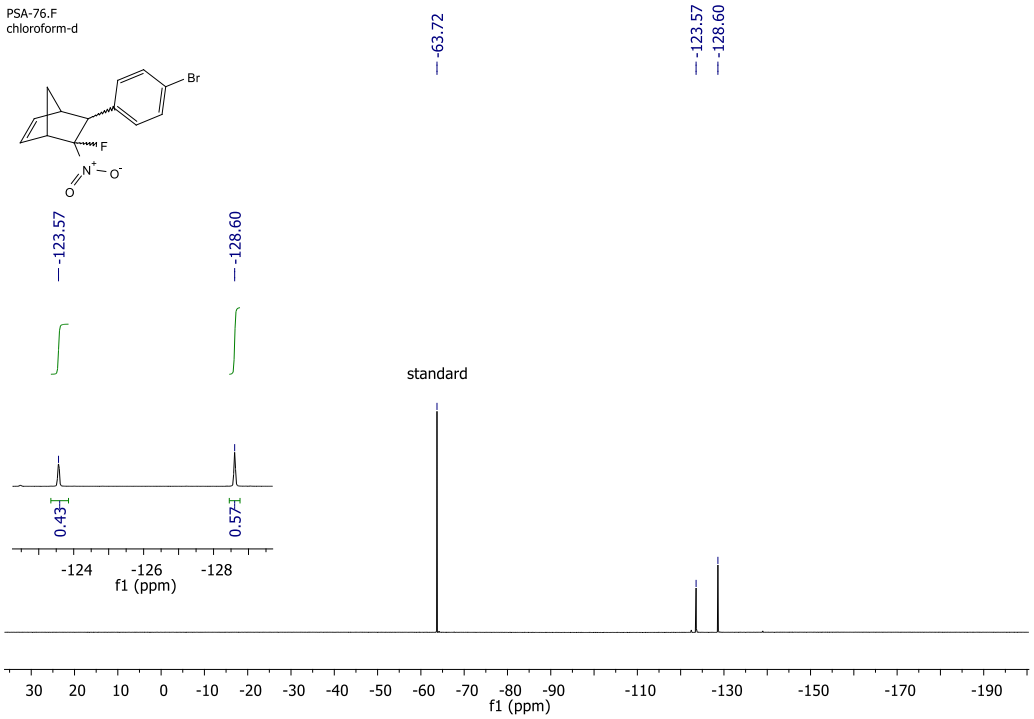

^{19}F NMR spectrum of 6-(4-bromophenyl)-5-fluoro-5-nitrobicyclo[2.2.1]hept-2-ene (**2f**)

S19

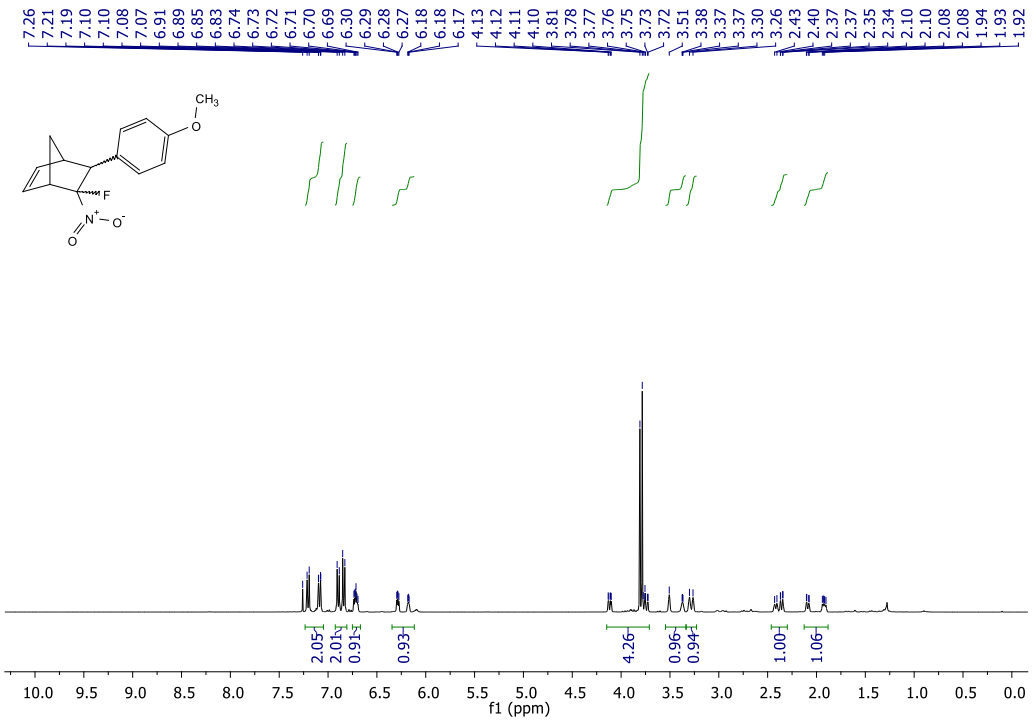

^{1}H NMR spectrum of 5-fluoro-6-(4-methoxyphenyl)-5-nitrobicyclo[2.2.1]hept-2-ene (**2g**)

S20

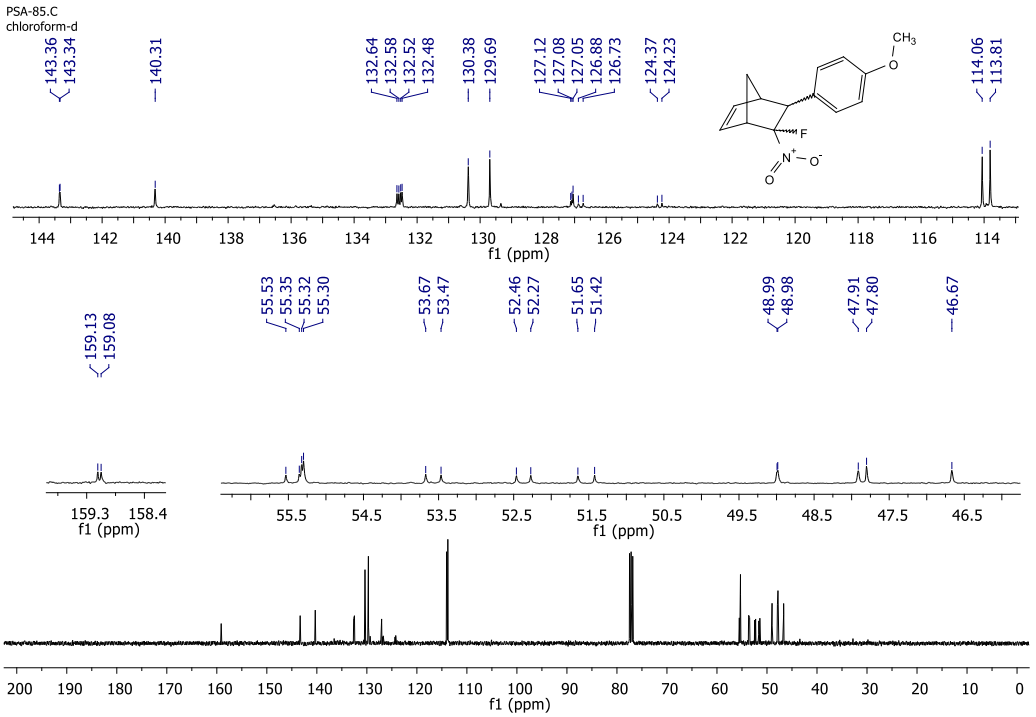

^{13}C NMR spectrum of 5-fluoro-6-(4-methoxyphenyl)-5-nitrobicyclo[2.2.1]hept-2-ene (**2g**)

S21

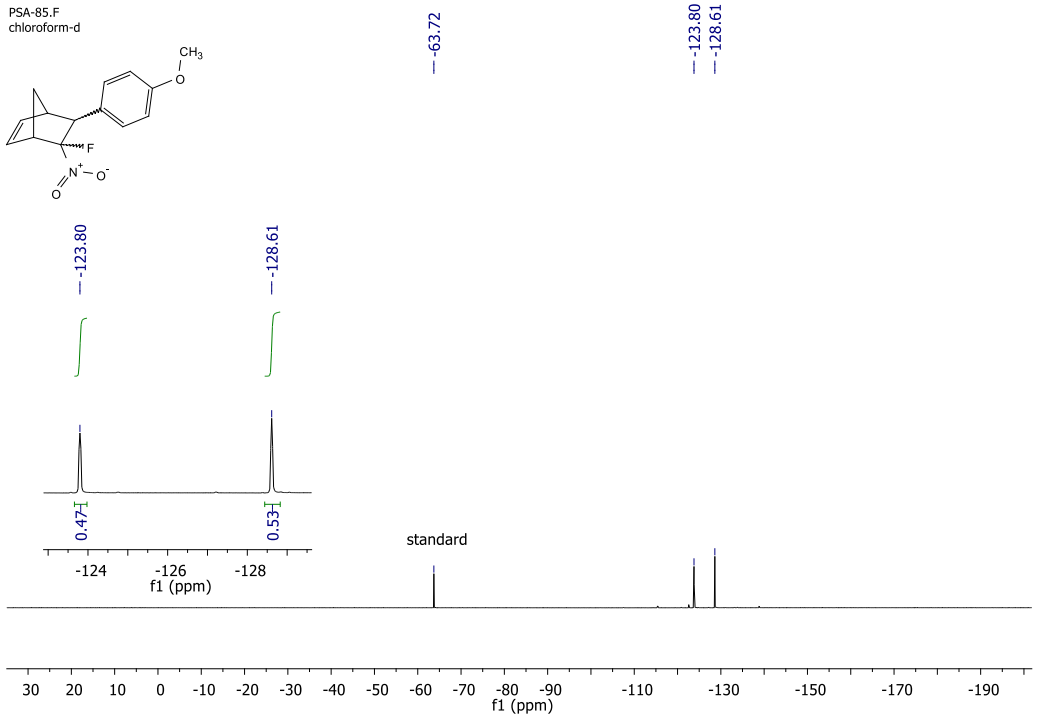

^{19}F NMR spectrum of 5-fluoro-6-(4-methoxyphenyl)-5-nitrobicyclo[2.2.1]hept-2-ene (**2g**)

S22

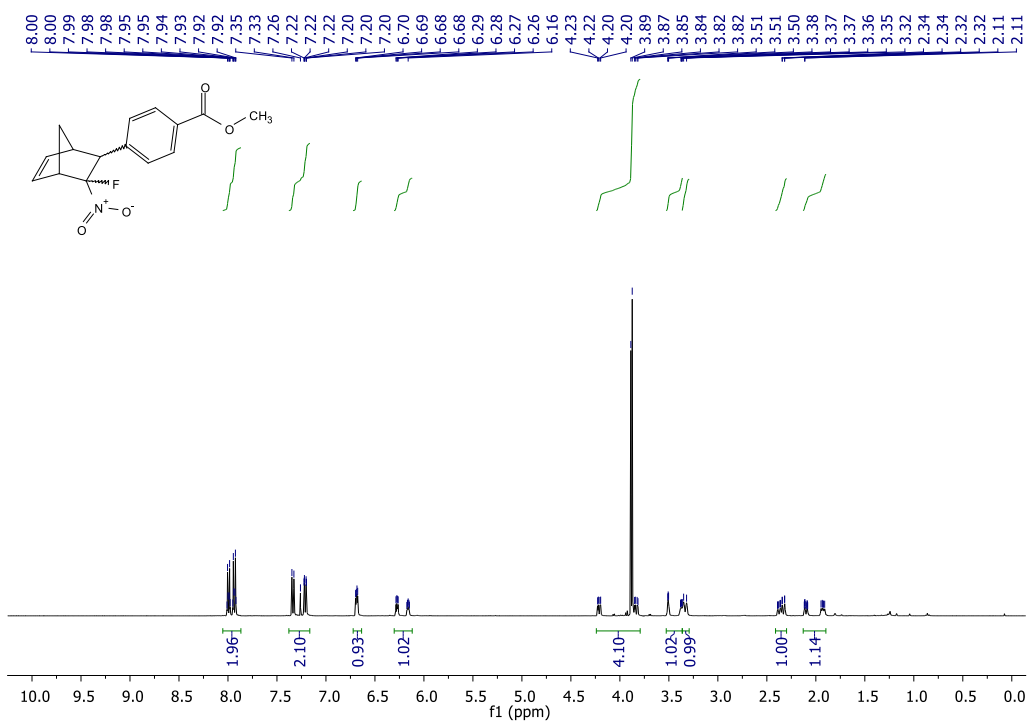

^{1}H NMR spectrum of methyl 4-(3-fluoro-3-nitrobicyclo[2.2.1]hept-5-en-2-yl)benzoate (**2h**)

S23

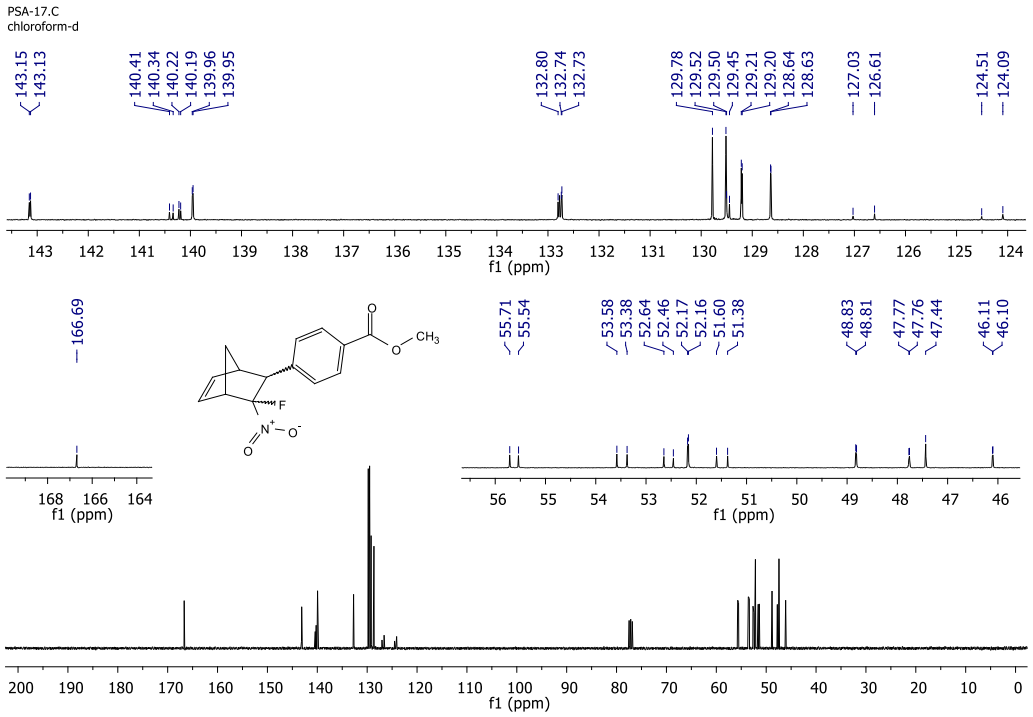

^{13}C NMR spectrum of methyl 4-(3-fluoro-3-nitrobicyclo[2.2.1]hept-5-en-2-yl)benzoate (**2h**)

S24

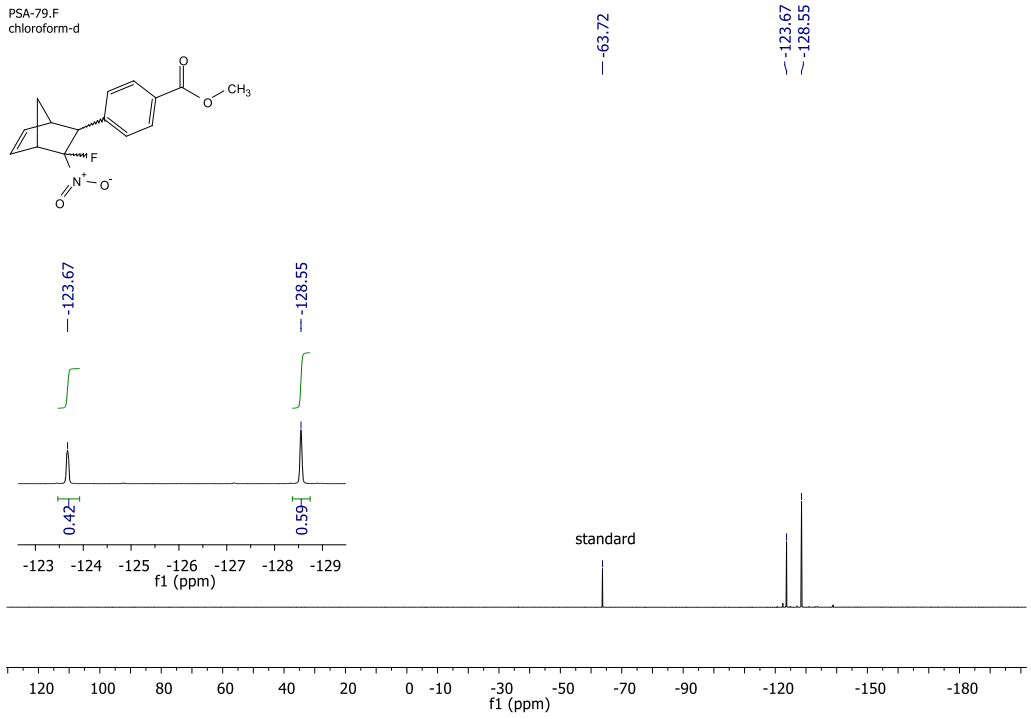

^{19}F NMR spectrum of methyl 4-(3-fluoro-3-nitrobicyclo[2.2.1]hept-5-en-2-yl)benzoate (**2h**)

S25

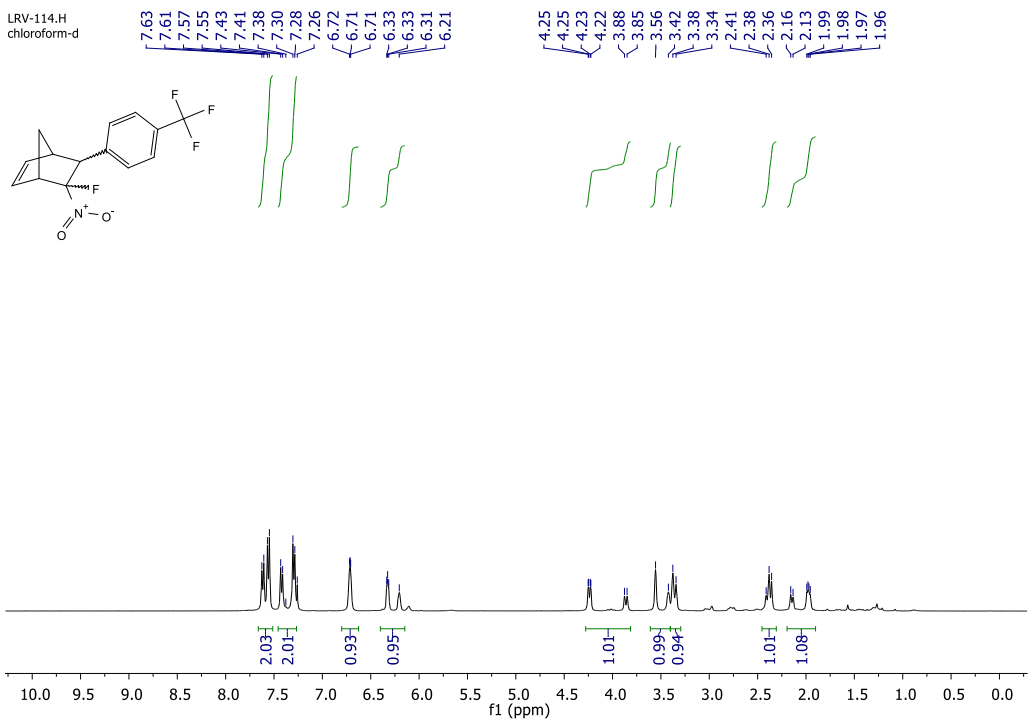

^{1}H NMR spectrum of 5-fluoro-5-nitro-6-(4-(trifluoromethyl)phenyl)bicyclo[2.2.1]hept-2-ene (**2i**)

S26

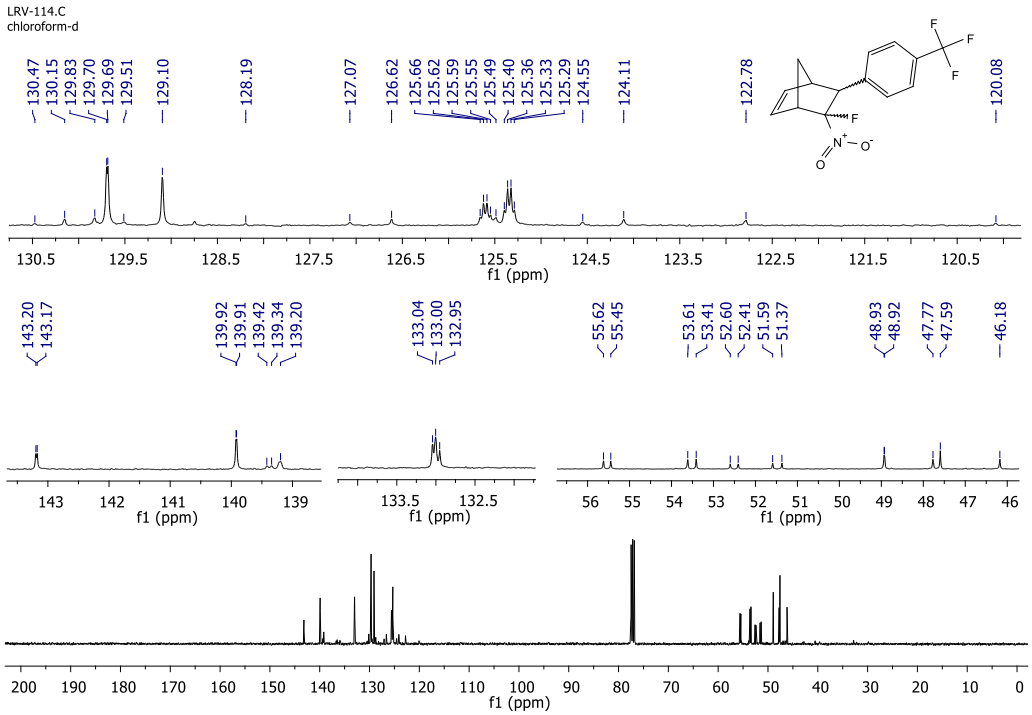

^{13}C NMR spectrum of 5-fluoro-5-nitro-6-(4-(trifluoromethyl)phenyl)bicyclo[2.2.1]hept-2-ene (**2i**)

S27

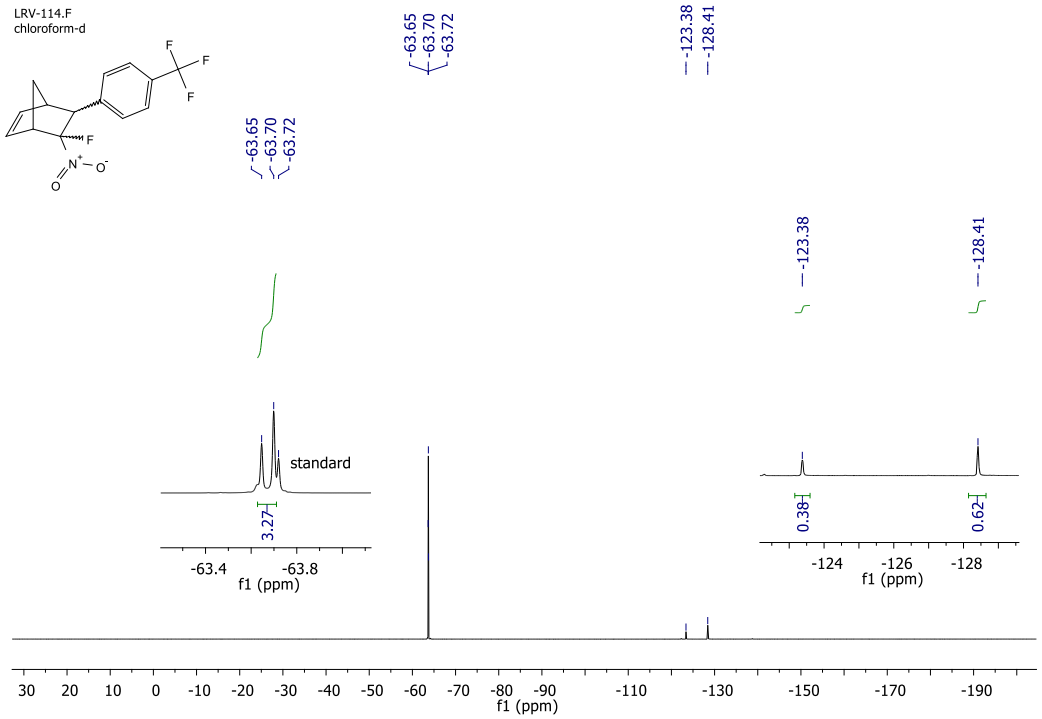

^{19}F NMR spectrum of 5-fluoro-5-nitro-6-(4-(trifluoromethyl)phenyl)bicyclo[2.2.1]hept-2-ene (**2i**)

S28

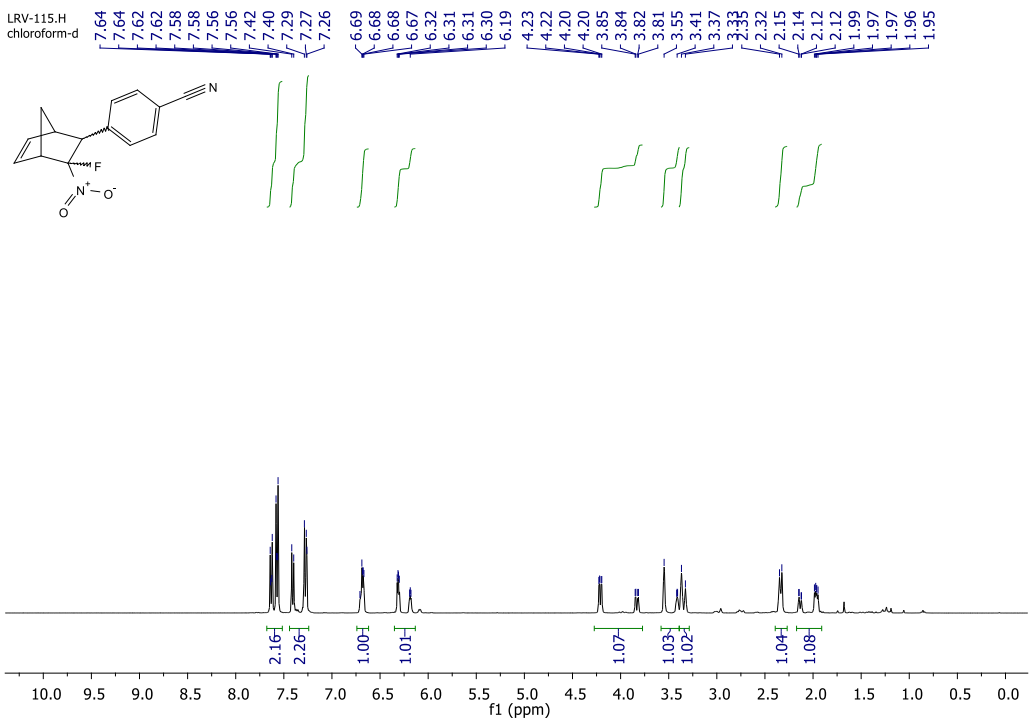

^{1}H NMR spectrum of 4-(3-fluoro-3-nitrobicyclo[2.2.1]hept-5-en-2-yl)benzonitrile (**2j**)

S29

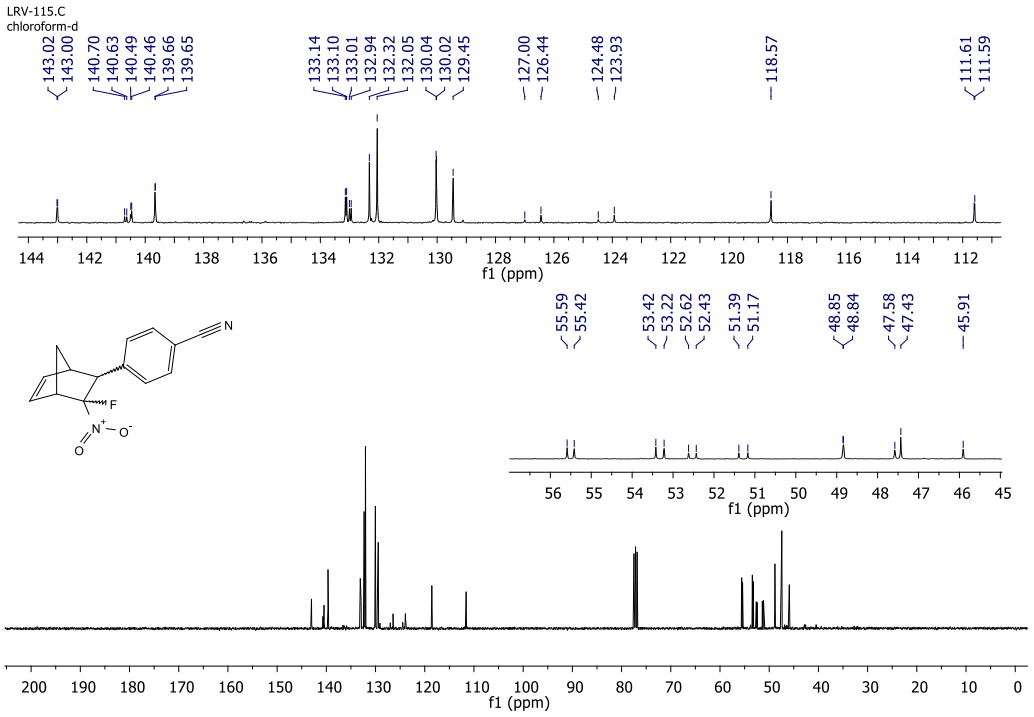

^{13}C NMR spectrum of 4-(3-fluoro-3-nitrobicyclo[2.2.1]hept-5-en-2-yl)benzonitrile (**2j**)

S30

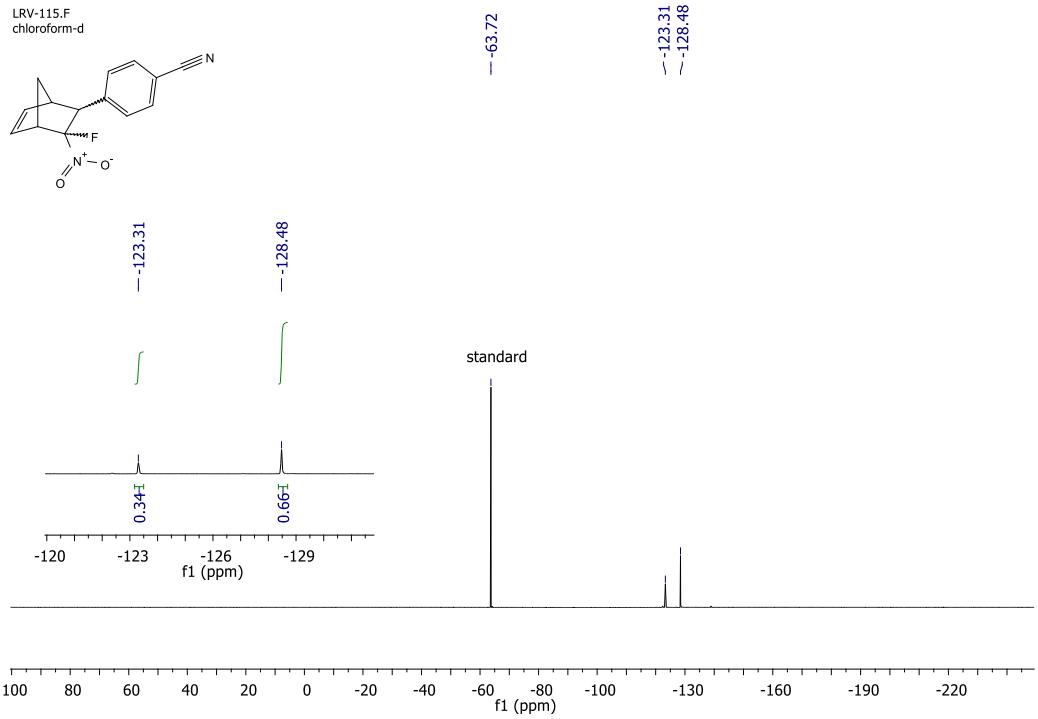

^{19}F NMR spectrum of 4-(3-fluoro-3-nitrobicyclo[2.2.1]hept-5-en-2-yl)benzonitrile (**2j**)

S31

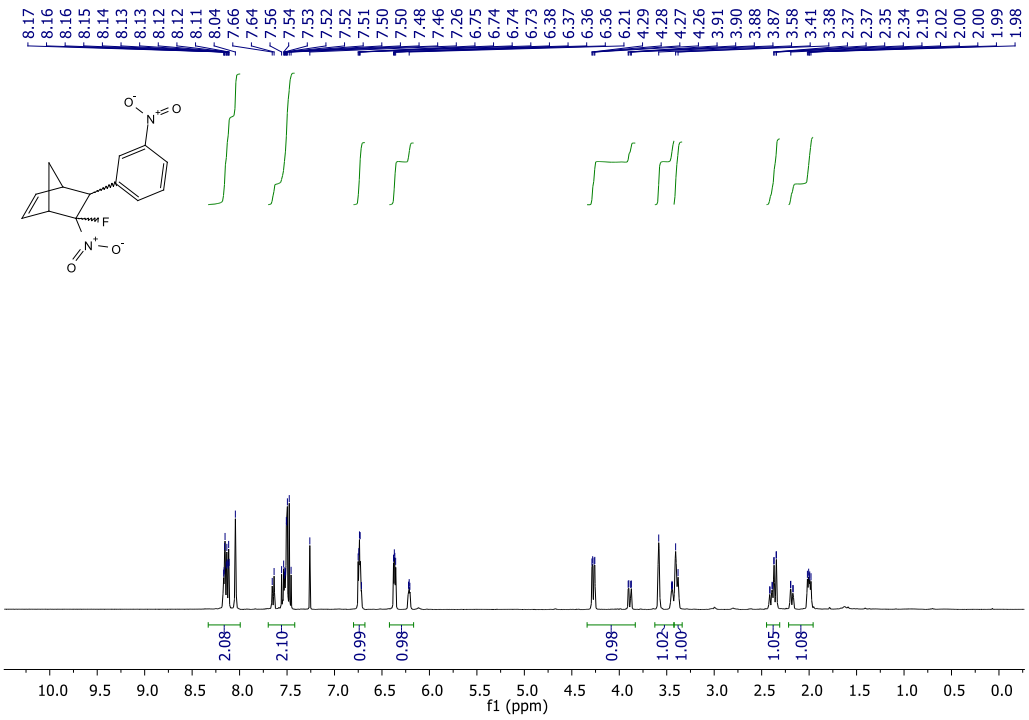

^{1}H NMR spectrum of 5-fluoro-5-nitro-6-(3-nitrophenyl)bicyclo[2.2.1]hept-2-ene (**2k**)

S32

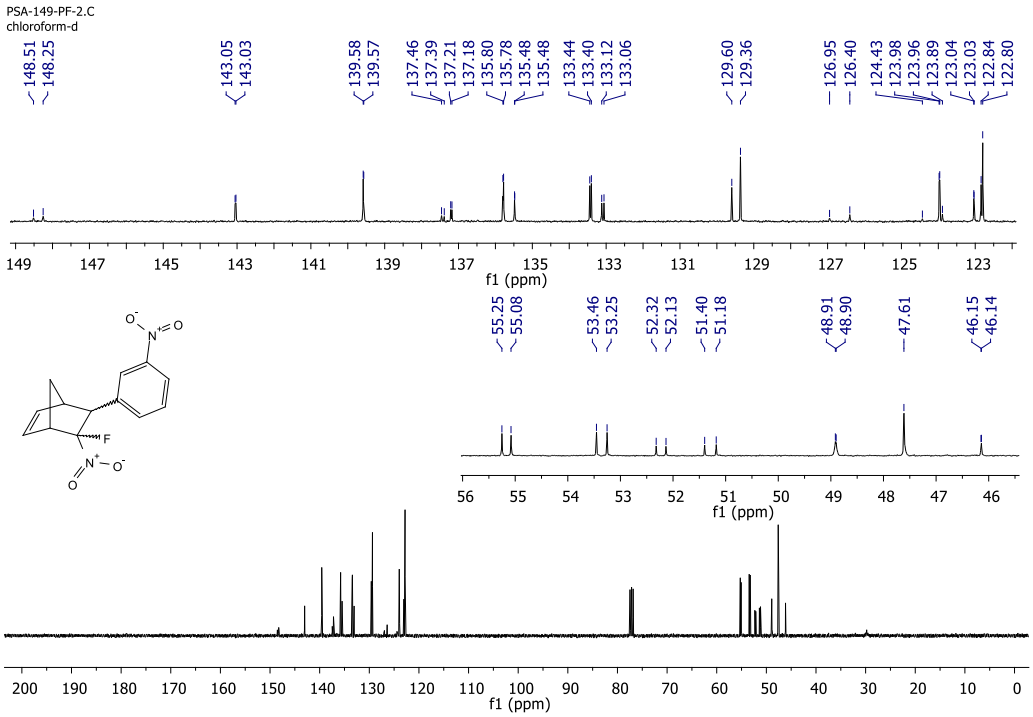

^{13}C NMR spectrum of 5-fluoro-5-nitro-6-(3-nitrophenyl)bicyclo[2.2.1]hept-2-ene (**2k**)

S33

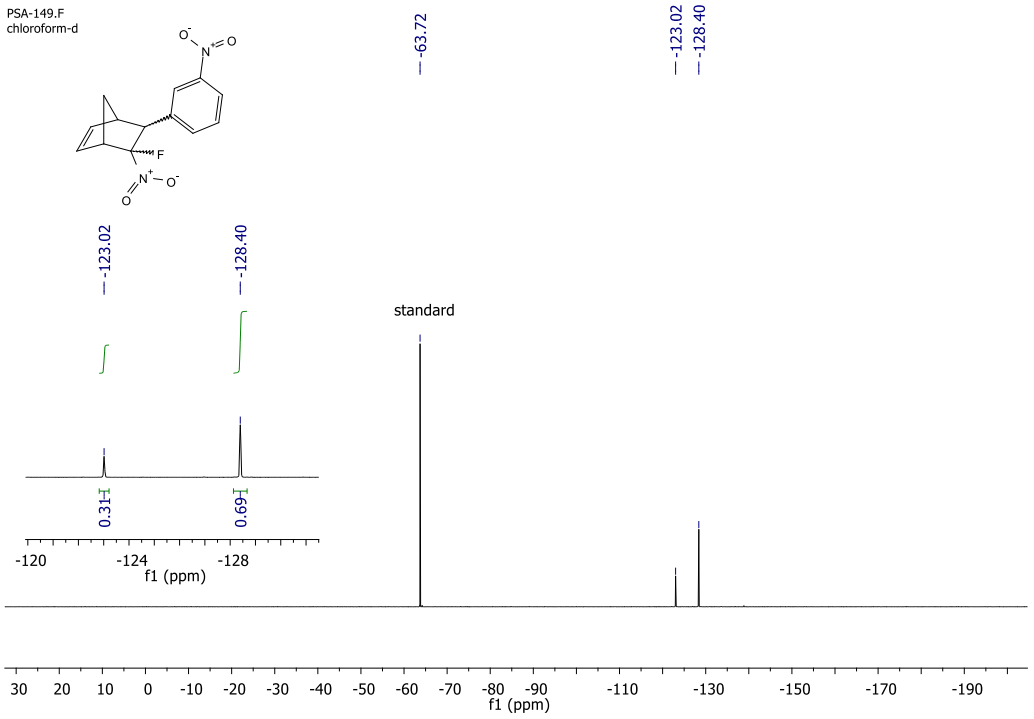

^{19}F NMR spectrum of 5-fluoro-5-nitro-6-(3-nitrophenyl)bicyclo[2.2.1]hept-2-ene (**2k**)

S34

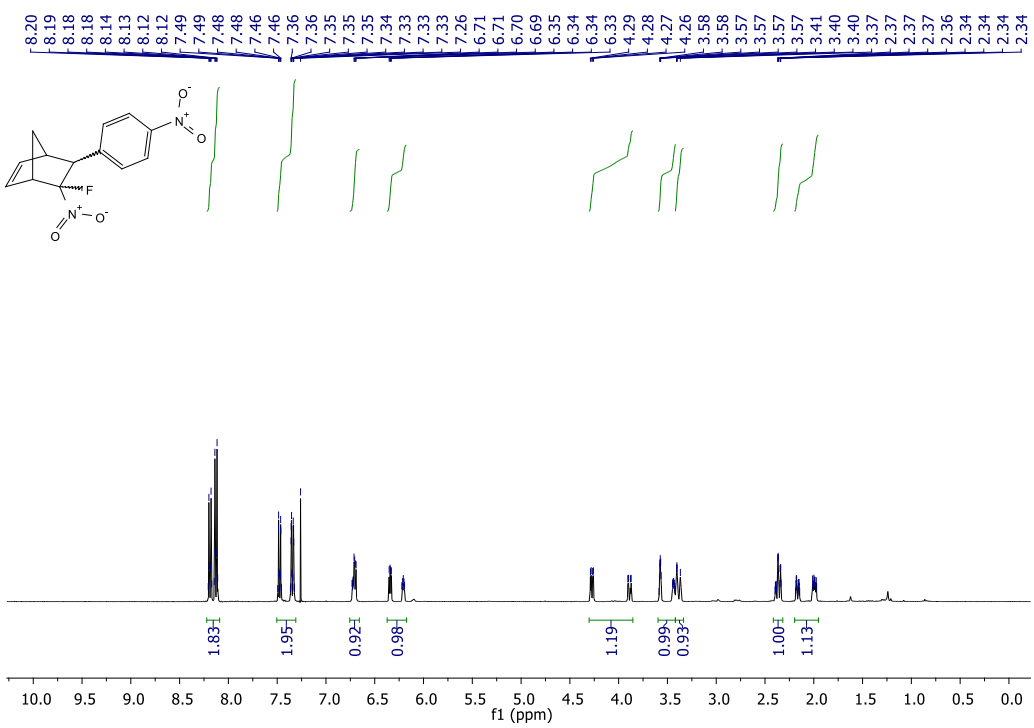

^{1}H NMR spectrum of 5-fluoro-5-nitro-6-(4-nitrophenyl)bicyclo[2.2.1]hept-2-ene (**2l**)

S35

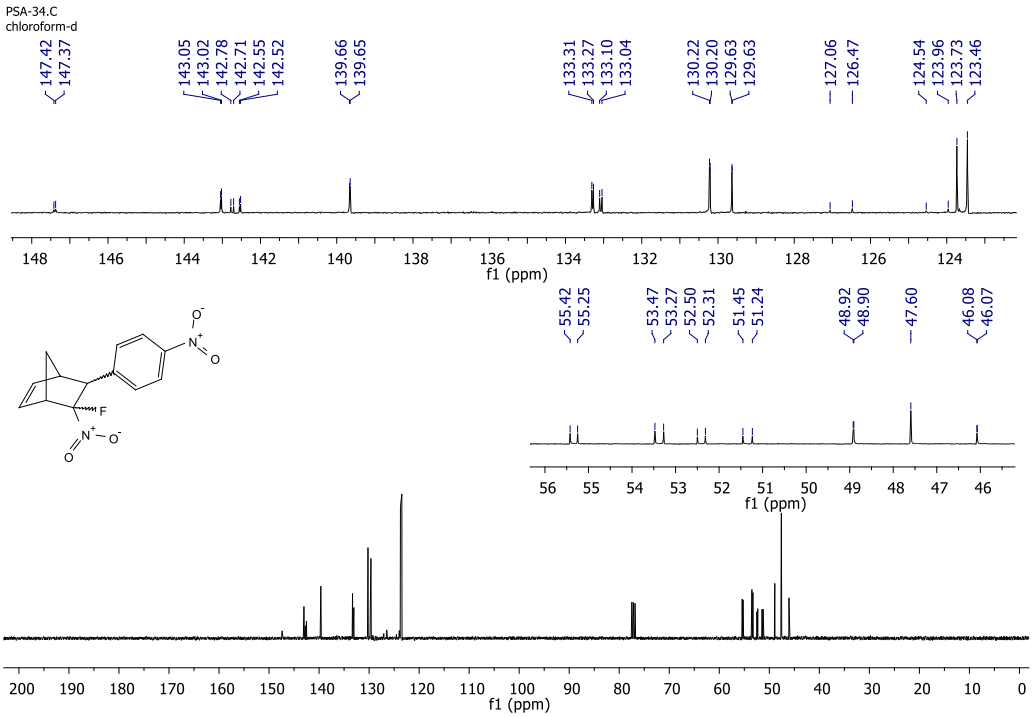

^{13}C NMR spectrum of 5-fluoro-5-nitro-6-(4-nitrophenyl)bicyclo[2.2.1]hept-2-ene (**2l**)

S36

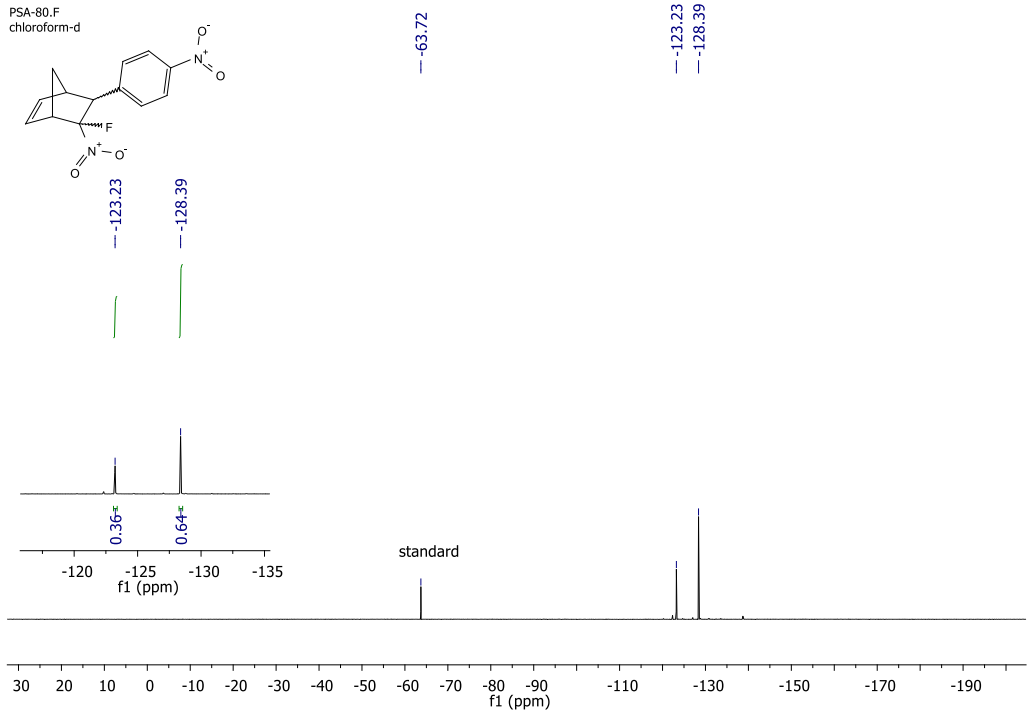

^{19}F NMR spectrum of 5-fluoro-5-nitro-6-(4-nitrophenyl)bicyclo[2.2.1]hept-2-ene (**2l**)

S37

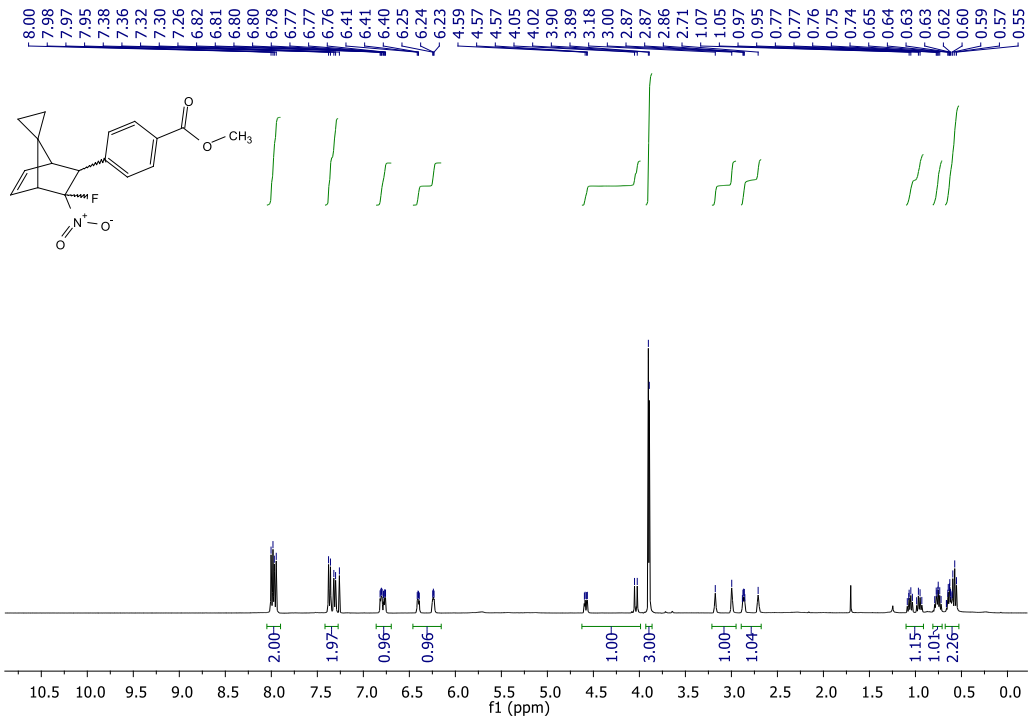

^{1}H NMR spectrum of methyl 4-(5-fluoro-5-nitrospiro[bicyclo[2.2.1]hept[2]ene-7,1'-cyclopropan]-6-yl)benzoate (**2m**)

S38

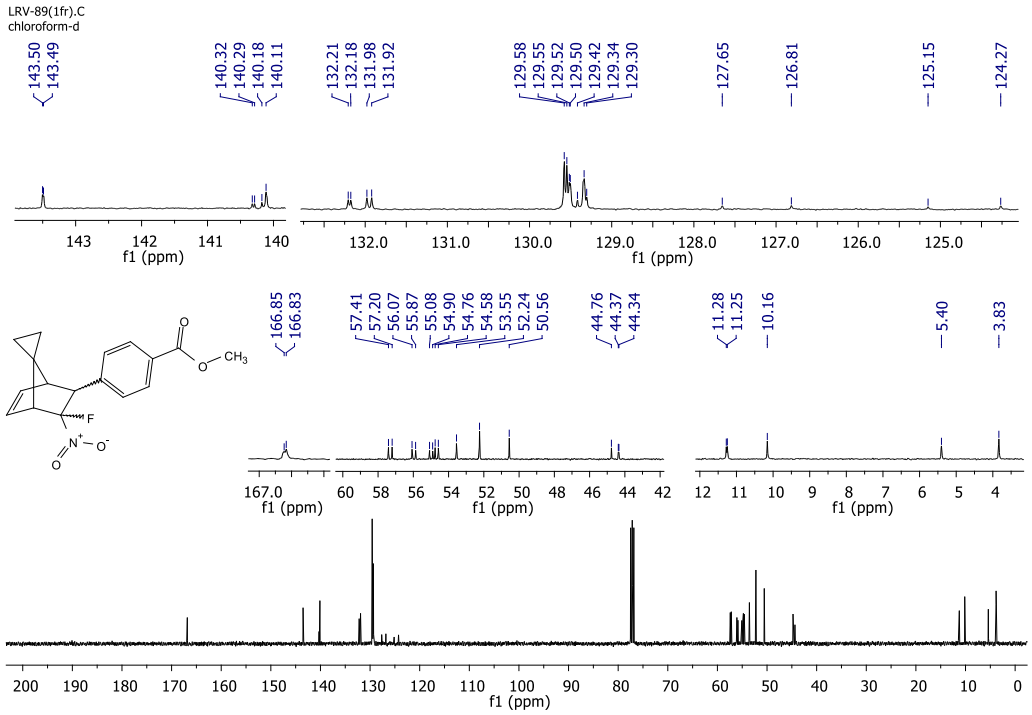

^{13}C NMR spectrum of methyl 4-(5-fluoro-5-nitrospiro[bicyclo[2.2.1]hept[2]ene-7,1'-cyclopropan]-6-yl)benzoate (**2m**)

S39

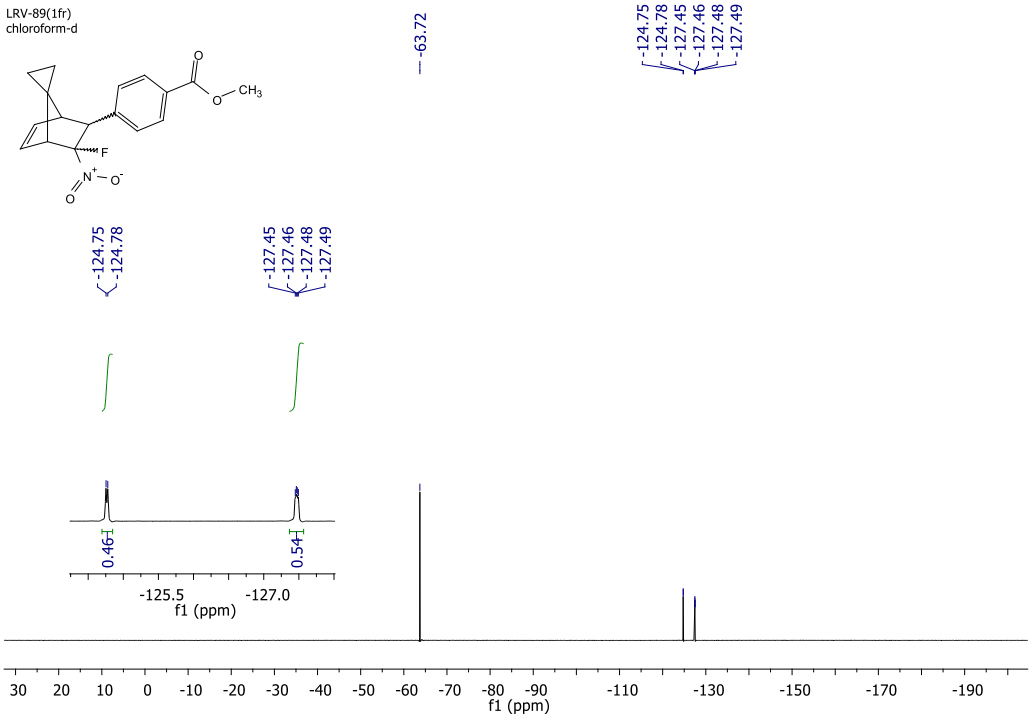

^{19}F NMR spectrum of methyl 4-(5-fluoro-5-nitrospiro[bicyclo[2.2.1]hept[2]ene-7,1'-cyclopropan]-6-yl)benzoate (**2m**)

S40

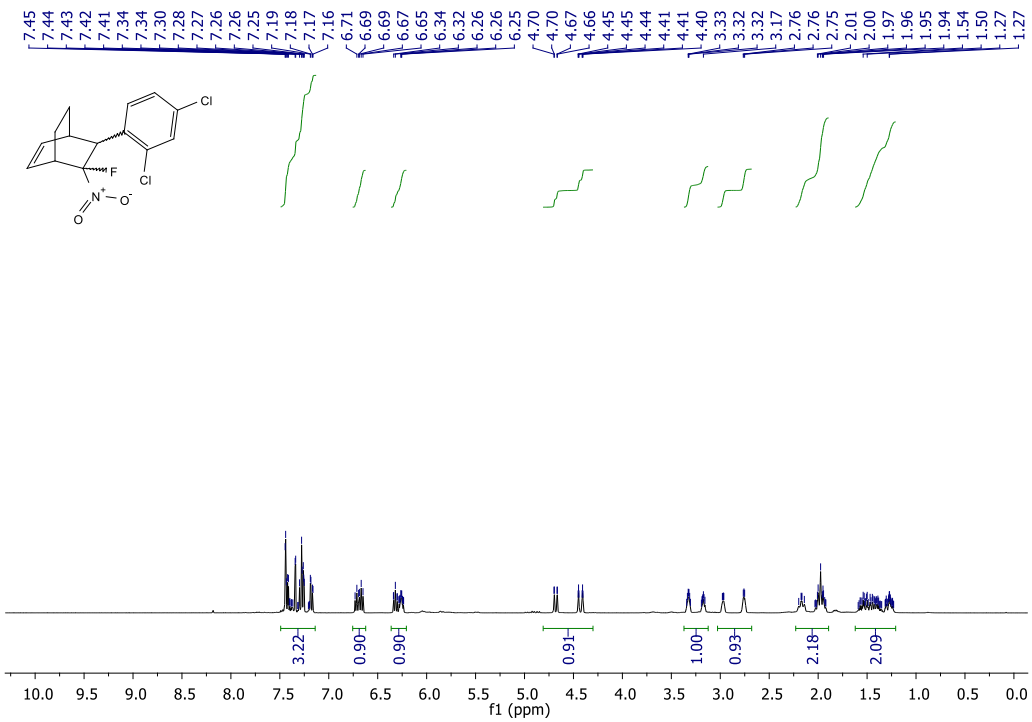

^{1}H NMR spectrum of 6-(2,4-dichlorophenyl)-5-fluoro-5-nitrobicyclo[2.2.2]oct-2-ene (**3a**)

S41

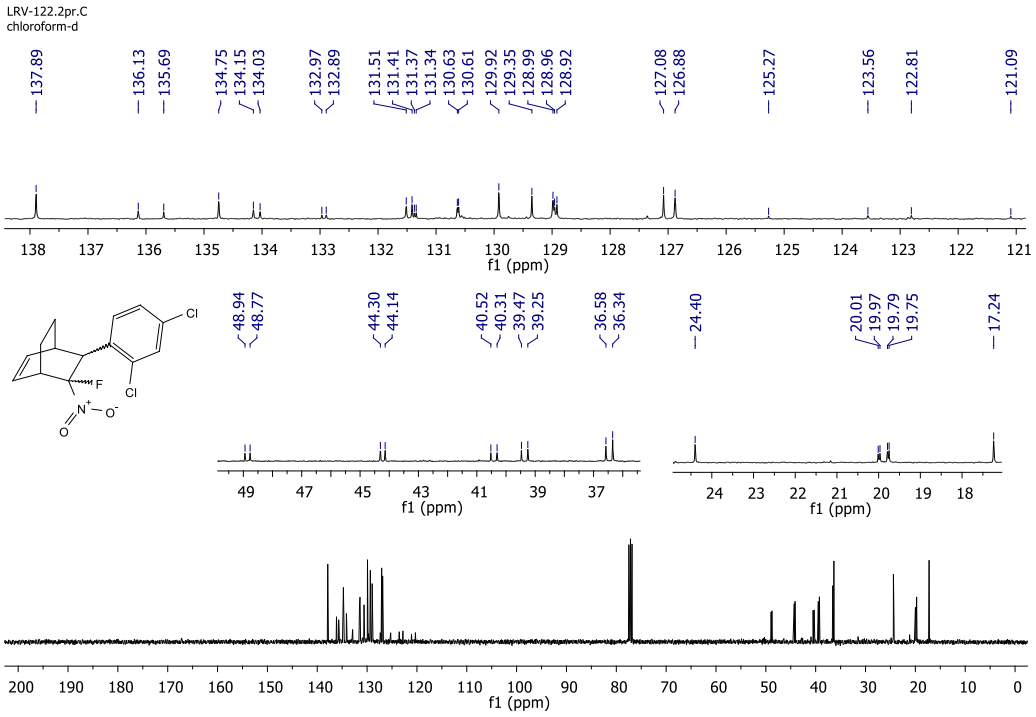

^{13}C NMR spectrum of 6-(2,4-dichlorophenyl)-5-fluoro-5-nitrobicyclo[2.2.2]oct-2-ene (**3a**)

S42

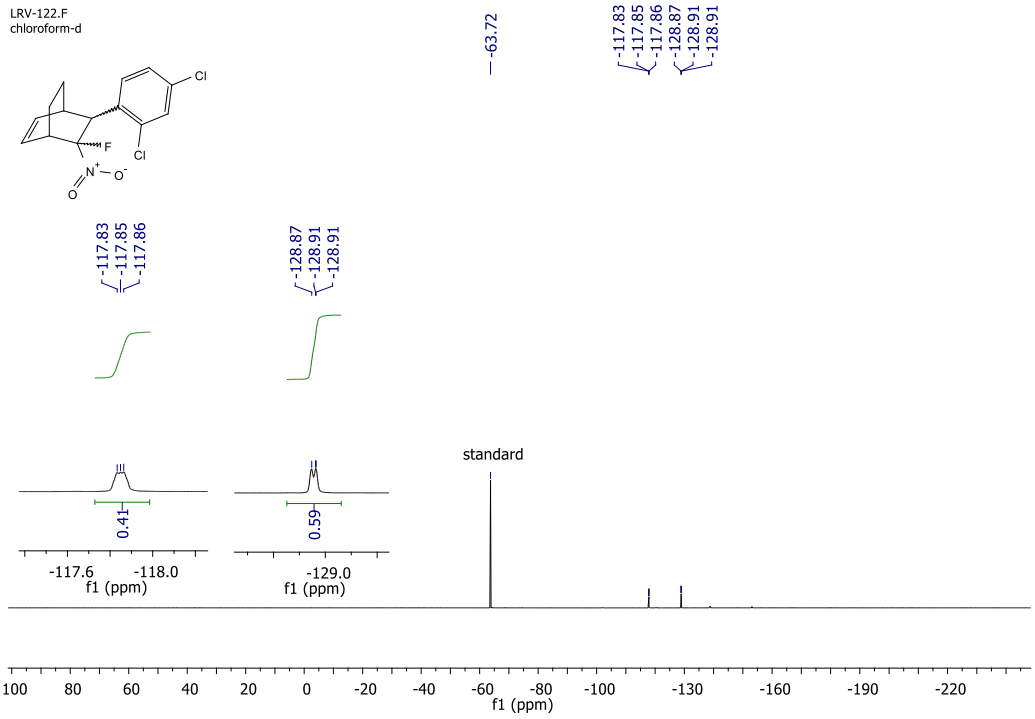

^{19}F NMR spectrum of 6-(2,4-dichlorophenyl)-5-fluoro-5-nitrobicyclo[2.2.2]oct-2-ene (**3a**)

S43

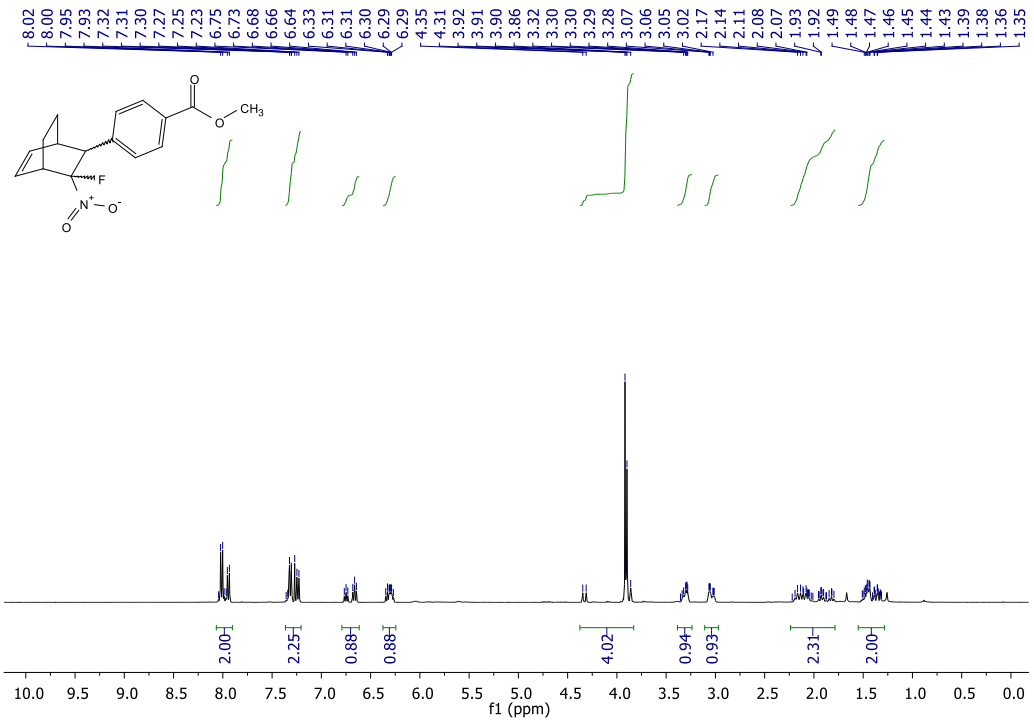

^{1}H NMR spectrum of methyl 4-(3-fluoro-3-nitrobicyclo[2.2.2]oct-5-en-2-yl)benzoate (**3b**)

S44

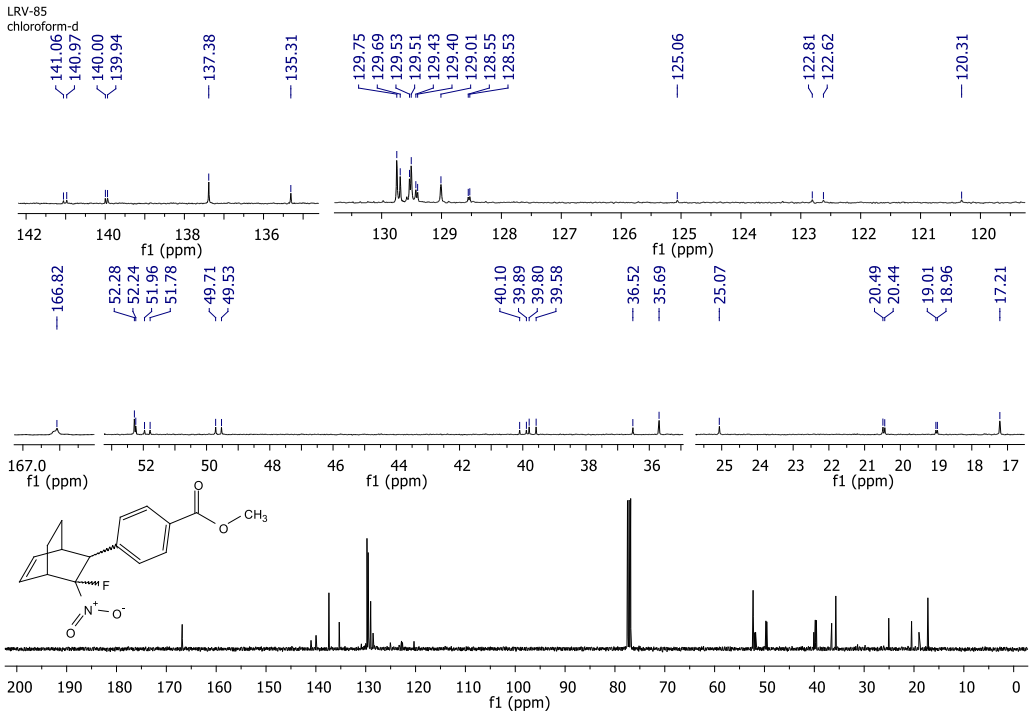

^{13}C NMR spectrum of methyl 4-(3-fluoro-3-nitrobicyclo[2.2.2]oct-5-en-2-yl)benzoate (**3b**)

S45

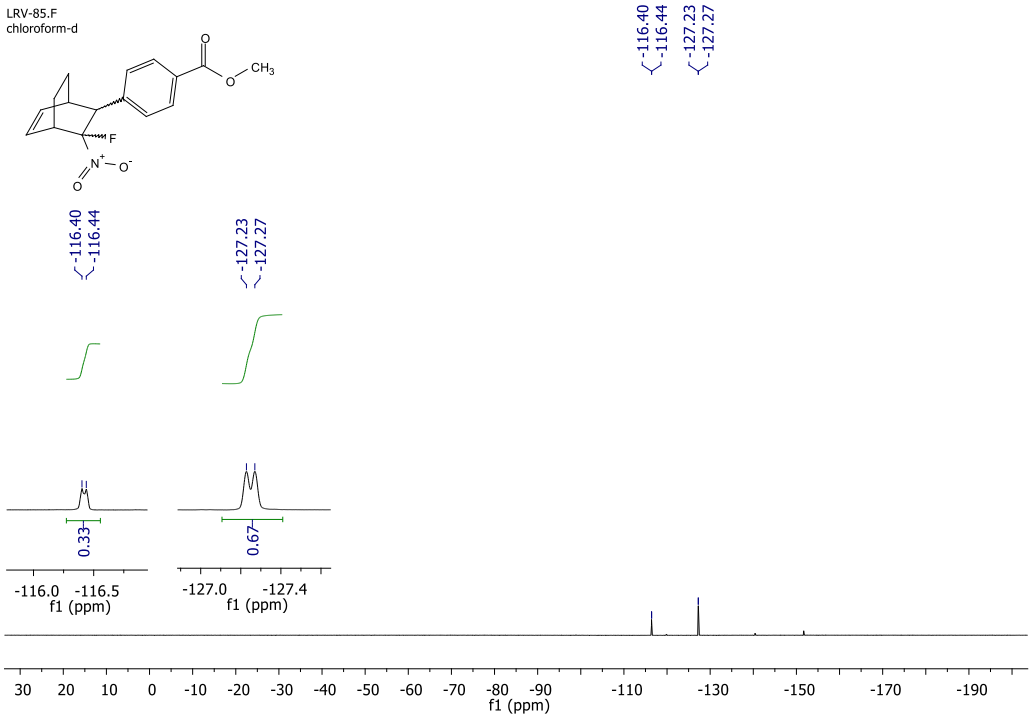

^{19}F NMR spectrum of methyl 4-(3-fluoro-3-nitrobicyclo[2.2.2]oct-5-en-2-yl)benzoate (**3b**)

S46

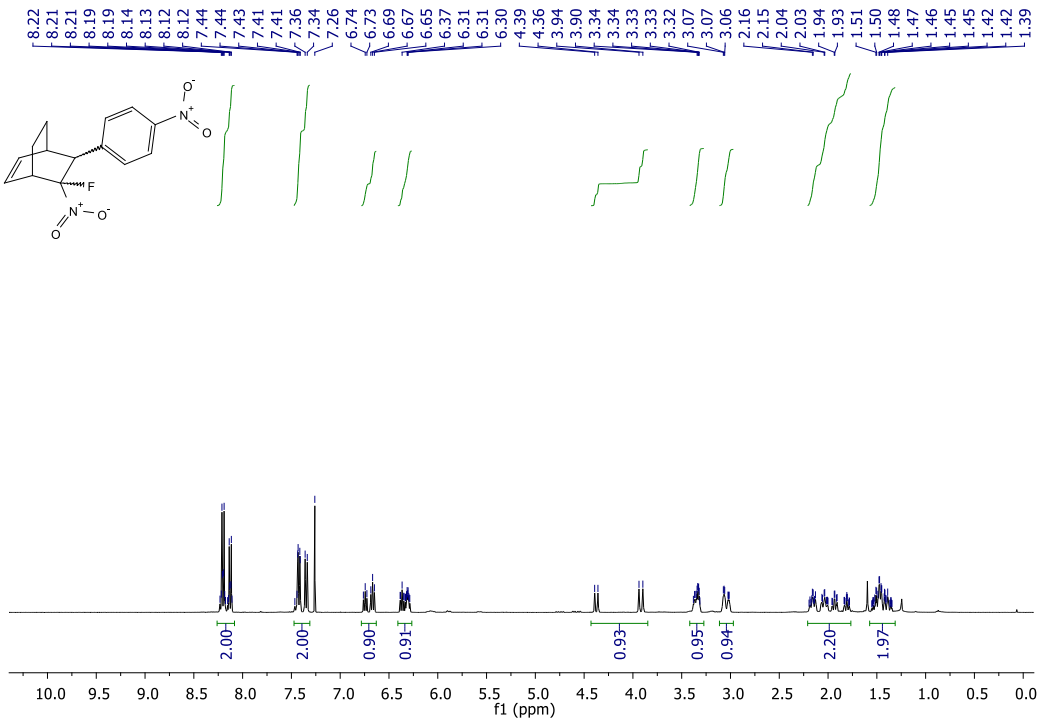

^{1}H NMR spectrum of 5-fluoro-5-nitro-6-(4-nitrophenyl)bicyclo[2.2.2]oct-2-ene (**3c**)

S47

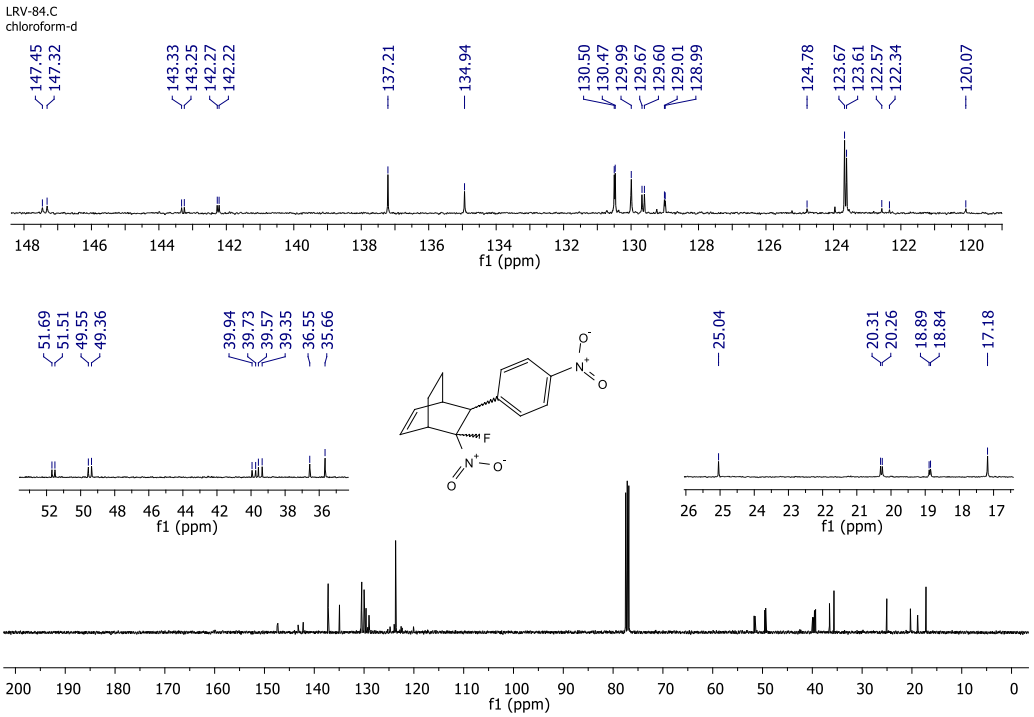

^{13}C NMR spectrum of 5-fluoro-5-nitro-6-(4-nitrophenyl)bicyclo[2.2.2]oct-2-ene (**3c**)

S48

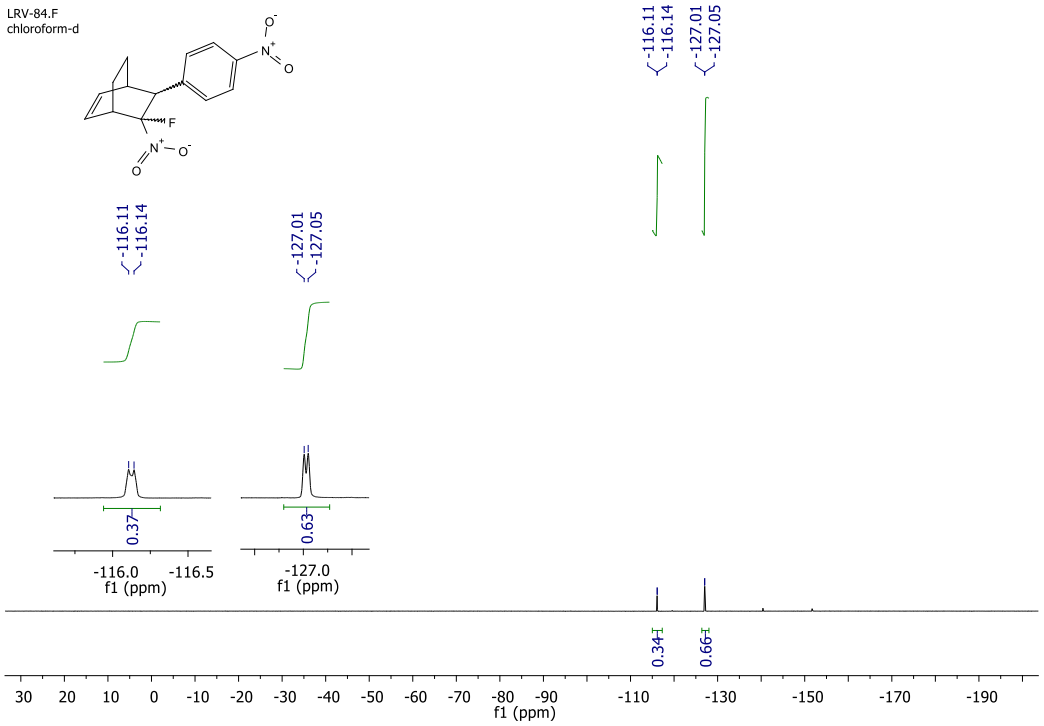

^{19}F NMR spectrum of 5-fluoro-5-nitro-6-(4-nitrophenyl)bicyclo[2.2.2]oct-2-ene (**3c**)

S49

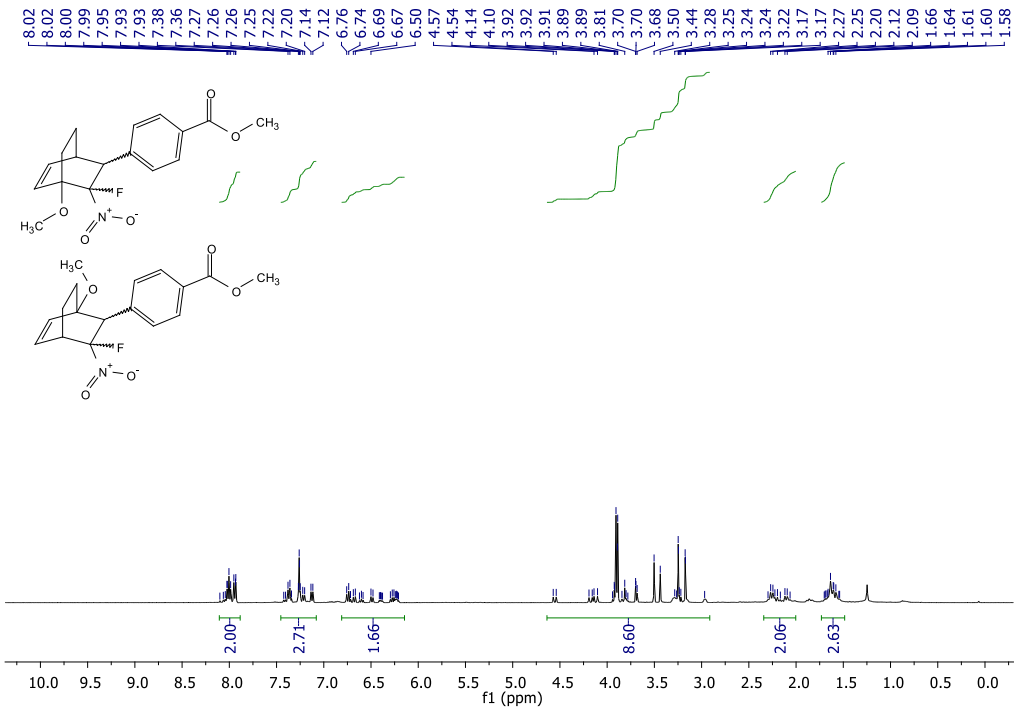

^{1}H NMR spectrum of methyl 4-(3-fluoro-4-methoxy-3-nitrobicyclo[2.2.2]oct-5-en-2-yl)benzoate and methyl 4-(3-fluoro-1-methoxy-3-nitrobicyclo[2.2.2]oct-5-en-2-yl)benzoate (**3d**)

S50

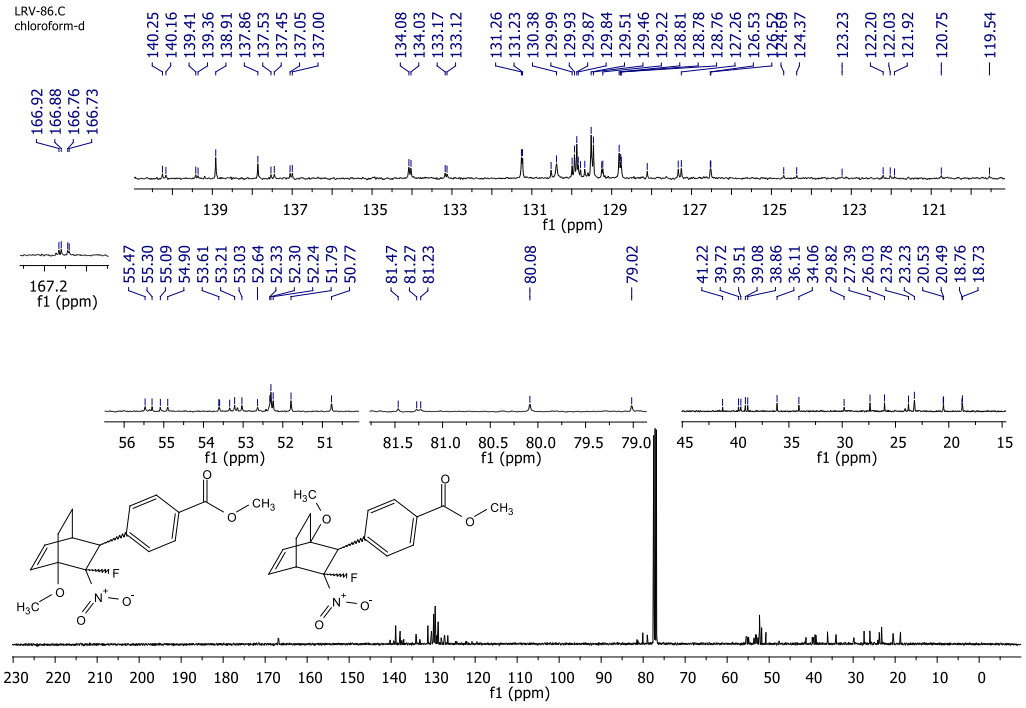

^{13}C NMR spectrum of methyl 4-(3-fluoro-4-methoxy-3-nitrobicyclo[2.2.2]oct-5-en-2-yl)benzoate and methyl 4-(3-fluoro-1-methoxy-3-nitrobicyclo[2.2.2]oct-5-en-2-yl)benzoate (**3d**)

S51

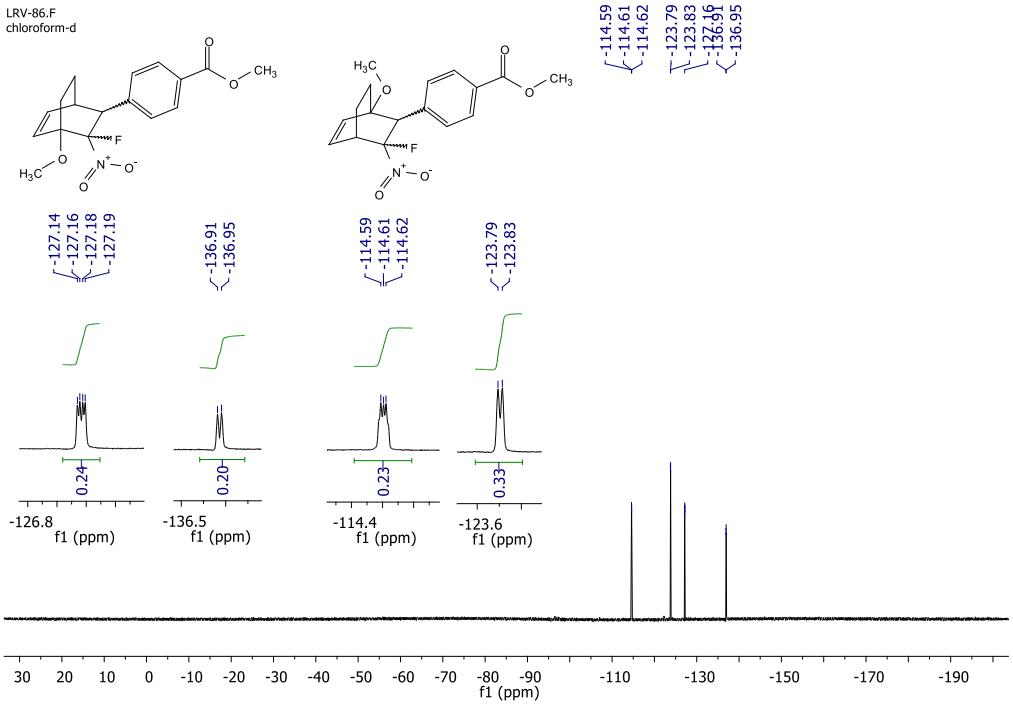

^{19}F NMR spectrum of methyl 4-(3-fluoro-4-methoxy-3-nitrobicyclo[2.2.2]oct-5-en-2-yl)benzoate and methyl 4-(3-fluoro-1-methoxy-3-nitrobicyclo[2.2.2]oct-5-en-2-yl)benzoate (**3d**)

S52

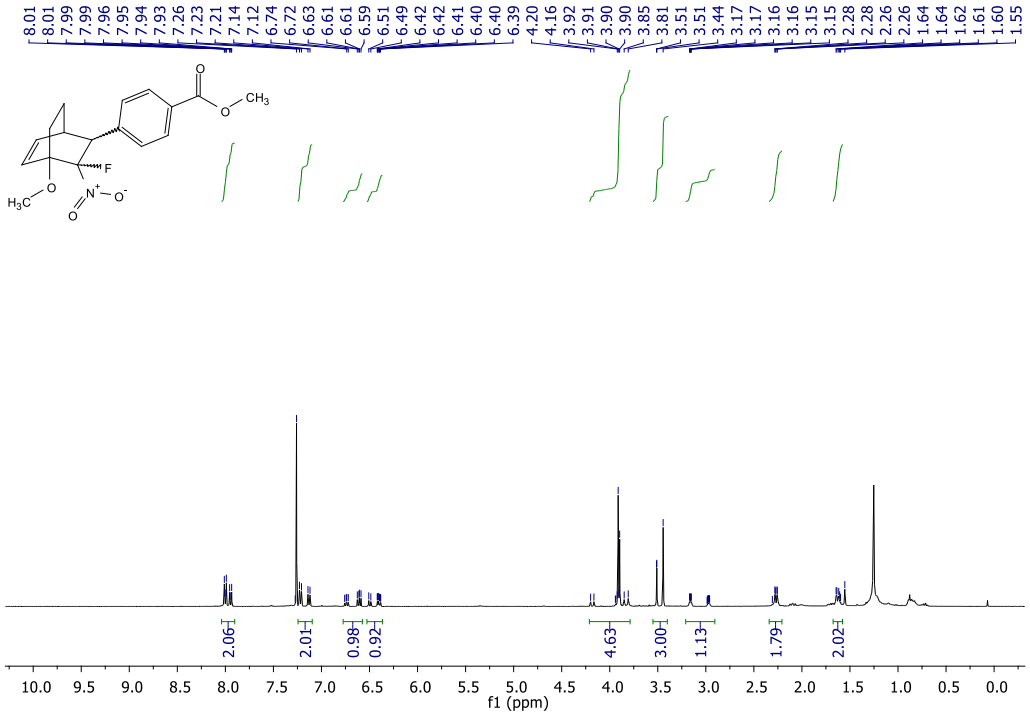

^{1}H NMR spectrum of methyl 4-(3-fluoro-4-methoxy-3-nitrobicyclo[2.2.2]oct-5-en-2-yl)benzoate (**3d**)

S53

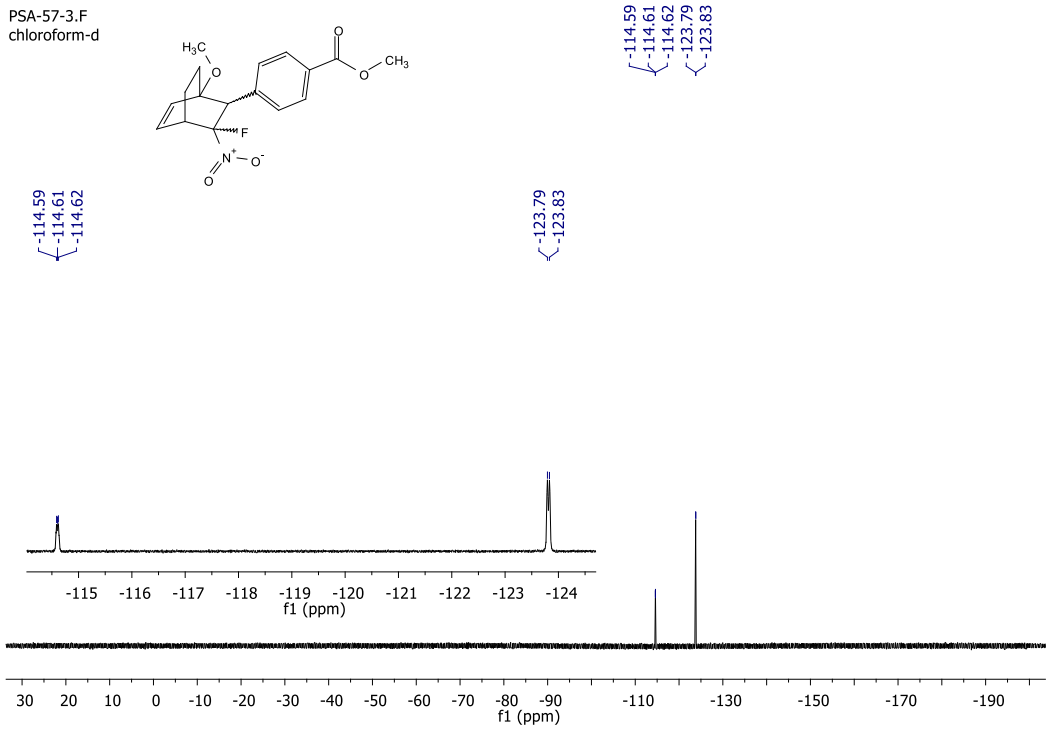

^{19}F NMR spectrum of 4-(3-fluoro-1-methoxy-3-nitrobicyclo[2.2.2]oct-5-en-2-yl)benzoate (**3d**)

S54

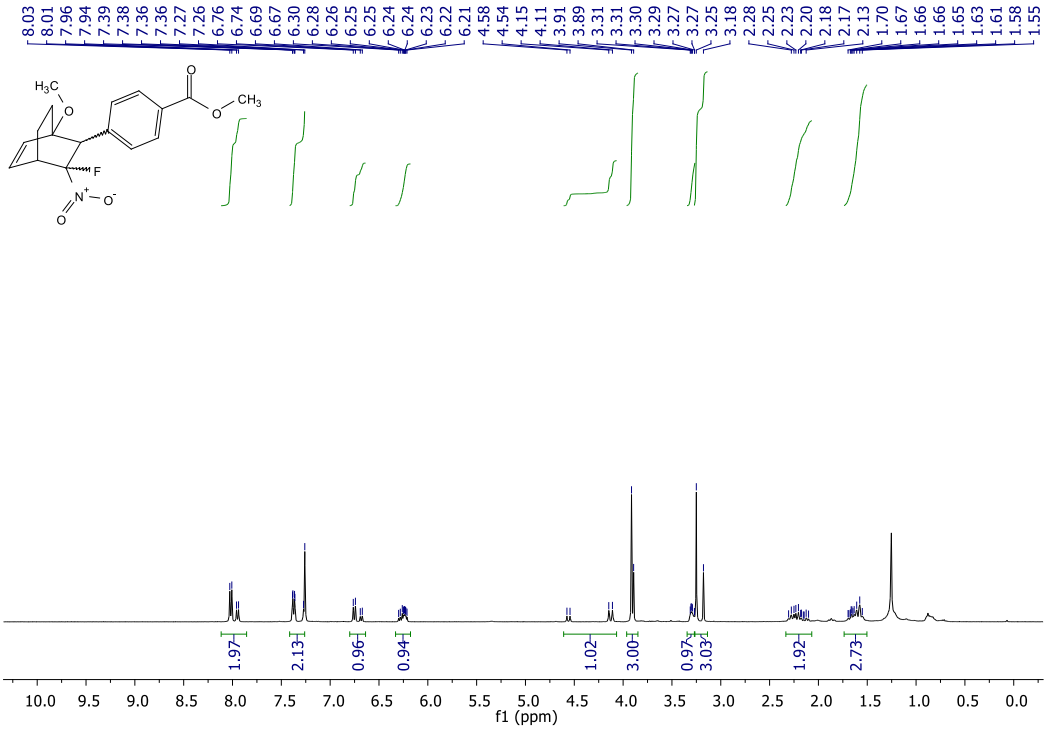

[1]H NMR spectrum of 4-(3-fluoro-1-methoxy-3-nitrobicyclo[2.2.2]oct-5-en-2-yl)benzoate (**3d**)

S55

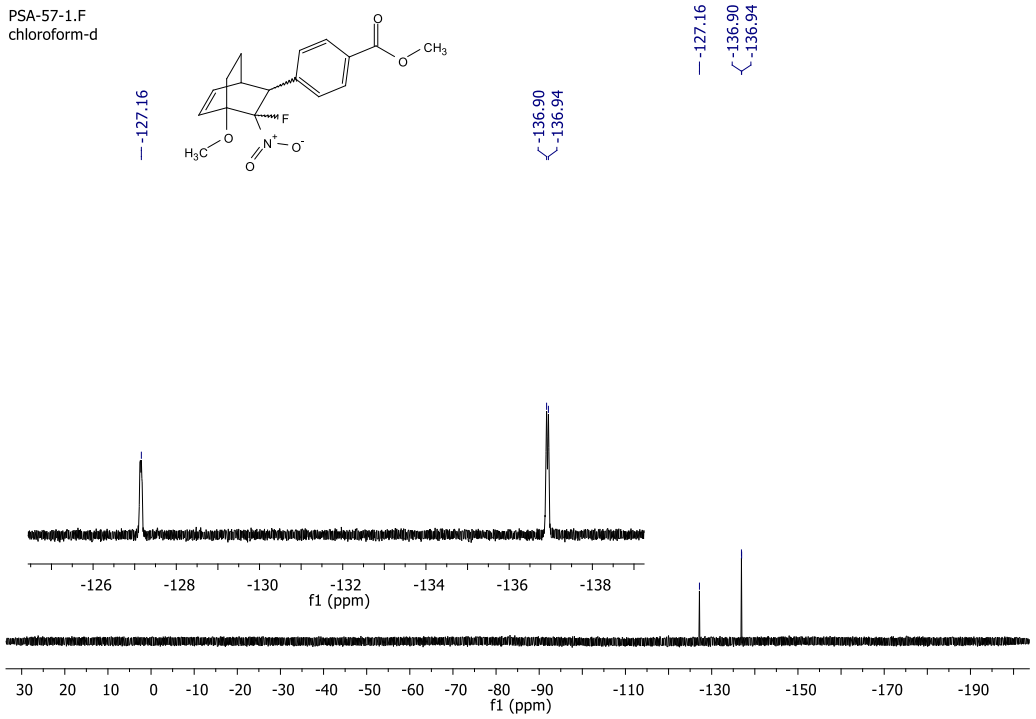

^{19}F NMR spectrum of methyl 4-(3-fluoro-4-methoxy-3-nitrobicyclo[2.2.2]oct-5-en-2-yl)benzoate (**3d**)

S56

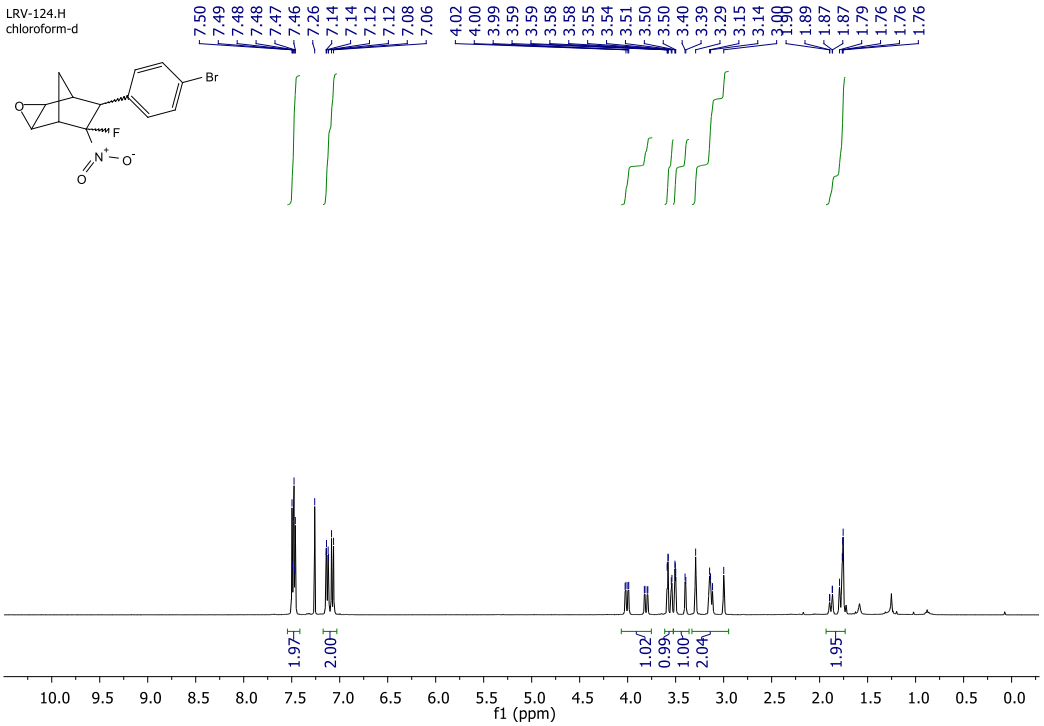

^{1}H NMR spectrum of 7-(4-bromophenyl)-6-fluoro-6-nitro-3-oxatricyclo[3.2.1.0^{2,4}]octane (**4a**)

S57

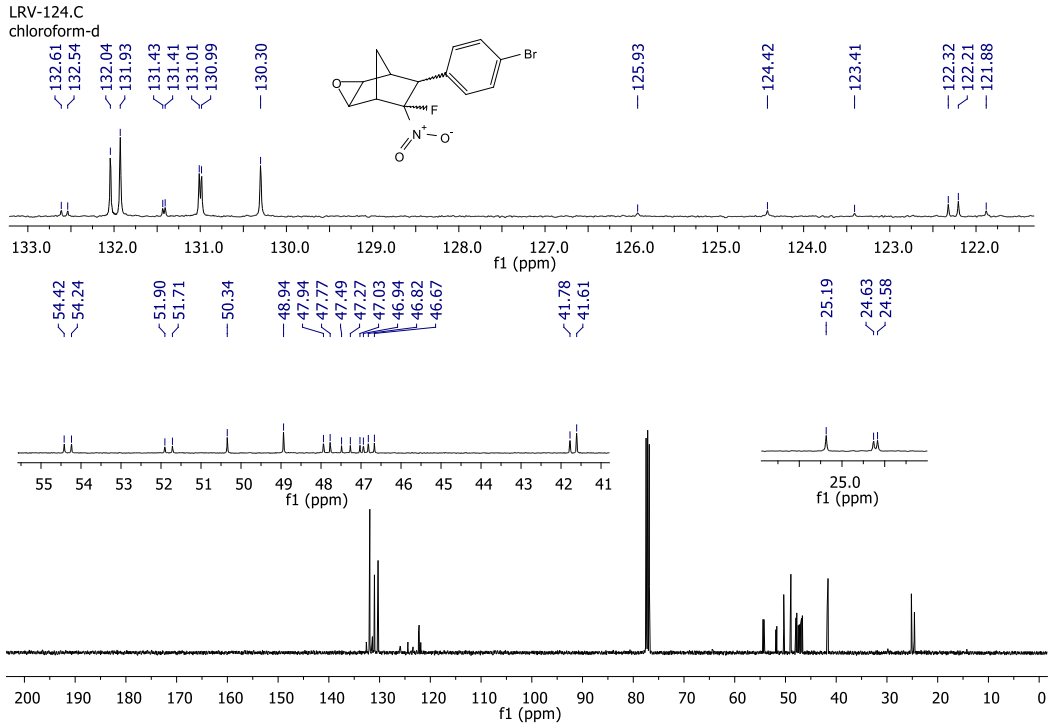

^{13}C NMR spectrum of 7-(4-bromophenyl)-6-fluoro-6-nitro-3-oxatricyclo[3.2.1.0^{2,4}]octane (**4a**)

S58

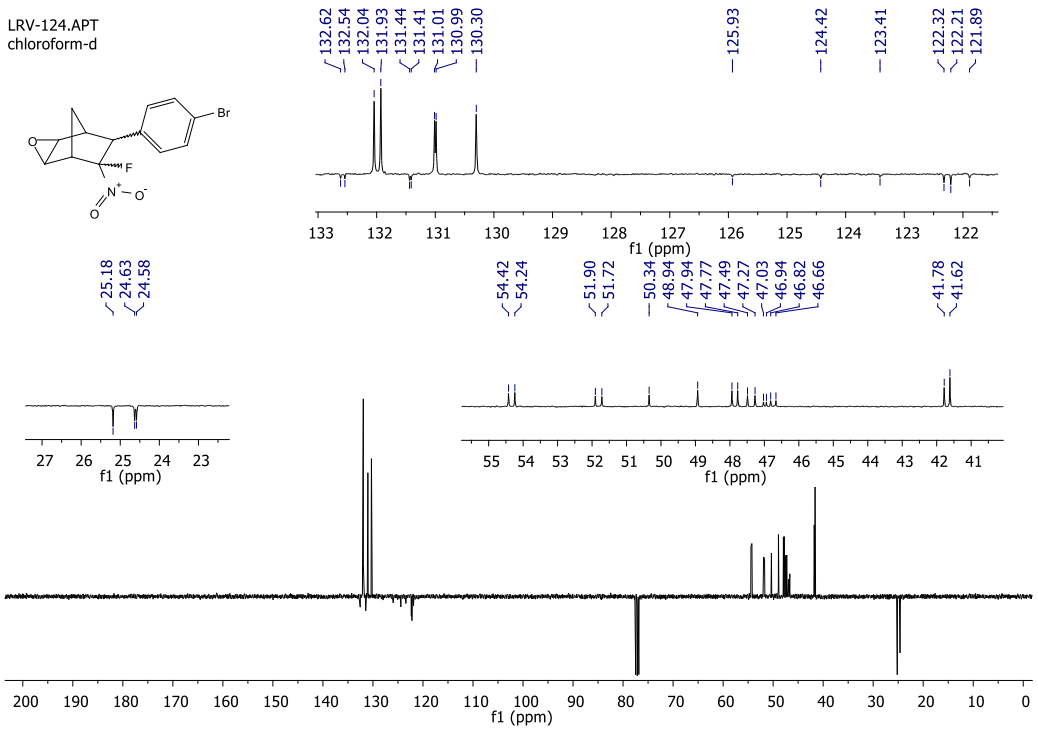

^{13}C APT NMR spectrum of 7-(4-bromophenyl)-6-fluoro-6-nitro-3-oxatricyclo[3.2.1.0^{2,4}]octane (**4a**)

S59

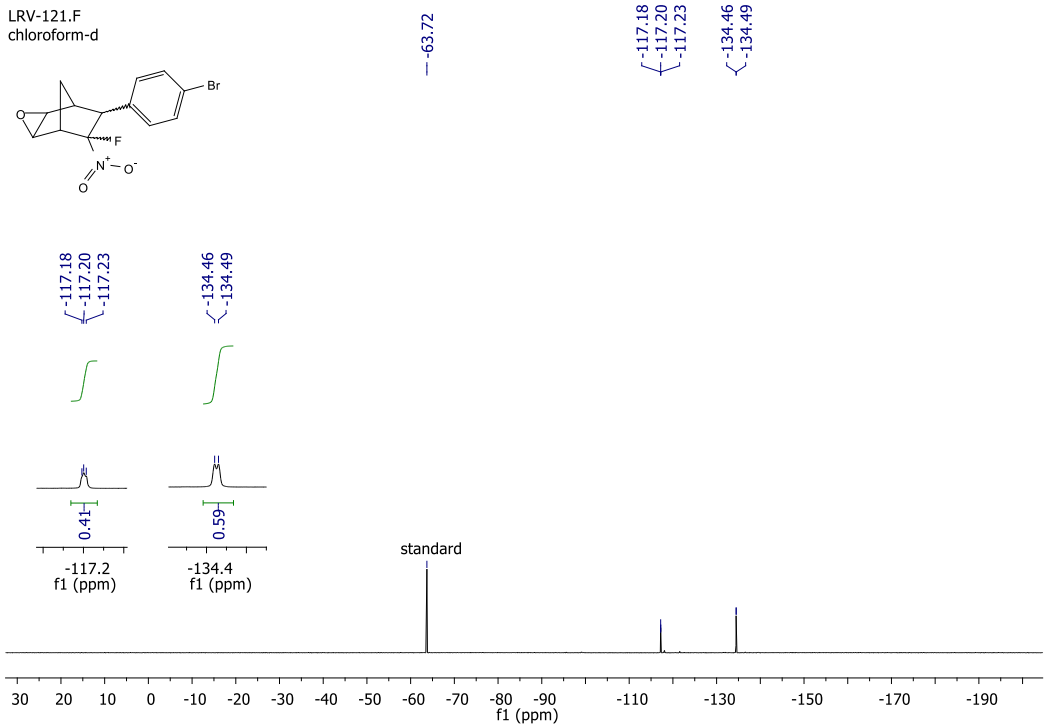

^{19}F NMR spectrum of 7-(4-bromophenyl)-6-fluoro-6-nitro-3-oxatricyclo[3.2.1.0^{2,4}]octane (**4a**)

S60

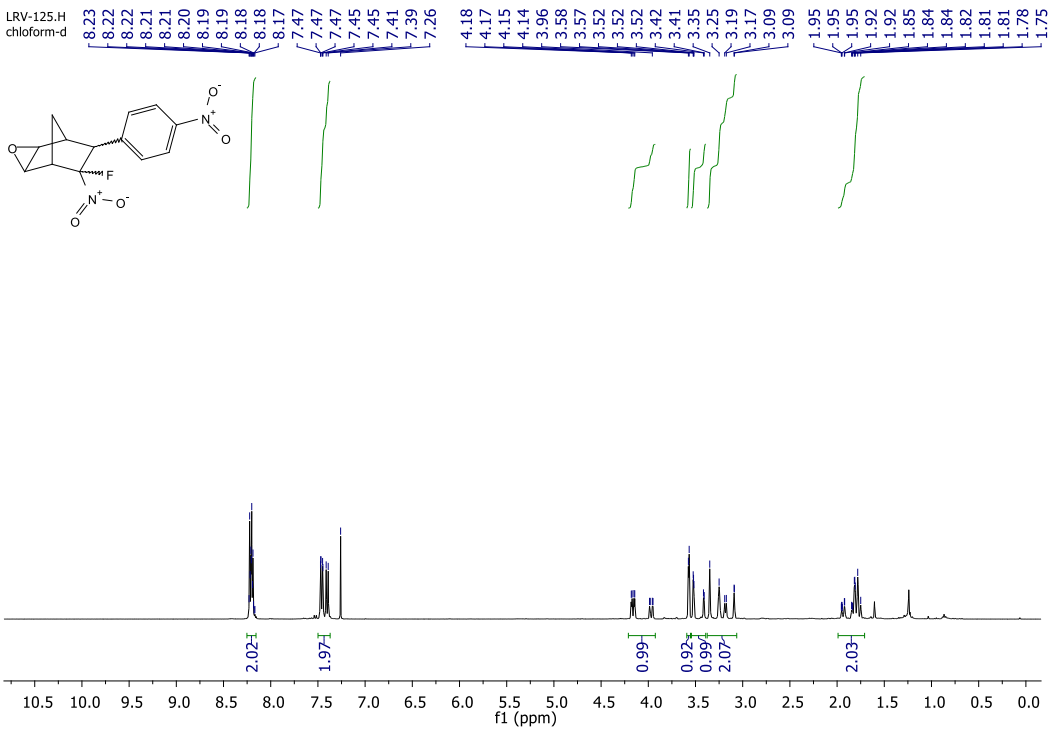

^{1}H NMR spectrum of 6-fluoro-6-nitro-7-(4-nitrophenyl)-3-oxatricyclo[3.2.1.0^{2,4}]octane (**4b**)

S61

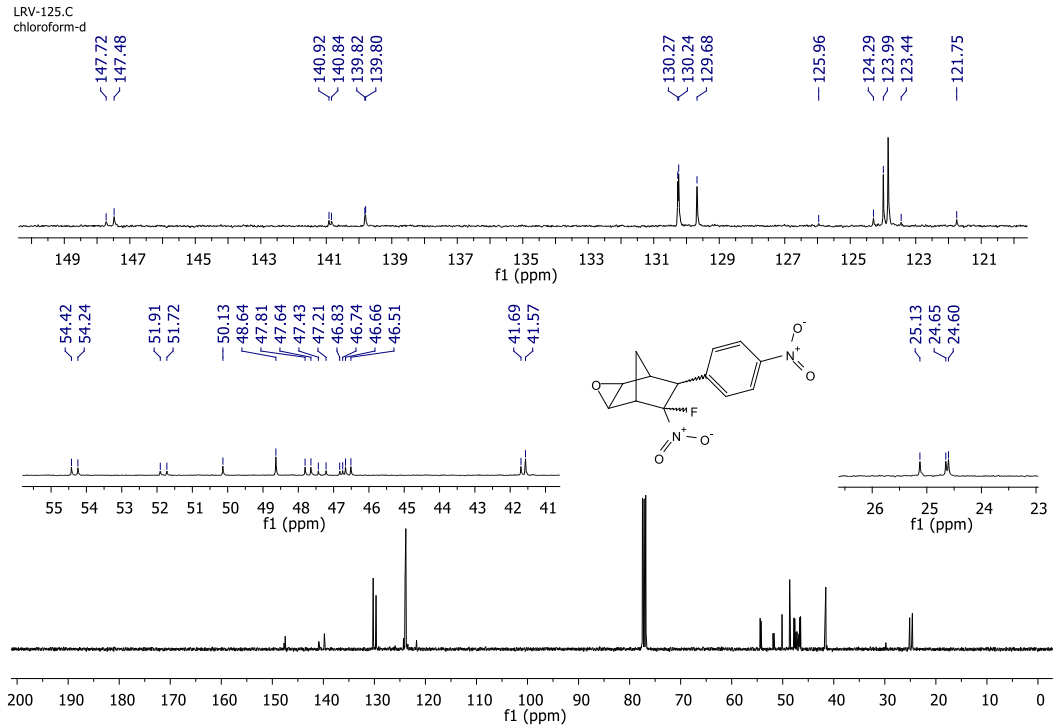

^{13}C NMR spectrum of 6-fluoro-6-nitro-7-(4-nitrophenyl)-3-oxatricyclo[3.2.1.0^{2,4}]octane (**4b**)

S62

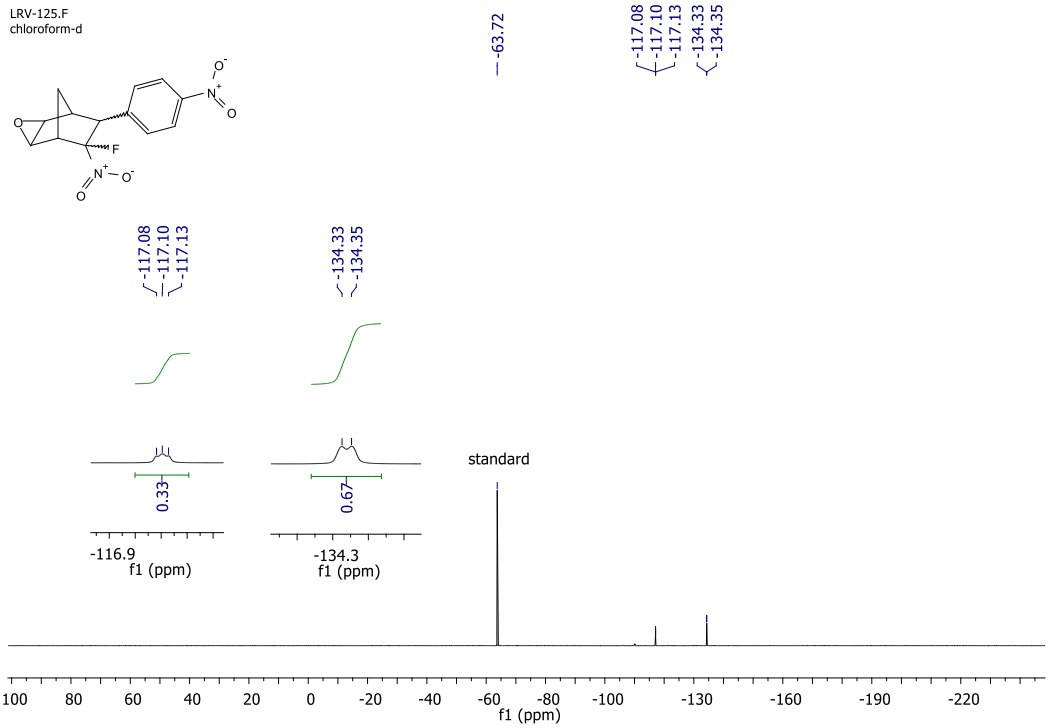

^{19}F NMR spectrum of 6-fluoro-6-nitro-7-(4-nitrophenyl)-3-oxatricyclo[3.2.1.0^{2,4}]octane (**4b**)

S63

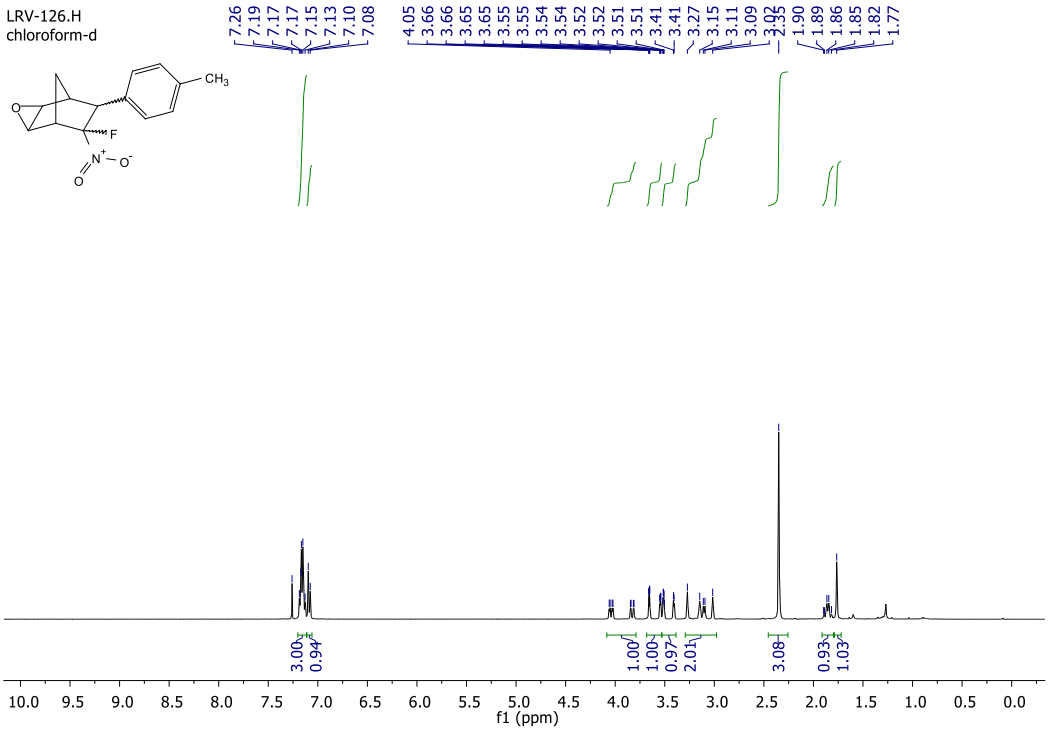

^{1}H NMR spectrum of 6-fluoro-6-nitro-7-(p-tolyl)-3-oxatricyclo[3.2.1.0^{2,4}]octane (**4c**)

S64

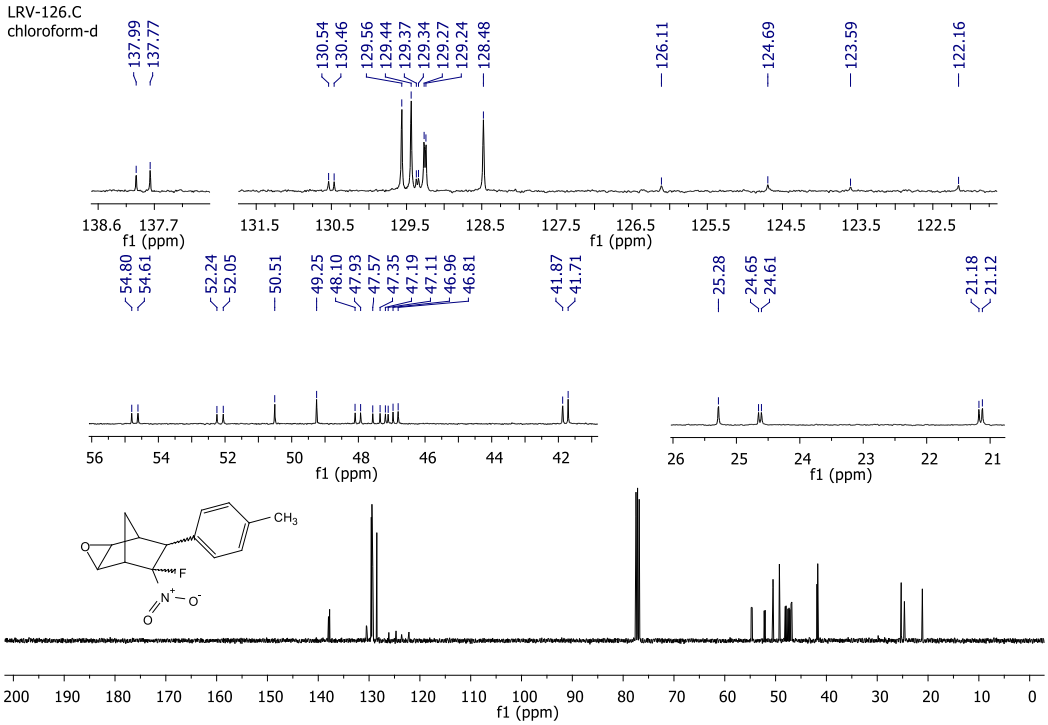

^{13}C NMR spectrum of 6-fluoro-6-nitro-7-(p-tolyl)-3-oxatricyclo[3.2.1.0^{2,4}]octane (**4c**)

S65

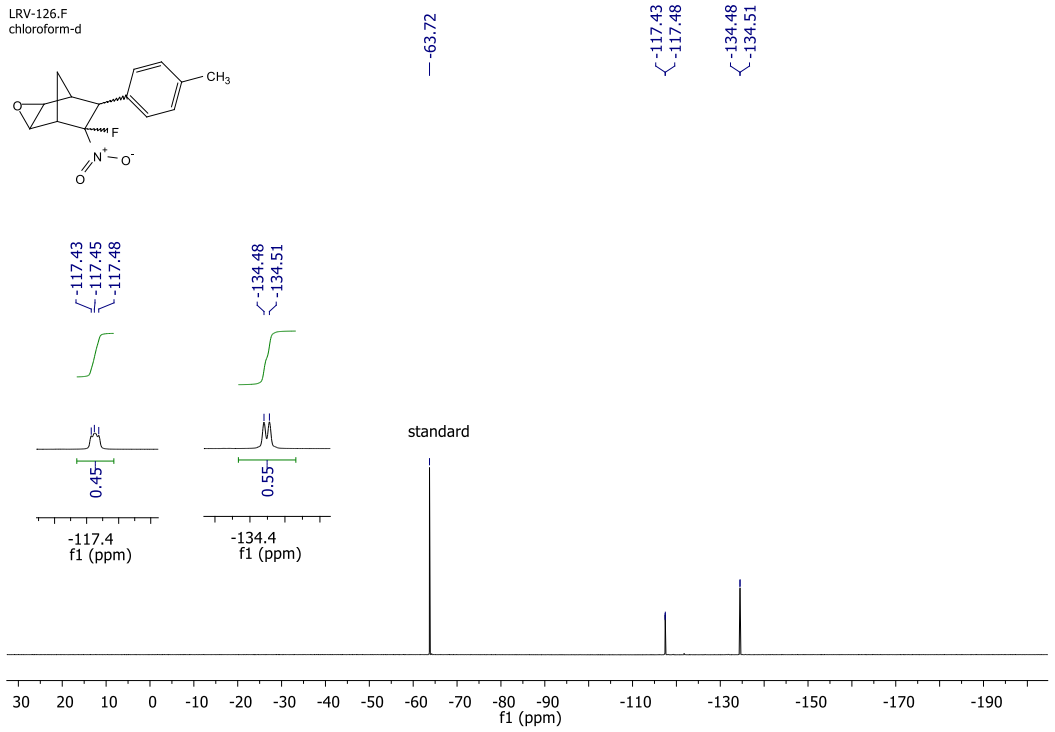

^{19}F NMR spectrum of 6-fluoro-6-nitro-7-(p-tolyl)-3-oxatricyclo[3.2.1.0^{2,4}]octane (**4c**)

S66

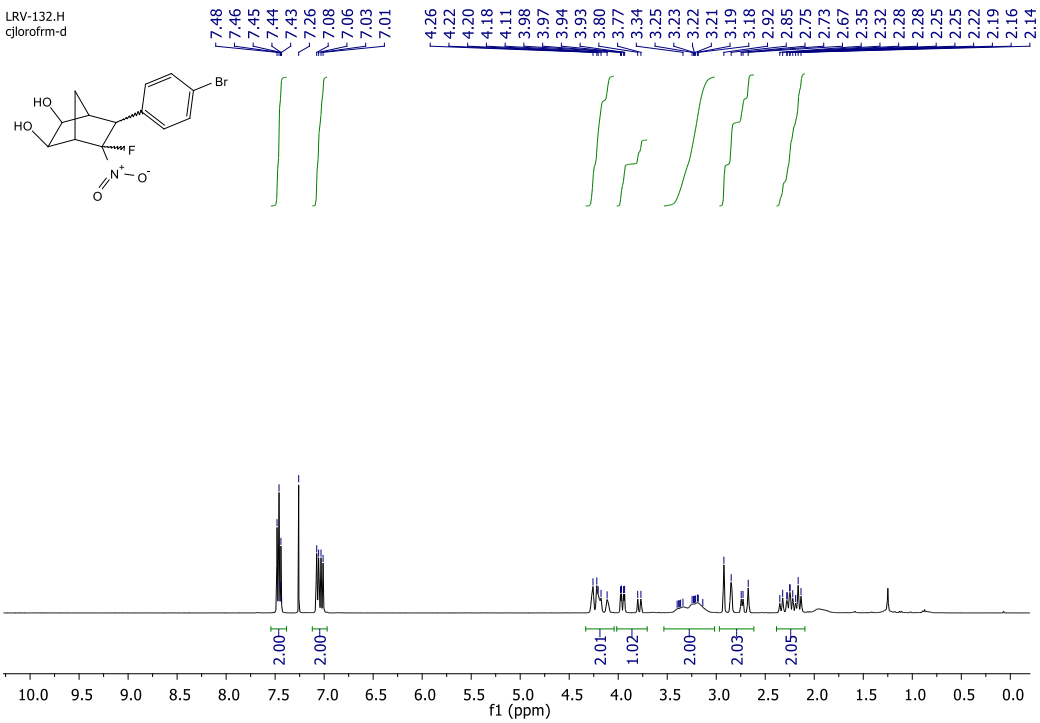

^{1}H NMR spectrum of 6-(4-bromophenyl)-5-fluoro-5-nitrobicyclo[2.2.1]heptane-2,3-diol (**5**)

S67

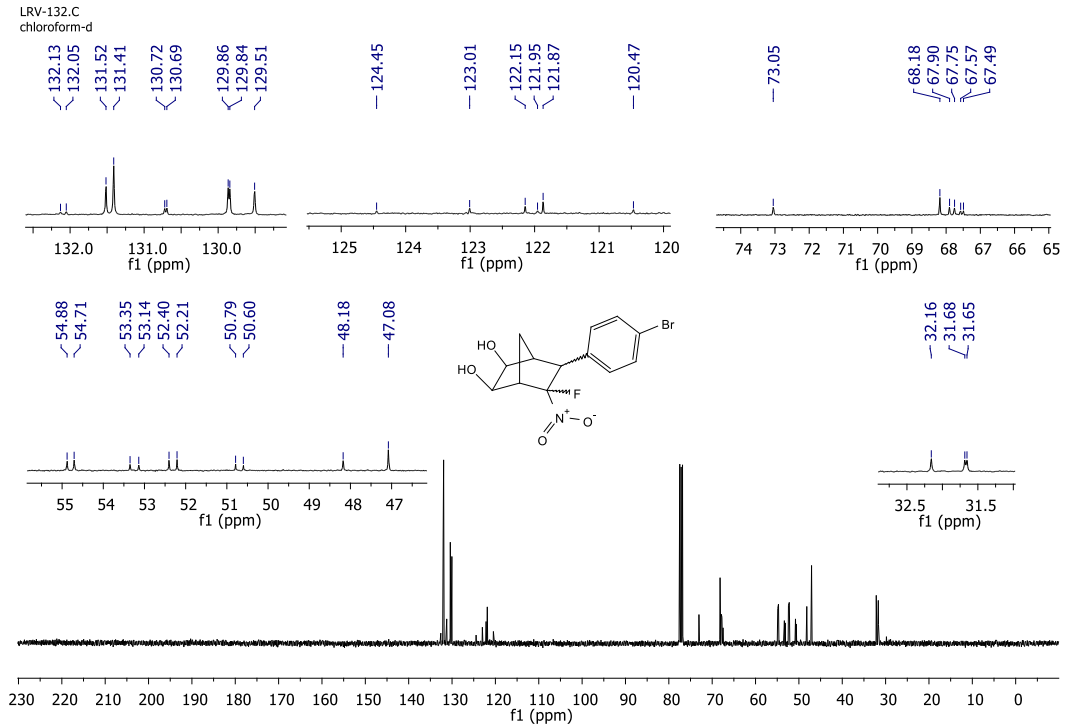

^{13}C NMR spectrum of 6-(4-bromophenyl)-5-fluoro-5-nitrobicyclo[2.2.1]heptane-2,3-diol (**5**)

S68

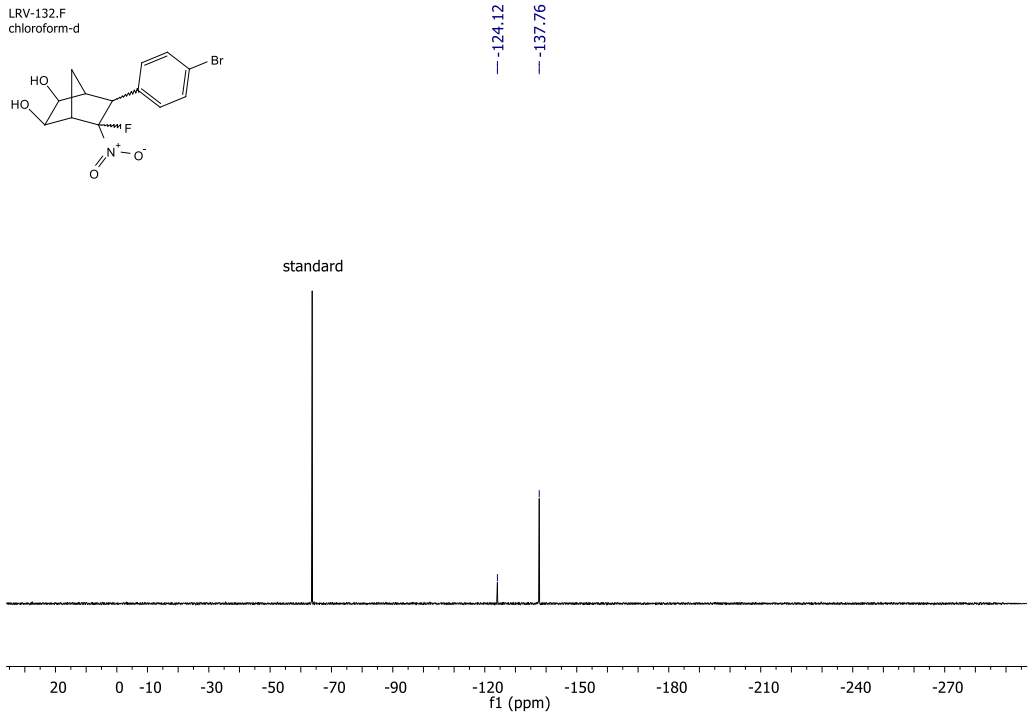

^{19}F NMR spectrum of 6-(4-bromophenyl)-5-fluoro-5-nitrobicyclo[2.2.1]heptane-2,3-diol (**5**)

S69

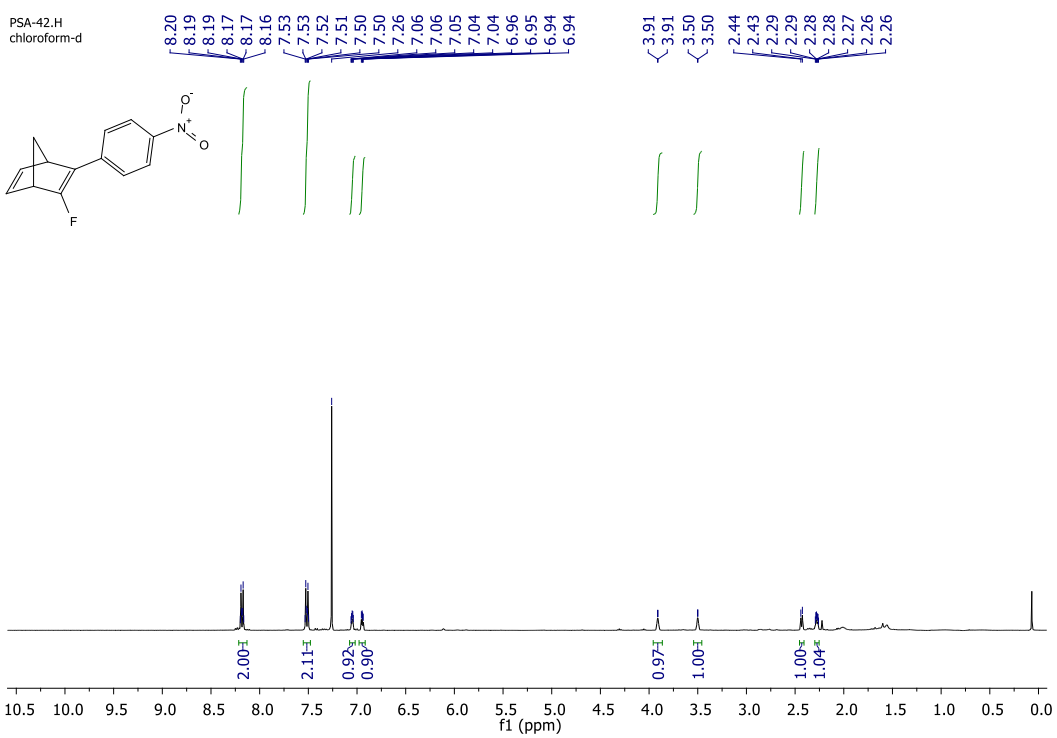

^{1}H NMR spectrum of 2-fluoro-3-(4-nitrophenyl)bicyclo[2.2.1]hepta-2,5-diene (**6**)

S70

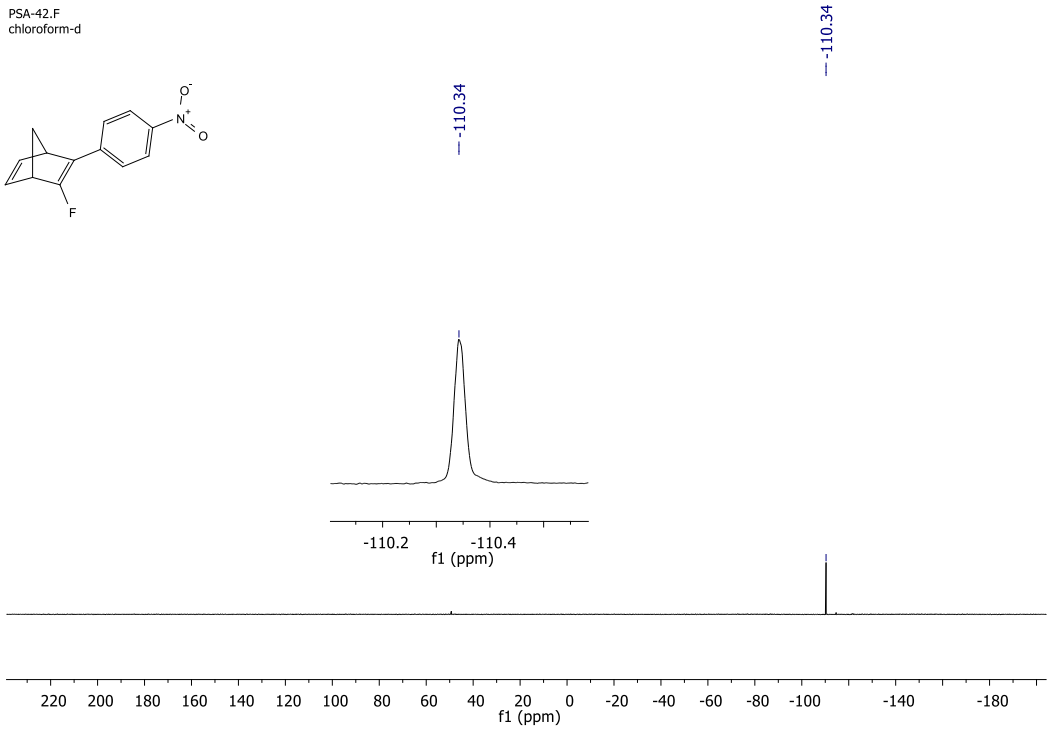

^{19}F NMR spectrum of 2-fluoro-3-(4-nitrophenyl)bicyclo[2.2.1]hepta-2,5-diene (**6**)

S71

2. Experimental section

All reagents were purchased from commercial sources and used without any further purification. CPD was prepared by monomerization of dicyclopentadiene (DCPD). *o*-Xylene was dried before use by passing through a column charged with activated neutral alumina [1]. Melting points (M.p.) were measured with a Büchi B-545 melting point apparatus. NMR (^{1}H, ^{13}C and ^{19}F) spectra were obtained with Bruker AV-400 and Agilent 400-MR spectrometers using deuterated chloroform ($CDCl_3$). Chemical shifts for ^{1}H NMR spectroscopic data were referenced to internal tetramethylsilane (δ = 0.0 ppm) and the residual solvent resonance (δ = 7.26 ppm); chemical shifts for ^{13}C NMR spectroscopic data were referenced to the residual solvent resonance (δ = 77.16 ppm); chemical shifts for ^{19}F NMR spectroscopic data were referenced to $PhCF_3$ (δ = −63.72 ppm). Data are reported as follows: chemical shift, integration multiplicity (s = singlet, d = doublet, t = triplet, q = quadruplet, qui = quintet, sext = sextet, sept = septet, br = board, m = multiplet, dd = *doublet of doublets*, ddd = *doublet of doublet of doublets*) and coupling constants (Hz). The starting β-fluoro-β-nitrostyrenes were prepared according to the described procedure and all are known compounds [2,3].

General procedure for the Diels–Alder reaction of β-fluoro-β-nitrostyrenes and 1,3-dienes

Analogous as described in [3], in a typical experiment, β-fluoro-β-nitrostyrene **1** (0.5 mmol, 1 mol equiv), *o*-xylene (0.2 mL), and diene (2.5–5.0 mmol, 5–10 mol equiv) were successively loaded into a screw-top vial filled with argon. After the cap was screwed tightly, the reaction mixture was heated at 110–130 °C with vigorous stirring for the appropriate time (8–24 h). After completion of the reaction (^{1}H NMR analysis monitoring), the excess of the diene and *o*-xylene were evaporated under vacuum. The pure product was isolated by column chromatography using mixture of Hex/DCM as eluent.

(1*R,4*S**,5*R**,6*R**)-5-Fluoro-5-nitro-6-phenylbicyclo[2.2.1]hept-2-ene** (*endo*-**2a**; major isomer) and **(1*R**,4*S**,5*S**,6*S**)-5-fluoro-5-nitro-6-phenylbicyclo[2.2.1]hept-2-ene** (*exo*-**2a**; minor isomer). Eluent: Hex/DCM 4:1, Hex/DCM 1:1; 0.097 g (74 %); *dr* = 45:55; yellowish oil. Anal. calcd for $C_{13}H_{12}FNO_2$ (%): C, 66.94; H, 5.19; N, 6.01; Found: C, 66.88; H, 5.31; N, 6.21. ^{1}H NMR (400 MHz, $CDCl_3$): (major isomer) δ = 1.88 – 2.00 (m, 1H), 2.38 (dd, *J* = 9.6, 0.7 Hz, 1H), 3.37 (s, 1H), 3.52 (s, 1H), 4.21 (dd, *J* = 9.4, 3.0 Hz, 1H), 6.30 (dd, *J* = 5.3, 3.5 Hz, 1H), 6.68 – 6.80 (m, 1H), 7.18 (d, *J* = 7.5 Hz, 1H), 7.26 – 7.45 (m, 4H) ppm; (minor isomer) δ = 2.12 (dd, *J* = 9.6, 1.3 Hz, 1H), 2.45 (d, *J* = 9.5 Hz, 1H), 3.34 (s, 1H), 3.38 – 3.42 (m, 1H), 3.84 (dd, *J* = 10.9, 2.8 Hz, 1H), 6.17 – 6.22 (m, 1H), 6.68 – 6.80 (m, 1H), 7.18 (d, *J* = 7.5 Hz, 1H), 7.26 – 7.45 (m, 4H) ppm; ^{13}C NMR (100 MHz, $CDCl_3$): (major isomer) δ = 47.6, 48.9 (d, $^{3}J_{CF}$ = 1.1 Hz), 53.6 (d, $^{2}J_{CF}$ = 20.5 Hz), 55.9 (d, $^{2}J_{CF}$ = 17.8 Hz), 125.6 (d, $^{1}J_{CF}$ = 252.3 Hz), 127.7, 128.4, 128.7, 132.5 (d, $^{3}J_{CF}$ = 4.4 Hz), 135.1 (d, $^{3}J_{CF}$ = 3.4 Hz), 140.3 (d, $^{4}J_{CF}$ = 1.2 Hz) ppm; (minor isomer) δ = 46.4, 48.0, 51.6 (d, $^{2}J_{CF}$ = 22.5 Hz), 52.8 (d, $^{2}J_{CF}$ = 19.2 Hz), 125.8 (d, $^{1}J_{CF}$ = 253.2 Hz), 127.7, 128.6, 129.2 (d, $^{4}J_{CF}$ = 1.1 Hz), 132.7 (d, $^{3}J_{CF}$ = 6.3 Hz), 135.2 (d, $^{3}J_{CF}$ = 7.1 Hz), 143.4 (d, $^{4}J_{CF}$ = 2.2 Hz) ppm; ^{19}F NMR (376 MHz, $CDCl_3$): (major isomer) δ = -127.56 (s) ppm; (minor isomer) δ = -122.81 (s) ppm.

(1*R,4*S**,5*R**,6*R**)-5-Fluoro-5-nitro-6-(*p*-tolyl)bicyclo[2.2.1]hept-2-ene** (*endo*-**2b**; major isomer) and **(1*R**,4*S**,5*S**,6*S**)-5-fluoro-5-nitro-6-(*p*-tolyl)bicyclo[2.2.1]hept-2-ene** (*exo*-**2b**; minor isomer). Eluent: Hex/DCM 3:1; Hex/DCM, 2:1; Hex/DCM, 1:1. 0.238 g (70 %); *dr* = 48:52; yellowish oil. Anal. calcd for $C_{14}H_{14}FNO_2$ (%):C, 68.00; H, 5.71; N, 5.66; Found: C, 68.19; H, 5.67; N, 5.58. ^{1}H NMR (400 MHz, $CDCl_3$): (major isomer) δ = 1.93 – 2.00 (m, 1H), 2.41 (s, 3H), 2.55 – 2.51 (m, 1H), 3.37 (s, 1H), 3.54 (s, 1H), 4.20 (dd, *J* = 9.4, 3.0 Hz, 1H), 6.31 (dd, *J* = 5.4, 3.4 Hz, 1H), 6.78 (dd, *J* = 5.6, 2.9 Hz, 1H), 7.17 (d, *J* = 8.1 Hz, 2H), 7.23 (s, 2H) ppm; (minor isomer) δ = 2.14 (dd, *J* = 9.6, 1.3 Hz, 1H), 2.38 (s, 3H), 2.39 – 2.44 (m, 1H), 3.33 (s, 1H), 3.39 – 3.44 (m, 1H), 3.83 (dd, *J* = 10.8, 2.8 Hz, 1H), 6.18 – 6.25 (m, 1H), 6.72 – 6.76 (m, 1H), 7.11 (d, *J* = 7.6 Hz, 2H), 7.23 (s, 2H) ppm; ^{13}C NMR (100 MHz, $CDCl_3$): (major isomer) δ = 21.0, 47.5, 48.9 (d, $^3J_{CF}$ = 1.0 Hz), 53.5 (d, $^2J_{CF}$ = 20.5 Hz), 55.65 (d, $^2J_{CF}$ = 17.8 Hz), 125.5 (d, $^1J_{CF}$ = 252.0 Hz), 129.1, 129.3, 132.0 (d, $^3J_{CF}$ = 3.5 Hz), 132.3 (d, $^3J_{CF}$ = 4.4 Hz), 137.4, 140.3 (d, $^4J_{CF}$ = 1.1 Hz) ppm; (minor isomer) δ = 21.1, 46.4, 47.0, 51.5 (d, $^2J_{CF}$ = 22.5 Hz), 52.5 (d, $^2J_{CF}$ = 19.2 Hz), 125.7 (d, $^1J_{CF}$ = 252.7 Hz), 128.4, 129.1, 132.1 (d, $^3J_{CF}$ = 7.3 Hz), 132.5 (d, $^3J_{CF}$ = 6.2 Hz), 137.3, 143.3 (d, $^4J_{CF}$ = 2.3 Hz) ppm. ^{19}F NMR (376 MHz, $CDCl_3$): (major isomer) δ = -128.64 (s) ppm; (minor isomer) δ = -123.79 – -123.79 (m) ppm.

(1*R,4*S**,5*R**,6*R**)-6-(4-(*tert*-Butyl)phenyl)-5-fluoro-5-nitrobicyclo[2.2.1]hept-2-ene** (*endo*-**2c**; major isomer) and **(1*R**,4*S**,5*S**,6*S**)-6-(4-(*tert*-butyl)phenyl)-5-fluoro-5-nitrobicyclo[2.2.1]hept-2-ene** (*exo*-**2c**; minor isomer). Eluent: Hex/DCM 4:1, Hex/DCM 2:1; 0.114 g (88 %); *dr* = 48:52; yellowish oil. Anal. calcd for $C_{17}H_{20}FNO_2$ (%): C, 70.57; H, 6.97; N, 4.84, Found: C, 70.37; H, 7.17; N, 4.85. ^{1}H NMR (400 MHz, $CDCl_3$): (major isomer) δ = 1.32 (s, 9H), 1.89 – 1.97 (m, 1H), 2.38 (dd, *J* = 9.6, 0.9 Hz, 1H), 3.35 (s, 1H), 3.50 – 3.54 (m, 1H), 4.18 (dd, *J* = 9.5, 3.0 Hz, 1H), 6.30 (dd, *J* = 5.5, 3.4 Hz, 1H), 6.76 (dd, *J* = 5.6, 2.9 Hz, 1H), 7.07 – 7.14 (m, 2H), 7.31 – 7.37 (m, 2H) ppm; (minor isomer) δ = 1.34 (s, 9H), 2.11 (dd, *J* = 9.6, 1.4 Hz, 1H), 2.42 – 2.49 (m, 1H), 3.31 (s, 1H), 3.37 – 3.42 (m, 1H),), 3.79 (dd, *J* = 11.0, 2.8 Hz, 1H), 6.16 – 6.22 (m, 1H), 6.68 – 6.74 (m, 1H), 7.23 (d, *J* = 8.3 Hz, 2H), 7.37 – 7.43 (m, 2H) ppm; ^{13}C NMR (100 MHz, $CDCl_3$): (major isomer) δ = 31.4, 34.5, 47.7, 49.0 (d, $^3J_{CF}$ = 1.0 Hz), 53.7 (d, $^2J_{CF}$ = 20.5 Hz), 55.7 (d, $^2J_{CF}$ = 18.0 Hz), 125.3, 125.6 (d, $^1J_{CF}$ = 252.0 Hz), 128.3, 132.1 (d, $^3J_{CF}$ = 3.4 Hz), 132.4 (d, $^3J_{CF}$ = 4.4 Hz), 140.4 (d, $^4J_{CF}$ = 1.1 Hz), 150.6 ppm; (minor isomer) δ = 31.4, 34.6, 46.6, 48.0, 51.6 (d, $^2J_{CF}$ = 22.4 Hz), 52.6 (d, $^2J_{CF}$ = 19.4 Hz), 125.6, 125.8 (d, $^1J_{CF}$ = 253.0 Hz), 129.0 (d, $^4J_{CF}$ = 1.0 Hz), 132.1 (d, $^3J_{CF}$ = 7.3 Hz), 132.6 (d, $^3J_{CF}$ = 6.1 Hz), 143.4 (d, $^4J_{CF}$ = 2.3 Hz), 150.6 ppm. ^{19}F NMR (376 MHz, $CDCl_3$): (major isomer) δ = -128.55 (s) ppm; (minor isomer) δ = -123.90 – - 123.81 (m) ppm.

(1*R,4*S**,5*R**,6*R**)-6-(4-Chlorophenyl)-5-fluoro-5-nitrobicyclo[2.2.1]hept-2-ene** (*endo*-**2d**; major isomer) and **(1*R**,4*S**,5*S**,6*S**)-6-(4-chlorophenyl)-5-fluoro-5-nitrobicyclo[2.2.1]hept-2-ene** (*exo*-**2d**; minor isomer). Eluent: Hex/DCM 4:1, Hex/DCM 2:1; 0.123 g (90 %) [scale-up: 1.057 g (83 %)], *dr* = 41:59; colorless oil. Anal. calcd for $C_{13}H_{11}ClFNO_2$ (%): C, 58.33; H, 4.14; N, 5.23, Found: C, 58.61; H, 4.09; N, 5.31. ^{1}H NMR (400 MHz, $CDCl_3$): (major isomer) δ = 1.89 – 1.99 (m, 1H), 2.35 (dd, *J* = 9.8,

0.9 Hz, 1H), 3.32 (s, 1H), 3.53 (s, 1H), 4.14 (dd, *J* = 9.3, 3.1 Hz, 1H), 6.30 (dd, *J* = 5.5, 3.4 Hz, 1H), 6.66 – 6.73 (m, 1H), 7.09 (d, *J* = 7.2 Hz, 2H), 7.24 – 7.30 (m, 2H) ppm; (minor isomer) δ = 2.11 (dd, *J* = 9.7, 1.4 Hz, 1H), 2.34- 2.40 (m, 1H), 3.28 (s, 1H), 3.36 – 3.43 (m, 1H), 3.76 (dd, *J* = 10.7, 2.8 Hz, 1H), 6.15 – 6.22 (m, 1H), 6.66 – 6.74 (m, 1H), 7.22 (d, *J* = 8.5 Hz, 2H), 7.30 – 7.36 (m, 2H) ppm; ^{13}C NMR (100 MHz, $CDCl_3$): (major isomer) δ = 47.6, 48.9 (d, $^3J_{CF}$ = 1.2 Hz), 53.5 (d, $^2J_{CF}$ = 20.4 Hz), 55.3 (d, $^2J_{CF}$ = 17.7 Hz), 125.3 (d, $^1J_{CF}$ = 252.2 Hz), 128.5, 130.6 (d, $^4J_{CF}$ = 1.3 Hz), 132.8 (d, $^3J_{CF}$ = 4.5 Hz), 133.6 (d, $^3J_{CF}$ = 3.1 Hz), 133.7, 140.0 (d, $^4J_{CF}$ = 1.1 Hz); (minor isomer) δ = 46.3, 47.7, 51.4 (d, $^2J_{CF}$ = 22.3 Hz), 52.2 (d, $^2J_{CF}$ = 19.0 Hz), 125.6 (d, $^1J_{CF}$ = 252.8 Hz), 128.79, 130.0, 132.8 (d, $^3J_{CF}$ = 6.0 Hz), 133.6, 133.7 (d, $^3J_{CF}$ = 7.3 Hz), 143.2 (d, $^4J_{CF}$ = 2.2 Hz) ppm; ^{19}F NMR (376 MHz, $CDCl_3$): (major isomer) δ = -128.63 (s) ppm; (minor isomer) δ = -123.69 – -123.53 (m) ppm.

(1*R,4*S**,5*R**,6*R**)-6-(2,4-Dichlorophenyl)-5-fluoro-5-nitrobicyclo[2.2.1]hept-2-ene** (*endo*-**2e**; major isomer) and **(1*R**,4*S**,5*S**,6*S**)-6-(2,4-dichlorophenyl)-5-fluoro-5-nitrobicyclo[2.2.1]hept-2-ene** (*exo*-**2e**; minor isomer). Eluent: Hex/DCM 4:1, Hex/DCM 1:1; 0.125 g (97 %), *dr* = 46:54; yellowish solid; M.p. 93-94 °C. Anal. calcd for $C_{13}H_{10}Cl_2FNO_2$ (%): C, 51.68; H, 3.34; N, 4.64; found: C, 51.97; H, 3.59; N, 4.71. ^{1}H NMR (400 MHz, $CDCl_3$): (major isomer) δ = 1.93 (dd, *J* = 9.4, 5.1 Hz, 1H), 2.44 (d, *J* = 9.6 Hz, 1H), 3.31 (s, 1H), 3.45 (s, 1H), 4.78 (dd, *J* = 10.0, 2.8 Hz, 1H), 6.32 (dd, *J* = 8.7, 3.5 Hz, 1H), 6.74 (dd, *J* = 5.4, 2.8 Hz, 1H), 7.09 – 7.22 (m, 1H), 7.28 (s, 1H), 7.32 – 7.42 (m, 1H) ppm; (minor isomer) δ = 2.10 (d, *J* = 9.4 Hz, 1H), 2.34 (d, *J* = 9.3 Hz, 1H), 3.25 (s, 1H), 3.36 (s, 1H), 4.10 (dd, *J* = 10.3, 2.5 Hz, 1H), 6.16 (s, 1H), 6.70 (s, 1H), 7.09 – 7.22 (m, 1H), 7.28 (s, 1H), 7.32 – 7.42 (m, 1H) ppm; ^{13}C NMR (100 MHz, $CDCl_3$): (major isomer) δ = 47.5, 49.2 (d, $^3J_{CF}$ = 1.1 Hz), 51.5 (d, $^2J_{CF}$ = 17.4 Hz), 54.4 (d, $^2J_{CF}$ = 20.2 Hz), 125.0 (d, $^1J_{CF}$ = 254.1 Hz), 127.0, 129.4, 130.6 (d, $^3J_{CF}$ = 3.8 Hz), 131.95 (d, $^3J_{CF}$ = 2.6 Hz), 132.9, 132.9, 136.2, 140.1 ppm; (minor isomer) δ = 46.8, 48.4, 50.4 (d, $^2J_{CF}$ = 18.6 Hz), 53.0 (d, $^2J_{CF}$ = 22.2 Hz), 123.3 (d, $^1J_{CF}$ = 256.7 Hz), 127.4, 129.0, 129.5, 132.9, 132.9 (d, $^3J_{CF}$ = 5.3 Hz), 134.2, 136.4, 141.7 (d, $^4J_{CF}$ = 2.5 Hz) ppm; ^{19}F NMR (376 MHz, $CDCl_3$): (major isomer) δ = -128.84 (s) ppm; (minor isomer) δ = -126.50 (s) ppm.

(1*R,4*S**,5*R**,6*R**)-6-(4-Bromophenyl)-5-fluoro-5-nitrobicyclo[2.2.1]hept-2-ene** (*endo*-**2f**; major isomer) and **(1*R**,4*S**,5*S**,6*S**)-6-(4-bromophenyl)-5-fluoro-5-nitrobicyclo[2.2.1]hept-2-ene** (*exo*-**2f**; minor isomer). Eluent: Hex/DCM 4:1, Hex/DCM 2:1; 0.115 g (90 %) [scale-up: 0.926 g (73 %)]; *dr* = 43:57; yellowish oil. Anal. calcd for $C_{13}H_{11}BrFNO_2$ (%): C, 50.02; H, 3.55; N, 4.49; found: C, 50.02; H, 3.67; N, 4.40. ^{1}H NMR (400 MHz, $CDCl_3$): (major isomer) δ = 1.88 – 1.98 (m, 1H), 2.34 (d, *J* = 9.8 Hz, 1H), 3.32 (s, 1H), 3.52 (s, 1H), 4.12 (dd, *J* = 9.3, 3.0 Hz, 1H), 6.30 (dd, *J* = 5.4, 3.5 Hz, 1H), 6.64 – 6.74 (m, 1H), 7.03 (d, *J* = 7.6 Hz, 2H), 7.39 – 7.45 (m, 2H) ppm; (minor isomer) δ = 2.10 (dd, *J* = 9.7, 1.3 Hz, 1H), 2.36 (d, *J* = 9.8 Hz, 1H), 3.27 (s, 1H), 3.39 (s, 1H), 3.75 (dd, *J* = 10.7, 2.7 Hz, 1H), 6.15 – 6.21 (m, 1H), 6.64 – 6.74 (m, 1H), 7.16 (d, *J* = 8.4 Hz, 2H), 7.44 – 7.52 (m, 2H) ppm; ^{13}C NMR (100 MHz, $CDCl_3$):

(major isomer) δ = 47.6, 48.9 (d, $^{3}J_{CF}$ = 1.0 Hz), 53.5 (d, $^{2}J_{CF}$ = 20.4 Hz), 55.3 (d, $^{2}J_{CF}$ = 17.7 Hz), 121.9, 125.3 (d, $^{1}J_{CF}$ = 252.2 Hz), 131.0 (d, $^{4}J_{CF}$ = 1.2 Hz), 131.6, 132.86 (d, $^{3}J_{CF}$ = 4.2 Hz), 134.1 (d, $^{3}J_{CF}$ = 3.4 Hz), 140.0 ppm; (minor isomer) δ = 46.3, 47.8, 51.5 (d, $^{2}J_{CF}$ = 22.2 Hz), 52.3 (d, $^{2}J_{CF}$ = 19.1 Hz), 121.8, 125.6 (d, $^{1}J_{CF}$ = 253.2 Hz), 130.4, 131.8, 132.9 (d, $^{3}J_{CF}$ = 6.3 Hz), 134.3 (d, $^{3}J_{CF}$ = 7.2 Hz), 143.2 (d, $^{4}J_{CF}$ = 2.3 Hz) ppm; ^{19}F NMR (376 MHz, $CDCl_3$): (major isomer) δ = -128.60 (s) ppm; (minor isomer) -123.57 (s) ppm.

(1*R,4*S**,5*R**,6*R**)-5-Fluoro-6-(4-methoxyphenyl)-5-nitrobicyclo[2.2.1]hept-2-ene** (*endo*-**2g**; major isomer) and **(1*R**,4*S**,5*S**,6*S**)-5-fluoro-6-(4-methoxyphenyl)-5-nitrobicyclo[2.2.1]hept-2-ene** (*exo*-**2g**; minor isomer). Eluent: Hex/DCM 10:1, Hex/DCM 5:1; 0.095 g (68 %); *dr* = 45:55; pale brown oil. Anal. calcd for $C_{14}H_{14}FNO_3$ (%): C, 63.87; H, 5.36; N, 5.32; Found: C, 63.92; H, 5.40; N, 5.27. ^{1}H NMR (400 MHz, $CDCl_3$): (major isomer) δ = 1.88 –1.96 (m, 1H), 2.36 (dd, *J* = 9.6, 0.9 Hz, 1H), 3.30 (s, 1H), 3.51 (s, 1H), 3.78 (s, 3H), 4.12 (dd, *J* = 9.5, 3.0 Hz, 1H), 6.29 (dd, *J* = 5.4, 3.4 Hz, 1H), 6.67 – 6.75 (m, 1H), 6.81 – 6.87 (m, 2H), 7.09 (dd, *J* = 8.8, 0.7 Hz, 2H) ppm; (minor isomer) δ = 2.09 (dd, *J* = 9.6, 1.3 Hz, 1H), 2.42 (d, *J* = 9.5 Hz, 1H), 3.26 (s, 1H), 3.43 – 3.41 (m, 1H), 3.74 (dd, *J* = 10.5, 2.3 Hz, 1H), 3.81 (s, 3H), 6.14 – 6.22 (m, 1H), 6.67 – 6.75 (m, 1H), 6.81 – 6.87 (m, 2H), 7.20 (d, *J* = 8.6 Hz, 2H) ppm; ^{13}C NMR (100 MHz, $CDCl_3$): (major isomer) δ = 47.8, 49.0 (d, $^{3}J_{CF}$ = 1.2 Hz), 53.6 (d, $^{2}J_{CF}$ = 20.5 Hz), 55.3, 55.4 (d, $^{2}J_{CF}$ = 18.1 Hz), 113.8, 125.5 (d, $^{1}J_{CF}$ = 251.6 Hz), 127.1 (d, $^{3}J_{CF}$ = 4.0 Hz), 129.7, 132.5 (d, $^{3}J_{CF}$ = 4.4 Hz), 140.32 (d, $^{4}J_{CF}$ = 1.2 Hz), 159.1 ppm; (minor isomer) δ = 46.7, 47.9, 51.5 (d, $^{2}J_{CF}$ = 22.5 Hz), 52.4 (d, $^{2}J_{CF}$ = 19.3 Hz), , 55.3, 114.1, 125.6 (d, $^{1}J_{CF}$ = 252.6 Hz), 127.1 (d, $^{3}J_{CF}$ = 7.0 Hz), , 130.4 (d, $^{4}J_{CF}$ = 1.0 Hz), 132.6 (d, $^{3}J_{CF}$ = 6.2 Hz), 143.4 (d, $^{4}J_{CF}$ = 2.3 Hz), 159.2 ppm; ^{19}F NMR (376 MHz, $CDCl_3$): (major isomer) δ = -128.61 (s) ppm, (minor isomer) δ = -123.8 (s) ppm.

Methyl 4-((1*R,2*R**,3*R**,4*S**)-3-fluoro-3-nitrobicyclo[2.2.1]hept-5-en-2-yl)benzoate** (*endo*-**2h**; major isomer) and **methyl 4-((1*R**,2*S**,3*S**,4*S**)-3-fluoro-3-nitrobicyclo[2.2.1]hept-5-en-2-yl)benzoate** (*exo*-**2h**; minor isomer). Eluent: Hex/DCM 2:1, Hex/DCM 1:1, Hex/DCM 1:2; 0.127 g (95 %), *dr* = 45:55; pale yellow solid; M.p. 72-75 °C. Anal. calcd for $C_{15}H_{14}FNO_4$ (%): C, 61.85; H, 4.84; N, 4.81, Found: C, 62.11; H, 4.90; N, 4.94. ^{1}H NMR (400 MHz, $CDCl_3$): (major isomer) δ = 1.88 – 1.97 (m, 1H), 2.33 (dd, *J* = 9.7, 1.0 Hz, 1H), 3.35 (br s, 1H), 3.48 – 3.53 (m, 1H), 3.87 (s, 3H), 4.21 (dd, *J* = 9.2, 3.1 Hz, 1H), 6.27 (dd, *J* = 5.6, 3.4 Hz, 1H), 6.69 (dd, *J* = 5.5, 2.9 Hz, 1H), 7.14 – 7.24 (m, 2H), 7.90 – 7.97 (m, 2H) ppm; (minor isomer) δ = 2.07 – 2.14 (m, 1H), 2.35 – 2.41 (m, 1H), 3.32 (br s, 1H), 3.35 – 3.40 (m, 1H), 3.83 (dd, *J* = 10.5, 3.2 Hz, 1H), 3.89 (s, 3H), 6.11 – 6.20 (m, 1H), 6.69 (dd, *J* = 5.5, 2.9 Hz, 1H), 7.31 – 7.36 (m, 2H), 7.97 –8.01 (m, 2H) ppm; ^{13}C NMR (100 MHz, $CDCl_3$): (major isomer) δ = 47.4, 48.8 (d, $^{3}J_{CF}$ = 1.5 Hz), 52.2, 53.5 (d, $^{2}J_{CF}$ = 20.4 Hz), 55.6 (d, $^{2}J_{CF}$ = 17.6 Hz), 125.4 (d, $^{1}J_{CF}$ = 252.7 Hz), 129.2 (d, $^{4}J_{CF}$ = 1.8 Hz), 129.4, 129.5, 132.8 (d, $^{3}J_{CF}$ = 4.5 Hz), 140.0 (d, $^{4}J_{CF}$ = 1.5 Hz), 140.2 (d, $^{3}J_{CF}$ = 3.4 Hz), 166.7 ppm; (minor

isomer) δ = 46.1 (d, $^{3}J_{CF}$ = 0.9 Hz), 47.8 (d, $^{3}J_{CF}$ = 1.1 Hz), 51.5 (d, $^{2}J_{CF}$ = 22.2 Hz), 52.2, 52.6 (d, $^{2}J_{CF}$ = 19.0 Hz), 125.8 (d, $^{1}J_{CF}$ = 253.4 Hz), 128.6 (d, $^{4}J_{CF}$ = 0.7 Hz), 129.5, 129.8, 132.8 (d, $^{3}J_{CF}$ = 6.3 Hz), 140.4 (d, $^{3}J_{CF}$ = 7.2 Hz), 143.1 (d, $^{4}J_{CF}$ = 2.4 Hz), 166.7 ppm; ^{19}F NMR (376 MHz, $CDCl_3$): (major isomer) δ = -128.55 (s) ppm; (minor isomer) -123.67 (s) ppm.

(1*R,4*S**,5*R**,6*R**)-5-Fluoro-5-nitro-6-(4-(trifluoromethyl)phenyl)bicyclo[2.2.1]hept-2-ene** (*endo*-**2i**; major isomer) and **(1*R**,4*S**,5*S**,6*S**)-5-fluoro-5-nitro-6-(4-(trifluoromethyl)phenyl)bicyclo[2.2.1]hept-2-ene** (*exo*-**2i**; minor isomer). Eluent: Hex/DCM, 5:1, Hex/DCM, 2:1; 0.130 g (80 %); *dr* = 38:62; colorless oil. Anal. calcd for $C_{14}H_{11}F_4NO_2$: C, 55.82; H, 3.68; N, 4.65; found: C, 56.06; H, 3.50; N, 4.49. ^{1}H NMR (400 MHz, $CDCl_3$): (major isomer) δ = 1.92 – 2.03 (m, 1H), 2.31 – 2.46 (m, 1H), 3.38 (s, 1H), 3.56 (s, 1H), 4.24 (dd, *J* = 9.0, 2.1 Hz, 1H), 6.29 – 6.37 (m, 1H), 6.65 – 6.77 (m, 1H), 7.29 (d, *J* = 7.9 Hz, 2H), 7.56 (d, *J* = 8.1 Hz, 2H) ppm; (minor isomer) δ = 2.15 (d, *J* = 9.5 Hz, 1H), 2.31 – 2.46 (m, 1H), 3.34 (s, 1H), 3.42 (s, 1H), 3.86 (dd, *J* = 10.6, 1.6 Hz,1H), 6.17– 6.24 (m, 1H), 6.65 – 6.77 (m, 1H), 7.42 (d, *J* = 8.0 Hz, 2H), 7.62 (d, *J* = 8.0 Hz, 2H) ppm; ^{13}C NMR (100 MHz, $CDCl_3$): (major isomer) δ = 47.6, 48.9 (d, $^{3}J_{CF}$ = 1.0 Hz), 53.5 (d, $^{2}J_{CF}$ = 20.3 Hz), 55.5 (d, $^{2}J_{CF}$ = 17.5 Hz), 124.1 (q, $^{1}J_{CF}$ = 272.1 Hz), 125.3 (q, $^{3}J_{CF}$ = 3.6 Hz), 125.4 (d, $^{1}J_{CF}$ = 252.6 Hz), 129.7 (d, $^{4}J_{CF}$ = 1.2 Hz), 130.0 (q, $^{2}J_{CF}$ = 32.0 Hz), 133.0 (d, $^{3}J_{CF}$ = 4.0 Hz), 139.2, 139.9 (d, $^{4}J_{CF}$ = 0.9 Hz) ppm; (minor isomer) δ = 46.2, 47.8, 51.5 (d, $^{2}J_{CF}$ = 22.2 Hz), 52.5 (d, $^{2}J_{CF}$ = 19.0 Hz), 124.1 (q, $^{1}J_{CF}$ = 272.1 Hz), 125.6 (q, $^{3}J_{CF}$ = 3.6 Hz), 125.8 (d, $^{1}J_{CF}$ = 253.4 Hz), 129.1, 130.0 (q, $^{2}J_{CF}$ = 32.0 Hz), 133.0 (d, $^{3}J_{CF}$ = 5.2 Hz), 139.4 (d, $^{3}J_{CF}$ = 7.9 Hz), 143.2 (d, $^{4}J_{CF}$ = 2.2 Hz) ppm; ^{19}F NMR (376 MHz, $CDCl_3$): (major isomer) δ = -128.41 (s, 1F), -63.70 (s, 3F) ppm; (minor isomer) δ = 123.38 (s, 1F), -63.65 (s, 3F) ppm.

4-((1*R,2*R**,3*R**,4*S**)-3-Fluoro-3-nitrobicyclo[2.2.1]hept-5-en-2-yl)benzonitrile** (*endo*-**2j**; major isomer) and **4-((1*R**,2*S**,3*S**,4*S**)-3-fluoro-3-nitrobicyclo[2.2.1]hept-5-en-2-yl)benzonitrile** (*exo*-**2j**; minor isomer). Eluent: Hex/DCM, 1:1; Hex/DCM, 1:2; 0.101 g (75 %); *dr* = 34:66; colorless oil. Anal. calcd for $C_{14}H_{11}FN_2O_2$ (%): C, 65.11; H, 4.29; N, 10.85; Found: C, 65.38; H, 4.32; N, 10.51. ^{1}H NMR (400 MHz, $CDCl_3$): (major isomer) δ = 1.91 – 2.01 (m, 1H), 2.32 (s, 1H), 3.37 (s, 1H), 3.55 (s, 1H), 4.21 (dd, *J* = 9.1, 3.0 Hz, 1H), 6.31 (dd, *J* = 5.4, 3.4 Hz, 1H), 6.66 – 6.73 (m, 1H), 7.25 – 7.30 (m, 2H), 7.61 – 7.66 (m, 2H) ppm; (minor isomer) δ = 2.13 (dd, *J* = 9.8, 1.4 Hz, 1H), 2.35 (s, 1H), 3.33 (s, 1H), 3.39 – 3.43 (m, 1H), 3.83 (dd, *J* = 10.7, 2.8 Hz, 1H), 6.16 – 6.21 (m, 1H), 6.66 – 6.73 (m, 1H), 7.41 (d, *J* = 8.2 Hz, 2H), 7.60 – 7.67 (m, 2H) ppm. ^{13}C NMR (100 MHz, $CDCl_3$): (major isomer) δ = 47.4, 48.8 (d, $^{3}J_{CF}$ = 1.1 Hz), 53.3 (d, $^{2}J_{CF}$ = 20.3 Hz), 55.5 (d, $^{2}J_{CF}$ = 17.4 Hz), 111.6, 118.6, 125.2 (d, $^{1}J_{CF}$ = 252.7 Hz), 130.0 (d, $^{4}J_{CF}$ = 1.5 Hz), 132.1, 133.1 (d, $^{3}J_{CF}$ = 4.4 Hz), 139.7 (d, $^{4}J_{CF}$ = 1.0 Hz), 140.5 (d, $^{3}J_{CF}$ = 3.1 Hz) ppm; (minor isomer) δ = 45.9, 47.6, 51.28 (d, $^{2}J_{CF}$ = 22.1 Hz), 52.53 (d, $^{2}J_{CF}$ = 18.9 Hz), 111.6, 118.6, 125.74 (d, $^{1}J_{CF}$ = 253.2 Hz), 129.45, 132.32, 133.0 (d, $^{3}J_{CF}$ = 6.2 Hz), 140.67 (d, $^{3}J_{CF}$ = 7.4 Hz), 143.01 (d, $^{4}J_{CF}$ = 2.2 Hz) ppm; ^{19}F NMR (376 MHz, $CDCl_3$): (major isomer) δ = -128.48 (s) ppm ; (minor isomer) δ = -123.31 (s) ppm.

(1*R,4*S**,5*R**,6*R**)-5-Fluoro-5-nitro-6-(3-nitrophenyl)bicyclo[2.2.1]hept-2-ene** (*endo*-**2k**; major isomer) and **(1*R**,4*S**,5*S**,6*S**)-5-fluoro-5-nitro-6-(3-nitrophenyl)bicyclo[2.2.1]hept-2-ene** (*exo*-**2k**; minor isomer). Eluent: Hex/DCM, 3:1, Hex/DCM, 2:1; 0.112 g (80%); *dr* = 31:69; greenish oil. Anal. calcd for $C_{13}H_{11}FN_2O_4$ (%): C, 56.12; H, 3.98; N, 10.07; Found: C, 56.33; H, 3.99; N, 9.95; ^{1}H NMR (400 MHz, $CDCl_3$): (major isomer) δ = 1.93 – 2.06 (m, 1H), 2.36 (dd, *J* = 9.8, 1.0 Hz, 1H), 3.41 (s, 1H), 3.58 (s, 1H), 4.27 (dd, *J* = 9.1, 3.1 Hz, 1H), 6.37 (dd, *J* = 5.5, 3.4 Hz, 1H), 6.69 – 6.78 (m, 1H), 7.44 – 7.52 (m, 2H), 8.04 (s, 1H), 8.09 – 8.19 (m, 1H) ppm; (minor isomer) δ = 2.18 (dd, *J* = 9.9, 1.3 Hz, 1H), 2.40 (dd, *J* = 9.9, 1.2 Hz, 1H), 3.38 (s, 1H), 3.45 (dd, *J* = 8.5, 6.7 Hz, 1H), 3.89 (dd, *J* = 10.6, 2.7 Hz, 1H), 6.15 – 6.27 (m, 1H), 6.69 – 6.78 (m, 1H), 7.44 – 7.57 (m, 1H), 7.65 (d, *J* = 7.8 Hz, 1H), 8.09 – 8.19 (m, 2H) ppm; ^{13}C NMR (100 MHz, $CDCl_3$): (major isomer) δ = 47.6, 48.9 (d, $^3J_{CF}$ = 1.5 Hz), 53.4 (d, $^2J_{CF}$ = 20.3 Hz), 55.2 (d, $^2J_{CF}$ = 17.4 Hz), 122.8, 124.0 (d, $^4J_{CF}$ = 1.8 Hz), 125.1 (d, $^1J_{CF}$ = 252.5 Hz), 129.4, 133.4 (d, $^3J_{CF}$ = 4.3 Hz), 135.8 (d, $^3J_{CF}$ = 1.8 Hz), 137.2 (d, $^3J_{CF}$ = 3.4 Hz), 139.6 (d, $^4J_{CF}$ = 1.5 Hz), 148.3 ppm; (minor isomer) δ = 46.1 (d, $^3J_{CF}$ = 0.6 Hz), 47.6, 51.3 (d, $^2J_{CF}$ = 22.1 Hz), 52.2 (d, $^2J_{CF}$ = 18.8 Hz), 122.9, 123.0 (d, $^4J_{CF}$ = 0.6 Hz), 125.7 (d, $^1J_{CF}$ = 253.1 Hz), 129.6, 133.1 (d, $^3J_{CF}$ = 6.2 Hz), 135.5 (d, $^3J_{CF}$ = 0.5 Hz), 137.4 (d, $^3J_{CF}$ = 7.5 Hz), 143.0 (d, $^4J_{CF}$ = 2.3 Hz), 148.5 ppm; ^{19}F NMR (376 MHz, $CDCl_3$): (major isomer) δ = -128.40 (s) ppm; (minor isomer) δ = -123.02 (s) ppm.

(1*R,4*S**,5*R**,6*R**)-5-Fluoro-5-nitro-6-(4-nitrophenyl)bicyclo[2.2.1]hept-2-ene** (*endo*-**2l**; major isomer) and **(1*R**,4*S**,5*S**,6*S**)-5-fluoro-5-nitro-6-(4-nitrophenyl)bicyclo[2.2.1]hept-2-ene** (*exo*-**2l**; minor isomer). Eluent: Hex/DCM, 3:1; Hex/DCM, 2:1; 0.089 g (67 %) [scale-up: 0.705 g (71 %)]; *dr* = 40:60; brown oil. Anal. calcd for $C_{13}H_{11}FN_2O_4$ (%): C, 56.12; H, 3.98; N, 10.07, Found: C, 56.36; H, 4.18; N, 9.95. ^{1}H NMR (400 MHz, $CDCl_3$): (major isomer) δ = 1.96 – 2.03 (m, 1H), 2.32 – 2.41 (m, 1H), 3.38 – 3.42 (m, 1H), 3.56 – 3.59 (m, 1H), 4.27 (dd, *J* = 9.1, 3.1 Hz, 1H), 6.34 (dd, *J* = 5.6, 3.4 Hz, 1H), 6.70 (dd, *J* = 5.7, 2.8 Hz, 1H), 7.32 – 7.37 (m, 2H), 8.10 – 8.16 (m, 2H) ppm; (minor isomer) δ = 2.17 (dtd, *J* = 9.8, 2.8, 1.5 Hz, 1H), 2.32 – 2.41 (m, 1H), 3.34 – 3.39 (m, 1H), 3.41 – 3.46 (m, 1H), 3.89 (dd, *J* = 10.7, 2.9 Hz, 1H), 6.18 – 6.23 (m, 1H), 6.71 – 6.75 (m, 1H), 7.44 – 7.51 (m, 2H), 8.16 – 8.22 (m, 2H) ppm; ^{13}C NMR (100 MHz, $CDCl_3$): (major isomer) δ = 47.6, 48.9 (d, $^3J_{CF}$ = 1.5 Hz), 53.4 (d, $^2J_{CF}$ = 20.2 Hz), 55.3 (d, $^2J_{CF}$ = 17.3 Hz), 123.5, 125.2 (d, $^1J_{CF}$ = 252.8 Hz), 130.2 (d, $^4J_{CF}$ = 1.9 Hz), 133.3 (d, $^3J_{CF}$ = 4.3 Hz), 139.7 (d, $^4J_{CF}$ = 1.6 Hz), 142.5 (d, $^3J_{CF}$ = 3.2 Hz), 147.3 ppm; (minor isomer) δ = 46.1 (d, $^3J_{CF}$ = 0.6 Hz), 47.6, 51.3 (d, $^2J_{CF}$ = 21.9 Hz), 52.4 (d, $^2J_{CF}$ = 18.7 Hz), 123.7, 125.8 (d, $^1J_{CF}$ = 253.6 Hz), 129.6 (d, $^4J_{CF}$ = 0.6 Hz), 133.1 (d, $^3J_{CF}$ = 6.2 Hz), 142.7 (d, $^3J_{CF}$ = 7.3 Hz), 143.0 (d, $^4J_{CF}$ = 2.4 Hz), 147.4 ppm; ^{19}F NMR (376 MHz, $CDCl_3$): (major isomer) δ = -128.39 (s) ppm; (minor isomer) δ = -123.23 (s) ppm.

Methyl 4-((1*R,4*S**,5*S**,6*S**)-5-Fluoro-5-nitrospiro[bicyclo[2.2.1]heptane-7,1'-cyclopropan]-2-en-6-yl)benzoate** (*exo*-**2m**; major isomer) and **methyl 4-((1*R**,4*S**,5*R**,6*R**)-5-fluoro-5-nitrospiro[bicyclo[2.2.1]heptane-7,1'-cyclopropan]-2-en-6-yl)benzoate** (*endo*-**2m**; minor isomer).

Eluent: Hex/DCM, 2:1; Hex/DCM, 1:1; Hex/DCM, 1:3; 0.070 g (44 %); *dr* = 44:56; yellowish oil. Anal. calcd for $C_{17}H_{16}FNO_4$ (%): C, 64.35; H, 5.08; N, 4.41; found: C, 64.18; H, 5.18; N, 4.24. ^{1}H NMR (400 MHz, $CDCl_3$): (major isomer) δ = 0.53 – 0.68 (m, 2H), 0.71 – 0.81 (m, 1H), 0.96 (dd, *J* = 14.8, 7.6 Hz, 1H), 2.84 – 2.89 (m, 1H), 3.00 (br s, 1H), 3.90 (s, 3H), 4.04 (d, *J* = 11.8 Hz, 1H), 6.21 – 6.27 (m, 1H), 6.81 (dd, *J* = 5.8, 3.2 Hz, 1H), 7.37 (d, *J* = 8.3 Hz, 2H), δ 7.99 (d, *J* = 8.4 Hz, 2H) ppm; (minor isomer) δ = 0.53 – 0.68 (m, 2H), 0.71 – 0.81 (m, 1H), 1.01 – 1.11 (m, 1H), 2.68 – 2.74 (m, 1H), 3.18 (br s, 1H), 3.89 (s, 3H), 4.58 (dd, *J* = 9.6, 3.2 Hz, 1H), 6.40 (dd, *J* = 5.5, 3.5 Hz, 1H), 6.77 (dd, *J* = 5.7, 2.8 Hz, 1H), 7.31 (d, *J* = 7.5 Hz, 2H), 7.96 (d, *J* = 8.4 Hz, 2H) ppm; ^{13}C NMR (100 MHz, $CDCl_3$): (major isomer) δ = 10.2, 11.3 (d, $^4J_{CF}$ = 2.9 Hz), 44.8, 50.6, 52.2, 54.7 (d, $^2J_{CF}$ = 18.3 Hz), 57.3 (d, $^2J_{CF}$ = 21.0 Hz), 125.5 (d, $^1J_{CF}$ = 256.3 Hz), 129.3, 129.5 (d, $^4J_{CF}$ = 1.1 Hz), 129.6, 132.0 (d, $^3J_{CF}$ = 5.8 Hz), 140.1, 140.1 (d, $^3J_{CF}$ = 6.4 Hz), 166.8 ppm; (minor isomer) δ = 3.8, 5.4, 44.4 (d, $^3J_{CF}$ = 3.5 Hz), 52.2, 53.6, 55.0 (d, $^2J_{CF}$ = 17.7 Hz), 56.0 (d, $^2J_{CF}$ = 20.4 Hz), 126.4 (d, $^1J_{CF}$ = 252.0 Hz), 129.3, 129.4, 129.6, 132.2 (d, $^3J_{CF}$ = 3.1 Hz), 140.3 (d, $^3J_{CF}$ = 3.5 Hz), 143.5 (d, $^4J_{CF}$ = 1.5 Hz), 166.9 ppm; ^{19}F NMR (376 MHz, $CDCl_3$): (major isomer) δ = -127.47 (dd, *J* = 10.8, 5.7 Hz) ppm; (minor isomer) δ = -124.77 (d, *J* = 9.3 Hz) ppm;

(1*R,4*S**,5*S**,6*S**)-6-(2,4-Dichlorophenyl)-5-fluoro-5-nitrobicyclo[2.2.2]oct-2-ene** (*exo*-**3a**; major isomer) and **(1*R**,4*S**,5*R**,6*R**)-6-(2,4-dichlorophenyl)-5-fluoro-5-nitrobicyclo[2.2.2]oct-2-ene** (*endo*-**3a**; minor isomer). Eluent: Hex/DCM, 3:1; 0.051 g (32 %); [scale-up under microwave activation: 0.119 g (35 %)]; *dr* = 41:59; viscous pale yellow oil. Anal. calcd for $C_{14}H_{12}Cl_2FNO_2$: C, 53.19; H, 3.83; N, 4.43; found: C, 53.45; H, 3.87: N, 4.25; ^{1}H NMR (400 MHz, $CDCl_3$): (major isomer) δ = 1.32 – 1.62 (m, 2H), 1.88 –2.06 (m, 2H), 2.71 – 2.80 (m, 1H), 3.27 – 3.38 (m, 1H), 4.43 (dt, *J* = 14.4, 1.8 Hz, 1H), 6.22 – 6.29 (m, 1H), 6.67 (t, *J* = 7.4 Hz, 1H), 7.22 – 7.51 (m, 3H) ppm; (minor isomer) δ = 1.20 – 1.33 (m, 2H), 2.11 – 2.24 (m, 2H), 2.93 – 3.01 (m, 1H), 3.14 – 3.21 (m, 1H), 4.68 (dd, *J* = 12.4, 1.3 Hz, 1H), 6.29 – 6.35 (m, 1H), 6.71 (t, *J* = 7.3 Hz, 1H), 7.15 – 7.21 (m, 1H), 7.22 – 7.51 (m, 2H) ppm; ^{13}C NMR (100 MHz, $CDCl_3$): (major isomer) δ = 17.2, 19.8 (d, $^3J_{CF}$ = 3.9 Hz), 36.3, 39.4 (d, $^2J_{CF}$ = 21.9 Hz), 44.2 (d, $^2J_{CF}$ = 16.5 Hz), 124.0 (d, $^1J_{CF}$ = 247.6 Hz), 127.1, 128.99, 129.92, 130.62 (d, $^4J_{CF}$ = 2.2 Hz), 131.41, 134.09 (d, $^3J_{CF}$ = 11.6 Hz), 136.13, 137.89 ppm; ^{13}C NMR (100 MHz, $CDCl_3$): (minor isomer) δ = 19.99 (d, $^3J_{CF}$ = 4.3 Hz), 24.40, 36.58, 40.41 (d, $^2J_{CF}$ = 21.4 Hz), 48.85 (d, $^2J_{CF}$ = 17.6 Hz), 122.32 (d, $^1J_{CF}$ = 247.8 Hz), 126.88, 128.94 (d, $^3J_{CF}$ = 4.1 Hz), 129.35, 131.36 (d, $^4J_{CF}$ = 3.2 Hz), 131.51, 132.93 (d, $^3J_{CF}$ = 7.6 Hz), 134.75, 135.69 ppm; ^{19}F NMR (376 MHz, $CDCl_3$): (major isomer) δ = -128.89 (dd, *J* = 14.4, 2.1 Hz) ppm; (minor isomer) δ = -117.92 – -117.79 (m) ppm

Methyl 4-((1*R,2*S**,3*S**,4*S**)-3-fluoro-3-nitrobicyclo[2.2.2]oct-5-en-2-yl)benzoate** (*exo*-**3b**; major isomer) and **methyl 4-((1*R**,2*R**,3*R**,4*S**)-3-fluoro-3-nitrobicyclo[2.2.2]oct-5-en-2-yl)benzoate** (*endo*-**3b**; minor isomer). Eluent: Hex/DCM, 1:1; Hex/DCM, 2:3; Hex/DCM, 1:3; Hex/DCM, 1:5; Hex/DCM, 1:10; DCM; 0.042 g (28 %); *dr* = 33:67; yellowish oil. Anal. calcd for $C_{16}H_{16}FNO_4$ (%): C, 62.95; H, 5.28; N, 4.59; Found: C, 63.14; H, 5.27; N, 4.59. ^{1}H NMR (400 MHz, $CDCl_3$): (major isomer) δ = 1.40 – 1.55

(m, 2H), 1.98 – 2.25 (m, 2H), 3.03 – 3.10 (m, 1H), 3.25 – 3.34 (m, 1H), 3.88 (d, $^3J_{HF}$ = 15.8 Hz, 1H), 3.92 (s, 3H), 6.25 – 6.33 (m, 1H), 6.66 (t, *J* = 7.4 Hz, 1H), 7.27 – 7.38 (m, 2H), 7.97 – 8.07 (m, 2H) ppm; (minor isomer) δ = 1.30 – 1.41 (m, 2H), 1.77 – 1.97 (m, 2H), 3.02 (dd, *J* = 2.9, 1.6 Hz, 1H), 3.31 – 3.36 (m, 1H), 3.90 (s, 3H), 4.33 (d, $^3J_{HF}$ = 13.6 Hz, 1H), 6.29 – 6.36 (m, 1H), 6.75 (t, *J* = 7.2 Hz, 1H), 7.24 (d, *J* = 8.2 Hz, 2H), 7.91 – 7.98 (m, 2H) ppm; ^{13}C NMR (100 MHz, $CDCl_3$): (major isomer) δ = 17.2, 20.5 (d, $^3J_{CF}$ = 5.2 Hz), 35.7, 39.7 (d, $^2J_{CF}$ = 22.2 Hz), 49.6 (d, $^2J_{CF}$ = 18.7 Hz), 52.3, 121.6 (d, $^1J_{CF}$ = 250.9 Hz), 129.0, 129.4 (d, $^3J_{CF}$ = 3.0 Hz), 129.5, 129.8, 137.4, 140.0 (d, $^3J_{CF}$ = 5.4 Hz), 166.8 ppm; (minor isomer) δ = 19.0 (d, $^3J_{CF}$ = 4.2 Hz), 25.1, 36.5, 40.0 (d, $^2J_{CF}$ = 21.5 Hz), 51.9 (d, $^2J_{CF}$ = 17.8 Hz), 52.2, 123.8 (d, $^1J_{CF}$ = 245.6 Hz), 128.5 (d, $^3J_{CF}$ = 2.6 Hz), 129.0, 129.5, 129.7, 135.3, 141.0 (d, $^3J_{CF}$ = 8.2 Hz), 166.8 ppm; ^{19}F NMR (376 MHz, $CDCl_3$): (major isomer) δ = -127.25 (d, $^3J_{HF}$ = 15.8 Hz) ppm; (minor isomer) δ = -116.42 (d, $^3J_{HF}$ = 13.6 Hz) ppm

(1*R,4*S**,5*S**,6*S**)-5-Fluoro-5-nitro-6-(4-nitrophenyl)bicyclo[2.2.2]oct-2-ene** (*exo*-**3c**; major isomer) and **(1*R**,4*S**,5*R**,6*R**)-5-fluoro-5-nitro-6-(4-nitrophenyl)bicyclo[2.2.2]oct-2-ene** (*endo*-**3c**; minor isomer). Eluent: Hex/DCM, 2:1; Hex/DCM, 1:1; 0.038 g, (26 %); *dr* = 37:63; viscous pale brown oil. Anal. calcd for $C_{14}H_{13}FN_2O_4$ (%): C, 57.53; H, 4.48; N, 9.59; Found : C, 57.81; H, 4.49; N, 9.42. ^{1}H NMR (400 MHz, $CDCl_3$): (major isomer) δ = 1.44 – 1.56 (m, 2H), 1.98 – 2.10 (m, 1H), 2.11 – 2.22 (m, 1H), 3.04 – 3.10 (m, 1H), 3.30 – 3.41 (m, 1H), 3.92 (d, $^3J_{HF}$ = 15.7 Hz, 1H), 6.28 – 6.34 (m, 1H), 6.67 (t, *J* = 7.3 Hz, 1H), 7.38 – 7.50 (m, 2H), 8.16 – 8.27 (m, 2H) ppm; (minor isomer) δ = 1.33 – 1.44 (m, 2H), 1.76 – 1.86 (m, 1H), 1.94 (td, *J* = 9.4, 2.8 Hz, 1H), 2.99 – 3.05 (m, 1H), 3.30 – 3.41 (m, 1H), 4.38 (d, *J* = 13.5 Hz, 1H), 6.34 – 6.40 (m, 1H), 6.75 (t, *J* = 7.2 Hz, 1H), 7.35 (d, *J* = 8.8 Hz, 2H), 8.10 – 8.17 (m, 2H) ppm; ^{13}C NMR (100 MHz, $CDCl_3$): (major isomer) δ = 17.2, 20.3 (d, $^3J_{CF}$ = 5.1 Hz), 35.7, 39.5 (d, $^2J_{CF}$ = 22.1 Hz), 49.5 (d, $^2J_{CF}$ = 18.6 Hz), 121.3 (d, $^1J_{CF}$ = 250.6 Hz), 123.7, 129.6 (d, $^3J_{CF}$ = 7.1 Hz), 130.5 (d, $^4J_{CF}$ = 3.0 Hz), 137.2, 142.2 (d, $^3J_{CF}$ = 5.4 Hz), 147.3 ppm; (minor isomer) δ = 18.9 (d, $^3J_{CF}$ = 4.2 Hz), 25.04, 36.6, 39.8 (d, $^2J_{CF}$ = 21.3 Hz), 51.6 (d, $^2J_{CF}$ = 17.6 Hz), 123.6 (d, $^1J_{CF}$ = 245.8 Hz), 123.6, 129.0 (d, $^3J_{CF}$ = 2.4 Hz), 130.0, 134.9, 143.3 (d, $^3J_{CF}$ = 8.2 Hz), 147.5 ppm; ^{19}F NMR (376 MHz, $CDCl_3$): (major isomer) δ = -127.03 (d, $^3J_{HF}$ = 15.7 Hz) ppm; (minor isomer) δ = -116.12 (d, $^3J_{HF}$ = 13.5 Hz) ppm.

Methyl 4-((1*R,2*R**,3*S**,4*R**)-3-fluoro-4-methoxy-3-nitrobicyclo[2.2.2]oct-5-en-2-yl)benzoate** (*exo*-**3d**-5-F; 24 %) and **methyl 4-((1*R**,2*S**,3*R**,4*R**)-3-fluoro-4-methoxy-3-nitrobicyclo[2.2.2]oct-5-en-2-yl)benzoate** (*endo*-**3d**-5-F; 20 %) and **(methyl 4-((1*S**,2*R**,3*S**,4*S**)-3-fluoro-1-methoxy-3-nitrobicyclo[2.2.2]oct-5-en-2-yl)benzoate** (*endo*-**3d**-6-F; 33 %) and **methyl 4-((1*S**,2*S**,3*R**,4*S**)-3-fluoro-1-methoxy-3-nitrobicyclo[2.2.2]oct-5-en-2-yl)benzoate** (*exo*-**3d**-6-F; 23 %). Eluent: Hex/DCM, 1:1; Hex/DCM, 2:3; Hex/DCM, 1:3; Hex/DCM, 1:5; Hex/DCM, 1:10; DCM. 0.067 g (40 %); isomers ratio = (24:20) : (23:33); yellowish oil; Anal. calcd for $C_{17}H_{18}FNO_5$ (%): C, 60.89; H, 5.41; N, 4.18; found: C, 60.85; H, 5.66; N, 4.08. ^{1}H NMR (400 MHz, $CDCl_3$): (*exo*-**3d**-5-F) δ = 1.57 – 1.68 (m, 2H), 2.22 – 2.32 (m, 2H), 2.94 – 3.01 (m, 1H), 3.51 (d, *J* = 1.3 Hz, 3H), 3.90 (s, 3H), 4.18 (d, $^3J_{HF}$ = 13.7 Hz, 1H), 6.50

(d, *J* = 8.6 Hz, 1H), 6.74 (dd, *J* = 8.6, 6.4 Hz, 1H), 7.13 (d, *J* = 8.4 Hz, 2H), 7.92 – 7.97 (m, 2H) ppm; (*endo*-**3d**-5-F) δ = 1.57 – 1.68 (m, 2H), 2.22 – 2.32 (m, 2H), 3.11 – 3.21 (m, 1H), 3.44 (s, 3H), 3.83 (d, $^{3}J_{HF}$ = 17.0 Hz, 1H), 3.91 (s, 3H), 6.37 – 6.44 (m, 1H), 6.61 (dd, *J* = 8.6, 6.7 Hz, 1H), 7.22 (d, *J* = 8.2 Hz, 2H), 7.98 – 8.02 (m, 2H) ppm; (*endo*-**3d**-6-F) δ = 1.51 – 1.74 (m, 2H), 2.07 – 2.34 (m, 2H), 3.25 (s, 3H), 3.26 – 3.34 (m, 1H), 3.91 (s, 3H), 4.13 (d, $^{3}J_{HF}$ = 15.0 Hz, 1H), 6.19 – 6.32 (m, 1H), 6.75 (d, *J* = 8.8 Hz, 1H), 7.37 (dd, *J* = 8.2, 1.4 Hz, 2H), 8.02 (d, *J* = 8.3 Hz, 2H) ppm; (*exo*-**3d**-6-F) δ = 1.51 – 1.74 (m, 2H), 2.07 – 2.34 (m, 2H), 3.18 (s, 3H), 3.26 – 3.34 (m, 1H), 3.89 (s, 3H), 4.56 (d, $^{3}J_{HF}$ = 12.7 Hz, 1H), 6.19 – 6.32 (m, 1H), 6.68 (d, *J* = 8.4 Hz, 1H), 7.27 (d, *J* = 5.2 Hz, 2H), 7.95 (d, *J* = 8.3 Hz, 2H) ppm; ^{13}C NMR (100 MHz, $CDCl_3$): δ = 18.7, 18.8, 20.5 (d, $^{3}J_{CF}$ = 3.4 Hz), 23.2, 23.8, 26.0, 27.4, 29.8, 34.1, 36.1, 39.0 (d, $^{2}J_{CF}$ = 22.2 Hz), 39.6 (d, $^{2}J_{CF}$ = 21.7 Hz), 41.2, 50.8, 51.8, 52.2, 52.3, 52.3, 53.1 (d, $^{2}J_{CF}$ = 18.5 Hz), 53.2 (d, $^{2}J_{CF}$ = 19.7 Hz), 53.6 (d, $^{3}J_{CF}$ = 2.1 Hz), 55.0 (d, $^{2}J_{CF}$ = 18.7 Hz), 55.4 (d, $^{2}J_{CF}$ = 17.7 Hz), 77.4, 79.0, 80.1, 81.3 (d, $^{3}J_{CF}$ = 4.3 Hz), 81.5, 120.8 (d, $^{1}J_{CF}$ = 250.1 Hz), 122.0 (d, $^{1}J_{CF}$ = 249.9 Hz), 123.1 (d, $^{1}J_{CF}$ = 246.4 Hz), 123.5 (d, $^{1}J_{CF}$ = 250.5 Hz), 126.5 (d, $^{4}J_{CF}$ = 1.2 Hz), 127.3 (d, $^{3}J_{CF}$ = 7.8 Hz), 128.1, 128.8 (d, $^{4}J_{CF}$ = 1.7 Hz), 128.8, 129.2 (d, $^{4}J_{CF}$ = 2.8 Hz), 129.4, 129.5, 129.7 (d, $^{3}J_{CF}$ = 10.9 Hz), 129.8, 129.9, 129.9, 130.0, 130.4, 130.5, 131.3 (d, *J* = 2.7 Hz), 133.2 (d, $^{3}J_{CF}$ = 4.6 Hz), 134.1 (d, $^{3}J_{CF}$ = 5.3 Hz), 137.0 (d, $^{3}J_{CF}$ = 5.6 Hz), 137.5 (d, $^{3}J_{CF}$ = 8.4 Hz), 137.9, 138.9, 139.4 (d, $^{3}J_{CF}$ = 5.8 Hz), 140.2 (d, $^{3}J_{CF}$ = 8.6 Hz), 166.7, 166.8, 166.9, 166.9 ppm. ^{19}F NMR (376 MHz, $CDCl_3$): (*exo*-**3d**-5-F) δ = -127.17 (dd, *J* = 13.7, 6.2 Hz) ppm; *(endo*-**3d**-5-F) δ = -136.93 (d, *J* = 17.0 Hz) ppm; (*endo*-**3d**-6-F) δ = -123.81 (d, *J* = 15.0 Hz) ppm; (*exo*-**3d**-6-F) δ = -114.71 – -114.50 (m) ppm.

General procedure for the epoxidation of cycloadducts 2. In a typical experiment, *m*-chloroperbenzoic acid (0.6 mmol) was added to solution of norbornene **2** (0.2 mmol) in DCM (1 mL). The reaction mixture was stirred overnight at room temperature. The reaction was monitored by TLC. After completion of the reaction the reaction mixture was poured into a saturated solution of $Na_2S_2O_3$ (10 mL) The resulting mixture was then extracted with DCM (3 × 15 mL). The combined organic layer was washed with saturated solution of $NaHCO_3$ (3 × 50 mL), dried over Na_2SO_4, filtered, and concentrated under vacuum. The pure product was isolated by column chromatography on neutral alumina using mixture of Hex/DCM in an appropriate ratio as the eluent.

(1*S,2*S**,4*R**,5*S**,6*S**,7*R**)-7-(4-Bromophenyl)-6-fluoro-6-nitro-3-oxatricyclo[3.2.1.02,4]octane** (*endo*-**4a**; major isomer) and **(1*S**,2*S**,4*R**,5*S**,6*R**,7*S**)-7-(4-bromophenyl)-6-fluoro-6-nitro-3-oxatricyclo[3.2.1.0^{2,4}]octane** (*exo*-**4a**; minor isomer). Eluent: Hex/DCM, 3:1; Hex/DCM, 2:1; 0.051 g, (81 %); *dr* = 41:59; yellowish viscous oil; HRMS (ESI-TOF) m/z: calcd for $C_{13}H_{12}{}^{80}BrFNO_3$ $[M+H]^+$ = 327.9985; found 327.9985. ^{1}H NMR (400 MHz, $CDCl_3$): (major isomer) δ = 1.73 – 1.78 (m, 2H), 3.08 – 3.19 (m, 1H), 3.29 (s, 1H), 3.47 – 3.52 (m, 1H), 3.58 (dd, *J* = 3.4, 0.8 Hz, 1H), 4.01 (dd, *J* = 11.2, 3.5 Hz, 1H), 7.13 (dd, *J* = 8.4, 1.4 Hz, 2H), 7.44 – 7.52 (m, 2H) ppm; (minor isomer) δ = 1.79 (br s, 1H), 1.85 – 1.92 (m, 1H), 3.00 (s, 1H), 3.08 –3.19 (m, 1H), 3.40 (d, *J* = 2.9 Hz, 1H), 3.54 (d, *J* = 2.9 Hz, 1H), 3.81 (dd,

J = 11.8, 2.7 Hz, 1H), 7.07 (d, *J* = 8.4 Hz, 2H), 7.44 –7.52 (m, 2H) ppm; ^{13}C NMR (100 MHz, $CDCl_3$): (major isomer) δ = 24.6 (d, $^3J_{CF}$ = 4.7 Hz), 41.6, 46.7 (d, $^3J_{CF}$ = 15.3 Hz), 47.9 (d, $^2J_{CF}$ = 16.8 Hz), 48.9, 54.3 (d, $^2J_{CF}$ = 18.5 Hz), 122.2, 123.2 (d, $^1J_{CF}$ = 255.4 Hz), 131.0 (d, $^4J_{CF}$ = 2.7 Hz), 131.4 (d, $^3J_{CF}$ = 2.8 Hz), 131.9 ppm; (minor isomer) δ = 25.2, 41.8, 47.0 (d, $^3J_{CF}$ = 8.6 Hz), 47.4 (d, $^2J_{CF}$ = 22.0 Hz), 50.3, 51.8 (d, $^2J_{CF}$ = 19.0 Hz), 122.3, 124.7 (d, $^1J_{CF}$ = 253.2 Hz), 130.3, 132.0, 132.6 (d, $^3J_{CF}$ = 7.5 Hz) ppm; ^{19}F NMR (376 MHz, $CDCl_3$): (major isomer) δ = -134.48 (d, $^3J_{HF}$ = 11.2 Hz) ppm, (minor isomer) δ = -117.21 (dd, *J* = 11.8, 7.3 Hz) ppm.

(1*S,2*S**,4*R**,5*S**,6*S**,7*R**)-6-Fluoro-6-nitro-7-(4-nitrophenyl)-3-oxatricyclo[3.2.1.0^{2,4}]octane** (*endo*-**4b**; major isomer) and **(1*S**,2*S**,4*R**,5*S**,6*R**,7*S**)-6-fluoro-6-nitro-7-(4-nitrophenyl)-3-oxatricyclo[3.2.1.02,4]octane** (*exo*-**4b**; minor isomer). Eluent: Hex/DCM, 2:1; Hex/DCM, 1:1; Hex/DCM, 1:2; 0.048 g, (85 %); *dr* = 33:67; pale brown viscous oil; HRMS (ESI-TOF) m/z: calcd for $C_{13}H_{12}FN_2O_5$ $[M+H]^+$ = 295.0730; found 295.0723; ^{1}H NMR (400 MHz, $CDCl_3$): (major isomer) δ = 1.71 – 1.87 (m, 2H), 3.25 (br s, 1H), 3.35 (br s, 1H), 3.50 – 3.54 (m, 1H), 3.57 (d, *J* = 3.3 Hz, 1H), 4.16 (dd, *J* = 11.3, 3.5 Hz, 1H), 7.43 – 7.50 (m, 2H), 8.16 – 8.25 (m, 2H) ppm; (minor isomer) δ = 1.71 – 1.87 (m, 1H), 1.90 – 1.98 (m, 1H), 3.09 (d, *J* = 1.0 Hz, 1H), 3.18 (d, *J* = 6.9 Hz, 1H), 3.41 (d, *J* = 3.2 Hz, 1H), 3.57 (d, *J* = 3.2 Hz, 1H), 3.97 (dd, *J* = 11.8, 2.8 Hz, 1H), 7.40 (d, *J* = 8.7 Hz, 2H), 8.25 – 8.16 (m, 2H) ppm; ^{13}C NMR (100 MHz, $CDCl_3$): (major isomer) δ = 24.6 (d, $^3J_{CF}$ = 4.8 Hz), 41.6, 46.6 (d, $^3J_{CF}$ = 15.4 Hz), 47.7 (d, $^2J_{CF}$ = 16.7 Hz), 54.3 (d, $^2J_{CF}$ = 18.3 Hz), 48.6, 123.0 (d, $^1J_{CF}$ = 255.8 Hz), 123.8, 130.3 (d, $^4J_{CF}$ = 2.9 Hz), 139.8 (d, $^3J_{CF}$ = 2.4 Hz), 147.5 ppm; (minor isomer) δ = 25.1, 41.7, 46.8 (d, $^3J_{CF}$ = 8.6 Hz), 47.3 (d, $^2J_{CF}$ = 21.9 Hz), 50.1, 51.8 (d, $^2J_{CF}$ = 18.7 Hz), 124.0, 124.7 (d, $^1J_{CF}$ = 253.5 Hz), 129.7, 140.9 (d, $^3J_{CF}$ = 7.6 Hz), 147.7 ppm; ^{19}F NMR (376 MHz, $CDCl_3$): (major isomer) δ = -134.34 (d, $^3J_{HF}$ = 11.3 Hz) ppm; (minor isomer) δ = -117.10 (dd, *J* = 11.8, 7.3) ppm.

(1*S,2*S**,4*R**,5*S**,6*S**,7*R**)-6-Fluoro-6-nitro-7-(*p*-tolyl)-3-oxatricyclo[3.2.1.0^{2,4}]octane** (*endo*-**4c**; major isomer) and **(1*S**,2*S**,4*R**,5*S**,6*R**,7*S**)-6-fluoro-6-nitro-7-(*p*-tolyl)-3-oxatricyclo[3.2.1.02,4]octane** (*exo*-**4c**; minor isomer). Eluent: Hex/DCM, 3:1; Hex/DCM, 2:1; 0.051 g, (87 %); *dr* = 45:55; pale yellow viscous oil; HRMS (ESI-TOF) m/z: calcd for $C_{14}H_{15}FNO_3$ $[M+H]^+$ = 264.1036; found 264.1032. ^{1}H NMR (400 MHz, $CDCl_3$): (major isomer) δ = 1.77 (s, 1H), 1.79 –1.92 (m, 1H), 2.35 (s, 3H), 3.15 (br s, 1H), 3.27 (s, 1H), 3.51 (dt, *J* = 3.4, 1.6 Hz, 1H), 3.66 (dd, *J* = 3.4, 1.1 Hz, 1H), 4.04 (dd, *J* = 11.7, 3.4 Hz, 1H), 7.09 (d, *J* = 8.1 Hz, 1H), 7.11 – 7.21 (m, 3H) ppm; (minor isomer) δ = 1.77 (s, 1H), 1.79 –1.92 (m, 1H), 2.35 (s, 3H), 3.02 (s, 1H), 3.10 (d, *J* = 6.6 Hz, 1H), 3.41 (d, *J* = 2.6 Hz, 1H), 3.54 (dd, *J* = 3.3, 1.1 Hz, 1H), 3.83 (dd, *J* = 11.9, 2.4 Hz, 1H), 7.09 (d, *J* = 8.1 Hz, 1H), 7.11 – 7.21 (m, 3H) ppm; ^{13}C NMR (100 MHz, $CDCl_3$): (major isomer) δ = 21.1, 24.6 (d, $^3J_{CF}$ = 4.6 Hz), 41.7, 46.9 (d, $^3J_{CF}$ = 15.5 Hz), 48.0 (d, $^2J_{CF}$ = 16.8 Hz), 49.3, 54.7 (d, $^2J_{CF}$ = 18.7 Hz), 123.4 (d, $^1J_{CF}$ = 255.2 Hz), 129.3 (d, $^4J_{CF}$ = 2.4 Hz), 129.4 (d, $^3J_{CF}$ = 2.9 Hz), 129.4, 137.8 ppm; (minor isomer) δ = 21.2, 25.3, 41.9, 47.2 (d, $^3J_{CF}$ = 8.5 Hz), 47.5 (d, $^2J_{CF}$ = 22.2 Hz), 50.5, 52.2 (d, $^2J_{CF}$ = 19.2 Hz), 124.9 (d, $^1J_{CF}$ = 253.0 Hz), 128.5, 129.6, 130.5

(d, $^3J_{CF}$ = 7.4 Hz), 138.0 ppm; ^{19}F NMR (376 MHz, $CDCl_3$): (major isomer) δ = -134.50 (d, *J* = 11.7 Hz) ppm; (minor isomer): δ = -117.45 (dd, *J* = 11.9, 7.3 Hz) ppm.

Dihydroxylation of the cycloadduct 2f. *N*-Methylmorpholine *N*-oxide (0.031 g, 1.5 mol equiv) was added to a solution of **2f** (0.056 g, 1 mol equiv) in 1.2 mL of acetone/water 3:1. Then, 100 µL of OsO_4 1% solution (0.001 g, 2 mol %) was added. Then reaction mixture was stirred for 5 h at room temperature. After reaction completion (TLC monitoring), the reaction mixture was concentrated under vacuum, poured in 20 mL of water and then extracted with EtOAc (3 × 20 mL). The combined organic extract was dried over Na_2SO_4, filtrated, and concentrated under vacuum. The pure product was isolated by column chromatography on silica using mixture of Hex/EtOAc as the eluent.

(1*S,2*S**,3*R**,4*S**,5*S**,6*R**)-6-(4-Bromophenyl)-5-fluoro-5-nitrobicyclo[2.2.1]heptane-2,3-diol** (*endo*-**5,** major isomer) and **(1*S**,2*S**,3*R**,4*S**,5*R**,6*S**)-6-(4-bromophenyl)-5-fluoro-5-nitrobicyclo[2.2.1]heptane-2,3-diol** (*exo*-**5,** minor isomer). Eluent: Hex/EtOAc 1:1, Hex/EtOAc 1:2; 0.040 g (65 %); colorless solid. HRMS (ESI) m/z: calcd for $C_{13}H_{13}{}^{107}Ag^{81}BrFNO_4$ $[M+Ag]^+$ = 453.9042; found 453.9042; ^{1}H NMR (400 MHz, $CDCl_3$): (major isomer) δ = 2.15 (d, *J* = 11.7 Hz, 1H), 2.26 (dd, *J* = 11.8, 1.5 Hz, 1H), 2.85 (s, 1H), 2.92 (s, 1H), 3.05 – 3.29 (m, 2H), 3.96 (dd, *J* = 12.7, 4.1 Hz, 1H), 4.22 (s, 1H), 4.26 (s, 1H), 7.07 (d, *J* = 7.7 Hz, 2H), 7.47 (d, *J* = 7.7 Hz, 2H) ppm; (minor isomer) δ = 2.20 (d, *J* = 11.7 Hz, 1H), 2.34 (d, *J* = 11.7 Hz, 1H), 2.67 (s, 1H), 2.74 (d, *J* = 7.4 Hz, 1H), 3.29 – 3.47 (m, 2H), 3.78 (d, *J* = 13.1 Hz, 1H), 4.11 (s, 1H), 4.18 (s, 1H), 7.02 (d, *J* = 8.4 Hz, 2H), 7.45 (d, *J* = 8.4 Hz, 2H) ppm. ^{13}C NMR (100 MHz, $CDCl_3$): (major isomer) δ = 31.7 (d, $^3J_{CF}$ = 3.1 Hz), 47.1, 52.4 (d, $^2J_{CF}$ = 19.6 Hz), 54.7 (d, $^2J_{CF}$ = 17.2 Hz), 67.8 (d, $^3J_{CF}$ = 14.6 Hz), 68.2, 121.7 (d, $^1J_{CF}$ = 255.6 Hz), 121.8, 130.5 (d, $^4J_{CF}$ = 2.3 Hz), 131.2 (d, $^3J_{CF}$ =2.9 Hz), 131.9 ppm; (minor isomer) δ = 32.2, 48.2, 50.7 (d, $^2J_{CF}$ = 19.0 Hz), 53.2 (d, $^2J_{CF}$ = 21.3 Hz), 67.5 (d, $^3J_{CF}$ = 8.3 Hz), 73.0, 122.1, 123.2 (d, $^1J_{CF}$ = 251.2 Hz), 130.0, 132.0, 132.6 (d, $^3J_{CF}$ = 7.8 Hz) ppm. ^{19}F NMR (376 MHz, $CDCl_3$): (major isomer) δ = - 137.76 (s) ppm; (minor isomer) δ =-124.12 (s) ppm.

Base-induced nitrous acid elimination from cycloadduct 3l. Cycloadduct **2l** (0.052 g, 1 mol equiv) was dissolved in THF (1 mL) and the solution was loaded into a vial covered with aluminum foil. Then, potassium *tert*-butoxide (2 mol equiv) was added in the darkness in several portions over 20 min to the vigorously stirred reaction mixture. The reaction mixture was stirred overnight at room temperature and the reaction was monitored by TLC. After completion of the reaction the reaction mixture was passed through a column charged with alumina and covered with an aluminum foil using DCM as eluent. The solution of the pure product **6** was collected in a flask covered with aluminum foil and then concentrated under vacuum.

2-Fluoro-3-(4-nitrophenyl)bicyclo[2.2.1]hepta-2,5-diene (**6**). 0.034 g (77 %); yellow oil; ^{1}H NMR (400 MHz, $CDCl_3$) δ = 2.28 (ddd, *J* = 6.5, 4.7, 1.9 Hz, 1H), 2.41 – 2.46 (m, 1H), 3.47 – 3.53 (m, 1H), 3.88 – 3.94 (m, 1H), 6.95 (dd, *J* = 4.5, 3.1 Hz, 1H), 7.05 (dt, *J* = 4.6, 2.2 Hz, 1H), 7.47 – 7.56 (m, 2H), 8.16 – 8.20

(m, 2H) ppm; ^{19}F NMR (376 MHz, $CDCl_3$): δ = -110.34 (s) ppm. The analysis of the sample was consistent with the previously reported data [4].

Kinetic studies

Experimental procedure. Analogous as described in [3], in a typical kinetic experiment, nitrostyrene **1h** (0.025 mmol; 1 mol equiv), *o*-xylene (0.1 mL), and 1,3-cyclopentadiene (0.1 mL; 49 mol equiv) or 1,3-cyclohexadiene (0.1 mL; 43 mol equiv) were successively loaded into a series of screw-top vials filled with argon. After the caps were screwed tightly, the reaction mixtures were heated in a thermostat at preset temperature (50–130 °C) with vigorous stirring for the set time. After the heating completion, the reaction mixtures were cooled, diluted with DCM, passed through a silica pad, and concentrated under vacuum. The resulting mixtures were analyzed by ^{1}H NMR spectroscopy. The ratio of isomers and conversions (*F*) were calculated from the integral values of characteristic peaks of the starting nitrostyrene **1h** and the products.

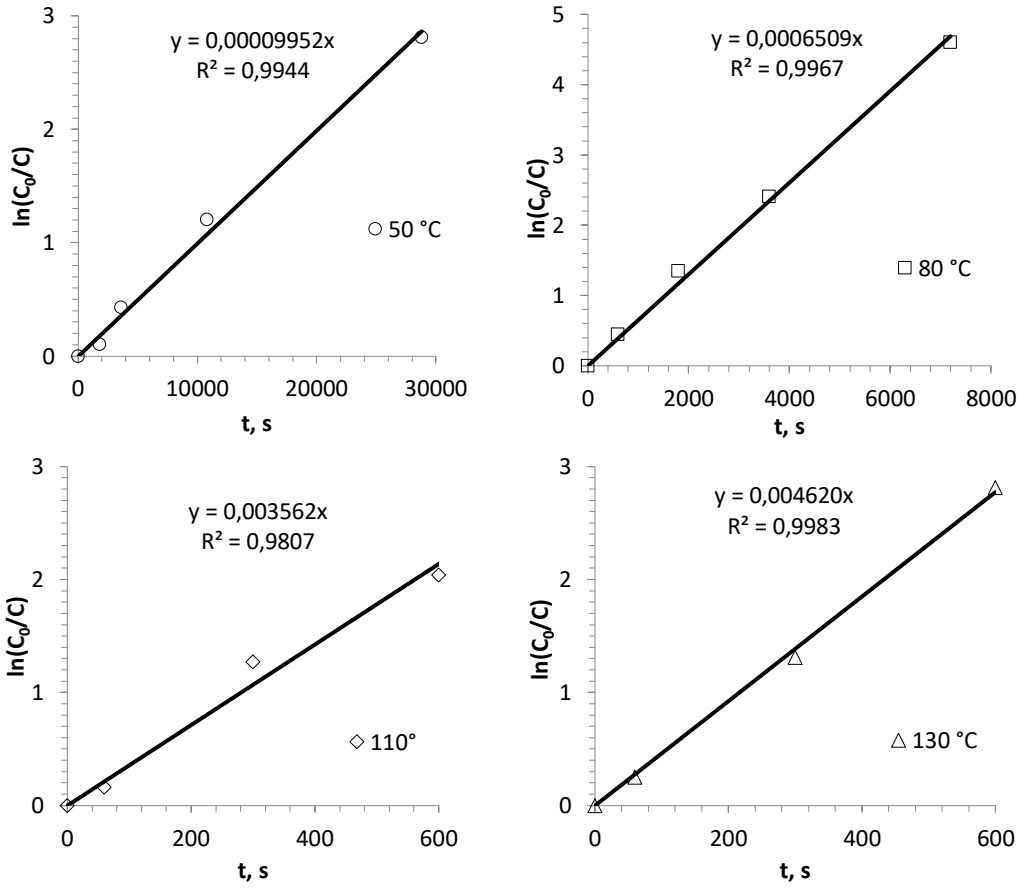

Figure S1: Plot of ln(C_0/C) *versus t* for the reactions of nitrostyrene **1h** with 1,3-cyclopentadiene at 50–130 °C.

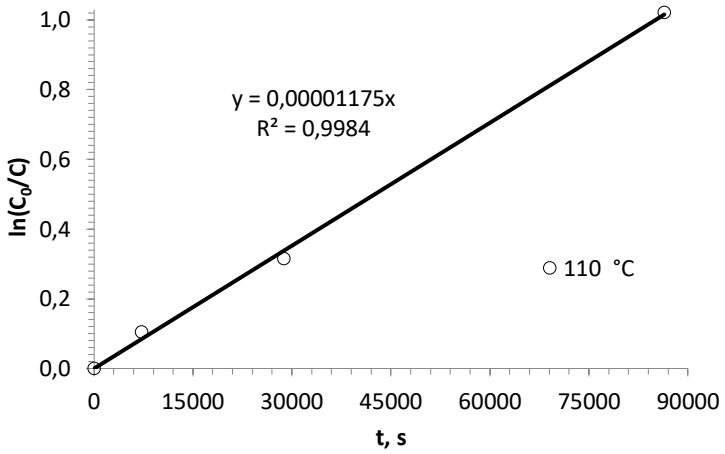

Figure S2: Plot of ln(C_0/C) *versus* t for the reaction of nitrostyrene **1h** with 1,3-cyclohexadiene at 110 °C.

3. Computational details

DFT calculations were performed using Gaussian 16, Rev. A.03[5]. The B3LYP [6,7,8] and M062X [9] functionals were used in conjunction with the 6-311+G(d,p) Pople basis set [10,11] and IEFPCM [12] solvation for *o*-xylene. The calculated ground states (GS) and transition states (TS) were confirmed by vibrational frequency analysis (GS: $N_{imag} = 0$, TS: $N_{imag} = 1$). Initial guesses for transition states were based on relaxed bond-length scan calculations (M062X/6-31G [13,14]) of the newly formed σ-bonds in the Diels–Alder reaction. Furthermore, IRC calculations confirmed that the transition states lead to the corresponding products and starting materials. Visual assessment of the vibration belonging to the imaginary frequency of the transition state using GaussView 6 [15] provided further confirmation of the transition state. In contrast to the geometry calculations, the frequency calculations for the thermochemical relevant energies were calculated at 383.15K with the corresponding optimized geometry.

Input Lines

Geometry optimization of a ground state:

#p opt=tight freq=noraman b3lyp/6-311+g(d,p) scrf=(iefpcm,solvent=o-xylene)

#p opt=tight freq=noraman m062x/6-311+g(d,p) scrf=(iefpcm,solvent=o-xylene)

Scan calculation (7 steps á 0.2 Å):

#p opt=modredundant m062x/6-31g scrf=(iefpcm,solvent=o-xylene)

Geometry optimization of a transition state:

#p opt=(calcfc,tight,ts,noeigen) freq=noraman scf=qc b3lyp/6-311+g(d,p) scrf=(iefpcm,solvent=o-xylene)

#p opt=(calcfc,tight,ts,noeigen) freq=noraman scf=qc m062x/6-311+g(d,p) scrf=(iefpcm,solvent=o-xylene)

IRC calculation of a transition state:

#p irc=(calcall,maxcyc=100) b3lyp/6-311+g(d,p) scrf=(iefpcm,solvent=o-xylene)

#p irc=(calcall,maxcyc=100) m062x/6-311+g(d,p) scrf=(iefpcm,solvent=o-xylene)

Frequency calucations for the thermochemical relevant energies:

#p freq=noraman b3lyp/6-311+g(d,p) scrf=(iefpcm,solvent=o-xylene) temperature=383.15

#p freq=noraman m062x/6-311+g(d,p) scrf=(iefpcm,solvent=o-xylene) temperature=383.15

Number of imaginary frequencies, enthalpies, electronic- and Gibbs energies calculated with B3LYP/6-311G+(d,p) and M062X/6-311G+(d,p) in *o*-xylene at 383.15K

(Colorcode: light grey: hydrogen, grey: carbon, red: oxygen, light blue: fluorine, blue: nitrogen)

Cyclopentadiene

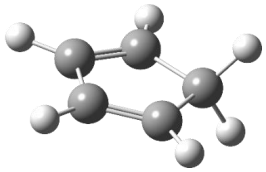

B3LYP

SCF Done: E(RB3LYP) = -194.157367733

Sum of electronic and thermal Enthalpies = -194.060247

Sum of electronic and thermal Enthalpies (383.15 K)= -194.057478

Sum of electronic and thermal Free Energies: = -194.091953

Sum of electronic and thermal Free Energies (383.15 K)= -194.101341

Number of imaginary frequencies = 0

M062X

SCF Done: E(RM062X) = -194.060330837

Sum of electronic and thermal Enthalpies = -193.962200

Sum of electronic and thermal Enthalpies (383.15 K)= -193.959451

Sum of electronic and thermal Free Energies = -193.993889

Sum of electronic and thermal Free Energies (383.15 K)= -194.003265

Number of imaginary frequencies = 0

β-Fluoro-β-nitrostyrene **1h**

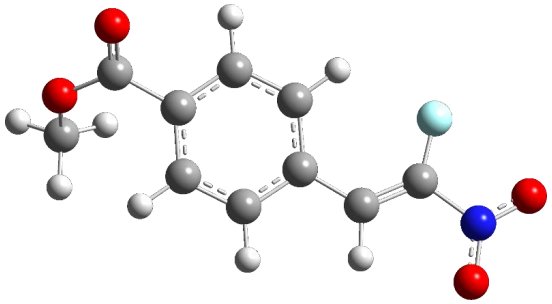

B3LYP

SCF Done: E(RB3LYP) = -841.490693409

Sum of electronic and thermal Enthalpies = -841.305171

Sum of electronic and thermal Enthalpies (383.15 K)= -841.297053

Sum of electronic and thermal Free Energies: = -841.365128

Sum of electronic and thermal Free Energies (383.15 K)= -841.383244

Number of imaginary frequencies = 0

M062X

SCF Done: E(RM062X) = -841.157231614

Sum of electronic and thermal Enthalpies = -840.968876

Sum of electronic and thermal Enthalpies (383.15 K)= -840.960875

Sum of electronic and thermal Free Energies = -841.028147

Sum of electronic and thermal Free Energies (383.15 K)= -841.046052

Number of imaginary frequencies = 0

endo-**TS**

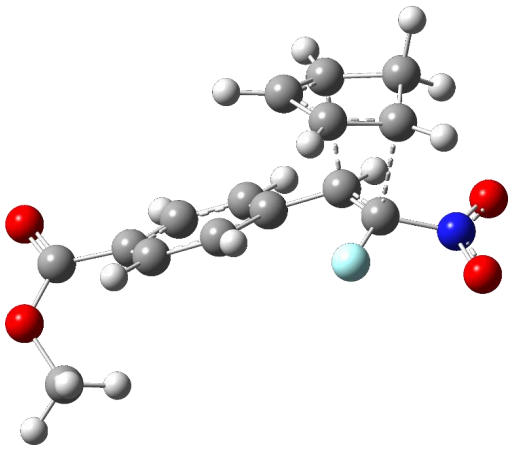

B3LYP

SCF Done: E(RB3LYP) = -1035.61479970

Sum of electronic and thermal Enthalpies = -1035.330728

Sum of electronic and thermal Enthalpies (383.15 K)= -1035.319748

Sum of electronic and thermal Free Energies: = -1035.399147

Sum of electronic and thermal Free Energies (383.15 K)= -1035.420031

Number of imaginary frequencies = 1

M062X

SCF Done: E(RM062X) = -1035.20424511

Sum of electronic and thermal Enthalpies = -1034.916372

Sum of electronic and thermal Enthalpies (383.15 K)= -1034.905558

Sum of electronic and thermal Free Energies = -1034.983311

Sum of electronic and thermal Free Energies (383.15 K)= -1035.003750

Number of imaginary frequencies = 1

exo-**TS**

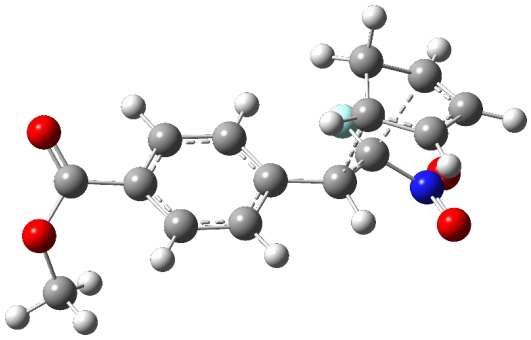

B3LYP

SCF Done: E(RB3LYP) = -1035.61454155

Sum of electronic and thermal Enthalpies = -1035.330383

Sum of electronic and thermal Enthalpies (383.15 K)= -1035.319400

Sum of electronic and thermal Free Energies: = -1035.398579

Sum of electronic and thermal Free Energies (383.15 K)= -1035.419401

Number of imaginary frequencies = 1

M062X

SCF Done: E(RM062X) = -1035.20415586

Sum of electronic and thermal Enthalpies = -1034.916118

Sum of electronic and thermal Enthalpies (383.15 K)= -1035.003376

Sum of electronic and thermal Free Energies = -1034.982962

Sum of electronic and thermal Free Energies (383.15 K)= -1034.905309

Number of imaginary frequencies = 1

Norbornene *endo*-**2h**

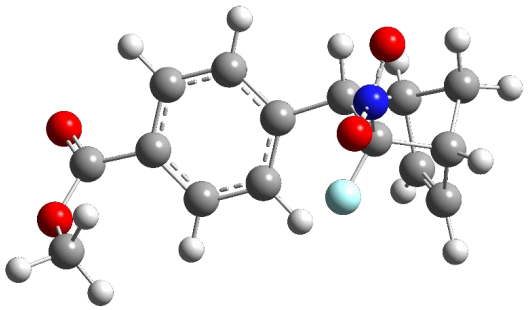

B3LYP

SCF Done: E(RB3LYP) = -1035.669464660

Sum of electronic and thermal Enthalpies = -1035.381415

Sum of electronic and thermal Enthalpies (383.15 K)= -1035.370605

Sum of electronic and thermal Free Energies: = -1035.447906

Sum of electronic and thermal Free Energies (383.15 K)= -1035.468215

Number of imaginary frequencies = 0

M062X

SCF Done: E(RM062X) = -1035.271688850

Sum of electronic and thermal Enthalpies = -1034.979554

Sum of electronic and thermal Enthalpies (383.15 K)= -1034.968939

Sum of electronic and thermal Free Energies = -1035.045276

Sum of electronic and thermal Free Energies (383.15 K)= -1035.065341

Number of imaginary frequencies = 0

Norbornene *exo*-**2h**

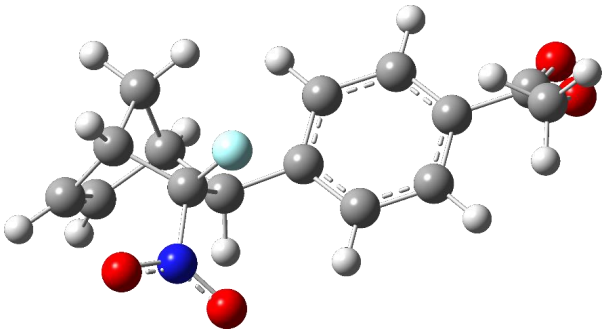

B3LYP

SCF Done: E(RB3LYP) = -1035.668394740

Sum of electronic and thermal Enthalpies = -1035.380504

Sum of electronic and thermal Enthalpies (383.15 K)= -1035.369679

Sum of electronic and thermal Free Energies: = -1035.447762

Sum of electronic and thermal Free Energies (383.15 K)= -1035.468292

Number of imaginary frequencies = 0

M062X

SCF Done: E(RM062X) = -1035.271008860

Sum of electronic and thermal Enthalpies = -1034.978820

Sum of electronic and thermal Enthalpies (383.15 K)= -1034.968197

Sum of electronic and thermal Free Energies = -1035.044396

Sum of electronic and thermal Free Energies (383.15 K)= -1035.064422

Number of imaginary frequencies = 0

References

[1] Williams, D. B. G.; Lawton, M. *J. Org. Chem.* **2010**, *75*, 8351–8354
[2] Motornov, V. A.; Muzalevskiy, V. M.; Tabolin, A. A.; Novikov, R. A.; Nelyubina, Yu. V.; Nenajdenko, V.G.; Ioffe, S. L. *J. Org. Chem.* **2017**, *82*, 5274–5284
[3] Larkovich, R. V.; Ponomarev, S. A.; Aldoshin, A. S.; Tabolin, A. A.; Ioffe, S. L.; Nenajdenko, V.G. *Eur. J. Org. Chem.* **2020**, 2479–2492
[4] Shastin, A. V.; Nenajdenko, V. G.; Muzalevskiy, V. M.; Balenkova, E. S.; Fröhlich, R.; Haufe, G. *Tetrahedron* **2008**, *64*, 9725- 9732
[5] Frisch, M. J.; Trucks, G. W.; Schlegel, H. B.; Scuseria, G. E.; Robb, M. A.; Cheeseman, J. R.; Scalmani, G.; Barone, V.; Petersson, G. A.; Nakatsuji, H.; Li, X.; Caricato, M.; Marenich, A. V.; Bloino, J.; Janesko, B. G.; Gomperts, R.; Mennucci, B.; Hratchian, H. P.; Ortiz, J. V.; Izmaylov, A. F.; Sonnenberg, J. L.; Williams; Ding, F.; Lipparini, F.; Egidi, F; Goings, J.; Peng, B.; Petrone, A.; Henderson, T.; Ranasinghe, D.; Zakrzewski, V. G.; Gao, J.; Rega, N.; Zheng, G.; Liang, W.; Hada, M.; Ehara, M.; Toyota, K.; Fukuda, R.; Hasegawa, J.; Ishida, M.; Nakajima, T.; Honda, Y.; Kitao, O.; Nakai, H.; Vreven, T.; Throssell, K.; Montgomery Jr., J. A.; Peralta, J. E.; Ogliaro, F.; Bearpark, M. J.; Heyd, J. J.; Brothers, E. N.; Kudin, K. N.; Staroverov, V. N.; Keith, T. A.; Kobayashi, R.; Normand, J.; Raghavachari, K.; Rendell, A. P.; Burant, J. C.; Iyengar, S. S.; Tomasi, J.; Cossi, M.; Millam, J. M.; Klene, M.; Adamo, C.; Cammi, R.; Ochterski, J. W.; Martin, R. L.; Morokuma, K.; Farkas, O.; Foresman, J. B.; Fox, D. J.Wallingford, CT, **2016**
[6] Lee, C.; Yang, W.; Parr, R. G. *Phys. Rev. B* **1988**, *37*, 785-789
[7] Becke, A. D. *J. Chem. Phys.* **1993**, *98*, 5648-5652
[8] Vosko, S. H.; Wilk, L.; Nusair, M. *Can. J. Phys.* **1980**, *58*, 1200-1211
[9] Zhao, Y.; Truhlar, D. G. *Theor. Chem. Acc.* **2008**, *120*, 215-241
[10] Krishnan, R.; Binkley, J. S.; Seeger, R.; Pople, J. A. *J. Chem. Phys.* **1980**, *72*, 650-654
[11] Frisch, M. J.; Pople, J. A.; Binkley, J. S. *J. Chem. Phys.* **1984**, *80*, 3265-3269
[12] Tomasi, J.; Mennucci, B.; Cancès, E. *J. Mol. Struct.* **1999**, *464*, 211-226
[13] Hehre, W. J.; Ditchfield, R.; Pople, J. A. *J. Chem. Phys.* **1972**, *56*, 2257-2261
[14] Hariharan, P. C.; Pople, J. A. *Theor. Chim. Acta* **1973**, *28*, 213-222
[15] Dennington, R.; Keith, T. A.; Millam, J. M. Semichem Inc. Shawnee Mission KS, **2016**

B.1.3 Zusatzmaterial der Publikation zur Reaktivität verschiedener *N*-Carbonsäureanhydride in einer ringöffnenden Synthese von Polypeptiden

Im Folgenden ist die *supporting information* der Publikation „An insight into the synthesis of *N*-methylated polypeptides“ abgedruckt.[556]

Electronic Supplementary Material (ESI) for Polymer Chemistry.

Supporting Information for:

An insight into the synthesis of *N*-methylated polypeptides

Christian Muhl,[†,‡] Lydia Zengerling,[†,‡] Jonathan Groß,[†] Paul Eckhardt,[†] Till Opatz,[†] Pol Besenius,[†,] Matthias Barz[†,*]*

[†]Department of Chemistry, Johannes Gutenberg University Mainz, 55099 Mainz

Table of Content

1 Experimental procedures

1.1 Materials

SCHLENK techniques were used at those reactions with air and moisture sensitive reagents or intermediates, performed under argon atmosphere, using laboratory glassware, dried under high vacuum at 120 °C with a hot air gun. In these instances, solvents and reagents were added through septa by disposable syringes and cannulas.

All used solvents and reagents were purchased from commercial sources. The respective suppliers are ACROS ORGANICS (Thermo Scientific GmbH, Nidderau), ALFA AESAR (Alfer Aesar GmbH & Co. KG, Karlsruhe), CARBOLUTION CHEMICALS (Carbolution Chemicals GmbH, Saarbrücken), IRIS BIOTECH (Iris Biotech GmbH, Markredwitz), MERCK (Merck KGaA, Darmstadt), SIGMA-ALDRICH (Sigma-Aldrich Chemie GmbH, Taufkirchen) and TCI (TCI Deutschland GmbH, Eschborn. Those chemicals were utilized without further purification unless stated otherwise.

Prior to use, water was demineralized, using PURELAB® flex by Elga. Solvents used for air or moisture sensitive reactions were bought anhydrous. DCM was dried using a solvent purification system. Solvents used as the mobile phase at flash- or thin layer chromatography were purchased in technical quality and applied without further purification.

1.2 Chromatography

All performed qualitative thin layer chromatography (TLC) were carried out using silica coated aluminum sheets (60 Å, F_{254}), purchased from MACHEREY-NAGEL (MN GmbH & Co. KG, Düren). Detection of the analytes was performed by the use of UV light (λ = 254 nm) and detection reagents of ninhydrin (0.1 g, 50 mL ethanol, 1.5 mL acetic acid) or $KMnO_4$ (0.75 g, 200 mL H_2O, 2.5 g $NaHCO_3$).

Flash chromatography (FC) was performed for purification by using silica gel with an average grain size of 15-40 µm, provided from ACROS Organics™.

1.3 Medium Pressure Liquid Chromatography

Purification was performed on a Sepacore® Easy Purification System (BÜCHI Labortechnik AG) equipped with a UV-Photometer C-640 (BÜCHI) and a Fraction Collector C-660 (BÜCHI). All runs were performed on a CHROMABOND Flash RS 120 C_{18} column (MACHEREY-NAGEL GmbH & Co. KG).

1.4 Gel permeation chromatography

Gel permeation chromatography (GPC) was performed with hexaflouroisopropanol (HFIP) containing 3 g L-1 potassium trifluoroacetate (KTFA) as eluent at 40 °C. The columns were packed with modified silica (PFG column particle size: 7 µm, porosity: 100 and 4000 Å, purchased from PSS Polymer Standards Service GmbH). For calibration polymethyl methacrylate (PMMA, Polymer Standards

Services GmbH) was used and toluene as the internal standard. A refractive index detector (G1362A RID) and an UV/VIS detector (at 230 nm, Jasco UV-2075 Plus) were used for polymer detection.

1.5 Mass spectroscopy

All mass spectra were recorded on an electrospray ionization spectrometer (ESI) QT of Ultima. The used samples were prepared at a concentration of 0.1 mg/mL in methanol or water as the solvent. The theoretical masses of the respective compounds were calculated by using the molecule editor ChemDraw® Professional 15.0.

1.6 Matrix-assisted laser desorption/ionization (MALDI)

MALDI-ToF mass spectra were recorded using a Bruker rapifleX MALDI-ToF mass spectrometer equipped with a 337 nm N_2 laser. Acceleration of the ions was performed with pulsed ion extraction (PIE, Bruker) at a voltage of 20 kV. The analyzer was operated in reflection mode and the ions were detected using a microchannel plate detector. Mass spectra were processed by the X-TOF 5.1.0 software (Bruker (Billerica, MA, USA)). Sample preparation was performed using trans-2-[3-(4-tert-Butylphenyl)-2-methyl-2-propenylidene]malononitrile (DCTB) as the matrix and sodium trifluoroacetate as the cationizing salt and dichloromethane as solvent.

1.7 NMR spectroscopy

All NMR-spectra were recorded on BRUKER Avance II 400 spectrometer and the measurements carried out in deuterated solvents ($CDCl_3$, DMSO-d_6, D_2O). The chemical shifts (δ) are reported in parts per million (ppm), relative to the chemical shifts of the residual protons of the deuterated solvents. The spin multiplicity of the signals is stated as follows: s = singlet, d = doublet, t = triplet, q = quartet, m = multiplet. The measured coupling constants (*J*) were calculated in hertz (Hz). All received NMR-spectra were analyzed using the NMR processing software MestReNova v12.0.0.

1.8 Circular dichroism (CD) spectroscopy

CD spectroscopy was performed on a Jasco J-815 spectrometer at 20 °C. The spectra was analyzed with Spectra Manager 2.0. Each measurement were repeated three times and average corrected. The concentrations were adjusted to keep the photomultiplier's high voltage (HV) below 600 V in the range of interest. All spectra were recorded using a quartz cell with a path length of 1 mm at a concentration of c = 0.25 g L^{-1} polymer in HFIP. θ_{MR} was calculated from the following equation:

$$\theta_{MR} = \frac{\theta \cdot M_{repeating\ unit}}{10 \cdot c_M \cdot l} [\mathrm{deg} \cdot cm^2 \cdot dmol^{-1}]$$

with $M_{repeating\ unit}$ = 147.1 g mol^{-1}, c_M = 0.25 g L^{-1} and l = 0.1 cm.

1.9 Polarimetry

All measurements of optical rotation were carried out with a Perkin Elmer 241 polarimeter at 589 nm. A quartz glass cuvette with a path length of 10 cm was used.

2 Synthetic Route

Synthesis of *N*-methyl-alanine

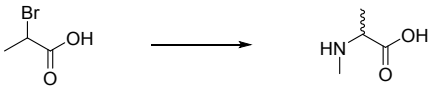

Synthesis of *N*-methyl-L-methionine

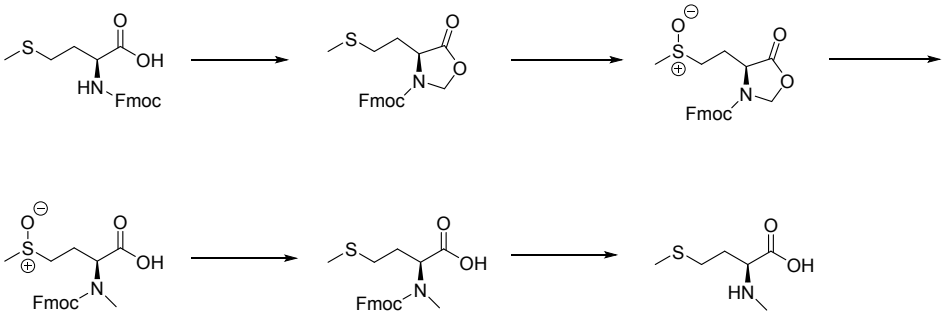

Synthesis of *N*-methyl-L-leucine

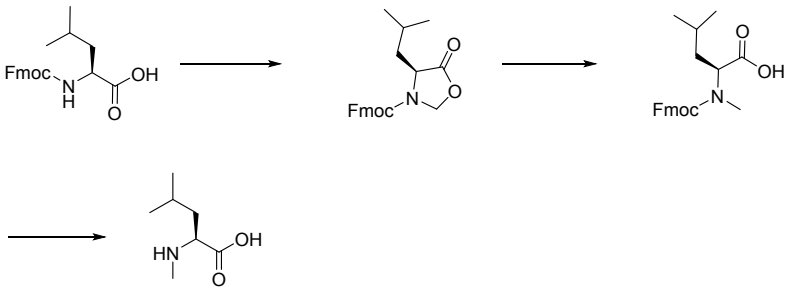

Scheme S1: Synthesis of *N*-methylated amino acids.

2.1 *N*-Methyl-alanine

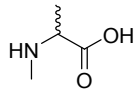

2-Bromopropanoic acid (4.6 g, 30 mmol, 1.0 eq.) was dissolved in ethanol (24 ml) at 0 °C and methylamine (33% wt in EtOH, 15 ml, 120 mmol, 4 eq.) was added to the stirred solution. The reaction mixture was then stirred at rt for 48 h and then evaporated under reduced pressure. Acetone was added and the product precipitated, which was filtered and the product obtained as a white solid (2.5 g, 24 mmol, 80%).[1]

Chemical formula: $C_4H_9NO_2$.

^{1}H-NMR (400 MHz, $CDCl_3$): δ [ppm] = 3.78 (q, *J* = 7.4 Hz, 1H, -α-CH-), 2.67 (s, 3H, -NCH_3), 1.45 (d, *J* = 7.4 Hz, -(α-CHC$\underline{H}_3$)).

2.2 9H-fluoren-9-ylmethyl (*S*)-4-isobutyl-5-oxo-1,3-oxazolidine-3-carboxylate

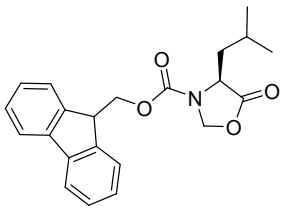

Fmoc-L-Leu-OH (12.0 g, 33.96 mmol, 1.0 eq.), paraformaldehyde (6.83 g, 227.50 mmol, 6.7 eq.) and *p*TsOH (0.585 g, 3.40 mmol, 0.1 eq.) were added to toluene (400 mL) and the suspension was stirred under reflux for 3 h in a DEAN-STARK apparatus. The resulting clear solution was cooled to room temperature, washed with a saturated $NaHCO_3$ solution (4 x 100 mL) and dried over Na_2SO_4. A yellow oil was obtained (product + traces of toluene :15.97 g, 33.96 mmol, quant.) and used without further purification.[2]

Molecular formula: $C_{22}H_{23}NO_4$.

^{1}H-NMR (400 MHz, DMSO-d_6): δ [ppm] = 7.89 (d, J = 7.4 Hz, 2H, -CH^{Fmoc}-), 7.66 (dd, J = 7.0, 3.9 Hz, 2H, -CH^{Fmoc}-), 7.42 (t, J = 8.0 Hz, 2H, -CH^{Fmoc}-), 7.34 (t, J = 7.4, 2.5, 1.2, 2H, -CH^{Fmoc}-), 5.32 (d, J = 4.3 Hz, 1H, NCH_2O), 5.19 (bs, 1H, NCH_2O), 4.90 – 4.40 (m, 2H, -C$\underline{H}_2$CH^{Fmoc}-), 4.30 (t, J = 5.4 Hz, 1H, -CH$_2$C$\underline{H}^{Fmoc}$-), 4.16 – 3.64 (m, 1H, -α-CH-), 1.77 – 1.16 (m, 3H, -CHC$\underline{H}_2$CH-), 0.71 (bs, 6H, -CH(C$\underline{H}_3$)$_2$).

^{13}C-NMR (101 MHz, DMSO-d_6): δ [ppm] = 172.7 (COOH), 143.6 (CH^{Fmoc}), 140.8 (CH^{Fmoc}), 128.9 (-CH^{Fmoc}-), 128.2 (-CH^{Fmoc}-), 127.7 (-CH^{Fmoc}-), 127.1 (-CH^{Fmoc}-), 125.3 (-CH^{Fmoc}-), 120.1 (-CH^{Fmoc}-), 77.4 (-NCH_2O-), 53.1 (-α-CH-), 46.7 (-CH$_2$C$\underline{H}^{Fmoc}$-), 22.5 (-CH(C$\underline{H}_3$)$_2$), 21.04 (-C$\underline{H}$(CH$_3$)$_2$).

2.3 Fmoc-*N*-Me-L-Leu-OH

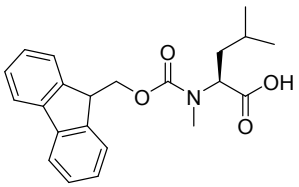

The crude mixture of 9H-fluoren-9-ylmethyl (*S*)-4-isobutyl-5-oxo-1,3-oxazolidine-3-carboxylate (12.4 g, 33.9 mmol, 1.0 eq.) was dissolved in $CHCl_3$ (80 mL). Triethylsilane (16.27 ml, 101.9 mmol, 3.0 eq.) and TFA (78 mL, 1018.6 mmol, 30.0 eq.) were added and the resulting solution was stirred at room temperature for 2 days. The $CHCl_3$ and TFA were removed under reduced pressure. The residue was co-distilled three times with toluene and further purified by FC on silica gel (DCM:MeOH = 99:2 + 0.05 v/v % HCOOH and then DCM:MeOH (100:0 to 99:1 + 0.05 v/v % HCOOH). A slightly yellow solid (9.560 g, 26.0 mmol, 77% over two steps) was obtained.[2]

Molecular formula: $C_{22}H_{23}NO_4$.

R_f: 0.28 (CH_2Cl_2:MeOH, 98:2 + 0.1 v/v % HCOOC).

^{1}H-NMR (400 MHz, DMSO-d_6): δ [ppm] = 12.76 (s, 1H, -COOH), 7.91 – 7.86 (m, 2H, -CH^{Fmoc}-), 7.66 (m, 2H, -CH^{Fmoc}-), 7.44 – 7.35 (m, 2H, -CH^{Fmoc}-), 7.35 – 7.27 (m, 2H, -CH^{Fmoc}-), 4.61 (dd, 1H, -α-CH-), 4.44 – 4.23 (m, 3H, -C$\underline{H}_2$CH^{Fmoc}-), 2.70 (s, 3H, -NCH_3), 1.74 – 1.44 (m, 2H, -CHC$\underline{H}_2$CH$(CH_3)_2$), 1.38 – 1.30 (m, 1H, -C$\underline{H}(CH_3)_2$), 0.90 – 0.67 (m, 6H, -CH(C$\underline{H}_3)_2$).

^{13}C-NMR (101 MHz, DMSO-d_6): δ [ppm] = 173.0 (-COOH), 163.4 (-OCON-), 156.1 (-CH^{Fmoc}-), 155.7 (-CH^{Fmoc}-), 143.9 (-CH^{Fmoc}-), 140.8 (-CH^{Fmoc}-), 127.6 (-CH^{Fmoc}-), 127.1 (-CH^{Fmoc}-), 125.0 (-CH^{Fmoc}-), 120.1 (-CH^{Fmoc}-), 66.7 (-COO$\underline{C}H_2$), 56.1 (-α-CH-), 56.0 (-α-CH-), 46.8 (-COOCH$_2\underline{C}$H-), 46.7 (-COOCH$_2\underline{C}$H-), 37.0 (-α-CH$\underline{C}H_2$-), 36.7 (-α-CH$\underline{C}H_2$-), 30.1 (-NCH_3), 29.9 (-NCH_3), 24.4 (-CH$\underline{C}H_2$CH$(CH_3)_2$), 23.1 (-CH$\underline{C}H_2$CH$(CH_3)_2$), 22.9 (-$\underline{C}$H$(CH_3)_2$), 21.0 (-CH($\underline{C}H_3)_2$), 20.9 (-CH($\underline{C}H_3)_2$).

ESI-MS (MeOH) (m/z): Calculated for: $[C_{22}H_{23}NO_4+H]^+$: 368.1856, found: 368.1859; $[C_{22}H_{23}NO_4+Na]^+$: 390.1676, found: 390.1675.

2.4 *N*-Me-L-Leu-OH

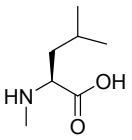

Fmoc-*N*-Me-L-Leu-OH (1.179 g, 3.21 mmol, 1.0 eq.) was dissolved in DCM (27 ml) and a methanolic solution of 3 N NaOH (3 ml, 9 mmol, 2.8 eq.) was added and the mixture was stirred at room temperature. The reaction was monitored by thin layer chromatography (TLC). After 30 min the starting material was completely converted and the solution became cloudy. Then the solvents were removed under vacuum. The residue was solved in water (20 ml) and extracted with diethyl ether (3 x 30 ml) to remove the fulvene. The aqueous phase was cooled and acidified with conc. HCl to pH 2. Excess of HCl was removed at the SCHLENK line. The salts were removed by MPLC on a CHROMABOND® Flash RS 120 C_{18} column. The aqueous solution was freeze dried and a withe powder (0.317 g, 2.18 mmol, 68%) was obtained.[3]

Molecular formula: $C_7H_{15}NO_2$.

^{1}H-NMR (400 MHz, D_2O): δ [ppm] = 3.57 – 3.53 (m, 1H, -α-CH-), 2.68 (s, 3H, -NCH_3), 1.76 – 1.61 (m, 2H, -CHC$\underline{H}_2$-), 0.94 – 0.92 (m, 6H, -CH(C$\underline{H}_3$)$_2$).

^{13}C-NMR (101 MHz, D_2O): δ [ppm] = 173.6 (-COOH), 62.0 (-$\underline{C}HCH_2$-), 38.9 (-CH$\underline{C}H_2$-), 31.7 (-NCH_3), 24.3 (-CH($\underline{C}H_3$)$_2$), 21.8 (-CH($\underline{C}H_3$)$_2$), 21.3 (CH($\underline{C}H_3$)$_2$).

ESI-MS (H_2O) (m/z): Calculated for: $[C_7H_{15}NO_2+H]^+$: 146.1176, found: 146.1178; $[C_7H_{15}NO_2+Na]^+$: 168.0995, found: 168.0998.

2.5 Fmoc-L-4-(2-methylthioethyl)-1,3-oxazolidin-5-one

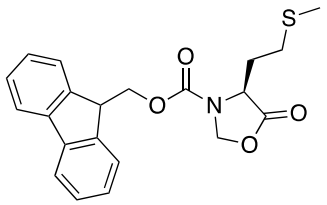

Fmoc-L-Met-OH (15.0 g, 40.38 mmol, 1.0 eq.), paraformaldehyde (8.12 g, 270.52 mmol, 6.7 eq.) and *p*TsOH (696 mg, 4.04 mmol, 0.1 eq.) were added to toluene (400 mL) and the suspension was stirred under reflux for 3 h in a DEAN-STARK apparatus. The resulting clear solution was cooled to room temperature, washed with a saturated $NaHCO_3$ solution (4 x 100 mL) and dried over $MgSO_4$. Thereby 14.00 g (35.0 mmol, 87%) of a colorless gum could be obtained.[2]

Chemical formula: $C_{21}H_{21}NO_4S$.

R_f: 0.36 (Cyclohexane:EtOAc, 3:1 + 0.1 v/v % HCOOH).

^{1}H-NMR (400 MHz, $CDCl_3$): δ [ppm] = 7.78 (d, *J* = 7.5 Hz, 2H, -CH^{Fmoc}-), 7.59 – 7.52 (m, 2H, -CH^{Fmoc}-), 7.42 (t, *J* = 7.4 Hz, 2H, -CH^{Fmoc}-), 7.33 (td, *J* = 7.5, 1.1 Hz, 2H, -CH^{Fmoc}-), 5.50 – 5.16 (m, 1H, -CH_2^{Oxaz}-), 5.12 (d, *J* = 4.0 Hz, 1H, -CH_2^{Oxaz}-), 4.93 – 4.45 (m, 2H, -C$\underline{H}_2$CH^{Fmoc}-), 4.24 (t, *J* = 5.0 Hz, 1H, -CH_2C$\underline{H}^{Fmoc}$-), 4.07 – 3.65 (m, 1H, -α-CH-), 2.64 – 1.50 (m, 7H, -C$\underline{H}_2$-/ -SC$\underline{H}_2$-/ -C$\underline{H}_3$).

ESI-MS (MeOH) (m/z): Calculated for: $[C_{21}H_{21}NO_4S+H]^+$: 384.1264, found: 384.1253.

2.6 Fmoc-L-4-(2-methylsulfinylethyl)-1,3-oxazolidin-5-one

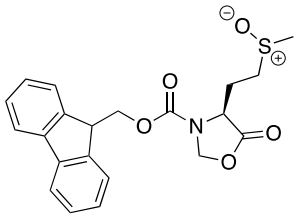

Fmoc-L-4-(2-methylthioethyl)-1,3-oxazolidin-5-one (14.0 g, 35.0 mmol, 1.0 eq.) was dissolved in DCM (300 mL) and cooled to 0 °C. A solution of *m*CPBA (6.9 g, 40.2 mmol, 1.1 eq.) in DCM (150 mL) was cooled to 0 °C as well and added dropwise to the stirred solution. After the addition the mixture was stirred for 20 min at room temperature and then washed with a Na_2CO_3-solution (10 w/v %, 4 x 100 mL). The aqueous layers were combined, and remaining product extracted with DCM (2 x 100 mL). The organic layers were combined and dried over $MgSO_4$. The volatiles were removed *in vacuo* to obtain 14.45 g (36.1 mmol, 99%) of a colorless hygroscopic solid.[2]

Chemical formula: $C_{21}H_{21}NO_5S$.

R_f: 0.30 ($CHCl_3$:MeOH, 98:2 + 0.1 v/v % HCOOH).

^{1}H-NMR (400 MHz, DMDO-d_6): δ [ppm] = 7.90 (d, *J* = 7.4 Hz, 2H, -CH^{Fmoc}-), 7.69 – 7.66 (m, 2H, -CH^{Fmoc}-), 7.43 (t, *J* = 7.4 Hz, 2H, -CH^{Fmoc}-), 7.35 (m, 2H, -CH^{Fmoc}-), 5.36 – 5.35 (m, 1H, -CH_2^{Oxaz}-), 5.32 – 5.20 (m, 1H, -CH_2^{Oxaz}-), 4.53 – 4.38 (m, 2H, -C<u>H</u>$_2$$CH^{Fmoc}$-), 4.35 – 4.28 (m, 1H, -CH_2C<u>H</u>^{Fmoc}-), 4.25 – 4.03 (m, 1H, -α-CH-), 2.86 – 1.73 (m, 7H, -CH_2-/ -SCH_2-/ -CH_3).

^{13}C-NMR (101 MHz, $CDCl_3$): δ [ppm] = 171.2 (-CH<u>C</u>OOCH_2-), 153.0 (-COONH-), 143.3 (-CH^{Fmoc}-), 141.5 (-CH^{Fmoc}-), 128.2 (-CH^{Fmoc}-), 127.5 (-CH^{Fmoc}-), 124.6 (-CH^{Fmoc}-), 120.3 (-CH^{Fmoc}-), 53.9 (-α-CH-), 53.8 (-α-CH-), 47.2 (-CH_2<u>C</u>H^{Fmoc}-), 38.7 (-CH_3).

ESI-MS (MeOH) (m/z): Calculated for: $[C_{21}H_{21}NO_5S+H]^+$: 400.1213, found: 400.1219, $[C_{21}H_{21}NO_5S+K]^+$: 438.0772, found: 438.0780, $[2C_{21}H_{21}NO_5S+3H]^{3+}$: 267.0833, found: 267.1722, $[2C_{21}H_{21}NO_5S+Na]^+$: 821.2173, found: 821.2178 .

2.7 Fmoc-*N*-methyl-L-methionine sulfoxide

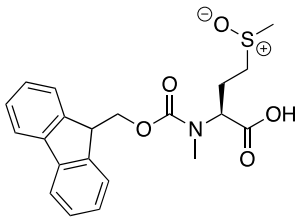

Fmoc-L-4-(2-methylsulfinylethyl)-1,3-oxazolidin-5-one (15.0 g, 37.6 mmol, 1.0 eq.) was dissolved in $CHCl_3$ (80 mL). Triethylsilane (13.11 g, 112.8 mmol, 3.0 eq.) and TFA (86 mL, 1127.5 mmol, 30.0 eq.) were added and the resulting solution was stirred at room temperature for 3 days. The product (11.6 g, 28.9 mmol, 77% was used without further purification.[2]

Chemical formula: $C_{21}H_{23}NO_5S$.

R_f: 0.31 ($CHCl_3$:MeOH, 96.25:3.75 + 0.1 v/v % HCOOC).

^{1}H-NMR (400 MHz, DMSO-d_6): δ [ppm] = 7.90 (t, J = 6.5 Hz, 2H, -CH^{Fmoc}-), 7.67 – 7.62 (m, 2H, -CH^{Fmoc}-), 7.44 – 7.40 (m, 2H, -CH^{Fmoc}-), 7.36 – 7.29 (m, 2H, -CH^{Fmoc}-), 4.59 – 4.41 (m, 1H, -α-CH-), 4.39 – 4.21 (m, 3H, -C$\underline{H}_2$C$\underline{H}^{Fmoc}$-), 2.79 – 2.75 (m, 3H, -NCH_3), 2.54 – 2.51 (m, 3H, -SCH_3-), 2.30 – 1.92 (m, 4H, -SC$\underline{H}_2$-, -C$\underline{H}_2$-).

ESI-MS (MeOH) (m/z): Calculated for: $[C_{21}H_{23}NO_5S+H]^+$: 402.1370, found: 402.1371; $[2C_{21}H_{23}NO_5S+Na]^+$: 825.2486, found: 825.2503.

2.8 Fmoc-*N*-methyl-L-methionine

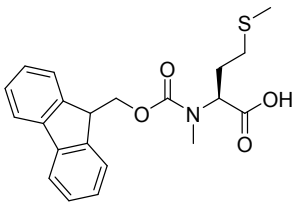

The crude mixture of Fmoc-*N*-methyl-L-methionine sulfoxide (15.894 g, 39.6 mmol, 1.0 eq.) in chloroform and TFA was cooled to 0 °C and dimethyl sulfide (8.68 ml, 118.8 mmol, 3.0 eq.) was added. Then portion wise ammonium iodide (17.213 g, 118.8 mmol, 3.0 eq.) was added and the solution turned brown. The solution was stirred for 3 h at 0 °C and then the volatiles were removed at the SCHLENK line, which was connected with a big cooling trap. The residue was solved in DCM (50 ml), transferred in a separatory funnel and washed with a 5% thiosulfate solution (150 ml). The organic layer was extracted with a sat. $NaHCO_3$ solution (100 ml). The combined aqueous layers were extracted ones with DCM (150 ml). Then the combined organic layers were dried over $NaSO_4$, filtered, the solvent removed under reduced pressure and three times co-distilled with toluene. The product was purified by FC on silica gel (DCM:EtOAC = 9:1 + 0.05 v/v % HCOOH) and afterwards by FC on silica gel (DCM:MeOH = 99:1 + 0.05 v/v % HCOOH). 9.88 g (25.6 mmol, 65% over two steps) of a colorless product were obtained.[2]

Molecular formula: $C_{21}H_{23}NO_4S$.

^{1}H-NMR (400 MHz, DMSO-d_6): δ [ppm] = 12.89 (s, 1H, COOH), 7.89 (t, *J* = 7.2 Hz, 2H, -CH^{Fmoc}-), 7.65 (d, *J* = 7.2 Hz, 2H, -CH^{Fmoc}-), 7.42 (td, *J* = 7.4, 2.9 Hz, 2H, -CH^{Fmoc}-), 7.35-7.28 (m, 2H, -CH^{Fmoc}-), 4.56 (ddd, *J* = 27.6, 10.4, 4.7 Hz, 1H, -α-CH-), 4.42-4.22 (m, 3H, -C<u>H</u>C<u>H$_2$</u>^{Fmoc}-), 2.75 (s, 3H, -NCH_3), 2.42-2.19 (m, 2H, -SCH_2-), 2.11-1.85 (m, 5H, -SC<u>H$_3$</u>-, -C<u>H$_2$</u>-).

^{13}C-NMR (101 MHz, DMSO-d_6): δ [ppm] = 172.3 (-COOH), 156.0 (-COONH-), 143.8 (-CH^{Fmoc}-), 140.8 (-CH^{Fmoc}-), 127.7 (-CH^{Fmoc}-), 127.1 (-CH^{Fmoc}-), 125.05 (-CH^{Fmoc}-), 120.1(-CH^{Fmoc}-), 66.7 (-<u>C</u>H$_2$CH^{Fmoc}-), 57.6 (-α-CH-), 46.7 (-CH$_2$<u>C</u>H^{Fmoc}-) , 31.0 (-NCH_3) , 30.0 (-SCH_2-), 27.8 (-CH_2-), 14.6 (-SCH_3).

ESI-HRMS (MeOH) (m/z): Calculated for $[C_{21}H_{23}NO_4S+H]^+$: 386.1421, found: 386.1420, $[C_{21}H_{23}NO_4S+Na]^+$: 408.1240, found 408.1235.

2.9 *N*-Methyl-L-methionine

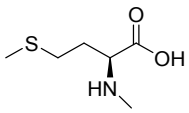

Fmoc-*N*-methyl-L-methionine (5.592 g, 1.25 mmol, 1.0 eq.) was dissolved in a solution of 20% piperidine in DMF (10 mL) and stirred for 2 h at room temperature. The precipitated colorless solid was filtered and washed with a slight amount of DCM to yield 1.007 g (0.63 mmol, 42%) of the colorless water-soluble product.

Molecular formula: $C_6H_{13}NO_2S$.

^{1}H-NMR (400 MHz, D_2O): δ [ppm] = 3.69 (t, *J* = 6.0 Hz, 1H, -α-CH-), 2.71 (s, 3H, -NCH_3), 2.62 – 2.57 (m, 2H, -SCH_2-), 2.18 – 2.12 (m, 5H, -$SC\underline{H}_3$, -$C\underline{H}_2$-).

^{13}C-NMR (101 MHz, D_2O): δ [ppm] = 173.0 (-COOH), 62.7 (-α-CH-), 31.8 (-NCH_3), 28.7 (-CH_2-), 28.5 (-SCH_2-), 14.0 (-SCH_3).

ESI-HRMS (MeOH) (m/z): Calculated for $[C_6H_{13}NO_2S + Na]^+$:186.0559, found 186.1141.

2.10 *N*-Methyl-DL-methionine

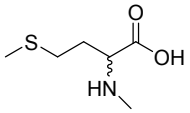

N-Methyl-L-methionine (500 mg, 3.063 mmol, 1.00 eq.) was dissolved in glacial acid (15 ml) and salicylaldehyde (18.7 mg, 0.153 mmol, 0.05 eq.) was added. The solution was stirred and heated at 100 °C for 2 days. Then the solvents were removed *in vacuo* and recrystallized in MeOH to yield a slightly yellow solid (200 mg, 1.225 mmol, 40%).[4]

$[\alpha]_D^{24.5}$: 0 ± 0.02 (c = 1.0, 3 M HCl).

3 FT-IR Spectra

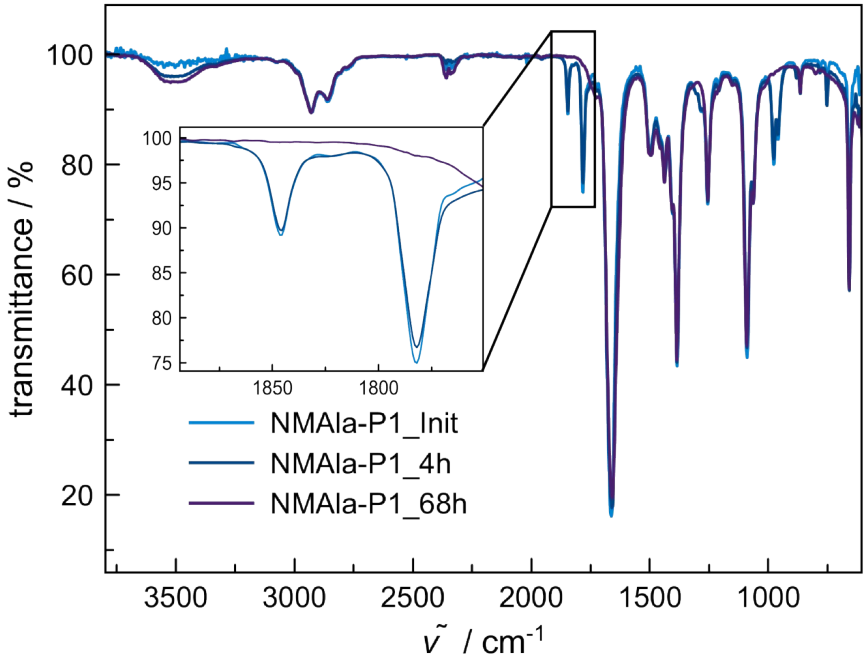

Figure S1: Generic FT-IR spectrum of a polymerization of NMAla-NCA in DMF (liquid film). Full conversion was ensured in all cases by FT-IR monitoring of the carbonyl attributed peaks at 1782 and 1845 cm^{-1}.

4 NMR Spectra

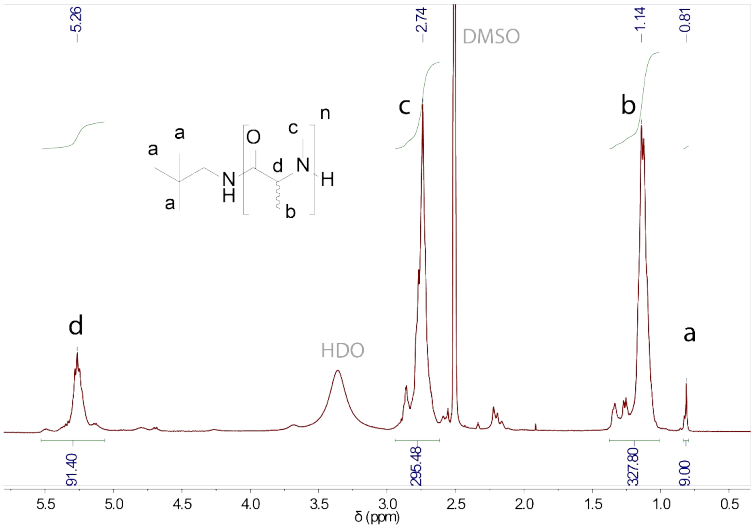

Figure S2: ^{1}H NMR spectrum of NMAla-P1 in d_6-DMSO.

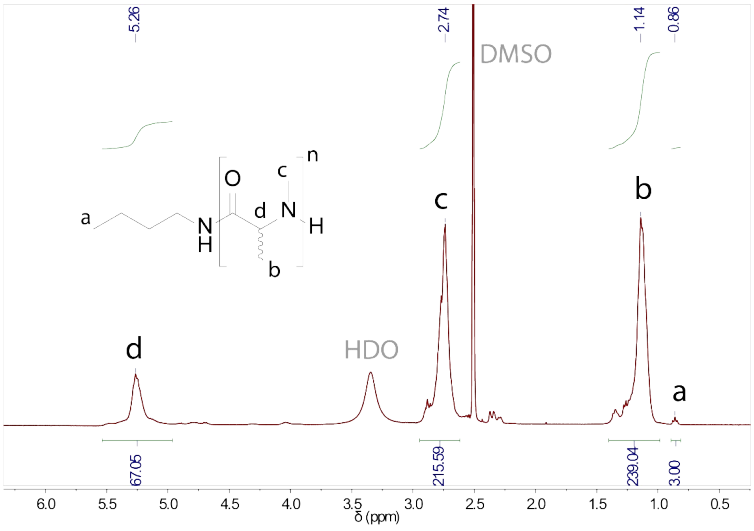

Figure S3: ^{1}H NMR spectrum of NMAla-P3 in d_6-DMSO.

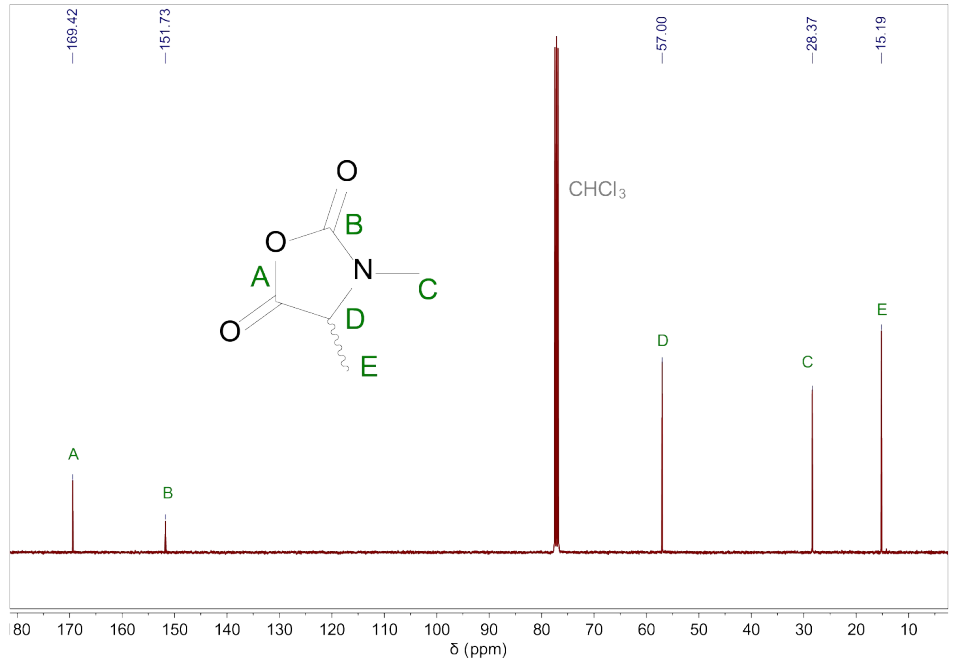
169.42
151.73
57.00
28.37
15.19
CHCl3
A
B
C
D
E
δ (ppm)

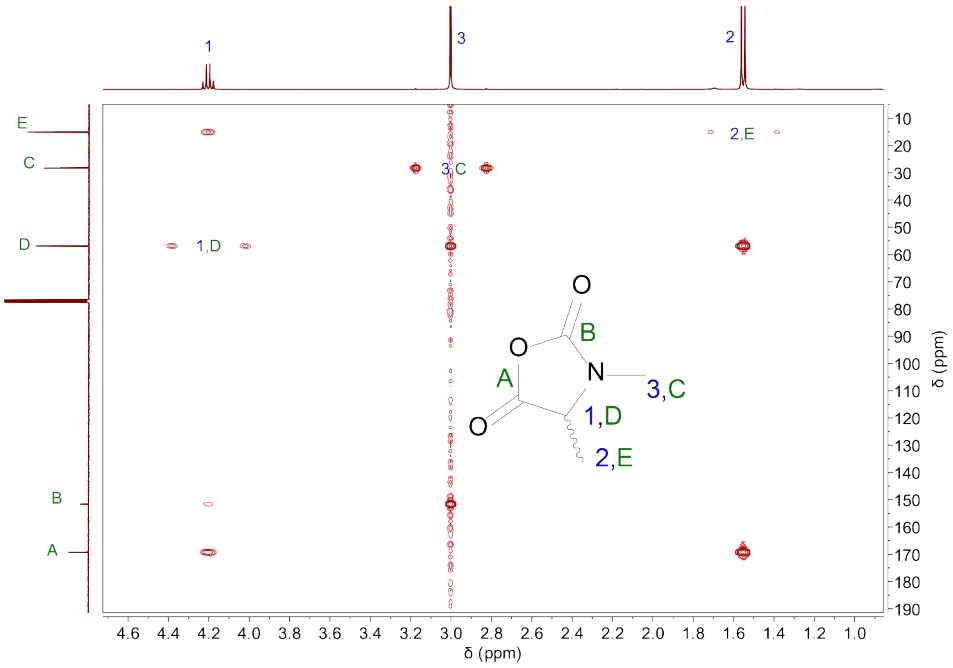
1
3
2
E
C
D
B
A
2,E
3,C
1,D
δ (ppm)

18

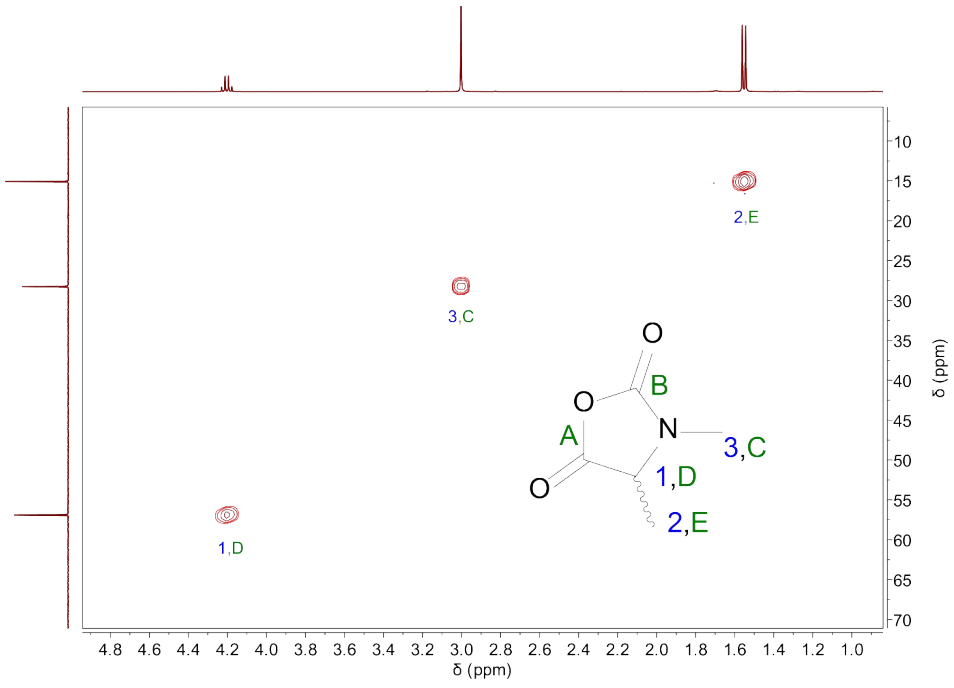
2,E
3,C
1,D
O
B
O
N
A
3,C
O
1,D
2,E
δ (ppm)
δ (ppm)

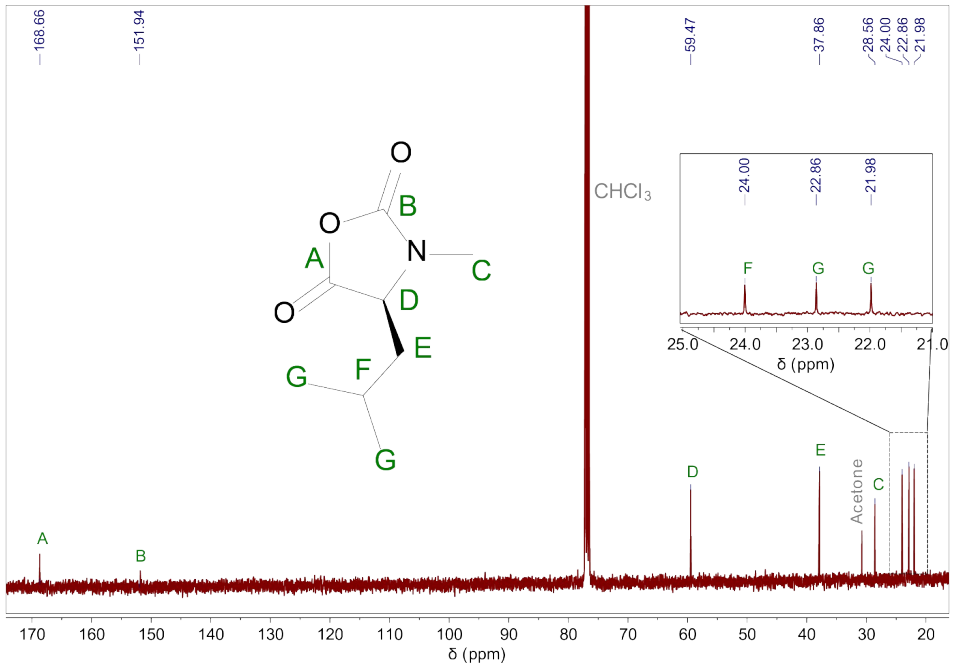
168.66
151.94
59.47
37.86
28.56
24.00
22.86
21.98
CHCl3
O
B
O
N
C
A
O
D
E
G
F
G
24.00
22.86
21.98
F
G
G
δ (ppm)
A
B
D
E
C
Acetone
δ (ppm)

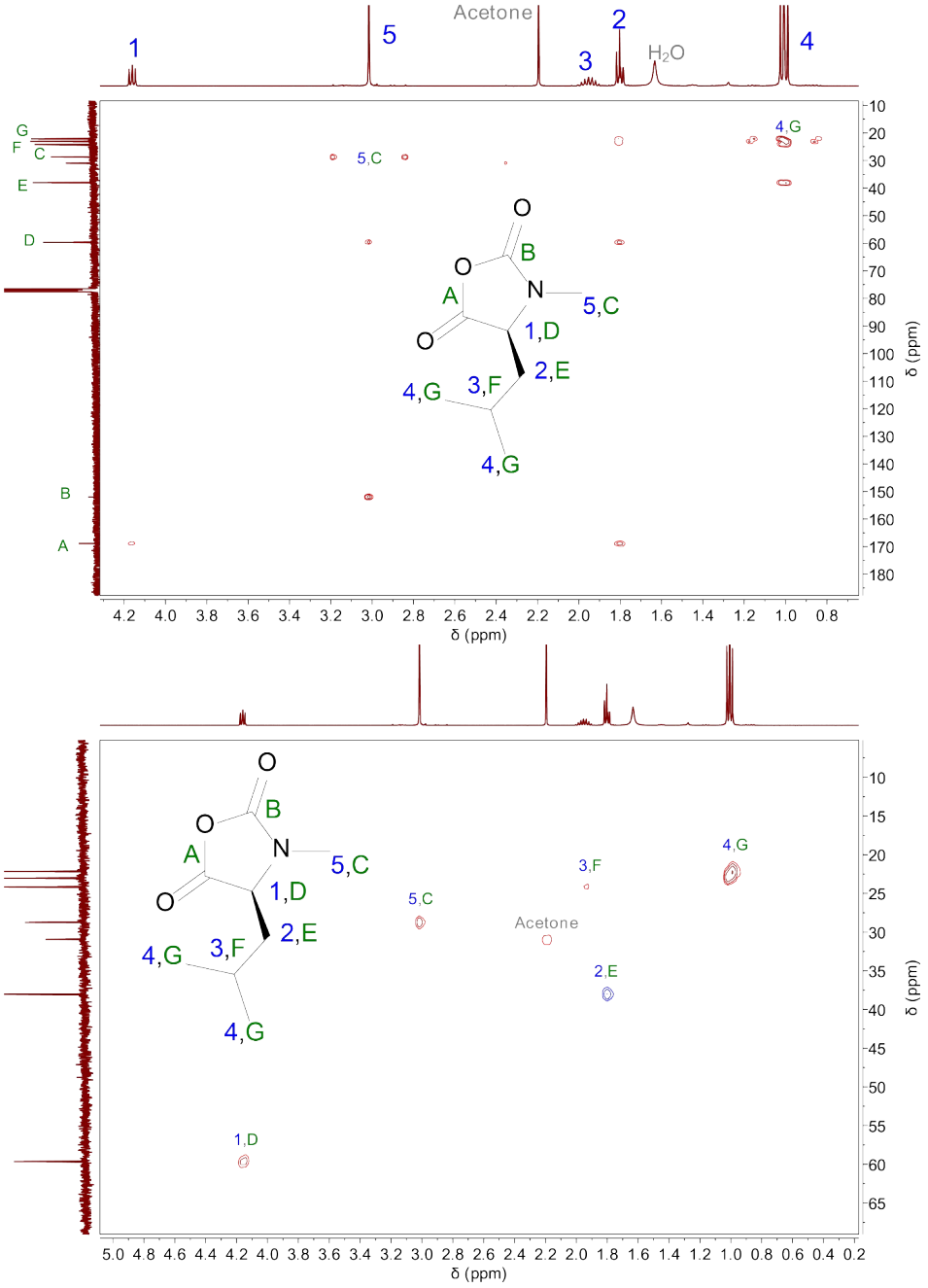
Acetone
1
5
2
3
H2O
4
G
F
C
E
D
B
A
4,G
5,C
O
B
O
N
A
5,C
O
1,D
2,E
4,G
3,F
4,G
δ (ppm)
3,F
4,G
5,C
Acetone
2,E
1,D
δ (ppm)

20

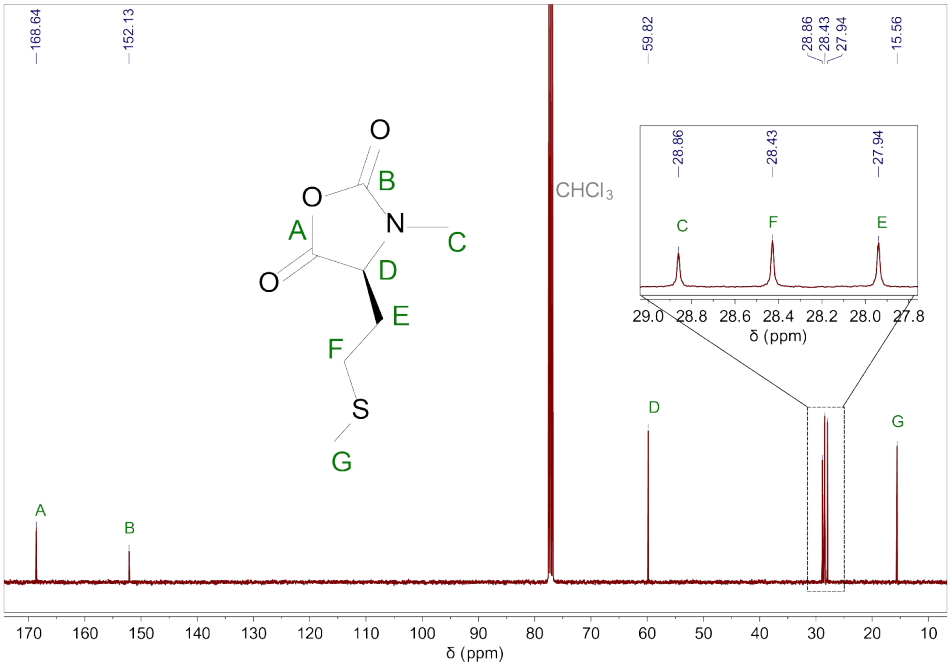
168.64
152.13
59.82
28.86
28.43
27.94
15.56
CHCl3
A
B
C
D
E
F
G
δ (ppm)

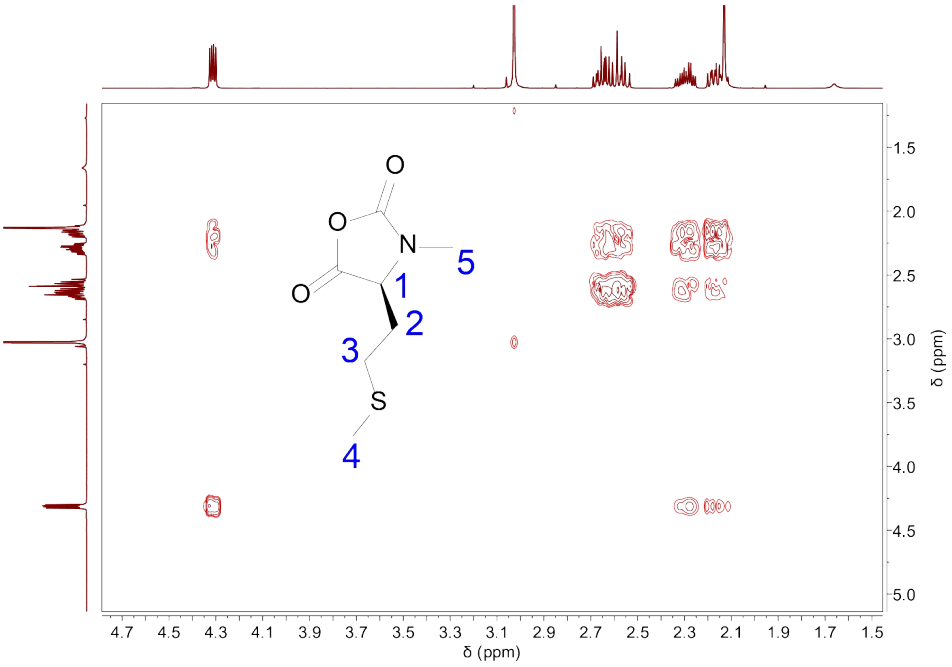
1
2
3
4
5
δ (ppm)
δ (ppm)

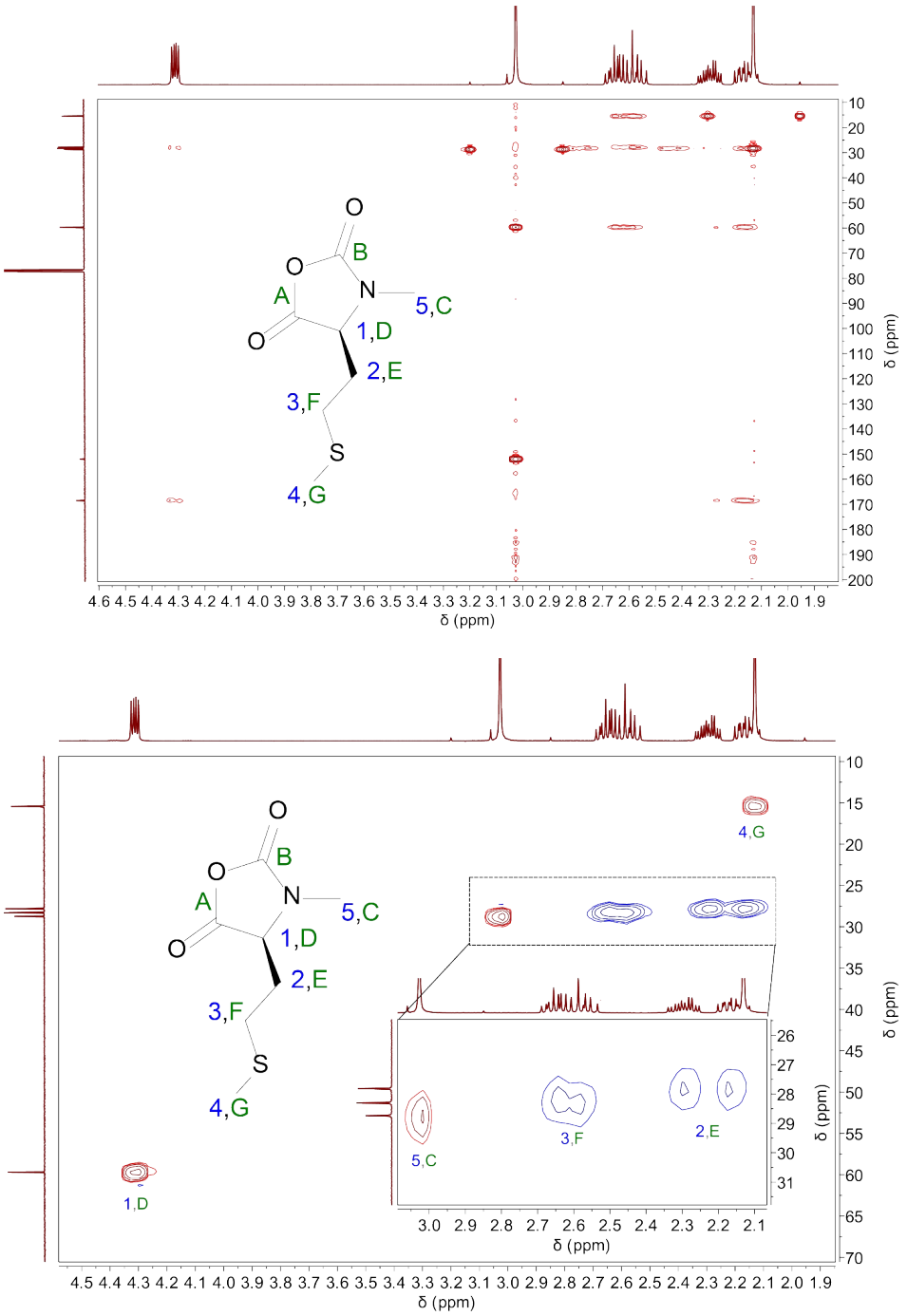

22

5 MALDI-ToF data

Table S1: Values of the peaks shown in the magnified area of the MALDI-ToF spectrum of figure 4 (Poly(N-methyl-DL-alanine)).

Initiator	X_n	Additional Ion	m/z (found)	m/z (calc)
*n*Bu	22	Na^+	1968,39	1968,68
*n*Bu	23	Na^+	2053,46	2053,8
NPA	22	Na^+	1981,83	1982,7
NPA	23	Na^+	2066,89	2067,82
H_2O	23	Na^+	1998,32	1998,66
H_2O	23	K^+	2011,39	2014,86
H_2O	24	Na^+	2083,42	2083,78
H_2O	24	K^+	2096,41	2099,98

Table S2: Values of the peaks shown in the magnified area of the MALDI-ToF spectrum of figure 6 (Poly(N-methyl-L-methionine)).

Initiator	X_n	Additional Ion	m/z (found)	m/z (calc)
H_2O	6	-	889,55	889,44
H_2O	6	Na^+	911,42	912,43
H_2O	6	K^+	925,42	928,54
H_2O	7	-	1034,64	1034,68
*n*Bu	6	-	943,42	944,58
*n*Bu	6	Na^+	966,46	967,57
*n*Bu	6	K^+	982,51	983,68
NPA	6	-	958,64	958,58

6 GPC data

Table S3: Molecular weights and dispersities determined *via* HFIP-GPC (based on PMMA standards)

Sample	M_n	M_w	PDI
DL-NMMet-P1	1639	2532	1.55
NMMet-P1	971	1965	2.02
NMMet-P2	2223	2401	1.49
NMMet-P3	2357	3306	1.40
NMMet-P4	713	1425	2.11
$pMet_{50}$	7683	10066	1.31
NMAla-P1	2285	2761	1.21
NMAla-P2	2880	3460	1.20
NMAla-P3	4213	5073	1.20
NMLeu-P1	526	713	1.89
$pSar_{50}$	15768	16115	1.17

7 Coupled cluster (CC) calculations

For the monomers NMMet-NCA and Met-NCA the molecule related parameters were obtained from x-ray data. These structures and the structure of ethylamine were optimized with Gaussian 16, Rev. A.03[5] using DFT methods and the IEFPCM solvation model[6] for DMF. All conformers were confirmed as local minima by frequency analysis ($N_{imag} = 0$). The B3LYP functional[7–10] was used in conjunction with the 6-311G(d,p) Pople basis set.[11,12]

Energy and NBO calculations were performed using orca 4.1.0[13] with the DLPNO-CCSD(T)[14] method and the cc-pVDZ[15,16] and cc-pVDZ/C[17,18] basis sets. The frontier orbitals were visualized using Chemcraft (Version 1.8, build 562b).[19]

Computational input lines

DFT optimization and frequency calculation:

```
#p opt=tight freq=noraman b3lyp/6-311g(d,p) scrf=(iefpcm,solvent=n,n-dimethylformamide)
```

The following keyword lines were used as input for Orca:

```
! DLPNO-CCSD(T) cc-pVDZ cc-pVDZ/C
%nbo
NBOKEYLIST      = "$NBO NBO NPA AONBO=C ARCHIVE PLOT $END"
end
```

XYZ Coordinates

NMMet-NCA

0 1

C	0.57042	0.19486	1.15955
H	1.02180	0.14514	2.15959
C	0.21999	-1.23469	0.77790
O	1.05547	-1.62537	-0.23674
C	1.90238	-0.55984	-0.59642

N	1.58544	0.51141	0.16506
O	-0.58072	-1.96905	1.27700
O	2.73557	-0.68981	-1.45263
C	2.41079	1.71043	0.20947
H	2.97324	1.75604	1.14631
H	1.79281	2.60485	0.11978
H	3.10581	1.67453	-0.62660
C	-0.62690	1.15677	1.23560
H	-0.30656	2.06045	1.76292
H	-1.37497	0.68419	1.87720
C	-1.24288	1.58808	-0.09709
H	-0.50278	2.09051	-0.72226
H	-2.04422	2.30422	0.09560
S	-1.90197	0.25827	-1.17507
C	-3.28552	-0.38570	-0.17045
H	-2.91951	-0.92971	0.69981
H	-3.83595	-1.07330	-0.81272
H	-3.94840	0.42522	0.13360

Met-NCA

0 1

C	0.41926	0.15203	-0.16057
H	-0.10741	0.21788	-1.11914
C	1.47598	1.24418	-0.11595
O	2.71413	0.65234	-0.09020
C	2.57990	-0.75255	-0.11782

N	1.26026	-1.03289	-0.10747
H	0.93578	-1.97446	-0.26459
O	1.32740	2.42878	-0.09083
O	3.53896	-1.47108	-0.13997
C	-0.58922	0.28924	0.98731
H	-0.05676	0.21369	1.94088
H	-1.01151	1.29559	0.93436
C	-1.70364	-0.76092	0.97106
H	-2.33469	-0.63800	1.85324
H	-1.29112	-1.77147	1.01261
S	-2.78545	-0.75451	-0.51273
C	-3.72422	0.79375	-0.25730
H	-4.23898	0.77299	0.70386
H	-4.46288	0.84171	-1.05734
H	-3.07940	1.66981	-0.32029

Ethylamine

0 1

N	-1.21209	-0.32640	-0.12258
C	-0.04788	0.55918	0.05385
H	-2.06468	0.22615	-0.08952
H	-1.26950	-0.95940	0.67196
H	-0.06996	1.30180	-0.75019
C	1.25079	-0.23799	-0.02697
H	-0.07014	1.11998	1.00120
H	1.31376	-0.77450	-0.97757

H	1.30709	-0.97515	0.78077
H	2.12060	0.41878	0.06016

6 References

(1) Etxabe, J.; Izquierdo, J.; Landa, A.; Oiarbide, M.; Palomo, C. Catalytic Enantioselective Synthesis of N,Cα,Cα-Trisubstituted α-Amino Acid Derivatives Using 1H-Imidazol-4(5H)-Ones as Key Templates. *Angew. Chemie - Int. Ed.* **2015**, *54* (23), 6883–6886.

(2) Aurelio, L.; Box, J. S.; Brownlee, R. T. C.; Hughes, A. B.; Sleebs, M. M. An Efficient Synthesis of N-Methyl Amino Acids by Way of Intermediate 5-Oxazolidinones. *J. Org. Chem.* **2003**, *68* (7), 2652–2667.

(3) Theodorou, V.; Alagiannis, M.; Ntemou, N.; Brentas, A.; Voulgari, P.; Polychronidou, V.; Gogou, M.; Giannelos, M.; Skobridis, K. Mild Alkaline Hydrolysis of Hindered Esters in Non-Aqueous Solution. *Arkivoc* **2018**, *2018* (7), 308–319.

(4) Yamada, S.; Hongo, C.; Yoshioka, R.; Chibata, I. Method for the Racemization of Optically Active Amino Acids. *J. Org. Chem.* **1983**, *48* (6), 843–846.

(5) Frisch, M. J.; Trucks, G. W.; Schlegel, H. B.; Scuseria, G. E.; Robb, M. A.; Cheeseman, J. R.; Scalmani, G.; Barone, V.; Petersson, G. A.; Nakatsuji, H.; Li, X.; Caricato, M.; Marenich, A. V.; Bloino, J.; Janesko, B. G.; Gomperts, R.; Mennucci, B.; Hratchian, H. P.; Ortiz, J. V.; Izmaylov, A. F.; Sonnenberg, J. L.; Williams-Young, D.; Ding, F.; Lipparini, F.; Egidi, F.; Goings, J.; Peng, B.; Petrone, A.; Henderson, T.; Ranasinghe, D.; Zakrzewski, V. G.; Gao, J.; Rega, N.; Zheng, G.; Liang, W.; Hada, M.; Ehara, M.; Toyota, K.; Fukuda, R.; Hasegawa, J.; Ishida, M.; Nakajima, T.; Honda, Y.; Kitao, O.; Nakai, H.; Vreven, T.; Throssell, K.; Montgomery, J. A., Jr.; Peralta, J. E.; Ogliaro, F.; Bearpark, M. J.; Heyd, J. J.; Brothers, E. N.; Kudin, K. N.; Staroverov, V. N.; Keith, T. A.; Kobayashi, R.; Normand, J.; Raghavachari, K.; Rendell, A. P.; Burant, J. C.; Iyengar, S. S.; Tomasi, J.; Cossi, M.; Millam, J. M.; Klene, M.; Adamo, C.; Cammi, R.; Ochterski, J. W.; Martin, R. L.; Morokuma, K.; Farkas, O.; Foresman, J. B.; Fox, D. J. Gaussian, Inc., Wallingford CT, **2016**.

(6) Tomasi, J.; Mennucci, B.; Cancès, E. The IEF Version of the PCM Solvation Method: An Overview of a New Method Addressed to Study Molecular Solutes at the QM Ab Initio Level. *J. Mol. Struct. THEOCHEM* **1999**, *464* (1–3), 211–226.

(7) Vosko, S. H.; Wilk, L.; Nusair, M. Accurate Spin-Dependent Electron Liquid Correlation Energies for Local Spin Density Calculations: A Critical Analysis. *Can. J. Phys.* **1980**, *58* (8), 1200–1211.

(8) Lee, C.; Yang, W.; Parr, R. G. Development of the Colle-Salvetti Correlation-Energy Formula into a Functional of the Electron Density. *Phys. Rev. B* **1988**, *37* (2), 785.

(9) Becke, A. D. Density-functional Thermochemistry. III. The Role of Exact Exchange. *J. Chem. Phys.* **1993**, *98* (7), 5648–5652.

(10) Becke, A. D. Density-Functional Exchange-Energy Approximation with Correct Asymptotic Behavior. *Phys. Rev. A* **1988**, *38* (6), 3098.

(11) Krishnan, R.; Binkley, J. S.; Seeger, R.; Pople, J. A. Self-Consistent Molecular Orbital Methods. XX. A Basis Set for Correlated Wave Functions. *J. Chem. Phys.* **1980**, *72* (1), 650–654.

(12) Frisch, M. J.; Pople, J. A.; Binkley, J. S. Self-Consistent Molecular Orbital Methods 25. Supplementary Functions for Gaussian Basis Sets. *J. Chem. Phys.* **1984**, *80* (7), 3265–3269.

(13) Neese, F. The ORCA Program System. *Wiley Interdiscip. Rev. Comput. Mol. Sci.* **2012**, *2* (1), 73–78.

(14) Guo, Y.; Riplinger, C.; Becker, U.; Liakos, D. G.; Minenkov, Y.; Cavallo, L.; Neese, F. Communication: An Improved Linear Scaling Perturbative Triples Correction for the Domain Based Local Pair-Natural Orbital Based Singles and Doubles Coupled Cluster Method [DLPNO-CCSD(T)]. *J. Chem. Phys.* **2018**, *148* (1).

(15) Dunning Jr., T. H. Gaussian Basis Sets for Use in Correlated Molecular Calculations. I. The Atoms Boron through Neon and Hydrogen. *J. Chem. Phys.* **1989**, *90* (2), 1007–1023.

(16) Prascher, B. P.; Woon, D. E.; Peterson, K. A.; Dunning Jr., T. H.; Wilson, A. K. Gaussian Basis Sets for Use in Correlated Molecular Calculations. VII. Valence, Core-Valence, and Scalar Relativistic Basis Sets for Li, Be, Na, and Mg. *Theor. Chem. Acc.* **2011**, *128* (1), 69–82.

(17) Weigend, F.; Köhn, A.; Hättig, C. Efficient Use of the Correlation Consistent Basis Sets in Resolution of the Identity MP2 Calculations. *J. Chem. Phys.* **2002**, *116* (8), 3175–3183.

(18) Hättig, C. Optimization of Auxiliary Basis Sets for RI-MP2 and RI-CC2 Calculations: Core–Valence and Quintuple-ζ Basis Sets for H to Ar and QZVPP Basis Sets for Li to Kr. *Phys. Chem. Chem. Phys.* **2005**, *7* (1), 59–66.

(19) Zhurko, G. *Ivanovo. Available online at: https://chemcraftprog.com* **2019**.

B.1.4 Zusatzmaterial der Publikation zur Bestimmung des Substituenteneinflusses bei der photochemischen Dehydrierung von N-Heterozyklen

Im Folgenden ist die *supporting information* der Publikation „Synthesis of 2,3-Dihydro-4-pyridones, 4-Quinolones, and 2,3-Dihydro-4-azocinones by Visible-Light Photocatalytic Aerobic Dehydrogenation“ abgedruckt.[557]

Supporting Information

Synthesis of 2,3-Dihydro-4-pyridones, 4-Quinolones, and 2,3-Dihydro-4-azocinones by Visible-Light Photocatalytic Aerobic Dehydrogenation

Adrian Sevenich, Paulina Sophie Mark, Torsten Behrendt, Jonathan Groß, and Till Opatz*

ejoc201900584-sup-0001-SupMat.pdf

Table of contents

I. Light sources and irradiation setup

The following light sources and irradiation setups were used:

1.) **Low power green LED stripe** (12 V, 4.8 W/m) was purchased from led-konzept.de (https://www.led-konzept.de/LED-Streifen-12V-gruen-24W-pro-5m). The spectral distribution can be found on the web page of the supplier. For the irradiation setup 2.75 m (~13 W) of the green LED stripe was wound in a hollow glass cylinder (h = 10 cm, ø = 10 cm) covered with aluminum foil. The glass cylinder was placed above a stirring plate and a cooling fan was installed on top to ensure cooling to ambient temperature (figure S1, center).

2.) **High power RGB LED stripe** (24 V, 29 W/m) was purchased from led-konzept.de (https://www.led-konzept.de/RGB-LED-Streifen-24V-29W-m) and set to the appropriate color (green or blue). The spectral distribution can be found on the web page of the supplier. For the irradiation setup 2.75 m (~80 W) of the RGB-LED-stripe was wound in a hollow glass cylinder (h = 10 cm, ø = 10 cm) covered with aluminum foil. The glass cylinder was placed above a stirring plate and a cooling fan was installed on top to ensure cooling to ambient temperature (figure S1, center and right).

3.) **High power blue LED** (100 W, HPR40E-48K100BG (GaInN/GaN), wavelength 462 nm ± 3 nm) was purchased from Huey Jann Electronic Industry CO, LTD., Taiwan. This LED is integrated into a custom-built case with cooling heat sink. The LED was placed in front of a stirring plate with ~5 cm distance to the reaction vial and a cooling fan was installed on top to ensure cooling to ambient temperature (figure S1, left).

4.) **High power green LED** (100 W, HPR40E-43K100G (GaInN/GaN), wavelength 520 nm ± 5 nm) was purchased from Huey Jann Electronic Industry CO, LTD., Taiwan. This LED is integrated into a custom-built case with cooling heat sink. The LED was placed in front of a stirring plate with ~5 cm distance to the reaction vial and a cooling fan was installed on top to ensure cooling to ambient temperature (figure S1, left).

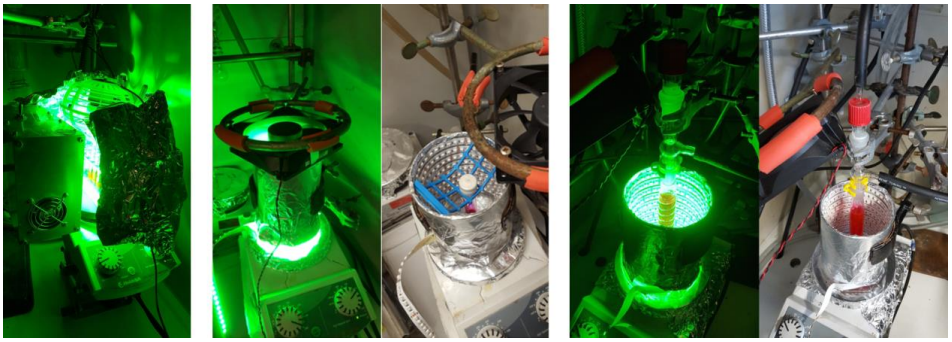

Figure S1. Setup for irradiation with high power green or blue LED (left), low power green LED stripe or high power RGB LED stripe (center) and reaction under oxygen bubbling with high power RGB LED stripe (right).

II. Optimization Studies for the photoredox catalyzed dehydrogenation

General procedure for screening reactions:

A 10 mL glass vial was charged with **1a** (generally 0.300 mmol), one of the photocatalysts **3-7** and anhydrous solvent (generally 1.00 mL). The vial was sealed with a rubber septum and the mixture was stirred until the catalyst was completely dissolved. The reaction vessel was flooded with oxygen for 2 minutes and the mixture was stirred under irradiation for the mentioned time. Water was added and the mixture was extracted with Et_2O to remove most of DMF. The organic phases were combined and the solvent was removed in vacuo. The yield was judged by ^{1}H-NMR using 1,4-bis(trimethylsilyl)benzene as internal standard.

Table S1. Screening of photocatalysts.[(a)]

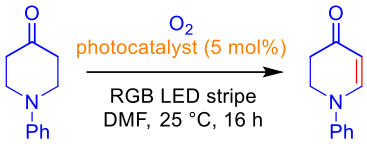

1a **2a**

Entry	Photocatalyst	LED color	**1a** (%)	**2a** (%)
1	fluoresceine (**3**)	blue	<1	58
2	rose Bengal (**5**)	green	<1	36
3	eosin Y (**4**)	green	<1	49
4	rhodamine B (**6**)	green	13	53
5	rhodamine 6G (**7**)	green	15	61

[(a)]Reaction conditions: **1a** (0.3 mmol), 1 ml dry DMF, high power RGB LED stripe.

Table S2. Screening of solvents.[(a)]

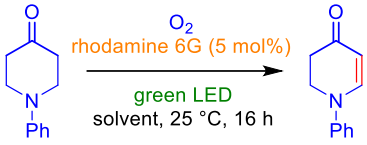

1a **2a**

Entry	Solvent	**1a** (%)	**2a** (%)
1	DMF	15	61
2	DMSO	58	21

3	MeOH	96	2
4	DCM	42	35
5	PhMe	85	9

[a]Reaction conditions: **1a** (0.3 mmol), 1 ml dry DMF, high power RGB LED stripe on green.

Table S3. Miscellaneous screenings.[a]

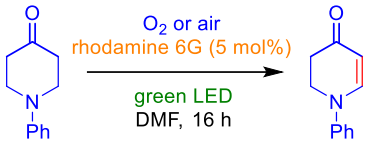

1a **2a**

Entry	Deviation from standard conditions	**1a** (%)	**2a** (%)
1	standard conditions (25 °C, O_2)	15	61
2	no cooling fan (40 °C)	<1	58
3	flooded with air instead of oxygen	65	24

[a]Reaction conditions: **1a** (0.3 mmol), 1 ml dry DMF, high power RGB LED stripe on green.

Table S4. Optimization of catalyst loading.[a]

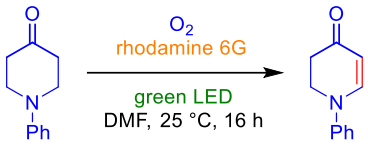

1a **2a**

Entry	Catalyst loading (mol%)	**1a** (%)	**2a** (%)
1	10	29	47
2	5	15	61
3	2	10	66
4	1.5	<1	72
5	1	<1	77 (70)[b]
6	0.5	4	68
7	0.1	7	59

[a]Reaction conditions: **1a** (0.3 mmol), 1 ml dry DMF, high power RGB LED stripe on green.
[b]Isolated yield in brackets.

Table S5. Screening of light sources.[a]

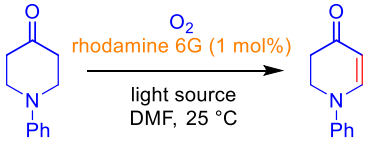

1a **2a**

Entry	Light source	time (h)	**1a** (%)	**2a** (%)
1	Low power green LED stripe (~13 W)	16	conversion <50%	
2	High power RGB LED stripe on green (~80 W)	16	<1	77
3	High power green LED (100 W)	16	15	61
4	High power blue LED (100 W)	16	<1	56
5	High power RGB LED stripe on white (~80 W)	6	3	65
6	High power RGB LED stripe on white (~80 W)	4	19	48

[(a)]Reaction conditions: **1a** (0.3 mmol), 1 ml dry DMF.

Table S6. Screening of additives (bases, acids, lewis acids).[(a)]

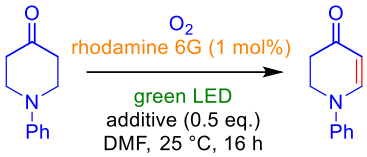

1a **2a**

Entry	Additive	**1a** (%)	**2a** (%)
1	no additive	<1	77
2	2,6-lutidine	14	59
3	NEt_3	<1	73
4	NaOAc	39	37
5	K_2HPO_4	13	63
6	Al_2O_3, neutral	2	69
7	HOAc	4	70
8	$LiBF_4$	5	66

[(a)]Reaction conditions: **1a** (0.3 mmol), 1 ml dry DMF, high power RGB LED stripe on green.

Table S7. Screening of concentration, scale and oxygen supply.[(a)]

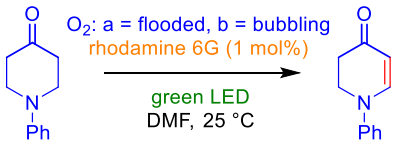

1a **2a**

Entry	**1a** (mmol)	solvent (ml)	O_2 supply	time (h)	**1a** (%)	**2a** (%)
1	0.9	3	a	16	<1	61
2	0.6	2	a	16	<1	67
3	0.3	1	a	16	<1	77
4	0.3	0.5	a	16	16	54
5	0.3	3	a	16	<1	64
6	0.3	2	b	12	4	62

7	0.3	5	b	8	9	58
8	0.3	10	b	4	12	49

[a]Reaction conditions: **1a** (0.3 mmol), 1 ml dry DMF, high power RGB LED stripe on green.
Explanation: For heterogeneous photoreactions in vials, both light absorption and oxygen availability depend strongly on scale and concentration, due to the area-to-volume ratio. At higher scale (but same concentration and same glass vial diameter) light absorption should be similar or slightly better but oxygen availability is lower, leading to decreased yields. At lower concentration (more solvent) light absorption should be more sufficient but on the other hand the surface area is lower, leading to less sufficient oxygen availability. Bubbling a steady stream of oxygen through the reaction mixture was tested as alternative oxygen supply to overcome this issue. Indeed, the reaction was faster but overall yields were lower.

Table S8. Control experiments.[a]

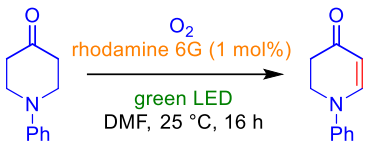

1a **2a**

Entry	Deviation from standard conditions	**1a** (%)	**2a** (%)
1	without catalyst	96	0
2	in the dark	98	0
3	flooded with argon instead of oxygen	96	0

[a]Reaction conditions: **1a** (0.3 mmol), 1 ml dry DMF, high power RGB LED stripe on green.
[b]Isolated yield in brackets.

III. Computational calculations

Conformational searches were performed using Spartan '10.[1] DFT calculations were performed using Gaussian 16, Rev. A.03.[2] The B3LYP functional[3] was used in conjunction with the 6-311+G(d,p) Pople basis set[4] and IEFPCM[5] solvation for *N*,*N*-dimethylformamide. The calculated structures were confirmed as local minima by vibrational frequency analysis.

Optimized structures of the lowest energy conformers in *N*,*N*-dimethylformamide:

(Gray: carbon; blue: nitrogen; red: oxygen; green: chlorine; hydrogen: omitted)

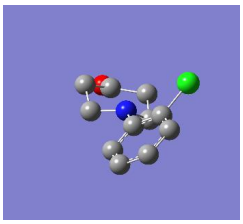

Figure S2: Lowest energy conformer of 1-(2-chlorophenyl)-piperidin-4-one **2x** (B3LYP/6-311+G(d,p)).

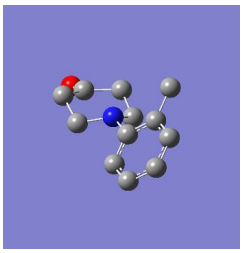

Figure S3: Lowest energy conformer of 1-(2-methylphenyl)-piperidin-4-one **2w** (B3LYP/6-311+G(d,p)).

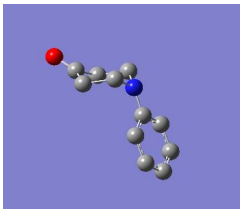

Figure S4: Lowest energy conformer of 1-phenylpiperidin-4-one **2a** (B3LYP/6-311+G(d,p)).

Input Lines

Conformational analysis with Spartan:

SEARCHMETHOD=THOROUGH KEEPALL FINDBOATS CONF_SELECTION_RULE=5

DFT calculations with Gaussian:

#p opt=tight freq b3lyp 6-311+g(d,p) scrf=(iefpcm,solvent=n,n-dimethylformamide)

Atomic coordinates, number of imaginary frequencies and total energies and Gibbs energies and for 1-(2-chlorophenyl)-piperidin-4-one in *N*,*N*-dimethylformamide:

Conformer2

SCF Done: E(RB3LYP) = -1016.74630202

Sum of electronic and thermal Free Energies= -1016.575802

Number of imaginary frequencies = 0

C	2.45395	0.98893	0.67218
C	1.08656	0.41317	1.06772
N	0.45403	-0.25710	-0.08093
C	1.25211	-1.39683	-0.53550
C	2.62826	-0.91373	-1.02505
C	3.32999	-0.04316	-0.00445
O	4.51811	-0.15526	0.24193
C	-0.94435	-0.45079	0.01928
C	-1.51789	-1.72060	0.19868
C	-2.89753	-1.89855	0.26646
C	-3.75156	-0.80313	0.17328
C	-3.21385	0.46970	-0.00819
C	-1.83642	0.63439	-0.09526
Cl	-1.22464	2.26012	-0.41675
H	2.29910	1.80328	-0.04595

H	2.97547	1.39428	1.54091
H	1.21101	-0.30068	1.89803
H	0.44415	1.21609	1.42284
H	1.39631	-2.14103	0.26435
H	0.73283	-1.89130	-1.35700
H	3.26906	-1.75882	-1.28205
H	2.48785	-0.30418	-1.92584
H	-0.86977	-2.58216	0.29443
H	-3.30025	-2.89530	0.40433
H	-4.82582	-0.93007	0.23076
H	-3.85981	1.33329	-0.10397

Atomic coordinates, number of imaginary frequencies and total energies and Gibbs energies and for 1-(2-methylphenyl)-piperidin-4-one in *N*,*N*-dimethylformamide:

Conformer5

SCF Done: E(RB3LYP) = -596.451050089

Sum of electronic and thermal Free Energies= -596.243392

Number of imaginary frequencies = 0

C	2.40943	1.10675	0.57758
C	1.00568	0.63112	0.98374
N	0.35355	-0.08479	-0.12210
C	1.10158	-1.28948	-0.48027
C	2.50694	-0.91330	-0.98186
C	3.23941	-0.01405	-0.00971
O	4.41514	-0.17322	0.26963
C	-1.06322	-0.21009	-0.01068

C	-1.66851	-1.44382	0.27271
C	-3.05444	-1.56701	0.35538
C	-3.86140	-0.44916	0.16435
C	-3.26670	0.77832	-0.12570
C	-1.87981	0.92595	-0.22738
C	-1.29931	2.26717	-0.60361
H	2.31217	1.87622	-0.19798
H	2.93815	1.54389	1.42642
H	1.08050	-0.02234	1.86917
H	0.40204	1.48918	1.27258
H	1.20126	-1.98149	0.37250
H	0.56839	-1.81840	-1.27108
H	3.10634	-1.80521	-1.17248
H	2.40871	-0.35916	-1.92315
H	-1.05308	-2.31940	0.43692
H	-3.49521	-2.53323	0.57483
H	-4.94069	-0.53045	0.22606
H	-3.89467	1.64589	-0.30269
H	-0.99789	2.84824	0.27475
H	-0.41321	2.14787	-1.23080
H	-2.03660	2.86338	-1.14475

Atomic coordinates, number of imaginary frequencies and total energies and Gibbs energies and for 1-phenylpiperidin-4-one in *N*,*N*-dimethylformamide:

Conformer1

SCF Done: E(RB3LYP) = -557.125983471

Sum of electronic and thermal Free Energies= -556.943912

Number of imaginary frequencies = 0

C	-1.94678	-1.30357	-0.09323
C	-1.12206	-0.96557	1.17443
N	-0.27143	0.20542	0.98744
C	-1.08778	1.38443	0.69781
C	-1.91128	1.20415	-0.60338
C	-2.70220	-0.08706	-0.58629
O	-3.86951	-0.14160	-0.93590
C	1.00453	0.07120	0.41199
C	1.82084	1.20244	0.19364
C	3.10684	1.07446	-0.32016
C	3.63688	-0.17803	-0.63319
C	2.84360	-1.30297	-0.42091
C	1.54997	-1.18782	0.08534
H	-1.26435	-1.61712	-0.89228
H	-2.64951	-2.11792	0.09287
H	-1.80834	-0.74334	1.99695
H	-0.53185	-1.82379	1.48880
H	-1.76698	1.53909	1.54109
H	-0.47524	2.27810	0.62177
H	-2.59005	2.04404	-0.76353
H	-1.21693	1.15958	-1.45145
H	1.46474	2.19204	0.44597

H	3.70236	1.96902	-0.46792
H	4.64003	-0.27248	-1.03145
H	3.22481	-2.29029	-0.65887
H	0.97215	-2.09194	0.21693

IV. Determination of the double bond geometry of the azocinones

To determine the geometry of double bonds, $^{3}J_{C\text{-}H}$ coupling constants between the methine protons and corresponding carbons were measured by CLIP-HSQMBC[6] and compared to literature values. Usually a *cis*-arrangement between C and H has lower values than a *trans*-arrangement (figure S2).[7] Consequently, the (2*E*,4*E*)-geometry was rationalized for all azocinones **12**.

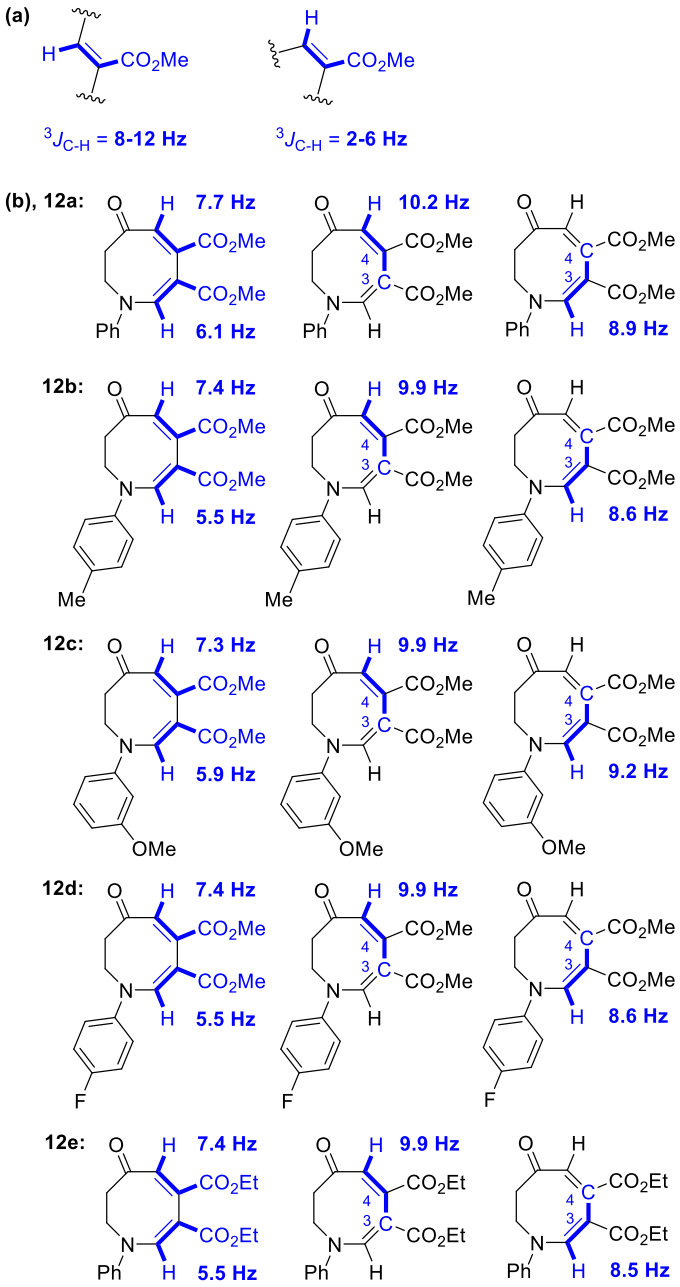

Figure S2. Comparison of measured coupling constants (b) with typical literature values (a).

V. NMR Spectra

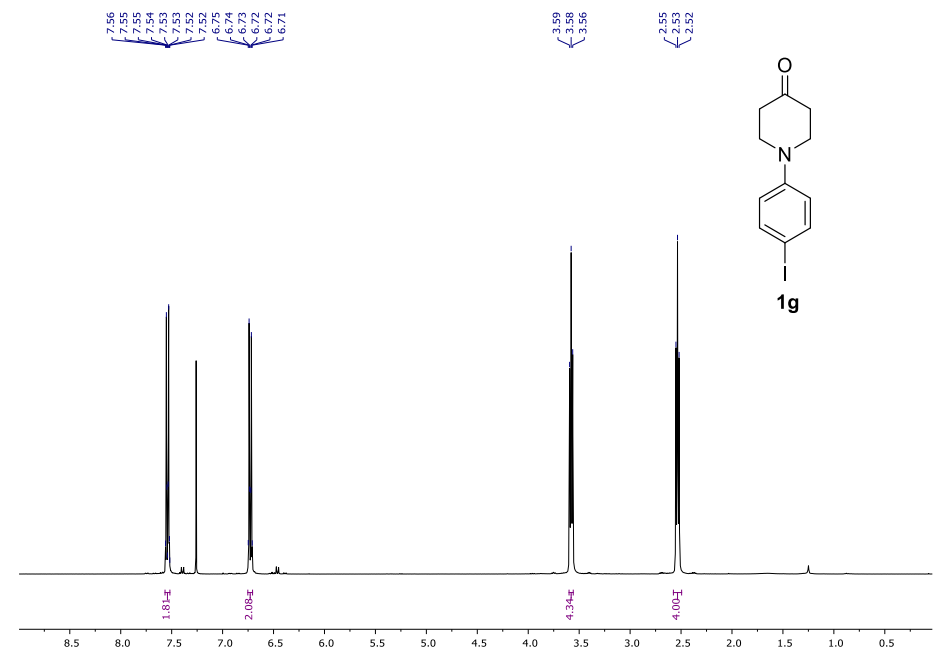

^{1}H-NMR (400 MHz, $CDCl_3$) of **1g**.

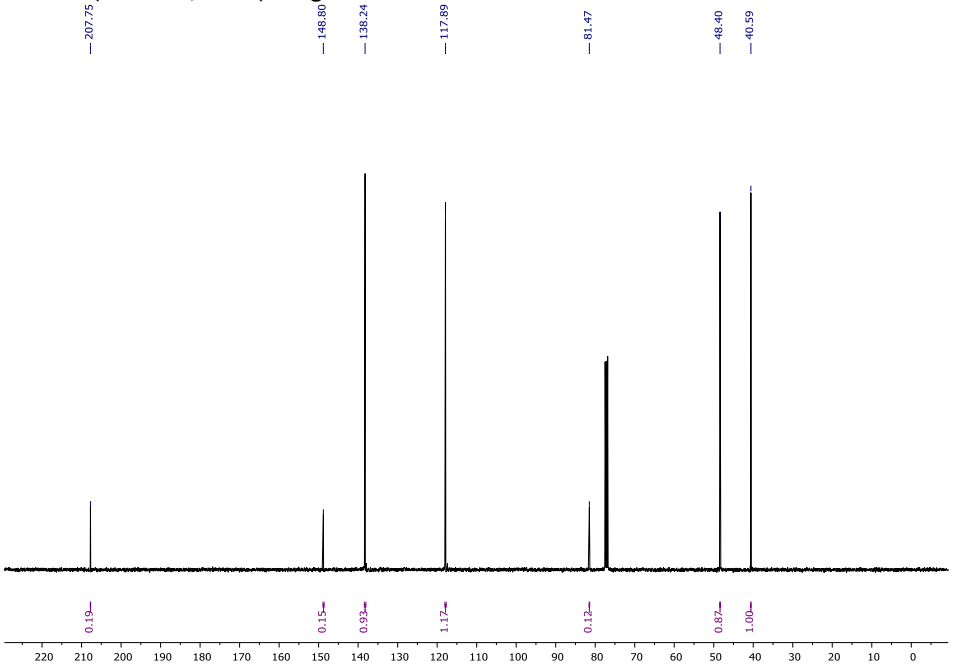

^{13}C-NMR (101 MHz, $CDCl_3$) of **1g**.

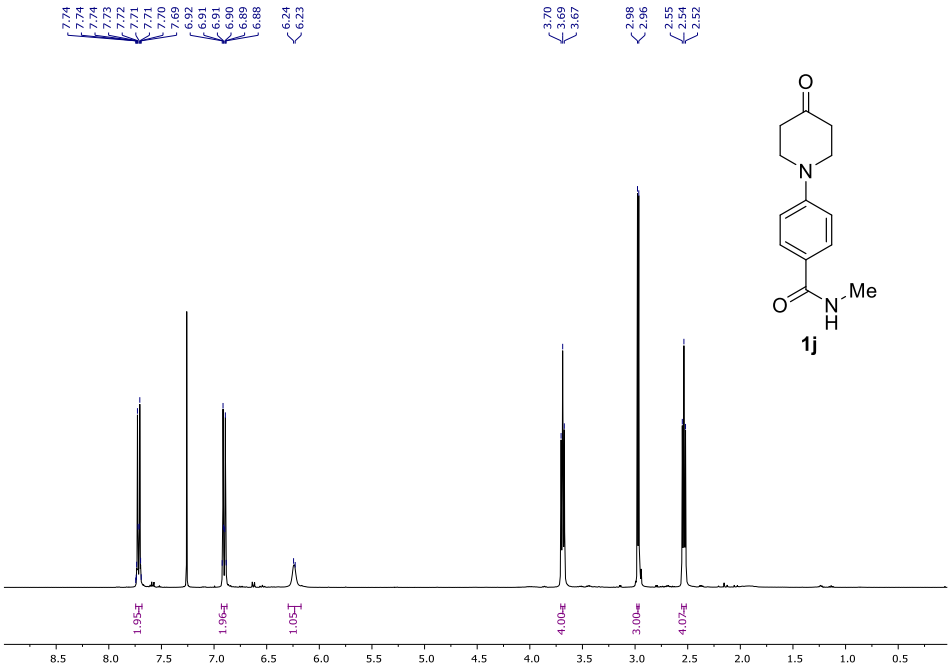

^{1}H-NMR (400 MHz, $CDCl_3$) of **1j**.

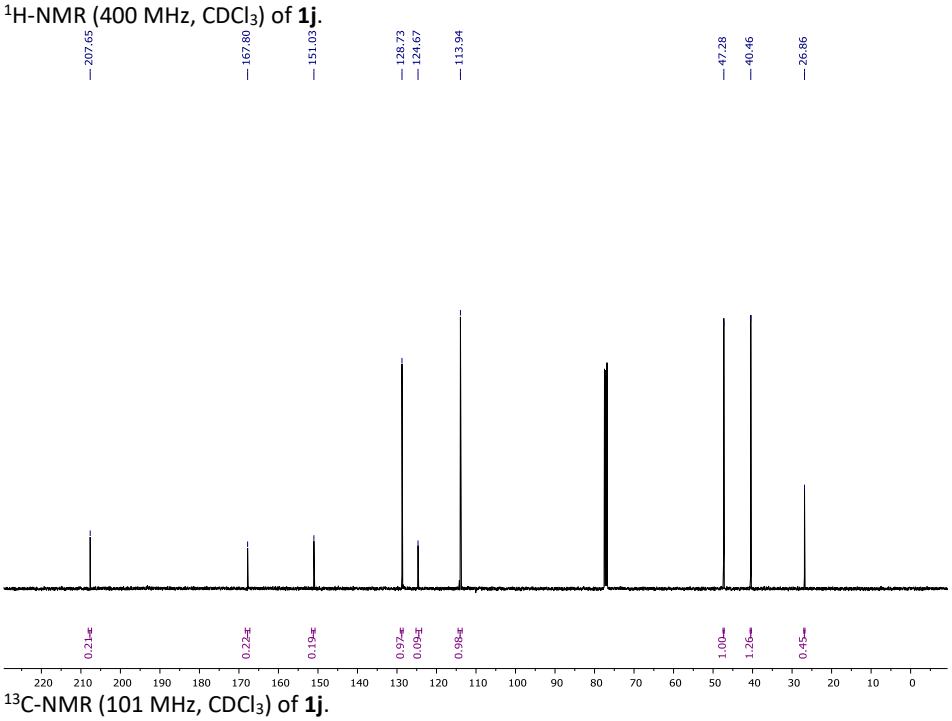

^{13}C-NMR (101 MHz, $CDCl_3$) of **1j**.

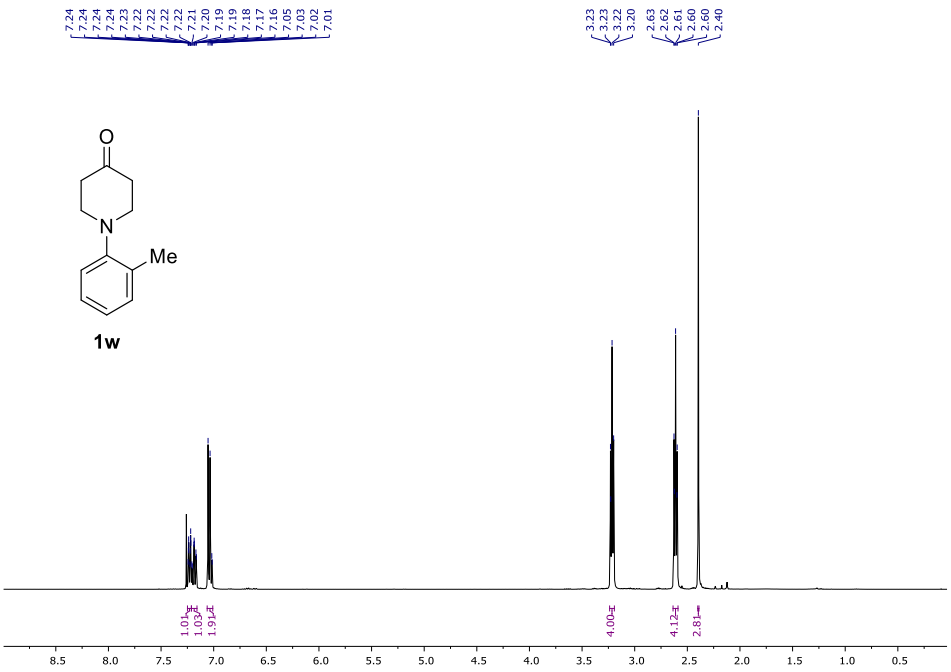

^{1}H-NMR (400 MHz, $CDCl_3$) of **1w**.

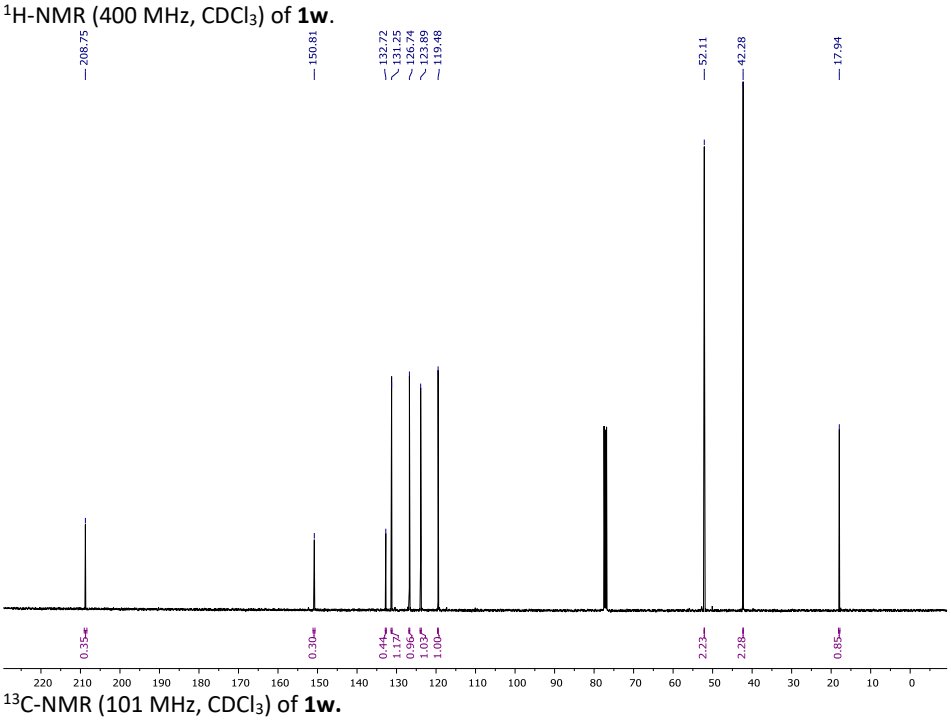

^{13}C-NMR (101 MHz, $CDCl_3$) of **1w.**

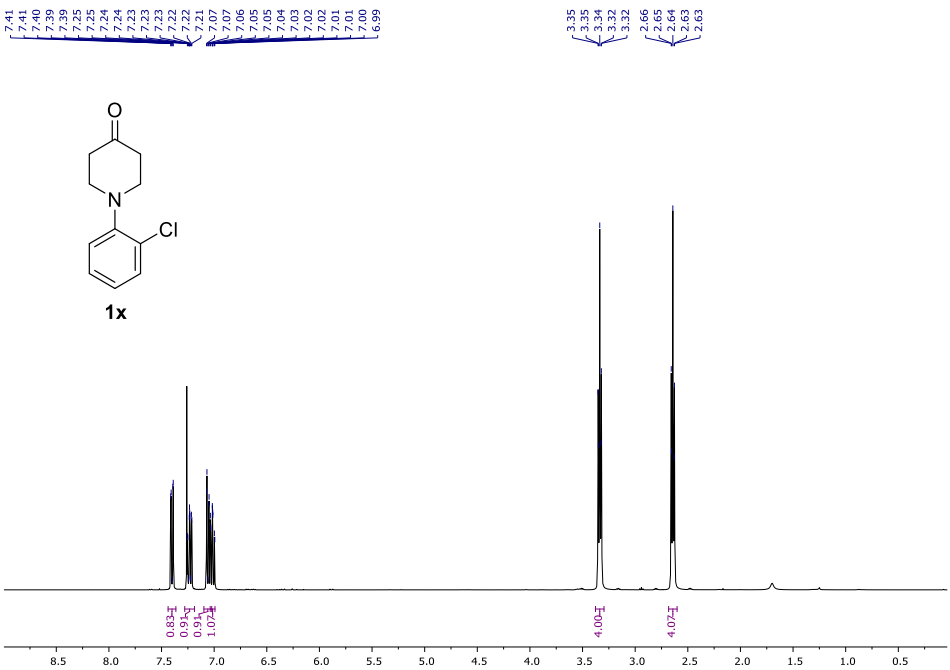

^{1}H-NMR (400 MHz, $CDCl_3$) of **1x**.

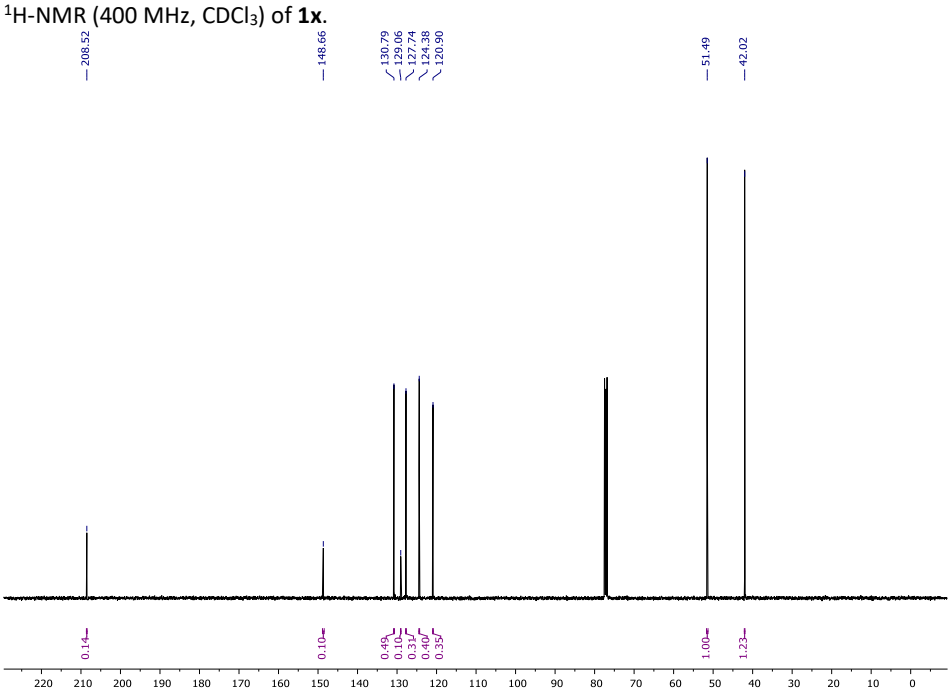

^{13}C-NMR (101 MHz, $CDCl_3$) of **1x.**

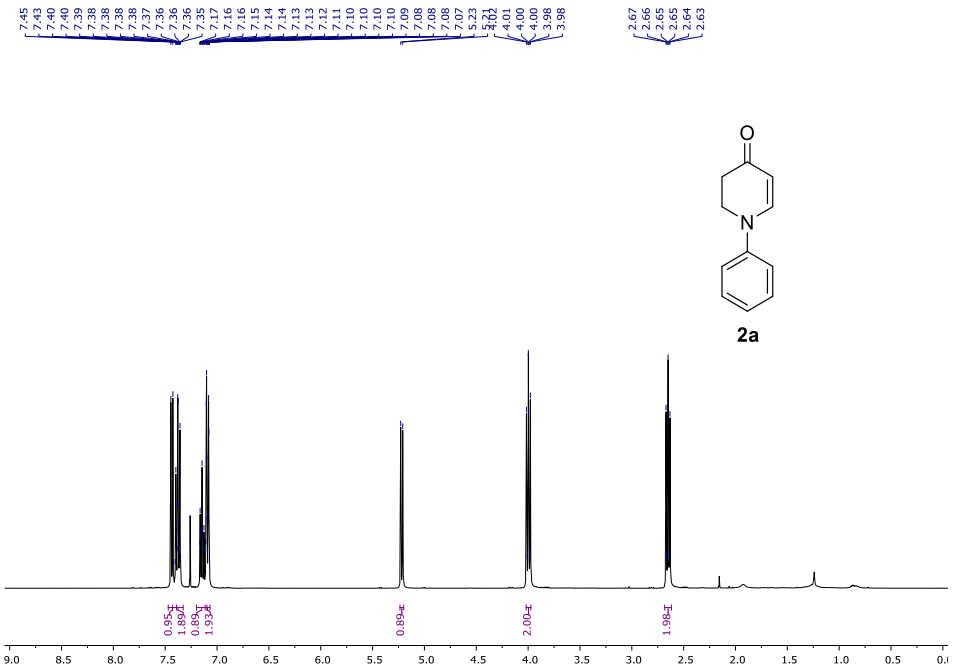

^{1}H-NMR (400 MHz, $CDCl_3$) of **2a**.

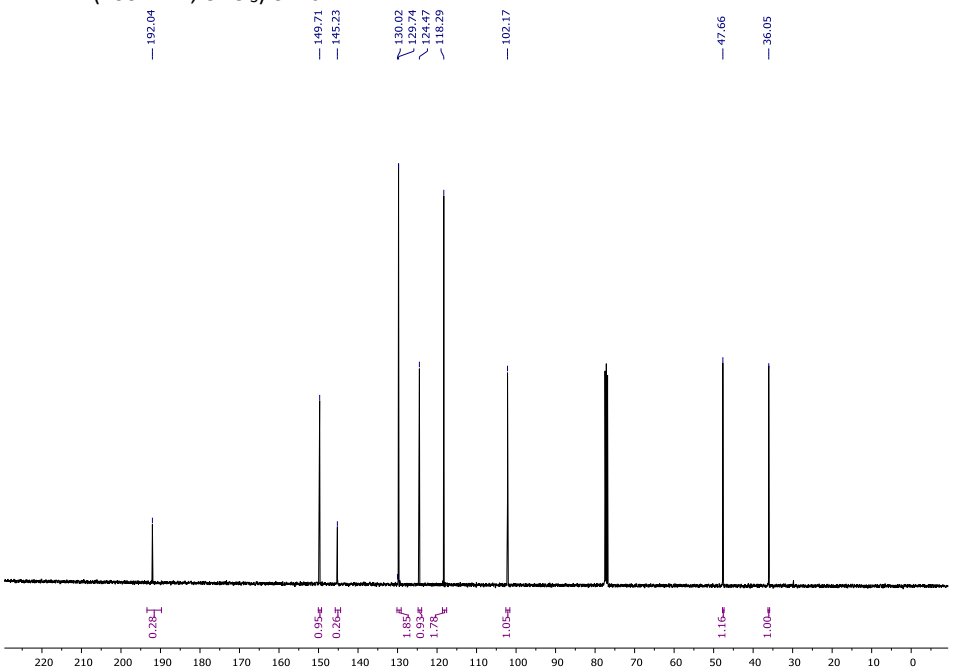

^{13}C-NMR (101 MHz, $CDCl_3$) of **2a.**

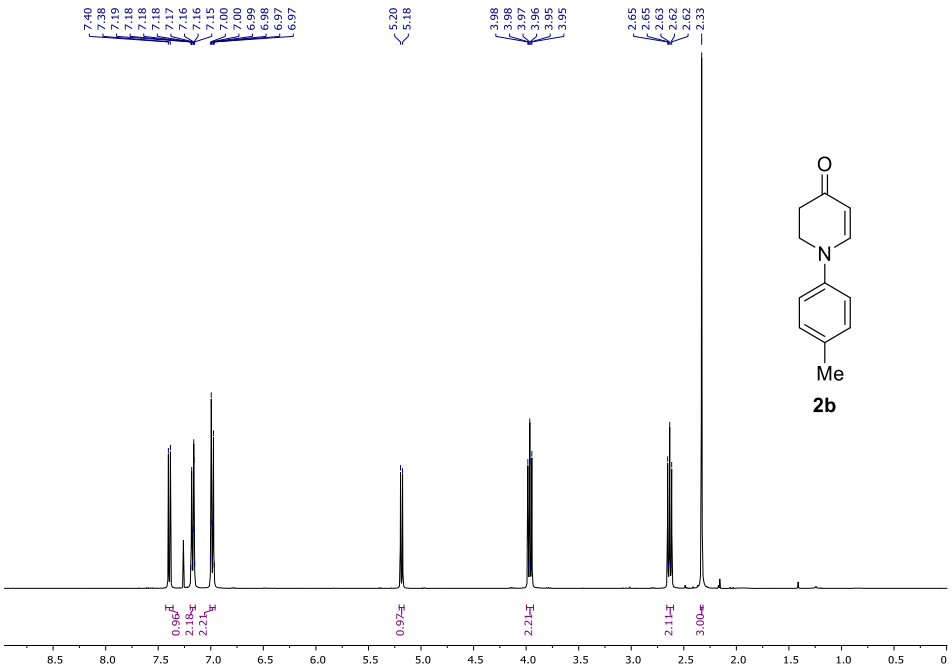

^{1}H-NMR (400 MHz, $CDCl_3$) of **2b**.

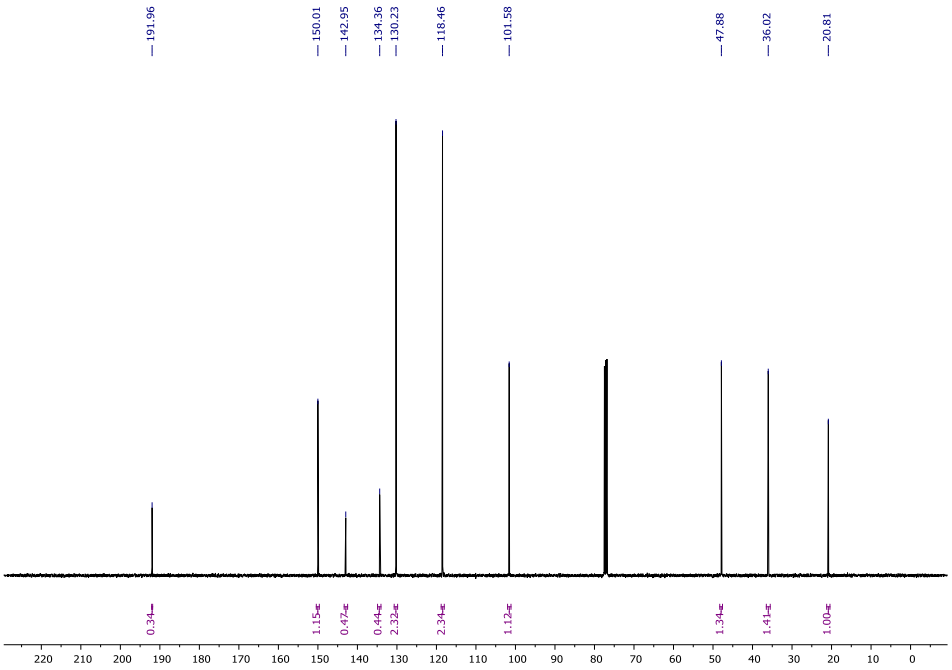

^{13}C-NMR (101 MHz, $CDCl_3$) of **2b**.

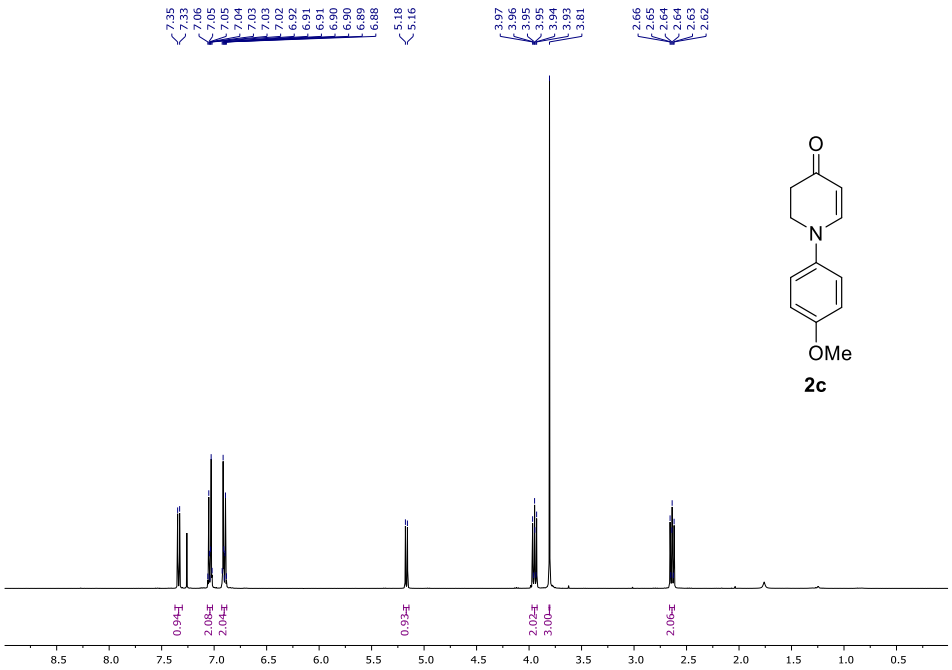

^{1}H-NMR (400 MHz, $CDCl_3$) of **2c**.

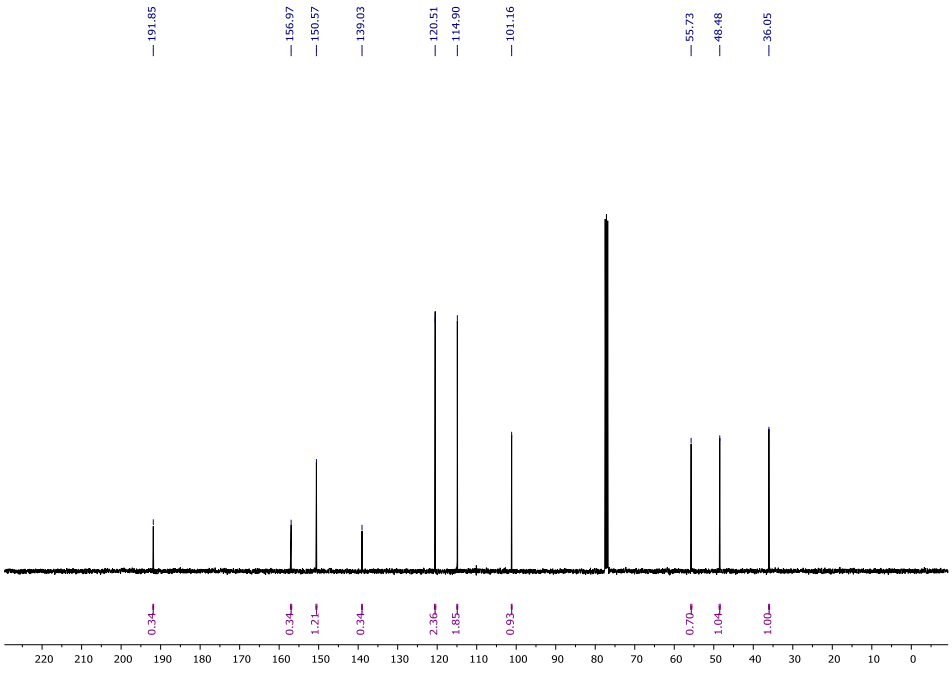

^{13}C-NMR (101 MHz, $CDCl_3$) of **2c**.

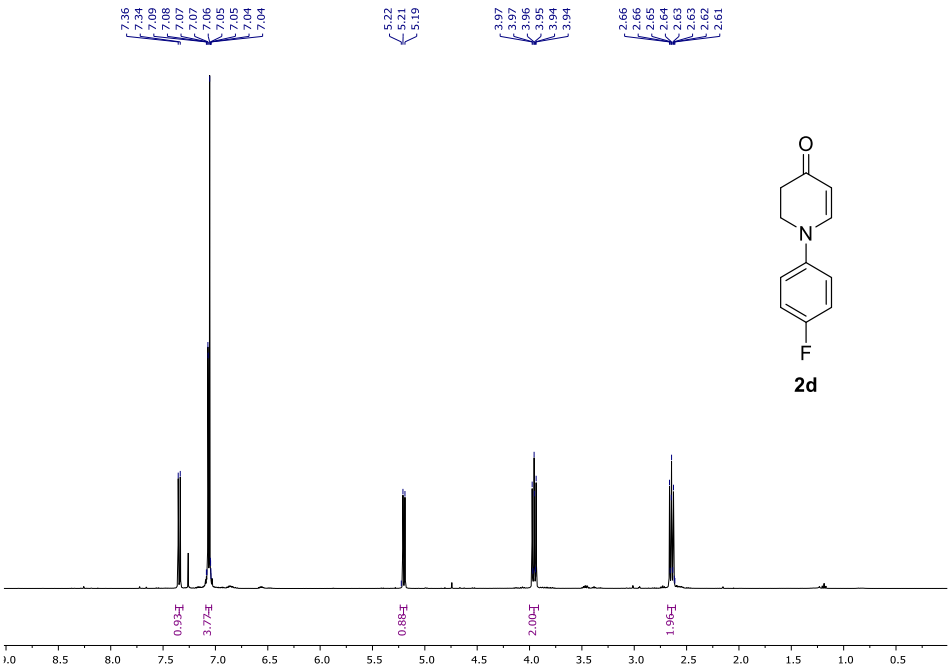

^{1}H-NMR (400 MHz, $CDCl_3$) of **2d**.

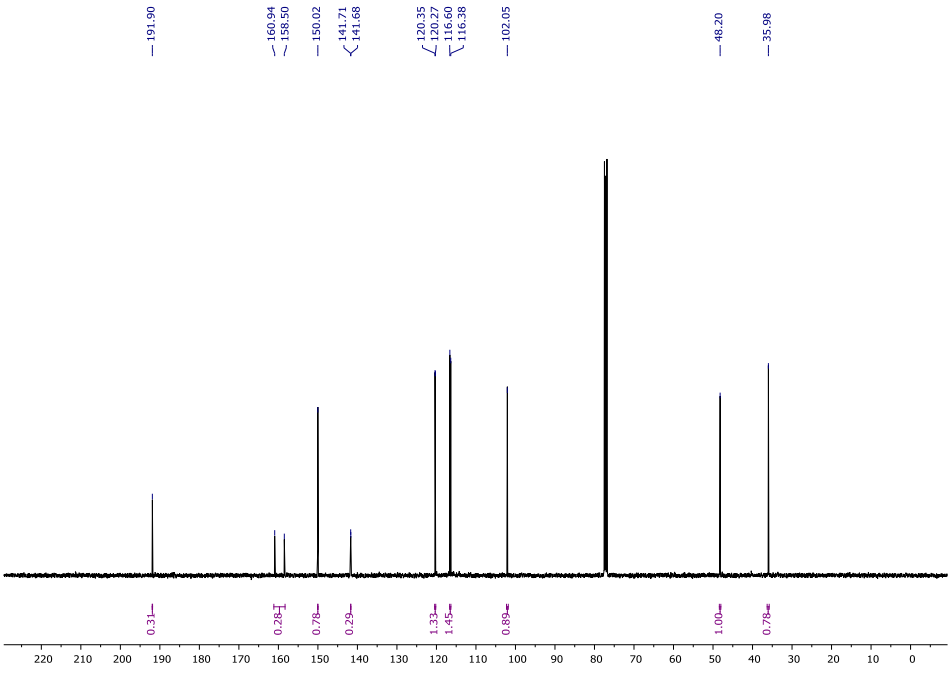

^{13}C-NMR (101 MHz, $CDCl_3$) of **2d**.

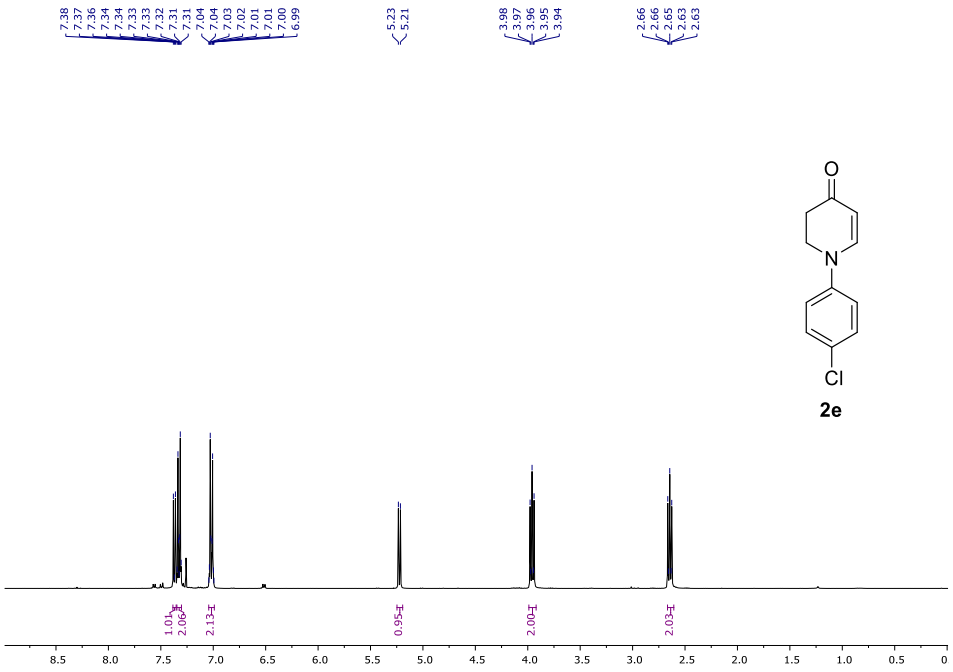

^{1}H-NMR (400 MHz, $CDCl_3$) of **2e**.

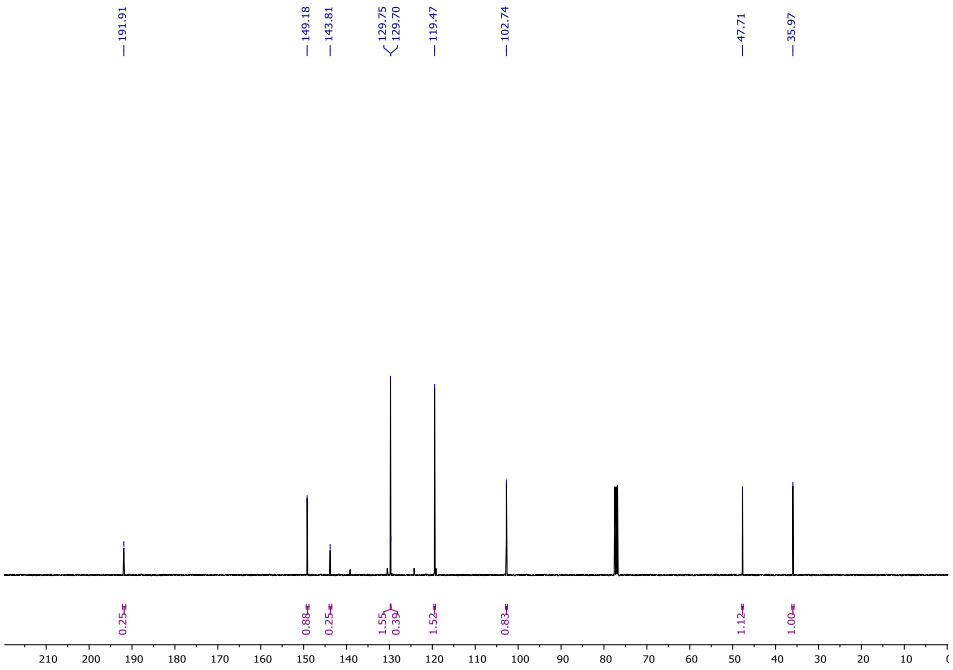

^{13}C-NMR (101 MHz, $CDCl_3$) of **2e**.

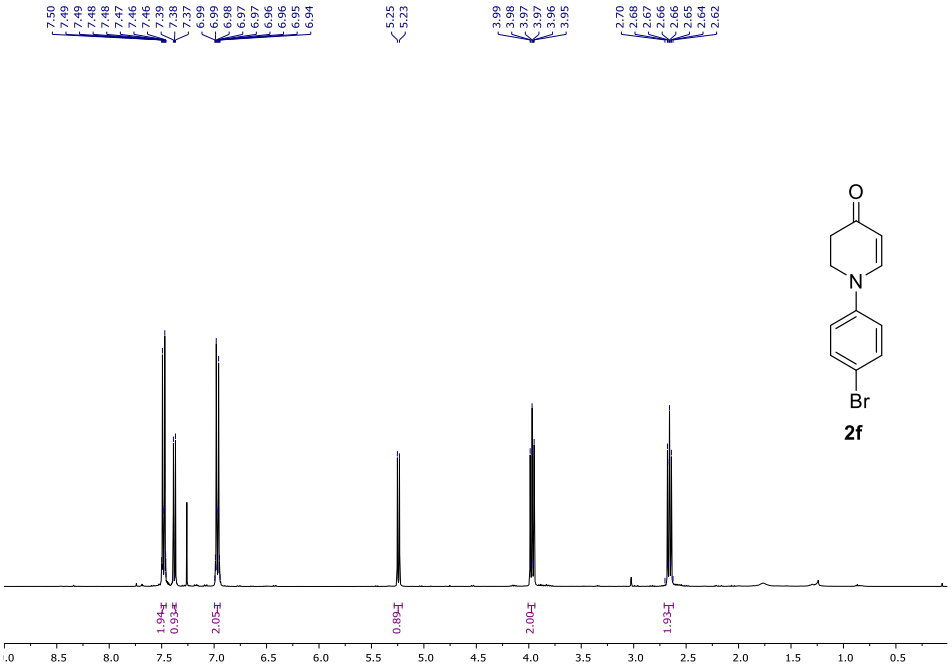

^{1}H-NMR (400 MHz, $CDCl_3$) of **2f**.

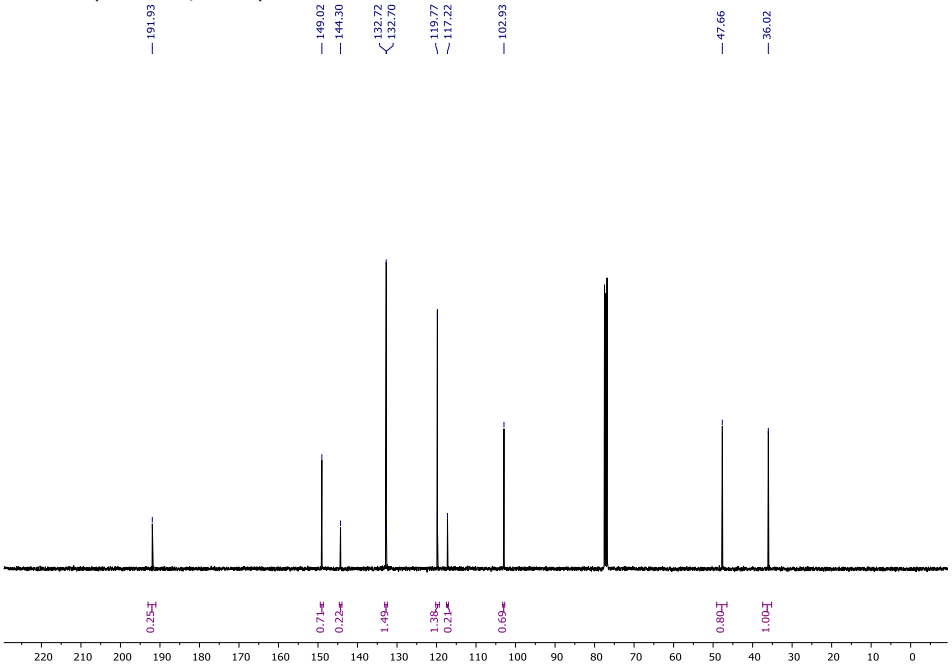

^{13}C-NMR (101 MHz, $CDCl_3$) of **2f**.

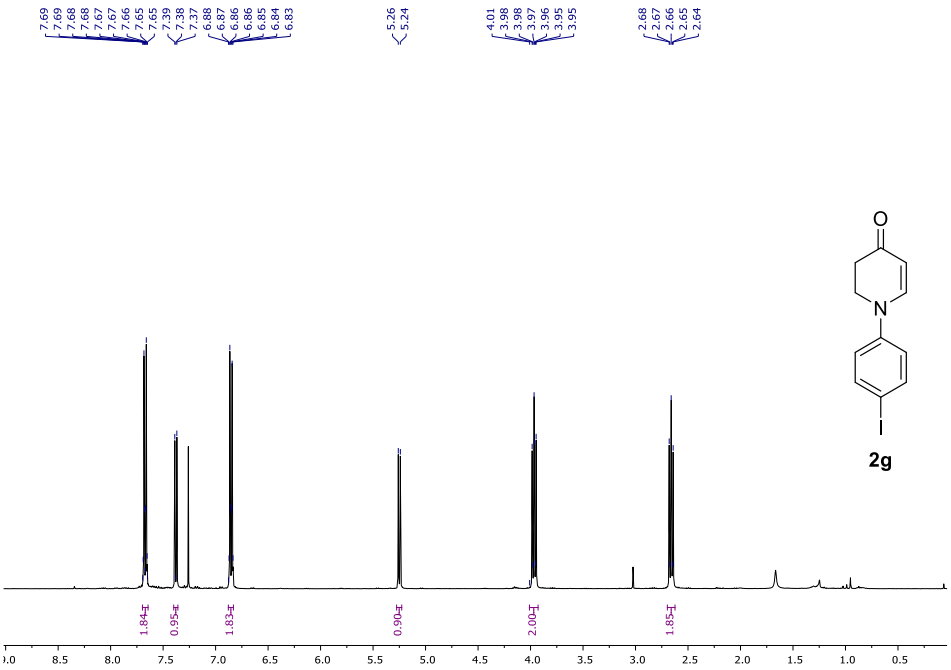

^{1}H-NMR (400 MHz, $CDCl_3$) of **2g**.

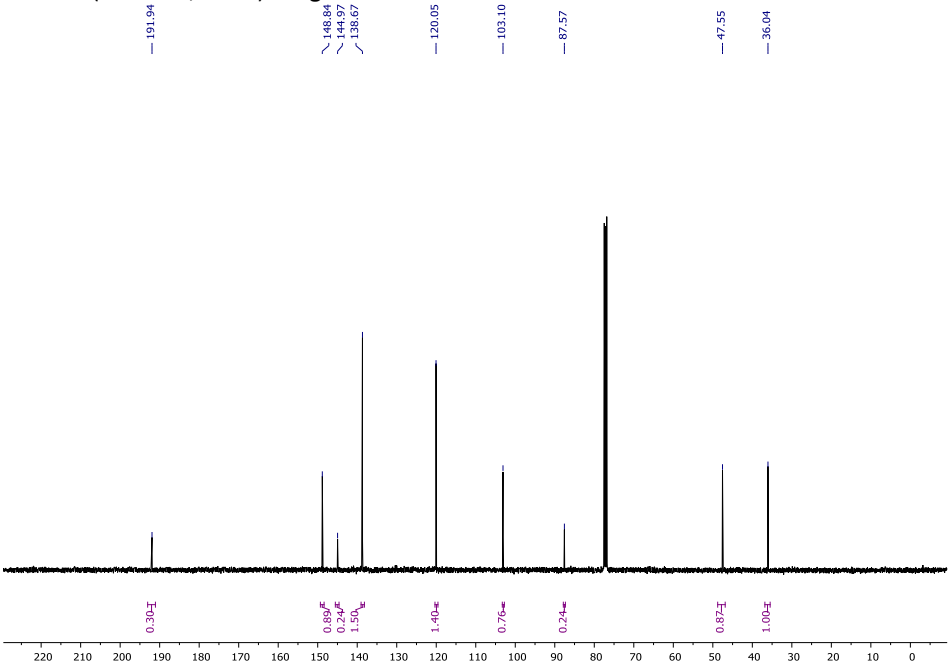

^{13}C-NMR (101 MHz, $CDCl_3$) of **2g**.

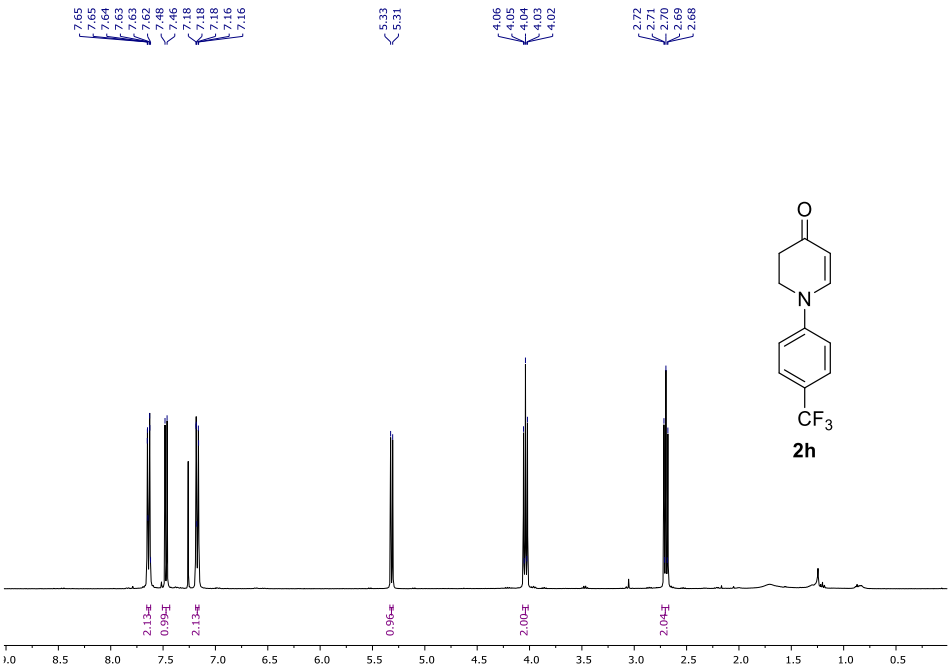

^{1}H-NMR (400 MHz, $CDCl_3$) of **2h**.

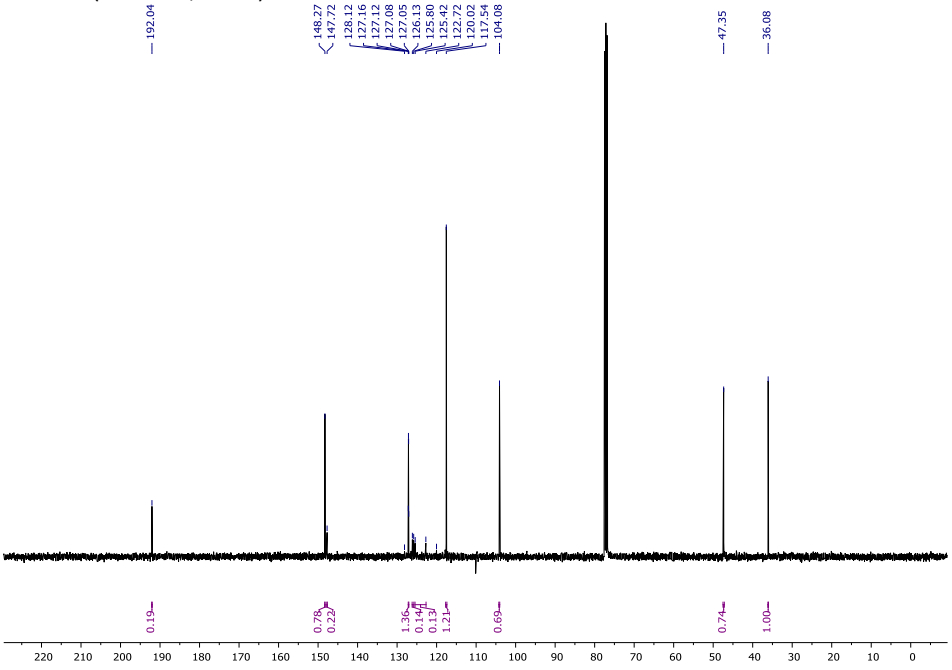

^{13}C-NMR (101 MHz, $CDCl_3$) of **2h**.

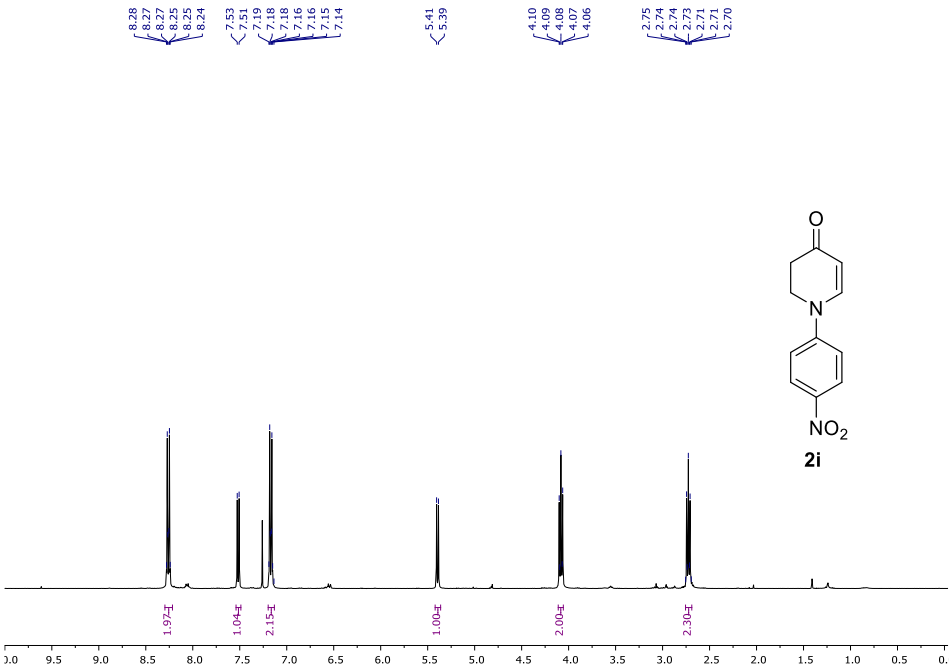

^{1}H-NMR (400 MHz, $CDCl_3$) of **2i**.

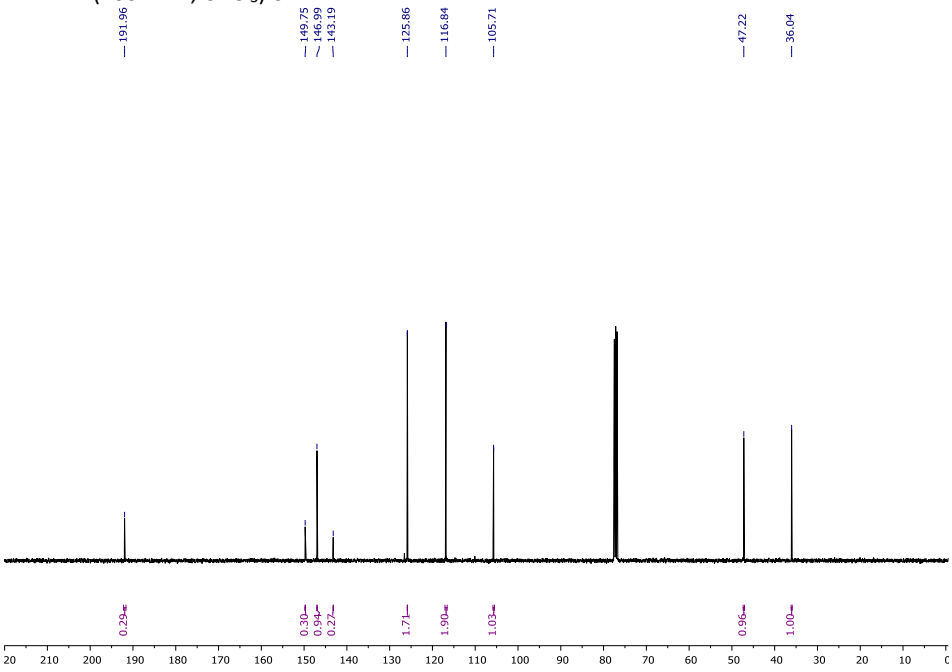

^{13}C-NMR (101 MHz, $CDCl_3$) of **2i**.

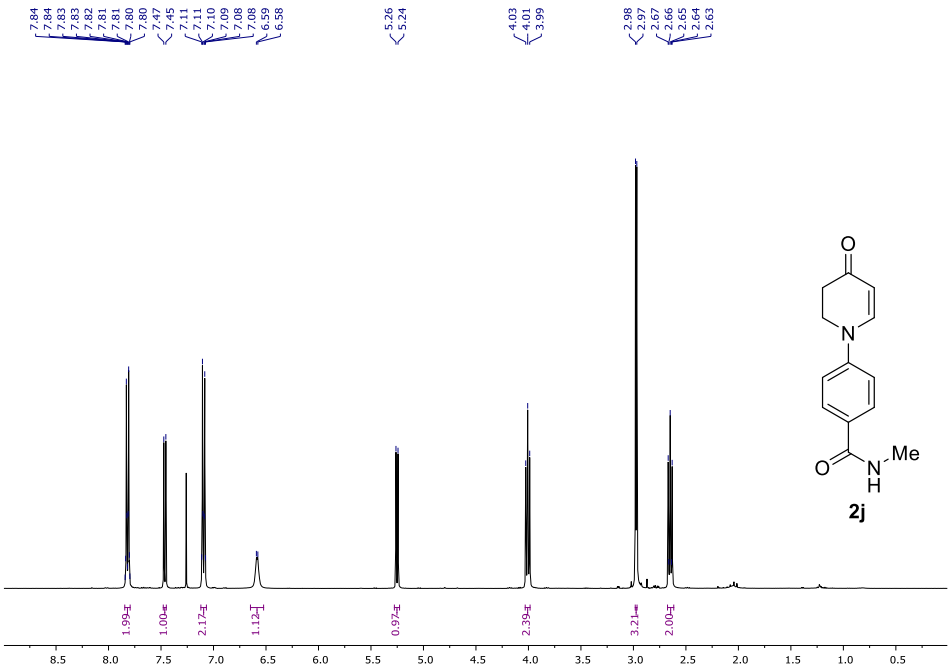

^{1}H-NMR (400 MHz, $CDCl_3$) of **2j**.

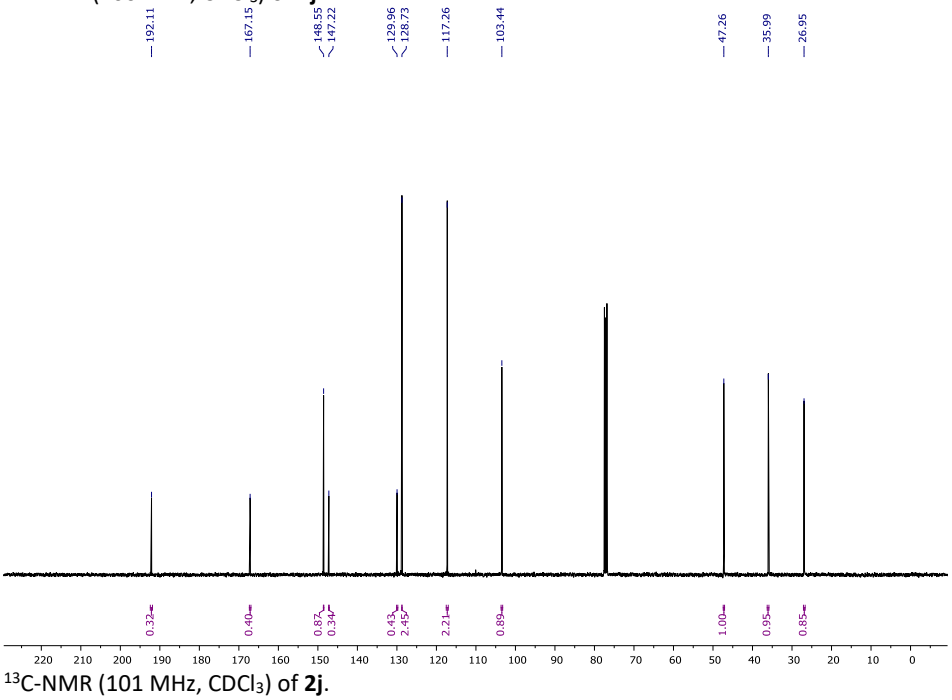

^{13}C-NMR (101 MHz, $CDCl_3$) of **2j**.

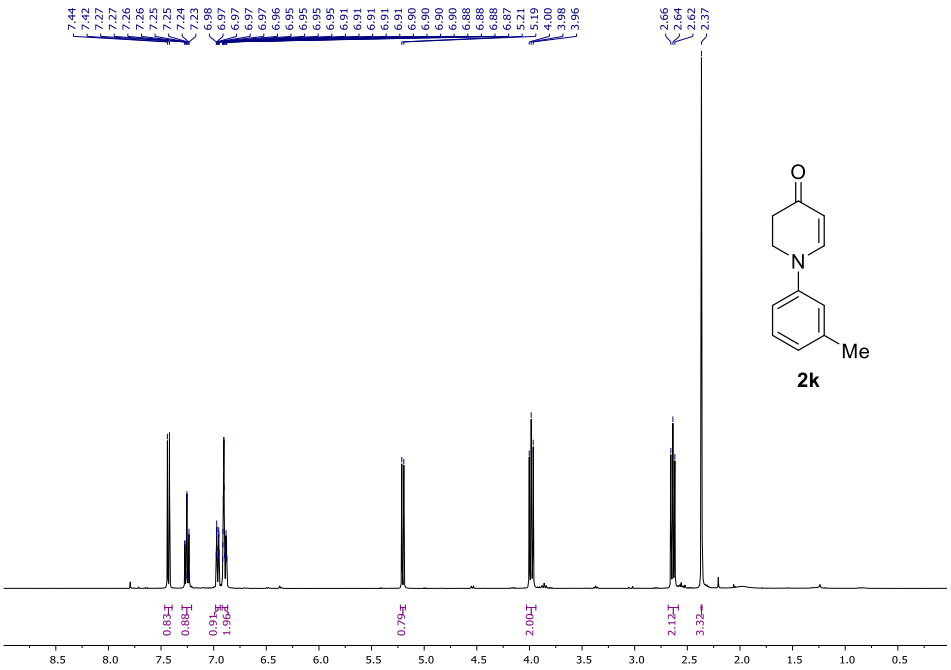

^{1}H-NMR (400 MHz, $CDCl_3$) of **2k**.

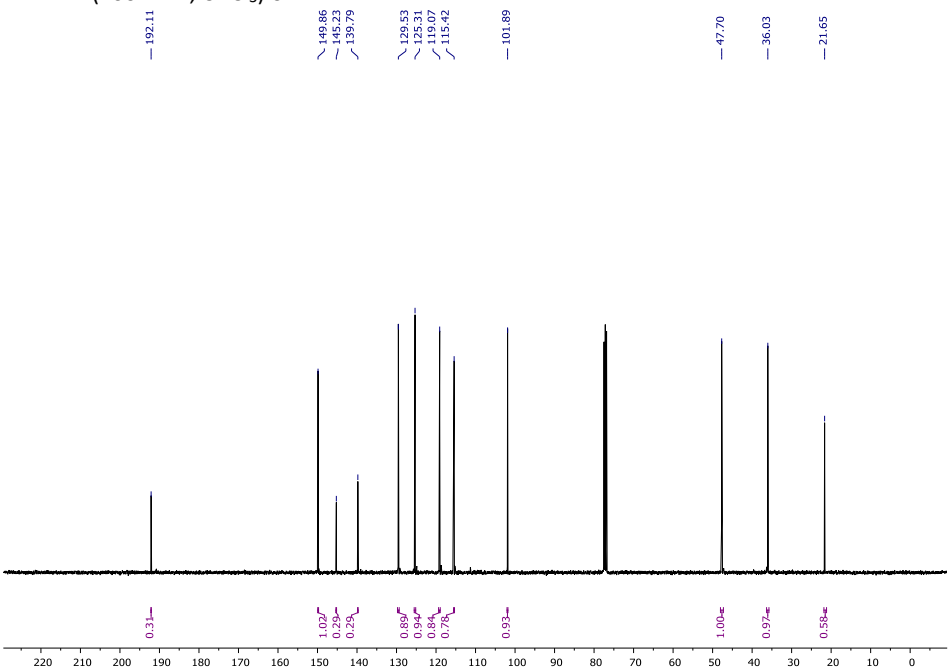

^{13}C-NMR (101 MHz, $CDCl_3$) of **2k**.

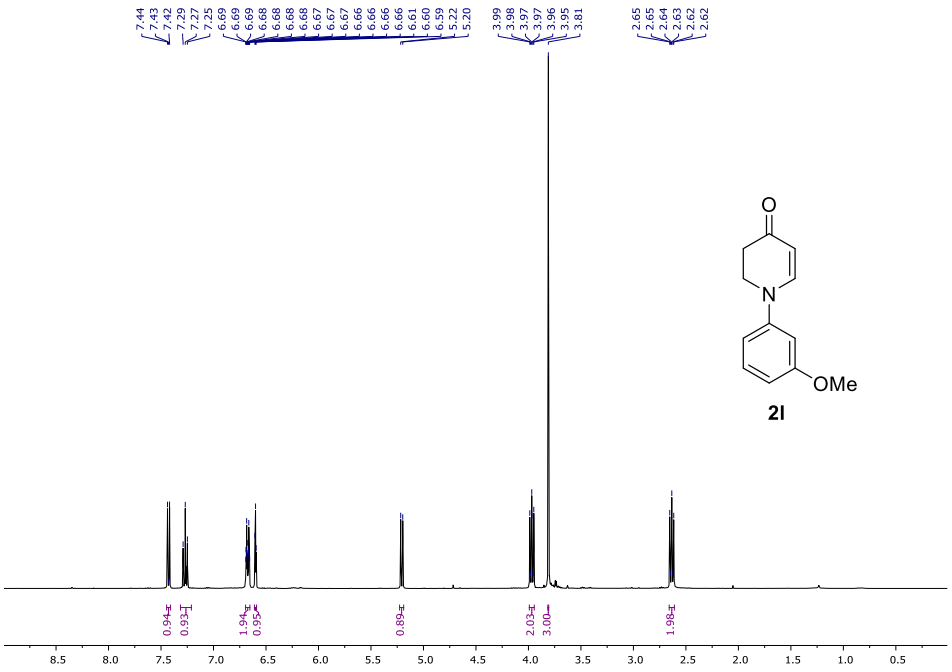

^{1}H-NMR (400 MHz, $CDCl_3$) of **2l.**

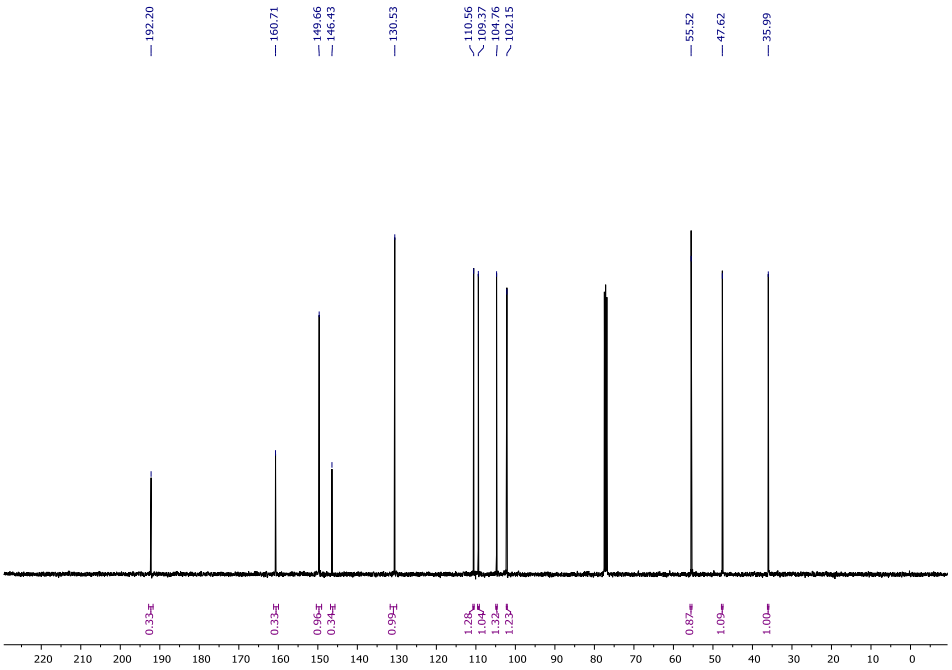

^{13}C-NMR (101 MHz, $CDCl_3$) of **2l**.

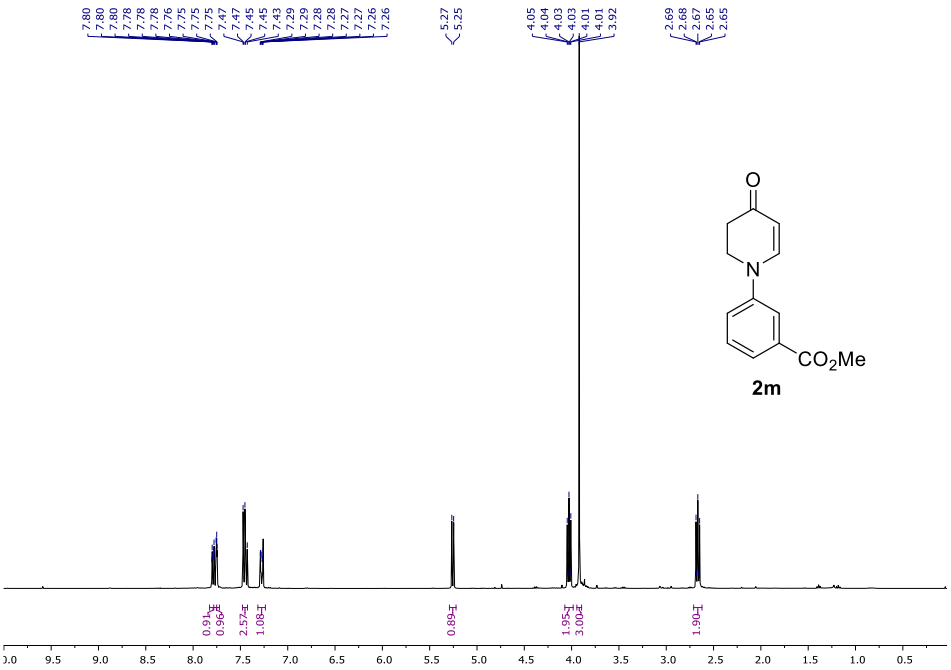

^{1}H-NMR (400 MHz, $CDCl_3$) of **2m.**

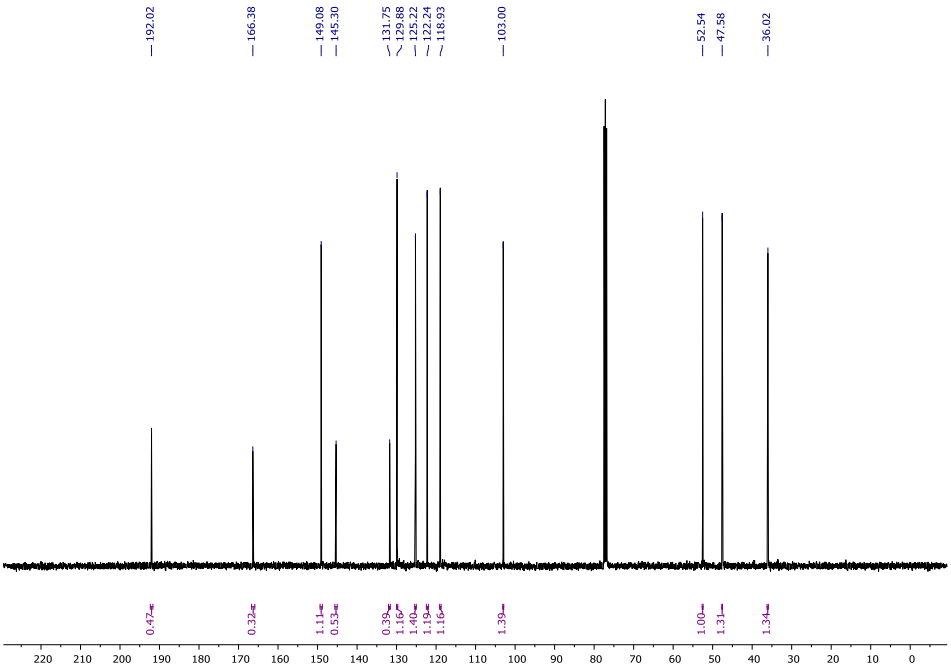

^{13}C-NMR (101 MHz, $CDCl_3$) of **2m**.

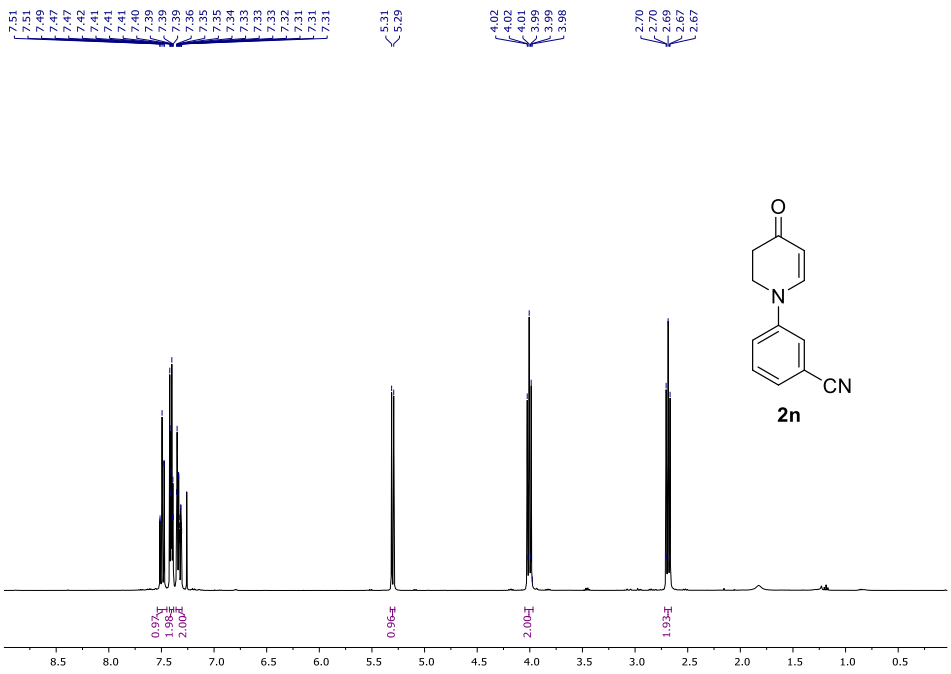

^{1}H-NMR (400 MHz, $CDCl_3$) of **2n**.

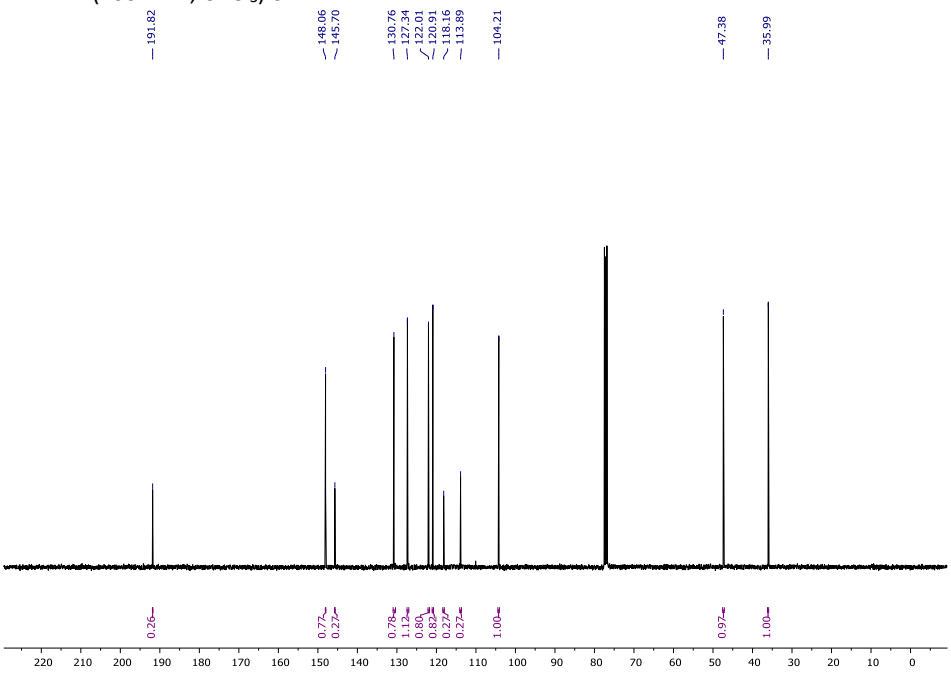

^{13}C-NMR (101 MHz, $CDCl_3$) of **2n**.

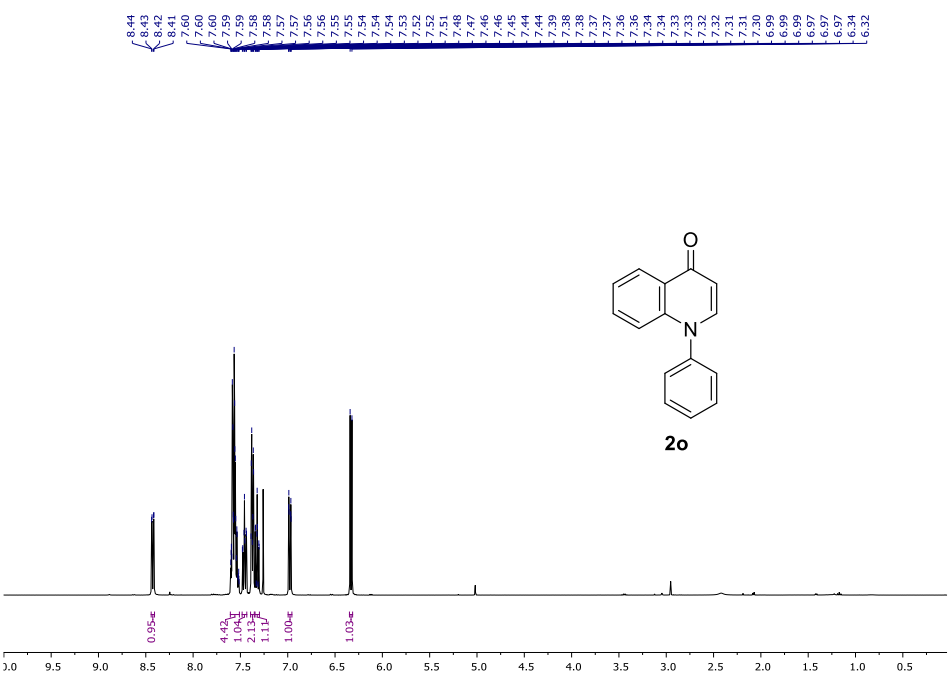

^{1}H-NMR (400 MHz, $CDCl_3$) of **2o**.

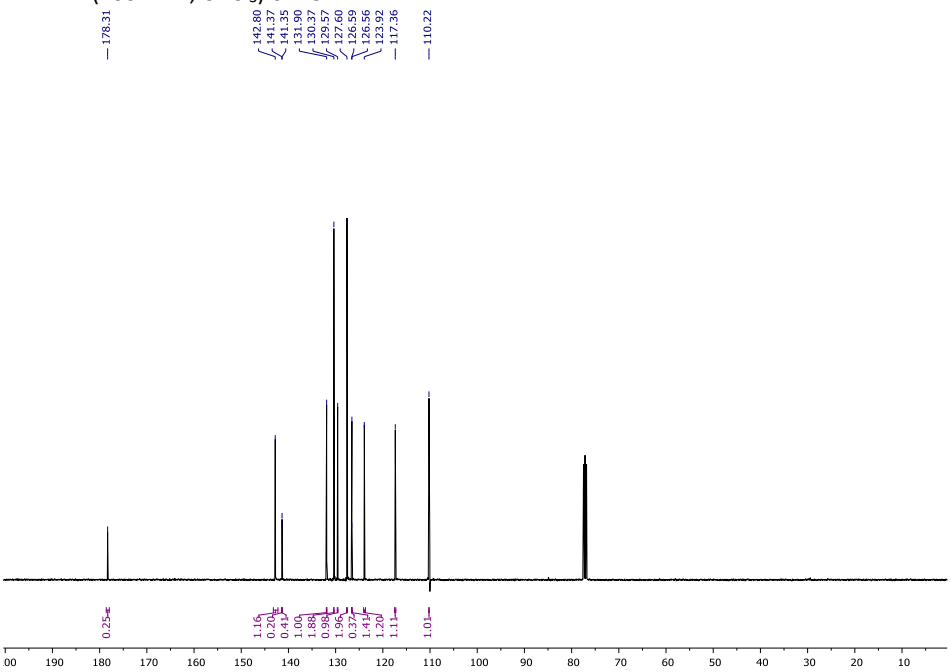

^{13}C-NMR (101 MHz, $CDCl_3$) of **2o.**

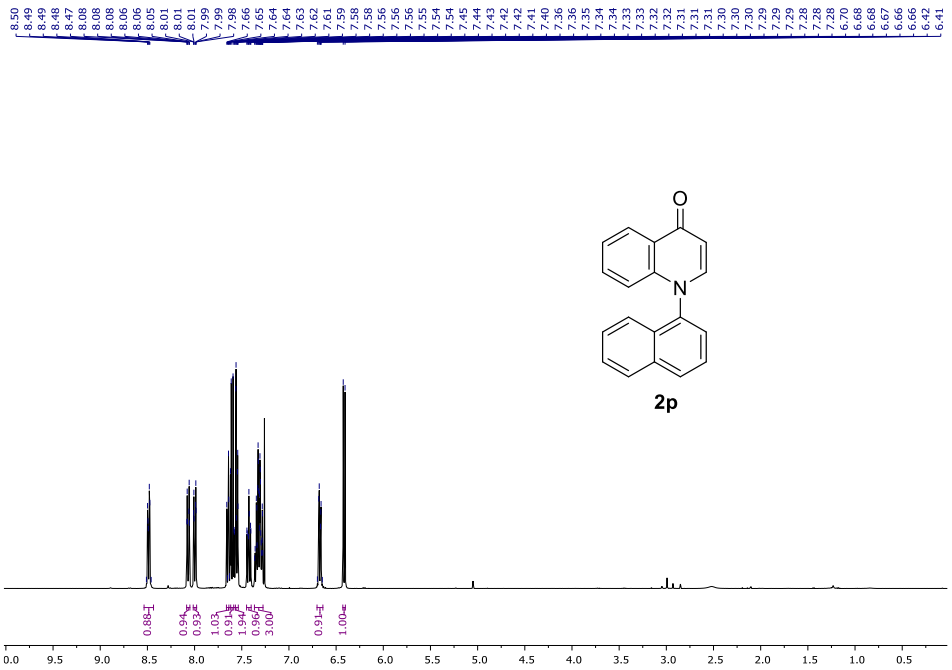

^{1}H-NMR (400 MHz, $CDCl_3$) of **2p.**

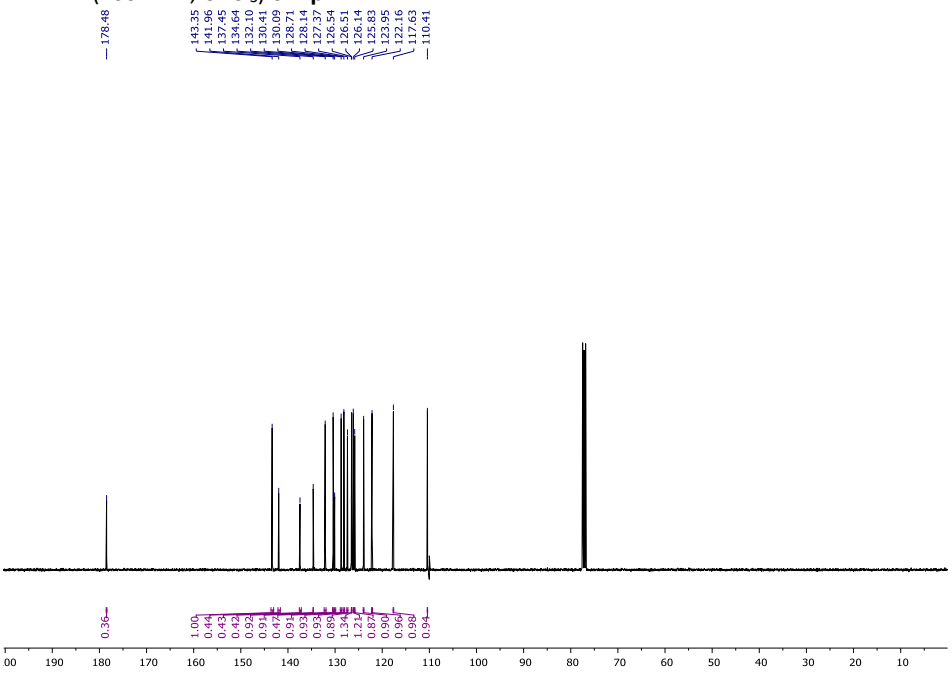

^{13}C-NMR (101 MHz, $CDCl_3$) of **2p.**

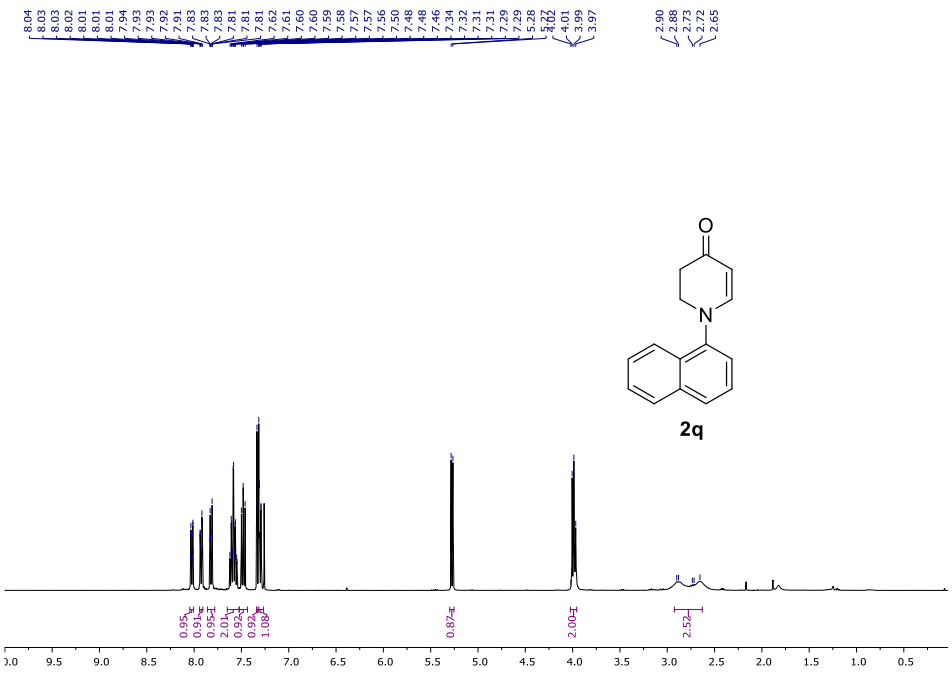

^{1}H-NMR (400 MHz, $CDCl_3$) of **2q**.

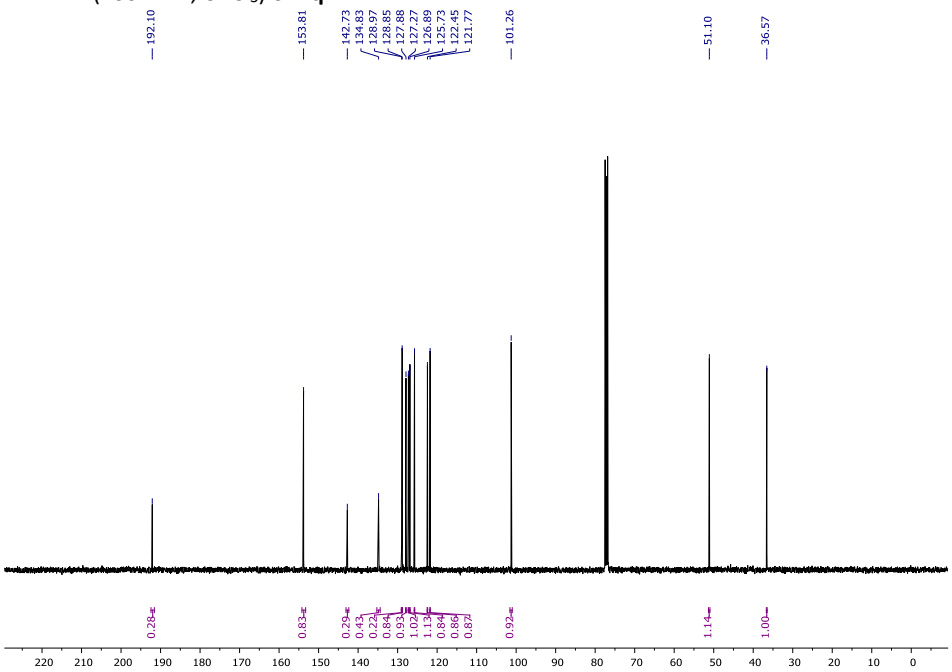

^{13}C-NMR (101 MHz, $CDCl_3$) of **2q.**

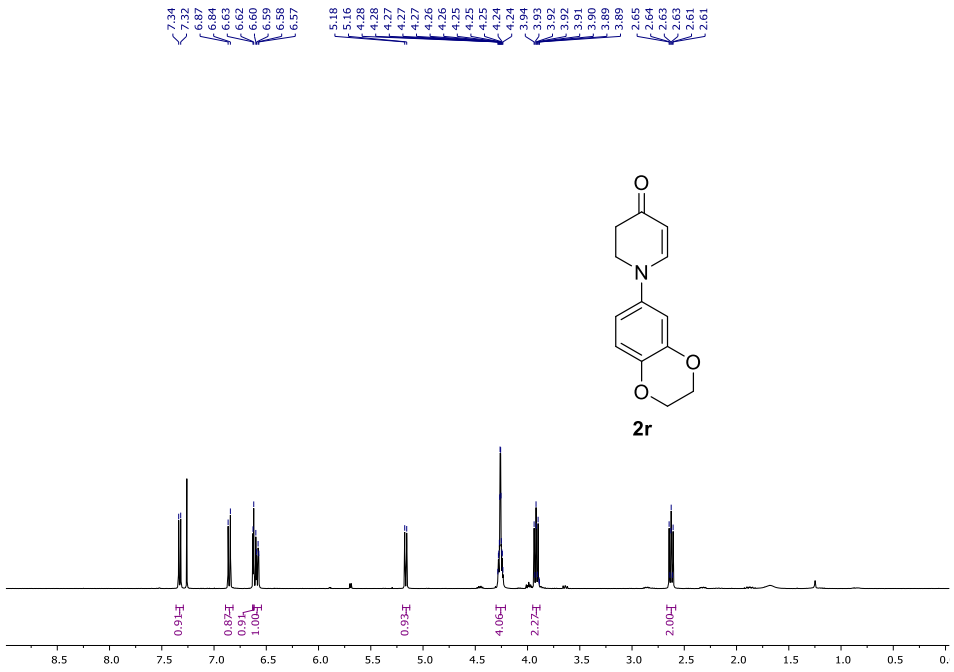

^{1}H-NMR (400 MHz, $CDCl_3$) of **2r**.

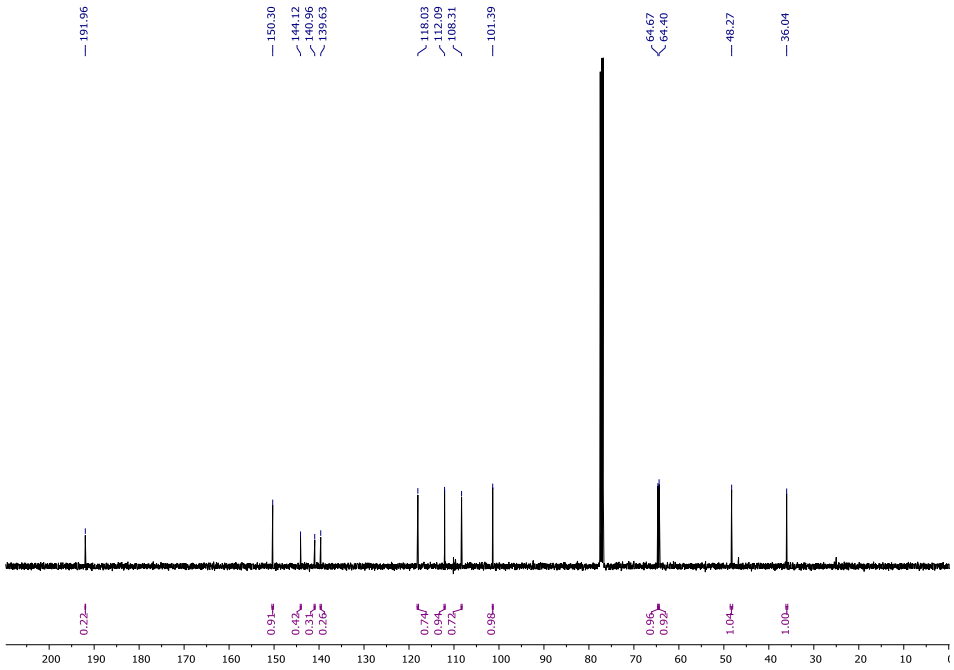

^{13}C-NMR (101 MHz, $CDCl_3$) of **2r**.

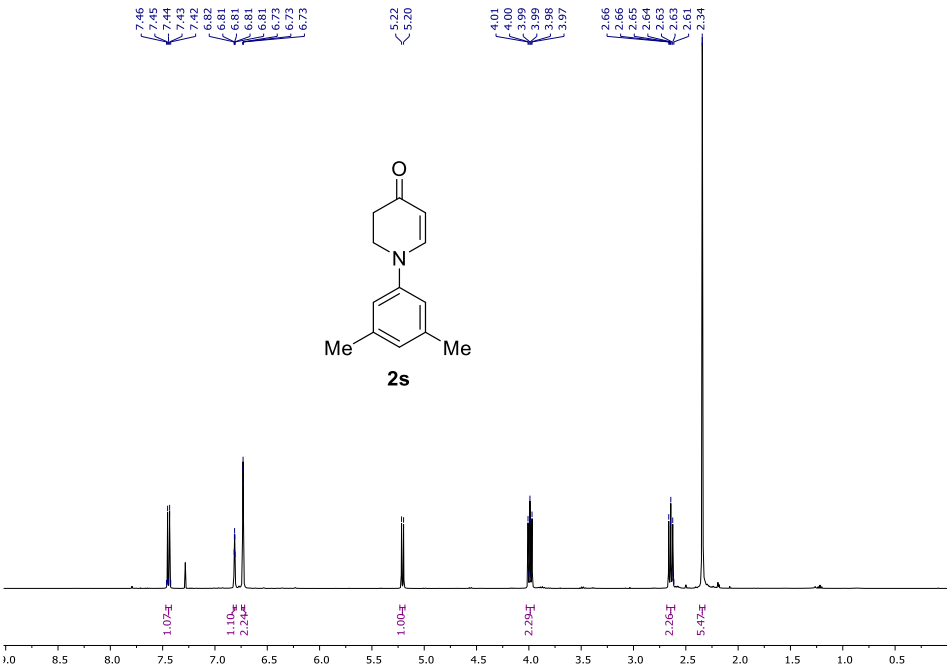

^{1}H-NMR (400 MHz, $CDCl_3$) of **2s**.

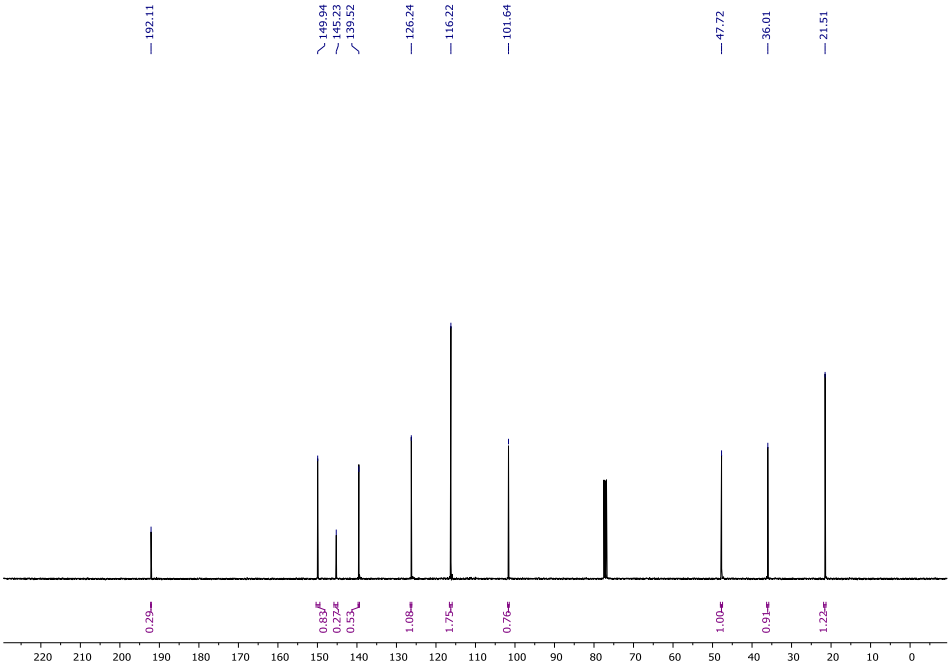

^{13}C-NMR (101 MHz, $CDCl_3$) of **2s**.

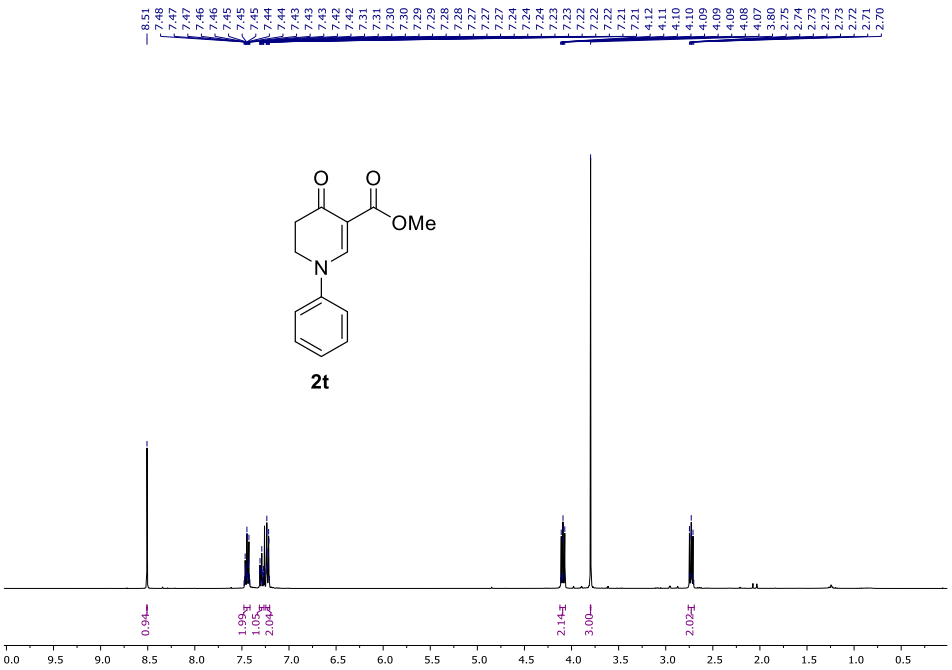

^{1}H-NMR (400 MHz, $CDCl_3$) of **2t**.

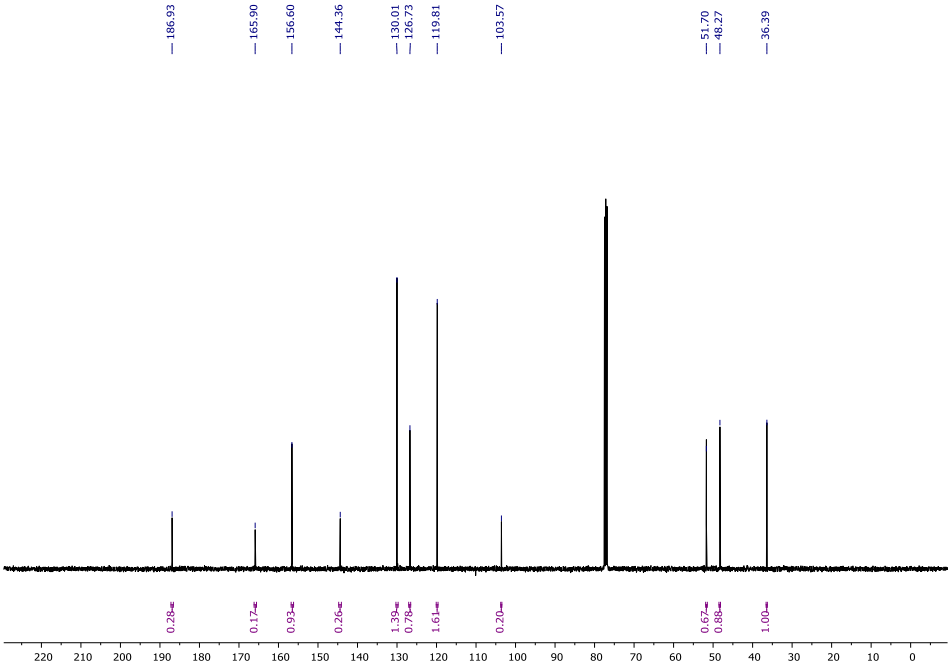

^{13}C-NMR (101 MHz, $CDCl_3$) of **2t.**

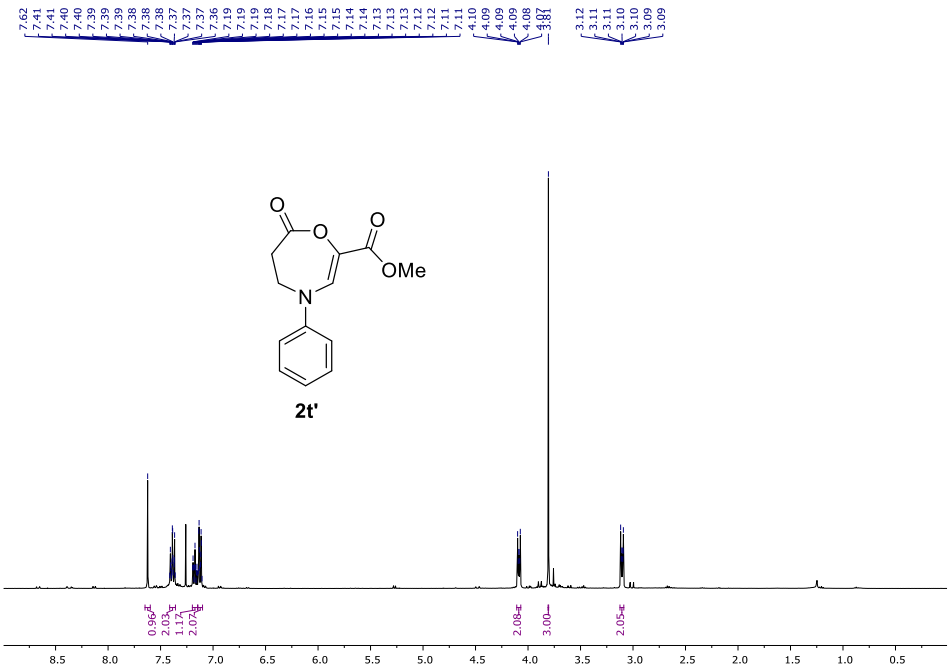

^{1}H-NMR (400 MHz, $CDCl_3$) of **2t'**.

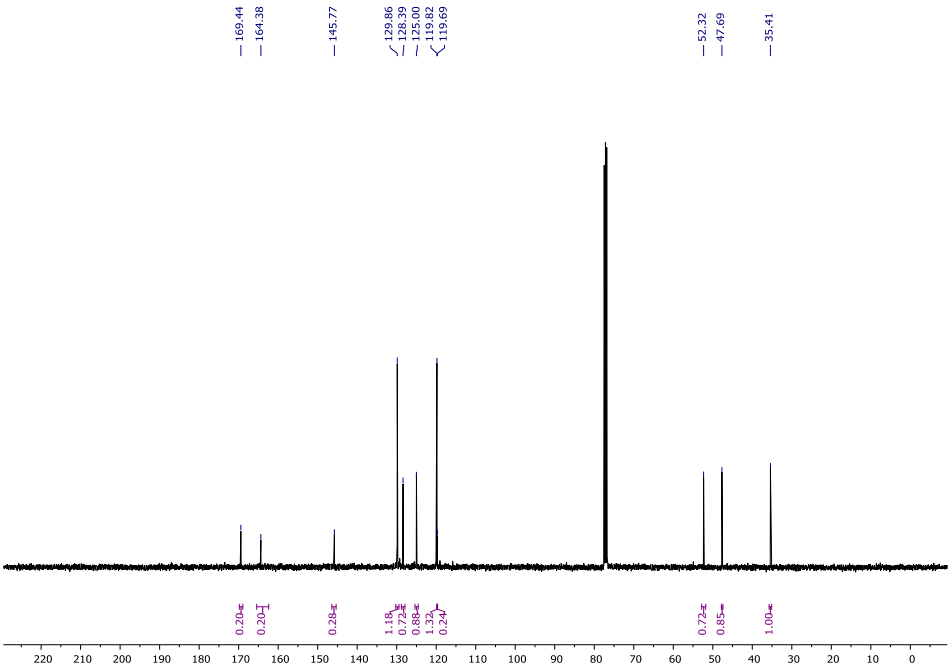

^{13}C-NMR (101 MHz, $CDCl_3$) of **2t'**.

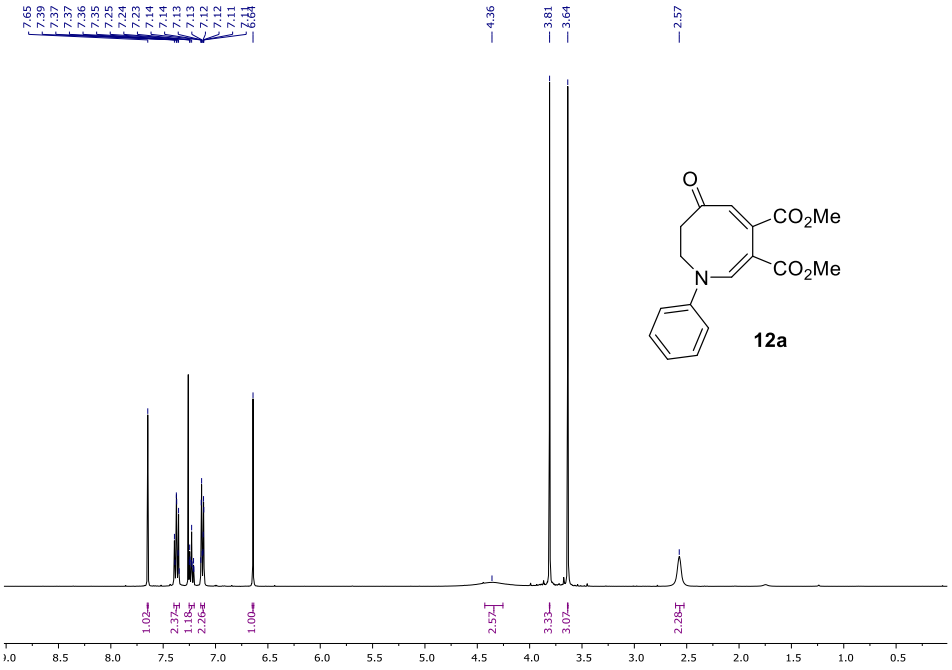

^{1}H-NMR (400 MHz, $CDCl_3$) of **12a**.

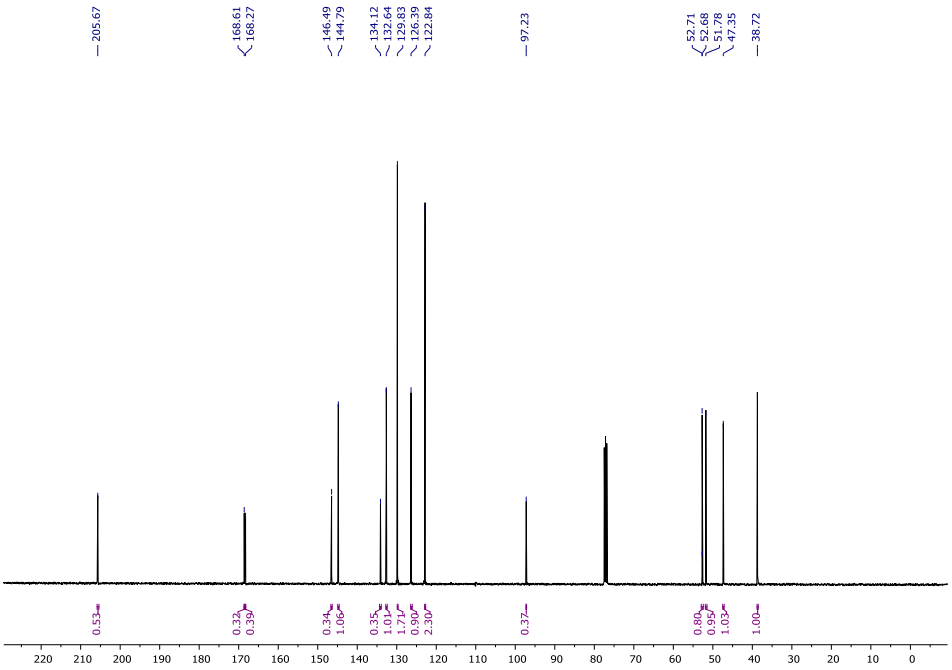

^{13}C-NMR (101 MHz, $CDCl_3$) of **12a.**

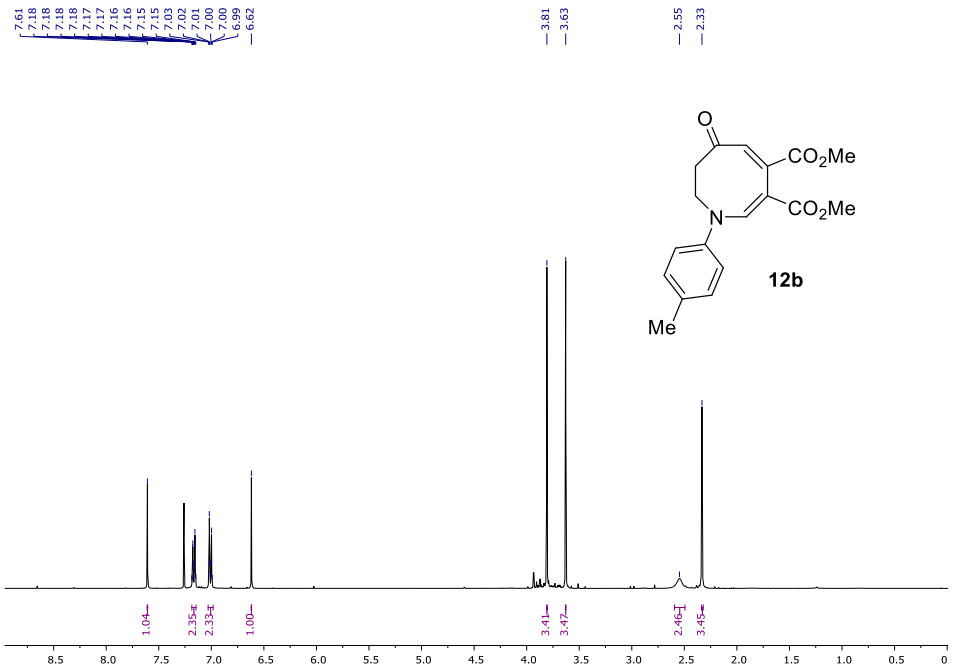

^{1}H-NMR (400 MHz, $CDCl_3$) of **12b**.

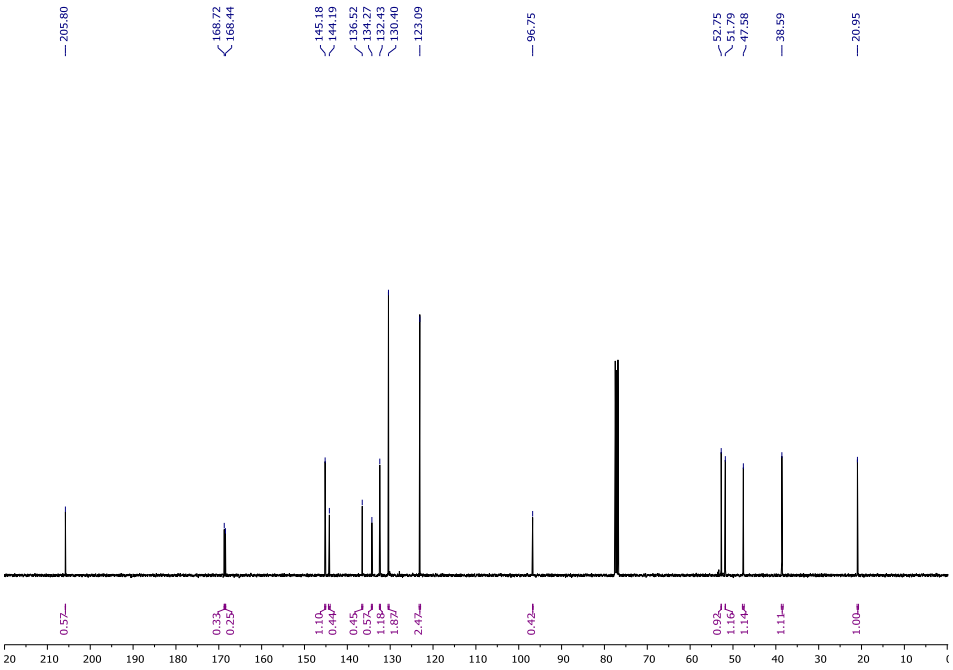

^{13}C-NMR (101 MHz, $CDCl_3$) of **12b.**

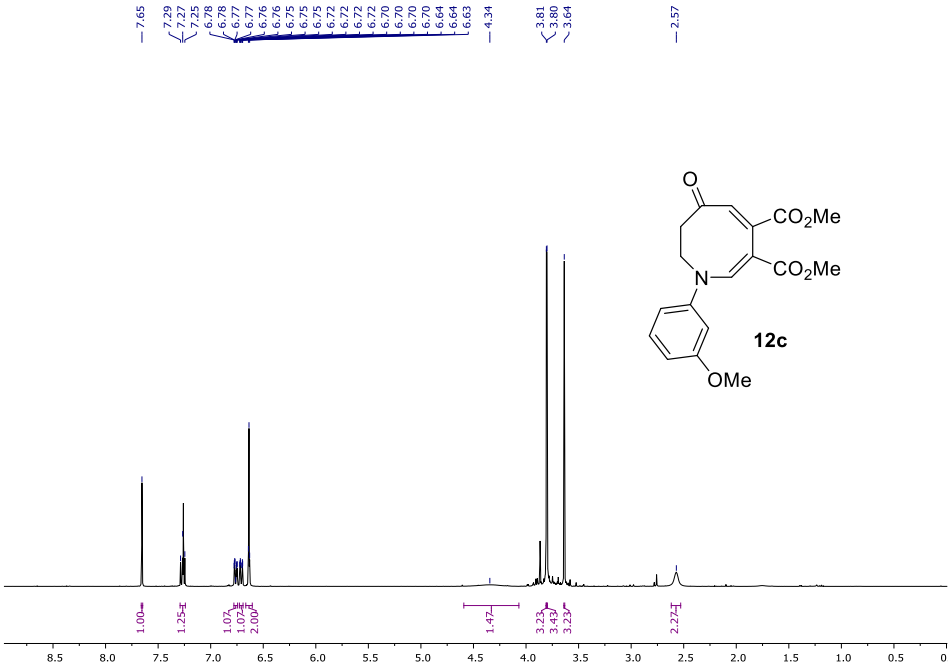

^{1}H-NMR (400 MHz, $CDCl_3$) of **12c**.

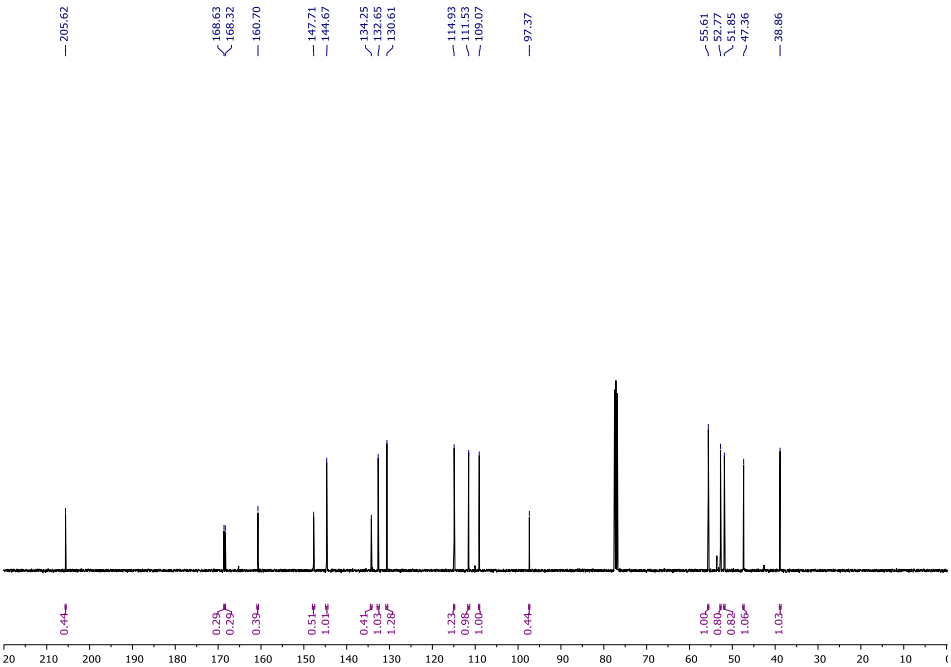

^{13}C-NMR (101 MHz, $CDCl_3$) of **12c.**

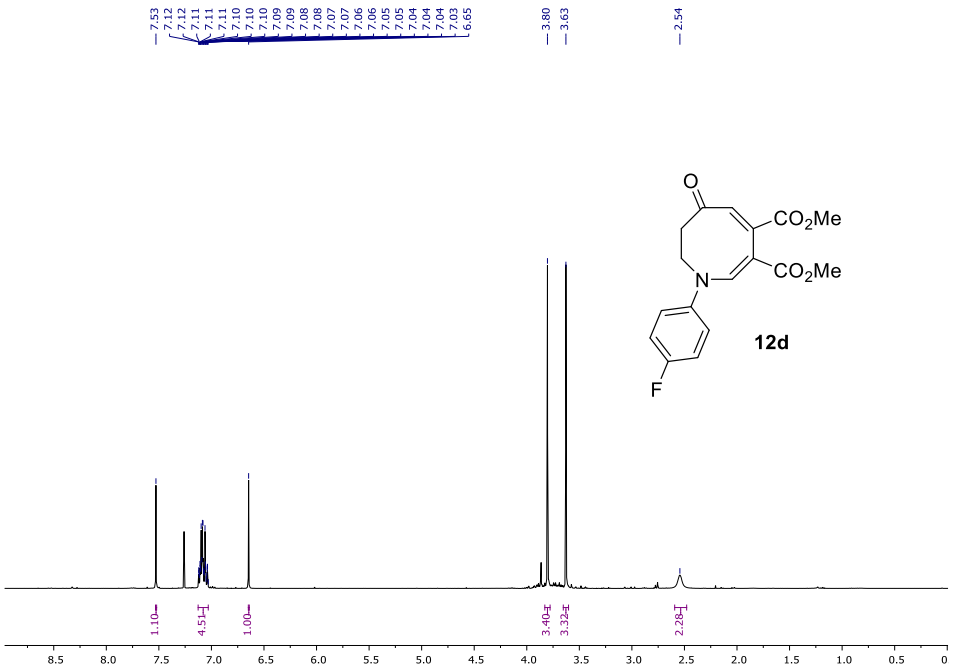

^{1}H-NMR (400 MHz, $CDCl_3$) of **12d**.

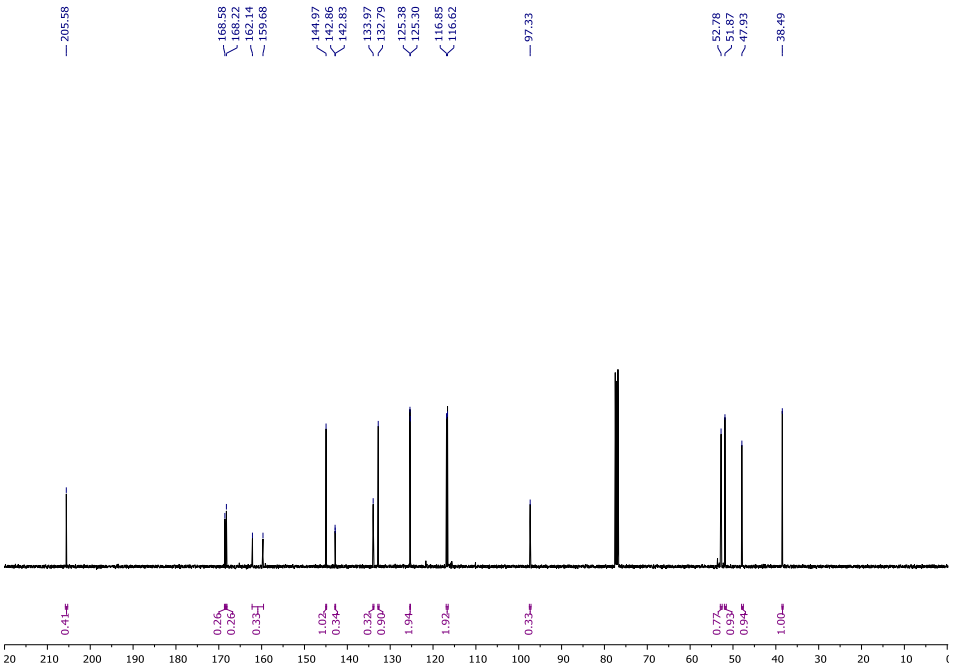

^{13}C-NMR (101 MHz, $CDCl_3$) of **12d.**

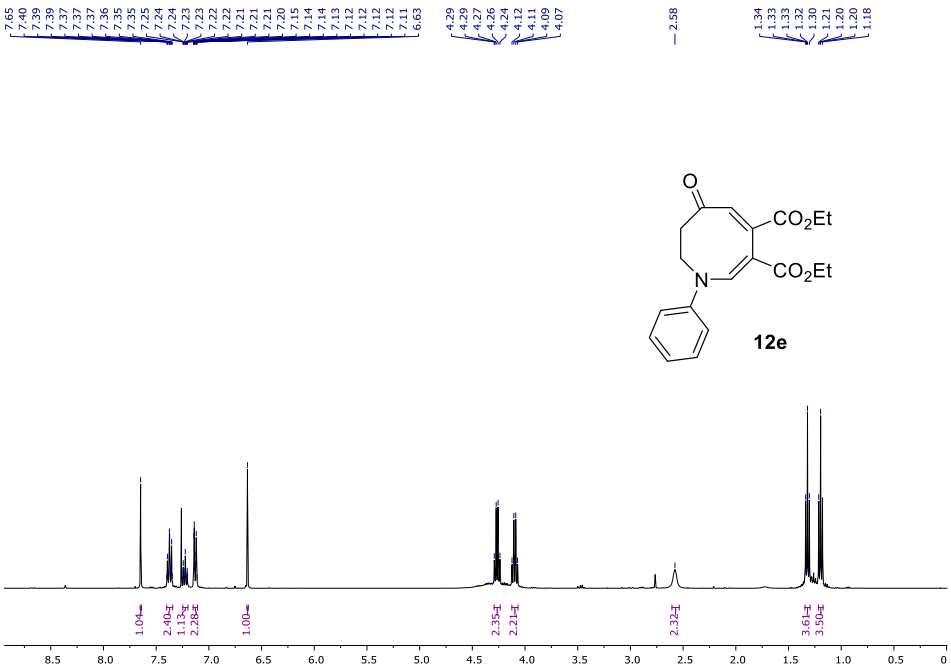

^{1}H-NMR (400 MHz, $CDCl_3$) of **12e**.

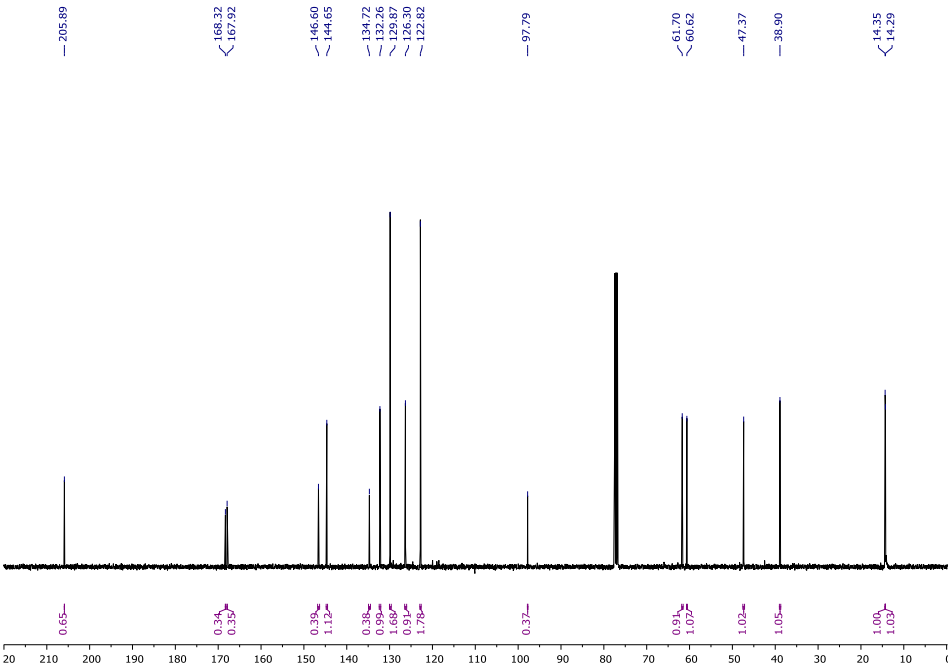

^{13}C-NMR (101 MHz, $CDCl_3$) of **12e.**

VI. References

[1] *Spartan'10*, Wavefunction, Inc., Irvine, CA, USA, **2009**.

[2] G. W. T. M. J. Frisch, H. B. Schlegel, G. E. Scuseria, M. A. Robb, J. R. Cheeseman, G. Scalmani, V. Barone, G. A. Petersson, H. Nakatsuji, X. Li, M. Caricato, A. V. Marenich, J. Bloino, B. G. Janesko, R. Gomperts, B. Mennucci, H. P. Hratchian, J. V. Ortiz, A. F. Izmaylov, J. L. Sonnenberg, Williams, F. Ding, F. Lipparini, F. Egidi, J. Goings, B. Peng, A. Petrone, T. Henderson, D. Ranasinghe, V. G. Zakrzewski, J. Gao, N. Rega, G. Zheng, W. Liang, M. Hada, M. Ehara, K. Toyota, R. Fukuda, J. Hasegawa, M. Ishida, T. Nakajima, Y. Honda, O. Kitao, H. Nakai, T. Vreven, K. Throssell, J. A. Montgomery Jr., J. E. Peralta, F. Ogliaro, M. J. Bearpark, J. J. Heyd, E. N. Brothers, K. N. Kudin, V. N. Staroverov, T. A. Keith, R. Kobayashi, J. Normand, K. Raghavachari, A. P. Rendell, J. C. Burant, S. S. Iyengar, J. Tomasi, M. Cossi, J. M. Millam, M. Klene, C. Adamo, R. Cammi, J. W. Ochterski, R. L. Martin, K. Morokuma, O. Farkas, J. B. Foresman, D. J. Fox, *Gaussian 16, Revision A.03*, Wallingford, CT, **2016**.

[3] a) S. H. Vosko, L. Wilk, M. Nusair, *Can. J. Phys.* **1980**, *58*, 1200-1211; b) C. Lee, W. Yang, R. G. Parr, *Physical Review B* **1988**, *37*, 785-789; c) A. D. Becke, *The Journal of Chemical Physics* **1993**, *98*, 5648-5652; d) A. D. Becke, *Phys. Rev. A* **1988**, *38*, 3098-3100.

[4] a) R. Krishnan, J. S. Binkley, R. Seeger, J. A. Pople, *The Journal of Chemical Physics* **1980**, *72*, 650-654; b) M. J. Frisch, J. A. Pople, J. S. Binkley, *The Journal of Chemical Physics* **1984**, *80*, 3265-3269.

[5] J. Tomasi, B. Mennucci, E. Cancès, *Journal of Molecular Structure: THEOCHEM* **1999**, *464*, 211-226.

[6] J. Saurí, T. Parella, J. F. Espinosa, *Org. Biomol. Chem.* **2013**, *11*, 4473-4478.

[7] a) J. Bezenšek, T. Koleša, U. Grošelj, J. Wagger, K. Stare, A. Meden, J. Svete, B. Stanovnik, *Tetrahedron Lett.* **2010**, *51*, 3392-3397; b) J. Bezensek, T. Kolesa, U. Groselj, A. Meden, K. Stare, J. Svete, B. Stanovnik, *Curr. Org. Chem.* **2011**, *15*, 2530-2539.

B.2 Computergestützte Strukturaufklärung kleiner organischer Moleküle

B.2.1 Zusatzmaterial der Benchmarkstudie über die Genauigkeit von DFT-Methoden in der VCD-Spektroskopie

Im Folgenden ist die *supporting information* der Publikation „Comparison of different density functional theory methods for the calculation of vibrational circular dichroism spectra“ abgedruckt.[558]

Supporting Information

Comparison of Different Density Functional Theory (DFT) Methods for the Calculation of Vibrational Circular Dichroism (VCD) Spectra

Jonathan Groß,[1,2] Jonas Kühlborn,[1,2] Stefan Pusch,[1] Carina Weber,[1] Lars Andernach,[1] Galit Renzer,[1] Paul Eckhardt,[1] Jan Brauer,[1] and Till Opatz[1,*]

Johannes Gutenberg University

Department of Chemistry

Duesbergweg 10–14, 55128 Mainz (Germany)

E-mail: opatz@uni-mainz.de

Table of Contents

1. Technical Details

All solvents and reagents were obtained from commercial suppliers and were used without prior purification, unless stated otherwise. If necessary, solvents were dried and purified by appropriate standard procedures.[1] Reactions requiring anhydrous conditions were performed under inert atmosphere (nitrogen or argon) in flame-dried glassware using standard Schlenk technique. Flash-chromatographic purifications were performed on silica gel (35–70 µm, Acros Organics) using a semiautomatic Biotage Isolera One system with integrated UV detector and silica cartridges. Thin-layer chromatography was done on silica plates purchased from Merck (TLC Silica 60 F254). Visualization of the compounds on these TLC-plates was accomplished by radiation with UV-A light (λ = 254 nm) or by immersion in a suitable staining solution and heating. The following solutions were used: $KMnO_4$ (3 g), K_2CO_3 (20 g), aqueous NaOH (5%, 5 mL) and water (300 mL). Nuclear magnetic resonance (NMR-) spectra were recorded on a Bruker Avance-II (^{1}H-NMR: 400 MHz, ^{13}C-NMR: 100.6 MHz) spectrometer using 5 mm probes and standard pulse sequences. All chemical shifts (δ) are referenced to the residual solvent signals ($CDCl_3$: δ_{1H} = 7.26 ppm, δ_{13C} = 77.16 ppm) and reported in parts per million (ppm) relative to tetramethylsilane (TMS). The following abbreviations are used for multiplicities of NMR signals: s = singlet, m = multiplet. ESI-HRMS spectra were recorded on an Agilent 6545 QTOF-MS with a suitable external calibrant. The reported high-resolution masses refer to the corresponding cationic species. Melting points were determined in open capillary tubes using an electrothermal Krüss-Optronic KSP 1 N apparatus with digital thermometer using a heating rate of 1 °C min^{-1}. Optical rotations were measured with a Perkin-Elmer 241 polarimeter at 589 nm. The infrared (IR) and vibrational circular dichroism (VCD) spectra were recorded with a Tensor 27 IR spectrometer (Bruker Optics) equipped with a PMA50 module for polarization modulation measurements. The photoelastic modulator was optimized for 1400 cm^{-1}. VCD spectra were measured in solution in CCl_4 with the below mentioned concentrations for each compound respectively in a 100 µm BaF_2 sample cell, except for caripyrin (**2**), which was measured in a 30 µm BaF_2 sample cell. An accumulation time of 6 h was applied (25,560 scans in 20 x 20 min single scans with two being excluded afterwards). The spectral range was set 1800–800 cm^{-1} for VCD measurements. Beforehand, the IR data were collected with the same sample cell within 16 scans in a range of 4000–800 cm^{-1} in transmission. The IR and VCD spectra were baseline corrected by subtraction of a solvent spectrum recorded using the same measurement parameters.

Table 1 Concentration of the measured compound solutions in CCl_4.

Compound	Concentration molL^{-1}
Camphor **1**	0.79
Caripyrin **2**	1.27
Phenethylamine **3**	1.31
Propylene oxide **4**	3.76
Methyl *p*-tolyl sulfoxide **5**	1.30
Thiocamphor **6**	1.62

1.1. Experimental Details

1.1.1. Synthesis of (*R*)-methyl *p*-tolyl sulfoxide (5)

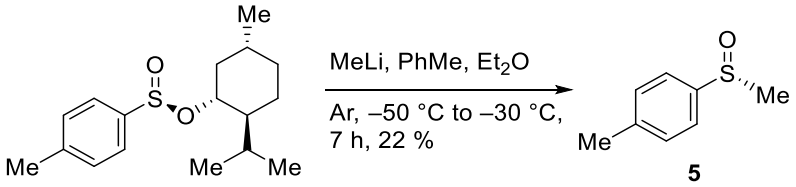

Dry toluene (25 mL) was added to a solution of methyl lithium in diethyl ether (1.6 M, 9.3 mL, 14.9 mmol, 8.8 eq.) under argon atmosphere and cooled to –50 °C. A solution of (1*R*,2*S*,5*R*)-(−)-menthyl-(*S*)-*p*-toluenesulfinate (509 mg, 1.7 mmol, 1 eq.) in dry toluene (25 mL) was added during 30 min while maintaining the temperature of the mixture at –30 °C. The mixture was stirred for 6 h at this temperature until another portion of methyl lithium in diethyl ether (1.6 M, 9.1 mL, 14.6 mmol, 8.6 eq.) was added. After stirring for 1 h sat. NH_4Cl solution (25 mL) was added and the resulting mixture was extracted with EtOAc (2 x 25 mL). The combined organic extracts were evaporated, and the crude product was purified by column chromatography (SiO_2, EtOAc in cyclohexane 0–100%) to yield the product as a colourless solid (60.0 mg, 0.38 mmol, 22%). **Mp** = 72.7–73.4 °C. **IR** (ATR): $\tilde{\nu}$ = 1495, 1407, 1090, 1057, 1016, 953 cm^{-1}. **^{1}H-NMR, COSY** (300 MHz, $CDCl_3$): δ = 7.56–7.52 (m, 2H, H-2, -6), 7.34–7.31 (m, 2H, H-3, -5), 2.70 (s, 3H, S-CH_3), 2.42 (s, 3H, Ar-CH_3) ppm. **^{13}C-NMR, HSQC, HMBC** (76 MHz, $CDCl_3$): δ = 142.5 (C-1), 141.5 (C-4), 130.0 (2C, C-3, -5), 123.5 (2C, C-2, -6), 44.0 (S-*C*H_3), 21.4 (Ar-*C*H_3).[2] $[\alpha]_D^{23}$ = +113.7 (*c* = 0.76, CCl_4).

ESI-HRMS: *m*/*z*: $[M+H]^+$, calculated for $[C_8H_{11}OS]^+$: 155.0525, found 155.0525; $[M+Na]^+$, calculated for $[C_8H_{10}NaOS]^+$: 177.0345, found 177.0345.

The analytical data are in accordance with the literature.[2-4]

1.2. Computational Details

1.2.1. Input lines

Conformational Analysis performed with Spartan '10:[5]

```
SEARCHMETHOD=THOROUGH FINDBOATS KEEPALL CONF_SELECTION_RULE=5
```

DFT Optimization and Frequency Calculation using Gaussian 16 Revision A.03:[6]

```
#p opt=tight freq=noraman FUNC BASIS scrf=(SOLV,solvent=ccl4)
```

`FUNC`, `BASIS` and `SOLV` were substituted by the respective functionals, basis sets and solvation models mentioned below.

Software: Spartan '10,[5] Gaussian 16 Revision A.03,[6] *SpecDis* 1.71.[7-9]

"FUNC": B3LYP,[10-13] B3P86,[10,14] B3PW91,[10,15-19] B97-D3,[20-23] BP86,[14] CAM-B3LYP,[24] LC-ωPBE,[17,18,25] M06-2X,[19] mPW1PW91,[17-19,25-27] PBE0,[27] PBE,[28,29] PW6B95,[30] TPSS,[31] TPSSh,[16,32] ωB97X-D.[33,34]

"BASIS": 6-31G,[35] 6-31G(d),[35-37] 6-31G(d,p),[35-37] 6-31+G(d,p),[35-38] 6-31++G(d,p),[35-38] 6-311G,[29,39] 6-311G(d),[29,36,37,39] 6-311G(d,p),[29,36,37,39] 6-311+G(d,p),[29,36-39] 6-311++G(d,p),[29,36-39] def2-SVP,[40-44] def2-TZVP,[40-44] def2-TZVPP,[40-44] cc-pVDZ,[45,46] cc-pVTZ,[45,46] aug-cc-pVTZ.[47]

"SOLV": IEFPCM,[48-50] SMD.[51]

1.2.2. Calculation of VCD spectra and ESI-values

For the calculation of the VCD spectra, conformational searches for the respective molecules were performed first on a semi-empirical level of theory (PM6)[52] using Spartan '10.[5] Afterwards, DFT-based geometry reoptimization and calculation of vibrational frequencies was conducted using Gaussian 16[6] at the combination of functionals, basis sets and solvation models of interest for each conformer (if applicable). Vibrational frequency analysis (N_{imag} = 0) confirmed all structures to be local minima. For caripyrin (**2**) and phenethylamine (**3**), Boltzmann-weighting was performed since it had more than one conformer. For the comparison of the experimental and theoretical spectra as well as for the calculation of the ESI values ($|f–f^*|$) *SpecDis* 1.71[7-9] was used.
The fitting of the calculated IR spectra to the experimental in *SpecDis* was done using the following parameters for every single compound, respectively. The range of wavelength ($\tilde{\nu}$) was determined by the regions were both curves showed distinct peaks. Afterwards, the similarity factors were generated by comparison of the VCD and ESI values were computed.

Table 2 Detailed parameters used for the fitting of the calculated to the experimental IR and VCD spectra.

Compound	Parameter		
	Scaling	Band width	$\tilde{\nu}$ / cm^{-1}
Camphor **1**	0.9–1.1	2–10	900–1550
Caripyrin **2**	0.9–1.1	2–10	900–1650
Phenethylamine **3**	0.9–1.1	2–10	900–1550
Propylene oxide **4**	0.9–1.1	2–10	850–1600
Methyl *p*-tolyl sulfoxide **5**	0.9–1.1	2–10	850–1550
Thiocamphor **6**	0.9–1.1	2–10	850–1600

The optimized geometries of the conformers used for the computation of the VCD spectra can be found in the attached zip-file in the form of xyz-files.

1.2.3. Comparison of the experimental spectra with selected simulated spectra

To illustrate the differences of the investigated combinations of *functional/basis set/solvation model*, the experimental spectra of (1*R*,4*R*)-camphor (**1**) were plotted with two of the simulated spectra (figure 1). With the applied parameters, the best combination (blue) achieved an ESI value of 0.9088 while the worst (red) produced an ESI value of 0.0392.

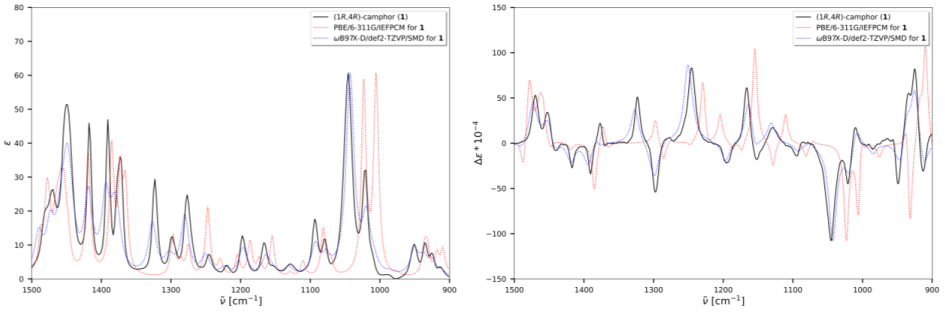

Figure 1 Comparison of the experimental IR (left) and VCD (right) spectra with the simulated results. PBE/6-311G/IEFPCM: ESI = 0.0392, scaling factor = 0.987, band width = 4 cm^{-1}; ωB97X-D/def2-TZVP/SMD: ESI = 0.9088, scaling factor = 0.971, band width = 7 cm^{-1}.

The very low ESI value obtained for PBE/6-311G/IEFPCM in this example (red dotted line) underestimates the general quality of the calculated VCD spectrum. Contrary to a visual comparison, the employed cross section algorithm of *SpecDis* mathematically minimizes the area between the curves in the IR spectrum, sometimes resulting in a scaling factor that displays the calculated VCD spectra with a considerable shift, although the band pattern only shows a limited deviation from the experimental spectrum.[7]

To check the effect of other fitting runs, it is possible to limit the *SpecDis* algorithm to a smaller wavenumber range (figures 2–3). Alternatively, these parameters for an optimal spectral overlap can be determined on the basis of the VCD spectra (figure 4).

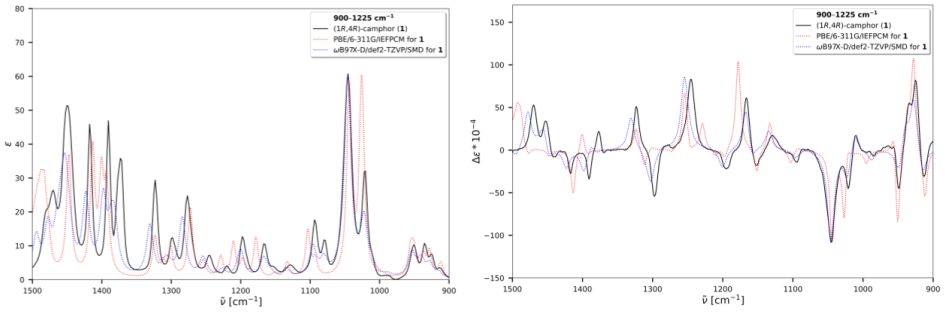

Figure 2 The entire spectrum of the IR (left) and the VCD (right) is shown, while the parameters and the ESI value only being determined in the range of 900–1225 cm^{-1}. PBE/6-311G/IEFPCM: ESI = 0.7646, scaling factor = 1.007, band width = 4 cm^{-1}; ωB97X-D/def2-TZVP/SMD: ESI = 0.9456, scaling factor = 0.974, band width = 6 cm^{-1}.

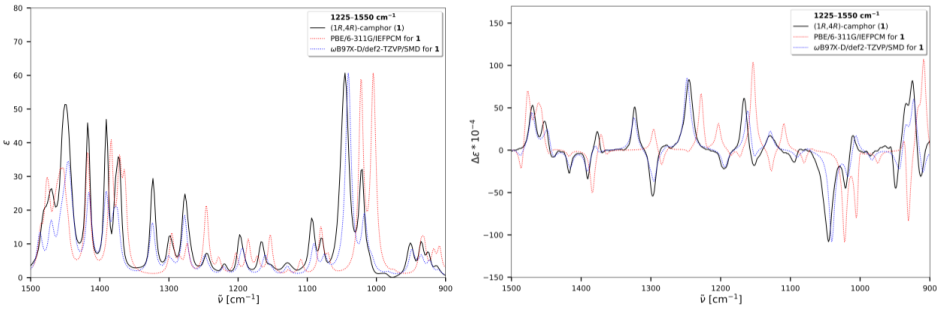

Figure 3 The entire spectrum of the IR (left) and the VCD (right) is shown, while the parameters and the ESI value only being determined in the range of 1225–1550 cm^{-1}. PBE/6-311G/IEFPCM: ESI = 0.2368, scaling factor = 0.986, band width = 4 cm^{-1}; ωB97X-D/def2-TZVP/SMD: ESI = 0.9572, scaling factor = 0.969, band width = 5 cm^{-1}.

Contrary to the full-range evaluation approach in this study, if the fitting is based on a smaller wavenumber range, in this example 900–1225 and 1225–1550 cm^{-1}, respectively, a different spectral overlap resulting in different ESI values is obtained. In these cases, different scaling factors as well as line broadening values were determined by *SpecDis*. However, the spectral overlap in the VCD spectrum in the other range becomes worse. This effect is much more pronounced for the PBE/6-311G/IEFPCM data while the ωB97X-D/def2-TZVP/SMD data still match relatively well in the "passive" part of the spectrum, which was not used for fitting. Therefore, the ESI values obtained with ωB97X-D/def2-TZVP/SMD remain high in all cases, while those for PBE/6-311G/IEFPCM fluctuate and can in part be very low.

Although local adjustment, as presented in the examples above, can result in higher ESI values, it is advisable to choose a reasonably large wavenumber range when an unbiased molecular chirality assignment is desired. To avoid misassignments, all available vibrational bands should be included in the evaluation process.

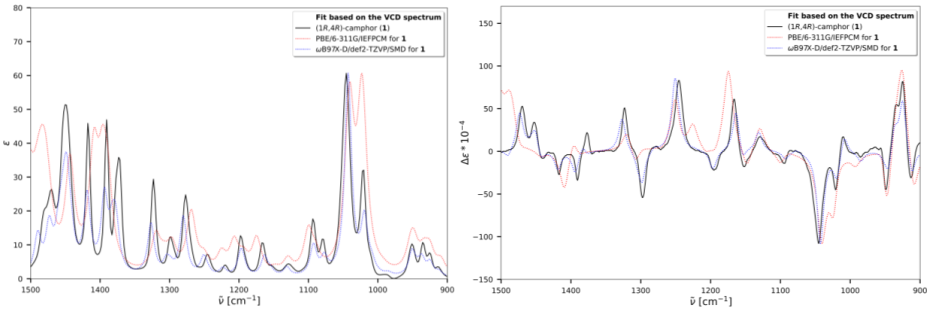

Figure 4 Determination of the spectral parameters after fitting of the simulated results to the experimental bands in the VCD spectra (right). PBE/6-311G/IEFPCM: ESI = 0.6614, scaling factor = 1.004, band width = 8 cm^{-1}; ωB97X-D/def2-TZVP/SMD: ESI = 0.9089, scaling factor = 0.971, band width = 6 cm^{-1}.

A fitting based on the VCD spectrum (corresponding to an approach opposite to the study conducted herein) can generate parameters that allow a proper overlap of bands for this molecule, similar to a visual comparison. Since the configuration of the enantiomer in this example is known, figure 4 shows the best-case scenario with which the selected functional/basis set can reproduce the experimental spectrum. However, this procedure and the generated ESI value must not be used for AC determination of chiral organic molecules since *SpecDis* only maximises the spectral overlap, which can easily lead to misassignments.

1.2.4. Evaluation of the computational results

The detailed results of this study (similarity factors *f* and *f**, resulting ESI-values, means, standard deviations, top and bottom 100 combinations) which were used for the generation of the graphs can be found in the attached excel file. This file is constructed in the following way:

Table 3 Explanation of the additional excel file containing detailed data used for the evaluation of the presented results.

#	Sheet	Content
1	Camphor **1**	*f*, *f** and ESI values sorted by combinations as well as ESI values
2	Caripyrin **2**	*f*, *f** and ESI values sorted by combinations as well as ESI values
3	Phenethylamine **3**	*f*, *f** and ESI values sorted by combinations as well as ESI values
4	Propylene oxide **4**	*f*, *f** and ESI values sorted by combinations as well as ESI values
5	Methyl *p*-tolyl sulfoxide **5**	*f*, *f** and ESI values sorted by combinations as well as ESI values
6	Thiocamphor **6**	*f*, *f** and ESI values sorted by combinations as well as ESI values
7	ESI-Overview	*f*, *f** and ESI values of all compounds as well as the mean values and standard deviations of the ESI values of all combinations sorted by combinations
8	ESI-Ranking (means)	Mean values and standard deviations of all combinations as well as top and bottom 100 combinations sorted by the mean values (used for figure 3 and 5)
9	ESI-Ranking (means – std.dev.)	means and standard deviations of all combinations as well as top and bottom 100 combinations sorted by the difference between mean values and standard deviation (used for figure 4 and 5)
10	ESI > 80%	combinations that reached ESI values >80% for at least one compound sorted by the combinations (used for figure 6)
11	ESI > 80% (mult. occ.)	combinations that reached ESI values >80% for multiple compounds separated by the compounds and sorted by the combinations (used for figure 6)
12	Diagrams	large scale copies of the graphs depicted in figure 2–6 and the occurrences of the functionals, basis sets and solvation models of the bottom 100 ESI mean values and the difference between mean value and standard deviation.

3. References

1. Ernzerhof M, Scuseria GE. Assessment of the Perdew–Burke–Ernzerhof exchange-correlation functional. *J Chem Phys.* **1999**;110(11):5029-5036.
2. Liao S, Čorić I, Wang Q, List B. Activation of H2O2 by Chiral Confined Brønsted Acids: A Highly Enantioselective Catalytic Sulfoxidation. *J Am Chem Soc.* **2012**;134(26):10765–10768.
3. Bauder C. A Non-Aldol Preparation of Enantiopure Propionate-Derived Motifs with the Assistance of Chiral Sulfoxides: Application to a Convergent Synthesis of the Lactone Core of Octalactins. *Eur J Org Chem.* **2015**;2015(24):5402–5413.
4. Gelat F, Jayashankaran J, Lohier J-F, Gaumont A-C, Perrio S. Organocatalytic Asymmetric Synthesis of Sulfoxides from Sulfenic Acid Anions Mediated by a Cinchona-Derived Phase-Transfer Reagent. *Org Lett.* **2011**;13(12):3170–3173.
5. Spartan'10. Irvine, CA, USA: Wavefunction, Inc.; **2009**.
6. Frisch MJ, Trucks GW, Schlegel HB, Scuseria GE, Robb MA, Cheeseman JR, Scalmani G, Barone V, Petersson GA, Nakatsuji H, Li X, Caricato M, Marenich AV, Bloino J, Janesko BG, Gomperts R, Mennucci B, Hratchian HP, Ortiz JV, Izmaylov AF, Sonnenberg JL, Williams, Ding F, Lipparini F, Egidi F, Goings J, Peng B, Petrone A, Henderson T, Ranasinghe D, Zakrzewski VG, Gao J, Rega N, Zheng G, Liang W, Hada M, Ehara M, Toyota K, Fukuda R, Hasegawa J, Ishida M, Nakajima T, Honda Y, Kitao O, Nakai H, Vreven T, Throssell K, Montgomery Jr. JA, Peralta JE, Ogliaro F, Bearpark MJ, Heyd JJ, Brothers EN, Kudin KN, Staroverov VN, Keith TA, Kobayashi R, Normand J, Raghavachari K, Rendell AP, Burant JC, Iyengar SS, Tomasi J, Cossi M, Millam JM, Klene M, Adamo C, Cammi R, Ochterski JW, Martin RL, Morokuma K, Farkas O, Foresman JB, Fox DJ. Gaussian 16, Revision A.03. Wallingford, CT; **2016**.
7. Bruhn T, Schaumlöffel A, Hemberger Y, Bringmann G. SpecDis: Quantifying the Comparison of Calculated and Experimental Electronic Circular Dichroism Spectra. *Chirality.* **2013**;25(4):243-249.
8. Bruhn T, Schaumlöffel A, Hemberger Y, Pescitelli G. SpecDis, Version 1.71. Berlin, Germany; **2017**.
9. Pescitelli G, Bruhn T. Good Computational Practice in the Assignment of Absolute Configurations by TDDFT Calculations of ECD Spectra. *Chirality.* **2016**;28(6):466-474.
10. Becke AD. Density-functional thermochemistry. III. The role of exact exchange. *J Chem Phys.* **1993**;98(7):5648-5652.
11. Lee C, Yang W, Parr RG. Development of the Colle-Salvetti correlation-energy formula into a functional of the electron density. *Phys Rev B.* **1988**;37(2):785-789.
12. Stephens PJ, Devlin FJ, Chabalowski CF, Frisch MJ. Ab Initio Calculation of Vibrational Absorption and Circular Dichroism Spectra Using Density Functional Force Fields. *J Phys Chem.* **1994**;98(45):11623-11627.
13. Vosko SH, Wilk L, Nusair M. Accurate spin-dependent electron liquid correlation energies for local spin density calculations: a critical analysis. *Can J Phys.* **1980**;58(8):1200-1211.
14. Perdew JP. Density-functional approximation for the correlation energy of the inhomogeneous electron gas. *Phys Rev B.* **1986**;33(12):8822-8824.
15. Staroverov VN, Scuseria GE, Tao J, Perdew JP. Comparative assessment of a new nonempirical density functional: Molecules and hydrogen-bonded complexes. *J Chem Phys.* **2003**;119(23):12129-12137.
16. Staroverov VN, Scuseria GE, Tao J, Perdew JP. Comparative assessment of a new nonempirical density functional: Molecules and hydrogen-bonded complexes. *J Chem Phys.* **2003**;119(23):12129–12137.
17. Vydrov OA, Heyd J, Krukau AV, Scuseria GE. Importance of short-range versus long-range Hartree-Fock exchange for the performance of hybrid density functionals. *J Chem Phys.* **2006**;125(7):074106.

18. Vydrov OA, Scuseria GE. Assessment of a long-range corrected hybrid functional. *J Chem Phys.* **2006**;125(23):234109.
19. Zhao Y, Truhlar DG. The M06 suite of density functionals for main group thermochemistry, thermochemical kinetics, noncovalent interactions, excited states, and transition elements: two new functionals and systematic testing of four M06-class functionals and 12 other functionals. *Theor Chem Acc.* **2008**;120(1):215-241.
20. Sadlej J, Dobrowolski JC, Rode JE. VCD spectroscopy as a novel probe for chirality transfer in molecular interactions. *Chem Soc Rev.* **2010**;39(5):1478-1488.
21. Hill JG. Gaussian basis sets for molecular applications. *Int J Quantum Chem.* **2013**;113(1):21-34.
22. Grimme S, Ehrlich S, Goerigk L. Effect of the damping function in dispersion corrected density functional theory. *J Comput Chem.* **2011**;32(7):1456-1465.
23. Nafie LA. Vibrational optical activity: principles and applications: John Wiley & Sons; **2011**.
24. Yanai T, Tew DP, Handy NC. A new hybrid exchange–correlation functional using the Coulomb-attenuating method (CAM-B3LYP). *Chem Phys Lett.* **2004**;393(1–3):51-57.
25. Vydrov OA, Scuseria GE, Perdew JP. Tests of functionals for systems with fractional electron number. *J Chem Phys.* **2007**;126(15):154109.
26. Cotton A. Dispersion rotatoire anomale des corps absorbants. *Compt. Rend.* **1895**;120:1044.
27. Adamo C, Barone V. Toward reliable density functional methods without adjustable parameters: The PBE0 model. *J Chem Phys.* **1999**;110(13):6158-6170.
28. Zhurko G. Chemcraft-Graphical Program for Visualization of Quantum Chemistry Computations, Version 1.8. *Ivanovo. Available online at: https://chemcraftprog. com.* **2019**.
29. Krishnan R, Binkley JS, Seeger R, Pople JA. Self-consistent molecular orbital methods. XX. A basis set for correlated wave functions. *J Chem Phys.* **1980**;72(1):650-654.
30. Zhao Y, Truhlar DG. Design of Density Functionals That Are Broadly Accurate for Thermochemistry, Thermochemical Kinetics, and Nonbonded Interactions. *J Phys Chem A.* **2005**;109(25):5656-5667.
31. Tao J, Perdew JP, Staroverov VN, Scuseria GE. Climbing the Density Functional Ladder: Nonempirical Meta-Generalized Gradient Approximation Designed for Molecules and Solids. *Phys Rev Lett.* **2003**;91(14):146401.
32. Stephens PJ, Devlin FJ, Pan J-J. The determination of the absolute configurations of chiral molecules using vibrational circular dichroism (VCD) spectroscopy. *Chirality.* **2008**;20(5):643-663.
33. Chai J-D, Head-Gordon M. Long-range corrected hybrid density functionals with damped atom-atom dispersion corrections. *Phys Chem Chem Phys.* **2008**;10(44):6615-6620.
34. Chai J-D, Head-Gordon M. Systematic optimization of long-range corrected hybrid density functionals. *J Chem Phys.* **2008**;128(8):084106.
35. Hehre WJ, Ditchfield R, Pople JA. Self—Consistent Molecular Orbital Methods. XII. Further Extensions of Gaussian—Type Basis Sets for Use in Molecular Orbital Studies of Organic Molecules. *J Chem Phys.* **1972**;56(5):2257-2261.
36. Francl MM, Pietro WJ, Hehre WJ, Binkley JS, Gordon MS, DeFrees DJ, Pople JA. Self-consistent molecular orbital methods. XXIII. A polarization-type basis set for second-row elements. *J Chem Phys.* **1982**;77(7):3654–3665.
37. Hariharan PC, Pople JA. The influence of polarization functions on molecular orbital hydrogenation energies. *Theor Chim Acta.* **1973**;28(3):213-222.
38. Clark T, Chandrasekhar J, Spitznagel GW, Schleyer PvR. Efficient diffuse function-augmented basis sets for anion calculations. III. The 3-21+G basis set for first-row elements, Li–F. *J Comput Chem.* **1983**;4(3):294-301.
39. McLean AD, Chandler GS. Contracted Gaussian basis sets for molecular calculations. I. Second row atoms, Z=11–18. *J Chem Phys.* **1980**;72(10):5639-5648.
40. Schäfer A, Horn H, Ahlrichs R. Fully optimized contracted Gaussian basis sets for atoms Li to Kr. *J Chem Phys.* **1992**;97(4):2571-2577.

41. Jensen F. Atomic orbital basis sets. *WIREs Computational Molecular Science.* **2013**;3(3):273-295.
42. Goerigk L, Grimme S. Double-hybrid density functionals. *WIREs Computational Molecular Science.* **2014**;4(6):576-600.
43. Weigend F, Ahlrichs R. Balanced basis sets of split valence, triple zeta valence and quadruple zeta valence quality for H to Rn: Design and assessment of accuracy. *Phys Chem Chem Phys.* **2005**;7(18):3297-3305.
44. Zheng J, Xu X, Truhlar D. Minimally augmented Karlsruhe basis sets. *Theor Chem Acc.* **2011**;128(3):295-305.
45. Bijvoet JM, Peerdeman AF, van Bommel AJ. Determination of the Absolute Configuration of Optically Active Compounds by Means of X-Rays. *Nature.* **1951**;168(4268):271-272.
46. Woon DE, Dunning TH. Gaussian basis sets for use in correlated molecular calculations. III. The atoms aluminum through argon. *J Chem Phys.* **1993**;98(2):1358-1371.
47. Van't Hoff JH. La chimie dans l'espace: Bazendijk; **1875**.
48. Mennucci B, Cammi R. Continuum solvation models in chemical physics: from theory to applications. Chichester, England: John Wiley & Sons; **2007**.
49. Covington CL, Polavarapu PL. Similarity in Dissymmetry Factor Spectra: A Quantitative Measure of Comparison between Experimental and Predicted Vibrational Circular Dichroism. *J Phys Chem A.* **2013**;117(16):3377-3386.
50. Tomasi J, Mennucci B, Cancès E. The IEF version of the PCM solvation method: an overview of a new method addressed to study molecular solutes at the QM ab initio level. *J Mol Struct: THEOCHEM.* **1999**;464(1–3):211-226.
51. Marenich AV, Cramer CJ, Truhlar DG. Universal Solvation Model Based on Solute Electron Density and on a Continuum Model of the Solvent Defined by the Bulk Dielectric Constant and Atomic Surface Tensions. *J Phys Chem B.* **2009**;113(18):6378-6396.
52. Stewart JJP. Optimization of parameters for semiempirical methods V: Modification of NDDO approximations and application to 70 elements. *J Mol Model.* **2007**;13(12):1173-1213.

B.2.2 Zusatzmaterial der Publikation zur Differenzierung von Diastereomeren in der Synthese eines HIV-Integrase-Inhibitors

Im Folgenden ist die *supporting information* der Publikation „Six-Step Gram Scale Synthesis of the HIV Integrase Inhibitor Dolutegravir Sodium“ abgedruckt.[559]

Supporting Information

Six-Step Gram Scale Synthesis of the Human Immunodeficiency Virus Integrase Inhibitor Dolutegravir Sodium

Jule-Philipp Dietz,[a] Tobias Lucas,[a] Jonathan Groß,[a] Sebastian Seitel,[a] Jan Brauer,[a] Dorota Ferenc,[a] B. Frank Gupton,[b] and Till Opatz,[a]*

Table of content

1. Optimization studies

Table S 1: Screening for the cyclization to ring A using $MgCl_2$ as an additive

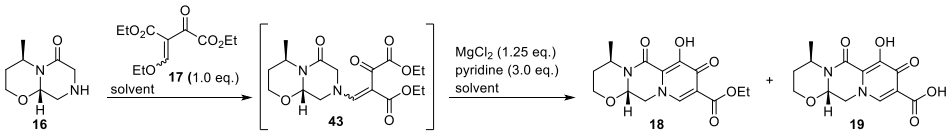

entry	solvent	*T* [°C]	*t* [h]	area% 18 [a]		area% 19 [a]	
				254 nm	315 nm	254 nm	315 nm
1	DCM	r.t.	24	no conversion			
2	DMF	60	8	no conversion			
3	THF	60	8	no conversion			
4	MeCN	r.t.	64	24	18	-	-
5	MeCN	60	6	83	52	-	-
6 [b]	MeCN	82	6	81	72	3	3
		82	24	57	52	29	31
		82	48	33	30	49	53
7 [b,c]	MeCN	82	24	65	60	17	19

Reactions were performed on a 20 mg scale using oven-dried Schlenk flasks under nitrogen atmosphere (balloon). [a] determined by LC-MS and UV-absorption. [b] reaction flask was additionally equipped with a reflux condenser. [c] 0.5 g scale.

Table S 2: Screening of the aminolysis in toluene using HOAc as an additive

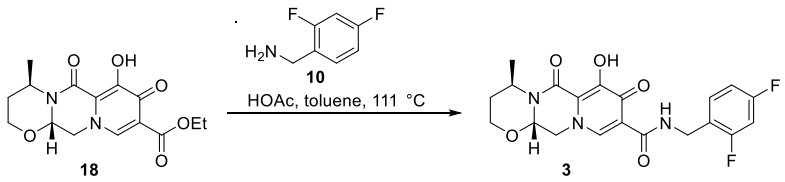

entry	eq. 10	eq. HOAc	*T* [°C]	area% 3 [a]		
				t [h]		
				8	**24**	**24 (100 °C)** [b]
1	1.5	0.3	90	22	26	-
2	1.5	1	90	55	61	-
3	2	2	90	71	84	85
4	2.5	2.5	90	78	90	91
5	3	3	90	87	95	-
6	3	1	90	81	88	-
7	3	2	90	79	90	93
8	3	4	90	81	90	92
9	2	1	100	50	54 [e]	80
10	3	3	100	84	87 [e]	95
11 [c]	2	2	111	81	95	-
12 [c]	2.5	2.5	111	-	99	-
13 [c,d]	2.5	2.5	111	-	100	-

Reactions were performed on a 30–40 mg scale using oven-dried Schlenk flasks under nitrogen atmosphere (balloon). [a] determined by LC-MS and UV-absorption at 315 nm only considering area of **18** and **3.** [b] temperature was increased to 100 °C after 24 h at 90 °C. [c] reaction flask was additionally equipped with a reflux condenser. [d] 0.3 g scale. [e] 2.0 eq. of HOAc were added before heating to 100 °C.

2. Chromatograms

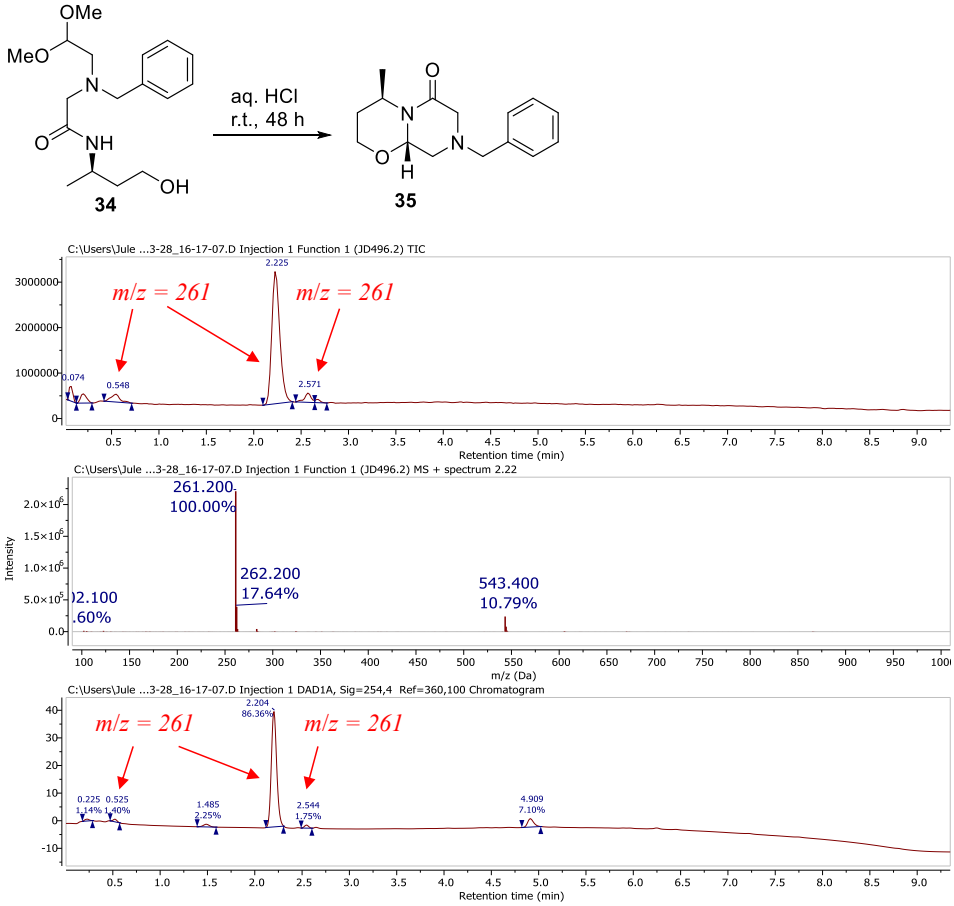

Figure S 1: LC-MS + UV-trace of the reaction mixture after 48 h (column: Ascentis Express C18, gradient MeCN:H_2O (+ 0.1% formic acid): 10:90 for 0.2 min, 10:90 to 90:10 in 7.5 min, 90:10 for 2.5 min, λ = 254 & 315 nm).

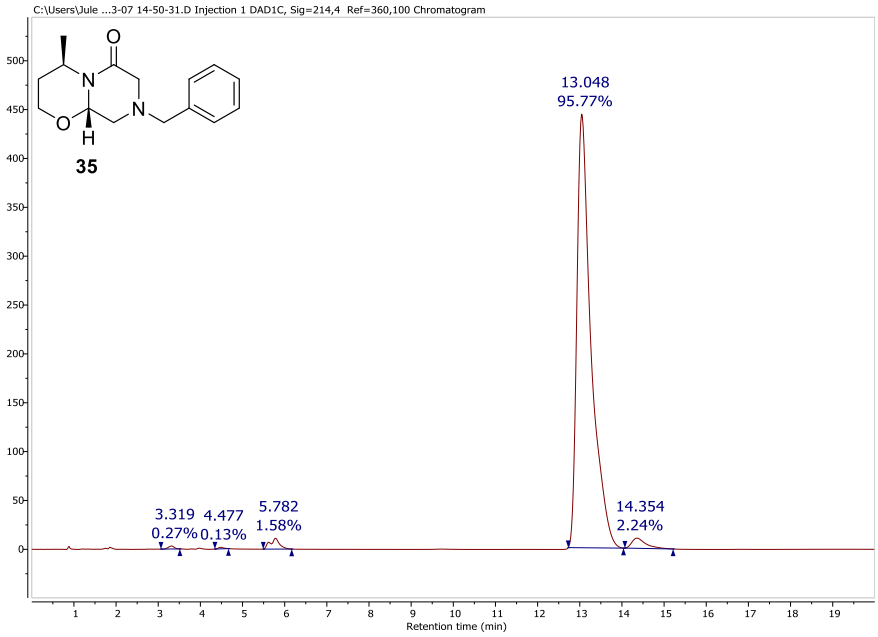

Figure S 2: Chromatogram of isolated crude **35** (column: ACE C18 PFP column, isocratic MeCN:H_2O (+ 0.1% formic acid) = 30:70, λ = 214 nm).

Supposing that the impurity at t_R = 14.35 min displays the undesired diastereomer of **35**, the dr would be 44:1.

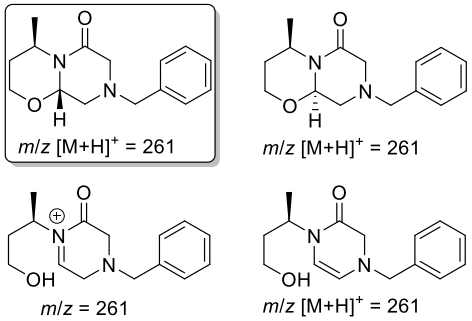

Figure S 3: Potentially detectable compounds showing *m/z* = 261.

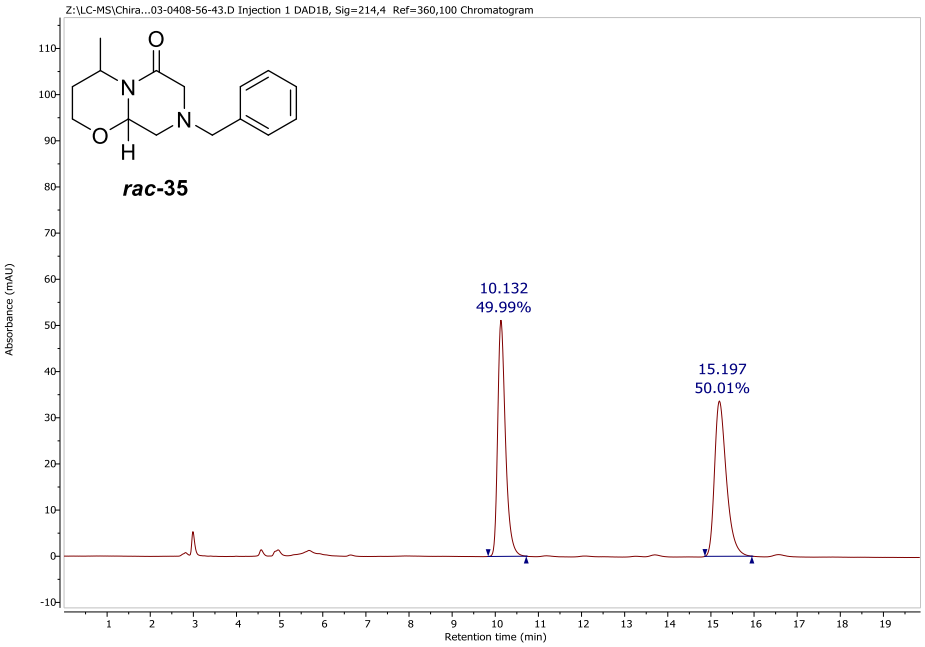

Figure S 4: Chromatogram of crude rac-**35** (column: Chiralpak IF-3, 40 °C, isocratic *n*-hexane:EtOH = 80:20, 1 mL/min, λ = 214 nm).

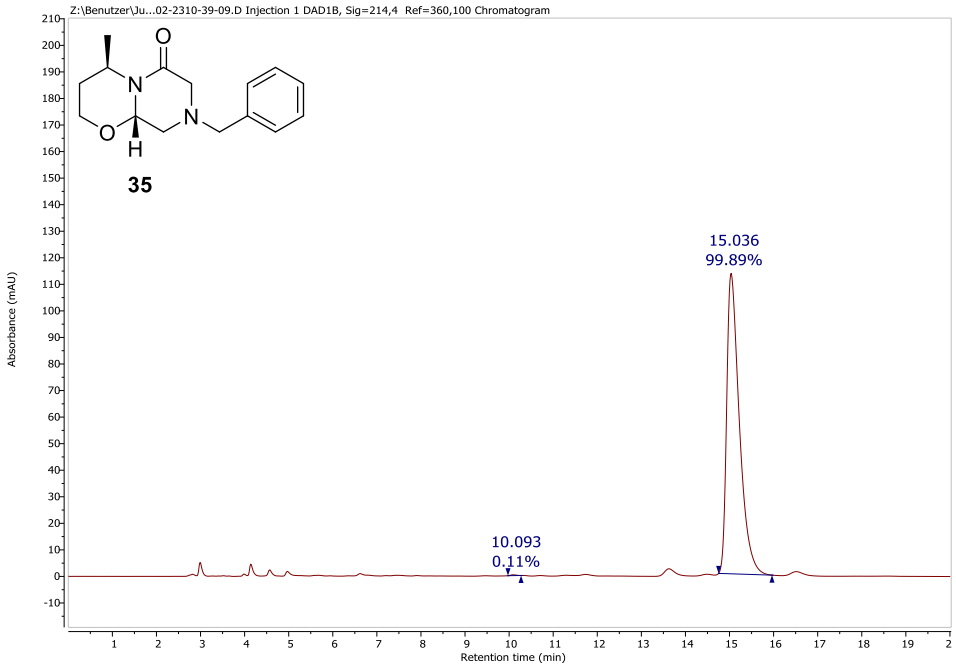

Figure S 5: Chromatogram of crude **35** (column: Chiralpak IF-3, 40 °C, isocratic *n*-hexane:EtOH = 80:20, 1 mL/min, λ = 214 nm).

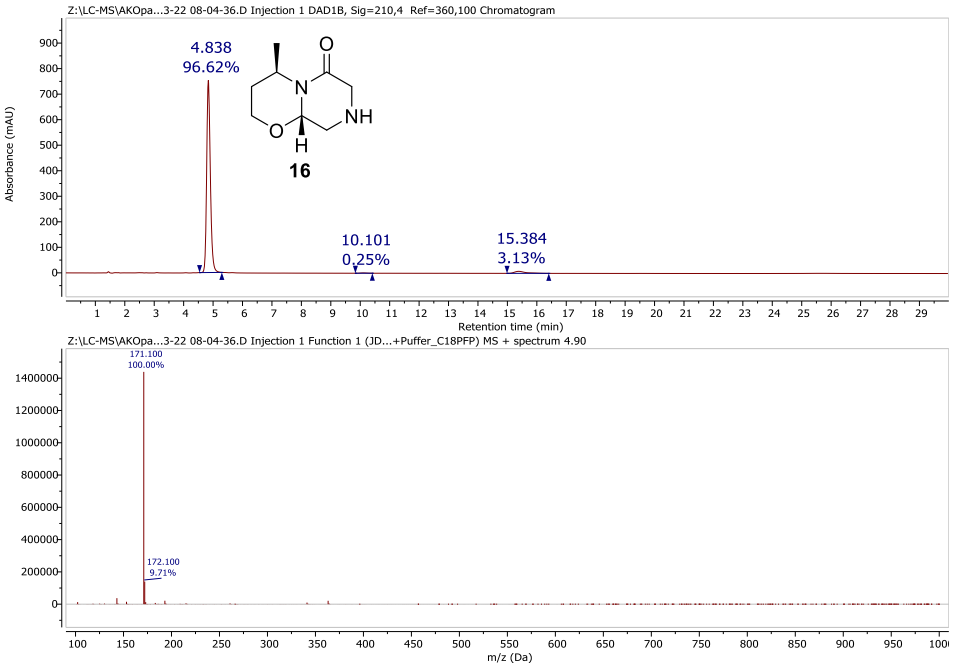

Figure S 6: LC-MS + UV-trace of crude amine **16** (column: ACE C18 PFP, isocratic MeOH:NH_4CO_3 buffer (15 mmol, pH = 8.0) = 15:85, 1 mL/min, λ = 210 nm).

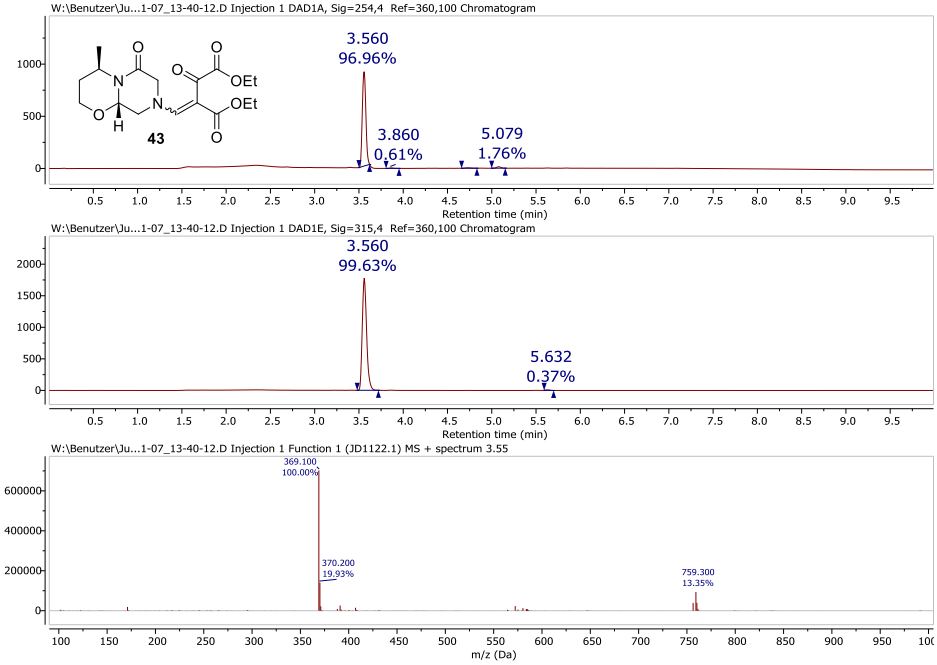

Figure S 7: LC-MS + UV-trace of crude ester **18** (column: Ascentis Express C1, gradient MeCN:H_2O (+ 0.1% formic acid): 5:95 for 0.2 min, 5:95 to 95:5 in 7.5 min, 95:5 for 2.5 min, λ = 254 & 315 nm).

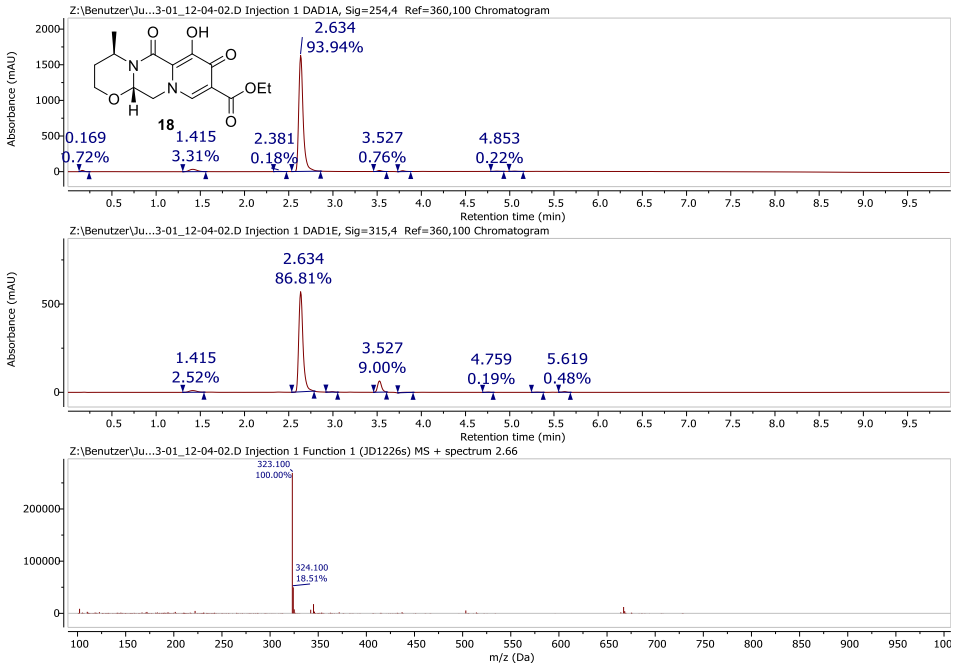

Figure S 8: LC-MS + UV-trace of crude ester **18** (column: Ascentis Express C18, gradient MeCN:H_2O (+ 0.1% formic acid): 5:95 for 0.2 min, 5:95 to 95:5 in 7.5 min, 95:5 for 2.5 min, λ = 254 & 315 nm).

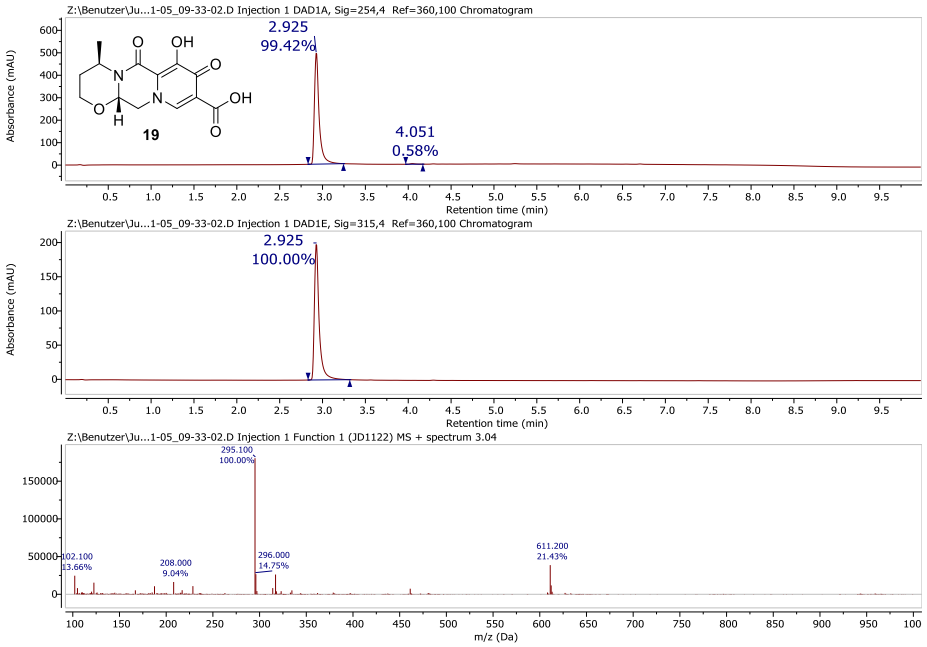

Figure S 9: LC-MS + UV-trace of isolated acid **19** (column: Ascentis Express C18, gradient MeCN:H_2O (+ 0.1% formic acid): 5:95 for 0.2 min, 5:95 to 95:5 in 7.5 min, 95:5 for 2.5 min, λ = 254 & 315 nm).

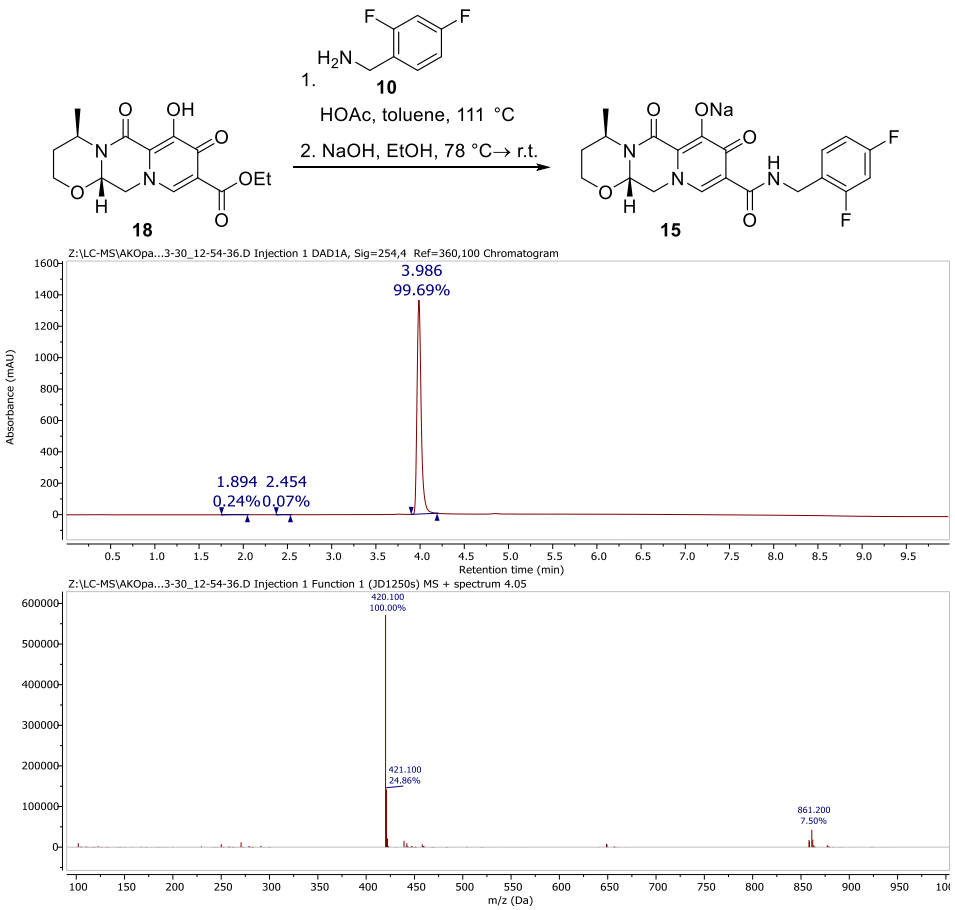

Figure S 10: LC-MS + UV-trace of isolated DTG-Na **15** from aminolysis of ester **18** (column: Ascentis Express C18, gradient MeCN:H_2O (+ 0.1% formic acid): 5:95 for 0.2 min, 5:95 to 95:5 in 7.5 min, 95:5 for 2.5 min, λ = 254 nm).

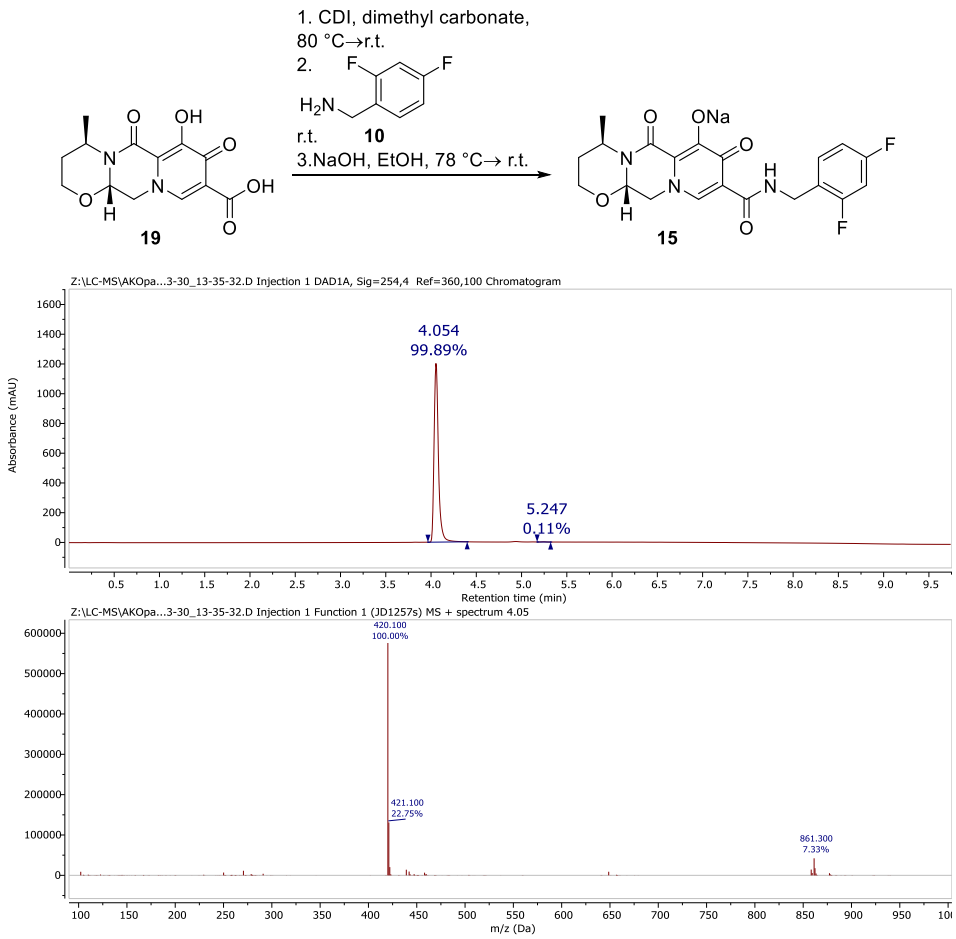

Figure S 11: LC-MS + UV-trace of isolated DTG-Na **15** from amid coupling with acid **19** with aqueous workup (column: Ascentis Express C18, gradient MeCN:H_2O (+ 0.1% formic acid): 5:95 for 0.2 min, 5:95 to 95:5 in 7.5 min, 95:5 for 2.5 min, λ =254 nm).

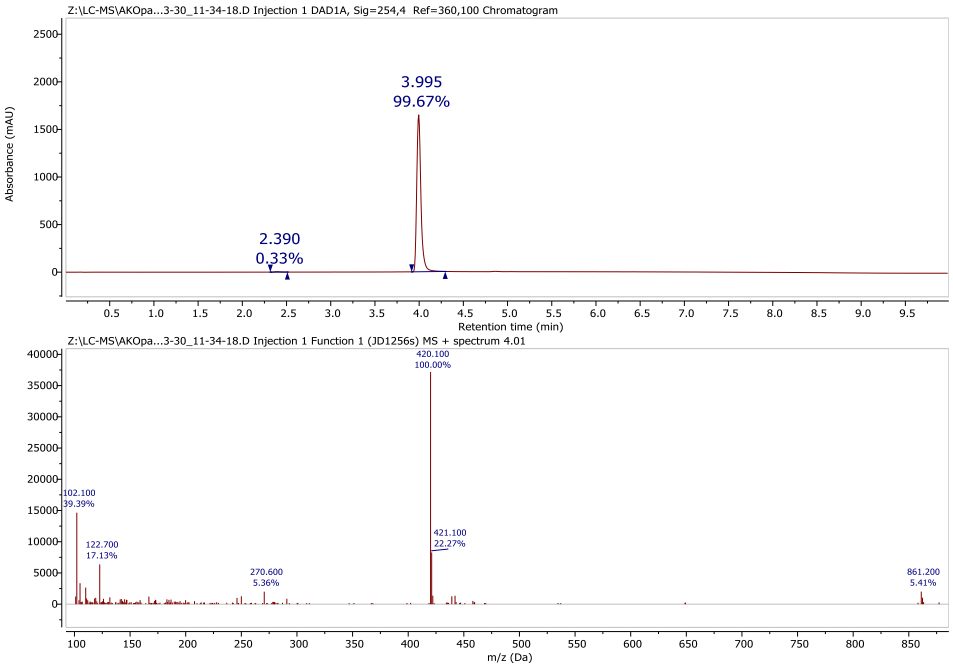

Figure S 12: LC-MS + UV-trace of isolated DTG-Na **15** from amid coupling with acid **19** without aqueous workup (column: Ascentis Express C18, gradient MeCN:H_2O (+ 0.1% formic acid): 5:95 for 0.2 min, 5:95 to 95:5 in 7.5 min, 95:5 for 2.5 min, λ = 254 nm).

3. Vibrational Circular Dichroism (VCD) Spectroscopy

The vibrational circular dichroism (VCD) and infrared (IR) spectra of **35** were measured with a Tensor 27 IR spectrometer equipped with a photoelastic modulator optimized for 1400 cm^{-1}. To obtain the VCD spectra, a solution of compound **35** in carbon tetrachloride (CCl_4) (0.58 mol/L) was measured for an accumulation time of 360 min with a resolution of 4 cm^{-1} in the spectral range of 1800–800 cm^{-1} in a 100 µm BaF_2 sample cell. The IR data was obtained with the same solution of **35** in the spectral range of 4000–800 cm^{-1} with 16 scans. Both spectra were baseline corrected by subtraction of a solvent spectrum recorded with the same parameters. A spectrum of the experimental noise was obtained by subtraction of two solvent spectra from each other.

4. Computational details

Conformational analysis was performed using Spartan '10 at a semiempirical level of theory (PM6).[1] Geometry optimizations and frequency calculations were performed using Gaussian 16, Rev. A.03 with the B3LYP functional,[2–5] the Pople basis set 6-31G(d,p)[6–8] and the IEFPCM solvation model[9] for CCl_4. Optimized geometries were confirmed as local minima via frequency analysis (N_{imag} = 0). Subsequently, VCD spectra were calculated at the same level of theory. All relevant xyz files of the geometry optimized conformers can be found in a separate ZIP file.

Input lines

Conformer Distribution

```
SEARCHMETHOD=THOROUGH FINDBOATS KEEPALL CONF_SELECTION_RULE=5
```

Geometry Optimization

```
#p opt=tight freq b3lyp/6-31g(d,p) scrf = (iefpcm, solvent =
carbontetrachloride)
```

VCD Calculation

```
#p freq=vcd b3lyp/6-31g(d,p) scrf = (iefpcm, solvent = carbontetrachloride)
```

Quantum mechanical assisted structure elucidation

VCD spectroscopy in combination with DFT based quantum mechanical simulations were conducted to determine which of the two possible diastereomers (4*R*9a*S*- vs. 4*R*9a*R*-) of oxazinone **35** was formed during the synthesis of dolutegravir sodium (**15**) (vide table 1). Based on the method developed by Bringmann *et al.*, similarity factors were calculated for the comparison of the experimental data with the simulated spectra of (4*R*9a*S*)-oxazinone **35** as well as with the simulated spectra of (4*R*9a*R*)-oxazinone **35b**.[10,11]

The software SpecDis 1.71 was used for the processing of the output files and the generation of Boltzmann weighted averaged spectra using the Gibbs free energies of the conformers. First, the Boltzmann weighted IR spectrum was fitted to the experimental data to determine the best scaling factor, the line broadening value γ as well as the applied shift. Subsequently, these obtained parameters were transferred onto the calculated VCD spectra for the comparison with the experimental data. In order to avoid artifacts due to solvent absorptions or the strong absorbing carbonyl region, the wavenumber region was set to 850–1300 cm^{-1}. A similarity factor of 76% was calculated for the comparison of the experimental VCD spectra with the (4*R*9a*S*)-oxazinone **35** diastereomer, whereas the other comparison yielded 25%. The comparison of the IR spectra yielded almost identical similarity factors (96% for (4*R*9a*S*)-**35** vs. 94% for (4*R*9a*R*)-**35b**). Thus, the configuration of 4*R*9a*S* was assigned to the synthesized oxazinone **35** and later confirmed by the successful preparation of dolutegravir sodium (**15**). The observed and calculated IR as well as the VCD spectra are shown in figure S13-S14.

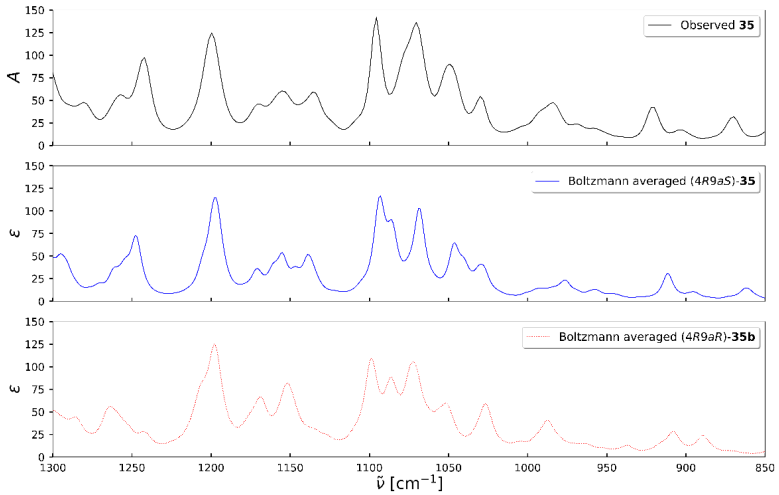

Figure S 13: Comparison of the observed oxazinone **35** (top) with the calculated IR spectra (middle: (4*R*9a*S*)-**35** and bottom: (4*R*9a*R*)-**35b**).

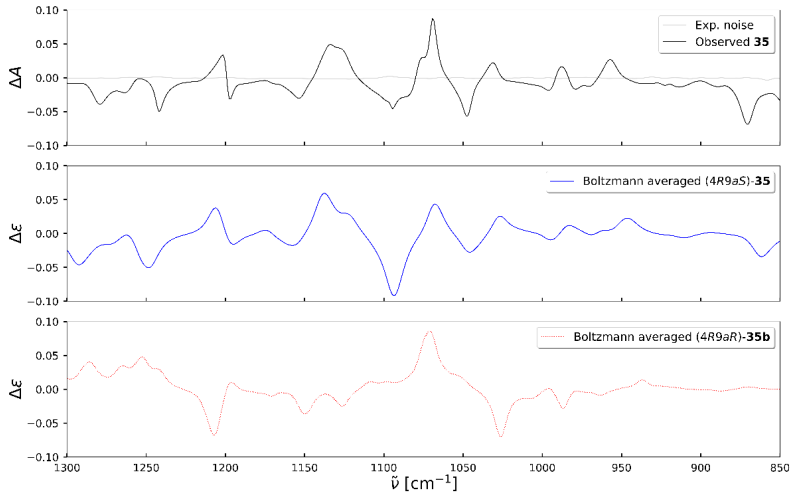

Figure S 14: Comparison of the observed VCD spectrum (top) of oxazinone **35** with the calculated spectra of both possible diastereomers (middle: (4*R*9a*S*)-**35** and bottom: (4*R*9a*R*)-**35b**).

5. NMR spectra

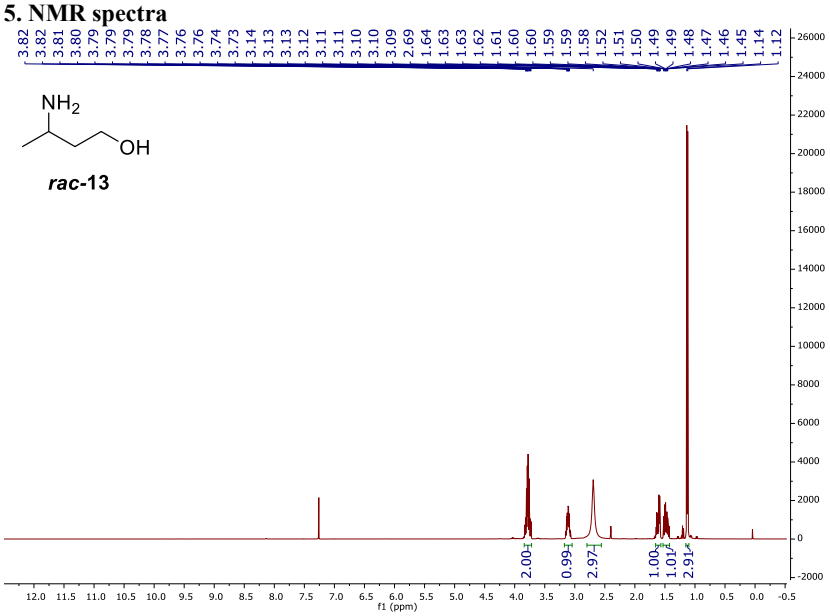

^{1}H-NMR-Spectrum (400 MHz, $CDCl_3$) of **13**.

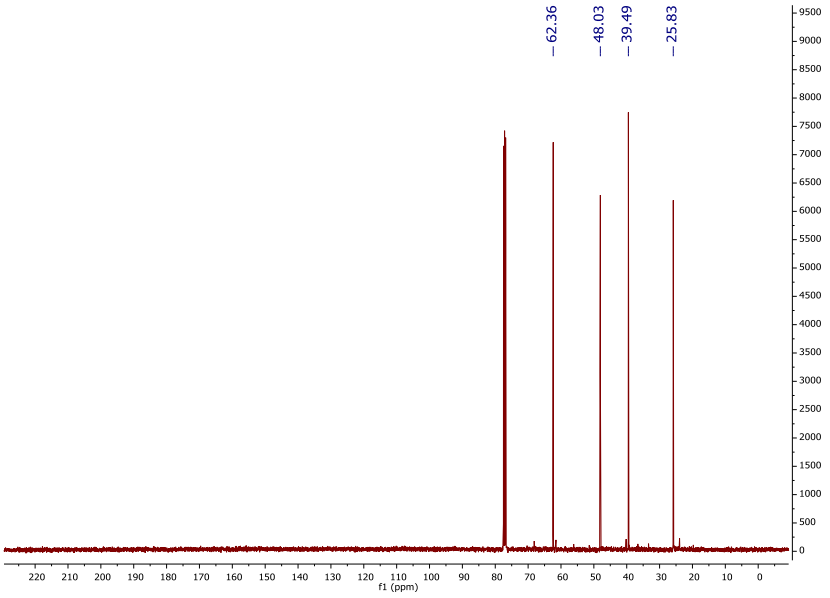

^{13}C-NMR-Spectrum (101 MHz, $CDCl_3$) of rac-**13.**

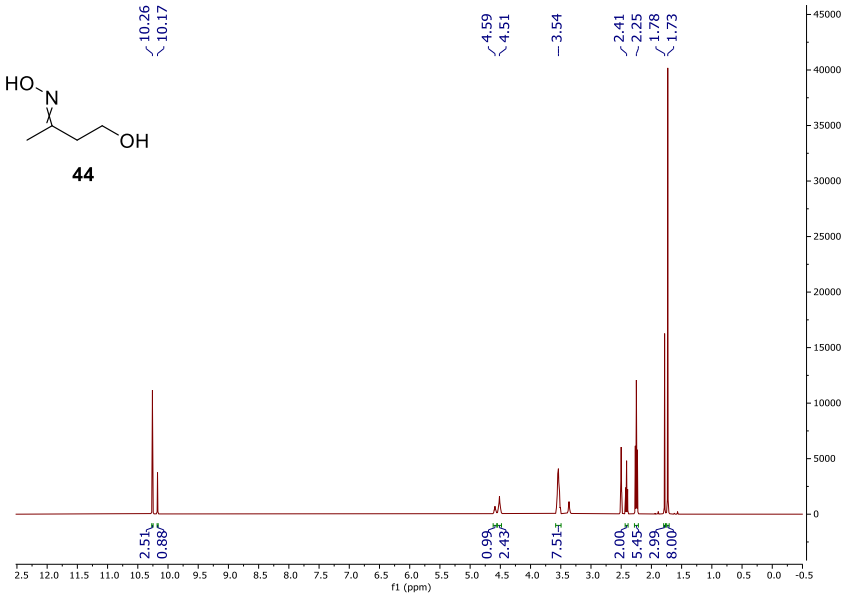

[1]H-NMR-Spectrum (400 MHz, DMSO-d_6) of **44**.

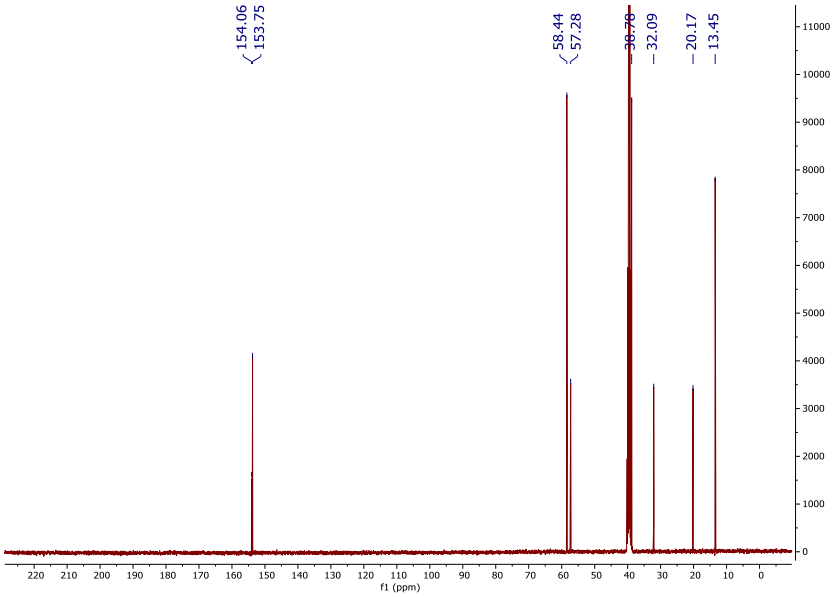

[13]C-NMR-Spectrum (101 MHz, DMSO-d_6) of **44**.

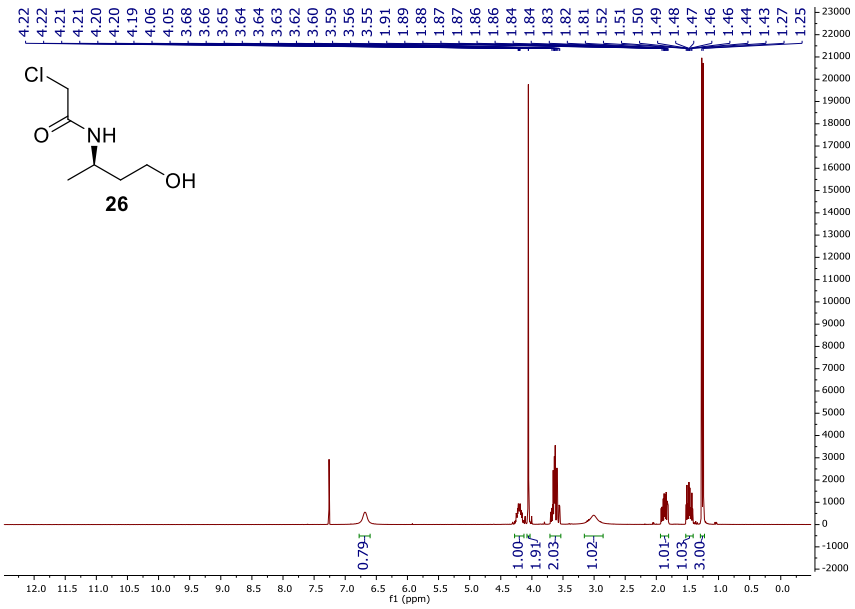

[1]H-NMR-Spectrum (300 MHz, $CDCl_3$) of **26**.

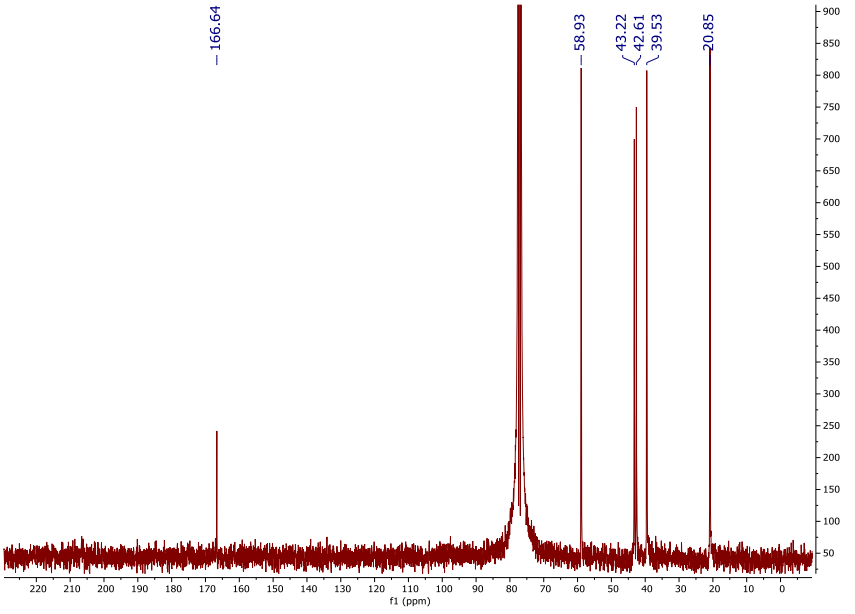

[13]C-NMR-Spectrum (75 MHz, $CDCl_3$) of **26.**

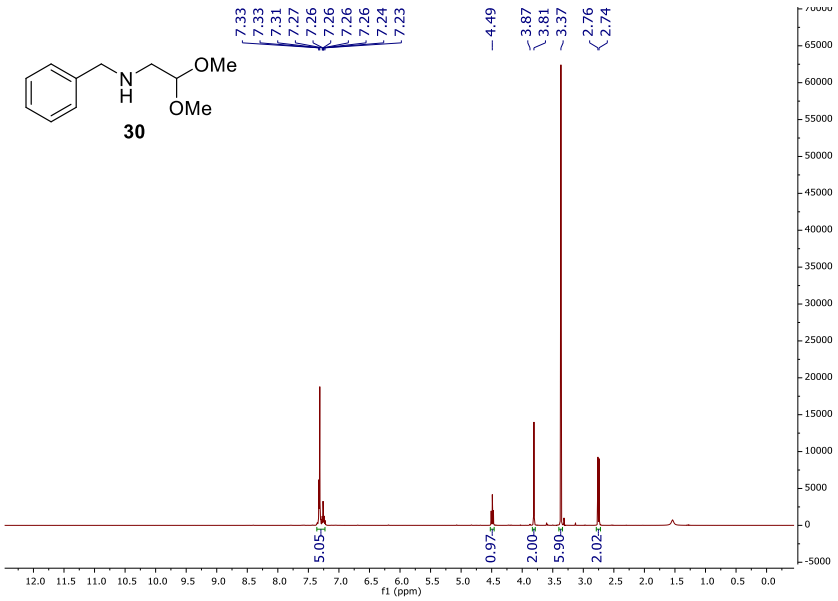

[1]H-NMR-Spectrum (300 MHz, $CDCl_3$) of **30**.

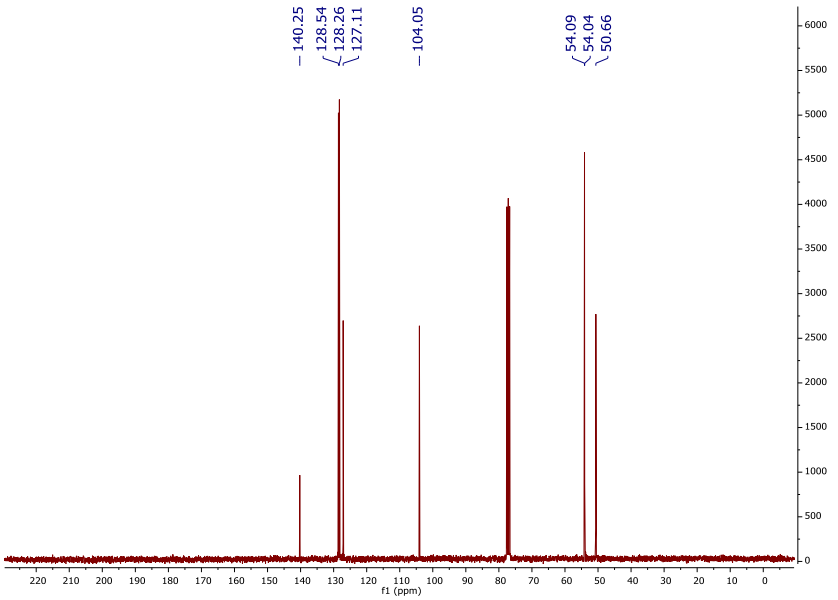

[13]C-NMR-Spectrum (75 MHz, $CDCl_3$) of **30.**

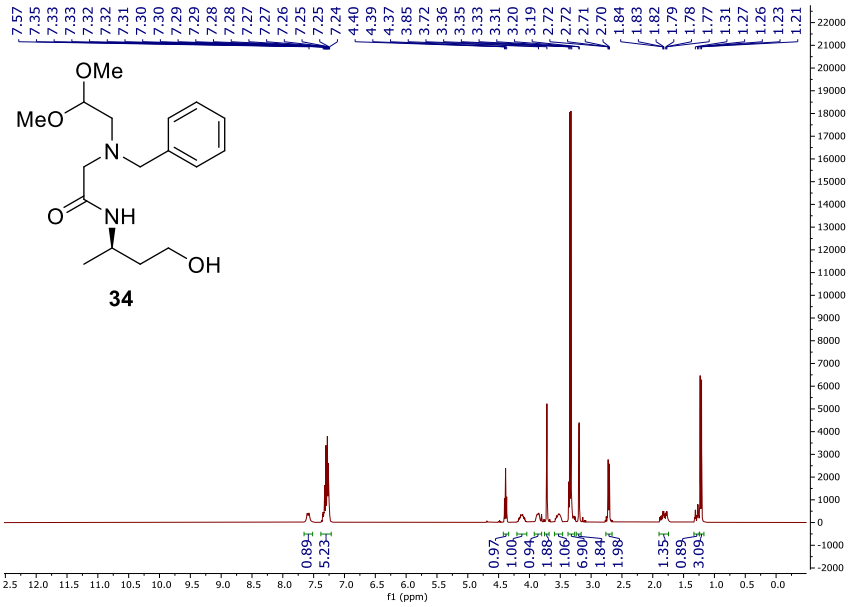

[1]H-NMR-Spectrum (300 MHz, $CDCl_3$) of **34**.

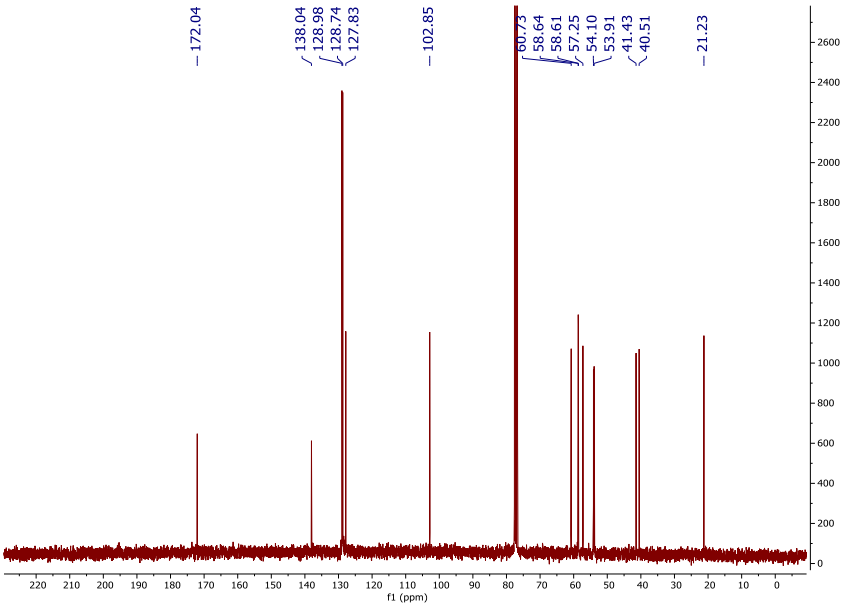

[13]C-NMR-Spectrum (75 MHz, $CDCl_3$) of **34.**

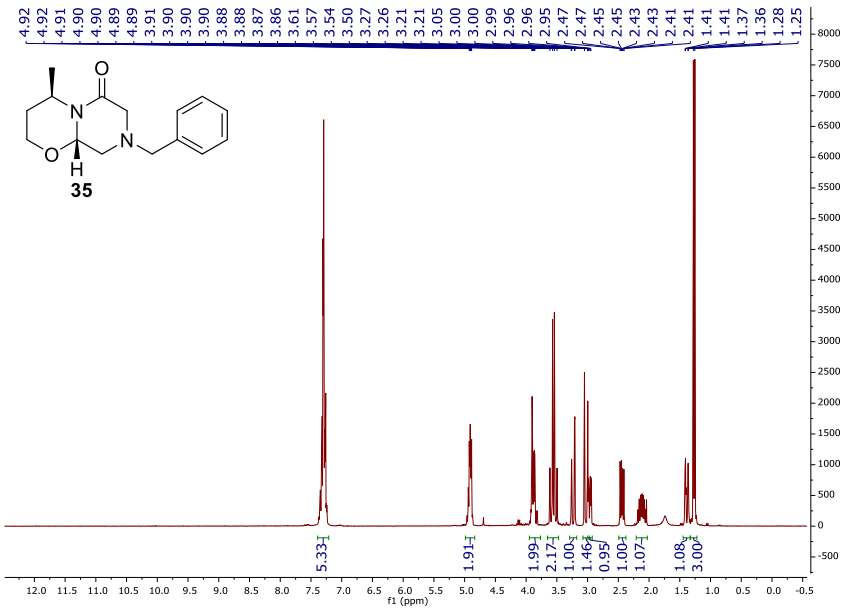

[1]H-NMR-Spectrum (300 MHz, $CDCl_3$) of crude **35**.

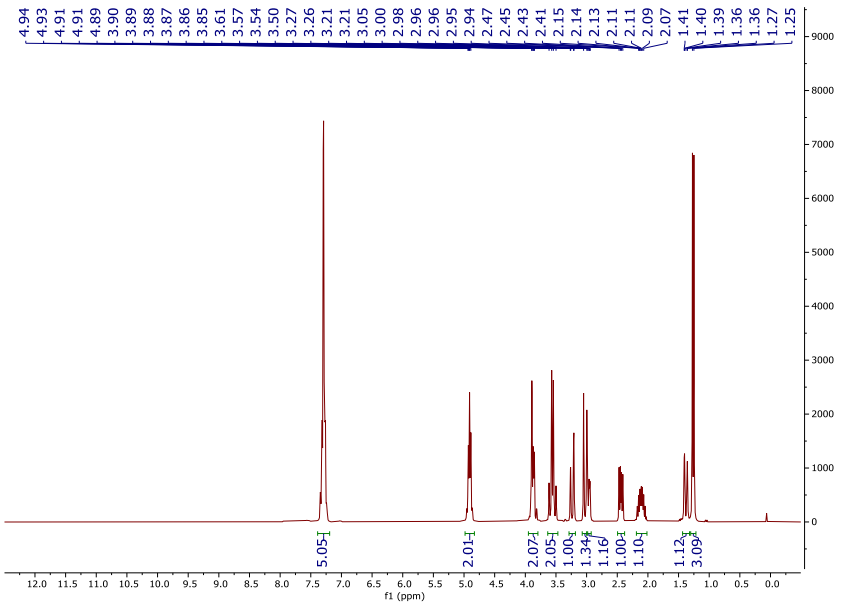

[1]H-NMR-Spectrum (300 MHz, $CDCl_3$) of purified **35**.

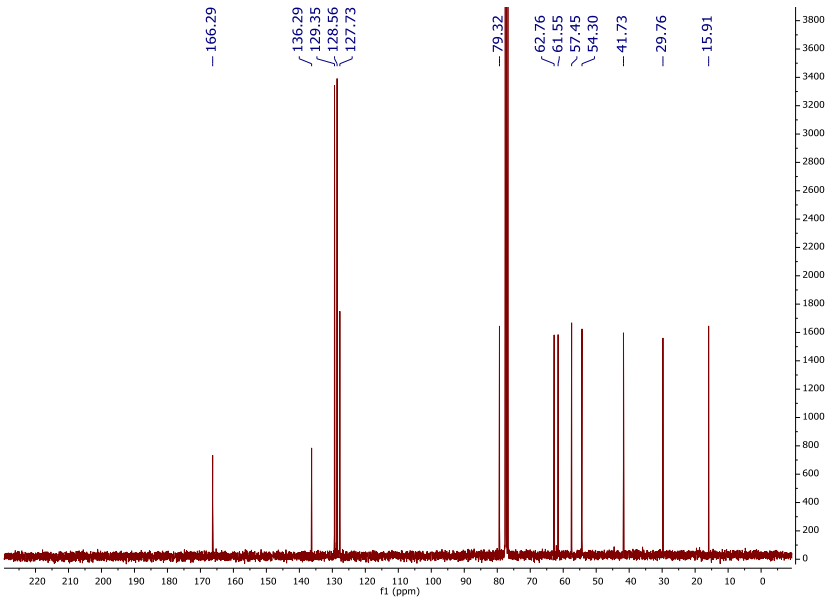

^{13}C-NMR-Spectrum (75 MHz, $CDCl_3$) of crude **35.**

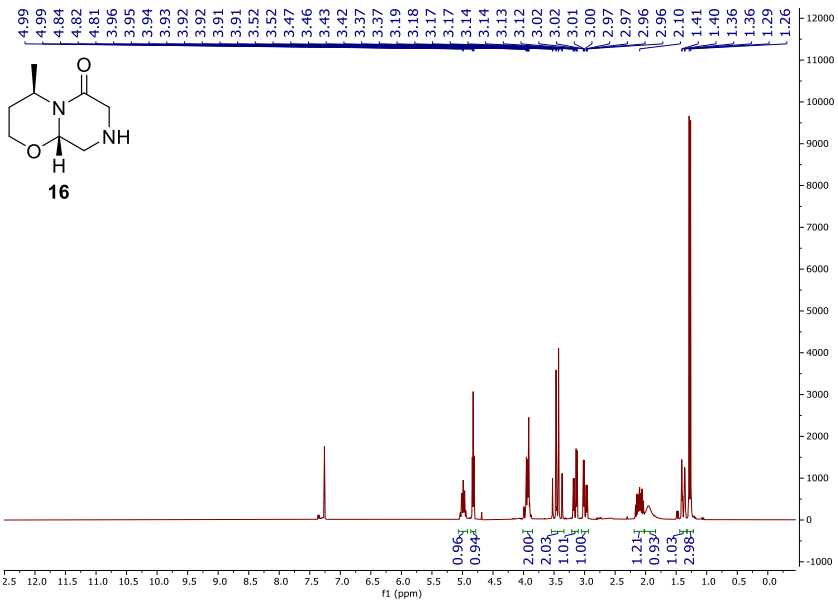

^{1}H-NMR-Spectrum (300 MHz, $CDCl_3$) of crude **16**.

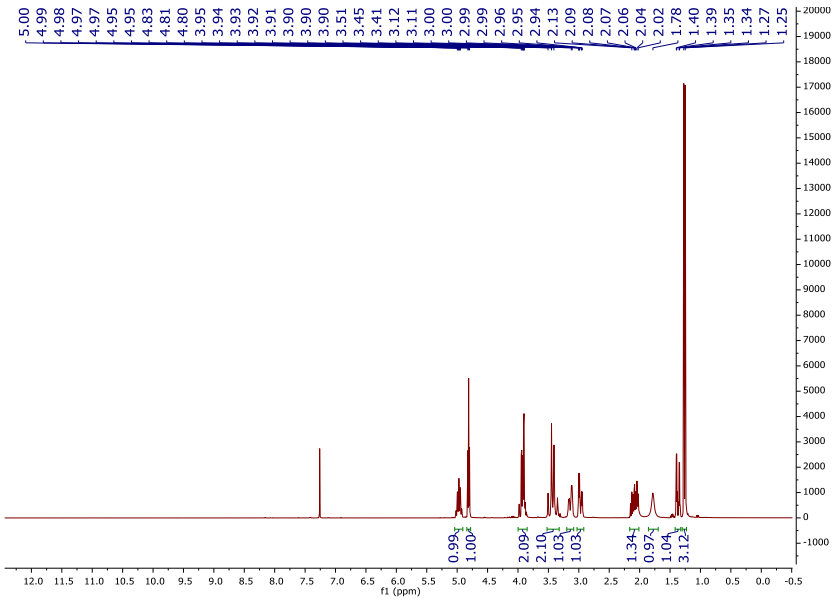

[1]H-NMR-Spectrum (300 MHz, $CDCl_3$) of purified **16**.

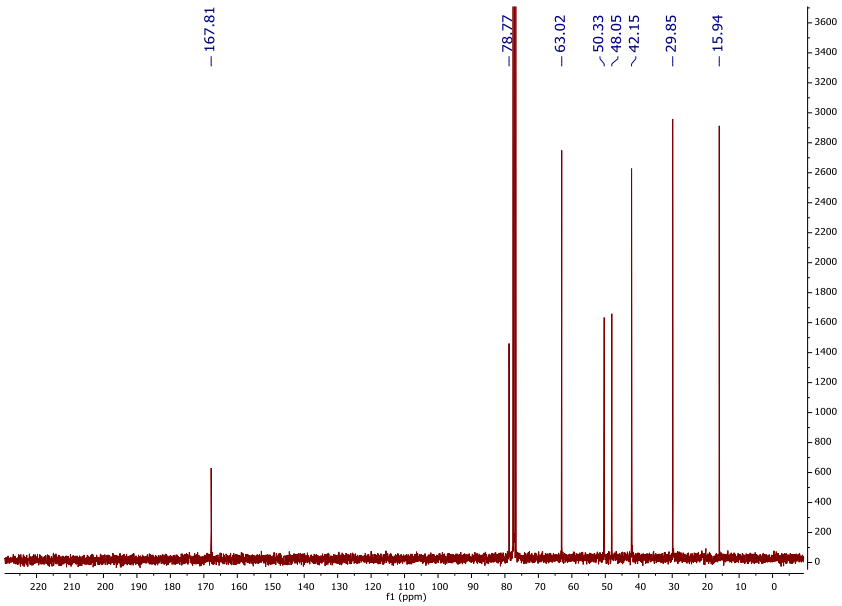

[13]C-NMR-Spectrum (75 MHz, $CDCl_3$) of purified **16.**

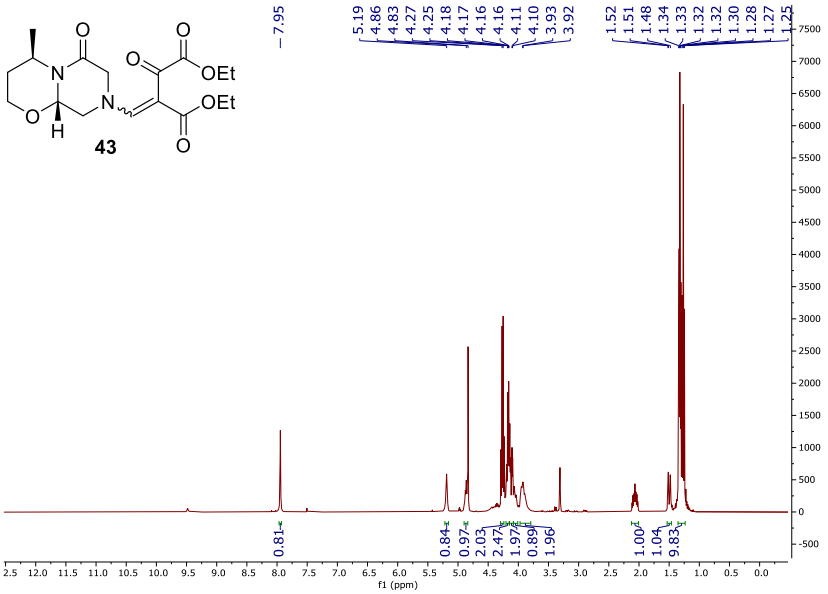

[1]H-NMR-Spectrum (400 MHz, MeOD) of crude **43**.

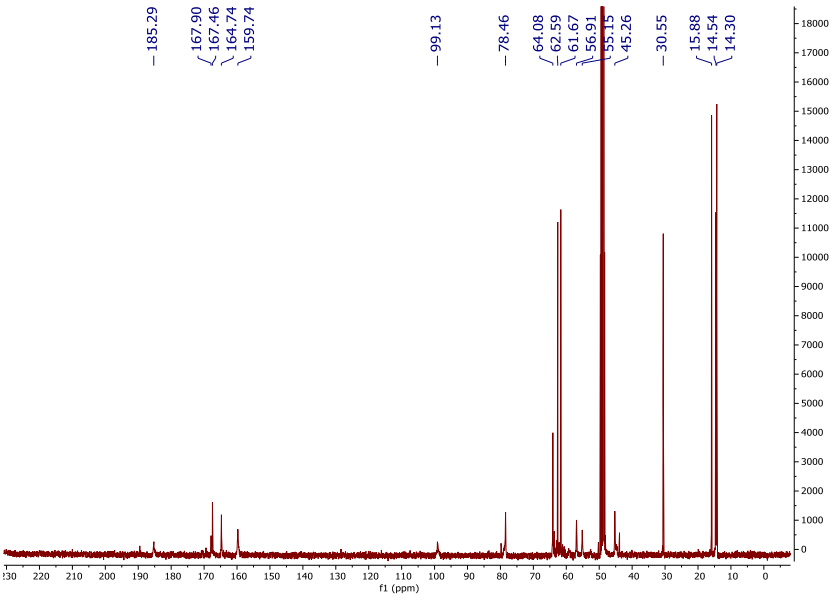

[13]C-NMR-Spectrum (101 MHz, $CDCl_3$) **43**.

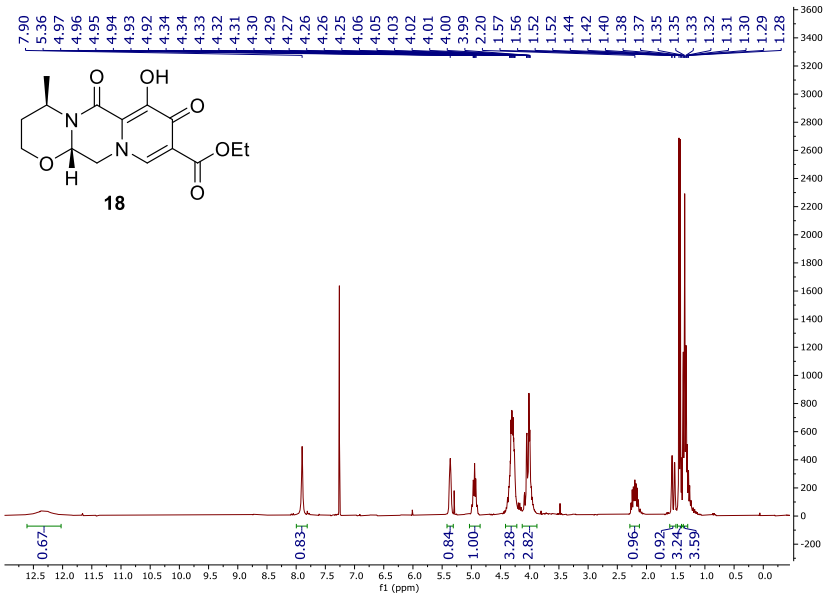

^{1}H-NMR-Spectrum (300 MHz, $CDCl_3$) of crude **18**.

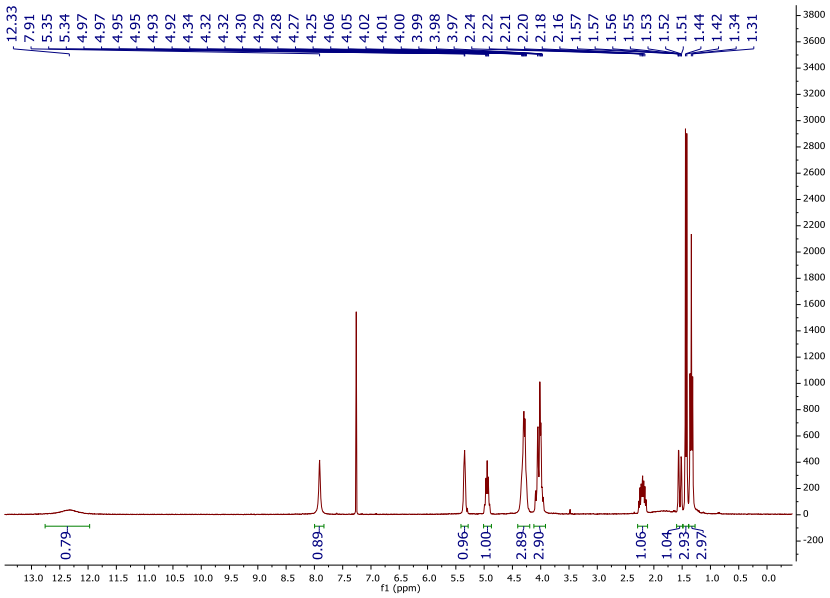

^{1}H-NMR-Spectrum (300 MHz, $CDCl_3$) of purified **18**.

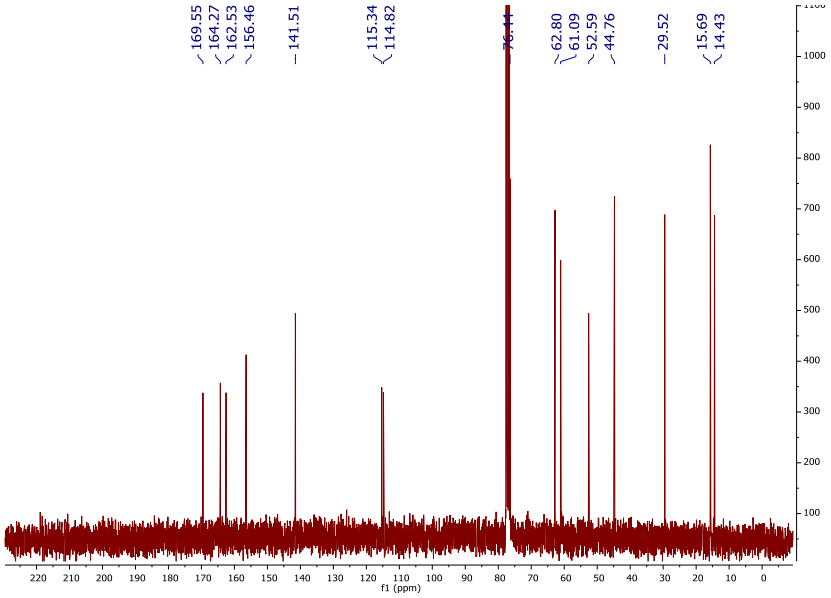

^{13}C-NMR-Spectrum (75 MHz, $CDCl_3$) of purified **18.**

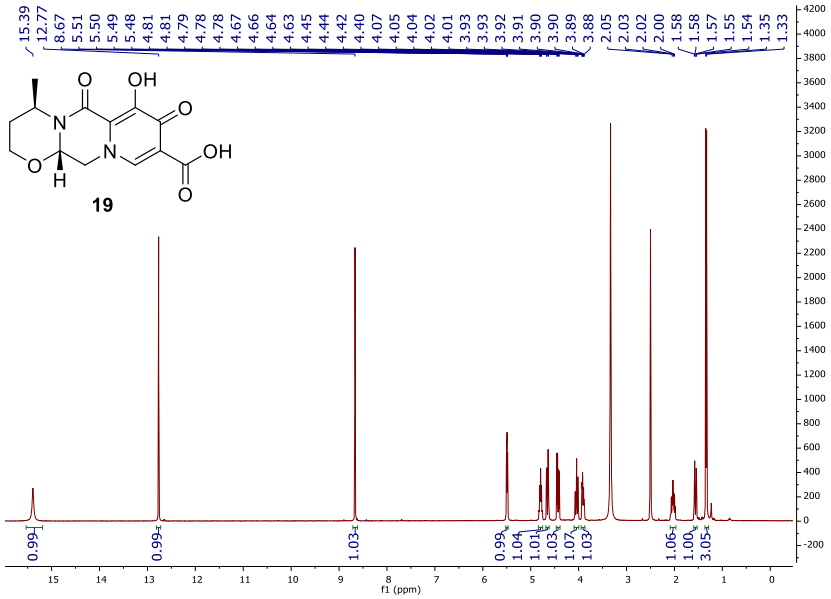

^{1}H-NMR-Spectrum (400 MHz, DMSO-d_6) of **19**.

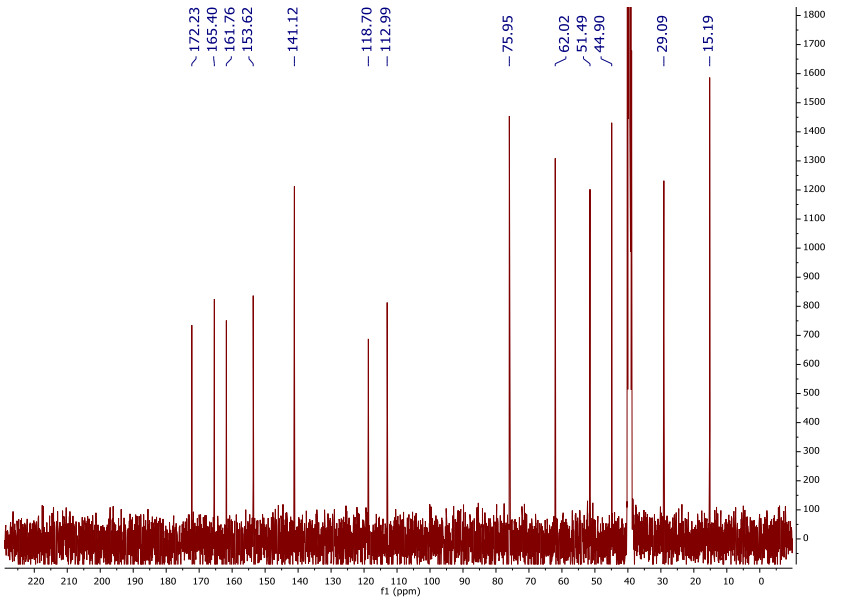

^{13}C-NMR-Spectrum (101 MHz, DMSO-d_6) of **19.**

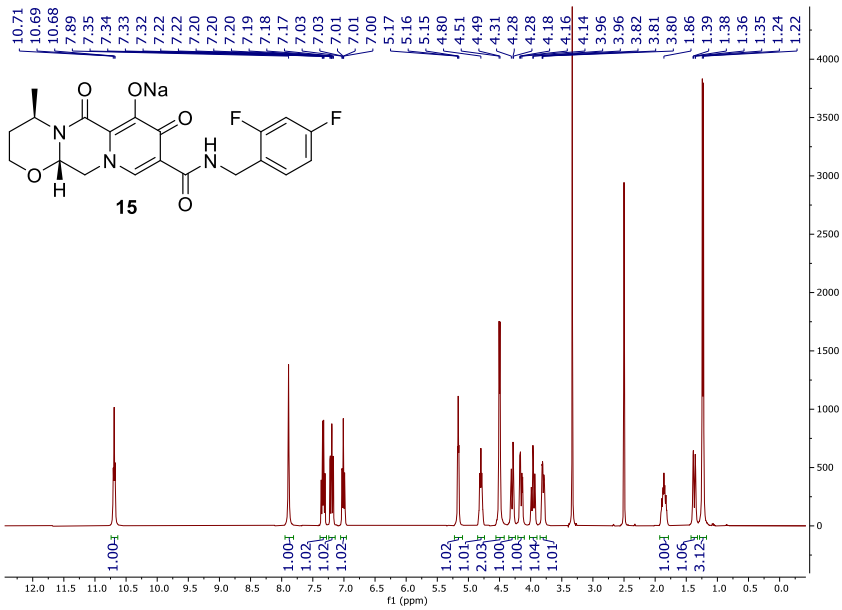

^{1}H-NMR-Spectrum (400 MHz, DMSO-d_6) of **15**.

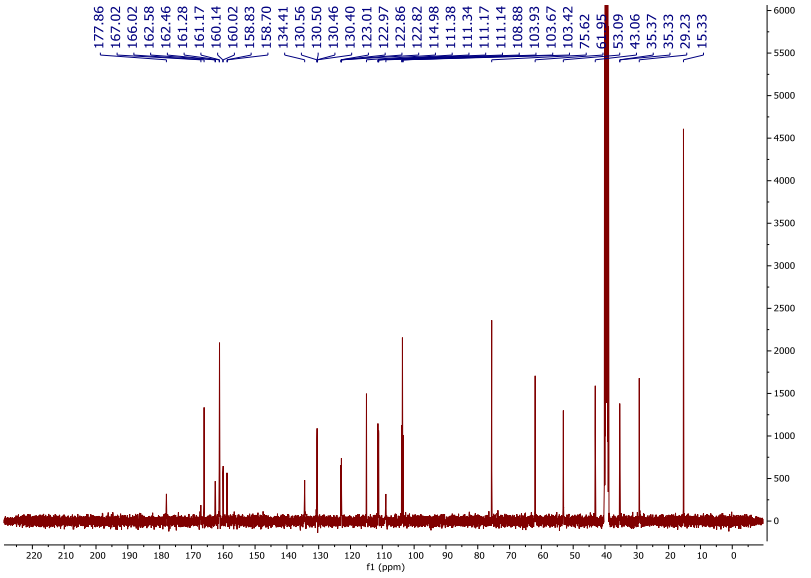

^{13}C-NMR-Spectrum (101 MHz, DMSO-d_6) of **15.**

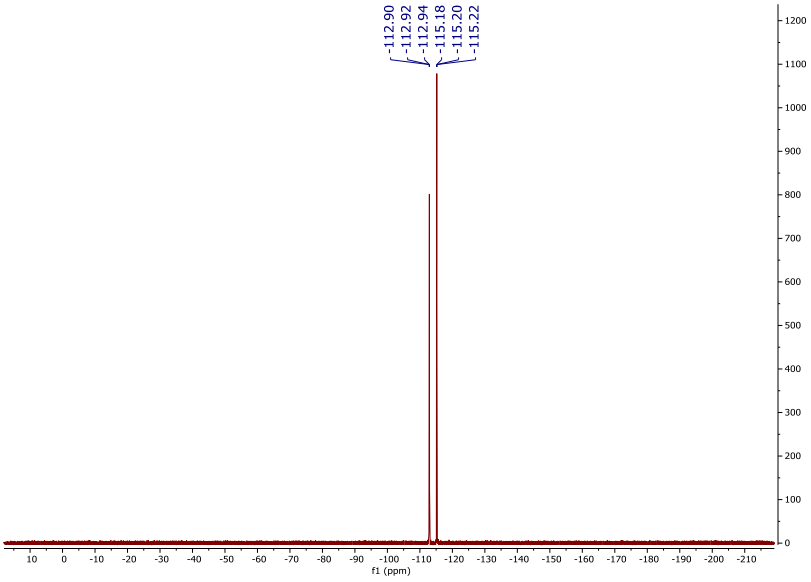

^{19}F-NMR-Spectrum (377 MHz, DMSO-d_6) of **15**.

6. References

(1) Stewart, J. J. P. Optimization of parameters for semiempirical methods V: Modification of NDDO approximations and application to 70 elements. *J. Mol. Model.* **2007**, *13*, 1173–1213.

(2) Vosko, S. H.; Wilk, L.; Nusair, M. Accurate spin-dependent electron liquid correlation energies for local spin density calculations: A critical analysis. *Can. J. Phys.* **1980**, *58*, 1200–1211.

(3) Lee; Yang; Parr. Development of the Colle-Salvetti correlation-energy formula into a functional of the electron density. *Phys. Rev. B, Condens. Matter* **1988**, *37*, 785–789.

(4) Becke, A. D. Density-functional thermochemistry. III. The role of exact exchange. *J. Chem. Phys.* **1993**, *98*, 5648–5652.

(5) Becke. Density-functional exchange-energy approximation with correct asymptotic behavior. *Phys. Rev. A, General Physics* **1988**, *38*, 3098–3100.

(6) Hariharan, P. C.; Pople, J. A. The influence of polarization functions on molecular orbital hydrogenation energies. *Theoret. Chim. Acta* **1973**, *28*, 213–222.

(7) Hehre, W. J.; Ditchfield, R.; Pople, J. A. Self—Consistent Molecular Orbital Methods. XII. Further Extensions of Gaussian—Type Basis Sets for Use in Molecular Orbital Studies of Organic Molecules. *J. Chem. Phys.* **1972**, *56*, 2257–2261.

(8) Francl, M. M.; Pietro, W. J.; Hehre, W. J.; Binkley, J. S.; Gordon, M. S.; DeFrees, D. J.; Pople, J. A. Self-consistent molecular orbital methods. XXIII. A polarization-type basis set for second-row elements. *J. Chem. Phys.* **1982**, *77*, 3654–3665.

(9) Tomasi, J.; Mennucci, B.; Cances, E. The IEF version of the PCM solvation method: an overview of a new method addressed to study molecular solutes at the QM ab initio level. *THEOCHEM* **1999**, *464*, 211–226.

(10) Bruhn, T.; Schaumlöffel, A.; Hemberger, Y.; Bringmann, G. SpecDis: Quantifying the comparison of calculated and experimental electronic circular dichroism spectra. *Chirality* **2013**, *25*, 243–249.

(11) Debie, E.; Gussem, E. de; Dukor, R. K.; Herrebout, W.; Nafie, L. A.; Bultinck, P. A confidence level algorithm for the determination of absolute configuration using vibrational circular dichroism or Raman optical activity. *ChemPhysChem* **2011**, *12*, 1542–1549.

B.2.3 Zusatzmaterial der Publikation zur Bestimmung der absoluten Konfiguration eines 13-Hydroxy-14-deoxyoxacyclododecindions

Im Folgenden ist die *supporting information* der Publikation „Total Synthesis and Biological Evaluation of the Anti-Inflammatory (13*R*,14*S*,15*R*)-13-Hydroxy-14-deoxyoxacyclododecindione“ abgedruckt.[560]

Total Synthesis and Biological Evaluation of the Anti-Inflammatory (13*R*,14*S*,15*R*)-13-Hydroxy-14-deoxyoxacyclododecindione

Kevin Seipp,[a] *Jonathan Groß*,[a] *Anna Maria Kiefer*,[b] *Gerhard Erkel*[b], *Till Opatz*[*a]

[a.]Department of Chemistry, Johannes Gutenberg-University, Duesbergweg 10–14, 55128 Mainz, Germany.

*E-mail: opatz@uni-mainz.de

[b.]Department of Molecular Biotechnology & Systems Biology, University of Kaiserslautern, Erwin-Schrödinger Str. 70, Building 70, 67663 Kaiserslautern, Germany.

Supporting Information

Table of contents

I. Synthetic Route of (13*R*,14*S*,15*R*)-13-Hydroxy-14-deoxyoxacyclododecindione (4)

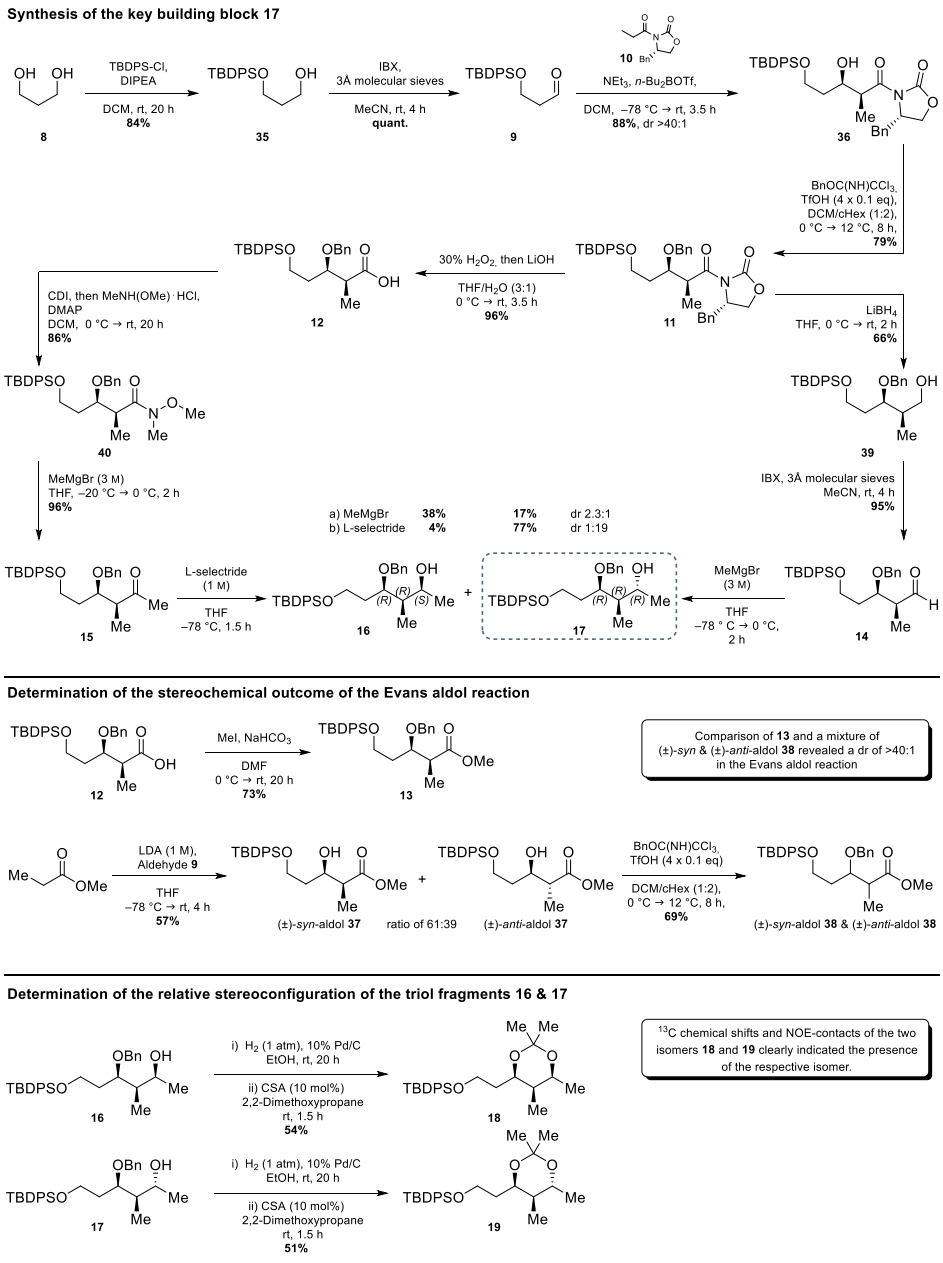

Scheme S1: Stepwise synthetic route of the stereoselective synthesis of the key building block **17** in the total synthesis of macrolactone **4**. Furthermore, the stereochemical outcome of the Evans aldol reaction and the determination of the relative configuration of the triol fragments **16** and **17** are presented.

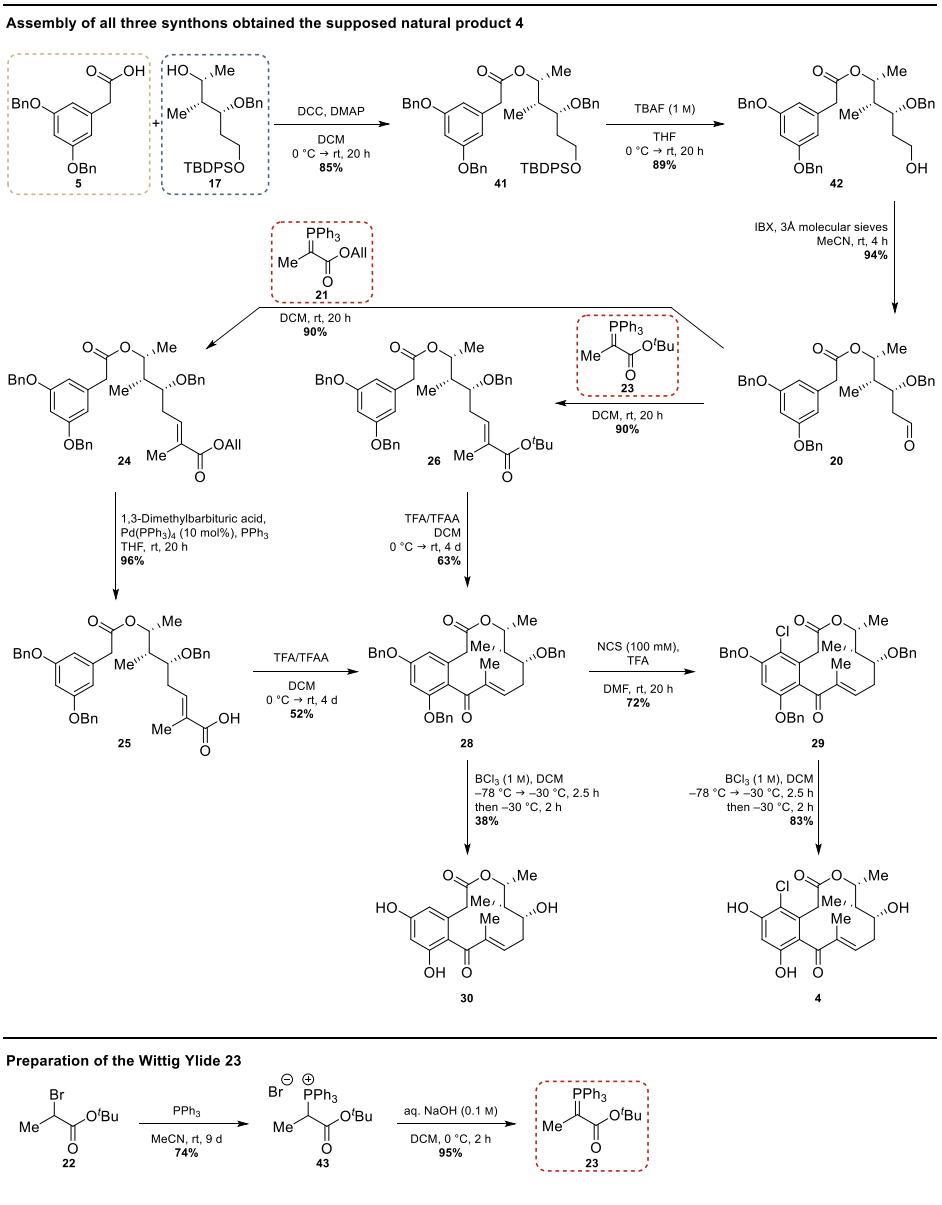

Scheme S2: Stepwise assembly of the three synthons resulting in the ring closure precursor **25** and **26**. IFCA, chlorination and deprotection led to (13*R*,14*S*,15*R*)-13-hydroxy-14-deoxyoxacyclododecindione (**4**). Furthermore, the preparation of the Wittig ylide **23** is presented.

II. ^{1}H- and ^{13}C{^{1}H}-NMR Spectra of Compounds

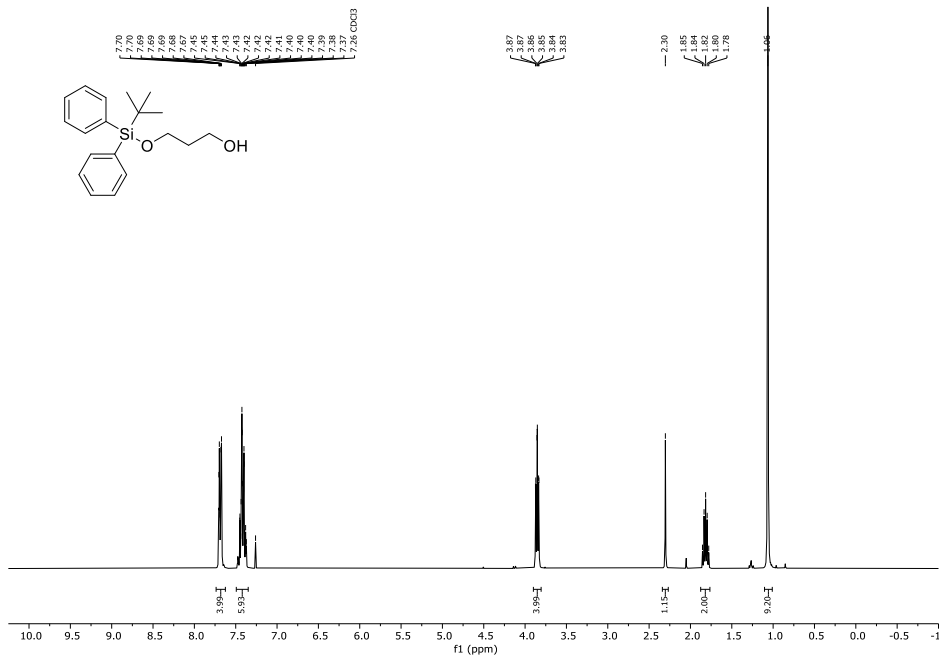

Figure S1: ^{1}H-NMR spectrum ($CDCl_3$, 400 MHz, 296 K) of 3-((*tert*-butyldiphenylsilyl)oxy)propan-1-ol (**35**).

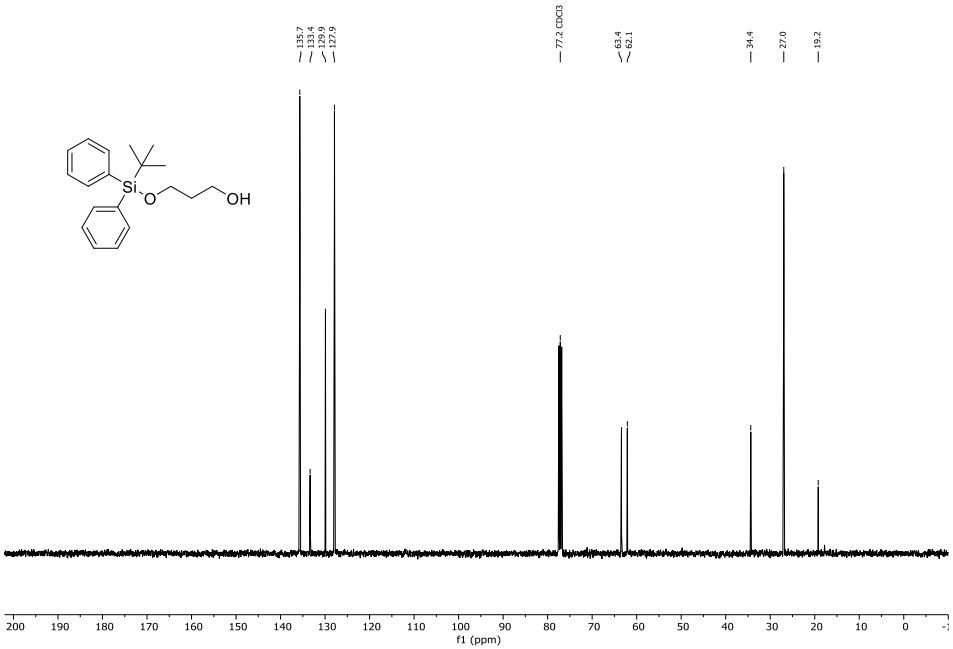

Figure S2: ^{13}C{^{1}H}-NMR spectrum ($CDCl_3$, 101 MHz, 296 K) of 3-((*tert*-butyldiphenylsilyl)oxy)propan-1-ol (**35**).

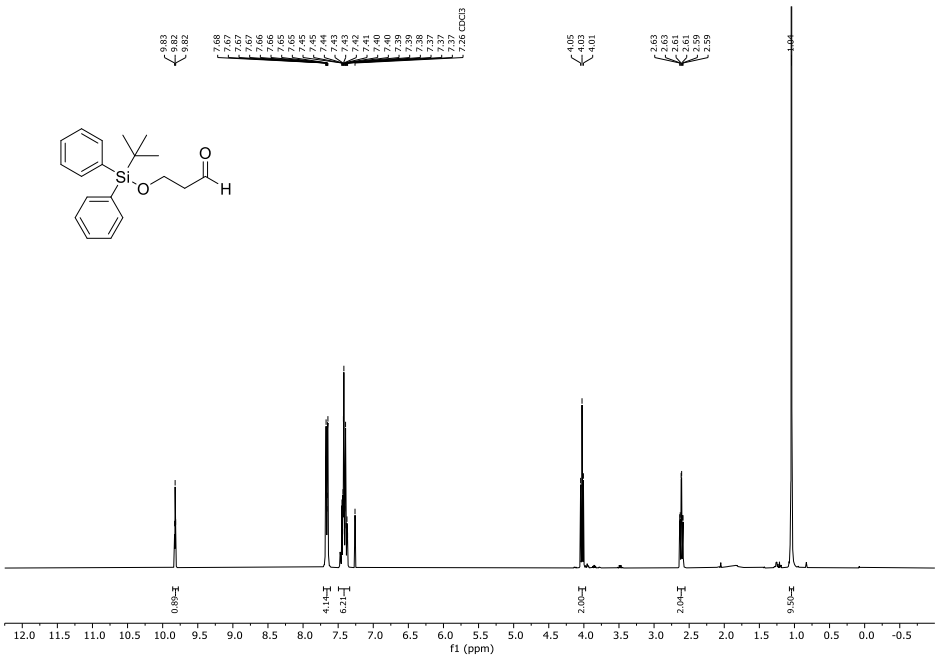

Figure S3: ^{1}H-NMR spectrum ($CDCl_3$, 300 MHz, 296 K) of 3-((*tert*-butyldiphenylsilyl)oxy)propanal (**9**).

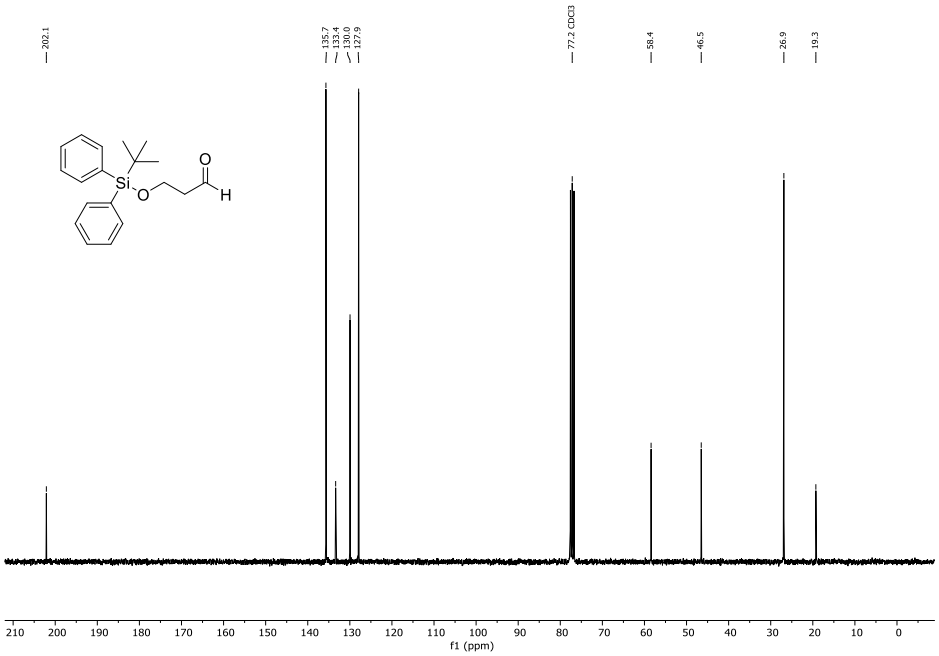

Figure S4: $^{13}C\{^{1}H\}$-NMR spectrum ($CDCl_3$, 75 MHz, 296 K) of 3-((*tert*-butyldiphenylsilyl)oxy)propanal (**9**).

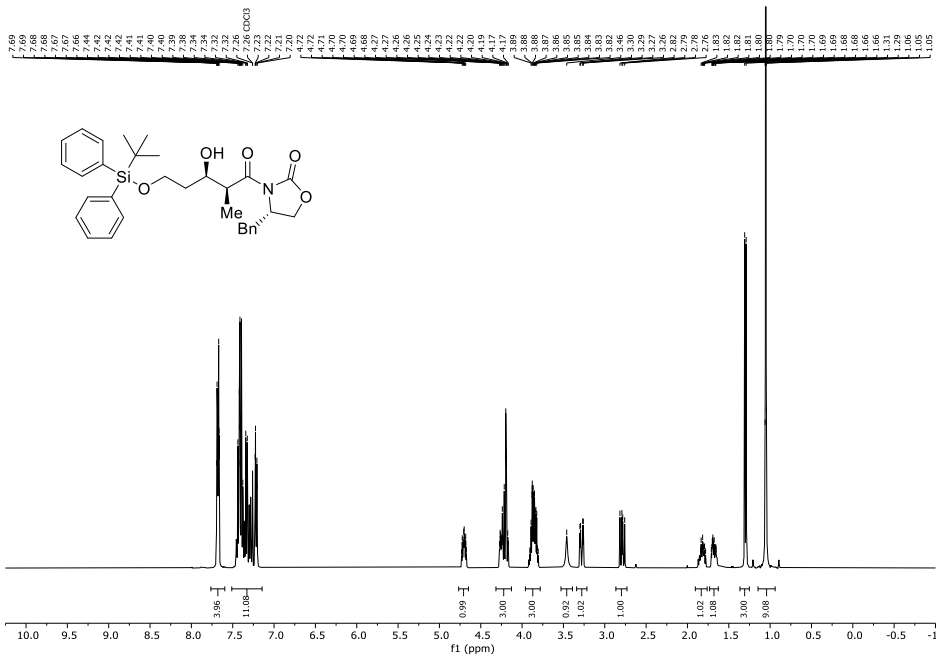

Figure S5: ^{1}H-NMR spectrum ($CDCl_3$, 400 MHz, 296 K) of (*S*)-4-benzyl-3-((2*S*,3*R*)-5-((*tert*-butyldiphenylsilyl)oxy)-3-hydroxy-2-methylpentanoyl)oxazolidin-2-one (**36**).

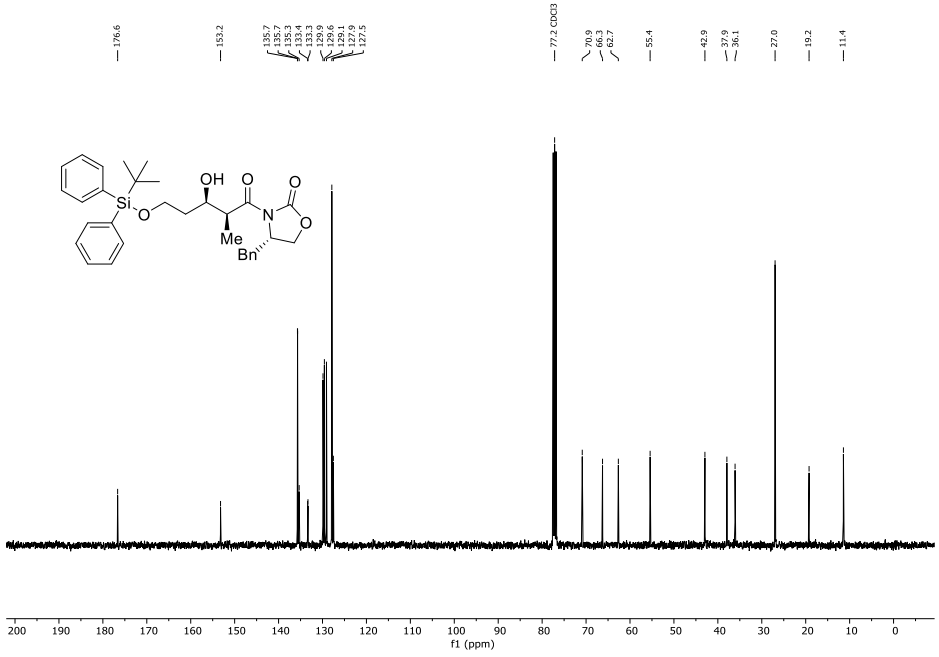

Figure S6: $^{13}C\{^{1}H\}$-NMR spectrum ($CDCl_3$, 101 MHz, 296 K) of (*S*)-4-benzyl-3-((2*S*,3*R*)-5-((*tert*-butyldiphenylsilyl)oxy)-3-hydroxy-2-methylpentanoyl)oxazolidin-2-one (**36**).

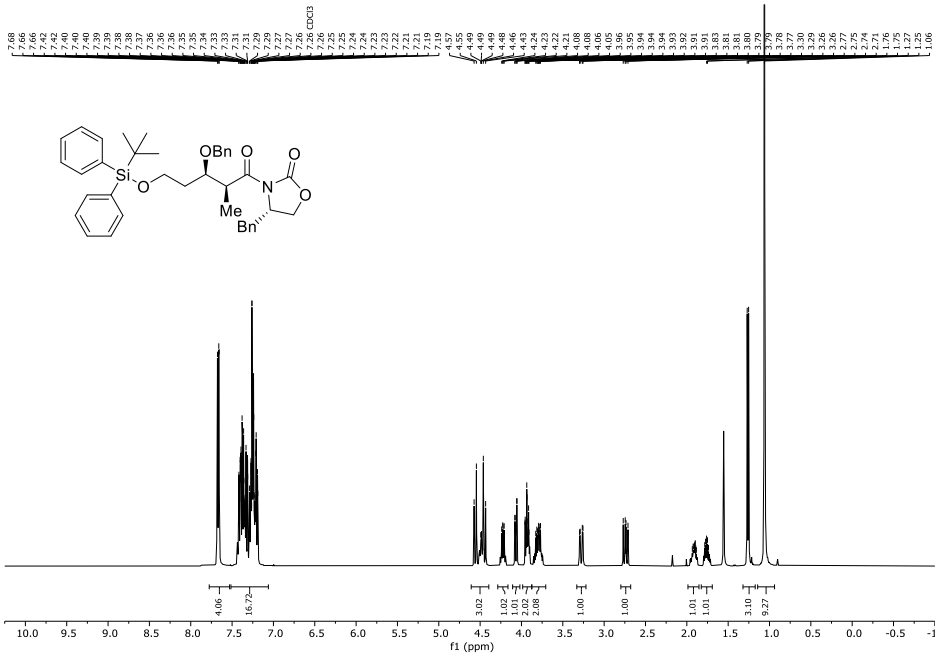

Figure S7: ^{1}H-NMR spectrum ($CDCl_3$, 400 MHz, 296 K) of (*S*)-4-benzyl-3-((2*S*,3*R*)-3-(benzyloxy)-5-((*tert*-butyldiphenylsilyl)oxy)-2-methylpentanoyl)oxazolidin-2-one (**11**).

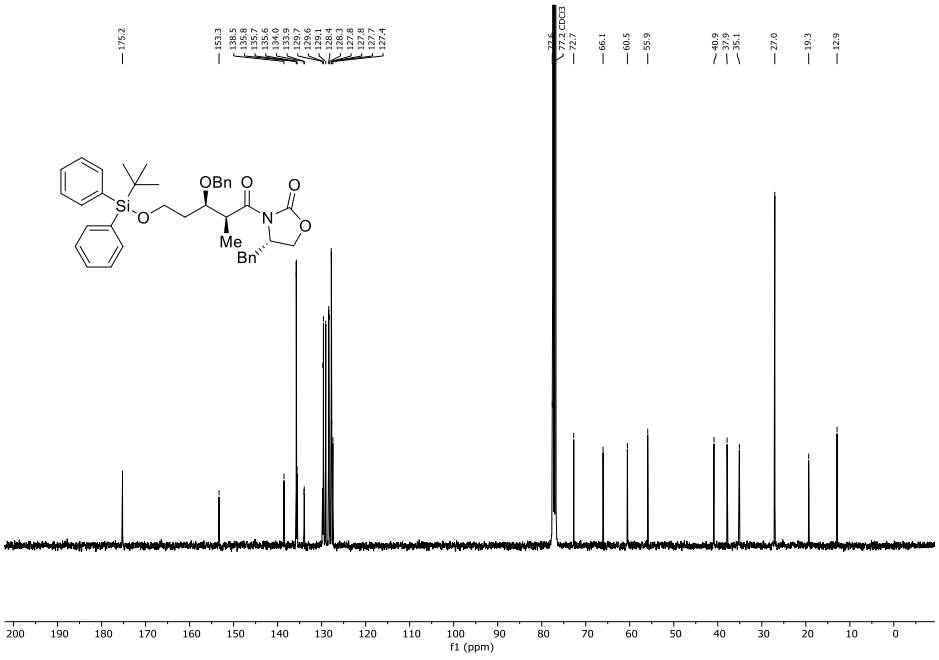

Figure S8: ^{13}C{^{1}H}-NMR spectrum ($CDCl_3$, 101 MHz, 296 K) of (*S*)-4-benzyl-3-((2*S*,3*R*)-3-(benzyloxy)-5-((*tert*-butyldiphenylsilyl)oxy)-2-methylpentanoyl)oxazolidin-2-one (**11**).

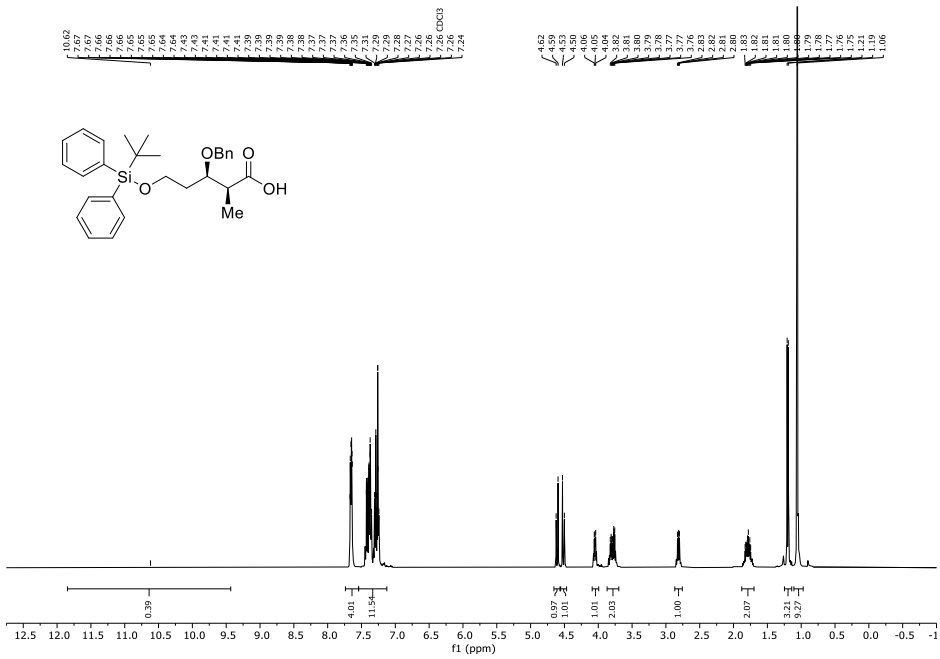

Figure S9: ^{1}H-NMR spectrum ($CDCl_3$, 400 MHz, 296 K) of (2*S*,3*R*)-3-(benzyloxy)-5-((*tert*-butyldiphenylsilyl)oxy)-2-methylpentanoic acid (**12**).

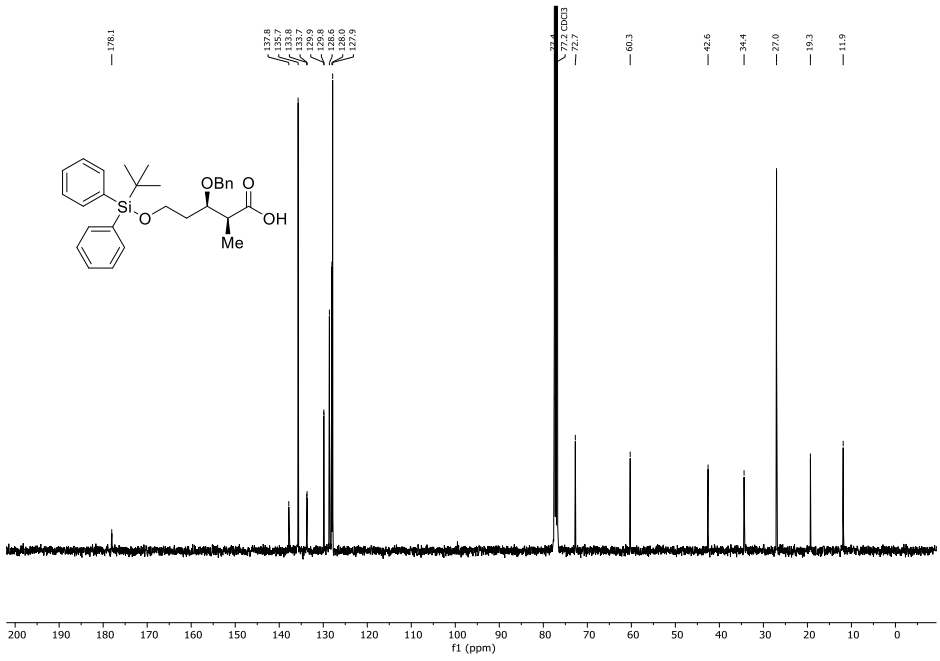

Figure S10: $^{13}C\{^{1}H\}$-NMR spectrum ($CDCl_3$, 400 MHz, 296 K) of (2*S*,3*R*)-3-(benzyloxy)-5-((*tert*-butyldiphenylsilyl)oxy)-2-methylpentanoic acid (**12**).

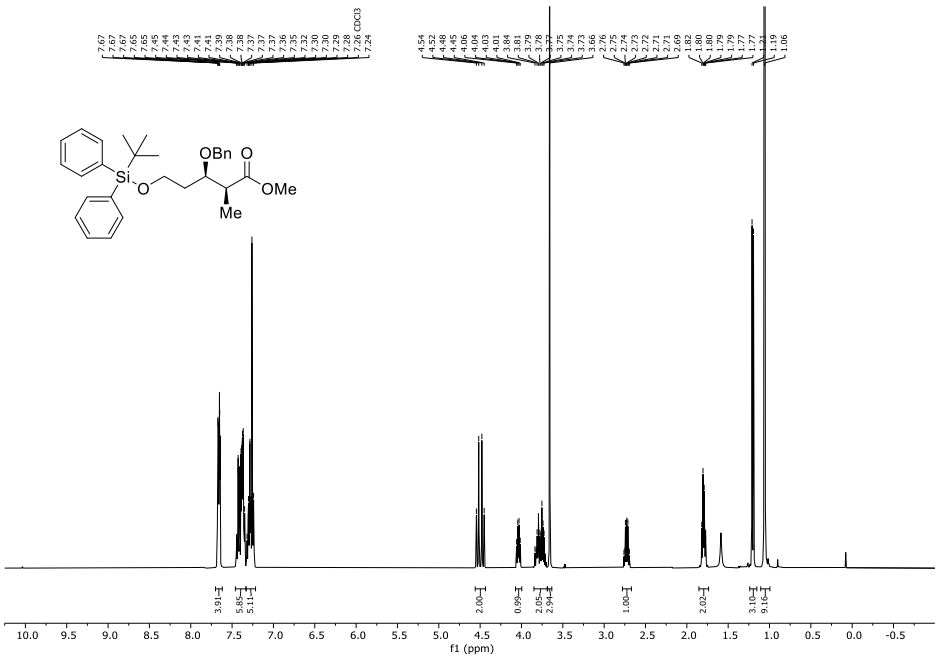

Figure S11: ^{1}H-NMR spectrum ($CDCl_3$, 400 MHz, 296 K) of methyl (2*S*,3*R*)-3-(benzyloxy)-5-((*tert*-butyldiphenylsilyl)oxy)-2-methylpentanoate (**13**).

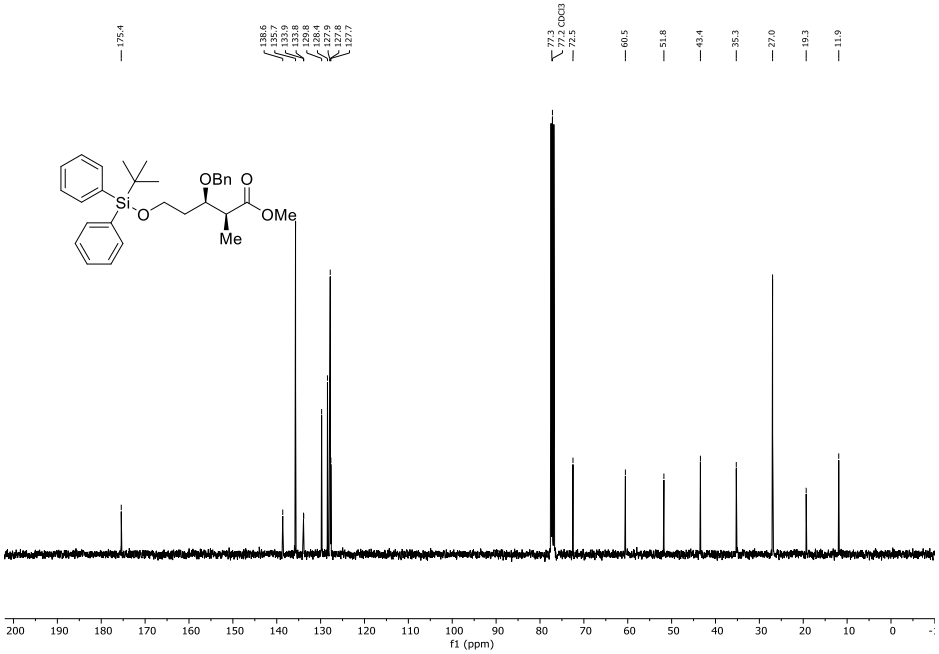

Figure S12: $^{13}C\{^{1}H\}$-NMR spectrum ($CDCl_3$, 101 MHz, 296 K) of methyl (2*S*,3*R*)-3-(benzyloxy)-5-((*tert*-butyldiphenylsilyl)oxy)-2-methylpentanoate (**13**).

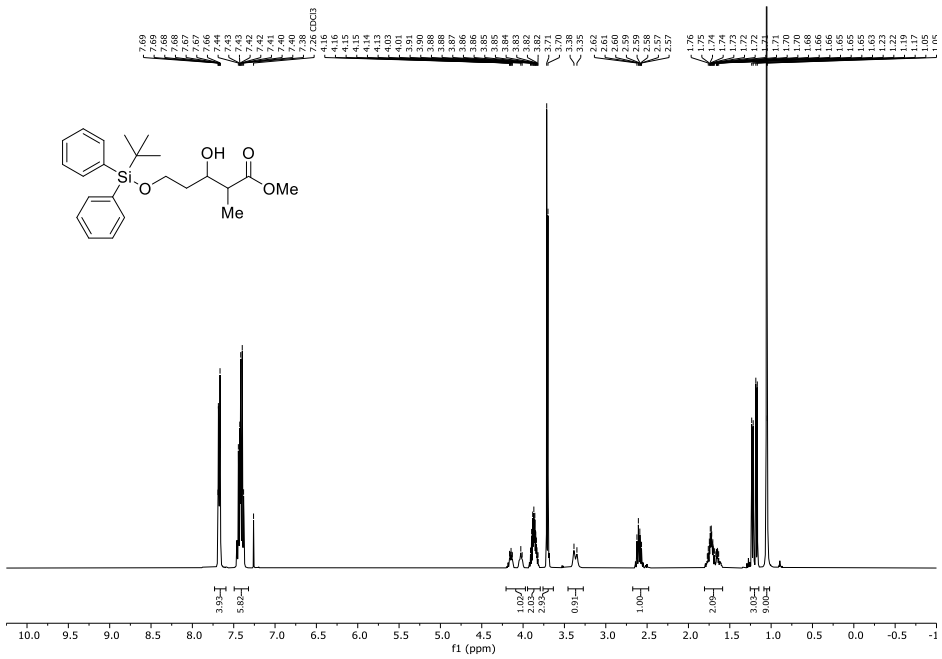

Figure S13: ^{1}H-NMR spectrum ($CDCl_3$, 400 MHz, 296 K) of methyl-5-((*tert*-butyldiphenylsilyl)oxy)-3-hydroxy-2-methylpentanoate (**37**).

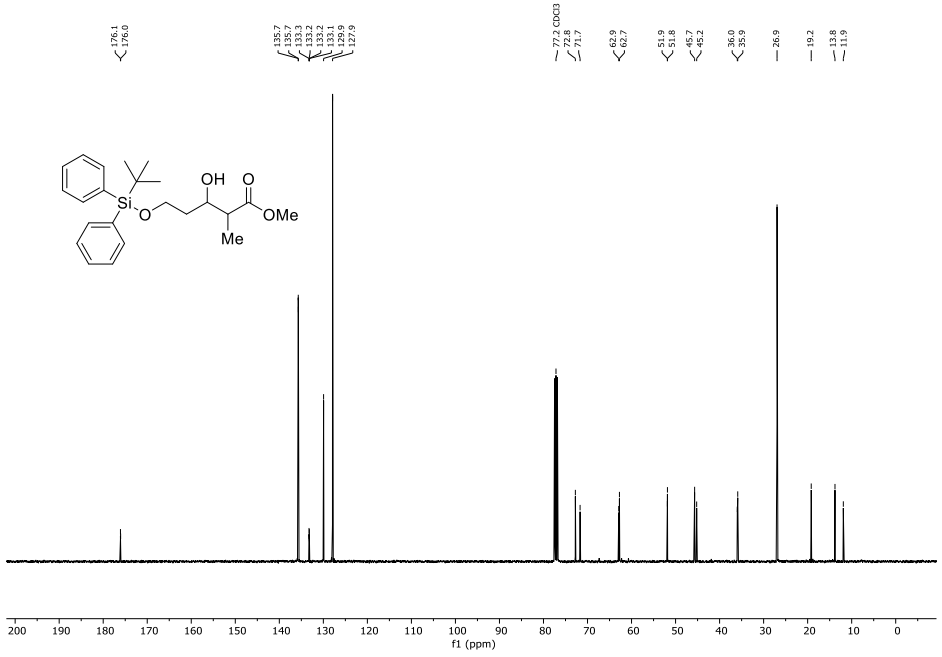

Figure S14: $^{13}C\{^{1}H\}$-NMR spectrum ($CDCl_3$, 101 MHz, 296 K) of methyl-5-((*tert*-butyldiphenylsilyl)oxy)-3-hydroxy-2-methylpentanoate (**37**).

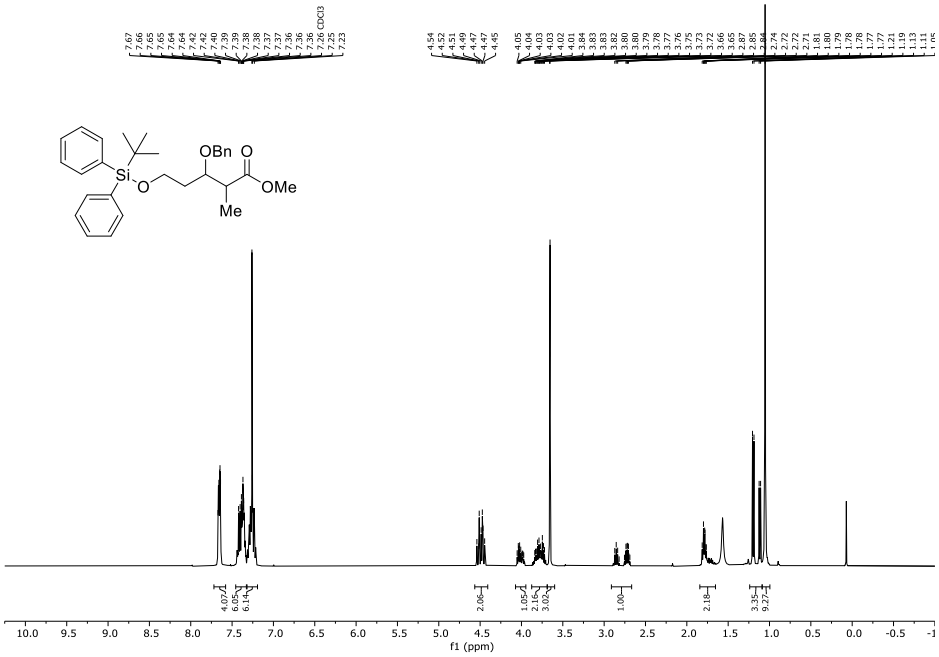

Figure S15: ^{1}H-NMR spectrum ($CDCl_3$, 400 MHz, 296 K) of methyl 3-(benzyloxy)-5-((*tert*-butyldiphenylsilyl)oxy)-2-methylpentanoate (**38**).

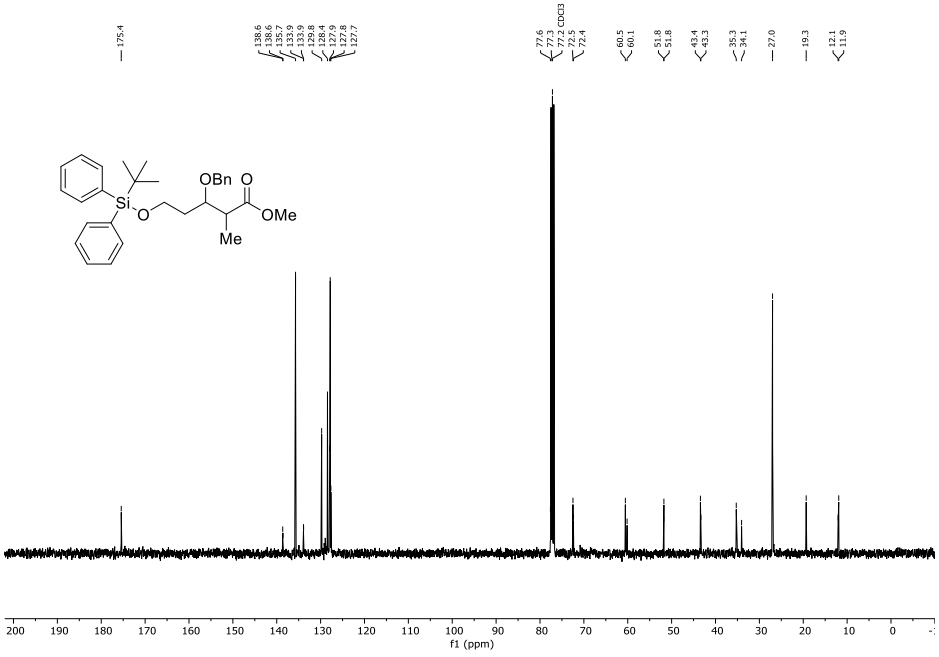

Figure S16: ^{13}C{^{1}H}-NMR spectrum ($CDCl_3$, 101 MHz, 296 K) of methyl 3-(benzyloxy)-5-((*tert*-butyldiphenylsilyl)oxy)-2-methylpentanoate (**38**).

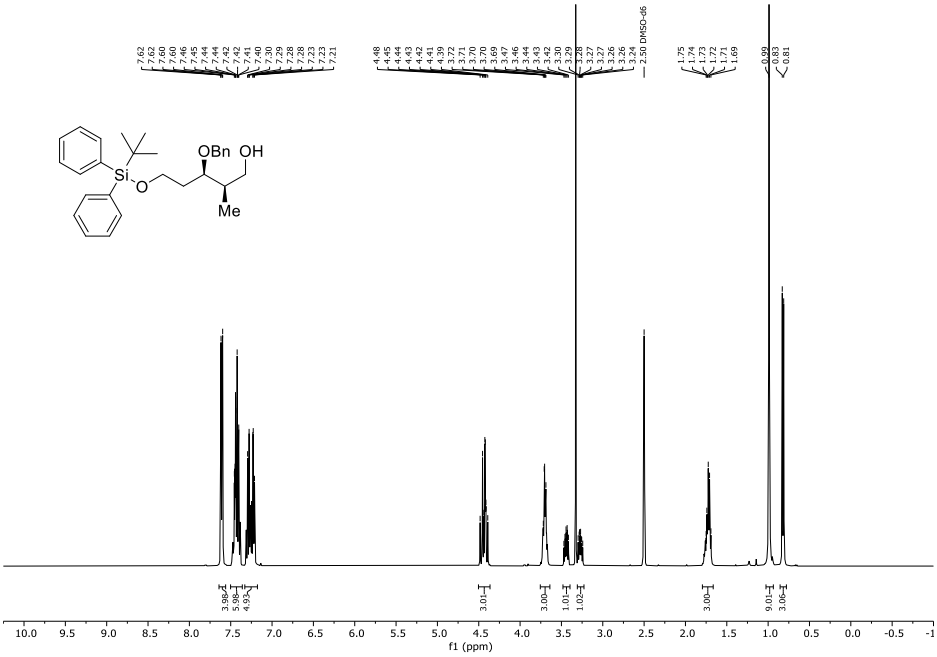

Figure S17: ^{1}H-NMR spectrum (DMSO-d_6, 400 MHz, 296 K) of (2*R*,3*R*)-3-(benzyloxy)-5-((*tert*-butyldiphenylsilyl)oxy)-2-methylpentan-1-ol (**39**).

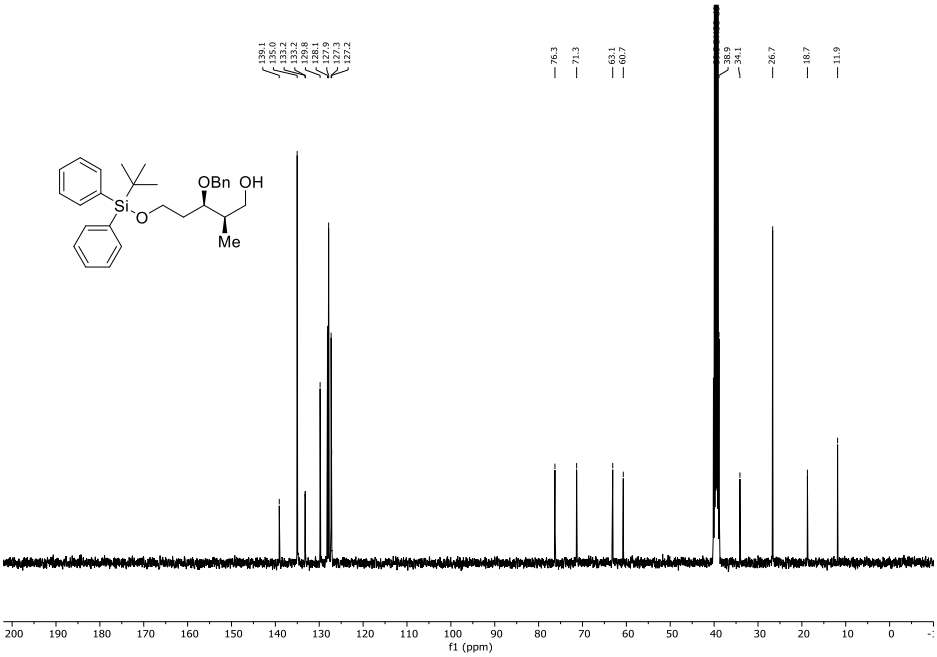

Figure S18: ^{13}C{^{1}H}-NMR spectrum (DMSO-d_6, 101 MHz, 296 K) of (2*R*,3*R*)-3-(benzyloxy)-5-((*tert*-butyldiphenylsilyl)oxy)-2-methylpentan-1-ol (**39**).

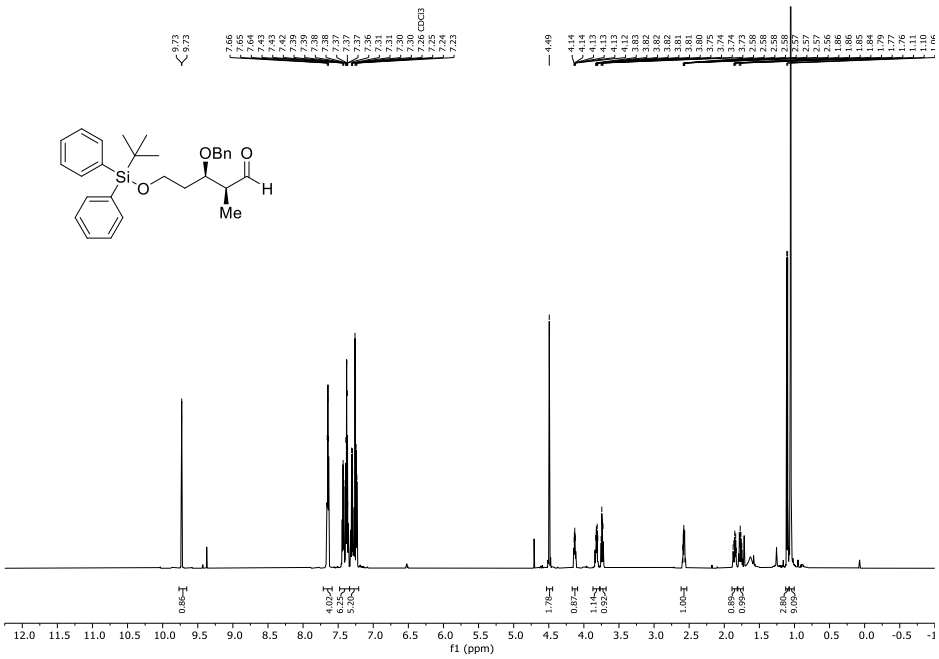

Figure S19: ^{1}H-NMR spectrum ($CDCl_3$, 600 MHz, 296 K) of (2*S*,3*R*)-3-(benzyloxy)-5-((*tert*-butyldiphenylsilyl)oxy)-2-methylpentanal (**14**).

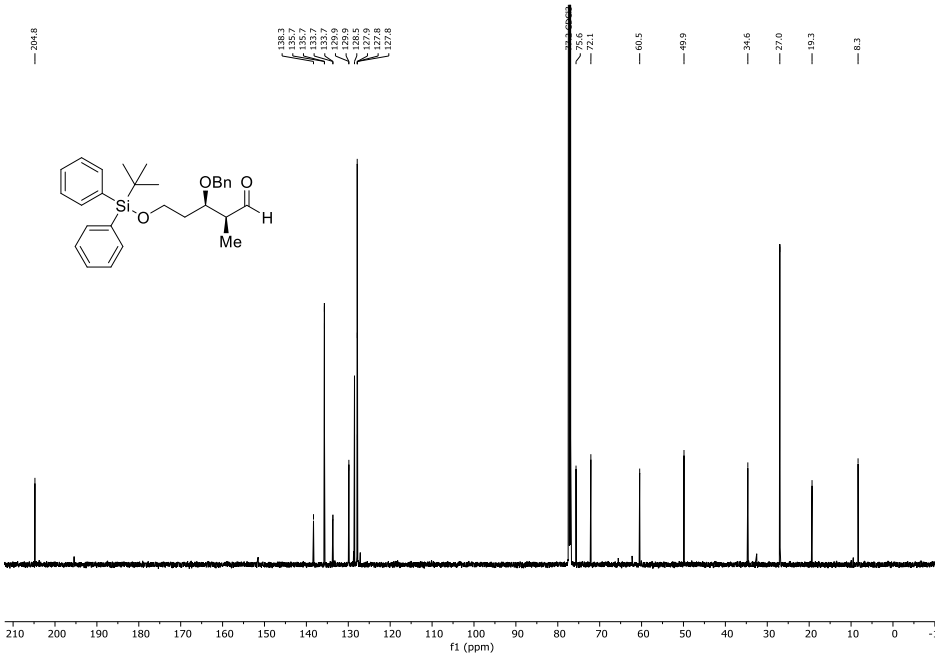

Figure S20: $^{13}C\{^{1}H\}$-NMR spectrum ($CDCl_3$, 151 MHz, 296 K) of (2*S*,3*R*)-3-(benzyloxy)-5-((*tert*-butyldiphenylsilyl)oxy)-2-methylpentanal (**14**).

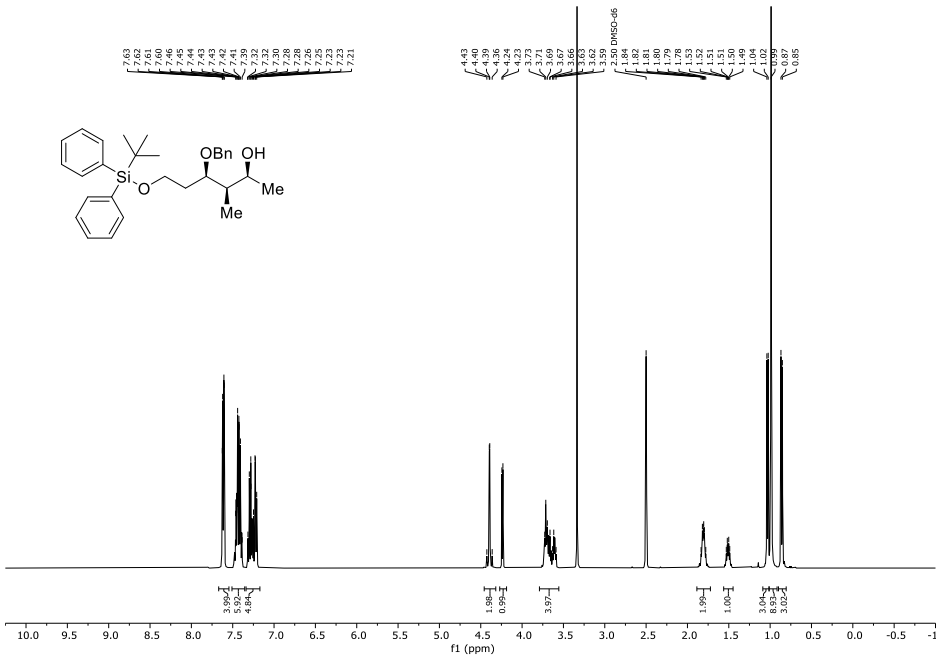

Figure S21: ^{1}H-NMR spectrum (DMSO-d_6, 400 MHz, 296 K) of (2*S*,3*R*,4*R*)-4-(benzyloxy)-6-((*tert*-butyldiphenylsilyl)oxy)-3-methylhexan-2-ol (**16**).

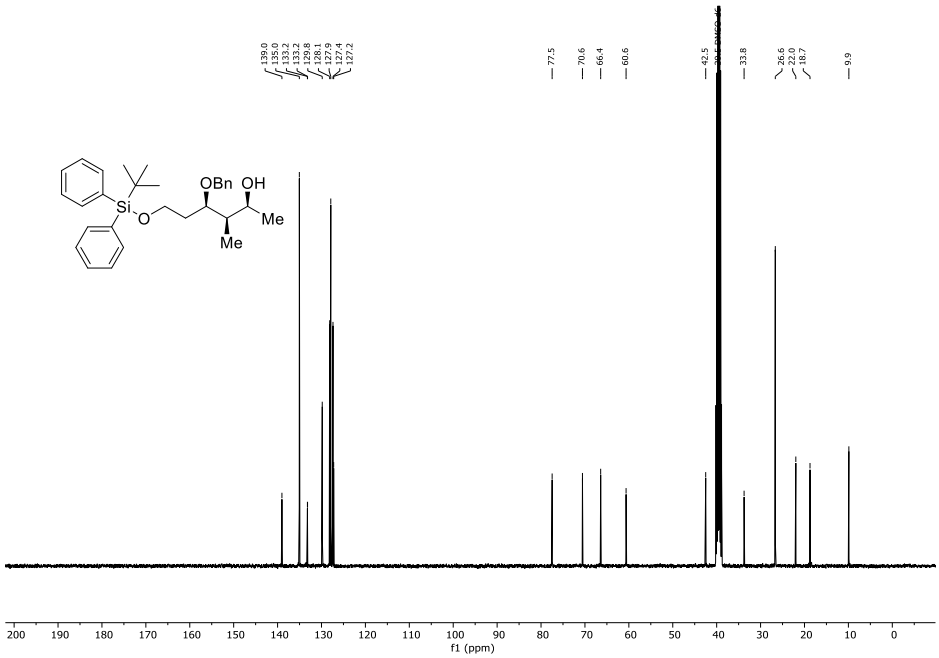

Figure S22: ^{13}C{^{1}H}-NMR spectrum (DMSO-d_6, 101 MHz, 296 K) of (2*S*,3*R*,4*R*)-4-(benzyloxy)-6-((*tert*-butyldiphenylsilyl)oxy)-3-methylhexan-2-ol (**16**).

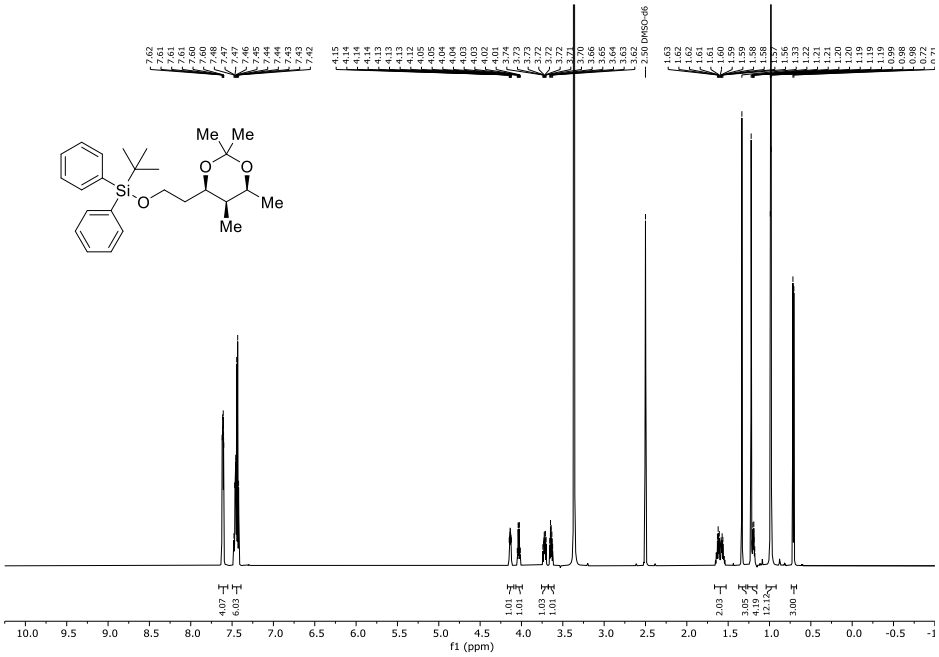

Figure S23: ^{1}H-NMR spectrum (DMSO-d$_6$, 600 MHz, 296 K) of *tert*-butyldiphenyl(2-((4*R*,5*R*,6*S*)-2,2,5,6-tetramethyl-1,3-dioxan-4-yl)ethoxy)silane (**18**).

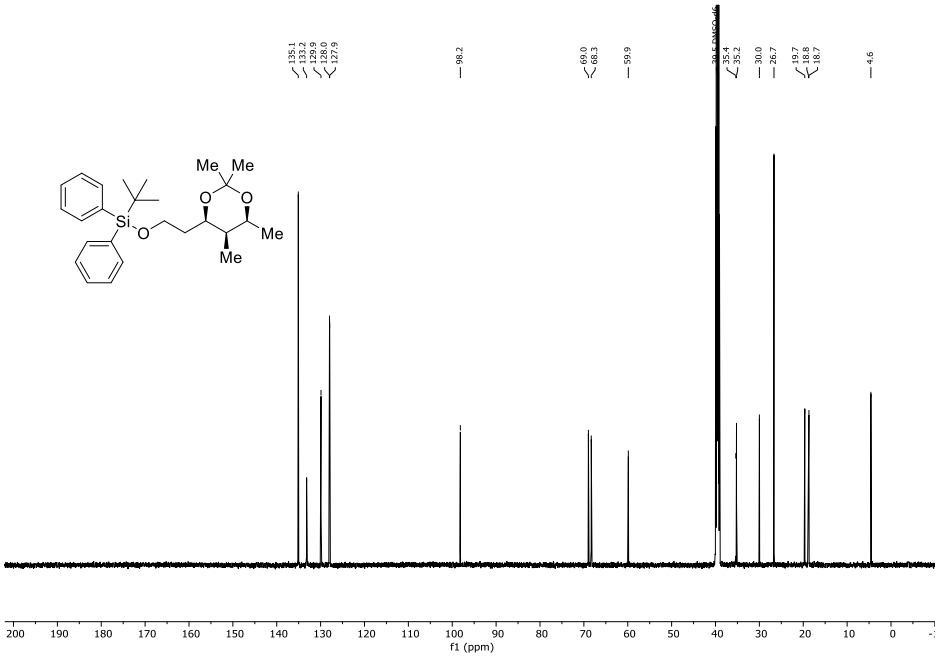

Figure S24: ^{13}C{^{1}H}-NMR spectrum (DMSO-d$_6$, 151 MHz, 296 K) of *tert*-butyldiphenyl(2-((4*R*,5*R*,6*S*)-2,2,5,6-tetramethyl-1,3-dioxan-4-yl)ethoxy)silane (**18**).

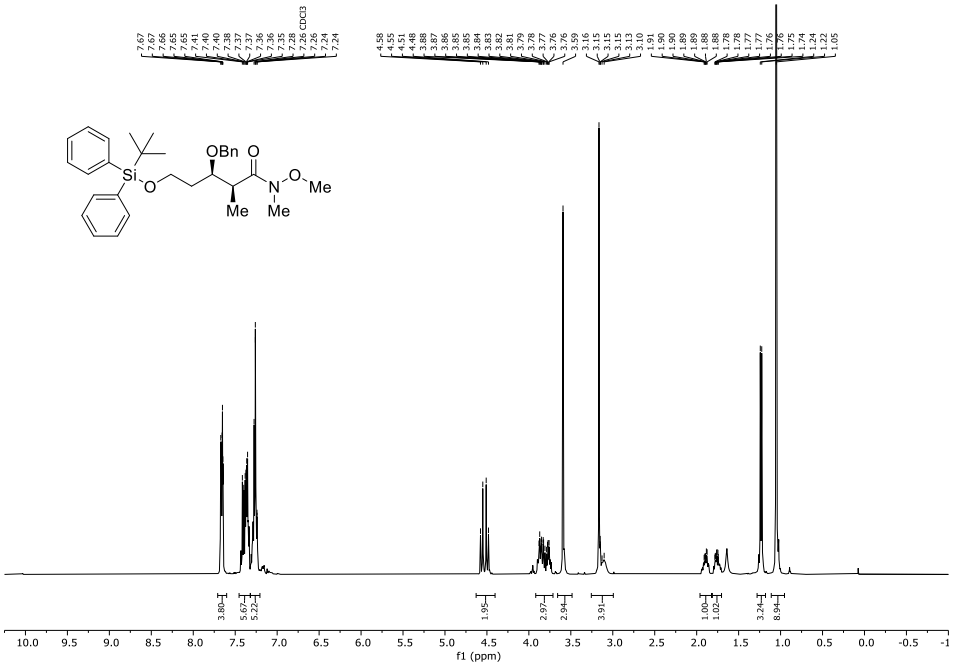

Figure S25: ^{1}H-NMR spectrum ($CDCl_3$, 400 MHz, 296 K) of (2*S*,3*R*)-3-(benzyloxy)-5-((*tert*-butyldiphenylsilyl)oxy)-*N*-methoxy-*N*,2-dimethylpentanamide (**40**).

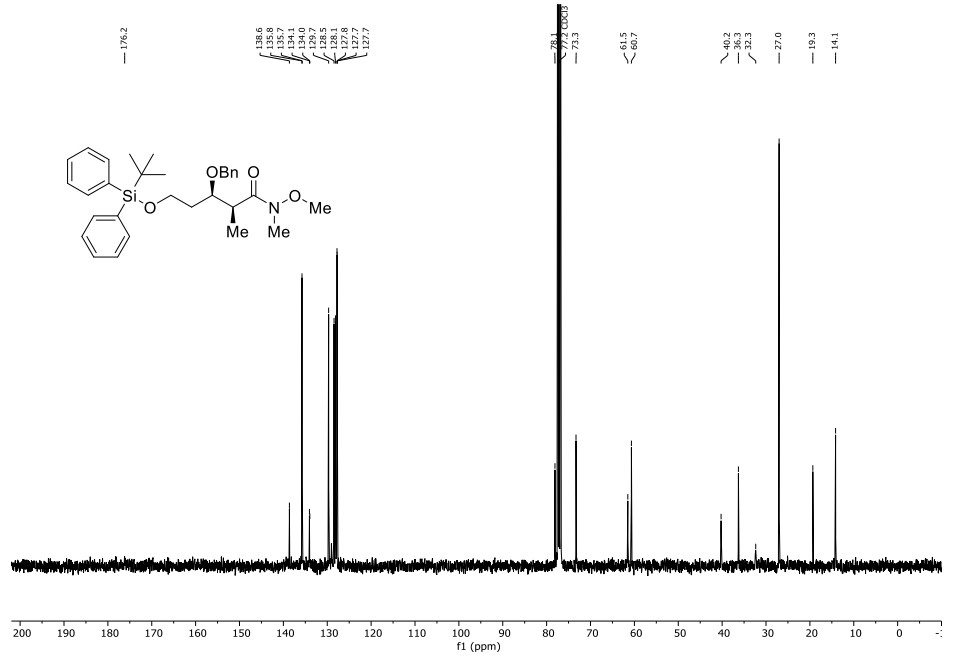

Figure S26: $^{13}C\{^{1}H\}$-NMR spectrum ($CDCl_3$, 101 MHz, 296 K) of (2*S*,3*R*)-3-(benzyloxy)-5-((*tert*-butyldiphenylsilyl)oxy)-*N*-methoxy-*N*,2-dimethylpentanamide (**40**).

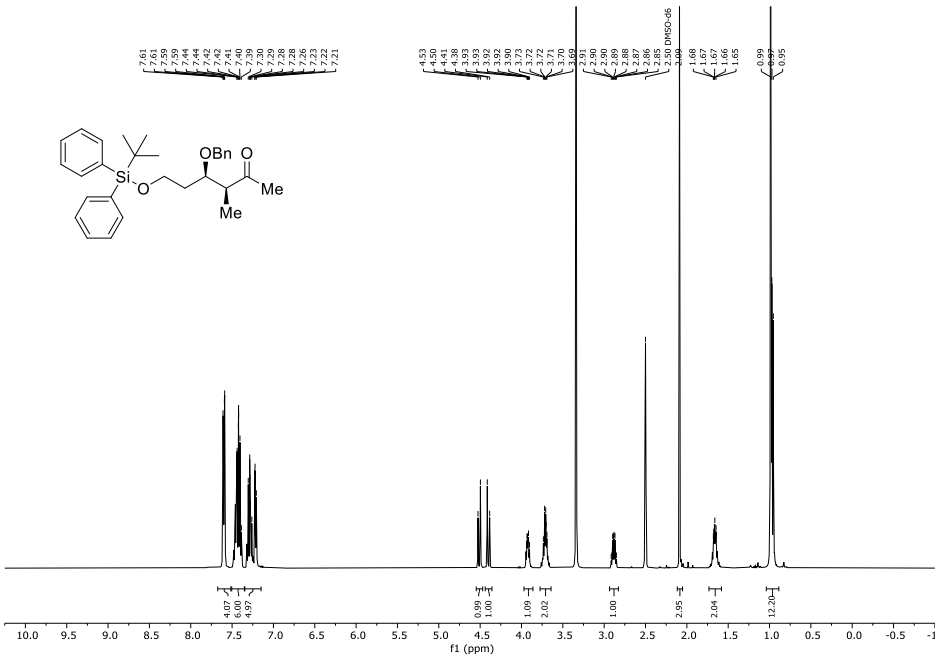

Figure S27: ^{1}H-NMR spectrum (DMSO-d$_6$, 400 MHz, 296 K) of (3*S*,4*R*)-4-(benzyloxy)-6-((*tert*-butyldiphenylsilyl)oxy)-3-methylhexan-2-one (**15**).

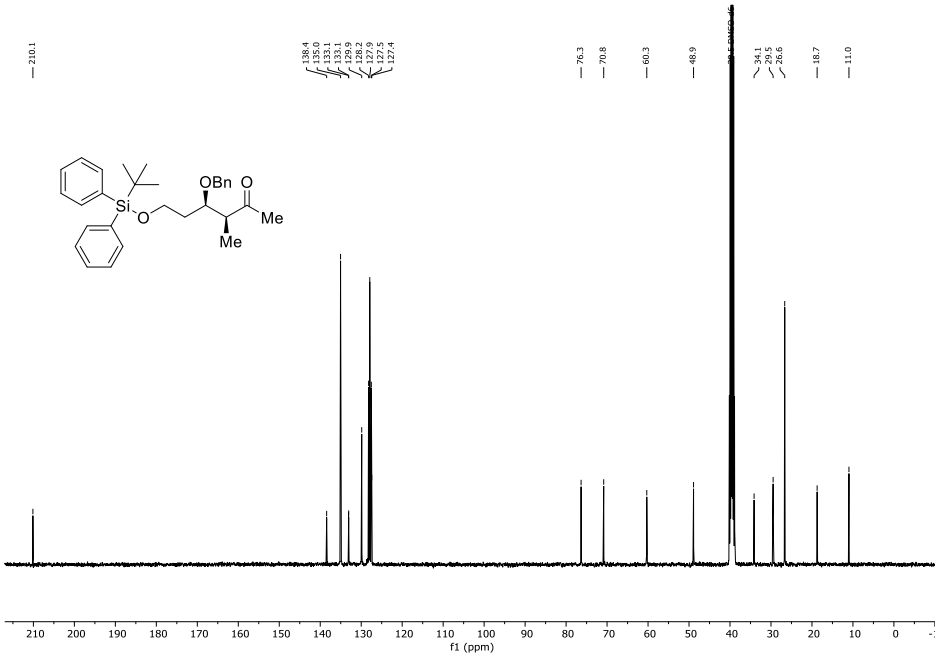

Figure S28: ^{13}C{^{1}H}-NMR spectrum (DMSO-d$_6$, 101 MHz, 296 K) of (3*S*,4*R*)-4-(benzyloxy)-6-((*tert*-butyldiphenylsilyl)oxy)-3-methylhexan-2-one (**15**).

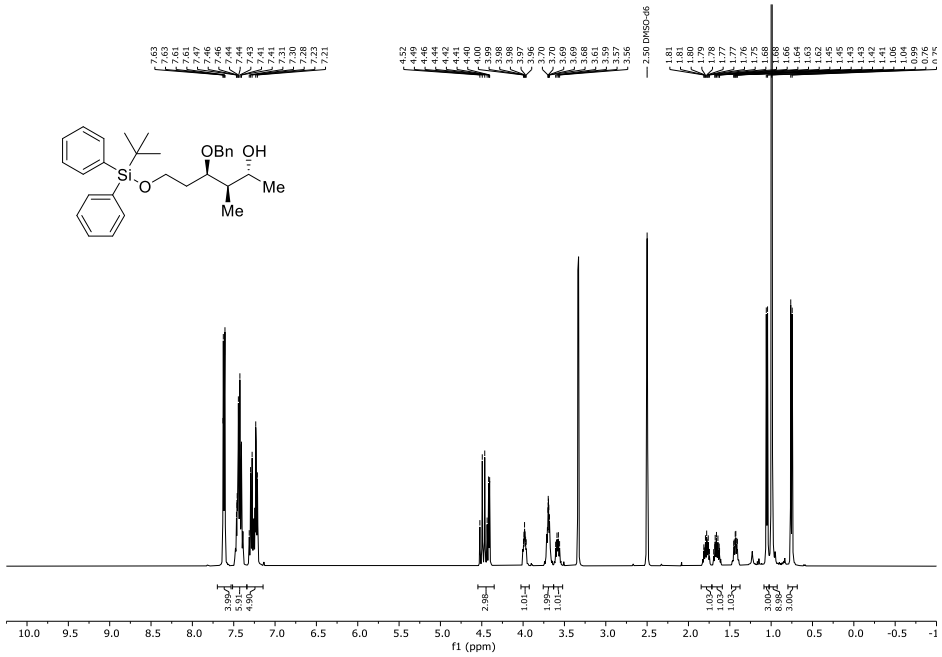

Figure S29: ^{1}H-NMR spectrum (DMSO-d$_6$, 400 MHz, 296 K) of (2*R*,3*R*,4*R*)-4-(benzyloxy)-6-((*tert*-butyldiphenylsilyl)oxy)-3-methylhexan-2-ol (**17**).

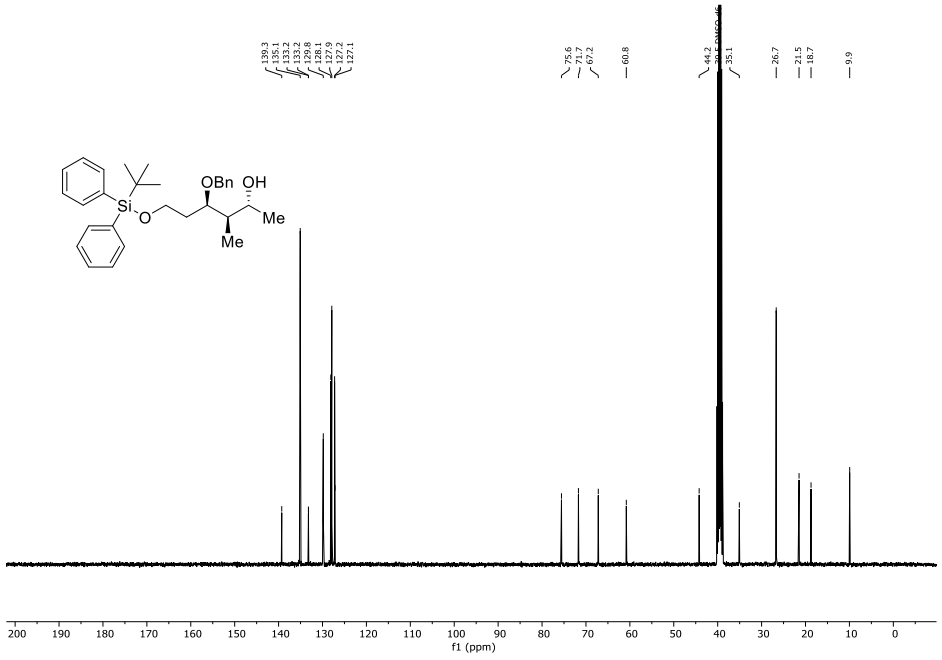

Figure S30: ^{13}C{^{1}H}-NMR spectrum (DMSO-d$_6$, 101 MHz, 296 K) of (2*R*,3*R*,4*R*)-4-(benzyloxy)-6-((*tert*-butyldiphenylsilyl)oxy)-3-methylhexan-2-ol (**17**).

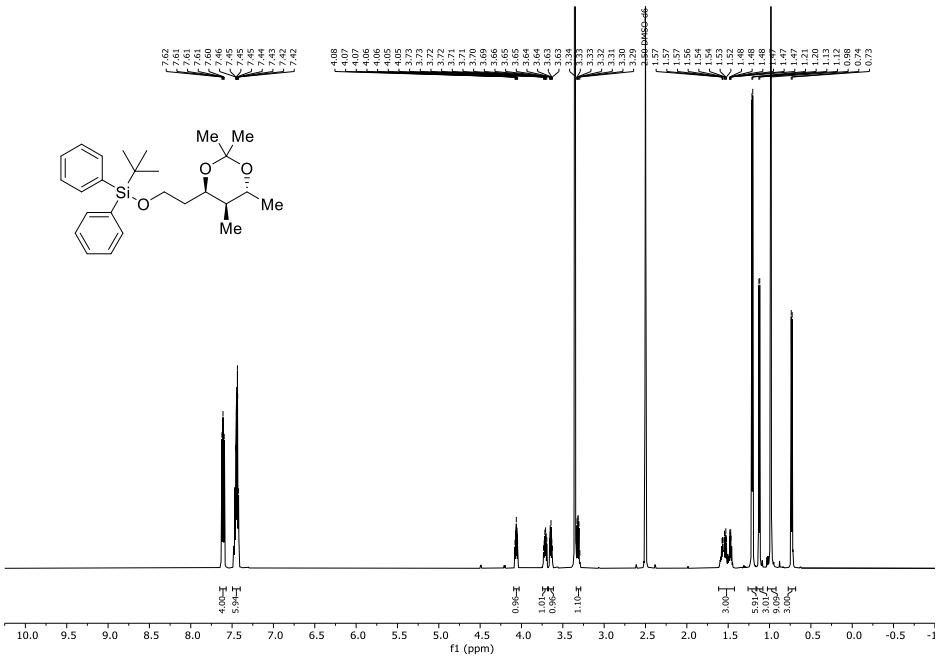

Figure S31: ^{1}H-NMR spectrum (DMSO-d$_6$, 600 MHz, 296 K) of *tert*-butyldiphenyl(2-((4*R*,5*R*,6*R*)-2,2,5,6-tetramethyl-1,3-dioxan-4-yl)ethoxy)silane (**19**).

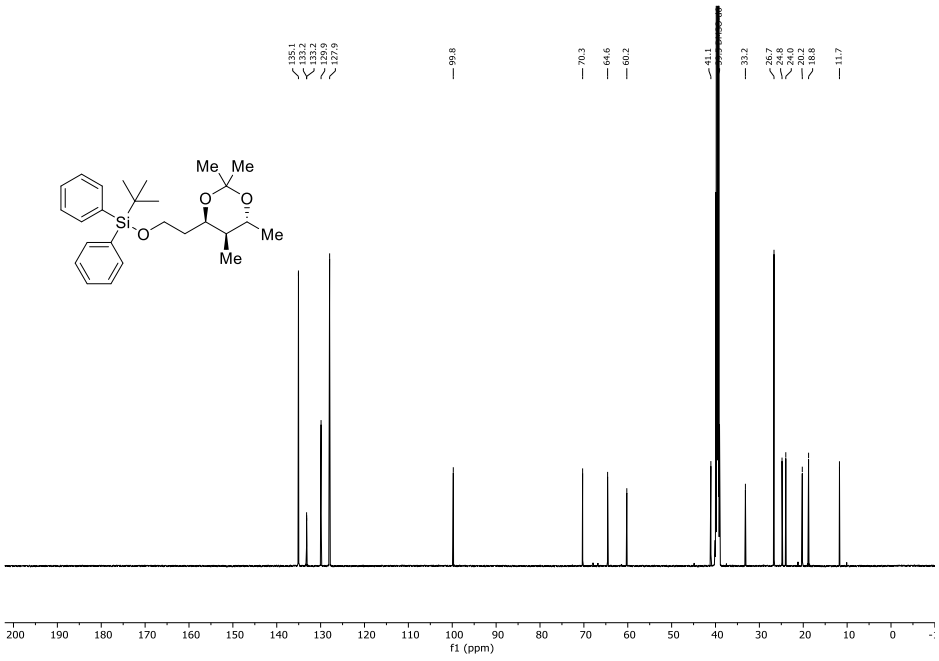

Figure S32: ^{13}C{^{1}H}-NMR spectrum (DMSO-d$_6$, 151 MHz, 296 K) of *tert*-butyldiphenyl(2-((4*R*,5*R*,6*R*)-2,2,5,6-tetramethyl-1,3-dioxan-4-yl)ethoxy)silane (**19**).

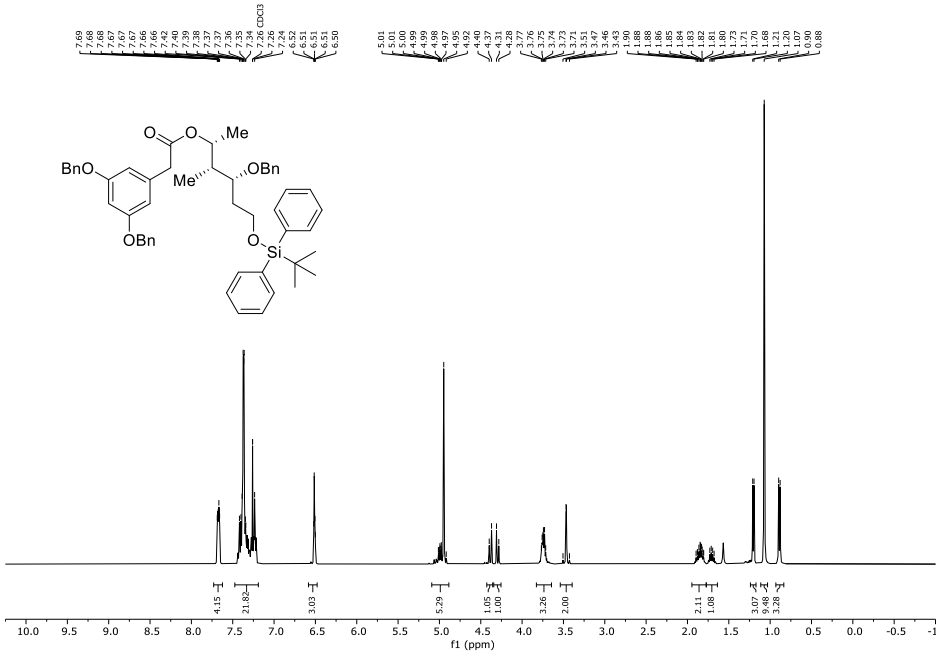

Figure S33: ^{1}H-NMR spectrum ($CDCl_3$, 400 MHz, 296 K) of (2*R*,3*R*,4*R*)-4-(benzyloxy)-6-((*tert*-butyldiphenylsilyl)oxy)-3-methylhexan-2-yl 2-(3,5-bis(benzyloxy)phenyl)acetate (**41**).

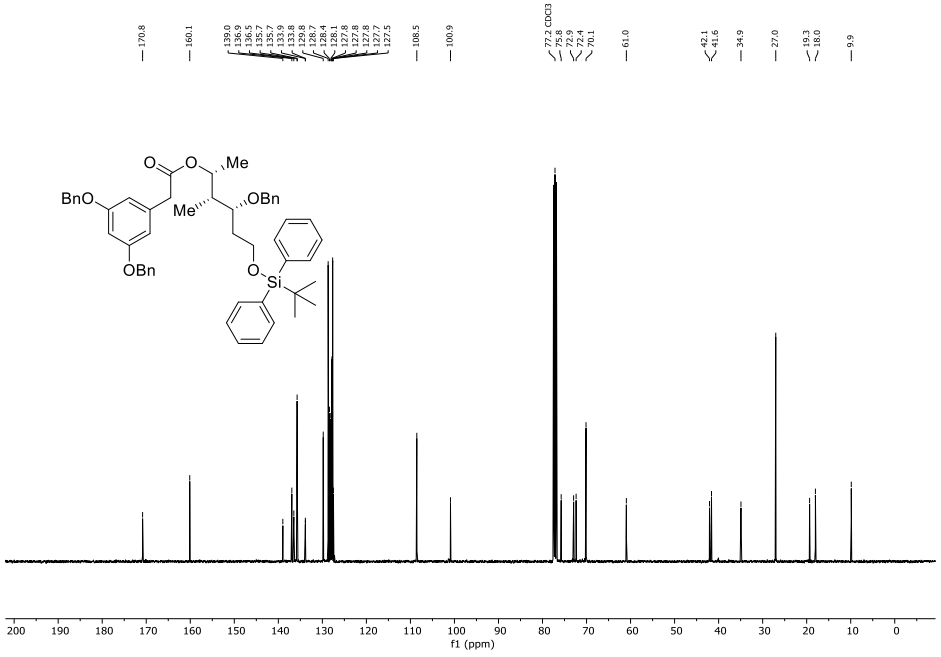

Figure S34: $^{13}C\{^{1}H\}$-NMR spectrum ($CDCl_3$, 101 MHz, 296 K) of (2*R*,3*R*,4*R*)-4-(benzyloxy)-6-((*tert*-butyldiphenylsilyl)oxy)-3-methylhexan-2-yl 2-(3,5-bis(benzyloxy)phenyl)acetate (**41**).

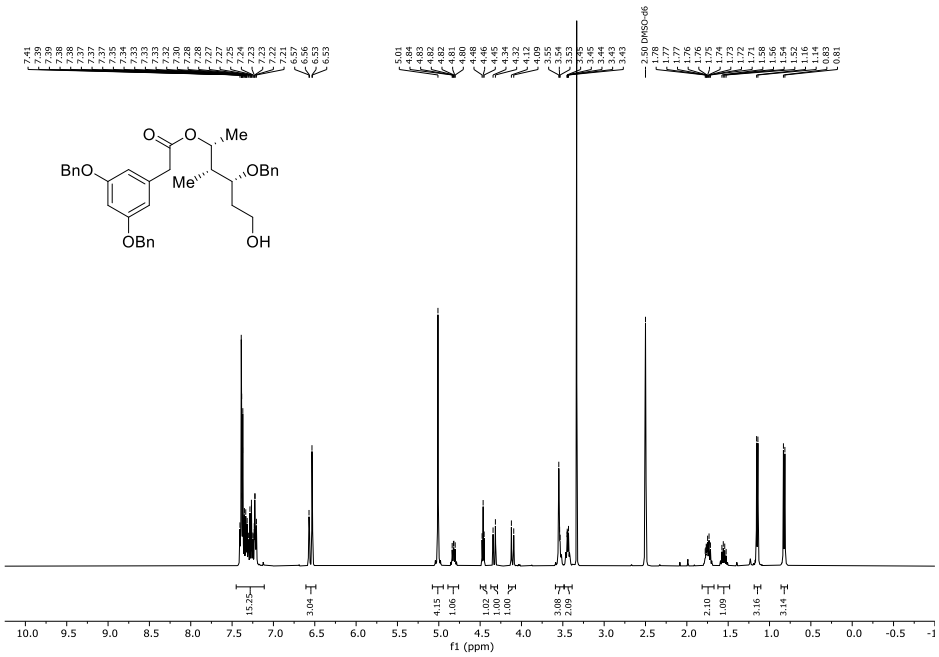

Figure S35: ^{1}H-NMR spectrum (DMSO-d$_6$, 400 MHz, 296 K) of (2*R*,3*R*,4*R*)-4-(benzyloxy)-6-hydroxy-3-methylhexan-2-yl 2-(3,5-bis(benzyloxy)phenyl)acetate (**42**).

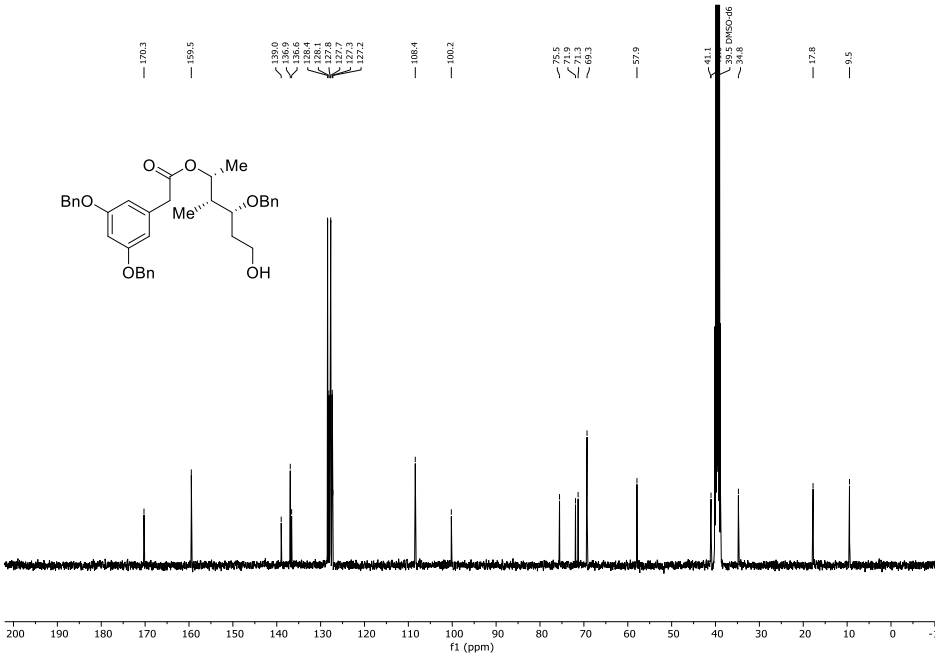

Figure S36: ^{13}C{^{1}H}-NMR spectrum (DMSO-d$_6$, 101 MHz, 296 K) of (2*R*,3*R*,4*R*)-4-(benzyloxy)-6-hydroxy-3-methylhexan-2-yl 2-(3,5-bis(benzyloxy)phenyl)acetate (**42**).

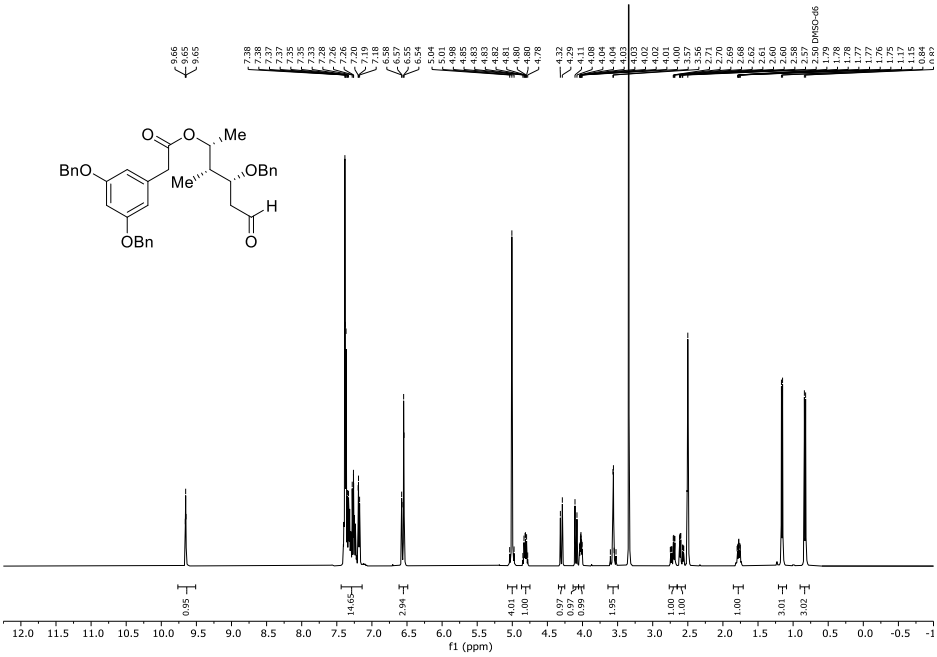

Figure S37: ^{1}H-NMR spectrum (DMSO-d_6, 400 MHz, 296 K) of (2*R*,3*R*,4*R*)-4-(benzyloxy)-3-methyl-6-oxohexan-2-yl 2-(3,5-bis(benzyloxy)phenyl)acetate (**20**).

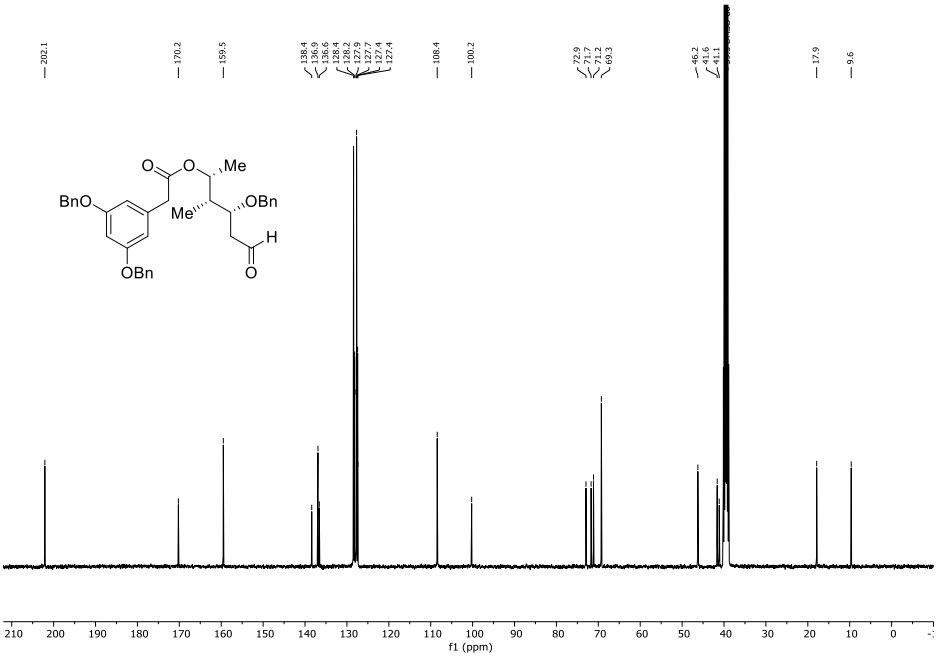

Figure S38: ^{13}C{^{1}H}-NMR spectrum (DMSO-d_6, 101 MHz, 296 K) of (2*R*,3*R*,4*R*)-4-(benzyloxy)-3-methyl-6-oxohexan-2-yl 2-(3,5-bis(benzyloxy)phenyl)acetate (**20**).

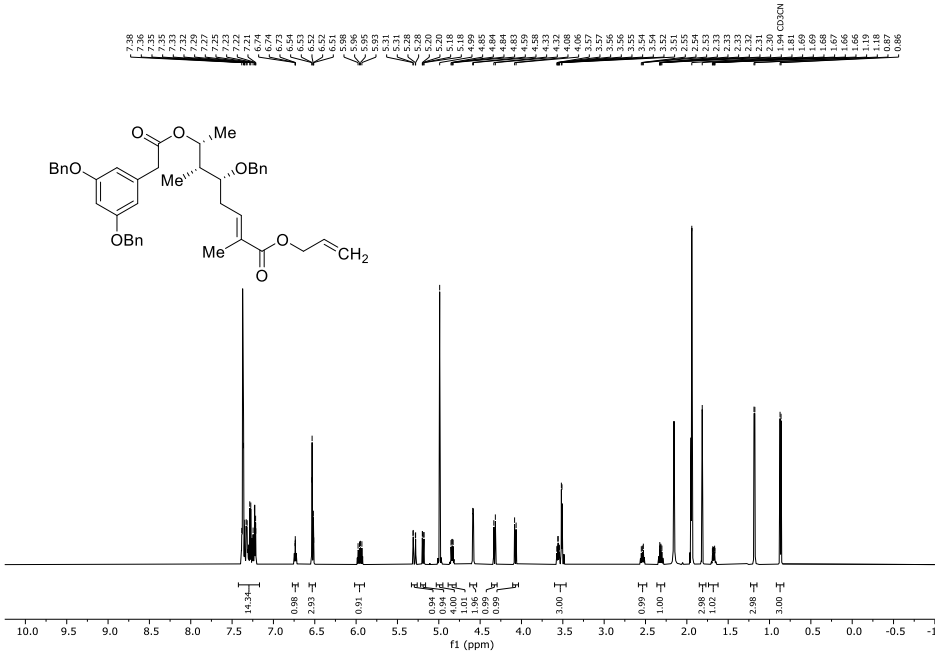

Figure S39: ^{1}H-NMR spectrum (MeCN-d_3, 600 MHz, 296 K) of allyl (5*R*,6*R*,7*R*,*E*)-5-(benzyloxy)-7-(2-(3,5-bis(benzyloxy)phenyl)acetoxy)-2,6-dimethyloct-2-enoate (**24**).

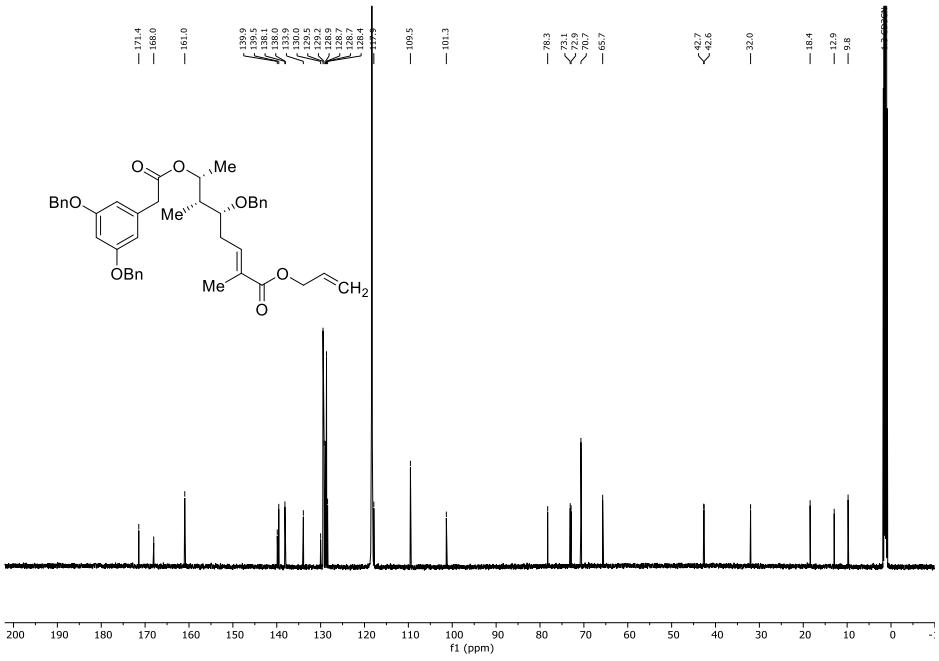

Figure S40: ^{13}C{^{1}H}-NMR spectrum (MeCN-d_3, 151 MHz, 296 K) of allyl (5*R*,6*R*,7*R*,*E*)-5-(benzyloxy)-7-(2-(3,5-bis(benzyloxy)phenyl)acetoxy)-2,6-dimethyloct-2-enoate (**24**).

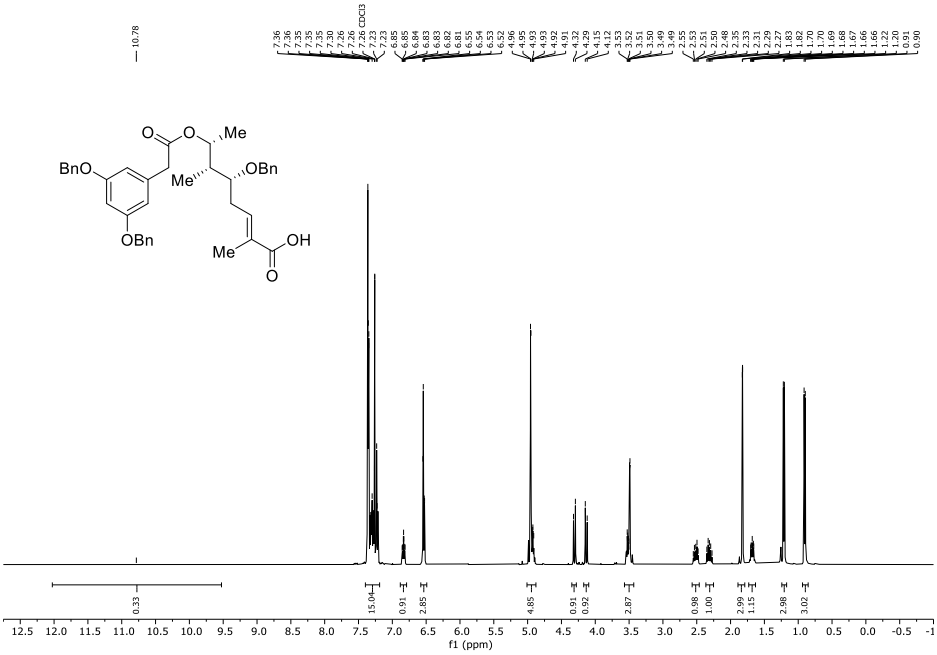

Figure S41: ^{1}H-NMR spectrum ($CDCl_3$, 400 MHz, 296 K) of (5*R*,6*R*,7*R*,*E*)-5-(benzyloxy)-7-(2-(3,5-bis(benzyloxy)phenyl)acetoxy)-2,6-dimethyloct-2-enoic acid (**25**).

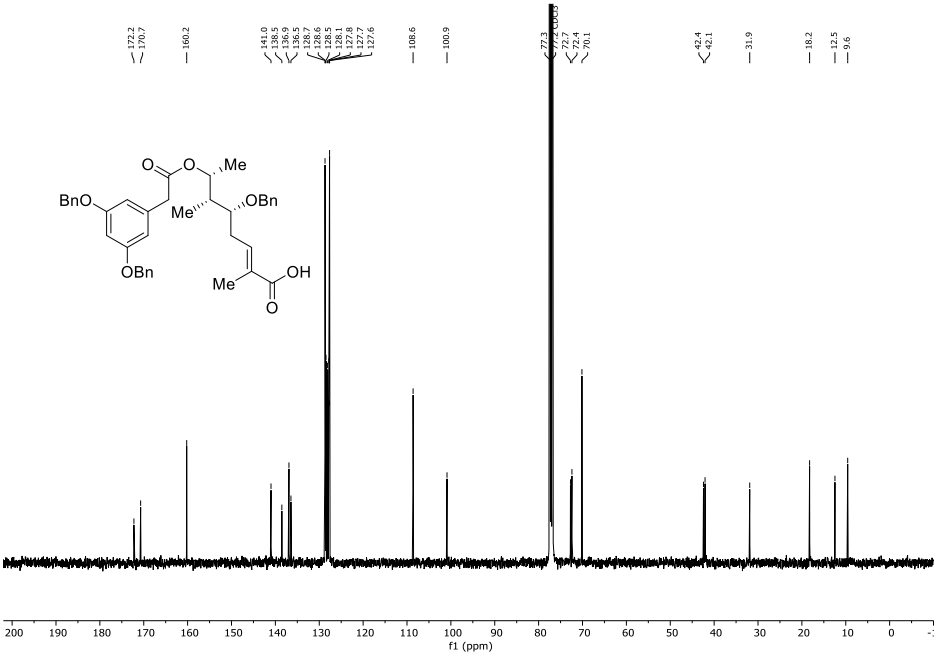

Figure S42: $^{13}C\{^{1}H\}$-NMR spectrum ($CDCl_3$, 101 MHz, 296 K) of (5*R*,6*R*,7*R*,*E*)-5-(benzyloxy)-7-(2-(3,5-bis(benzyloxy)phenyl)acetoxy)-2,6-dimethyloct-2-enoic acid (**25**).

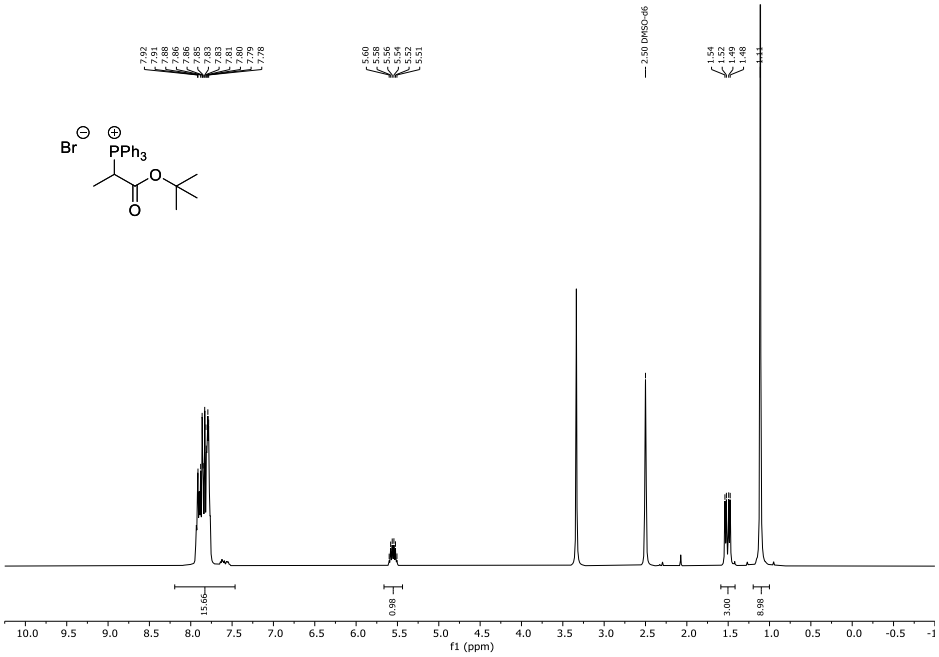

Figure S43: ^{1}H-NMR spectrum (DMSO-d_6, 400 MHz, 296 K) of (1-(*tert*-butoxy)-1-oxopropan-2-yl)triphenylphosphonium bromide (**43**).

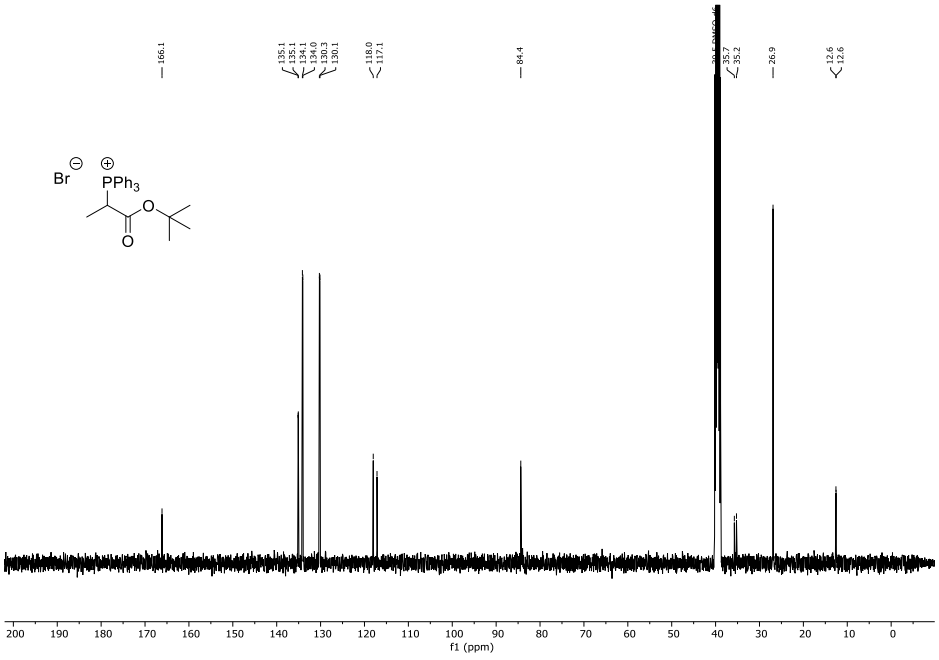

Figure S44: ^{13}C{^{1}H}-NMR spectrum (DMSO-d_6, 101 MHz, 296 K) of (1-(*tert*-butoxy)-1-oxopropan-2-yl)triphenylphosphonium bromide (**43**).

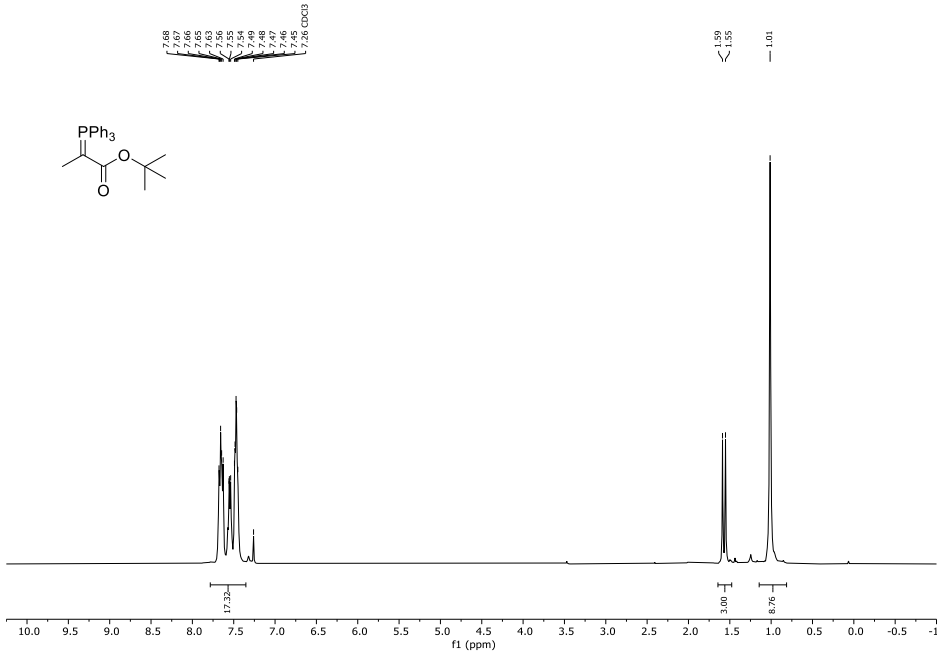

Figure S45: ^{1}H-NMR spectrum ($CDCl_3$, 400 MHz, 296 K) of *tert*-butyl 2-(triphenylphosphoranylidene)propanoate (**23**).

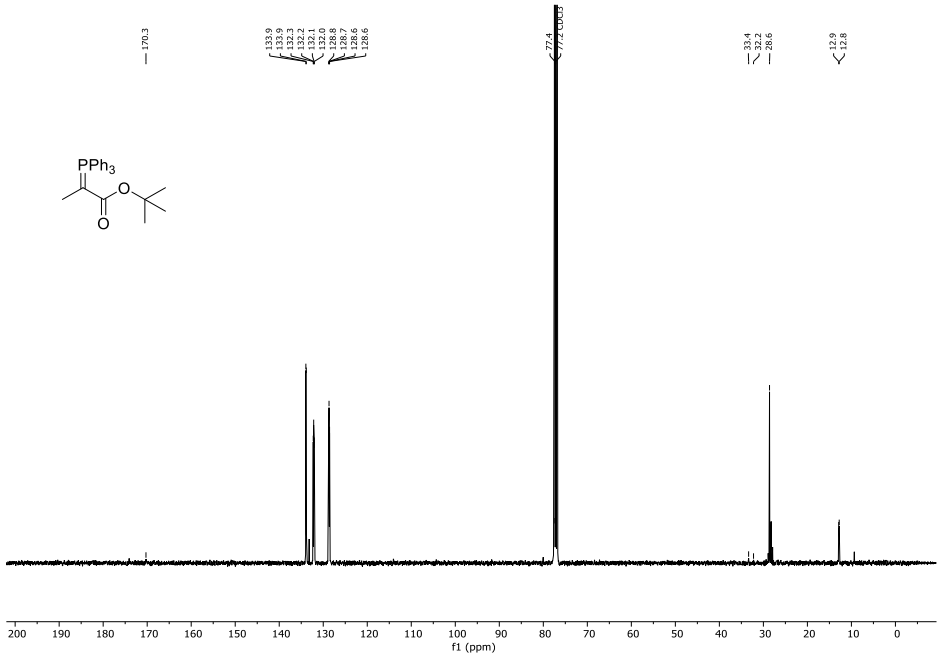

Figure S46: $^{13}C\{^{1}H\}$-NMR spectrum ($CDCl_3$, 101 MHz, 296 K) of *tert*-butyl 2-(triphenylphosphoranylidene)propanoate (**23**).

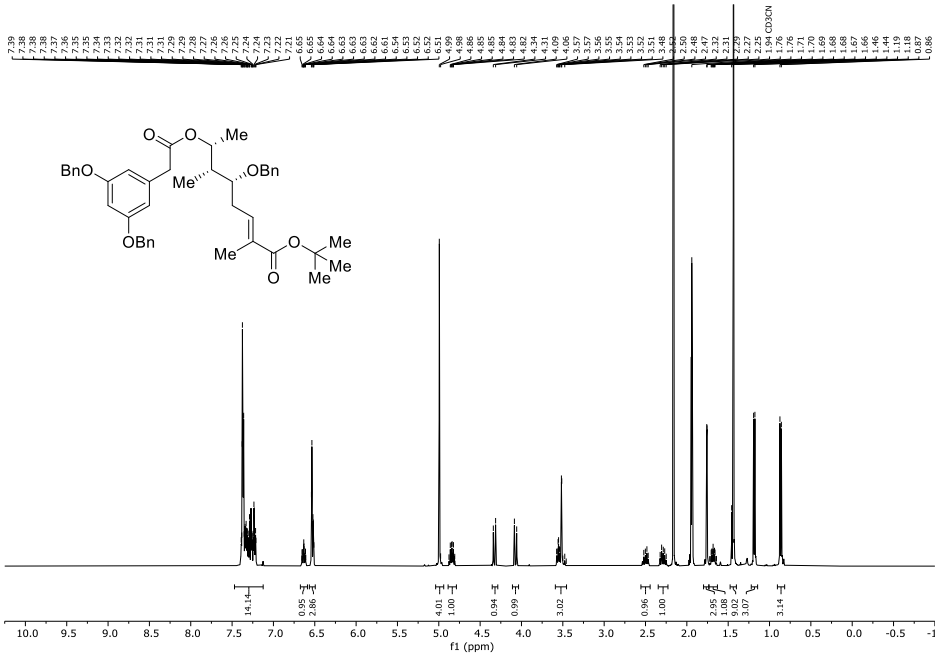

Figure S47: ^{1}H-NMR spectrum (MeCN-d_3, 400 MHz, 296 K) of *tert*-butyl (5*R*,6*R*,7*R*,*E*)-5-(benzyloxy)-7-(2-(3,5-bis(benzyloxy)phenyl)acetoxy)-2,6-dimethyloct-2-enoate (**26**).

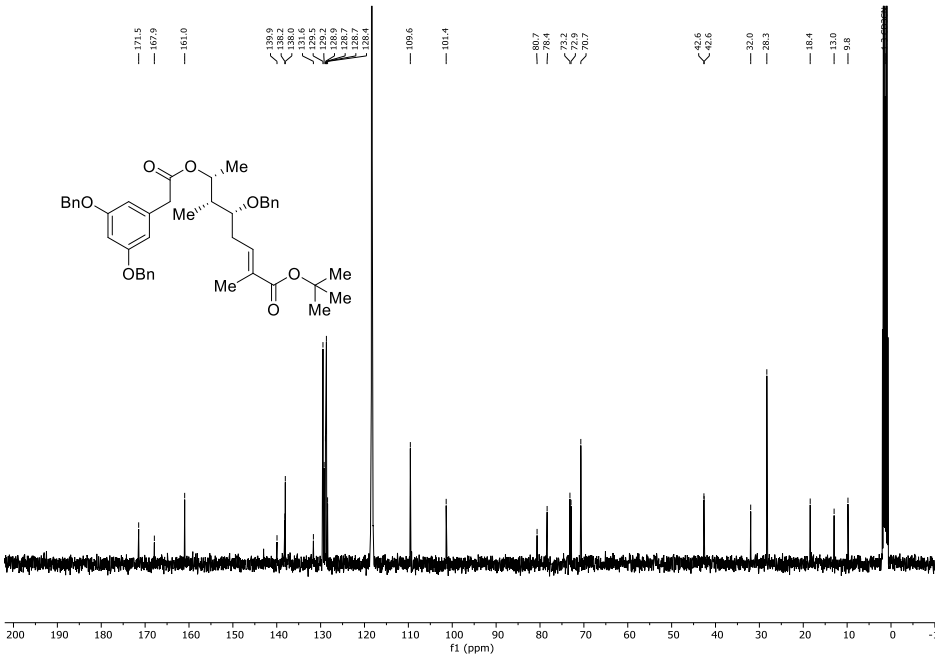

Figure S48: ^{13}C{^{1}H}-NMR spectrum (MeCN-d_3, 101 MHz, 296 K) of *tert*-butyl (5*R*,6*R*,7*R*,*E*)-5-(benzyloxy)-7-(2-(3,5-bis(benzyloxy)phenyl)acetoxy)-2,6-dimethyloct-2-enoate (**26**).

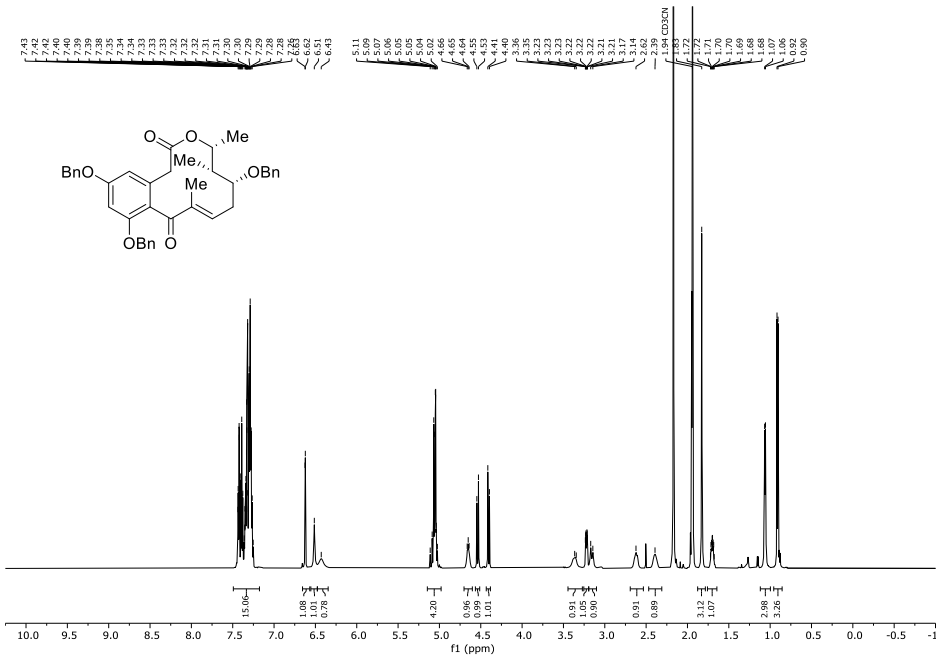

Figure S49: ^{1}H-NMR spectrum (MeCN-d$_3$, 600 MHz, 296 K) of (13*R*,14*R*,15*R*)-5,7,13-tris(benzyloxy)-4-dechloro-14-deoxyoxacyclododecindione (**28**).

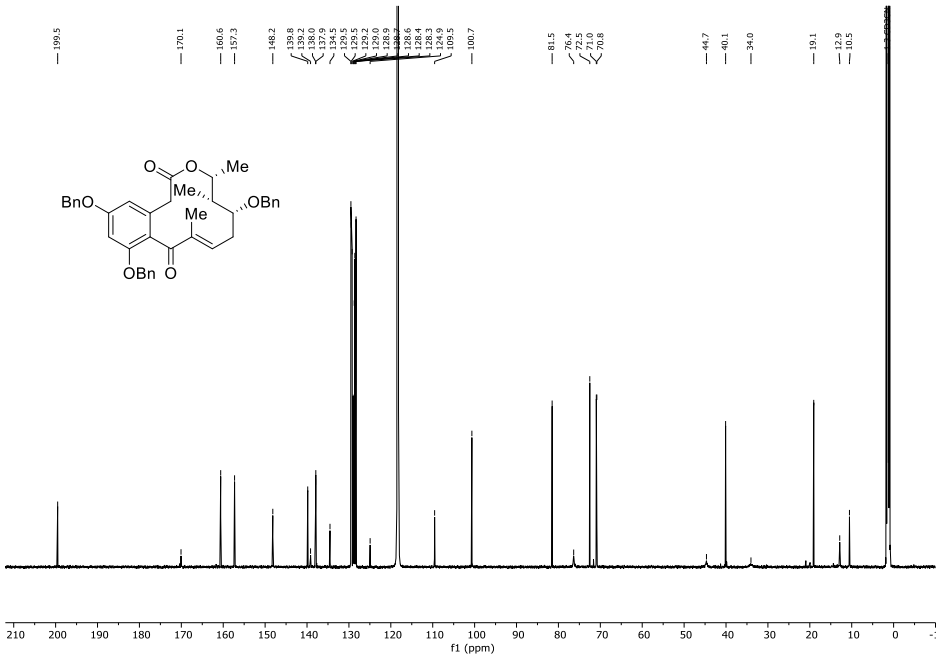

Figure S50: ^{13}C{^{1}H}-NMR spectrum (MeCN-d$_3$, 151 MHz, 296 K) of (13*R*,14*R*,15*R*)-5,7,13-tris(benzyloxy)-4-dechloro-14-deoxyoxacyclododecindione (**28**).

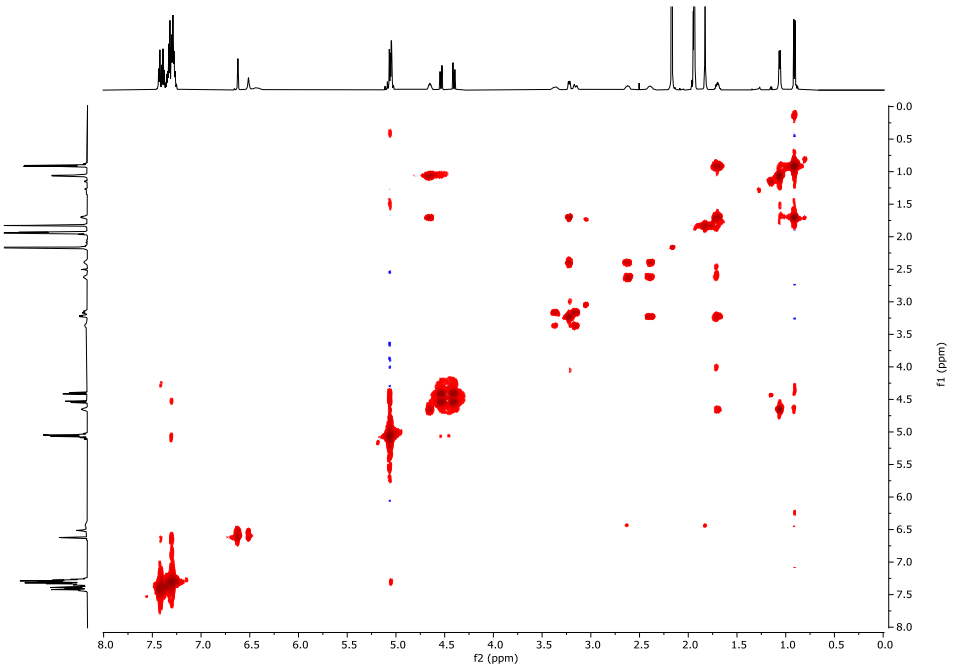

Figure S51: ^{1}H-^{1}H-COSY (MeCN-d_3, 600 MHz, 296 K) of (13*R*,14*R*,15*R*)-5,7,13-tris(benzyloxy)-4-dechloro-14-deoxyoxacyclododecindione (**28**).

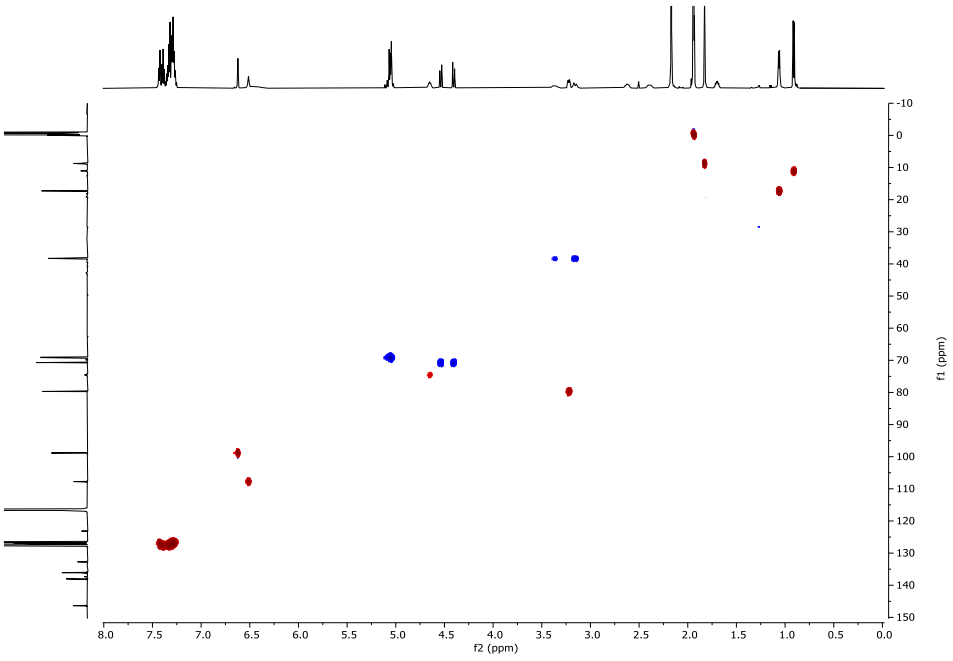

Figure S52: ^{1}H-^{13}C{^{1}H}-HSQC (MeCN-d_3, 600 MHz, 296 K) of (13*R*,14*R*,15*R*)-5,7,13-tris(benzyloxy)-4-dechloro-14-deoxyoxacyclododecindione (**28**).

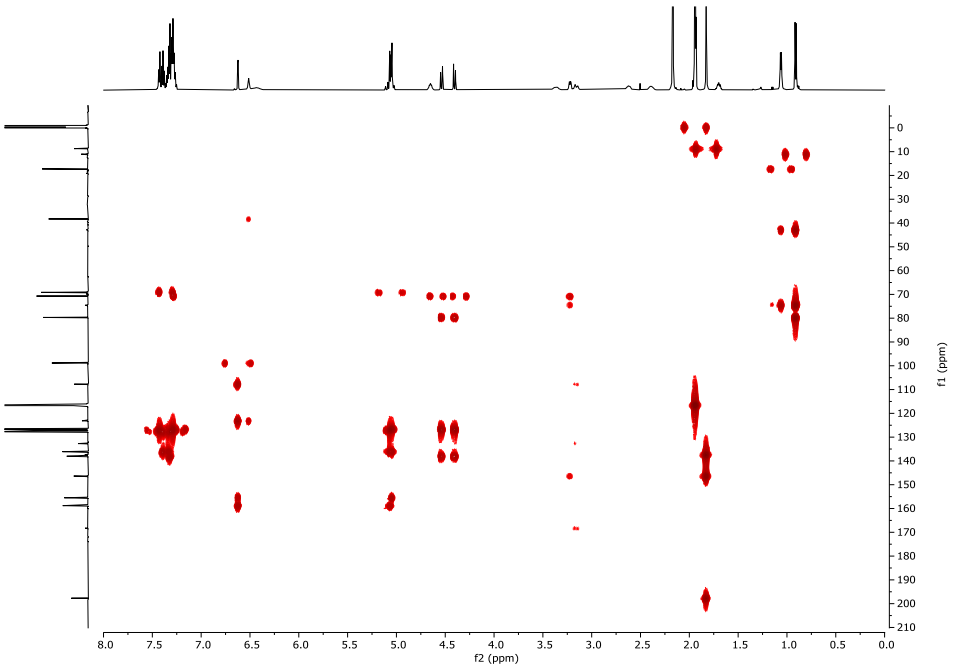

Figure S53: ^{1}H-^{13}C{^{1}H}-HMBC (MeCN-d$_3$, 600 MHz, 296 K) of (13*R*,14*R*,15*R*)-5,7,13-tris(benzyloxy)-4-dechloro-14-deoxyoxacyclododecindione (**28**).

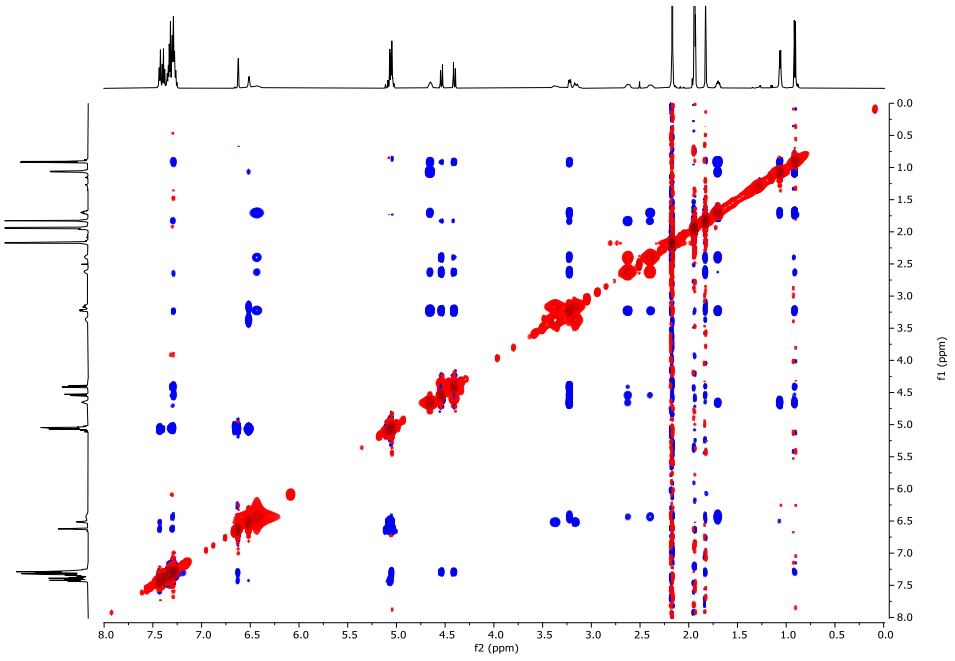

Figure S54: ^{1}H-^{1}H-NOESY (MeCN-d$_3$, 600 MHz, 296 K) of (13*R*,14*R*,15*R*)-5,7,13-tris(benzyloxy)-4-dechloro-14-deoxyoxacyclododecindione (**28**).

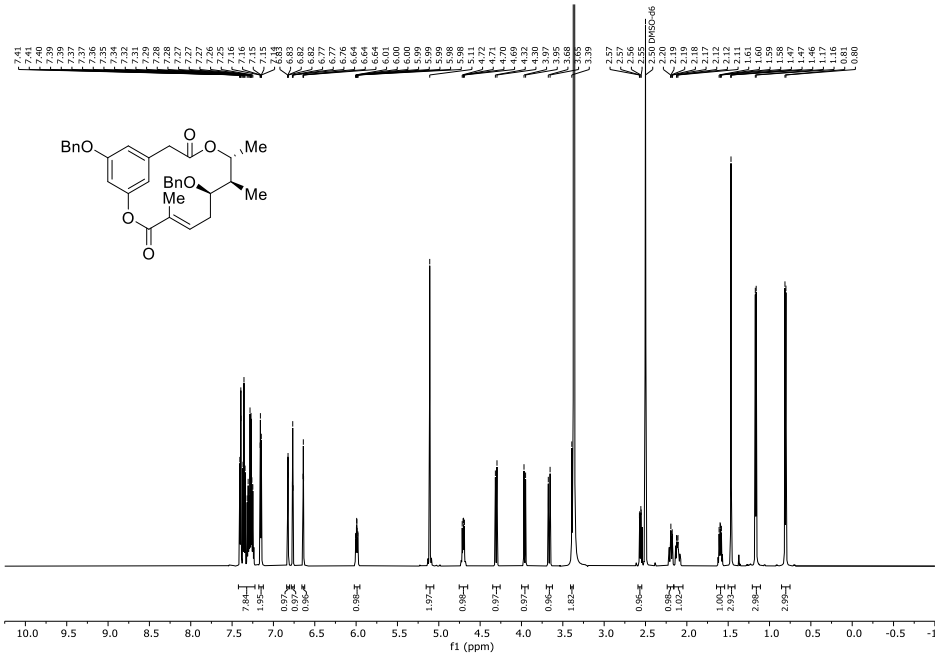

Figure S55: ^{1}H-NMR spectrum (DMSO-d$_6$, 600 MHz, 296 K) of (7*R*,8*R*,9*R*,*E*)-1^{5},7-bis(benzyloxy)-4,8,9-trimethyl-2,10-dioxa-1(1,3)-benzenacyclododecaphan-4-en-3,11-dione (**27**).

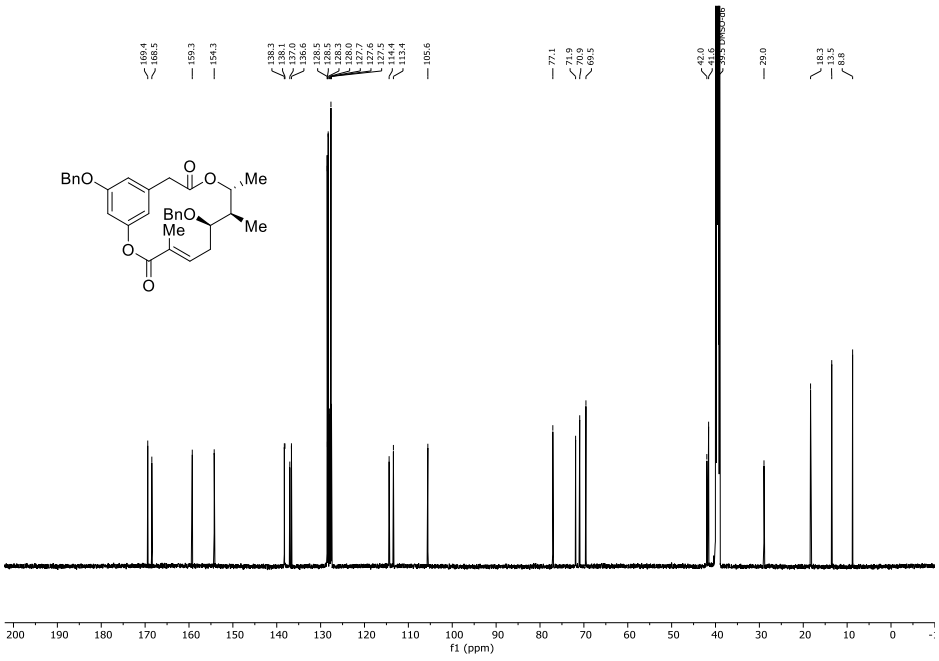

Figure S56: ^{13}C{^{1}H}-NMR spectrum (DMSO-d$_6$, 151 MHz, 296 K) of (7*R*,8*R*,9*R*,*E*)-1^{5},7-bis(benzyloxy)-4,8,9-trimethyl-2,10-dioxa-1(1,3)-benzenacyclododecaphan-4-en-3,11-dione (**27**).

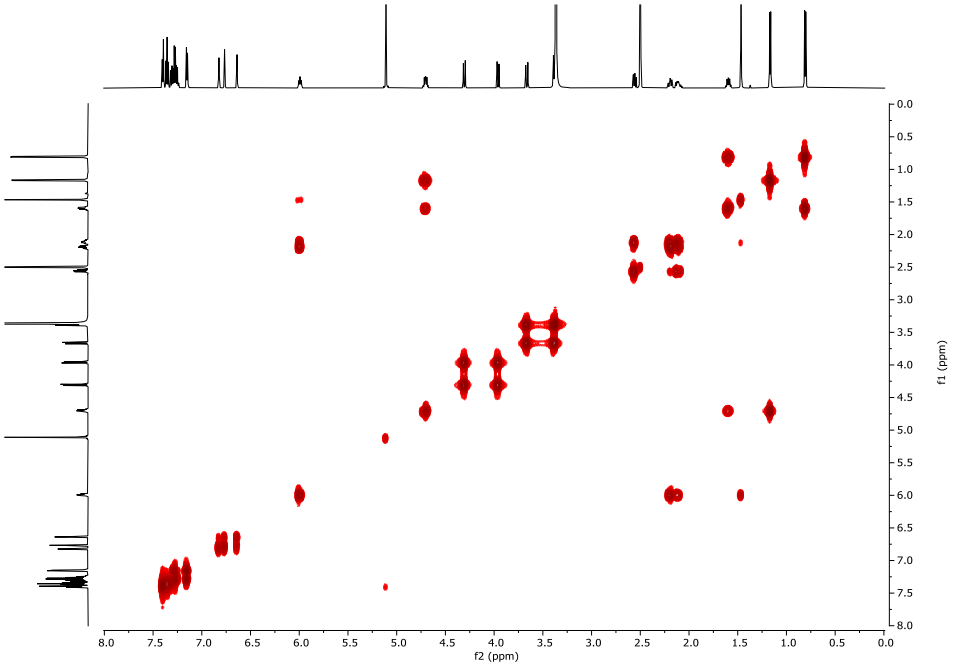

Figure S57: ^{1}H-^{1}H-COSY (DMSO-d$_6$, 600 MHz, 296 K) of (7*R*,8*R*,9*R*,*E*)-1^{5},7-bis(benzyloxy)-4,8,9-trimethyl-2,10-dioxa-1(1,3)-benzenacyclododecaphan-4-en-3,11-dione (**27**).

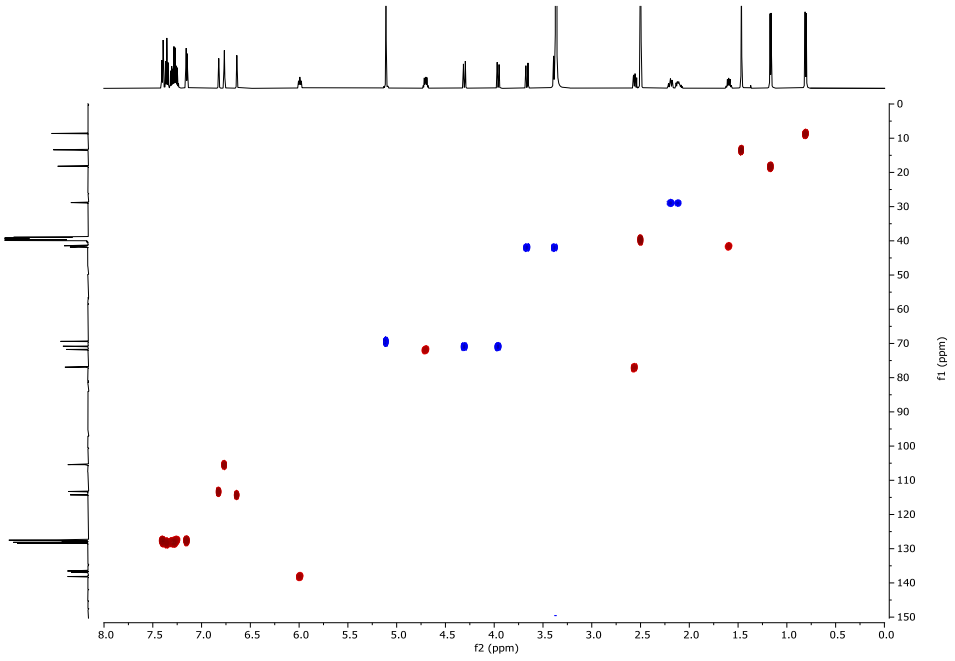

Figure S58: ^{1}H-^{13}C{^{1}H}-HSQC (DMSO-d$_6$, 600 MHz, 296 K) of (7*R*,8*R*,9*R*,*E*)-1^{5},7-bis(benzyloxy)-4,8,9-trimethyl-2,10-dioxa-1(1,3)-benzenacyclododecaphan-4-en-3,11-dione (**27**).

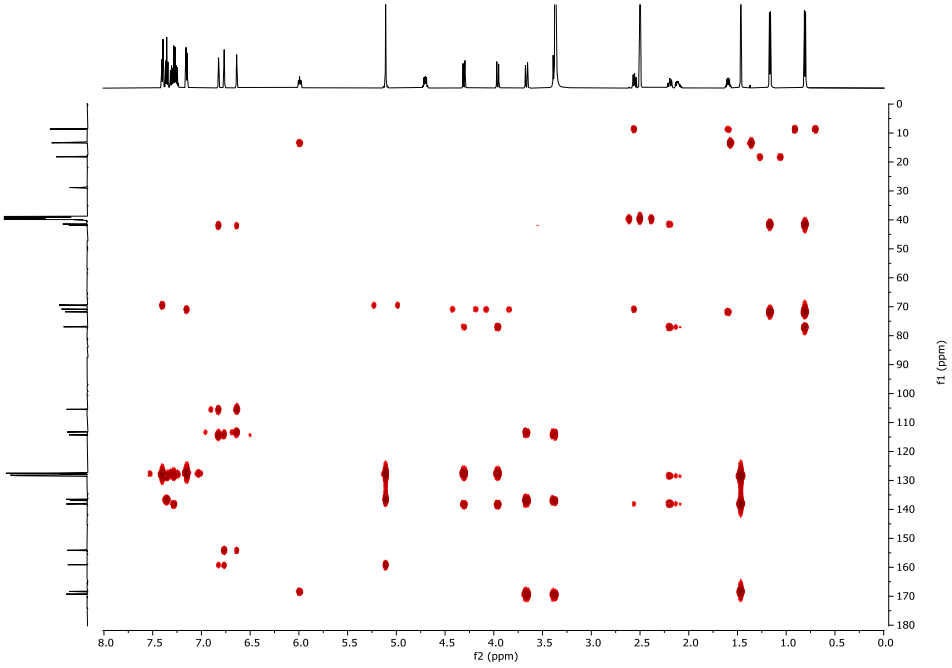

Figure S59: ^{1}H-^{13}C{^{1}H}-HMBC (DMSO-d$_6$, 600 MHz, 296 K) of (7*R*,8*R*,9*R*,*E*)-1^{5},7-bis(benzyloxy)-4,8,9-trimethyl-2,10-dioxa-1(1,3)-benzenacyclododecaphan-4-en-3,11-dione (**27**).

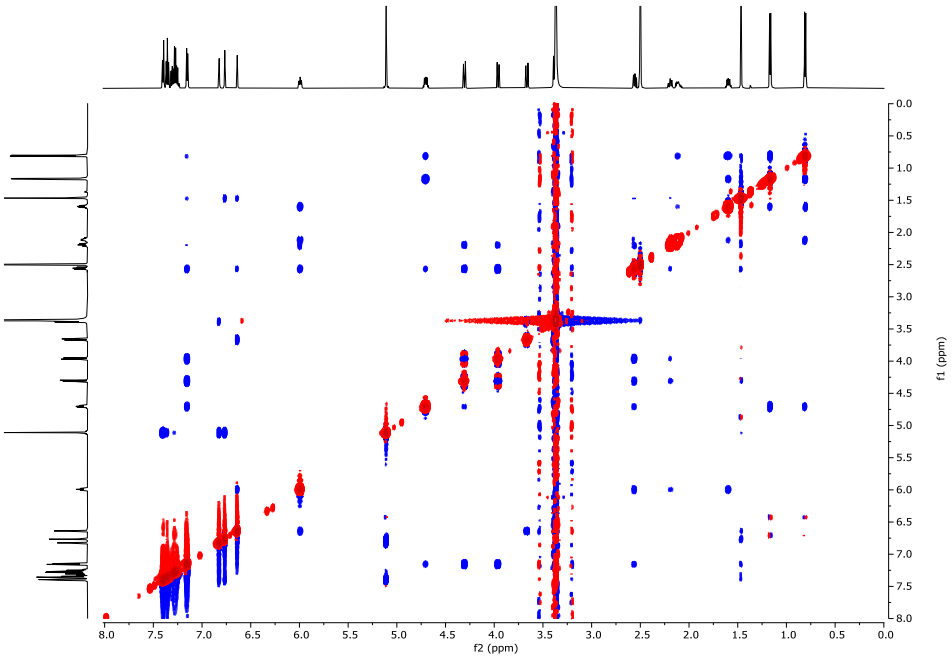

Figure S60: ^{1}H-^{1}H-NOESY (DMSO-d$_6$, 600 MHz, 296 K) of (7*R*,8*R*,9*R*,*E*)-1^{5},7-bis(benzyloxy)-4,8,9-trimethyl-2,10-dioxa-1(1,3)-benzenacyclododecaphan-4-en-3,11-dione (**27**).

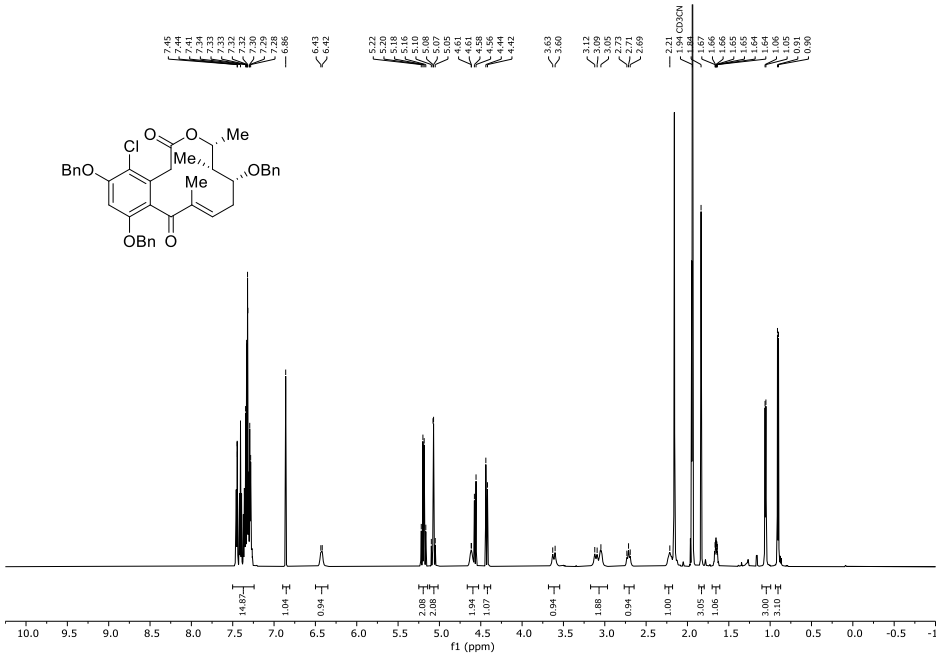

Figure S61: ^{1}H-NMR spectrum (MeCN-d$_3$, 600 MHz, 296 K) of (13*R*,14*R*,15*R*)-5,7,13-tris(benzyloxy)-14-deoxyoxacyclododecindione (**29**).

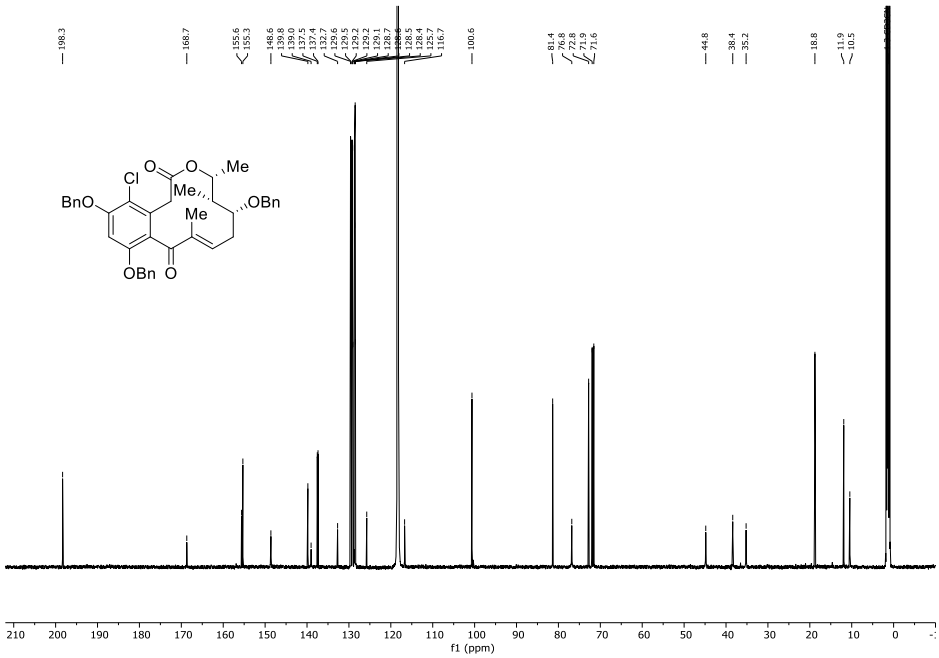

Figure S62: ^{13}C{^{1}H}-NMR spectrum (MeCN-d$_3$, 151 MHz, 296 K) of (13*R*,14*R*,15*R*)-5,7,13-tris(benzyloxy)-14-deoxyoxacyclododecindione (**29**).

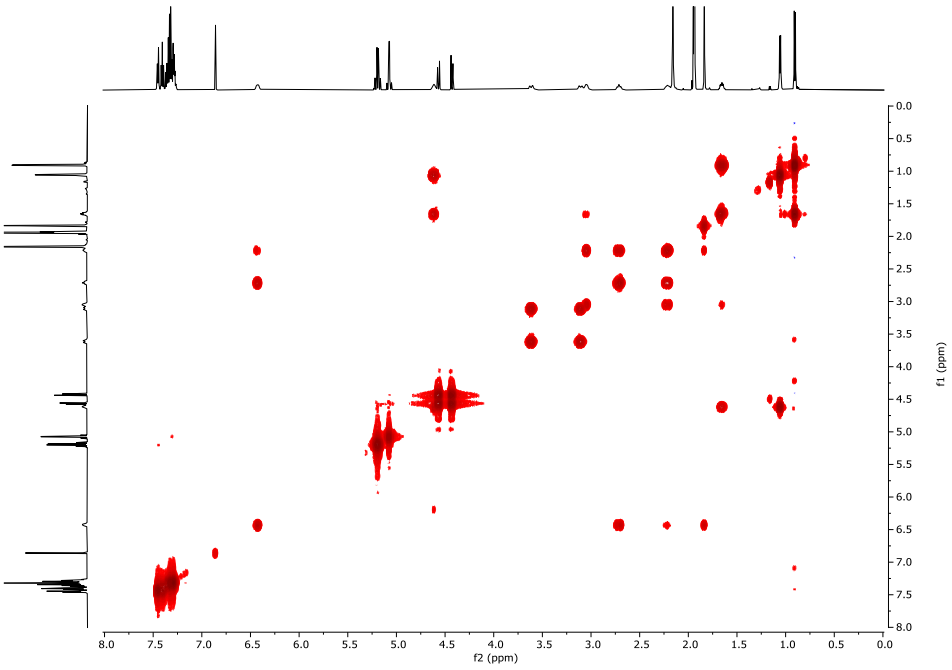

Figure S63: ^{1}H-^{1}H-COSY (MeCN-d$_3$, 600 MHz, 296 K) of (13*R*,14*R*,15*R*)-5,7,13-tris(benzyloxy)-14-deoxyoxacyclododecindione (**29**).

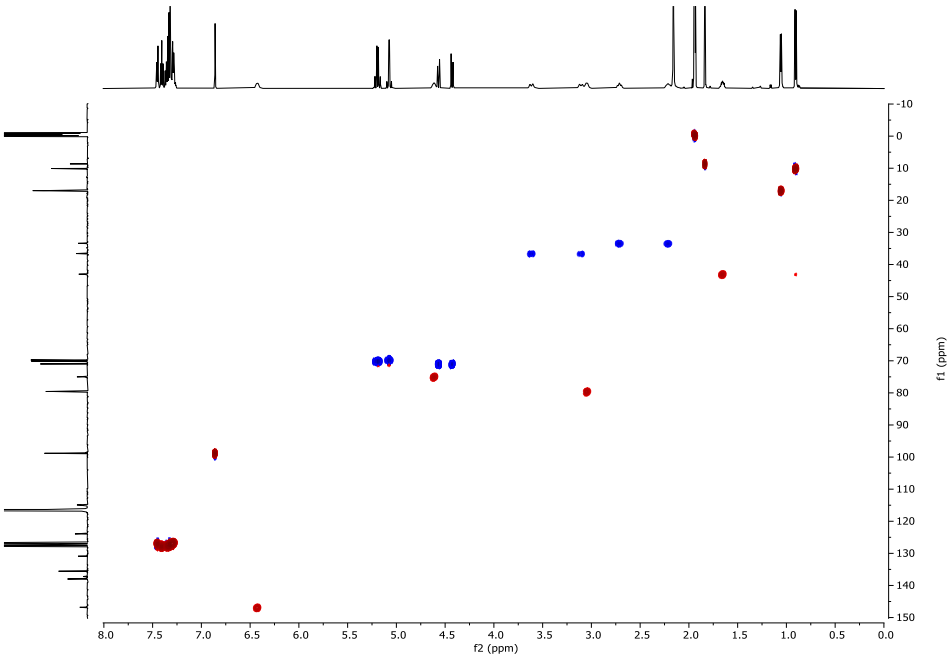

Figure S64: ^{1}H-^{13}C{^{1}H}-HSQC (MeCN-d$_3$, 600 MHz, 296 K) of (13*R*,14*R*,15*R*)-5,7,13-tris(benzyloxy)-14-deoxyoxacyclododecindione (**29**).

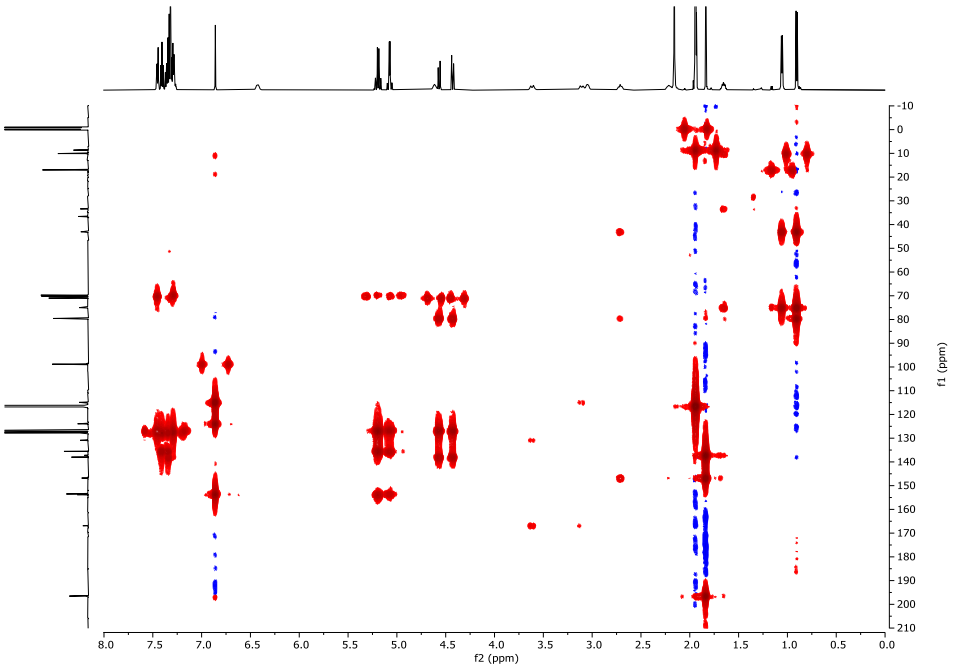

Figure S65: ^{1}H-^{13}C{^{1}H}-HMBC (MeCN-d_3, 600 MHz, 296 K) of (13*R*,14*R*,15*R*)-5,7,13-tris(benzyloxy)-14-deoxyoxacyclododecindione (**29**).

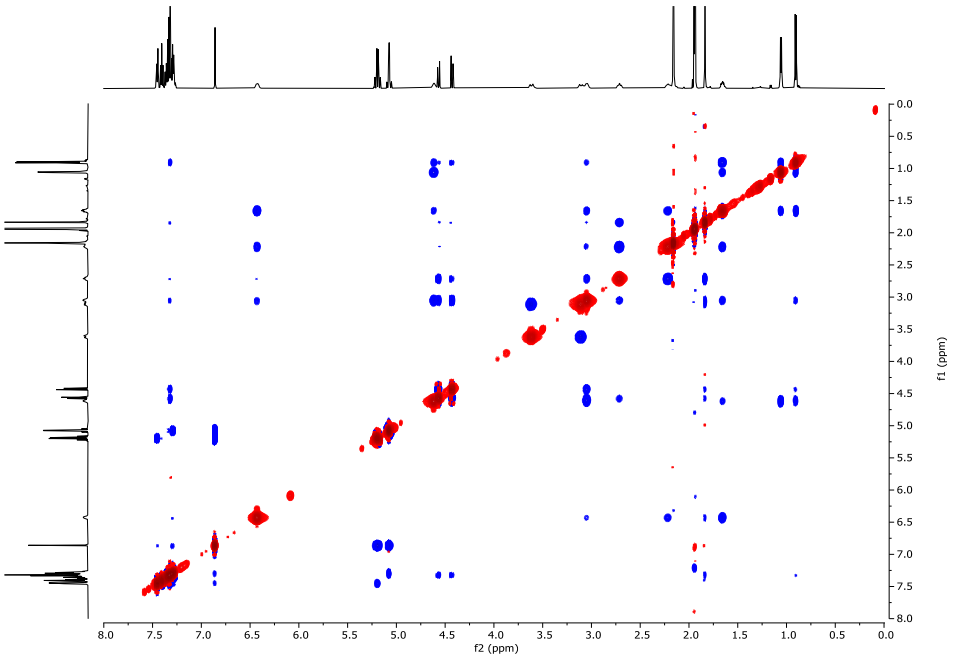

Figure S66: ^{1}H-^{1}H-NOESY (MeCN-d_3, 600 MHz, 296 K) of (13*R*,14*R*,15*R*)-5,7,13-tris(benzyloxy)-14-deoxyoxacyclododecindione (**29**).

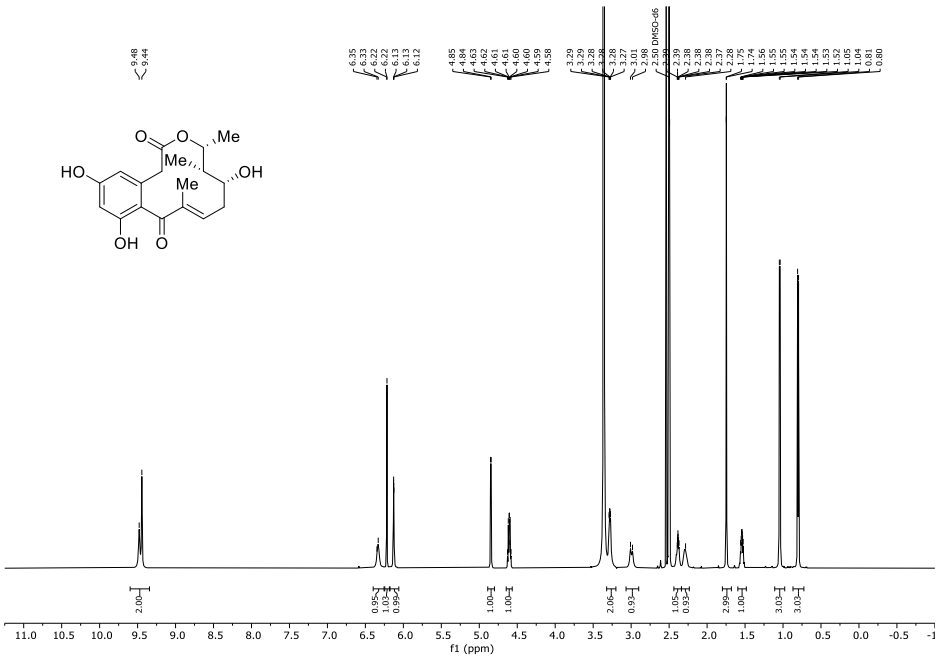

Figure S67: ^{1}H-NMR spectrum (DMSO-d$_6$, 600 MHz, 296 K) of (13*R*,14*S*,15*R*)-4-dechloro-13-hydroxy-14-deoxyoxacyclododecindione (**30**).

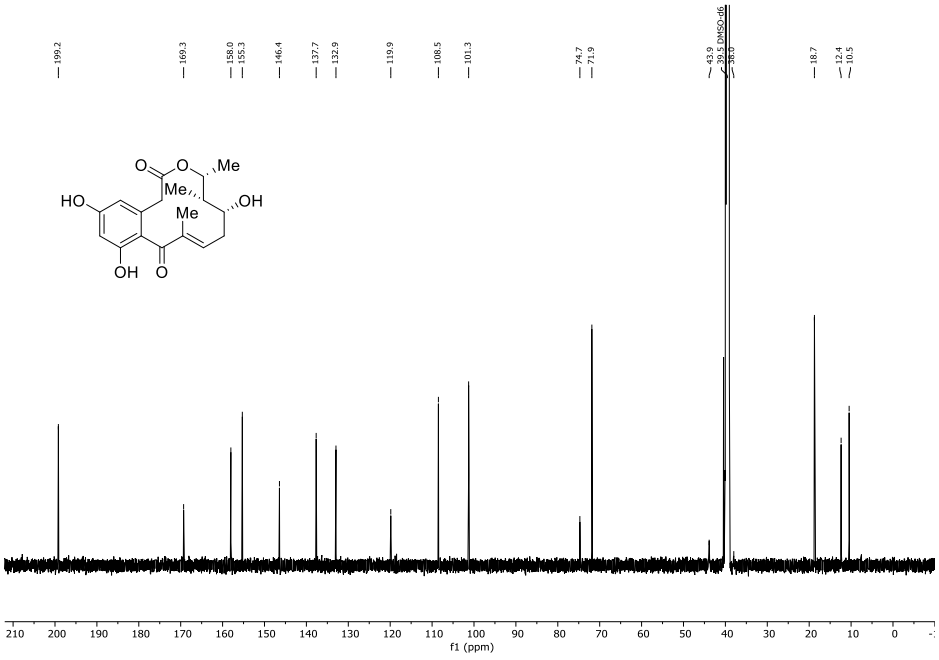

Figure S68: ^{13}C{^{1}H}-NMR spectrum (DMSO-d$_6$, 151 MHz, 296 K) of (13*R*,14*S*,15*R*)-4-dechloro-13-hydroxy-14-deoxyoxacyclododecindione (**30**).

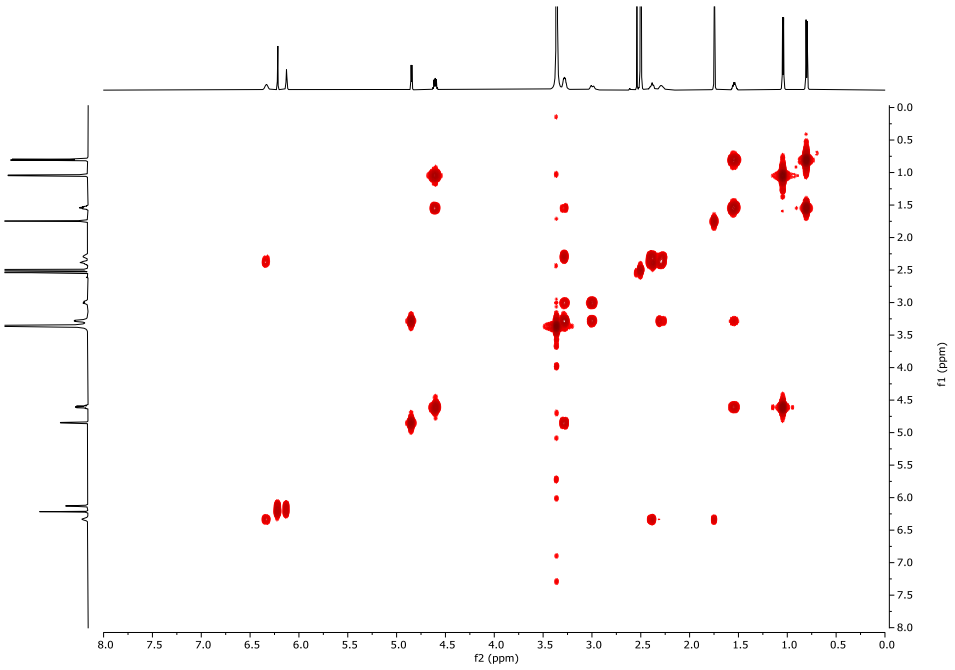

Figure S69: ^{1}H-^{1}H-COSY (DMSO-d$_6$, 600 MHz, 296 K) of (13*R*,14*S*,15*R*)-4-dechloro-13-hydroxy-14-deoxyoxacyclododecindione (**30**).

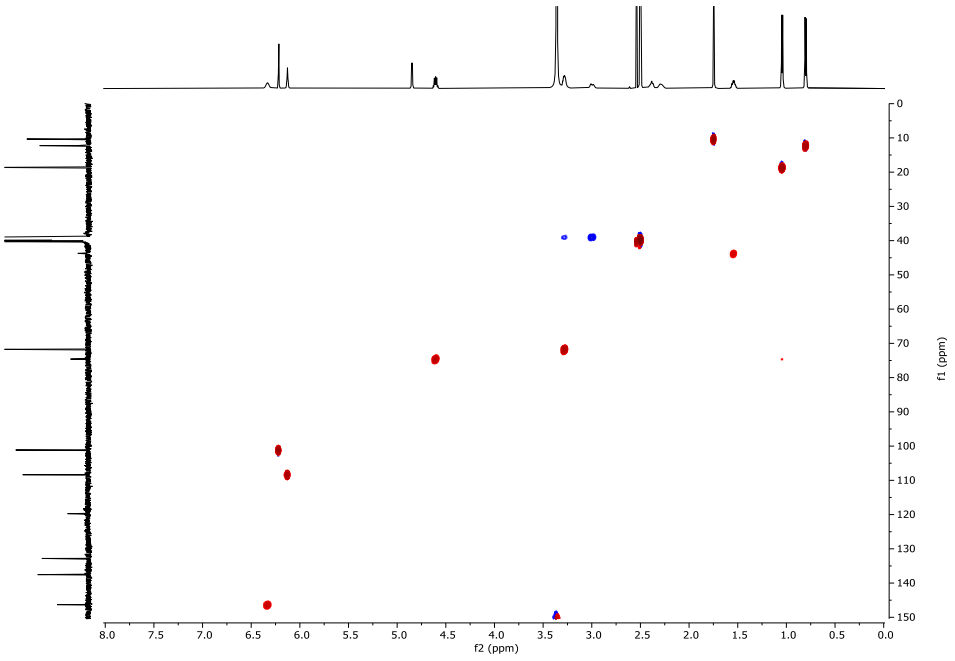

Figure S70: ^{1}H-^{13}C{^{1}H}-HSQC (DMSO-d$_6$, 600 MHz, 296 K) of (13*R*,14*S*,15*R*)-4-dechloro-13-hydroxy-14-deoxyoxacyclododecindione (**30**).

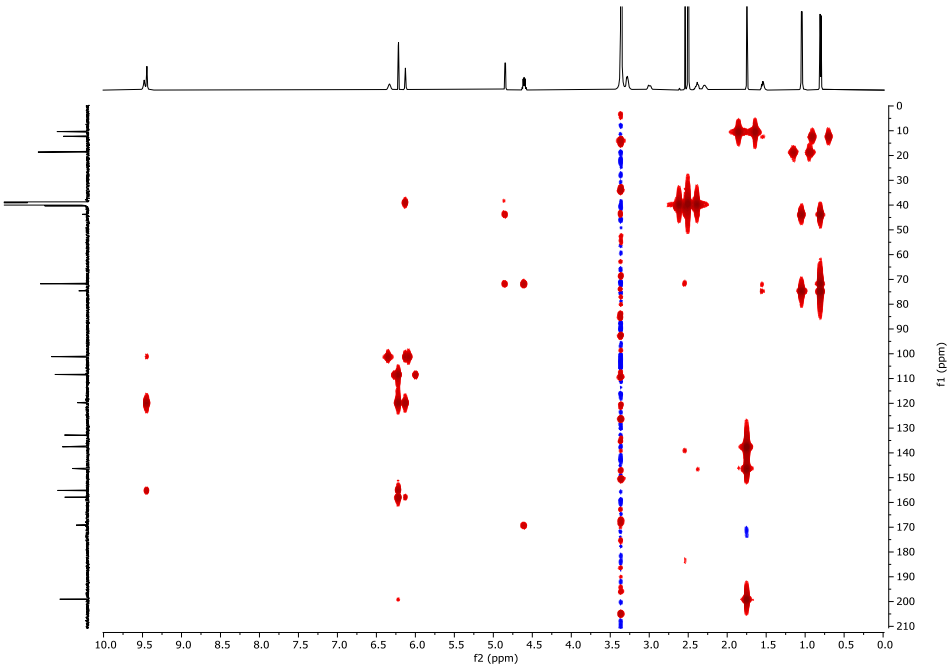

Figure S71: ^{1}H-^{13}C{^{1}H}-HMBC (DMSO-d$_6$, 600 MHz, 296 K) of (13*R*,14*S*,15*R*)-4-dechloro-13-hydroxy-14-deoxyoxacyclododecindione (**30**).

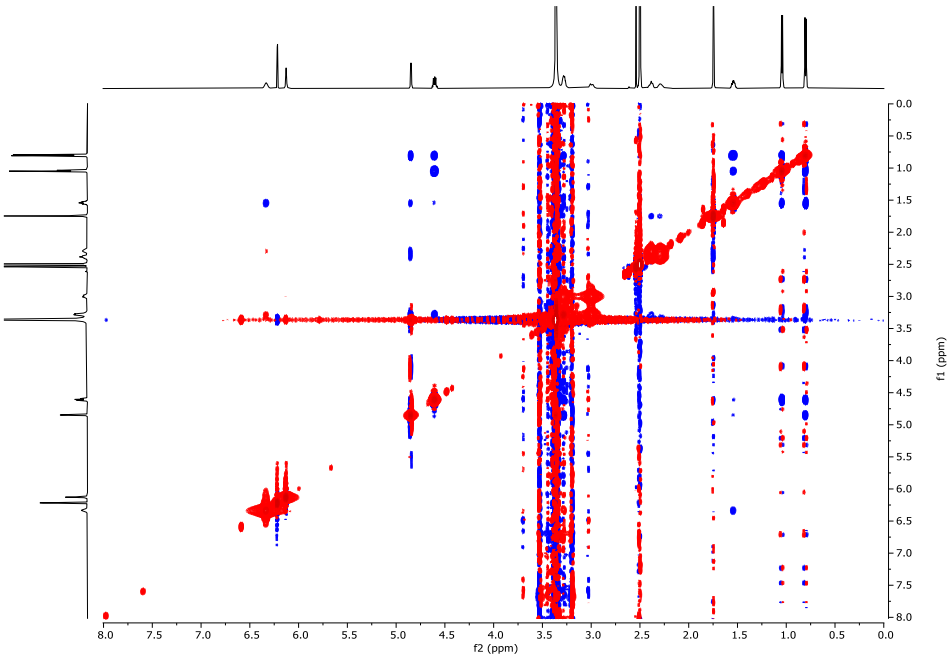

Figure S72: ^{1}H-^{1}H-NOESY (DMSO-d$_6$, 600 MHz, 296 K) of (13*R*,14*S*,15*R*)-4-dechloro-13-hydroxy-14-deoxyoxacyclododecindione (**30**).

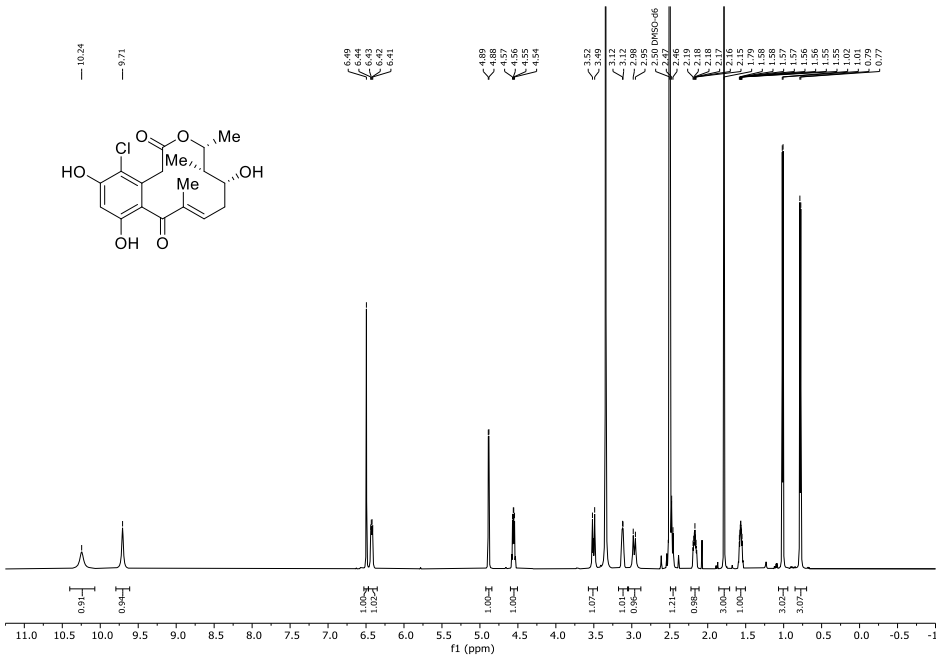

Figure S73: ^{1}H-NMR spectrum (DMSO-d_6, 600 MHz, 296 K) of (13*R*,14*S*,15*R*)-13-hydroxy-14-deoxyoxacyclododecindione (**4**).

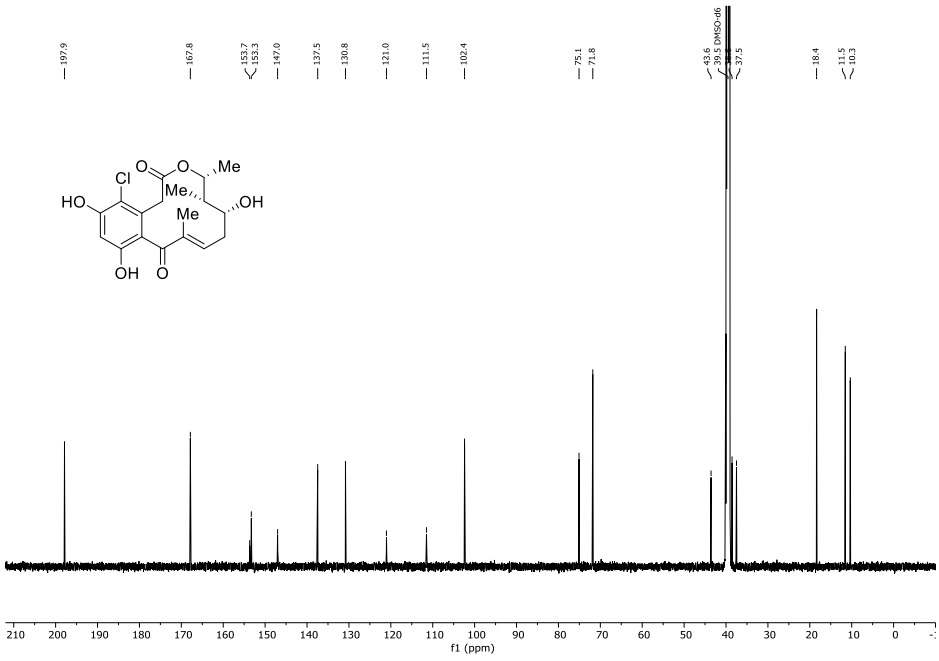

Figure S74: ^{13}C{^{1}H}-NMR spectrum (DMSO-d_6, 151 MHz, 296 K) of (13*R*,14*S*,15*R*)-13-hydroxy-14-deoxyoxacyclododecindione (**4**).

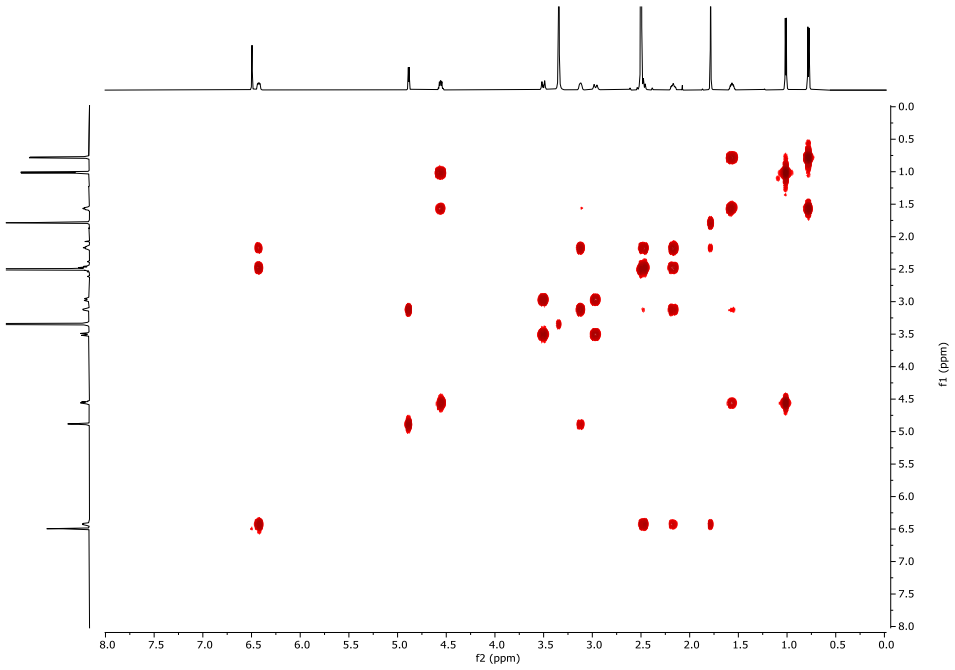

Figure S75: ^{1}H-^{1}H-COSY (DMSO-d$_6$, 600 MHz, 296 K) of (13*R*,14*S*,15*R*)-13-hydroxy-14-deoxyoxacyclododecindione (**4**).

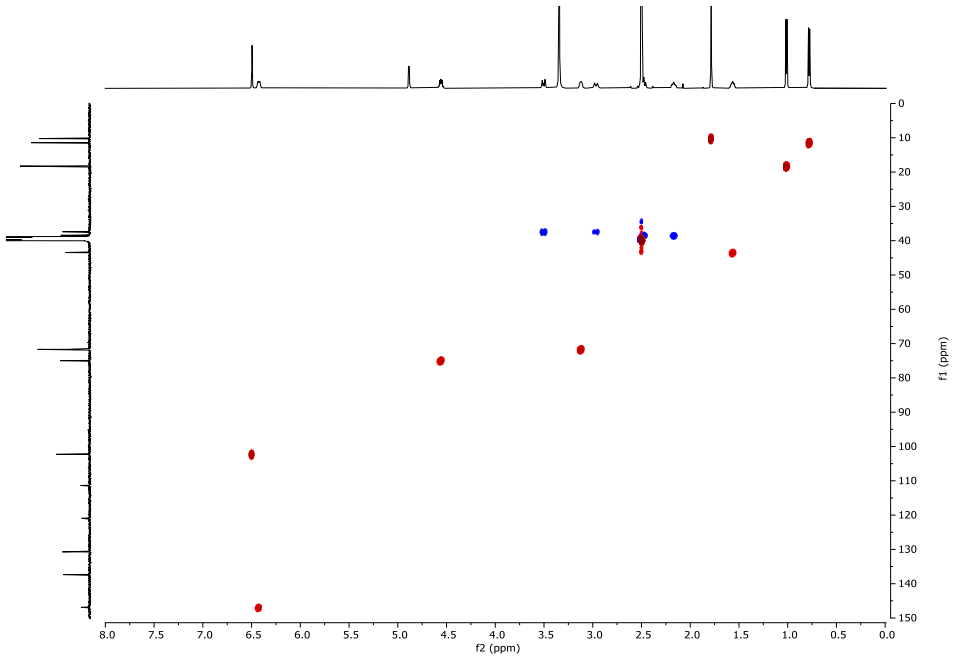

Figure S76: ^{1}H-^{13}C{^{1}H}-HSQC (DMSO-d$_6$, 600 MHz, 296 K) of (13*R*,14*S*,15*R*)-13-hydroxy-14-deoxyoxacyclododecindione (**4**).

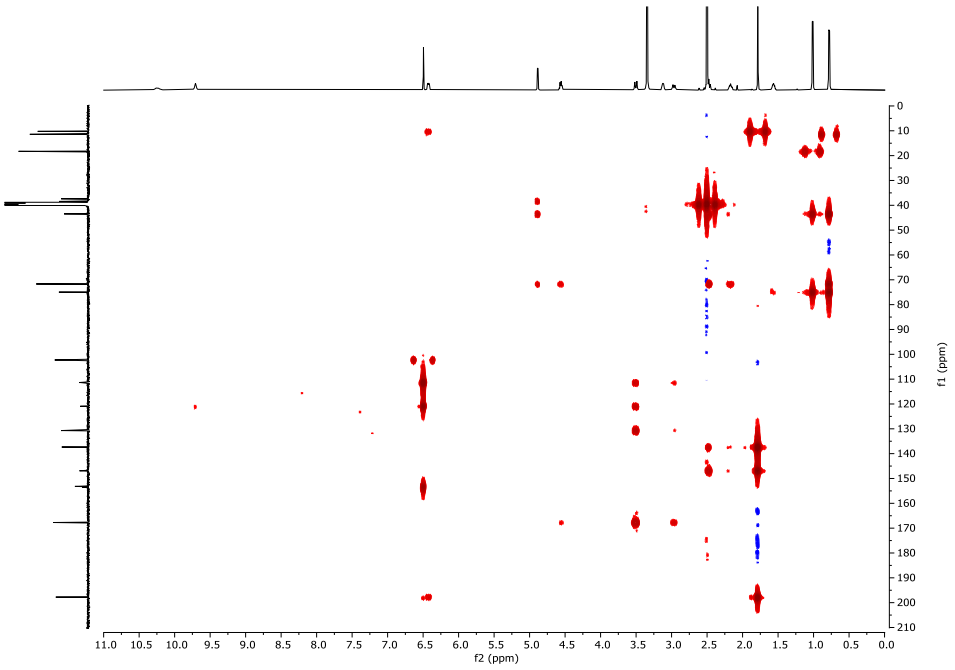

Figure S77: ^{1}H-^{13}C{^{1}H}-HMBC (DMSO-d$_6$, 600 MHz, 296 K) of (13*R*,14*S*,15*R*)-13-hydroxy-14-deoxyoxacyclododecindione (**4**).

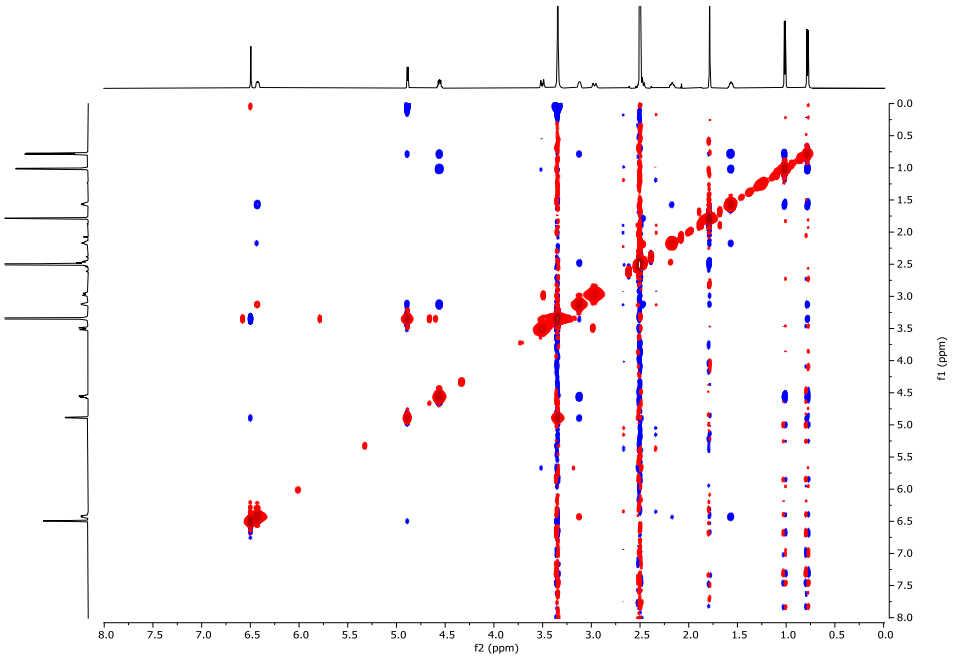

Figure S78: ^{1}H-^{1}H-NOESY (DMSO-d$_6$, 600 MHz, 296 K) of (13*R*,14*S*,15*R*)-13-hydroxy-14-deoxyoxacyclododecindione (**4**).

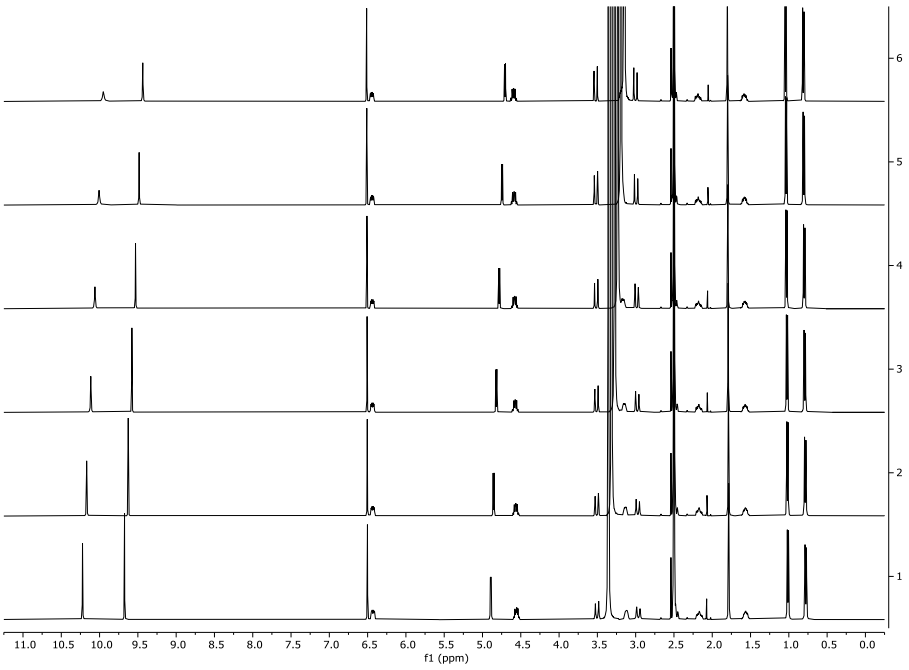

Figure S79: ^{1}H-NMR spectra temperature gradient (DMSO-d_6, 600 MHz, 296 K) of (13*R*,14*S*,15*R*)-13-hydroxy-14-deoxyoxacyclododecindione (**4**) within a range of 293 K to 343 K (ascending order).

III. *E*/*Z* Isomerization of (13*R*,14*S*,15*R*)-13-Hydroxy-14-deoxyoxacyclododecindione (4 & 34)

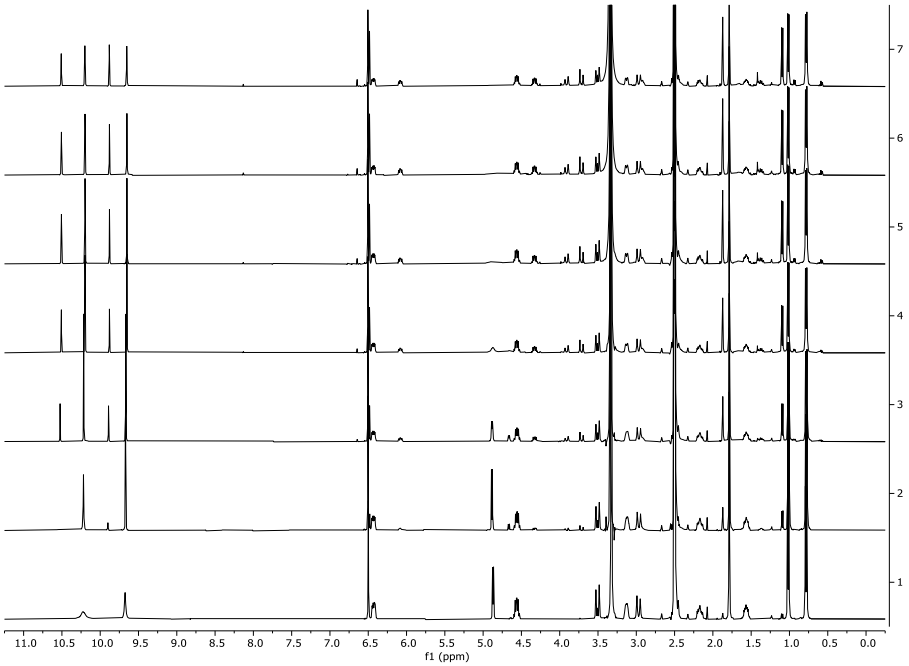

Figure S80: ^{1}H-NMR spectra (DMSO-d_6, 600 MHz, 296 K) of (13*R*,14*S*,15*R*)-13-hydroxy-14-deoxyoxacyclododecindione (**4** & **34**) within a time period of 0 d to 42 d.

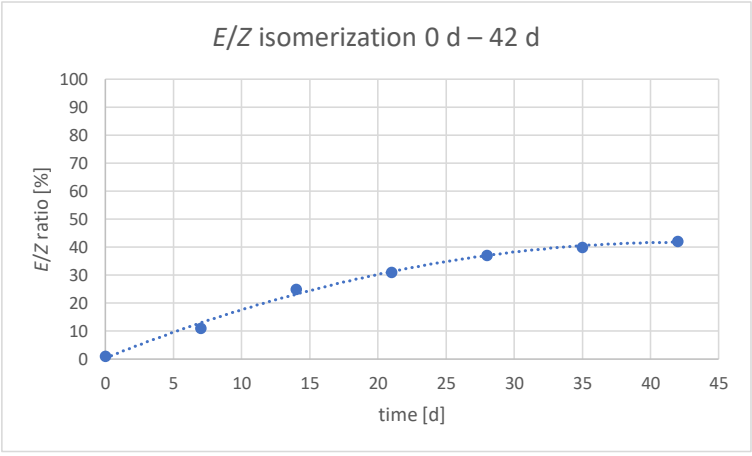

Figure S81: Kinetic representation of the *E*/*Z*-isomerization of (13*R*,14*S*,15*R*)-13-hydroxy-14-deoxyoxacyclododecindione (**4** & **34**) within a time period of 42 d. Ratio [%] is based on ^{1}H-NMR integration.

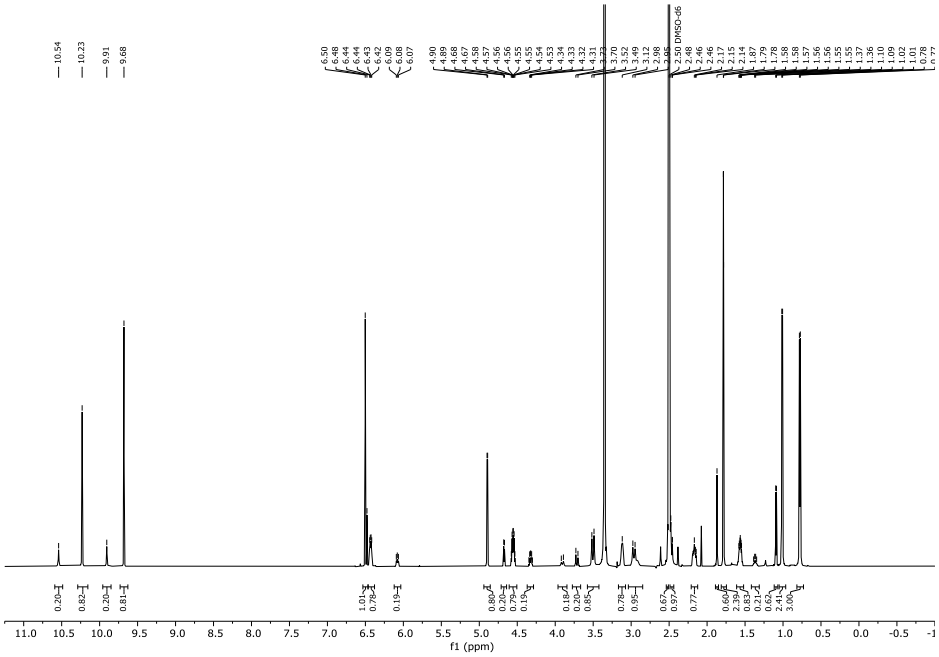

Figure S82: ^{1}H-NMR spectrum (DMSO-d_6, 600 MHz, 296 K) of the isomerized (13*R*,14*S*,15*R*)-13-hydroxy-14-deoxyoxacyclododecindione (**4** & **34**) after 18 d showing an *E*/*Z*-ratio of 80:20.

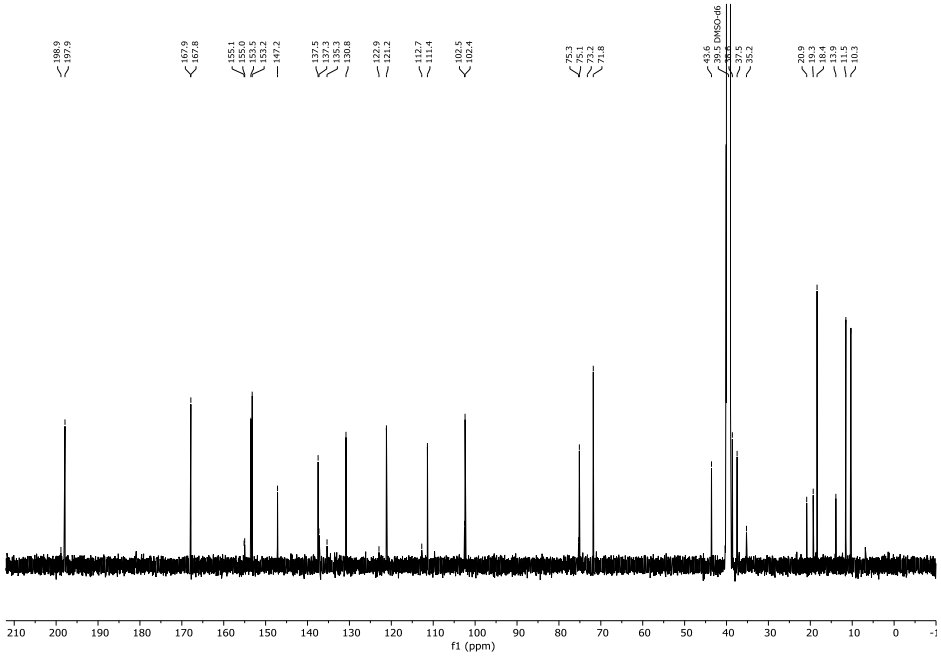

Figure S83: ^{13}C{^{1}H}-NMR spectrum (DMSO-d_6, 151 MHz, 296 K) of the isomerized (13*R*,14*S*,15*R*)-13-hydroxy-14-deoxyoxacyclododecindione (**4** & **34**) after 18 d showing an *E*/*Z*-ratio of 80:20.

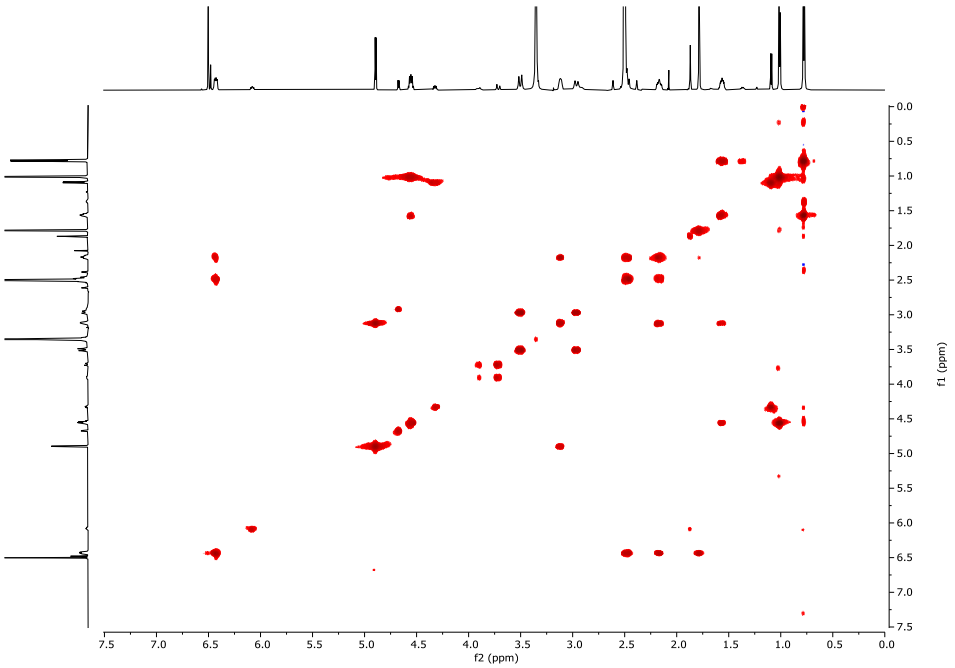

Figure S84: ^{1}H-^{1}H-COSY (DMSO-d$_6$, 600 MHz, 296 K) of the isomerized (13*R*,14*S*,15*R*)-13-hydroxy-14-deoxyoxacyclododecindione (**4** & **34**) after 18 d showing an *E*/*Z*-ratio of 80:20.

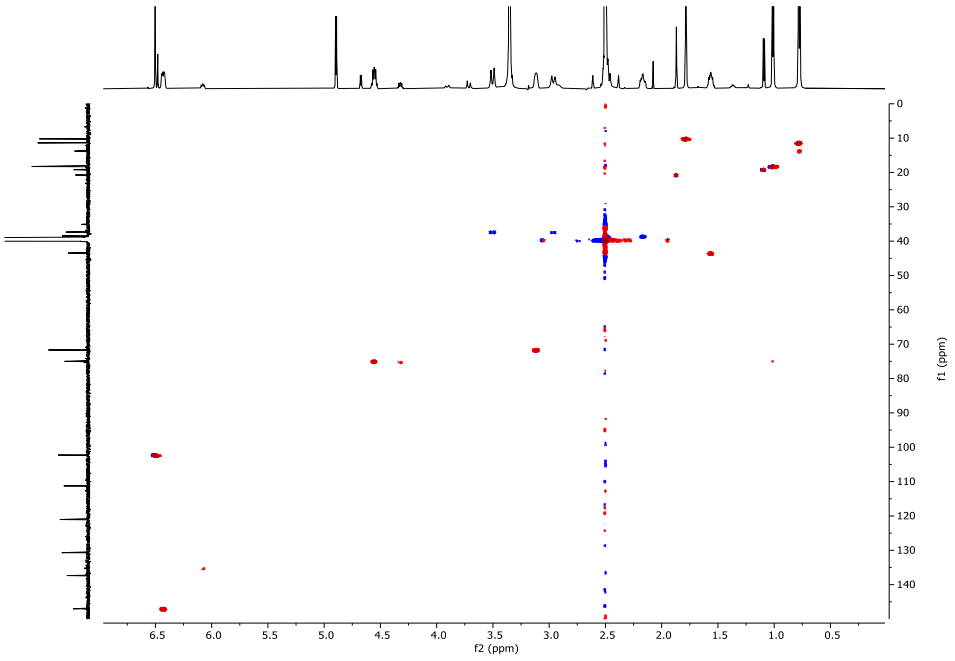

Figure S85: ^{1}H-^{13}C{^{1}H}-HSQC (DMSO-d$_6$, 600 MHz, 296 K) of the isomerized (13*R*,14*S*,15*R*)-13-hydroxy-14-deoxyoxacyclododecindione (**4** & **34**) after 18 d showing an *E*/*Z*-ratio of 80:20.

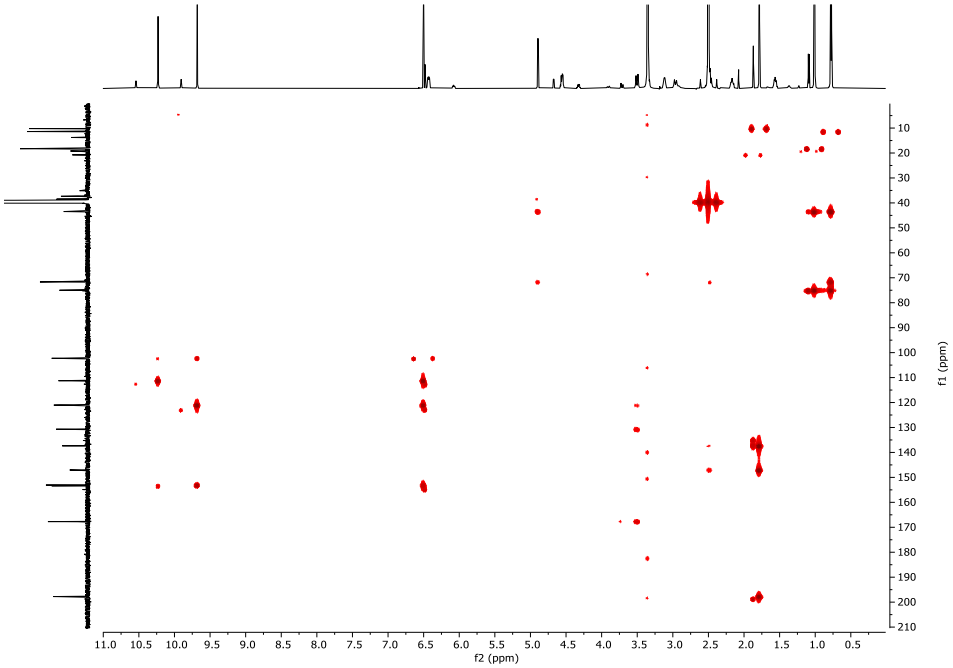

Figure S86: ^{1}H-^{13}C{^{1}H}-HMBC (DMSO-d$_6$, 600 MHz, 296 K) of the isomerized (13*R*,14*S*,15*R*)-13-hydroxy-14-deoxyoxacyclododecindione (**4** & **34**) after 18 d showing an *E*/*Z*-ratio of 80:20.

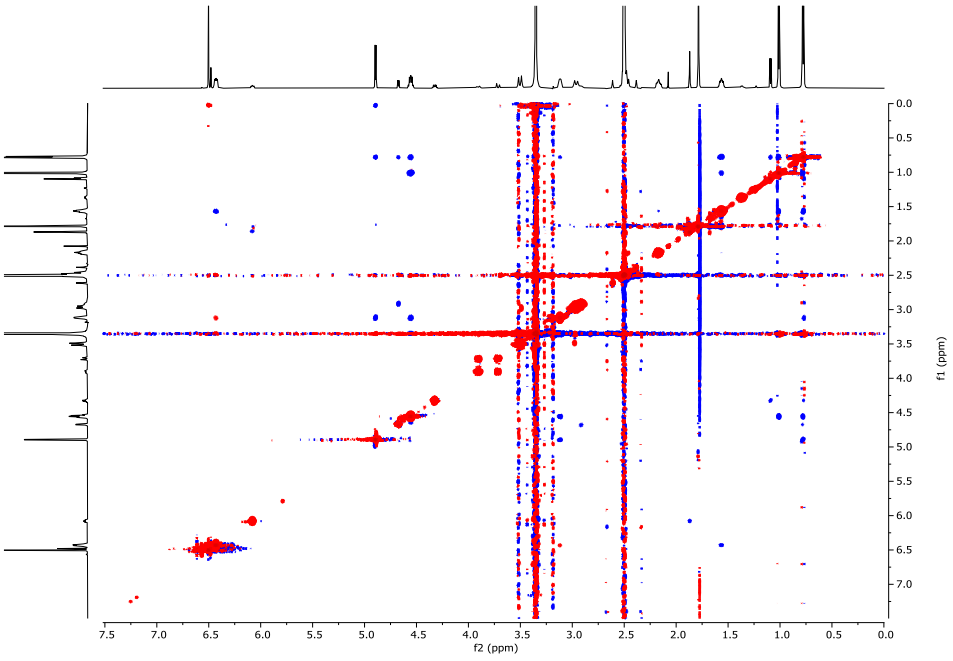

Figure S87: ^{1}H-^{1}H-NOESY (DMSO-d$_6$, 600 MHz, 296 K) of the isomerized (13*R*,14*S*,15*R*)-13-hydroxy-14-deoxyoxacyclododecindione (**4** & **34**) after 18 d showing an *E*/*Z*-ratio of 80:20.

IV. X-ray Crystallographic Analysis

X-ray molecular structure was obtained for (13*R*,14*S*,15*R*)-13-hydroxy-14-deoxyoxacyclododecindione (**4**).

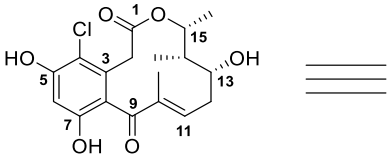

(+)-**4**

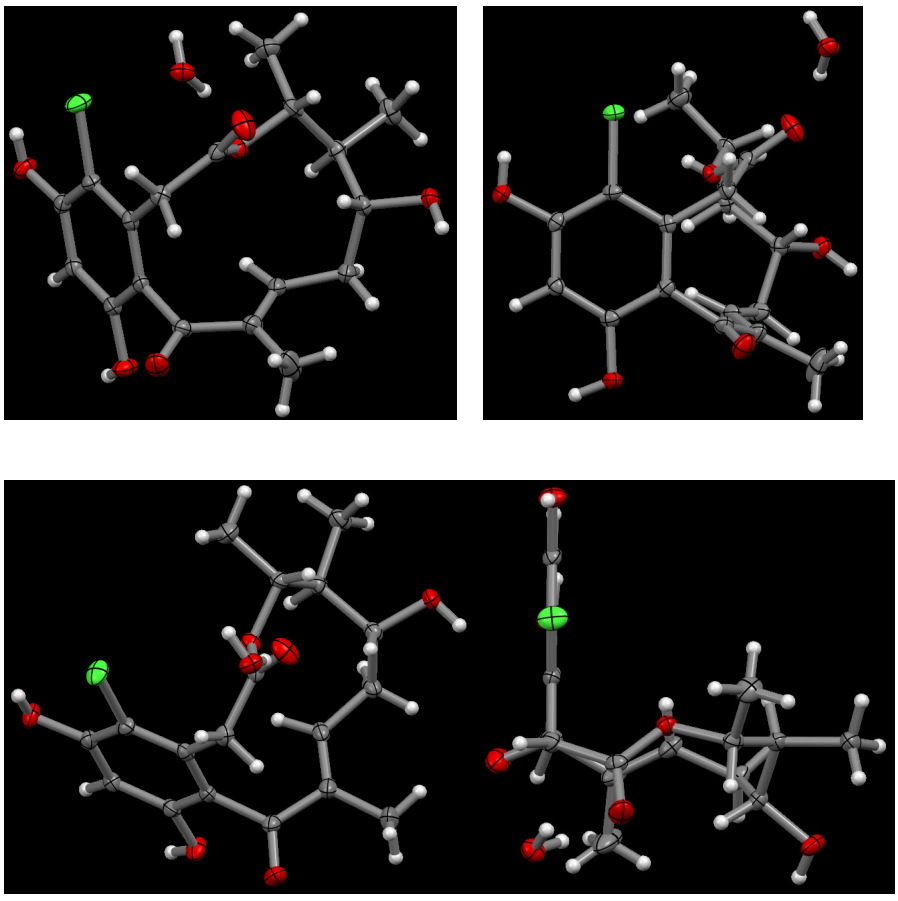

Figure S88: X-ray molecular structures of (13*R*,14*S*,15*R*)-13-hydroxy-14-deoxyoxacyclododecindione (**4**) from different perspectives, showing the unique structural features of the oxacyclododecindione class. **CCDC Number:** 2209471

Table S1: Crystal structure determination of compound **4**.

Empirical formula	$C_{18}H_{23}Cl_1O_7$
moiety formula	$C_{18}H_{23}Cl_1O_7, H_2O$
Formula weight	386.81
Temperature	120(2) K
Wavelength, radiation type	0.71073Å, MoKα
Diffractometer	STOE IPDS 2T
Crystal system	Orthorombic
Space group name, number	P $2_12_12_1$, (19)
Unit cell dimensions	a = 8.7011(3) Å b = 11.0375(4) Å c = 19.5633(6) Å
Volume	1878.83(11) $Å^3$
Number of reflections and range used for lattice parameters	27009 2.78° <=θ<= 28.40°
Z	4
Density (calculated)	1.367 Mg/m^3
Absorption coefficient	0.240 mm^{-1}
Absorption correction	Integration
Max. and min. transmission	0.9623 and 0.9259
F(000)	816
Crystal size, colour and form	0.150 x 0.260 x 0.470 mm^3, colourless plate
Theta range for data collection	2.782 to 27.881°.
Index ranges	-11<=h<=11, -14<=k<=14, -25<=l<=25
Number of reflections: collected independent observed [I>2sigma(I)] Completeness to theta = 25.2°	 13625 4497 [R(int) = 0.0168] 4361 99.8 %
Refinement method	Full-matrix least-squares on F^2
Data / restraints / parameters	4497 / 0 / 318
Goodness-of-fit on F^2	1.091
Final R indices [I>2sigma(I)]	R1 = 0.0263, wR2 = 0.0659
R indices (all data)	R1 = 0.0276, wR2 = 0.0675
Flack parameter	–0.02(2)
Largest diff. peak and hole	0.284 and -0.152 $eÅ^{-3}$
remark	all hydrogen atoms localized and isotropically refined.

V. Electronic Circular Dichroism (ECD) and Vibrational Circular Dichroism (VCD) Analysis

Computational details and quantum mechanical assisted structure elucidation

The conformational analysis of each investigated diastereomer was conducted using Spartan '10[1] on a MMFF level of theory[2], whereas all DFT calculations were performed using Gaussian 16, Rev. C.01.[3]

Each conformer was optimized on semi empirical level using pm7[4], doublets were removed and only the conformers were kept within the range of 4.5 kcal/mol from the respective diastereomer with the lowest energy. Each conformer was confirmed as local minima by frequency analysis (number of imaginary frequencies = 0).

For ECD calculation, the structure of each conformer was refined using a combination of the B3LYP functional[5-8], the 6-31g(d) basis set[9,10] and the IEFPCM solvation model[11] for methanol. The electronic excitations were calculated with a combination of CAM-B3LYP and 6-311+g(2d,p). To deliver comparable results, the Boltzmann weighted averaged spectra were simulated using SpecDis 1.71 with a half-bandwidth of 0.3 eV, as it was originally published by Shang and Lin et al.[12]

Rotational strengths for the simulation of vibrational circular dichroism (VCD) spectra were calculated with a combination of B3LYP/6-311+g(2d,p) and the IEFPCM solvation model for acetonitrile, after a geometry optimization at the same level of theory. The software SpecDis 1.71 was used for the generation of Boltzmann weighted averaged spectra using the Gibbs free energies from the output files of each conformer. In the first step, the simulated IR was fitted to the experimental spectrum to identify the best values for the numerical shift, the line broadening as well as the scaling factor. Secondly, the Boltzmann weighted VCD spectrum was compared with the observed spectrum by transferring the previously obtained parameters and the (enantiomeric) similarity factors for both spectra (IR and VCD) were calculated to determine which enantiomer of the four possible diastereomers fits the experimental VCD spectrum best, in the range of 1100–1500 cm^{-1}, based on the method developed by Bringmann et al.[13,14]

The observed and simulated spectra are shown in figure 89–91.

Input Lines

ECD:

Ground State

#p opt=tight freq b3lyp 6-31g(d) scrf=(iefpcm,solvent=methanol)

Electronic Excitations

#p td=(nstates=100) cam-b3lyp 6-311+g(2d,p) scrf=(iefpcm,solvent=methanol)

VCD:

Ground State

#p opt=tight freq b3lyp 6-311+g(2d,p) scrf=(iefpcm,solvent=acetonitrile)

Rotational strengths

#p freq=vcd b3lyp 6-311+g(2d,p) scrf=(iefpcm,solvent=acetonitrile)

VI. ECD Results

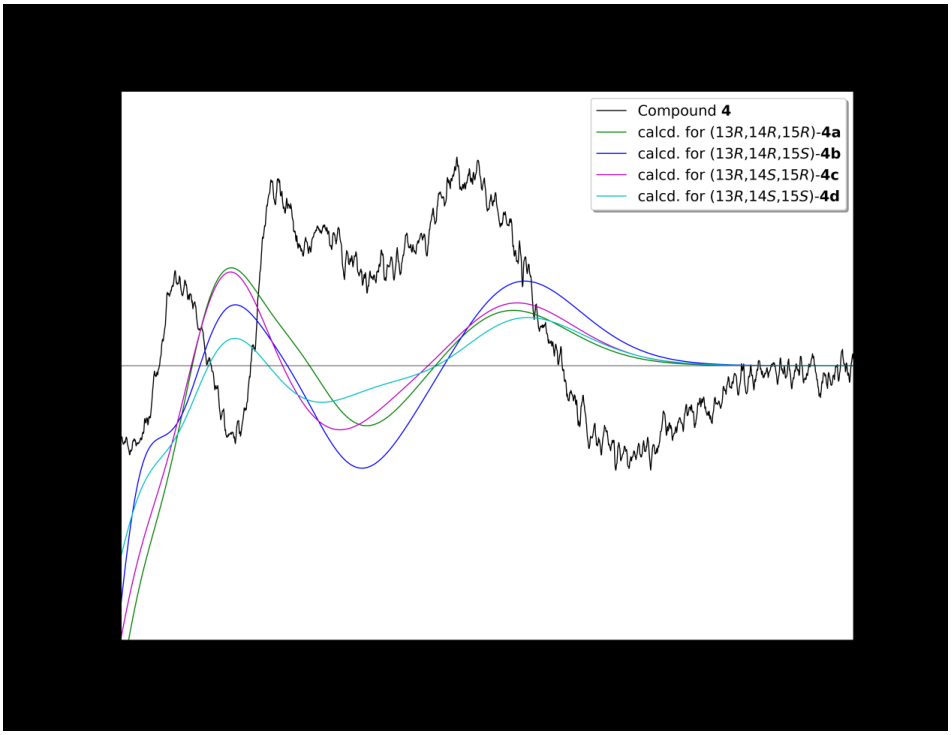

Figure S89: The experimental ECD spectrum of **4** (black) in methanol as well as the Boltzmann averaged simulated spectra for each diastereomer (**4a**–**4d**).

VII. IR and VCD Results

Figure S90 shows a comparison of the observed and simulated IR spectra.

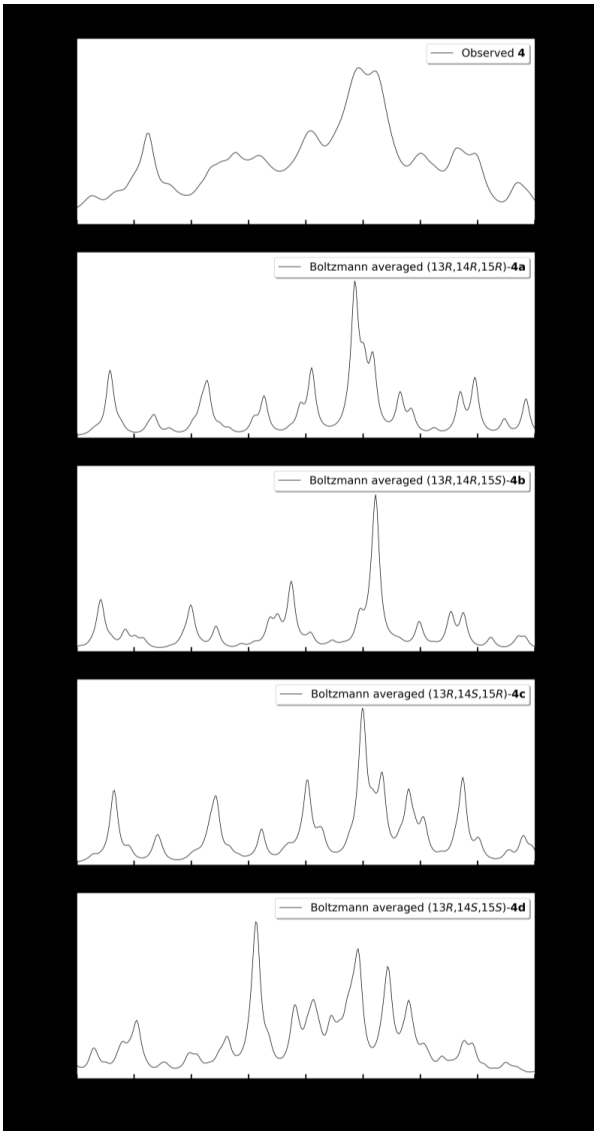

	(13*R*,14*R*,15*R*)-**4a**	(13*R*,14*R*,15*S*)-**4b**	(13*R*,14*S*,15*R*)-**4c**	(13*R*,14*S*,15*S*)-**4d**
Similarity factor *S*	77%	75%	87%	88%

Figure S90: Comparison of the observed IR spectrum of compound **4** (top) with the simulated spectra of each possible diastereomer (**4a**–**4d**) and the calculated similarity factors using SpecDis.

Figure S90 shows a comparison of the observed and simulated VCD spectra.

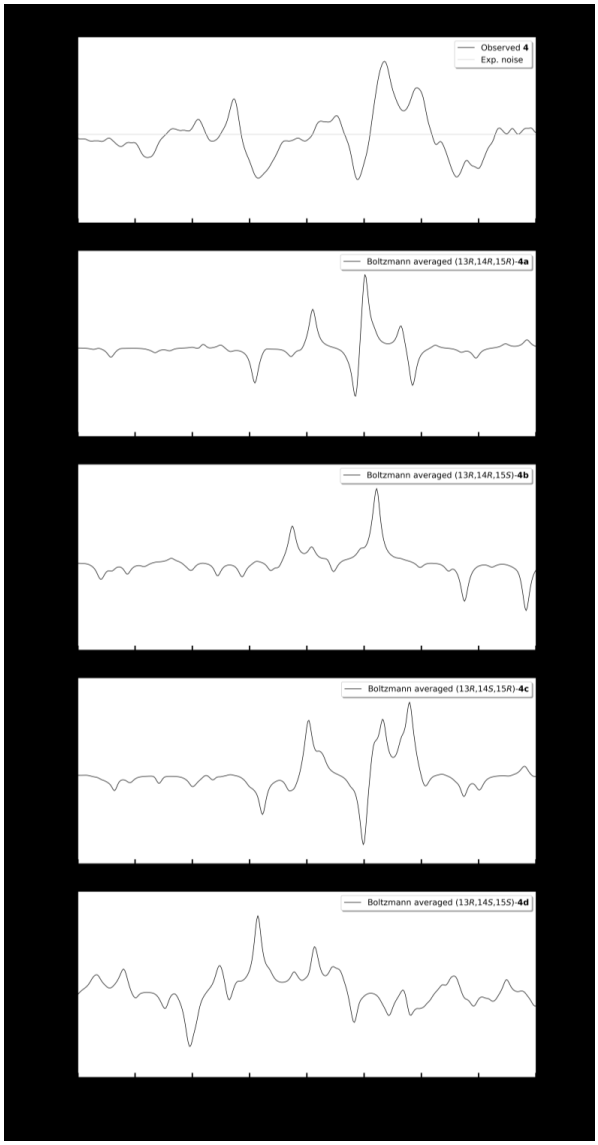

	(13*R*,14*R*,15*R*)-**4a**	(13*R*,14*R*,15*S*)-**4b**	(13*R*,14*S*,15*R*)-**4c**	(13*R*,14*S*,15*S*)-**4d**
Similarity factor *S*	29%	15%	73%	19%
Enantiomeric similarity factor *S**	20%	31%	2%	50%

Figure S91: Comparison of the observed VCD spectrum of compound **4** (top) with the simulated spectra of each possible diastereomer (**4a**–**4d**) and the calculated (enantiomeric) similarity factors using SpecDis.

VIII. References

(1) Wavefunction, Inc.: Irvine, CA, USA, 2009.

(2) Halgren, T. A. *J. Comput. Chem.* **1996**, *17*, 490-519.

(3) Frisch, M. J.; Trucks, G. W.; Schlegel, H. B.; Scuseria, G. E.; Robb, M. A.; Cheeseman, J. R.; Scalmani, G.; Barone, V.; Petersson, G. A.; Nakatsuji, H.; Li, X.; Caricato, M.; Marenich, A. V.; Bloino, J.; Janesko, B. G.; Gomperts, R.; Mennucci, B.; Hratchian, H. P.; Ortiz, J. V.; Izmaylov, A. F.; Sonnenberg, J. L.; Williams; Ding, F.; Lipparini, F.; Egidi, F.; Goings, J.; Peng, B.; Petrone, A.; Henderson, T.; Ranasinghe, D.; Zakrzewski, V. G.; Gao, J.; Rega, N.; Zheng, G.; Liang, W.; Hada, M.; Ehara, M.; Toyota, K.; Fukuda, R.; Hasegawa, J.; Ishida, M.; Nakajima, T.; Honda, Y.; Kitao, O.; Nakai, H.; Vreven, T.; Throssell, K.; Montgomery Jr., J. A.; Peralta, J. E.; Ogliaro, F.; Bearpark, M. J.; Heyd, J. J.; Brothers, E. N.; Kudin, K. N.; Staroverov, V. N.; Keith, T. A.; Kobayashi, R.; Normand, J.; Raghavachari, K.; Rendell, A. P.; Burant, J. C.; Iyengar, S. S.; Tomasi, J.; Cossi, M.; Millam, J. M.; Klene, M.; Adamo, C.; Cammi, R.; Ochterski, J. W.; Martin, R. L.; Morokuma, K.; Farkas, O.; Foresman, J. B.; Fox, D. J. Gaussian, Inc., Gaussian 16, Revision C.01, Wallingford CT, 2019.

(4) Stewart, J. J. P. *J. Mol. Model.* **2013**, *19*, 1-32.

(5) Vosko, S. H.; Wilk, L.; Nusair, M. *Can. J. Phys.* **1980**, *58*, 1200-1211.

(6) Lee, C.; Yang, W.; Parr, R. G. *Phys. Rev. B* **1988**, *37*, 785-789.

(7) Becke, A. D. *Int. J. Chem. Phys.* **1993**, *98*, 5648-5652.

(8) Becke, A. D. *Phys. Rev. A* **1988**, *38*, 3098.

(9) Hariharan, P. C.; Pople, J. A. *Theor. Chim. Acta* **1973**, *28*, 213-222.

(10) Hehre, W. J.; Ditchfield, R.; Pople, J. A. *J. Chem. Phys.* **1972**, *56*, 2257-2261.

(11) Tomasi, J.; Mennucci, B.; Cancès, E. *Comput. Theor. Chem* **1999**, *464*, 211-226.

(12) Lin, P.-C.; Wu, Y.-Z.; Bao, T.-W.; Wang, Y.-N.; Shang, X.-Y.; Lin, S. *J. Asian Nat. Prod. Res.* **2018**, *20*, 1093-1100.

(13) Bruhn, T.; Schaumlöffel, A.; Hemberger, Y.; Bringmann, G. *Chirality* **2013**, *25*, 243-249.

(14) Debie, E.; De Gussem, E.; Dukor, R. K.; Herrebout, W.; Nafie, L. A.; Bultinck, P. *ChemPhysChem* **2011**, *12*, 1542-1549.

B.3 Strukturaufklärung isolierter Naturstoffe mittels computergestützter Spektroskopie

B.3.1 Zusatzmaterial der Publikation zur Bestimmung der absoluten Konfiguration von Perylenchinonen

Im Folgenden ist die *supporting information* der Publikation „Structure elucidation and biological activities of perylenequinones from an *Alternaria* species“ abgedruckt.[563]

SUPPLEMENTARY MATERIAL

Structure elucidation and biological activities of perylenequinones from an *Alternaria* species

Anna Kiefer[1], Marcel Arnholdt[1], Viktoria Grimm[1], Leander Geske[2], Jonathan Groß[2], Nina Vierengel[2], Till Opatz[2,§], Gerhard Erkel[1,§]

Author's institution/affiliation

[1]Molecular Biotechnology & Systems Biology, RPTU, Paul-Ehrlich-Straße 23, D-67663 Kaiserslautern, Germany

[2]Department of Chemistry, Johannes Gutenberg-University, Duesbergweg 10-14, D-55128 Mainz, Germany

[§]Corresponding authors: Gerhard Erkel (erkel@bio.uni-kl.de); Till Opatz (opatz@uni-mainz.de)

Electroporation parameters

	Voltage	Pulse Length [msec]	Pulse Interval [msec]	Number of Pulses	Decay Rate [%]	Polarity
Poring Pulse	220	5	50	2	10	+
Transfer Pulse	20	50	50	5	40	+/-

Quantitative real time PCR Primer

SOD3 (NM_003102.4)	
Sense	ACGCTGGCGAGGACGACCTG
Antisense	GCTTCTTGCGCTCTGAGTGCTC
PRDX1 (NM_181696.3)	
sense	CTGCCAAGTGATTGGTGCTTCTG
antisense	AATGGTGCGCTTCGGGTCTGAT
TXNRD1 (NM_182743.3)	
Sense	GTTACTTGGGCATCCCTGGTGA
Antisense	CGCACTCCAAAGCGACATAGGA
NRF2 (NM_006164.5)	
Sense	CACATCCAGTCAGAAACCAGTGG
Antisense	GGAATGTCTGCGCCAAAAGCTG
HMOX1 (NM_002133.3)	
Sense	ATGACACCAAGGACCAGAGC
Antisense	GTGTAAGGACCCATCGGAGA
NQO1 (NM_000903.3)	
Sense	CAGTGGTTTGGAGTCCCTGCC
Antisense	TCCCCGTGGATCCCTTGCAG
Cyp1A1 (NM_000499)	
Sense	GATTGAGCACTGTCAGGAGAAGC
Antisense	ATGAGGCTCCAGGAGATAGCAG
Cyp1A2 (NM_000761)	
Sense	TCATCCTGGAGACCTTCCGACA
Antisense	GCCACTGGTTTACGAAGACACAG
GAPDH (NM_002046)	
Sense	CCTCCGGGAAACTGTGG
Antisense	AGTGGGGACACGGAAG

1. Experimental data:

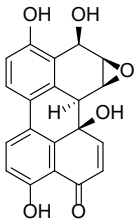

(1*S*,2*R*,3*R*,12a*R*,12b*S*)-Alterperylenepoxide A isomer, (+)-**1**): Yellow solid. **^{1}H NMR (600 MHz, CD_3OD):** δ [ppm] = 8.02 (d, *J* = 8.8 Hz, 1H), 7.68 (d, *J* = 10.3 Hz, 1H), 7.66 (d, *J* = 8.4 Hz, 1H), 7.03 (d, *J* = 8.8 Hz, 1H), 6.85 (d, *J* = 8.4 Hz, 1H), 6.51 (d, *J* = 10.3 Hz, 1H), 5.18 (t, *J* = 1.5 Hz, 1H), 3.99 (d, *J* = 3.7 Hz, 1H), 3.59–3.57 (m, 1H), 3.38–3.35 (m, 1H). **^{13}C NMR (151 MHz, CD_3OD):** δ [ppm] = 191.7, 161.5, 158.2, 148.7, 140.5, 133.1, 129.6, 127.7, 126.7, 125.7, 125.3, 119.1, 115.4, 114.0, 67.2, 60.5, 54.7, 43.7. **HR-ESI-MS (neg):** found m/z = 349.0715, calc. m/z = 349.0717. **LC-ESI-MS (neg):** found m/z = 349.0, calc. m/z = 349.1. **IR**: $\tilde{\nu}$ [cm^{-1}] = 3404, 2922, 2852, 1625, 1460, 1395, 1232, 1078, 1039. $[\alpha]_D^{21}$ = +230.0 (*c* = 0.26; MeOH).

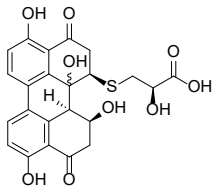

Compound **2**: Yellow solid. **^{1}H NMR (600 MHz, CD_3OD):** δ [ppm] = 8.01 (d, *J* = 8.8 Hz, 1H), 7.97 (d, *J* = 8.8 Hz, 1H), 7.03 (d, J = 8.8 Hz, 1H), 6.93 (dd, *J* = 8.8, 1.0 Hz, 1H), 4.70 (t, *J* = 3.3 Hz, 1H), 4.66 (ddd, *J* = 9.8, 8.3, 5.2 Hz, 1H), 4.32 (dd, *J* = 6.9, 4.3 Hz, 1H), 4.15 (d, *J* = 8.3 Hz, 1H), 3.73 (dd, *J* = 17.3, 3.3 Hz, 1H), 3.22–3.15 (m, 1H), 3.09 (dd, *J* = 17.4, 3.3 Hz, 1H), 3.05–2.95 (m, 3H). **^{13}C NMR (151 MHz, CD_3OD):** δ [ppm] = 205.2, 205.2, 163.2, 163.1, 139.0, 138.0, 133.4, 133.2, 125.6, 125.3, 120.2, 118.1, 117.3, 115.7, 73.1, 72.2, 67.3, 52.0, 41.6, 38.0. **HR-ESI-MS (neg):** found m/z = 471.0739, calc. m/z = 471.0755. **LC-ESI-MS (neg):** found m/z = 471.1, calc. m/z = 471.1. **IR**: $\tilde{\nu}$ [cm^{-1}] = 3407, 2925, 1641, 1461, 1357, 1242, 1199, 1082, 1040. $[\alpha]_D^{21}$ = +110.8 (*c* = 0.76; MeOH).

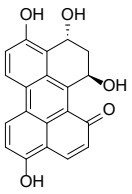

(10*R*,12*R*)-Compound (+)-**3**: Orange-red solid. **^{1}H NMR (600 MHz, CD_3OD):** δ [ppm] = 9.07 (d, *J* = 9.3 Hz, 1H), 8.74 (d, *J* = 10.1 Hz, 1H), 8.72 (d, *J* = 9.3 Hz, 2H), 7.42 (d, *J* = 9.1 Hz, 1H), 7.41 (d, *J* = 9.2 Hz, 1H), 6.98 (d, *J* = 10.0 Hz, 1H), 5.96 (t, *J* = 3.4 Hz, 1H), 5.68 (dd, *J* = 11.2, 5.0 Hz, 1H), 2.75 (dt, *J* = 13.0, 4.4 Hz, 2H), 2.20 (ddd, *J* = 12.9, 11.3, 3.1 Hz, 2H). **^{13}C NMR (151 MHz, CD_3OD):** δ [ppm] = 190.0, 170.2, 167.8, 155.8, 141.0, 140.8, 134.4, 128.1, 127.9, 127.6, 126.1, 124.6, 123.9, 123.5, 122.8, 120.8, 119.9, 112.8, 66.3, 64.1, 40.4. **HR-ESI-MS (neg):** found m/z = 333.0763, calc. m/z = 333.0768. **LC-ESI-MS (neg):** found m/z = 333.1, calc. m/z = 333.1. **IR**: $\tilde{\nu}$ [cm^{-1}] = 3356, 2920, 2851, 1624, 1516, 1467, 1390, 1356, 1234, 1175, 1046. $[\alpha]_D^{21}$ = +149.9 (*c* = 0.41; MeOH).

1. Spectra

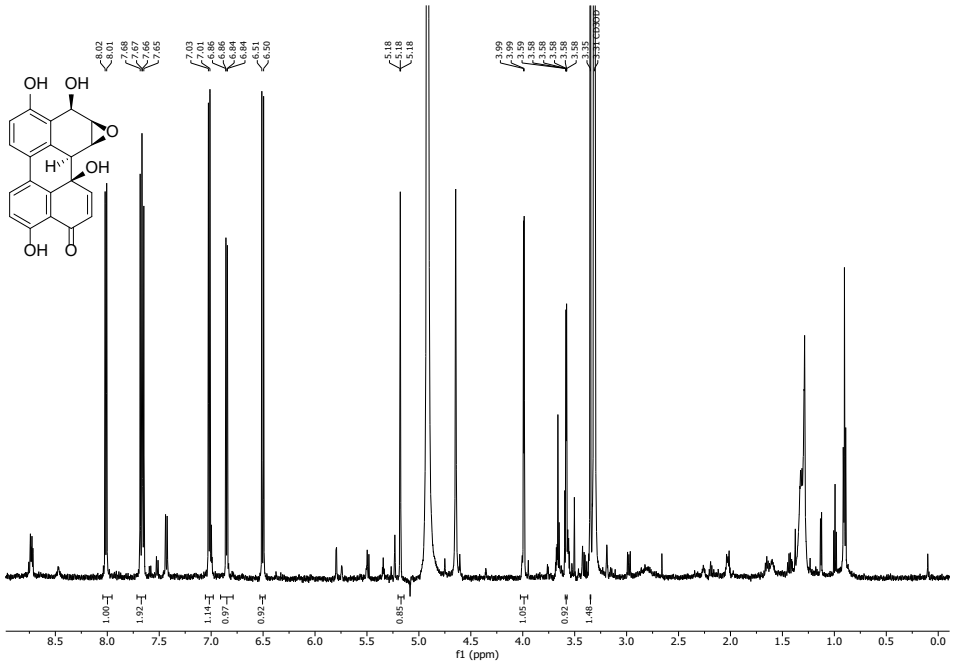

Figure 1 ^{1}H NMR (600 MHz, CD_3OD): Compound (+)-**1**.

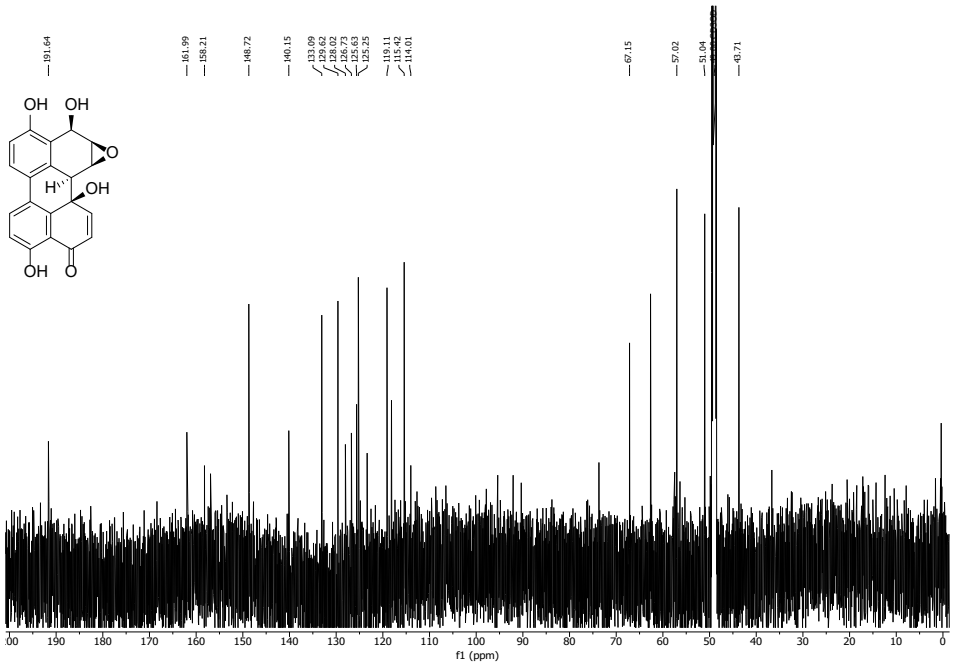

Figure 2 ^{13}C NMR (150 MHz, CD_3OD): Compound (+)-**1**.

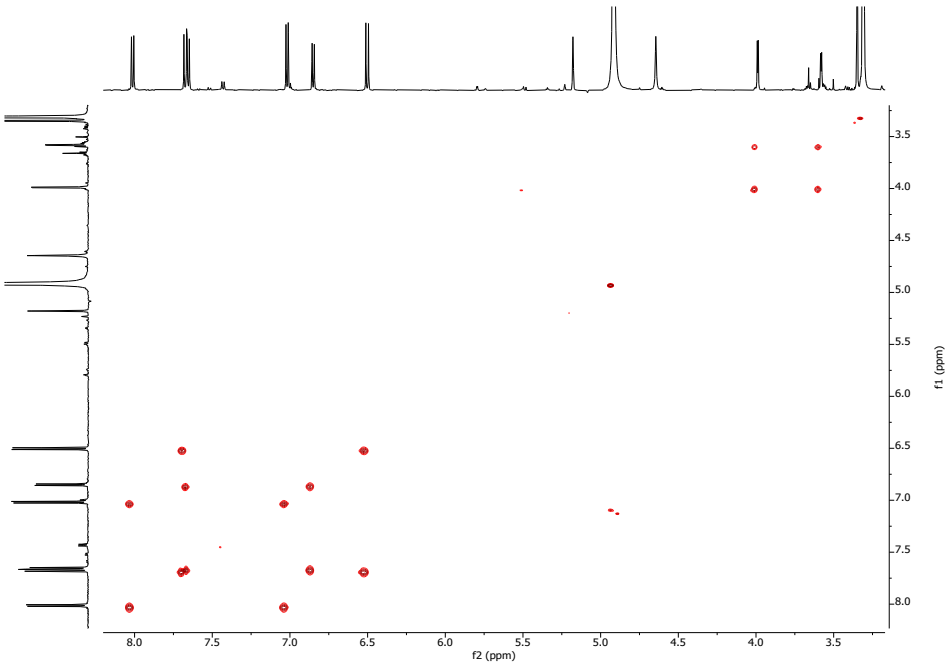

Figure 3 ^{1}H–^{1}H-COSY (CD_3OD): Compound (+)-**1**.

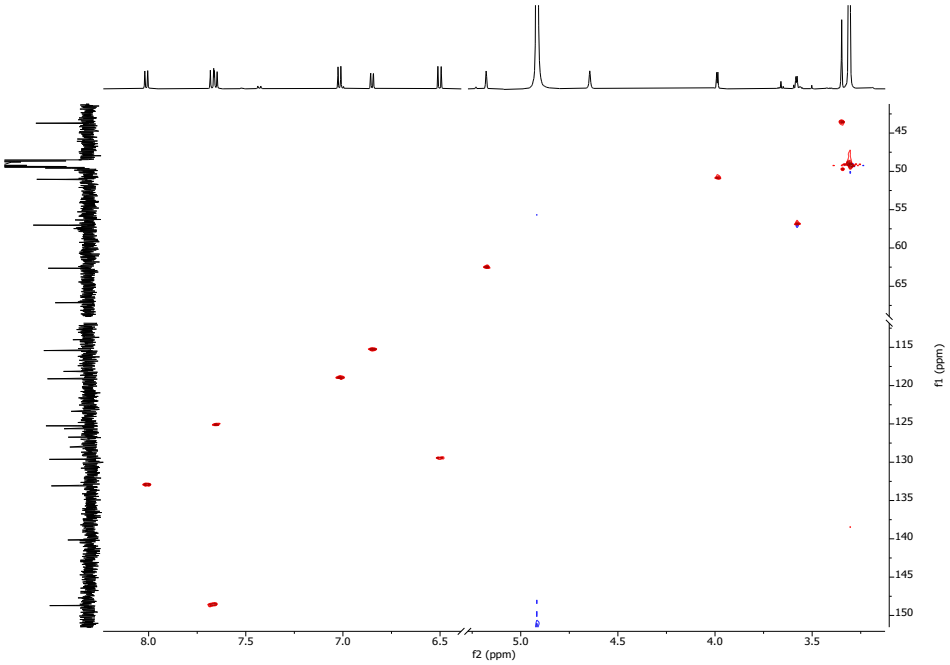

Figure 4 ^{1}H–^{13}C HSQC (CD_3OD): Compound (+)-**1**.

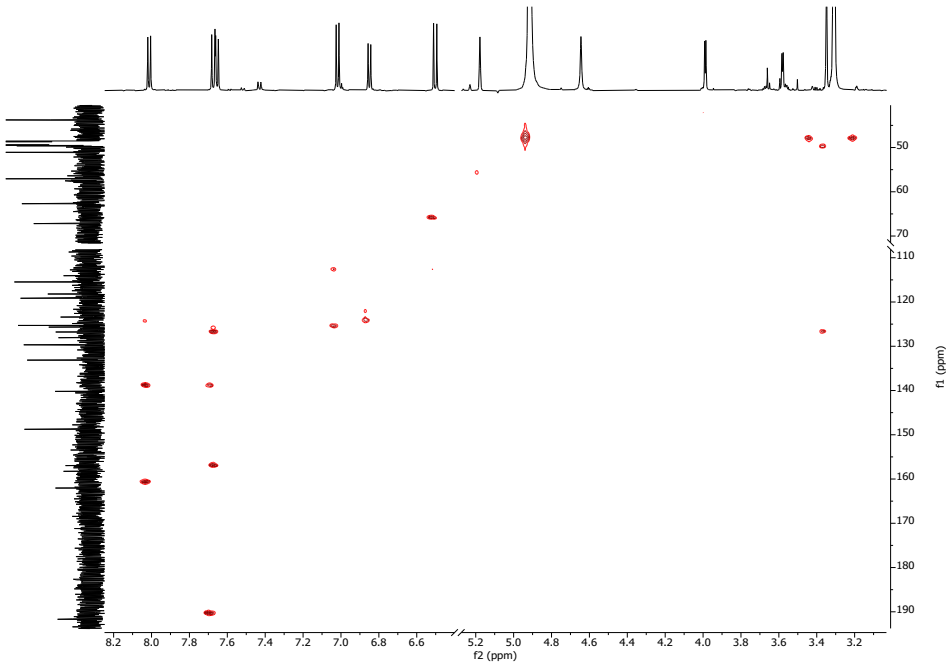

Figure 5 ^{1}H–^{13}C HMBC (CD_3OD): Compound (+)-**1**.

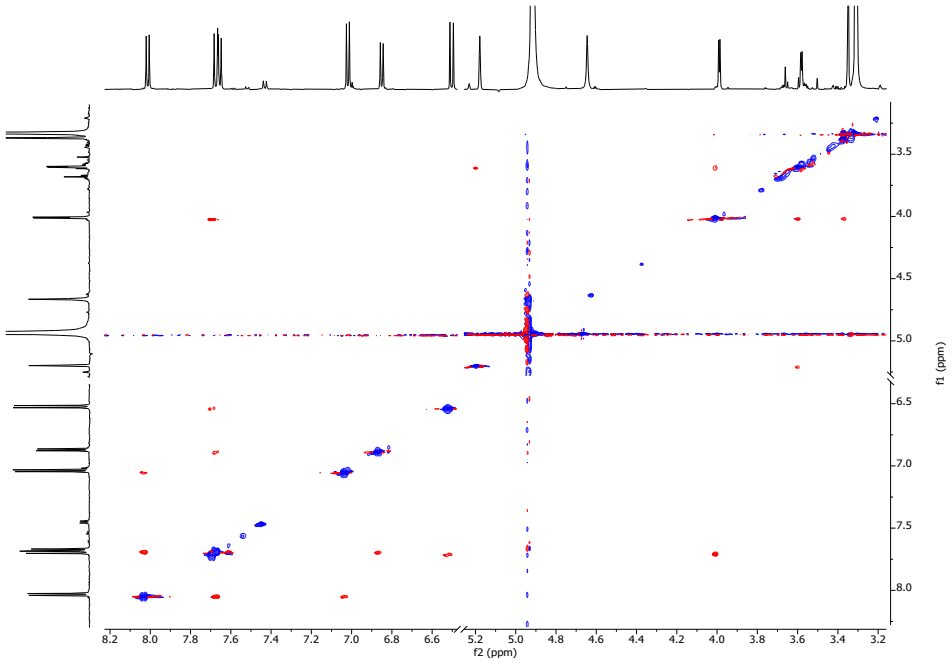

Figure 6 ^{1}H–^{1}H-NOESY (CD_3OD): Compound (+)-**1**.

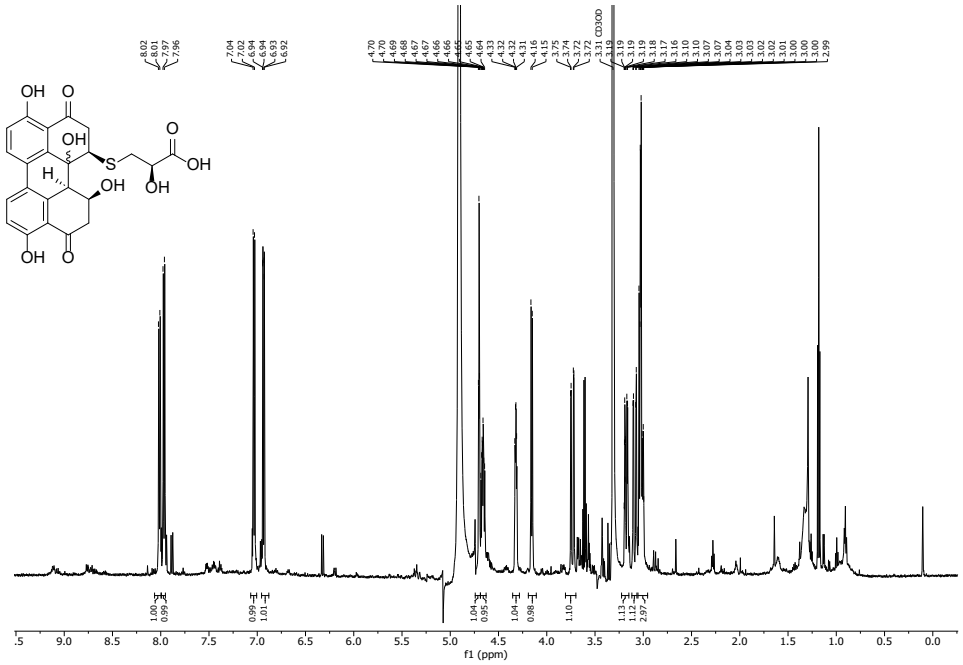

Figure 7 ^{1}H NMR (600 MHz, CD_3OD): Compound **2**.

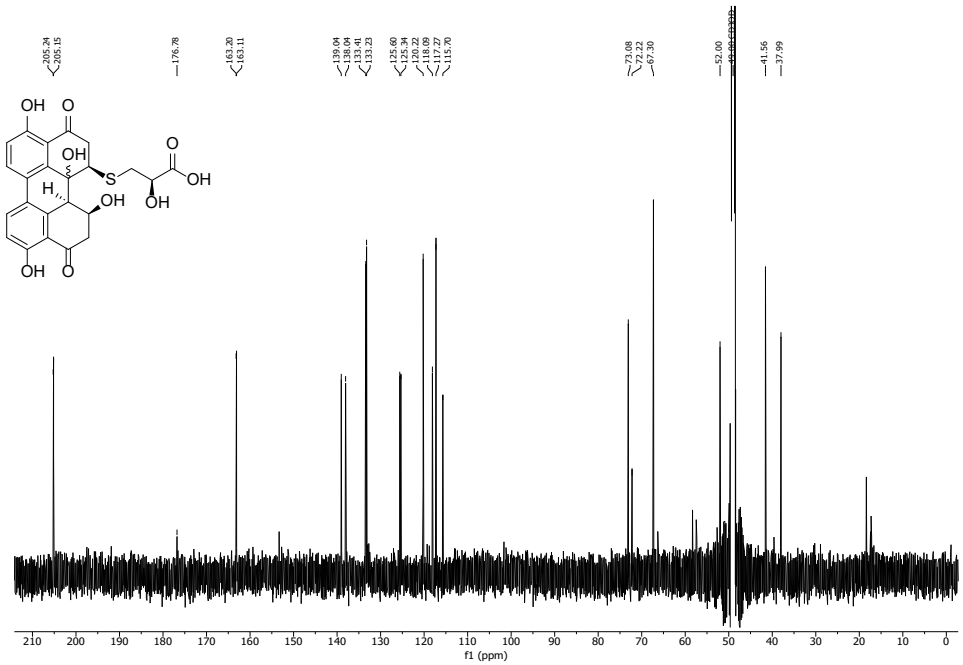

Figure 8 ^{13}C NMR (150 MHz, CD_3OD): Compound **2**.

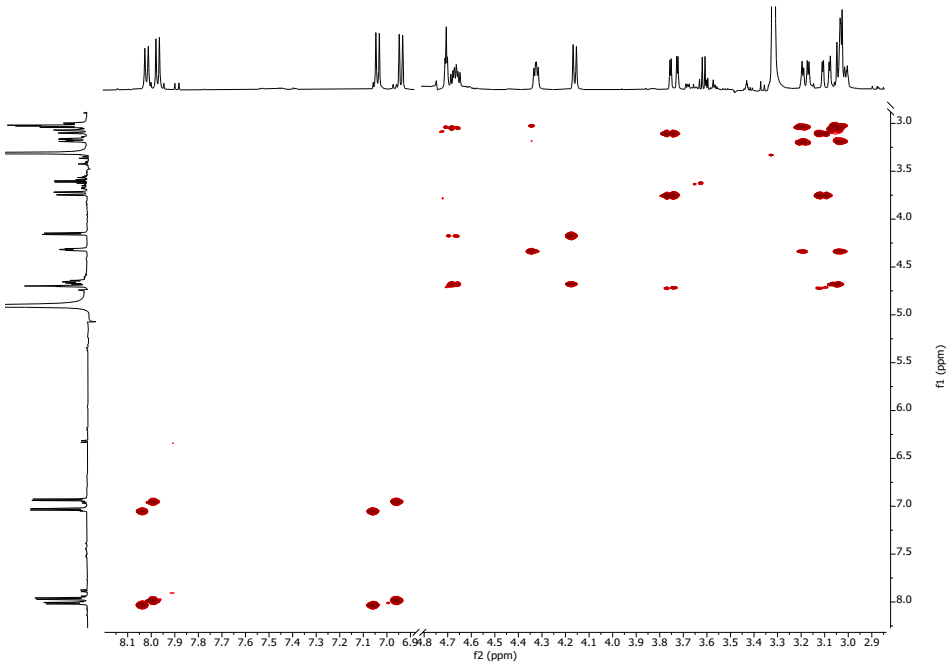

Figure 9 ^{1}H–^{1}H-COSY (CD_3OD): Compound **2**.

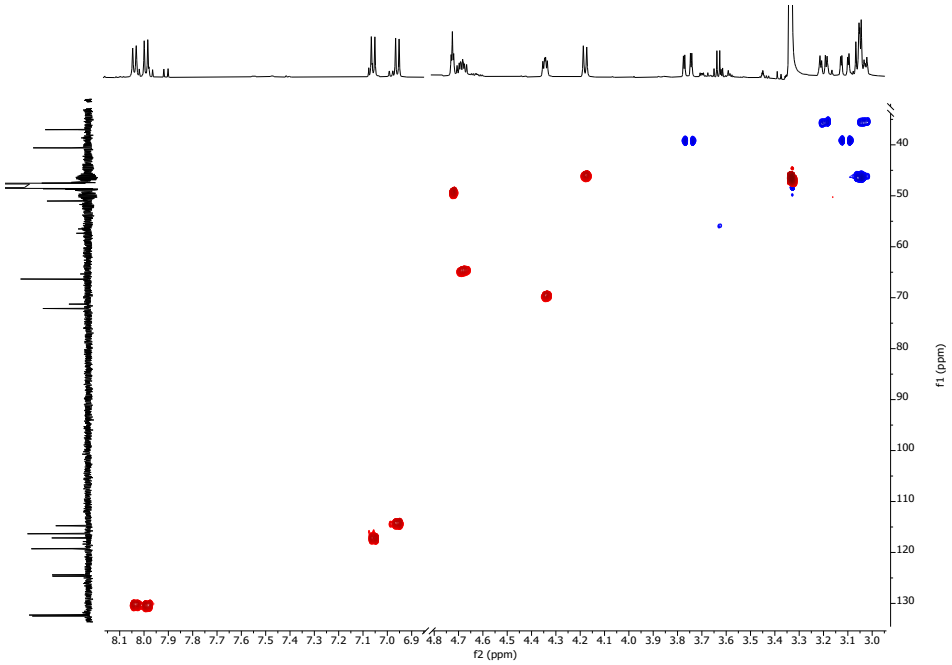

Figure 10 ^{1}H–^{13}C HSQC (CD_3OD): Compound **2**.

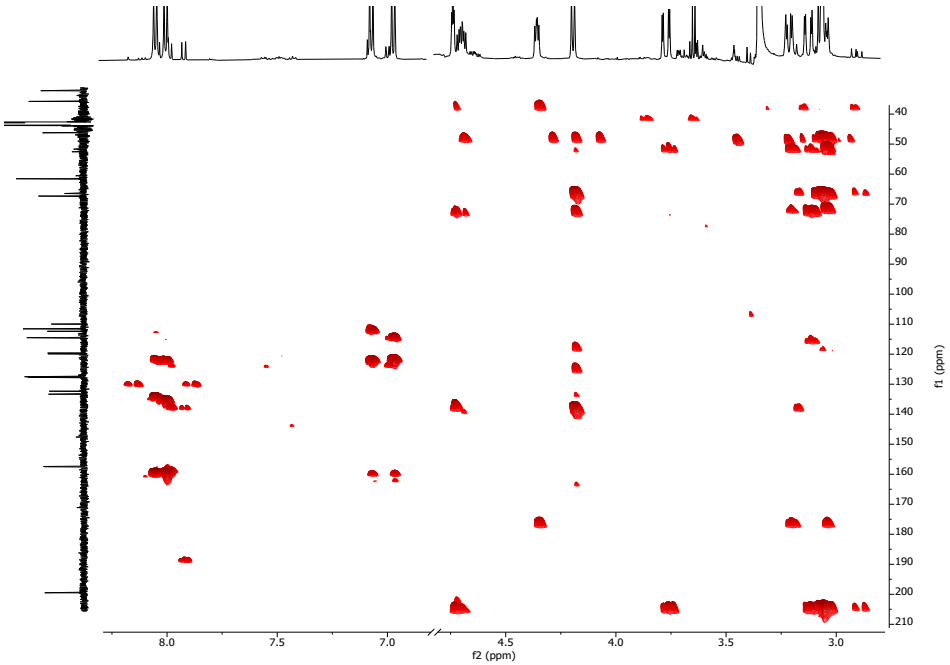

Figure 11 ^{1}H–^{13}C HMBC (CD_3OD): Compound **2**.

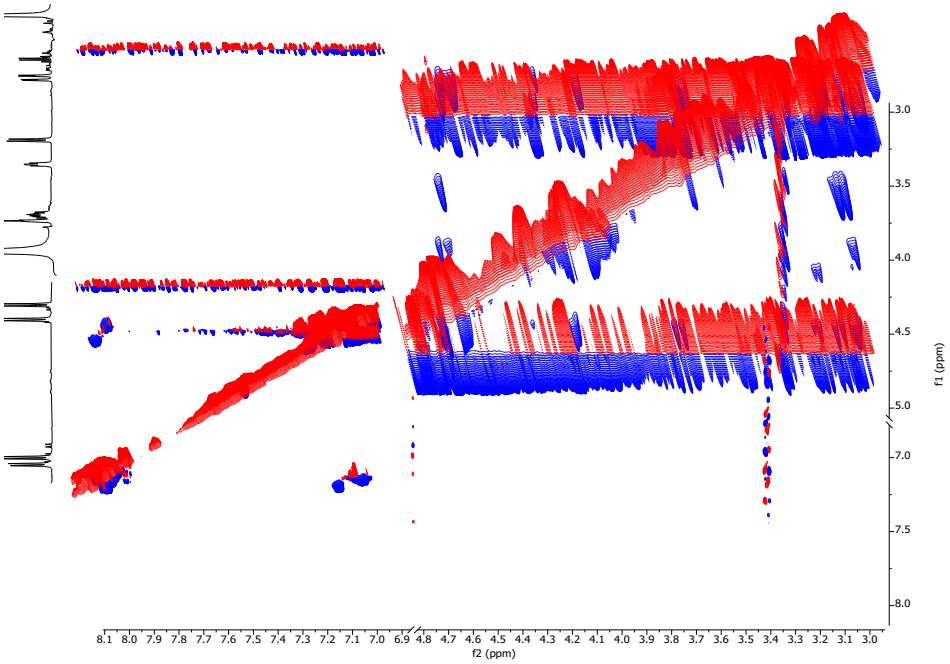

Figure 12 ^{1}H–^{1}H-NOESY (CD_3OD): Compound **2**.

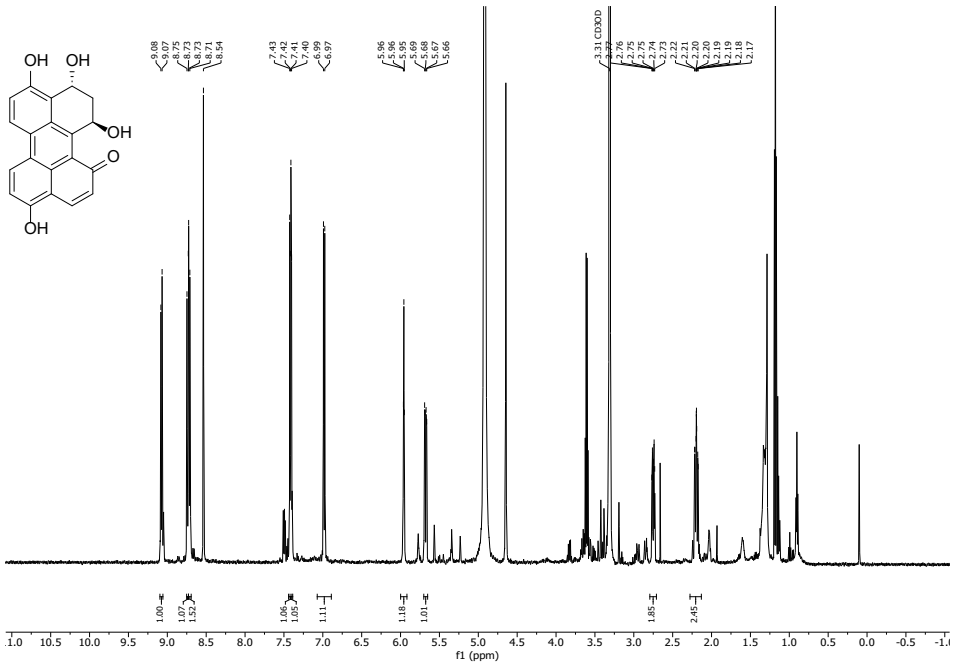

Figure 13 ^{1}H NMR (600 MHz, CD_3OD): Compound (+)-**3**.

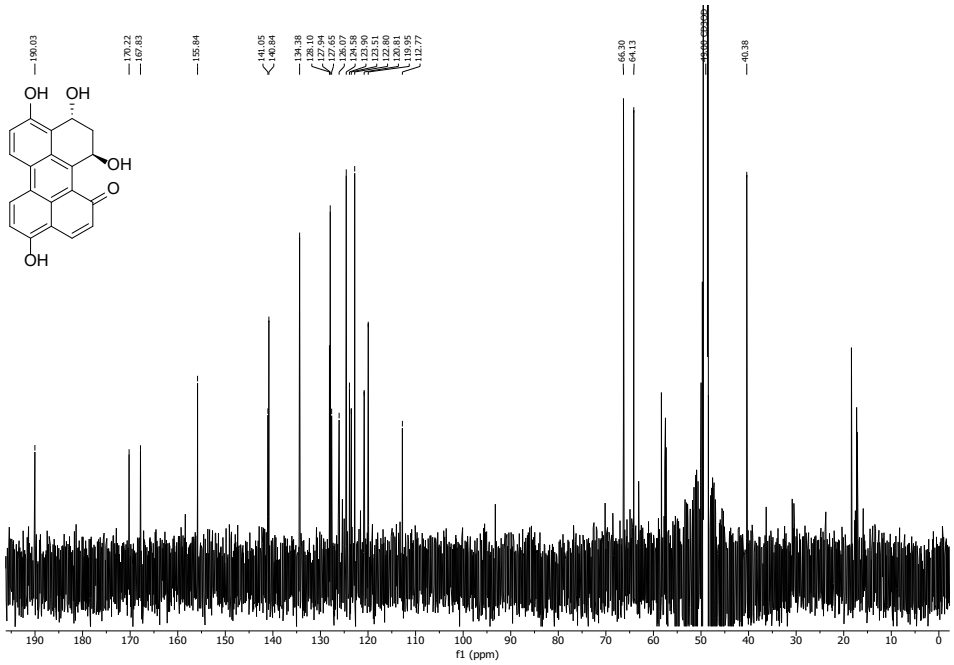

Figure 14 ^{13}C NMR (150 MHz, CD_3OD): Compound (+)-**3**.

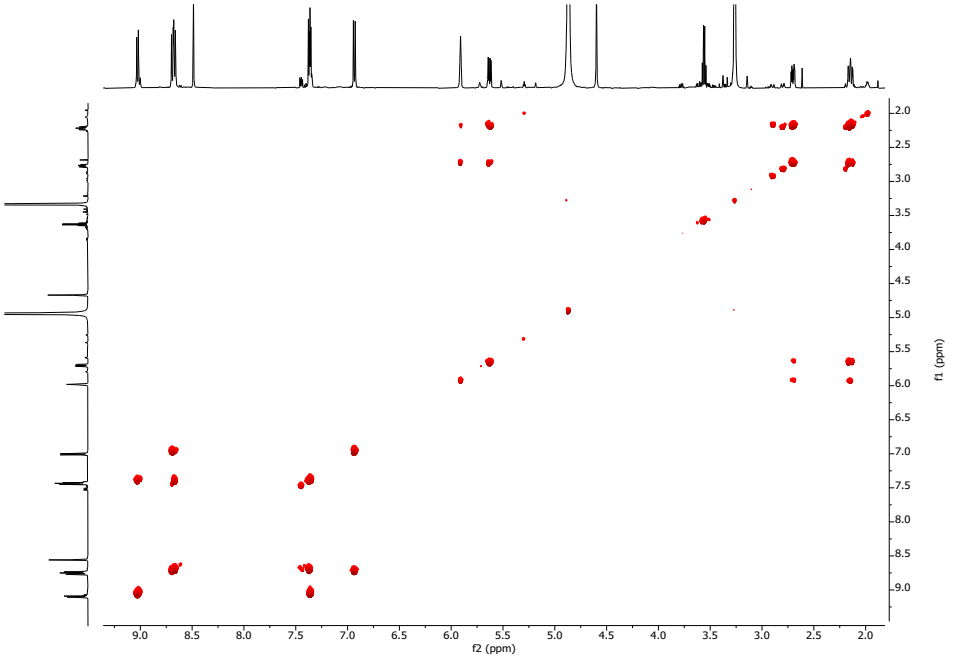

Figure 15 ^{1}H–^{1}H-COSY (CD_3OD): Compound (+)-**3**.

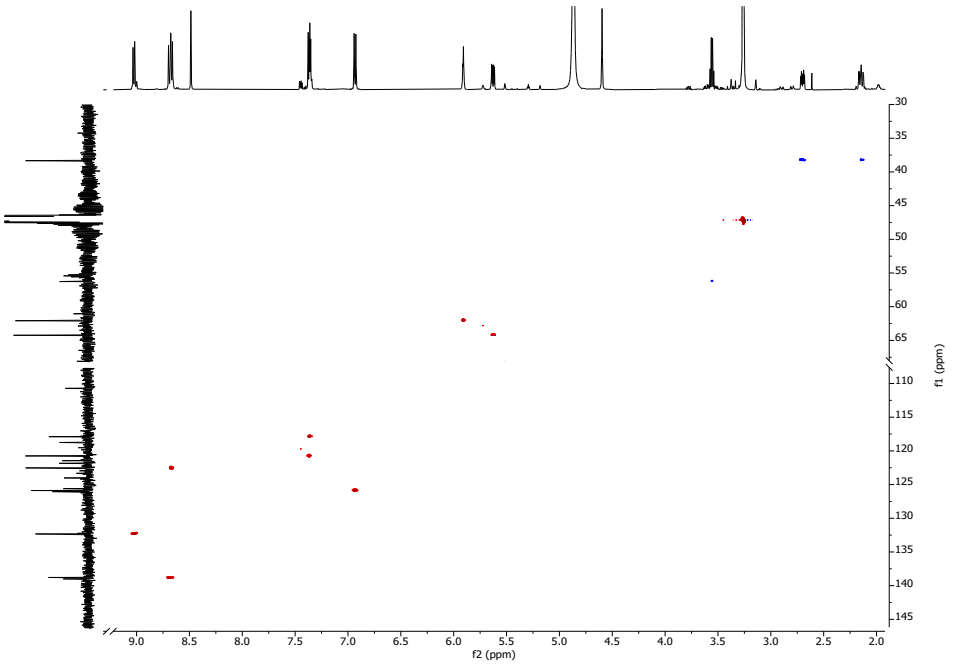

Figure 16 ^{1}H–^{13}C-HSQC (CD_3OD): Compound (+)-**3**.

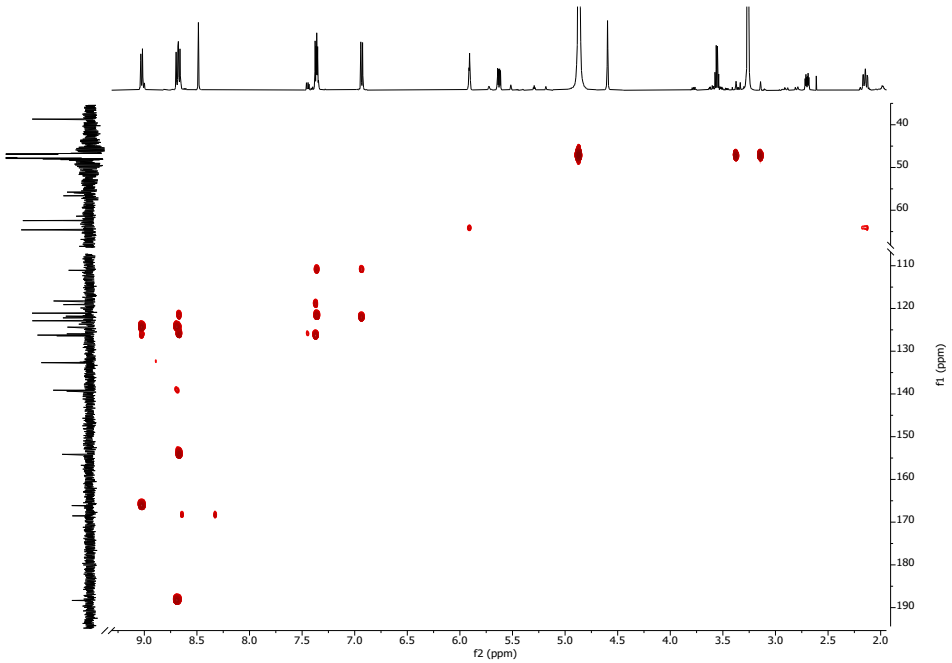

Figure 17 ^{1}H–^{13}C-HMBC (CD_3OD): Compound (+)-**3**.

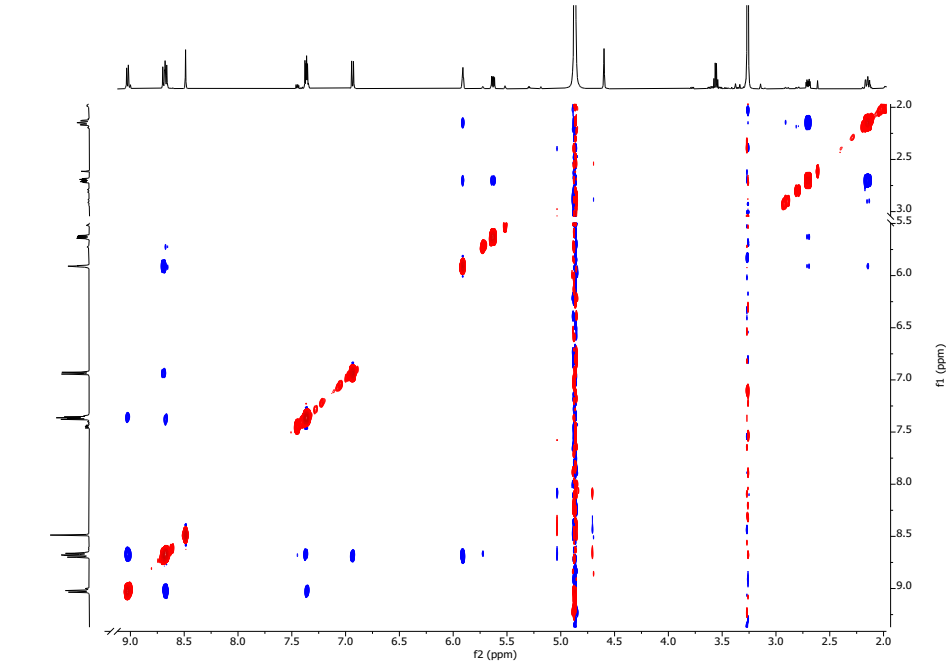

Figure 18 ^{1}H–^{1}H-NOESY (CD_3OD): Compound (+)-**3**.

2. Computational Details

For each compound (+)-**1** and (+)-**3**, a conformational analysis was performed using Spartan '10[1] at a semiempirical level of theory (PM6).[2] Geometry optimizations and frequency calculations at DFT level as well as the calculation of electronic excitations using time-dependent DFT[3] were performed using Gaussian 16, Rev. C.01.[4] Geometry optimization of each conformer was performed with the B3LYP functional,[5-8] the Pople basis set 6-311+G(2d,p)[9-11] and the IEFPCM solvation model[12] for methanol. For the simulation of electronic CD spectra, the electronic excitations were calculated based on the DFT optimized conformers. Based on the calculated values of each conformer, Boltzmann averaged CD spectra were created using SpecDis v1.71.[13] An empirical shift (in the range of -30–30 nm) and an empirical bandwidth (0.1–0.3 eV) were applied for the comparison of simulated with measured data.

The respective xyz coordinate files of the geometry optimized conformers can be found in a separate ZIP file.

Input Lines

Conformer Distribution

```
SEARCHMETHOD=THOROUGH FINDBOATS KEEPALL CONF_SELECTION_RULE=5
```

Geometry Optimization

```
#p opt=tight freq b3lyp 6-311+G(2d,p) scrf=(iefpcm,solvent=methanol)
```

Electronic Excitations

```
#p td=(nstates=60) b3lyp 6-311+G(2d,p) scrf=(iefpcm,solvent=methanol)
```

3. ECD Spectra

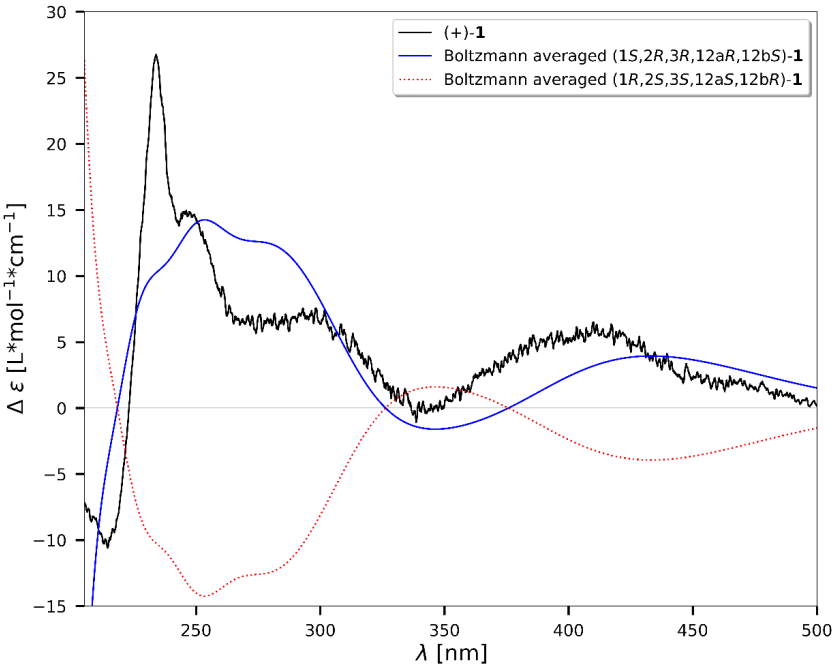

Similarity factor (1*S*,2*R*,3*R*,12a*R*,12b*S*) = 0.843
Similarity factor (1*R*,2*S*,3*S*,12a*S*,12b*R*) = 0.009
Δ (Enantiomeric Similarity Index) = 83.4%

Figure 19 Comparison of the observed (+)-**1** (c = 0.1 mM in MeOH; black) with the Boltzmann averaged calculated CD spectra (1*S*,2*R*,3*R*,12a*R*,12b*S*; 205–500 nm; -8 nm shift; 0.3 eV band width; blue). Similarity factors for both possible enantiomers as well as the resulting Δ(ESI), determined with SpecDis v1.71.[13-15]

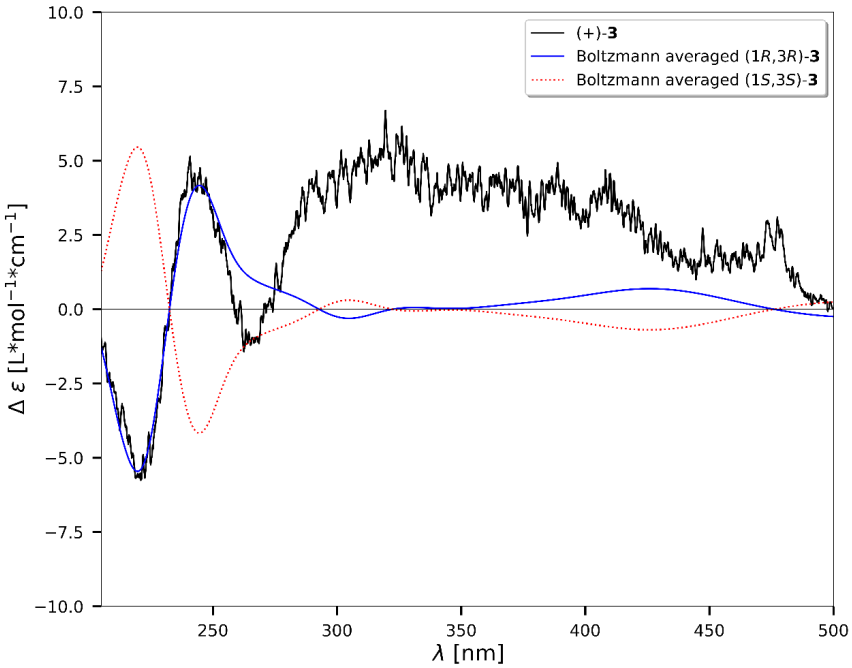

Similarity factor (1*R*,3*R*) =	0.542
Similarity factor (1*S*,3*S*) =	0.025
Δ (Enantiomeric Similarity Index) =	51.7%

Figure 20 Comparison of the observed (+)-**3** (c = 0.1 mM in MeOH; black) with the Boltzmann averaged calculated CD spectra (1*R*,3*R*; 205–500 nm; +21 nm shift; 0.3 eV band width; blue). Similarity factors for both possible enantiomers as well as the resulting Δ(ESI), determined with SpecDis v1.71.[13-15]

4. HPLC Data

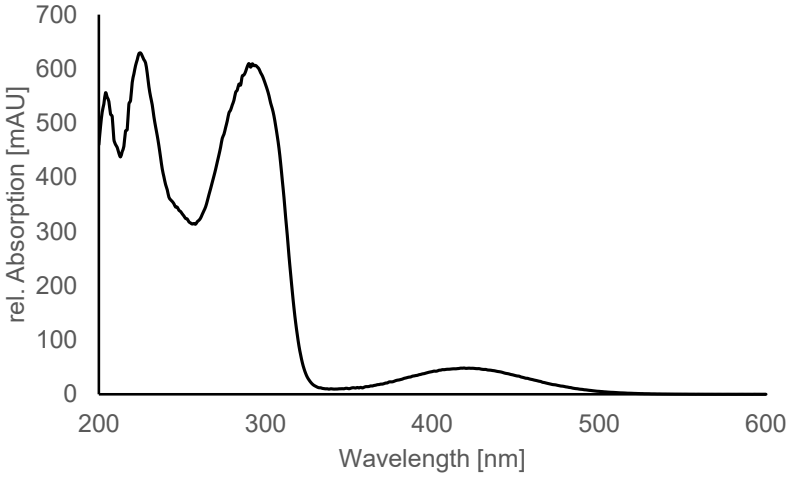

Figure 21 UV-Spectrum of compound (+)-**1**

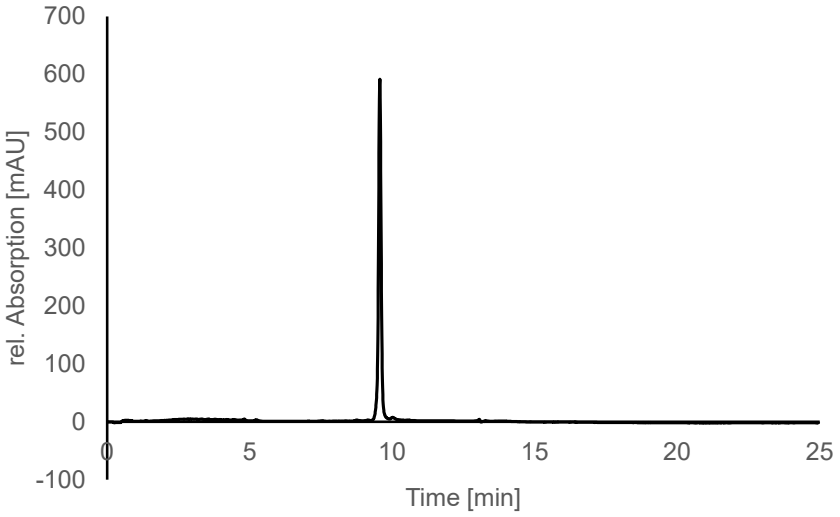

Figure 22 Chromatogram at 300 nm of compound (+)-**1**. Measured with Lichrospher 100 RP18 column (125 x 4 mm, 5 µm, Macherey-Nagel) using water and acetonitrile; Flow 1 mL/min. Starting with 99% water and 1% acetonitrile, to 100 % acetonitrile in 20 minutes. 5 minutes at 100 % acetonitrile.

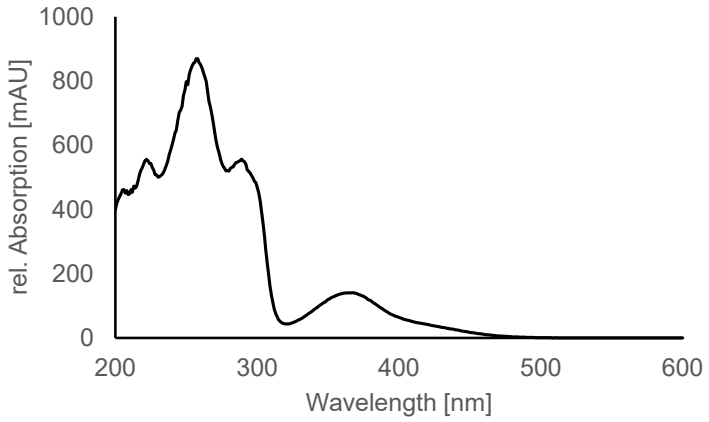

Figure 23 UV-Spectrum of ATX-I

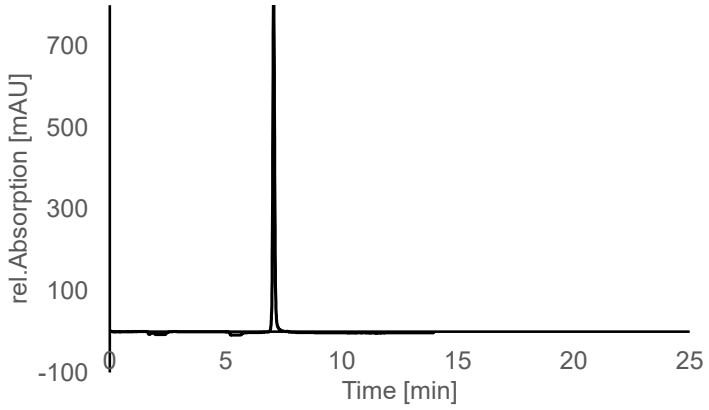

Figure 24 Chromatogram at 300 nm of ATX-I. Measured with Lichrospher 100 RP18 column (125 x 4 mm, 5 µm, Macherey-Nagel) using water and acetonitrile; Flow 1 mL/min. Starting with 99% water and 1% acetonitrile, to 100 % acetonitrile in 20 minutes. 5 minutes at 100 % acetonitrile.

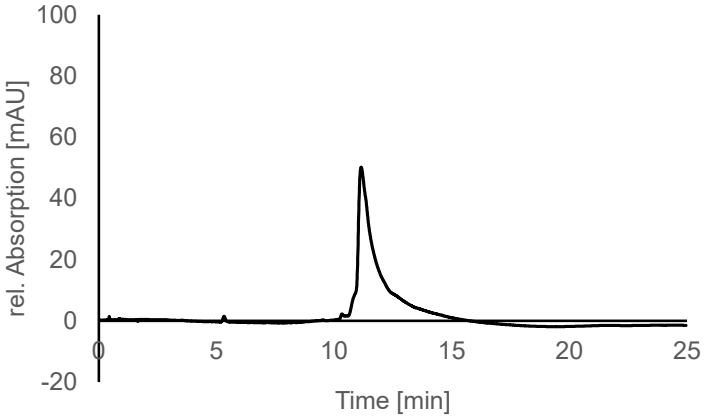

Figure 25 Chromatogram at 300 nm of compound (+)-**3**. Measured with Lichrospher 100 RP18 column (125 x 4 mm, 5 µm, Macherey-Nagel) using water and acetonitrile; Flow 1 mL/min. Starting with 99% water and 1% acetonitrile, to 100 % acetonitrile in 20 minutes. 5 minutes at 100 % acetonitrile.

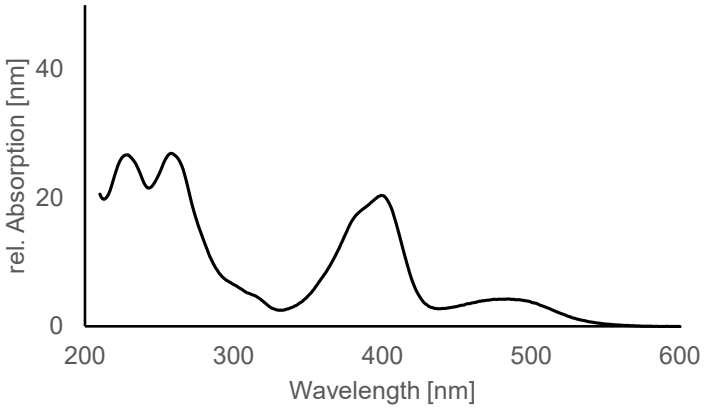

Figure 26 UV-Spectrum of compound (+)-**3**

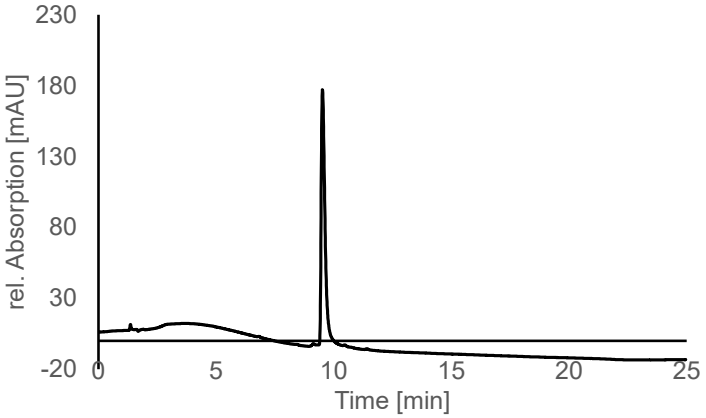

Figure 27 Chromatogram at 300 nm of compound (+)-**2**. Measured with Lichrospher 100 RP18 column (125 x 4 mm, 5 µm, Macherey-Nagel) using water and acetonitrile; Flow 1 mL/min. Starting with 99% water and 1% acetonitrile, to 100 % acetonitrile in 20 minutes. 5 minutes at 100 % acetonitrile.

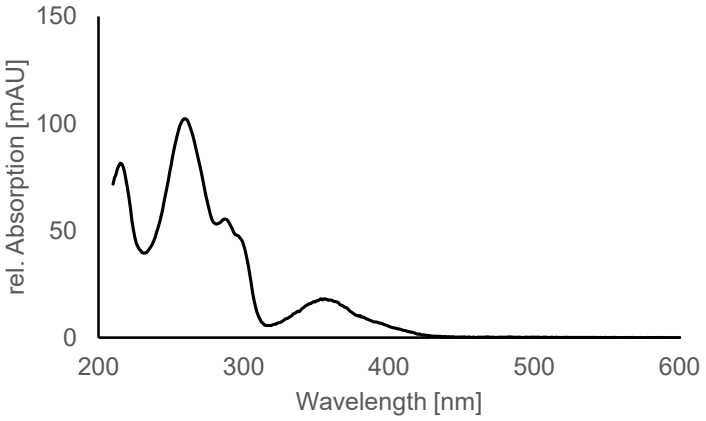

Figure 28 UV-Spectrum of compound (+)-**2**

5. HPLC/MS Data

ATX-I

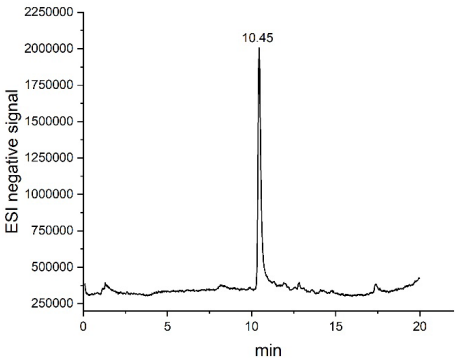

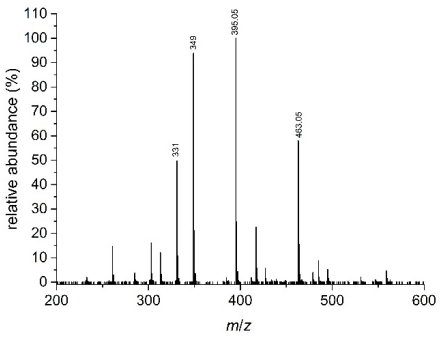

(+)-**1**

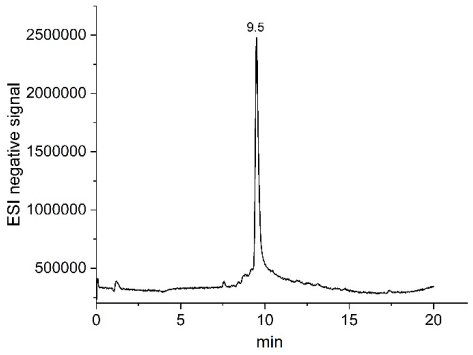

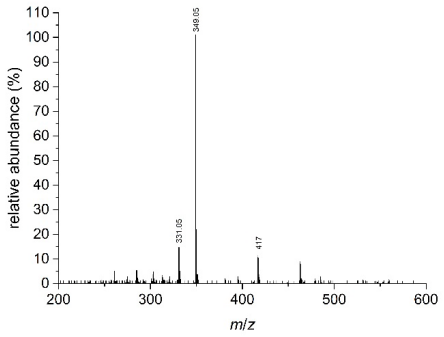

(+)-**2**

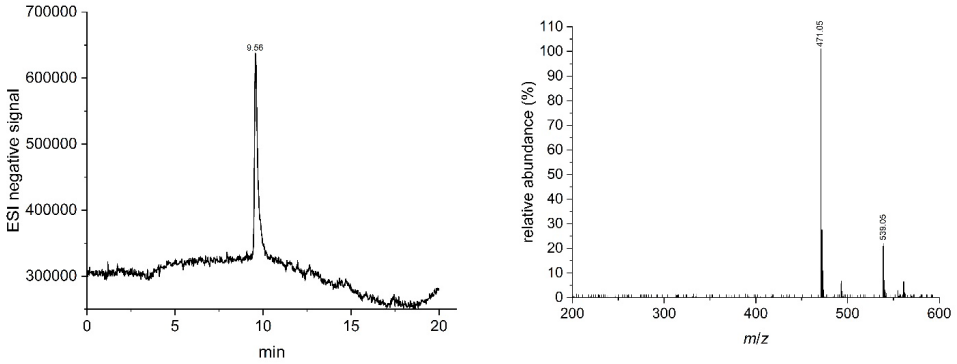

(+)-**3**

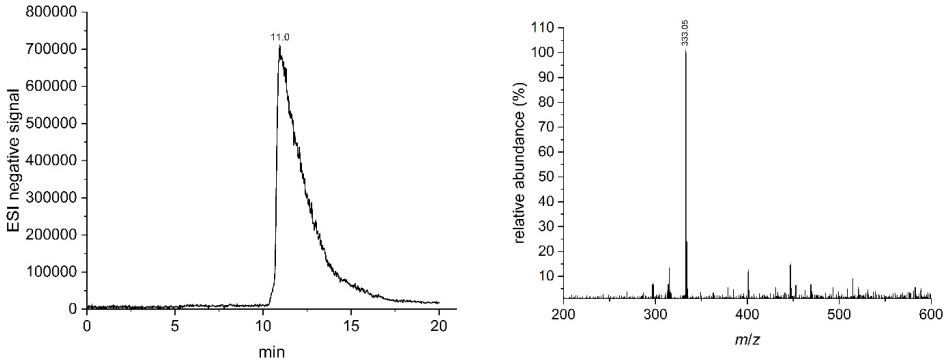

Figure 29 Mass spectra of ATX-I and compounds **1**-**3** obtained using an ESI interface. Analyses of the purified compounds by detection of ESI-negative signal fragments and single-quadrupole mass spectra showing the quasi-molecular ions.

The mass UV spectra were analyzed with a Shimadzu HPLC-LCMS-2020 mass spectrometer fitted with a Superspher RP18 column (125 x 2 mm, 4 µm particle size, Merck).

The chromatographic conditions consisted of a gradient from 1% to 100% acetonitrile in 20 min, and an isocratic step at 100% acetonitrile for 1 min at 40^0C and 10 µl injection volume was used. The flow rate was 0.45 ml/min. The detector voltage was set to 1.1 kV, the interface voltage was set to -3.5 kV in the negative ESI mode, DL-Voltage was set to 1.5 V, Q-Array RF-Voltage was set to 60 V and the evaporator temperature was set to 400°C.

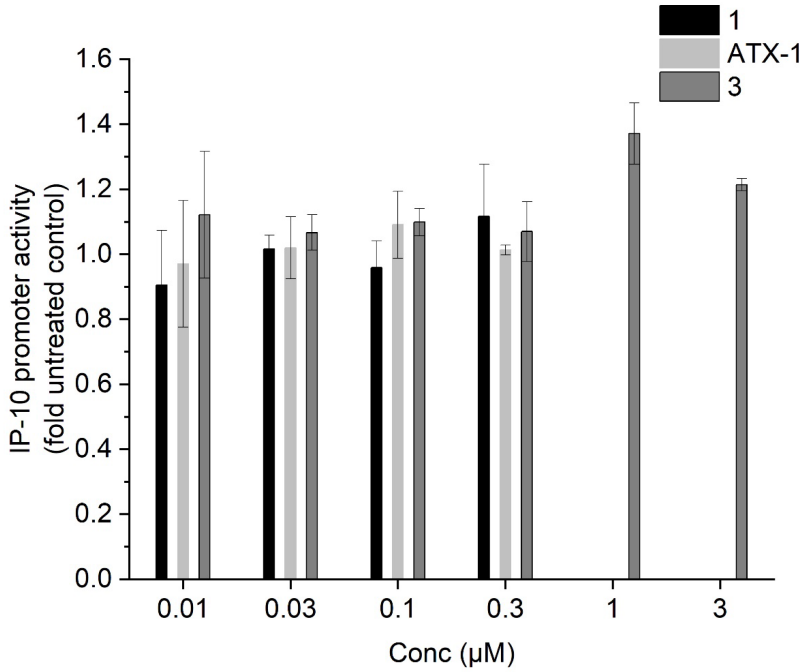

Figure 30 Influence of compounds (+)-**1**, (+)-**3**, and ATX-1 on IP-10 (CXCL-10) promoter activity.

BEAS-2B cells were transiently transfected with a human IP-10-promoter dependent reporter plasmid by electroporation and stimulated with 10 ng/mL TNF-α, 10 ng/mL IFN-γ and 5 ng/mL IL-1β for 24 h with and without test compounds. Control: stimulation only. The expression of the reporter gene was determined as described in the experimental section. Data represent the mean ± SEM of at least three independent experiments.

Sequencing results of the ITS1-5.8S rDNA-ITS2 region of nuclear DNA of the producer strain with ITS4 und ITS5 primer.[16]

Sequenz forward (5'→3'):

ATTACACAATATGAAGGCGGGCTGGACACCCTCCAGCCGGGCACTGCTTCACGGCGTGCGCGGCTGGAGCCGGCC
CTGCTGAATTATTCACCCGTGTCTTTTGCGTACTTCTTGTTTCCTGGGTGGGCTCGCCCGCCATCAGGACCAACC
ATAAACCTTTTTGTAATAGCAATCAGCGTCAGTAACAACGTAATTAATTACAACTTTCAACAACGGATCTCTTGG
TTCTGGCATCGATGAAGAACGCAGCGAAATGCGATACGTAGTGTGAATTGCAGAATTCAGTGAATCATCGAATCT
TTGAACGCACATTGCGCCCTTTGGTATTCCAAAGGGCATGCCTGTTCGAGCGTCATTTGTACCCTCAAGCTTTGC
TTGGTGTTGGGCGTCTTTTGTCTCCAGCTCGCTGGAGACTCGCCTTAAAGTCATTGGCAGCCGGCCTACTGGTTT
CGGAGCGCAGCACAAGTCGCGCTCTTGCCCAGCCAAGGTCAGCGTCCAGCAAGCCTTTTTTCAACCTTTGACCTC
GGATCAGGTAGGGATACCCGCTGAACTTAAGCATATCAA

Sequenz reverse (5'→3'):

```
AAAGGTTGAAAAAAGGCTTGCTGGACGCTGACCTTGGCTGGGCAAGAGCGCGACTTGTGCTGCGCTCCGAAACCA
GTAGGCCGGCTGCCAATGACTTTAAGGCGAGTCTCCAGCGAGCTGGAGACAAAAGACGCCCAACACCAAGCAAAG
CTTGAGGGTACAAATGACGCTCGAACAGGCATGCCCTTTGGAATACCAAAGGGCGCAATGTGCGTTCAAAGATTC
GATGATTCACTGAATTCTGCAATTCACACTACGTATCGCATTTCGCTGCGTTCTTCATCGATGCCAGAACCAAGA
GATCCGTTGTTGAAAGTTGTAATTAATTACGTTGTTACTGACGCTGATTGCTATTACAAAAAGGTTTATGGTTGG
TCCTGATGGCGGGCGAGCCCACCCAGGAAACAAGAAGTACGCAAAAGACACGGGTGAATAATTCAGCAGGGCCGG
CTCCAGCCGCGCACGCCGTGAAGCAGTGCCCGGCTGGAGGGTGTCCAGCCCGCCTTCATATTGTGTAATGATCCC
TCCGCAGGTTCACCTACGGAGACCTTGTTACGC
```

6. References

[1] Wavefunction, Inc., Irvine, CA, USA, **2009**.
[2] J. J. P. Stewart, *J. Mol. Model.* **2007**, *13*, 1173-1213.
[3] E. Runge, E. K. U. Gross, *Physical Review Letters* **1984**, *52*, 997-1000.
[4] M. J. Frisch, G. W. Trucks, H. B. Schlegel, G. E. Scuseria, M. A. Robb, J. R. Cheeseman, G. Scalmani, V. Barone, G. A. Petersson, H. Nakatsuji, X. Li, M. Caricato, A. V. Marenich, J. Bloino, B. G. Janesko, R. Gomperts, B. Mennucci, H. P. Hratchian, J. V. Ortiz, A. F. Izmaylov, J. L. Sonnenberg, Williams, F. Ding, F. Lipparini, F. Egidi, J. Goings, B. Peng, A. Petrone, T. Henderson, D. Ranasinghe, V. G. Zakrzewski, J. Gao, N. Rega, G. Zheng, W. Liang, M. Hada, M. Ehara, K. Toyota, R. Fukuda, J. Hasegawa, M. Ishida, T. Nakajima, Y. Honda, O. Kitao, H. Nakai, T. Vreven, K. Throssell, J. A. Montgomery Jr., J. E. Peralta, F. Ogliaro, M. J. Bearpark, J. J. Heyd, E. N. Brothers, K. N. Kudin, V. N. Staroverov, T. A. Keith, R. Kobayashi, J. Normand, K. Raghavachari, A. P. Rendell, J. C. Burant, S. S. Iyengar, J. Tomasi, M. Cossi, J. M. Millam, M. Klene, C. Adamo, R. Cammi, J. W. Ochterski, R. L. Martin, K. Morokuma, O. Farkas, J. B. Foresman, D. J. Fox, Gaussian 16, Revision C.01, Wallingford, CT, **2019**.
[5] S. H. Vosko, L. Wilk, M. Nusair, *Can. J. Phys.* **1980**, *58*, 1200-1211.
[6] C. Lee, W. Yang, R. G. Parr, *Phys. Rev. B* **1988**, *37*, 785-789.
[7] A. D. Becke, *Int. J. Chem. Phys.* **1993**, *98*, 5648-5652.
[8] A. D. Becke, *Phys. Rev. A* **1988**, *38*, 3098.
[9] M. J. Frisch, J. A. Pople, J. S. Binkley, *Int. J. Chem. Phys.* **1984**, *80*, 3265-3269.
[10] R. Krishnan, J. S. Binkley, R. Seeger, J. A. Pople, *Int. J. Chem. Phys.* **1980**, *72*, 650-654.
[11] T. Clark, J. Chandrasekhar, G. W. Spitznagel, P. V. R. Schleyer, *J. Comput. Chem.* **1983**, *4*, 294-301.
[12] J. Tomasi, B. Mennucci, E. Cancès, *Comput. Theor. Chem* **1999**, *464*, 211-226.
[13] T. Bruhn, A. Schaumlöffel, Y. Hemberger, G. Pescitelli, Berlin, Germany, **2017**.
[14] T. Bruhn, A. Schaumlöffel, Y. Hemberger, G. Bringmann, *Chirality* **2013**, *25*, 243-249.
[15] E. Debie, E. De Gussem, R. K. Dukor, W. Herrebout, L. A. Nafie, P. Bultinck, *ChemPhysChem* **2011**, *12*, 1542-1549.
[16] T. J. White, T. Bruns, S. Lee, J. Taylor, in *PCR Protocols* (Eds.: M. A. Innis, D. H. Gelfand, J. J. Sninsky, T. J. White), Academic Press, San Diego, **1990**, pp. 315-322.

B.3.2 Zusatzmaterial der Publikation zur Bestimmung der absoluten Konfiguration eines Dihydroxanthons

Im Folgenden ist die *supporting information* der Publikation „Anti-inflammatory dihydroxanthones from a *Diaporthe* species“ abgedruckt.[565]

Anti-inflammatory dihydroxanthones from a *Diaporthe* species

Markus Rohr, Anna Maria Kiefer, Ulrich Kauhl, Jonathan Groß, Till Opatz, Gerhard Erkel

Supplementary material

Chiral HPLC Analysis

A chiral HPLC analysis (normal phase, isocratic mode with ethanol:*n*-hexane = 70:30) was performed using Chiralpak ID-3, IE-3, IF-3 columns (Daicel Corporation) as well as an Infinity Lab Poroshell 120 Chiral-V column (Agilent). Due to the limited stability of compound **2** under these conditions, dehydration at C-1/C-2 proceeded (see total chromatograms below). The degradation product (the less polar peak) was identified via LC-MS analysis (Figure S1).

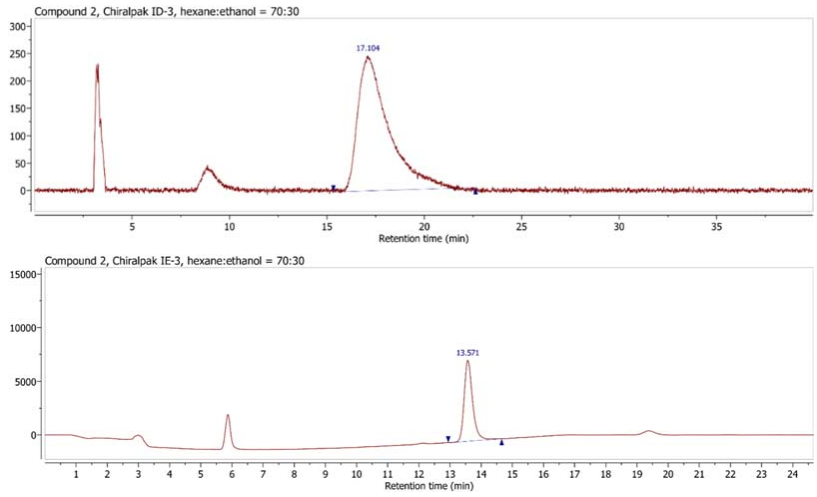

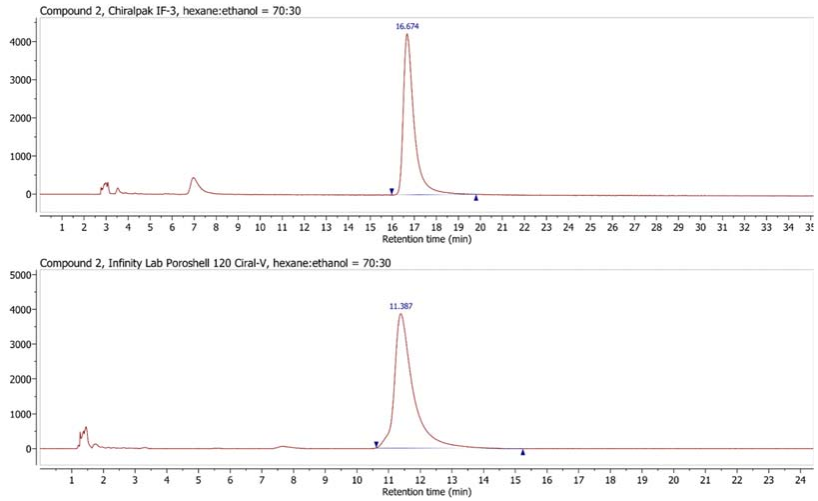

*Figure S1: Total Chromatograms of compound **2** using a Chiralpak ID-3, IE-3, IF-3 column as well as an Infinity Lab Poroshell 120 Chiral-V column in isocratic mode with ethanol:n-hexane = 70:30.*

When a Chiralpak IA-3 column (mobile phase: *n*-hexane:EtOH = 85:15, 1 mL min^{-1}, λ =190-400 nm, 40 °C) was used, chromatograms of compound **2** revealed an additional peak in the trailing flank of the main signal (Figure S2). The signals at 37 min and 40 min retention time showed no difference in their UV spectra and therefore the second signal may corresponded to the enantiomer of compound **2** although this remains uncertain. The depicted chromatograms display the best separation that could be obtained. The tangent skim integration method was used for the determination of the hypothetical *enantiomeric excess* = 76% (*enantiomeric ratio* = 7.3:1). The area percentages are given in Table S1.

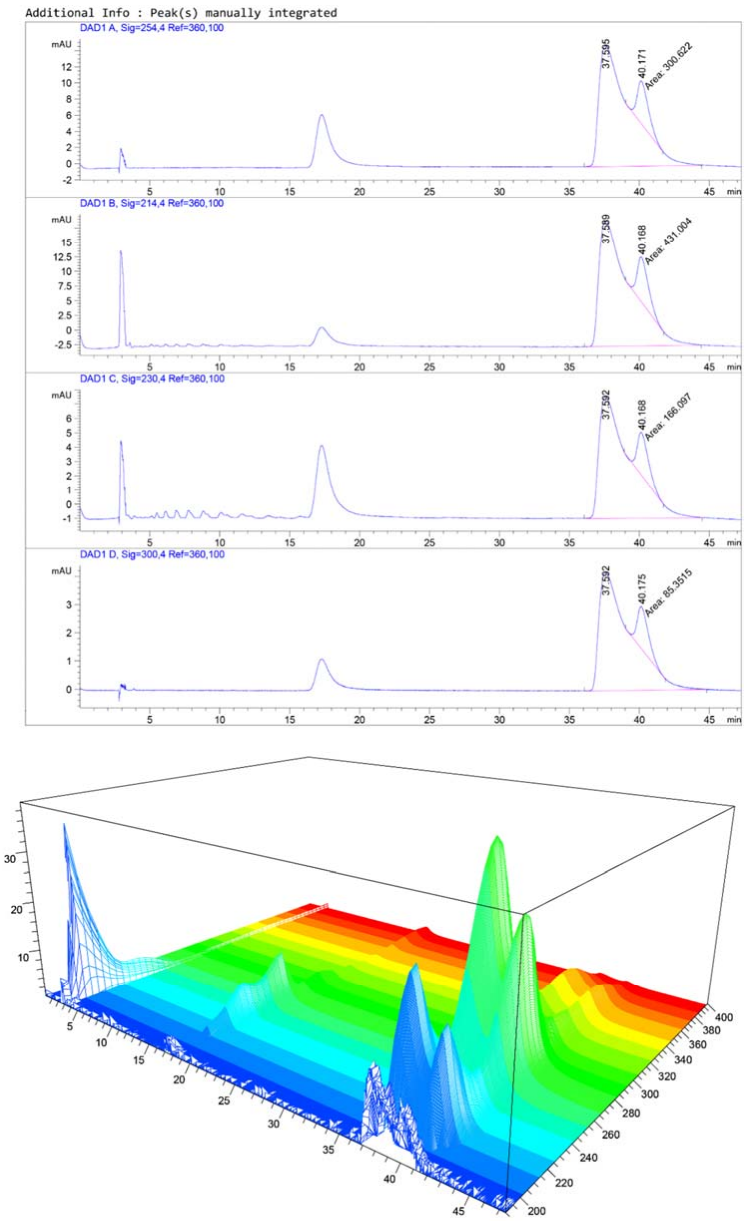

*Figure S2: DAD traces of compound **2** using a Chiralpak IA-3 column in isocratic mode with ethanol:n-hexane = 85:15.*

*Table S1: The area percent report of the respective DAD signals of compound **2**.*

	Peak #	Retention Time [min]	Width [min]	Area [mAU*s]	Height [mAU]	Area %
Signal: 254 nm	1	37.595	2.2924	2333.21509	15.02205	88.5862
	2	40.171	1.0020	300.62195	5.33489	11.4138
Signal: 214 nm	1	37.589	2.5778	3336.38647	21.57160	88.5596
	2	40.168	1.0016	431.00433	7.68469	11.4404
Signal: 230 nm	1	37.592	2.5989	1334.82800	8.56030	88.9337
	2	40.168	0.9246	166.09726	2.99395	11.0663
Signal: 300 nm	1	37.592	2.5828	653.94946	4.21996	88.4551
	2	40.175	0.9428	85.35149	1.50882	11.5449

If compound **2** was indeed a scalemic mixture, the determination of the absolute configuration of the major component would still be valid: Division of the experimental $[\alpha]_D$ of compound **2** ($[\alpha]_D^{29}$ –72.6 (c = 0.2, MeOH)) by the putative enantiomeric excess, the hypothetical optical rotation of the pure enantiomer (–)-**2** can be estimated ($[\alpha_{est.}]_D^{29}$ –95.5 (c = 0.2, MeOH)). The difference of this value and the calculated value of the *RR* enantiomer lies within Stephens' error margin of 57.8 (–46.3 – –95.5 = 49.2), whereas the difference with its antipode is > 57.8 (+46.3 – –95.5 = 141.8). Therefore, the AC of the (–)-enantiomer of compound **2** can be assigned with >95% confidence.

Computational details and input lines for the calculation of chemical shifts and the optical rotation of compound 2.

Conformational analysis was performed using Spartan '10[1] (MMFF level of theory[2]):

SEARCHMETHOD=SPARSE FINDBOATS KEEPALL CONF_SELECTION_RULE=5

All DFT calculations were performed using Gaussian 16, Rev. A.03.[3] Geometry optimizations with the B3LYP functional[4-7], the Pople basis set 6-31G(d)[8, 9] and the IEFPCM solvation model[10] for methanol:

#p opt=tight freq=noraman b3lyp 6-31g(d) scrf=(iefpcm,solvent=methanol)

NMR calculations for the DP4+-method using the mpw1pw91 functional[11] with the 6-311+G(d,p) basis set[12-14]:

#p nmr= giao mpw1pw91 6-311+g(d,p) scrf= (iefpcm,solvent=methanol)

NMR calculations for the *J*-DP4-method:

#p nmr=(giao,spinspin) b3lyp/6-31g(d,p)

Calculation of the optical rotation using the optrot method[15, 16]and the Dunning basis set aug-cc-pVTZ[17, 18]:

#p temperature=302.15 polar=optrot cphf=rdfreq b3lyp/aug-cc-pVTZ scrf=(iefpcm,solvent=methanol)

Table S2: DP4+-probabilities for the *RR* and the *RS* configuration of compound **2**.

		RR	*RS*
*s*DP4+	(H data)	0.96%	99.04%
*s*DP4+	(C data)	99.86%	0.14%
*s*DP4+	(all data)	87.14%	12.86%
*u*DP4+	(H data)	60.20%	39.80%
*u*DP4+	(C data)	99.93%	0.07%
*u*DP4+	(all data)	99.95%	0.05%
DP4+	(H data)	1.45%	98.55%
DP4+	(C data)	100.00%	0.00%
DP4+	**(all data)**	**99.99%**	**0.01%**

Table S3: *J*-DP4-probabilities for the *RR* and the *RS* configuration of compound **2**.

	RR	*RS*
H	0.24%	99.76%
C	5.45%	94.55%
H+C	0.01%	99.99%
J	62.20%	37.80%
all data	**0.02%**	**99.98%**

References

[1] Wavefunction, Inc., Irvine, CA, USA, **2009**.
[2] T. A. Halgren, *J. Comput. Chem.* **1996**, *17*, 490–519.
[3] M. J. Frisch, G. W. Trucks, H. B. Schlegel, G. E. Scuseria, M. A. Robb, J. R. Cheeseman, G. Scalmani, V. Barone, G. A. Petersson, H. Nakatsuji, X. Li, M. Caricato, A. V. Marenich, J. Bloino, B. G. Janesko, R. Gomperts, B. Mennucci, H. P. Hratchian, J. V. Ortiz, A. F. Izmaylov, J. L. Sonnenberg, Williams, F. Ding, F. Lipparini, F. Egidi, J. Goings, B. Peng, A. Petrone, T. Henderson, D. Ranasinghe, V. G. Zakrzewski, J. Gao, N. Rega, G. Zheng, W. Liang, M. Hada, M. Ehara, K. Toyota, R. Fukuda, J. Hasegawa, M. Ishida, T. Nakajima, Y. Honda, O. Kitao, H. Nakai, T. Vreven, K. Throssell, J. A. Montgomery Jr., J. E. Peralta, F. Ogliaro, M. J. Bearpark, J. J. Heyd, E. N. Brothers, K. N. Kudin, V. N. Staroverov, T. A. Keith, R. Kobayashi, J. Normand, K. Raghavachari, A. P. Rendell, J. C. Burant, S. S. Iyengar, J. Tomasi, M. Cossi, J. M. Millam, M. Klene, C. Adamo, R. Cammi, J. W. Ochterski, R. L. Martin, K. Morokuma, O. Farkas, J. B. Foresman, D. J. Fox, Wallingford, CT, **2016**.

[4] S. H. Vosko, L. Wilk, M. Nusair, *Can. J. Phys.* **1980**, *58*, 1200–1211.
[5] C. Lee, W. Yang, R. G. Parr, *Phys. Rev. B* **1988**, *37*, 785–789.
[6] A. D. Becke, *Int. J. Chem. Phys.* **1993**, *98*, 5648–5652.
[7] A. D. Becke, *Phys. Rev. A* **1988**, *38*, 3098.
[8] P. C. Hariharan, J. A. Pople, *Theor. Chim. Acta* **1973**, *28*, 213–222.
[9] W. J. Hehre, R. Ditchfield, J. A. Pople, *J. Chem. Phys.* **1972**, *56*, 2257–2261.
[10] J. Tomasi, B. Mennucci, E. Cancès, *Comput. Theor. Chem* **1999**, *464*, 211–226.
[11] C. Adamo, V. Barone, *Int. J. Chem. Phys.* **1998**, *108*, 664–675.
[12] M. J. Frisch, J. A. Pople, J. S. Binkley, *Int. J. Chem. Phys.* **1984**, *80*, 3265–3269.
[13] R. Krishnan, J. S. Binkley, R. Seeger, J. A. Pople, *Int. J. Chem. Phys.* **1980**, *72*, 650–654.
[14] T. Clark, J. Chandrasekhar, G. W. Spitznagel, P. V. R. Schleyer, *J. Comput. Chem.* **1983**, *4*, 294–301.
[15] P. J. Stephens, F. J. Devlin, J. R. Cheeseman, M. J. Frisch, *J. Phys. Chem. A* **2001**, *105*, 5356–5371.
[16] B. Mennucci, J. Tomasi, R. Cammi, J. R. Cheeseman, M. J. Frisch, F. J. Devlin, S. Gabriel, P. J. Stephens, *J. Phys. Chem. A* **2002**, *106*, 6102–6113.
[17] T. H. Dunning, *Int. J. Chem. Phys.* **1989**, *90*, 1007–1023.
[18] R. A. Kendall, T. H. Dunning Jr., R. J. Harrison, *Int. J. Chem. Phys.* **1992**, *96*, 6796–6806.

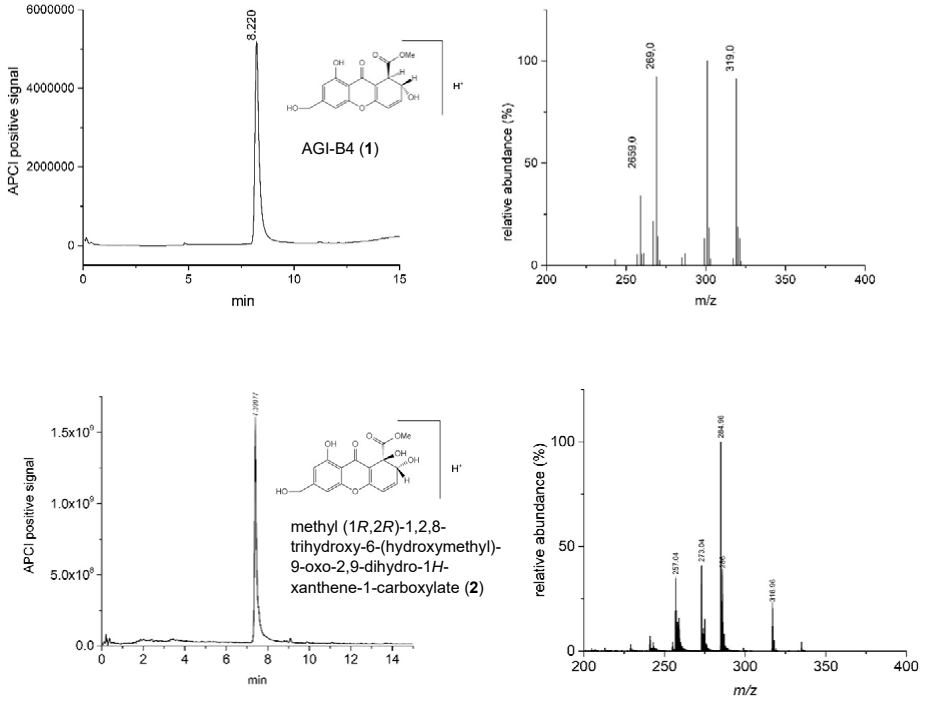

Mass spectra of AGI-B4 (**1**) and methyl (1*R*,2*R*)-1,2,8-trihydroxy-6-(hydroxymethyl)-9-oxo-2,9-dihydro-1*H*-xanthene-1-carboxylate (**2**) obtained using an atmospheric pressure chemical ionization interface. Analyses of the purified compounds by detection of APCI-positive signal fragments and single-quadrupole mass spectrum showing the quasi-molecular ions.

The mass and UV spectra were analyzed with a Hewlett-Packard Series 1100LC-instrument coupled to an AB Sciex 4000 QT mass spectrometer fitted with a Superspher RP18 column (125 x 2 mm, 4 µm particle size, Merck). The chromatographic conditions consisted of a gradient from 1% to 100% acetonitrile in 20 min, and an isocratic step at 100% acetonitrile for 1 min at 40^{0}C and 10 µl injection volume was used. The flow rate was 0.45 ml/min. The fragmentor voltage was set to 90 V, the collision energy was set to 10 V in the positive APCI mode and the evaporator

temperature was set to 400°C. The purity of the isolated compounds was analyzed by HPLC-DAD/MS using the conditions described above. The purity of the compounds was greater than 98.5% as determined by HPLC equipped with diode-array detection and mass spectrometry analysis.

Supplement Rohr et al.

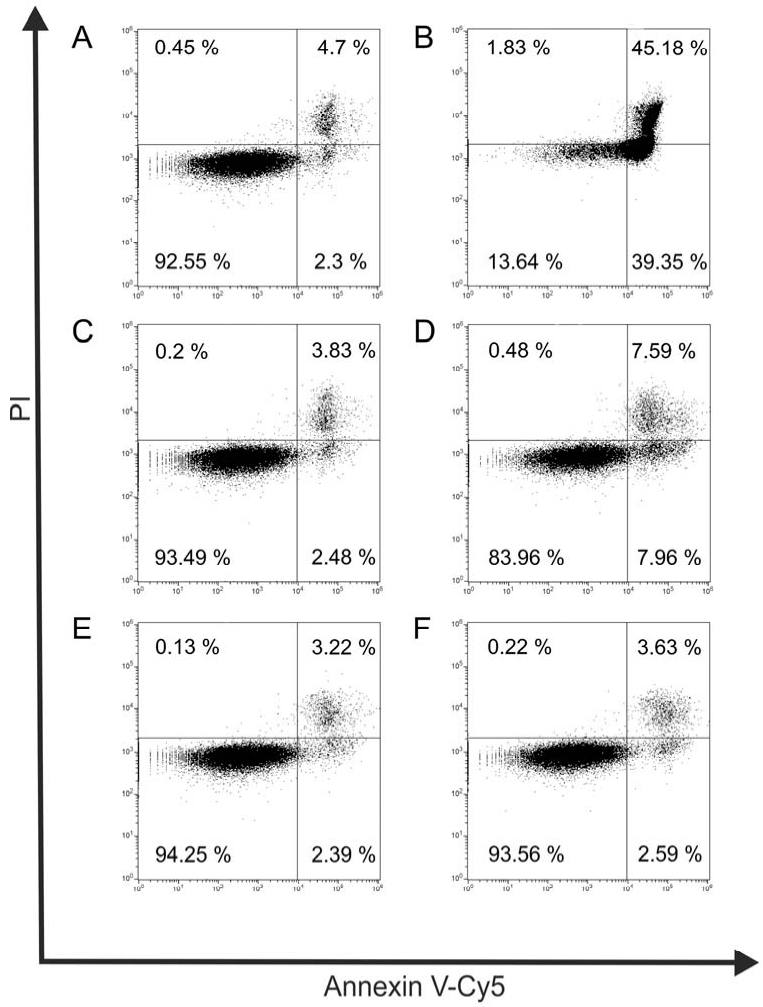

Effect of compound **1**, **2** and H_2O_2 on induction of necrosis and apoptosis in MonoMac6 cells. 2 x 10^6 cells were left untreated (**A**), incubated for 2 hours with 500 µM H_2O_2 (**B**) or incubated with various concentrations auf compound **1** and **2** for 24 hours. **C:** 6.26 µM **1**; **D:** 12.52 µM **1**; **E:** 3 µM **2**; **F:** 6 µM **2**. Analysis of viable cells was done using Annexin V-Cy5/PI staining by flow cytometry as described in Materials and methods. The data shown is representative of 3 independent experiments.

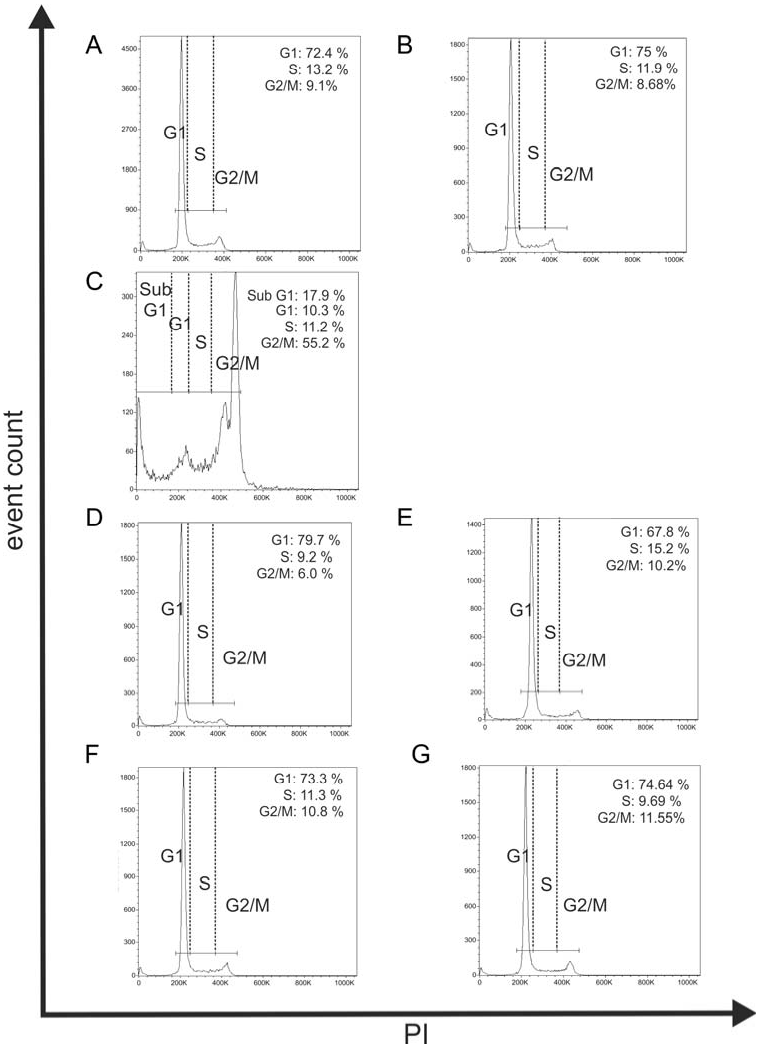

Cell cycle analysis of MonoMac6 cells treated with taxol and different concentrations of compound **1** and **2**. As a control we used untreated cells (**A**) and cells with 4 µl DMSO added (**B**). **C:** 0.5 µg/ml Taxol; **D**: 6.26 µM **1**; **E:** 12.52 µM **1**; **F:** 3 µM **2**; **G:** 6 µM **2.** Analysis was done after RNA digestion with PI staining. The data shown are representative for three independent experiments.

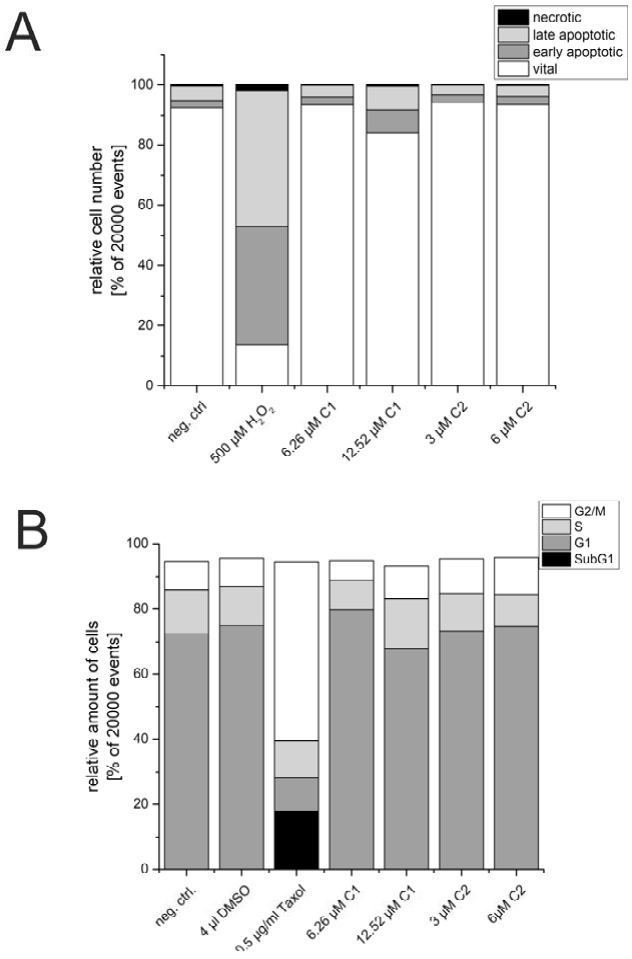

A: Annexin V PI staining of MonoMac6 cells. **B:** Cell cycle analysis of MonoMac6 cells after treatment with compound **1** or **2**.

B.3.3 Zusatzmaterial der Publikation zur Bestimmung der relativen Konfiguration eines Sesquiterpenlactons

Im Folgenden ist die *supporting information* der Publikation „Sesquiterpene Lactones from *Vernonia tufnelliae*: Structural Features, Stereochemistry, and Biological Evaluation“ abgedruckt.[567]

SUPPLEMENTARY INFORMATION

Sesquiterpene Lactones from *Vernonia tufnelliae*: Structural Characterization and Biological Evaluation

Gabin Thierry M. Bitchagno,[*,†,‡] Anja Schüffler, Jonathan Gross, Matthias Krumb, Pierre Tane,[#] and Till Opatz[*,†]

[†]*Department of Chemistry, Johannes Gutenberg-University of Mainz, Duesbergweg 10-14, D-55128 Mainz, Germany*

[‡]*Department of Chemistry, University of Dschang, P.O. Box 67, Dschang, Cameroon*

[§]*Institut für Biotechnologie und Wirkstoff-Forschung gGmbH (IBWF), Hanns-Dieter-Hüsch-Weg 17, 55128 Mainz, Germany*

[#]*Deceased*

TABLE OF CONTENTS

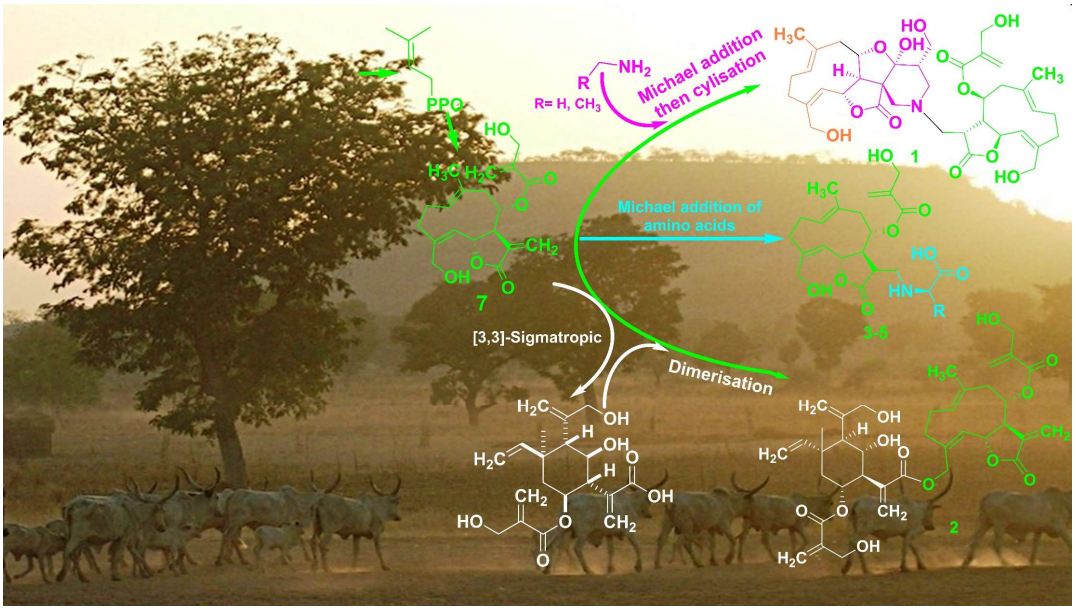

Scheme S1. Completed graphical abstract. General thoughts to the biosynthesis of compounds **1-5**

Page **6** sur **36**

Data File	1011138.d	**Sample Name**	VC-D4-2-p4
Sample Type	Sample	**Position**	P1a10
Instrument Name	Instrument 1	**User Name**	
Acq Method	ESI_pos_ACN_above1000.m	**Acquired Time**	7/26/2019 8:39:33 AM (UTC+02:00)
IRM Calibration Status	Success	**DA Method**	Report_standard.m
Comment	Bitchagno, Opatz		
Sample Group		**Info.**	
Stream Name	LC 1	**Acquisition Time (Local)**	7/26/2019 8:39:33 AM (UTC+02:00)
Acquisition SW Version	6200 series TOF/6500 series Q-TOF B.08.00 (B8058.0)	**QTOF Driver Version**	8.00.00
QTOF Firmware Version	20.698	**Tune Mass Range Max.**	3200

Spectra

Fragmentor Voltage	Collision Energy	Ionization Mode
50	0	ESI

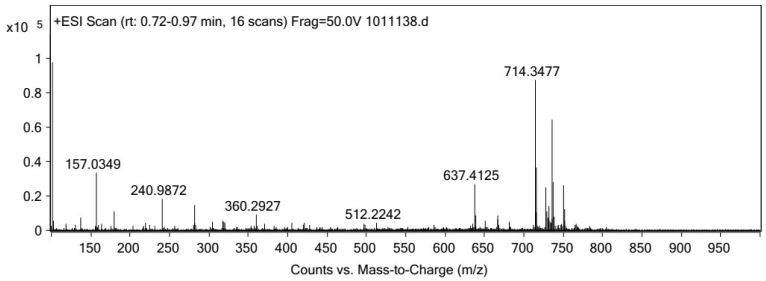

Figure S1. HR-ESI mass spectrum of **1**

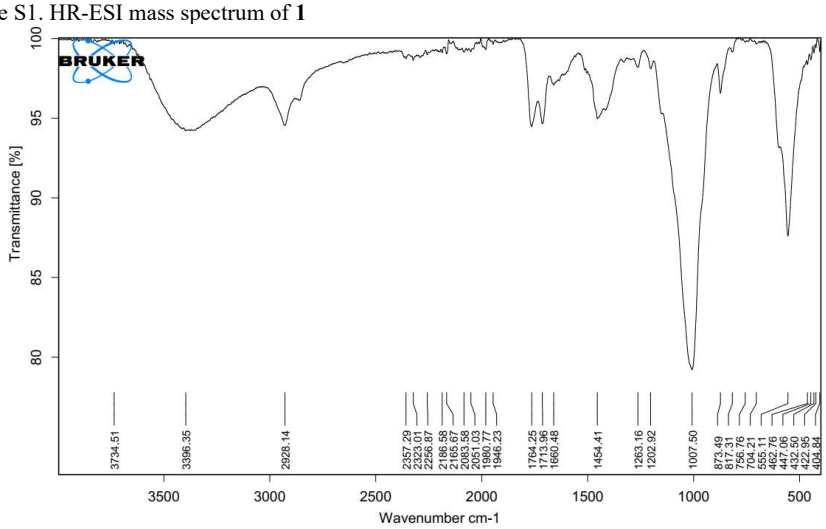

Figure S2. IR spectrum of **1**

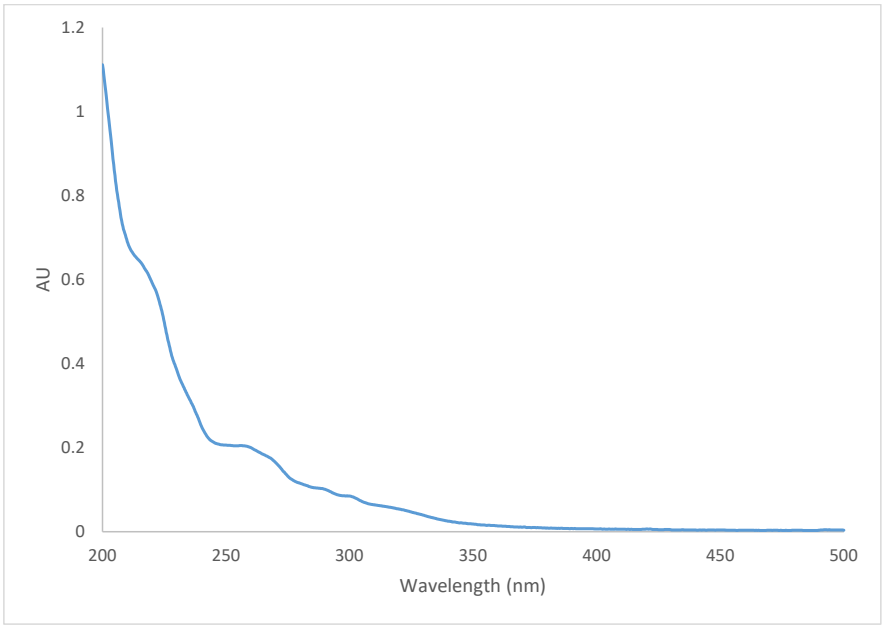

Figure S3. UV spectrum of **1** in acetonitrile

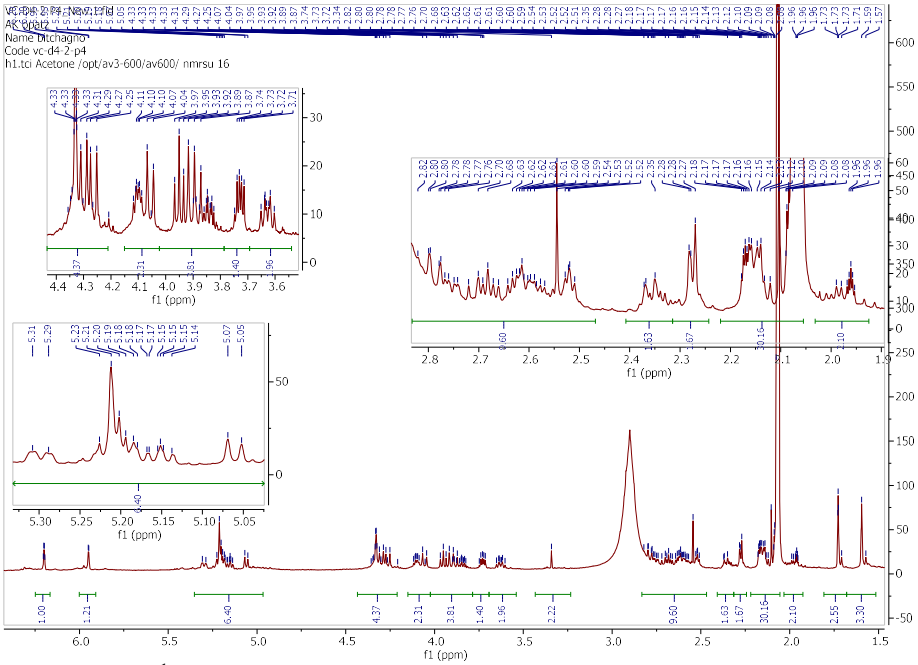

Figure S4. Full ^{1}H NMR spectrum (Acetone-d_6, 600 MHz) of **1**

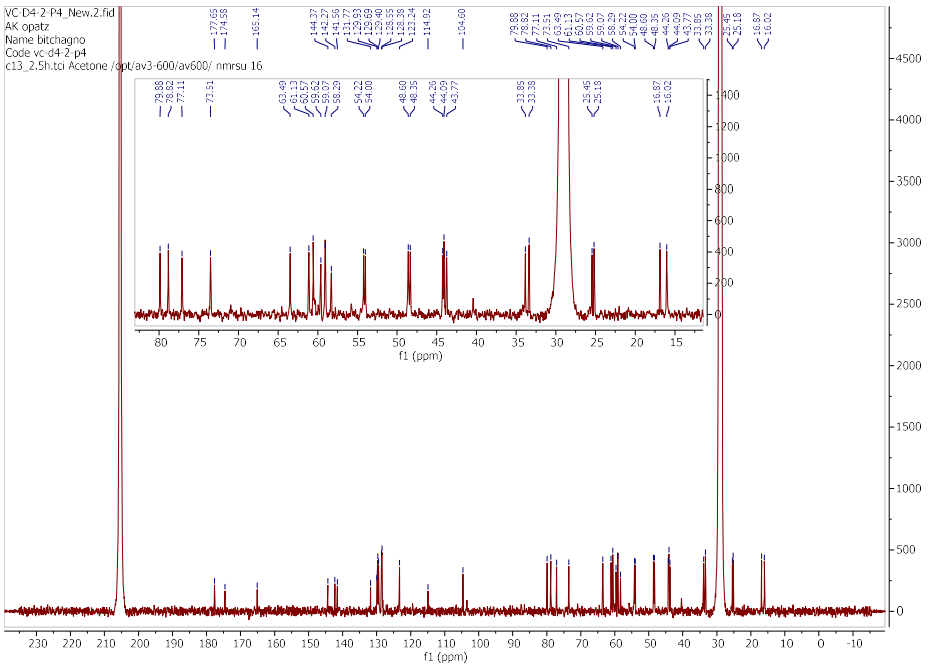

Figure S5. Full ^{13}C NMR spectrum (Acetone-d_6, 150 MHz) of **1**

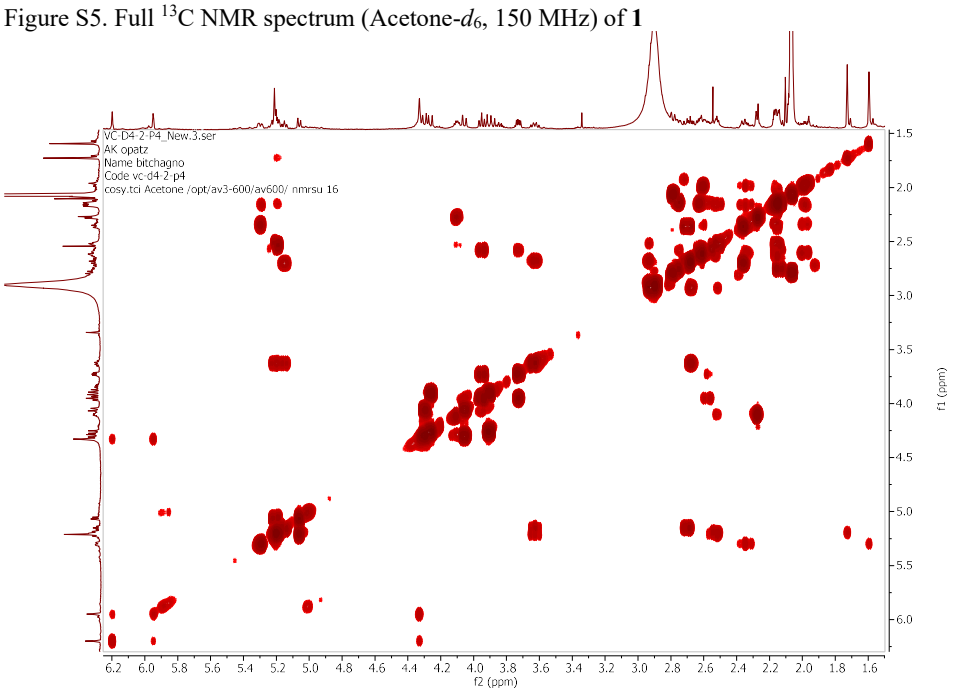

Figure S6. Full ^{1}H-^{1}H COSY spectrum of **1**

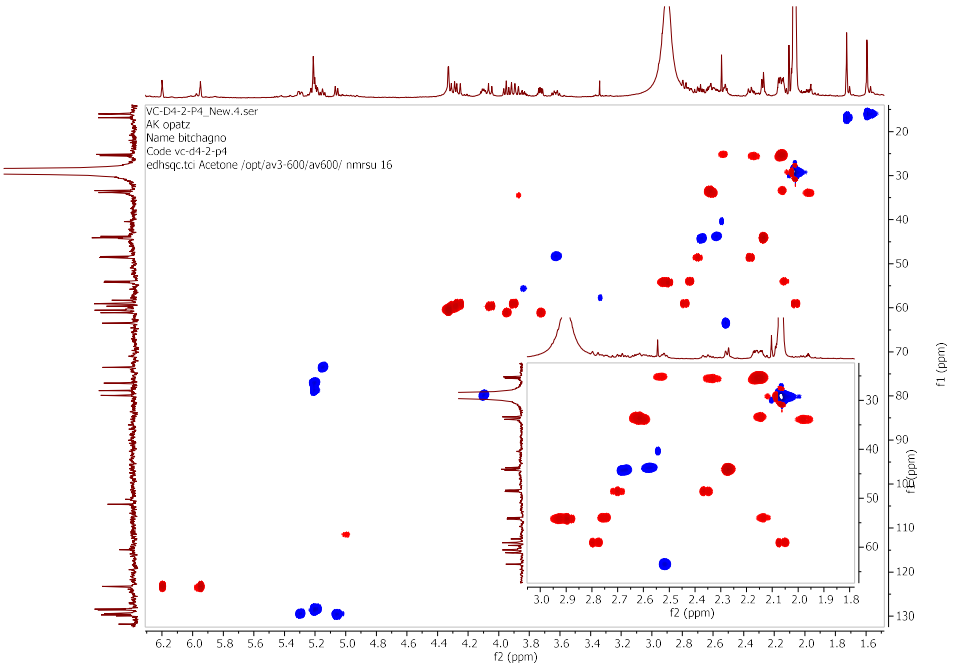

Figure S7. Full HSQC spectrum of **1**

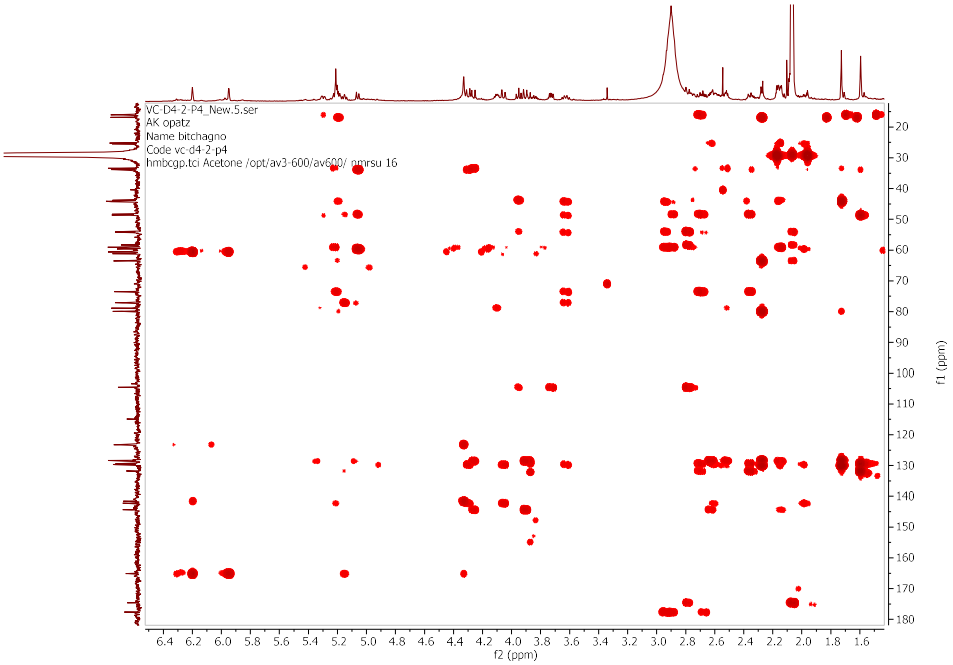

Figure S8. Enlarged HMBC spectrum of **1**

Page **10** sur **36**

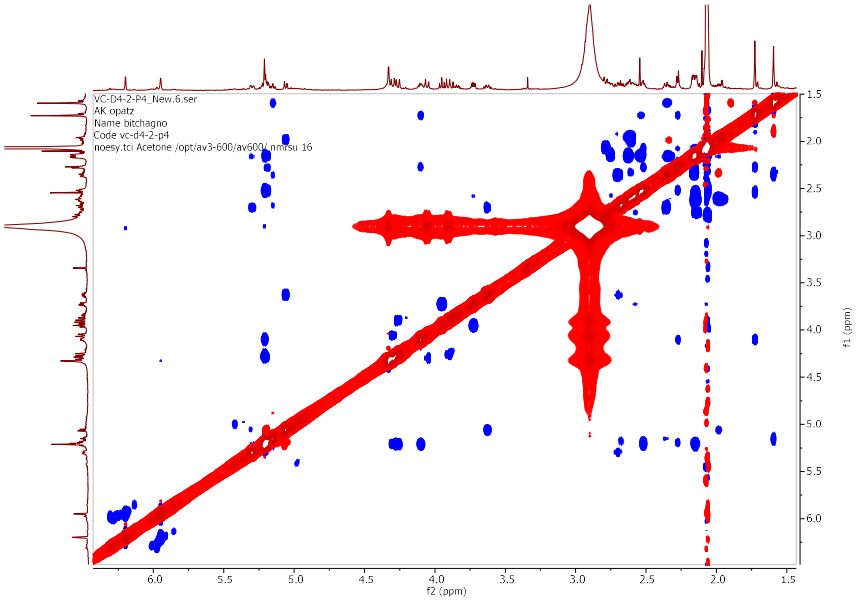

Figure S9. Full NOESY spectrum of **1**

Data File	1011139.d	**Sample Name**	VC-D4-2-p6
Sample Type	Sample	**Position**	p2a1
Instrument Name	Instrument 1	**User Name**	
Acq Method	ESI_pos_ACN_above1000.m	**Acquired Time**	7/26/2019 8:43:46 AM (UTC+02:00)
IRM Calibration Status	Success	**DA Method**	Report_standard.m
Comment	Bitchagno, Opatz		
Sample Group		**Info.**	
Stream Name	LC 1	**Acquisition Time (Local)**	7/26/2019 8:43:46 AM (UTC+02:00)
Acquisition SW Version	6200 series TOF/6500 series Q-TOF B.08.00 (B8058.0)	**QTOF Driver Version**	8.00.00
QTOF Firmware Version	20.698	**Tune Mass Range Max.**	3200

Spectra

Fragmentor Voltage	Collision Energy	Ionization Mode
50	0	ESI

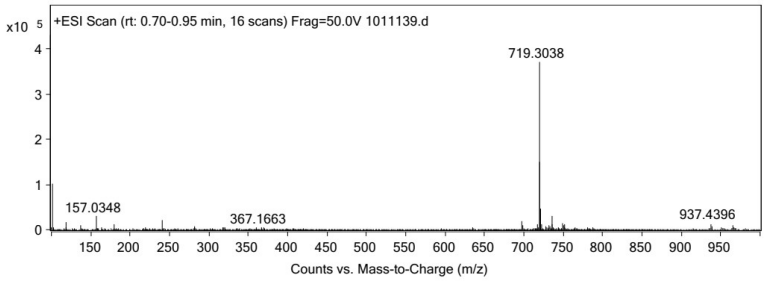

Figure S10. HR-ESI mass spectrum of **2**

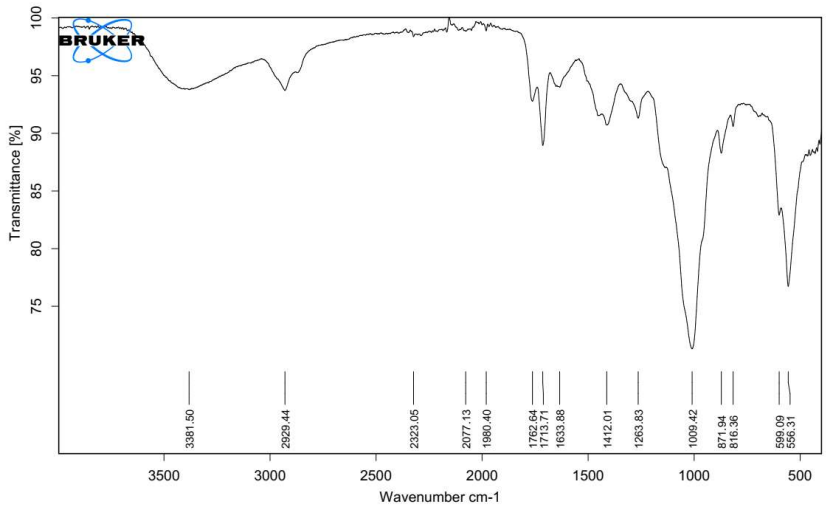

Figure S11. IR spectrum of **2**

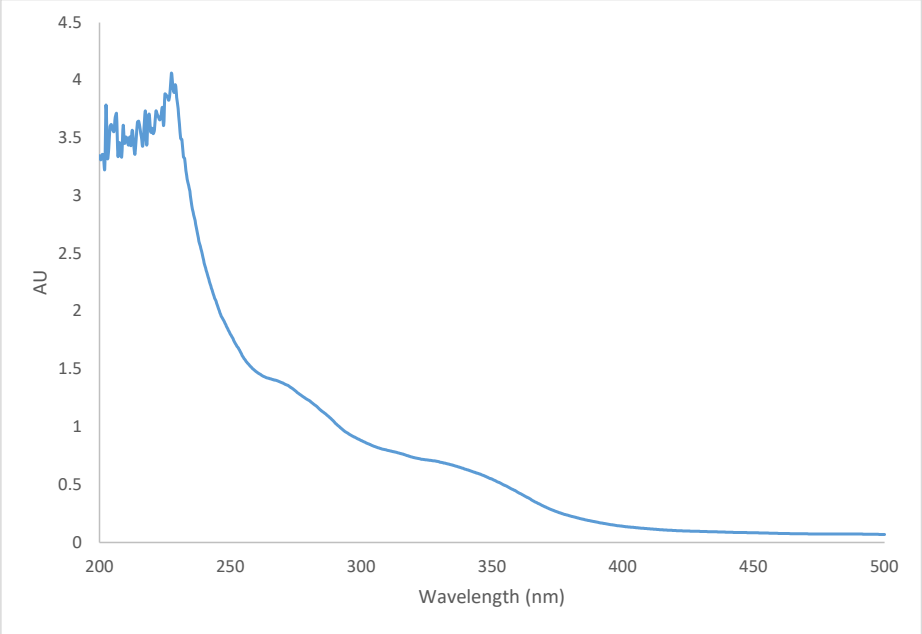

Figure S12. UV spectrum of **2** in acetonitrile

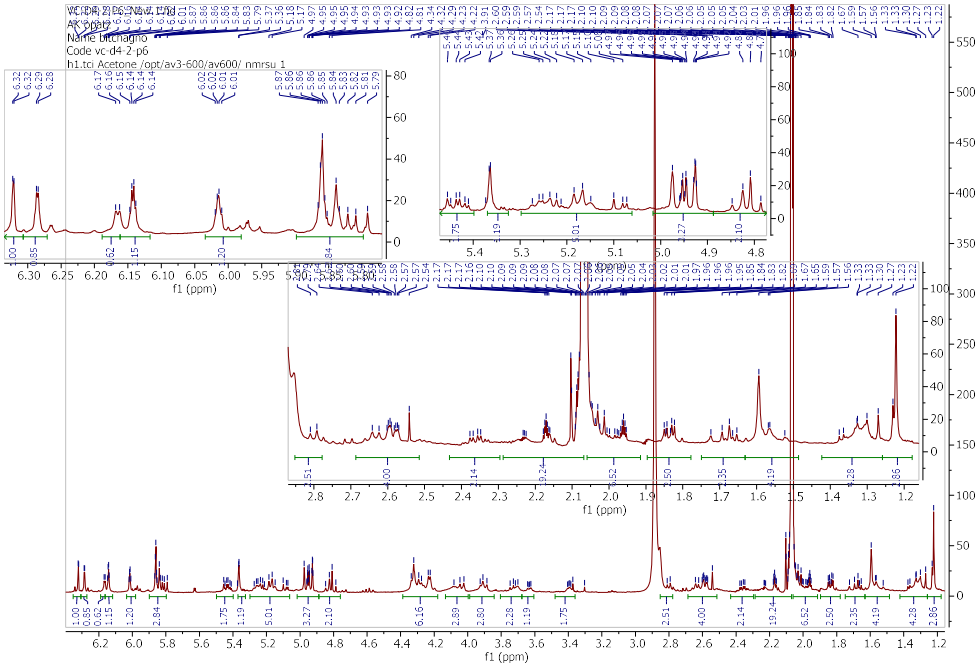

Figure S13. Full ^{1}H NMR spectrum (Acetone-d_6, 600 MHz) of **2**

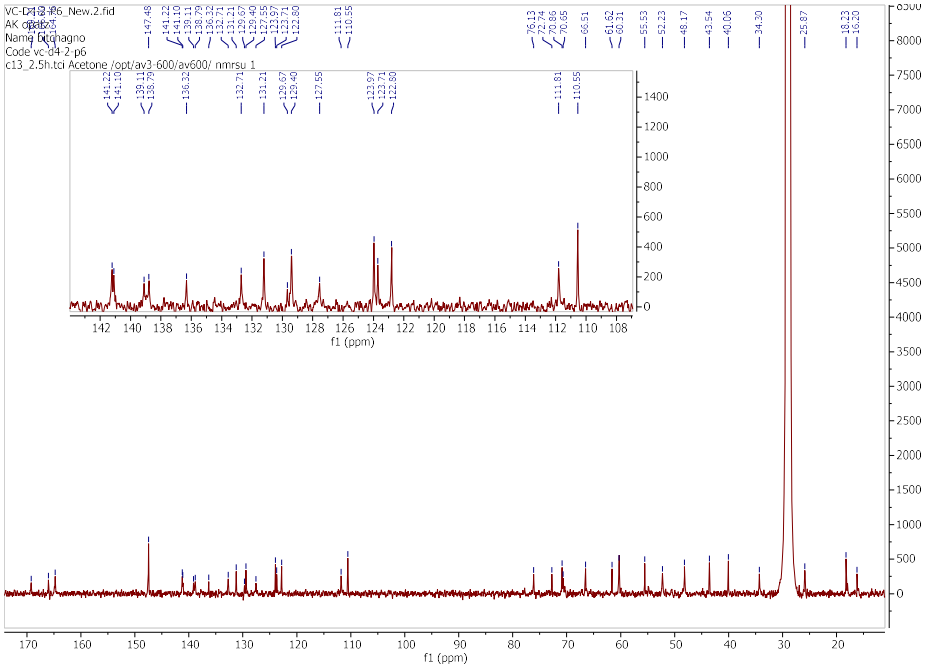

Figure S14. Full ^{13}C NMR spectrum (Acetone-d_6, 150 MHz) of **2**

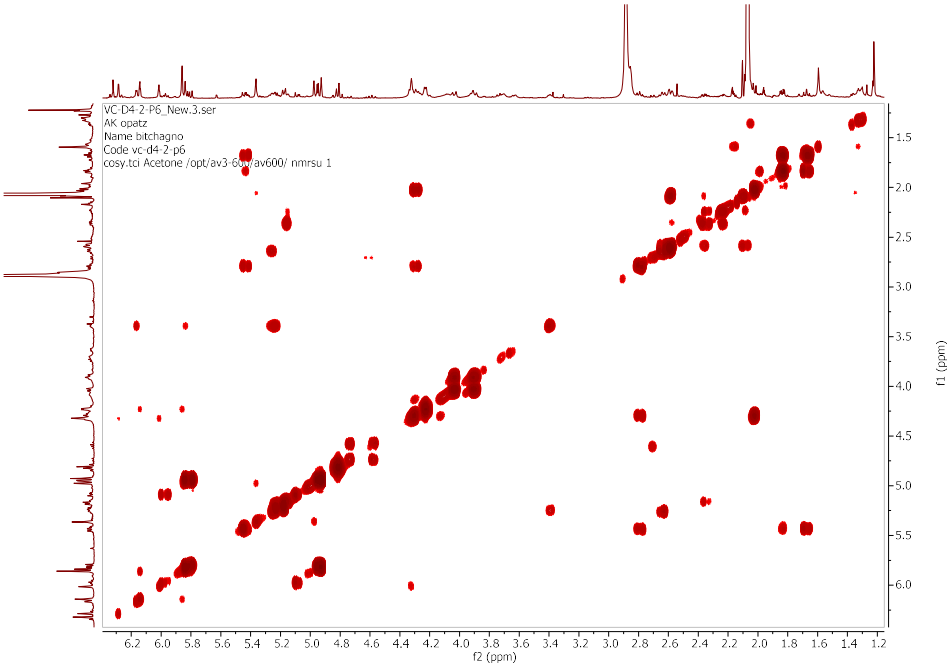

Figure S15. Full ^{1}H-^{1}H COSY spectrum of **2**

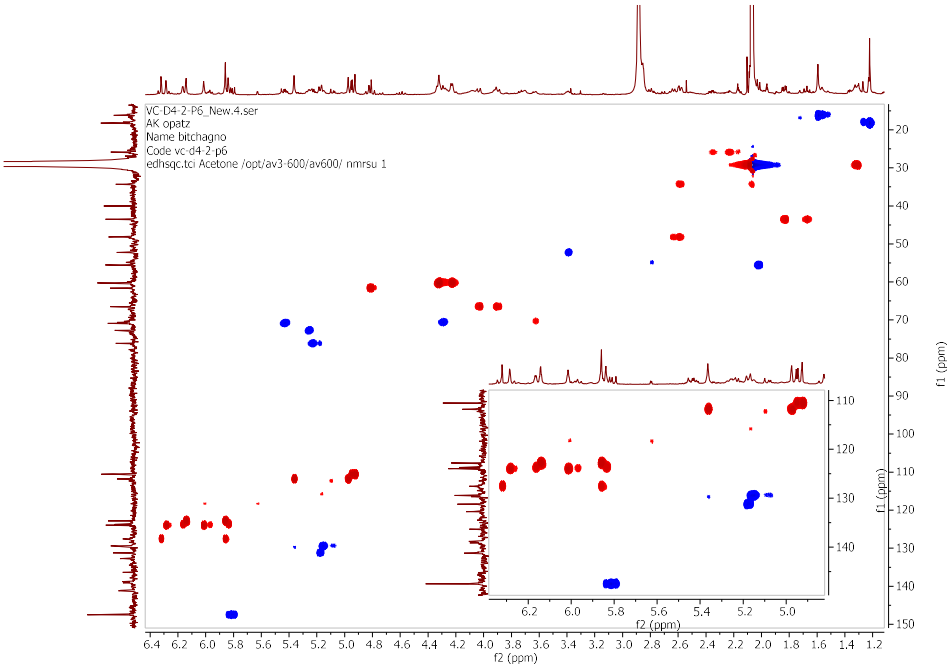

Figure S16. Full HSQC spectrum of **2**

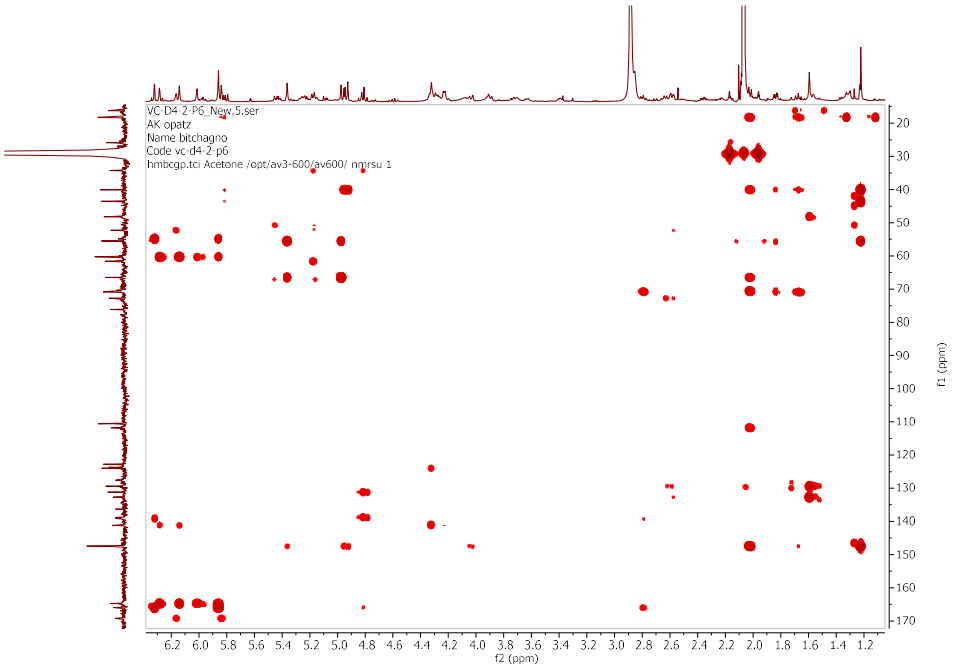

Figure S17. Full HMBC spectrum of **2**

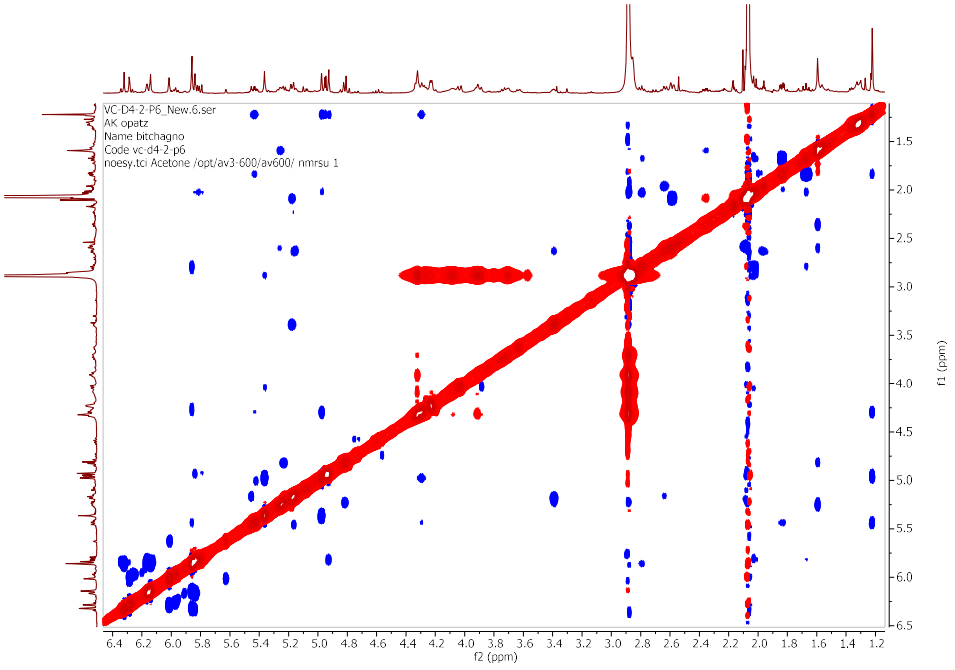

Figure S18. Full NOESY spectrum of **2**

Page **15** sur **36**

Data File	1011256.d	**Sample Name**	VC-D1B-A1
Sample Type	Sample	**Position**	P2a8
Instrument Name	Instrument 1	**User Name**	
Acq Method	ESI_pos_ACN_below1000.m	**Acquired Time**	8/2/2019 9:10:35 AM (UTC+02:00)
IRM Calibration Status	Success	**DA Method**	Report_standard.m
Comment	Bitchagno, Opatz		
Sample Group		**Info.**	
Stream Name	LC 1	**Acquisition Time (Local)**	8/2/2019 9:10:35 AM (UTC+02:00)
Acquisition SW Version	6200 series TOF/6500 series Q-TOF B.08.00 (B8058.0)	**QTOF Driver Version**	8.00.00
QTOF Firmware Version	20.698	**Tune Mass Range Max.**	3200

Spectra

Fragmentor Voltage	Collision Energy	Ionization Mode
80	0	ESI

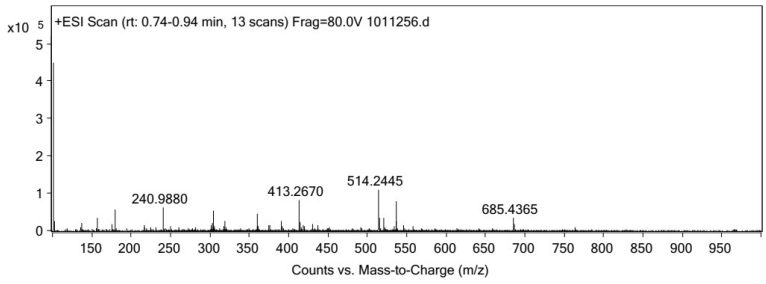

Figure S19. HR-ESI mass spectrum of **3**

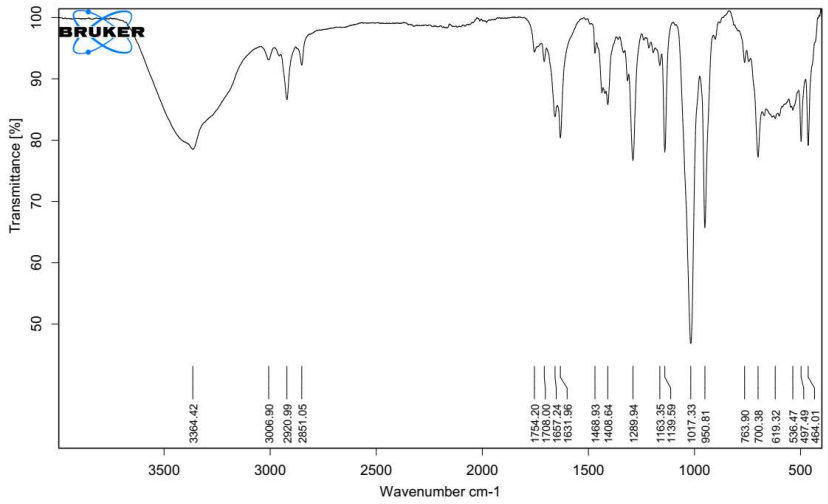

Figure S20. IR spectrum of **3**

Page **16** sur **36**

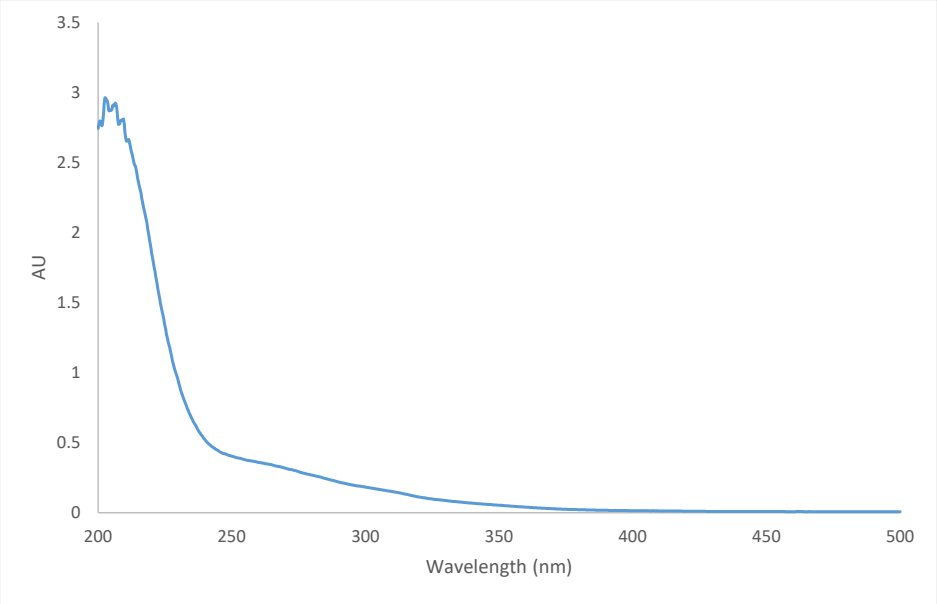

Figure S21. UV spectrum of **3** in acetonitrile

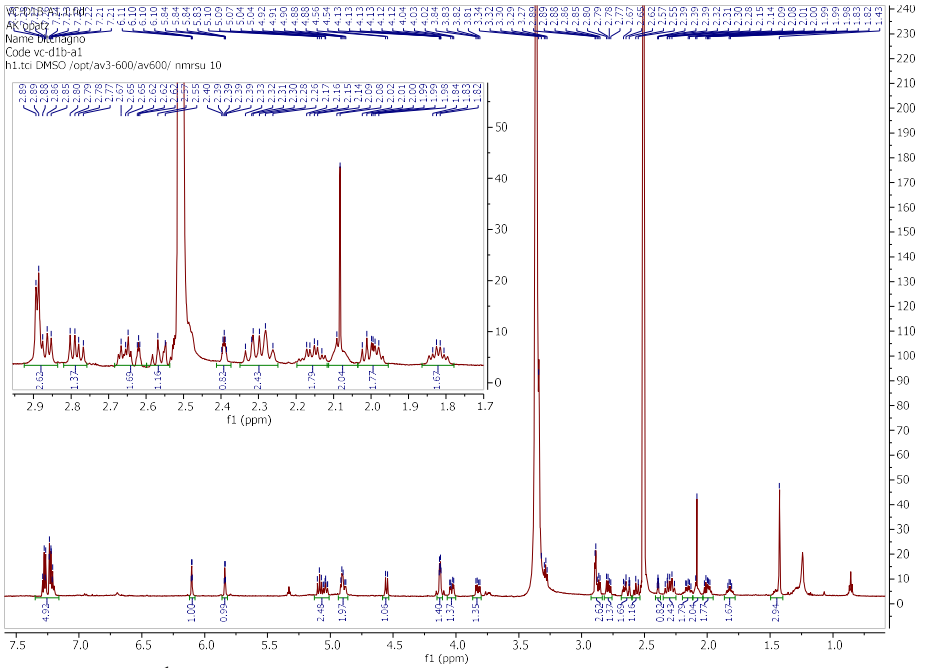

Figure S22. Full ^{1}H NMR spectrum (DMSO-d_6, 600 MHz) of **3**

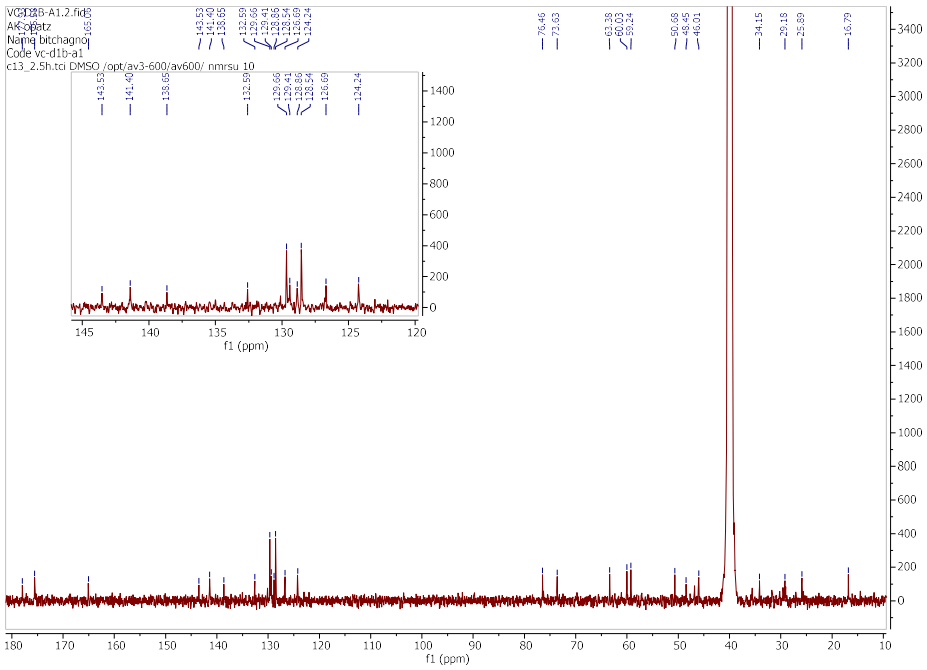

Figure S23. Full ^{13}C NMR spectrum (DMSO-d_6, 150 MHz) of **3**

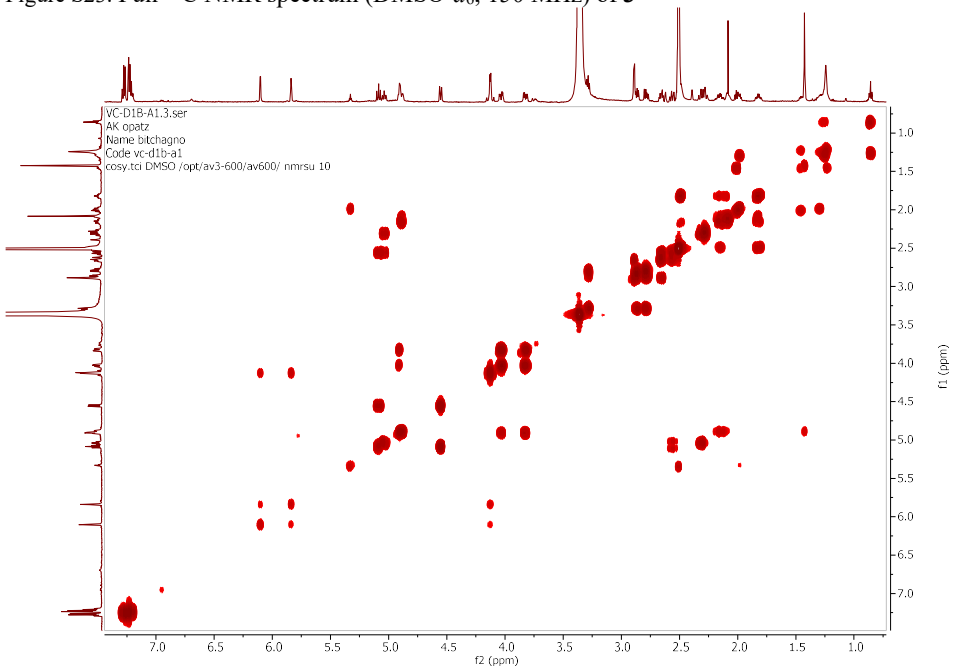

Figure S24. Full ^{1}H-^{1}H COSY spectrum of **3**

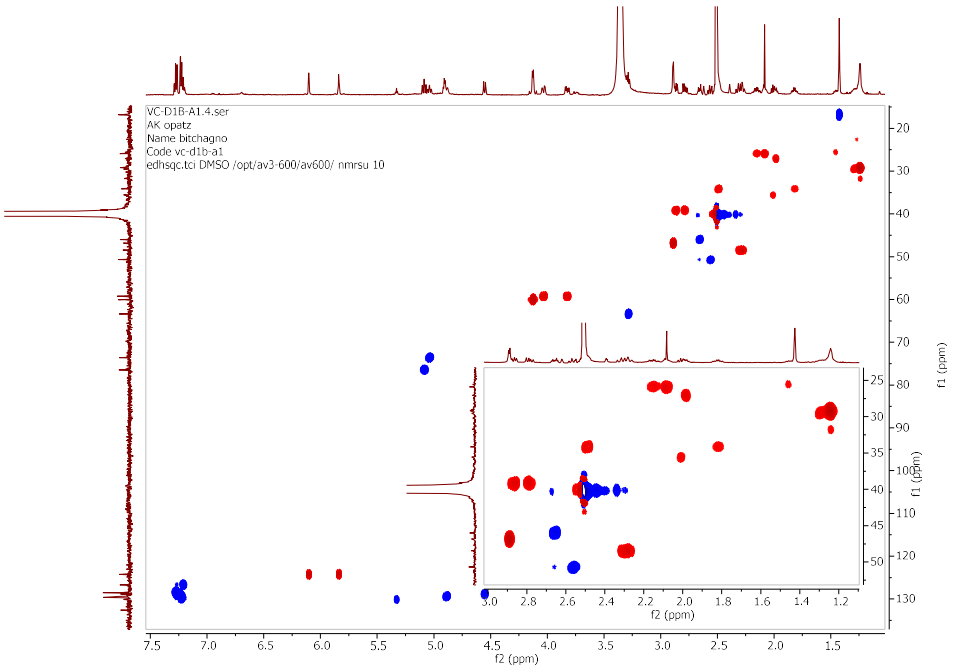

Figure S25. Full HSQC spectrum of **3**

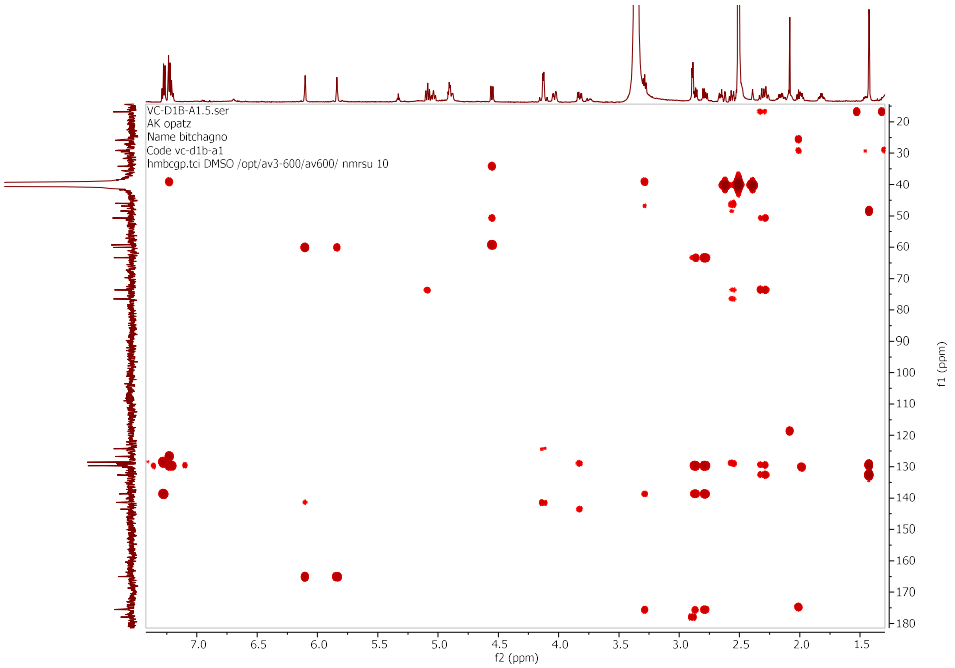

Figure S26. Full HMBC spectrum of **3**

Page **19** sur **36**

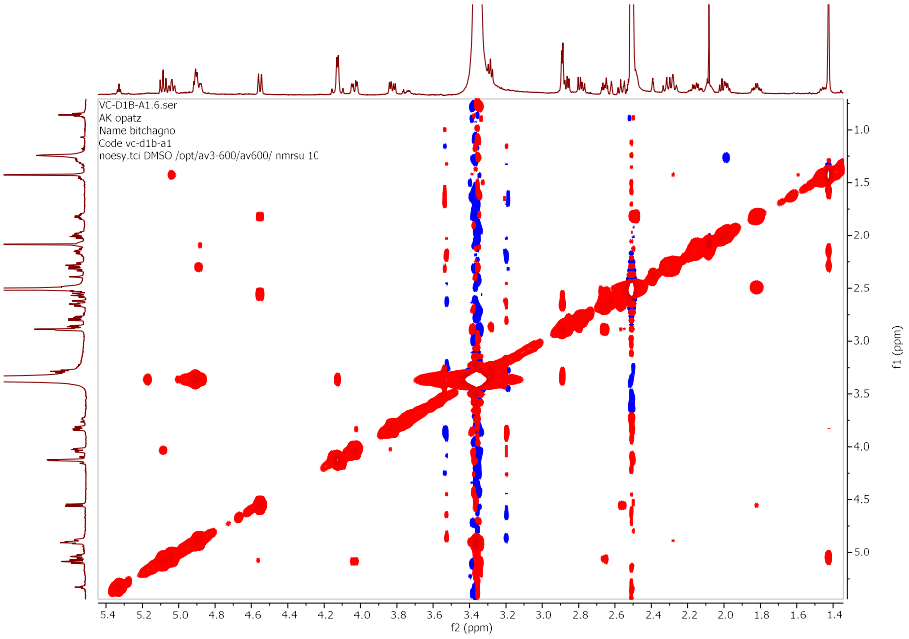

Figure S27. Full NOESY spectrum of **3**

Data File	1011136.d	**Sample Name**	VC-E-P1
Sample Type	Sample	**Position**	P1a5
Instrument Name	Instrument 1	**User Name**	
Acq Method	ESI_pos_ACN_above1000.m	**Acquired Time**	7/26/2019 8:34:38 AM (UTC+02:00)
IRM Calibration Status	Success	**DA Method**	Report_standard.m
Comment	Bitchagno, Opatz		
Sample Group		**Info.**	
Stream Name	LC 1	**Acquisition Time (Local)**	7/26/2019 8:34:38 AM (UTC+02:00)
Acquisition SW Version	6200 series TOF/6500 series Q-TOF B.08.00 (B8058.0)	**QTOF Driver Version**	8.00.00
QTOF Firmware Version	20.698	**Tune Mass Range Max.**	3200

Spectra

Fragmentor Voltage	Collision Energy	Ionization Mode
50	0	ESI

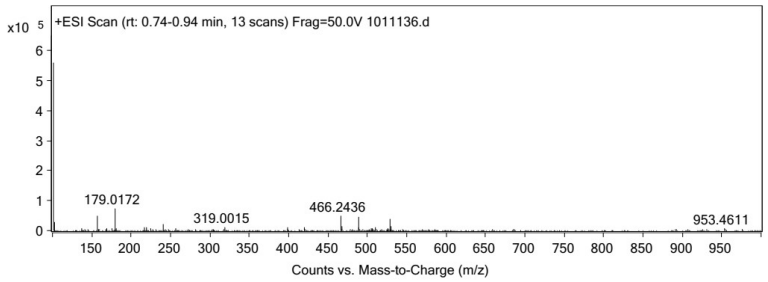

Figure S28. HR-ESI mass spectrum of **4**

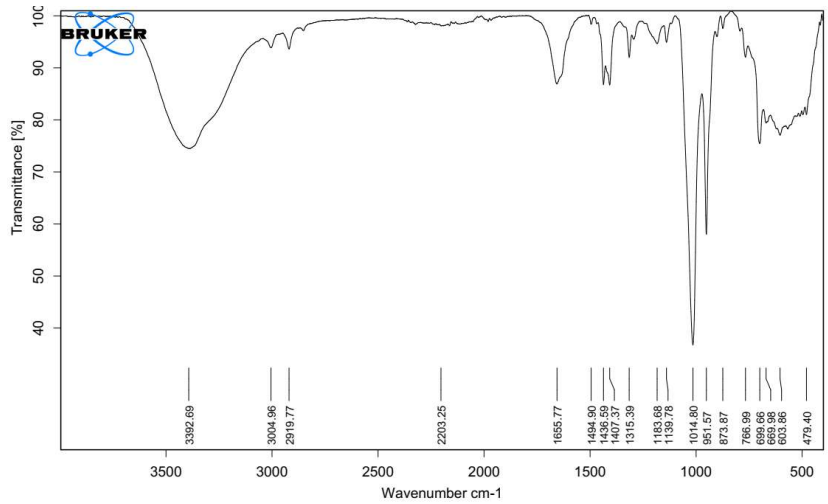

Figure S29. IR spectrum of **4**

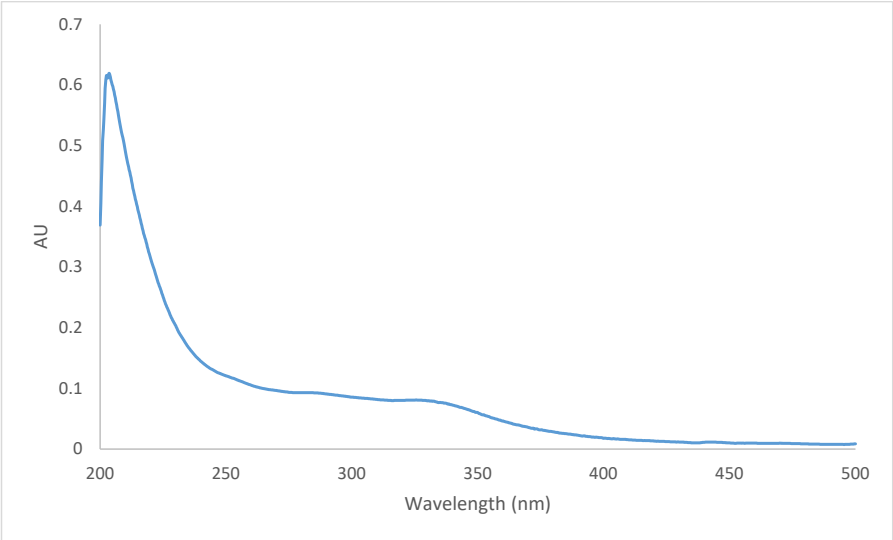

Figure S30. UV spectrum of **4** in methanol

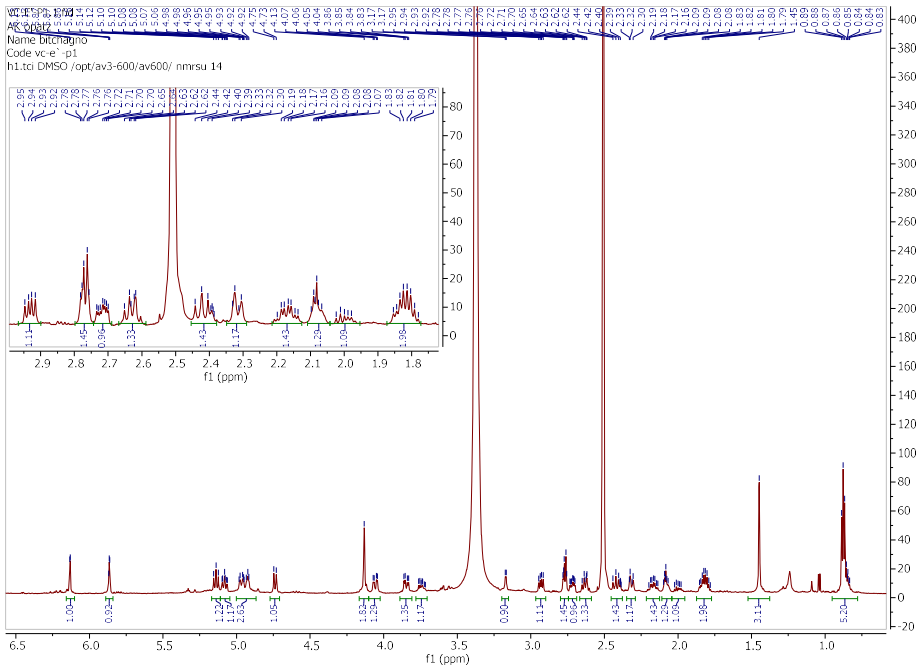

Figure S31. Full ^{1}H NMR spectrum (DMSO-d_6, 600 MHz) of **4**

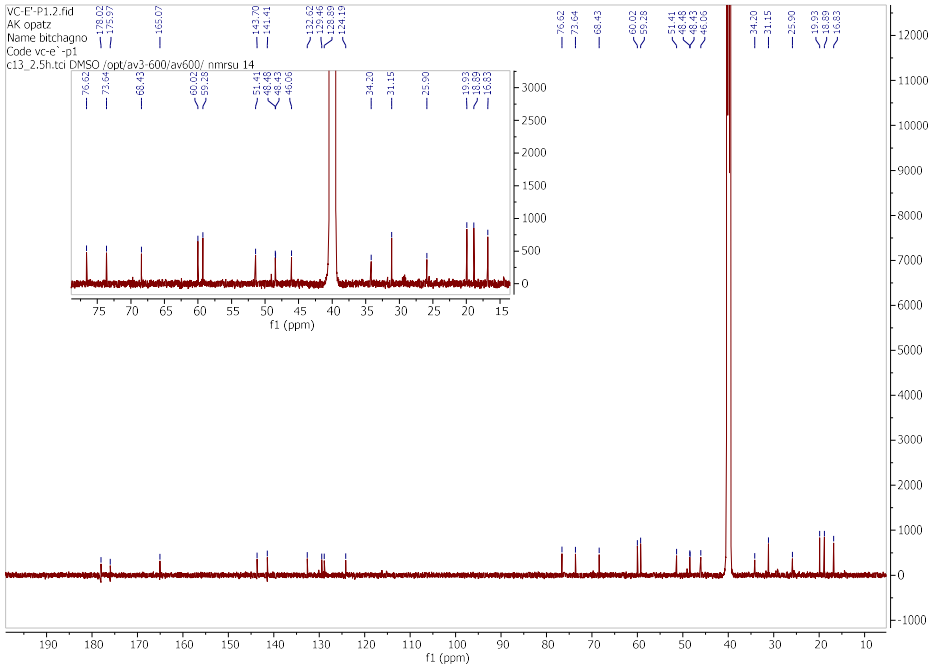

Figure S32. Full ^{13}C NMR spectrum (DMSO-d_6, 150 MHz) of **4**

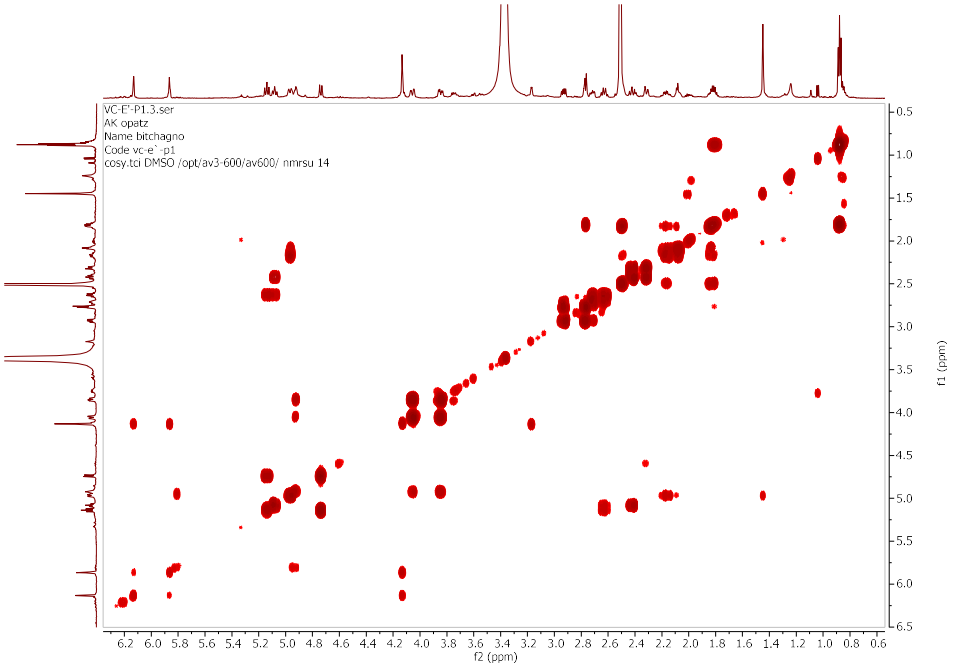

Figure S33. Full HMBC spectrum of **4**

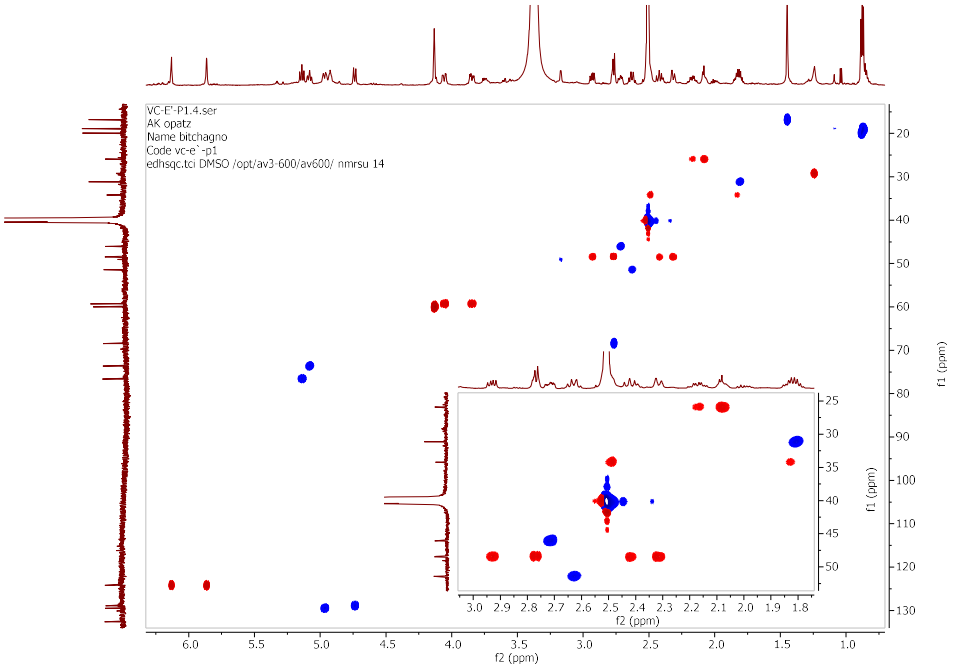

Figure S34. Full HSQC spectrum of **4**

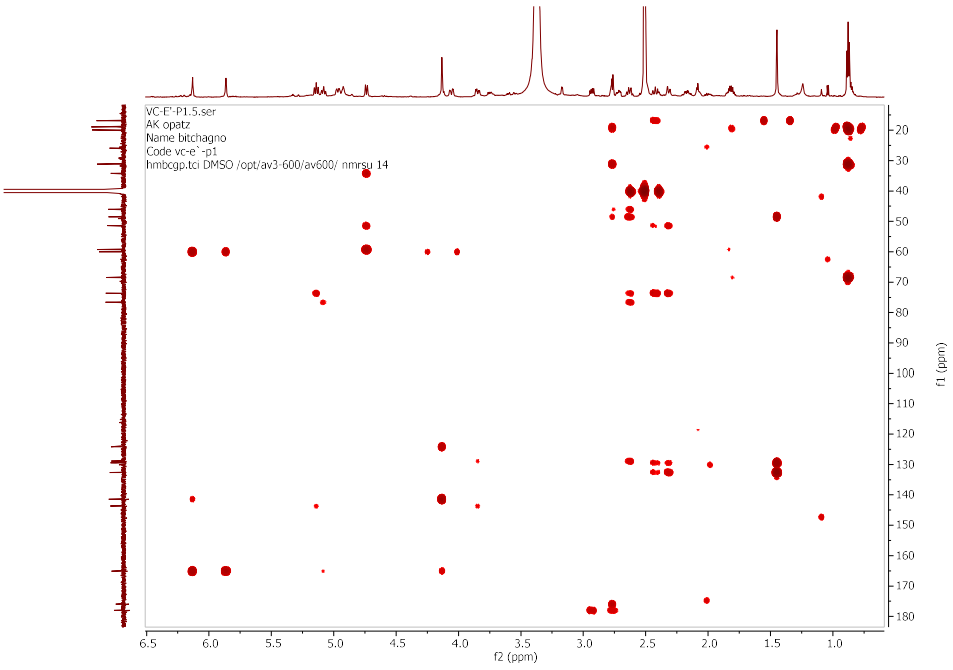

Figure S35. Full HMBC spectrum of **4**

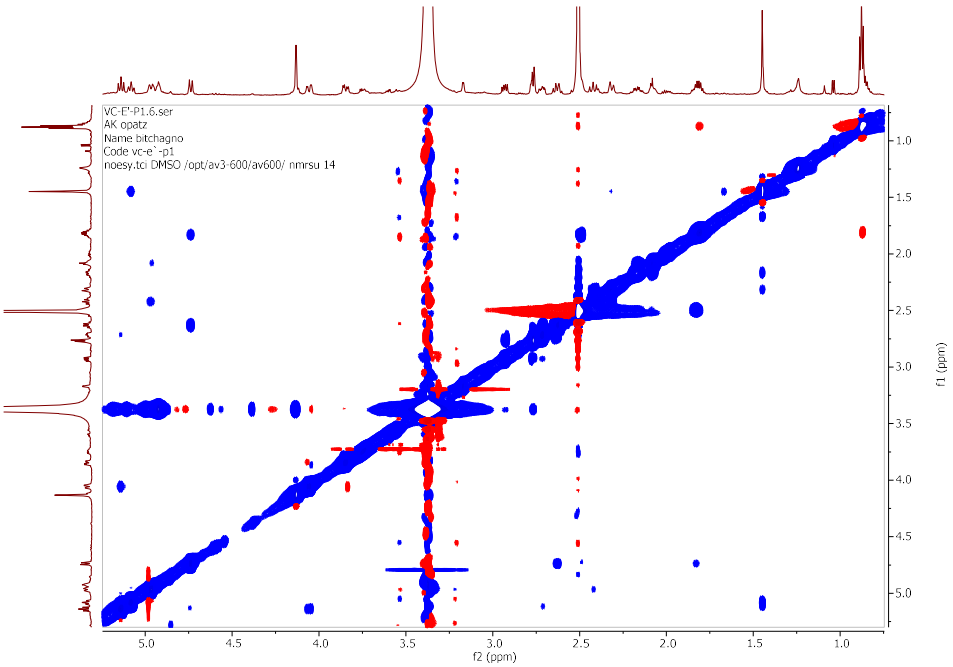

Figure S36. Full NOESY spectrum of **4**

Page **24** sur **36**

Data File	1011261.d	**Sample Name**	VC-D1F-A1
Sample Type	Sample	**Position**	P2a7
Instrument Name	Instrument 1	**User Name**	
Acq Method	ESI_pos_ACN_below1000.m	**Acquired Time**	8/2/2019 9:23:04 AM (UTC+02:00)
IRM Calibration Status	Success	**DA Method**	Report_standard.m
Comment	Bitchagno, Opatz		
Sample Group		**Info.**	
Stream Name	LC 1	**Acquisition Time (Local)**	8/2/2019 9:23:04 AM (UTC+02:00)
Acquisition SW Version	6200 series TOF/6500 series Q-TOF B.08.00 (B8058.0)	**QTOF Driver Version**	8.00.00
QTOF Firmware Version	20.698	**Tune Mass Range Max.**	3200

Spectra

Fragmentor Voltage	Collision Energy	Ionization Mode
80	0	ESI

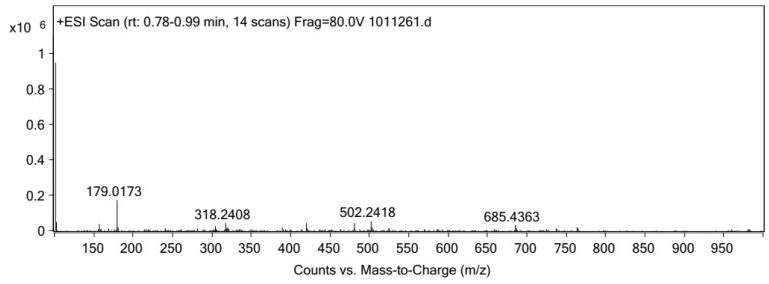

Figure S37. HR-ESI mass spectrum of **5**

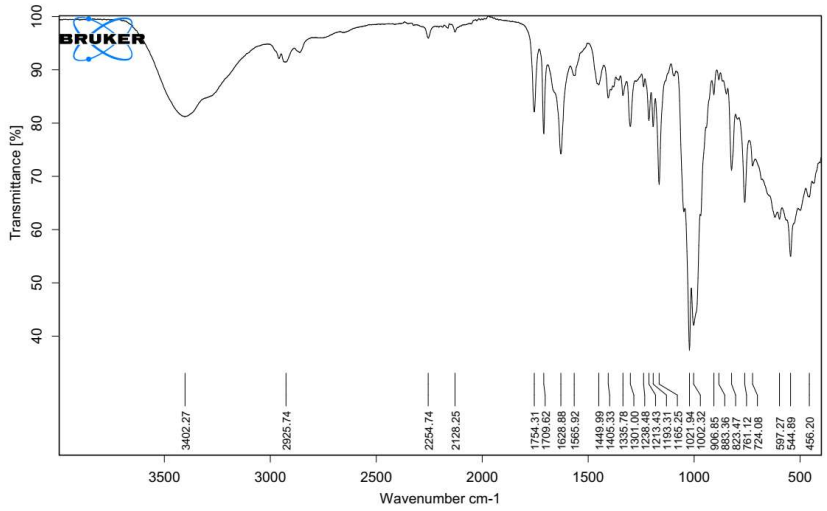

Figure S38. IR spectrum of **5**

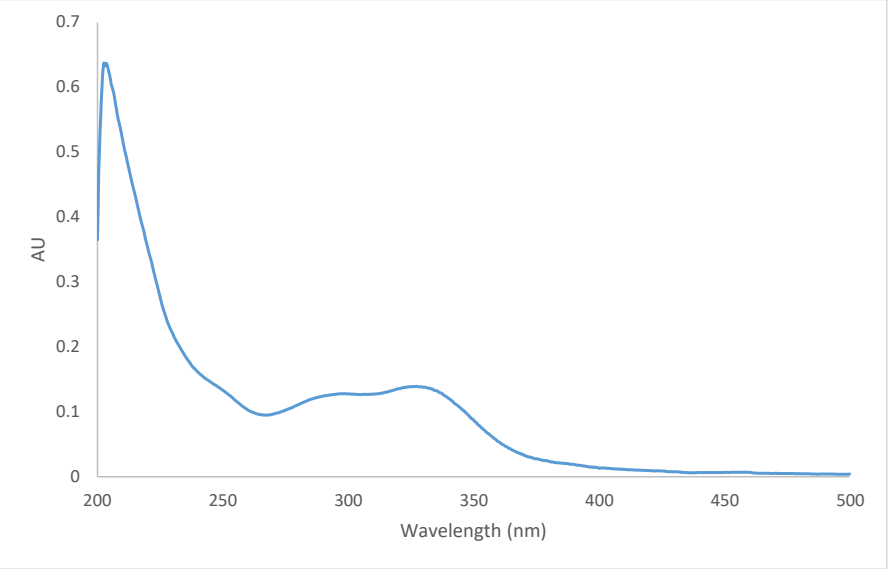

Figure S39. UV spectrum of **5** in methanol. The signals in the UVB region likely result from impurities or decomposition.

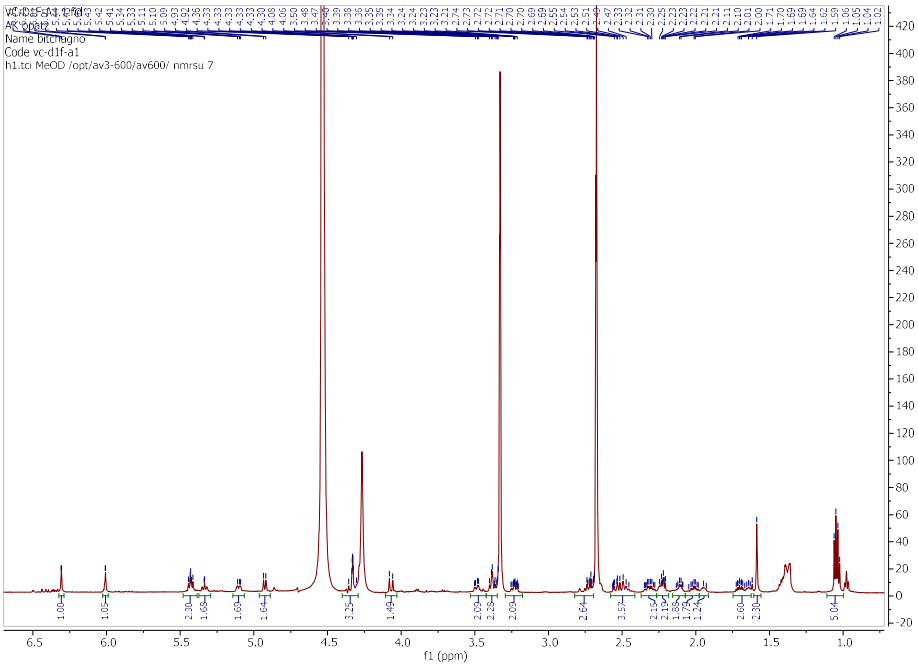

Figure S40. Full ^{1}H NMR spectrum (DMSO-d_6-CH_3OH-d_4, 600 MHz) of **5**

Page **26** sur **36**

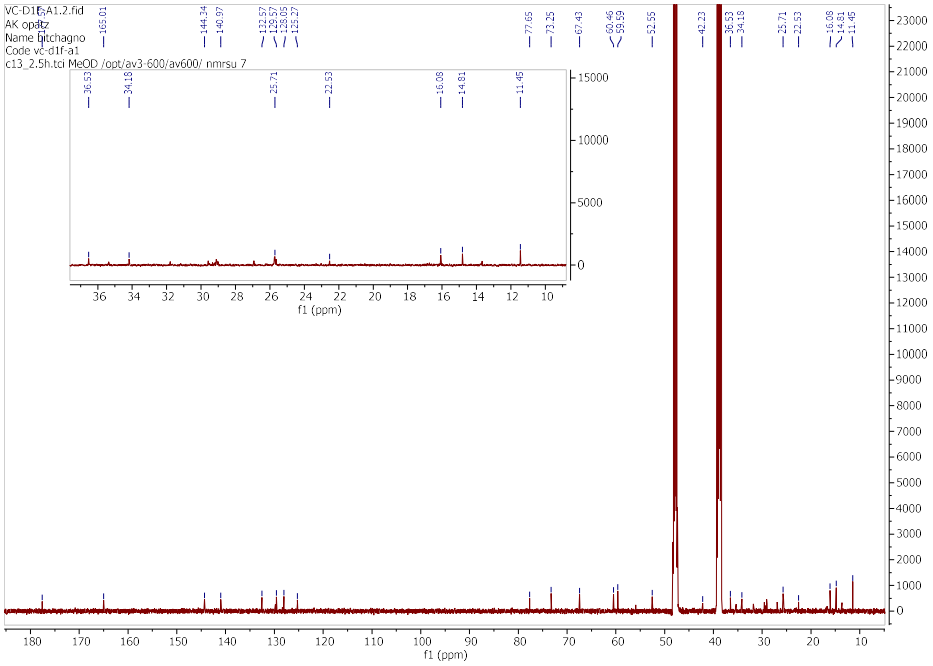

Figure S41. Full ^{13}C NMR spectrum (DMSO-d_6-CH_3OH-d_4, 150 MHz) of **5**

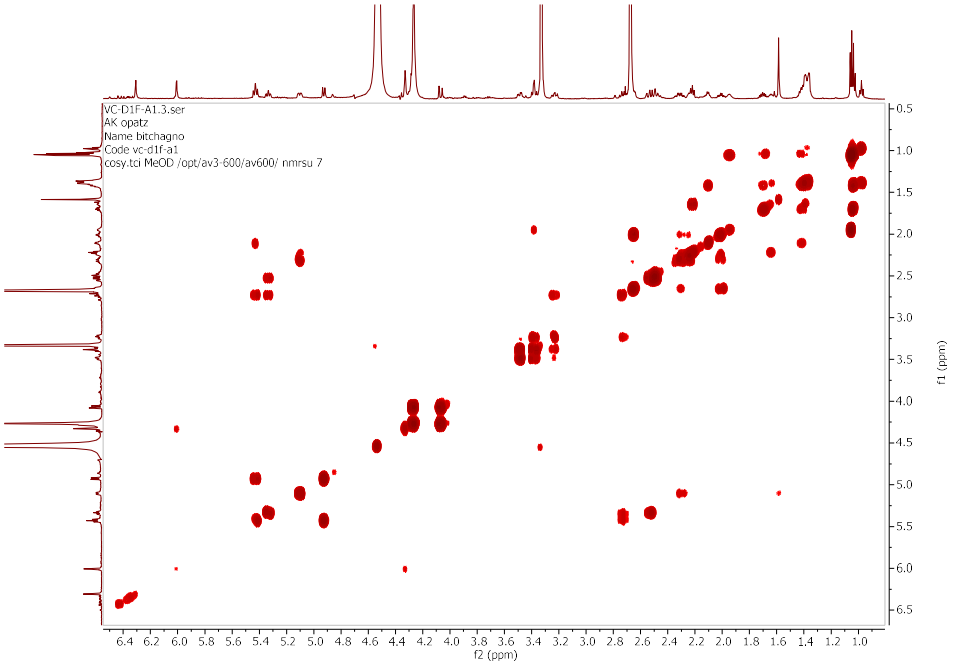

Figure S42. Full ^{1}H-^{1}H NMR spectrum of **5**

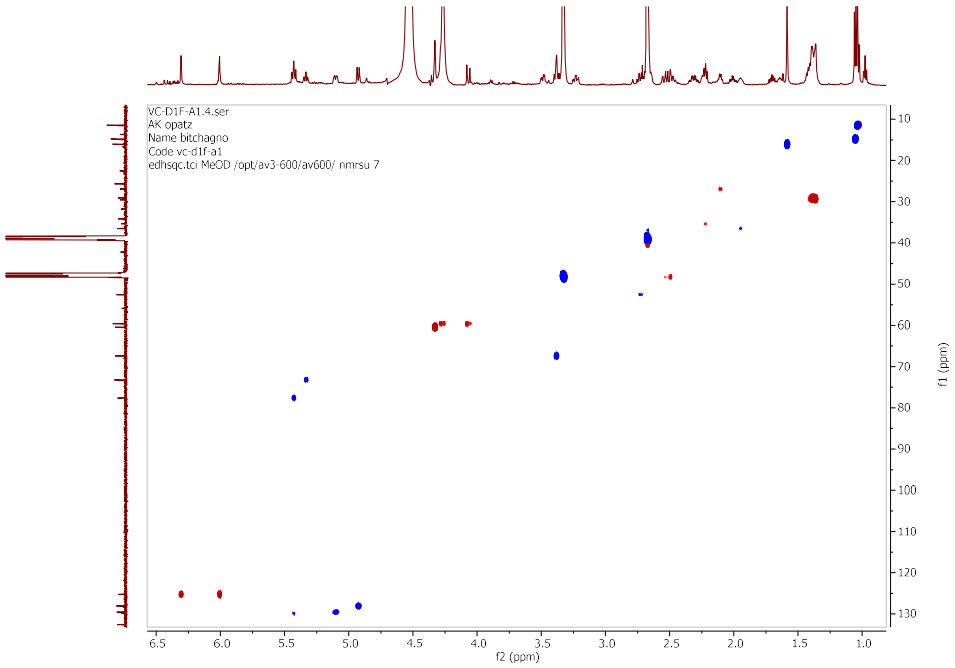

Figure S43. Full HSQC spectrum of **5**

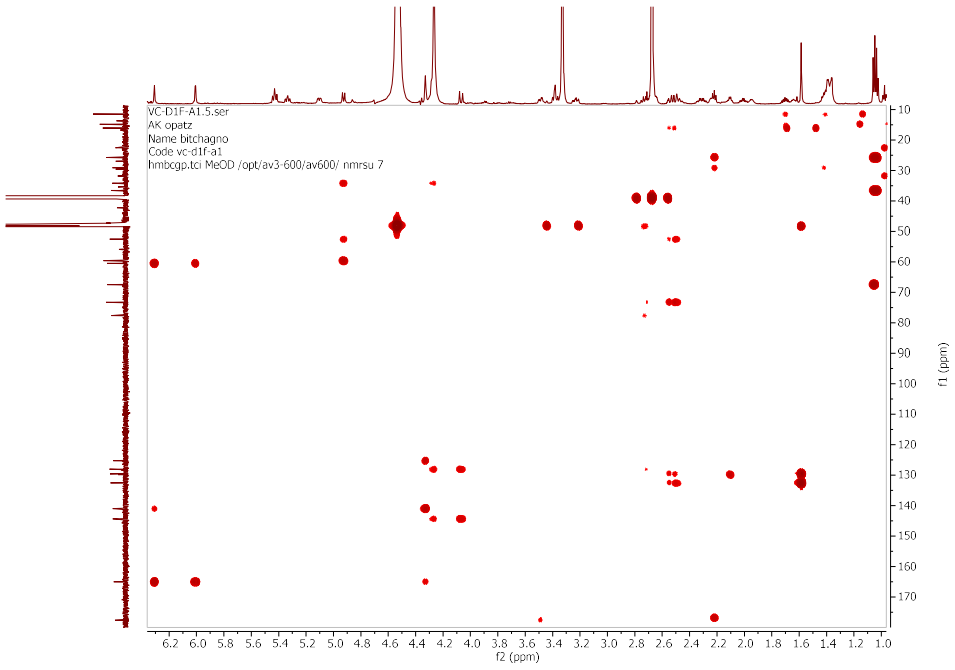

Figure S44. Full HMBC spectrum of **5**

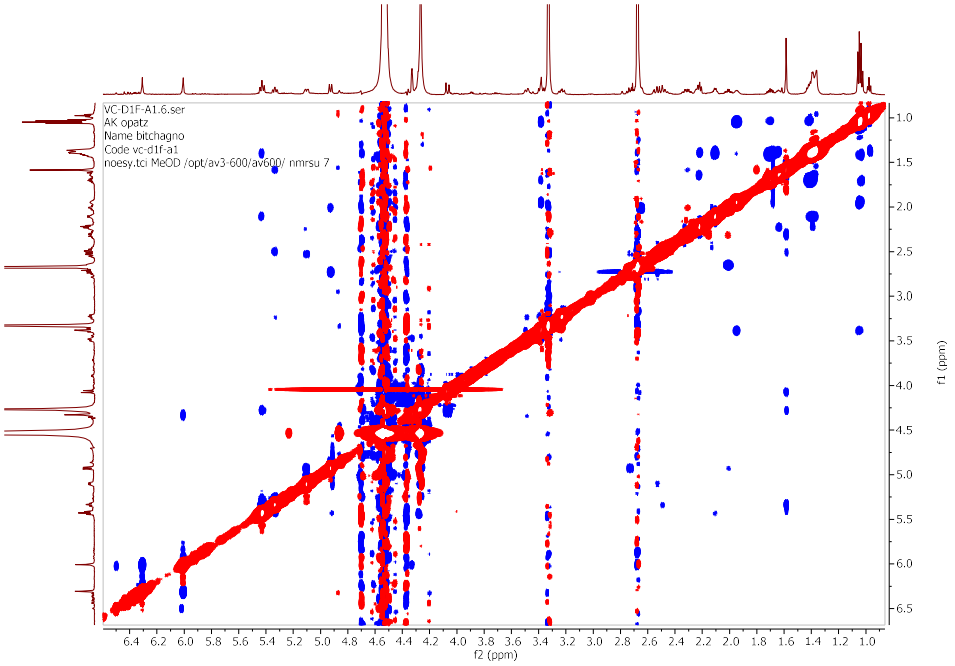

Figure S45. Full NOESY spectrum of **5**

Notice.

Maxima or shoulders above 250 nm displayed in the UV spectra of compounds **1**-**5** could result from a sample degradation; samples were isolated in 2019, and UV spectra were newly recorded during review process.

Appendix to the SI

Computational details for the calculation of the chemical shifts of compound 1

Conformational analysis for each possible isomer (e.g. 11*R*,16*R*,17*R*) of compound **1** was performed using Spartan '10[1] (MMFF level of theory[2]). All DFT calculations were performed using Gaussian 16, Rev. C.01.[3] Geometry optimization of each conformer was performed with the B3LYP functional[4–7] in combination with the Pople basis set 6-31G(d).[8,9] All conformations of one isomer, within 4.5 kcal/mol from the respective B3LYP global minimum, were taken into account for NMR analysis, after removal of duplicates. For the shielding tensors calculations, the mpw1pw91 functional[10] was used with the 6-31+G(d,p) basis set[11,12] and the IEFPCM solvation model[13] for acetone.

Computational details for the calculation of the CD spectra and the specific rotation values

Based on the DFT optimized conformer distribution, electronic excitations for the simulation of electronic CD spectra were calculated using time-dependent DFT[14] with the CAM-B3LYP[15] functional, the 6-311g(d,p)[11,16] basis set and the IEFPCM solvation model for methanol. Additionally, specific rotation values were computed with the B3LYP functional in conjunction with 6-311+g(2d,p) [11,12,16] as well as the IEFPCM solvation model for acetone. The calculated values for each conformer were subsequently Boltzmann averaged. Molecular orbital (MO) analysis was performed with GaussView 6.0.16.[17]

Input lines

Spartan:

SEARCHMETHOD=SPARSE FINDBOATS KEEPALL CONF_SELECTION_RULE=5

NMR:

#p opt=tight freq=noraman b3lyp 6-31g(d)

#p nmr=giao mpw1pw91 6-31+g(d,p) scrf=(iefpcm,solvent=acetone)

Electronic excitation

#p cam-b3lyp 6-311g(d,p) scrf=(iefpcm,solvent=methanol) td=(nstates=50) pop=full

Specific rotation:

#p temperature=295.15 polar=optrot cphf=rdfreq b3lyp 6-311+g(2d,p) scrf=(iefpcm,solvent=acetone)

At the end of each input file:

589.3nm

Detailed Results

Table S2: DP4+-probabilities for the eight possible diastereoisomers of compound **1**.

		11*R*,16*R*,17*R*	11*R*,16*R*,17*S*	11*R*,16*S*,17*R*	11*R*,16*S*,17*S*	11*S*,16*R*,17*R*	11*S*,16*R*,17*S*	11*S*,16*S*,17*R*	11*S*,16*S*,17*S*
*s*DP4+	(H data)	0.00%	0.00%	0.00%	100.00 %	0.00%	0.00%	0.00%	0.00%
*s*DP4+	(C data)	0.12%	0.00%	0.00%	0.00%	0.00%	0.00%	0.03%	99.86%
*s*DP4+	(all data)	0.01%	0.00%	0.00%	99.65%	0.00%	0.00%	0.00%	0.35%
*u*DP4+	(H data)	99.83%	0.00%	0.00%	0.00%	0.00%	0.06%	0.01%	0.10%
*u*DP4+	(C data)	2.68%	0.00%	0.00%	0.00%	0.00%	0.00%	0.05%	97.26%
*u*DP4+	(all data)	96.66%	0.00%	0.00%	0.00%	0.00%	0.00%	0.00%	3.34%
DP4+	(H data)	99.99%	0.00%	0.00%	0.00%	0.00%	0.01%	0.00%	0.00%
DP4+	(C data)	0.00%	0.00%	0.00%	0.00%	0.00%	0.00%	0.00%	100.00 %
DP4+	**(all data)**	**43.00%**	**0.00%**	**0.00%**	**0.00%**	**0.00%**	**0.00%**	**0.00%**	**57.00%**

Electronic CD spectra and specific rotation value results

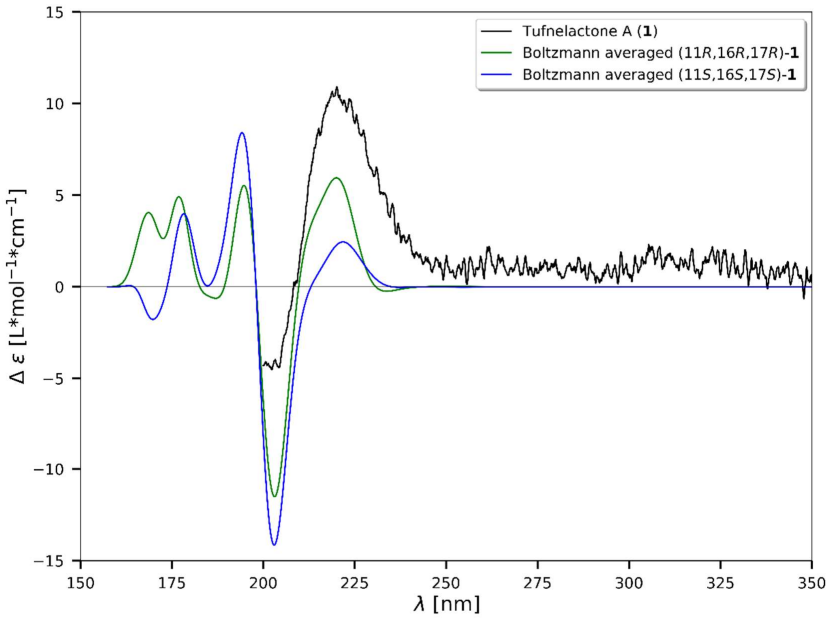

Figure S46 Comparison of the observed tufnelactone A (**1**, *c* = 0.1 mM in MeOH, black) with the calculated CD spectra (green: 11*R*,16*R*,17*R*; blue: 11*S*,16*S*,17*S*).

To investigate which electronic excitation contributed to the CD curve at 220 nm (Figure S46), the molecular orbitals of the conformer with the highest contribution to the Boltzmann distribution (sss-M7 conformer, excited state 5) were analyzed. While a complete MO analysis would go be beyond the scope of this article, the MOs with the largest contribution to this CD signal were evaluated exemplarily for the 11*S*,16*S*,17*S* diastereomer of compound **1**. This revealed a major contribution of a π–π* transitions in the onopordopicrin-part of molecule **1** as seen in Figure S47**.**

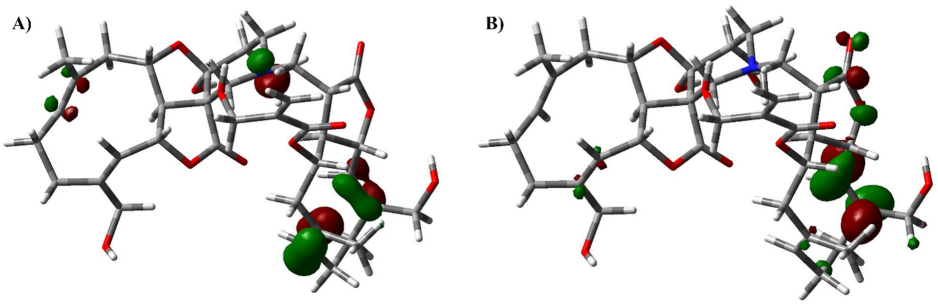

Figure S47 The occupied (A) and virtual (B) orbitals that contribute the most to the electron excitation at 220 nm are displayed with an isovalue of 0.06. This transition represents a π–π* excitation.

The Boltzmann averaged specific rotation values ($[\alpha]_D^{22}$) for the 11*R*,16*R*,17*R* as well as the 11*S*,16*S*,17*S* diastereomers were calculated to be -16.9 deg dm^{-1} $(g/mL)^{-1}$ and -76.4 deg dm^{-1} $(g/mL)^{-1}$, respectively. Unfortunately, no clear assignment is possible with the obtained values.

Table S2. Growth inhibition against cell line HelaS3 (given in % growth inhibition, evaluated by visual inspection) and a variety of fungi and bacteria (given in % inhibition, evaluated by OD and/or microscopy)

Compound ID	Name	MW [Da]	HelaS3					*Aneurinibacillus migulans*		*Staphylococcus aureus*		*Candida albicans*		*Rhizomucor miehei*	
			2.5 µg/mL	5 µg/mL	10 µg/mL	25 µg/mL	50 µg/mL	25µg/mL	50µg/mL	25µg/mL	50µg/mL	25µg/mL	50µg/mL	25µg/mL	50µg/mL
-	crude extract	-	0%	0%	25%	100%	100%	0%	0%	0%	0%	0%	0%	0%	0%
1	Tufnelactone A	713	0%	0%	0%	0%	25% [70.1 µM]	0%	0%	0%	0%	0%	0%	0%	0%
2	Tufnelactone B	696	0%	0%	0%	75% [35.9 µM]	100% [71.8 µM]	0%	0%	0%	0%	0%	0%	0%	0%
3	Tufnelactone C	513	0%	0%	0%	0%	0%	0%	0%	0%	0%	0%	0%	0%	0%
4	Tufnelactone D	465	0%	0%	0%	0%	0%	0%	0%	0%	0%	0%	0%	0%	0%
5	Tufnelactone E	479	0%	0%	0%	0%	0%	0%	0%	0%	0%	0%	0%	0%	0%
7	Onopordopicrin	348	0%	0%	0%	75% [71.8 µM]	100% [143.7 µM]	0%	0%	0%	0%	0%	0%	0%	0%
8		145	0%	0%	0%	0%	0%	0%	0%	0%	0%	0%	0%	0%	0%
9		270	0%	0%	cytostatic [37 µM]	100% [92.6 µM]	100% [185.2 µM]	0%	0%	0%	0%	0%	0%	0%	0%
10		316	0%	0%	0%	0%	0%	0%	0%	0%	0%	0%	0%	0%	0%
12		446	0%	0%	0%	0%	0%	0%	0%	0%	0%	0%	0%	0%	0%
13		462	0%	0%	0%	0%	0%	0%	0%	0%	0%	0%	0%	0%	0%
14		200	0%	0%	0%	0%	0%	0%	0%	0%	0%	0%	0%	0%	0%
15		200	0%	0%	0%	0%	0%	0%	0%	0%	0%	0%	0%	0%	0%

Table S2 (continuation)

Compound ID	Name	*Penicillium chrysogenum*		*Peacilomyces variotii*		*Pyricularia oryzae* in H20		*Botrytis cinerea*		*Phytophthora infestans*		*Pyricularia oryzae* in CM		*Pseudomonas aeruginosa*	
		25µg/mL	50µg/mL	25µg/mL	50µg/mL	25µg/mL	50µg/mL	25µg/mL	50µg/mL	25µg/mL	50µg/mL	25µg/mL	50µg/mL	25µg/mL	50µg/mL
-	crude extract	0%	0%	0%	0%	0%	0%	0%	0%	0%	0%	0%	0%	0%	0%
1	Tufnelactone A	0%	0%	0%	0%	0%	0%	0%	0%	0%	0%	0%	0%	0%	0%
2	Tufnelactone B	0%	0%	0%	0%	0%	0%	0%	0%	0%	0%	0%	0%	0%	0%
3	Tufnelactone C	0%	0%	0%	0%	0%	0%	0%	0%	0%	0%	0%	0%	0%	0%
4	Tufnelactone D	0%	0%	0%	0%	0%	0%	0%	0%	0%	0%	0%	0%	0%	0%
5	Tufnelactone E	0%	0%	0%	0%	0%	0%	0%	0%	0%	0%	0%	0%	0%	0%
7	Onopordopicrin	0%	0%	0%	0%	0%	0%	0%	0%	0%	0%	0%	0%	0%	0%
8		0%	0%	0%	0%	0%	0%	0%	0%	0%	0%	0%	0%	0%	0%
9		0%	0%	0%	0%	0%	0%	0%	0%	0%	0%	0%	0%	0%	0%
10		0%	0%	0%	0%	0%	0%	0%	0%	0%	0%	0%	0%	0%	0%
12		0%	0%	0%	0%	0%	0%	0%	0%	0%	0%	0%	0%	0%	0%
13		0%	0%	0%	0%	0%	0%	0%	0%	0%	0%	0%	0%	0%	0%
14		0%	0%	0%	0%	0%	0%	0%	0%	0%	0%	0%	0%	0%	0%
15		0%	0%	0%	0%	0%	0%	0%	0%	0%	0%	0%	0%	0%	0%

REFERENCES

(1) Wavefunction, Inc.; Irvine, CA, USA 2009.

(2) Halgren, T. A. *J. Comput. Chem.* **1996**, *17*, 490–519.

(3) Frisch, M. J.; Trucks, G. W.; Schlegel, H. B.; Scuseria, G. E.; Robb, M. A.; Cheeseman, J. R.; Scalmani, G.; Barone, V.; Petersson, G. A.; Nakatsuji, H.; Li, X.; Caricato, M.; Marenich, A. V.; Bloino, J.; Janesko, B. G.; Gomperts, R.; Mennucci, B.; Hratchian, H. P.; Ortiz, J. V.; Izmaylov, A. F.; Sonnenberg, J. L.; Williams-Young, D.; Ding, F.; Lipparini, F.; Egidi, F.; Goings, J.; Peng, B.; Petrone, A.; Henderson, T.; Ranasinghe, D.; Zakrzewski, V. G.; Gao, J.; Rega, N.; Zheng, G.; Liang, W.; Hada, M.; Ehara, M.; Toyota, K.; Fukuda, R.; Hasegawa, J.; Ishida, M.; Nakajima, T.; Honda, Y.; Kitao, O.; Nakai, H.; Vreven, T.; Throssell, K.; Montgomery, J. A.; Jr.; Peralta, J. E.; Ogliaro, F.; Bearpark, M. J.; Heyd, J. J.; Brothers, E. N.; Kudin, K. N.; Staroverov, V. N.; Keith, T. A.; Kobayashi, R.; Normand, J.; Raghavachari, K.; Rendell, A. P.; Burant, J. C.; Iyengar, S. S.; Tomasi, J.; Cossi, M.; Millam, J. M.; Klene, M.; Adamo, C.; Cammi, R.; Ochterski, J. W.; Martin, R. L.; Morokuma, K.; Farkas, O.; Foresman, J. B.; Fox, D. J. Gaussian 09, Revision A.02; Gaussian Inc., 2016.

(4) Vosko, S. H.; Wilk, L.; Nusair, M. *Can. J. Phys.* **1980**, *58*, 1200–1211.

(5) Lee, C.; Yang, W.; Parr, R. G. *Phys. Rev. B* **1988**, *37*, 785–789.

(6) Becke, A. D. *J. Chem. Phys.* **1993**, *98*, 5648–25652.

(7) Becke, A. D. *Phys. Rev. A* **1988**, *38*, 3098–23100.

(8) Hariharan, P. C.; Pople, J. A. *Theor. Chim. Acta* **1973**, *28*, 213–222.

(9) Hehre, W. J.; Ditchfield, K.; Pople, J. A. *J. Chem. Phys.* **1972**, *56*, 2257.

(10) Adamo, C.; Barone, V. *J. Chem. Phys.* **1998**, *108*, 664–675.

(11) Frisch, M. J.; Pople, J. A.; Binkley, J. S. *J. Chem. Phys.* **1984**, *80*, 3265–33269.

(12) Clark, T.; Chandrasekhar, J.; Spitznagel, G. W.; Schleyer, P. V. R. *J. Comput. Chem.* **1983**, *4*, 294–301.

(13) Tomasi, J.; Mennucci, B.; Cance, E. *J. Mol. Struct.* **2018**, *464*, 211–226.

(14) Li, T. C.; Tong, P. Q. *Phys. Rev. A* **1986**, *34*, 529–532.

(15) Yanai, T.; Tew, D. P.; Handy, N. C. *Chem. Phys. Lett.* **2004**, *393*, 51–57.

(16) Krishnan, R.; Binkley, J. S.; Seeger, R.; Pople, J. A. *J. Chem. Phys.* **1980**, *72*, 650–654.

(17) Dennington, R.; Keith, T. A.; Millam, J. M. Semichem Inc.; Shawnee Mission. KS, USA 2016.

Lebenslauf

[redacted]

[redacted]	[redacted]
[redacted]	[redacted]
[redacted]	[redacted]
[redacted]	[redacted]
[redacted]	[redacted]

[redacted]

[redacted]	[redacted]
[redacted]	[redacted]
[redacted]	[redacted]
[redacted]	[redacted]

[redacted]

Publikationen

- **Structure elucidation and biological activities of perylenequinones from an Alternaria species**
  A. Kiefer, M. Arnholdt, V. Grimm, L. Geske, J. Groß, N. Vierengel, T. Opatz, G. Erkel, *Mycotoxin Res.* **2023**, *39*, 303–316.

- **An In Vitro Study of Local Oxygen Therapy as Adjunctive Antimicrobial Therapeutic Option for Patients with Periodontitis**
  L. K. Müller-Heupt, A. Eckelt, J. Eckelt, J. Groß, T. Opatz, N. Kommerein, *Antibiotics* **2023**, *12*, 990.

- **Comparison of Different Density Functional Theory Methods for the Calculation of Vibrational Circular Dichroism Spectra**
  J. Groß,[†] J. Kühlborn,[†] S. Pusch, C. Weber, L. Andernach, G. Renzer, P. Eckhardt, J. Brauer, T. Opatz, *Chirality* **2023**, *35*, 1–13.

- **Diplomeroterpenoid G: An unusual meroterpenoid from *Mimosa pudica* Linn. (Mimosaceae)**
  C. F. Kenmogne, P. Eckhardt, R. T. Tchuenguem, J. Groß, F. T. Ngouafong, B. K. Ponou, J. P. Dzoyem, R. B. Teponno, T. Opatz, L. A. Tapondjou, *Tetrahedron* **2023**, 154451.

[†] Geteilte Erstautorenschaft

- **Oxygen-Releasing Hyaluronic-Acid Based Dispersion with Controlled Oxygen Delivery for Enhanced Periodontal Tissue Engineering**
  L. K. Müller-Heupt, N. Wiesmann-Imilowski, S. Schröder, J. Groß, P. C. Ziskoven, P. Bani, P. W. Kämmerer, E. Schiegnitz, A. Eckelt, J. Eckelt, U. Ritz, T. Opatz, B. Al-Nawas, C. Synatschke, J. Deschner, *Int. J. Mol. Sci.* **2023**, *24*, 5936.

- **Total Synthesis and Biological Evaluation of the Anti-Inflammatory (13*R*, 14*S*,15*R*)-13-Hydroxy-14-deoxyoxacyclododecindione**
  K. Seipp, J. Groß, A. Kiefer, G. Erkel, T. Opatz, *J. Nat. Prod.* **2023**, *86*, 924–938.

- **Complementary Mechanochemical and Biphasic Approaches for the Synthesis of Organic Thiocyanates using Hexacyanoferrates as Non-Toxic Cyanide Sources**
  C. Grundke,† J. Groß,† N. Vierengel, J. Sirleaf, M. Schmitz, L. Krieger, T. Opatz, *Org. Biomol. Chem.* **2023**, *21*, 644–650.

- **Extracts of *Rheum palmatum* and *Aloe vera* Show Beneficial Properties for the Synergistic Improvement of Oral Wound Healing**
  L. K. Müller-Heupt, N. Wiesmann, S. Schröder, Y. Korkmaz, N. Vierengel, J. Groß, R. Dahm, J. Deschner, T. Opatz, J. Brieger, B. Al-Nawas, P. W. Kämmerer, *Pharmaceutics* **2022**, *14*, 2060.

- **Ethyl Hydroxyethyl Cellulose—A Biocompatible Polymer Carrier in Blood**
  A. Eckelt, F. Wichmann, F. Bayer, J. Eckelt, J. Groß, T. Opatz, K. Jurk, C. Reinhardt, K. Kiouptsi, *Int. J. Med. Sci.* **2022**, *23*, 6432.

- **Constituents of *Desmodium salicifolium* (Poir.) DC (Fabaceae) with antifungal activity**
  A. P. T. Donkia, P. Eckhardt, B. T. Tsafack , R. T. Tchuenguem, J. Groß, B. K. Ponou, R. B. Teponno, J. P. Dzoyem, T. Opatz, L. Barboni, L. A. Tapondjou, *Phytochem. Lett.* **2022**, *50*, 100–105.

† Geteilte Erstautorenschaft

- **Sesquiterpene Lactones from *Vernonia tufnelliae*: Structural Features, Stereochemistry, and Biological Evaluation**
  G. Bitchagno, A. Schueffler, J. Groß, M. Krumb, P. Tané, T. Opatz, *J. Nat. Prod.* **2022**, *85*, 1681–1690.

- **Antiplanktonic and Antibiofilm Activity of *Rheum palmatum* against *Streptococcus oralis* and *Porphyromonas gingivalis***
  N. Kommerein, N. Vierengel, J. Groß, T. Opatz, B. Al-Nawas, L. K. Müller-Heupt, *Microorganisms* **2022**, *10*, 965.

- **Vinylcyclopropane [3+2] Cycloaddition with Acetylenic Sulfones Based on Visible Light Photocatalysis**
  A. Luque, J. Groß, T. J. B. Zähringer, C. Kerzig, T. Opatz, *Chem. Eur. J.* **2022**, *28*, e2021043.

- **Antimicrobial Activity of *Eucalyptus globulus, Azadirachta indica, Glycyrrhiza glabra, Rheum palmatum* Extracts and Rhein against *Porphyromonas gingivalis***
  L. K. Müller-Heupt, N. Vierengel, J. Groß, T. Opatz, J. Deschner, F. D. von Loewenich, *Antibiotics* **2022**, *11*, 186.

- **Xylochemicals and Where to Find Them**
  J. Groß,† C. Grundke,† J. Rocker,† A. J. Arduengo III, T. Opatz, *Chem. Commun.* **2021**, *57*, 9979–9994.

- **Anti-inflammatory dihydroxanthones from a Diaporthe species**
  M. Rohr, U. Kauhl, J. Groß, T. Opatz, G. Erkel, *Biol. Chem.* **2022**, *403*, 89–101.

- **Six-Step Gram Scale Synthesis of the HIV Integrase Inhibitor Dolutegravir Sodium**
  J.-P. Dietz, T. Lucas, J. Groß, S. Seitel, J. Brauer, D. Ferenc, B. F. Gupton, T. Opatz, *Org. Process Res. Dev.* **2021**, *25*, 1898–1910.

†Geteilte Erstautorenschaft

- **C-28/C-30 oxidized cycloartanes from the leaves and twigs of *Caloncoba dusenii* Gilg**
  L. Zeufack Nguetsa, J. D. Simo Mpetga, G. T. M. Bitchagno, J. Delain Tadjuidje, J. Groß, B.N. Lenta, T. Opatz, N. Sewald, M. Tene, *Phytochem. Lett.* **2021**, *43*, 145–149.

- **Diels-Alder Reaction of β-Fluoro-β-nitrostyrenes with Cyclic Dienes**
  S. A. Ponomarev, R. V. Larkovich, A. S. Aldoshin, A. A. Tabolin, S. L. Ioffe, J. Groß, T. Opatz, V. G. Nenajdenko, *Beilstein J. Org. Chem.* **2021**, *17*, 283–292.

- **An insight into the synthesis of *N*-methylated polypeptides**
  C. Muhl, L. Zengerling, J. Groß, P. Eckhardt, T. Opatz, P. Besenius, M. Barz, *Polym. Chem.* **2020**, *11*, 6919–6927.

- **Antimicrobial secondary metabolites from the medicinal plant *Crinum glaucum* A. Chev. (Amaryllidaceae)**
  B. Y. Kianfé, J. Kühlborn, R. T. Tchuenguem B. T. Tchegnitegni, B. K. Ponou, J. Groß, R. B. Teponno, J. P. Dzoyem, T. Opatz, L. A. Tapondjou, *S. Afr. J. Bot.* **2020**, *133*, 161–166.

- **Applications of Xylochemistry from Laboratory to Industrial Scale**
  J. Groß,† J. Kühlborn,† T. Opatz, *Green Chem.* **2020**, *22*, 4411–4425.

- **Making Natural Products from Renewable Feedstocks: Back to the Roots?**
  J. Kühlborn,† J. Groß,† T. Opatz, *Nat. Prod. Rep.* **2019**, *37*, 380–424.

- **Structure, Biosynthesis, and Bioactivity of Photoditritide from *Photorhabdus temperata* Meg1**
  L. Zhao, R. M. Awori, M. Kaiser, J. Groß, T. Opatz, H. B. Bode, *J. Nat. Prod.* **2019**, *82*, 3499–3503.

- **Synthesis of 2,3-Dihydro-4-Pyridones, 4-Quinolones and 2,3-Dihydro-4-Azocinones by Visible-Light Photocatalytic Aerobic Dehydrogenation**
  A. Sevenich, P. S. Mark, T. Behrendt, J. Groß, T. Opatz, *Eur. J. Org. Chem.* **2020**, *82*, 1505–1514.

†Geteilte Erstautorenschaft

- **Xylochemical Synthesis of Cytotoxic 2-Aminophenoxazinone-Type Natural Products Through Oxidative Cross Coupling**
  J. Kühlborn, M. Konhäuser, J. Groß, P. Wich, T. Opatz, *ACS Sustainable Chem. Eng.* **2019**, *7*, 4414–4419.